Chemical Research in Toxicology

pubs.acs.org/crt

Review

A Review on the Recent Applications of Deep Learning in Predictive Drug Toxicological Studies

Krishnendu Sinha,* Nabanita Ghosh, and Parames C. Sil*

Cite This: https://doi.org/10.1021/acs.chemrestox.2c00375

Read Online

ACCESS | Metrics & More | Article Recommendations

ABSTRACT: Drug toxicity prediction is an important step in ensuring patient safety during drug design studies. While traditional preclinical studies have historically relied on animal models to evaluate toxicity, recent advances in deep-learning approaches have shown great promise in advancing drug safety science and reducing animal use in preclinical studies. However, deep-learning-based approaches also face challenges in handling large biological data sets, model interpretability, and regulatory acceptance. In this review, we provide an overview of recent developments in deep-learning-based approaches for predicting drug toxicity, highlighting their potential advantages over traditional methods and the need to address their limitations. Deep-learning models have demonstrated excellent performance in predicting toxicity outcomes from various data sources such as chemical structures, genomic data, and high-throughput screening assays. The potential of deep learning for automated feature engineering is also discussed. This review emphasizes the need to address ethical concerns related to the use of deep learning in drug toxicity studies, including the reduction of animal use and ensuring regulatory acceptance. Furthermore, emerging applications of deep learning in drug toxicity prediction, such as predicting drug−drug interactions and toxicity in rare subpopulations, are highlighted. The integration of deep-learning-based approaches with traditional methods is discussed as a way to develop more reliable and efficient predictive models for drug safety assessment, paving the way for safer and more effective drug discovery and development. Overall, this review highlights the critical role of deep learning in predictive toxicology and drug safety evaluation, emphasizing the need for continued research and development in this rapidly evolving field. By addressing the limitations of traditional methods, leveraging the potential of deep learning for automated feature engineering, and addressing ethical concerns, deep-learning-based approaches have the potential to revolutionize drug toxicity prediction and improve patient safety in drug discovery and development.

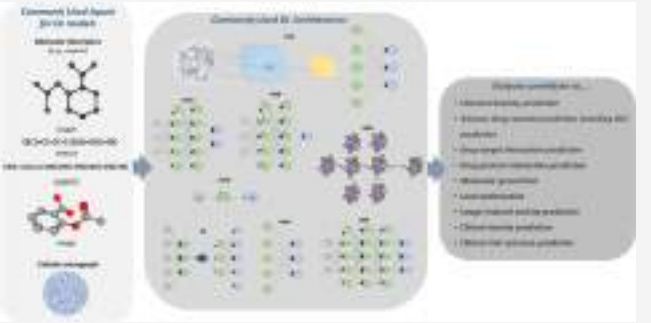

CONTENTS

Received: November 28, 2022

1. INTRODUCTION

The utilization of big data has emerged as a leading factor driving contemporary research in toxicology and drug discovery. An immense volume of data about biomedical and toxicity assessments, such as high-throughput screening, omics, image, and signal data, has been amassed and has the potential to provide valuable insights for healthcare and biological research.[1] The industrial and academic sectors are heavily involved in research and development, producing cutting-edge technologies such as OpenAI'sGenerative Pretrained Transformer (GPT) models, Deep Mind's AlphaFold, and others.[2−5] IBM's Watson for Oncology, for instance, analyzes patients' medical data to aid clinicians in identifying potential treatment options. Similarly, DeepMind, following its successful creation of AlphaGo in the game of Go, has launched DeepMind Health with a focus on the development of effective healthcare technologies.[2,6] Recently, DeepMind's AlphaFold has achieved a significant breakthrough in tackling one of the most difficult challenges in biology, the determination of the tertiary structure of a protein from its primary sequence.[7,8] In recent years, machine learning (ML) has become a widely used approach for knowledge extraction from big data in bioinformatics, predictive toxicology, and drug discovery research.[1,9,10] However, traditional ML algorithms like random forests (RF), support vector machines (SVM), and logistic regressions (LR) require well-defined features to classify patterns in high-dimensional biological data.[11−15] This poses a challenge for researchers to identify which features are most relevant for the task at hand and to develop a feature extractor to transform raw data into suitable input forms.[12,16,17] In contrast, representation learning, particularly deep learning, has shown significant promise for overcoming this limitation.[9,10] Deep learning (DL) is a specialized subfield of ML that utilizes neural networks to learn and discover internal representations of raw data.[11,12] Recent advances in parallel and distributed computing, sophisticated algorithms, and applications in speech and image recognition have led to the widespread popularity of deep learning in analyzing big data.[1,18,19] Deep learning has also been transforming biomedical research by enabling accurate radiological studies, molecular biological studies, and chemical and drug toxicity predictions.[8,10,20−30] In the field of drug toxicity prediction, deep learning has shown significant potential for improving safety assessment studies by enabling more reliable and efficient predictive models. Deep-learning-based approaches have demonstrated state-of-the-art performance in predicting toxicity outcomes from various data sources such as chemical structures, genomic data, and high-throughput screening assays. Deep learning has also been used to predict drug−drug interactions and toxicity in rare subpopulations, highlighting its emerging applications in this field.[31−35]

Drugs are often necessary to treat illnesses, but they can also cause negative reactions, which are referred to as adverse drug reactions (ADRs).[9,10,30] Therefore, it is crucial to monitor and manage ADRs closely to ensure drug safety and reduce risks associated with clinical trials. To achieve this, predictive drug toxicological studies are essential, beginning with in vitro and in vivo studies during the drug development process and continuing through clinical trials and postmarketing surveillance.[10] Despite these efforts, ADRs still lead to a significant number of clinical trial failures and drug withdrawals.[36,37] The current approaches used for assessing drug toxicity have limitations and challenges, making them less than ideal. For example, traditional in vitro and in vivo assays can be costly, time-consuming, and ethically questionable.[10,38] Moreover, these methods are heavily dependent on animal models, which goes against the principles of the 3R approach (i.e., Replacement, Reduction, and Refinement) of humane treatment toward animals.[38,39] Additionally, animal studies may not always be reliable predictors of human toxicity due to differences in physiology and metabolism between species, which can lead to unexpected adverse effects during clinical trials.[40] Furthermore, these traditional approaches have limited throughput and may not capture the complex interactions that occur within biological systems, making it difficult to predict toxicity for large numbers of compounds or to accurately identify the mechanisms underlying toxicity. Traditional tools are also facing great challenges in future toxicity prediction efforts due to increased polypharmacy and patient diversity.[41−44] Finally, the integration and interpretation of toxicity data from different sources can be challenging due to differences in experimental protocols, data formats, and quality. These limitations and challenges highlight the need for alternative methods for toxicity assessment, such as in silico approaches, which can complement and enhance traditional methods.

In silico methods are gaining popularity as a cost-effective and efficient alternative for drug toxicity assessment, with QuantitativeStructure−Activity Relationship (QSAR) being a commonly used approach.[45−47] However, QSAR has limitations, such as the requirement for large and diverse data sets, and the lack of standardization in experimental design and data reporting.[48,49] To overcome these limitations, researchers are exploring other in vitro/in vivo assay data such as omics data and high-content imaging.[50−52] ML/DL algorithms have also aided in silico methods for toxicity prediction, but their reliability and interpretability in real-world scenarios are limited.[53,54] Address-

https://doi.org/10.1021/acs.chemrestox.2c00375
Chem. Res. Toxicol. XXXX, XXX, XXX−XXX

ing these limitations, such as using diverse and high-quality data sets and robust validation protocols, is necessary for accurate and reliable prediction of drug toxicity.[53−58]

This review covers the importance of predictive drug toxicological studies, as well as their limitations, including traditional computational techniques like QSAR. The focus then shifts to the advantages of deep-learning algorithms over traditional methods in predicting drug toxicity. Various deep-learning paradigms, architectures, and models used in drug toxicological studies such as self-supervised learning, graph neural networks (GNNs), convolutional neural networks (CNNs), recurrent neural networks (RNNs), and autoencoders, are discussed. The evaluation metrics and interpretability of deep-learning models are also explained, along with success stories in predictive drug toxicological studies. Additionally, useful databases with their advantages and disadvantages are highlighted. Finally, this review concludes with an overview of existing models, challenges, emerging trends, future directions, ethical considerations, and societal implications of deep learning in drug toxicological studies.

2. QSAR AND ITS LIMITATIONS

QSAR analysis is the most commonly used in silico method in predictive toxicology.[59,60] QSAR is a computational modeling technique that uses mathematical and statistical methods to predict the biological activity or toxicity of chemical compounds based on their chemical structures.[59] QSAR models are typically constructed by correlating the physicochemical properties of a set of compounds with their corresponding biological activities or toxicities using a variety of statistical methods such as multiple linear regression (MLR), partial least-squares regression (PLS), or support vector regression (SVR).[61−63]

The development of QSAR models involves the identification and calculation of molecular descriptors, which are mathematical representations of structural features that are related to the activity or toxicity of the compound.[64−67] Molecular descriptors can be calculated using various algorithms and software tools, such as Morderd, Dragon, PaDEL-Descriptor, ChemAxon, etc.[68−72] There are numerous descriptors available, including geometric, electronic, and topological descriptors.[69] The chemical structures of the compounds are represented by a set of molecular descriptors, which are calculated based on their three-dimensional (3D-QSAR) or two-dimensional structures.[70] The molecular descriptors are numerical values that quantify the physicochemical properties of the compounds, such as molecular weight, electronic charge distribution, lipophilicity, hydrogen bonding capacity, and steric properties. The molecular descriptors are then used as input variables in the QSAR model.[69−76] Regression analysis is then used to establish a quantitative relationship between the molecular descriptors and the activity or toxicity of the compound.[61,63,64] The resulting QSAR equation is typical of the following form: *Activity/toxicity* = *f*(*Descriptor*1, *Descriptor*2, ..., *DescriptorN*), where *Activity/toxicity* is the biological activity or toxicity of the compound, *Descriptor*1−*DescriptorN* are the molecular descriptors, and *f* is a mathematical function that relates the descriptors to the *Activity/toxicity*.

The performance of QSAR models is evaluated using cross-validation and validation metrics, and the applicability domain of the model should be carefully considered to ensure reliable and accurate predictions.[61,77,78] Cross-validation is a common technique used to evaluate the predictive power of QSAR models. This technique involves dividing the data set into training and validation subsets, with the model being trained on the training subset and tested on the validation subset.[77] This process is repeated several times using different subsets of the data, and the results are averaged to obtain an estimate of the model's predictive power. Validation metrics such as *R*-squared (R^2; the coefficient of determination, indicating how well the model fits the data), the root-mean-square error (*RMSE*; the average deviation of predicted values from observed values), and the mean absolute error (*MAE*; indicating the average magnitude of prediction errors regardless of direction) are used to evaluate the performance of QSAR models.[77−79] R^2 measures the proportion of variance in the activity/toxicity that can be explained by the QSAR model, while *RMSE* and *MAE* measure the difference between the predicted and actual values of the activity/toxicity.[77−80]

QSAR models can be used to predict the biological activity or toxicity of new compounds based solely on their chemical structures. However, there are several limitations to QSAR models that need to be considered.

QSAR models, which assume that similar compounds have similar toxicity outcomes, often struggle to accurately predict activity cliffs (ACs) where this assumption does not hold.[81−83] ACs refer to pairs of small molecules that share high structural similarity but display a significant difference in their binding affinity toward a specific pharmacological target.[81] Despite the difficulties posed by ACs, they provide a substantial understanding of the structure−activity relationship (SAR), which holds great value. AC clusters can be found across different compound activity categories and offer valuable insights into SAR. Computational techniques can effectively organize and extract SAR information from these clusters.[84] Nevertheless, the extraction and application of SAR information from AC clusters present considerable challenges and require systematic approaches to access SAR information.[85] For example, AC prediction by QSAR models generally improved when one compound's activity is known.[81] Also, graph isomorphism features performed competitively for AC classification, while extended-connectivity fingerprints were best for general QSAR prediction.[81] Traditional methods use a fixed potency difference, regardless of the target. The current study introduces a computational approach for AC identification and analysis with three components: variable potency difference criteria based on target sets, extraction from analog series (ASs), and analysis of multisite ACs using individual substitutions.[84] A benchmarking study was conducted, evaluating several ML/DL approaches, and it was found that machine learning with molecular descriptors outperforms complex deep-learning methods.[82] The need for activity-cliff-centered metrics and novel algorithms is emphasized. In response to this, Molecule-ACE, an open-access benchmarking platform on GitHub, was created.[82]

Additionally, the quality and completeness of the data used to build QSAR models can greatly affect the accuracy of the predictions. QSAR analysis relies on the availability of experimental toxicity data to train and validate the models. If the data is limited, biased, or inconsistent, the QSAR model may not be accurate or reliable.[86,87] Additionally, QSAR models are often developed for specific types of toxicity end points, such as acute toxicity or genotoxicity, and may not apply to other types of toxicity. QSAR models require large and diverse data sets to ensure that the models can capture the variability and complexity of the toxicity outcomes. However, the availability of high-quality toxicity data is often limited, and the data sets

https://doi.org/10.1021/acs.chemrestox.2c00375
Chem. Res. Toxicol. XXXX, XXX, XXX−XXX

used to build QSAR models may be biased or incomplete.[88,89] Then the selection of descriptors is a critical step in QSAR analysis as it determines the accuracy, reliability, and robustness of the model, and there are limitations to using chemical descriptors for toxicity prediction.[90] Chemical descriptors capture only the structural properties of a chemical and do not consider other factors, such as metabolism, bioavailability, and toxicokinetics. Therefore, QSAR models built solely on chemical descriptors may not be able to accurately predict the toxicity of a chemical in vivo.[91,92] Also, one should remember that QSAR models may not apply to all types of biological activity/toxicity or all chemical classes of compounds. The predictions of QSAR models should always be confirmed experimentally before making any decisions based on them.[91,92]

QSAR remains valuable in early stage drug development for screening compounds, but exploring new methods is essential for expanding its capabilities. Researchers are incorporating additional data sources like omics data and high-content imaging to address limitations and complement QSAR.[91] Omics data provides a comprehensive view of how the body reacts to chemicals, while high-content imaging captures structural and functional changes in cells and tissues.[93] Machine-learning algorithms combined with these data types have led to predictive models for toxicity.[94−98] However, challenges exist, including the need for high-quality experimental data, complex analysis, and integration with existing knowledge. While these methods complement QSAR, they may have limitations in reproducibility and interpretability. Integrating in silico approaches enhances drug toxicity models, and interdisciplinary collaboration is vital for advancing the field.

3. A BRIEF ACCOUNT ON DEEP LEARNING

ML is a technique for computers to learn from data without explicit programming. It uses algorithms to learn rules from data and produce results (Figure 1).[99] Traditional ML requires manual feature extraction, simplifying data for algorithm.[99] In complex data sets like toxicological data, this process becomes complex.[100] Deep learning, a type of ML, is better in such cases. It models the world as nested concepts and uses a multilayer architecture inspired by the brain to automatically extract features (Figure 1).[14] Its advantage is processing raw data, extracting features, and learning complex relationships. Artificial neural networks (ANNs) are fundamental to deep learning. They use linear units, taking inputs with weights and biases to give output. Dense layers, stacking linear units, form a deep neural network (DNN).[101] DNNs have input and output layers, with hidden layers in-between. Activation functions (e.g., rectified linear unit or ReLU) add nonlinearity between dense layers.[14101,102] Deep learning hierarchically processes data, with layers gaining a more profound understanding, representing complex associations.

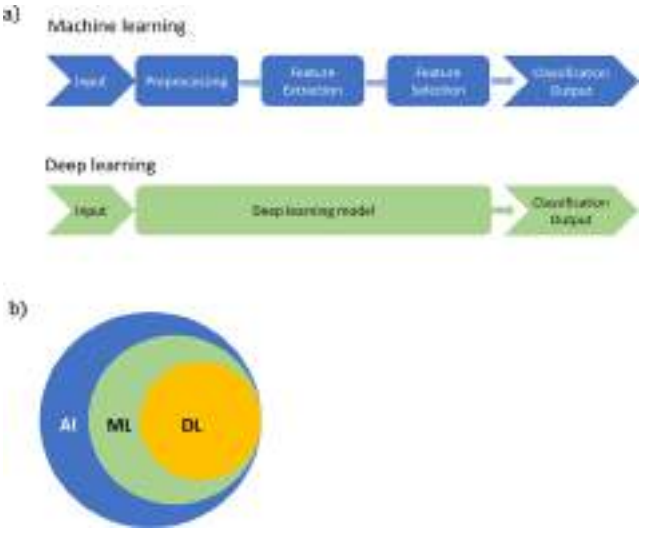

Figure 1. (a) Differences between the workflow of machine learning and deep learning; (b) interrelation between artificial intelligence (AI), machine learning (ML), and deep learning (DL).

3.1. Basic Types of Deep-Learning Models and Model Training Types. ANNs have various architectures used by different deep-learning models for different problem types, and understanding task-specific categories and model training types is important before exploring these architectures.[103]

3.1.1. Generative and Discriminative Models. Deep-learning models are broadly divided into two fundamental categories, namely, discriminative and generative.[103,104] Discriminative models learn the conditional probability distribution $p(y|x)$ of the output variable given the input variables x and corresponding label y. More specifically, discriminative models aim to find a function $f(x)$ that maps input x to output y. They focus on modeling the decision boundary between different classes directly from the input features.[104] Generative models learn the joint probability distribution $p(x,y)$ of the input and output variables and generate new data points by sampling from it.[104] Discriminative models predict the output based on the input, while generative models learn how the data were generated to create new instances.[104] Discriminative models are used for supervised learning, while generative models are suited for unsupervised learning and probabilistic distribution problems.[103] For example, discriminative models include classification and regression, while generative models include autoencoders and generative adversarial networks.[99]

3.1.2. Types of Model Training. Deep-learning models can be trained through five fundamental ways of learning: supervised, unsupervised, semisupervised, self-supervised, and reinforcement learning.[12,13,103−109] Supervised learning involves using labeled data, represented as $\{(x_i,y_i)\}_{i=1}^{n}$, where x_i is a feature vector and y_i is the corresponding label.[110] Each dimensional value is a feature, represented as $x_i^{(j)}$. Feature defines an instance. The goal is to train a model that can classify unlabeled feature vectors accurately. In unsupervised learning, there is no labeled data set, and the training data is represented as $\{x_i\}_{i=1}^{n}$, consisting of unlabeled feature vectors, x_i.[99] Unsupervised learning models transform these vectors to solve various problems, such as pattern identification or classification.[111] Semisupervised learning combines both supervised and unsupervised techniques to extract important features from high-dimensional data sets that contain labeled and unlabeled information. It addresses the challenge of extracting meaningful features from such data.[104,111] Self-supervised learning (SSL) is an emerging paradigm in deep learning that utilizes unlabeled data and contrastive learning to learn representations without human supervision.[112] SSL replaces the need for labeled data sets by leveraging co-occurrence relationships in data.[112−116] It can be categorized into generative, contrastive, and generative−contrastive methods.[112] SSL consists of a pretext task, where the model learns to extract features, and a downstream task, where the learned representations improve performance on target tasks like image classification.[112−115,117] The goal is to learn generic

https://doi.org/10.1021/acs.chemrestox.2c00375
Chem. Res. Toxicol. XXXX, XXX, XXX−XXX

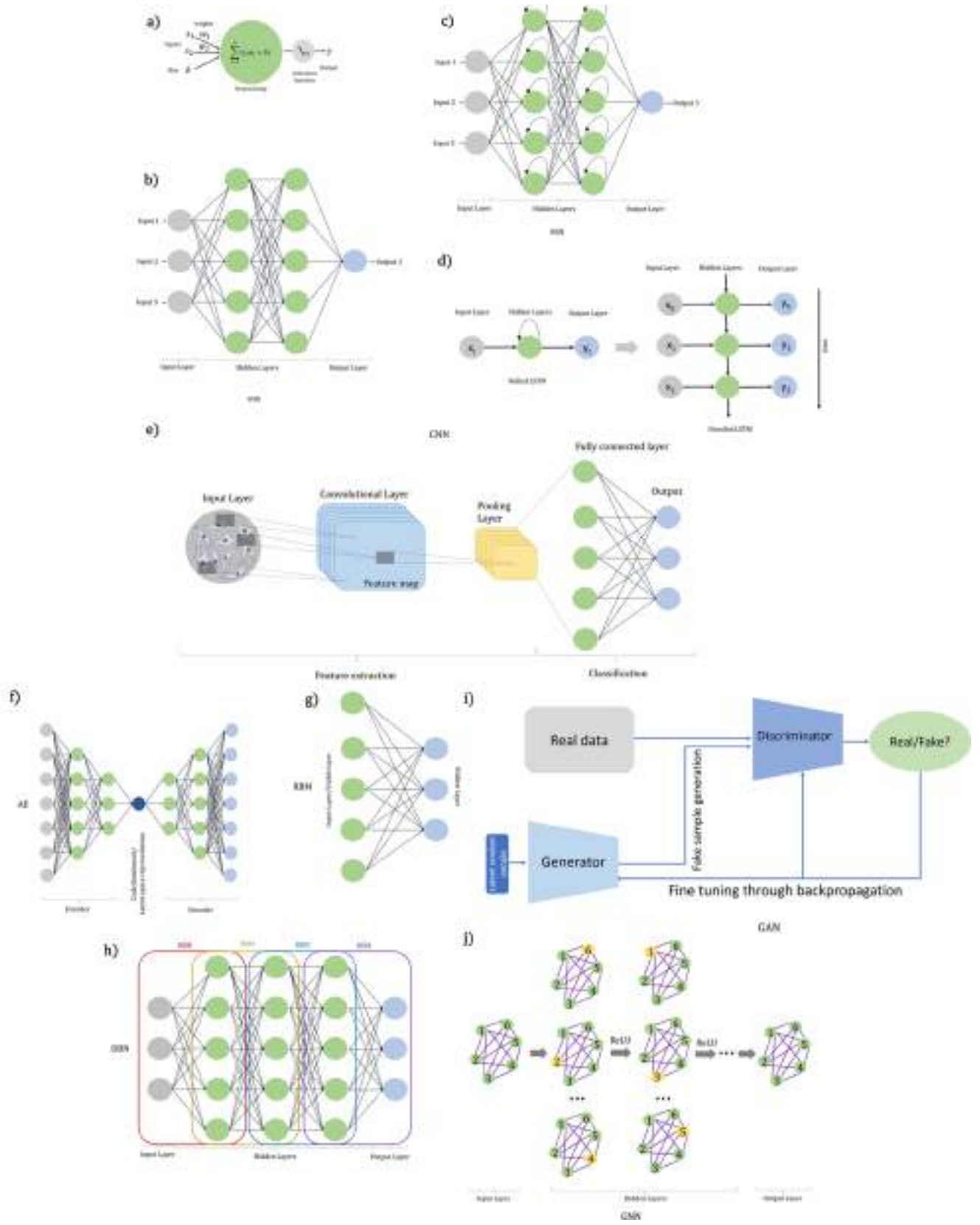

Figure 2. Architecture of artificial neuron/perceptron (a), feed-forward neural network (FNN) (b); recurrent neural network (RNN) (c); long–short-term memory network (LSTM) (d); convolutional neural network (CNN) (e); autoencoder (AE) (f); restricted Boltzmann machine (RBM) (g); deep belief network (DBN) (h); generative adversarial network (GAN) (i); and graph neural network (GNN) (j).

representations transferable to various tasks. SSL shows promise when labeled data sets are scarce or costly.[117]

3.2. ANN Architectures. ANN architectures organize neurons (Figure 2a) and layers, influencing information flow

https://doi.org/10.1021/acs.chemrestox.2c00375
Chem. Res. Toxicol. XXXX, XXX, XXX−XXX

and processing. Examples include feed-forward networks (FNNs) with unidirectional flow, recurrent neural networks (RNNs) with bidirectional flow, and Kohonen Self-Organizing Neural Networks (SOMs) with lateral flow.[11,118−122] RNNs capture temporal dependencies, while SOMs compete to identify the best matching unit (BMU).[118] Researchers optimize ANNs for specific tasks by adjusting parameters. FNNs handle classification and regression, RNNs process language and speech, and SOMs aid clustering and visualization in drug toxicity studies. FNNs, generally known as DNNs (when there is more than one hidden layer, which is true in almost all cases) or multilayer perceptrons (MLPs), are highly utilized neural network architectures (Figure 2b). They consist of multiple fully connected hidden layers between input and output layers. The networks are unidirectional, with information flowing from input to output, and lack feedback between layers. Each node in a layer performs a weighted summation of inputs, applies an activation function, and passes the output to the next layer, except for the output layer, which produces the classification result.

RNNs are commonly used for sequential and time series data. They have hidden layers with feedback connections, allowing information from one instance to be used as input for the next (Figure 2c).[123] These connections help retain the memory of past inputs and capture temporal dependencies. Long−short-term memory (LSTM), a popular RNN architecture, addresses the vanishing gradient problem and includes recurrent connections with gates controlling information flow (Figure 2d). RNNs are trained using the back propagation through time (BPTT) algorithm.

SOMs are neural networks primarily used for unsupervised learning.[124] However, some variations of SOMs can be used in supervised learning.[125] They organize input data into clusters based on similarity while preserving topological properties. SOMs have input and output layers, with the output layer represented as a two-dimensional grid. The network learns by iteratively updating the weights of output neurons. Information flows laterally in the output layer, with neurons competing based on weight similarity to input data, forming new clusters.

CNNs are neural networks designed to learn spatial hierarchies of features.[11,120,126] They consist of convolutional layers, pooling layers, and fully connected layers (Figure 2e). Convolutional layers use filters to generate feature maps, while pooling layers downsample the input. Fully connected layers operate on flattened inputs, introducing nonlinearities through activation functions like ReLU.[120,127] CNNs process data as arrays, such as 2D arrays for images or 3D arrays for video data.

Visual neural network (VNN) is a unique deep-learning model that interprets the relationship between gene-level measurements and cellular behavior.[128] Inspired by molecular subsystems, VNN models identify key pathways and processes by analyzing interconnected nodes representing genes and proteins.[128] They achieve an accuracy-interpretability balance by incorporating biological ontologies. VNNs have been used successfully in predicting yeast cell growth, drug response, and cancer patient stratification.[128−130] They have broad applications in drug discovery, disease diagnosis, and personalized medicine, revolutionizing our approach to healthcare.

Restricted Boltzmann Machines (RBMs) are probabilistic, unsupervised, generative ANNs with only two layers: the input/visible layer and the hidden layer (Figure 2g).[131,132] RBMs calculate the probability distribution of the training set using a stochastic approach, and each neuron gets activated randomly at the beginning of training. RBMs can be stacked to form deep belief networks (DBNs), which are pretrained and then fine-tuned for specific tasks. RBMs are also known as generative models as they reconstruct input differently from the original input.[133]

An autoencoder (AE) is an unsupervised neural network that compresses data while minimizing reconstruction errors (Figure 2f).[134,135] It consists of an encoder and a decoder, which are symmetrical deep belief networks (DBNs) (Figure 2h), and a hidden layer called the latent space representation or code.[136,137] The encoder generates a reduced feature representation and stores it in the code, while the decoder reconstructs the initial input. There are different types of autoencoders, such as variational autoencoders (VAEs), denoising autoencoders (DAEs), and adversarial autoencoders (AAEs), each with unique architectures and applications.[135,138,139] VAEs are generative models used for high-dimensional data, while DAEs prevent the network from learning only the identity function by corrupting input data. AAEs combine autoencoders and generative adversarial networks (GANs) to generate realistic data samples.[138] Autoencoders are useful for noise reduction, compression, dimensionality reduction, anomaly detection, and feature extraction.

GANs are unsupervised generative models consisting of a generator and a discriminator (Figure 2i).[140] The generator produces fake data samples to deceive the discriminator, while the discriminator tries to differentiate between fake and real data. Through training, both networks improve iteratively, leading to the generation of high-quality synthetic data.[141] GANs have applications in various fields, including medicine, drug discovery, pandemics, 3D object generation, face detection, image processing, anomaly detection, texture transfer, and traffic control.

Normalizing flows (NFs) are a family of generative models that can efficiently sample and evaluate probability densities.[142] NFs use invertible neural networks to transform a simple base density into complicated distributions with strong correlations and multimodality.[143] They have been applied in various fields, including image, audio, and graph generation, and they are useful for efficient sampling and density estimation.[144] However, NFs can be computationally expensive for high-dimensional data.

Diffusion models are a type of generative model that use a Markov chain of diffusion steps to gradually introduce random noise to the data and then learn to reverse the process to generate desired samples.[145] Diffusion models capture the underlying structure and dependencies of the data by estimating the probability density function of the data set.[145,146] Unlike other generative models like VAE or flow models, diffusion models use a fixed learning procedure and maintain the same high dimensionality as the original data.[145,147] They are used for generative tasks to produce new data from the training data set.

Autoregressive models predict the output at the current time step based on the output of previous time steps.[148] These models measure the correlation between past observations and the next time step to make predictions.[148] A positive or negative correlation indicates whether variables change in the same or opposite directions.[148] They come in feed-forward, recurrent, and convolutional forms and are used in molecular graph generation, language modeling, speech recognition, and time series prediction.[149,150]

GNNs are neural networks designed to process graph-structured data, making them suitable for tasks such as molecular

https://doi.org/10.1021/acs.chemrestox.2c00375
Chem. Res. Toxicol. XXXX, XXX, XXX−XXX

Table 1. List of Highly Used DL Models along with Their Applications

Deep-Learning Model/Architecture	Best Suited for	Applications
Convolutional Neural Networks (CNN)	Image-Based Toxicity Studies	High-dimensional imaging data, such as histopathology slides, cellular micrographs, etc.
Recurrent Neural Networks (RNN)	Time-Series Toxicity Studies	Longitudinal toxicity data, such as time-series gene expression data or longitudinal imaging data
Generative Adversarial Networks (GAN)	Augmenting Small Toxicity Data Sets	Generating synthetic data for training is particularly useful when training data is limited, such as in rare toxicity events or in cases where data collection is costly or time-consuming
Autoencoders	Feature Extraction	Reducing high-dimensional data, such as reducing the number of features in high-dimensional molecular data, or extracting key features from complex toxicity data sets
Visual Neural Networks (VNN)	Visualizing Chemical Structures	Identifying patterns in chemical structures, useful for predicting toxicity based on molecular structures
Graph Neural Networks (GNN)	Modeling Molecular Interactions	Learning from graph-structured data, such as predicting toxicity based on molecular interactions and relationships
Kohonen Self-Organizing Maps (SOM)	Clustering and Visualization	Clustering and visualizing toxicity data, such as identifying subgroups of toxicity in a given data set
Normalizing Flow-Based Models	Modeling Toxicity Distributions	Modeling the distribution of toxicity scores for a given data set
Autoregressive Models	Learning Conditional Probability Distributions	Identifying the probability of toxicity given a set of inputs, such as molecular or phenotypic data
Diffusion Models	Handling High-Dimensional Data	Learning a diffusion process to model the underlying probability distribution of high-dimensional data
Deep Belief Networks (DBN)	Predictive Modeling	Handling missing data and imbalanced data sets is particularly useful when there is a large amount of missing data or when the data is imbalanced
Transfer Learning	Pretraining on Related Toxicity Data	Limited toxicity data sets are particularly useful when the available data is limited or the training set is small, or when the model is transferred from related fields, such as image analysis or natural language processing
Attention-Based Models	Multimodal Data Integration	Combining different types of toxicity data, such as combining molecular and imaging data, or clinical and genetic data

Table 2. List of Commonly Used Evaluation Metrics

Metric	Formula	Interpretation	Limiting Values
Accuracy	$\frac{TP+TN}{TP+TN+FP+FN}$	The proportion of correctly classified instances. Higher is better.	$0 \le Accuracy \le 1$
Precision	$TP/(TP+FP)$	The proportion of correctly predicted positive instances. Higher is better.	$0 \le Precision \le 1$
Recall (Sensitivity or *TPR*)	$TP/(TP+FN)$	The proportion of actual positive instances correctly predicted as positive. Higher is better.	$0 \le Recall \le 1$
*F*1 Score	$\frac{2 \times Precision \times Recall}{Precision + Recall}$	Higher the value better the precision and recall.	$0 \le F1\,Score \le 1$
Specificity (*TNR*)	$TN/(TN+FP)$	The proportion of actual negative instances correctly predicted as negative. Higher is better.	$0 \le Specificity \le 1$
FPR	$FP/(TN+FP)$	The proportion of actual negative instances incorrectly predicted as positive. Lower is better.	$0 \le FPR \le 1$
AUROC	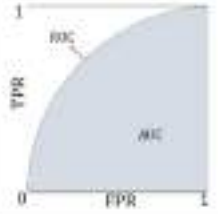	A measure of the performance of a binary classifier at different classification thresholds. The higher the AUROC, the better the model predicts.	$0 \le AUROC \le 1$
MSE	$\frac{1}{N}\sum_{i=1}^{N}(y_i-\hat{y}_i)^2$	Measures how close a model's prediction is to an actual data point. The lower the MSE, the better the model predicts.	$0 \le MSE \le \infty$
MAE	$\frac{1}{N}\sum_{i=1}^{N}\lvert y_i-\hat{y}_i\rvert$	A measure of how far off the predictions are from the actual values. The lower the MAE, the better the model predicts.	$0 \le MAE \le \infty$
RMSE	$\sqrt{\frac{1}{N}\sum_{i=1}^{N}(y_i-\hat{y}_i)^2}$	A measure of how accurately the model predicts the response. The lower the RMSE, the better the model predicts.	$0 \le RMSE \le \infty$
R^2 Score	$1-\frac{\sum(y_i-\hat{y}_i)^2}{\sum(y_i-\bar{y}_i)^2}$	A measure of how well the model fits the data. The closer the R2 value is to 1, the better the fit.	$0 \le R^2\,Score \le 1$

https://doi.org/10.1021/acs.chemrestox.2c00375
Chem. Res. Toxicol. XXXX, XXX, XXX−XXX

structure analysis (Figure 2j).[151] GNNs use a message-passing mechanism to allow nodes in a graph to exchange information with their neighbors.[151] This process is repeated multiple times, enabling nodes to refine their embeddings based on information from neighbors GNNs learn node and graph-level embeddings, enabling graph classification, link prediction, and clustering.[151−154] In recent years, GNNs have seen various advancements such as graph convolutional networks (GCN), graph attention networks (GAT), graph recurrent networks (GRN), etc., which have shown remarkable results in deep-learning tasks.[155−159] GCNs treat each atom in a molecule as a node and use the chemical bonds between atoms to connect these nodes.[160] The aim is to allow the nodes to share information, which helps to build a complete picture of the molecular structure. The graph convolution process iteratively collects information from the neighboring atoms for each node (atom), resulting in a more complete understanding of the local and global features of the molecule.[161]

Attention mechanisms in deep-learning models capture the relevance or importance of input features or positions. These mechanisms assign weights or scores to each input feature, indicating its relative importance.[161] Transformers, a type of neural network architecture, process sequential data by attending to different parts of the input sequence simultaneously.[162] They use multihead attention mechanisms to learn global dependencies and positional encodings to distinguish the position of each element.[163] Transformers are widely used in natural language processing tasks, offering the ability to model long-range dependencies without the vanishing gradient problem in RNN.[163,164]

Please note that Table 1 provides specific scenarios for the use of different deep-learning models in toxicity studies, but it may not cover all situations and can be modified or adapted based on the research scope and toxicity data being studied.

3.3. Performance Evaluation, Interpretability, and Utility of Deep-Learning Models. Deep-learning models excel in complex tasks but lack interpretability, requiring a balance between evaluation metrics and understanding the prediction process for dependable and credible results.[189−191]

Classification and regression deep-learning models are evaluated using various metrics such as accuracy, precision, recall, specificity, *F*1 score, receiver operating characteristic (*ROC*) curve, the area under the curve (*AUROC* or *AUC*), the area under the precision-recall curve (*AUPRC*), *MAE*, *MSE*, *RMSE*, and R^2 (Table 2).[165−167] These metrics assess the performance of a model by measuring factors like correct identification of outcomes, false positives and negatives, and trade-offs between precision and recall. Instead, evaluating implicit generative models, like GANs and diffusion models, is challenging due to the absence of likelihood values.[168] Common metrics like inception score (IS) and Frechet inception distance (FID) are heuristic, and their meaning is not fully understood. Studies have shown that FID and IS can vary significantly in ranking similar models.[168] Researchers have explored different evaluation paradigms for generated text, including discriminative and generative metrics. A combined framework called T5Score has been proposed, which outperforms existing metrics.[169] This metric uses both supervised and unsupervised[169] signals. Additionally, a method based on Riemannian geometry has been proposed to address the issue of densely covered latent space in neural samplers like VAEs and GANs, allowing for principled distance measurement.[170] Finally, note that the metrics discussed here are not exhaustive, and there are many more out there used contextually. It is important to carefully select appropriate metrics that align with the objectives of the problem and avoid metrics that may introduce bias or prioritize certain types of errors.

Interpretability is vital in drug toxicological studies for understanding and trusting deep-learning models. Advanced interpretability methods have emerged, including visualization techniques like saliency maps, class activation maps, and feature importance maps.[171] These techniques allow researchers to identify the important features in the input data that contribute to the model's predictions, aiding in the discovery of potential biomarkers for drug toxicity. Surrogate models provide simplified approximations of deep-learning models, shedding light on the most influential features and the decision-making process.[172] LIME offers interpretable explanations for classifier predictions, while activation maximization and layer-wise relevance propagation (LRP) techniques enhance interpretability.[173,174] Adversarial examples help uncover model vulnerabilities, while model-agnostic methods provide a general framework for interpreting machine-learning models.[175,176] The SHAP (Shapley Additive exPlanations) framework unifies various methods, assigning importance values to each feature for specific predictions, improving performance, and aligning with human intuition.[177] Explainable artificial intelligence (XAI) addresses the lack of transparency in traditional "black box" models, promoting trust and responsible use.[178] Attention mechanisms, including self-attention in transformer-based models, show promise in enhancing interpretability, particularly in drug toxicity prediction.[179−181] Despite these advancements, challenges such as misleading interpretations and overfitting must be carefully considered when applying interpretability methods in drug toxicological studies.

Deep-learning models in predictive toxicology offer key features such as generalizability, transfer learning, robustness, scalability, abstract descriptor generation, and a universal learning approach.[182−185] However, training deep-learning models comes with challenges such as premature convergence, overfitting, vanishing gradients, exploding gradients, adversarial attacks, interpretability, scalability, and data bias.[186−197] Researchers have developed techniques like regularization methods, optimization strategies, proper activation functions, weight initialization, gradient clipping, adversarial training, and interpretability methods to address these challenges.[182,186,187,198−200] Scalability is addressed through distributed training, model parallelism, and data parallelism, while data bias can be mitigated by using diverse and representative training data. Common data bias scenarios in predictive drug toxicology include imbalanced representation, outdated data, and nonhuman models.

4. DEEP LEARNING IN PREDICTIVE DRUG TOXICITY STUDIES

Different approaches can help to identify potential drug toxicity and guide drug design and optimization to ensure the safety and efficacy of new drugs. This section will deal with different aspects of traditional drug toxicity prediction approaches and how these are aided by modern deep-learning approaches (Table 1).

4.1. Chemical Toxicity Prediction. Chemical toxicity prediction uses computational models to identify potential hazards associated with a chemical compound early in the drug development process. This approach involves the use of QSAR models trained on toxicological data to predict toxicity based on the chemical structure of a compound. Mostly molecular

https://doi.org/10.1021/acs.chemrestox.2c00375
Chem. Res. Toxicol. XXXX, XXX, XXX−XXX

descriptors and simplified molecular input line entry system (SMILES) representations of chemical compounds are used for this purpose. Molecular descriptors and SMILES are two different ways of representing chemical compounds. Molecular descriptors represent chemical compounds using numerical or binary values, while SMILES represent them using textual strings. However, by predicting toxicity, researchers can make informed decisions about the safety and efficacy of potential drug candidates. Significant progress has been made in recent times by deep-learning models in the task of toxicity prediction and assisting QSAR. This will be discussed in further detail below.

4.1.1. DNN. The first study that used deep-learning for computational toxicity prediction tasks was done by Mayr et al.[30] The team developed the DeepTox pipeline, which utilizes an ensemble approach with a DNN backbone for toxicity prediction.[30] DeepTox normalizes chemical representations, computes chemical descriptors as input, trains and evaluates models, and combines the best-performing models to form ensembles.[30] In the Tox21 Data Challenge, DeepTox had the highest performance, winning the grand challenge and several other categories. The pipeline outperformed other computational approaches, such as naive Bayes, support vector machines, and random forests.[30] Idakwo et al. compared the performance of deep-learning and shallow-learning algorithms for chemical toxicity prediction using two-cell-based androgen receptor (AR) activity data sets.[201] DNN outperformed the shallow-learning algorithm random forest by a significant margin for multiple metrics, including precision, recall, F-measure, AUPRC, and AUROC.[201] The study also provided insights into structural alerts for AR agonists/antagonists and inactive/inconclusive compounds, which may aid in toxicity prediction modeling.[201]

Carcinogenicity has the potential to be a crucial toxicity of any drug compound. For that purpose, conventional studies involved 2-year rodent animal studies, which are both inhumane and time-consuming.[202] Li et al. propose DNN bases DeepCarc model for predicting the carcinogenicity of small molecules using deep-learning-based model-level representations, as a faster, more humane, and more reliable alternative to the traditional animal model.[202,203] The model follows the same architecture of DeepDILI, which is discussed under the ADRs section.[202] However, DeepCarc was evaluated on a data set of 692 compounds and outperformed four advanced deep-learning models, with an average improvement rate of 37%.[202,203] The model could also be used to screen the carcinogenicity potential of compounds from DrugBank and Tox21 and could serve as an early detection tool for carcinogenicity assessment.

4.1.2. CNN. Epoxides are often formed by cytochromes P450, and identifying the specific site of epoxidation can aid in developing safer drugs. Hughes et al. developed a model to predict sites of epoxidation on drug molecules, which can help identify potential toxicity caused by electrophilic reactive metabolites.[204] The model was built using a database of 702 epoxidation reactions and a CNN, with an accuracy of 94.9% for identifying sites of epoxidation and separating epoxidized and nonepoxidized molecules with 79.3% accuracy. The model is the first of its kind and can be accessed at http://swami.wustl.edu/xenosite.

The detection of motifs and unknown functional groups using SMILES-based CNNs can aid in drug toxicity research by identifying potential toxicophores and improving understanding of the mechanism of toxicity. Hirohara et al. created a deep-learning model for compound classification by using SMILES notation, which linearly represents a compound structure.[205] This approach allows the team to process all types of compounds and incorporates a wide range of structure information. SMILES allowed for processing all types of compounds while incorporating a broad range of structure information, and a low-dimensional representation of input features were automatically acquired by CNN's representation learning. The chemical space consisting of the features learned by SMILES-based representation learning adequately expressed a richer feature space that enabled the accurate discrimination of compounds.[205] The source code of the model is available at http://www.dna.bio.keio.ac.jp/smiles/.

Most deep-learning methods for toxicity prediction use SMILES as input, neglecting spatial information. The grid method extracts molecular characteristics, but only using van der Waals force is inadequate to represent the molecule's structure. In a recent study, a grid-based approach was introduced, combining van der Waals forces and hydrogen bonding properties for improved accuracy.[206] The study proposed a multichannel CNN model based on a two-dimensional grid of molecules for predicting molecular toxicity in drug design.[206] Multichannel grids were generated by calculating the van der Waals force and hydrogen bond based on different molecular descriptors to provide more detailed information for toxicity prediction. These grids were fed into a convolutional neural network, which outperformed traditional deep-learning and machine-learning methods on the evaluation data set (Tox21).[206] Future research could focus on introducing more accurate molecular descriptors and the grid generation method to improve the accuracy of prediction.

4.1.3. LSTM. Though CNNs are being successfully used to predict molecular toxicity, Nath and Goswami showed an efficient and comparatively fast method for detecting toxicity in new drug candidates by using LSTM.[207] The team used simplified molecular-input line-entry system (SMILES) as a parameter for developing LSTM-based models to examine new drug toxicity.[207] However, it is cautioned that imbalanced data may affect the reliability of the model's predictions, and thus sampling is adapted to balance the data.[207] Experiments with different batch sizes show an increase in training accuracy, but testing accuracy and AUROC remain almost constant.[207] Promising results are observed in the study with LSTM, but better-balanced data is needed for accuracy improvement.

4.1.4. GNN. A fundamental task in chemistry and drug discovery is learning discriminative representations of molecules. Discriminative representations of molecules are key to their molecular property and toxicity prediction.[208] Graph representation learning is a natural way to capture molecular representations, but limited labeled data can cause overfitting and poor generalization in GNNs; and by its inherent nature GNNs are data-hungry. Researchers have addressed GNN's data-hungry nature in a different yet relatable manner. Contrastive learning seems to have good promise here.[209] Contrastive Leave One Out boost for Molecule Encoders (CLOOME) is a self-supervised contrastive learning method that combines image and structure-based representations for molecule encoders.[210] It aims to enhance transferability and shows promise for activity prediction and bioisosteric replacement tasks. Though CLOOME utilizes a descriptor-based fully connected network, authors considered graphs good alternative options for structure encoders with appropriate pooling operations.[208,210] In a related study, Zheng et al. propose Molecular graph and hIgh content imaGe Alignment

https://doi.org/10.1021/acs.chemrestox.2c00375
Chem. Res. Toxicol. XXXX, XXX, XXX−XXX

(MIGA), a novel cross-modal graph-and-image pretraining framework.[208] The approach leverages the correspondence between molecular structures and phenotypic perturbations and uses cross-modal pretraining with various contrastive loss functions.[208] MIGA enhances GNNs by incorporating phenotypic features from cellular images during pretraining, bringing biological knowledge to the network for transfer to downstream tasks.[208] The proposed model utilizes high-content cell microscopy images to assist in learning molecular representation, leveraging the rich morphological information contained in stained cell images that reflect the biological changes induced by chemical structures on cell cultures, thereby improving the generalization capability in the domains of molecular property prediction.[208] MIGA is a three-stage cross-modal learning approach that aligns molecular graph representations with high-content cellular images.[208] The first stage is molecular graph encoding, where the molecule and cell microscopy images are encoded independently with a molecular graph encoder and an image encoder.[208] The second stage involves aligning graph embeddings with the image embeddings through three contrastive modules: graph-image contrastive (GIC) learning, masked graph modeling (MGM), and generative graph-image matching (GGIM).[208] The three modules are complementary and enable the encoders to perform cross-modal learning by capturing structural and localized information.[208] The final stage involves evaluating models on a benchmark data set that contains 750k molecular graph-cellular image pairs and a new biological meaningful retrieval task specific to graph-image cross-modal learning.[208] The learned representations improve performance in downstream tasks with extensive biological priors, such as achieving gains in molecular property prediction, graph-image retrieval, and clinical outcome prediction over existing models. In another study, Sun et al. pretrained GNNs in an unsupervised manner using GCL, which maximizes the mutual information between paired graph augmentations.[211] However, this approach has limitations in its augmentation design and its focus on local perturbations. To improve this, a study by Sun et al. proposed a novel framework called MoCL, which utilizes domain knowledge at both a local and global level to assist representation learning in the context of the biomedical domain where molecular graphs are present.[211] The model is trained using a double contrast objective and achieves state-of-the-art performance on various molecular data sets.[211]

Molecular graph representation learning via GNN models has gained popularity in drug toxicity studies. Pretraining models through self-supervised learning and using GNN encoders to create a representation vector for each molecule have been successful in molecular property prediction.[212] These models are then followed by a prediction model for the specific property. Zang et al. propose Hierarchical Molecular Graph Self-Supervised Learning (HiMol) as a solution to the challenges faced by molecular representation learning.[213] HiMol consists of two main components: a Hierarchical Molecular Graph Neural Network (HMGNN), which is a GNN-based hierarchical molecule encoder that captures the molecular structure and incorporates motifs, and Multilevel Self-supervised Pretraining (MSP), which uses multilevel pretext tasks to provide supervision signals for pretraining.[213] HiMol improves molecular property prediction results and captures chemical semantic information and properties, thanks to its hierarchical GNN, construction of motifs based on chemical rules, graph-level node augmentation, and multilevel self-supervised pretraining tasks.[213] Future work should include extending the model to molecule generation and optimization tasks. Another line of development for GNNs is the use of graph contrastive learning (GCL) methods. The scarcity of labeled data remains a significant obstacle to achieving high prediction performance in GNN models for QSAR analysis. For some computational drug discovery tasks, collecting labeled data can be prohibitively expensive.GCL has shown promising performance in many applications where there is a lack of labeled data through existing GCL methods that may alter the fundamental properties of a molecule.[208] To address this, a new method called GeomGCL has been proposed, which uses both 2D and 3D views of a molecule's geometry.[212] A dual-view geometric message passing network (GeomMPNN) is used to leverage both views, and a novel geometric graph contrastive scheme is designed to improve the generalization ability of GeomMPNN.[208] Experimental results on seven real-life molecular data sets show the effectiveness of GeomGCL against state-of-the-art baselines.[212]

Another approach for molecular property prediction under limited labeled data is forwarded by Wang et al., which is termed Molecular Contrastive Learning of Representations via Graph Neural Networks (MolCLR).[167] It is a self-supervised learning framework that utilizes large unlabeled data to learn differentiable representations via GNN encoders and three-molecule graph augmentations.[167] The contrastive learning framework significantly improves the performance of GNN encoders on various molecular property benchmarks, achieving state-of-the-art results on several challenging benchmarks after fine-tuning. MolCLR also learns to embed molecules into representations that can distinguish chemically reasonable molecular similarities.[167] Duvenaud et al. addressed a similar problem by introducing GCNs.[214] Circular fingerprints can encode the substructure of each atom in a molecule.[215] Duvenaud et al. proposed neural fingerprints that use a real-valued vector to represent a molecule instead of a binary vector.[214] The encoding procedure is convolutional, and the final representation is obtained by aggregating representations of all atoms, with the softmax layer enabling the interpretation of learned features.[215]

Limitations of existing self-supervised pretraining frameworks for GNNs are their inability to capture rich information in subgraphs or graph motifs, which are important for the accurate prediction of molecular properties. To address these limitations, Zhang et al. propose a novel self-supervised motif generation framework for GNNs called Motif-based Graph Self-supervised Learning (MGSSL), which extracts functional groups (subgraphs) from molecular graphs to capture rich information that node or graph-level approaches cannot, leading to better performance on downstream benchmark tasks.[216]

4.1.5. GCN. Recent advancements in neural machinery have produced promising results for molecular property prediction, particularly through DNNs applied to computed molecular fingerprints or expert-crafted descriptors and GCN; however, which method is superior for generalizing to new chemical space and for industrial use has yet to be determined, and the study by Yang et al. benchmarks and introduces a GCN that outperforms existing models on both public and proprietary data sets.[217] In a recent study, Chen et al. aimed to improve compound toxicity prediction using a GCN and semisupervised learning.[218] To address the lack of annotated toxicity data, they proposed using semisupervised learning algorithms, such as the Mean Teacher semisupervised learning algorithm, in combination with GCN.[218] Using Tox21 data, the authors found that the semisupervised learning-GCN models outperformed the GCN models trained by supervised learning and conventional

https://doi.org/10.1021/acs.chemrestox.2c00375
Chem. Res. Toxicol. XXXX, XXX, XXX−XXX

machine-learning methods by 6% on 12 toxicological end points, achieving an average AUROC score of 0.757 in the test set.[218] They also found that unlabeled data was advantageous for model training, and the optimal unannotated to annotated data ratio ranged from 1:1 to 4:1.[218] The study demonstrates the success of semisupervised learning in chemical toxicity prediction and suggests potential applications in other chemical property prediction tasks. However, the authors note limitations in terms of data diversity, interpretability of the graph convolution model, and the unresolved issue of activity cliffs.[218] Kearnes et al. proposed a graph convolution framework to learn molecular representations for data-driven tasks.[219] In addition to node features or labels, edge information is also important and can be encoded in graph convolution.[215] Liu et al. developed a system to predict ADME properties using GCN.[220] Li et al. introduced an alternative approach to generating graph-level representation using GCN by introducing a dummy super node.[221] The early spectral GCN fixed graph structure without training, but Li et al. constructed graph convolution that accepts flexible graph inputs and learned additional topology information for each input graph.[221] The previous frameworks were all built on spatial graph convolution, while spectral graph convolution was less employed in QSAR tasks.[215]

GCN models have been successful in classifying the activity of therapeutic drugs using complex information. However, Sakai et al. found that with enough experimental data and hidden layers, a simple representation of compounds could predict activity accurately.[222] The study developed activity prediction models for 127 target proteins in ChEMBL, using only two-dimensional structural information on compounds through a GCN architecture.[222] The study extended the range of hyperparameters and found that ensemble learning improved predictive performance. The study showed that GCN models built using ChEMBL data performed better than CNN, RF, and FNN models.[222] Structural diversity had minimal effect on prediction performance.[222] The study also demonstrated the potential applications of activity prediction models in drug discovery research, including drug repositioning, prioritizing strategies, finding polypharmacological drugs, and elucidating molecular mechanisms.[222] The GCN architecture developed in this study could be a useful tool in drug discovery research, as it identified a novel serotonin transporter inhibitor (SERT)-acting compound with activity comparable to a clinically effective drug. Further investigation is needed to improve the prediction performance of the models, such as using different data preprocessing methods.

4.1.6. MPNN. Deep learning in computational chemistry aims to predict molecular properties from configurations; message-passing neural networks capture molecular features as a graph, but previous studies assumed all features contribute equally regardless of the task. One proposed model overcomes this limitation by learning heterogeneous molecular features with different scales, which are trained flexibly based on the prediction target.[223] The proposed model is a dual-branched neural network that combines the message-passing framework of neural networks with standard multilayer perceptron networks for predicting molecular properties based on molecular configurations.[223] The message-passing framework allows the model to capture molecular geometric features by treating a molecule as a graph. The model learns heterogeneous molecular features with different scales and trains them flexibly based on the prediction target.[223] In addition, a discrete branch is introduced to learn single-atom features without local aggregation. The proposed model outperforms other recent models with sparser representations and considers the diverse chemical nature of targets for improved performance and generalizability. Liu et al. propose a novel neural network architecture called Atom-Bond Transformer-based Message-Passing Neural Network (ABT-MPNN) that combines the strengths of GCNs and Transformers for better molecular representation in predicting molecular properties.[224] The method integrates molecular representations at the bond, atom, and molecule levels in an end-to-end way by designing attention mechanisms in the message-passing and readout phases of MPNN. The model outperforms state-of-the-art baseline models in quantitative structure−property relationship tasks, including predicting the growth inhibitors of *Mycobacterium tuberculosis*.[224] The model's visualization modality of attention at the atomic level helps to investigate molecular atoms or functional groups associated with desired biological properties, which increases the interpretability of traditional MPNNs and can help understand the mechanism of action of drugs.

The construction of appropriate molecule representations is essential for tasks such as drug toxicity study, drug design, etc. Often, GNN models for molecular representation learning either miss higher-order graph properties or do not fully utilize edge information.[225] To address this, a new model called Communicative Message Passing Transformer (CoMPT) is proposed, which uses a message diffusion mechanism to leverage graph connectivity and reinforce interactions between nodes and edges.[225] CoMPT outperformed state-of-the-art baselines by around 4% on seven chemical property data sets and two chemical shift data sets, and visualization studies showed better representation capacity.[225]

4.1.7. SOM. SOMs are suitable for estimating the toxic properties of chemicals for risk assessment and classification for regulatory purposes. They can also be used in drug research to consider diverse data sets more effectively with nonlinear methods. The study of nonlinear descriptor-target relationships is important in drug discovery. The selection of relevant descriptors is a general problem in QSAR modeling, and neural networks including SOMs are often used to select important descriptors.[226] The SOM shows promise in modeling and decoding these relationships. The SOM and the counter propagation neural network (CP NN) are presented as powerful tools in QSAR modeling by Vracko.[226] The study showed two areas of applications, the estimation of toxic properties in environmental research and the utilization of these techniques in drug research.[226] Xiao et al. combined simulated annealing with the supervised SOM to create high-quality QSAR models.[125] The technique was tested on six data sets with different biological end points, and model quality was confirmed through external validation.[125] Cross-validation and dynamic partitioning techniques were also introduced to address model overfitting and assessment.[125]

Rallo et al. used HTS assays and SOM to evaluate the toxicity response of a murine macrophage cell line to metal and metal oxide nanoparticles.[227] The SOM approach identified similarities in toxicity response and aided in developing predictive quantitative-structure relations.[227] Though this study is not directly related to drug toxicity prediction, this approach has the potential to be applied to drug toxicity studies, where it could be used to identify and classify toxicity response patterns among different drugs.

4.1.8. Contrastive Learning Approach. Self-supervised learning, especially contrastive learning, has gained attention

https://doi.org/10.1021/acs.chemrestox.2c00375
Chem. Res. Toxicol. XXXX, XXX, XXX−XXX

in molecular property predictions, but most molecular SSL methods neglect unique cheminformatics and multilevel graphical structures of molecules, so Wang et al. propose iMolCLR, which improves Molecular Contrastive Learning of Representations with GNNs in two ways, and experiments show that iMolCLR significantly improves GNN models' performance on various molecular property predictions, surpassing supervised learning models on most benchmarks and embedding molecule similarities.[228] The proposed iMolCLR model with improved molecular contrastive learning has the potential to enhance the prediction of molecular properties and could be a valuable tool for drug toxicity research.

BioassayCLR is a machine-learning method that utilizes textual bioassay descriptions along with chemical structures of molecules to predict activity.[229] This approach employs contrastive learning to learn representations of molecules and bioassays, which are similar if the molecule−bioassay pair is active and dissimilar if the pair is inactive.[229] The molecule and bioassay encoders have a feature extraction component and a learned component, both learned using a contrastive approach. Molecular descriptors are extracted and passed to an FNN for the molecule encoder, while text descriptions of bioassays are processed with either Latent Semantic Analysis (LSA) or BioBERT as a feature extractor and passed to a neural network for the bioassay encoder.[229] BioassayCLR outperforms baselines using simple textual similarity and other QSAR methods on a strict temporal hold-out set with 615 unseen bioassays and 248,290 unseen molecules, reaching an AUROC of 63.97 ± 0.47.[229] This method is the first to directly use a textual representation of a bioassay in a QSAR model, allowing for zero-shot transfer learning in drug discovery.[229] The study is exceptional in the sense that it shows how a predictive model can achieve high AUROCs without any activity measurement and solely based on the textual description of a bioassay, suggesting that virtual screening for active molecules can be performed without the bioassay even existing physically. The study also found that the sentence structure and grammar of the bioassay descriptions do not significantly affect the predictive modeling.[229] The trained molecule encoders potentially contain more information than encoders trained purely on activity data, making them suitable for transferring to other prediction tasks.[229] BioassayCLR could become a useful tool in early stage drug discovery, and architectural improvements could further improve its performance.

4.2. Adverse Drug Reactions (ADRs). ADRs are negative and unwanted effects that occur as a result of taking medication. They are an important consideration in drug toxicity research as they can have serious consequences for patient health and safety. Drug-induced liver injury (DILI) is one of the most prominent aspects of ADRs. It is important in drug toxicity research as it can result in serious and sometimes fatal liver damage. Identifying the risk of DILI is crucial in drug development, clinical trials, and postmarketing surveillance.[10,230,231] Efforts to mitigate the risk of DILI are critical for ensuring the safety of new drugs and protecting public health. Overall, understanding the incidence and mechanisms of adverse drug reactions can help researchers develop safer and more effective drugs.

4.2.1. DNN. A DNN model was developed to predict DILI using gene expression data by Feng et al.[232] The model achieved high accuracy, sensitivity, and specificity compared to a previous machine-learning algorithm, making it a useful tool for drug safety assessment and clinical drug use. Nguyen-Voet al. have introduced a computational framework inspired by the concept of word embeddings in natural language processing (NLP).[233] Molecular fingerprints, derived directly from SMILES converted to an embedded matrix. Then the molecular fingerprint-embedded features were used to identify DILI compounds, through CNNs.[233] The results show significant improvement compared to previous models, with an average accuracy of 0.89, MCC of 0.80, and an AUC of 0.96.[233] A molecular fingerprint-embedded featurizer is an effective molecular representation for future studies. Li et al. developed DeepDILI, a DNN-based DILI prediction model, using Mold2 descriptors and the DILIst data set, with a model-level representation generated through five conventional ML algorithms (i.e., LR, KNN, SVM, RF, and XGBoost) trained through aDNN.[202] DeepDILI was developed using pre-1997 drugs and evaluated on those approved thereafter.[202] The model aims to provide an explainable approach to DILI risk prediction and improve prediction performance.[202] The DeepDILI model outperformed other methods and demonstrated potential for real-world application. One of the critical aspects of the model is its explainability, which is achieved through a feature selection strategy that identifies important descriptors. The model's performance can be further improved by investigating different molecular representations and diverse biological end points.

Evaluating DILI models is challenging due to inconsistent classification and sample size variation. Efforts to standardize classification include data sets like LTKB Benchmark, DILIrank, and DILIst. Limited DILI-negative compounds constrain predictive model development. High-throughput screen technologies like L1000 and TempO-Seq could improve generalization. Evaluation of deep-learning algorithms for DILI prediction is urgently needed. These issues have been addressed by Li et al.[234] Li et al.developed a DNN model to predict DILI using transcriptomic profiles of human cell lines.[234] The model demonstrated superior performance compared to conventional machine-learning algorithms, achieving an AUC of 0.802 and 0.798, balanced accuracy of 0.741 and 0.721, and a balanced sensitivity of 0.839 and specificity of 0.603 for training and an independent validation set, respectively.[234] The genes driving the predictions were analyzed for their relevance to the underlying mechanisms of DILI, and the DNN model showed a more balanced sensitivity and specificity.[234] This model provides a promising tool for the early detection of DILI potential in preclinical settings, especially for oncology drugs. Kang et al. developed a new tool for identifying DILI risk and evaluating drug safety using extended connectivity fingerprints of diameter 4 (ECFP4)-based DNN model in a study with an almost equal number of DILI-positive and DILI-negative drugs from the DILIrank and LiverTox databases.[235] Integer ECFP4 fingerprint bits were used to define the applicability domain of the developed model, with each bit corresponding to a specific substructure.[235] The applicability domain refers to the range of compounds for which the model can accurately predict DILI risk. The researchers used integer ECFP4 fingerprint bits to define this domain and calculated the ratio of bits outside the domain for each compound, which they called the "endurance level".[235] This helped them develop a more reliable model by ensuring that predictions were based only on compounds within the applicability domain. The model was constructed using curated data sets and achieved an accuracy of 0.731, sensitivity of 0.714, and specificity of 0.750 on the validation data set. The model was evaluated on four external data sets and achieved an accuracy of 0.867 on 15 drugs with DILI cases reported since 2019.[235]

https://doi.org/10.1021/acs.chemrestox.2c00375
Chem. Res. Toxicol. XXXX, XXX, XXX−XXX

4.2.2. LSTM. Electronic health records (EHRs) are being increasingly utilized in drug toxicity studies due to their ability to provide a large amount of patient data, including demographic information, medication history, and adverse events. This data can be used to identify drug toxicity patterns and potential drug interactions, aiding in the development of safer drugs and better patient care. Santiso et al. used the Joint AB-LSTM network, a subclass of the Bidirectional LSTM network on the finding of ADRs in EHRs inscribed in Spanish.[236] ADRs tend to be undercited due to the workload on experts, and these efforts could provide an automated text mining-based solution to alleviate the workload and increase the rate of ADR reports.[236] An augmented amount of data on ADRs should help data-driven decisions in the preclinical testing of similar leads and also provide data for building robust predictive models in the future.[236]

4.2.3. GNN. To improve the performance of DILI prediction models, researchers have explored various approaches such as developing new annotation schemes, using different machine-learning models, and using ensemble computational models with different molecular descriptors. However, these approaches are limited by the availability of labeled DILI data. To address this, the researchers propose a property augmentation strategy that combines more drugs with other toxic properties, such as PLD28, to create a larger training data set.[237] This strategy uses multiview GNN (MV-GNN) models to learn molecular vector representation based on graph structure and underlying atom/bond level features.[237] This helps generate more accurate molecular representations and improves the accuracy of DILI prediction.

Xu et al. successfully used an undirected graph recursive neural networks (UGRNN) molecular encoding approach that was developed for predicting DILI, outperforming previous models with an accuracy of 86.9%, a sensitivity of 82.5%, specificity of 92.9%, and AUC of 0.955 on an external validation set.[230] Important molecular structure features related to DILI were identified.[230] The models have the potential to improve DILI risk prediction in human architecture in DILI prediction.[230] In this context, it is better to mention that a recursive neural network (RvNN) is just a generalization of anRNN. RNN shows a linear structure, whereas RvNN shows a treelike hierarchical structure.[238]

4.2.4. VNN. VNNs can address the limitations of toxicity prediction models by incorporating pathway knowledge, resulting in high interpretability. DTox, a VNN model, was developed to predict compound response to toxicity assays and to identify VNN paths that can explain toxicity outcomes.[129] The DTox models were used to perform virtual screening of compounds and linked predicted cytotoxicity scores with clinical phenotypes of DILI.[129] The DTox interpretation framework will benefit in silico mechanistic studies and generate testable hypotheses for further investigation.[129] The code for DTox is available openly at https://github.com/yhao-compbio/DTox.

4.2.5. Normalizing Flow and Diffusion Model. The majority of machine-learning approaches to design new molecules have been in the unconditional setting, where the goal is to generate molecules without regard to a specific purpose. This can produce "druglike" molecules, but it does not consider a specific target receptor that the molecules are intended to bind with. In contrast, the conditional setting involves generating ligand molecules to bind to a target receptor, which is more applicable to drug design. Rozenberg et al. present a method for generating ligand molecules that can bind to a given receptor molecule based on a conditional generative model.[239] In other words, this conditional generative model generates target-specific ligands that have the potential to lessen the risk of nonspecific ADRs. The algorithm uses a continuous normalizing flow to learn a distribution that is invariant to rigid body transformations and permutations of the ligand and receptor atoms.[239] The flow is implemented using a GNN architecture that can handle large differences in size between the ligand and receptor.[239] Authors tested their approach on the CrossDocked2020 data set, achieving better results in binding affinity than with other methods.[239]

Proteins can be modulated by ligands, making molecular docking a crucial task in drug design. Traditional approaches rely on scoring functions and optimization algorithms, but they are slow and inaccurate. Recent deep-learning models treat docking as a regression problem, but accuracy remains an issue. Corso et al. propose framing docking as a generative modeling problem to learn a distribution over ligand poses.[240] They present a new approach to molecular docking using deep learning, called DIFFDOCK, which frames the problem as a generative modeling task.[240] DIFFDOCK uses diffusion generative models to accelerate the development of new drugs and reduce the likelihood of adverse side effects.[240] The authors use this diffusion generative model over the non-Euclidean manifold of ligand poses by mapping the manifold to the product space of the degrees of freedom involved in docking (translational, rotational, and torsional).[240] Most molecular docking tools used for in silico drug design take a "sampling and scoring" approach, which is time-consuming and costly. DIFFDOCK's generative modeling approach assumes that there is a distribution of possible answers, which is critical in the presence of uncertainty.[240] This "blind docking" approach creates new opportunities to take advantage of AlphaFold 2's computationally folded protein structures to help identify new drug mechanisms of action.[240] Empirically, DIFFDOCK outperforms traditional docking and deep-learning methods with a 38% top-1 success rate on PDB-Bind.[240] Additionally, DIFFDOCK maintains high precision when docking on computationally folded structures and provides confidence estimates with high selective accuracy, while also having fast inference times.

4.2.6. Transformers. The FDA regulates 25% of the U.S. market, including foods, medications, and tobacco, with the responsibility of ensuring safe and effective products while promoting innovation. To achieve this, regulatory science is required to develop reliable evaluation and surveillance methods. The fast-evolving healthcare field, including AI, presents challenges in retrieving information from a vast number of documents. AI-based NLP offers a promising solution to speed up the process.A team of researchers used Bidirectional Encoder Representations from Transformers (BERT) to develop an NLP model for classifying DILI risk based on FDA drug-labeling documents.[241] The model's performance was statistically validated using internal and external procedures, and it showed excellent results.[241] The study demonstrated that the model could capture the semantic meanings of complex text in drug labeling and was portable across agencies, indicating the potential for using AI technologies to modernize and advance regulatory science. Another similar study used BERT-powered NLP to automatically filter out DILI literature from around 28,000 papers provided by the CAMDA challenge.[242] The model using TF-IDF and logistic regression achieved an accuracy of 0.957 with an ensemble model fine-tuned to lower

https://doi.org/10.1021/acs.chemrestox.2c00375
Chem. Res. Toxicol. XXXX, XXX, XXX−XXX

false-negative cases, achieving an accuracy of 0.954 and an F1 score of 0.955.[242] The ensemble model identified important words in positive/negative predictions, providing researchers with a rapid filter for DILI-related literature. Overall, these research studies aim to assist regulatory activities in evaluating drug safety and identifying potential DILI risks, making it indirectly related to active drug toxicity prediction efforts.

4.3. Drug−Target Interaction (DTI) and Drug−Protein Interaction (DPI). DTI and DPI are essential in understanding the mechanisms underlying drug toxicity. A drug's therapeutic effect depends on its ability to bind to and modulate specific target proteins. However, off-target binding can lead to adverse side effects. Therefore, predicting DPIs and identifying potential off-target effects are critical in evaluating a drug's safety and efficacy. A similar concept to DPI is compound−protein interaction (CPI), which refers to the interaction between small molecules (compounds) and proteins, whereas DPI specifically refers to the interaction between a drug molecule and a protein target. CPI research can be useful in drug discovery, while DPI research is important for understanding how specific drugs interact with their protein targets. Advances in deep-learning and experimental methods have facilitated the identification and characterization of DTIs/DPIs/CPIs, enabling researchers to develop safer and more effective drugs.

4.3.1. GNN. Recent work proposes a new computational approach called CPI-IGAE for predicting compound−protein interactions (CPIs) in drug development.[243] The approach transforms a compound−protein heterogeneous graph into a homogeneous graph and uses an Inductive Graph AggrEgator (IGAE)-based framework to learn low-dimensional representations of compounds and proteins in an end-to-end manner.[243] The results show that CPI-IGAE outperforms some state-of-the-art methods, and the model architecture and feature extraction process are advantageous, as validated by an ablation study and visualization of embeddings. Some of the top-ranked CPIs predicted by CPI-IGAE have been validated by recent literature reviews. Data and source codes are available at https://github.com/wanxiaozhe/CPI-IGAE.

4.3.2. RBM and DBM. Though in recent times RBMs are mostly getting replaced by GANs, their use in predictive drug toxicology is evident. As already discussed earlier, drug target interactions are vital to predict ADRs and DDIs. But, as very low known drug target pairs have been proved to show drug targets in the drug target space (less than 0.3%), it became hard to represent the whole sample space with these small interaction pairs. Due to this scarcity of labeled data, unsupervised learning algorithms became beneficial in drug target predictions. Wen et al. employed DBN to develop DeepDTIs, which precisely forecast new DTIs within FDA-approved drugs and targets.[244] RBMs are stacked to form a DBN that was trained greedily.[244−246,38,39] The team used five-layers-deep DBN. Each adjacent two layers (excluding the last two layers, which form the logistic regression classifier) were made up of RBMs. The training procedure of DBN has been divided into two successive processes. The greedy layer-wise unsupervised training process and the supervised fine-tuning process use the output of the last hidden layer as the input of the logistic regression classifier (LR).[244] In the mini batches, size, pretraining learning rate, fine-tuning learning rate, and the number of hidden layers were optimized to 128, 0.1, 0.1, and 4, respectively, and the model yielded the AUC, accuracy, sensitivity, and specificity of the test set of 0.9158, 0.8588, 0.8227, and 0.8953, respectively.[244] The team implemented the DBN algorithm using the DeepLearningTutorials package.[244] In another interesting study, Wang et al. showed the utility of capsule networks (CapsNets) in drug toxicity assessment studies.[247,248] They developed CNN and RBM feature extractor-based CapsNets called CNN-CapsNet and RBM-CapsNet, respectively, to classify hERG blockers and nonblockers.[247] Drugs with hERG blockade activity are alleged to have a latent hazard of cardiotoxicity.[247] Both models showed excellent results (RBM-CapsNet with the marginally better result) with prediction accuracies of 91.8% for Conv-CapsNet and 92.2% for RBM-CapsNet models.[247,248]

4.3.3. AEs. Machine-learning methods like matrix factorization gained attention in DTI prediction.[249,250] However, the sparsity of interaction matrixes decreases prediction performance. To address this, some methods utilize side information and a combination of matrix factorization and denoising autoencoders.[249] The proposed hybrid model includes two steps: preprocessing the interaction matrix and using similarity matrixes of drugs and targets to address sparsity. The method shows good results in predicting interactions on reference data sets and achieves high accuracy on golden standard data sets using 10-fold cross-validation.[249] A graphical representation of the hybrid model combining matrix factorization with denoising autoencoders with the help of drug and target side information is provided.[249]

Wang et al. projected a novel deep-learning architecture MDADTI for DTIs prediction based on Multimodal Deep Autoencoder (MDA).[251] MDA can learn high-level features automatically by fusing multiple similarities of data.[251,252] With the help of the Random Walk with Restart (RWR) method and Positive Pointwise Mutual Information (PPMI), the MDA take out low-dimensional features, which were fed into a DNN to predict DTIs.[251] Their outcomes showed the superiority of MDADTI in efficiently identifying previously unidentified DTIs.

In another study, Shayakhmetov et al. developed an AE-based model called Bidirectional Adversarial Autoencoder, which could infer drug molecules with the potential to induce desired changes in the gene expression.[253] The model generates molecular structures in the SMILES format.[253] Along with the induction of a given gene expression's modification, it could envisage a gene expression variance after incubation of a given molecular structure.[253] Generating leads with desirable effects could be of great help in preclinical studies.

The identification of drug−protein interactions is crucial in drug development. Existing methods for predicting these interactions have not fully integrated the attribute information on drug−protein pairs and their attribute distribution. To address this, the authors propose a new method called GVDTI, which encodes multiple pairwise representations, including attention-enhanced topological representation, attribute representation, and attribute distribution.[254] The method combines a graph convolutional autoencoder with a trilayer heterogeneous network to learn pairwise representations, which are then fused for drug−protein interaction prediction.[254] Experimental results demonstrate that GVDTI outperforms seven other state-of-the-art methods, with improved recall rates and case studies that confirm its ability to discover potential candidate drug-related proteins.[254]

Matrix factorization is an unsupervised method used in DTI prediction. However, it suffers from cold start problems and sparsity issues. To address these problems, a novel unsupervised deep-learning model, AutoDTI++, learns the latent factors from the matrix interaction.[255] The AutoDTI++ uses a denoising autoencoder and drug fingerprint feature to build a nonsparse

https://doi.org/10.1021/acs.chemrestox.2c00375
Chem. Res. Toxicol. XXXX, XXX, XXX−XXX

interaction matrix.[255] By preprocessing the DTI matrix and using AUPR and AUC as performance measures, AutoDTI++ outperforms other state-of-the-art methods, especially in the presence of missing DTIs in the training data.[255] The drug fingerprint feature provides additional information to build an accurate model and handle the sparse interaction matrix, leading to better performance. The method is especially effective for IC data sets, where the sparsity is low, and performs worse for E data sets with high sparsity. This method was compared with six other state-of-the-art methods and achieved better performance in predicting left-out interactions.[255]

4.3.4. Contrastive Learning. Graph-learning-based methods have shown certain advantages in predicting DTIs, but labeled data can be limited and expensive to obtain. Li et al. show the use of supervised contrastive learning for DTIs prediction. The proposed end-to-end supervised graph cocontrastive learning model for DTI prediction directly from heterogeneous networks generates a contrastive loss to guide the model optimization in a supervised manner.[256] The work showed how supervised contrastive learning gives an aligned representation of drug and protein pairs (DPPs) node representations with the same class label.[256] In embedding space, DPP node representations with the same label are pulled together, and those with different labels are pushed apart.[256] Experiments on three public data sets demonstrate that the model outperforms existing methods significantly, especially in the case of cold start, and provides a new research perspective of contrastive learning for DTI prediction.[256]

4.3.5. Transformer and Attention. Many studies on DTI ignore the essential correlations between atoms when encoding drug compounds and model the interaction of drug−target pairs simply by concatenation. This may result in suboptimal DTI predictions. Zeng et al. propose a new model for predicting DTI using multiple attention blocks.[257] The model addresses these limitations by using a relation-aware self-attention block to encode atom correlations and a multihead attention block to model drug−target interactions.[257] The approach outperforms existing methods on two benchmark data sets, and we also determine the best max relative position length value (M1). Authors apply our model to predict the DTI of COVID-19-related genome sequences and FDA-approved drugs (M2).[257]

To address the issue of traditional methods being unable to effectively extract features of complex drug and protein structures, Liu et al. propose a novel transformer-based method for DTI prediction.[258] The method uses only the sequence information on drugs and proteins and can effectively extract deep features through the attention mechanism in the transformer.[258] To improve the performance of the approach, the researchers conducted a lot of adjustment experiments and optimized the parameters to analyze and compare the experimental results.[258] Tests on two benchmark data sets demonstrated the effectiveness and accuracy of their method.

4.3.6. Multiobjective Neural Networks with GCN and CNN. A multiobjective neural network (MONN) is a type of neural network that is specifically designed to optimize multiple objectives simultaneously.[161] As an example, MONN can predict both the noncovalent interactions and binding affinities between compounds and proteins in drug development.[161] This makes it particularly useful in situations where the objectives are interdependent or conflicting. Researchers have developed structure-free models for predicting CPI to overcome the limitations of structure-based computational methods, which require high-quality 3D-structure data of the protein targets (e.g., molecular docking).[161] These structure-free models use deep-learning-based methods that fully exploit the local features of input compound structures and protein sequences to predict their binding affinities. Neural attention has been applied to these models to capture local binding sites mediated by noncovalent interactions.[161,259] However, these models have difficulty in automatically capturing the accurate local noncovalent interactions without extra supervised guidance.[161] To address this issue, Li et al. developed a multiobjective neural network called MONN that can learn both pairwise noncovalent interactions and binding affinities between compounds and proteins.[161] MONN is capable of handling large data sets with low computational complexity and requires only the input of graph representations of compounds and primary sequences of proteins.[161] It utilizes GCNs and CNNs to process this input information and does not rely on any specific structure. However, in addition to a traditional GCN, MONN uses a graph warp module to learn both global and local features of compounds and contains a pairwise interaction prediction module that captures noncovalent interactions between atoms of a compound and residues of a protein.[161] MONN successfully learns pairwise noncovalent interactions and uses the results to predict binding affinities and outperformed other state-of-the-art attention-based methods in predicting binding affinities.

DNNs that can learn from symbolic data (like words in NLP) have shown great performance on challenging problems. In the case of predicting CPIs, the data are represented symbolically as graphs for compounds (with atoms as vertices and chemical bonds as edges) and sequences of amino acids for proteins. In this context, Tsubaki et al. put forward a novel approach for CPIs prediction that combines a GNN for compounds and a CNN for proteins representation to achieve competitive or better performance compared to existing methods.[160] An attention mechanism is also used to help understand which parts of a protein are important for predicting interactions with a drug compound.[160]

4.4. Molecular Generation and Lead Optimization. Molecular generation and lead optimization are crucial processes in drug development, especially in drug toxicity research. They involve designing and refining drug candidates using computational methods to optimize their properties, including potency, selectivity, pharmacokinetic properties, and safety. These processes are important for reducing the risk of toxicity and increasing the success of drug candidates in clinical trials, while also speeding up the drug discovery process and reducing costs.

4.4.1. RNN. Segler et al. use novel computational strategies to design new molecules for biological targets using RNN.[260] RNNs are trained as generative models for molecular structures.[260] The model can be fine-tuned with small sets of known active molecules to create libraries of new molecules with high affinity. The model accurately reproduced a significant percentage of test molecules for *Staphylococcus aureus* and *Plasmodium falciparum*.[260] When combined with a scoring function, the model can perform complete de novo drug design to create large sets of new molecules for drug discovery.[260]

4.4.2. LSTM. Though deep learning is considerably contributing to predictive toxicological research, its demand for a huge amount of data imposes a constraint on its use, especially in the lead optimization stage. The lead optimization stage of drug discovery relies on limited data, making it a fundamentally low-data problem.[261] Altae-Tran et al. significantly reduces the need for data by introducing deep one-shot

https://doi.org/10.1021/acs.chemrestox.2c00375
Chem. Res. Toxicol. XXXX, XXX, XXX−XXX

learning to lead optimization problem.[261] The team proposed the iterative refinement LSTM, a novel architecture, that significantly advances the learning of meaningful distance metrics over small molecules in combination with graph convolutional neural networks.[261] This review introduces an architecture for low-data learning in drug discovery that outperforms simpler methods, particularly for Tox21 and SIDER collections.[261] One-shot learning is effective for small biological data sets but struggles with diverse scaffolds as shown in MUV data sets.[261] The architecture uses iterative refinement LSTMs that can generalize to new experimental assays. Future work can investigate the limits of one-shot models and the structure of embeddings learned by the LSTM modules.[261] The DeepChem library has open-sourced all graph-convolutional primitives and scripts used in the experiments.

4.4.3. AAE. When data are scarce in the training data set, GANs generate novel data that are strikingly similar to the training data set.[141] This feature is greatly being utilized by predictive toxicological research to contextually fill the gap between low data volume and predictive deep-learning models. Kadurin et al. proposed a deep generative adversarial model, a generative AAE, for complete in silico generation of biologically relevant novel compounds that make use of existing biological and chemical data.[138,262] They created the first seven-layer AAE-based application for generating novel molecular fingerprints with a defined set of parameters.[262,263] The AAE-based workflow was capable of generating anticancer molecules based on concentrations and fingerprints as sole inputs.[262] The approach is capable of shortening the drug discovery timeline by providing robust biologically relevant predictions that, in turn, increase the rate of the drug discovery workflow and reduces the redundant use of lab animals.[262] In another related study, Kadurin et al. developed a model named druGAN, based on the generative AAE architecture.[263] druGAN is used for de novo in silico generation of novel leads with user-defined specific anticancer properties.[263] This advanced AAE has demonstrated its enhanced capacity and efficiency over VAE through its adjustability in molecular fingerprint generations, molecular big data processing, and efficient unsupervised pretraining for a regression model.[263] We hope generating molecules with specific desirable properties would significantly relieve the burden of preclinical toxicity and related loss of animal resources.

4.4.4. Variational Graph Autoencoders. Drug repurposing existing drugs for new therapeutic indications has gained popularity due to its potential to save time and resources in drug development. In drug toxicity research, identifying existing drugs with a known safety profile can be valuable, as it can reduce the time and cost of drug development while providing new treatments for diseases where current treatments are inadequate.[264] However, traditional experimental methods can be costly and time-consuming. In recent years, the development of deep-learning-based methods has greatly facilitated drug repositioning.[264] Zhang et al. propose a novel end-to-end model called GCMM, which incorporates known drug−disease relations, drug−drug chemical similarity, drug−drug therapeutic similarity, disease−disease semantic similarity, and disease−disease target-based similarity into a heterogeneous network and uses a GCN encoder and multimodal attention layer to predict drug−disease relationships with higher accuracy than four recently proposed deep-learning models, as demonstrated through fivefold cross-validation evaluations and a case study on Alzheimer's disease.[265] In another similar study, the authors propose a new drug repositioning method called VGAEDR, which is based on a heterogeneous network that includes multiple drug attributes and a variational graph autoencoder.[250] The authors establish a drug−disease network based on three drug attributes, disease semantic information, and known drug−disease associations.[250] They then use a variational graph autoencoder and a multilayer convolutional module to learn low-dimensional feature representations of this network. Finally, the feature representation is fed to a fully connected layer and a Softmax layer to predict new drug−disease associations.[250] The authors conduct comparative experiments with other baseline methods on three data sets, and the results demonstrate that VGAEDR performs excellently.[250] The authors also conduct a case study where they predict the top 10 possible anti-COVID-19 drugs using the existing drug and disease data, and six of these predictions are later verified by other studies.[250]

4.4.5. Graph Convolutional Autoencoders. Current methods of drug repositioning focus on multisource data for predicting drug−disease associations, but they fail to fully integrate different drug similarities and exploit the topology structures of multiple drug−disease heterogeneous networks. To address this issue, GFPred proposes a method using a graph convolutional autoencoder and a fully connected autoencoder with an attention mechanism to predict drug-related diseases.[266] Three drug−disease heterogeneous networks are constructed, and the topology representations and attribute representations of drug and disease nodes are integrated using the attribute-level attention mechanism.[266] GFPred achieves better performance than several state-of-the-art prediction methods and can retrieve more actual drug−disease associations.[266] This is helpful for biologists to discover real associations through experiments.

Existing methods for drug repositioning or drug-related disease prediction mainly focus on single or multiple drug−disease networks. However, these networks lack specific information between drug nodes and disease nodes.[267] To address this, a new model, CTST, is designed to extract and integrate common and specific topologies in multiple heterogeneous networks and subnets.[267] CTST uses graph convolutional autoencoders and attention mechanisms to learn informative representations of drug and disease nodes.[267] Experimental results confirm the effectiveness of CTST in discovering potential candidate diseases.

4.4.6. Normalizing Flow and Diffusion Model. Generative models in machine learning have advanced drug discovery by enabling distribution learning and molecular property optimization. Distribution learning produces novel compounds, while property optimization searches for molecules with desirable properties. Researchers often combine these tasks by training a distributed learning model and using its latent codes for property optimization. Proper latent codes are crucial for navigating the molecular space. Kuznetsov et al. propose MolGrow for generating proper latent code. MolGrow is a new graph generative model that uses a novel hierarchical normalizing flow model for generating molecular graphs.[268] The model is modular, invertible, and hierarchical, allowing for precise control over the resulting graph. This model can create new molecular structures by splitting every node recursively.[268] The model starts with a single node and iteratively splits every node into two, mapping molecular structures onto a fixed-size hierarchical manifold.[268] A hierarchical manifold is a mathematical concept that refers to a space with multiple levels of structure. In this study, the top levels of the manifold correspond to the global features of the molecules, while the bottom levels

https://doi.org/10.1021/acs.chemrestox.2c00375
Chem. Res. Toxicol. XXXX, XXX, XXX−XXX

represent local features. The use of a hierarchical manifold allows for the generation of complex molecular structures in a controlled and structured manner. Perturbations in the first layer of the hierarchical latent codes cause global structural changes, while perturbations in the subsequent layers affect the molecule only marginally.[268] MolGrow outperforms existing generative graph models on distribution learning and enables successful optimization of chemical properties. This model can be used to generate molecules with desirable properties with minimal toxicity.

3D molecular generation can help in toxicity prediction studies by simulating the real-world behavior of molecules, providing insights into their interactions with biological targets, and designing safer drug candidates. Leveraging geometric symmetries in molecular data is important for good generalization as molecules live in physical 3D space. E(n) equivariant layers can be used for molecule generation in 3D. Autoregressive models have integrated E(n) equivariant layers, but they are difficult to scale during sampling. Continuous-time normalizing flows or E-NF are expensive to train to lead to limited performance and scalability. In recent work, the authors introduce E(3) Equivariant Diffusion Models (EDMs) that learn to denoise a diffusion process operating on both continuous coordinates and categorical atom types in a significantly less expensive manner.[269] EDMs can generate molecules in 3D space without requiring a particular atom ordering and can be trained more efficiently than normalizing flows.[269] The authors show that EDMs outperform previous molecule generation models in log-likelihood and molecule stability.[269] In another related study, Morehead et al. used denoising diffusion probabilistic models (DDPMs), which are making strides in generative modeling, including text-guided image generation and structure-guided protein design.[270] GCDM is a new geometry-complete diffusion model that leverages graph neural networks for state-of-the-art 3D molecule diffusion generation, providing insights into physical inductive biases.[270] Source code and data are available at https://github.com/BioinfoMachineLearning/bio-diffusion.

Generating druglike molecules with high binding affinity using structure-based generative chemistry can be used in drug toxicity research to identify potential safety concerns and toxicity risks associated with these molecules, which can then be refined to improve their safety and efficacy. Huang et al. present a novel approach called PMDM for generating druglike molecules with high binding affinity to specific proteins using structure-based generative chemistry.[271] PMDM incorporates a dual equivariant diffusion model framework to efficiently generate 3D molecules that fit specified target proteins.[271] It considers the conditioned protein semantic and spatial information to generate chemically and conformationally valid molecules that suitably fit pocket holes.[271] PMDM outperforms state-of-the-art models in generating druglike, synthesis-accessible, novel, and high-binding affinity molecules targeting specific proteins. The generated molecules are rational compared to the reference molecules, and PMDM can generate bioactive molecules highly binding to targeted proteins not included in the training set.

4.4.7. Contrastive Learning. Retrosynthesis is also useful in drug toxicity research for predicting and designing molecules with reduced toxicity based on their metabolic pathways and structural features. Lee et al. propose RetCL, a new approach for deep learning in retrosynthesis, which reformulates it into a reactant selection problem from a candidate set of commercially available molecules using GNN and contrastive training.[272] RetCL achieves high accuracy and generalizes well to unseen templates.[272]

4.5. Image-Based Toxicity Prediction. Different types of images, such as molecular images, microscopy images, and medical imaging modalities, are important in drug toxicity research as they provide a comprehensive view of the effects of drugs on the body. By combining information from multiple imaging modalities, researchers can obtain a detailed understanding of the mechanisms underlying drug toxicity, identify potential biomarkers for toxicity, and develop more effective treatments, ultimately leading to safer and more effective drug development.

4.5.1. CNN. Drug-induced neurotoxicity has farsighted effects on health.[273] With the introduction of whole slide imaging (WSI), different deep-learning algorithms are significantly contributing to different areas of neurotoxicological analysis like deep-learning-assisted automated brain image segmentation, detection and analysis of toxicity in different regions of the brain, etc.[273] Wang et al. used a CNN model to automatically detect focal cerebral ischemia-reperfusion-injured neurons in label-free two-photon microscopic (TPM) images.[274] This model significantly improves diagnostic accuracy compared with standard histology and detects the location of the injured neuron without prior knowledge of histopathology.[274] The study used 64 × 64 pixels input images to be fed into a Residual Network CNN (ResNet CNN), which reduces the spatial resolution of the input.[274] Though this study is not directly related to drug-induced toxicity, the approach could be extrapolated to neurotoxicological analysis to yield robust toxicity quantification tools that in turn shall reduce the need of using more laboratory animals to get robust results.[273,274]

Drug-induced toxicity is tightly related to hepatic and cardiac adverse effects of drugs, and more than 75% of postmarketing withdrawals of drugs are due to these two causes.[275−277] These toxicities are intricately related to the disruption of the subcellular structures.[277] Changes in the nuclear parameters like morphology, density, etc. have proven to be excellent parameters for cytotoxicity assessments.[278−282] Hence, analysis of subcellular structures from micrographs and videos at the finer level yields much information about the nature of toxicity, though it is considered to be a fairly challenging task for conventional image-analysis techniques, and due to human-based visual analysis, it is mostly regarded as a qualitative tool for cellular health analysis.[277,282] Maddah et al. developed an CNN model of enumerating drug-induced structural changes using hiPSC-derived cardiomyocytes and hepatocytes, named PhenoTox.[277] They harnessed the power of transfer learning by using an 18-layer-deep CNN, the ResNet18 architecture, with a reliable set of hyperparameters (an initial learning rate of 0.01 and several epochs of 20) for all training operations.[277] The model was able to detect the dynamics of drug-induced structural alterations in both cells with superior performance in assessing toxicity in comparison to conventional methods.[277] Another similar study used deep CNNs to build a quantitative toxicity prediction model that was capable of predicting toxicity from images of fluorescently stained (using DAPI) nuclei of several drugs' pretreated cells without using specific toxicity labeling.[10,282] They developed two CNN models, Tox_CNN and Tox_RCNN (Tox_Region-based CNN), for classifying cells based on their health status.[282] The Tox_CNN depends on prior cell segmentation and cropping of nuclei images, while Tox_RCNN performed fully automated cell detection and

https://doi.org/10.1021/acs.chemrestox.2c00375
Chem. Res. Toxicol. XXXX, XXX, XXX−XXX

classification.[282] Both models output robust screening data, capable of sensing prelethal toxicity. The results were validated for a wide assemblage of toxicity pathways and cell assays.[282] These methods should be useful for robust in vitro toxicity screening in the drug discovery pipeline, which we hope shall reduce and or replace the unnecessary use of laboratory animals.[282]

A fully automated 3DCNN framework was found useful for structure-based protein analysis and probing a protein microenvironment for its structural impact without the need for previous knowledge or feature assumptions.[283] It also forecasts the mutation's effect on protein structure.[10,283] This approach confirmed a twofold increase in the accuracy of prediction over certain models that require hand-selected features.[10,283] This model has the potential to aid predictive drug toxicity research by analyzing the effects of the drug in the protein microenvironment and related changes in the protein's structure and function, which leads to ADRs in many instances.

Cytochrome P450s (CYPs) and peroxidases metabolically oxidize drugs into highly reactive electrophilic quinone species that are primarily responsible for idiosyncratic adverse drug reactions (IADRs).[284−288] IDARs are the most common adverse reactions of an approved drug and lead to severe mortality and morbidity in more than 70% of cases.[288] CNN has been used for accurate predictions of quinone formation by modeling both one- and two-step quinone formation reactions.[288] The model is robustly built with one molecule layer, one input layer, three hidden layers, and three output layers.[288] It forecasts the probability of a candidate molecule to form quinone with the help of its output described as molecule quinone formation score (MQS) (it is predicted by integrating atom quinone formation score (AQS) and pair-level quinone formation score (PQS), which are generating two of the output layers).[288] The model could be beneficial as a robust and rapid screening tool in drug toxicity risk prediction in an early stage of drug development studies. Another CNN model has been beautifully crafted by Tandon et al. to execute robust binary and multiclass classifications on digital micrographs of chemically exposed undifferentiated (proliferating) and differentiated 2D cultures of HepaRG cells and primary human hepatocytes generated from high-throughput toxicology assay.[184] This model significantly advances the analysis of the high volume of these micrographs, which earlier was limited by time-consuming and error-prone manual analysis. The binary classifier classifies altered and healthy cell classes with above 98% accuracy, and the multiclass classifier classifies altered, intermediate, and healthy classes with an accuracy above 95%.[184] The team used transfer learning by training ResNet-50 (a 50-layer deep CNN, pretrained with over a million images from the ImageNet database) with the prepared micrographs using the fast.ai deep-learning library.[289−291] To get a more reliable result using ResNet-50, they retrain the model using their prepared micrographs by using discriminative learning rates and gradual unfreezing.[184] They also employed Class Activation Maps (CAM) to get a grasp on the internal workings of the CNN for better optimization.[184,292] Their findings raise hopes of an automated strong classifier of cellular images with the possibility to enhance high-throughput toxicological studies.

4.5.2. SOM. Recent advancements in neuronal imaging to measure cellular activity after drug treatment has the potential for accurately predicting neuronal activity over time, but the complex pattern of neuronal activity over time poses a challenge in predicting the corresponding drug dose. The problem was addressed by a recent study that discusses the use of SOM to cluster and classify drug-induced Ca^{2+} response in hippocampal neurons at different drug doses.[293] By implementing SOM, the study provides a visualization and prediction tool to analyze high-dimensional data into a low-dimensional SOM grid, enabling the classification of unknown neuronal responses based on the extent of drug levels present in the system.[293] This technique could be generalized to other drug-induced cellular responses and holds promise in high-content imaging analysis.

4.5.3. Contrastive Learning. The use of contrastive learning in self-supervised representation learning has improved computer vision and NLP. Contrastive learning has been successful in producing transferable representations of language and image data in Contrastive Language-Image Pretraining (CLIP) and Contrastive Leave One Out Boost (CLOOB).[210,294,295] However, contrastive learning has not yet been applied to the multimodal data sets in drug discovery, even though it could provide a solution to the costly labeling process.[210] It has immense potential to simultaneously compare image-based toxicity data with chemical structural information for predicting more accurate and state-of-the-art predictions. Sanchez-Fernandez et al. used this possibility to propose a method using a self-supervised contrastive learning approach for molecule encoders that combines image and structure-based representations.[210] Authors call this approach Contrastive Leave One Out boost for Molecule Encoders (CLOOME), and it builds on the success of recent contrastive learning methods in computer vision and natural language processing and is used for image-based and structure-based representations of small molecules for drug discovery.[210] CLOOMElearns representations of molecules using microscopy images and chemical structures.[210] By applying this approach to biological imaging and drug discovery, authors aim to improve the transferability of molecule encoders beyond their current limitations.[210] They demonstrate the transferability of their method on a benchmark data set and suggest that the learned representations could be used for activity prediction and bioisosteric replacement tasks.[210] But currently, the method has some limitations in terms of the type of microscopy images it can work with and the amount of available data.[210] Hyperparameters and architecture space are also underexplored, but the authors suggest that the representations obtained with CLOOME could be useful for drug discovery efforts.[210]

4.6. Clinical Toxicity Prediction. Multitask learning (MTL) has emerged as a superior approach to single-task learning in drug discovery.[296,297] A MTL model accurately predicts toxicity for all end points, including clinical, as indicated by the area under the ROC curve and balanced accuracy.[298] By jointly modeling multiple properties, MTL exploits relationships and dependencies among tasks, resulting in enhanced predictive performance.[297] It also improves data efficiency by leveraging shared information and enabling knowledge transfer. MTL provides synergistic insights into relationships between properties, facilitates feature learning, and has translational applications in toxicity prediction and multimodal therapy development.[296] Overall, MTL holds immense promise for accelerating drug discovery and developing more effective therapies.[296,297] A study by Sharma et al. used a deep-learning framework with two different molecular-input representations and accurately predicted toxicity for all end points, including clinical. The use of pretrained molecular SMILES embeddings improved clinical toxicity predictions compared to existing models.[298] The study also indicated that in vivo data is minimally required for clinical

https://doi.org/10.1021/acs.chemrestox.2c00375
Chem. Res. Toxicol. XXXX, XXX, XXX−XXX

toxicity predictions.[298] A post hoc contrastive explanation method was used to explain the model's predictions and returned known mutagenic and reactive toxicophores.[298] This method captured more in vitro and in vivo end points and uncovered a preference toward this experimental data.[298] This is the first contrastive explanation for predictions of clinical and in vivo molecular toxicity. Also, clinical trials are a critical aspect of drug toxicity prediction in the target organism. Clinical trials are important in the development of new drugs, which are expensive and time-consuming, and have a low success rate. Deep-learning models excel at modeling biomedical data but often struggle with multimodal data sets that have diverse characteristics and demand domain-specific knowledge, which are important criteria for clinical trial prediction. Fu et al. propose a new GNN method called Hierarchical Interaction Network (HINT), which tries to overcome these challenges associated with clinical trial outcome prediction.[299] HINT can handle complex interaction patterns from multimodal data, including graphs, text, and categorical variables, with missing values.[299] HINT encodes multimodal data into embeddings, trains knowledge-embedding modules using drug pharmacokinetic and historical trial data, and finally uses a hierarchical interaction graph to connect all the embeddings and predict trial outcomes.[299] The authors curated and released a large and labeled benchmark data set of 17,538 clinical trials for trial outcome predictions, and the code is available on GitHub (https://github.com/futianfan/clinical-trial-outcome-prediction).[299] HINT was trained and validated on 1160 phase I, 4449 phase II, and 3436 phases III trials and significantly outperformed the best baseline method on most metrics.[299] In future, the work can support more trial types and animal trials to more accurately predict the outcome in the cost of minimal life.

5. DATABASES FOR DEEP LEARNING

The primary requirement of deep learning is the accessibility to big data. Luckily, with the improvement of technology, advanced chemical toxicity screening programs have generated a stirring quantity of biological activity data.[9] These data are typically public and hosted by pronoun databases. A few prominent databases are discussed here, and a table (Table 3) containing a few more relevant databases (along with the databases discussed) is presented. The list is neither exclusive nor exhaustive.

PubChem is the chief public chemical database containing information about a compound's toxicity, pharmaceutical activity, and genomic data.[9,300−303] The National Center for Biotechnology Information established PubChem in 2004.[303,304] Today, it contains the data of more than 12 million compounds, 298 million substances, and 301 million bioactivities.[304]

ChEMBL is another open database under the control of EMBL-EBI containing data of more than 2.3 million compounds, 1.5 million assays, 14,000 drugs, and many more properties.[305−309] U.S. National Toxicology Program (NTP) designed another public online toxicology resource, the Chemical Effects in Biological Systems (CEBS) repository that contains experiential toxicology data.[9,310] It is a unified public data repository for toxicogenomics data. It integrates toxicity data and study design through proteomics and microarray data, clinical chemistry, and histopathology findings.[311] CEBS is a public resource and has received depositions of data from academic, industrial, and governmental laboratories.[311] CEBS stores data in a relational database, designed to display data in the context of biology and study design.[310] It also allows data integration for knowledge generation, cross-study analysis, and novel meta analysis.[310,311]

The Comparative Toxicogenomics Database (CTD) is another publicly available robust database that intends to advance one's understanding of the outcome of environmental exposures of toxins on human health.[312−315] It offers manually curated data about chemical−gene/protein interactions, and chemical−disease and gene−disease associations.[314] It harmonizes cross-species heterogeneous data for chemical exposures and their biological impacts by manually curating and interrelating chemical, exposure content, gene, phenotype, anatomy, taxa, and disease from the published literature.[312,314] Currently, it contains data for more than 17,100 chemicals, 54,300 genes, 6100 phenotypes, 7270 diseases, and 202,000 exposure statements.[312,314,315]

The Toxin and Toxin Target Database (T3DB), or the Toxic Exposome Database, is another excellent openly accessible bioinformatics resource that combines detailed toxin data with complete toxin target information.[316−318] The database presently comprises more than 3678 toxins described by 41,602 synonyms, including pollutants, pesticides, drugs, and food toxins, linked to 2073 corresponding toxin target records.[316,317] These data have been obtained from over 18,143 sources, which consist of other databases, scientific literature, government documents, and books.[317] This project is sponsored by the Canadian Institutes of Health Research, Canada Foundation for Innovation, and The Metabolomics Innovation Centre (TMIC), a nationally funded research and core facility that helps to sustain a broad array of cutting-edge metabolomic studies.[9,316,317]

DrugBank Online is a comprehensive, unrestricted, online database that has information on drugs and drug targets.[319] It contains both bioinformatics and cheminformatics resources. The database combines detailed drug data with complete drug target information including sequence, structure, and pathway.[320] DrugBank is widely used by all starting from medical professionals to the general public. It began in 2006 at the University of Alberta in Dr. Wishart's lab as a project to aid academic researchers to get comprehensive structured information relating to drugs.[319] Later in 2011, it became a part of The Metabolomics Innovation Center (TMIC). The project grew further in scope and popularity and became a part of OMx Personal Health Analytics Inc. in 2015. Today, DrugBank is one of the leading drug databanks across the data-oriented medicine industry due to its comprehensive referencing, broad scope, and complete data description detailing. The DrugBank project initially was funded by the Canadian Institutes of Health Research, Alberta Innovates - Health Solutions, and by The Metabolomics Innovation Centre (TMIC). ZINC is another free-to-access database of commercially available compounds for virtual screening.[321] It covers more than 230 million purchasable compounds in 3D formats, ready-to-dock.[321] It also contains more than 750 million purchasable compounds whose analogues can be searched for.[321] This database is provided by the Irwin and Shoichet Laboratories, Department of Pharmaceutical Chemistry at the University of California, San Francisco (UCSF). They get financial support from NIGMS (GM71896).

Toxicogenomics is a field that examines compound safety by analyzing gene expression profiles. Large toxicogenomics databases are more effective than small ones in identifying biomarkers for predicting and evaluating drug safety based on a compound's toxicological mechanisms in animal organs.[322] The

https://doi.org/10.1021/acs.chemrestox.2c00375
Chem. Res. Toxicol. XXXX, XXX, XXX−XXX

Table 3. List of Databases for Drug Toxicity Study with Their Pros and Cons

Database Name	Link	Primary Usefulness	Limitations
ACToR	https://actor.epa.gov/actor/faces/Home.xhtml	Access is provided to thousands of chemicals and hundreds of thousands of toxicity testing records through a comprehensive collection of chemical data from multiple sources, for environmental and human health research.	The focus of the data is primarily on environmental effects, and comprehensive toxicity data may not be provided. Some types of toxicity, such as developmental and reproductive toxicity, have limited data.
ADMETlab	http://admet.scbdd.com/	A platform for predicting the ADMET (Absorption, Distribution, Metabolism, Excretion, and Toxicity) properties of chemicals online.	Comprehensive experimental data may not be provided, and actual toxicity may not be accurately reflected, as predictions are limited to in silico methods.
ChEMBL	https://www.ebi.ac.uk/chembl/	Integration of chemical, bioactivity, and genomic data	Limited toxicity data and characterization
Chemical Effects in Biological Systems (CEBS)	https://www.niehs.nih.gov/cebs-df/	An integrated database of toxicology and exposure data	Limited data on specific toxicity end points may not fully represent human toxicity
ChemIDplus	https://chem.nlm.nih.gov/chemidplus/	Access is provided to chemical structure, names, and properties through a comprehensive chemical database that identifies substances and their properties, with information on over 400,000 chemicals.	Limited data on toxicity
ChemSpider	https://www.chemspider.com/	A comprehensive database of chemical structures and properties	Limited toxicity data and characterization
Comparative Toxicogenomics Database (CTD)	http://ctdbase.org/	Integration of chemical−gene, chemical−disease, and gene−disease interactions	Limited data on specific toxicity end points may not fully represent human toxicity
CSISSFRRA	https://csiss.org/data/FRRA/	A framework for risk assessment of chemicals in the environment is provided by a collection of environmental data sets.	All available toxicity data may not be included, and the focus may be limited to environmental risk assessment.
DART	https://www.dartlibrary.org/	Data on developmental and reproductive toxicity is provided by the database for chemicals.	Developmental and reproductive toxicity is limited to the available data.
DrugBank	https://www.drugbank.ca/	Information on drugs and drug targets is contained in a comprehensive database.	Toxicity data and characterization are limited, and nondrug chemicals are not included.
DrugMatrix	https://discoverx.com/portfolio/drugmatrix	Gene expression data on drug-induced effects in rats and mice is provided by a database of in vivo pharmacology data for drug discovery and development.	Limited to drug-related toxicity data
DSSTox	https://www.epa.gov/chemical-research/distributed-structure-searchable-toxicity-dsstox-database-network	A suite of toxicity data and predictive models is provided by a comprehensive collection of chemical data for toxicity assessment and chemical screening.	Limited toxicity data are available for some chemicals and limited data on some types of toxicity, such as developmental and reproductive toxicity.
EFED (Environmental Fate and Effects Division)	https://www.epa.gov/efed	Provides environmental hazard and risk assessment data	Limited to environmental toxicity and risk assessment
EPA CompTox	https://comptox.epa.gov/	Access is provided to toxicity data and predictive models through a database containing information on thousands of chemicals, including experimental and predicted data on toxicity and exposure.	Limited information on some compounds and lack of standardization in toxicity testing protocols. Also, limited data on some types of toxicity, such as developmental and reproductive toxicity
eTox (Electronic Toxicology)	http://www.e-tox.net/	Provides a database of in vitro toxicology data	Limited to in vitro toxicity data
GDSC (Genomics of Drug Sensitivity in Cancer)	https://www.cancerrxgene.org/	Provides genomic data on the sensitivity of cancer cells to drugs	Limited to drug-related toxicity and cancer cell sensitivity
Lhasa Limited	https://www.lhasalimited.org/	A range of toxicity prediction software and services are provided by the collaborative data-sharing platform for toxicology and chemistry data.	Subscription-based, may not be accessible for all users. Limited to predicted data and may not accurately reflect actual toxicity.
Open TG-GATEs		Offers a wide range of toxicogenomic data and metadata primarily of drug compounds to assess compound safety and predict drug toxicity.	Focusing primarily on animal target organs and its reliance on gene expression profiles. Currently archived and last updated on 2021.
PharmaPendium	https://pharmapendium.com/	Access to preclinical and clinical drug development data is provided by a comprehensive database of drug efficacy, safety, and toxicity information for regulatory and research purposes.	Subscription-based, may not be accessible for all users. Limited to drug-related toxicity data.
PharmGKB	https://www.pharmgkb.org/	Information about the relationships between genetic variation and drug response is contained in a comprehensive resource for pharmacogenomic knowledge and medication dosing guidelines suitable for clinical implementation.	Not specifically focused on toxicity data and may not provide comprehensive information on adverse effects. Limited to drug-related toxicity and genetic variation.

https://doi.org/10.1021/acs.chemrestox.2c00375
Chem. Res. Toxicol. XXXX, XXX, XXX−XXX

Table 3. continued

Database Name	Link	Primary Usefulness	Limitations
PubChem	https://pubchem.ncbi.nlm.nih.gov/	Comprehensive information on chemical properties and biological activities is provided by a large database of chemical substances with various biological activities.	Limited toxicity data and characterization. Provides limited information on toxicity and can include many false positives.
T3DB	http://www.t3db.ca/	Comprehensive information is provided about toxins, their targets, and their mechanisms of toxicity through a curated database of toxic compounds, including information on toxicity mechanisms and health effects.	Limited coverage of chemicals and mainly focused on environmental toxins. Limited to toxin-related toxicity data.
Tox21	https://tripod.nih.gov/tox21/challenge/	High-throughput screening for toxicity end points	With a limited number of chemicals tested, end points may not fully represent human toxicity
ToxCast	https://www.epa.gov/chemical-research/toxicity-forecaster-toxcasttm-data	Toxicity end points are screened through a high-throughput screening program using automated chemical screening technologies. Toxicology, hazardous chemicals, environmental health, and toxic releases are covered by a collection of databases that provide access to information on these topics.	With a limited number of chemicals tested, end points may not fully represent human toxicity. Limited information on the toxicity of some compounds. Data is fragmented across multiple databases and may require significant effort to obtain comprehensive information. Limited to curated data and may not include all available toxicity data
U.S. National Toxicology Program (NTP)	https://ntp.niehs.nih.gov/	Provides toxicology data and information on potentially hazardous substances	Limited to substances tested by NTP
ZINC	http://zinc15.docking.org/	A database of commercially available compounds for virtual screening	Limited to commercially available compounds
Antimicrobial Chemotherapeutics Database (ACD)	https://acd.ucdavis.edu/	A database of antibiotics, antifungals, and antivirals	Limited to antimicrobial compounds

Japanese Toxicogenomics Project consortium (TGP) has developed a comprehensive toxicogenomics database over the past decade, incorporating data from 170 compounds, primarily drugs, to enhance drug safety assessment.[322] The project's data, including gene expression, pathology, and lot numbers, are freely accessible to the public through Open TG-GATEs (Toxicogenomics Project-Genomics Assisted Toxicity Evaluation System).[322] The Life Science Database Archive in Japan securely preserves and maintains the Open TG Database. This comprehensive repository ensures long-term stability and accessibility of the valuable toxicogenomics data it contains.

Another useful database is the MDL Drug data report (MDDR), created by Accelrys and Prous Science, which contains more than 180,000 biologically relevant compounds and well-defined derivatives, with updates appending around 10,000 a year to the database.[323] The MDDR Finder permits the user to search the database by structure or across relevant data fields.[323] The database focuses on drugs launched or under development, descriptions of therapeutic action and biological activity, and tracking of compounds through development phases.

The antimicrobial chemotherapeutics database (ACD) is also an important database for antimicrobial or antibiotic drug researchers, which contains around 4100 synthetic antimicrobial compounds as well as near about 1030 active antimicrobial peptides, mostly being biological sources but some are synthetic.[324]

6. CONCLUSION

Deep-learning-based approaches have great potential for drug toxicity prediction, which can advance drug safety science and support the 3R principle of replacement, reducing, and refining animal testing in preclinical studies. Deep learning can automatically learn complex features from large data sets. It also can extract representation from raw data, such as images or text. In the case of drug toxicity prediction, this means that deep-learning models can extract meaningful features from molecular structures and other data related to drug compounds. To train deep-learning models for drug toxicity prediction, large amounts of data are required. This data can come from a variety of sources, including chemical structural data (e.g., SMILES, molecular graphs, etc.), genomic data (e.g., gene expression, DNA methylation, chromatin accessibility, etc.), protein structural data (e.g., PDB files, protein sequences, etc.), AlphaFold 2 generated artificially folded protein structural data, cell, and tissue images (e.g., histology, microscopy, MRI etc.), pharmacological data (e.g., drug−target interactions, drug efficacy and potency, etc.), clinical data (e.g., patient demographics, adverse events, medical histories, etc.), electronic health records (EHRs), etc. One of the challenges of using these data is that it can be noisy, incomplete, and unlabeled (Table 3). However, deep-learning models can handle noisy and incomplete data, as they can learn from patterns and correlations within the data. Self-supervised learning is one deep-learning technique that can leverage unlabeled data to learn useful representations of molecular structures, and thanks to its advancement, deep learning now upgraded its ability to learn from unlabeled data. This is particularly important in the context of drug toxicity prediction and drug discovery, where labeled data can be scarce and expensive to obtain. Today, by training a model on unlabeled data, such as molecular graphs, to predict certain features of a molecule, such as its 3D structure or binding affinity, based on its 2D representation, the model can learn to

https://doi.org/10.1021/acs.chemrestox.2c00375
Chem. Res. Toxicol. XXXX, XXX, XXX−XXX

Figure 3. A guideline for probable use of DL architectures under different scenarios. This flowchart is intended to provide general guidance and may not be exhaustive or applicable to every situation. The specific scenarios may vary depending on the scope of your research and the type of toxicity data you are working with. One may need to modify or adapt this flowchart to fit the specific context of their study.

encode relevant information about the molecule in a lower-dimensional space. This can be useful for predicting the toxicity of new compounds, as it allows the model to generalize to unseen data. Contrastive self-supervised learning also aids in multimodal learning like comparing different types of data, e.g., drug toxicity image data and molecular graph data of the drug, to give completely novel before-seen insight. Another modern deep-learning architecture that has shown promise in drug toxicity prediction is GNNs. GNNs are designed to handle graph-structured data, such as molecular graphs, which are abundant in chemical toxicity studies. It also can be employed under different learning paradigms to deal with labeled, partially labeled, or unlabeled data. GNNs can learn to capture the structural features of molecules represented as graphs, which can be useful in predicting toxicity by identifying structural features associated with it.

When choosing a deep-learning architecture for toxicity studies, one must take into account the data type, labeling, and study objectives, as well as the strengths and limitations of various DL techniques. The selection of an appropriate deep-learning architecture should also consider the specific characteristics and features of the molecules of interest to ensure optimal performance. Though a hierarchical flowchart has been provided to aid in selecting models, this flowchart is intended to provide

https://doi.org/10.1021/acs.chemrestox.2c00375
Chem. Res. Toxicol. XXXX, XXX, XXX−XXX

general guidance and is not exhaustive or applicable to every situation (Figure 3). The specific scenarios may vary depending on the scope of your research and the type of toxicity data you are working with. One needs to modify or adapt this flowchart to fit the specific context of their study.

In addition to the deep-learning models themselves, the availability of large-scale molecular data sets is also important for training accurate toxicity prediction models. One example of such a data set is the Tox21 data set, which contains toxicity measurements for thousands of compounds across multiple assays (Table 3). By training models on such data sets, DL methods can learn to generalize to a wide range of compounds and toxicity end points.

Deep learning is a promising approach in drug toxicology research, with potential benefits in drug development and safety testing. However, there are challenges associated with this approach that must be carefully considered and addressed. One of the main challenges is the acquisition and quality of data. Data is often scarce and heterogeneous and of varying quality due to measurement errors, batch effects, and missing data, which can adversely affect the performance of deep-learning models. Researchers are exploring the integration of different types of data sources, such as genomics, proteomics, and metabolomics data, to address these issues and improve the performance of deep-learning models. Combining chemical structure and genomic data can enhance the accuracy of toxicity prediction models. Integrating transcriptomics data with chemical structure data has also been shown to improve the accuracy of predictions.

In addition to data integration, the development of more interpretable deep-learning models is crucial. While deep learning has demonstrated high levels of accuracy in predicting drug toxicity, its black-box nature can make it challenging to understand the underlying biological mechanisms or features that contribute to toxicity prediction. Researchers are working on developing methods to explain the predictions made by deep-learning models, such as using attention mechanisms to highlight important features. The development of explainable AI models is an emerging trend in drug toxicology research, and researchers are developing novel methods for interpreting deep-learning models to improve model transparency and interoperability.

Ethical concerns are also a crucial consideration in drug toxicology research. The complexity of deep-learning models can make it difficult to interpret their predictions and raise concerns about potential biases and discrimination. Ensuring that deep learning is used responsibly and ethically, with proper consideration given to issues such as privacy, bias, and fairness, is crucial.

Personalized medicine is another area where deep learning has the potential to make a significant impact by predicting an individual's response to a particular drug based on their unique genetic makeup and other factors. By tailoring drug treatments to individual patients, it may be possible to reduce the risk of adverse drug reactions and improve patient outcomes. In this context, reinforcement learning can leverage its ability to learn from feedback loops from the environment to optimize drug dosages and mitigate adverse drug reactions. For example, a reinforcement learning agent can be trained on patient data to predict the optimal drug dosage that maximizes the desired therapeutic effect while minimizing toxicity. The agent then interacts with the patient in real time, receiving feedback on the efficacy and toxicity of the drug. Based on this feedback, the agent can adjust the drug dosage and optimize the treatment for the patient, effectively creating a feedback loop between the agent and the patient's response to the drug. Similarly, reinforcement learning can be used to monitor patients for adverse drug reactions and adjust treatment accordingly. The agent receives feedback on the patient's response to the drug, including any adverse reactions, and adjusts the treatment to mitigate those reactions. By continually monitoring and adjusting treatment based on feedback from the patient, the agent can effectively create a feedback loop that optimizes the drug treatment for the individual patient.

As discussed throughout the text, the potential for improving drug development and approval processes exists with deep learning in drug toxicological studies. However, the potential improvement of drug development and approval processes through deep learning in drug toxicological studies is overshadowed by ethical and societal concerns that must be addressed. Ethical considerations include potential biases in data and models, misuse of the technology, and removal of human judgment. Data privacy and societal implications such as decreased animal testing and impact on the job market are also important to consider. To ensure ethical and responsible use of deep-learning models, new regulations and guidelines along with ongoing discussions and collaboration among stakeholders are necessary to ensure responsible and ethical application of these technologies. Validation and testing of models and careful consideration of the implications of the technology are important for responsible and ethical application.

In conclusion, deep-learning algorithms have revolutionized drug toxicological studies, offering new opportunities and possibilities for drug development. However, there are still many challenges to overcome, such as the need for large and high-quality data sets, ethical considerations, and the interpretability of deep-learning models. Therefore, future research should focus on developing novel algorithms that integrate the strengths of deep learning with other machine-learning techniques and incorporate interpretability and transparency in the models. Furthermore, efforts should be made to ensure that deep learning is used ethically and that the benefits of these technologies are distributed equitably across different groups of people.

AUTHOR INFORMATION

Corresponding Authors

Krishnendu Sinha − *Department of Zoology, Jhargram Raj College, Jhargram 721507 West Bengal, India*; Email: dr.krishnendusinha@gmail.com

Parames C. Sil − *Division of Molecular Medicine, Bose Institute, Kolkata 700054 West Bengal, India*; orcid.org/0000-0003-0190-5904; Email: paremes@jcbose.ac.in

Author

Nabanita Ghosh − *Department of Zoology, Maulana Azad College, Kolkata 700013 West Bengal, India*

Complete contact information is available at: https://pubs.acs.org/10.1021/acs.chemrestox.2c00375

Author Contributions

CRediT: **Krishnendu Sinha** conceptualization, data curation, visualization, writing-original draft, writing-review & editing; **Nabanita Ghosh** writing-original draft, writing-review & editing; **Parames C Sil** supervision, writing-review & editing.

Funding

No funding was received.

https://doi.org/10.1021/acs.chemrestox.2c00375
Chem. Res. Toxicol. XXXX, XXX, XXX−XXX

Notes

The authors declare no competing financial interest.

Biographies

Dr. Krishnendu Sinha, an assistant professor in Zoology holds a position at the Jhargram Raj College, located in the Jhargram district of West Bengal, India. He obtained his bachelor's degree in Zoology from the Presidency College in Kolkata, followed by a master's degree in Zoology from the University of Calcutta in Kolkata. Additionally, he earned a Ph.D. in molecular toxicology and applied pharmacology from the prestigious Bose Institute in Kolkata. Dr. Sinha's primary research interests revolve around the utilization of AI/ML within the realms of toxicology and pharmacology. He is currently engaged in ongoing work related to this area of study.

Dr. Nabanita Ghosh, an assistant professor in Zoology at the Maulana Azad College, Kolkata, India, holds a bachelor's and a master's degree in Zoology from the University of Calcutta, Kolkata. She earned her Ph.D. in applied neuroscience, focusing on Parkinson's disease, from the same university. Her passion lies in exploring the utilization of AI/ML in the realm of applied neuroscience. Currently, her research centers around conducting cognitive behavioral studies using mice models.

Prof. Parames C. Sil is a professor of Molecular Medicine at the prestigious Bose Institute in Kolkata, India. He holds a Bachelor's degree in Chemistry, a Master's degree in Physical Chemistry, and a Ph.D. in Chemistry from the University of Calcutta and the Bose Institute. With over a decade of experience at the Cleveland Clinic Foundation in Cleveland, Ohio, United States, his research covers cardiac hypertrophy, heart failure, molecular toxicology, pharmacology, nanotechnology, and AI/ML. Currently, Dr. Sil serves as an Associate Editor for Toxicology Reports and is an editorial board member for journals like Biochemical Pharmacology and Chemical Research in Toxicology.

REFERENCES

(1) Min, S.; Lee, B.; Yoon, S. Deep learning in bioinformatics. *Brief Bioinform.* **2017**, *18* (5), 851−869.

(2) Powles, J.; Hodson, H. Google DeepMind and healthcare in an age of algorithms. *Health Technol. (Berl).* **2017**, *7* (4), 351−367.

(3) Ferrucci, D.; Brown, E.; Chu-Carroll, J.; Fan, J.; Gondek, D.; Kalyanpur, A. A.; Lally, A.; Murdock, J. W.; Nyberg, E.; Prager, J.; Schlaefer, N.; Welty, C. Building Watson: An Overview of the DeepQA Project. *AI Mag.* **2010**, *31* (3), 59−79.

(4) *IBM Watson*. https://www.ibm.com/in-en/watson?utm_content=SRCWW&p1=Search&p4=43700052660680860&p5=e&gclid=Cj0KCQiA4OybBhCzARIsAIcfn9nKCckPc1jlnJWe_SLdTcmkFBGN9BfytAnPVD9Lfz24Ua-zGbSou0caAuFIEALw_wcB&gclsrc=aw.ds (accessed 2022-11-21).

(5) Bavarian, M.; Jun, H.; Tezak, N.; Schulman, J.; McLeavey, C.; Tworek, J.; Chen, M. Efficient Training of Language Models to Fill in the Middle. *arXiv*, July 28, 2022, 2207.14255 (accessed 2023-04-18).

(6) Silver, D.; Huang, A.; Maddison, C. J.; Guez, A.; Sifre, L.; Van Den Driessche, G.; Schrittwieser, J.; Antonoglou, I.; Panneershelvam, V.; Lanctot, M.; Dieleman, S.; Grewe, D.; Nham, J.; Kalchbrenner, N.; Sutskever, I.; Lillicrap, T.; Leach, M.; Kavukcuoglu, K.; Graepel, T.; Hassabis, D. Mastering the game of Go with deep neural networks and tree search. *Nature 2016 529:7587.* **2016**, *529* (7587), 484−489.

(7) *AlphaFold*. https://www.deepmind.com/research/highlighted-research/alphafold (2022-11-22).

(8) Jumper, J.; Evans, R.; Pritzel, A.; Green, T.; Figurnov, M.; Ronneberger, O.; Tunyasuvunakool, K.; Bates, R.; Žídek, A.; Potapenko, A.; Bridgland, A.; Meyer, C.; Kohl, S. A. A.; Ballard, A. J.; Cowie, A.; Romera-Paredes, B.; Nikolov, S.; Jain, R.; Adler, J.; Back, T.; Petersen, S.; Reiman, D.; Clancy, E.; Zielinski, M.; Steinegger, M.; Pacholska, M.; Berghammer, T.; Bodenstein, S.; Silver, D.; Vinyals, O.; Senior, A. W.; Kavukcuoglu, K.; Kohli, P.; Hassabis, D. Highly accurate protein structure prediction with AlphaFold. *Nature 2021 596:7873.* **2021**, *596* (7873), 583−589.

(9) Tang, W.; Chen, J.; Wang, Z.; Xie, H.; Hong, H. Deep learning for predicting toxicity of chemicals: a mini review. *J. Environ. Sci. Health C Environ. CarcinogEcotoxicol Rev.* **2018**, *36* (4), 252−271.

(10) Basile, A. O.; Yahi, A.; Tatonetti, N. P. Artificial Intelligence for Drug Toxicity and Safety. *Trends Pharmacol. Sci.* **2019**, *40* (9), 624−635.

(11) Lecun, Y.; Bengio, Y.; Hinton, G. Deep learning. *Nature 2015 521:7553.* **2015**, *521* (7553), 436−444.

(12) Alzubaidi, L.; Zhang, J.; Humaidi, A. J.; Al-Dujaili, A.; Duan, Y.; Al-Shamma, O.; Santamaría, J.; Fadhel, M. A.; Al-Amidie, M.; Farhan, L. Review of deep learning: concepts, CNN architectures, challenges, applications, future directions. *Journal of Big Data 2021 8:1.* **2021**, *8* (1), 1−74.

(13) Géron, A. Hands-on machine learning with Scikit-Learn, Keras and TensorFlow: concepts, tools, and techniques to build intelligent systems. *O'Reilly Media*. Published online 2019. https://www.oreilly.com/library/view/hands-on-machine-learning/9781492032632/ (accessed 2022-11-22).

(14) *Deep Learning*. https://www.deeplearningbook.org/ (accessed 2023-03-12).

(15) Chollet, F. Introduction to Keras. In *Deep Learning with Python*. Published online 2017. https://www.manning.com/books/deep-learning-with-python (accessed 2022-11-22).

(16) Greener, J. G.; Kandathil, S. M.; Moffat, L.; Jones, D. T. A guide to machine learning for biologists. *Nat. Rev. Mol. Cell Biol.* **2022**, *23* (1), 40−55.

(17) Deo, R. C. Machine Learning in Medicine. *Circulation* **2015**, *132* (20), 1920−1930.

https://doi.org/10.1021/acs.chemrestox.2c00375
Chem. Res. Toxicol. XXXX, XXX, XXX−XXX

(18) McCulloch, W. S.; Pitts, W. A logical calculus of the ideas immanent in nervous activity. *bulletin of mathematical biophysics 1943 5:4.* **1943**, *5* (4), 115−133.
(19) Emmert-Streib, F.; Yang, Z.; Feng, H.; Tripathi, S.; Dehmer, M. An Introductory Review of Deep Learning for Prediction Models With Big Data. *Front ArtifIntell.* **2020**, *3*, 4.
(20) Echle, A.; Rindtorff, N. T.; Brinker, T. J.; Luedde, T.; Pearson, A. T.; Kather, J. N. Deep learning in cancer pathology: a new generation of clinical biomarkers. *Br J. Cancer.* **2021**, *124* (4), 686−696.
(21) Zhang, M.; Young, G. S.; Chen, H.; Li, J.; Qin, L.; McFaline-Figueroa, J. R.; Reardon, D. A.; Cao, X.; Wu, X.; Xu, X. Deep-Learning Detection of Cancer Metastases to the Brain on MRI. *J. MagnReson Imaging.* **2020**, *52* (4), 1227−1236.
(22) Hosny, A.; Parmar, C.; Quackenbush, J.; Schwartz, L. H.; Aerts, H.J.W.L. Artificial intelligence in radiology. *Nat. Rev. Cancer.* **2018**, *18* (8), 500−510.
(23) Wang, S.; Hou, Y.; Li, X.; Meng, X.; Zhang, Y.; Wang, X. Practical Implementation of Artificial Intelligence-Based Deep Learning and Cloud Computing on the Application of Traditional Medicine and Western Medicine in the Diagnosis and Treatment of Rheumatoid Arthritis. *Front Pharmacol.* **2021**, *12*, 12.
(24) Üreten, K.; Maraş, H. H. Automated Classification of Rheumatoid Arthritis, Osteoarthritis, and Normal Hand Radiographs with Deep Learning Methods. *J. Digit Imaging.* **2022**, *35* (2), 193−199.
(25) Wu, M.; Wu, H.; Wu, L.; Cui, C.; Shi, S.; Xu, J.; Liu, Y.; Dong, F. A deep learning classification of metacarpophalangeal joints synovial proliferation in rheumatoid arthritis by ultrasound images. *J. Clin Ultrasound.* **2022**, *50* (2), 296−301.
(26) Karthik, R.; Menaka, R.; Johnson, A.; Anand, S. Neuroimaging and deep learning for brain stroke detection - A review of recent advancements and future prospects. *Comput. Methods Programs Biomed.* **2020**, *197*, 105728.
(27) Jaganathan, K.; KyriazopoulouPanagiotopoulou, S.; McRae, J. F.; Darbandi, S. F.; Knowles, D.; Li, Y. I.; Kosmicki, J. A.; Arbelaez, J.; Cui, W.; Schwartz, G. B.; Chow, E. D.; Kanterakis, E.; Gao, H.; Kia, A.; Batzoglou, S.; Sanders, S. J.; Farh, K. K. H. Predicting Splicing from Primary Sequence with Deep Learning. *Cell.* **2019**, *176* (3), 535−548.
(28) Regan, K.; Saghafi, A.; Li, Z. Splice Junction Identification using Long Short-Term Memory Neural Networks. *Curr. Genomics.* **2021**, *22* (5), 384−390.
(29) Zhang, Y.; Liu, X.; MacLeod, J.; Liu, J. Discerning novel splice junctions derived from RNA-seq alignment: a deep learning approach. *BMC Genomics.* **2018**; *19* (1). DOI: 10.1186/s12864-018-5350-1.
(30) Mayr, A.; Klambauer, G.; Unterthiner, T.; Hochreiter, S. DeepTox: Toxicity prediction using deep learning. *Front Environ. Sci.* **2016**, *3* (FEB), 80.
(31) Kong, W.; Midena, G.; Chen, Y.; Athanasiadis, P.; Wang, T.; Rousu, J.; He, L.; Aittokallio, T. Systematic review of computational methods for drug combination prediction. *Comput. Struct Biotechnol J.* **2022**, *20*, 2807−2814.
(32) Ingber, D. E. Human organs-on-chips for disease modelling, drug development and personalized medicine. *Nature Reviews Genetics* **2022**, *23* (8), 467−491.
(33) Ingelman-Sundberg, M.; Mkrtchian, S.; Zhou, Y.; Lauschke, V. M. Integrating rare genetic variants into pharmacogenetic drug response predictions. *Hum Genomics.* **2018**, *12* (1), 26.
(34) Lauschke, V. M.; Ingelman-Sundberg, M. The Importance of Patient-Specific Factors for Hepatic Drug Response and Toxicity. *International Journal of Molecular Sciences.* **2016**, *17* (10), 1714.
(35) Terranova, N.; Venkatakrishnan, K.; Benincosa, L. J. Application of Machine Learning in Translational Medicine: Current Status and Future Opportunities. *AAPS Journal.* **2021**, *23* (4), 74.
(36) Segall, M. D.; Barber, C. Addressing toxicity risk when designing and selecting compounds in early drug discovery. *Drug Discov Today.* **2014**, *19* (5), 688−693.
(37) Onakpoya, I. J.; Heneghan, C. J.; Aronson, J. K. Worldwide withdrawal of medicinal products because of adverse drug reactions: a systematic review and analysis. *Crit. Rev. Toxicol.* **2016**, *46* (6), 477−489.
(38) Raies, A. B.; Bajic, V. B. In silico toxicology: computational methods for the prediction of chemical toxicity. *Wiley Interdiscip Rev. Comput. Mol. Sci.* **2016**, *6* (2), 147−172.
(39) *The 3Rs | NC3Rs.* https://www.nc3rs.org.uk/who-we-are/3rs (accessed 2022-11-15).
(40) Lin, Z.; Chou, W. C. Machine Learning and Artificial Intelligence in Toxicological Sciences. *Toxicol. Sci.* **2022**, *189* (1), 7.
(41) Luo, J.; Wu, M.; Gopukumar, D.; Zhao, Y. Big Data Application in Biomedical Research and Health Care: A Literature Review. *Biomed Inform Insights.* **2016**, *8*, BII.S31559.
(42) Rajkomar, A.; Dean, J.; Kohane, I. Machine Learning in Medicine. *New England Journal of Medicine.* **2019**, *380* (14), 1347−1358.
(43) Tatonetti, N. P.; Ye, P. P.; Daneshjou, R.; Altman, R. B. Data-driven prediction of drug effects and interactions. *Sci. Transl Med.* **2012**, *4* (125), 125ra31.
(44) Tannenbaum, C.; Day, D. Age and sex in drug development and testing for adults. *Pharmacol. Res.* **2017**, *121*, 83−93.
(45) Agamah, F. E.; Mazandu, G. K.; Hassan, R.; Bope, C. D.; Thomford, N. E.; Ghansah, A.; Chimusa, E. R. Computational/in silico methods in drug target and lead prediction. *Brief Bioinform.* **2020**, *21* (5), 1663.
(46) Raunio, H. In silico toxicology non-testing methods. *Front Pharmacol.* **2011**, *2*, 33.
(47) Cronin, M. T. D.; Enoch, S. J.; Madden, J. C.; Rathman, J. F.; Richarz, A. N.; Yang, C. A review of in silico toxicology approaches to support the safety assessment of cosmetics-related materials. *Computational Toxicology.* **2022**, *21*, 100213.
(48) Cherkasov, A.; Muratov, E. N.; Fourches, D.; Varnek, A.; Baskin, I. I.; Cronin, M.; Dearden, J.; Gramatica, P.; Martin, Y. C.; Todeschini, R.; Consonni, V.; Kuz'Min, V. E.; Cramer, R.; Benigni, R.; Yang, C.; Rathman, J.; Terfloth, L.; Gasteiger, J.; Richard, A.; Tropsha, A. QSAR Modeling: Where have you been? Where are you going to? *J. Med. Chem.* **2014**, *57* (12), 4977.
(49) Fourches, D.; Muratov, E.; Tropsha, A. Trust, but verify: on the importance of chemical structure curation in cheminformatics and QSAR modeling research. *J. Chem. Inf Model.* **2010**, *50* (7), 1189−1204.
(50) Kim, S.; Thiessen, P. A.; Bolton, E. E.; Chen, J.; Fu, G.; Gindulyte, A.; Han, L.; He, J.; He, S.; Shoemaker, B. A.; Wang, J.; Yu, B.; Zhang, J.; Bryant, S. H. PubChem Substance and Compound databases. *Nucleic Acids Res.* **2016**, *44* (D1), D1202−D1213.
(51) Pognan, F.; Beilmann, M.; Boonen, H. C. M.; Czich, A.; Dear, G.; Hewitt, P.; Mow, T.; Oinonen, T.; Roth, A.; Steger-Hartmann, T.; Valentin, J. P.; Van Goethem, F.; Weaver, R. J.; Newham, P. The evolving role of investigative toxicology in the pharmaceutical industry. *Nature Reviews Drug Discovery* **2023**, *22*, 317.
(52) Li, S.; Xia, M. Review of High-content Screening Applications in Toxicology. *Arch. Toxicol.* **2019**, *93* (12), 3387.
(53) Cavasotto, C. N.; Scardino, V. Machine Learning Toxicity Prediction: Latest Advances by Toxicity End Point. *ACS Omega.* **2022**, *7* (51), 47536−47546.
(54) Judson, R.; Houck, K.; Martin, M.; Knudsen, T.; Thomas, R. S.; Sipes, N.; Shah, I.; Wambaugh, J.; Crofton, K. In Vitro and Modelling Approaches to Risk Assessment from the U.S. Environmental Protection Agency ToxCast Programme. *Basic Clin PharmacolToxicol.* **2014**, *115* (1), 69−76.
(55) Vamathevan, J.; Clark, D.; Czodrowski, P.; Dunham, I.; Ferran, E.; Lee, G.; Li, B.; Madabhushi, A.; Shah, P.; Spitzer, M.; Zhao, S. Applications of machine learning in drug discovery and development. *Nat. Rev. Drug Discovery* **2019**, *18* (6), 463.
(56) Daina, A.; Michielin, O.; Zoete, V. SwissADME: a free web tool to evaluate pharmacokinetics, drug-likeness and medicinal chemistry friendliness of small molecules. *Scientific Reports 2017 7:1.* **2017**, *7* (1), 1−13.
(57) Kuroda, M.; Watanabe, R.; Esaki, T.; Kawashima, H.; Ohashi, R.; Sato, T.; Honma, T.; Komura, H.; Mizuguchi, K. Utilizing public and private sector data to build better machine learning models for the

https://doi.org/10.1021/acs.chemrestox.2c00375
Chem. Res. Toxicol. XXXX, XXX, XXX−XXX

prediction of pharmacokinetic parameters. *Drug Discov Today*. **2022**, *27* (11), 103339.
(58) Gadaleta, D.; Lombardo, A.; Toma, C.; Benfenati, E. A new semi-automated workflow for chemical data retrieval and quality checking for modeling applications. *J. Cheminform.* **2018**, *10* (1), 60.
(59) Gad, S. C. QSAR. *Encyclopedia of Toxicology: Third Edition*; Academic Press: 2014; pp 1−9.
(60) Roy, K.; Kar, S.; Das, R. N. Newer QSAR Techniques. In *Understanding the Basics of QSAR for Applications in Pharmaceutical Sciences and Risk Assessment*; Academic Press: 2015; pp 319−356.
(61) Gini, G. QSAR Methods. *Methods Mol. Biol.* **2022**, *2425*, 1−26.
(62) Leszczynski, J. *Advances in QSAR Modeling*; Springer: 2017. DOI: 10.1007/978-3-319-56850-8
(63) Topliss, J. G. *Quantitative structure−activity relationships of drugs*; Elsevier: 1983; Vol. *19*.
(64) Karelson, M.; Lobanov, V. S.; Katritzky, A. R. Quantum-chemical descriptors in QSAR/QSPR studies. *Chem. Rev.* **1996**, *96* (3), 1027−1043.
(65) Akamatsu, M. Current State and Perspectives of 3D-QSAR. *Curr. Top Med. Chem.* **2002**, *2* (12), 1381−1394.
(66) Verma, J.; Khedkar, V.; Coutinho, E. 3D-QSAR in Drug Design - A Review. *Curr. Top Med. Chem.* **2010**, *10* (1), 95−115.
(67) Mauri, A.; Consonni, V.; Todeschini, R. Molecular Descriptors. *Handbook of Computational Chemistry* **2016**, 1−29.
(68) Yap, C. W. PaDEL-descriptor: an open source software to calculate molecular descriptors and fingerprints. *J. Comput. Chem.* **2011**, *32* (7), 1466−1474.
(69) Todeschini, R.; Consonni, V.. Handbook of molecular descriptors. In *Methods and Principles in Medicinal Chemistry*; Wiley: 2000; p 667.
(70) Chuang, K. V.; Gunsalus, L. M.; Keiser, M. J. Learning Molecular Representations for Medicinal Chemistry. *J. Med. Chem.* **2020**, *63* (16), 8705−8722.
(71) Danishuddin; Khan, A. U. Descriptors and their selection methods in QSAR analysis: paradigm for drug design. *Drug Discov Today*. **2016**, *21* (8), 1291−1302.
(72) Moriwaki, H.; Tian, Y. S.; Kawashita, N.; Takagi, T. Mordred: A molecular descriptor calculator. *J. Cheminform.* **2018**, *10* (1), 4.
(73) Verma, J.; Khedkar, V.; Coutinho, E. 3D-QSAR in drug design−a review. *Curr. Top Med. Chem.* **2010**, *10* (1), 95−115.
(74) Dapson, R. W. Alternative methods for estimating common descriptors for QSAR studies of dyes and fluorescent probes using molecular modeling software: 1. Concepts and procedures. *Biotech Histochem.* **2013**, *88* (8), 477−488.
(75) Sabando, M. V.; Ponzoni, I.; Milios, E. E.; Soto, A. J. Using molecular embeddings in QSAR modeling: does it make a difference? *Brief Bioinform.* **2022**, *23* (1), bbab365.
(76) Sahoo, S.; Adhikari, C.; Kuanar, M.; Mishra, B. A Short Review of the Generation of Molecular Descriptors and Their Applications in Quantitative Structure Property/Activity Relationships. *CurrComput. Aided Drug Des.* **2016**, *12* (3), 181−205.
(77) Roy, K.; Kar, S.; Das, R. N.Validation of QSAR Models. In *Understanding the Basics of QSAR for Applications in Pharmaceutical Sciences and Risk Assessment*; Elsevier: 2015; pp 231−289.
(78) Davis, A. M. Quantitative Structure-Activity Relationships. *Comprehensive Medicinal Chemistry III* **2017**, *3−8*, 379−392.
(79) Kiralj, R.; Ferreira, M. M. C. Basic validation procedures for regression models in QSAR and QSPR studies: theory and application. *J. Braz Chem. Soc.* **2009**, *20* (4), 770−787.
(80) Alexander, D. L. J.; Tropsha, A.; Winkler, D. A. Beware of R2: simple, unambiguous assessment of the prediction accuracy of QSAR and QSPR models. *J. Chem. Inf Model.* **2015**, *55* (7), 1316.
(81) Dablander, M.; Hanser, T.; Lambiotte, R.; Morris, G. M. Exploring QSAR models for activity-cliff prediction. *Journal of Cheminformatics 2023 15:1.* **2023**, *15* (1), 1−16.
(82) Van Tilborg, D.; Alenicheva, A.; Grisoni, F. Exposing the Limitations of Molecular Machine Learning with Activity Cliffs. *J. Chem. Inf Model.* **2022**, *62* (23), 5938−5951.
(83) Stumpfe, D.; Hu, H.; Bajorath, J. Evolving Concept of Activity Cliffs. *ACS Omega.* **2019**, *4* (11), 14360.
(84) Stumpfe, D.; Hu, H.; Bajorath, J. Computational method for the identification of third generation activity cliffs. *MethodsX* **2020**, *7*, 100793.
(85) Dimova, D.; Stumpfe, D.; Hu, Y.; Bajorath, J. Activity cliff clusters as a source of structure-activity relationship information. *Expert Opin Drug Discovery* **2015**, *10* (5), 441−447.
(86) Rácz, A.; Bajusz, D.; Héberger, K. Intercorrelation Limits in Molecular Descriptor Preselection for QSAR/QSPR. *Mol. Inform.* **2019**, *38* (8−9), 1800154.
(87) Martin, Y. C. 3D QSAR: Current State, Scope, and Limitations. In *3D QSAR in Drug Design*; Springer: 2002; pp 3−23.
(88) Kolmar, S. S.; Grulke, C. M. The effect of noise on the predictive limit of QSAR models. *J. Cheminform.* **2021**, *13* (1), 92.
(89) Rácz, A.; Bajusz, D.; Héberger, K. Intercorrelation Limits in Molecular Descriptor Preselection for QSAR/QSPR. *Mol. Inform.* **2019**, *38* (8−9), 1800154.
(90) Orosz, Á; Héberger, K.; Rácz, A. Comparison of Descriptor- and Fingerprint Sets in Machine Learning Models for ADME-Tox Targets. *Front Chem.* **2022**, *10*, 486.
(91) Danishuddin; Khan, A. U. Descriptors and their selection methods in QSAR analysis: paradigm for drug design. *Drug Discov Today*. **2016**, *21* (8), 1291−1302.
(92) Jagiello, K.; Grzonkowska, M.; Swirog, M.; Ahmed, L.; Rasulev, B.; Avramopoulos, A.; Papadopoulos, M. G.; Leszczynski, J.; Puzyn, T. Advantages and limitations of classic and 3D QSAR approaches in nano-QSAR studies based on biological activity of fullerene derivatives. *Journal of Nanoparticle Research.* **2016**, *18* (9), 256.
(93) Eicher, T.; Kinnebrew, G.; Patt, A.; Spencer, K.; Ying, K.; Ma, Q.; Machiraju, R.; Mathé, E. A. Metabolomics and Multi-Omics Integration: A Survey of Computational Methods and Resources. *Metabolites.* **2020**, *10* (5), 202.
(94) Cavasotto, C. N.; Scardino, V. Machine Learning Toxicity Prediction: Latest Advances by Toxicity End Point. *ACS Omega.* **2022**, *7* (51), 47536−47546.
(95) Kapsiani, S.; Howlin, B. J. Random forest classification for predicting lifespan-extending chemical compounds. *Scientific Reports 2021 11:1.* **2021**, *11* (1), 1−13.
(96) Chen, T.; Cao, Y.; Zhang, Y.; Liu, J.; Bao, Y.; Wang, C.; Jia, W.; Zhao, A. Random Forest in Clinical Metabolomics for Phenotypic Discrimination and Biomarker Selection. *Evid Based Complement Alternat Med.* **2013**, *2013*, 298183.
(97) Wang, H.; Liu, R.; Schyman, P.; Wallqvist, A. Deep neural network models for predicting chemically induced liver toxicity endpoints from transcriptomic responses. *Front Pharmacol.* **2019**, *10* (FEB), 42.
(98) Li, T.; Tong, W.; Roberts, R.; Liu, Z.; Thakkar, S. Deep Learning on High-Throughput Transcriptomics to Predict Drug-Induced Liver Injury. *Front BioengBiotechnol.* **2020**, *8*, 1366.
(99) Sinha, K.; Ghosh, J.; Sil, P. C. Machine Learning in Drug Metabolism Study. *Curr. Drug Metab.* **2022**, *23* (13), 1012−1026.
(100) Wu, L.; Yan, B.; Han, J.; Li, R.; Xiao, J.; He, S.; Bo, X. TOXRIC: a comprehensive database of toxicological data and benchmarks. *Nucleic Acids Res.* **2023**, *51* (D1), D1432−D1445.
(101) Chollet, F.. *Deep Learning with Python*, 2021. ISBN 9781617296864.
(102) Bishop, C. M. *Pattern Recogniton and Machine Learning*; Springer-Verlag: New York, 2006. https://www.springer.com/gp/book/9780387310732 (accessed 2022-06-18).
(103) Sarker, I. H. Deep Learning: A Comprehensive Overview on Techniques, Taxonomy, Applications and Research Directions. *SN Comput. Sci.* **2021**, *2* (6), 420.
(104) Shrestha, A.; Mahmood, A. Review of deep learning algorithms and architectures. *IEEE Access.* **2019**, *7*, 53040−53065.
(105) Arulkumaran, K.; Deisenroth, M. P.; Brundage, M.; Bharath, A. A. Deep reinforcement learning: A brief survey. *IEEE Signal Process Mag.* **2017**, *34* (6), 26−38.

https://doi.org/10.1021/acs.chemrestox.2c00375
Chem. Res. Toxicol. XXXX, XXX, XXX−XXX

(106) Francois-Lavet, V.; Henderson, P.; Islam, R.; Bellemare, M. G.; Pineau, J. An Introduction to Deep Reinforcement Learning. *Foundations and Trends in Machine Learning*. **2018**, *11* (3−4), 219−354.
(107) Chai, W.; Wang, G. Deep Vision Multimodal Learning: Methodology, Benchmark, and Trend. *Applied Sciences 2022, Vol 12, Page 6588*. **2022**, *12* (13), 6588.
(108) LeCun, Y.I now call it "self-supervised learning". *Facebook*. https://www.facebook.com/722677142/posts/10155934004262143/ (accessed 2023-03-19).
(109) Self-supervised learning: The dark matter of intelligence. *Facebook*. https://ai.facebook.com/blog/self-supervised-learning-the-dark-matter-of-intelligence/ (accessed 2023-03-19.)
(110) Burkov, A. *Machine Learning Engineering*. Published online 2020. https://www.saint-gobain.co.in/sites/saint-gobain.co.in/files/webform/apply_for_indec/_sid_/machine-learning-engineering-andriy-burkov-pdf-download-free-book-c6498c8.pdf (accessed 2022-06-15).
(111) LeCun, Y.; Kavukcuoglu, K.; Farabet, C. Convolutional networks and applications in vision. In *ISCAS 2010 - 2010 IEEE International Symposium on Circuits and Systems: Nano-Bio Circuit Fabrics and Systems*; IEEE: 2010; pp 253−256.
(112) Liu, X.; Zhang, F.; Hou, Z.; Wang, Z.; Mian, L.; Zhang, J.; Tang, J. Self-supervised Learning: Generative or Contrastive. *IEEE Trans Knowl Data Eng.* **2021**, *35* (1), 857−876.
(113) Beyer, L.; Zhai, X.; Oliver, A.; Kolesnikov, A. S4L: Self-Supervised Semi-Supervised Learning. In *Proceedings of the IEEE International Conference on Computer Vision*; IEEE: 2019; pp 1476−1485. DOI: 10.1109/ICCV.2019.00156.
(114) Jaiswal, A.; Babu, A. R.; Zadeh, M. Z.; Banerjee, D.; Makedon, F. A Survey on Contrastive Self-Supervised Learning. *Technologies 2021, Vol 9, Page 2*. **2021**, *9* (1), 2.
(115) Gutmann, M.; Hyvärinen, A. Noise-contrastive estimation: A new estimation principle for unnormalized statistical models. In *Proceedings of the Thirteenth International Conference on Artificial Intelligence and Statistics*; ML Research Press: 2010; pp 297−304. https://proceedings.mlr.press/v9/gutmann10a.html (accessed 2023-03-28).
(116) Chen, T.; Kornblith, S.; Norouzi, M.; Hinton, G. A Simple Framework for Contrastive Learning of Visual Representations. In *37th International Conference on Machine Learning, ICML 2020*; JMLR.org: 2020; pp 1575−1585.
(117) Rani, V.; Nabi, S. T.; Kumar, M.; Mittal, A.; Kumar, K. Self-supervised Learning: A Succinct Review. *Archives of Computational Methods in Engineering*. **2023**, *30*, 2761−2775.
(118) Naskath, J.; Sivakamasundari, G.; Begum, A. A. S. A Study on Different Deep Learning Algorithms Used in Deep Neural Nets: MLP SOM and DBN. *WirelPersCommun.* **2023**, *128* (4), 2913−2936.
(119) What are Recurrent Neural Networks? *IBM*. https://www.ibm.com/cloud/learn/recurrent-neural-networks#toc-what-are-r-btVB33l5 (accessed 2022-11-26).
(120) *CS 230 - Recurrent Neural Networks Cheatsheet*. https://stanford.edu/~shervine/teaching/cs-230/cheatsheet-recurrent-neural-networks (accessed 2022-11-26).
(121) Pascanu, R.; Mikolov, T.; Bengio, Y. On the difficulty of training recurrent neural networks. In *Proceedings of the 30th International Conference on Machine Learning*; MLR Press: 2013; pp 1310−1318. https://proceedings.mlr.press/v28/pascanu13.html (accessed 2023-04-02).
(122) Bengio, Y. Learning Deep Architectures for AI. *FNT Machine Learning* **2009**, *2* (1), 1−127.
(123) Sharma, D. K.; Chatterjee, M.; Kaur, G.; Vavilala, S. Deep learning applications for disease diagnosis. In *Deep Learning for Medical Applications with Unique Data*; Academic Press: 2022; pp 31−51;
(124) Kohonen, T. The Self-Organizing Map. *Proceedings of the IEEE* **1990**, *78* (9), 1464−1480.
(125) Xiao, Y.-D.; Harris, R.; Bayram, E.; Santago, P.; Schmitt, J. D. Supervised Self-Organizing Maps in Drug Discovery. 2. Improvements in Descriptor Selection and Model Validation. *J. Chem. Inf Model.* **2006**, *46* (1), 137−144.
(126) Yamashita, R.; Nishio, M.; Do, RK G; Togashi, K. Convolutional neural networks: an overview and application in radiology. *Insights Imaging*. **2018**, *9* (4), 611−629.
(127) Albawi, S.; Mohammed, T. A.; Al-Zawi, S. Understanding of a convolutional neural network. In *Proceedings of 2017 International Conference on Engineering and Technology*; ICET: 2018; pp 1−6. DOI: 10.1109/ICENGTECHNOL.2017.8308186.
(128) Huang, X.; Huang, K.; Johnson, T.; Radovich, M.; Zhang, J.; Ma, J.; Wang, Y. ParsVNN: parsimony visible neural networks for uncovering cancer-specific and drug-sensitive genes and pathways. *NAR GenomBioinform.* **2021**, *3*, 4.
(129) Hao, Y.; Romano, J. D.; Moore, J. H. Knowledge-guided deep learning models of drug toxicity improve interpretation. *Patterns*. **2022**, *3* (9), 100565.
(130) Roy, G. G.; Geard, N.; Verspoor, K.; He, S. MPVNN: Mutated Pathway Visible Neural Network Architecture for Interpretable Prediction of Cancer-specific Survival Risk. *Bioinformatics* **2022**, *38* (22), 5026−5032.
(131) Le Roux, N.; Bengio, Y. Representational power of restricted boltzmann machines and deep belief networks. *Neural Comput.* **2008**, *20* (6), 1631−1649.
(132) Ali, A. Restricted Boltzmann Machine (RBM) with Practical Implementation. *Medium*. Wavy AI Research Foundation. https://medium.com/machine-learning-researcher/boltzmann-machine-c2ce76d94da5 (accessed 2022-11-27).
(133) Ghojogh, B; Ghodsi, A; Karray, F.; Crowley, M. Restricted Boltzmann Machine and Deep Belief Network: Tutorial and Survey. *arXiv*, August 6, 2022, 2107.12521 (accessed 2023-03-12).
(134) Kunapuli, S. S.; Bhallamudi, P. C. A review of deep learning models for medical diagnosis. In *Machine Learning, Big Data, and IoT for Medical Informatics*; Elsevier: 2021; pp 389−404
(135) Intro to Autoencoders. *TensorFlow Core*. https://www.tensorflow.org/tutorials/generative/autoencoder (accessed 2022-11-27).
(136) Abirami, S.; Chitra, P. Energy-efficient edge based real-time healthcare support system. *Advances in Computers*. **2020**, *117* (1), 339−368.
(137) Dertat, A. Applied Deep Learning - Part 3: Autoencoders. *Towards Data Science*. https://towardsdatascience.com/applied-deep-learning-part-3-autoencoders-1c083af4d798 (accessed 2022-11-27).
(138) Makhzani, A.; Shlens, J.; Jaitly, N.; Goodfellow, I.; Frey, B. Adversarial Autoencoders. *arXiv*, November 18, 2015, 1511.05644 (accessed 2023-02-25). DOI: 10.48550/arxiv.1511.05644.
(139) Zhai, J.; Zhang, S.; Chen, J.; He, Q. Autoencoder and Its Various Variants. In *Proceedings - 2018 IEEE International Conference on Systems, Man, and Cybernetics, SMC 2018*; IEEE: 2019; pp 415−419.
(140) Goodfellow, I. J.; Pouget-Abadie, J.; Mirza, M.; Xu, B.; Warde-Farley, D.; Ozair, S.; Courville, A.; Bengio, Y. Generative Adversarial Networks. *Sci. Robot.* **2014**, *3*, 2672−2680.
(141) Aggarwal, A.; Mittal, M.; Battineni, G. Generative adversarial network: An overview of theory and applications. *International Journal of Information Management Data Insights*. **2021**, *1* (1), 100004.
(142) Kobyzev, I.; Prince, SJ D; Brubaker, M. A. Normalizing Flows: An Introduction and Review of Current Methods. *IEEE Trans Pattern Anal Mach Intell.* **2021**, *43* (11), 3964−3979.
(143) Winkler, C.; Worrall, D.; Hoogeboom, E.; Welling, M. Learning Likelihoods with Conditional Normalizing Flows. *arXiv*, November 29, 2019, 1912.00042, ver. 1. https://arxiv.org/abs/1912.00042v1 (accessed 2023-04-07).
(144) Liu, J.; Kumar, A.; Ba, J.; Kiros, J.; Research, G.; Swersky, K. Graph Normalizing Flows. *Adv. Neural Inf Process Syst.* **2019**, 32.
(145) Yang, L.; Zhang, Z.; Song, Y.; Hong, S.; Xu, R.; Zhao, Y.; Shao, Y.; Zhang, W.; Cui, B.; Yang, M. H. Diffusion Models: A Comprehensive Survey of Methods and Applications. *arXiv*, September 2, 2022, 2209.00796, ver. 10. https://arxiv.org/abs/2209.00796v10 (accessed 2023-04-07).
(146) Luo, C. Understanding Diffusion Models: A Unified Perspective. *arXiv*, August 25, 2022, 2208.11970, ver. 1. https://arxiv.org/abs/2208.11970v1 (accessed 2023-04-07).

https://doi.org/10.1021/acs.chemrestox.2c00375
Chem. Res. Toxicol. XXXX, XXX, XXX−XXX

(147) What are Diffusion Models? *Lil'Log*. https://lilianweng.github.io/posts/2021-07-11-diffusion-models/ (accessed 2023-04-07).
(148) Dalal, M.; Li, A. C.; Taori, R. Autoregressive Models: What Are They Good For? *arXiv*, October 17, 2019, 1910.07737, ver. 1. https://arxiv.org/abs/1910.07737v1 (accessed 2023-06-16).
(149) Xu, X. S.; Wang, H.; Vermeulen, A. Modeling delayed drug effect using discrete-time nonlinear autoregressive models: a connection with indirect response models. *J. PharmacokinetPharmacodyn.* **2011**, *38* (3), 353−367.
(150) Shi, C.; Xu, M.; Zhu, Z.; Zhang, W.; Zhang, M.; Tang, J. GraphAF: a Flow-based Autoregressive Model for Molecular Graph Generation. *arXiv*, January 26, 2020, 2001.09382, ver. 2. https://arxiv.org/abs/2001.09382v2 (accessed 2023-06-16).
(151) Zhou, J.; Cui, G.; Hu, S.; Zhang, Z.; Yang, C.; Liu, Z.; Wang, L.; Li, C.; Sun, M. Graph neural networks: A review of methods and applications. *AI Open.* **2020**, *1*, 57−81.
(152) Zhang, X. M.; Liang, L.; Liu, L.; Tang, M. J. Graph Neural Networks and Their Current Applications in Bioinformatics. *Front Genet.* **2021**, *12*, 1073.
(153) Bronstein, M. M.; Bruna, J.; Cohen, T.; Veličković, P. Geometric Deep Learning: Grids, Groups, Graphs, Geodesics, and Gauges. *arXiv*, April 27, 2021, 2104.13478, ver. 2. https://arxiv.org/abs/2104.13478v2 (accessed 2023-04-03).
(154) Liao, W.; Bak-Jensen, B.; Radhakrishna Pillai, J.; Wang, Y.; Wang, Y. A Review of Graph Neural Networks and Their Applications in Power Systems. *Journal of Modern Power Systems and Clean Energy.* **2022**, *10* (2), 345−360.
(155) Choudhary, K.; DeCost, B.; Chen, C.; Jain, A.; Tavazza, F.; Cohn, R.; Park, C. W.; Choudhary, A.; Agrawal, A.; Billinge, SJ L; Holm, E.; Ong, S. P.; Wolverton, C. Recent advances and applications of deep learning methods in materials science. *npj Computational Materials 2022 8:1*. **2022**, *8* (1), 1−26.
(156) Veličković, P.; Casanova, A.; Liò, P.; Cucurull, G.; Romero, A.; Bengio, Y. Graph Attention Networks. *arXiv*, October 30, 2017, 1710.10903 (accessed 2023-04-22). DOI: 10.48550/arxiv.1710.10903.
(157) Schlichtkrull, M.; Kipf, T. N.; Bloem, P.; van den Berg, R.; Titov, I.; Welling, M. Modeling Relational Data with Graph Convolutional Networks. In *Lecture Notes in Computer Science (including subseries Lecture Notes in Artificial Intelligence and Lecture Notes in Bioinformatics)*; Springer: 2017; Vol. *10843*, pp 593−607. DOI: 10.48550/arxiv.1703.06103.
(158) Xu, K.; Jegelka, S.; Hu, W.; Leskovec, J. How Powerful are Graph Neural Networks?. *arXiv*, October 1, 2018, 1810.00826 (accessed 2023-01-20). DOI: 10.48550/arxiv.1810.00826.
(159) Chen, Z.; Bruna, J.; Li, L. Supervised Community Detection with Line Graph Neural Networks. *arXiv*, May 23, 2017, 1705.08415 (accessed 2023-03-15). DOI: 10.48550/arxiv.1705.08415.
(160) Tsubaki, M.; Tomii, K.; Sese, J. Compound−protein interaction prediction with end-to-end learning of neural networks for graphs and sequences. *Bioinformatics.* **2019**, *35* (2), 309−318.
(161) Li, S.; Wan, F.; Shu, H.; Jiang, T.; Zhao, D.; Zeng, J. MONN: A Multi-objective Neural Network for Predicting Compound-Protein Interactions and Affinities. *Cell Syst.* **2020**, *10* (4), 308−322.
(162) Chorowski, J. K.; Bahdanau, D.; Serdyuk, D.; Cho, K.; Bengio, Y. Attention-Based Models for Speech Recognition. *arXiv*, June 24, 2015, 1506.07503 (accessed 2023-03-21).
(163) Vaswani, A.; Shazeer, N.; Parmar, N.; Uszkoreit, J.; Jones, L.; Gomez, A. N.; Kaiser, Ł.; Polosukhin, I. Attention Is All You Need. In *NIPS'17: Proceedings of the 31st International Conference on Neural Information Processing Systems*; NIPS: 2017; pp 5999−6009. https://arxiv.org/abs/1706.03762v5 (accessed 2023-04-09).
(164) Cordonnier, J. B.; Loukas, A.; Jaggi, M. Multi-Head Attention: Collaborate Instead of Concatenate. *arXiv*, June 29, 2020, 2006.16362, ver. 2.https://arxiv.org/abs/2006.16362v2 (accessed 2023-04-09).
(165) Carrington, A. M.; Manuel, D. G.; Fieguth, P. W.; Ramsay, T.; Osmani, V.; Wernly, B.; Bennett, C.; Hawken, S.; Magwood, O.; Sheikh, Y.; Mcinnes, M.; Holzinger, A. Deep ROC Analysis and AUC as Balanced Average Accuracy, for Improved Classifier Selection, Audit and Explanation. *IEEE Trans Pattern Anal Mach Intell.* **2023**, *45* (1), 329−341.
(166) Boyd, K.; Eng, K. H.; Page, C. D. Area under the precision-recall curve: Point estimates and confidence intervals. In *Lecture Notes in Computer Science (including subseries Lecture Notes in Artificial Intelligence and Lecture Notes in Bioinformatics)*; Springer: 2013; Vol. *8190* (3), pp 451−466.
(167) Wang, Y.; Wang, J.; Cao, Z.; BaratiFarimani, A. Molecular contrastive learning of representations via graph neural networks. *Nature Machine Intelligence.* **2022**, *4* (3), 279−287.
(168) Betzalel, E.; Penso, C.; Navon, A.; Fetaya, E. A Study on the Evaluation of Generative Models. *arXiv*, June 22, 2022, 2206.10935, ver. 1. https://arxiv.org/abs/2206.10935v1 (accessed 2023-04-10).
(169) Qin, Y.; Yuan, W.; Neubig, G.; Liu, P. T5Score: Discriminative Fine-tuning of Generative Evaluation Metrics. *arXiv*, December 12, 2022, 2212.05726, ver. 1. https://arxiv.org/abs/2212.05726v1 (accessed 2023-04-10).
(170) Chen, N.; Klushyn, A.; Kurle, R.; Jiang, X.; Bayer, J.; van der Smagt, P. Metrics for Deep Generative Models. In *International Conference on Artificial Intelligence and Statistics, AISTATS 2018*; MLR Press: 2018; pp 1540−1550. First published online November 3, 2017, 1711.01204. https://arxiv.org/abs/1711.01204v2 (accessed 2023-04-10).
(171) Simonyan, K.; Vedaldi, A.; Zisserman, A. Deep Inside Convolutional Networks: Visualising Image Classification Models and Saliency Maps. In *2nd International Conference on Learning Representations, ICLR 2014 - Workshop Track Proceedings*; *arXiv*, December 20, 2013, 1312.6034. https://arxiv.org/abs/1312.6034v2 (accessed 2023-04-10).
(172) Thakur, A.; Chakraborty, S. A deep learning based surrogate model for stochastic simulators. *Probabilistic Engineering Mechanics.* **2022**, *68*, 103248.
(173) Ribeiro, M. T.; Singh, S.; Guestrin, C. "Why Should I Trust You?": Explaining the Predictions of Any Classifier. In *NAACL-HLT 2016 - 2016 Conference of the North American Chapter of the Association for Computational Linguistics: Human Language Technologies, Proceedings of the Demonstrations Session*; Association for Computational Linguistics: 2016; pp 97−101; published online February 16, 2016.
(174) Montavon, G.; Binder, A.; Lapuschkin, S.; Samek, W.; Müller, K. R. Layer-Wise Relevance Propagation: An Overview. In *Lecture Notes in Computer Science (including subseries Lecture Notes in Artificial Intelligence and Lecture Notes in Bioinformatics)*; LNCS: 2019; Vol. *11700*, pp 193−209. DOI: 10.1007/978-3-030-28954-6_10/COVER.
(175) Szegedy, C.; Zaremba, W.; Sutskever, I.; Bruna, J.; Erhan, D.; Goodfellow, I.; Fergus, R. Intriguing properties of neural networks. In *2nd International Conference on Learning Representations, ICLR 2014 - Conference Track Proceedings*. *arXiv*, February 19, 2014, 1312.6199, ver. 4. https://arxiv.org/abs/1312.6199.
(176) *Interpretable Machine Learning*. https://christophm.github.io/interpretable-ml-book/ (accessed 2023-04-11).
(177) Lundberg, S. M.; Lee, S. I. A Unified Approach to Interpreting Model Predictions. In *31st Conference on Neural Information Processing Systems (NIPS 2017)*; 2017; pp 4766−4775. *arXiv*, November 25, 2017, 1705.07874 https://arxiv.org/abs/1705.07874v2 (accessed 2023-04-11).
(178) Vilone, G.; Longo, L. Explainable Artificial Intelligence: a Systematic Review. *arXiv*, October 12, 2020, 2006.00093, ver. 4. https://arxiv.org/abs/2006.00093v4 (accessed 2023-04-11).
(179) Liu, Q.; Xie, L. TranSynergy: Mechanism-driven interpretable deep neural network for the synergistic prediction and pathway deconvolution of drug combinations. *PLoSComput. Biol.* **2021**, *17* (2), No. e1008653.
(180) Askr, H.; Elgeldawi, E.; Aboul Ella, H.; Elshaier, Y. A. M. M.; Gomaa, M. M.; Hassanien, A. E. Deep learning in drug discovery: an integrative review and future challenges. *Artif. Intell. Rev.* **2023**, *56* (7), 5975−6037.
(181) Dollar, O.; Joshi, N.; Beck, DA C; Pfaendtner, J. Attention-based generative models for de novo molecular design. *Chem. Sci.* **2021**, *12* (24), 8362−8372.

https://doi.org/10.1021/acs.chemrestox.2c00375
Chem. Res. Toxicol. XXXX, XXX, XXX−XXX

(182) Singh, G.; Shawe-Taylor, J. Faster Convergence & Generalization in DNNs. *arXiv*, October 10, 2018, 1807.11414. ver. 3. https://arxiv.org/abs/1807.11414v3 (accessed 2023-04-02).
(183) Guan, S.; Loew, M. Analysis of Generalizability of Deep Neural Networks Based on the Complexity of Decision Boundary. In *Proceedings - 19th IEEE International Conference on Machine Learning and Applications, ICMLA 2020*. IEEE: 2020; pp 101−106.
(184) Tandon, A.; Howard, B.; Ramaiahgari, S.; Maharana, A.; Ferguson, S.; Shah, R.; Merrick, B. A. Deep Learning Image Analysis of High-Throughput Toxicology Assay Images. *SLAS Discovery* **2022**, *27* (1), 29−38.
(185) Kazius, J.; McGuire, R.; Bursi, R. Derivation and validation of toxicophores for mutagenicity prediction. *J. Med. Chem.* **2005**, *48* (1), 312−320.
(186) Schmidhuber, J. Deep Learning in Neural Networks: An Overview. *Neural Networks.* **2015**, *61*, 85−117.
(187) Huesmann, K.; Klemm, S.; Linsen, L.; Risse, B. Exploiting the Full Capacity of Deep Neural Networks while Avoiding Overfitting by Targeted Sparsity Regularization. *arXiv*, February 21, 2020, 2002.09237. https://arxiv.org/abs/2002.09237v1 (accessed 2023-04-02).
(188) Yang, Z.; Yu, Y.; You, C.; Steinhardt, J.; Ma, Y. Rethinking Bias-Variance Trade-off for Generalization of Neural Networks. In *Proceedings of the 37th International Conference on Machine Learning*; MLR Press: November 21, 2020; pp 10767−10777. https://proceedings.mlr.press/v119/yang20j.html (accessed 2023-04-02).
(189) Geman, S.; Bienenstock, E.; Doursat, R. Neural Networks and the Bias/Variance Dilemma. *Neural Comput.* **1992**, *4* (1), 1−58.
(190) Strigl, D.; Kofler, K.; Podlipnig, S. Performance and scalability of GPU-based convolutional neural networks. In *Proceedings of the 18th Euromicro Conference on Parallel, Distributed and Network-Based Processing, PDP 2010*; 2010; pp 317−324.
(191) Keuper, J.; Preundt, F. J. Distributed Training of Deep Neural Networks: Theoretical and Practical Limits of Parallel Scalability. *2016 2nd Workshop on Machine Learning in HPC Environments (MLHPC)*; IEEE: 2017; pp19−26.
(192) Zhang, Y.; Tino, P.; Leonardis, A.; Tang, K. A Survey on Neural Network Interpretability. *IEEE Trans Emerg Top ComputIntell.* **2021**, *5* (5), 726−742.
(193) Tang, H.; Ma, G.; Chen, Y.; Guo, L.; Wang, W.; Zeng, B.; Zhan, L. Adversarial Attack on Hierarchical Graph Pooling Neural Networks. *arXiv*, May 23, 2020, 2005.11560. https://arxiv.org/abs/2005.11560v1 (accessed 2023-04-02).
(194) Philipp, G.; Song, D.; Carbonell, J. G. The exploding gradient problem demystified - definition, prevalence, impact, origin, tradeoffs, and solutions. *arXiv*, December 15, 2017, 1712.05577. https://arxiv.org/abs/1712.05577v4 (accessed 2023-04-02).
(195) Rehmer, A.; Kroll, A. On the vanishing and exploding gradient problem in Gated Recurrent Units. *IFAC-PapersOnLine.* **2020**, *53* (2), 1243−1248.
(196) Hu, Z.; Zhang, J.; Ge, Y. Handling Vanishing Gradient Problem Using Artificial Derivative. *IEEE Access.* **2021**, *9*, 22371−22377.
(197) Hochreiter, S. The Vanishing Gradient Problem During Learning Recurrent Neural Nets and Problem Solutions. *Int. J. Unc. Fuzz. Knowl. Based Syst.* **1998**, *6* (2), 107−116.
(198) Xu, Y.; Zhang, H. Convergence of Deep Convolutional Neural Networks. *Neural Networks.* **2022**, *153*, 553−563.
(199) *A Gentle Introduction to Premature Convergence - MachineLearningMastery.com*. https://machinelearningmastery.com/premature-convergence/ (accessed 2023-04-02).
(200) Nadimi-Shahraki, M. H.; Taghian, S.; Mirjalili, S.; Ewees, A. A.; Abualigah, L.; Abd Elaziz, M. MTV-MFO: Multi-Trial Vector-Based Moth-Flame Optimization Algorithm. *Symmetry* **2021**, *13* (12), 2388.
(201) Idakwo, G.; Thangapandian, S.; Luttrell, J.; Zhou, Z.; Zhang, C.; Gong, P. Deep Learning-Based Structure-Activity Relationship Modeling for Multi-Category Toxicity Classification: A Case Study of 10K Tox21 Chemicals With High-Throughput Cell-Based Androgen Receptor Bioassay Data. *Front Physiol.* **2019**, *10*, 1044.
(202) Li, T.; Tong, W.; Roberts, R.; Liu, Z.; Thakkar, S. DeepDILI: Deep Learning-Powered Drug-Induced Liver Injury Prediction Using Model-Level Representation. *Chem. Res. Toxicol.* **2021**, *34* (2), 550−565.
(203) Li, T.; Tong, W.; Roberts, R.; Liu, Z.; Thakkar, S. DeepCarc: Deep Learning-Powered Carcinogenicity Prediction Using Model-Level Representation. *Front Artif. Intell.* **2021**, *4*, 176.
(204) Hughes, T. B.; Miller, G. P.; Swamidass, S. J. Modeling Epoxidation of Drug-like Molecules with a Deep Machine Learning Network. *ACS Cent Sci.* **2015**, *1* (4), 168−180.
(205) Hirohara, M.; Saito, Y.; Koda, Y.; Sato, K.; Sakakibara, Y. Convolutional neural network based on SMILES representation of compounds for detecting chemical motif. *BMC Bioinformatics.* **2018**, *19* (19), 83−94.
(206) Yuan, Q.; Wei, Z.; Guan, X.; Jiang, M.; Wang, S.; Zhang, S.; Li, Z. Toxicity Prediction Method Based on Multi-Channel Convolutional Neural Network. *Molecules* **2019**, *24* (18), 3383.
(207) Mriganka, N.; Subhasish, G. Toxicity Detection in Drug Candidates using Simplified Molecular-Input Line-Entry System. *Int. J. Comput. Appl.* **2020**, *175* (21), 1−4.
(208) Zheng, S.; Rao, J.; Zhang, J.; Li, C.; Yang, Y. Cross-modal Graph Contrastive Learning with Cellular Images. *bioRxiv*, 2022.06.05.494905, September 25, 2022 (accessed 2023-03-21).
(209) Fang, Y.; Zhang, Q.; Zhang, N.; Chen, Z.; Zhuang, X.; Shao, X.; Fan, X.; Chen, H. Knowledge graph-enhanced molecular contrastive learning with functional prompt. *Nature Machine Intelligence* **2023**, *5* (5), 542−553.
(210) Sanchez-Fernandez, A.; Rumetshofer, E.; Hochreiter, S.; Klambauer, G. Contrastive learning of image- and structure-based representations in drug discovery. In *ICLR2022 Machine Learning for Drug Discovery*; published online May 24, 2022 https://openreview.net/forum?id=OdXKRtg1OG.
(211) Sun, M.; Wang, H.; Zhou, J.; Xing, J.; Chen, B.; Zhou, J. MoCL: Data-driven Molecular Fingerprint via Knowledge-aware Contrastive Learning from Molecular Graph. In *KDD '21: Proceedings of the 27th ACM SIGKDD Conference on Knowledge Discovery & Data Mining*; 2021; Vol. *10*, pp 3585−3594. .
(212) Li, S.; Zhou, J.; Xu, T.; Dou, D.; Xiong, H. GeomGCL: Geometric Graph Contrastive Learning for Molecular Property Prediction. *Proceedings of the AAAI Conference on Artificial Intelligence.* **2022**, *36* (4), 4541−4549.
(213) Zang, X.; Zhao, X.; Tang, B. Hierarchical Molecular Graph Self-Supervised Learning for property prediction. *Communications Chemistry 2023 6:1.* **2023**, *6* (1), 1−10.
(214) Duvenaud, D.; Maclaurin, D.; Aguilera-Iparraguirre, J.; Gómez-Bombarelli, R.; Hirzel, T.; Aspuru-Guzik, A.; Adams, R. P. Convolutional Networks on Graphs for Learning Molecular Fingerprints. In *Adv. Neural Inf Process Syst*; 2015; pp 2224−2232. *arXiv*, 1509.09292. https://arxiv.org/abs/1509.09292v2 (accessed 2023-04-03).
(215) Sun, M.; Zhao, S.; Gilvary, C.; Elemento, O.; Zhou, J.; Wang, F. Graph convolutional networks for computational drug development and discovery. *Brief Bioinform.* **2020**, *21* (3), 919−935.
(216) Zhang, Z.; Liu, Q.; Wang, H.; Lu, C.; Lee, C. K. Motif-based Graph Self-Supervised Learning for Molecular Property Prediction. In *Adv. Neural Inf Process Syst.*; 2021; Vol. *34*, pp 15870−15882. https://github.com/zaixizhang/MGSSL (accessed 2023-04-12).
(217) Yang, K.; Swanson, K.; Jin, W.; Coley, C.; Eiden, P.; Gao, H.; Guzman-Perez, A.; Hopper, T.; Kelley, B.; Mathea, M.; Palmer, A.; Settels, V.; Jaakkola, T.; Jensen, K.; Barzilay, R. Analyzing Learned Molecular Representations for Property Prediction. *J. Chem. Inf. Model.* **2019**, *59* (8), 3370−3388.
(218) Chen, J.; Si, Y. W.; Un, C. W.; Siu, S. W. I. Chemical toxicity prediction based on semi-supervised learning and graph convolutional neural network. *J. Cheminform.* **2021**, *13* (1), 93.
(219) Kearnes, S.; McCloskey, K.; Berndl, M.; Pande, V.; Riley, P. Molecular graph convolutions: moving beyond fingerprints. *J. Comput. Aided Mol. Des.* **2016**, *30* (8), 595−608.
(220) Liu, K.; Sun, X.; Jia, L.; Ma, J.; Xing, H.; Wu, J.; Gao, H.; Sun, Y.; Boulnois, F.; Fan, J. Chemi-net: a graph convolutional network for

accurate drug property prediction. *arXiv*, March 16, 2018, 1803.06236. https://arxiv.org/abs/1803.06236v2 (accessed 2023-04-03).
(221) Li, J.; Cai, D.; He, X. Learning Graph-Level Representation for Drug Discovery. *arXiv*, September 12, 2017, 1709.03741, ver. 2. https://arxiv.org/abs/1709.03741v2 (accessed 2023-04-03).
(222) Sakai, M.; Nagayasu, K.; Shibui, N.; Andoh, C.; Takayama, K.; Shirakawa, H.; Kaneko, S. Prediction of pharmacological activities from chemical structures with graph convolutional neural networks. *Scientific Reports 2021 11:1*. **2021**, *11* (1), 1−14.
(223) Jo, J.; Kwak, B.; Lee, B.; Yoon, S. Flexible Dual-Branched Message-Passing Neural Network for a Molecular Property Prediction. *ACS Omega* **2022**, *7* (5), 4234−4244.
(224) Liu, C.; Sun, Y.; Davis, R.; Cardona, S. T.; Hu, P. ABT-MPNN: an atom-bond transformer-based message-passing neural network for molecular property prediction. *J. Cheminform.* **2023**, *15* (1), 29.
(225) Chen, J.; Zheng, S.; Song, Y.; Rao, J.; Yang, Y. Learning Attributed Graph Representations with Communicative Message Passing Transformer. In *IJCAI International Joint Conference on Artificial Intelligence*; July 19, 2021; pp 2242−2248. DOI: 10.24963/ijcai.2021/309.
(226) Vracko, M. Kohonen Artificial Neural Network and Counter Propagation Neural Network in Molecular Structure-Toxicity Studies. *Current Computer Aided-Drug Design.* **2005**, *1* (1), 73−78.
(227) Rallo, R.; France, B.; Liu, R.; Nair, S.; George, S.; Damoiseaux, R.; Giralt, F.; Nel, A.; Bradley, K.; Cohen, Y. Self-organizing map analysis of toxicity-related cell signaling pathways for metal and metal oxide nanoparticles. *Environ. Sci. Technol.* **2011**, *45* (4), 1695−1702.
(228) Wang, Y.; Magar, R.; Liang, C.; BaratiFarimani, A. Improving Molecular Contrastive Learning via Faulty Negative Mitigation and Decomposed Fragment Contrast. *J. Chem. Inf Model.* **2022**, *62* (11), 2713−2725.
(229) Vall, A.; Hochreiter, S.; Klambauer, G. BioassayCLR: Prediction of biological activity for novel bioassays based on rich textual descriptions. ELLIS Machine Learning for Molecule Discovery Workshop, 2021.
(230) Xu, Y.; Dai, Z.; Chen, F.; Gao, S.; Pei, J.; Lai, L. Deep Learning for Drug-Induced Liver Injury. *J. Chem. Inf Model.* **2015**, *55* (10), 2085−2093.
(231) Atienzar, F. A.; Blomme, E. A.; Chen, M.; Hewitt, P.; Kenna, J. G.; Labbe, G.; Moulin, F.; Pognan, F.; Roth, A. B.; Suter-Dick, L.; Ukairo, O.; Weaver, R. J.; Will, Y.; Dambach, D. M. Key Challenges and Opportunities Associated with the Use of in Vitro Models to Detect Human Dili: Integrated Risk Assessment and Mitigation Plans. *Biomed Res. Int.* **2016**, *2016*, 9737920.
(232) Feng, C.; Chen, H.; Yuan, X.; Sun, M.; Chu, K.; Liu, H.; Rui, M. Gene Expression Data Based Deep Learning Model for Accurate Prediction of Drug-Induced Liver Injury in Advance. *J. Chem. Inf Model.* **2019**, *59* (7), 3240−3250.
(233) Nguyen-Vo, T. H.; Nguyen, L.; Do, N.; Le, P. H.; Nguyen, T. N.; Nguyen, B. P.; Le, L. Predicting Drug-Induced Liver Injury Using Convolutional Neural Network and Molecular Fingerprint-Embedded Features. *ACS Omega.* **2020**, *5* (39), 25432−25439.
(234) Li, T.; Tong, W.; Roberts, R.; Liu, Z.; Thakkar, S. Deep Learning on High-Throughput Transcriptomics to Predict Drug-Induced Liver Injury. *Front BioengBiotechnol.* **2020**, *8*, 1366.
(235) Kang, M. G.; Kang, N. S. Predictive Model for Drug-Induced Liver Injury Using Deep Neural Networks Based on Substructure Space. *Molecules 2021, Vol 26, Page 7548.* **2021**, *26* (24), 7548.
(236) Santiso, S.; Pérez, A.; Casillas, A. Exploring Joint AB-LSTM With Embedded Lemmas for Adverse Drug Reaction Discovery. *IEEE J. Biomed Health Inform.* **2019**, *23* (5), 2148−2155.
(237) Ma, H.; An, W.; Wang, Y.; Sun, H.; Huang, R.; Huang, J. Deep Graph Learning with Property Augmentation for Predicting Drug-Induced Liver Injury. *Chem. Res. Toxicol.* **2021**, *34* (2), 495−506.
(238) Irsoy, O, Cardie, C. Deep Recursive Neural Networks for Compositionality in Language. In *NIPS'14: Proceedings of the 27th International Conference on Neural Information Processing Systems*; 2014; Vol. 2, pp 2096−2104.
(239) Rozenberg, E.; Freedman, D. Semi-Equivariant Continuous Normalizing Flows for Target-Aware Molecule Generation. *arXiv*, November 9, 2022, 2211.04754. https://arxiv.org/abs/2211.04754v1 (accessed 2023-04-07).
(240) Corso, G.; Stärk, H.; Jing, B.; Barzilay, R.; Jaakkola, T. DiffDock: Diffusion Steps, Twists, and Turns for Molecular Docking. *arXiv*, October 4, 2022, 2210.0177. https://arxiv.org/abs/2210.01776v2 (accessed 2023-04-07).
(241) Wu, Y.; Liu, Z.; Wu, L.; Chen, M.; Tong, W. BERT-Based Natural Language Processing of Drug Labeling Documents: A Case Study for Classifying Drug-Induced Liver Injury Risk. *Front Artif. Intell.* **2021**, *4*, 190.
(242) Zhan, X.; Wang, F.; Gevaert, O. Filter Drug-induced Liver Injury Literature with Natural Language Processing and Ensemble Learning. *IEEE J. Biomed Health Inform.* **2022**, *26* (10), 5033−5041.
(243) Wan, X.; Wu, X.; Wang, D.; Tan, X.; Liu, X.; Fu, Z.; Jiang, H.; Zheng, M.; Li, X. An inductive graph neural network model for compound−protein interaction prediction based on a homogeneous graph. *Brief Bioinform.* **2022**, *23* (3), bbac073.
(244) Wen, M.; Zhang, Z.; Niu, S.; Sha, H.; Yang, R.; Yun, Y.; Lu, H. Deep-Learning-Based Drug-Target Interaction Prediction. *J. Proteome Res.* **2017**, *16* (4), 1401−1409.
(245) Mishra, S.; Gupta, P.; Ojha, S.; Sharma, V.; Anthony, V.; Sharma, D. Deep Learning Advancements in Target Delivery. *Deep Learning for Targeted Treatments.* **2022**, 101−125.
(246) Mishra, P. S.; Mishra, R.; Mazumder, R. Deep Learning on Site-Specific Drug Delivery System. *Deep Learning for Targeted Treatments.* **2022**, 77−100.
(247) Wang, Y.; Huang, L.; Jiang, S.; Wang, Y.; Zou, J.; Fu, H.; Yang, S. Capsule networks showed excellent performance in the classification of hERG blockers/nonblockers. *Front Pharmacol.* **2020**, *10*, 1631.
(248) Sabour, S.; Frosst, N.; Hinton, G. E.*Dynamic routing between capsules*. 31st Conference on Neural Information Processing Systems (NIPS 2017), Long Beach, CA, USA, 2017, https://proceedings.neurips.cc/paper_files/paper/2017/file/2cad8fa47bbef282badbb8de5374b894-Paper.pdf.
(249) Sajadi, S. Z.; ZareChahooki, M. A.; Tavakol, M.; Gharaghani, S. Matrix factorization with denoising autoencoders for prediction of drug-target interactions. *Mol. Divers.* **2023**, *27*, 1333.
(250) Liu, B.; Papadopoulos, D.; Malliaros, F. D.; Tsoumakas, G.; Papadopoulos, A. N. Multiple similarity drug-target interaction prediction with random walks and matrix factorization. *Brief Bioinform.* **2022**, *23* (5), bbac353.
(251) Wang, H.; Wang, J.; Dong, C.; Lian, Y.; Liu, D.; Yan, Z. A novel approach for drug-target interactions prediction based on multimodal deep autoencoder. *Front Pharmacol.* **2020**, *10*, 1592.
(252) Gligorijević, V.; Barot, M.; Bonneau, R. deepNF: deep network fusion for protein function prediction. *Bioinformatics.* **2018**, *34* (22), 3873−3881.
(253) Shayakhmetov, R.; Kuznetsov, M.; Zhebrak, A.; Kadurin, A.; Nikolenko, S.; Aliper, A.; Polykovskiy, D. Molecular Generation for Desired Transcriptome Changes With Adversarial Autoencoders. *Front Pharmacol.* **2020**, *11*, 269.
(254) Xuan, P.; Fan, M.; Cui, H.; Zhang, T.; Nakaguchi, T. GVDTI: Graph convolutional and variational autoencoders with attribute-level attention for drug-protein interaction prediction. *Brief Bioinform.* **2022**, *23* (1), bbab453.
(255) Sajadi, S. Z.; ZareChahooki, M. A.; Gharaghani, S.; Abbasi, K. AutoDTI++: deep unsupervised learning for DTI prediction by autoencoders. *BMC Bioinformatics* **2021**, *22* (1). DOI: 10.1186/s12859-021-04127-2.
(256) Li, Y.; Qiao, G.; Gao, X.; Wang, G. Supervised graph co-contrastive learning for drug−target interaction prediction. *Bioinformatics.* **2022**, *38* (10), 2847−2854.
(257) Zeng, Y.; Chen, X.; Luo, Y.; Li, X.; Peng, D. Deep drug-target binding affinity prediction with multiple attention blocks. *Brief Bioinform.* **2021**, *22* (5), bbab117.
(258) Liu, J.; Jiang, T.; Lu, Y.; Wu, H. Drug-Target Interaction Prediction Based on Transformer. *Lecture Notes in Computer Science*

(including subseries Lecture Notes in Artificial Intelligence and Lecture Notes in Bioinformatics). **2022**, 13394 LNCS, 302−309.
(259) Lim, S.; Lu, Y.; Cho, C. Y.; Sung, I.; Kim, J.; Kim, Y.; Park, S.; Kim, S. A review on compound-protein interaction prediction methods: Data, format, representation and model. *Comput. Struct Biotechnol J.* **2021**, *19*, 1541.
(260) Segler, M. H. S.; Kogej, T.; Tyrchan, C.; Waller, M. P. Generating Focused Molecule Libraries for Drug Discovery with Recurrent Neural Networks. *ACS Cent Sci.* **2018**, *4* (1), 120−131.
(261) Altae-Tran, H.; Ramsundar, B.; Pappu, A. S.; Pande, V. Low Data Drug Discovery with One-Shot Learning. *ACS Cent Sci.* **2017**, *3* (4), 283−293.
(262) Kadurin, A.; Aliper, A.; Kazennov, A.; Mamoshina, P.; Vanhaelen, Q.; Khrabrov, K.; Zhavoronkov, A. The cornucopia of meaningful leads: Applying deep adversarial autoencoders for new molecule development in oncology. *Oncotarget.* **2017**, *8* (7), 10883.
(263) Kadurin, A.; Nikolenko, S.; Khrabrov, K.; Aliper, A.; Zhavoronkov, A. druGAN: An Advanced Generative Adversarial Autoencoder Model for de Novo Generation of New Molecules with Desired Molecular Properties in Silico. *Mol. Pharmaceutics* **2017**, *14* (9), 3098−3104.
(264) Kim, Y.; Jung, Y. S.; Park, J. H.; Kim, S. J.; Cho, Y. R. Drug-Disease Association Prediction Using Heterogeneous Networks for Computational Drug Repositioning. *Biomolecules.* **2022**, *12* (10), 1497.
(265) Zhang, F.; Hu, W.; Liu, Y. GCMM: graph convolution network based on multimodal attention mechanism for drug repurposing. *BMC Bioinformatics.* **2022**, *23* (1). DOI: 10.1186/s12859-022-04911-8.
(266) Xuan, P.; Gao, L.; Sheng, N.; Zhang, T.; Nakaguchi, T. Graph Convolutional Autoencoder and Fully-Connected Autoencoder with Attention Mechanism Based Method for Predicting Drug-Disease Associations. *IEEE J. Biomed Health Inform.* **2021**, *25* (5), 1793−1804.
(267) Gao, L.; Cui, H.; Zhang, T.; Sheng, N.; Xuan, P. Prediction of drug-disease associations by integrating common topologies of heterogeneous networks and specific topologies of subnets. *Brief Bioinform* **2022**, *23* (1), bbab467.
(268) Kuznetsov, M.; Polykovskiy, D. MolGrow: A Graph Normalizing Flow for Hierarchical Molecular Generation. *Proceedings of the AAAI Conference on Artificial Intelligence.* **2021**, *35* (9), 8226−8234.
(269) Hoogeboom, E.; Satorras, V. G.; Vignac, C.; Welling, M. Equivariant Diffusion for Molecule Generation in 3D. In *Proceedings of the 39th International Conference on Machine Learning*; June 28, 2022; pp 8867−8887. https://proceedings.mlr.press/v162/hoogeboom22a.html (accessed 2023-04-07).
(270) Morehead, A.; Cheng, J. Geometry-Complete Diffusion for 3D Molecule Generation. *arXiv*, February 8, 2023, 2302.04313.http://arxiv.org/abs/2302.04313 (accessed 2023-04-12).
(271) Huang, L.; Xu, T.; Yu, Y.; Zhao, P.; Wong, K. C.; Zhang, H. A dual diffusion model enables 3D binding bioactive molecule generation and lead optimization given target pockets. *bioRxiv*, January 30, 2023, 2023.01.28.526011 (accessed 2023-04-28).
(272) Lee, H.; Ahn, S.; Seo, S. W.; Song, Y. Y.; Yang, E.; Hwang, S. J.; Shin, J. RetCL: A Selection-based Approach for Retrosynthesis via Contrastive Learning. In *IJCAI International Joint Conference on Artificial Intelligence*; 2021; pp 2673−2679.
(273) Srivastava, A.; Hanig, J. P. Quantitative neurotoxicology: Potential role of artificial intelligence/deep learning approach. *Journal of Applied Toxicology.* **2021**, *41* (7), 996−1006.
(274) Wang, S.; Lin, B.; Lin, G.; Lin, R.; Huang, F.; Liu, W.; Wang, X.; Liu, X.; Zhang, Y.; Wang, F.; Lin, Y.; Chen, L.; Chen, J. Automated label-free detection of injured neuron with deep learning by two-photon microscopy. *J. Biophotonics* **2020**, *13* (1), No. e201960062.
(275) Weaver, R. J.; Valentin, J. P. Today's Challenges to De-Risk and Predict Drug Safety in Human "Mind-the-Gap. *Toxicol. Sci.* **2019**, *167* (2), 307−321.
(276) Brown, G. E.; Khetani, S. R. Microfabrication of liver and heart tissues for drug development. *Philosophical Transactions of the Royal Society B: Biological Sciences* **2018**, *373* (1750), 20170225.
(277) Maddah, M.; Mandegar, M. A.; Dame, K.; Grafton, F.; Loewke, K.; Ribeiro, A. J. S. Quantifying drug-induced structural toxicity in hepatocytes and cardiomyocytes derived from hiPSCs using a deep learning method. *J. PharmacolToxicol Methods.* **2020**, *105*, 106895.
(278) Sinha, K.; Das, J.; Pal, P. B.; Sil, P. C. Oxidative stress: The mitochondria-dependent and mitochondria-independent pathways of apoptosis. *Arch. Toxicol.* **2013**, *87* (7), 1157−1180.
(279) Orrenius, S.; Nicotera, P.; Zhivotovsky, B. Cell death mechanisms and their implications in toxicology. *Toxicol. Sci.* **2011**, *119* (1), 3−19.
(280) Kerr, J. F. R.; Wyllie, A. H.; Currie, A. R. Apoptosis: a basic biological phenomenon with wide-ranging implications in tissue kinetics. *Br J. Cancer.* **1972**, *26* (4), 239−257.
(281) Trump, B. F.; Berezesky, I. K.; Chang, S. H.; Phelps, P. C. The pathways of cell death: oncosis, apoptosis, and necrosis. *ToxicolPathol.* **1997**, *25* (1), 82−88.
(282) Jimenez-Carretero, D.; Abrishami, V.; Fernández-de-Manuel, L.; Palacios, I.; Quílez-Álvarez, A.; Díez-Sánchez, A.; del Pozo, M. A.; Montoya, M. C. Tox_(R)CNN: Deep learning-based nuclei profiling tool for drug toxicity screening. *PLoSComput. Biol.* **2018**, *14* (11), No. e1006238.
(283) Torng, W.; Altman, R. B. 3D deep convolutional neural networks for amino acid environment similarity analysis. *BMC Bioinformatics.* **2017**, *18* (1), 302.
(284) Flynn, N. R.; Ward, M. D.; Schleiff, M. A.; Laurin, C. M. C.; Farmer, R.; Conway, S. J.; Boysen, G.; Swamidass, S. J.; Miller, G. P. Bioactivation of Isoxazole-Containing Bromodomain and Extra-Terminal Domain (BET) Inhibitors. *Metabolites 2021, Vol 11, Page 390.* **2021**, *11* (6), 390.
(285) Schleiff, M. A.; Payakachat, S.; Schleiff, B. M.; Swamidass, S. J.; Boysen, G.; Miller, G. P. Impacts of diphenylamine NSAID halogenation on bioactivation risks. *Toxicology.* **2021**, *458*, 152832.
(286) Sharma, M.; Sharma, N.; Muddassir, M.; Rahman, Q. I.; Dwivedi, U. N.; Akhtar, S. Structure-based pharmacophore modeling, virtual screening and simulation studies for the identification of potent anticancerous phytochemical lead targeting cyclin-dependent kinase 2. *https://doi.org/101080/07391102202119361778* **2022**, *40*, 9815.
(287) Cui, S.; Yu, Y.; Zhan, T.; Zhang, C.; Zhuang, S. 2,6-Di-tert-butylphenol and its quinone metabolite trigger aberrant transcriptional responses in C57BL/6 mice liver. *Science of The Total Environment.* **2021**, *778*, 146322.
(288) Hughes, T. B.; Swamidass, S. J. Deep Learning to Predict the Formation of Quinone Species in Drug Metabolism. *Chem. Res. Toxicol.* **2017**, *30* (2), 642−656.
(289) Howard, J.; Gugger, S. Fastai: A Layered API for Deep Learning. *Information 2020, Vol 11, Page 108.* **2020**, *11* (2), 108.
(290) Deng, J.; Dong, W.; Socher, R.; Li, L. J.; Kai, L.; Li, F.-F. ImageNet: A large-scale hierarchical image database. In *2009 IEEE Conference on Computer Vision and Pattern Recognition*: IEEE: 2010; pp 248−255. .
(291) He, K.; Zhang, X.; Ren, S.; Sun, J. Deep Residual Learning for Image Recognition. In *Proceedings of the IEEE Computer Society Conference on Computer Vision and Pattern Recognition*; IEEE: 2016; pp 770−778.
(292) Jung, H.; Oh, Y. Towards Better Explanations of Class Activation Mapping. In *Proceedings of the IEEE International Conference on Computer Vision*; IEEE: 2021: pp 1316−1324
(293) Saxena, A.; Dhyani, V.; Jana, S.; Giri, L. Application of kohonen-self organizing map to cluster drug induced ca2+ response in hippocampal neurons at different drug dose. In *26th National Conference on Communications, NCC 2020*; 2020; DOI: 10.1109/NCC48643.2020.9056031.
(294) Fürst, A.; Rumetshofer, E.; Lehner, J.; Tran, V.; Tang, F.; Ramsauer, H.; Kreil, D.; Kopp, M.; Klambauer, G.; Bitto-Nemling, A.; Hochreiter, S. CLOOB: Modern Hopfield Networks with InfoLOOB Outperform CLIP. *arXiv*, October 21, 2021, 2110.11316. https://arxiv.org/abs/2110.11316v4 (accessed 2023-04-03).
(295) Radford, A.; Kim, J. W.; Hallacy, C.; Ramesh, A.; Goh, G.; Agarwal, S.; Sastry, G.; Askell, A.; Mishkin, P.; Clark, J.; Krueger, G.; Sutskever, I. Learning Transferable Visual Models From Natural Language Supervision. In *Proceedings of the 38th International*

Conference on Machine Learning; MLR Press: 2021; pp 8748−8763.https://proceedings.mlr.press/v139/radford21a.html (accessed April 3, 2023).
(296) Sosnin, S.; Vashurina, M.; Withnall, M.; Karpov, P.; Fedorov, M.; Tetko, I. V. A Survey of Multi-task Learning Methods in Chemoinformatics. *Mol. Inform.* **2019**, *38* (4), 1800108.
(297) Sosnin, S.; Karlov, D.; Tetko, I. V.; Fedorov, M. V. Comparative Study of Multitask Toxicity Modeling on a Broad Chemical Space. *J. Chem. Inf Model.* **2019**, *59* (3), 1062−1072.
(298) Sharma, B.; Chenthamarakshan, V.; Dhurandhar, A.; Pereira, S.; Hendler, J. A.; Dordick, J. S.; Das, P. Accurate clinical toxicity prediction using multi-task deep neural nets and contrastive molecular explanations. *Scientific Reports.* **2023**, *13* (1), 1−16.
(299) Fu, T.; Huang, K.; Xiao, C.; Glass, L. M.; Sun, J. HINT: Hierarchical interaction network for clinical-trial-outcome predictions. *Patterns.* **2022**, *3* (4), 100445.
(300) Kim, S.; Thiessen, P. A.; Bolton, E. E.; Chen, J.; Fu, G.; Gindulyte, A.; Han, L.; He, J.; He, S.; Shoemaker, B. A.; Wang, J.; Yu, B.; Zhang, J.; Bryant, S. H. PubChem Substance and Compound databases. *Nucleic Acids Res.* **2016**, *44* (D1), D1202−D1213.
(301) Wang, Y.; Suzek, T.; Zhang, J.; Wang, J.; He, S.; Cheng, T.; Shoemaker, B. A.; Gindulyte, A.; Bryant, S. H. PubChem BioAssay: 2014 update. *Nucleic Acids Res.* **2014**, *42* (D1), D1075−D1082.
(302) Wang, Y.; Xiao, J.; Suzek, T. O.; Zhang, J.; Wang, J.; Zhou, Z.; Han, L.; Karapetyan, K.; Dracheva, S.; Shoemaker, B. A.; Bolton, E.; Gindulyte, A.; Bryant, S. H. PubChem's BioAssay Database. *Nucleic Acids Res.* **2012**, *40* (D1), D400−D412.
(303) Kim, S.; Chen, J.; Cheng, T.; Gindulyte, A.; He, J.; He, S.; Li, Q.; Shoemaker, B. A.; Thiessen, P. A.; Yu, B.; Zaslavsky, L.; Zhang, J.; Bolton, E. E. PubChem in 2021: new data content and improved web interfaces. *Nucleic Acids Res.* **2021**, *49* (D1), D1388−D1395.
(304) *PubChem*. https://pubchem.ncbi.nlm.nih.gov/ (accessed 2022-11-12).
(305) *ChEMBL Database*. https://www.ebi.ac.uk/chembl/ (accessed 2022-11-12).
(306) Mendez, D.; Gaulton, A.; Bento, A. P.; Chambers, J.; De Veij, M.; Félix, E.; Magariños, M. P.; Mosquera, J. F.; Mutowo, P.; Nowotka, M.; Gordillo-Marañón, M.; Hunter, F.; Junco, L.; Mugumbate, G.; Rodriguez-Lopez, M.; Atkinson, F.; Bosc, N.; Radoux, C. J.; Segura-Cabrera, A.; Hersey, A.; Leach, A. R. ChEMBL: Towards direct deposition of bioassay data. *Nucleic Acids Res.* **2019**, *47* (D1), D930−D940.
(307) Gaulton, A.; Bellis, L. J.; Bento, A. P.; Chambers, J.; Davies, M.; Hersey, A.; Light, Y.; McGlinchey, S.; Michalovich, D.; Al-Lazikani, B.; Overington, J. P. ChEMBL: a large-scale bioactivity database for drug discovery. *Nucleic Acids Res.* **2012**, *40* (D1), D1100−D1107.
(308) Bento, A. P.; Gaulton, A.; Hersey, A.; Bellis, L. J.; Chambers, J.; Davies, M.; Krüger, F. A.; Light, Y.; Mak, L.; McGlinchey, S.; Nowotka, M.; Papadatos, G.; Santos, R.; Overington, J. P. The ChEMBL bioactivity database: an update. *Nucleic Acids Res.* **2014**, *42* (D1), D1083−D1090.
(309) Gaulton, A.; Hersey, A.; Nowotka, M. L.; Bento, A. P.; Chambers, J.; Mendez, D.; Mutowo, P.; Atkinson, F.; Bellis, L. J.; Cibrian-Uhalte, E.; Davies, M.; Dedman, N.; Karlsson, A.; Magarinos, M. P.; Overington, J. P.; Papadatos, G.; Smit, I.; Leach, A. R. The ChEMBL database in 2017. *Nucleic Acids Res.* **2017**, *45* (D1), D945−D954.
(310) Waters, M.; Stasiewicz, S.; Alex Merrick, B.; Tomer, K.; Bushel, P.; Paules, R.; Stegman, N.; Nehls, G.; Yost, K. J.; Johnson, C. H.; Gustafson, S. F.; Xirasagar, S.; Xiao, N.; Huang, C. C.; Boyer, P.; Chan, D. D.; Pan, Q.; Gong, H.; Taylor, J.; Choi, D.; Rashid, A.; Ahmed, A.; Howle, R.; Selkirk, J.; Tennant, R.; Fostel, J. CEBS—Chemical Effects in Biological Systems: a public data repository integrating study design and toxicity data with microarray and proteomics data. *Nucleic Acids Res.* **2007**, *36*, D892−D900.
(311) *Chemical Effects in Biological Systems*. https://cebs.niehs.nih.gov/cebs/ (accessed 2022-11-12).
(312) Davis, A. P.; Wiegers, T. C.; Johnson, R. J.; Sciaky, D.; Wiegers, J.; Mattingly, C. J. Comparative Toxicogenomics Database (CTD): update 2023. *Nucleic Acids Res.* **2023**, *51*, D1257.
(313) Davis, A. P.; Grondin, C. J.; Johnson, R. J.; Sciaky, D.; King, B. L.; McMorran, R.; Wiegers, J.; Wiegers, T. C.; Mattingly, C. J. The Comparative Toxicogenomics Database: update 2017. *Nucleic Acids Res.* **2017**, *45* (D1), D972−D978.
(314) *The Comparative Toxicogenomics Database | CTD*. http://ctdbase.org/ (accessed 2022-11-12).
(315) Mattingly, C. J.; Rosenstein, M. C.; Davis, A. P.; Colby, G. T.; Forrest, J. N.; Boyer, J. L. The Comparative Toxicogenomics Database (CTD): A Cross-Species Resource for Building Chemical-Gene Interaction Networks. *Toxicol. Sci.* **2006**, *92* (2), 587.
(316) Lim, E.; Pon, A.; Djoumbou, Y.; Knox, C.; Shrivastava, S.; Guo, A. C.; Neveu, V.; Wishart, D. S. T3DB: a comprehensively annotated database of common toxins and their targets. *Nucleic Acids Res.* **2010**, *38*, D781.
(317) *T3DB*. http://www.t3db.ca/ (accessed 2022-11-12).
(318) Wishart, D.; Arndt, D.; Pon, A.; Sajed, T.; Guo, A. C.; Djoumbou, Y.; Knox, C.; Wilson, M.; Liang, Y.; Grant, J.; Liu, Y.; Goldansaz, S. A.; Rappaport, S. M. T3DB: the toxic exposome database. *Nucleic Acids Res.* **2015**, *43* (D1), D928−D934.
(319) Wishart, D. S.; Knox, C.; Guo, A. C.; Cheng, D.; Shrivastava, S.; Tzur, D.; Gautam, B.; Hassanali, M. DrugBank: a knowledgebase for drugs, drug actions and drug targets. *Nucleic Acids Res.* **2008**, *36*, D901.
(320) Wishart, D. S.; Feunang, Y. D.; Guo, A. C.; Lo, E. J.; Marcu, A.; Grant, J. R.; Sajed, T.; Johnson, D.; Li, C.; Sayeeda, Z.; Assempour, N.; Iynkkaran, I.; Liu, Y.; MacIejewski, A.; Gale, N.; Wilson, A.; Chin, L.; Cummings, R.; Le, Di; Pon, A.; Knox, C.; Wilson, M. DrugBank 5.0: a major update to the DrugBank database for 2018. *Nucleic Acids Res.* **2018**, *46* (D1), D1074−D1082.
(321) Sterling, T.; Irwin, J. J. ZINC 15 - Ligand Discovery for Everyone. *J. Chem. Inf. Model.* **2015**, *55* (11), 2324−2337.
(322) Igarashi, Y.; Nakatsu, N.; Yamashita, T.; Ono, A.; Ohno, Y.; Urushidani, T.; Yamada, H. Open TG-GATEs: a large-scale toxicogenomics database. *Nucleic Acids Res.* **2015**, *43*, D921−D927.
(323) *MDDR - MDL Drug Data Report*. http://www.akosgmbh.de/accelrys/databases/mddr.htm (accessed 2022-11-27).
(324) Azam, M. W.; Kumar, A.; Khan, A. U. ACD: Antimicrobial chemotherapeutics database. *PLoS One.* **2020**, *15* (6), e0235193.

https://doi.org/10.1021/acs.chemrestox.2c00375
Chem. Res. Toxicol. XXXX, XXX, XXX−XXX

UTTAR PRADESH JOURNAL OF ZOOLOGY

43(7): 52-59, 2022
ISSN: 0256-971X (P)

SHORT-TERM EFFECT OF *Naja naja* SHED SKIN EXTRACT ON HISTOPATHOLOGY OF TESTIS, EPIDIDYMIS AND VAS DEFERENS OF SWISS ALBINO MICE

RAJARSHI GHOSH [a*], SOUBHIK DAS [a], DEEPSHIKHA MITRA [a], PRADIP BHATTACHARJEE [a] AND SUBIR CHANDRA DASGUPTA [a]

[a] Post-Graduate Department of Zoology, Maulana Azad College, 8 Rafi Ahmed Kidwai Road, Kolkata - 700013, West Bengal, India.

AUTHORS' CONTRIBUTIONS

This research work has been carried out in collaboration among all authors. Author RG designed the study, wrote the protocol and first draft of the manuscript. Authors SD, DM and PB performed the experiments and interpreted the data. Author PB managed the literature survey. Author SCD has made substantial contributions to the final checking of the manuscript. All authors read and approved the final manuscript.

Article Information

Editor(s):
(1) Dr. Villagomez Cortes Jose Alfredo Santiago, University of Veracruz, Mexico.
Reviewers:
(1) Amina Abd Al-Rahman Fayad, University of Baghdad, Iraq.
(2) Said Ahmed Mohamed Hassan, Suez Canal University, Egypt.
(3) Gunasekar Manoharan, New Jersey Bio Science Centre, USA.

Received: 01 March 2022
Accepted: 04 May 2022
Published: 09 May 2022

Original Research Article

ABSTRACT

Ancient literature reveals that snake shed skin had been frequently used to treat several diseases like glaucoma, hernia, psoriasis, hemorrhoids, etc. Previously, it was reported that *Naja naja* shed skin extract causes temporary cessation of the estrous cycle and altered female reproductive hormones in rodents, and the probable bioactive molecule behind such alterations was also identified. Based on this information, the present study was designed to establish the effect of *Naja naja* shed skin extract on the male reproductive system of Swiss albino mice. The extract was prepared with physiological saline and was injected intraperitoneally in the male mice for 7 consecutive days @ 10 mg kg^{-1} body weight. The short-term histopathological studies were performed by Haematoxylin and Eosin staining and the sperm morphology was analyzed by using bright-field microscopy. The snake skin extract markedly changed the gross histological architecture of the seminiferous tubules including disorganization of germinal epithelial cells, accumulation of exfoliated cells in the lumen, tailless sperm in the epididymis, disorganized basal cells in vas deferens as well as marked alteration of sperm morphology. The present work with snake shed skin strongly indicates that it is not simply a biological waste, but it might be a treasure house of many bioactive compounds.

Keywords: *Naja naja*; histopathology; male reproductive system; shed snake skin extract.

**Corresponding author: Email: 1977rajarshighosh@gmail.com;*

1. INTRODUCTION

Out of a million venomous animals, the snakes are the most feared but, at the same time, the most worshipped living creatures on earth. Different body components of the snakes including fat, bile, and shed skin have been used in folk and ethnomedicine of various cultures since ancient times [1,2,3]. Skin shedding or ecdysis is a dynamic event that occurs throughout the lifetime of a snake [4]. A healthy snake sheds its skin in a single piece, like an inverted sock. As soon as a shedding cycle is complete, a new cycle begins, and it is repeated throughout the life of the snake [5,6]. The use of snake shed skin (SSS) in different pathophysiological conditions such as wound healing, burn, glaucoma and eczema has been mentioned in folk medicine [7]. In the traditional medicine concept of China, the SSS has long been used in various diseases such as furuncles, carbuncles and mammary abscesses and was also reported to be useful in curing the inguinal hernia [1]. Based on the concept of traditional healers and ancient medicinal practices of using SSS in reproductive disorders in the South-Eastern part of Asia and India, it could be stated that the SSS could be associated with alteration of the reproductive functions [8].

The SSS, thought to be a biological waste initially, could be a potential source of bioactive molecules [8]. Limited scientific data are available to establish the therapeutic uses of such moleculesobtained from SSS in health and diseases [2,9,10]. Though largely used by traditional naturopaths for treating various female reproductive disorders, the role of aqueous shed skin extract of Indian cobra, *Naja naja* on the estrous cycle of female mice was well documented [7]. It caused a cessation of the estrous cycle, especially at the diestrus phase. From SSS extract, a small crystalline peptide was isolated as bioactive molecule from *Naja naja* shed skin called NNSS2 which probably was responsible for the estrous cycle inhibition [8]. Further extensive studies have been carried out to investigate the effects of SSS extract on the female reproductive system in mice. But there is no scientific evidence regarding the bioactivity of the SSS on the male reproductive system. Therefore, the present study is targeted to evaluate the role of the aqueous extract of *Naja naja* shed skin on the histopathology of the male reproductive system in Swiss albino mice.

2. MATERIALS AND METHODS

2.1 Specimen Collection and Maintenance

Male Swiss albino mice of 10-12 weeks old were purchased from the approved animal breeders of Maulana Azad College, Kolkata. They were acclimatized for 7 days in polypropylene cages at 25 ± 2°C in a light-controlled environment (12 h in light and dark conditions alternatively). All the animals were fed a standard laboratory diet and had free access to food and water *ad libitum*.

2.2 Collection of *Naja naja* Shed Skin and Maintenance

Fresh *Naja naja* shed skin of both sexes were collected from North 24-Parganas District of West Bengal, India through field collection as per the permission granted by the office of the Principal Chief Conservator of Forests (Wildlife) and Chief Wildlife Warden, West Bengal, India (memo no. C-28011/11/2020, dated 17.01.2020). The skins were identified by the Zoological Survey of India, Kolkata. The shed skins were stored in desiccators at room temperature and an aqueous extraction was made as per requirement.

2.3 Preparation of Snake Shed Skin Aqueous Extract and Estimation of Protein

Freshly powdered shed skin of *Naja naja* was soaked in physiological mammalian saline (0.9 % NaCl solution) overnight at 4°C and it was then centrifuged at 5000 rpm at 4°C for 20 min. The supernatant was collected and expressed in terms of protein content [11].

2.4 Experimental Design

For the study with an aqueous extract of SSS, the male Swiss albino mice were randomized into 2 groups (n=5). One group was considered as control where mice were injected with normal mammalian physiological saline and to the mice of the experimental group, the SSS extract (10 mg kg^{-1} body weight) was administered through the intraperitoneal route for 7 consecutive days (total of 7 exposures). The dose of the SSS extract in this present work has been standardized following the previous experiment which was performed on female Swiss albino mice for investigating the effects of SSS of *Naja naja* on histopathology of ovary and uterus [7]. After 24 h of the last dose being injected, male mice were sacrificed by cervical dislocation. For histopathological analysis of the male reproductive system, testes, epididymis and vas deferens were dissected carefully and freed from adhering tissues.

2.5 Histopathological Studies

The testis, vas deferens and epididymis from control and SSS-treated male mice were isolated, washed in

saline, and fixed in 10 % buffered formalin for 18 h. Then, tissues were dehydrated in upgraded alcoholic series, immersed in cedar wood oil followed by embedding in molten paraffin (melting point: 56-58°C). Serial paraffin thin sections (5 µm) were cut using a rotary microtome. The tissue sections were stained with Haematoxylin and Eosin (HE) following standard protocol and mounted in Dibutylphthalate Polystyrene Xylene (DPX). Finally, the stained tissue sections were observed under a bright-field microscope.

2.6 Sperm Morphology Analysis

The epididymis from the control and SSS-treated male mice was finely minced by anatomical scissors in 1 mL of isotonic saline solution kept in a Petri dish. It was completely squashed with the help of tweezers for 2 min. Then it was incubated for 4h at room temperature to provide the migration of all spermatozoa from epididymal tissue to fluid. The inner content of epididymis was taken out in saline and the material was thoroughly shaken to suspend the sperm in saline solution. The sperm suspension was filtered with the help of cell strainer (PluriSelect, USA; mesh size: 40 µm) to remove the debris and the filtrate was collected in a graduated tube; more saline was added to make the volume 10 mL. The sperm suspension, thus collected, was put in the centre of the clean slide over which 0.02 mL methanol was added, air-dried overnight at room temperature. A drop of diluted Giemsa stock solution (6:1) was put on the material. The material was covered with a cover glass sealed temporarily for observation under bright-field microscope as per the routine procedure.

3. RESULTS AND DISCUSSION

3.1 Effect of Snake Shed Skin (SSS) Extract on the Testis

The histological structure of the normal testis treated with physiological saline showed the usual characteristics; the seminiferous tubules exhibited spermatogenic activity with successive stages of sperm development, healthy germinal epithelium, and presence of interstitial cells of Leydig in between the tubules (Fig. 1A). Significant alterations were observed in the histoarchitecture of the testes treated with SSS extract. The degenerative changes in the seminiferous tubules were not uniformly distributed. Within the same section, some tubules were found to have a greater extent of disturbances than others. The diameter of the tubules significantly decreased, and the interstitial space became wider as compared to the control (Fig. 1B). The germinal epithelial cells became reduced in height, showed increased disorganization with the accumulation of cellular debris in the lumen. As a result, the epithelial covering of the seminiferous tubules became thinner and resulted in the arrest of spermatogenesis (Fig. 1C). Few of the interstitial cells underwent cellular necrosis (Fig. 1D). The necrotic effect on the spermatogenic cells was evident in the sections with elevated cellular congestion and hemorrhage. This is one of the major reasons for testicular weight loss [12, 13,14]. In some sections, the presence of giant cells containing abnormal spermatid nuclei was evident (Fig. 1E). This type of cell is suggested to be formed from multiple nuclear divisions without cytoplasmic separation of the cells [15]. An increased accumulation of cells in the interstitial space was also noticed in the treated mice testis (Fig. 1F). In general, the affected seminiferous tubules showed degeneration of the epithelial layer, intraepithelial vacuolation, degradation of the sperm cells, and the presence of a mixed type of spermatogenic cells in different stages of spermatogenesis.

3.2 Effect of Snake Shed Skin (SSS) Extract on Caput Epididymis

The epididymis of the control mice was shown to have normal histological features; it consisted of several tubules lined with pseudostratified columnar epithelium having stereocilia and the lumen was filled with sperm bundles. The tubules were separated by connective tissue having blood vessels (Fig. 2A).The caput epididymis was taken for comparison from the SSS-treated mice. The tubular diameter increased, although not so significantly. There were few tubules without any sperm in the lumen (Fig. 2B). This might be due to the partial arrest of spermatogenesis after treatment with SSS extract which led to the loss of spermatogenic cells from tubular epithelium or hormonal impairment [16,17]. The most prominent effect of SSS extract in the caput epididymis was the dislodging of the stereocilia (Fig. 2C). The lumen was often found to contain exfoliated germ cells that are the resultants of the loss of premature cell adhesion to the processes of Sertoli cells [17]. These caused the accumulation of germ cell elements into the lumen of seminiferous tubules [18].

3.3 Effects of Snake Shed Skin (SSS) Extract on Vas Deferens

In control mice, the vas deferens consisted of three distinct muscular layers, viz. the outer longitudinal, middle circular and inner longitudinal layers. The lamina propria was also prominent in between the

longitudinal muscle layer and pseudostratified epithelial cells having stereo cilia (Fig. 3A). Basal cells are regularly arranged in the endothelium. The epithelial layer was folded so as to form a stellate lumen containing the sperm bundles (Fig. 3C). On the contrary, the endothelium showed swelling in SSS-treated mice as compared to the control. The cellular height of the epithelial cells did not change much, but it showed nuclear pyknosis, especially in the regions of folds (Fig. 3B). The regular arrangement of the basal cells was affected in the treated mice. The flattening of the endothelial lining consisting of remnants of stereo cilia was also visible along with some endothelial lesions (Fig. 3D).The atrophy in the tubular epithelial cells and loss of proper spermatogenic activities might be due to the functional interruption of the Sertoli cells [19]. This study implied the involvement of hormonal misbalance especially testosterone due to the application of SSS extract into mice [20,21,22,23].

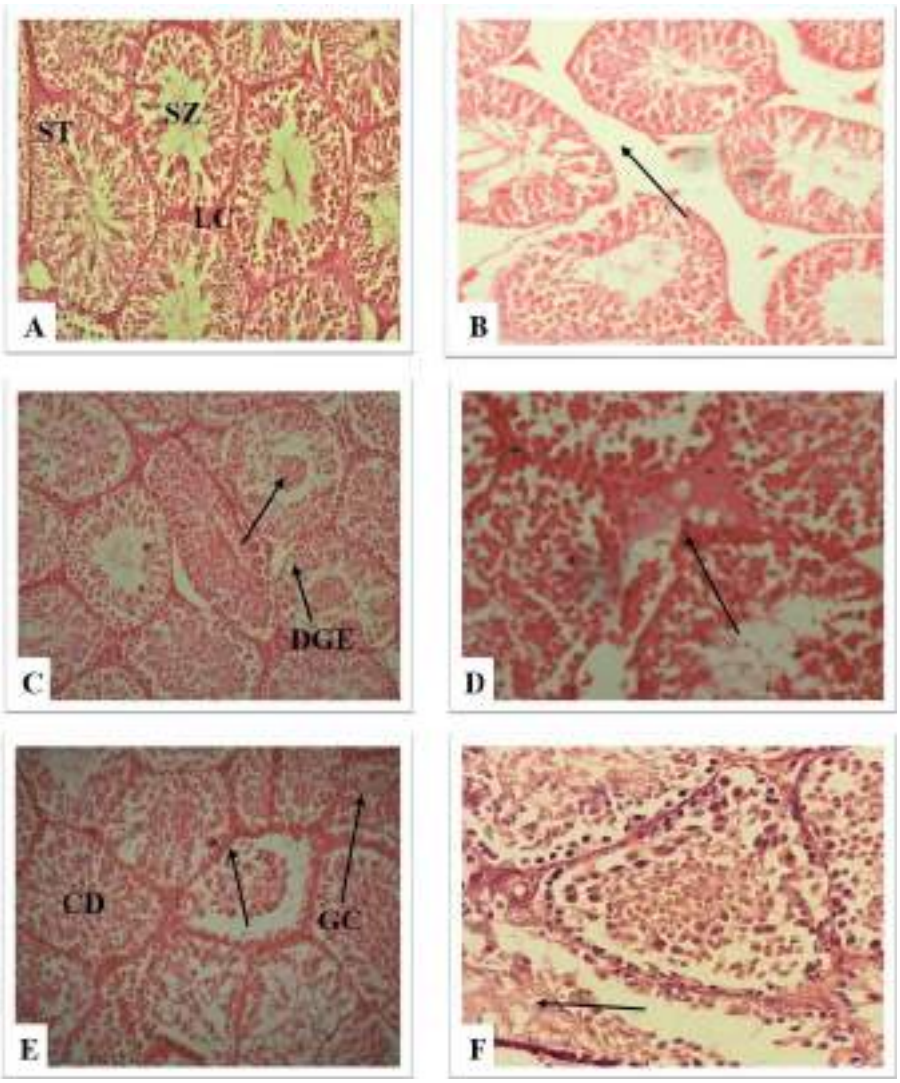

Fig. 1. Photomicrographs of histopathological analysis of testes; [A] The sectional view of testis from control Swiss albino mice showing seminiferous tubules (ST), interstitial cells of Leydig (LC) and spermatozoa (SZ), HE staining (200X); [B] testes of SSS-treated mice showing an enlargement of the interstitial space between the tubules as indicated by the black arrow, HE staining (100X); [C] Testes of SSS-treated mice showing denudation of the epithelial cells into the lumen as indicated by black arrow and disarrayed germinal epithelium (DGE), HE staining (200X); [D] Initiation of cellular necrosis in interstitial spaces, indicated by the black arrow, HE staining (400X); [E] cellular debris in the lumen (CD) and degradation of the spermatogenic cells due to arrest of spermatogenesis (black arrow) and presence of giant cell (GC), HE staining (200X); [F] Increased cellular accumulation in the interstitial space, indicated by the black arrow, HE staining (400X)

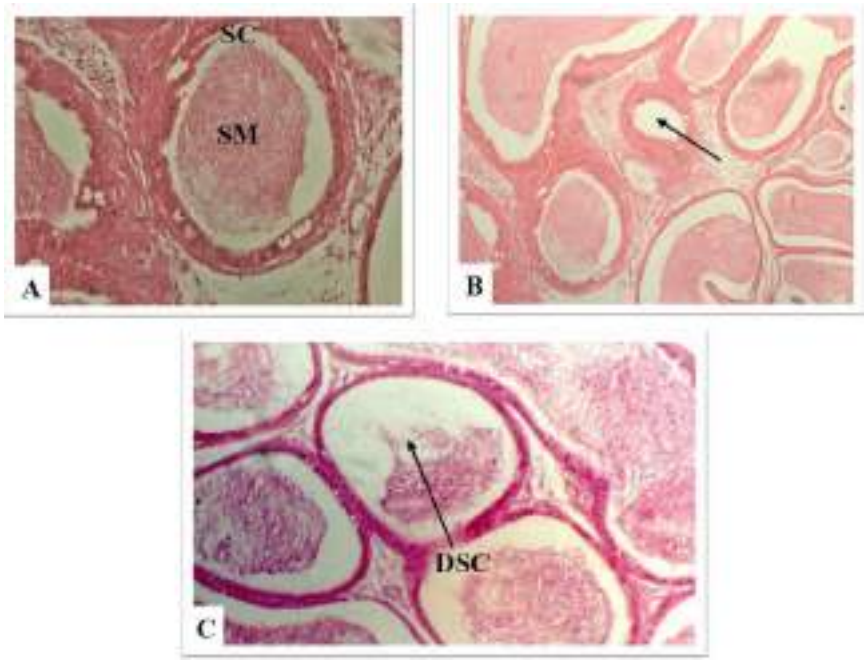

Fig. 2. Photomicrographs of histopathological analysis of caput epididymis; [A] The control caput epididymis showing the usual arrangement of stereo cilia (SC) and spermatozoa (SM), HE staining (200X); [B] Tubule without sperm in SSS-treated mice as indicated by the black arrow, HE staining (100X); [C] Epithelial layer of treated caput epididymis with dislodged stereo cilia (DSC) and debris of spermatozoa and abnormal sperm cells as indicated by black arrow, HE staining (200X)

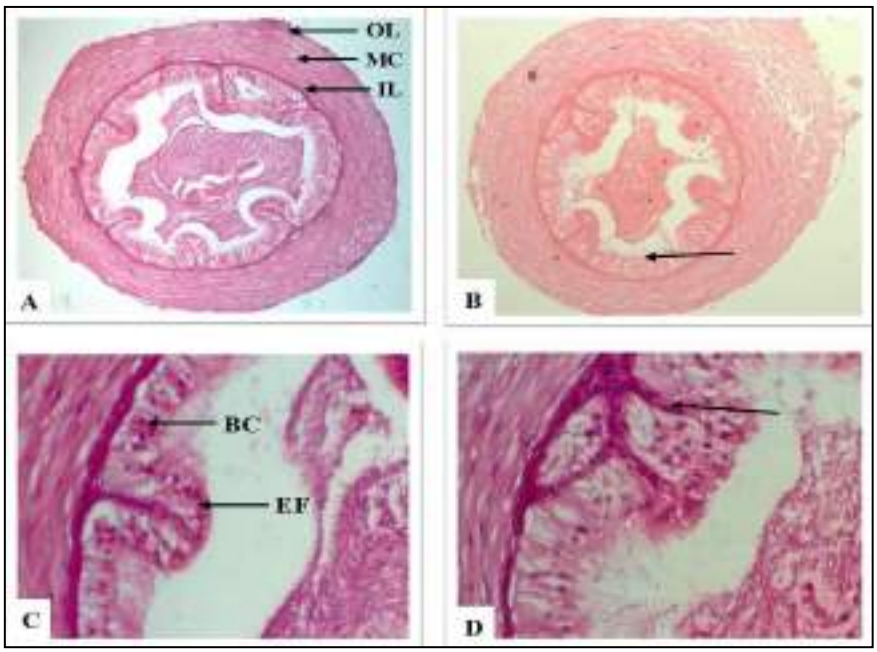

Fig. 3. Photomicrographs of histopathological analysis of vas deferens; [A] Vas deferens in control mice showing three layers of muscles viz. outermost longitudinal (OL), middle circular (MC) and innermost longitudinal (IL) layers, HE staining (200X); [B] Swelling of the endothelium with remnants of stereocilia in treated mice, indicated by black arrow, HE staining (200X); [C] Normal vas deferens showing a regular arrangement of basal cells (BC) within the basement membrane and epithelial fold (EF), HE staining (400X); [D] Irregularly distributed basal cells as indicated by black arrow and disturbed epithelial fold, HE staining (400X)

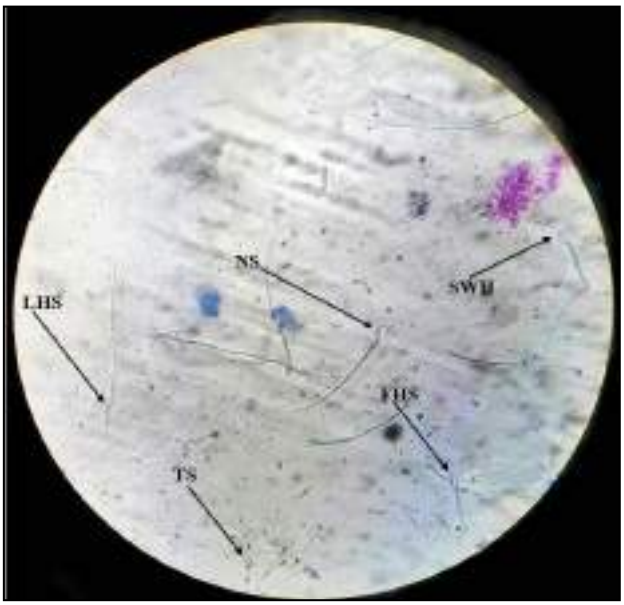

Fig. 4. Changes in sperm morphology in mice treated with snake shed skin (SSS) extract. Normal sperm with hook and tail (NS), long-headed sperm (LHS), tailless sperm (TS), forked-headed sperm (FHS) and sperm without hook (SWH) were also observed when treated with SSS, Giemsa staining (400X)

3.4 Changes in Sperm Morphology

The direct effects of SSS extract on sperm morphology are quite evident from the obtained data. Certain types of abnormal sperm morphs were visible following the treatment of SSS extract in mice. A normal motile sperm contains a marked hook and a distinct tail which is a unique and important characteristic to predict the fertilization capacity [24]. When the SSS extract was administered to the mice, the number of abnormal sperms including long-headed and tailless sperm increased significantly (Fig. 4) which reduced sperm motility to a greater extent resulting in a decreased fertilizing capacity of mice [25]. A number of forked-headed sperm was also observed in treated mice groups. It was also observed that SSS extract could lead to the production of sperm without any hook (Fig. 4). Reduced sperm motility associated with morphological changes might be due to low levels of ATP that drive its movements [26,27] and abnormalities in male gonadotropins [19,28,29,30]. The extract possibly had direct effects on Sertoli cells of seminiferous tubules, the principal player in spermiogenesis [31]. Any disorganization in the epithelial layer or testicular tubular atrophy can alter Sertoli cell functions and thereby decrease normal and healthy sperm production [32].

4. CONCLUSION

The present study reflected the effects of aqueous extract of *Naja naja* shed skin on the histological characteristics of the male reproductive system in mice. It showed marked alterations in the gross histopathology of the overall reproductive organs including degeneration of epithelial cells of the seminiferous tubules, accumulation of cellular debris in the lumen, temporary arrest of spermatogenesis, tubules without sperm, abnormal and reduced sperm motility, degradation of the stereo cilia in the epididymis, disorganized basal cells and eventually reduced fertility.

The necrotic changes and reduced spermatogenic activities that occurred followed by the administration of the SSS extract might have caused a reduction in the weight of testes. The direct effect on the functional integrity of Sertoli cells was reflected in the arrest of spermatogenesis and degradation of spermatogenic cells. The increased cellular debris in the interstitial space was a clear indicator of the fact that testosterone secretion was being affected in the treated mice. Testosterone is crucial for the maintenance of the interstitial cells of Leydig, which in turn is important for the structural integrity of the seminiferous tubules and proper spermatogenetic activities. Decreased sperm motility, as in the case of tailless sperm observed in SSS- treated samples may be associated with infertility in male mice. There might be several reasons behind alteration of the sperm morphology and its effects on fertilization ability. Altered enzymatic activities of oxidative processes and subsequently low levels of ATP content could be the major issues determining sperm motility. The sperm count, on the other hand, was

also crucial for usual fertility, which was affected after SSS extract injection.

The overview of the SSS extract on the male reproductive system and the possible reasons behind them clearly indicate that the SSS is a potential source of active biomolecules with therapeutic advantages. Future works are required to evaluate the hormonal and biochemical changes due to SSS extract administration into male mice and to investigate the nature of active biomolecules present in the shed skin of *Naja* and other snakes.

ETHICAL APPROVAL

The experimental protocols used for this study were approved by the Institutional Animal Ethical Committee of Maulana Azad College and followed strictly.

COMPETING INTERESTS

Authors have declared that no competing interests exist.

REFERENCES

1. Lev E. Traditional healing with animals (zootherapy): Medieval to present-day Levantine practice. Journal of Ethnopharmacology. 2003;85:107. DOI: 10.1016/s0378- 8741(02)00377-x
2. Costa-Neto EM. Animal-based medicines: biological prospection and the sustainable use of zootherapeutic resources. Anais da Academia Brasileira de Ciencias. 2005;77:33. DOI: 10.1590/s0001-37652005000100004
3. Soewu DA. Wild animals in ethnozoological practices among the Yorubas of southwestern Nigeria and the implications for biodiversity conservation. African Journal of Agricultural Research. 2008;6:421.
4. Kardong KV. Vertebrates: Comparative Anatomy, Function, Evolution (5th ed.). New York: McGraw Hill. 2009;216-217. ISBN: 978-007-127033-5.
5. Mattison C. The new encyclopedia of snakes. Princeton: Princeton University Press;2007.
6. Parker HW. Snakes- A natural history talks. London: Cornell University Press; 1977.
7. Mukherjee S, Dasgupta SC, Gomes A. Effect of *Naja naja* Laurenti shed skin extract on estrous cycle, hormone- cytokine profiles, histopathology of ovary and uterus of Swiss albino mice. Indian Journal of Experimental Biology. 2013;51:235-240.
8. Mukherjee S, Dasgupta SC, Gomes A. Estrous cycle cessation caused via activating the apoptotic pathway by NNSS2 isolated from *Naja naja* shedded skin. Journal of Toxins. 2016;3(1):3.
9. El-Kamali HH. Folk medicinal use of some animal products in Central Sudan. Journal of Ethnopharmacology. 2000;72:279-289. DOI: 10.1016/s0378-8741(00)00209-9
10. Adeola MO. Importance of wild animals and their parts in the culture, religious festivals, and traditional medicine, of Nigeria. Environmental Conservation. 1992;19:125-134. DOI:https://doi.org/10.1017/S0376892900030605
11. Lowry OH, Rosenburg NJ, Farr AL, Roudall R. Protein measurement with the Folinphenol reagent. Journal of Biological Chemistry. 1951;193:265-275.
12. Lue Y, Sinha HAP, Wang C, Leung A, Baravarian S, Reutrakul V, Sangsawan R, Chaichana S, Swerdloff RS. Triptolide: a potential male contraceptive. Journal of Andrology. 1998;19(4):479-486.
13. Takihara H, Cossentino MJ, Sakotoku J, Cockett ATK. Significance of testicular size measurements in andrology II. Correlation of testicular size with testicular function. Journal of Urology. 1987;137:416-419. DOI: 10.1016/s0022-5347(17)44053-5
14. Udoh P, Kehinde A. Studies on anti-fertility effect of pawpaw seeds (*Carica papaya*) on the gonads of male albino rats. Phytotherapy Research. 1999;13(3):226-228. DOI: 10.1002/(sici)1099-1573(199905)13:3<226::aid-ptr396>3.0.co;2-e
15. Mishra RK, Singh SK. Effect of aqueous leaf extract of *Azadirachta indica* on the reproductive organs in male mice. Indian Journal of Experimental Biology. 2005;43: 1093-1103.
16. Creasy DM. Pathogenesis of male reproductive toxicity. Toxicologic Pathology. 2001;29:64-76. DOI: 10.1080/019262301301418865
17. Vidal JD, Whitney KM. Morphologic manifestations of testicular and ependymal toxicity. Spermatogenesis. 2014;4:e979099. DOI: 10.4161/21565562.2014.979099
18. Donmez YB, Kizilay G, Topcu-Tarladacalisir Y. MAPK immunoreactivity in streptozotocin-induced diabetic rat testis. Acta Cirurgica Brasileira. 2014;29:644-650. DOI: 10.1590/S0102-8650201400160004
19. Crews D, Williangham E, Skipper JK. Endocrine disruptors: Present issues, future

directions. The Quarterly Review of Biology. 2000;75:243-260.
DOI: 10.1086/393498

20. Bartke A. Pituitary-Testis relationship. Reproductive Biology. 1991;1:136-152.
21. Sharpe RM, Maddocks S, Kerr JB. Cell-cell interactions in the control of spermatogenesis as studied using Leydig cell destruction and testosterone replacement. American Journal of Anatomy. 1990;188:3-20.
DOI: 10.1002/aja.1001880103
22. Xu Y, Lei H, Guan R, Gao R, Li H, Wang L, Song W, Gao B, Xin Z. Studies on the mechanism of testicular dysfunction in the early stage of a streptozotocin induced diabetic rat model. Biochemical and Biophysical Research Communications. 2014;450:87-92.
DOI: 10.1016/j.bbrc.2014.05.067
23. Kianifard D, Sadrkhanlou RA, Hasanzadeh S. The ultrastructural changes of the sertoli and leydig cells following streptozotocin induced diabetes. Iranian Journal of Basic Medical Sciences. 2012;15:623-635.
24. Aitken RJ, Best FSM, Warner P, Templeton A. A prospective study of the relationship between semen quality and fertility in the case of unexplained infertility. International Journal of Andrology. 1984;5:297-303.
DOI: 10.1002/j.1939-4640.1984.tb00792.x
25. Murugavel T, Ruknudin A, Thangavelu S, Akbarsha MA. Antifertility effect of *Vinca rosea* (Linn.) leaf extract on male albino mice. A sperm parametric study. Current Science. 1989;58(19):1102-1103.
26. Tso WW, Lee CS. Effect of gossypol on boar spermatozoa *in vitro*. Archives of Andrology. 1981;7:85-88.
DOI: 10.3109/01485018109009381
27. Iamsaard S, Burawat J, Kanla P, Arun S, Sukhorum W, Sripanidkulchai B, Uabundit N, Wattathorn J, Hipkaeo W, Fongmoon D, Kondo H. Antioxidant activity and protective effect of *Clitoriaternatea*flower extract on testicular damage induced by ketoconazole in rats. Journal of Zhejiang University-Science B. 2014;15(6):548-555.
DOI: 10.1631/jzus.B1300299
28. Adamkovicova M, Toman R, Martiniakova M, Omelka R, Babosova R, Krajcovicova V, Grosskopf B, Massanyi P. Sperm motility and morphology changes in rats exposed to cadmium and diazinon. Reproductive Biology and Endocrinology. 2016;14:42.
DOI: 10.1186/s12958-016-0177-6
29. Singh SK, Pandey RS. Effect of subchronicendosulfan on plasma gonadotropins, testosterone, testicular testosterone and enzymes of androgen biosynthesis. Indian Journal of Experimental Biology. 1990;28:953-956.
30. Bodding PO. Studies in Santhal Medicine and Connected Folklore. Calcutta: Baptist Mission Press, The Royal Asiatic Society of Bengal; 1925.
31. Bedford JM. Significance of the need for sperm capacitation before fertilization in eutherian mammals. Biology Reports. 1983; 28:108-120.
DOI: 10.1095/biolreprod28.1.108
32. Bardin CW, Cheng CY, Musto NA, Gunsalus GL. The Sertoli cell. In: The Physiology of Reproduction (Ed., Knobil E, Neill J). Raven Press, New York. 1988; 933-974.

Zootaxa 5200 (1): 051–062
https://www.mapress.com/zt/

Article

ISSN 1175-5326 (print edition)
ZOOTAXA
ISSN 1175-5334 (online edition)

https://doi.org/10.11646/zootaxa.5200.1.4
http://zoobank.org/urn:lsid:zoobank.org:pub:C4A97ADB-42ED-45B7-831A-BB3C66928CC1

Two new species of *Pseudosmittia* Edwards, 1932 from India with a key to Oriental species adult males (Diptera: Chironomidae: Orthocladiinae)

TUHAR MUKHERJEE[1,3], DIPAK KUMAR SOM[2,4] & NILADRI HAZRA[1,5*]
[1]*Entomology Research Unit, Department of Zoology, The University of Burdwan, Burdwan, India, 713104*
[2]*Post Graduate Department of Zoology, Maulana Azad College, Government of West Bengal, Kolkata, India, 700013*
[3] tuharmukherjeeofficial@gmail.com, https://orcid.org/0000-0002-9449-5985
[4] dipaksom@gmail.com
[5]*Corresponding author* nhazra@zoo.buruniv.ac.in; https://orcid.org/0000-0001-8149-9445

Abstract

In this study, we described and illustrated two new species, *Pseudosmittia luna* and *Pseudosmittia valida* based on the adult males from the plains of West Bengal, India. A DNA barcode of *Pseudosmittia luna* **sp. n.** compared with selected congeneric sequences from NCBI GenBank, indicates that the species is sister to an unknown species with accession number MG301870. Additionally, we provided a key for the adult males of the Oriental species of the genus.

Key words: New species, taxonomy, *Pseudosmittia*, Orthocladiinae, Orient

Introduction

Pseudosmittia Edwards, 1932 is one of the most speciose and heterogeneous genera within the subfamily Orthocladiinae of the family Chironomidae. Knowledge of their taxonomy and biogeography is lacking in the Oriental region, so among 128 species discovered, only twelve species are known from the Oriental region (Ferrington & Sæther 2011; Ashe & O'Connor 2012; Hazra *et al.* 2016). Mazumdar *et al.* (1997) reported *Pseudosmittia dupla* (Tokunaga, 1936), from the Sundarbans Mangrove areas of West Bengal, India. However, after careful examination of the type material, it was found to be a new species of the genus *Pseudosmittia*. *Pseudosmittia* is divided into thirteen species groups based on parsimony analysis of morphological characteristics of adults and immatures (Ferrington and Sæther 2011). Among them, only *xanthostola* and *brachydicrana* groups are known from South Asia and the Indo-Pacific region, while most other groups are reported in other zoogeographical regions (Ferrington and Sæther 2011). DNA barcoding using COX1 sequence has successfully delineated the Indian chironomids in the past (Mukherjee *et al.* 2020; Mondal *et al.* 2021). However, DNA barcodes of very few orthoclad species from India have been made till date. In this paper, we have sequenced the Cytochrome Oxidase I (COX1) gene of *P. luna*. Molecular analysis of COX1 gene of *P. luna* with available sequences in BOLD indicates that species form a sister group to an unknown *Pseudosmittia* species with an accession number of ACU8963.

This paper on Indian orthoclads contains descriptions of two new species of the genus *Pseudosmittia* and for the first time a key for identification of the males of species of this genus reported from the Oriental region. This study helps to improve our knowledge on the diversity of *Pseudosmittia* in the Orient.

Material and methods

Sample collection and preparation

We collected the adult midges using white light traps (8W CFL lamp) and sweep nets from the Golapbag campus of The University of Burdwan and mangrove forests of Kakdwip, West Bengal (Figure 1). We mounted the midge carcasses on glass slides following Wirth and Marston's Phenol-Balsam method (1968). All material examined temporarily retained in the collection of insects in the Entomology Division, Department of Zoology, The University of Burdwan, West Bengal, India are deposited in the National Zoological Collections (NZC), Kolkata.

Accepted by B. Rossaro: 16 Sept. 2022; published: 26 Oct. 2022

UTTAR PRADESH JOURNAL OF ZOOLOGY

43(22): 61-66, 2022
ISSN: 0256-971X (P)

MICROPLASTIC IN INDIA A SHODDY AFFAIR

ABHISHEK MUKHERJEE [a*], ARCHISMAN BHATTACHARJEE [a] and AOISHIK ROY [a]

[a] Maulana Azad College, Kolkata, India.

AUTHORS' CONTRIBUTIONS

This work was carried out in collaboration among all authors. All authors read and approved the final manuscript.

Article Information

DOI: 10.56557/UPJOZ/2022/v43i223233

Editor(s):
(1) Dr. Osama Anwer Saeed, University of Anbar, Iraq.
Reviewers:
(1) Richard Ciotola, the Ohio State University, U.S.A.
(2) Veeranuch Srakaew, Chandrakasem Rajabhat University, Thailand.

Received: 18 September 2022
Accepted: 23 November 2022
Published: 02 December 2022

Review Article

ABSTRACT

Small sized fragmented plastic or microplastic contamination is widespread and considered as one of the major problems of aquatic environment. Ability to resist bio-degradation amplifies longevity, long transportation and aggregation, enables microplastics to find their sink in the drinking water. The situation in India is more critical as sources of microplastics are far too many and the high sediment flux in the rivers may easily facilitate the process of fragmentation during typical tropical climate, making the aquatic ecosystem of India extremely vulnerable. Detailed research and careful monitoring activities could bring clearer picture of the scenario and assess the impact of plastics on environment and biota. Some mechanism through which the emissions at the source could be checked or some other ways to reduce and reuse plastic waste or some new novel business solutions are essential to tackle this problem.

Keywords: Microplastic; freshwater; globally distributed; industrial efflux; pollution.

1. INTRODUCTION

Plastics have become omnipresent and a pervasive compelling force of contemporary industrialized world. It has become indispensable because of its exceptional properties in an affordable price. Chemicals such as lead, cadmium and mercury used in production of plastic are toxic and detrimental to human body. When larger plastic wastes are exposed to different environmental conditions it undergoes weathering and leads to formation of microplastics. Microplastics are very small plastic pieces (less than 5 mm long) which are harmful to all types of life forms [1]. Because of their small size, they can penetrate the biological barriers and accumulate in tissues which produce a series of hazardous effects on feeding, growth, reproduction, immunity and genetics [1].

Microplastics have become an alarming concern for living fraternity around the world. The most common

**Corresponding author: Email: 2007.mukherjee@gmail.com;*

and concerning reason which makes microplastics threatening is solely because they are not completely biodegradable and have a propensity to accumulate in environment [2]. Researchers have also thrown light on how the microplastics are accumulated in each trophic level (bioaccumulation) and magnify (biomagnifications) [3].

Microplastics have been found in all continents (except Antarctica) out of which Asia accounts for majority of it and Australia least [4]. With over 1.2 billion population and improper infrastructure for waste management, India is one of the world's leading plastics consumers and waste generator, with over 40-45% of its waste remains uncollected and dumped indiscriminately into rivers, lakes, ponds, oceans and seas [5]. Due to rampant disposal and dispersal in aquatic environments plastics and eventually microplastics interfere with marine and freshwater life. India predominantly being a rural country and with less than 40% of its rural population having access to safe drinking water between 2016-2020 [6], uses freshwater sources as the primary source of water for day-to-day activities (bathing, washing utensils and clothes), farming and most importantly, drinking. Clothes, cosmetics, personal care products, plastic bottles, paints etc. have different forms of plastic materials [like - polyvinyl chloride (PVC), polyethylene (PE), polystyrene (PS), polypropylene (PP), and polyethylene terephthalate (PET) etc.] that get accumulated in the water and while fishing gears and other nets used in freshwater bodies are also accumulator of plastic materials [7]. This amounts to microplastics loading in freshwater sources and has serious adverse effects in health. Urban population use relatively less natural freshwater source for day-to-day activities but the rampant industrialization in order to meet the demands of ever expanding population releases toxic waste materials containing plastics into freshwater sources. The plastics dumped under the soil as land fill may reach the groundwater in microplastic form and contaminate drinking water sources for urban population that can have damaging ramifications to health [8]. Indian rivers are fed by tremendous amount of monsoon rains receiving from both South-West and North-East monsoon, leading to flooding and microplastics loading in freshwater sources [9]. Though proper health concerns due to microplastic pollution and accumulation are undeciphered but eventually they will be evident.

The reason for microplastics being omnipresent is owing to its low cost, easy availability and its multidimensional use by human fraternity. If examined, their presence can be traced from the mighty remote Himalayas to the abysmal depths of oceans. Plastics have become an inescapable truth of daily life .Escalating demand for plastic use and soaring plastic wastes cannot be the gospel of life. Remedial measures to overcome and reduce this problem of microplastic pollution are the need of time. Certain countries despite being surrounded by ocean have controlled microplastic pollution effectively through proper awareness and strict directive measures like imposing ban on single use plastics switching to more convenient and natural mode to do away with this invisible threat [10].

Thus in this review we discuss the extent of microplastics' contamination in freshwater sources across Indian subcontinent and try to enlighten the possible remedies to deal with this problem.

2. ORIGIN AND ABUNDANCE OF MICROPLASTIC

Creation of new synthetic chemicals in collaboration with competence of mass production has made plastic one of the most available commodity in modern world. Most standard plastics such as polypropylene, polystyrene, PVC and polyethylene terephthalate are non-biodegradable and their increasing aggregation in the environment is a warning to planet.

Small size plastic particles are described as macroplastics as >5 mm, mesoplastics as 5 to >1 mm, microplastics as 1 mm to >0.1 μm, and nanoplastics as 0.1 μm by Lambert et al. [11]. However, generally accepted upper limit size of microplastic is < 5 mm [12] and are a crucial adulterant dispersed throughout freshwater and marine ecosystem and posing notable threat to the living organisms. Microplastics are present in diverse morphologies like beads, fragments, fibers, films. Microplastics can be originated from variety of sources like ingredients in cigarette filters, textile fibers and cleaning items such as sponges and cosmetic care products for personal use and dust from vehicular tires, as well as from larger plastic products released into the aquatic environment through cosmetics, textiles, land application, waste from domestic and industry are degraded down by natural and artificial processes such as photo degradation, biodegradation, mechano-chemical, photo-oxidative degradation, thermal, and catalytic action. Weathering of plastic greatly increases the surface area which has detrimental effect on organisms. Hydrophobic chemicals can be adsorbed on microplastic and desorbed into the digestive system thus increasing bioavailability of pollutants leading to bioaccumulation. Certain microorganisms, such as fungi (Actinomycetes) and bacteria (mutated *Pseudomonas putida*) are capable of breakdown of

larger plastics, specifically thermocol, polycarbonate, low-density polyethylene etc. into microplastics [13]. Microplastics are dispersed in the environment as mishandled wastes that haphazardly adulterate water, soil and air. Environmental contamination by microplastic is augmented by anthropogenic factors, such as low efficiency of urban waste water treatment and application of sewage sludge to fields. Natural factors such as wind, storms and floods contribute to the distribution of microplastic [14]. The concentration of microplastic is measured in items/m^3 (freshwater) and items/m^2 (marine environment). Asia followed by Europe and America are the most polluted continents where as Africa and Oceania are least polluted with microplastic [15].

3. STATUS OF MICROPLASTIC IN INDIA

Microplastic and India: India accounts for about 16% of the world's population sustaining on only 4% of world's freshwater sources. These diminishing freshwater sources are getting polluted with microplastics. Microplastic owing to its ability to withstand biodegradation increases its durability, transportation capability and accumulation and thus sinking in the drinking water.

India being an industrialized nation and in the path of becoming a developed nation is farfetched because there is little or no control on release of industrial efflux on freshwater sources resulting in aggregation of microplastics like low density polyethylene (LDPE), polyethylene terephthalate (PET), polystyrene (PS), polyvinyl chloride (PVC), polyurethane (PUR), polybutylene terephthalate (PBT) in freshwater sources [9]. On the basis of primary techniques like sieving and filtration microplastics in aquatic environment are predominantly classified on their size, shape, colour, and polymer type. Fourier transform infrared spectroscopy (FT-IR) is the most common spectroscopy used to identify polymer of microplastics based on their functional groups. Microplastic studies in India are mostly conducted on surface water and sediment sections of lake and river lacking substantial study in the arena of groundwater [16].

Appearance of microplastic in freshwaters of India is an emergent issue and is very recently explored. The principal source of microplastic contamination in freshwater is fragmentation, degradation and weathering of plastic debris like fishing ropes, pipes, synthetic textiles, it can also occur due to leakage of primary microplastic from cosmetic industries, runoff activities during rain and dry deposits in lakes. Latest studies have estimated that billion microplastics discharge into Bay of Bengal, Brahmaputra and Meghna river [16]. Wind patterns and wind velocity of cyclones and storms and moisture laden winds of South-West and North-East monsoon leads to accumulation and transportation of microplastic.

Indian economy being an agrarian one where 50% of the total work force is dependent on agriculture based work owing to high demand in the market, there is a pursuit of high productivity and increase the profit per unit of agricultural input hence excess pesticides are used which are polluting the freshwater sources long with microplastics. It's estimated that world accounts for 6.46 billion tons of plastic [9], due to insufficient waste management. The situation in India is censorious as source of microplastics are superabundant. This can be directly associated with the livelihood of huge Indian population. Microplastics have been recovered from different parts of the country.

- **Vembanad Lake** the largest brackish wetland ecosystem in Southern India. Microplastic particles were retrieved on sampling [17].
- **Dal Lake, Kashmir, India** contains microplastics. The lake serves many people as a means of income, whether they are fishermen, tourist guides or owners of Shikara boats which is attributed as the main reason for microplastic pollution [18].
- Floodplains of two gigantic population sustaining rivers of the world- **Ganga and Brahmaputra** carry microplastics as well as heavy metal pollution. Co-occurrence of microplastic and heavy metals can be attributed to the fact that microplastics act as a vector for heavy metal transportation, the heavy metals adsorb on microplastics, thus with trophic transfer it leads to bioaccumulation of both microplastics and heavy metals [9].

Microplastic pollution in Indian urban industrialized areas are equal to the rural contributes. Availability of safe and drinkable water continues to be an aspiration of rural population in parts of India. Maharashtra State Health Department has stated that 25% of the rural water available is unfit to drink. Traces of microplastic and microbial contamination have been found in the water bodies of rural India [19]. This can be attributed due to discharge of domestic sewage directly or indirectly into water bodies, agricultural run-off during rainy season containing chemical fertilizers and pesticides as well as effluents from agro-based industries and from day to day activities of bathing and washing.

In India, people suffering from different health issues in the coastal region and river banks can be mostly traced backed to microplastic pollution. Toxicity of microplastic creates a colossal modification of environmental compositions, biomagnifications and bioaccumulations in aquatic and terrestrial ecosystems. The abundance and characteristics of microplastics in the aquatic environment, the aquatic biota mistaking them for food, leads to a serious concern both for aquatic organisms and people who depend on them for food. Microplastics are generally found in seafood and copepods which harm their body functions, these microplastic contaminated seafood are a potential threat to human health. It was detected in the gut of the fish species in Tuticorin, the south east coast of India. Polystyrene in the soft tissues of *Pernavirdis* was found in the fishing harbor of Chennai [20].

The presence of heavy metals like Cd, Pb, Hg and Cr in the additives that are used extensively in the manufacture of plastics make microplastics more hazardous to the aquatic environment [21]. To avoid this problem of bioaccumulation the fish should be degutted before consumption.

Data on microplastic pollution is largely inadequate and is mostly confined to the regions of Tamil Nadu and Pondicherry. Extensive coastlines of Andhra Pradesh, Orissa, and West Bengal remain unexplored.

Tackling the unseen:Occurrence, transportation and effect of microplastic pollution has been discussed effectively. It requires better mastery over microplastics for control and removal strategies. Control of microplastics can be divided into three stages- (i) production stages, (ii) application stages and (iii) discharge stages.

(i) Production stage is involved in understanding the inauspicious effects of microplastic. The consciousness about single use plastic bags and microbeads are important sources of microplastic. Inadequate productions will reduce microplastic discharging in aquatic environment. Stopping the spread of microplastic pollution begins with holding the companies accountable who use plastic. While that requires government intervention and laws, proper industrial protocol to incorporate social responsibility, covering all the ethical, legal, and economic dimensions. Using more of biodegradable polymers or bio-based plastics rather than fossil-based plastics may help to limit microplastic pollution to some extent. Though, more detailed study is also needed on the toxicity of those biodegradable polymers or bio-based plastics.

(ii) Application stage strategies and **laws** have been furnished by different governments to lessen plastic applications. The policies involve in banning the sell of plastic bags, charging customers for light weight bags and imposing taxes from manufacturers, for example, Indian Central Government had implemented the "Plastic Waste Management Amendment Rules", 2021 for prohibiting all identified single use plastic items by 2022. Changes in washing behaviors, reduction in detergent dosage and recycling plastics in a sustainable way may reduce microfibers in aquatic environments.

Some remedies to control microplastics are –

- **Change in doing laundry**- the polyester is a cheap and versatile material popularly used in making t-shirt or yoga pants but clothing made from this plastic is one of the biggest sources of microplastic pollution in the world as well as in India. A single load of laundry can release more than 1 million microplastic fibers into the environment.
  Remedies- filters can be installed in a washing machine that catches microplastics. Traditional mode of hand washing reduces the microplastic pollution. Decreasing the amount of detergent in laundry led to substantial decrease in microfibers.
- **Buy clothes from natural materials-** instead of garments made of plastic; seek out brands that only use natural resources such as cotton, silk, wool, hemp and linen. Use of polyamide fabric with glycidyl-methaacrylate-modified pectin may reduce microplastic released by 90% on washing.
- **Stop using single use plastics-**buying reusable water bottle, tote bags for groceries, and multi-use straws.
- **Use public transportation-**as cars move on roads the tires break down and shed plastic particles due to wear and tear which accumulate in air.
- **Use of plastic free cosmetics-**lotions and skin creams often include plastic to promote absorption, while toothpastes and exfoliators often contain microbeads.

(iii) Discharge stage-after releasing microplastics into aquatic environment it becomes difficult to separate owing to their miniature size and very low concentration. Wastewater treatment plays a noteworthy role in controlling microplastic discharge into aquatic environments. Before tertiary treatment 88% of microplastics were removed and after tertiary treatment 97% were

removed [22]. Different removal technologies were used like-

Filtration-is used to separate solid plastic particles.

Density separation-isolation of microplastics from sediments, lighter microplastics float in upper layer.

Coagulation-due to small size suspended microplastics form unstable colloid on addition of coagulant for physical separation.

Agglomeration-formation of macromolecular networks can sustainably remove microplastics by hydrolysis and condensation.

Adsorption removal- removal of microplastics by using Zn-Al layered double hydroxide (LDH).

Oil film separation- for microplastic removal it is a hydrophobicity based method.

Froth flotation- achieved through a selective adherence of bubbles on target materials.

4. CONCLUSION

This society becomes increasingly plastic reliant since the initiation of commercial production began in 1950 [23]. Owing to their versatility, stability, light weight and low production costs have fueled global demand. The present estimation states that amount of microplastic in water bodies are predicted to double by 2030 [24]. Around the world, human produces an estimated 300 million tons of plastic waste every year, and at least 3.5% of it ends up in our water bodies [25].

Microplastic pollution sources can be traced back to products like tea bags, cloth washing and glitter. These pose a risk of trophic transfer in aquatic biota via ingestion, bioaccumulation and biomagnifications [3].

Recent studies have made us realize that we inhale and ingest microplastics round the clock during our daily lives. A study in 2019 by researchers at the University of New Castle found that "globally people might ingest an average of 5g plastic every week-equivalent to a credit card" [26]. The impact of this diet in our body is still poorly understood.

Chemicals used in plastics have, however been linked to a range of health problems including cancer, heart disease and poor fetal development, it can also cause oxidative stress, inflammation and respiratory problems [27]. One more concern is that plastics could carry pathogens which bind themselves to different materials. Though the proper health concern due to microplastic accumulation in human body is potentially undeciphered but sooner or later the consequences will be in front of our eyes [27]. Actions should be immediately taken in countries around the world and immediate ban should be imposed on single-use plastic products to get rid of this apparent miniature threat which with subsequent time can jeopardize the environmental harmony between biotic communities throughout the world. So plastic is not just a problem of the health of our environment but really a problem that concerns our own health.

Microplastic pollution should be dealt with concern and proper measures should be taken to control it at both individual and authoritative levels. We as individuals can cut down unnecessary use of plastic and shift more towards sustainable products. International concerns should be raised to discuss in global forums about the potential threat and possible measures to control this unforeseen threat. A strong governing body with international participation should be created immediately to overcome this grim situation as well as harsh retribution should be introduced in order to reform this potentially invincible threat in the name of microplastic.

ACKNOWLEDGEMENTS

We are thankful to Prof. Subir Chandra Dasgupta (HOD), Department of Zoology, Maulana Azad College for providing necessary facilities.

COMPETING INTERESTS

Authors have declared that no competing interests exist.

REFERENCES

1. Arthur C, Baker J, Bamford H. Proceedings of the international research workshop on ther occurrence, effects and fate of microplastic marine debris. Tacoma, WA, USA;2008.
2. Barnes DKA, Galgani F, Thompson RC, Barlaz M. Accumulation and fragmentation of plastic debris in global environments. Philos Trans R Soc Lond B Biol Sci. 2009;364(1526):1985-98.
3. Miller ME, Hamann M, Kroon FJ. 'Bioaccumulation and biomagnification of microplastics in marine organisms: A review and meta-analysis of current data'. PLoS on. 2020;15(10):e0240792.
4. Cera A, Cesarini G, Scalici M. Microplastic in freshwater: what is the news from the world? Diversity. 2020;12(7):1-19.

5. Vanapalli KR, Dubey BK, Bhattacharya J. Assessment of microplastic pollution in aquatic ecosystems-An Indian perspective. Case Studies in Chemical and Environmental. Engineering. 2021;3/100071:1-7.
6. WHO/UNICEF. Annual report of joint monitoring programme for water supply, sanitation and hygiene (JMP);2017. Available: https://washdata.org
7. Crawford CB, Quinn B. Plastic production, waste and legislation. In: Crawford CB, Quinn B, editors. Microplastic pollutants. Amsterdam: Elsevier Science. 2017;39-56.
8. Afrin S, Uddin MK, Rahman MM. Microplastics contamination in the soil from Urban Landfill site, Dhaka, Bangladesh.Uddin, and Md. M. Rahman. Heliyon. 2020;6(11):e05572.
9. Pandey D, Singh A, Ramanathan A, Kumar M. The combined exposure of microplastic and toxic contaminants in the floodplains of North India: a review. J Environ Manage. 2021;279:111557.
10. Paterson HL, Stead JL, Crutchett T, Hovey RK, Ford BM, Speldewinde P et al. Battling the known unknowns: a synoptic review of aquatic plastics research from Australia, the United Kingdom and China. Environ Sci Process Impacts. 2021;23(11):1663-80.
11. Lambert S, Sinclair CJ, Boxall ABA. Occurrence, degradation and effects of polymer based materials in the environment. Rev Environ Contam Toxicol. 2014;227:1-53.
12. GESAMP. Sources, fate and effects of microplastics in the marine environment: a global assessment. Joint Group Experts Sci Aspects Mar Environ Prot Rep Stud. 2015;90.
13. Shah AA, Hasan F, Hameed A, Ahmed S. Biological degradation of plastics: A comprehensive review. Biotechnol Adv. 2008;26(3):246-65.
14. Lechthaler S, Waldschläger K, Sandhani CG, Sannasiraj SA, Sundar V, Schwarzbauer J et al. Baseline study on microplastics in Indian Rivers under different Anthropogenic Influences. Water. 2021;13(12):1648.
15. Rodrigues MO, Abrantes N, Gonçalves FJM, Nogueira H, Marques JC, Gonçalves AMM. Spatial and temporal distribution of microplastics in water and sediments of freshwater system (Antua River, Portugal). Sci Total Environ. 2018;633:1549-59.
16. Vaid M, Sarma K, Gupta A. Microplastic pollution in aquatic environment with special emphasis on riverine systems: current understanding and way forward. J Environ Manage. 2021;293:112860.
17. Sruthy S, Ramasamy EV. Microplastic pollution in Vembanad Lake, Kerala, India: the first report of microplastics in lake and estuarine sediments in India. Environ Pollut. 2017;222:315-22.
18. Firdous J, Mathur YK, Jeelani M, Aziz A, Azmat S, Mudasir S. Preliminary studies on the microplastic pollution in Dal lake, Kashmir (first report). Adv Environ Res. 2020;9/4:275-84.
19. Amrutha K, Warrier AK. The first report on the source-to-sink characterization of microplastic pollution from a riverine environment in tropical India. Sci Total Environ. 2020; 739:140377.
20. Davis EK, Raja S. Sources and impact of microplastic pollution in Indian Aquatic Ecosystem: a review. Curr World Environ. 2020;15/1;Special Issue:01-9.
21. Zhou Y, Liu X, Wang J. Characterization of microplastics and the association of heavy metals with microplastics in suburban soil of central China. Sci Total Environ. 2019;694:133798.
22. Zhang Y, Jiang H, Bian K, Wang H, Wang C. A critical review of control and removal strategies for microplastics from aquatic environments. J Environ Chem Eng. 2021;9(4):105463.
23. Carpenter EJ, Smith KL. Plastics on the Sargasso sea surface. Science. 1972; 175(4027):1240-1.
24. Isobe A, Iwasaki S, Uchida K, Uchida K, Tokai T. Abundance of non-conservativemicroplastics in the upper ocean from 1957 to 2066. Nat Commun. 2019; 10(1):417.
25. Zhang Y, Gao T, Kang S, Shi H, Mai L, Allen D et al. Current status and future perspectives of microplastic pollution in typical cryospheric regions. Earth Sci Rev. 2022;226:103924.
26. Palanisami T. Plastic ingestion by people could be equating to a credit card a week; 2019. Newcastle University news. Available:https://www.newcastle.edu.au/newsroom/featured/plastic-ingestion-by-people-could-be-equating-to-a-credit-card-a-week.
27. Campanale C, Massarelli C, Savino I, Locaputo V, Uricchio VF. A detailed review study on potential effects of microplastics and additives of concern on human health. Int J Environ Res Public Health. 2020;17(4):1212.

Indian J. Applied & Pure Bio. Vol. 37(1), 135-149 (2022). **ISSN: 0970-2091**
A web of Science Journal

A study on the vegetative and flowering phenology including insect visitors of *Rhododendron arboreum* Sm. (Ericaceae Juss.) in Darjeeling Himalaya (India)-Phase-I

Subhasis Panda[1,2], Priyankar Roy[1] and Dipak Kumar Som[3]

[1]Angiosperm Taxonomy & Biodiversity Conservation Laboratory,
Department of Botany, Maulana Azad College (University of Calcutta), 8,
Rafi Ahmed Kidwai Road, Kolkata-700013 (India)
Email: bgc.panda@gmail.com (Principal Investigator & JRF)
[2]Biodiversity Conservation Laboratory, Government General Degree College, Chapra
(Kalyani University), Village, Shikra, PO. Padmamala, Nadia-741123 (Present posting).
[3]Division of Entomology, Post-Graduate Department of Zoology, Maulana Azad College, 8,
Rafi Ahmed Kidwai Road, Kolkata-700013 (India)
Email: dipaksom@gmail.com (Co-Principal Investigator)

Corresponding Author: bgc.panda@gmail.com

Abstract

During field studies at different places of Darjeeling Himalaya including Singalila National Park since May 2019 till February 2021 under State Government-funded Major Research Project, an attempt was made to assess the diversity of vegetative phenology and insect visitors reflecting flowering phenology of *Rhododendron arboreum* Sm.

During field studies at different places of Darjeeling Himalaya including Singalila National Park since May 2019 till February 2021 under DST & BT-funded major Research Project, an attempt was made to assess the diversity of vegetative phenology and insect visitors reflecting flowering phenology of *Rhododendron arboreum* Sm. in and around Singalila National Park as well as in other localities of Darjeeling hills. Flowering phenological data include inflorescence nature, number of flowers per rachis, colour change observation in all flowers, bracts/bracteoles-nature & number, indumentums/scales, presence of any mucilage like substances/not, flowering time, flower-buds to flower formation duration, flower colour and colour change, odour if any, floral parts in detail, calyx-nature, colour, union, indumentums etc., corolla-nature, indumentums, colour, inside colour markings for pollinator path etc., stamens-nature, number, size, colour, anther lobes nature etc., bracts/bracteoles—nature, number, colour; fruiting (duration, colour, maturity etc, persistent/not), seeds, insect flower visitors and pollination time.

Besides flowering phenology, variation in different vegetative phenological features

for a particular locality are also studied along with leaf and bark associates and their specificity to this species. Vegetative phenological data include nature of habit, indumentums/scales if any, nature of axillary and terminal buds, leaf phyllotaxy, leaf-colour (both surface), leaf-nature, indumentums/ scales types, size-range, petiole ranges, leaf galls/protuberances, number of individual plants per locality.

For insect visitor study, a range of different sampling methods have been employed with special reference to net sweeping, aspiration sampling and pan trap sampling. Each of sampling has its own effectiveness based on time, location and accessibility to resource of flowering plants. In net sampling, the number and type of visiting insects were recorded from 08:00 to 16:00 h on sunny days during the flowering season at altitudes ranging from 2500 m – 3636 m at different places of Darjeeling hills. Vegetation of *R. arboreum* flowering plants was selected for pan trap sampling at BK Bhanjang, 2 km down Sandakphu. A combination of red, yellow and blue pans was set from 10.00 to 10.00 h. The vast array of insects belonging to orders Hymenoptera, Thysanoptera, Coleoptera and Diptera is the indicative of flowering phenology of *Rhododendron arboreum* Sm. in Singalila National Park of Darjeeling Himalaya. Out of these orders, Diptera and Coleoptera were considered as the most diversed groups. The order Diptera is represented by two sub-orders Nematocera and Brachycera. Out of these two groups, Nematocera was observed to be more diversed in number and forms. Among the Coleopteran families notable flower visitors are Coccinellidae, Elateridae, Scarabeidae, Nitidulidae, Dermestidae, Phalacridae and Tipulidae. Adaptive modifications of these minute sized beetles have also been noted to find their suitability in the extraction of nectar from flowers of *R. arboretum* so far studied. Very interestingly, a few Collembolan hexapods have been found from the pan trap sample of *Collembola* having unknown association with *Rhododendron arboreum*.

Probably J. D. Hooker[11] was first to explore the present area extensively in April-August, 1848 during his voyage to the Himalayas and he published "*The Rhododendron of Sikkim Himalayas*" in 1849, in which Darjeeling-Kalimpong areas was included under Sikkim. Since Hooker, several other workers like C. B. Clarke[5], Hara[10], Biswas[2], Mukherjee[14], Pradhan & Lachungpa[16], Long[13], Das[6,7], Chhetri *et al.*[4], Bhattacharyya & Sanjappa[1], Rai *et al.*[18], Ghosh & Mallick[9], Panda & Kirtinia[15] surveyed the area and documented floristic elements in various ways, but very little or no investigations regarding vegetative and floral phenology and flower visitors were made.

For Phenological Studies: Relevant Taxonomic references and herbarium specimens consultation were done in CAL (Central National Herbarium), BSIS (Industrial Section Indian Museum, Kolkata), Lloyd Botanical Garden Herbarium, Darjeeling for preliminary information and species identification purpose. Field visits are carried out at the end of every month for the same taxon at different areas of Darjeeling Himalayas. Phenological data include nature of ***Stem***-bark, stem-bark-associated plants like mosses, leafy liverworts etc., branch-stem nature, indumentums/scales if any, ***leaves***-colour (both surface), indumen-

tums/scales types, size-range, then their leaf nature, leaf-associated bryophytes *etc*., ***inflorescence*** nature, number of flowers per rachis, colour change observation in all flowers, bracts/bracteoles-nature & number, indumentums/scales, presence of any mucilage like substances/not, ***flowering*** (time of beginning, peak & end—duration), flower-buds to flower formation duration, flower colour and colour change, odour if any, flowering time change if any (early or late) if unusually flower in other season, unusual flower nature in detail, floral parts in detail, *calyx*-nature, colour, union, indumentums *etc*., *corolla*-nature, indumentums, colour, inside colour markings for pollinator path *etc*., *stamens*-nature, number, size, colour, anther lobes nature, colour, indumentums *etc*., *flower-nectar in detail*; ***Bracts/ bracteoles***—nature, number, colour; fruiting (duration, colour, maturity etc, persistent/not), maturity of seeds after how many days of fruit formation, fruit is formed/not, nature of seeds, time of inflorescence emergence (from main or branch shoot), flower visitors (only type viz., insect/birds/butterfly/moth etc) and pollination time. Field data are written on specially prepared Field Note Book along with GPS data for each taxon available at different localities/ single locality. Live photography were done for different populations using CANON 1500D DSLR Camera along with its Micro lens. Each and every parts were also studied under Dissecting Binocular Microscope for detailed study purpose in the Laboratory of Maulana Azad College, Kolkata.

Descriptive terminology for Phenological-morphology followed Lawrence[12], Featherly[8], Stearn[19], Radford[17] and Veldkamp in Vogel[20] and Chamberlain *et al*.[3]. Botanical identity will be confirmed with consulting herbarium specimens in Central National Herbarium (CAL), Online Type images (Kew Herbarium) and relevant Taxonomic References. Important voucher specimens are deposited in the laboratory of Angiosperm Taxonomy, Botany Deptt., Maulana Azad College, Kolkata, also one sample specimen will be deposited in CAL.

Flower visitors: As variations in the flowering phenology of *Rhododendron* spp. are greatly reflected by the diversity of insect pollinators, and major Insects (usually belong to orders Hymenoptera, Diptera and Lepidoptera) visiting the flowers also showing temporal variation in the flowering season, two commonly used sampling methods are employed for collecting such pollinators----pan traps and net sweeping which are considered to be effective at capturing the most species and highest abundance of pollinators.

Net sweeping*:* Flower-visiting invertebrates were to be sampled along each 100 m 65 m belt transect. Four collectors were deployed among the eight transects at each site: two at each location. Collectors were sampled flower-visitors using nets from all plant species along transects for two hours and fulfilled these conditions: concurrent sampling of crest and swale between collectors. Each transect would be sampled for 30 minutes by each collector. These measures would help to negate any effect of collector's bias. Flower-visitors were then be caught using nets and plastic containers, and were transferred into 5 ml vials for transportation. Net sampling at each site were conducted for three consecutive days in morning and afternoon sessions, the timing of which might be varied to best match

the activity patterns of invertebrates. To increase the representation at the transect and above levels, and to minimise any potential effects of weather on captures, sampling were performed during fine weather, and pooled over the three day period. Sites were sampled in random order for each survey.

***Pan traps**:* Pan Traps were deployed along each 100 m transect at B.K. Bhanjang from 10.00 am to 10.00 am (24 hours). Pans are made from polyethylene plastic bowls (400 ml, 110 mm diameter, 70 mm high) painted in either UV fluorescent yellow, blue or white paint. These colours are equally effective for capturing of a broad range of invertebrates. Six pans (two of each colour) were to be placed along each transect, 15 m apart, in alternating colours. In each pan we placed 100 ml of detergent mixture (5 ml of non-odorous detergent in 1.5 litre water). Pans were checked and cleared of captures after 24 hours at 10.00 am of the next day. Specimens were stored in 70% ethanol for microscopic study.

Table-1. Collection no, locality, time, altitude, habit-habitat of *R. arboreum* Sm. in Darjeeling Himalaya

Coll No.	Place of Collection	Month of Collection	Altitude (m)	Habit	Habitat
49	T.N. Road, Alubari	July	2257	Tree	Loose Rocky soil
50	T.N. Road, Alubari	July	2257	Tree	Loose Rocky soil
52	Jungle Busty	JUly	2045	Tree	Rocky soil
54	Jungle Busty	July	2063	Tree	Near Jhora
55	Jungle Busty	July	2063	Tree	Loose Rocky soil
60	Tumling	July	2937	Tree	Rocky soil
65	Tumling	July	2993	Tree	Loose Rocky soil
70	Bhutta Kheti, Sonada	July	1814	Tree	Loose Rocky soil
71	Darjeeling Mall Road	July	1898	Tree	Rocky soil
77	Rambhi Busty	August	2205	Tree	Near Jhora
89	Betw Kayakatta & Kalpokhari	September	2897	Tree	Rocky soil
95	1km above BKB	September	3190	Tree	Hill slopes
96	1.1 km above Gairibas to Sandakphu	September	2968	Tree	Hill slopes
100	Sandakphu-Gurudum road	September	3361	Tree	Rocky soil
84	1km above Gairibas to Sandakphu	September	2608	Tree	Loose Rocky soil
93	Between Kalpokhari and BKB	September	3065	Tree	Loose Rocky soil

Field Images Of Vegetative, Flowering & Fruiting Phenology Of *Rhododendron Arboreum* In Darjeeling Himalaya:-

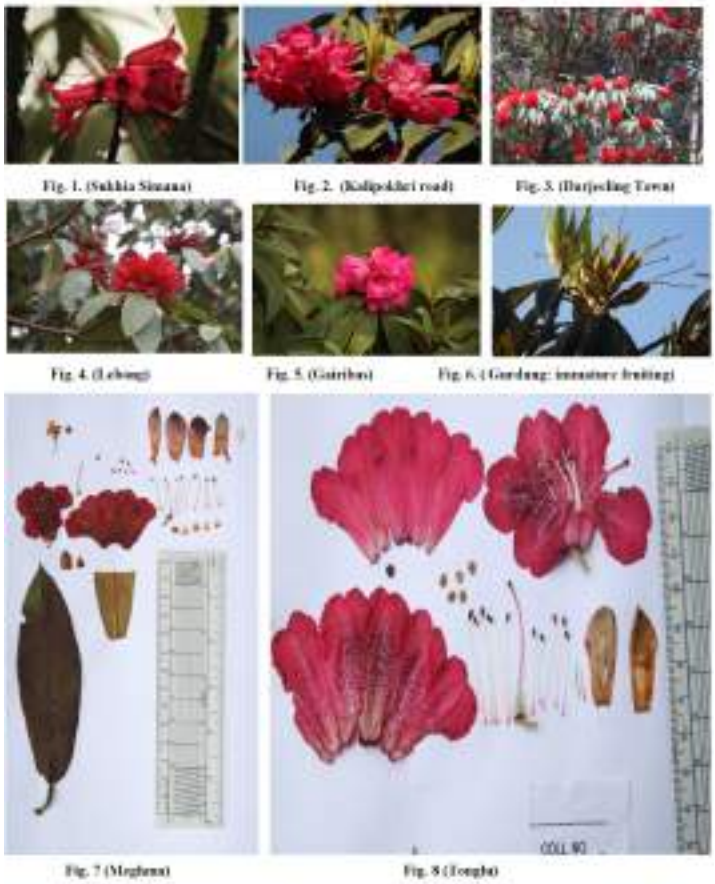

Figs.1-8. Flowering phenology observation in *R. arboreum* subsp. *arboreum* in Darjeeling in May, 2019.

Fig. 9 (near Sandakphu) Fig. 10 (near Sandakphu) Fig. 11 (Sandakphu-Phalut Road)

Figs.9-11: Flowering phenology observation in May, 2019

Fig.12 Fig. 13 Fig. 14 Fig. 15

Figs.12-15: Fruiting phenology & Lichen-association with stem observed along BK Bhanjyang-Sandakphu Road in Sept. 2019.

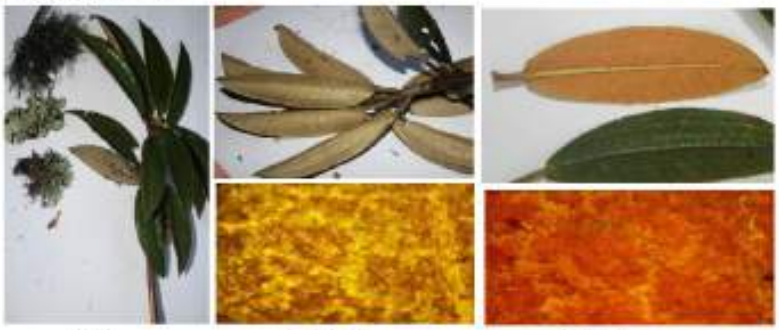

Fig. 16 Figs.17-18 Figs.19-20

Fig.16. Lichen-association observation at Kalipokhri-BK Bhanjyang Road in Sept. 2019. Figs.17-18: Leaf abaxial surface showing golden yellowish scales observed at BK Bhanjyang in Sept. 2019. Figs.19-20: Leaf abaxial surface showing brownish scales observed at Sandakphu-Gurdung Road in Sept. 2019.

Figs.9-20. *R. arboreum* subsp. *cinnamomeum* var. *cinnamomeum* in Darjeeling Himalaya in May-September, 2019 (Kalipokhri-BK Bhanjang-Sandakphu-Gurdung).

Fig. 21 Fig. 22 Fig. 23 Fig. 24

Figs.21-23: Flowering phenology observation at Tonglu in May, 2019; Fig. 24. Fruiting phenology observation at Tonglu in Sept. 2019.

Fig. 25 (Tumling) Fig.26 (BK Bhanjyang) Fig.27 (BKB) Fig.28 (BKB)

Figs.25-28: Flowering phenology observation in May, 2019

Fig.29 Fig.30 Figs.31-32 Fig.33

Figs.29-33: Lichen-Bryophyte-Pteridophytic association with stem observed at Tumling in Sept.19

Figs.21-33. *R. arboreum* subsp. *cinnamomeum* var. *roseum* in Darjeeling Himalaya in May-September, 2019 (Tonglu-Kalipokhri-BK Bhanjang).

Figs. 34-35. Insect visitors observed at Kalipokhri in May 2019

Fig. 36. Family: Tipulidae (Crane fly); **Fig. 37**. Family: Tipulidae; **Fig. 38**. Family: Coccinalidae

Figs. 34-38. Insect visitors observed in *R. arboreum* subsp. *cinnamomeum* var. *roseum* in and around Kalipokhri-B.K. Bhanjyang Road based on NET SWEEPING

Fig. 39. Insect visitors observed in *R. arboreum* subsp. *cinnamomeum* var. *cinnamomeum* in and around Kalipokhri-B.K. Bhanjyang Road based on PAN TRAP & NET SWEEPING

Fig. 40. Insect visitors observed in *R. arboreum* subsp. *arboreum* in and around Kalipokhri-B.K. Bhanjyang Road based on NET SWEEPING

Table 2. Height, girth & colour of stem, bark association & phyllotaxy of *R. arboretum* in Darjeeling Himalaya:-

Coll No.	Height (m)	Girth of Stem	Color of Stem	Bark association	Phyllotaxy
49	3m	42cm	Redish Brown	BR., PT., LI.	Sub-alternate
50	4.5m	36cm	Redish Brown	BR., LI.	Sub-alternate
52	6m	68cm	Redish Brown	BR., PT., LI.	Sub-alternate
54	3m	60cm	Brown	BR., PT., LI.	Sub-alternate
55	7.5m	140cm	Brown	BR., PT., LI.	Sub-alternate
60	3m	77cm	Redish Brown	BR., LI.	Sub-alternate
65	6m	103cm	Redish Brown	BR., PT., LI.	Sub-alternate
70	7m	120cm	Redish Brown	BR., PT., OR.	Sub-alternate
71	3.5m	64cm	Brown	BR., PT., OR.	Sub-alternate
77	2m	72cm	Redish Brown	LI.	Sub-alternate
89	2.5m	52cm	Redish Brown	LI.	Sub-alternate
95	4.5m	125cm	Redish Brown	BR., LI.	Sub-alternate
96	2.5m	32cm	Redish Brown	BR.	Sub-alternate
100	5.25m	97.5cm	Brown	LI.	Sub-alternate
84	4m	97cm	Light Brown	BR.	Sub-alternate
93	4.5m	115cm	Light Brown	BR., LI.	Sub-alternate

BR=Bryophyte; PT=Pteridophyte; LI=Lichen; OR=Orchid

Table 2. Localities like Table 1

In the first phase, present work embodies 19 populations of *R. arboreum* including its two subspecies viz., subsp. *arboreum* and subsp. *cinnamomeum* studied and documented from 19 different localities in Darjeeling Himalaya (vegetative phenological data were documented from 16 populations and flowering phenological data were documented from 3 other populations). 10 vegetative and 12 floral characters including character-states were observed and documented from the said localities (Table 1 – 14). Following 14 tables show comparative vegetative, floral, fruiting and insect visitors diversity in 19 populations of *R. arboreum* Sm. Data were collected in respect to stem and leaf indumentum, leaf-size, shape, colour, venation, scales, petiole nature, stem-colour, bark, bud-scales and branches, axillary and terminal branching, leaf & bark-association *etc*.

Table 3. leaf apex, margin, surfaces, length & breadth of *R. arboreum* in Darjeeling

Lf apex	Lf margin	Lf surface ad	Lf surface ab	Lf length	Lf breadth
Mucronate	Entire	Glabrous	Dense brown scales	79-128mm	20-38mm
Mucronate	Entire	Glabrous	Silver scales	84-170mm	24-45mm
Acuminate	Entire	Glabrous	Silver brown scales	58-106mm	20-32mm
Acuminate	Entire	Glabrous	Silvery white hairs	85-140mm	20-41mm
Mucronate	Entire	Glabrous	Silvery white hairs	62-155mm	16-58mm
Mucronate	Entire-wavy	Glabrous	greenish-white scales	46-75mm	16-40mm
Acuminate	Entire-wavy)	Glabrous	Silver brown scales	64-136mm	17-47mm
Mucronate	Entire	Glabrous	Silvery White scales	118-154mm	28-39mm
Mucronate	Entire	Glabrous	Silvery White scales	34-110mm	11-27mm
Mucronate	Entire	Glabrous	Silvery white scales	72-100mm	15-30mm
Mucronate	Entire	Glabrous	orange-brown scales	58-128mm	17-38mm
Mucronate	Entire	Glabrous	Orange-brown scales	82-100mm	26-55mm
Acute	Entire	Glabrous	light brown scalers	86-111mm	18-28mm
Mucronate	Entire	Glabrous	Brownish scales	67-104mm	22-34mm
Acute	Entire	Glabrous	Light brown scales	42-104mm	14-31mm
Mucronate	Entire	Glabrous	Light brown scales	42-83mm	16-27mm

Lf=Leaf; ad=adaxial surface; ab=abaxial surface

Table 3. Coll no. & Localities like Table 1

Table 4. Petiole length and indumentum of *R. arboreum* in Darjeeling

Coll No.	Adaxial petiole	Abaxial Petiole	Petiole length
49	Red, brown scales		10-20mm
50	Light green, glabrous	Light green to Yellow scales	10-18mm
52	Brown scales	Light green to Sparsely silver scales	7-19mm
54	Light green-whitish scales	Light green to sparsely brown scales	4-13mm
55	Light green-whitish scales	Green to slightly white scales	7-25mm
60	Greenish-brown, glabrous	brown-green to green-white scales	10-11mm
65	Yellowish green, glabrous	Light green to silver brown scales	10-18mm
70	Light green, glabrous	Green, Silver scales	5-7mm
71	Greenish-white scales	Green, Brown scalers	15-20mm
77	Green, glabrous	Silver-white dense scales	10-15mm
89	Light green to brown scales	Light green to brown scales	15-20mm
95	Green, glabrous	Light Green to brown scales	15-17mm
96	Green, brown scales	Green-Brown scales	18-20mm
100	Green, Brownish scales	orange-brown scales	16-23mm
84	Green, Reddish Brown scales	Greenish scales	16-20mm
93	Reddish brown scales	Light green to brown scales	17-23mm

Table 4. Localities like Table 1

Table 5. Altitudinal height-girth variation of stems of *Rhododendron arboreum* subsp. *arboreum* in Darjeeling Himalaya

Coll No.	Month	Altitude (m)	Habit	Habitat	Girth of St	Height of St	Height/ Girth
49	July	1814	Tree	hilly slope	120cm	700cm	5.83
50	July	1898	Tree	moist open rocky soil	64cm	350cm	5.46
52	July	2045	Tree	shaded rocky soil	68cm	600cm	8.82
54	July	2063	Tree	near Jhora	60cm	300cm	5
55	July	2063	Tree	loose open rocky soil	140cm	750cm	5.35
60	August	2205	Tree	near Jhora	72cm	200cm	2.77
65	July	2257	Tree	loose open rocky soil	42cm	300cm	7.14
70	July	2257	Tree	loose wet rocky soil	36cm	450cm	12.5
71	Sept.	2608	Tree	loose wet rocky soil	97cm	400cm	4.12
77	Sept.	2897	Tree	open moist rocky soil	52cm	250cm	4.8
89	July	2937	Tree	open moist rocky soil	77cm	300cm	3.89
95	Sept.	2968	Tree	hilly slopes	32cm	250cm	7.81
96	July	2993	Tree	loose rocky soil	103cm	600cm	5.82
100	Sept.	3065	Tree	loose rocky soil	115cm	450cm	3.91
84	Sept.	3190	Tree	hilly slopes	125cm	450cm	3.6
93	Sept.	3361	Tree	loose wet rocky soil	97.5cm	525cm	5.38

Localities like Table 1.

FLOWERING PHENOLOGY

Table 6. Flowering phenology of *Rhododendron arboreum* in Darjeeling Himalaya: Part A

Name of the species	Coll no.	Locality	Fl bract	No of fl/ infl
R. arboreum subsp. *cinnamomeum*	14	Kalapokhari	2-3: 16-18mm long	8-flowered
R. arboreum subsp. *cinnamomeum var. roseum*	41	Sandakphu-BKB	1: 16-20mm long	12-14-flowered
R. arboreum subsp. *arboreum*	3	Sukhia Simana	6-7: 14-18mm long	12-flowered

Fl=flowers; infl=inflorescence

Table 7. Flowering phenology of *Rhododendron arboreum* in Darjeeling Himalaya: B

Name of the species	corolla colour	corolla scent	corolla shape	corolla size
R. arboreum subsp. *cinnamomeum*	rose-purple red	Not-scented	tubulo-campanulate	38-46x35-38mm
R. arboreum subsp. *cinnamomeum var. roseum*	Rose-red	Not-scented	tubulo-campanulate	32-40x28-34mm
R. arboreum subsp. *arboreum*	Blood red	Not-scented	tubulo-campanulate	45x50mm

Table 7. locality and coll no similar to Table 6

Table 8. Flowering phenology of *Rhododendron arboreum* in Darjeeling Himalaya: Part C

Name of the species	corolla indumentum	calyx length	calyx indumentum	calyx color
R. arboreum subsp. *cinnamomeum*	Glabrous	1mm	glabrous	purple red
R. arboreum subsp. *cinnamomeum var. roseum*	Smooth	1mm	glabrous	rose-red
R. arboreum subsp. *arboreum*	Smooth	1.5mm	apical hairy	pinkish-green

Table 8. Coll no. & locality similar to Table 6

Table 9. Flowering phenology of *Rhododendron arboreum* in Darjeeling Himalaya: Part D

Name of the species	No of Stamens	Length of Stamens	Length of Filaments	Filament Indumentum
R. arboreum subsp. *cinnamomeum*	10 (-8)	18-34mm	16-32mm long	Glabrous
R. arboreum subsp. *cinnamomeum var. roseum*	10	10-32mm	7.5-29mm long	Glabrous
R. arboreum subsp. *arboreum*	8	26-37mm	25-36mm long	Glabrous

Table 9. Coll no. & locality similar to Table 6

Table 10. Flowering phenology of *Rhododendron arboreum* in Darjeeling Himalaya: Part E

Name of the species	colour of filament	anther length	anther colour	Anther indumentum
R. arboreum subsp. *cinnamomeum*	light purple	2mm long	Brown	Glabrous
R. arboreum subsp. *cinnamomeum var. roseum*	white to light pink	2.5mm long	Dark brown	Glabrous
R. arboreum subsp. *arboreum*	white with basal pink	1mm long	Dark brown	Smooth

Table 10. Coll no. & locality similar to Table 6

Table 11. Flowering phenology of *Rhododendron arboreum* in Darjeeling Himalaya: Part F

Name of the species	pistil length	Ovary size	Ovary shape	Ovary colour	Ovary indumentum
R. arboreum subsp. *cinnamomeum*	42mm long	5-6x3mm	oblong	white	tomentose
R. arboreum subsp. *cinnamomeum var. roseum*	36mm long	6x3mm	oblong	light green	tomentose
R. arboreum subsp. *arboreum*	42-43mm	7-8x3mm	oblong green	light	tomentose

Table 11. Coll no. & locality similar to Table 6

Table 12. Flowering phenology of *Rhododendron arboreum* in Darjeeling Himalaya: Part G

Name of the species	Style length	Style colour	Stigma
R. arboreum subsp. *cinnamomeum*	32-34mm	purple red	dark purple
R. arboreum subsp. *cinnamomeum var. roseum*	30mm	light green	dark red
R. arboreum subsp. *arboreum*	35mm	purple pink	purple

Table 12. Coll no. & locality similar to Table 6

Table 13. Fruiting phenology of *R. arboreum* in Darjeeling Himalaya

Coll no.	Locality	Time	Fr colour (mature)	Fr colour (immature)	Fr indum	Fr length	Fr breadth
	Fruiting phenology of *R. arboreum* subsp. *arboreum* in Darjeeling						
49	T.N. Road, Alubari	July	green	brown	yellow hairs	25mm	8mm
50	T.N. Road, Alubari	July	green	brown	white hairs	20mm	6mm
52	Jungle Busty	July	light green	brown	brown hairs	25mm	11mm
54	Jungle Busty	July	light green	brown	white hairs	28mm	5mm
55	Jungle Busty	July	light green	brown	white hairs	26mm	7mm
60	Tumling	July	not found	not found	not seen	N/F	N/F
65	Tumling	July	light green	brown	not seen	33mm	7mm
70	Bhutta Kheti, Sonada	July	green	brown	white hairs	10mm	3mm
71	Darjeeling Mall Road	July	green	dark brown	not seen	15mm	7mmm
77	Rambhi Busty	Aug	N/F	N/F	not seen	N/F	N/F
	Fruiting phenology of *R. arboreum* subsp. *cinnamomeum* var. *cinnamomeum* in Darjeeling						
89	Kayakatta to Kalpokhari	Sept.	green	brown	white hairs	7mm	7mm
95	BKB to Sandakphu	Sept.	red-green	brown	reddish hairs	7mm	7mm
96	Gairibas to Sandakphu	Sept.	green	brown	brown hairs	8mm	8mm
100	Sandakphu-Gurdum	Sept.	green	brown	white hairs	7mm	7mm
	Fruiting phenology of *R. arboreum* subsp. *cinnamomeum* var. roseum in Darjeeling						
84	Gairibas to Sandakphu	Sept.	green	brown	red hairs	8mm	8mm
93	Kalapokhari to BKB	Sept.	not seen	not seen	not seen	not seen	not seen
	Fr=fruit; indum=indumentum;						

Table 14. Insect Flower Visitors: Following Orders & Families observed in *R. arboreum* subsp. *arboreum*, subsp. *cinnamomeum* var. *cinnamomeum* and var. *roseum* in Kalipokhri-BK Bhanjyang Road based on PAN TRAP & NET SWEEPING.

Sl no.	Order	Family
1.	Hymenoptera	Apidae
2.	Coleoptera	Phalacridae
3.	Coleoptera	Coccinalidae
4.	Thyasanoptera	Phaleotripidae
5.	Coleoptera	Scarabaeidae
6.	Coleoptera	Scarabaeidae
7.	Coleoptera	Scarabaeidae
8.	Diptera	Calliphoridae
9.	Hymenoptera	Apidae
10.	Coleoptera	Nitidulidae
11.	Diptera	Tipulidae
12.	Hymenoptera	Apidae
13.	Coleoptera	Elataridae
14.	Coleoptera	Nitidulidae
15.	Coleoptera	Elataridae
16.	Coleoptera	Dermestidae
17.	Coleoptera	Phalacridae

#Genus and Species level identification is under process in ZSI

Detailed vegetative and floral phenological data of *R. arboreum* Sm. based on 19 different local natural populations in Darjeeling Himalaya may help to understand range of variation as well as the raw materials for climate change study when these will compare with past data (if and when available). Documentation of insect flower visitors including specific pollinators of *R. arboreum* Sm. are urgently required for biodiversity as well as *Rhododendron* conservation, not only in Darjeeling but also throughout Indian Himalayas. This work will be a raw material cum model for future climate change study not only in *Rhododendron* but also for other plants in respect to biodiversity conservation.

We are thankful to Department of Science & Technology and Biotechnology, Govt of West Bengal for providing financial assistance to carry out this project. We are also grateful to Dr. Subhasis Dutta, Principal of Maulana Azad College for providing necessary help during field trip to Singalila National Park, to PCCF Wildlife Warden, Govt of West Bengal for kind permission to survey the National Park and to DFO Wildlife Warden, Darjeeling for his valuable suggestions and cooperation during field survey.

References :

1. Bhattacharyya, D. and M. Sanjappa, (2014). *Rhododendron arboreum* Sm. In: Sanjappa, M. and A.R.K. Sastry (Eds.), Fascicles of Flora of India: Fascicle 25 Ericaceae. pp. 87. *Botanical Survey of India, Kolkata*.
2. Biswas, K.P. (1966). Plants of Darjeeling and Sikkim Himalayas. pp. 540. Calcutta.
3. Chamberlain, D.F., R. Hyam, G. Argent, G. Fairweather, and K.S. Walter, (1996). The genus *Rhododendron*: Its classification and synonymy: 1-184. Royal Botanic Garden, Edinburgh.
4. Chhetri, D.R., D. Basnet, P.F. Chiu, S. Kalikotay, G. Chhetri, and S. Parajuli, (2005). *Current Sci*. *89*(2): 264-268.
5. Clarke, C.B. (1882). Ericaceae. In Hooker, J.D., Flora of British India, vol. 3. pp. 465, Reeve & Co., London.
6. Das, A.P. (2004). Floristic Studies in Darjeeling Hills. *Bull. Bot. Surv. India 43* (1-4): 1-18.
7. Das, A.P. (1995). Diversity of angiospermic flora of Darjeeling hills. In *Taxonomy and Biodi*versity (ed. A.K.Pandey), pp. 118-127. CBS Publishers and Distributors, New Delhi.
8. Featherly, H. I. (1954). *Taxonomic Terminology of the Higher Plants*. pp. 1-166. Ames, Iowa, USA.
9. Ghosh, D. K. and J. K. Mallick, (2014) *Rhododendron cinnabarinum* Hook. f. Flora of Darjeeling Himalaya and Foothills (Angiosperms). Bishen Singh Mahendra Pal Singh, Dehra Dun. pp. 199.
10. Hara, H., (1966). The Flora of Eastern Himalaya – Results of the Botanical Expedition to Eastern Himalaya organized by the University of Tokyo, 1960 – 1963. 1st Report. pp. 1-744. University of Tokyo Press, Japan.
11. Hooker, J.D. (1849). *J. Asiat. Soc. Bengal 18:* 419-449.
12. Lawrence, G.H.M. (1951). *Taxonomy of Vascular Plants.* pp.1-823. Macmillan

Co., New York, USA.

13. Long, D.G. (1991). Ericaceae. In: Grierson, A.J.C., Long, D.G. (eds.), Flora of Bhutan *2*(1): 372. Royal Botanic Garden, Edinburgh.
14. Mukherjee, A. (1988). *Flowering Plants of Darjeeling*. Pp. 1-287. Atma Ram & Sons, Delhi.
15. Panda, S. and I. Kirtania, (2016). Variation in *Rhododendron arboreum* Sm. complex (Ericaceae): Insights from exomorphology, leaf anatomy and pollen morphology. *Modern Phytomorphology 9:* 27-49.
16. Pradhan, U.C. and S.T. Lachungpa (1990) Sikkim Himalayan *Rhododendons*. Primulaceae Books, Kalimpong, Darjeeling, India. pp. 75.
17. Radford, A.E. (1986). Ericaceae. *Fundamentals of Plant Systematics*. pp. 365-367. Harpers & Row, New York, USA.
18. Rai, U., D. Lama, N. Thapa, and S. Rai, (2013) *Pleione 7* (2): 434. 2013.
19. Stearn, W.T. (1983). *Botanical Latin*.pp. 1-541. 3rd revised ed. David & Charles Inc., USA.
20. Veldkamp, J.F. (1987). *Manual for the description of Flowering Plants*. In: Vogel, E. F., Manual of Herbarium Taxonomy: Theory and Practice: UNESCO Regional Office, Jakarta (Indonesia).pp. 20 – 64.

Volume 66, Issue 5, 2022
Journal of Scientific Research
Institute of Science,
Banaras Hindu University, Varanasi, India.

Next Generation Antivenoms and Their Neutralizing Efficacy against Snakebite Envenoming

Pradip Bhattacharjee[1*], Sanjukta Manna[2], Subir Chandra Dasgupta[3]

[*1]Department of Zoology, Maulana Azad College, Kolkata-700013, India, Email- pradip21@iisertvm.ac.in
[2]Department of Zoology, Maulana Azad College, Kolkata-700013, India, Email- Sanjukta_manna@rediffmail.com
[3]Department of Zoology, Maulana Azad College, Kolkata-700013, India, Email- subirdgupta@gmail.com

Abstract:**Snake envenomation is a major neglected tropical disease and remains a serious threat in many countries at the present day. The impoverished rural populations are vulnerable to snakebite envenoming which eventually strengthens the cycle of poverty. The highly diversified components of snake venoms are primarily responsible for severe clinical manifestations in the victim. The only available treatment is the use of animal-derived broad-spectrum polyvalent antivenoms having a very low level of case-specific antibodies. A significant number of drawbacks of this antivenom are possessing a key challenge in snakebite treatments. The recent advancements into the toxin-specific monoclonal antibodies proved to be promising for future envenoming treatments, although its use is still in a naïve stage since it also holds some limitations in neutralizing the complex snake venoms. In the emerging fields of molecular biology along with transcriptomic and proteomic analysis protocols, the snake venom constituents have been well characterized and this holds another promising approach to using DNA immunization for next-generation therapeutics. This strategy is more compatible with the human immune system and exerts the least adverse effects. In this review, the comparative analysis of present polyvalent antivenom and future therapeutic protocols has been discussed.**

Index Terms:**Antivenom, Envenomation, Recombinant, Therapeutics, Toxicity.**

I. INTRODUCTION

Envenomation caused by snakes is one of the major problems in tropical countries and is considered a 'neglected tropical disease'. An estimated extent of snakebites occurring per year in the world is within the range of 1.8 to 2.7 million. India ranks first in the number of deaths occurring due to snakebites, with an average of 50,000 per year ((Chippaux, 2017; Mohapatra et al., 2011). The increasing human-snake conflict in tropical countries and lack of efficiency in the proper diagnosis of snakebite is causing an elevation in the number of victims globally.The detrimental consequences of such cases include economic degradation in the families of snakebite victims, mental health implications in the survivors with an increased risk of depressive and post-traumatic stress disorders (Williams et al., 2019). Lack of proper knowledge about snakes and snakebite imparts one of the major inhibitors of improving snakebite victims.Neglecting or postponement of the initiation of treatment can lead to several health issues such as tissue necrosis, amputation, and compartmental syndromedepending on the type of snake and its venom composition. Thus, snakebite is not only a public health issue but also one of the major reasons for socioeconomic degradation. The significant numbers of mortality along with other public health concerns are due to the action of snake venoms which are cocktails of toxic and non-toxic constituents. The toxic components contain both enzymatic and non-enzymatic molecules affecting different organ systems of the victim leading to its death (Alangode et al., 2020).

Upon incorporation of snakebite as a 'neglected tropical disease' by WHO, it has been a focus to look at with strategic improvements in its defensefrom both educational and medical facilities. Currently, 22 countries from the 5 continents are involved in the resolution of fighting against this so-called 'disease of the poor', and it has been taken into action at the 71st World Health Assembly.Data from a global survey from 2020 showed the presence of 22 antivenom manufacturers for 65 distinct products, but the availability and gross yearly production are unclear (Potet et al., 2021). The annual bite cases in India alone are quite high, and when this number is combined with Sub-Saharan countries the supply of antivenom vials is insignificant rendering high mortality in the rural areas. It was earlier reported that the antivenom vials intended to be used in India in a year can reach up to 2 million (Whitaker andWhitaker, 2012). But it is still not determined how many vials are effective to neutralize the actions of snake venom in Indiadue to variations in efficacy of the polyvalent antivenom currently in use. These represent a serious need for producing more antivenom vials annually or changing the approach to antivenom production.

The conventional medical treatment to neutralize snakebite toxicity is the use of heterologous antivenoms, a century-old nonspecifictreatment protocol that is still giving lives to thousands of snakebite victims. This type of antivenom is obtained from horse immunization with sub-lethal doses of respective snake venoms (Laustsen et al., 2018). The conventional heterologous antivenom is the only effective procedure implemented against snakebite envenomation, but it contains several unwanted health problems due to the toxins that may vary between taxa, geographic range, age, and sex of the snakes. One of the major concerns in the neutralization of the toxic effects is the batch variation of snake venoms. Apart from this, the negative reactions elicited by the polyvalent antivenom such as pyrogenic reactions, serum sickness, allergic reactions, etc. are imposing the bigger limitations in its use and induces the urge to innovate and implement new and effective antivenom strategies.

To reduce or eliminate the drawbacks caused by the current antivenom, there is an urgent requirement to innovate another therapeutic approach for the effective treatment of snakebite envenomation. Different alternative strategies have been proposed including the use of monoclonal antibodies, DNA immunization, synthetic epitope strings, etc.Introduction of monoclonal antibodies against snake venom toxins may be of great advantage in the future by using antibody library based on phage display technique as it can overcome the existing limitations of polyvalent antivenom. But low half-life stability, high production cost, and low immunogenicity of monoclonal antivenom are the hindrances in pushing it into clinical trials. Although broadly neutralizing monoclonal antibodies can be an answer to this (Fernandes et al., 2010).

Another recent advancement in the field of antivenoms is the use of recombinant antibodies and antibody fragments specific to the toxic components within a venom (Laustsen et al., 2018). These proposed antivenom strategies are well-investigated and do not exert any undesirable reaction in the bodyof model organisms such as mice. The recombinant antibodies of human origin are compatible with the human immune system and thus represent better safety profiles. Broadly neutralizing monoclonal antibodies only target the therapeutically active toxins not only of snake venoms, but also of the scorpion, spider, and bee venoms. But the use of monoclonal antivenom possesses the limitation of not being cost-effective. Moreover, the selection of specific toxins and the production of antibodies against them require extensive steps, and more investigations are required to identify different isoforms of very complex snake venoms (Ahmadi et al., 2020). There are certain proposed low molecular weight formats of recombinant antivenoms such as single-chain variable fragments (scFvs), Fab, diabodies, bivalent formulations, etc. that have lower chances to induce adverse immune reactions in the body. Pharmacokinetic considerations are also needed to be balanced to implement such therapeutic approaches (Laustsen et al., 2018).

Recently with the emergence of advanced biotechnological protocols, the study of DNA immunization with transcriptomic analysis has also expanded the horizons in the field of snakebite envenomation. In this elegant and robust process, specific DNA coding sequences of toxic antigens is directly injected into the cells andexpressed in an immunized animal. This technique is comparatively much easier to develop specific antibodies without the involvement of recombinant technologies and purification of proteins from heterologous organisms such as *Escherichia coli* (Suntravat et al., 2013). This approach can be beneficial to the proposed antivenom strategies for its cost-effective production and least harmful effects on the victim. Not only the aforementioned advantages are there, but the DNA immunization can be highly specific for other venomous animals also (Liu et al., 2021).

In this present review, the neutralizing efficacy of the present Indian polyvalent antivenom is compared to the recombinant antivenoms with a directional view on the DNA immunization against the snakebite envenomation.

II. DIVERSITY OF SNAKE VENOM COMPONENTS

Treatment of snakebites is highly difficult due to the intense variability of snake venoms which is again dependent on the taxonomic and geographical diversity of venomous snakes worldwide (Shashidharamurthy and Kemparaju, 2007). The venomous species along with their subspecies add further diversity in the composition of venoms due to the differences at the genetic level. There are many more unexplored species than the world currently deals with, and it is again another cause of additional venom diversity in the snakes. Even after such disparity, the venoms contain many similarities too. They all are complex mixtures consisting of different hydrolytic enzymes, non-enzymatic proteins, and several other peptide components (Williams et al., 2019; Gutierrez et al., 2017). The enzymatic components exert principal toxic effects in the snakebite victims through several diverse mechanisms which are listed in the table-1. Although enzymatic components are the main players in toxicological aspects of snakebite envenomation, numerous non-enzymatic constituents may have similar pathophysiological consequences. Not all of them are toxic to the body, and therefore need not to be neutralized. Some of the main non-enzymatic components are listed here in the table-2.

Table I. Enzymatic components of snake venom

Phospholipase A_2 (PLA_2)	Group I PLA_2	Present in the venoms of elapid and colubrid snakes. They are basically β-neurotoxins affecting voltage-gated ion channels to block pre-synaptic transmission of nerve impulses and sometimes can cause permanent neurotoxicity by hydrolysing phospholipids at the nerve terminals (Williams et al., 2018).
	Group II PLA_2	Present in the members of Viperidae, primarily acts as cytotoxic components causing myonecrosis (Dixon and Harris, 1996).
Snake Venom Metalloproteases (SVMPs)	P-I/ Group I	Present in all groups and comprise just a metalloprotease domain. They hydrolyse the components of the endothelial cell basement around blood capillaries (Mackessy, 2010).
	P-II/ Group II	Contain an additional disintegrin domain. Function in the integrin shedding and have myotoxic effects (Siigur and Siigur, 1991).

	P-III/ Group III	Cysteine-rich domains and disintegrin domains are present. Inhibit collagen-induced platelet aggregation and induce inflammation (Chatrath et al., 2011).
	P-IV/Group IV	Two C-type lectin-like domains along with Cysteine-rich and disintegrin domains. They activate platelets by activating tyrosine kinase-dependent receptors (Ferreira et al., 2018).
Snake Venom Serine Proteases (SVSPs)		They degrade blood components proteolytically and thus affect the haemostasis of the body (Serrano and Maroun, 2005). The major effect of these components is cleaving fibrinogen to promote coagulation; but can act as anticoagulants in some cases (Sanchez et al., 2000). They are also found to dilate the blood vessels, activate prothrombin, and alter blood pressure to cause blood clotting (Kisiel et al., 1987).
L-Amino Acid Oxidases (LAAOs)		They are found in the venoms of elapids and vipers (Tasoulis and Isbister, 2017). They function in the oxidative deamination of amino acids and produce ammonia and hydrogen peroxide as side products that have several cytotoxic effects and may induce oedema, apoptosis, and may act as anticoagulants (Meléndez-Martínez et al., 2017; Sharma et al., 2015).
Acetylcholinesterase		Hydrolyses the neurotransmitter acetylcholine synaptically and blocks effective neuronal transmission (Schetinger et al., 2009).
Hyaluronidases		They hydrolyse the hyaluronic acid in the interstitial space and facilitate the diffusion of other toxins across the body (Isoyama et al., 2006).

Table II. Non-enzymatic components of snake venom

Three-finger Toxins	Predominant in elapid venoms, and some viper and colubrid venoms (Aird et al., 2013). They are generally neurotoxic or cytotoxic having a variety of biological effects such as they block neuromuscular transmission by binding to the post-synaptic nicotinic receptors in the skeletal muscle, form ion pores and cause cell lysis, block calcium channels and inhibit platelet aggregation (Heyborne and Mackessy, 2013; Kini and Doley, 2010).
Cysteine-rich Secretory Proteins	Found in all the venomous families. These single-chain polypeptides exert their effect by blocking calcium and potassium ion channels and thereby affecting signal transmission and smooth muscle contractions (Fox and Serrano, 2005).
Kunitz-type Proteinase Inhibitors	Present in vipers and elapids (Yuan et al., 2008), and functions to inhibit serine proteases and numerous ion channels. One of the notable groups of Kunitz peptides is the dendrotoxins found in the mambas, they interact with voltage-gated ion channels and cause involuntary muscle contractions (Laustsen et al., 2015).
Disintegrins	Present in viper venoms inhibits the collagen-induced activation of platelets (Williams et al., 2019).
Natriuretic Peptides	Found in elapids and vipers, promote natriuresis affecting myocardial actions as well as causing hypotension (Collins et al., 2000).
Snake C-type Lectin-like Proteins (Snaclecs)	Both activate and inhibit platelets through various types of receptors (Clemetson et al., 2005).
Bradykinin-potentiating Peptides (BPPs)	Inhibit the angiotensin-converting enzyme and cleave bradykinin resulting in potent hypotensive actions (Sciani and Pimenta, 2017).
Nerve Growth Factor (NGF)	Helps in the prey incapacitation. Cause mast cells to release chemical mediators and increase vascular permeability to facilitate dispersal of other venom components (Sunagar et al., 2013).

III. TOXIC EFFECTS OF SNAKE ENVENOMING

Venomous snakes contain a specialized biting mechanism to deliver their venoms into the body of the prey. The biting apparatus contains a pair of fangs that may be located anterior to the maxillary bones in the cases of viperids, elapids, or posteriorly in the colubrids known as non-front-fanged snakes. The size of the fangs determines whether the venom is injected subcutaneously or intramuscularly. Once inside the body, the venom is translocated with the help of the blood and lymphatic system to several organs inside the body and exert their pathological effects. There are significant differences in the toxicological effects between diverse groups of venomous snakes. But they exert some similar pathophysiological effects in the victimized prey such as local tissue damage, inflammation, haemostatic alterations(Gutierrez et al., 2017).

A. Local Tissue Damage

Almost all of the venomous snakes induce local tissue injuries, but the most potent effects are exerted by the vipers. SVMPs induce hydrolysis of blood vessel walls that causes haemorrhage of the local tissue and the venom spreads quickly in the body. The spread of venom is also promoted by the hyaluronidases(Escalante et al., 2011). PLA_2 induce blistering and oedema at the injured location(Dixon and Harris, 1996). These components can also induce necrosis in the softer tissues. SVMPs degrade the dermal-epidermal interface causing blisters. Hyaluronidases along with SVMPs hydrolyse extracellular matrix components, including collagen, proteoglycans, hyaluronic acid that alter the structure and function of tissue

components inducing local tissue damage (Gutierrez et al., 2016). The local intra-muscular nerves and vasculature also get damaged due to the actions of the toxin components. The envenomed tissue develops an extensive inflammatory response following the synthesis and release of several inflammatory mediators inducing pain in the tissue (Rucavado et al., 2016).

B. Haemotoxicity

Snake venom components destroy basement membrane components resulting in the reduced mechanical stability of the blood vessels. SVSPs and SVMPs modulate the factors involved in coagulation and can prevent or promote blood clots. Many other components including the three-finger toxins, snaclecs, disintegrins, cysteine-rich secretory proteins dysregulate the platelet aggregation (Kini and Koh, 2016). The SVMP-induced vascular damage causes disruption of the endothelial cell-to-cell adhesions (Escalante et al., 2011).They enhance haemorrhaging and may induce thrombocytopenia. Natriuretic peptides increase vasodilation. High concentration of PLA_2 causes haemolysis in elapid bites. Bleeding is also associated with snakebite envenomation. Intracranial bleeding causes ischaemia, stroke and several neurological symptoms (Del Brutto and Del Brutto, 2011). Hypovolaemia can result from increased vascular permeability caused by SVSPs. The viperid venoms include bradykinin-potentiating peptides that inhibit the angiotensin-converting enzyme and may also contribute to haemostatic alterations(Hayashi and Camargo, 2005).

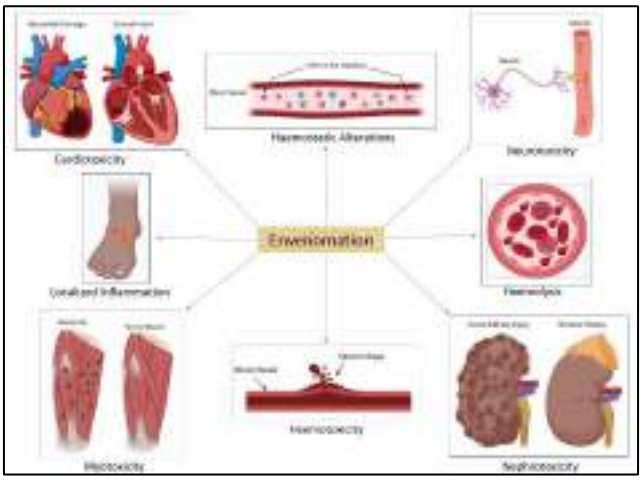

Fig.1. Toxicological effects of snake venoms

C. Myotoxicity

Myotoxic effects are majorly due to the actions of PLA_2 and three-finger toxins that can disrupt the integrity of the myofibrils via pore formations. They also cause hydrolysis of the phospholipids in the cell membrane. Following disturbances in the membrane structures, a rapid influx of calcium ions dysregulates the normal contractile mechanism of the myofilaments and causes other degenerative muscular events leading to irreversible muscle damage. SVMPs cause myotoxicity by cleaving collagen and other basement membrane components. The myotoxic effects are also caused by ischaemiaand localized oedema that alters tissue vasculature. Moreover, as a consequence of vascular and nervous damage of the tissues, muscular regeneration is impaired, often leading to permanent sequelae (Gutierrez et al., 2017; Ferreira et al., 2018).

D. Neurotoxicity

The nervous system is more affected in elapid envenomation and viperids generally do not severely act on the neurons, although crotoxin of some viper species such as *Daboia russelii* shows significant levels of neurotoxicity. The elapid venoms contain notable neurotoxins that cause neuromuscular paralysis resulting in respiratory failure and blockade of swallowing. Alpha-neurotoxins belonging to the three-finger toxin family acts post-synaptically and bind with the cholinergic receptors at the neuromuscular junction. Thus, they block the interactions of acetylcholine and induce flaccid paralysis (Barber et al., 2013). Beta-neurotoxins are predominantly PLA_2s that act pre-synaptically. These neurotoxins upon binding to their appropriate receptors cause enzymatic degradation of the membrane phospholipids causing neurotoxicity. Moreover, with the generation of lysophospholipids and fatty acids, the alterations in the cell cause immature fusion and release of synaptic vesicles (Rossetto and Montecucco, 2008). With an increased membrane permeability to ions followed by calcium influx and depolarization of the nerve membrane, the synaptic reserve vesicles are depleted due to exocytosis. These events ultimately lead to degenerative intracellular mechanisms resulting in degradation of the nerve terminals (Harris et al., 2000). These are the underlying causes for prolonged paralysis in snakebite victims. Some PLA_2s can act by blocking voltage-gated ion channels in the neuronal membrane (Pungercar and Krizaj, 2007). Other snake venom components may also contribute to severe neurotoxicity such as acetylcholinesterase hydrolyses the acetylcholine and thus blocks neuromuscular signal transduction, cysteine-rich secretory proteins block specific ion channels (Ca^{2+} and K^{+}) to dysregulate the membrane potential (Harvey and Robertson, 2004).

E. Nephrotoxicity

Acute kidney injury is also connected with snake-bite envenomation. Haemodynamic disturbances caused by systemic bleeding and vascular damage often result in decreased renal blood flow that can cause kidney damage. SVMPs often hydrolyse the basement membrane components in the glomerular capillaries in the kidneys. Thrombotic microangiopathy may also develop due to the deposition of microthrombi. Some cytotoxic PLA_2s exert their effect directly by damaging tubular cells in the kidney. In some cases, cytotoxic and proteolytic activity can cause accumulation of myoglobin in the renal tubules resulting in severe nephrotoxicity (Sitprija and Sitprija, 2012).

F. Cardiotoxicity

Cardiotoxic effects are mainly caused by natriuretic peptides which mediate their effects by causing hyponatremia. The haemodynamic alterations also influence cardiological toxicity. In some elapid venoms, cardiotoxins directly cause myocardial damage. SVMPs often lead to cardiovascular shock from the haemodynamic changes due to venom-induced bleeding in the body (Hayashi and Camargo, 2005; Hojer et al., 2010).

G. Cytotoxicity

The major cytotoxic components are the PLA_2s and three-finger toxins. These constituents induce localized necrosis due to their cytotoxic effects. Three-finger toxins reduce the stability of the plasma membrane in different cell types through non-enzymatic mechanisms. Group-II PLA_2s can directly induce cytotoxic effects causing myogenic damage (Rivel et al., 2016; Duboyskii and Utkin, 2014).

IV. Conventional polyclonal antivenom

The anti-snake venom serum (ASVS) currently in use is a polyvalent antivenom extracted from horse serum after the animal is injected with respective snake venoms. The antivenom, also called antivenin, is F(ab')-based equine polyspecific antibodies developed using the venoms of four Indian venomous snakes which are Russel's viper (*Daboiarusselii*), Spectacled cobra (*Najanaja*), Common krait (*Bungarus caeruleus*), and Saw-scaled viper (*Echiscarinatus*) (Kini et al., 2018).

This conventional antivenom is produced through a multi-step process. First of all, the snakes are milked for obtaining the required venom from their venom glands and the venom is injected into a larger mammal, mostly horse or in some cases sheep to immunize the animal against snake venom toxins. After successful immunization of the animal, blood is collected from the body in a sufficient amount, and erythrocytes are separated from the plasma. Different precipitation techniques are employed to isolate manufactured IgG antibodies from the plasma. The concentration and formulations are tested before marketing as vials and administered into the snakebite victims (Kini et al., 2018).

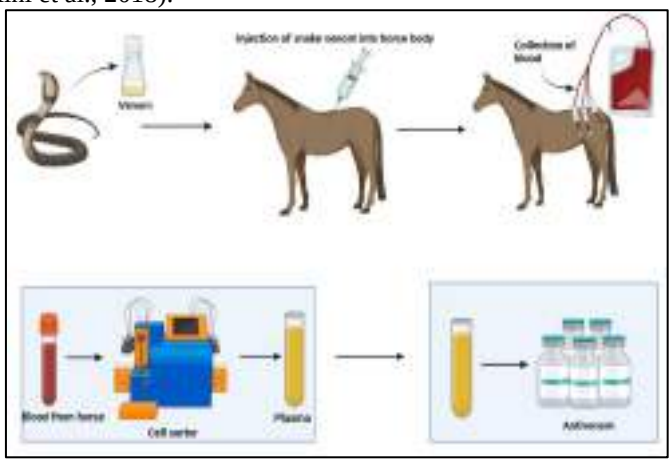

Fig.2. Manufacturing the conventional polyclonal antivenom

A. Limitations

1) Complexity

The process of manufacturing polyclonal antivenoms is largely dependent on the availability of associated snake venom and the immune system of the individual horse. The production system is also very much invasive and requires multiple tedious steps to produce a sufficient number of polyclonal antibodies.

2) Serum sickness

Serum sickness is a type of delayed-type hypersensitive reaction that occurs in several victims administered with the antivenom. The polyvalent antivenom contains only 5-36% antibodies able to bind to the snake venom toxins, and this is the major reason for administering multiple vials of antivenom (Segura et al., 2013). The high dosage of such poor neutralizing components increases the risk of serum sickness in the snakebite victims (Lavonas et al., 2011).

3) Inability to abolish local tissue damage

The local tissue damaged by snake venom components cannot be reverted back to its normal condition upon antivenom administration. The antibodies present in the administered antivenom have the limited pharmacokinetic properties to reach the deep layers of tissues and neutralize the catastrophic pathophysiology induced by multiple toxins in the snake venom (Gutierrez et al., 2017). This antivenom may not be effective to treat venom-induced consumption coagulopathy (VICC) which is one of the major outcomes of envenomation by elapid and viper species (Gulati et al., 2013). VICC being irreversible poses a great challenge to be neutralized by the polyvalent antibodies, and it has been shown to be less effective against *Echis*envenomation (Rogalski et al., 2017).

4) Allergic reactions

The horse-derived antivenoms are foreign to the human body and may act as antigens rather than acting as antibodies against snake venom toxins. These can lead to acute anaphylactic shock followed by severe allergic reactions in the victims (Lalloo and Theakston, 2003).

5) Unable to neutralize venoms from different regions

The chemical composition varies with geographical distribution in the venomous snakes. In certain cases, the antivenom fails to neutralize snake venoms in the victims from different locations and is the most potent failure of the currently available polyvalent antivenom (Goncalves-Machado, 2018). The neutralizing efficacy and the venom yield per bite are depicted in the given chart.

6) Lack of neutralizing ability against venoms of certain medically important snakes other than the 'big four'

The present antivenom cannot properly neutralize the toxins from the venomous species all over the country that are less known yet medically significant and also cause a good proportion of envenomation. There are about 29 unique venom components between *Najanaja*and *Najakaouthia*, and it exerts the resistance in neutralizing ability of the antivenom against the venom from *N. kaouthia* at the same level as that of *N.*

naja(Parvatam, 2018; Mukherjee, 2020). It is unable to reverse the myotoxic effects induced by the venom of Sri Lankan *Najanaja* once it has already begun damaging the tissue (Madhushani et al., 2021).

7) Expensive

Antivenom production takes several steps and diverse biological systems and thus it is much more expensive in clinical uses (Kini et al., 2018).

8) Pharmacodynamic consideration

Pharmacodynamics is the ability of therapeutic components to act *in vivo* to neutralize the toxins of venom and it is one of the key determinants of antivenom efficacy. The polyclonal antivenom has several limitations that make the measurements complicated. A single epitope in a toxin may be recognized by several antibodies with different affinities. Again, a particular antibody component in polyclonal antivenom may bind to homologous toxins with different specificities. The concentrations of individual antibody component that binds with a single epitope cannot be measured in this antivenom (Vauquelin and Charlton, 2013).

V. Requirements of alternate strategies

There are numerous reasons to find out effective intervention methodologies to treat snakebite envenomation. Currently available therapeutic strategies may be viable to some extent but possess several side effects and also have high mortality even after the application of the therapeutics. In snakebite envenomation, there is no incubation period for the toxins, although there may be some delay in starting the pathogenesis of systemic toxins that need to be transported through the blood from the site of biting. This is the reason to start treatment of envenomation as early as possible with effective measurements (Laustsen, 2019).

Larger snakes can inject a high dose of toxins into the body that can exert their effects immediately. This leads to the need for high amounts of antivenom that should be used against the venom (Harrison and Gutierrez, 2016). The higher dosage of antivenom influences the economic side of antivenom production. Effective and sound treatment protocol cannot be employed in the rural areas of India where the snake bite mortality is higher if the cost of antivenom is not within the limit (Laustsen and Dorrestin, 2018). Moreover, snake venoms are complex mixtures of different enzymes and chemicals considered as toxins. Therefore, it needs to be used a mixture of antivenom components. But it should be monitored which toxins are needed to be neutralized as some venom constituents may not be medically significant for the body. This will reduce the complexities in therapeutic methodologies (Laustsen et al., 2015; Laustsen, 2016).

The envenomation is not transmissible into a population and production of a suitable antivenom is sufficient as it will not require the development of herd immunity. Therefore, the development of a vaccine against snake venoms will be of limited value. There is a very low probability of developing resistance against the antivenoms, because of very slow mutation rates in reptiles, and the medically important toxins will barely change their composition in long periods of time (Laustsen, 2019). The polyvalent antivenoms, directed against the venom components after immunization of a host animal, contain several antibodies against those antigens that the host has encountered during its entire life. As a result, the antivenom carries a huge portion of antibodies that are not relevant for snakebite victims (Segura et al., 2013).

VI. Monoclonal antivenom

Monoclonal antibodies (mAbs) have been reported to be effective therapeutic tools in several pathological states. The production of toxin-specific mAbs is one of the finest advancements in recombinant technology and it theoretically promises to overcome the limitation of ensuring that each of the IgGs in therapy is efficient to neutralize a toxin. There are other recombinant antibodies besides the mAb such as the single-chain variable fragments (scFvs), nanobodies, and antigen-binding fragments (Fab and $F(ab')_2$s) that have been studied to neutralize several toxins of different animal venoms (Richard et al., 2013; Boyer et al., 2013).

The first fully human-originated oligoclonal IgGs against animal toxins were reported recently. Carefully selecting the oligoclonal mixtures of human monoclonal IgGs can abolish the neurotoxicity caused by the dendrotoxins of the infamous black mamba (*Dendroaspispolylepis*) (Laustsen, 2018).

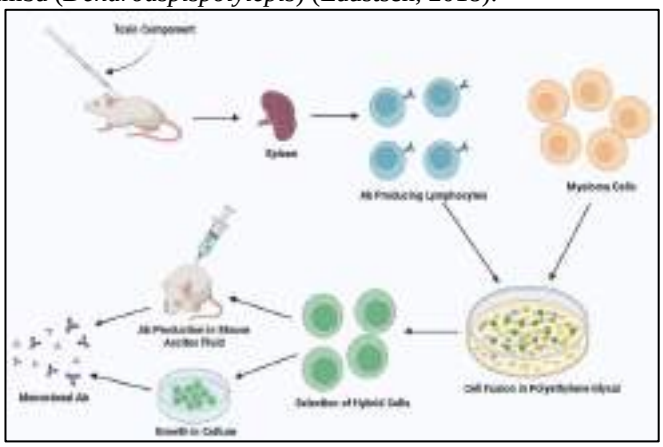

Fig.3. Schematic representation of producing monoclonal antibodies

The snake venom-mediatedhaemotoxicity can be addressed by using specific mAbs for species-specific toxins (Tanjoni et al., 2003). Successful evaluation of neutralizing efficacy for mAbs has been done against West African carpet viper (*Echis* sp.) (Idddon et al., 1988), Western diamondback rattlesnake (*Crotalus atrox*) (Perez et al., 1984), and *Bothrops*snakes (Fernandes et al., 2010). These approaches include mAb-induced antivenom responses only for very similar epitopes of a particular toxin of the whole venoms. They showed significant inefficacy against other venoms.

MAbs against the factor X activators present in the venom of Russel's viper is also investigated and proved to be effective in neutralizing the toxic component (Pukrittayakamee et al., 1983). A successful investigation has been done to find out the neutralization effects of myotoxic components of *Bothrops asper* snake venom (Lomonte et al., 1992). There are several studies regarding the neutralization efficacy of the mAbs raised against neurotoxic substances of snake venom as well. The specific

mAb against toxin alpha of *Najanigricolis* neutralizes its effects both *in vivo* and *in vitro* (Boulain et al., 1982). There are instances when mAbs neutralized long-chain neurotoxic curaremimetic toxins of snake venoms. Alpha-cobratoxin is also a type of these long-chain neurotoxins found in *Najakaouthia* snake venom (Pillet, 1992).

Human-originatedscFvs have also been proved to neutralize several toxins from distinct animal venoms, mostly scorpions (Riano-Umbarila et al., 2019; Rodriguez-Rodriguez et al., 2016).The injections of LD_{50} of whole venoms of certain scorpion species such as *Centruroides elegans, C. tecomanus, C. limpidus*, etc. caused death in all of the mice except in those administered with scFvs. It is more effective than using against the snake venoms, perhaps because the scorpion venoms are not so complex and even the molecular and pathological considerations are well distinguished for them (Riano-Umbarila et al., 2019; Bahraoui et al., 1988).Moreover, snake-bite deaths are more common than due to scorpions. Although to eliminate the less efficacy of such small molecule antivenoms it is better to find out potential toxic components from the venom. Another unusual class of antibodies lacking the light chains and the first constant portion of the heavy chain was obtained from camelid serum. This type of antibody often referred to as nanobodies or heavy-chain antibodies comprises only the variable domain of a classical antibody molecule (VHH) but is still able to neutralize antigens (Kunz et al., 2017). Nanobodies can be easily produced on large scale and also hold promising advancements over conventional antivenom such as high specificity to venom toxins, highly thermostable, and fewer chances of immunogenic reactions in humans because of high sequence identity (Fernandes et al., 2021). The very small size of such molecules enables their better distribution throughout the body which is crucial for removing toxicological effects at the cellular level. But the usage of nanobodies is still in the naïve stage and to bring it to the clinical level, extensive studies should be performed.

The high mono-specificity of the above-mentioned mAbs is not favorable in the case of highly complex snake venoms containing multiple antigens. It is, therefore, required to use broadly neutralizing mAbs that are able to act against numerous similar or dissimilar antigens (Ahmadi et al., 2020).This kind of mAbs has been generated against *Najanigricolis, N. mossambica*, and *N. melanoleuca*, and subsequently assayed with cell line viability tests only. To make its neutralizing capacity effective to be used in humans, it has to be used in several other combinations of venoms depending upon the tropical countries. Apart from a cell line, mice models should be employed with LD_{50} of venom combinations. It would be beneficial over the conventional antivenom due to its less cross-reactive properties and thus will reduce the chances of serum sickness.Although there are successes in using mAbs as neutralizing agents against animal-derived toxins, the difficulties in identifying specific isoforms of toxins and the complexities of snake venoms are discouraging the extensive usage of mAbs against snake venom toxins. These situations still possess resistances in generating toxin-specific mAbs to treat the systemic pathophysiology in snakebite envenomation (Harrison et al., 2011).

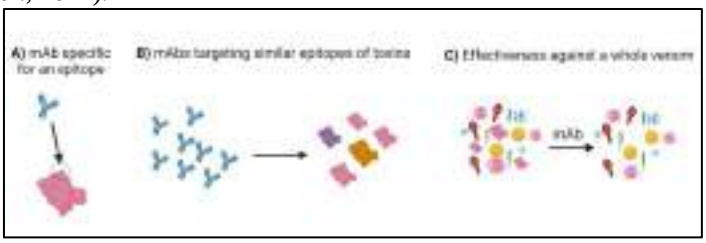

Fig.4. Efficacy of mAb-based antivenom

VII. RECOMBINANT ANTIVENOM

The rapidly emerging fields of recombinant technology allow the insertion of a gene of interest into a heterologous host genome and investigate the consequent expression of that gene product. Different protein expression systems have been employed for the purification of specific gene products and used in numerous biotechnological interests. The protein products can be further injected into larger animals either for the production of vaccines or for the generation of specific antibodies in the body that can be collected and used for therapeutic purposes.

With the advent of more efficient gene delivery methods, they are being used together with gene optimization techniques resulting in an enhancement of the levels of protein expressions. These strategies along with the beginning of using DNA vaccines have been proving to elicit more effective cellular immune responses (Yan et al., 2007) and also induce the production of a higher number of antibodies (Yadava and Ockenhouse, 2003; Smith et al., 2004).

The very promising protocols of genetic immunization may have a better solution to the above-mentioned limitations in developing the most effective snake antivenom for the medically important snakes of India. This would be an easier approach to present correctly folded toxins from snake venom to a host with the concurrent production of most probable neutralizing antibodies against the toxin.Structural conformations and immunogenic properties of toxins within whole venom are very easy to determine. Inducing antibody production against particular toxin by combining it with other carrier molecules may enhance the immunogenic property. Development of suitable expression systems for such recombinant toxins and re-introducing them into large animals would increase the availability of antivenom compared to the present scenario.

The *Escherichia coli* system has been widely used to study the expression of toxic components including α-neurotoxic protein of the Mexican coral snake, *Micrurus laticollaris* (Carbajal-Saucedo et al., 2013), SVMPs from the broad-banded copperhead, *Agkistrodon contortrix laticinctus (Selistre-de-Araujo et al., 2000)*, post-synaptically acting neurotoxins from *Pseudonaja textilis* (Gong et al., 1999). The snake venom toxins are very complex polypeptides having correctly folded conformation established by disulfide bonds, that are again necessary for eliciting their toxic effects. Therefore, the use of a prokaryotic host imposes several limitations in the production of such polypeptide toxins. The toxins cannot be produced in higher quantities, there is a high chance that the molecules would not be correctly folded and hence, become less active (Selistre-de-Araujo et al., 2000; Moura-da-Silva et al., 1999) To

overcome the issues, eukaryotic host systems, such as *Pichia pastoris*, has been shown to be more effective and may be an alternative approach for the expression of recombinant toxins of snake venom (Pinyachat, 2011).

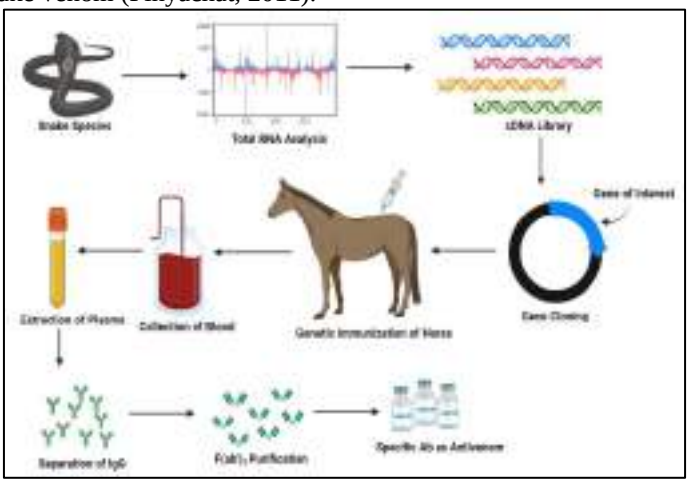

Fig.5. Schematic representation for the production of recombinant antivenom

The first DNA immunization strategy as an attempt to develop antivenom capable of neutralizing the toxicological effects elicited by the snake venom was done using the Jararhagin of *Bothrops jararaca*. The specific carboxyl-disintegrin and cysteine-rich domains of this metalloprotease were targeted in this approach and a significant reduction of around 77% in the hemorrhagic lesion was found. It was later found that the immunoglobulins have high reactivity to the components of snake venoms of a particular species which promotes the potential use of this strategy to produce toxin-specific antibodies with polyspecific cover (Harrison et al., 2003). This type of early work demonstrated the probability of using DNA immunization as an alternative approach for the next generation of antivenom therapies.

Although it is not effective to target a single toxin within the snake venom, it was found that targeting a specific toxin is able to reduce the toxic effects caused by the whole venom. The work done with *Echis ocellatus* that display a large molecular diversification of SVMPs far exceeding that observed in the case of *B. jararaca* implicated that an adequate neutralization of the toxicological activities caused by a certain venom would be accomplished by the production of antibodies targeting the antigenic epitopes present in most of the diverse SVMP isoforms (Francischetti et al., 2004; Junqueira-de-Azevedo and Ho, 2002; Kashima et al., 2004; Wagstaff et al., 2006).There has been works with cloning and cDNA sequence analysis from the total RNA extracts of a venom. In such cases, immunopotentiators are also used to increase the antibody titer. Co-administration of such venom toxins and potentiators have shown increased production of antibodies in mice models decreasing the venom-induced tissue damage (Ramos and Ho, 2015).

This clearly indicates that using the bioinformatics analysis of the venom components and even the venom gland transcriptome can be a great way to enhance the neutralization efficacy of the snake antivenom.

The initial works paved the way for new antivenom therapeutics, but still, there is no record of using recombinant toxins to synthesize the antivenoms. The snake venoms are very complex mixtures of diverse toxic components, therefore, targeting only one toxin and making antibodies against it may not be always beneficial for the neutralization of pathogenesis. To produce an adequate amount of recombinant toxins, the host must be feasible enough, but this is again very costly. By developing an appropriate database regarding the most abundant epitopes in the complex mixture of venom and using bioinformatic tools the sequence tags may be identified, that can direct the future progress in this domain of antivenom production.

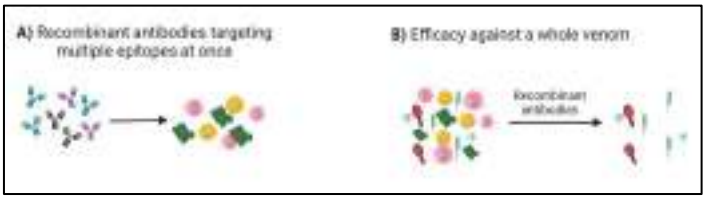

Fig.6. Efficacy of recombinant antivenom

CONCLUSION

Innovation of new antivenom for the future is not so simple. Purification of the toxins from crude venom is very complex and it does not allow the collection of enough toxins for immunization studies. Most of the elapids deliver a very small quantity of venoms per bite, yet they are medically important as they are responsible for significant mortalities in tropical and sub-tropical countries including India. Heterologous expression systems may be a better alternative for the production of important toxin molecules. Future research should be done on developing a much compatible and cost-effective antivenom having no harmful side effects or least number of side effects. Selection of most abundant epitopes from specific snake venom and developing cDNA libraries for the medically important snake species are yet to be focused. More types of recombinant toxins may be generated to neutralize the whole venoms of elapids, vipers, and colubrids. The antivenom strategy involving DNA immunization can be a great tool for antivenom development in the near future. Several aspects involving this strategy are yet to be dealt with and further studies should be done to make it available clinically.

ACKNOWLEDGMENT

We would like to thank Dr. Subhasis Dutta, Honourable Principal of Maulana Azad College, Kolkata for his permission and enthusiastic approach to conduct this study.

REFERENCES

Ahmadi, S., Pucca, M.B., Jurgensen, J.A., Janke, R., Ledsgaard, L., Schoof, E.M., Sorensen, C.V., Caliskan, F., &Laustsen, A.H. (2020). An in vitro methodology for discovering broadly neutralizing monoclonal antibodies. *Scientific Reports*, 10, 10765.

Aird, S.D., Watanabe, Y., Villar-Briones, A., Roy, M.C., Terada, K., &Mikheyev, A.S. (2013). Quantitative high-

throughput profiling of snake venom gland transcriptomes and proteomes (*Ovophisokinavensis* and *Protobothropsflavoviridis*). *BMC Genomics*, 14, 790.

Alangode, A., Rajan, K., & Nair, B.G. (2020). Snake Antivenom: challenges and alternate approaches. *Biochemical Pharmacology*, 181, 114135.

Azofeifa-Cordero, G., Arce-Estrada, V., Flores-diaz, M., Alape-Giron, A. (2008). Immunization with cDNA of a novel P-III type metalloproteinase from the rattlesnake *Crotalus durissusdurissus* elicits antibodies which neutralize 69 % of the hemorrhage induced by the whole venom. *Toxicon*, 52(2), 302-308.

Bahraoui, E., Pichon, J., Muller, J.M., Darbon, H., Elayeb, M., Granier, C., Marvaldi, J., Rochat, H. (1988). Monoclonal antibodies to scorpion toxins. Characterization and molecular mechanisms of neutralization. *Journal of Immunology*, 141, 214-220.

Barber, C.M., Isbister, G.K., & Hodgson, W.C. (2013). Alpha neurotoxins. *Toxicon*, 66, 47-58.

Boulain, J.C., Menez, A., Couderc, J., Faure, G., Liacopoulos, P., &Fromageot, P. (1982). Neutralizing monoclonal antibody specific for *Najanigricollis* toxin alpha: preparation, characterization, and localization of the antigenic binding site. *Biochemistry*, 21, 2910-2915.

Boyer, L.V., Chase, P.B., Degan, J.A., Figge, G., Buelna-Romero, A., Luchetti, C., &Alagon, A. (2013). Subacute coagulopathy in a randomized, comparative trial of Fab and $F(ab')_2$ antivenoms. *Toxicon*, 74, 101-108.

Carbajal-Saucedo, A., Lopez-Vera, E., Benard-Valle, M., Smith, E.N., Zamudio, F., & de Roodt, A.R. (2013). Isolation, characterization, cloning and expression of an alpha-neurotoxin from the venom of the Mexican coral snake *Micrurus laticollaris* (Squamata: Elapidae). *Toxicon*, 66, 64-74.

Chippaux, J.P. (2017). Snakebite envenomation turns again into a neglected tropical disease! *Journal of Venomous Animals and Toxins Including Tropical Diseases*, 23, 38.

Clemetson, K.J., Lu, Q., &Clemetson JM (2005) Snake C-type lectin-like proteins and platelet receptors.PathophysiolHaemostThromb 34:150-155

Collins, E., Bracamonte, M.P., Burnett Jr, J.C., & Miller, V.M. (2000) Mechanism of relaxations to *Dendroaspis* natriuretic peptide in canine coronary arteries. *Journal of Cardiovascular Pharmacology*, 35, 614-618.

Del Brutto, O.H., & Del Brutto, V.J. (2011). Neurological complications of venomous snake bites: A review. *Acta Neurologica Scandinavica*, 125, 363-372.

Dixon, R.W., & Harris, J.B. (1996). Myotoxic activity of the toxic phospholipase, notexin, from the venom of the Australian tiger snake. *Journal of Neuropathology and Experimental Neurology*, 55, 1230-1237.

Dubovskii, P.V., &Utkin, Y.N. (2014). Cobra cytotoxins: Structural organization and antibacterial activity. *Acta Naturae*, 6, 11-18.

Escalante, T., Rucavado, A., Fox, J.W., & Gutierrez, J.M. (2011). Key events in microvascular damage induced by snake venom hemorrhagic metalloproteinases. *Journal of Proteomics*, 74, 1781-1794.

Fernandes, I., Assumpcao, G.G., Silveira, C.R.F., Faquim-Mauro, E.L., Tanjoni, I., Carmona, A.K., Alves, M.F.M., Takehara, H.A., Ramos, O.H.P., Moura-da-Silva, A.M., & Gutierrez, J.M. (2010). Immunochemical and biological characterization of monoclonal antibodies against BaP1, a metalloproteinase from *Bothrops asper* snake venom. *Toxicon*, 56, 1059-1065.

Fernandes, C.F.C., Pereira, S.S., Luiz, M.B. (2021). Engineering of single-domain antibodies for next-generation snakebite antivenoms. *International Journal of Biological Macromolecules*, 185, 240-250.

Ferreira, B.A., Deconte, S.R., de Moura, F.B.R., Tomiosso, T.C., Clissa, P.B., Andrade, S.P., & Araújo, F.D.A. (2018). Inflammation, angiogenesis and fibrogenesis are differentially modulated by distinct domains of the snake venom metalloproteinase jararhagin. *International Journal of Biological Macromolecules*, 119, 1179-1187.

Francischetti, I.M., My-Pham, V., Harrison, J., Garfield, M.K., Ribeiro, J.M. (2004). *Bitis gabonica* (Gaboon viper) snake venom gland: toward a catalog for the full-length transcripts (cDNA) and proteins. *Gene*, 337, 55-69.

Goncalves-Machado, L. (2016). Combined venomics, venom gland transcriptomics, bioactivities, and antivenomics of two *Bothrops jararaca* populations from geographic isolated regions within the Brazilian Atlantic rainforest. *Journal of Proteomics*, 135, 73-89.

Gong, N., Armugam, A., &Jeyaseelan, K. (1999). Postsynaptic short-chain neurotoxins from Pseudonaja textilis. cDNA cloning, expression and protein characterization. *European Journal of Biochemistry*, 265(3), 982-989.

Gulati, A., Isbister, G.K., &Duffull, S.B. (2013). Effect of Australian elapid venoms on blood coagulation: Australian Snakebite Project (ASP-17). *Toxicon*, 61, 94-104.

Gutierrez, J.M., Calvete, J.J., Habib, A.G., Harrison, R.A., Williams, D.J., &Warrell, D.A. (2017). Snakebite envenoming. *Nature Reviews Disease Primers*, 3, 17063.

Gutierrez, J., Escalante, T., Rucavado, A., Herrera, C., & Fox, J. (2016). A comprehensive view of the structural and functional alterations of extracellular matrix by snake venom metalloproteases (SVMPs): novel perspectives on the pathophysiology of envenoming. *Toxins (Basel)*, 8, 304.

Harris, J.B., Grubb, B.D., Maltin, C.A., & Dixon, R. (2000). The neurotoxicity of the venom phospholipase A2, notexin and taipoxin. *Experimental Neurology*, 161, 517-526.

Harrison, R.A., Cook, D.A., Renjifo, C., Casewell, N.R., Currier, R.B., & Wagstaff, S.C. (2011). Research strategies to improve snakebite treatment: Challenges and progress. *Journal of Proteomics*, 74, 1768-1780.

Harrison, R.A., & Gutiérrez, J.M. (2016). Priority actions and progress to substantially and sustainably reduce the mortality, morbidity and socioeconomic burden of tropical snakebite. *Toxins*, 8(12), 351.

Harrison, R.A., Wuster, W., & Theakston, R.D. (2003). The conserved structure of snake venom toxins confers extensive

immunological cross-reactivity to toxin-specific antibody. *Toxicon*, 41(4), 441-449.

Harvey, A., & Robertson, B. (2004). Dendrotoxins: Structure-activity relationships and effects on potassium ion channels. *Current Medicinal Chemistry*, 11, 3065-3072.

Hayashi, M.A., & Camargo, A.C.M. (2005). The bradykinin-potentiating peptides from venom gland and brain of *Bothrops jararaca* contain highly site-specific inhibitors of the somatic angiotensin-converting enzyme. *Toxicon*, 45, 1163-1170.

Heyborne, W.H., &Mackessy, S.P. (2013). Identification and characterization of a taxon-specific three-finger toxin from the venom of the green vine-snake (*Oxybelisfulgidus*; family Colubridae). *Biochimie*, 95, 1923-1932.

Hojer, J., Tran Hung, H., &Warrell, D. (2010). Life-threatening hyponatremia after krait bite envenoming- a new syndrome. *Clinical Toxicology*, 48, 956-957.

Iddon, D., Hommel, M., & Theakston, R.D. (1988). Characterisation of a monoclonal antibody capable of neutralising the haemorrhagic activity of West African *Echiscarinatus* (carpet viper) venom. *Toxicon,* 26, 167-179.

Isoyama, T., Thwaites, D., Selzer, M.G., Carey, R.I., Barbucci, R., &Lokeshwar, V.B. (2006). Differential selectivity of hyaluronidase inhibitors toward acidic and basic hyaluronidases. *Glycobiology*, 16, 11-21.

Junqueira-de-Azevedo, I.L., & Ho, P.L. (2002). A survey of gene expression and diversity in the venom glands of the pitviper snake *Bothropsinsularis* through the generation of expressed sequence tags (ESTs). *Gene*, 299, 279-291.

Juste, M. (2007). Using a recombinant bispecific antibody to block Na^+ -channel toxins protects against experimental scorpion envenoming. *Cellular and Molecular Life Sciences*, 64, 206-218.

Kashima, S., Roberto, P.G., Soares, A.M., Astolfi-Filho, S., Pereira, J.O., &Giuliati, S. (2004). Analysis of *Bothropsjararacussu* venomous gland transcriptome focusing on structural and functional aspects: I–gene expression profile of highly expressed phospholipases A2. *Biochimie*, 86(3), 211-219.

Kini, R.M., &Doley, R. (2010). Structure, function and evolution of three-finger toxins: Mini proteins with multiple targets. *Toxicon*, 56, 855-867.

Kini, R.M., & Koh, C. (2016). Metalloproteases affecting blood coagulation, fibrinolysis and platelet aggregation from snake venoms: definition and nomenclature of interaction sites. *Toxins (Basel)*, 8, 284.

Kini, R.M., Sidhu, S.S., &Laustsen, A.H. (2018). Biosynthetic oligoclonal antivenom (BOA) for snakebite and next-generation treatments for snakebite victims. *Toxins*, 10, 534.

Kisiel, W., Kondo, S., Smith, K.J., McMullen, B., & Smith, L.F. (1987). Characterization of a protein C activator from *Agkistrodon contortrix contortrix* venom. *Journal of Biological Chemistry*, 262, 12607-12613.

Kunz, P., Flock, T., Soler, N. (2017). Exploiting sequence and stability information for directing nanobody stability engineering. *Biochimica et Biophysica Acta*, 1861, 2196-2205.

Lalloo, D.G., & Theakston, R.D.G. (2003). Snake antivenoms. *Journal of Toxicology: Clinical Toxicology*, 41, 277-290.

Laustsen, A.H. (2016). Toxin synergism in snake venoms. *Toxin Reviews*, 35, 165-170.

Laustsen, A.H. (2018). Guiding recombinant antivenom development by omics technologies. *New Biotechnology*, 45, 19-27.

Laustsen, A.H. (2019). How can monoclonal antibodies be harnessed against neglected tropical diseases and other infectious diseases? *Expert Opinion on Drug Discovery*, 14(11), 1103-1112.

Laustsen, A.H., &Dorrestin, N. (2018). Integrating engineering, manufacturing, and regulatory considerations in the development of novel antivenoms. *Toxins*, 10, 309.

Laustsen, A.H., Karatt-Vellatt, A., & Masters, E.W. (2018). In vivo neutralization of dendrotoxin-mediated neurotoxicity of black mamba venom by oligoclonal human IgG antibodies. *Nature Communications*, 9, 3928.

Laustsen, A.H., Lohse, B., &Lomonte, B. (2015). Selecting key toxins for focused development of elapid snake antivenoms and inhibitors guided by a Toxicity Score. *Toxicon*, 104, 43-45.

Laustsen, A.H., Lomonte, B., Lohse, B., Fernández, J., & Gutiérrez, J.M. (2015). Unveiling the nature of black mamba (*Dendroaspispolylepis*) venom through venomics and antivenom immunoprofiling: Identification of key toxin targets for antivenom development. *Journal of Proteomics*, 119, 126-142.

Lavonas, E.J., Kokko, J., Schaeffer, T.H., Mlynarchek, S.L., Bogdan, G.M., & Dart, R.C. (2011). Short-term outcomes after Fab antivenom therapy for severe crotaline snakebite. *Annals of Emerging Medicine*, 57, 128-137.

Liu, B.S., Jiang, B.R., Hu, K.C., Liu, C.H., Hsieh, W.C., Lin, M.H., & Sung, W.C. (2021). Development of a broad-spectrum antiserum against cobra venoms using recombinant three-finger toxins. *Toxins*, 13, 556.

Lomonte, B., Gutierrez, J.M., Ramirez, M., & Diaz, C. (1992). Neutralization of myotoxic phospholipases A2 from the venom of the snake *Bothrops asper* by monoclonal antibodies. *Toxicon*, 30, 239-245.

Mackessy, S.P. (2010). Handbook of Venoms and Toxins of Reptiles. CRC Press: Boca Raton, FL, USA.

Madhushani, U., Thakshila, P., Hodgson, W.C., Isbister, G.K., & Silva, A. (2021). Effect of Indian polyvalent antivenom in the prevention and reversal of local myotoxicity induced by common cobra (*Najanaja*) venom from Sri Lanka in vitro. *Toxins*, 13, 308.

Meléndez-Martínez, D., Muñoz, J.M., Barraza-Garza, G., Cruz-Peréz, M.S., Gatica-Colima, A., Alvarez-Parrilla, E., &Plenge-Tellechea, L.F. (2017). Rattlesnake *Crotalus molossus nigrescens* venom induces oxidative stress on human erythrocytes. *Journal of Venomous Animals and Toxins Including Tropical Diseases*, 23, 24.

Mohapatra, B., Warrell, D.A., Suraweera, W., Bhatia, P., Dhingra, N., Jotkar, R.M., Rodriguez, P.S., Mishra, K., Whitaker, R., & Jha, P. (2011). Snakebite mortality in India: A nationally representative mortality survey. *PLoS Neglected Tropical Diseases*, 5, e1018.

Moura-da-Silva, A.M., Linica, A., Della-Casa, M.S., Kamiguti, A.S., Ho, P.L., & Crampton, J.M. (1999). Jararhagin ECD-containing disintegrin domain: Expression in *Escherichia coli* and inhibition of the platelet-collagen interaction. *Archives of Biochemistry and Biophysics*, 369(2), 295-301.

Mukherjee, A. K. (2020). Species-specific and geographical variation in venom composition of two major cobras in Indian subcontinent: Impact on polyvalent antivenom therapy, *Toxicon*, 188, 150-158.

Parvatam, S. (2018). India battles snakebite scourge. SciDev Net.

Perez, J.C., Garcia, V.E., & Huang, S.Y. (1984). Production of a monoclonal antibody against hemorrhagic activity of *Crotalus atrox* (western diamondback rattlesnake) venom. *Toxicon*, 22, 967-973.

Pillet, L. (1992). Anti-idiotypic and anti-anti-idiotypic responses to a monoclonal antibody directed to the acetylcholine receptor binding site of curaremimetic toxins. *Biochimica et Biophysica Acta*, 1138, 282-289.

Pinyachat, A., Rojnuckarin, P., Muanpasitporn, C., Singhamatr, P., &Nuchprayoon, S. (2011). Albocollagenase, a novel recombinant P-III snake venom metalloproteinase from green pit viper (*Cryptelytropsalbolabris*), digests collagen and inhibits platelet aggregation. *Toxicon*, 57(5), 772-780.

Potet, J., Beran, D., Ray, N., Alcoba, G., Habib, A.G., et al. (2021). Access to antivenoms in the developing world: A multidisciplinary analysis. *Toxicon: X*, 12, 100086.

Pukrittayakamee, S., Esnouf, M.P., & McMichael, A.J. (1983). Purification and inactivation of the factor X activator of Russell's viper venom with monoclonal antibodies. *Molecular Biology in Medicine*, 1, 123-135.

Ramos, H.R., & Ho, P.L. (2015). Developing snake antivenom sera by genetic immunization: A review. In Gopalakrishnakone, P. et al. (Ed.) *Clinical Toxinology in Asia Pacific and Africa. Toxinology* (pp. 402-411), Springer, Dordrecht.

Riaño-Umbarila, L., Gómez-Ramírez, I.V., &Ledezma-Candanoza, L.M. (2019). Generation of a broadly cross-neutralizing antibody fragment against several mexican scorpion venoms. *Toxins*, 11, 32.

Richard, G., Meyers, A.J., McLean, M.D., Arbabi-Ghahroudi, M., MacKenzie, R., & Hall, J.C. (2013). *In vivo* neutralization of alpha-cobratoxin with high-affinity llama single-domain antibodies (V_HHs) and a V_HH-Fc antibody. *PLoS ONE, 8, 2013.*

Rivel, M., Solano, D., Herrera, M., Vargas, M., Villalta, M., Segura, A., Arias, A.S., Leon, G., & Gutierrez, J.M. (2016). Pathogenesis of dermonecrosis induced by venom of the splitting cobra, *Najanigricollis*: An experimental study in mice. *Toxicon*, 119, 171-179.

Rogalski, A., Soerensen, C., op den Brouw, B., Lister, C., Dashvesky, D., Arbuckle, K., Gloria, A., Zdenek, C.N., Casewell, N.R., Gutiérrez, J.M., Wüster, W., Ali, S.A., Masci, P., Rowley, P., Frank, N., & Fry, B.G. (2017). Differential procoagulant effects of saw-scaled viper (Serpentes: Viperidae: *Echis*) snake venoms on human plasma and the narrow taxonomic ranges of antivenom efficacies. *ToxicologyLetters*, 280, 159-170.

Rossetto, O., &Montecucco, C. (2008). Presynaptic neurotoxins with enzymatic activities. Handbook of Experimental Pharmacology, 184, 129-170.

Rucavado, A., Nicolau, C.A., Escalante, T., Kim, J., Herrera, C., Gutierrez, J.M., & Fox, J.W. (2016). Viperid envenomation wound exudate contributes to increased vascular permeability via a DAMPs/TLR-4 mediated pathway. *Toxins (Basel)*, 8, 349.

Sanchez, E.F., Santos, C.I., Magalhaes, A., Diniz, C.R., Figueiredo, S., Gilroy, J., & Richardson, M. (2000). Isolation of a proteinase with plasminogen-activating activity from *Lachesis mutamuta* (bushmaster) snake venom. *Archives of Biochemistry and Biophysics*, 378, 131-141.

Schetinger, M.R., Rocha, J.B.T., Ahmed, M., &Morsch, V.M. (2009). Snake venom acetylcholinesterase. In S.P. Mackessy (Ed.), Handbook of Venoms and Toxins of Reptiles (pp. 207-219). CRC Press Inc., London, UK.

Sciani, J.M., &Pimenta, D.C. (2017). The modular nature of bradykinin-potentiating peptides isolated from snake venoms! *Journal of Venomous Animals and Toxins Including Tropical Diseases*, 23, 45.

Segura, A., Herrera, M., Villalta, M., Vargas, M., Gutiérrez, J.M., & León, G. (2013). Assessment of snake antivenom purity by comparing physicochemical and immunochemical methods. *Biologicals*, 41, 93-97.

Selistre-de-Araujo, H.S., de Souza, E.L., Beltramini, L.M., Ownby, C.L., & Souza, D.H. (2000). Expression, refolding, and activity of a recombinant nonhemorrhagic snake venom metalloprotease. *Protein Expression and Purification*, 19(1), 41-47.

Serrano, S.M., &Maroun, R.C. (2005). Snake venom serine proteinases: Sequence homology vs. substrate specificity, a paradox to be solved. *Toxicon*, 45,1115-1132.

Shashidharamurthy, R., &Kemparaju, K. (2007). Region-specific neutralization of Indian cobra (*Najanaja*) venom by polyclonal antibody raised against the eastern regional venom: A comparative study of the venoms from three different geographical distributions. *International Immunopharmacology*, 7, 61-69.

Siigur, E., &Siigur, J. (1991). Purification and characterization of lebetase, a fibrinolytic enzyme from *Viperalebetina* (snake) venom. *Biochimica et Biophysica Acta (BBA)-General Subjects*, 1074, 223-229.

Sitprija, V., &Sitprija, S. (2012). Renal effects and injury induced by animal toxins. *Toxicon*, 60, 943-953.

Smith, J.M., Amara, R.R., Campbell, D., Xu, Y., Patel, M., & Sharma, S. (2004). DNA/MVA vaccine for HIV type 1: Effects of codon-optimization and the expression of aggregates or virus-like particles on the immunogenicity of the DNA prime. *AIDS Research and Human Retroviruses*, 20(12), 1335-1347.

Sunagar, K., Fry, B.G., Jackson, T.N., Casewell, N.R., Undheim, E.A., Vidal, N., Ali, S.A., King, G.F., Vasudevan, K., & Vasconcelos, V. (2013). Molecular evolution of vertebrate neurotrophins: Co-option of the highly conserved nerve growth factor gene into the advanced snake venom arsenalf. *PLoS ONE*, 8, e81827.

Suntravat, M., Jia, Y., Lucena, S.E., Sanchez, E.E., & Perez, J.C. (2013). cDNA cloning of a snake venom metalloproteinase from the eastern diamondback rattlesnake (*Crotalus adamanteus*), and the expression of its disintegrin domain with anti-platelet effects. *Toxicon*, 64, 43-54.

Tanjoni, I., Butera, D., Spencer, P.J., Takehara, H.A., Fernandes, I., & Moura da Silva, A.M. (2003). Phylogenetic conservation of a snake venom metalloproteinase epitope recognized by a monoclonal antibody that neutralizes hemorrhagic activity. *Toxicon*, 42, 809-816.

Tasoulis, T., &Isbister, G.K. (2017). A Review and database of snake venom proteomes. *Toxins*, 9, 290.

Vauquelin, G., & Charlton, S.J. (2013). Exploring avidity: Understanding the potential gains in functional affinity and target residence time of bivalent and heterobivalent ligands. *British Journal of Pharmacology*, 168, 1771-1785.

Wagstaff, S.C., Laing, G.D., Theakston, R.D., Papaspyridis, C., & Harrison, R.A. (2006). Bioinformatics and multiepitope DNA immunization to design rational snake antivenom. *PLoS Medicine*, 3(6), e184.

Whitaker, R., & Whitaker, S. (2012). Venom, antivenom production and the medically important snakes of India. *Current Science*, 103, 635-643.

Williams, H.F., Hayter, P., Ravishankar, D., Baines, A., Layfield, H.J., Croucher, L., Wark, C., Bicknell, A.B., Trim, S., &Vaiyapuri, S. (2018). Impact of *Najanigricollis* venom on the production of methaemoglobin. *Toxins*, 10, 539.

Williams, H.F., Layfield, H.J., Vallance, T., Patel, K., Bicknell, A.B., Trim, S.A., &Vaiyapuri, S. (2019). The urgent need to develop novel strategies for the diagnosis and treatment of snakebites. *Toxins*, 11, 363.

Yadava, A., &Ockenhouse, C.F. (2003). Effect of codon optimization on expression levels of a functionally folded malaria vaccine candidate in prokaryotic and eukaryotic expression systems. *Infection and Immunity*, 71(9), 4961-4969.

Yan, J., Yoon, H., Kumar, S., Ramanathan, M.P., Corbitt, N., &Kutzler, M. (2007). Enhanced cellular immune responses elicited by an engineered HIV-1 subtype B consensus-based envelope DNA vaccine. *Molecular Therapeutics*, 15(2), 411-421.

Yuan, C.H., He, Q.Y., Peng, K., Diao, J.B., Jiang, L.P., Tang, X., & Liang, S.P. (2008). Discovery of a distinct superfamily of Kunitz-type toxin (KTT) from tarantulas. *PLoS ONE*, 3, e3414.

***

Indian J. Applied & Pure Bio. Vol. 37(2), 488-498 (2022). **ISSN: 0970-2091**
A web of Science Journal

Studies on some Haematological parameters including Cellular Phagocytosis interaction occurring in the larval stages as well as in imago of *Bombyx mori* L. (Lepidoptera: Bombycidae) Breeds

Dipak Kumar Som[1*], Somdip Mazumder[**], Jesmine Murshed[*], Monika Das[*] and Salil Raha[**]

*****Division of Entomology, Department of Zoology, Maulana Azad College, Kolkata-700013 (India)
******Department of Sericulture, Murshidabad University, Berhampore, Murshidabad-700013 (India)
[1]Corresponding author mail id: dipaksom@gmail.com

Abstract

The motive of the present work is to confer different haematological parameters in healthy larval and adult mulberry silkworm *Bombyx mori* L. on the three commercial breeds viz. hybrid (Nistari X M12W), bivoltine (NB4D2) and multivoltine (Nistari) along with cellular defensive role in diseased state. Five types of haemocytes, viz. prohaemocytes, plasmatocytes, granulocytes, Spherulocytes, and Oenocytoids are recorded in both healthy adults and 5th instar larvae in contrast to six types of haemocytes including imaginal Spherulocytes recorded prior this study. Discrete Total Haemocyte Count (THC) and Differential Haemocyte Count (DHC) values in the 5th instar larvae among these breeds showed significant differences with the values decreased in the order multivoltine breed, Nistari >bivoltine breed NB4D2. Under infected conditions, THC value in the 5th instar larvae increased in the order of multivoltine breed > bivoltine breed NB4D2 when counted from day 1 to day 4 of developing 5th instar larvae. In both cases declining haemocyte population turn down sharply on the day 5 of 5th instar larval development just prior spinning. Cellular defense response of Nistari breed, against bacterial infection was also studied in their functional aspects, and sequential steps followed in phagocytosis interaction to defend itself against infection from the beginning were also investigated. This comprehensive study may provide an additional reference for the future researches of insect immunity.

Haemocytes in insect's life play significant roles, either functioning alone or in alliance with the haemolymph. The mulberry Silkworm *B. mori* L. lacks an adaptive immune system but depends solely on innate immunity comprising of humoral and cellular immunity to fight against disease causing pathogens[9]. The "blood cells" in the Silkworm, *Bombyx mori* L. are classified into six types in adult viz. Prohaemocytes, Plasmatocytes, Granulocytes, Spherulocytes, Imaginal Spherulocytes (occasionally observed in pupa or the day before emergence) and Oenocytoids[12]. It was also established long ago that five types of haemocytes in *B. mori* L. larvae functioning in various ways including prevention of pathogenic microorganisms which are known as Prohaemocytes, Plasmatocytes, Granulocytes, Spherulocytes and Oenocytoids[2,3]. It has also been established that the number of haemocytes tend to increase during the larval instars peak in 5th instar and reducing the numbers as observed in the pupa and adult stages[12]. THC and DHC analyses indicate the susceptibility status of the insect which signifies the importance of haematological studies in the field of silkworm physiology. Keeping these in mind, we carried out THC and DHC determination of commercial silkworm breeds along with related haematological parameters to corroborate their susceptible tendencies in healthy and diseased conditions as haemocytes are basically influenced by environmental conditions and disease stresses[13]. Circulating haemocytes carry out cellular defence via phagocytosis, nodulation or encapsulation as reported earlier by Wood and Jasinto[16] and present study also emphasized on phagocytosis interaction against flacherie caused by *Bacillus thuringiensis*. The present study is restricted to the commercial Nistari (multivoltine), NB4D2 (bivoltine) and hybrid (Nistari X M12W) to give a comparable view of the distinct varieties of haemocytes present in both larval and adult stages and to recognize them instantly along with their functional aspects.

Healthy silkworm breeds viz. Nistari (multivoltine), NB4D2(bivoltine) and N X M12W (hybrid) were collected and reared at Krishnath College, Berhampore, Murshidabad presently Murshidabad University, West Bengal during both spring as well as summer season (2018-2020) in the laboratory as per standard rearing protocol with room temperature of 32^{o}C, humidity of 80%-95% and natural photoperiod. Larvae were fed on mulberry leaves S1 variety as per recommendation. The 3rd instar (Nistari, NB4D2), 4th instar (Nistari, NXM12W), 5th instar (NB4D2) larvae, pupae and adults (Nistari) were used for our experiments. Some flacherie infected 4th and 5th instar larvae were also procured from C.S.R & T.I, Government of India, Berhampore, West Bengal for our studies and these larval stocks were separately maintained in the bio-safety laboratory, Division of Entomology, Maulana Azad College, Kolkata with utmost care. Haemolymph collection, staining, THC and DHC determination were done following Jones[8] and Jalali & Salehi[7]. The smear was examined and visualized with a compound microscope (Magnus-MLXDX 11E634) at 40X magnification and after that images were acquired. Morphometric analyses were executed with the help of ocular and stage micrometer and the average size of the haemocyte types was

estimated by measuring the length and width of five cells of each type by calibration and standardization of the microscope. Close observations were made under Phase Contrast Microscope to study phagocytosis interactions of the haemocytes.

THC and DHC analysis of haemocytes showed significant differences with the values in observing seasonal and day to day occurrences among studied breeds under both healthy and infected conditions. Haemocytes of healthy mulberry silkworm larvae *Bombyx mori* L at their 4th and 5th instars were observed for THC (Table-1).

Table-1. THC values of silkworm breeds (Number/ mm^3) in two seasons.

Silkworm Breeds	Spring, 2019	Summer, 2019
Pure Mysore	9300	9800
Nistari Silkworm	9900	10600
NB4D2	8300	8200

Higher THC values in the healthy 5th instar larvae of multivoltine breeds occurring than the bivoltine breeds is due to the development of primary haemocytes.

Above findings of two commercial breeds of West Bengal in comparison to that of Pure Mysore race as reported earlier showed deviations with the results of Paul *et al.*,[14] and they explained that feeding efficiencies in the larval stages are responsible to increase the number of haemocytes in both the seasons. Our study is also adding another important factor that influencing increased haemocytes in both the breeds of *Bombyx mori* L. Higher THC value in multivoltine breeds is probably due to a large number of haemocyte populations producing from the haematopoietic organs as hematopoietic tissue (Fig-1). These primary haemocytes are prohaemocytes and plasmatocytes. These are pluripotent and the main sources for other cell types. Further, it can be explained as higher survival chances for multivoltine breed during summer due to increased number of haemocyte populations. In healthy 5th instar larvae THC values in both multivoltine and bivoltine breeds recorded significant differences during 1st day to 5th day of 5th instar. The present study showed that multivoltine breed was found to have greater THC value than the bivoltine breed on all the days of the 5th instar larvae. In both breeds THC was found to be gradually increasing from the first day to the last day of the 5thinstar (Table-2). In healthy 5thinstar larvae THC value of multivoltine breed, Nistari ranged from 6.4 x 10^3/mm^3 on the 1stday to 10 x 10^3/mm^3 on the 5thday and in bivoltine breed NB4D2 value recorded from 3.2 x 10^3/mm^3 on the 1stday to 6.4 x 10^3/mm^{3}on the 5thday (Fig- 2).

Table-2. Day wise THC records in the 5th instar larvae of a multivoltine (Nistari) and a bivoltine (NB4D2) breed of the mulberry silkworm, *Bombyx mori* L. always pointed out greater population

Days	Multivoltine breed (Nistari) (10^3/mm^3)	Bivoltine breed (NB4D2) (10^3/mm^3)
Day 1	6.4	3.2
Day 2	7.2	4.2
Day 3	8.2	4.4
Day 4	9.4	5.2
Day 5	10.0	6.4

So, all these records can be explained for normal growth of larvae during their developmental period to attain maturity. Differences of THC values also noted in both these breeds.

Table-3. Types of haemocytes form and state of larval haemocytes

Haemocytes	Appearance	Position of nucleus	Nature of cytoplasm
Prohaemocytes (PR)	Round or spherical	Central	Basophilic
Plasmatocytes (PL)	Elliptical, fusiform	Largely central	Basophilic
Granulocyte (GR)	Spherical or oval	Central or eccentric	Slightly acidophilic
Spherulocytes (SP)	Round or oval	Generally eccentric	Basophilic
Oenocytoids (OE)	Rounded	Eccentric	Slightly acidophilic

Table-4. Haemocyte types in Nistari, NB4D2 and NXM12W breeds

	Instars	Haemocyte types				
Nistari	3rd instar	PR	PL	GR	OE	-
	4th instar	PR	PL	GR	OE	SP
	5th instar	PR	PL	GR	OE	SP
NB4D2	3rd instar	PR	PL	GR	-	-
	4th instar	PR	PL	GR	OE	SP
NXM12W	4th instar	PR	PL	GR	-	-

Characterization of larval haemocytes, morphometric analysis and their immune functions:

Adult *Bombyx mori* L. was reported to contain six types of haemocytes viz. Prohaemocytes (PRs), Plasmatocytes (PLs), Granulocytes (GRs), Spherulocytes (SPs), Imaginal Spherulocytes and Oenocytoids (OEs). However, in the mature 5th instar larvae five types of haemocytes were recognized earlier (Table-3) based on their morphology and functions as known from the works of Akai and Sato[1]. Further Balavenkatasubbaiah *et al.*,[2]; Ling *et al.*,[10], and Nakahar *et al.*,[11] described in detail for better understanding of all these haemocytes though Jones[8]; Gupta[6] and recently Tan *et al.*,[15] explained lesser numbers of larval haemocytes observed in Silkworm. In the present study following observations have been noted in 3rd to 5th instar larvae of those commercial breeds (Table-4).

Haemocyte types and their characteristics in silkworm (***Bombyx mori* L.**) have been studied extensively and are known from a large number of literatures. Here for instant recognition of those haemocytes, typical

morphology of its type and morphometric analysis along with a particular role in immunological studies have been focused for further works in this area of study. Prohaemocytes (PRs) were the smallest among all haemocytes and the nucleus occupied most of the cytoplasm which forms a very thin layer around the nucleus. Plasmatocytes (PLs) were highly polymorphic cells and significantly larger than PRs and their irregular shapes were due to cytoplasmic projections. Granulocytes (GRs) were the most common in all larval instars having variable in shape and size and contained large amount of different sized granules in the cytoplasm. Oenocytoids (OEs) were opaque in appearance and the cytoplasm contained fine and weak granulations. Spherulocytes (SPs) were irregular in shape and the cytoplasm was characterized by large vesicles with membrane-bound vacuoles containing spherules and appeared as bulbous swellings on the cell surface.

Morphometric Analysis :

The average size of each haemocyte type for healthy silkworms were evaluated by measuring the length and width of five cells of each type with the help of ocular and stage micrometer. The morphometric analyses of distinct haemocytes were measured and are depicted in the table-5.

Table-5. Micrometric measurements (µm) of haemocyte types in studied multivoltine and bivoltine breeds

	Instars	PRs	PLs	GRs	OEs	SPs
Nistari	3rd instar larvae	L=13.55 W=12.3	L=12.4 W=8.1	L=15.5 W=13	L=18.2 W=16.6	-
	4th instar larvae	L=10.56 W=8.4	L=13.55 W=10.58	L=16.38 W=13.8	L=23.47 W=19.46	L=16.25 W=14.8
	5th instar larvae	L= 13 W= 12	L= 22 W= 17	L= 24 W= 21	L= 24 W= 22	L= 27 W= 12
	Pupae	L=10.82 W=9.32	L=13.15 W=10.32	L=12.98 W=10.49	L=19.49 W=14.82	L=25.82 W=20.41
	Adult	L=10.32 W=9.49	L=14.32 W=9.98	L=12.82 W=10.48	L=19.15 W=17.49	L=16.65 W=13.73
NB4D2	3rd instar larvae	L=13.99 W= 12.66	L=11.86 W=9.15	L=17.69 W= 15.41	-	-
	5th instar larvae	L=10.61 W=8.73	L=14.15 W=11.65	L=16.48 W=14.49	L=21.99 W=18.65	L=12.78 W=11.94
NXM12W	4th instar larvae	L=0.99 W=7.99	L=10.66 W=8.49	L=14.15 W=12.8		

Micrometric observations showed instar wise little deviations and noted Oenocytoids are the largest of Bombyx haemocytes.

Table-6. Measurements of Standard Error (SE) of haemocyte types in studied multivoltine and bivoltine breeds

	Instars	Mean ± SE	
		Length	Width
Nistari	3rd instar larvae	14.91 ± 1.09	12.5 ± 1.50
	4th instar larvae	16.04 ± 1.91	13.40 ± 1.69
	5th instar larvae	22 ± 2.13	16.8 ± 1.91
	Pupae	16.45 ± 2.46	13.07 ± 1.85
	Adult	14.65 ± 1.36	12.23 ± 1.35
NB4D2	3rd instar larvae	14.51 ± 1.38	12.40 ± 1.47
	5th instar larvae	15.20 ± 1.74	13.09 ± 1.48
NXM12W	4th instar larvae	8.6 ± 3.21	9.76 ± 1.24

Table-7. THC (*10^3/mm^3) of Bivoltine & Multivoltine Breed under infected condition

Breeds	Day 1	Day 2	Day 3	Day 4	Day 5
NB4D2 Bivoltine	1.68	1.98	3.03	2.48	1.74
Nistari Multivoltine	1.96	2.25	3.21	3.64	2.23

Total and Differential haemocyte count of flacherie infected larvae in Multivoltine and Bivoltine breeds :

Flacherie is the most common bacterial disease that inflicts the maximum damage to sericulture practices. Due to varied symptoms the disease is also named as Sotton disease, shrinking disease, softening disease, faecal disease etc. The changing of reactions of 5th larval instars against *Bacillus thuringiensis* in both the breeds revealed highly prominent changes in the THC (Table-7). It was noted that initially there is a sharp fall in the circulating haemocytes than normal THC levels in the 5th instar larvae. So, it is indicating the deployment of defence cells chiefly plasmatocytes and granulocytes to fight against bacteria. The initial decrease in the THC's is indicative of the quick deployment of cells to the infection site to combat the invading pathogens.

Day wise THC values of infected 5th instar larvae in two breeds showing multivoltine breed> bivoltine breed when analysed for comparison.

Under infected conditions, THC value showed in multivoltine breed from 1.96 x 10^3/ mm^3 on day 1 and increased to 3.64 x 10^3/ mm^3on the 4th day of 5th instar larvae. In contrast to above breed, THC value showing less in bivoltine breed from 1.68 x 10^3/mm^3on the 1stday and increased to 2.48 x 10^3/mm^3 on the 4th day of 5th instar larvae (Fig-3). With the commencement of spinning there was a sharp fall in THC which drastically reduced in

the pupal stage (0.340×10^3+-0.303/mm^3) and it was higher in adults. These results indicated capacity to endure against diseases and the differences in between the two breeds due to their acquired characters.

In our observations THC value in both larval groups showed increased level first and immediately declining phases started under flacherie infected conditions and sharply declined just before spinning.

Bacterial infection decreased the number of prohaemocytes, granulocytes, plasmatocytes and Oenocytoids as observed in differential haemocyte count (DHC). On the other hand, the infection of Bombyx mori 5^{th} larval instar with Bacillus thuringiensis gradually increased the granulocyte count but still less than healthy ones.

Cellular defence and Phagocytic Interaction :

The cellular immune response includes the identification of pathogens, phagocytosis of invasive bacteria and viruses, nodulation of large microbial pathogens such as fungi and bacterial clusters and encapsulation of multicellular (parasitic) organisms. Zafar *et al.*,[17] clearly mentioned immunological responses in silkworm are accomplished by circulating haemocytes which play a significant role in innate immune mechanism. Present study reveals that pathogenic bacteria invade into the haemocoel of *Bombyx mori* L. at larval stage led to humoral and cellular immune response. Due to bacterial infection haemocytes underwent considerable structural changes. The contents of the granulocytes seem to swell giving the cell an extremely vacuolated appearance. Haemocytes (plasmatocytes and granulocytes) that have phagocytic response to the bacteria tend to form aggregations. These unstructured aggregations may later be encapsulated by other haemocytes or by cells may be released from the aggregations. The aggregated haemocytes appeared in haemolymph due to *B. thuringiensis* infection. A number of phagocytosing plasmatocytes, granulocytes and attached bacteria were also observed. Oenocytoids showed to have numerous patches of crystal like inclusions in the cytoplasm. Hyperphagocytic haemocytes are involved in nodule formation. It was earlier demonstrated that granulocytes and plasmatocytes are the major cells that phagocytized pathogenic bacteria in the larval stages of *Bombyx mori* L. According to Carton and Nippi[4] phagocytosis, encapsulation and nodule formation is the main reaction for clearance of pathogen and other foreign particles. As we know that the process of phagocytosis is accomplished in a single cell, involving the identification, phagocytosis, destruction of invasive pathogens and death of cells occur as described by Gray and Botelho[5]. Our findings facilitated phagocytosis where phagocytic cells recognized foreign particles through a series of receptors on their cell membrane for pathogen associated molecules. These receptors in turn initiate a series of signaling pathway that instruct the cells to ingest and eventually destroy the foreign particles. Following steps have been evaluated during the process of phagocytosis- 1) when foreign particles or organisms are too large for either phagocytosis or nodule formation is completely destroyed by encapsulation. 2) At the initial stages foreign

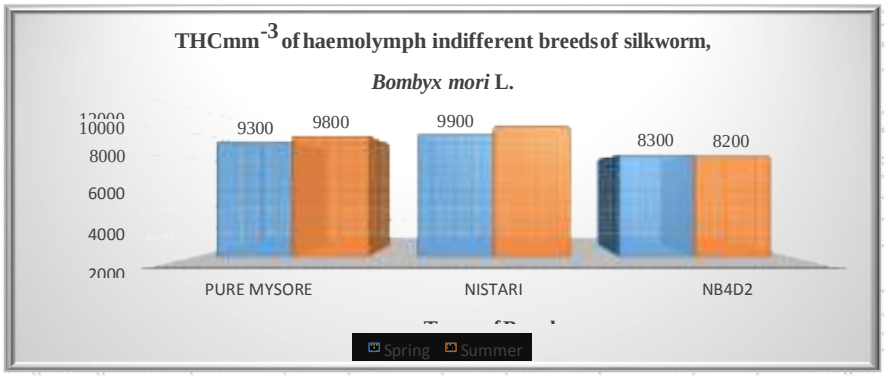

Fig. 1. Seasonal comparisons of THC values

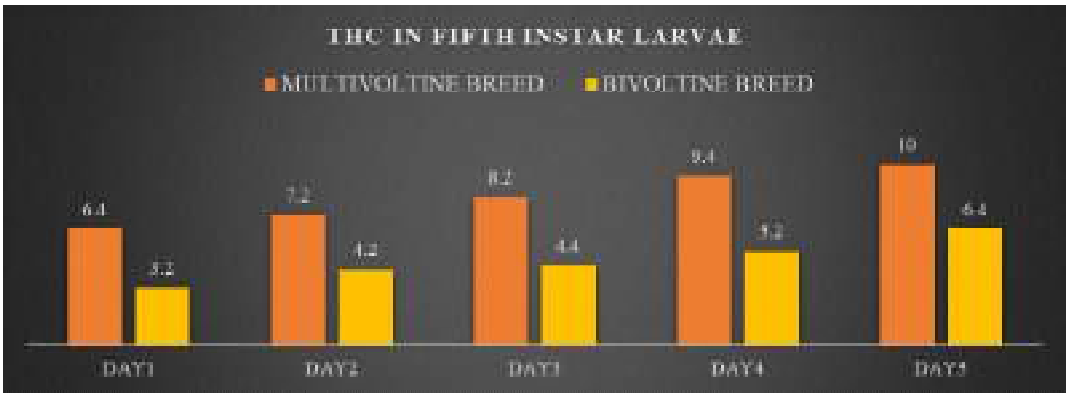

Fig. 2. Day wise THC analysis. Gradual increased THC values in both breeds indicating healthy larval growth

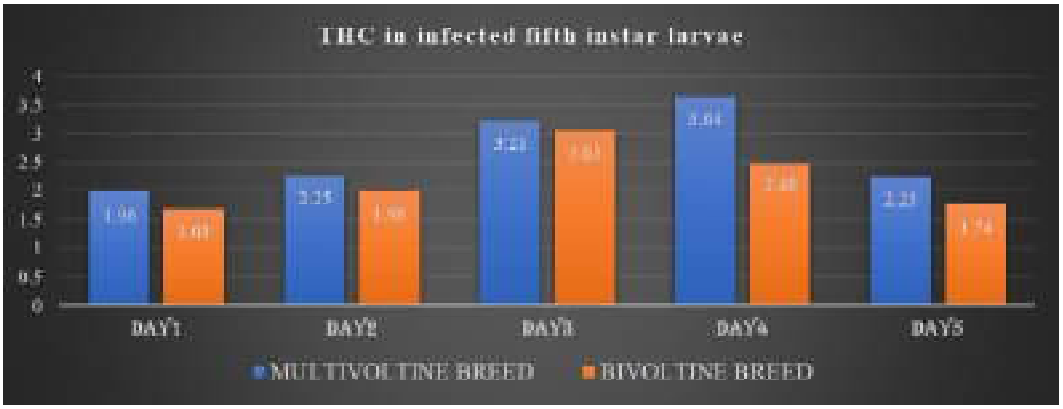

Fig. 3. Day wise THC values of infected 5th instar larvae in two breeds showing multivoltine breed> bivoltine breed when analysed for comparison

(A) (B)

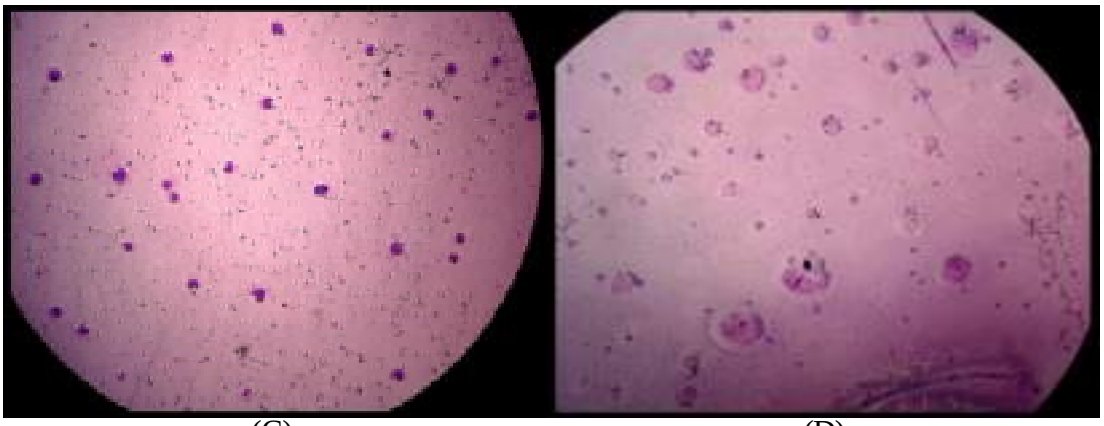

(C) (D)

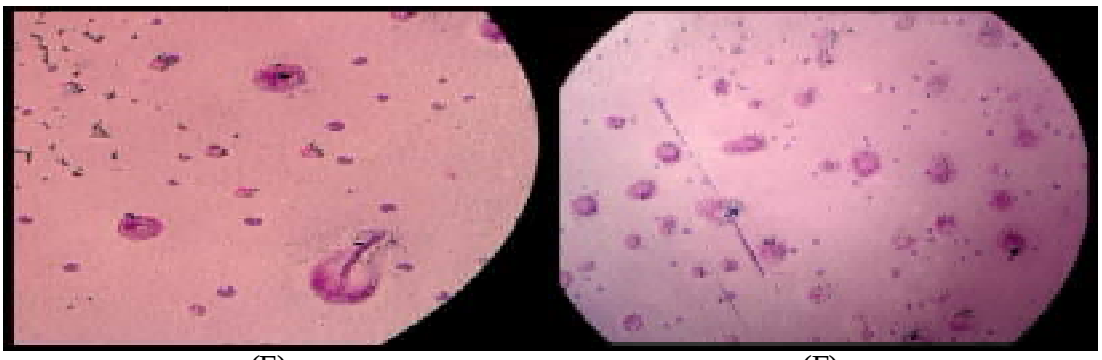

(E) (F)

ILLUSTRATIONS:

Fig-4

A – Healthy 5th instar larvae of Nistari	**B** – Infected 4th instar larvae of Nistari (First day)
C – Prohaemocytes (Nistari)	**D** – Granular haemocytes (Nistari)
E – Encapsulation	**F** – Lysis of Granulocytes

body is randomly contacted by a granulocyte which recognizes the particular existence. 3) The Granulocyte degranulates and material sticks to foreign body which is responded by additional granulocytes attacking to foreign bodies. 4) Lysis took place and granulocytes release a haemocytic recognition factor that attracts and recruits plasmatocytes to attach foreign body. 5) Plasmatocytes then flatten and spread over the foreign body surface increasing the number of layers around the foreign food so long that it is no longer recognized as foreign particles.

Information on the haemocyte population within an insect is essential for strengthening physiological studies. The haemocytes of *Bombyx mori* L. are also the examples of classic types as found in *Drosophila* (Diptera) which are engaged in different roles in host defence reactions. All our findings in regard to phagocytic response are consistent with the general idea that the nature of infecting bacteria influences interaction. The THC and DHC values in the 5^{th} instar larvae among the studied breeds showed significant differences with the values decreased in the order multivoltine breed, Nistari >bivoltine breed NB4D2. Finally, it is clear from the study that, under infected conditions, THC value in the 5^{th} instar larvae increased in the order of multivoltine breed > bivoltine breed NB4D2 when counted from day 1 to day 4 of developing 5^{th} instar larvae. In both cases declining haemocyte population turn down sharply on the day 5 of 5^{th} instar larval development just prior spinning. So, multivoltine of Silkworm contains more circulating cells and more defence cells against bacterial invasions than the bivoltine breed so far examined. Further investigations will certainly add more information about activation of haemocytes against different pathogens to defend.

The authors are grateful to the Department of Science & Technology and Biotechnology, Government of West Bengal for providing financial support to the present study (Vide Memo No. 204 (Sanc.)/ST/P/S & T/1G-45/2017 dated 21.03.2018 and Memo No. 640(Sanc.)/STBT-11012(27)/18/2020-ST SEC dated 21.12. 2020). The authors also express their sincere thanks to Dr. Sujata Bagchi Banerjee, Hon'ble Vice Chancellor, Murshidabad University, formerly Principal, Krishnath College, Berhampore, Murshidabad, West Bengal, Dr. Subhasis Dutta, Principal, Maulana Azad College, Kolkata, West Bengal and Dr. Subir Chandra Dasgupta, Professor and Head, Post Graduate Department of Zoology, Maulana Azad College, Kolkata for providing necessary facilities to complete this work.

References :

1. Akai, H., and S. Sato, (1973) *Int. J. Insect Morphol. Embryol. 2:* 207-231.
2. Balavenkatasubbaiah, M., B. Nataraju, V. Thiyagarajan, and R.K. Datta, (2001) *Indian J. Seric. 40*(2): 158- 162.
3. Balavenkatasubbaiah, M. and B. Nataraju (2005) *Madras Agricultural Journal, 92*(7-9): 431-437.
4. Carton, Y., and, A.J. Nippi (1997) *Parasitology today, 13:* 89-104.
5. Gray, M. and R.J. Botelho (2017) Springer,

New York.

6. Gupta, A.P. (1979) Cambridge University Press, Cambridge, London.
7. Jalali, J. and R. Salehi, (2008) *Munis Entomology and Zoology Journal, 3*(1): 199-216.
8. Jones, J.C. (1962) *Amer. Zoot. 2:* 209-246.
9. Lavine, M.D. and M.R. Strand, (2002) *Insect Biochemistry & Molecular Biology, 32:* 1295-1309.
10. Ling, E., K. Shirai, R. Kanekatsu, and K. Kiguchi, (2003) *Histochemistry and Cell Biology 120:* 505-511.
11. Nakahara, Y., S. Shimura, C. Ueno, Y. Kanamori, K. Mita, and M. Kiuchi, (2009) *Dev Comp Immunol. 33:* 439-448.
12. Nittono, Y. (1960) *Bull. Seric. Expt. Stn; 16:* 261-266.
13. Pandey, J.P., P.K. Mishra, D. Kumar, B.M.K. Singh, and B.C. Prasad, (2010) *Res J Immunol. 3: 1*69-177.
14. Paul, D.C., G. Subba, Rao and D.C. Deb, (1992) *Journal of Insect Physiology, 38:* 229-230.
15. Tan, J., M. Xu, K. Zhang, X. Wang, S. Chen, and T. Li, *et al.* (2013) *J. Insect Physiol. 59:* 595-603.
16. Wood, W. and A. Jasinto, (2007) *Nature reviews: Molecular cell Biology, 8:* 542-551.
17. Zafar, B., S.A. Wani, M.A. Malik, and M.A. Ganai, (2013) *Asian Journal of Science and Technology 4*(11): 157-166.

Cobra venom neutralization by gold nano particle-2-hydroxy-4-methoxy benzoic acid

Sir,

Snake envenomation have been treated by ASVS, with many limitations/side effects[1] but from ancient time herbs and herbal compounds were in use against snake bite. Herbs/herbal compounds may overcome the drawbacks of ASVS.[2] 2-Hydroxy-4-methoxy benzoic acid (HMBA), from Indian sarsaparilla had effective neutralization potential against Russell's viper venom.[2] HMBA conjugated with nano-sized gold particle enhanced efficacy against Russell's viper venom.[3,4] *Naja kaouthia* (cobra) found in south-east Asian countries, including India, causing fatal bites.[5] This study was an attempt to establish experimental neutralization potential of a herbal-nano compound (Gold nanoparticle [GNP]-HMBA) against *Naja kaouthia* venom (NKV).

GNP was conjugated with HMBA as reported earlier.[4] NKV was purchased and processed.[5] Albino Swiss male mice of 18–22 g were used as per the guidelines of IAEC and grouped ($n=6$): (1) control, (2) NKV treated, (3) NKV + HMBA treated, (4) NKV + GNP-HMBA treated, and (5) NKV + GNP treated. The minimum lethal dose (MLD) amount of NKV was incubated with HMBA/GNP-HMBA/GNP stored at 37°C and injected (intravenous [iv]) and efficacy of NKV neutralization was evaluated up to 24 h. Group 1, 2, 3, 4, and 5 animal's paw were injected (subplanter) with 0.9% saline, NKV, NKV + HMBA, NKV + GNP-HMBA and NKV + GNP, respectively, and the paw diameters were measured at 0 and 8 h for the minimum edema dose (MED) of NKV, i.e., 2 µg. For NKV induced oxidative toxicities and inflammatory changes, Group 2, 3, 4, and 5 animals were injected with 5 µg NKV (*s. c.*), after 1 h followed by injections (IV) of 0.9% saline (100 µl), HMBA (100 µl), GNP-HMBA (200 µl) and GNP (100 µl), respectively, and observed till 24 h and sacrificed for blood collection, serum preparation. The degree of neutralization of NKV Phospholipase was determined by mixing the venom (1–5 units) with HMBA/GNP-HMBA/GNP (37°C/15 min) and evaluating the PLA_2 activity. NKV-induced plasma recalcification neutralizing potential of HMBA/GNP-HMBA/GNP and hemolytic activity of NKV was tested by standard protocol. The significant differences between data (mean ± standard error of mean) were measured using one-way ANOVA at $P < 0.05$.

MLD of NKV in IV route was 5 µg. GNP and HMBA offered no protection against 1 MLD dose but GNP-HMBA showed protection against 1 MLD dose. NKV-induced MED was 2 µg. Protection offered by GNP-HMBA was 4 MED, as compared with HMBA (3MED) and GNP (1MED). Serum reduced glutathione (GSH), superoxide dismutase (SOD), catalase were decreased (35.39%, 57.42%, and 33.24%, respectively) and lipid peroxidation (LPO) was increased (147.4%) (significance at $P < 0.05$) in when compared with venom control group [Table 1]. Treatment with HMBA increased (significance at $P < 0.05$) GSH, SOD, and catalase (61.36%, 53.85%, and 62.54%, respectively) and decreased LPO (55.17%) when compared with venom control group. GNP-HMBA treatment increased (significance at $P < 0.05$) GSH, SOD, catalase (65.16%, 87.85%, and 101.39%, respectively) and decreased (significance at $P < 0.05$) LPO (66.32%) when compared with venom control group. Treatment with GNP offered no protection against venom-induced changes in oxidative stress and inflammatory markers when compared with venom control animals. NKV injection in venom control animals increased serum

Table 1: Effect of gold nanoparticle -2-hydroxy-4-methoxy benzoic acid on antioxidant parameters in *Naja kaouthia* venom induced stress on Swiss male albino mice

Animal group	Antioxidant parameters			
	GSH (µM/mg protein)	SOD (IU/mg protein)	Catalase (IU/mg Hb)	LPO (MDA/mg protein)
Group 1	120.15±11.05	51.06±3.05	38.71±6.25	7.97±9.27
Group 2	42.53±9.59#	29.32±8.92#	12.87±4.94#	19.72±7.28#
Group 3	110.08±6.03*	45.11±2.4*	20.92±4.11	8.84±2.43*
Group 4	122.08±3.13*	55.08±2.9*	25.92±4.32*	6.64±1.20*
Group 5	58.19±6.54	35.45±4.87	12.62±1.12	16.89±2.68

Group 1: Sham control, Group 2: Venom control, Group 3: HMBA treated, Group 4: GNP-HMBA treated, Group 5: GNP treated. Values were expressed as mean±standard error of mean (n=6), statistical analysis was done with one way ANOVA, #P<0.05 when compared to sham control group, *P<0.05 when compared to venom control group. GSH=Glutathione, SOD=Superoxide dismutase, LPO=Lipid peroxidation, GNP-HMBA=Gold nanoparticle -2-hydroxy-4-methoxy benzoic acid

cytokines (pro-inflammatory), i.e., tumor necrosis factor-alpha, interleukin 1 (IL1) β, and IL 17 and decreased serum antiinflammatory cytokine (IL-10) when compared with control animal. HMBA and GNP-HMBA decreased proinflammatory cytokines (significance at $P < 0.05$) and increased antiinflammatory cytokine when compared with venom control animals [Figure 1]. *In vitro* NKV PLA2 activity was neutralized by HMBA and GNP-HMBA. The degree of neutralization of NKV PLA2 was GNP-HMBA (3-fold) >HMBA (2-fold) >GNP (1-fold). NKV (4 μg) increased the plasma (goat) recalcification time by 60 s when compared with control group. The degree of neutralization of plasma recalcification time was GNP-HMBA (1fold) > HMBA and GNP (no protection). 1 HD_{50} of NKV was found to be 4 μg. The degree of neutralization of HD_{50} was GNP-HMBA (1.5-fold) >HMBA (1-fold) >GNP (no protection).

NKV PLA_2 activity was neutralized by GNP-HMBA, which may contribute to the protection of NKV-induced hemolysis, oxidative stress. NKV-induced decrease of GSH, SOD and catalase, and increase in LPO, suggesting oxidative stress. ASVS did not neutralize venom-induced oxidative stress.[5] Treatment with GNP-HMBA increased the GSH, SOD, catalase and decreased LPO, indicating the production of antioxidants inside the body and neutralizing the venom-induced prooxidant effects. Cobra envenomation increased the release of serum pro-inflammatory cytokines from T-cells and activated macrophages, and decrease in anti-inflammatory cytokine release leading to inflammation.[5] GNP-HMBA treatment significantly inhibited proinflammatory cytokines release and stimulated antiinflammatory cytokine production, resulting in restoration of serum cytokine equilibrium. GNP alone could not neutralize venom-induced inflammation and oxidative stress, but it may be suggested that GNP conjugation with HMBA leads to increase in the availability, uptake, and utilization of HMBA at local sites.

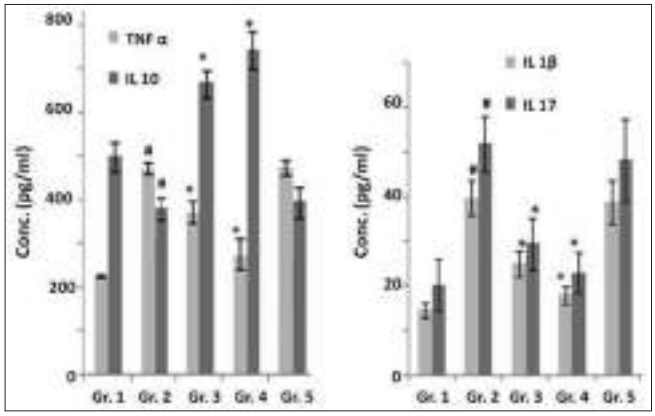

Figure 1: Effect of gold nanoparticle -2-hydroxy-4-methoxy benzoic acid on serum proinflammatory and antiinflammatory cytokines in *Naja kaouthia* venom-induced Swiss male albino mice. Gr. 1, sham control, Gr. 2 Venom control, Gr. 3 2-hydroxy-4-methoxy benzoic acid treated, Gr. 4 Gold nanoparticle -2-hydroxy-4-methoxy benzoic acid treated, Gr. 5 Gold nanoparticle treated. Values were expressed as mean ± standard error of the mean ($n = 6$), statistical analysis was done with one way ANOVA, $^{\#}P < 0.05$ when compared to sham control group, $^{*}P < 0.05$ when compared to Venom control group

In conclusion, the present study indicated the increased NKV neutralization potential of HMBA after the conjugation with GNP, i.e., GNP-HMBA significantly neutralized NKV-induced toxicity in experimental *in vivo* and *in vitro* models which may be utilized for designing supportive treatment against snake (Naja) bite.

Acknowledgment
UGC, Government of India.

Financial support and sponsorship
Nil.

Conflicts of interest
There are no conflicts of interest.

Kalyani Saha, Sourav Ghosh, Aparna Gomes[1], Subir Chandra Dasgupta[2], Antony Gomes

Department of Physiology, Laboratory of Toxinology and Experimental Pharmacodynamics, University of Calcutta, [1]Department of Physiology, CSIR-Indian Institute of Chemical Biology, [2]Department of Zoology, Maulana Azad College, Kolkata, West Bengal, India

Address for correspondence:
Antony Gomes,
Department of Physiology, Laboratory of Toxinology and Experimental Pharmacodynamics, University of Calcutta, 92, A. P. C. Road, Kolkata - 700 009, West Bengal, India.
E-mail: agomescu@gmail.com

Submitted: 19-Jul-2018
Revised: 02-May-2019
Accepted: 18-Mar-2021
Published: 28-Apr-2021

References

1. Chippaux JP, Goyffon M. Antivenom serotherapy: Its applications, its limitations, its future. Bull Soc Pathol Exot 1991;84:286-97.
2. Alam MI, Auddy B, Gomes A. Isolation purification and partial characterization of viper venom neutralizing factor from the root extract of Indian medicinal plant Sarsaparilla (Hemidesmus indicus R. Br.). Toxicon 1994;32;155.
3. Gomes A, Sengupta J, Ghosh S, Gomes A. Application of gold nanoparticle conjugation with 2-hydroxy-4-methoxy benzoic

acid (HMBA) from Hemidesmus indicus Root Enhancing Neutralization of Snake (Viper) Venom Activity. J Nanosci Nanotechnol 2016; 16: 8322-9.

4. Saha K, Gomes A. Russell's viper venom induced nephrotoxicity, myotoxicity, hepatotoxicity: Neutralization with gold nanoparticle conjugated 2-hydroxy-4-methoxy benzoic acid (GNP-HMBA) in experimental animal models. Indian J Exp Biol 2017;55:7-14.
5. Saha K, Ghosh S, Ghosh S, Dasgupta SC, Gomes A, Gomes A. Neutralization of *Naja kaouthia* venom induced toxicity and stress response by Vitex negundo-gold nanoparticle (VN-GNP) in experimental animal models. J Toxins 2015;2:8.

Access this article online	
Quick Response Code:	Website: www.ijp-online.com
	DOI: 10.4103/ijp.IJP_370_18

How to cite this article: Saha K, Ghosh S, Gomes A, Dasgupta SC, Gomes A. Cobra venom neutralization by gold nano particle-2-hydroxy-4-methoxy benzoic acid. Indian J Pharmacol 2021;53:73-5.

Biomedical
Communication

BBRC
Bioscience Biotechnology
Research Communications

Biosc.Biotech.Res.Comm. Vol 14 No (1) Jan-Feb-March 2021 Pp 66-73

Emerging Applications of Nanotechnology in Neurological Disorders: Recent Review

Rajarshi Ghosh*, Pradip Bhattacharjee and Anish Pal
Department of Zoology, Maulana Azad College, Kolkata, West Bengal, India

ABSTRACT

The neurological disorders include Alzheimer's disease (AD), Parkinson's disease (PD), Huntington's disease, stroke, epilepsy, brain tumours, multiple sclerosis etc. which are the leading health concerns in today's world. The conventional therapies are not yet successful in treating these diseases because of the presence of intracellular and extracellular barriers across the central nervous system (CNS), which poses the major challenge of drug delivery to the CNS. The field of nanotechnology promises revolutionary advances of treating these devastating neuronal human disorders and has shown great potential to overcome the problems related to the conventional treatment approaches. Gold nanoparticles, micelles, quantum dots, polymeric nanoparticles, liposomes, microparticles, carbon nanotubes, fullerenes and several other types of nanoscale materials have been engineered and utilized for various purposes including improvement of diagnosis, delivery of neurotherapeutic agents, treatment-response assessment etc. The nanomaterials cross those barriers, target specific cell or signalling pathway, respond to endogenous stimuli, act as a vehicle for gene delivery and also support nerve regeneration. Such frameworks may serve as effective drug delivery systems and can pave the way for effective treatments in the neuronal disorders. It has been found that the drugs encapsulated with nanomaterials have better efficacy in eradicating the diseases than the bulk materials used in conventional therapies. But there are several basic concerns related to the therapeutic approach of nanotechnology, including health issues and other problems because of the very small size of nanomaterials. This review mainly aims to focus on the barriers which guard the CNS, the nanomaterials as effective drug delivery systems, their preparation, mechanism of action, nanoformulations of different neuroprotective agents, nano-neurotoxicity and future perspectives.

KEY WORDS: BLOOD-BRAIN BARRIER, NANOMATERIALS, NEURONAL DISORDERS, THERAPEUTIC DRUGS.

INTRODUCTION

The term 'Neurological Disorders' refers to central and peripheral nervous system diseases including the brain, spinal cord, cranial nerves, peripheral nerves, nerve roots, autonomic nervous system (ANS), neuromuscular junction and muscles. These disorders include cerebrovascular diseases, Parkinson's disease, Alzheimer's disease, Huntington's disease, amyotrophic lateral sclerosis, multiple sclerosis, brain tumour, stroke, neuroinfections, autism spectrum disorder and schizophrenia (Chhabra et al., 2015). Unfortunately, many potent neuropharmaceuticals aimed at providing a treatment for such disorders proved inefficient in large scale clinical trials. The reason, at least in part, is the unsuccessful delivery of substances to their targeted site of action inside the body. A wide spectrum of potential drugs has been investigated to treat several neurological disorders but their therapeutic success is still limited due to range of challenges (Sahoo et al., 2017).

The difficulty of crossing the peripheral barriers viz. the blood-brain barrier (BBB) and blood-cerebrospinal fluid barrier (BCSFB), particularly the BBB, is the key challenge

ARTICLE INFORMATION

*Corresponding Author: rajarshi.ghosh@maulanaazadcollegekolkata.ac.in
Received 15th Dec 2020 Accepted after revision 23rd March 2021
Print ISSN: 0974-6455 Online ISSN: 2321-4007 CODEN: BBRCBA

Thomson Reuters ISI Web of Science Clarivate Analytics USA and Crossref Indexed Journal

NAAS Journal Score 2020 (4.31)

*Online Contents Available at: http//www.bbrc.in/
DOI: http://dx.doi.org/10.21786/bbrc/14.1/9*

in delivering therapeutic agents such as medicines, nucleic acids, proteins, imaging agents and other macromolecules to the CNS (Sahoo et al., 2017). Nanotechnology is an innovative and promising approach for delivering these neurotherapeutics across BBB. Although the assembly and use of nano-sized particles had taken place many years ago, nanomedicine was first established as an interdisciplinary science within the nineties of the last century. The nanotechnological approach was first framed within the 1950's and soon the constitutive force to determine nanomedicine gained importance as a paramount section in science and medical treatments (Krukemeyer et al., 2015 Sohail et al., 2020).

In the last few decades, due to its nano-size range, its unique physico-chemical properties and ability to exploit surface engineered biocompatible and biodegradable nanomaterials, drugs loaded inside nanoparticles (Table 1) have shown great potentials for efficient drug delivery to CNS (Aso et al., 2019). These nanoparticles can be made through different approaches which are illustrated in Table 2. Nanotechnology will gain importance in the coming decade in medical field, as it has the capability to improve the quality of life of the patients having neuronal disorders (Sohail et al., 2020). After the successful implementation of the strategies in nanotechnology, the growth of the field of neural circuitry has exponentially accelerated (Sohail et al., 2020).

Recent years have witnessed an explosion of research studies in the field of nanotechnology which opens up new probabilities in drug delivery, theranostics, tissue engineering, magnetofection and gene therapy (Krukemeyer et al., 2015). The effectiveness of nanotechnology is now well established and it has carved path for new and very efficient systems for drug delivery even to the most inaccessible regions such as CNS (Kumar and Singh, 2015). In this review, we strive to explain the applications of nanotechnology in neurological disorders by identifying the key principles, concepts and techniques, which will lead to further understanding in this topic and will call for much more research (Naqvi et al., 2020).

Blood Brain Barrier (BBB) and Blood Cerebrospinal Fluid Barrier (BCSFB): The brain has a very dense microvasculature with the average distance between the blood capillaries to be around 40 microns suggesting that each cell in the brain might have its own capillary (Duvernoy et al., 1983). The diffusion distances from nearest capillary to a neuron are approximately 10-20 nm (Schlageter et al., 1999). The epithelial cells of the choroid plexus (CP) contain tight junctions which limits the penetration of substances from blood to CSF.

But due to its low resistance (Saito, 1983), few substances penetrate from the blood into the CSF. For example, Azidothymidine (AZT) enters CSF through the choroid plexus epithelium but is tightly restricted at the BBB. The entry of a substance into the CSF may not allow its penetration into the brain parenchyma. The circumventricular organs are separated from the rest of the brain by the unique presence of ependymal and glial cells (Abbott et al., 2006) and penetration of substances from CSF to brain parenchyma is facilitated through diffusion. The large distances create a diffusion barrier that can be referred to as the CSF-brain barrier (CBB). The arachnoid barrier (AB) cells are present in subarachnoid space filled with CSF, which surrounds the brain and spinal cord which may act as a barrier and restrict the penetration of substances into the CSF (Yasuda et al., 2013; Sohail et al., 2020).

Strategies for Drug Delivery into CNS: Delivery of drugs through invasive techniques causes a number of problems like immunological inflammatory reactions, damage nervous system and many others. On the contrary, non-invasive technique such as nano drug delivery ensures drug delivery without damaging BBB (Jain, 2007). In this procedure, the targeted drug delivery in required quantity could be achieved by encapsulating the drug within a carrier system specially nanoparticles by the technique of nanotechnology. The nanoparticles should have a sufficient tensile strength to remain in the circulation for a long period without getting degraded. The delivery system may be either polymer based or lipid based (Naqvi et al., 2020).

Mechanism of Action of Drug Release with the help of Nanomaterials: Nanomaterials possessing positive surface charge electrostatically interact with the negative surface charge of endothelial cells present in brain, and further the lipophilic nature of nano-carriers facilitates adsorption process. The nanoparticles get absorbed by getting access to low density lipoprotein receptors on the brain capillary endothelial cells following normal endocytosis and transcytosis. Desorption occurs and then it re-enters into the blood stream, then on the surface of the blood brain barrier, the drug loaded nano carrier releases the encapsulated or adsorbed drug and further diffuses into brain parenchyma. Either passive, gradient-dependent (passive targeting) or active, energy-dependent (active targeting) pathways can lead to selective entry into the brain (Figure 1). The nano-carriers having a size less than 500 Da undergo transcellular transportation (Georgieva et al., 2014).

The nanoparticles can enter the cell through macropinocytosis, a vesicle mediated endocytosis or by phagocytosis which can be carried out through the following two pathways (Figure 2):

(i) Clathrin-Mediated Endocytosis: This mechanism occurs on all mammalian cells. The nano-carrier binds with a specific plasma membrane receptor, stimulating the polymerization of clathrin-1, a cytoplasmic protein just below the plasma membrane in order to form an inward budding leading to the engulf of cargo (Rappoport, 2008). The GTPase activity of dynamin pinches off the inward budding resulting into the formation of clathrin-coated vesicles. Actin helps in shedding of clathrin coat leading to the formation of early endosomes which deliver their content to late endosomes and finally to the lysosomes

where it is degraded off. During the transition from late endosomes to lysosomes, the pH gradually decreases, causing the release of the drug from the nano-vehicle and finally releasing the drug at the target site (Georgieva et al., 2014).

Table 1. Preparation of nanoparticles

Sr. No.	Techniques Used	Preparation Procedure	Types of Nanoparticles
1.	Solvent Evaporation	The polymer solutions are prepared in water-non-miscible, Organic volatile solvents ($CHCl_3$, $CHCl_2$, and C_4H8O_2). The Emulsion (o/w, w/o/w) undergoes evaporation of the solvent. The NPs are collected, washed, and lyophilized after ultracentrifugation	Poly (lactic-co-glycolic acid) (PLGA) nanoparticle isprepared by this method (Reis et al., 2006)
2.	Nanoprecipitation	A solution is prepared by dissolving polymer in water miscible organic solvent. For formation of colloidal suspension and its precipitation pipetting is done in stirring aqueous medium	Preparation of cyclosporine A loadedNPs (Allemann et al., 1998)
3.	Emulsification	The polymer is dissolved in partially water-soluble solvent in the presence of excess of water. This is then dissolved in aqueous solution having surfactant. Nano spheres or Nano capsules are produced depending on the concentration of oil and polymer	Doxorubicin (anti-cancer drug) loaded PLGA NPs is done by this method (Yoo et al., 1999)
4.	Salting Out	Drug and polymer are dissolved in a solvent(acetone). This is dissolved in an aqueous solution containing as calcium chloride or sucrose which acts as salting out agent and polyvinyl pyrrolidone acting as stabilizing agent. This forms o/w emulsion that is then diluted in excess water resulting in the production of Nano spheres	This technique is employed in formation of lipophilic drugs (Memisoglu et al., 2003)
5.	Supercritical Fluid Technology	In this process, rapid expansion of supercritical solution into liquid solvent (RESOLV) and rapid expansion of super critical fluids (RESS) was used	Submicron particles of cyclosporine, water insoluble drug (Young et al., 2000)
6.	Emulsion Polymerization	The monomer is dispersed in aqueous or organic non-soluble solvent followed by addition of surfactant. Polymerization is established either by adding an initiation molecule such as a free radical or by producing the radical by the monomer itself with the aid of radiation	Poly (styrene-methyl methacrylate) /SiO_2composite NPs (Mahdavian et al., 2007)

Table 1 Continue

7.	Ionic Gelation	A solution of a biodegradable polymer (chitosan or gelatin) and a di block polymer is produced and is then mixed with a solution of the drug to be incorporated. The molecules undergo electrostatic interactions resulting change of state form liquid to gel, the process is referred to as Gelation	Chitosan nanoparticles are produced by this process (Memisoglu et al., 2003)

Table 2. Nano approaches towards CNS drug delivery

Sr No.	Nanoparticles	Description	Uses
1.	Micelles	Micelles are the vesicles ranging from10 to 100 nm with outer hydrophilic portion and inner hydrophobic core (generally polypropylene glycols, phospholipids, fatty acids). They may be made up of either amphiphilic surfactants (non-polymeric micelles) or amphiphilic copolymers (polymeric micelles)	They help in the loading of hydrophobic drugsfor CNS delivery (Torchilin, 2007)
2.	Polymeric Nanoparticles	Polymeric nanoparticles (10-100 nm) are solid colloidal dispersion of biocompatible, biodegradable polymers. These have a core of dense polymer and a hydrophilic outer covering to provide steric stability	*Encapsulates lipophilic* drugs which may be encapsulated, adsorbed or chemically attached to the surface (Sahoo et al., 2017)
3.	Solid Lipid Nanoparticles (SLN)	They are aqueous colloidal nano-carrier system composed of lipids (triglycerides, fatty acids, steroids, etc.), introduced aqueous surfactant solution or water and enerally solidify on cooling	Quercetin loaded to treat AD, Atazanavir loaded against HIV-encephalitis (Chattopadhyay et al., 2008)
4.	Nano Emulsions	Nano emulsions (100-500nm) are o/w or w/o colloidal particulate systems which are made up of edible oils, surfactants and water.	Modification of nano emulsions helps in overcoming the BBB, helping in rapid distribution of drugs to peripheral sites, mainly the brain (Shah et al., 2013)
5.	Dendrimers	Dendrimers have 3-dimensional symmetrical structure having an inner core from which there is a number of hyper branches, ('generations') with functional groups at the peripheral terminal surface to be easily functionalized with many ligands	Dendrimers are used for hydrophobic and hydrophilic drug delivery (Tripathy and Das, 2013; Sohail et al., 2020)
6.	Carbon Nanotubes and Fullerenes	These are carbon allotropes which are characterized by a hollow structure and striking thermal, electrical and mechanical properties. Fullerenes are of two types- Spherical Fullerenes and Cylindrical Fullerenes or Nanotubes	These are successfully used in neuronal disorders like AD, PD, and ischemic stroke and in vivo in many diseases like bone ants, rheumatoid arthritis, osteoporosis, and cancer (Boridy et al., 2009)

(ii) Caveolar Pathway for Delivery in the Brain: This pathway escapes lysosomal delivery thus making it different from different from the clathrin-mediated pathway.

Caveolae are flask-shaped invaginations in the plasma membrane and three isoforms of caveolin proteins are present in mammalian cells: caveolin-1, caveolin-2, and caveolin-3 helps in transportation through this pathway. The Nano carriers are internalized after binding to caveolar receptor forming a vesicular structure known as cavicle. The cavicle then is drived with the help of energy derived from actin and is ultimately fused with caveosomes which have neutral pH and then moves toward the endoplasmic reticulum penetrating into the cytosol and finally gaining access to the nucleus through the nuclear pore complex (Rappoport, 2008).

Figure 1: Different ways of crossing the BBB. Source: (Teleanu et al., 2019)

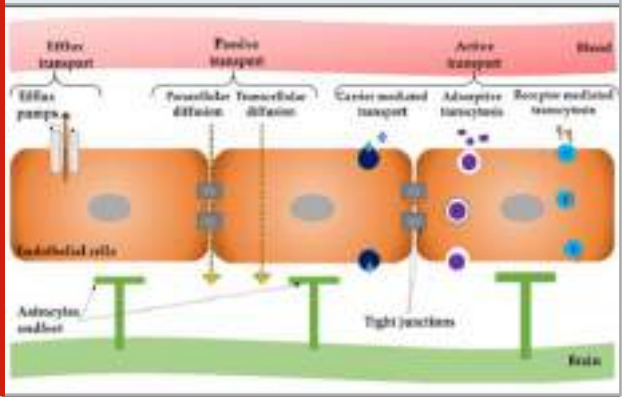

Applications of Nanotechnology in CNS Disorders: In Alzheimer's disease, polyethylene glycol (PEG) stabilized nanomicelles made up of phospholipids inhibit Ab-aggregation and attenuate Ab-induced neurotoxicity in SHSY-5Y human neuroblastoma cell line in vitro. Microemulsion nanoparticles loaded with copper chelator d-penicillamine were found to have capability of crossing the BBB and dissolving the pre-existing Ab aggregates in vitro (Vinogradow et al., 2004). The nanoliposomes made up of curcumin not only inhibits Ab aggregation but also enhanced its bioavailability. Besides, Fullerene has a neuroprotective action, has an ability to inhibit Ab peptide fibrillization and prevention of Ab-induced cognitive impairments after intraventricular administration (Taylor et al., 2011). In Parkinson's disease, the PEG and polyethylenimine nano gels complexes with antisense oligonucleotides can efficiently cross BBB *in vitro*. When injected intravenously, the oligonucleotides supply the brain more efficiently, particularly when the gels were functionalized with insulin (Mohanraj et al., 2013). The nerve growth factor (NGF) bound polybutylcyanoacrylate (PBCA) nanoparticles and L-Dopa encapsulated nanoparticles cross blood brain barrier (Siddiqi et al, 2018).

In Huntington's disease, fullerenols have ability to clear free radicals and reduce oxidative stress to cell.

Figure 2: Macropinocytosis and phagocytosis pathways for drug delivery into brain. Source: (Hillaireau and Couvreur, 2009)

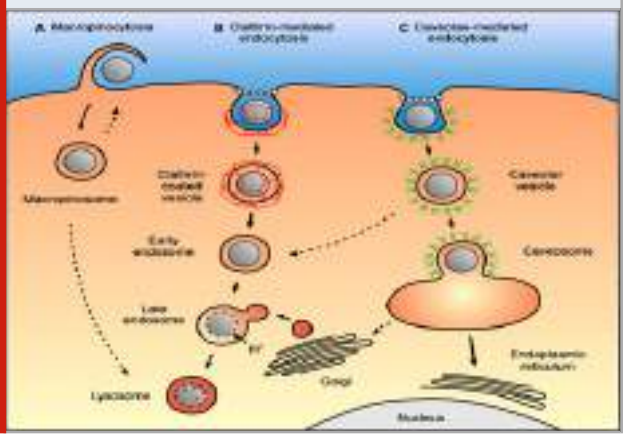

Nitrendipine encapsulated in SLNs showed higher uptake of drug in comparison of bulk drug. Short-interfering RNA (siRNA) encapsulated cyclodextrin nanoparticles reduce expression of Huntingtin (HTT) mRNA both in vivo as well as in vitro (Huang et al., 2012). In multiple sclerosis, the interaction of carbon nanotubes along with stem cell is a way for tissue engineering to explore and add to cell behaviour. In a preclinical study, ciliary neurotrophic factor (CNTF) loaded microcapsules demonstrated in situ sustained delivery of CNTF upon encapsulation into polymers. This does not cause any immune response and cytotoxic effect (Godinho et al., 2013). In amyotrophic lateral sclerosis, a superoxide dismutase (SOD)-coated gold nanoparticle along with SOD1 aggregates is used as colorimetric detection system for ALS diagnosis. Sometimes carboxyfullerenenanotubes with SOD can be used. Carbon NPs may be used to effectively and precisely deliver riluzole, a glutamate inhibitor, to the affected sites (Klyachko et al., 2013; Alexander et al., 2019).

In brain tumour, nanoformulations like PBCA nanoparticles filled with methotrexate and temozolamide have resulted in increased intracerebral drug concentration as compared with free drugs. Solid lipid nanoparticles (SLNs) of etoposide and paclitaxel, in vitro, then enhanced inhibitory effect on glioma cell line proliferation was shown to be more effective than the free drug alone (Kohane et al., 2002). SLNs filled with carbamazepine and PLGA nanoparticles loaded with b-carotene are effective in epilepsy. In rat model, liposomal muscimol formulation is found to suppress focal seizures while producing minimal histological alterations (Brioschi et al., 2012). Xenon gas loaded liposomes were found to be successful in rat models administered for up to 5 h after the onset of stroke with an acceptable dosage range of 7-14 mg/kg (Peng et al., 2013). In neuro-AIDS, enhanced targeted delivery of Azidothymidine (AZT) to macrophages is possible using poly (hexylcyanoacrylate) NPs. Poly (hexylcyanoacrylate) NPs can also be used to deliver Saquinavir in human monocytes or macrophages (Chhabra et al., 2015; Alexander et al., 2019).

Nanotechnology Based Delivery of Neuroprotective Drugs: The biologically active and key phenolic constituent of turmeric, Curcumin (diferuloylmethane), obtained from the rhizomes of *Curcuma longa*, has shown considerable therapeutic efficacy in several diseases (Chattopadhyay et al., 2008). Being a natural antioxidant, curcumin has been found to possess many pharmacological activities including anti-inflammatory, antimicrobial, anticancer, the neuroprotective effect in neurodegenerative disorders, in both preclinical and clinical studies. Despite the wide medicinal applications of curcumin, due to low solubility, physico-chemical instability, poor bioavailability and quick metabolism, its clinical implications are hindered (Chattopadhyay et al., 2008). However, these problems can be resolved by developing efficient delivery systems with the help of nanotechnological approach. Compared to bulk curcumin, curcumin loaded PLGA-PEG nanoparticles, curcumin-loaded polysorbate 80 modified with some (CPC) nanoparticles showed better stability, longer circulation period and higher permeation of curcumin nanoformulation (Naksuriya et al., 2014; Alexander et al., 2019).

Among growth factors, Nerve Growth factors (NGFs) have great therapeutic potential for various CNS disorders. Vascular endothelial growth factor (VEGF) has been shown to participate in the process of post-ischemic brain repair via promoting neurogenesis and cerebral angiogenesis. Successful neuroprotection and promotion of vascular regeneration in the ischemic brain have therefore been achieved by treatment with modified liposomes with VEGF loaded transferrin. Edaravone (EDR), a well-known lipophilic drug, is used as a free radical scavenger for not only neurodegenerative disease, but also cardiovascular disease and cancer (Hudson et al., 2013). In preclinical studies, EDR has shown great efficiency against AD and cerebral aneurysm via oral administration, although oral bioavailability of EDR is very limited (Cruz, 2018). The lipid-based nanosystem (LNS) loaded with EDR was developed to promote its successful oral delivery by increasing the oral bioavailability (Alexander et al., 2019).

Neurotoxicity of Nanomaterials (Nano-Neurotoxicity): While invading the barriers within neural networks, doors are open not only for drug delivery but also to toxicity. The scope and size of toxic events is a part of the challenge in determining nanotoxicology. They interact heavily with components and pathways in both the biochemical environment of the cell and physiological system (Karmakar et al., 2014). Metal oxide NPs are highly useful in various fields such as medicine and engineering.

However, these NPs have high chemical reactivity and toxicity as a consequence of their small size and large surface area. These NPs can accumulate in structures of the brain, such as the cerebellum and cortex (Valavanidis and Vlachogianni, 2016). For the use of multi walled carbon nanotubes (MWCNTs) as scaffolds, studies have inferred a substantial degree of genotoxicity (DNA interference) that is symptomatic of a broader problem posed by the use of nanomaterials. Hence, nanotoxicology profiling is a critical component of studies of nanomaterials (Kumar et al., 2017; Alexander et al., 2019).

CONCLUSION

In last few recent years brain-targeted drug delivery systems have been developed and gained large attention. Applications of nanotechnology have been developed in many fields in the last decade such as method of drug delivery, biological sensing, biomedical imaging, targeted anticancer drugs and antibiotic carriers. Within the realm of medicine, nanotechnology has found its way not only in improving drug delivery, but also in improving the required surgical procedures as seen in case of brain tumours. Compared to conventional implants that may cause neuroinflammation due to rigidity of the material, new polymeric implants are advantageous as they provide increased bioavailability with minimal or no neuroinflammation.

Though several nanoformulations have shown great efficacy in preclinical and clinical studies, there are several basic concerns which should be addressed in the future to achieve the successful clinical translation of nanoformulations. The nanomaterials should be effective and safe in brain-targeted drug delivery systems, as well as they must be easily biodegradable. The approaches for the development of nanomaterials should be eco-friendly. The physico-chemical properties attached to nanomaterials must be evaluated carefully for the development of effective brain targeted drug delivery systems. To avoid complications associated with invasive routes a non- invasive alternative method for drug delivery should be developed. More studies are required on the basic level to increase the possibility of the use of nanoparticles in clinical settings.

ACKNOWLEDGEMENTS

All the authors in this manuscript have made substantial contributions towards conception, design, acquisition of data, analysis and interpretation of the data, participated in drafting the manuscript and revising it critically for important intellectual content. The authors of this manuscript would like to thank Prof. Subir Chandra Dasgupta, Head, Department of zoology, Maulana Azad College, Kolkata for his constant support and useful insight during the preparation of this review paper.

Conflict of Interest: The authors declare that there is no conflict of interests.

REFERENCES

Abbott NJ, Rönnbäck L and Hansson E (2006). Astrocyte-endothelial interactions at the blood-brain barrier. Nature Reviews Neuroscience, 7(1): 41-53.

Alexander A, Agrawal M, Uddin A, Siddique S, Shehata AM and Shaker MA (2019). Recent expansions of novel strategies towards the drug targeting into the brain.

International Journal of Nanomedicine, 14: 5895-5909.

Allemann E, Leroux JC and Gurny R (1998). Polymeric nano-microparticles for the oral delivery of peptides and peptidomimetics. Advanced Drug Delivery Reviews, 34: 171-189.

Aso E, Martinsson I, Appelhans D, Effenberg C, Benseny-Cases N and Cladera J (2019). Poly (propylene imine) dendrimers with histidine-maltose shell as novel type of nanoparticles for synapse and memory protection. Nanomedicine and Nanotechnology, 17: 198-209.

Boridy S, Takahashi H, Akiyoshi K and Maysinger D (2009). The binding of pullulan modified cholesteryl nanogels to Ab oligomers and their suppression of cytotoxicity. Biomaterials, 30: 5583-5591.

Brioschi A, Zenga F, Zara GP, Gasco MR, Ducati A and Mauro A (2007). Solid lipid nanoparticles: could they help to improve the efficacy of pharmacologic treatments for brain tumors? Neurology Research, 29(3): 324-330.

Chattopadhyay N, Zastre J, Wong HL, Wu XY and Bendayan R (2008). Solid lipid nanoparticles enhance the delivery of the HIV protease inhibitor, atazanavir, by a human brain endothelial cell line. Pharmaceutical Research, 25: 2262-2271.

Chhabra R, Grabrucker AM and Tosi G (2015). Emerging use of nanotechnology in the treatment of neurological disorders. Current Pharmaceutical Design, 21: 3111-3130.

Cruz MP (2018). Edaravone (Radicava): a novel neuroprotective agent for the treatment of amyotrophic lateral sclerosis. Physical Therapy, 43: 25-28.

Duvernoy H, Delon S and Vannson JL (1983). The vascularization of the human cerebellar cortex. Brain Research Bulletin, 11: 419-480.

Georgieva J, Hoekstra D and Zuhorn I (2014). Smuggling drugs into the brain: an overview of ligands targeting transcytosis for drug delivery across the blood–brain barrier. Pharmaceutics, 6: 557-583.

Godinho BM, Ogier JR, Darcy R, O'driscoll CM and Cryan JF (2013). Self-assembling modified b-cyclodextrin nanoparticles as neuronal sirna delivery vectors: focus on Huntington's disease. Molecular Pharmaceutics, 10: 640-649.

Hillaireau H and Couvreur P (2009). Nanocarriers' entry into the cell: Relevance to drug delivery. Cellular and Molecular Life Sciences, 66(17): 2873-2896.

Huang YJ, Wu HC, Tai NH and Wang TW (2012). Carbon nanotube rope with electrical stimulation promotes the differentiation and maturity of neural stem cells. Small, 8: 2869-2877.

Hudson JS, Hoyne DS and Hasan DM (2013). Inflammation and human cerebral aneurysms: current and future treatment prospects. Future Neurology, 8: 663–676.

Jain K (2007). Nanobiotechnology-based drug delivery to the central nervous system. Neurodegenerative Diseases, 4: 287-291.

Karmakar A, Zhang Q and Zhang Y (2014). Neurotoxicity of nanoscale materials. Journal of Food and Drug Analysis, 22(1): 147-160.

Klyachko NL, Haney MJ and Zhao Y (2013). Macrophages offer a paradigm switch for CNS delivery of therapeutic proteins. Nanomedicine, 9:1403-1442.

Kohane DS, Holmes GL, Chau Y, Zurakowski D, Langer R and Cha BH (2002). Effectiveness of muscimol-containing microparticles against pilocarpine-induced focal seizures. Epilepsia,43: 1462-1468.

Krukemeyer MG, Krenn V, Huebner F, Wagner W and Resch R (2015). History and possible uses of nanomedicine based on nanoparticles and nanotechnological progress. Journal of Nanomedicine and Nanotechnology, 6(6): 1000336(1-7).

Kumar A and Singh A (2015). A review on Alzheimer's disease pathophysiology and its management: an update. Current Pharmacology Reports, 67: 195-203.

Kumar A, Tan A, Wong J, Spagnoli JC, Lam J, Blevins BD, Natasha G, Thorne L, Ashkan K, Xie J and Liu H (2017). Nanotechnology for neuroscience: Promising approaches for diagnostics, therapeutics and brain activity mapping. Advanced Functional Materials, 19: 27-39.

Mahdavian AR, Ashjari M and Makoo AB (2007). Preparation of poly (styrene-methyl methacrylate) /SiO2 composite nanoparticles via emulsion polymerization. An investigation into the compatiblization. European Polymer Journal, 336-344.

Memisoglu E, Bochot A, Ozalp M, Sen M, Duchene D and Hincal A (2003). Direct formation of nanospheres from amphiphilic betacyclodextrin inclusion complexes. Pharmaceutical Research, 20: 117-125.

Mohanraj K, Sethuraman S and Krishnan UM (2013). Development of poly (butylene succinate) microspheres for delivery of levodopa in the treatment of Parkinson's disease. Journal of Biomedical Materials Research Part B: Applied Biomaterials, 101: 840-847.

Naksuriya O, Okonogi S, Schiffelers RM and Hennink WE (2014). Curcumin nanoformulations: A review of pharmaceutical properties and preclinical studies and clinical data related to cancer treatment. Biomaterials, 35: 3365-3383.

Naqvi S, Panghal A and Flora SJS (2020). Nanotechnology: A promising approach for delivery of neuroprotective drugs. Frontiers in Neuroscience, 14(494): 1-26.

Peng T, Britton GL, Kim H, Cattano D, Aronowski J and Grotta J (2013). Therapeutic time window and dose

dependence of xenon delivered via echogenic liposomes for neuroprotection in stroke. CNS Neuroscience and Therapeutics, 19: 773-784.

Rappoport JZ (2008). Focusing on clathrin-mediated endocytosis. Biochemical Journal, 412: 415-423.

Reis CP, Neufeld RJ, Ribeiro AJ and Veiga F (2006). Nanoencapsulation I. Methods for preparation of drug-loaded polymeric nanoparticles. Nanomedicine: Nanotechnology, Biology and Medicine, 2: 8-21.

Sahoo SK, Misra R and Parveen S (2017). Nanoparticles: A boon to drug delivery, therapeutics, diagnostics and imaging. Nanomedicine, 8: 73-124.

Saito Y and Wright EM (1983). Bicarbonate transport across the frog choroid plexus and its control by cyclic nucleotides. Journal of Physiology, 336: 635-648.

Schlageter KE, Molnar P, Lapin GD and Groothuis DR (1999). Microvessel organization and structure in experimental brain tumors: microvessel populations with distinctive structural and functional properties. Microvascular Research, 58: 312-328.

Shah L, Yadav S and Amiji M (2013). Nanotechnology for CNS delivery of biotherapeutic agents. Drug Delivery and Translational Research, 3: 336-351.

Siddiqi KS, Husen A, Sohrab SS and Yassin MO (2018). Recent status of nanomaterial fabrication and their potential applications in neurological disease management. Nanoscale Research Letters, 13(231):1-17.

Sohail I, Bhatti IA, Ashar A, Sarim FM, Mohsin M, Naveed R, Yasir M, Iqbal M and Nazir A (2020). Polyamidoamine (PAMAM) dendrimers synthesis, characterization and adsorptive removal of nickel ions from aqueous solution. Journal of Materials Research and Technology, 9: 498-506.

Taylor M, Moore S, Mourtas S, Niarakis A, Re F and Zona C (2011). Effect of curcumin-associated and lipid ligand-functionalized nanoliposomes on aggregation of the Alzheimer's Ab peptide. Nanomedicine: Nanotechnology, Biology and Medicine, 7:541-550.

Teleanu DM, Negut I, Grumezescu V, Grumezescu AM and Teleanu RI (2019). Nanomaterials for drug delivery to the central nervous system. Nanomaterials, 9(371):1-18.

TorchilinVP (2007). Micellar nanocarriers: pharmaceutical perspectives. Pharmaceutical Research, 24(1): 1-16.

Tripathy S and Das MK (2013). Dendrimers and their applications as novel drug delivery carriers. Journal of Applied Pharmaceutical Science, 3: 142-149.

Valavanidis A and Vlachogianni T (2016). Engineered nanomaterials for pharmaceutical and biomedical products new trends, benefits and opportunities. Pharmaceutical Bioprocessing, 4(1): 13-24.

Vinogradov SV, Batrakova EV and Kabanov AV (2004). Nanogels for oligonucleotide delivery to the brain. Bioconjugate Chemistry, 15: 50-60.

Yasuda K, Cline C and Vogel P (2013). Drug transporters on arachnoid barrier cells contribute to the blood-cerebrospinal fluid barrier. Drug Metabolism and Disposition, 41(4): 923-931.

Yoo HS, Oh JE, Lee KH and Park TG (1999). Biodegradable nanoparticles containing PLGA conjugate for sustained release. Pharmaceutical Research, 16: 1114-1118.

Young TJ, Mawson S, Johnston KP, Henriksen IB, Pace GW and Mishra AK (2000). Rapid expansion from supercritical aqueous solution to produce submicron suspensions of water-insoluble drugs. Biotechnology Progress, 16(3): 402-407.

UTTAR PRADESH JOURNAL OF ZOOLOGY

42(17): 123-135, 2021
ISSN: 0256-971X (P)

MORPHOLOGY AND BIOLOGY OF FRESHWATER TANK GOBY, *Glossogobius giuris* (Hamilton, 1822) FROM INDIAN SUBCONTINENT: A REVIEW

RAJARSHI GHOSH[1*], SHREYOSREE GANGULY[2], PRADIP BHATTACHARJEE[1] AND ANISH PAL[1]

[1]Post Graduate Department of Zoology, Maulana Azad College, 8 Rafi Ahmed Kidwai Road, Kolkata-700013, West Bengal, India.
[2]Depatment of Industrial Fish and Fisheries, Asutosh College, 92 S.P. Mukherjee Road, Kolkata700026, West Bengal, India.

AUTHORS' CONTRIBUTIONS

This work was carried out in collaboration among all authors. All authors read and approved the final manuscript.

Article Information

Editor(s):
(1) Dr. Golam Mustafa, Center for Resource Development Studies Ltd., Bangladesh.
Reviewers:
(1) Byron Baron, University of Malta, Malta.
(2) B. Puvarajan, India.

Received: 20 June 2021
Accepted: 26 August 2021
Published: 01 September 2021

Review Article

ABSTRACT

Glossogobius giuris (Hamilton, 1822), commonly known as tank goby or Bele, is an important food fish of Indian subcontinents for being inexpensive and nutrient-rich. It is widely distributed in freshwater bodies of India, Bangladesh, Pakistan, and Myanmar. The morphological features of this fish are striking with distinct sexual dimorphism. The feeding habits vary with season and different age groups. Based on qualitative and quantitative analysis of gut contents, this fish has been categorized as carnivores. When young ones are abundant, cannibalism has also been observed in this fish group. It has a prolonged breeding period with prolific breeding habits and maximum availability during the rainy season. This fish is full of nutrients with a very low percentage of carbohydrate and lipid but with high protein content and thus increases the demand among fish lovers. The tank goby also drags the attention of aquarium keepers and is considered a small indigenous species in Bangladesh and India. The present review has been prepared to gather the published literature on different biological aspects of *Glossogobius giuris*, the further study of which will not only help to make fishery industry more vibrant and economically viable but also for conservation of this important food fish.

Keywords: *Glossogobius giuris*; morphology; food and feeding habits; breeding biology.

**Corresponding author: Email: 1977rajarshighosh@gmail.com;*

1. INTRODUCTION

The freshwater goby, *Glossogobius giuris* is a widespread species belongs to the order of Perciformes under the family of Gobiidae, the second largest teleost family next to Cyprinidae. Tank goby is generally found in tropical and sub-tropical freshwater, brackish water or marine water bodies even in estuarine region and both in lentic and lotic environment [1]. From a zoogeographic point of view, *G. giuris* is well distributed fish throughout the south and south- east Asian regions including India, Bangladesh, Myanmar, Pakistan, Thailand, Vietnam and also found in some areas of Indo-China, Africa, Central Australia and East Indies [2,3]. Fish proteins are comparatively cheap and abundant among the animal proteins. Most of the aqua culturists, therefore, would be interested to grow more fish and supply the cheap proteins specifically to meet the requirement of the low-middle class and poor people of the developing countries. *G. giuris* is well known commercial fish and has good consumer preference as it is of highly nutritive value [4]. This was also reported as small indigenous species [5] which draws the attention of people of South Asia for its exceptional taste, small size, low fat and high protein content [6] and therefore, forms an important capture fishery in many countries. The fish culturists are now trying to incorporate this fish in composite culture with carps [7]. Consequently, this fish species may be cultured in captive condition with carps. The species is also famous for its ornamental quality and thus becomes valuable for aquarium keepers to enhance foreign exchange. If the potential culture techniques as well as fish management system can improve further, it would be successful to earn huge foreign currency in near future. Indian Major Carps (IMCs) and several minor carps are being used at a large scale as commercially important aquatic species but they gradually become genetically weaker due to inbreeding and poor brood stock management practices. Therefore, fish farmers are now much more looking forward for species having new potentialities. In this scenario, *G. giuris* may appear as a good candidate and play a vital role in the enhancement of fish production as well as the upliftment of socio-economic condition in the country.

The morphological characteristics including sexual dimorphism are based on the previous study on *G. giuris* [8]. Although seasonal variation is well marked in its feeding behaviour, it mainly feeds on small crustaceans, insects and smaller fishes [9]. This species does not possess any particular breeding time, rather they are prolific breeders like Tilapia, i.e., they have more than one breeding peak [10]. According to some researchers, they migrate during their breeding period which, however, occurs many times during their life-time [11]. Information regarding the food and feeding habits, fecundity, breeding techniques, ecology of *G. giuris* from different geographical locations are fragmentary [10,12,13,14,15,16,17] and no one has so far attempted to describe a comprehensive account of the tank goby which would provide future investigations aimed to improve management of this important food fish. Therefore, the present review aims to amalgamate information of *G. giuris* from the different biological aspects.

2. NOMENCLATURE AND TAXONOMY

The tank goby holds numerous vernacular names such as Balia (India), Bele (West Bengal and Bangladesh), Weligouva (Sri Lanka), Bekukor (Malaysia), Bulla (Nepal) and Fareast [2]. The *Glossogobius giuris* was first describes as *Gobius giuris* by Hamilton, 1822 (type locality: all the ponds and freshwater rivers in Gangetic provinces in India). It was included under *Glossogobius* in the year 1822 based on its morphological studies (Greek, 'glossa' means tongue, and Latin 'gobius' means gudgeon). According to the International Code of Zoological Nomenclature (ICZN), the type species (*Gobius giuris* Hamilton, 1822, Fishes of Ganges: 51, pI. 33, Fig. 15) is named as *Glossogobius giuris giuris* [18] and modern system of classification has included this underthe sub-family Gobiinae (Fig. 1).

Kingdom- Animalia
Sub-Kingdom- Metazoa
Phylum- Chordata
Sub-Phylum- Vertebrata
Super-Class- Pisces
Division- Gnathostomata
Class- Osteichthyes
Sub-Class- Actinopterygii
Super-Order- Teleostei
Order- Perciformes
Sub-Order- Gobioidei
Family- Gobiidae
Sub-Family- Gobiinae
Genus- *Glossogobius*
Species- *Glossogobius giuris*

Fig. 1. Systematic Position of *Glossogobius giuris* [10]

3. EXTERNAL MORPHOLOGY

The morphological description of tank goby was well documented by a number of researchers in the past [19,20,21]. The colour of the body is generally

yellowish brown with five dark blotches on the flank, sometimes it may be olive green to blackish green above and lighter below [19]. The fish body (Fig. 2) is elongated and cylindrical in anterior part and compressed posteriorly with a flattened head [22]. The upper jaw, maxilla extends below the anterior part of eye and the lower jaw, mandible is longer too. Eyes are slightly larger in younger specimens than adults and iris is without process in pupil. The average length of the body ranges between 10 cm to 45 cm [23]. Lips are thick and mouth is slightly oblique. Lower lip is pointed but the upper one is short. Teeth are villiform in jaws, outer and inner rows are enlarged in front in both jaws [10]. The tongue is bilobate; few longitudinal mucous canals are also present on cheeks. The body is with 5 or 6 dark, rounded spots on both sides [24]. Scales are present on upper portion of the head, cheek, breast and belly and are of ctenoid type. Two dorsal fins are present but are separated with a thin division, and the fins are with brownish spots forming longitudinal stripes. The second dorsal fin and anal fin are pointed posteriorly and caudal fin is somewhere rounded [21]. Caudal fin is yellowish green with a dark spotted edge whereas pectoral fin is lightly spotted and grey in colour. Pelvic fins are grayish, jointed but connected to the body only at the anterior part. The finformula of *G. giuris* is D VI+I 8-9; P 16-21; A I 7-8 [25].

Fig. 2. Fresh specimen of *Glossogobius giuris*

4. FOOD AND FEEDING BEHAVIOUR

Studies on the food, feeding habit and feeding ecology are absolutely important in the management and life history analysis of fishes [25]. On the basis of their feeding habits, fishes can be categorized as detritivorous, carnivorous, herbivorous and omnivorous [10]. The available information of food and feeding behaviour of *G. giuris* is very limited in the Indian sub-continent and is mainly based on morphometric studies [26,27,28]. The quality and quantity of available food materials are important for the actual growth pattern and behaviour of the fish [29]. Types of food and feeding strategy depend on various stages of the stomach (relative length of the gut, RLG) and body forms, gut content, and even on sex. When the stomach is ¾th full, the fish would be considered as active feeder, moderate feeder when stomach is ½ full and poor feeder when¼ th or traces of the stomach is full [9,26]. The seasonal data regarding the percentage of fullness of gut of *G. giuris* clearly showed that peak active feeding was accomplished in February, moderate feeding in December, poor in May and most numbers of empty stomach were observed in October [27]. Similar kind of observations regarding monthly fluctuations in feeding intensity percentage of *G. giuris* was also reported earlier from Haor region of Kishoreganj, Bangladesh which was summarized in Fig. 3 [26].

4.1 Feeding Habits of Juveniles

The food of the juveniles may be strikingly different from that of the adults (Fig. 4). Juveniles of *G. giuris* are mainly insectivorous and planktonic feeders but adults are subsequently changed into carnivorous [29, 30]. Juveniles feed on crustaceans such as copepods, cladocerans, larvae or juvenile of prawns and polychaetes, fry of teleost fishes, amphipods, ostracods and stomatopods [25]. Among copepods, *Cyclops* constitutes the major part of gut content. The remaining part is held by a variety of fauna including post larval or juvenile stages of shrimp and prawn viz. *Penaeus, Metapenaeus, Acetes, Macrobrachium*; *Daphnia*, *Moina*, *Ceriodaphnia*, *Bosmina* among Cladocerans; *Cypris* and *Stenocypris* among Ostracods; *Nereis, Dendronereis* among polychaetes and larvae or immature stages of various insects like dragonflies, chironomids and mosquitoes. Crustaceans were the major gut content of the juvenile *G. giuris* which also feeds on filamentous algae like *Spirogyra* and *Cladophora* [9].

4.2 Feeding Habits of Adults

Adults are known to be piscivorous and also cannibalistic [1,31,32,33,34] as they feed on juvenile *G. giuris* and many other small fishes including carps. Cannibalism has frequently been observed when the juveniles are abundant [34]. Adults feed on a variety of animals and plants which include juveniles of teleost fishes, shrimps and prawns, semi-digested matters and traces of crabs, insects (mainly chironomids, trichopterans and nymph of dragonfly), aquatic hydrophilid beetles, molluscs (predominantly gastropods such as Thiara tuberculata and Physa acuta), annelids (chiefly Nereis and Dendronereis), nematodes, few algae (Chlorella, Spirogyra, Cladophora etc.) and also parts of higher plants such as Typha [35]. The fry of teleost is the major gut content of the adult *G. giuris* throughout the year except for months of July and August where shrimps and prawns form the major portion of food material [36].

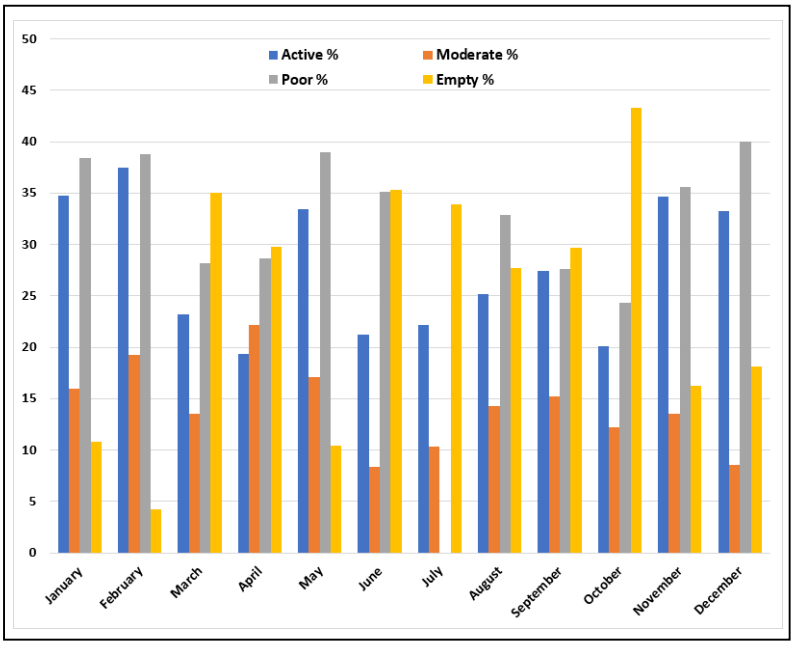

Fig. 3. Seasonal fluctuations in percentage of fullness of gut of *Glossogobius giuris*

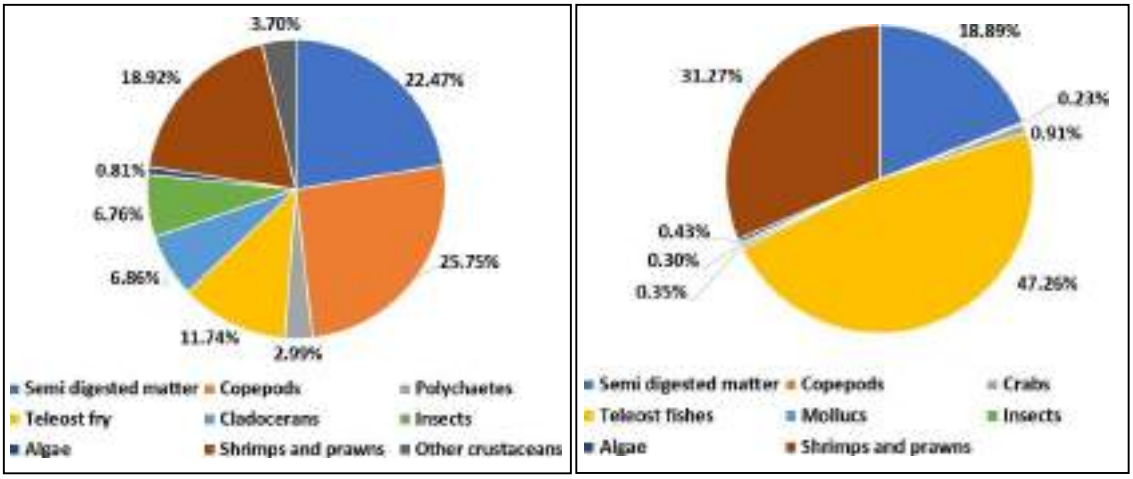

Fig. 4. Proportion of food materials of juveniles and adults *G. giuris* respectively

4.3 Gastro Somatic Index (GaSI)

Feeding intensity varies seasonally in different fish species [37,38]. The trend of seasonal variation in feeding behaviour of *G. giuris* was observed from the study of the Gastro Somatic Index (GaSI) of the fishes by various workers collected from different habitats (Fig. 5). The values of GaSI were obtained after dividing the weight (g) of the fish gut by the total fish weight (g) multiplied by 100. Recent findings suggest that the highest value for GaSI is found in the month of February [26]. Interestingly, the feeding intensity was recorded high in winter season (especially in months of January and February) in males and monsoon and post-monsoon periods (especially in June, July and October) in females of *G. giuris* while the lowest values of both sexes were reported in April. This relative variation is predominantly due to the environmental factors affecting the feeding habits of the fishes. The feeding activity of *G. giuris* is higher in winter than summer (spawning period) as preferable food availability is dominant in winter months [27].

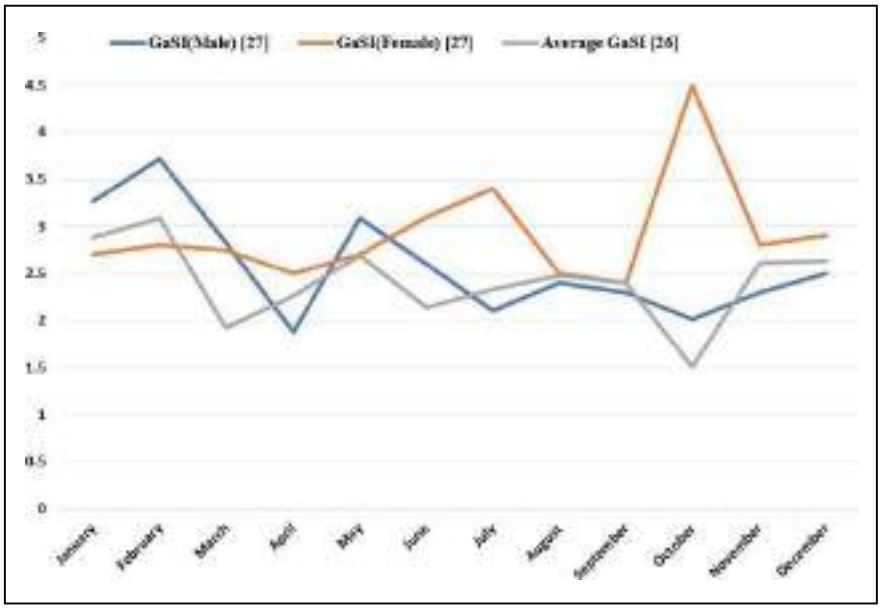

Fig. 5. Seasonal changes of GaSI of *G. giuris*

5. BREEDING BIOLOGY

5.1 Sexual Dimorphism

It is quite evident that the sexes of any fish species can be determined by examining the internal presence of gonads. Every time it is not possible to distinguish the sex of a fish by looking externally. The sexual dimorphism (Fig. 6) in *G. giuris* has been well studied which is summarized in Table 1 [1,39] though it cannot be determined until the species grows up to 60 mm [40].

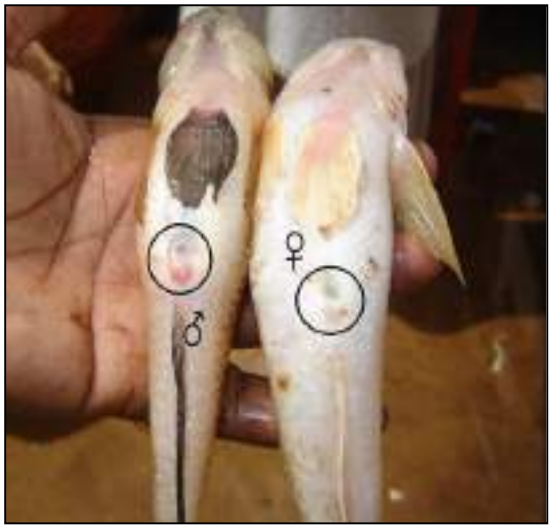

Fig. 6. Male and female of *G. giuris* [39]

5.2 Breeding Period

The species of tank goby has a prolonged breeding period, breeds throughout the year in both impoundment and running water body while the breeding reaches the peak point during April to June followed by a decline [1]. The fish breeds from May to July in Sri Lanka, and there is a substantial variation among the breeding periods throughout its habitats [41]. Length and body weight changes with maturity and sex and it attains maximum in months of August to September [42]. Adult females are observed to contain eggs in their ovaries in the months from March to June and also in November. It breeds almost throughout the year or twice a year with short gaps after the two seasons but the breeding period remains at peak during May to July [41].

5.3 Factors Influencing the Breeding Habits

Sexual maturity is an important factor for breeding and it is largely affected by environmental factors. Males mature at smaller sizes whereas the female ones are at larger. The age of the reproducing fishes is dependent on the concerned fish population and the area they inhabit [43]. A favorable environment promotes the growth of the fishes to attain sexual maturity in adults but when the environment is unfavorable for the survival of the adults, reproduction takes place at younger ages. Females tend to reproduce quickly as a means of natural selection [44]. The seasonal variation in both feeding and breeding behaviors of the species is mainly

dependent on the environmental factors present within the habitat. In some of the findings, they are described as prolific breeders [10], whereas in most of the studies they have been reported as seasonal breeders whose sexual activity declines after a certain period of the year [45].

5.4 Fecundity

The eggs of *G. giuris* are very small ranged from 0.17 to 0.75 mm and average fecundity ranges from 24,000 to 25,000. Fecundity generally varies with different environments and water parameter availability and even body parameter like length, weight, gonadal weight, etc. [46]. The shape of the oocytes, histology of gonad and other breeding parameters are also studied extensively [41]. The shape of the oocytes varies depending upon maturity stages like an oval in immature and elongated in mature stages [47].

5.5 Gonadosomatic Index (GSI)

The GSI is used to measure the stage of maturity and timing of spawning. It is calculated following the reproductive cycle of a particular species throughout the year at certain intervals and it is mathematically expressed as GSI= [(Gonad weight / Body weight) × 100].The breeding behavior throughout the year was studied with the help of GSI values (Fig. 7). The monthly variation in GSI value for male fishes has been more or less uniform throughout the year with a minute increase in August and October. In case of female *G. giuris*, the GSI value shows much more variation during the different months of the year with higher values in the months of March, June, August, October and November. This shows their prolonged breeding period with two breeding peaks in March and mid-October [42].

Table 1. Sexual dimorphism of *G. giuris*

Male *G. giuris*	Female *G. giuris*
Pelvic fins are darker in color (Fig. 6)	Pelvic fins are light in color (Fig. 6), although they become blackish during breeding season
Straight, thin and pointed genital papilla	Short, fleshy and circular genital papilla
They are comparatively smaller	These are larger than the males
Abdomen is flat, thin, and comparatively non-bulky	Soft, swollen, and bulky abdomen

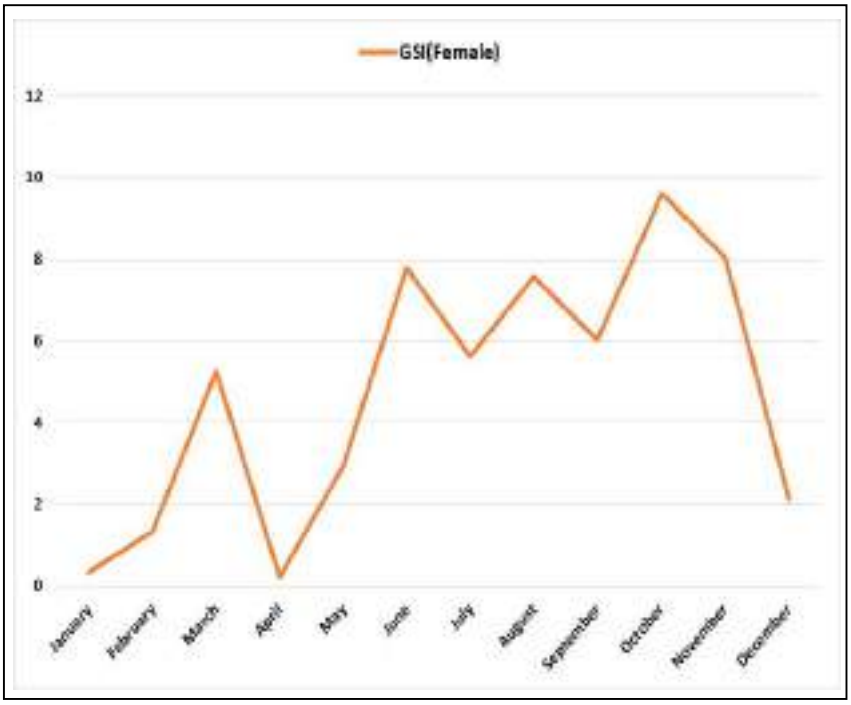

Fig. 7. Monthly changes in GSI in female *G. giuris*

5.6 Induced Breeding in *G. giuris*

Apart from natural breeding protocols, induced breeding techniques of *G. giuris* has been employed successfully to enhance its productions under captivity [48]. The optimum water conditions for the induced breeding differ according to the environment from which the fishes have been collected. In general, the temperature ranges from 27-32°C, pH rounds at 5.8 - 9, and dissolved oxygen content ranges around 4.5-12 mg/L [40]. The breeding behaviour of *G. giuris* has been studied mainly with the pituitary gland extract (PGE), HCG and ovaprim. There is no clear-cut data regarding the exact amount of dosage for these extracts and the most potent inducing reagent to date [49]. Most of the researchers have studied only with the PGE; some have tried to find out the influence of ovaprim and HCG also. Among them, induction with PGE is the most successful for breeding with highest spawning rate and maximum level of survival [40]. HCG can also be useful for the purpose, but ovaprim has not been able to produce any concluding result. Several researchers have suggested a range of dosage amounts according to the site of collection and other environmental factors. With the recent research done on the induced breeding behavior, a dosage of 8 mg Pituitary Gland / kg body weight of fish has been the most suitable inducing agent for *G. giuris* [49].

5.7 Problems of *G. giuris* Culture in Captivity

The production of *G. giuris* may be enhanced by the process of appropriate captive culture techniques. There are suitable water bodies for the culture of this species with other fishes or it can be cultured as a single species for local consumption or exported as a delicious expensive fish. So, *G. giuris* could be a suitable candidate for aquaculture as commercial farming. However, there are several issues associated with culture in captivity which must be addressed for effective farming.

5.7.1 Cultivation density

In the peak spawning season (September), the occurrence of the highest intensity of cannibalism has been noticed in *G. giuris* which might be due to the abundant availability of fry [49]. Cannibalism is not an accidental phenomenon at that period but it is merely intentional thereby affecting the density in captive breeding. Maintenance of an ideal population density during fish culture is very crucial because overcrowding often leads to an increase in physiological stress and transmission of parasitic diseases. An increase in stock density also raises the competition among members over food, mating partner and habitat.

5.7.2 Territorial behavior in males

Territorial behavior is related to the competition for suitable breeding areas, perfect mating partners, and ideal reproductive conditions [50]. *G. giuris*, being cannibalistic during the breeding period, may show some adverse effects in the territory. Different goby species perform distinct territorial behavior, but little is known about *G. giuris*. Most of the gobies have a special strategy characterized by male parental care of eggs and defending outsiders or intruders with aggressive behavior [51]. High stocking density of *G. giuris* in small confinement may increase the chance of aggressiveness and that may affect the fertilization rate. Pieces of evidence between mate guarding and sperm expenditure have been observed in some species of goby suggesting that both the plans are expensive in terms of time and energy [52].

5.7.3 Common diseases of *G. giuris* in culture

Diseases of freshwater fishes in the Indian subcontinent pose a severe threat to water bodies. About 15-20 % of the total aquaculture production is constrained by the increasing prevalence of parasitic infestations [53]. The reason behind this might be due to deterioration of environmental conditions coupled with increased virulence of the pathogens on a susceptible host species. Parasites interfere with host nutrition, metabolism, and secretary functions of the alimentary canal of fish and can even perturb the host nervous system [54]. They can cause ulceration and reduce the reproductive capacity of the fish. The parasitic infestation of *G. giuris* was studied from different wetlands, dams, and local fish markets of Bangladesh and India previously [55,56,57]. The majority of the parasitic infections are due to the presence of monogenetic (*Dactylogyrus cirrhini* and *D. glossogobi*) and digenetic trematodes (*Allocreadium glossogobium* and *A. handiai*), and few acanthocephalans (*Pallisentis nandai* and *P. gaboes*). The prevalence, intensity, and abundance of infections vary according to the season and sex of the *G. giuris*. Females are much more susceptible than those males [57]. The parasite abundance and prevalence showed the highest peak in December while the lowest was observed in April and May [57]. A similar kind of observations was found in the visceral organs of *G. giuris* infected with nematode parasite, *Rhabdochona garuaiin* [56]. Exposure to pesticides like Malathion and other abnormal environmental factors proved lethal to the population of *G. giuris* and its survival which caused devastating impacts on fish endocrinology, physiology and reproduction [58].

5.7.4 Proper management system

Although the highest availability of *G. giuris* is generally observed in the rainy season, its abundance in nature is decreasing day by day due to various human interferences. Therefore, Fish biologists should know the number of eggs, fry, and young that could be produced from an individual brood fish for better management and production. The Lower growth performances of *G. giuris could* be associated with the age and size of fish, species variations, protein supply, and environmental conditions. An effective management strategy has to be implemented for successful fish farming. Maturation of the brood fish, feeding and manuring in appropriate quantity, the dosage of proper hormones used in induced breeding, quality and ripeness of oocytes, and overall conducive environment is essential for the culture of *G. giuris* in captivity [49]. Immature eggs cannot be fertilized and thus requires intense care and observations. Only reliable artificial breeding and proper rearing techniques of larvae, fry, and fingerlings can ensure a steady supply of quality fish seeds. Fishes which breed in captivity are more susceptible to diseases than the ones in natural water bodies. Hence, necessary protocols for the eradication of the common diseases should be adopted at the proper time.

6. NUTRIENT PROFILES

The demand for various fresh water and marine fish is very high in India because of their nutrient contents. *G. giuris* is very much notable for its nutrient profile among the small indigenous species (SIS) which is shown in Table 2. Several authors [59,60,61] have studied the nutritional status of Bele and according to their reports, *G. giuris* is very rich in protein, vitamins, amino acids, minerals and moisture content but is poor in carbohydrates. This species is, therefore highly eligible in the criteria for human consumption. There is a substantial variation in nutritional components among male and female members of the species. In general, a fish is composed of about 72% water, 8% fat, 19% protein, 0.5% calcium, 0.25% phosphorus, 0.1% vitamins [62]. The nutrient profile is also dependent upon seasonal fluctuations [63]. Due to the availability of food in different seasons of the year, the tissue composition is directly influenced. The chemical composition is not only dependent on the environment, but also relies on several other factors like sex, habitat, feeding habit and age of the fishes [64]. Astonishing seasonal variations can be viewed in the contents of lipid, protein, moisture, whereas the content of ash and carbohydrates remain more or less constant [65].

Table 2. The nutrient composition of *G. giuris*

Nutrient content	Remarks
Moisture	It is the major component of fish meat, ranges between 78 % - 80 % depending on sex and behavioral pattern. In general, the female fishes have higher moisture content than the males [59].
Protein	14-16% (depends on season and sex). During breeding season, the protein content reaches at its peak in both of the sexes. The average proportion of protein is comparatively lower in females [66,67].
Amino acids	Essential amino acids are found to be around 33% of total amino acid content including Histidine 17.08%, Threonine 10.70 %, Lysine 1.46 %, Methionine 0.6%, Tryptophan 1.31 %, Valine 1.31%, Leucine 0.01 %, Isoleucine 0.01% and Phenylalanine 0.29 % [68].
Lipid	It varies between males and females within 1-2 %. The content increases during the pre-spawning period in the females, while it reachesmaximum in the males during the post-spawning period [59].
Carbohydrate	A small quantity (0.60-1.50 %, varies within sex) of carbohydrates, predominantly in the form of glycogen which is rapidly converted into lactic acid after death [68].
Minerals	*G. giuris* is also an important source of minerals. The major components are- potassium, sodium, calcium, phosphorus, iron, nickel, magnesium, manganese, copper and very low amount of Cadmium [61].
Ash content	It ranges from 2.15 % to 2.96 %. It is almost similar in both the sexes with a slight seasonal variation [59].

7. MIGRATION

G. giuris is known to migrate for breeding purposes. They travel to marine water for spawning when it comes to breeding. Although their migratory behaviour is not well marked, few researchers have studied them along with their habitat, starting from freshwater of the rivers to the marine waters of the estuary [11]. It is reported that *G. giuris* can breed not only in the impounded area but also in running freshwater and marine habitat [31]. They are amphidromous by nature, i.e., they travel between freshwater and marine water in both directions. But they are not classical migrators as no supportive evidence of migration over 100 km has been found sofar. The journey made by *G. giuris* is also not cyclical, and their migratory route is not predictable [69].

8. THREATS AND CONSERVATION STATUS

G. giuris is recorded under Least Concern category (LC) as per record in IUCN Red Data Book of Threatened Species, 2019 [70]. However, a few primary and common threats are regularly limiting the life history of freshwater fish groups [71]. The freshwater biodiversity group of IUCN has been working since the early 2000s for better assessment of conservation strategies and the common threats encountered by the freshwater fishes (Fig. 8). Major threats include pollution [72], habitat destruction and fragmentation [73], global climatic pattern change [74], effects of invasive species [75], anthropogenic stress [76] and most importantly overfishing and unscientific fishing [77]. The adverse effects of deforestation are also severe for the freshwater fishes including gobioids due to the associated sediment runoff [78].

9. CURRENT STATUS OF *G. giuris* ON THE MARKET (CUSTOMER RECEPTION)

Gobies are considered an essential food fish in many countries of the Indian subcontinent [79]. People have a special preference for *G. giuris* in their diet because of its special taste and low fat- high protein content [6,80]. About 80% of people of Bangladesh are dependent on SIS (small indigenous species) for the required supply of animal proteins because they are available at a reasonable price [10]. The tank goby also drags the attention of aquarium keepers in recent times. *G. giuris* sometimes looks expensive to common people due to high demand in the market which makes it debatable whether this fish is a family food for the middle class or higher class. In Bangladesh, the general price of large fresh fish is around 700-800 Taka/kg [49], whereas the same in India is about 400-450 INR/kg. The market price for *G. giuris* varies according to its size. Large-sized fish is notable in the southern part of Bangladesh, the price of which is comparatively higher than that of smaller ones. Different kinds of delicious food items can be prepared with the eggs of *G. giuris* such as 'jhuri' which is highly appreciated by people of India and Bangladesh. In recent times, it got beyond the buying capacity especially for the poor and middle-class families due to its uprising market value. To meet the level of such high demand, the culture of *G. giuris* in captivity is need of the hour compared to capture methods [48].

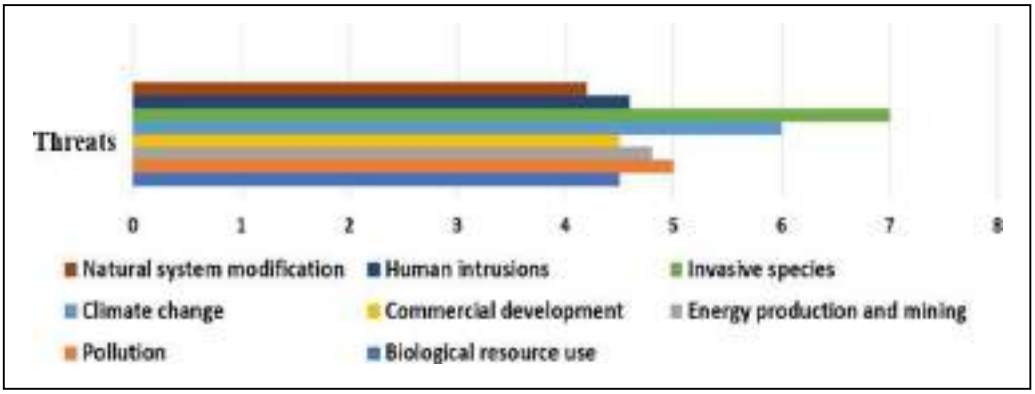

Fig. 8. Threats to freshwater fishes

10. CONCLUSIONS

The present study concluded with all the available information of food and feeding habits, reproductive biology, habitat and morphological variation of *G. giuris* along with some future perspectives and probable threats of the species. *G. giuris* is reported as small indigenous species (SIS) in India and Bangladesh region with a good taste and nutritional value. Many poor populations of India, Bangladesh and other south Asian countries depend on gobioids as they are available in large amounts and because of their reasonable market price. But availability in the local market is not sufficient which increases market cost day by day and thereby becomes one of the limitations to serve regularly on the plate. The maximum need is made by wild catch. This fish has a good range of feeding habits and a prolonged breeding period ranging from April to June. Thus, they are recorded as a very important cultivable species and need to enhance more captive propagation for more availability and commercialization. Moreover, the medicinal value of the fish has not yet been studied. Relevant steps must be taken to increase the availability and to reduce the pressure on natural stocks. This can be only achieved through artificial propagation or employing the species in a different culture system with other commercial species. This review focused on the overall biological aspects of *G. giuris* and will be indicative for future workers to look after the areas especially the conservation strategies of the species so that it can be elevated from semi- commercial to a highly economic commercial food product.

COMPETING INTERESTS

Authors have declared that no competing interests exist.

REFERENCES

1. Doha S. Investigation into the biology of the gobi, *Glossogobius giuris* (Hamilton-Buchanon). Bangladesh Journal of Zoology. 1974;2:95-106.
2. Larson H, Britz R, Sparks JS. *Glossogobius giuris*. The IUCN Red List of Threatened Species (Least Concern, ver 3.1); 2016.
   DOI: 10.2305/IUCN.UK.2016-3.RLTS.T166533A19011337.en
3. Hossain MAR, Wahab MA, Belton B. The checklist of the riverine fishes of Bangladesh. Fisheries and Aquaculture, News FAN, Bangladesh. 2012;2:17-18.
4. Dana EB, Jinoy VG, Mathew S. Assessment of nutritional quality in the tissue of euryhaline fish tank goby *Glossogobius giuris*, Hamilton 1822 caught from Vembanad Lake, Kerala, India. International Journal of Fisheries and Aquatic Studies. 2019;7(3):213-218.
5. Ali MY. Small indigenous fish species culture in Bangladesh. Proceedings of National Workshop on Small Indigenous Fish culture in Bangladesh, IFADEP-SP 2, Dhaka, Bangladesh; 1997.
6. Islam NM, Joaddar RAM. Seasonal variation of the proximate composition of freshwater gobi, *Glossogobius giuris* (Hamilton) from the River Padma. Pakistan Journal of Biological Sciences. 2005;8:532-536.
   DOI: 10.3923/pjbs.2005.532.536
7. Roos N, Wahhabi MA, Hossain MAR, Thilsted SH. Linking human nutrition and fisheries: incorporating micronutrient-dense, small indigenous fish species in carp polyculture production in Bangladesh. Food and Nutrition Bulletin. 2007;28:280-293.
   DOI: 10.1177/15648265070282S207
8. Hamilton F. An account of the fishes found in the river Ganges and its branches. Archibald Constable and Company, Edinburg. 1822;7: 148.
   DOI: https://doi.org/10.5962/bhl.title.6897
9. Rao LM, Rao PS. Food and Feeding Habits of *Glossogobius giuris* from Gosthani Estuary. Indian Journal of Fisheries. 2002;49:35-40.
10. Islam MN. Eco-biology of freshwater gobi, *Glossogobius giuris* (Hamilton) of the River Padma in relation to its fishery: A review. Journal of Biological Science. 2004;4:780-793.
    DOI: 10.3923/jbs.2004.780.793
11. Hora SL. Ecology and bioeconomics of the gobioid fishes of the Gangetic delta. 12th International Zoological Congress, Lisbon. 1936;63.
12. Inger RF, Kong CP. Freshwater fishes of North Bomeo. Fieldana, Zoology. Chicago Natural History Museum. 1962;5.
    DOI: https://doi.org/10.5962/bhl.title.2957
13. Mohsin AKM, Ambak MA. Freshwater Fishes of Peninsular Malaysia. Published by Penerbit University, Malaysia. 1983;284.
14. Devi KR. Gobioids of Ennore estuary and its vicinity. Record of Zoological Survey of India. 1992;90:161-189.
15. Islam MR, Mollah MFA. Morphological observation and PG-induced breeding of *Glossogobius giuris* (Hamilton, 1822). Journal of Science and Technology. 2013;171-180.

16. Rao S, Rao L. Sex ratio, fecundity, maturity and spawning details of *Glossogobius giuris* (Hamilton) from Gosthani Estuary near Visakhapatnam. Journal of Life Sciences. 2007;1:16-29.
17. Achakzai WM, Saddozai S, Baloch WA, Massod Z, Rehman HU, Mussarrat-ul-Ain. Food and Feeding Habits of *Glossogobius giuris* (Hamillton and Buchannan, 1822) collected from Manchar Lake distt. Jamshoro, Sindh, Pakistan. Global Veterinaria. 2015;14 (4):613-618.
DOI: 10.5829/idosi.gv.2015.14.04.9465
18. Koumans FP. Gobioid fishes of India. Memoirs of the Indian Museum. 1941;13(3): 256- 272.
19. Dorado EL, Torres MAJ, Demayo CG. Describing body shapes of the white goby, *Glossogobius giuris* of Lake Buluan in Mindanao, Philippines using landmark-based geometric morphometric analysis. International Research Journal of Biological Sciences. 2012; 1(7):33-37.
20. Rahman AKA. Freshwater Fishes of Bangladesh. The Zoological Society of Bangladesh, Dhaka. 2005;307-308.
21. Bhuiyan AL. Fishes of Dacca. Asiatic Society of Pakistan. 1964;13:113-114.
22. Nichols JT. The freshwater fishes of China. Natural history of Central Asia: Volume IX. The American Museum of Natural History, New York, USA. 1943;322.
DOI: https://doi.org/10.5962/bhl.title.12103
23. Hoese DF. Gobiidae. In Smith's sea fishes. Springer-Verlag, Berlin. 1986;774-807.
DOI: 10.1007/978-3-642-82858-4
24. Sit G, Jana A, Chanda A. Gobioid Fish of Paschim Medinipur and Jhargram District, West Bengal, India. Uttar Pradesh Journal of Zoology. 2019;40(4):146-153.
25. Datta Munshi JS, Singh ON, Singh DK. Food and feeding relationship of certain aquatic animals in Ganga ecosystem. Tropical Ecology. 1990;31(2):138-144.
26. Hossain S, Roy A, Mohammad RL. Food and feeding habit of Bele, *Glossogobius giuris* (Hamilton and Buchannan, 1822) collected from MithamainHaor of Kishoreganj districts, northeastern Bangladesh, International Journal of Fisheries and Aquatic Studies. 2016;4(5): 84-88.
27. Sonowal M, Abujam SK, Biswas SP. Feeding biology of *Glossogobius giuris* (Hamilton-Buchanan) from upper Assam. International Journal of Fisheries and Aquatic Studies. 2017; 5(5):369-371.
28. Azad MAK, Hossain MY, Khatun D, Parvin MF, Nawer F, Rahman O, Hossen MA. Morphometric relationships of the tank goby *Glossogobius giuris* (Hamilton, 1822) in the Gorai river using multilinear dimensions. Jordan Journal of Biological Science. 2018; 11:81-85.
29. Tandon KK. Biology of Channa punctatus (Bloch) and *Glossogobius giuris* (Hamilton). Research Bulletin, Punjab University. 1962;13 (3-4):257-262.
30. Mookerjee HK. On the food of *Glossogobius giuris* (Hamilton). Science and Culture. 1947; 13:162–163.
31. Alikunhi KH, Rao GL, Jacob PK. Bionomics and development of *Glossogobius giuris* (Hamilton). Journal of Madras University. 1951;21:238-248.
32. Bhowmick RM. Studies on some aspects of the biology of *Glossogobius giuris* (Hamilton) with notes on the fishery in the Hooghly estuary. Proceedings of Indo-Pacific Fisheries Council. 1965;11(2):99-115.
33. Bhuiyan AS, Haque S. Cannibalistic food habit of *Glossogobius giuris* (Hamilton) in relation to its size and sex. Bangladesh Journal of Zoology. 1984;12:111-113.
34. Islam MN. Cannibalism of freshwater gobi, *Glossogobius giuris* (Hamilton) in relation to its size, sex and season from the river Padma. University Journal of Zoology. 2002;21:63-64.
35. Roshni K, Renjithkumar CR, Kurup BM. Food and feeding habits of *Glossogobius giuris* in Chalakudy river, Southern Western Ghats, India. International Journal of Scientific Research in Science, Engineering and Technology. 2015;1(4):321-325.
36. Karamchandrani SJ. On the occurrence of associates of carp fry in the fry collection nets and the destructive role played by predatory fish. Indian Journal of Fisheries. 1957;4(1):47-61.
37. Dewan S, Shaha SN. Food and feeding habits of *Tilapia nilotica* (L.) (Perciformes: Cichlidae). II, Diel and seasonal patterns of feeding. Bangladesh Journal of Zoology. 1979; 7(2):75-80.
38. Mustafa G, Islam KR, Ali S. Seasonal patterns of feeding of the freshwater fish Colisafasciata (Bloch). Ibd. 1981;9(1):49-50.
39. Qambrani GR, Soomro AN, Palh ZA, Baloch WA, Tabasum S. Reproductive Biology of *Glossogobius giuris* (Hamilton), in Manchar Lake Sindh, Pakistan. Journal of Aquaculture Research and Development. 2015;6:392.
DOI: 10.4172/2155- 9546.1000392

40. Jahan DA, Kohinoor AHM, Khan MM, Monir MS. Gonad histology and biological aspects of freshwater gobi, *Glossogobius giuris* (Hamilton, 1822). Trends in Fishery Research. 2015;4:20-24.
41. Jabbar S, Liza SK. Breeding biology of freshwater goby *Glossogobius giuris* using gonadosomatic index and gonadal histology. Annals of Bangladesh Agriculture. 2019;23 (1):1-13.
42. Hossain MS. Reproductive Characteristics of Bele, *Glossogobius giuris* from Mithamoin Haor, Kissorgonj, Bangladesh. World Journal of Fish and Marine Sciences. 2014;6:537-543.
43. Moyle PB, Cech JJ. Reproduction. In Fishes: An Introduction to Ichthyology, 4thEdn, Prentice Hall Inc. 2000;123-144.
44. Raitaniemi J, Bergstrand E, Floystad L, Hokki R, Kleiven E, Rask M, Reizenstein M, Saksgard R, Angstrom C. The reliability of whitefish (*Coregonus lavaretus*) age determination- differences between methods and between readers. Ecology of Freshwater Fish. 1998;7:25-35.
45. Sonowal M, Abujam SK, Biswas SP. Certain aspects of reproductive biology of *Glossogobius giuris* (Hamilton-Buchanan) from Upper Assam. World Wide Journal of Multidisciplinary Research and Development. 2018; 4(1): 45-48.
46. Roy A, Hossain MS, Rahman ML, Salam MA, Ali MM. Fecundity and gonadosomatic index of *Glossogobius giuris* (Hamilton, 1822) from the Payra River, Patuakhali, Bangladesh. Journal of Fisheries. 2014;2:141-147.
47. Haque MA, Hossain MA. Sexual maturity and maturity of freshwater fish Mystus vittatus (Bloch) (Cypriniformes: Bagridae). University Journal of Zoology, Rajshahi University. 1993; 12:9-13.
48. Islam MS, Tuly DM, Hasnahena M, Bahadur P, Hasan MR. Induced breeding of freshwater gobi, *Glossogobius giuris* (Hamilton, 1822) in the captivity: A preliminary study. Journal of Fisheries and Aquatic Science. 2014;9:24-32. DOI: 10.3923/jfas.2014.24.32
49. Yeasmine S, Rahman MA, Sarower-E-Mahfuj M, Sku S, Hossen MN, Rahman MA, Mollah MFA. Development of induced breeding technique for freshwater fish gobi, *Glossogobius giuris* (Hamilton, 1822) using pituitary gland (PG) extract. Annual Research & Review in Biology. 2021;36(1):24-35. DOI: 10.9734/ARRB/2021/v36i130330
50. Ghosh S, Marudhupandi T, Kumar A, Balasubramanian T. Studies on sea anemone specificity in captive spawning of clownfish with special reference to Amphiprion oceallaris. Journal of Recent Trends in Biosciences. 2011;1(2):72-76.
51. Corkum LD, MacInnis AJ, Wickett RG. Reproductive habits of round gobies. Great Lake Research Reviews. 1998;3:13-20.
52. Candolin U, Reynolds JD. Adjustments of ejaculation rates in response to risk of sperm competition in a fish, the bitterling (Rhodeus sericeus). Proceedings of the Royal Society London. 2002;B269:1549-1553.
53. Chowdhury AK. Helminth parasite infestation and histopathological changes in snakehead fishes. M.Sc. Thesis, Department of Zoology, University of Dhaka, Dhaka; 1992.
54. Markov GS. Physiology of fish parasites. In: Parasitology of fishes (Dogiel, Petrushevesky and Polyansky eds.), English translation by Z. Kobata, Oliver and Boyd, Edinberg and London. 1961;117-139.
55. Chakrabarti KK. A new strigeid metacercaria, Tetracotyle glossogobii sp.n., from an Indian freshwater fish, *Glossogobius giuris* (Ham.), Helminthologia. 1970;11:77-82.
56. Leela B, Rama Rao K. Nematode parasites in a freshwater fish *Glossogobius giuris* (Hamilton-Buchanan, 1822) at lower Mannair Dam, Kaarsimnagar Dt. Andhra Pradesh, India. IOSR Journal of Pharmacy and Biological Sciences. 2014;9(2):37-40.
57. Sultana S. Organal distribution and their seasonal rate of infestation in *Glossogobius giuris*. International Research Journal of Biological Sciences. 2015;4(5):44-49.
58. Ramachandra MM. Sea water fish, *Glossogobius giuris* at last lives in fresh water now. Journal of Fisheries and Livestock Production. 2015;3:1. DOI: 10.4172/2332- 2608.1000123.
59. Wimalasena S, Jayasurya MNS. Nutrional analysis of some fresh water fishes. Journal of the National Science Foundation of Sri Lanka. 1996;24(1):21-26.
60. Bogard JR, Thilsted SH, Marks GC, Wahab MA, Hossain MAR, Jakobsend J, Stangoulis J. Nutrient composition of important fish species in Bangladesh and potential contribution to recommended nutrient intakes. Journal of Food Composition and Analysis. 2015;42:120-133. DOI:https://doi.org/10.1016/j.jfca.2015.03.002
61. Guha BC. The Role of Fish in Human Nutrition. In: Fish in Nutrition. Published by Fishing News (Books) Ltd., England. 1962; 39-42.
62. FAO. Fish for Food and Development. 1991; 1-49.

63. DoF (Directorate of Fisheries. Fisheries Resource Information of Bangladesh (1999-2000), Ministry of Fisheries and Live Stock, Government of the People's Republic of Bangladesh. 2001;65-76.
64. Love RM. The Biochemical Composition of Fish. In: The Physiology of Fishes (Ed., Brown, M. E.). Academic Press, London and New York. 1957;1:401-418.
65. Jafri AK, Khawaja DK, Qasim SZ. Studies on the biochemical composition of some freshwater fishes. Part-I. Muscle. Fish Technology. 1964;1:148-157.
66. Khuda MQ, De HN, Khan NM. Chemical composition and quantity of traditionally processed fish. Pakistan Journal of Scientific and Industrial Research. 1964;5:70-73.
67. Kamaluddin A, Malek MA, Sanaullah M. DeshioKhaidderPustiman (In Bengali). Institute of Nutrition and Food Science. 1977; 1-22.
68. Gopalam C, Ramasastri BV, Balasubramaniam SC. Nutritive value of Indian foods. National Institute of Nutrition, Indian Council of Medical Research, Hyderabad, India. 1978;46-103.
69. Froese R, Pauly D. *Glossogobius giuris* in Fish Base. Updated 01.2016.
70. IUCN. The IUCN Red List of Threatened Species. Version 2019-2.
71. Arthington AH, Dulvy NK, Gladstone W, Winfield IJ. Fish conservation in freshwater and marine realms: status, threats and management. Aquatic Conservation: Marine and Freshwater Ecosystems. 2016;26(5):838-857.
DOI: https://doi.org/10.1002/aqc.2712
72. Winfield IJ. Eutrophication and freshwater fisheries. In Freshwater Fisheries Ecology, JF Craig (ed.). John Wiley: Oxford. 2015;779-793.
DOI:https://doi.org/10.1002/9781118394380.ch54
73. Winfield IJ. Fish in the littoral zone: ecology, threats and management. Limnologica. 2004; 34:124–131.
DOI: 10.1016/S0075-9511(04)80031-8
74. Heino J, Erkinaro J, Huusko A, Luoto M. Climate change effects on freshwater fishes, conservation and management. In Conservation of Freshwater Fishes, GP Closs, M Krkosek, JD Olden (eds). Cambridge University Press: Cambridge. 2016;76–106.
DOI:https://doi.org/10.1017/CBO9781139627085
75. Snoeks J. How well known is the ichthyodiversity of the large East African lakes? Advances in Ecological Research. 2000; 31:17–38.
DOI: 10.1016/S0065- 2504(00)31005-4
76. Fagan WF. Connectivity, fragmentation, and extinction risk in dendritic metapopulations. Ecology. 2002;83:3243–3249.
DOI: https://doi.org/10.1890/0012-9658(2002)083[3243:CFAERI]2.0.CO;2
77. Dudgeon D, Arthington AH, Gessner MO, Kawabata ZI, Knowler DJ, Leveque C, Naiman RJ, Prieur-Richard AH, Soto D, Stiassny MLJ, Sullivan CA. Freshwater biodiversity: importance, threats, status and conservation challenges. Biological Reviews. 2006;81:163-182.
DOI: 10.1017/S1464793105006950
78. Benstead JP, De Rham PH, Gattoliat JL, Gibon FM, Loiselle PV, Sartori M, Sparks JS, Stiassny MLJ. Conserving Madagascar's freshwater biodiversity. Bioscience. 2003;53: 1101–1111.
DOI:10.1641/0006-3568(2003)053[1101:CMFB]2.0.CO;2
79. Joaddar MAR. Length-weight relationship and condition factor (Kn) of gobi, *Glossogobius giuris* (Hamilton) from "Atrai River" in the northern part of Bangladesh. Journal of Fisheries International. 2009;4(1): 1-4.
80. Ahmed ATA, Mustafa G, Alam MZ. Biochemical composition of seven species of gobi fish. Journal of Asiatic Society of Bangladesh. Science. 1984;10:107-111.

World Journal of Environmental Biosciences

Available Online at: **www.environmentaljournals.org**

Volume 10, Issue 2: 9-17

https://doi.org/10.51847/mhLv0Gijx5

ISSN 2277- 8047

COVID-19 Forced Lockdown: Nature's Strategy to Rejuvenate Itself

Koushik Sen[1]*, Tanmay Sanyal[2], Susanta Roy Karmakar[3]

[1]Department of Zoology, Jhargram Raj College, Jhargram, West Bengal, India.
[2]Department of Zoology, Krishnagar Government College, Krishnagar, West Bengal, India.
[3]Department of Zoology, Maulana Azad College, Kolkata, West Bengal, India.

ABSTRACT

Coronavirus diseases-2019 (COVID-19) pandemic emerged in late 2019 and many countries initially adopted partial or complete lockdown measures to restrict the transmission of the disease, as effective drugs or vaccines were unavailable till then. Imposing lockdown drastically reduced anthropogenic and commercial activity. All types of large and small industries and markets were closed; all sorts of public and commercial transportation, except for the essential ones, along with railways and flights were completely shut off. Worldwide reports and research indicating that COVID-19 induced lockdown might have a crucial impact on the global environment. During the lockdown, air and water quality improved significantly due to low atmospheric pollution, environmental noise reduced and wild lives are also blooming. COVID-19 may be nature's warning to the human being; when human beings are confined in homes for saving their lives, nature takes advantage and try to heal herself. Based on available research and media reporting, in this article, we try to summarize the episode of COVID-19 induced lockdown and its effect on the environment especially emphasizing the Indian context.

Keywords: *COVID-19, Environmental impact, Lockdown, SARS-COV-2*

Corresponding author: Koushik Sen
e-mail ✉ koushiksen1987@gmail.com
Received: 22 March 2021
Accepted: 08 June 2021

INTRODUCTION

Coronaviruses are a group of viruses that infect humans through zoonotic transmission. After Severe Acute Respiratory Syndrome (SARS) and Middle East Respiratory Syndrome (MERS) (Zhong *et al.*, 2003; Ramadan & Shaib 2019; Magomedova *et al.*, 2020) in the last two decades, in late December 2019, a novel infectious disease was identified in the Wuhan city of China (Rivas *et al.*, 2020). The International Committee on Taxonomy of Viruses (ICTV) named the virus "severe acute respiratory syndrome coronavirus 2" (SARS-CoV-2) (Gorbalenya *et al.*, 2020), and the disease was named COVID-19 (Chen *et al.*, 2020) on February 19, 2020, by World Health Organization (WHO). With affecting more than 175.5 million people and causing nearly 3.8 million deaths (as of 14th June 2021) in more than 200 countries, so far, the COVID-19 is the largest pandemic on the earth (WHO, 2020a). SARS-CoV2 is a member of the β-coronavirus subgroup under the Coronaviridae family (Pyrc *et al.*, 2007) having glycoprotein spikes like a crown on its surface with a diameter ranging between 65-125 nm. COVID-19 is transmitted from person to person through respiratory droplets expelled by the infected person's coughing, sneezing, talking, singing, or spread by touching fomites (Bouey *et al.*, 2020). Recently, WHO (on 9th July 2020) admitted that the virus can also be transmitted through the air (WHO, 2020b). This newly-born disease has a long incubation period ranging between 2-14 days with symptoms like breathing difficulty, dry cough, fever, mild pain or pressure in the chest, and blue lips (CDC, 2020). Initially, there are no specific effective drugs to prevent the disease (Cortegiani *et al.*, 2020). Some preexisting antibacterial and antiviral drugs such as favipiravir, remdesivir, tocilizumab, ivermectin, and lopinavir are used to combat this disease (Paital *et al.*, 2020). There are approximately 300 promising vaccine candidates under trial, among which 102 are under clinical trial and the rest are under preclinical evaluation (WHO, 2020c). National Regulatory Authorities recently approved sixteen vaccine candidates, for emergency mass vaccination purposes (WHO, 2021).

The emergency committee of WHO, on 30th January 2020, declared the disease as a global health emergency (WHO, 2020d). Initially, due to a lack of effective medicine or vaccine, the social lockdown was the only way to maintain less human interaction for preventing this disease from spreading (Paital *et al.*, 2020). Several countries implemented these lockdown measures at different stages of infection; China imposing lockdown from the end of January 2020 in Wuhan, whereas in Italy the nationwide lockdown was first applied from 09th March 2020, and in Spain, Australia, United Kingdom, and France, the lockdown measure was imposed on 14th March 23rd March, 23rd March, 17th March 2020, respectively (Wikipedia, 2020a).

In India, the first confirmed positive case of COVID-19 was reported from Kerala on 13th January 2020 (India Today, 2020) and now India holds 2nd position with 29,510,410 confirmed

cases and 374,305 deaths as of 14th June 2021 (Worldometer, 2020). With 500 confirmed cases, the Prime minister requested all the citizens of the country to observe a 14 hrs (7.00 A.M-9.00 P.M. IST) voluntarily social distancing campaign, observed as Janata curfew on 22nd March 2020 (The Hindu, 2020a), followed by a nationwide imposed locked down from 25th March 2020 with initial duration for 21 days and extended till June 30th. Step by step unlocking procedure was started but till now, to control the second wave of COVID-19, state governments are imposed a lockdown on a regional scale (Wikipedia 2020b; Indian Express, 2021). Different phases of lockdown are implemented with different rules and levels of restrictions to maintain strict social distancing as a measure to reduce the effects and transmission of Coronavirus (Somani *et al.*, 2020). In general, under the nationwide lockdown, all the academic institutions, industries, multiplex, shopping complexes, restaurants, and similar public places were closed. All sorts of transportation services including railways and flights were suspended except the essential one. The lockdown affected the Indian economy but led to a dramatic decrease in air pollution and improvement of overall environmental health including surface water quality, GHG emissions, noise level, and organic and inorganic west product generation.

The total or partial social lockdown around the planet to flatten the pandemic curve results in less anthropogenic and economic activity and human-environment interaction and led to a decrease in pollution (The Gurdian, 2020). In a nutshell COVID-19, the biggest pandemic and curse to human civilization to date may be a warning for us from Nature to stop destroying the natural resources, on the other side when we are quarantined at home to prevent this fatal disease, nature is trying to heal itself.

In this article, we try to sum up the impact of COVID-19-induced lockdown on the global environment almost on every aspect (air pollution, water pollution, noise pollution, greenhouse gas (GHG) emission, biodiversity, and wildlife) with emphasizing the Indian context using available literature, news from media and various regulatory authorities.

COVID-19 and status of air pollution

To live on the earth, ambient air quality is the essential one; although globally 91% of people live under poor air quality (WHO, 2016). Air pollution is responsible for 4.6 million deaths globally (Cohen *et al.*, 2017). The concentration of particulate matter (PM) is one of the major parameters to measure air quality. The high $PM_{2.5}$ is responsible for adverse health effects causing chronic obstructive pulmonary disease (COPD), respiratory infection (GBD, 2018), is declined in various cities all over the world due to lockdown measures. In Zaragoza (city of Spain) the $PM_{2.5}$ significantly decreased 58% in March 2020 compared to February 2020; in Rome, the average $PM_{2.5}$ value lowered 24 % in March 2020 compared to the value of February 2020. In Dubai (UAE) the $PM_{2.5}$ reduced by 11% during March 2020 compared to March 2019 (Chauhan & Singh 2020). According to the Copernicus Atmospheric Monitoring Service (CAMS) of the European Union, in a large area of China mean value of $PM_{2.5}$ reduced up to 20-30% in February when compared to the mean value of February 2017, 2018, and 2019 (Zambrano-Monserrate *et al.*, 2020). A study to analyze the $PM_{2.5}$ of fifty most polluted capital cities of different countries around the world reported an average 12% reduction in $PM_{2.5}$ concentration worldwide with the highest reduction in the African continent by 33% followed by a 22 % reduction in America and 16 % in Asia; finally, in European countries the reduction level was only 5% due to lockdown in last year **(Table 1)** (Rodríguez-Urrego & Rodríguez-Urrego, 2020). Nitrogen dioxide (NO_2) is a highly reactive air pollutant emitted from vehicles and industrial activity and causes inflammation, and respiratory distress (He *et al.*, 2020a; He *et al.*, 2020b). National Aeronautics and Space Administration (NASA) and European Space Agency (ESA) released images, of several nations before and during the lockdown, using Ozone Monitoring Instrument (OMI) through the AURA satellite and Tropospheric Monitoring Instrument (TROPOMI) through the Sentinel-5P satellite to capture the data suggests a reduction in NO_2 concentration up to 30 % with improved environmental quality **(Table 2)**. Heavy changes in NO_2 concentration were observed in the middle of March 2020, onwards in South Asia and South-East Asian countries including a large part in India, due to the closure of industries and transportation service. Similar changes were recorded in Western Africa and Europe (Lal *et al.*, 2020). Carbon dioxide (CO2), another major air pollutant has led to a sharp decline of approximately 17% by 7th April 2020 when compared to 2019 levels due to the peak in global lockdown. The carbon emission was reduced by 23.9 %, 30.7 %, and 31.6 % in China, UK, and USA, respectively. In India, carbon emission was reduced by 26 % (Le Quéré *et al.*, 2020).

In India, gradual improvement in the overall air quality was also observed. Air Quality Index is an important value to measure the overall air pollution due to principal air pollutants; the lower the AQI value and air quality are inversely related. During the complete lockdown period in 2020, the Air Quality Index (AQI) of the country was 30% reduced when compared to 2019. The north, south, east, west, and central regions of India experienced a 44, 33, 29, 32, and 15 % decline in AQI value, respectively (Sharma *et al.*, 2020). The average AQI of Delhi, which was around 300-400, drastically reduced to 94, during the lockdown phase. According to Sentinel-5P satellite captured data, the NO_2 concentration in India was reduced by almost 40-50% **(Figure 1)** across the major cities of India compared to the same time frame of the previous year (Lokhandwala & Gautam, 2020). During the initial lockdown period (16th March to 14th April 2020), in 22 cities of India PM10, PM2.5, carbon monoxide (CO) was reduced by 43, 31, and 10 %, respectively (Arora *et al.*, 2020). In Delhi and Mumbai, PM2.5 was reduced by 35% and 14%, respectively when compared to March 2019 (Chauhan & Singh, 2020) and a similar pattern of PM2.5 reduction was also observed in other cities of India**, (Table 3).** Even in this year, due to the second wave of COVID-19, after the starting of lockdown in mid-April 2021, the air quality is similar to that of last year, when a nationwide lockdown was implemented in March 2020. The average PM2.5 for May of both years is almost identical at about 55-56 $\mu g/m^3$. However, this value is about 42 percent lower than the value in May 2019, when there was no lockdown (India Today, 2021).

Table 1. Percentage of PM 2.5 Reduction in World's Different Cities Due of COVID-19 Lockdown

City	% Reduction in PM $_{2.5}$	Time	Source
Newyork, USA	20%	Feb 2020 and Mar 2020	Chauhan and Singh, 2020
Los Angles, USA	30%	Feb 2020 and Mar 2020	
Zaragoza, Spain	58%	Feb 2020 and Mar 2020	
Rome, Italy	24%	Feb 2020 and Mar 2020	
Dubai, UAE	11%	Mar 2019 and Mar 2020	
Delhi, India	35%	Mar 2019 and Mar 2020	
Dhaka, Bangladesh	24%	Feb 2020 and April 2020	
Tehran, Iran	39%	Feb 2020 and April 2020	Rodríguez-Urrego & Rodríguez-Urrego, 2020
Astana, Kazakhstan	18%	Feb 2020 and April 2020	
Santiago, Chile	10%	Feb 2020 and April 2020	

Table 2. Nitrogen dioxide (NO_2) Emission data of Different Countries during Lockdown

City	% Reduction in PM $_{2.5}$	Time	Source
Delhi	35%	Mar 2019 and Mar 2020	Chauhan & Singh, 2020
Mumbai	14%		
Chennai	32%	Mar- May 2019 and Mar-May 2020	Kumar *et al.*, 2020
Hydrabad	26%		
Kolkata	24%		
Jaipur	50.5%	Mar- May 2019 and Mar-May 2020	Navinya *et al.*, 2020
Lucknow	51.5%		
Ahemedabad	67.7%		
Nagpur	52.6%		
Bangalore	45.4%		
Chennai	30.2%		

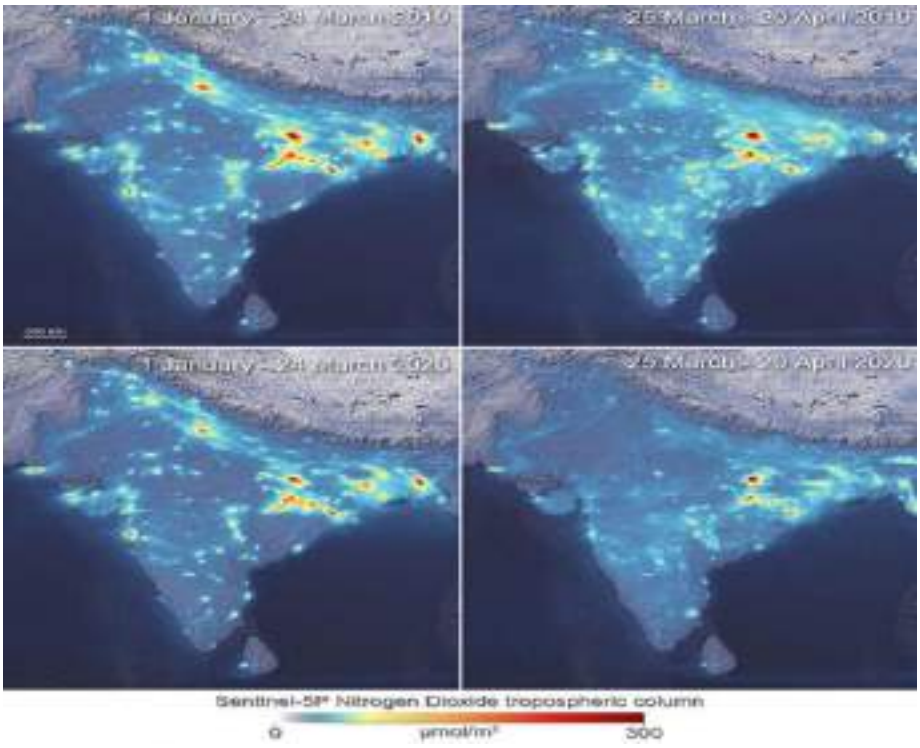

Figure 1. Nitrogen Dioxide (NO_2) Concentration Before and During COVID-19 Lockdown, 2020 in India (Image Source- Earthsky, 2020)

Table 3. Percentage of PM 2.5 Reduction in Different Cities of India Due to COVID-19 Lockdown

Location	Time	% Reduction	Source
Spain	Mar 2019 and Mar 2020	20-30%	Muhammad *et al.*, 2020
USA	Mar 2015–19 and Mar 2020	30 %	
France	Mar 2019 and Mar 2020	20-30%	
Italy	Mar 2019 and Mar 2020	20-30%	
China	Jan and Feb 2020	20-30%	
Europe	Mar 2019 and Mar 2020	20-30%	
India	Mar- Apr 2019 and Mar -Apr 2020	40-50%	Lokhandwala *et al.*, 2020

Impact on GHG emission and ozone hole

In the last few years, the amount of GHG emission throughout the world meets a new peak (Global Climate report, 2019). CO_2 emission rising by 1% per year for the last one decade without changing its pattern till 2019 (Le Quéré *et al.*, 2020). The International Energy Agency estimated a fall of 8 % in CO_2 emission (equivalent to 2600 Mt. CO_2) during this global lockdown. Some agencies have also expected a reduction in CO_2 emission by more than 5%, the highest annual reduction to date (Scientific American, 2020). Imposing Global lockdown at different times results in a daily reduction of global CO_2 emission by 17% by 7th April 2020. The change in global CO_2 emission rate was highest on 7th April during the last 4 months of 2020 (1st January to 30th April) with an average decrease of 26% in individual countries (Le Quéré *et al.*, 2020).

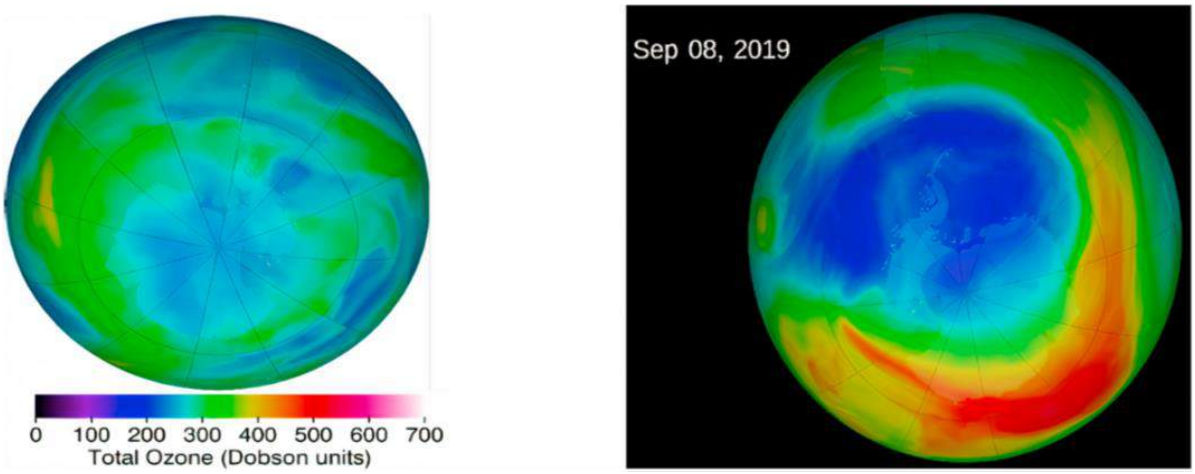

a) b)

Figure 2. The Hole in the ozone layer over Antarctica on 23rd May 2020 and September 08, 2019, respectively (Image source- Arora *et al.*, 2020)

Implementation of strict lockdown by the Indian government to reduce human interaction, also effectively decreased carbon emission by almost 15% during March 2020 and estimated to reach to 30% level at the end of April (Myllavirta & Dahiya, 2020). Just within 10 days of lockdown, the overall power consumption of India decreased up to 20% compared to the usual consumption level. The thermal power generation sector is one of the major GHG emitting sources, dropped GHG emissions by 31% within the first 21 days of April 2020. Following a similar trend in electricity demand, consumption of fossil fuels and natural gas was also reduced during this lockdown, which ultimately led to a significant reduction in GHG emissions (Myllavirta & Dahiya, 2020).

After implementing Montreal Protocol to save the ozone layer, the stratosphere healed 1-3% per decade in the last 20 years and expected to get back its heath as it was in 1980 in the next 50 years. NO_2, CO_2, and various GHG and ozone-depleting substances emissions were reduced during lockdown with a simultaneous increase in surface ozone concentration. During lockdown Copernicus, atmospheric monitoring services (CAMS) confirmed that the largest ozone hole of about 1 million square kilometers over the arctic region has been healed **(Figure 2)** (India Times, 2020). It has been presumed that healing of arctic ozone hole due to reduced emission of GHG and other pollutant triggering by COVID-19 lockdown. However, later scientists reported that ozone layer healing is due to the polar vortex unrelated to the change in lockdown-induced pollution level (Arora *et al.*, 2020).

COVID-19: impact on noise pollution

Anthropogenic activity generated unwanted sound can be defined as environmental noise, which is a prime factor for discomfort and disease of human population and also harmful for the environment and other animals of the earth (Zambrano-Monserrate *et al,* 2019). Most noise pollutions are generated due to anthropogenic activity (Paital, 2020). Long-time exposure to high noise may play a crucial role in irritation, mental stress, hypertension, concentration loss, and

insomnia (Öhrström, 1989; Stansfeld *et al.*, 1996; Rabinowitz, 2000; WHO 2005; Banerjee *et al.*, 2008). An extreme level of sound pollution can cause stroke, heart attack, and dementia (European Union, 2015). In major cities of India generally, the average noise level ranged between 45-86 decibels (db) during the day and 37-76 db during the night. In the residential area, the diurnal noise level is between 63-90 db and 46-78 db, whereas the same for the commercial area are 50-89 and 40-70 during day and night, respectively (Arora *et al.*, 2020). A steep reduction in the noise level has been observed during the lockdown period last year. Global data indicating traffic movement drop down by 54, 36, and 19% in the UK, US, and China, respectively (Somani *et al.*, 2020).

In India, after imposing lockdown, flights, trains, buses, and all other vehicles are stopped except some freight trains and vehicles associated with essential services. For the first time in Indian transportation history, no mail or passenger trains are in operation from 22 March 10:00 PM, 2020 (Hindustan Times, 2020a). With this cessation of transportation, there was a dramatic decrease in noise pollution in Indian cities with an estimated reduction in noise pollution ranged between 35-68 db from 8 AM to 4 PM. In Kolkata and Delhi, noise pollution was decreased by 50-75 db and 20-30 db, respectively in phase-I lockdown (Paital, 2020). In Bengaluru, the noise level was less than 45db in silk bored, JC road, and BTM areas. According to the West Bengal, pollution control board 50-75 % decrease in noise pollution in Kolkata, the city of joy, during the lockdown phase (NDTV, 2020).

COVID-19: impact on water quality

According to articles and media reports, lockdown for preventing COVID-19 has had a great effect on the aquatic ecosystem. The water quality of some major rivers in India including Ganga, Yamuna, Kavery, improved within a few weeks of imposing lockdown mainly due to less anthropogenic activity and closure of industries. Aquatic parameters of Ganga and Yamuna deteriorated over time due to a gradual increase in industrialization and urbanization (Chakrapani & Subramanian, 1996; Dudeja *et al.*, 2011; Deoli *et al.*, 2017). About 1072 industrial units, by releasing waste products, cause pollution of Ganga between Haridwar and Kanpur (Times of India, 2020a).

During pre-COVID time, 6500-6700 MLD (Million liters per day) toxic waste materials were dumped in Ganga in its UP stretch and onwards, about 10% of which is industrial waste. 100-150 tons of BOD, estimated at about 30% of the total BOD, comes from industrial toxicants (Arora *et al.*, 2020). Despite making and executing several consecutive programs almost over the past four decades by GOVT of India, initiated with Ganga Action Plan (GAP) in 1986, then GAP –II in 1993, and recently "Namami Gange" to clean and lean Ganga, but a load of pollutants and waste keep hike on in the Ganga River but nationwide lockdown improves this situation (Times of India, 2020b).

In upstream and downstream of Ganga Barrage, the average concentration of dissolved oxygen (DO) and biological oxygen demand (BOD), were respectively 8 mg/l, 2.1 mg/l, pH 7.9 and DO (7.90), BOD (2.1 mg/l), and pH (7.9) during COVID-19 induced forced lockdown period of March 2020 (Lokhandwala & Gautam, 2020). A study aimed to analyze the complete lockdown effect on water quality of Ganga in which samples were collected and analyzed before and during lockdown from five polluted sites. It showed that the DO increased up to 25-30% and BOD decreased up to 35-40% when compared to pre-lockdown and during the lockdown (Times of India, 2020b). The Data regarding fecal coliform of five mostly crowded areas of Uttarakhand, *i.e.,* Lakshmanjhula, Rishikesh, Bindughat, Dudhiavan, Har ki Pauri, and Jagjeetpur showed 47%, 46%, 25%, 25%, 34 %, and 27 % reduction, respectively (Hindustan times, 2020b). In the UP stretch of river Ganga, the water quality data analysis clearly showed that in a majority of the stations, DO and BOD was increased and decreased respectively in April 2020 when compared with April 2019 (**Figure 3)** (UPPCB, 2020). The water quality shown by 27 real-time water monitoring units out of the 36 units located along Ganga, suitable for 'bathing' and 'propagation of wildlife and fisheries' (Singhal & Matto, 2020). The upper stretch of Ganga showed the sharpest improvement. According to Uttarakhand Pollution Control Board, after more than 30 years the water of Har-ki-Pauri in Haridwar stunningly became 'fit for drinking' for the first time (Katariya, 2020). The sharp improvement in water quality at Haridwar and Rishikesh was due to a sudden and huge drop in the number of devotees and tourists along with a 500% decrease in sewage and industrial toxicants (Singhal & Matto, 2020). The overall water quality was also improved between Haridwar and Kanpur. A remarkable improvement was noticed during the lockdown phase across the entire stretch of Ganga, especially the up stretch of Kanpur (Dutta *et al.*, 2020). River Yamuna, the largest arm of Ganga, also appeared more transparent, blue, and natural after many years during the lockdown. The toxic foam floated on the river surface, originated due to a mix of detergents, chemicals from industrial effluents and sewage has almost totally wiped out in southeast Delhi's Kalindi Kunj (Lokhandwala & Gautam, 2020). The water quality data collected from Palla, Nizamuddin Bridge and Okhla upstream, Najafgarh and Shahdara Drain of Yamuna River comparison during lockdown period, April 2020 when compared with the same of April 2019, clearly showed that there is a significant reduction in the value of pH, BOD and COD by 1-10 %, 30-70%, 10-70% respectively due to low pollution as a result of complete lockdown. Yamuna Pollution Monitoring Committee Report, 2020). According to the Karnataka State Pollution Control board, River Kavery and its tributaries such as Hemabati, Kabini, Shimsa also rejuvenated due to less pollution (The Hindu, 2020b).

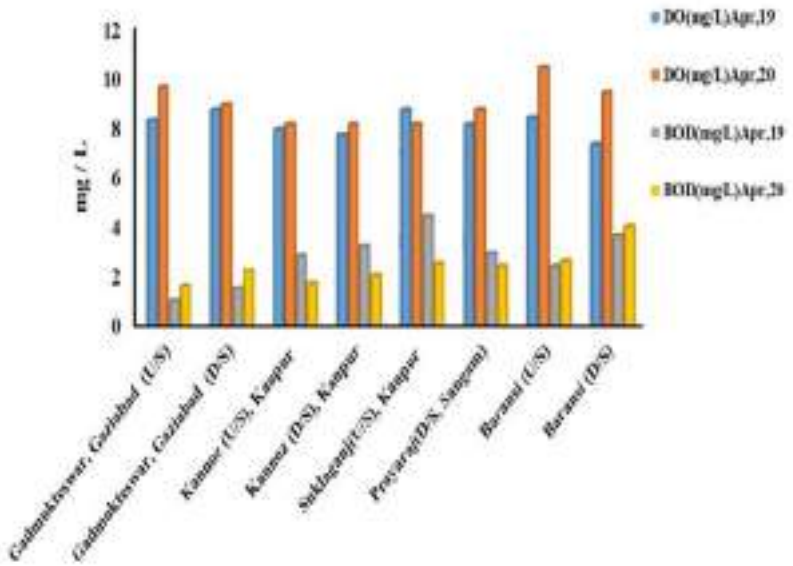

Figure 3. Impact of COVID-19 lockdown on water quality of Ganga in UP stretch [Data Source- UP Pollution Control Board (uppcb.com)]

COVID-19: effect on wild life and biodiversity

Global lockdown in the last year due to the appearance of the COVID-19 pandemic and restricted human interaction gives the wild animals and birds a free space that has never been seen before. During the complete lockdown period last year, many animals such as deers, elephants, monkeys, turtles, dolphins, and several kinds of birds were spotted very frequently. Animal behavior such as spotting of coyotes (that normally timid of traffic) on the Golden Gate Bridge in San Francisco, USA, deers are munching in Washington homes, a few miles away from the White House, wild boars are becoming bolder in Barcelona and Bergamo, Italy, peacocks have strutted through Bangor and goats through Llandudno and sheep in Wales (Loring, 2020). In North America, Killer whales have been spotted in the parts of Vancouver for the first time in decades due to less human interference (CSR News, 2020). Confining humans in their home, indicate the use of human zone by wild animals.

In India, the scenario is also stunning and promising for wildlife and biodiversity. A few days after implementing lockdown by Govt. of India at the end of March 2020, several wild animals were seen in urban areas, some of which are spotted after a long time. Asian antelopes, deers, Civet cats, peacocks; one-horned rhinos, and dolphins were spotted across the different cities of India. Peacocks were dancing in the streets of Mumbai, deer found in the locality **(Figure 4)**, similarly in Kozhikode, Kerala, an Indian civet cat was spotted on the road, while a Nilgai was spotted in Noida Sector-18, Delhi, walking leisurely on the road. In Chandigarh, a sambar deer was captured while crossing a road in the city (Economic times, 2020).

The aquatic life was also been thriving due to less water pollution. Several species of fishes were observed in Kolkata ghats after 30 years (Katariya, 2020). The lockdown period coincides with the annual nesting activity of the olive ridley turtle, in different coastal regions of India such as Odisha and Maharastra, came as a blessing for this endangered animal and nearly 2 crore Olive Ridley hatchlings have emerged and successfully made their way to sea (News18, 2020a). In National Chambal Sanctuary, Agra, 3170 Gharial offspring took birth in the last hatching season, June, 2020 whereas in 2019 and 2018 the number of offspring took birth was 2919 and 2800, respectively. According to Govt. officials, less human interference due to COVID-19 lockdown results in the high natality rate of Gharials in the last hatching season (Times of India, 2020c). Large numbers of migratory birds are returning to lakes and different water bodies and migrate freely due to less human interference (Arora *et al.*, 2020). Many bird species, which migrate from other parts of the country – known as partial migratory birds – have been extended their stay at the Therthangal and Melaselvanoor-Keelaselvanoor bird sanctuaries, Tamilnadu (The Hindu, 2020c). Reduced noise pollution makes the bird's mating call more audible to their mates than ever before, they also flap their wings and perform the mating dance (The Hindu, 2020d). In Kolkata, one of the busiest city of India, peoples spotted, saw, and heard the calls of different kinds of birds, such as Yellow-footed green pigeon, Purple sunbird, Coppersmith barbet, and several others, may be for the first time in their locality (Basu, 2020). Brahmakamal (*saussurea obvallata),* a rare flower and also the state flower of Uttarakhand, India. Generally, it blooms during mid-monsoon (July-August) in high altitude (3500-4800 meters) but the flower was found to bloom in the comparatively low altitude, Garhwal of Chamoli district, Uttarakhand, India, till October 2020 due to low pollution and tourist activity as a result of COVID-19 lockdown (Times of India, 2020d).

Figure 4. A peacock is seen on the road at Juhu, Mumbai, during the nationwide lockdown in India; A deer crashed through the roof of a house in Mumbai [Image Source-News 18, 2020b]

Among all these positivity for wildlife of India, a report regarding Indian wildlife amid the COVID-19 crisis indicates a hike in poaching of wild animals during the lockdown all around the country. Various cases of poaching have been reported from national parks, wildlife sanctuaries, bird sanctuaries, and others. Mainly 35 different wild animal species were targeted, of which 15 are listed in schedule I of the Wildlife Protection Act, 1972 of India. During the lockdown 88 poaching cases were reported by the media, which was significantly higher than the reported cases of poaching in pre lockdown time (TRAFFIC Report, India June 2020). However, the overall picture regarding nature and wildlife activity during this crisis period, clearly indicates that Nature presses the RE-SET button for rejuvenating itself, after experiencing that so-called nature's best creation (Human) doing nothing for it. So, we should learn from this experience and need to adapt the ways to live our lives in this post covid era so that we can use nature and its resources without harming it.

CONCLUSION

COVID-19, the largest global pandemic causing deadly threats to human life and its long-lasting, large-scale impact on human lifestyle and society may be a matter of research and arguing for the next decades. But despite several negative consequences of this pandemic, the environment healed itself during the lockdown period. All the major polluting industries were closed; vehicles are hard to be found on the road, which led to less carbon and GHG emission along with pure water in the river. Due to less pollution and a calm environment, animals were also enjoying the positive impacts of lockdown. All these positive environmental impacts may be temporary but from this situation, human beings should learn to know their limits of dominancy over nature before it is too late.

ACKNOWLEDGMENTS: I am grateful to Prof. Kousik Pramanick (Integrative Biology Research Unit, Dept. of Life Sciences, Presidency University, West Bengal, India) and Dr. Abhishek Guha (University of Alabama, Birmingham, USA) for their valuable suggestions.

CONFLICT OF INTEREST: None

FINANCIAL SUPPORT: None

ETHICS STATEMENT: None

REFERENCES

Arora, S., Bhaukhandi, K. D., & Mishra, P. K. (2020). Coronavirus lockdown helped the environment to bounce back. *Science of the Total Environment*, 29, 140573.

Banerjee, D., Chakraborty, S. K., Bhattacharyya, S., & Gangopadhyay, A. (2008). Evaluation and analysis of road traffic noise in Asansol: an industrial town of eastern India. *International Journal of Environmental Research and Public Health*, *5*(3), 165-171.

Basu, J. (2020). COVID-19: Sounds of Birds Replace Noise Pollution in Kolkata. (downtoearth.org.in)

Bouey, J. (2020, March). From SARS to 2019-Coronavirus (nCoV): US-China Collaborations on Pandemic Response: Addendum: Testimony of Jennifer Bouey, Before the US House Committee on Foreign Affairs, Subcommittee on Asia, the Pacific, and Nonproliferation, March 5, 2020. In *RAND Corporation*. RAND Corporation.

CDC, (2020). Symptoms of COVID-19 | CDC

Chakrapani, G. J., & Subramanian, V. (1996). Fractionation of heavy metals and phosphorus in suspended sediments of the Yamuna river, India. *Environmental Monitoring and Assessment*, *43*(2), 117-124.

Chauhan, A., & Singh, R. P. (2020). Decline in PM2. 5 concentrations over major cities around the world associated with COVID-19. *Environmental Research*, *187*, 109634.

Chen, Y., Liu, Q., & Guo, D. (2020). Emerging coronaviruses: genome structure, replication, and pathogenesis. *Journal of Medical Virology*, *92*(4), 418-423.

Cohen, A. J., Brauer, M., Burnett, R., Anderson, H. R., Frostad, J., Estep, K., Balakrishnan, K., Brunekreef, B., Dandona, L., Dandona, R., et al. (2017). Estimates and 25-year trends of the global burden of disease attributable to ambient air

pollution: an analysis of data from the Global Burden of Diseases Study 2015. *The Lancet, 389*(10082), 1907-1918.

Cortegiani, A., Ingoglia, G., Ippolito, M., Giarratano, A., & Einav, S. (2020). A systematic review on the efficacy and safety of chloroquine for the treatment of COVID-19. *Journal of Critical Care*, *57*, 279-283.

CSR News, (2020). Earth Day 2020 - Nature Heals During COVID-19 Lockdown - The CSR Journal.

Deoli, B. K., Bartarya, S. K., & Siddiqui, N. A. (2017). Assessment of surface and ground water Quality of Haridwar district of Uttarakhand. *International Journal of Chemtech Research*, *10*, 95-118.

Dudeja, D., Bartarya, S. K., & Biyani, A. K. (2011). Hydrochemical and water quality assessment of groundwater in Doon Valley of Outer Himalaya, Uttarakhand, India. *Environmental Monitoring and Assessment*, *181*(1), 183-204.

Dutta, V., Dubey, D., & Kumar, S. (2020). Cleaning the River Ganga: Impact of lockdown on water quality and future implications on river rejuvenation strategies. *Science of the Total Environment*, *743*, 140756.

Earthsky, (2020). Satellite images: Air pollution in India plummets | Earth | EarthSky

Economic Times, (2020). Retrieved from. Coronavirus lockdown: unusual sightings of animals in India - Nilgai in Noida | The Economic Times (indiatimes.com)

European Union, (2015). 47si.pdf (europa.eu)

GBD 2017 Risk Factor Collaborators. (2018). Global, regional, and national comparative risk assessment of 84 behavioural, environmental and occupational, and metabolic risks or clusters of risks for 195 countries and territories, 1990–2017: a systematic analysis for the Global Burden of Disease Study 2017. *Lancet (London, England)*, *392*(10159), 1923.

Global Climate Report, (2019). Retrieved from. https://www.ncdc.noaa.gov/sotc/global/201913

Gorbalenya, A. E., Baker, S. C., Baric, R., Groot, R. J. D., Drosten, C., Gulyaeva, A. A., Haagmans, B. L., Lauber, C., Leontovich, A. M., Neuman, B. W., et al. (2020). Severe acute respiratory syndrome-related coronavirus: The species and its viruses–a statement of the Coronavirus Study Group.

He, L., Zhang, S., Hu, J., Li, Z., Zheng, X., Cao, Y., Xu, G., Yan, M., & Wu, Y. (2020a). On-road emission measurements of reactive nitrogen compounds from heavy-duty diesel trucks in China. *Environmental Pollution*, *262*, 114280.

He, M. Z., Kinney, P. L., Li, T., Chen, C., Sun, Q., Ban, J., Wang, J., Liu, S., Goldsmith, J., & Kioumourtzoglou, M. A. (2020b). Short-and intermediate-term exposure to NO2 and mortality: a multi-county analysis in China. *Environmental Pollution*, *261*, 114165.

Hindustan Times, (2020a). Retrieved from. Covid-19: Only 4 trains operate as Railways comes to standstill amid lockdown | Latest News India - Hindustan Times.

Hindustan times, (2020b). Covid-19 lockdown: Pollution in Ganga declines as factories in UP, Uttarakhand remain shut | Latest News India - Hindustan Times.

India Times, (2020). Earth Finally Fixed Largest Ozone Layer Hole Above Arctic, Healing 1 million Square Km (indiatimes.com)

India Today, (2020). Kerala reports first confirmed coronavirus case in India - India News (indiatoday.in).

India Today, (2021). Delhi breathes easy as Covid-19 lockdown lowers pollution levels again - Cities News (indiatoday.in)

Indian Express, (2021). Covid-19 Second Wave: Here's a list of states that have imposed lockdowns (indianexpress.com)

Katariya, M. (2020). 10 Things That Have Happened for The First Time in Years During the Coronavirus Lockdown (scoopwhoop.com)

Kumar, P., Hama, S., Omidvarborna, H., Sharma, A., Sahani, J., Abhijith, K. V., Debele, S. E., Zavala-Reyes, J. C., Barwise, Y. & Tiwari, A. (2020). Temporary reduction in fine particulate matter due to 'anthropogenic emissions switch-off'during COVID-19 lockdown in Indian cities. *Sustainable Cities and Society*, *62*, 102382.

Lal, P., Kumar, A., Kumar, S., Kumari, S., Saikia, P., Dayanandan, A., Adhikari, D., & Khan, M. L. (2020). The dark cloud with a silver lining: Assessing the impact of the SARS COVID-19 pandemic on the global environment. *Science of the Total Environment*, *732*, 139297.

Le Quéré, C., Jackson, R. B., Jones, M. W., Smith, A. J., Abernethy, S., Andrew, R. M., De-Gol, A. J., Willis, D. R., Shan, Y., Canadell, J. G., et al. (2020). Temporary reduction in daily global CO 2 emissions during the COVID-19 forced confinement. *Nature Climate Change*, *10*(7), 647-653.

Lokhandwala, S., & Gautam, P. (2020). Indirect impact of COVID-19 on environment: A brief study in Indian context. *Environmental Research*, *188*, 109807.

Loring, K. (2020). In San Francisco, coyotes are your wildest neighbors | KALW

Magomedova, U. G., Khadartseva, Z. A., Grechko, V. V., Polivanova, M. N., Mishvelov, A. E., Povetkin, S. N., Demchenkov, E. L., & Shevchenko, Y. S., (2020). The Role of Covid-19 in the Acute Respiratory Pathology Formation in Children. *Pharmacophore*, *11*(5), 61-65.

Muhammad, S., Long, X., & Salman, M. (2020). COVID-19 pandemic and environmental pollution: A blessing in disguise?. *Science of the Total Environment*, *728*, 138820.

Myllavirta, L., & Dahiya, S. (2020). Analysis: India's CO2 emissions fall for first time in four decades amid coronavirus. Carbon Brief. Retrieved from. Analysis: India's CO2 emissions fall for first time in four decades amid coronavirus (carbonbrief.org)

Navinya, C., Patidar, G., & Phuleria, H. C. (2020). Examining effects of the COVID-19 national lockdown on ambient air quality across urban India. *Aerosol and Air Quality Research*, *20*(8), 1759-1771.

NDTV, (2020). World Environment Day 2020: This Is How The Environment Is Healing During The COVID-19 Lockdown | World Environment Day 2020 (ndtv.com)

NEWS 18, (2020a). Watch: Hundreds of Baby Olive Ridley Turtles Make Their Way to Sea in Odisha amid Lockdown (news18.com)

NEWS 18, (2020b). Wild Animals Are Strolling Public Places During Coronavirus Lockdown (news18.com)

Öhrström, E. (1989). Sleep disturbance, psycho-social and medical symptoms—a pilot survey among persons exposed to high levels of road traffic noise. *Journal of Sound and Vibration*, *133*(1), 117-128.

Paital, B. (2020). Nurture to nature via COVID-19, a self-regenerating environmental strategy of environment in global context. *Science of the Total Environment*, 139088.

Pyrc, K., Berkhout, B., & Van Der Hoek, L. (2007). Identification of new human coronaviruses. *Expert Review of Anti-Infective Therapy*, *5*(2), 245-253.

Rabinowitz, P. (2000). Noise-induced hearing loss. *American Family Physician*, *61*(9), 2749-2756.

Ramadan, N., & Shaib, H. (2019). Middle East respiratory syndrome coronavirus (MERS-CoV): A review. *Germs*, *9*(1), 35.

Rivas, D. V., Pino, M. M., Rivas, S. V., Bazan, E. D., Pérez, Y. P., Campaña, Z. G., Vasquez, M. G., Carrera, C. O., Calderón, L. R., Carranza, J. P., et al. (2020). Information Generation Rate and its Relationship with the Entropy of Non-Linear Models: Covid-19 Case, Peru 2020. *Journal of Biochemical Technology*, *11*(4), 8-14.

Rodríguez-Urrego, D., & Rodríguez-Urrego, L. (2020). Air quality during the COVID-19: PM2. 5 analysis in the 50 most polluted capital cities in the world. *Environmental Pollution*, 115042.

Scientific American, (2020). Why CO2 Isn't Falling More during a Global Lockdown - Scientific American

Sharma, S., Zhang, M., Gao, J., Zhang, H., & Kota, S. H. (2020). Effect of restricted emissions during COVID-19 on air quality in India. *Science of the Total Environment*, *728*, 138878.

Singhal, S., & Matto, M. (2020). COVID-19 lockdown: a ventilator for rivers. *Down to Earth*.

Somani, M., Srivastava, A. N., Gummadivalli, S. K., & Sharma, A. (2020). Indirect implications of COVID-19 towards sustainable environment: an investigation in Indian context. *Bioresource Technology Reports*, *11*, 100491.

Stansfeld, S., Gallacher, J., Babisch, W., & Shipley, M. (1996). Road traffic noise and psychiatric disorder: prospective findings from the Caerphilly Study. *BMJ*, *313*(7052), 266-267.

The Gurdian, (2020). Climate crisis: in coronavirus lockdown, nature bounces back – but for how long? | Greenhouse gas emissions | The Guardian.

The Hindu, (2020a). Janata Curfew | updates - The Hindu.

The Hindu, (2020b). Cauvery, tributaries look cleaner as pandemic keeps pollution away - The Hindu.

The Hindu, (2020c). Pandemic-induced lockdown gives migratory birds and animals a reason to cheer - The Hindu.

The Hindu, (2020d). How birds' mating calls have become more audible thanks to lower noise pollution - The Hindu.

Times of India, (2020a). Lockdown curbs rejuvenate Ganga in UP 's industrial hub | Kanpur News - Times of India (indiatimes.com)

Times of India, (2020b). How lockdown has been a gift for river Ganga - Times of India (indiatimes.com)

Times of India, (2020c). Over 3,000 critically endangered gharials born in Chambal | Agra News - Times of India (indiatimes.com)

Times of India, (2020d). Brahma kamal: Brahmakamal's October bloom stumps experts | India News - Times of India (indiatimes.com)

TRAFFIC, (2020). Wildlife-amidst-COVID-19-India.pdf (traffic.org)

UPPCB, (2020). UP Pollution Control Board, Lucknow (uppcb.com)

WHO, (2005). United Nations road safety collaboration: a handbook of partner profiles.

WHO, (2016). Water, sanitation, hygiene, and waste management for SARS-CoV-2, the virus that causes COVID-19 (who.int)

WHO, (2020a). Retrieved June 14, 2021 from Coronavirus disease (COVID-19) (who.int)

WHO, (2020b). Transmission of SARS-CoV-2: implications for infection prevention precautions (who.int)

WHO, (2020c). COVID-19 vaccine tracker and landscape (who.int)

WHO, (2020d). WHO Director-General's opening remarks at the media briefing on COVID-19 - 11 March 2020

WHO, (2021). Status_COVID_VAX_18May2021.pdf (who.int)

Wikipedia, (2020a). COVID-19 lockdowns - Wikipedia

Wikipedia, (2020b). COVID-19 lockdown in India - Wikipedia

Worldometer, (2020). Retrieved June 14, 2021 from https://www.worldometers.info/coronavirus/country/india/

Yamuna Pollution Monitoring Committee Report 2020. yamuna-revival.nic.in

Zambrano-Monserrate, M. A., Ruano, M. A., & Sanchez-Alcalde, L. (2020). Indirect effects of COVID-19 on the environment. *Science of the Total Environment*, *728*, 138813.

Zhong, N. S., Zheng, B. J., Li, Y. M., Poon, L. L. M., Xie, Z. H., Chan, K. H., Li, P. H., Tan, S. Y., Chang, Q., Xie, J. P., et al. (2003). Epidemiology and cause of severe acute respiratory syndrome (SARS) in Guangdong, People's Republic of China, in February, 2003. *The Lancet*, *362*(9393), 1353-1358.

International Journal of Experimental Research and Review (IJERR)

ISSN: 2455-4855 (Online) ***Review Article***
Received: 10th July, 2021; **Accepted:** 15th August, 2021; **Published:** 30th August, 2021
DOI: https://doi.org/10.52756/ijerr.2021.v25.009

The genetic aspect of musicality, perfect pitch and congenital Amusia

Amlan Mandal and Susanta Roy Karmakar*
Post Graduate Department of Zoology, Maulana Azad College, Kolkata-700013, West Bengal, India

***Corresponding Author:** subidar71@gmail.com

Abstract

As one of the most important aspects of art, music is also a part of human biology and has had a significant influence on human evolution and development. In addition, it is an essential component of cultural heritage. Both hereditary and environmental variables are thought to play a role in developing and manifesting musical talent. Although environmental variables affecting musical ability have been extensively studied, genetic influences are less well understood. The genetic influence was strongly supported in studies of a random population, twins, and families of talented musicians. Linkage analysis, variation in gene copy number, and scanning for whole-genome expression were among the modern biomolecular methods used to discover genes or chromosomal areas linked to musical ability. Singing and music perception have been linked to many loci on chromosome 4, while absolute pitch and music perception have been linked to specific loci on chromosome 8q. Music perception, memory, and listening have all been linked to the AVPR1A gene on chromosome 12q, while SLC6A4 on chromosome 17q has been linked to music memory and choir involvement.

Keywords: Amusia, music genetics, music perception, music production.

Introduction

Music is a universal language. The ability to perceive, create and reproduce music is recognized as a ubiquitous communication process that involves rhythm, pitch and timbre. However, music competency is diverse across individuals and that adds a driving force to the long-standing debate of whether musical reception and performance are of genetic or environmental background or both.

Compared to more comprehensive research done in the language domain, few studies have focused on the genetic foundation of musical skills (Newbury and Monaco, 2010; Carrion-Castillo et al., 2013). Furthermore, prior behavioural genetic studies of musical aptitude often lacked scientific accuracy or sample numbers (Coon and Carey, 1989). The advent of genetic research in the post-

genomic age offers much potential for this area, which is yet largely unexplored (Tan et al., 2014). Except for a few advances, such as individual variations in musicality explained by genetic background, the present level of knowledge of the genetic foundation of music talent has not been examined much since the development of molecular genetic research (Stewart, 2008; Peretz, 2016; Gingras et al., 2015). It was discovered via the showing of microRNA fraction overexpression in peripheral blood as soon as two hours after a classical music performance. has-miR-3909, has-miR-30d-5p, has-miR-92a-3p, has-miR-222-3p, and has-miR-30a-5p are the five microRNAs that were shown to be significant (Nair et al., 2019). Genes influencing auditory and creative involvement in music have recently been identified using genome-wide linkage and association scanning. The primary instruments for detecting gene copy number changes and estimating gene expression are now gene copy number changes and gene expression estimates, and the findings of this research will be given later on (Szyfter et al., 2020).

The goal of this review is to describe findings of the genetic background of musical ability, as well as new and previously established molecular techniques, to help music and genetic researchers gain a better understanding of this relatively new field, and to encourage increased research effort into uncovering the genetic basis of musical ability.

Inheritance of musical talent in renowned artists' families

The well-known truth is that musical talent runs in families. The family of Johann Sebastian Bach (1685–1750), one of the greatest musical geniuses of all time, is one of the most remarkable instances in music history. There has been a characteristic of hereditary musical talents for over 200 years, spanning six generations of artists. Out of 35 musicians, Johann Sebastian and at least six of his close relatives have left an indelible mark on the history of music: in the generation before Johan Sebastian, the flautist Johann Ambrosius and organist Johann Christoph, and two generations later, four sons, all outstanding composers—Wilhelm Friedemann, Carl Philip Emanuel, Johann Christian Friedr (Wolff, 1983). In reality, the Bach family only received training in the profession of musician, which was handed down from father to son and therefore provided a source of income. However, its difficult to explain the existence of seven famous musicians in one family, across generations, one of whom is an acknowledged genius, and at least two more who are extremely well-known, as the result of family practice alone (Szyfter et al., 2020).

Human genetic method

Various genetic analytical techniques may be used to examine the connection between genes and phenotypes. This section gives an overview of the behavioural and molecular genetic methods frequently utilized in human genetic research.

Behavioural genetic approaches

Familial aggregation

Family aggregation is the clustering of a few traits, behaviors, or syndromes in a given family. Family aggregation may arise thanks to genetic or environmental similarities. This issue may be addressed via familial aggregation, which compares

whether the prevalence of a characteristic is higher in a proband's family than in the general population (Naj et al., 2012). Families and controls are only asked to provide phenotypic evidence. The sibling recurrence-risk ratio (s), which estimates the percentage of proband siblings who also show the investigated feature compared to the population prevalence, is a typical metric resulting from familial aggregation. The size and shape of family associations discovered in domestic aggregation research may provide valuable information about genes and the environment's roles (Naj et al., 2012). A score as low as 1 indicates that genetic effects are negligible, while a value greater than 5 suggests that a genetic theory is worth investigating (Mitry et al., 2011).

The phrase musical aptitude was coined to describe the capacity to approximate rhythm, timbre, tone length, pitch, and music assembly to make the findings on musicality measurable and quantitative. Karma music test (KMT) is a measuring instrument that uses small abstract sound patterns that are repeated to create hierarchic structures (Karma, 1994). The Gaussian distribution of musical aptitude was discovered in the population, which corresponds to conclusions made from observations of brilliant musicians' families.

Ascertainment bias may exaggerate family aggregation measures, which are solely used to assess the presence of familial grouping (Guo, 1998). It does not say how much of the family grouping is caused by genetic or environmental factors. Follow-up research, such as twin and adoption studies, may provide answers to such questions.

Twin studies

Tests on identical or fraternal twins are known as twin studies. The goal is to highlight the significance of environmental and genetic influences on characteristics, phenotypes, and diseases. In behavioural genetics, twin research is regarded as a critical tool. Twin studies aid separates the relative importance of genetic and environmental variables in trait variation (Verweij et al., 2012). Identical or monozygotic (MZ) twins share almost all of their DNA, while fraternal or dizygotic (DZ) twins share just approximately half of their genes, just like any other sibling. As a result, if concordance for a trait is much more significant in the MZ twins, the trait is likely to be heritable.

Twin studies may be used to assess the effects of genetic influence, unique and shared environment on a characteristic using structural equation modelling and statistical tools like Mx (Neale et al., 2006).

Twin studies backed up the importance of genetic variables in the development of personal musicality (Oikkonen and Järvelä, 2014). The participants, who were monozygotic and dizygotic twin pairs of Caucasian ancestry, were instructed to distinguish between right and wrong sounds in well-known tunes (Drayna et al., 2001). The research was conducted using a distorted tunes test based on note identification, a famous melody with an erroneous pitch. Heritability was evaluated for 71% of the data (all data) and 80% once a specific limit value was presented. The scientists concluded that differences in musical pitch identification are primarily due to highly heritable differences in auditory processes. Separate research of Dutch twin pairs looked at music, arts, language, mathematics, chess, and sports

skills. It was shown that shared surroundings had a negligible impact on musical aptitude and talent abilities and that genetic factors play a significant role in musical diversity (Vinkhuyzen et al., 2009).

Family pedigree analysis

Family pedigrees may also be used to estimate heritability. The ratio of additive genetic variation to a total phenotypic variable variance is known as heritability in the narrow sense (h^2). Heritability estimate is a valuable prelude to molecular genetic research since the magnitude of h^2 may suggest the statistical power for finding the causative genes of a characteristic (Bochud, 2012). When several related characteristics' h^2 estimations are available, the trait with the best h^2 estimate may be selected for gene mapping. In human research, h^2 analyses below 0.2 are regarded low, those between 0.2 and 0.5 are considered moderate, and those over 0.5 are called high heritability (Tan et al., 2014). High h^2 values indicate that the genotype is tightly linked to the trait phenotype, but this does not mean that every gene linked to the trait significantly impacts the phenotype (Visscher et al., 2008).

Analysis of segregation

Segregation analysis is used to determine whether familial data for a specific disorder or other traits are compatible with particular inheritance methods. Modes of inheritance tried in segregation analyses contain Mendelian, digenic or polygenic models. The family data are fitted with several segregation models reflecting various attribute heritage patterns. Using maximum probability methods, the best suited genetic model is identifiable (i.e., the pattern of inheritance that best describes how the characteristic is passed down the family line). The segregation ratio is an essential measurement of the percentage of offspring that inherits that specific characteristic from a parent (Strachan and Read, 1999). For autosomal recessive and autosomal dominant inheritance, the expected segregation ratio is 0.5 and 0.25 correspondingly. These proportions are for Mendelian characteristics; a difference between these numbers shows that the trait may potentially have partial penetration, may be predisposed to various genes, or both environmental and genetic variables influence the quality. For example, in research, the absolute pitch had a segregation ratio of 0.089 (Theusch and Gitschier, 2011). This implies that the feature was not taken from the Mendelian pattern. The separation analysis often acts as a precursor to parametric connection analysis, which requires specifying the heritage pattern of the stated characteristic (Schnell and Sun, 2012).

Genetic-molecular methods

Analysis of linkages

Linkage analysis is a genetic technique that identifies chromosomal segments which co-segregate through families with the disease phenotype and is an analytical tool used to detect most lipodystrophic genes. Analysis of the link may be parametric or non-parametric.

Linkage analysis involves using single-nucleotide polymorphism (SNP) arrays for every family member of a big family or multiple family pedigrees. If it is thought that a genetic locus predisposes a characteristic, members with the same

markers should have a higher similarity to those who do not share the markers. The linkage analysis is thus intended to identify features in the SNP array which are frequently prevalent within and across pedigrees with interest (Tan et al., 2014). The non-parametric or model-free linking checks if relative characteristics share more alone than was mistakenly anticipated (Xu et al., 2012). Parametric (model-based) link analysis requires the inheritance mode specification provided by segregation analysis. Linkage is then evaluated by comparing the likelihood that the test data is obtained if a marker locus & trait locus are associated with the probability of the test data obtained if the 2 loci are not connected (Schnell and Sun, 2012). Computerized LOD analysis is an easy method to analyse complicated family pedigrees to determine the connection between Mendelian characteristics (or between a trait and a marker, or two markers). The LOD score (logarithm (base 10) of the odds) established by Newton Morton is a statistical measure often used in human, animal and plant linking. The LOD data compares the probability of obtaining the test data if the 2 loci are connected to the potential of simply by chance seeing the same data. Positive LOD values support the existence of a connection, whereas low LOD ratings suggest that the connection is not so probable. A LOD score for every three is generally seen as an essential indication of the connection, since it shows that the chances of the two loci being connected and legacy together exceed 1000–1. Alternatively, substantial evidence to deny the connection is taken into consideration as a LOD score −2. Generally, results within the range of $-2 < x < 3$ are considered to be nonconclusive evidence for connection with results between $2 < x < 3$, justifying further research (Tan et al., 2014).

Analysis of Association

Relationship analysis is a statistical technique used for determining the association between a genetic variation and a characteristic (Carey, 2003b). An association study may either use a population-based approach or a family-based design in which relatives control cases. Statistical analyses are conducted to evaluate whether a specific allele in the candidate gene approach has a greater frequency.

In this method, only specific allele variants are studied, which is a major drawback of the candidate gene approach. If multiple genes are involved or the trait under study is complex, this approach is unsuitable. This method relies heavily on the researcher's "educated guess".

Instead, genome-wide association study (GWAS) can be applied even without prior knowledge of potential candidate genes. It involves an agnostic search of the entire human genome, generally using SNP arrays with many common markers (Sun and Dimitromanolakis, 2012).

Exome sequencing

Exome sequencing is a genetic method for the sequencing of a genome's entire protein coding region. The first stage is only to choose the DNA subset that encodes proteins known as exons. It comprises two phases. The second stage involves sequencing exonic DNA with any high-performance DNA sequence technique.

Exome accounts for about 1.5% of the whole genome. Thus, exome sequencing,

like GWAS, may be carried out without previous knowledge of possible applicant genes or genetic variations. In addition, it can detect unusual causative variants with unique metabolic characteristics, which cannot be found by linking studies because of insufficient research power (Singleton, 2011).

CNV analysis

Copy number variations (CNVs) are genomic alterations that lead to abnormal copies of 1 or more genes. Structural genomic rearrangements like duplications, deletions, translocations, and inversions can cause CNVs. Microarray-based CNV analysis techniques generally use SNP arrays or aCGH (array comparative genomic hybridization) platforms to detect gains or losses of copy numbers within the test sample compared with a reference sample (Alkan et al., 2011).

Music perception abilities

Absolute pitch ability

Absolute pitch, often known as the perfect pitch, is unique music for identifying or producing pits without external reference. The prevalence estimated is less than 1 in 10,000 (Bachem, 1955; Profita and Bidder, 1988). In 1500, this estimate was updated to 1 (Gingras et al., 2015)

Various scholars via family studies have investigated the genetic basis of absolute pitch. Profita and Bidder (1988) performed one of the first segregation investigations with 35 AP probes in 19 families and found substantial family occurrence. In females of this sample, the absolute pitch was more frequent and vertical transmission was found. The segregation ratio was estimated to be between 0,24 and 0,37 and indicates an incomplete autosomal dominant gene. However, since no control participant was recruited, they were unable to establish any recurrence risk ratios.

A further family aggregation research generated an estimated sibling recurrence risk ratio of 20, which indicates that siblings with absolute pitch have an estimated 20 times higher probability of having final pitch than the general population (Gregersen and Kumar, 1996). Gregersen's team subsequently performed two more family aggregation studies which generated an estimated 8.3 and 12.2 relative sibling risk (sib RR) correspondingly (Gregersen et al., 1999 & 2001). Thus, Sib RR offers a more cautious approach than μs (Naj et al., 2012).

Gregersen's team also compared the occurrence of AP in Asian (n=36) and non-Asian (n=50) conservatory students and calculated it as 49.3% and 18.1%, respectively. This finding was reflected later in subsequent studies by Deutsch et al. 2006, Hove et al. 2010, Miyazaki et al. 2012. It was hypothesized that the differences in absolute pitch could be connected with speech development because of deep tonality in East-Asian languages (Deutsch et al., 2006). This impact on AP performance was also discussed in the study on 37 AP possessors of mixed ethnicity (Van Hedger and Nusbaum, 2019).

Studies on large samples of musicians presented that almost all displaying Absolute Pitch started their musical education by 7. It was also recommended that it is somewhat unlikely that an individual can develop Absolute Pitch if musical training has been created after the age of 11 (Sergeant, 1969). However, this view does not hold precisely in the face of

the most current information since Van Hedger et al., (2019) showed that Adults could learn absolute Pitch and the learned Absolute Pitch is indistinguishable from an inborn ability. In view of this, Baharloo et al., (1998) controlled for early music training by only examining families where the contributors & one or more of their siblings had received music training before 6 years of age. The λs was estimated to be approximately 7.5 (Gregersen, 1998). In a subsequent study, Baharloo and colleagues estimated λs for the most severe form of AP, termed "AP-1" (Baharloo et al., 2000). The AP-1 phenotype was defined by a reliably high level of pitch naming ability, falling at least three standard errors above the mean score of a randomized cluster of AP and non-AP musicians. Also controlling for early music training, the λs for AP-1 was estimated to fall within 7.8–15.1, with a greater likelihood of the true value being found near the upper end of this range. However, it is possible that even after controlling for early music training, the estimated λs may still be influenced by other shared environmental factors experienced by the AP-1 probands and their concordant siblings. The authors hence noted that the λs approximation might not wholly reflect genetic factors. Nonetheless, the high estimates of λs from various familial aggregation studies suggest a significant role for genetic influences on the development of AP and the possibility of a major-gene effect (Tan et al., 2014).

Morphometric brain structure investigations have discovered another factor that may influence AP development. AP musicians have left-hand asymmetry of a portion of the temporal lobe known as planum timescale (PT), an area traditionally linked to language and auditory processing.

Non-parametric multi-point linking analysis indicated the potential linking of the European/Ashkenazi Jewish/Indian Combined Dataset with chromosomes 8q24.21 (LOD = 2.330) and 8q21.11 (LOD = 2.069) (Table 1). One of the four genes identified in the neighbourhood of the linkage peak of 8q24.21 was ADCY8 (Adenylate cyclase 8), expressed nearly exclusively in the brain (Wong et al., 1999; Ludwig and Seuwen, 2002; De Quervain and Papassotiropoulos, 2006). Other peaks were observed in European families at loci 8q21.11 (LOD = 2.236), 7q22.3 (LOD = 2.074) and 9p21.3 (LOD = 2.048). Linkage area on 7q22.3 was also seen in a sub-set of 19 East Asian AP families, with a smaller connection point (LOD between 1 and 1.5).

AP segregation study was conducted in monozygous twins (78.6%), dizygous twins (45.2%) and their families by Theusch and Gitschier (2011). He also found that AP is likely to be genetically heterogeneous, not just mendelian inherited. Environmental, epigenetic, & stochastic variables probably contribute to the expression of Absolute Pitch.

Smith et al. investigated pitch discrimination in multiethnic ancestry people in 2017. The better presentation was linked to greater intelligence, East Asian background, male sex, younger age, and appropriate music instruction (especially before age 6). GWAS & gene-based analyses of collapse have examined a limited sample volume. While chromosomal areas (4q22, 4q23-4q26, chromosome 3) have previously demonstrated in connection with pitch perception, no significant correlations have been found.

Studies on huge samples of artists showed that nearly everyone with

Absolute Pitch began their musical instruction at seven. Furthermore, it was suggested that it is relatively improbable that someone would be able to acquire Absolute Pitch beyond the age of 11. (Sergeant, 1969). This concept does not exist in the face of the latest facts. Van Hedger et al., (2019) showed that certain adults can acquire absolute pitch, and that the taught final pitch is distinct from the innate ability.

Congenital Amusia

Congenital amus or tone deafness, despite its normal cognition, language and hearing skills, is a fine-grained perceptual impairment defined by an inability to identify incorrect notes in melodies (Peretz and Hyde, 2003). Congenital amus has an estimated frequency of 4% of the population (Kalmus and Fry, 1980). Although, however, a comprehensive investigation of the neurological foundation of congenital amusia was made (Peretz and Hyde, 2003; Hyde et al., 2007; Mandell et al., 2007; Loui et al., 2009; Mignault Goulet et al., 2012), there was little exploration of its genetic origin.

In the first congenital amusia family aggregation study, Peretz et al., (2007) conducted an online amusic diagnostic exam with 13 amusic probands and 17 controls, as well as 58 proband families (out of 9 prominent families) and 58 control family members (from 10 families). The findings have shown that 39% of first-degree relatives have congenitally amused, whereas only 3% of controls have been equally identified. Notably, the μs was 10.8 for amusia congenital, whereas the risk of recurrence of offspring was considerably lower at 2.3. While the high μs indicates a likely hereditary foundation for congenital amusa, Peretz et al., hypothesised that exposure to a musical environment created may reduce the risk of offspring of amusing evidence. However, Mignault Goulet et al. (2012) found that the music perception and electrophysiological measurements of seven amusing youngsters (ages 10–12) did not change basically after four weeks of daily listening to the music. This promotes that listening to everyday music is insufficient to enhance pitches' perception or stimulate brain plasticity in amusing progenies. Another study conducted in the same research group with a large cohort of Canadian participants found that 46% of first-degree proband family members had a prevalence of congenital amusia. Other associated problems such as dyslexia, speech dysfunction, memory problems or spatial placement problems have been identified in just a few amusing minorities. The scientists concluded that many interacting genes might affect congenital amus (Peretz & Vuvan, 2017). Deregulations of the aforementioned genes such as AVPR1A (12q), SLC6A4 (17q) and the loci identified on 8q and Chromosome 4 are suggested for the cause of the disease (Tan et al., 2014).

Gingras et al., (2015) focused on musical extremes such as congenital amusia and absolute pitch. The amusia genes FOXP2 (7q31.2) (Gingras et al., 2015) and locus 22q11 are particular genes (Gao et al., 2018). Previous gene mutations in humans produce serious speech and language impairments, such as developing verbal dyspraxia (Lai et al., 2001). In birds singing, his orthology is essential for song learning & the adult recital (Adam et al., 2016), and echolocation in bats (Li et al., 2007).

Table 1. Summary of molecular genetic studies investigating absolute pitch.

Study type	Participants	Ancestry	Locus implicated	Genetic variant(s) implicated	Gene implicated	Possible function(s) of the gene
Genome-wide linkage study (Theusch et al., 2009)	73 AP families	European, Ashkenazi Jewish, Indian, East Asian	8q24.21	SNP rs3057 LOD= 2.330 Eu/AJ/I LOD= 3.464 EU	ADCY8	Learning and memory
			7q22.3	SNP rs2028030 LOD = 2.074 Eu LOD~1–1.5 E Asian		
			8q21.11	SNP rs1007750 LOD = 2.069 Eu/AJ/I LOD = 2.236 for Eu		
			9p21.3	SNP rs2169325 LOD = 2.048 Eu		
Genome-wide linkage study: exome sequencing (Gregersen et al., 2013)	53 AP multiplex families	Caucasian, Asian	6q14.1-16.1		EPHA7	Neural connectivity and development
	36 synesthesia multiplex families		Peak LOD= 4.68			
		2q	SNP rs1482308 HLOD = 4.7 (combined data set) SNP rs6759330 HLOD = 3.93			

ADCY8: adenylate cyclase 8; AJ: Ashkenazi Jewish ancestry; E Asian: East Asian ancestry; EPHA7: ephrin type-A receptor 7; Eu: European ancestry; HLOD: heterogeneity logarithm of odds score; I: Indian ancestry; LOD: logarithm of odds score; SNP: single nucleotide polymorphism.

Source: Tan et al., 2014

Music perception

Studies of child musical behaviour have revealed that children may identify melodic or rhythmic changes in musical patterns and notice changes in pitch & rhythm (Trehub et al., 1984, 1987, 1999; Trainor and Trehub, 1992, 1993; Trainor and Heinmiller, 1998; Trainor et al., 2002, Trehub, 2006; Honing et al., 2009; Winkler et al., 2009). These findings and the omnipresent aspect of music across all civilizations (McDermott and Hauser, 2005) indicate that all people are endowed with an inherent form of musicality and that genetic components may be part of their expression.

Individual changes in ease of auditory ability indicate that auditory capacity is prone to change. Gaab et al. (2006) noted that fast learners engaged the supramarginal left gyrus and left Heschl's gyrus more often in the post-training period in conjunction with their slow learners (participants were designated as slow or fast learners in an auditory differentiation training task). Jäncke et al. (2001) revealed various short term functional activation patterns compared to those who had shown no progress in the frequency discrimination test. Zatorre et al. (2012) showed that individuals who had learned a micro-melody task faster had steeper fMRI BOLD responses, even before they trained on the task, to alter their auditive cortex. These findings indicate that inherent variations in brain function may affect the ability of the person to perceive music and develop musical talents.

Foster and Zatorre (2010) found that Heschl's sulcus & bilateral sulcus intraparietal performance with a relatively pitched test includes grey matter content and cortical thickness even after music instruction. These results are compatible with Relative Pitch processing genetic effects since substantial heritability (650–97%) for total brain volume and grey and white matter volumes have been repeatedly reported in behavioural genetics studies (Peper et al., 2007).

In one large twin study performed in 2001, 136 monozygotic twin pairs and 148 dizygotic twin pairs went through the Distorted Tunes Test (DTT), where they judged whether simple well-known melodies had incorrect pitches that could have rendered them “out-of-tune” (Drayna et al., 2001). Twin structural modeling revealed a very high heritability estimate of 71–80% with no effect of shared environment, thus indicating a substantial genetic component influencing melodic perception ability.

A study on 15 musical Finnish families investigated the genetic basis of music aptitude using: The Karma Music Test, and Seashore's pitch and rhythm discrimination tests (Pulli et al., 2008). The Seashore tasks use paired discrimination to measure pitch & rhythm perception (Radocy and Boyle, 2012), while the Karma Music Test evaluates the ability to distinguish patterns in sound sequences (Karma, 2007). Heritability estimates of 42, 57, 21, and 48% were obtained for the Karma Music Test, Seashore's pitch and rhythm discrimination tests, and the combined score on all three tests.

Genome-wide linkage analysis revealed proof of linkage on chromosome 4q22 (LOD = 3.33 near markers D4S423 and D4S2460) and linkage evidence on chromosome region 8q13-21 (LOD = 2.29) for the combined score. Interestingly, the linkage peak at 8q13-21 was close to the

linkage on chromosome 8q21.11 identified in the AP study by Theusch et al., (2009), pointing to a possible convergence of AP and general music perception abilities. UNC5C, netrin receptor, is the candidate gene at the tallest linkage peak of chromosome 4q22.

A follow-up candidate gene study involving 19 Finnish musical families found that the AVPR1A (arginine vasopressin 1a) haplotype RS1+RS3 on chromosome 12q has significant associations with performance on the Karma Music Test & the combined score on the Karma & Seashore music tasks (Ukkola et al., 2009). Analysis on the polymorphisms of other candidate genes such as SLC6A4, TPH1, & DRD2 produced weak and inconclusive results. Prior studies have revealed that arginine vasopressin (AVP) plays a key role in social cognition & behaviour (Ferguson et al., 2002; Bielsky et al., 2004; Depue and Morrone-Strupinsky, 2005; Hammock and Young, 2005) and in social & spatial memory (Aarde & Jentsch, 2006). In this research, its association with auditory pattern perception proposes a potential link between music perception & human social functioning.

In the rhythm domain, one study has described that mutation of the FOXP2 (Forkhead box protein P2) gene on chromosome 7q31 impairs rhythm perception & production while leaving pitch perception & production abilities intact (Alcock et al., 2000).

Music memory

Granot et al., (2007) investigated the potential connection between phonological and musical memory with the AVPR1A & SLC6A4 genes (solute carrier family VII [neurotransmitter transporter serotonin], member IV). A previously documented connection between arginine vasopressin (AVP) and spatial and social memory was provided to justify targeting these two genes (Ferguson et al., 2002; Aarde & Jentsch, 2006). Furthermore, Serotonin also interacts with AVP in the hypothalamus (Albers et al., 2002) and serotonin enhances arginine vasopressin production (Gálfi et al., 2005). This leads to a possible epistatic connection between the AVPR1A gene, which provides the blueprint for synthesising the arginine vasopressin receptor and the SLC6 A4 gene, the transporter of serotonin which is essential for serotonin receptor supplies. Granot et al. have generalised 82 individuals from its institution with little musical training for the AVPR1A (RS1 & RS3 haplotypes) & SLC6A4 (HTTLPR) versatility using population and family association studies. The participants' phonological and music memory performance was assessed using a broad range of tests. Results generated significant genes for two melodic memory tasks, 1 rhythmic memory task and1 phonological memory task, even after using stringent Bonferroni adjustments for many tests, via epistatic gene interactions between AVPR1A and SLC6A4 polymorphisms. This offers early evidence of an epistatic connection between AVPR1A and SLC6A4 polymorphisms that is likely associated with short-term music memory, or more often, phonological memory.

Music listening

Ukkola-Vuoti et al., (2011) investigated the behaviour of 31 Finnish households in listening to music using questionnaires. A family-based investigation of relationships has shown favourable correlations

between haplotypes of AVPR1A and active music listening. The RS1+AVR haplotype and the present active musical listening and the RS1+RS3 haplotype and lifetime activity listening were the most significant correlations. No notable connection between listening and the polymorphisms of the SLC6A4 has been found. In this research, active listening refers to concentrated listening, such as attending concerts. Since Ukkola et al., (2009) have demonstrated that the same AVPR1A promotor area (RS1+RS3) is connected with music perception, these results indicate a similar genetical foundation for active listening frequency and perception.

Singing

In 1008 individuals from 73 extended Mongolian families, Park et al., (2012) examined the genetic variables that underlie vocabulary via family-based linkages and association testing. They performed a pitch production accuracy test and discovered that the target pitches with variations under a semitone were precisely matched by 357 participants (35.4 percent). The heritability of singing accuracy was found at 40% with the use of pedigree data. A study was conducted on genome-wide linkages, the most significant linkage peak found on 4q23 (LOD = 3.1 at marker D4S2986). The results coincide with chromosome 4q areas, which show links for the perception of music (Pulli et al., 2008; Oikkonen et al., 2014). A familial association study at the hypothesised connection site showed that SNP rs12510781 on 4q26 was most closely linked with singing precision. The authors also used an exotic sequence to search for additional likely SNP candidates and discovered in UGT8 a non-synonymous SNP (rs4148254) on 4q26. Furthermore, CNV study employing a comparative genomic hybridization (aCGH) array showed that a loss copy number upstream of the UGT8 might be related to singing accurately at 5.6 kb (5600 base pairs).

Discussion

As discussed in this article, much research has started to provide insights into music's genetic basis. Several promising and convergent findings have begun to emerge to date. Several chromosomal locations 8q were involved with two or more musical features. For example, loci 8q21 and locus 8q24 were involved with Absolute Pitch and perception of music (Pulli et al., 2008; Theusch et al., 2009; Ukkola-Vuoti et al., 2013). Similarly, loci 4p14 and 4q22 on chromosome 4 were linked with perception of music, especially with pitch identification (Pulli et al., 2008; Oikkonen et al., 2014), while the nearby locus 4q23 was associated with the precision of the pitch of singing ability (Park et al., 2012).

To date, several genes have been very significant in music genetics research. For example, the AVPR1A gene on chromosome 12q has been linked with music listening and music memory (Ukkola-Vuoti et al., 2011), perception of music (Ukkola et al., 2009). (Granot et al., 2007). On the other hand, the SLC6A4 gene was linked with the recollection of music (Granot et al., 2007) (Morley et al., 2012).

It is essential to reproduce the current research findings to validate the obtained data, particularly in small sample size studies (e.g., Granot et al., 2007, Pulli et al., 2008; Ukkola-Vuoti et al., 2013). For example, an existing big genome study (Oikkonen et al., 2014) failed to identify

the linkages between AVPR1A and music perception, which the same research group had previously revealed during another candidate gene analysis (Ukkola et al., 2009). The polymorphisms of genes such as AVPR1A & SLC6A4 were selected for many candidate-gene association studies based on the results of previous music studies. However, the multi-faceted character of musical ability may make a candidate gene, along with one musical function, a poor candidate for another musical function. This is shown by Morley et al. (2012), who discovered, despite their statistical power, no relationship between AVPR1A polymorphisms with involvement in choruses. Researchers may thus be more sensitive to choose potential genes based on supporting evidence from linkage analyses or GWAS of linked musical capacity.

For future researchers, it will be essential to utilise other populations and more extensive samples to reproduce the findings of the present investigations. In addition, many molecular genetic investigations have been conducted in different Finnish multigenerational families. Therefore, extending the findings of these families to other ethnic groups will help substantiate the connections mentioned.

Since molecular genes are still new, many of the studies here utilise older molecular genetic techniques, such as mapping the linkage or the candidate gene approach. Researchers in music genetics may explore combining CNV, SNP methods and results from CNV analysis may supplement the findings from SNP analysis (Stranger et al., 2007). Other recent procedures include exom sequencing as well as methylation studies to explore the possible role of epigenetic effects and the underlying molecular and biological processes (Rowe and Tenesa, 2012).

The possible impact of epistasis, gene-environmental interactions and epigenetic effects on music abilities are another major route in music genetic research. These factors may illustrate why many of the genetic variations involved in complex characteristics can only explain a small proportion of family study heritage predicted (Stranger et al., 2011). Therefore, researchers should increase awareness and concentrate on gene-environment interaction. For example, apparent environmental processes such as brain plasticity caused by training may be influenced by genetics (Brans et al., 2010; Vinkhuyzen et al., 2010). Likewise, environmental factors may change genetic expression via epigenetic processes (Fagiolini et al., 2009; Sweatt, 2013).

While the collected results to far seem encouraging, a more detailed study is needed. Most research has utilised assessments of music's capacity to work on music, giving unfair relevance to some perceptional skills, such as detecting pitch and rhythm while disregarding others.

Music impairments, such as tonal deafness (Peretz et al., 2007) & beat deafness (Phillips-Silver et al., 2011), may offer fruitful paths for future research since deficiencies are often more distinct than capacities to phenotype. However, at now, relatively few genetic studies based on music impairments have been conducted.

Our present understanding is restricted to the conclusion that FOXP2 may play a part in the processing of music rhythms, language and speech (Alcock et al., 2000; Lai et al., 2001). Thus, comparative

genomic study between music and language skills may help us understand the common and un-common genetic and neurological processes for music and language and can help to address important issues regarding music & language origins (Peretz, 2009).

To conclude, research into the genetics of music has produced encouraging findings, which emphasise the necessity for further study in this area. Enlightenment of musical talent's genetic foundation may be difficult because many natural elements need thorough identification, classification, and genetic research. In conjunction with the successful pace at which molecular genetics and statistical designs advance, an ever more precise picture of genetic processes underlying the genesis of musical characteristics are beginning to emerge. These mechanisms may then be linked with neuroscientific findings of the neurological basis of certain musical functions and behaviour. This will eventually enable us to understand better how interactions between nature and nutrition influence the development of human musical capabilities throughout our lifetime.

Acknowledgement

The authors appreciate the Maulana Azad College Principal for their kind assistance. In addition, the authors are grateful for their kind assistance and support to all professors and non-teachers in the Department of Zoology, Maulana Azad College.

References

Aarde, S. M. and Jentsch, J. D. (2006). Haploinsufficiency of the arginine-vasopressin gene is associated with poor spatial working memory performance in rats. *Horm. Behav*. 49: 501–508.

Adam, I., Mendoza, E., Kobalz, U., Wohlgemuth, S. and Scharff, C. (2016). FoxP2 directly regulates the reelin receptor VLDLR developmentally and by singing. *Molecular and Cellular Neuroscience.* 74: 96–105.

Albers, H. E., Karom, M. and Smith, D. (2002). Serotonin and vasopressin interact in the hypothalamus to control communicative behavior. *Neuroreport.* 13: 931–933.

Alcock, K. J., Passingham, R. E., Watkins, K. and Vargha, K. F. (2000). Pitch and timing abilities in inherited speech and language impairment. *Brain Lang*. 75: 34–46.

Alkan, C., Coe, B. P. and Eichler, E. E. (2011). Genome structural variation discovery and genotyping. *Nat. Rev. Genet*. 12: 363–376.

Bachner-Melman, R., Dina, C., Zohar, A. H., Constantini, N., Lerer, E., Hoch, S., Sella, S., Nemanov, L., Gritsenko, I., Lichtenberg, P., Granot, R. and Ebstein, R. P. (2005). AVPR1a and SLC6A4 gene polymorphisms are associated with creative dance performance. *PLoS Genet.* 1: e42.

Baharloo, S., Johnston, P. A., Service, S. K., Gitschier, J. and Freimer, N. B. (1998). Absolute pitch: an approach for identification of genetic and nongenetic components. *Am. J. Human. Genet.* 62: 224–231.

Baharloo, S., Service, S. K., Risch, N., Gitschier, J. and Freimer, N. B. (2000). Familial aggregation of absolute pitch. *Am. J. Hum. Genet.* 67: 755–758.

Bielsky, I. F., Hu, S. B., Szegda, K. L., Westphal, H. and Young, L. J. (2004). Profound impairment in social recognition and reduction in anxiety-like behavior in vasopressin V1a receptor knockout mice. *Neuropsychopharmacology.* 29: 483–493.

Bochud, M. (2012). Estimating heritability from nuclear family and pedigree data. In: Elston R. C., Satagopan J. M., Sun S. (eds) (New York, NY: Humana Press; Springer). *Statistical Human Genetics: Methods and Protocols*. Pp. 171–186.

Brauchli, C., Leipold, S. and Jäncke, L. (2019). Univariate and multivariate analyses of functional networks in absolute pitch. *Neuroimage.* 189:241–247.

Brans, R. G. H., Kahn, R., Schnack, H. G., Van, Baal, G. C. M., Posthuma, D. and Van, H. N. E. M. (2010). Brain plasticity and intellectual ability are influenced by shared genes. *J. Neurosci.* 30: 5519–5524.

Carrion-Castillo, A., Franke, B. and Fisher, S. E. (2013). Molecular genetics of dyslexia: an overview. *Dyslexia.* 19: 214–240.

Coon, H. and Carey, G. (1989). Genetic and environmental determinants of musical ability in twins. *Behav. Genet.* 19: 183–193.

Depue, R. A. and Morrone-Strupinsky, J. V. (2005). A neurobehavioral model of affiliative bonding: implications for conceptualizing a human trait of affiliation. *Behav. Brain Sci.* 28: 313–350.

De-Quervain, D. J. F. and Papassotiropoulos, A. (2006). Identification of a genetic cluster influencing memory performance and hippocampal activity in humans. *Proc. Natl. Acad. Sci. U.S.A.* 103: 4270–4274.

Deutsch, D., Henthorn, T., Marvin, E. and Xu, H. (2006). Absolute pitch among American and Chinese conservatory studentsd: prevalence differences, and evidence for a speech-related critical period. *J. Acoust. Soc. Am.* 119719-119722.

Dovern, A., Fink, G. R., Fromme, A. C. B., Wohlschläger, A. M., Weiss, P. H. and Riedl, V. (2012). Intrinsic network connectivity reflects consistency of synesthetic experiences. *J. Neurosci.* 32: 7614–7621.

Drayna, D., Manichaikul, A., De, Lange, M., Snieder, H. and Spector, T. (2001). Genetic correlates of musical pitch recognition in humans. *Science.* 291: 1969–1972.

Foster, N. E. V. and Zatorre, R. J. (2010). Cortical structure predicts success in performing musical transformation judgments. *Neuroimage.* 53: 26–36.

Gaab, N., Gaser, C. and Schlaug, G. (2006). Improvement-related functional plasticity following pitch memory training. *Neuroimage.* 31: 255–263.

Gao, L., Tang, S. X. and Yi, J. J. (2018). Musical auditory processing, cognition, and psychopathology in 22q11.2 deletion syndrome. *Am. J. Med. Genet. B. Neuropsychiatr. Genet*. 177: 765–773.

Gingras, B., Honing, H., Peretz, I., Trainor, L. J. and Fisher, S. E. (2015). Defining the biological bases of individual differences in musicality. *Philosoph. Transact. B.* 370: e20140092.

Goycoolea, M. V., Mena, I., Neubauer, S. G., Levy, R. G., Grez, M. F. and Berger, C. G. (2007). Musical brains: a study of spontaneous and evoked musical sensations without external auditory stimuli. *Acta Otolaryngol.* 127: 711–721.

Granot, R. Y., Frankel, Y., Gritsenko, V., Lerer, E., Gritsenko, I. and Bachner-Melman, R. (2007). Provisional evidence that the arginine vasopressin 1a receptor gene is associated with musical memory. *Evolut. Hum. Behav.* 28: 313–318.

Grayton, H. M., Fernandes, C., Rujescu, D. and Collier, D. A. (2012). Copy number variations in neurodevelopmental disorders. *Prog. Neurobiol.* 99: 81–91.

Gregersen, P. K. (1998). Instant recognition: the genetics of pitch perception. *Am. J. Hum. Genet.* 62: 221–223.

Gregersen, P. K., Kowalsky, E., Kohn, N. and Marvin, E. W. (1999). Absolute pitch: prevalence, ethnic variation, and estimation of the genetic component. *Am. J. Hum. Genet.* 65: 911–913.

Gregersen, P. K., Kowalsky, E., Kohn, N. and Marvin, E. W. (2001). Early childhood music education and predisposition to absolute pitch: teasing apart genes and environment. *Am. J. Med. Genet.* 98: 280–282.

Gregersen, P. K., Kowalsky, E., Lee, A., Baron-Cohen, S., Fisher, S. R., Asher, J. E., Ballard, D., Freudenberg, J. and Li, W. (2013). Absolute pitch exhibits phenotypic and genetics overlap with synesthesia. *Human Molec. Genet.* 22: 2097–2104.

Gregersen, P. K. and Kumar, S. (1996). The genetics of perfect pitch. *Am. J. Hum. Genet.* 59 (Suppl.): A179.

Guo, S. W. (1998). Inflation of sibling recurrence-risk ratio, due to ascertainment bias and/or overreporting. *Am. J. Hum. Genet.* 63: 252–258.

Henthorn, T. and Deutsch, D. (2007). Ethnicity versus early environment: comment on 'Early childhood music education and predisposition to absolute pitch: teasing apart genes and environment' by Peter K. Gregersen, Elena Kowalsky, Nina Kohn, and Elizabeth West Marvin [2000]. *Am. J. Med. Genet.* A143: 102–103.

Honing, H., Ladinig, O., Háden, G. P. and Winkler, I. (2009). Is beat induction innate or learned: probing emergent meter perception in adults and newborns using event-related brain potentials. *Ann. N.Y. Acad. Sci.* 1169: 93–96.

Hove, M. J., Sutherland, M. E. and Krumhansi, C. L. (2010). Ethnicity effects in relative pitch. *Psychon. Bull. Rev.* 17: 310–316.

Hyde, K. L., Lerch, J. P., Zatorre, R. J., Griffiths, T. D., Evans, A. C. and Peretz, I. (2007). Cortical thickness in congenital amusia: when less is better than more. *J. Neurosci.* 27: 13028–13032.

Järvelä, I. (2018). Genomics studies on musical aptitude, music perception, and practice. *Ann. N. Y. Acad. Sci*. 1423: 82–91.

Kalmus, H. and Fry, D. B. (1980). On tune deafness (dysmelodia): frequency, development, genetics and musical

background. *Ann. Hum. Genet.* 43: 369–382.

Karma, K. (1994). Auditory and visual temporal structuring: how important is sound to musical thinking. *Psychol. Music.* 22: 20–30.

Keenan, J. P., Thangaraj, V., Halpern, A. R. and Sclaug, G. (2001). Absolute pitch and planum temporale. *NeuroImage.* 14: 1402–1408.

Ku, C. S., Cooper, D. N., Polychronakos, C., Naidoo, N., Wu, M. and Soong, R. (2012). Exome sequencing: dual role as a discovery and diagnostic tool. *Ann. Neurol.* 71: 5–14.

Lai, C. S. L., Fisher, S. E., Hurst, J. A., Vargha-Khadem, F. and Monaco, A. P. (2001). A forkhead-domain gene is mutated in a severe speech and language disorder. *Nature.* 413: 519–523.

Lathrop, G. M., Lalouel, J. M., Julier, C. and Ott, J. (1984). Strategies for multilocus linkage analysis in humans. *Proc. Natl. Acad. Sci. U.S.A.* 81: 3443–3446.

Levitin, D. J. (2012). What does it mean to be musical? *Neuron.* 73: 633–637.

Lewis, C. M. and Knight, J. (2012). Introduction to genetic association studies. *Cold Spring Harb. Protoc.* 7: 297–306.

Li, C. C., Chakravarti, A. and Halloran, S. L. (1987). Estimation of segregation and ascertainment probabilities by discarding the single probands. *Genet. Epidemiol.* 4: 185–191.

Li, C. C. and Mantel, N. (1968). A simple method of estimating the segregation ratio under complete ascertainment. *Am. J. Hum. Genet.* 20: 61–81.

Li, G., Wang, J., Rossiter, S. J., Jones, G., Cotton, J. A. and Zhang, S. (2008). The hearing gene Prestin reunites echolocating bats. *Proceedings of the National Academy of Sciences.* 105 (37): 13959–13964.

Liu, X., Kanduri, C. and Oikkonen, J. (2016). Detecting signatures of positive selection associated with musical aptitude in the human genome. *Sci. Rep.* 6: 21198.

Loui, P., Alsop, D. and Schlaug, G. (2009). Tone deafness: a new disconnection syndrome? *J. Neurosci.* 29: 10215–10220.

Mariath, L. M., Silva, A. M., Kowalski, T. W., Gattino, G. S., Araujo, G. A., Figueiredo, F. G., Tagliani-Ribeiro, A., Roman, T., Vianna, F. S. L., Schuler-Faccini, L. and Schuch, J. B. (2017). Music genetics research: association with musicality of a polymorphism in the AVPR1A gene. *Genet. Molec. Biol.* 40: 421–429.

Mandell, J., Schulze, K. and Schlaug, G. (2007). Congenital amusia: an auditory-motor feedback disorder? *Restor. Neurol. Neurosci.* 25: 323–334.

McDermott, J. and Hauser, M. (2005). The origins of music: innateness, uniqueness, and evolution. *Music Percept.* 23: 29–59.

Mignault, G. G., Moreau, P., Robitaille, N. and Peretz, I. (2012). Congenital amusia persists in the developing brain after daily music listening. *PLoS ONE.* 7: e36860.

Mitry, D., Williams, L., Charteris, D. G., Fleck, B. W., Wright, A. F. and Campbell, H. (2011). Population-based estimate of the sibling recurrence risk ratio for

rhegmatogenous retinal detachment. *Invest. Ophthalmol. Vis. Sci.* 52: 2551–2555.

Morgan and Linkage. (2003a). In: Carey G. (ed.). Thousand Oaks, CA: Sage Publications, Inc. Chapter 10: *Human Genetics for the Social Sciences.* Pp. 161–180.

Morley, A. P., Narayanan, M., Mines, R., Molokhia, A., Baxter, S. and Craig, G. (2012). AVPR1A and SLC6A4 polymorphisms in choral singers and non-musicians: a gene association study. *PLoS ONE.* 7: e31763.

Naj, A. C., Park, Y. S. and Beaty, T. H. (2012). Detecting familial aggregation. In: Elston R. C., Satagopan J. M., Sun S. (eds.) (New York, NY: Humana Press; Springer). *Statistical Human Genetics: Methods and Protocols*. Pp. 119–150.

Nandram, B., Jai-Won, C. and Hongyan, X. (2011). Maximum likelihood estimation for ascertainment bias in sampling siblings. *J. Data Sci.* 9: 23.

Neale, M. C., Boker, S. M., Xie, G. and Maes, H. H. (2006). *Mx: Statistical Modeling*. Richmond, VA: Department of Psychiatry.

Newbury, D. F. and Monaco, A. P. (2010). Genetic advances in the study of speech and language disorders. *Neuron.* 68: 309–320.

Oikkonen, J., Huang, Y., Onkamo, P., Ukkola-Vuoti, L., Raijas, P. and Karma, K. (2015). A genome-wide linkage and association study of musical aptitude identifies loci containing genes related to inner ear development and neurocognitive functions. *Mol. Psychiatry*. 20(2): 275-282.

Oikkonen, J. and Järvelä, I. (2014). Genomics approaches to study musical aptitude. *Bioessays.* 36: 1102–1108.

Park, H., Lee, S., Kim, H. J., Ju, Y. S., Shin, J. Y., Hong, D., von, Grotthuss, M., Lee, D. S., Park, C., Kim, J. H., Kim, B., Yoo, Y. J., Cho, S. I., Sung, J., Lee, C., Kim, J. I. and Seo, J. S. (2012). Comprehensive genome analyses associate UGT8 variants with musical ability in a Mongolian population. *J. Med. Genet.* 49: 747–752.

Peretz, I. (2009). Music, language and modularity framed in action. *Psychol. Belg.* 49: 157–175.

Peretz, I., Cummings, S. and Dubé, M. P. (2007). The genetics of congenital amusia (tone deafness): a family-aggregation study. *Am. J. Hum. Genet.* 81: 582–588.

Peretz, I. and Vuvan, D. T. (2017). Prevalence of congenital amusia. *Eur. J. Human Genet.* 25: 625–630.

Profita, J. and Bidder, T. G. (1988). Perfect pitch. *Am. J. Med. Genet.* 29: 763–771.

Pulli, K., Karma, K., Norio, R., Sistonen, P., Göring, H. H. H. and Järvelä, I. (2008). Genome-wide linkage scan for loci of musical aptitude in Finnish families: evidence for a major locus at 4q22. *J. Med. Genet.* 45: 451–456.

Ross, D. A., Olson, I. R. and Gore, J. C. (2003). Absolute pitch does not depend on early musical training. *Ann. N.Y. Acad. Sci.* 999: 522–526.

Schnell, A. H. and Sun, X. (2012). Model-based linkage analysis of a quantitative trait. In: Elston R. C., Satagopan J. M., Sun S. (eds.) (New York, NY: Humana Press; Springer).

Statistical Human Genetics: Methods and Protocols. Pp. 263–284.

Sergeant, D. (1969). Experimental investigation of absolute pitch. *J. Res. Music Educ.* 17: 135–143.

Singleton, A. B. (2011). Exome sequencing: a transformative technology. *Lancet Neurol.* 10: 942–946.

Spencer, C. C. A., Su, Z., Donnelly, P. and Marchini, J. (2009). Designing genome-wide association studies: sample size, power, imputation, and the choice of genotyping chip. *PLoS Genet.* 5: e1000477.

Strachan, T. and Read, A. P. (1999). Complex diseases: theory and results. In: New York, NY: Wiley-Liss *Human Molecular Genetics*, 2nd edn.

Sun, L. and Dimitromanolakis, A. (2012). Identifying cryptic relationships. In: Elston R. C., Satagopan J. M., Sun S. (eds.) (New York, NY: Humana Press; Springer). *Statistical Human Genetics: Methods and Protocols*. Pp. 47–58.

Szyfter, K. and Witt, M. P. (2020). How far musicality and perfect pitch are derived from genetic factors? *J. Appl. Genet. Sep*. 61(3): 407-414.

Tan, Y. T., McPherson, G. E., Peretz, I., Berkovic, S. F. and Wilson, S. J. (2014). The genetic basis of music ability. *Front. Psychol.* 5: Art. 658.

The association study. (2003b). In: Carey G. (ed.). Thousand Oaks, CA: Sage Publications, Inc. Chapter 11: *Human Genetics for the Social Sciences.* Pp. 181–192.

Theusch, E., Basu, A. and Gitschier, J. (2009). Genome-wide study of families with absolute pitch reveals linkage to 8q24.21 and locus heterogeneity. *Am. J. Hum. Genet.* 85: 112–119.

Theusch, E. and Gitschier, J. (2011). Absolute pitch twin study and segregation analysis. *Twin Res. Hum. Genet.* 14: 173–178.

Trainor, L. J. and Heinmiller, B. M. (1998). The development of evaluative responses to music: infants prefer to listen to consonance over dissonance. *Infant Behav. Dev.* 21: 77–88.

Trainor, L. J. and Trehub, S. E. (1992). A comparison of infants' and adults' sensitivity to Western musical structure. *J. Exp. Psychol. Hum. Percept. Perform.* 18: 394–402.

Trainor, L. J. and Trehub, S. E. (1993). What mediates infants' and adults' superior processing of the major over the augmented triad? *Music Percept.* 11: 185–196.

Trainor, L. J., Tsang, C. D. and Cheung, V. H. W. (2002). Preference for sensory consonance in 2- and 4-month-old infants. *Music Percept.* 20: 187–194.

Trehub, S. E. (2003). The developmental origins of musicality. *Nat. Neurosci.* 6: 669–673.

Trehub, S. E. (2006). Infants as musical connoisseurs. In: McPherson G. E. (ed.) (New York, NY: Oxford University Press). *The Child as Musician: A Handbook of Musical Development*. Pp. 33–49.

Trehub, S. E., Bull, D. and Thorpe, L. A. (1984). Infants' perception of melodies: the role of melodic contour. *Child Dev.* 55: 821–830.

Trehub, S. E., Schellenberg, E. G. and Kamenetsky, S. B. (1999). Infants' and adults' perception of scale

structure. *J. Exp. Psychol. Hum. Percept. Perform.* 25: 965–975.

Trehub, S. E., Thorpe, L. A. and Morrongiello, B. A. (1987). Organizational processes in infants' perception of auditory patterns. *Child Dev.* 58: 741–749.

Ukkola, L. T., Onkamo, P., Raijas, P., Karma, K. and Järvelä, I. (2009). Musical aptitude is associated with AVPR1A-haplotypes. *PLoS ONE* 4: e5534.

Ukkola-Vuoti, L., Kanduri, C., Oikkonen, J., Buck, G., Blancher, C. and Raijas, P. (2013). Genome-wide copy number variation analysis in extended families and unrelated individuals characterized for musical aptitude and creativity in music. *PLoS ONE* 8: e56356.

Ukkola-Vuoti, L., Oikkonen, J., Onkamo, P., Karma, K., Raijas, P. and Järvelä, I. (2011). Association of the arginine vasopressin receptor 1A (AVPR1A) haplotypes with listening to music. *J. Hum. Genet.* 56: 324–329.

Verweij, K. J. H., Mosing, M. A., Zietsch, B. P. and Medland, S. E. (2012). Estimating heritability from twin studies. In: Elston R. C., Satagopan J. M., Sun S. (eds.) (New York, NY: Humana Press; Springer). *Statistical Human Genetics: Methods and Protocols*. Pp. 151–170.

Vinkhuyzen, A. A. E., Van-Der, S. S., De-Geus, E. J. C., Boomsma, D. I. and Posthuma, D. (2010). Genetic influences on "environmental" factors. *Genes Brain Behav.* 9: 276–287.

Vinkhuyzen, A. A. E., Van-Der, Sluis, S., Posthuma, D. and Boomsma, D. I. (2009). The heritability of aptitude and exceptional talent across different domains in adolescents and young adults. *Behav. Genet.* 39: 380–392.

Visscher, P. M., Hill, W. G. and Wray, N. R. (2008). Heritability in the genomics era-concepts and misconceptions. *Nat. Rev. Genet.* 9: 255–266.

Watts, C., Murphy, J. and Barnes, B. K. (2003). Pitch matching accuracy of trained singers, untrained subjects with talented singing voices, and untrained subjects with nontalented singing voices in conditions of varying feedback. *J. Voice.* 17: 185–194.

Weeks, D. E., Lehner, T., Squires, W. E., Kaufmann, C. and Ott, J. (1990). Measuring the inflation of the LOD score due to its maximization over model parameter values in human linkage analysis. *Genet. Epidemiol.* 7: 237–243.

Winkler, I., Háden, G. P., Ladinig, O., Sziller, I. and Honing, H. (2009). Newborn infants detect the beat in music. *Proc. Natl. Acad. Sci. U.S.A.* 106: 2468–2471.

Xu, W., Bull, S. B., Mirea, L. and Greenwood, C. M. T. (2012). Model-free linkage analysis of a binary trait. In: Elston R. C., Satagopan J. M., Sun S. (eds.) (New York, NY: Humana Press; Springer). *Statistical Human Genetics: Methods and Protocols*. Pp. 317–345.

UTTAR PRADESH JOURNAL OF ZOOLOGY

42(10): 10-18, 2021
ISSN: 0256-971X (P)

LARVICIDAL EFFECT OF *Coffea arabica* L., *Camellia sinensis* (L.) Kuntz, AND *Punica granatum* L. ON *Aedes albopictus* (Skuse), THE VECTOR OF DENGUE AND CHIKUNGUNYA

DIPAK KUMAR SOM[1*], PALLABI LAHA[1] AND SUPRIYA MONDAL[1]

[1]Post Graduate Department of Zoology, Maulana Azad College, 8 Rafi Ahmed Kidwai Road, Kolkata 700 013, West Bengal, India.

AUTHORS' CONTRIBUTIONS

This work was carried out in collaboration among all authors. Author DKS has made substantial contributions to conception, design of experiment, interpretation of data and final checking of manuscript. Author PL has performed the experiment and analysed the data and wrote the first draft of manuscript with literature survey. Author SM has assisted in performing the experiment, data analysis and statistical analyses. All authors read and approved the final manuscript.

Article Information

Editor(s):
(1) Dr. Sirigireddy Sivajothi, Sri Venkateswara Veterinary University, India.
Reviewers:
(1) Charles S. Apperson, North Carolina State University, North Carolina.
(2) Anupam Ghosh, Bankura Christian College, India.
(3) Raimundo N. Colares Camargo Júnior, Federal Institute of Education, Science and Technology of Pará, Brazil.

Received: 23 February 2021
Accepted: 01 May 2021
Published: 06 May 2021

Original Research Article

ABSTRACT

The purpose of the present study is to envisage the larvicidal activities of three common plant extracts in controlling *Aedes albopictus* (Skuse), a potential vector of Dengue and Chikungunya. Chloroform extract of green coffee beans, *Coffea arabica* L.; methanol extract of green tea leaves, *Camellia sinensis* (L.) Kuntz and chloroform extract of pomegranate fruit peel *Punica granatum* L. were tested against late 3rd instar/ early 4th instar larvae of *Ae. albopictus* under laboratory condition following WHO methodology, 2005. LC_{50} values were determined using the probit analysis with 95% confidence limit. The result indicated that after 24 hours and 48 hours of treatment, LC_{50} values for green coffee bean extract, green tea leaves extract and pomegranate fruit peel extract against *Ae. albopictus* larvae were 0.08, and 0.06, 0.13 and 0.06, 0.09 and 0.06 respectively. Our findings revealed that chloroform extract of green coffee beans and methanol extract of green tea leaves are the most effective in controlling *Aedes albopictus* larvae showing 100% mortality after 48 hours of exposure than chloroform extract of pomegranate fruit peel that shows 66% mortality after 48 hours of treatment. The overall larvicidal trend with reference to LC_{50} after 24 hours and 48 hours was green coffee > green tea > pomegranate. The larvae exposed to green coffee bean

**Corresponding author: Email: dipaksom@gmail.com;*

crude extract showed deformities related to moulting behavior and larval morphology. As these plants are widely distributed in India, their formulation might manifest effective eco-friendly alternatives for combating this upcoming potential vector of Dengue and Chikungunya.

Keywords: *Aedes albopictus*; botanicals as larvicides; dengue; Chikungunya; plant extract; vector control.

1. INTRODUCTION

The medical importance of mosquitoes as vectors for the transmission of life threatening diseases that causes morbidity, mortality, economic loss and social disruption such as dengue, Chikungunya, malaria, Japanese B encephalitis, lymphatic filariasis etc. are well recorded. Dengue is regarded as one of the most important arboviral infections in the world transmitted by *Aedes* mosquitoes, mainly *Aedes (Stegomyia) aegypti* and *Aedes albopictus* (Skuse) [1]. The incidence of Dengue has grown dramatically around the world in recent decades. Over 40% of world's population is now at risk from dengue [2]. *Aedes aegypti* is of supreme concern because of its wide distribution and close association with human [3]. *Aedes albopictus* (Skuse), commonly called 'the banded mosquito of Bengal', is now playing the role of secondary vector of Dengue and Chikungunya in rural and suburban regions of West Bengal [4]. This vector is now proliferating at a very fast rate due to high survivality in a wide range of environmental parameters throughout the world including India [5]. *Ae. albopictus*, is generally associated with human-outdoor areas but are gradually becoming a much potential vector for transmission of Dengue and Chikungunya virus in West Bengal due to rapid urbanization and deforestation [6].

Use of chemical insecticides has several drawbacks, such as these produce resistance among vectors [7], produce undesirable effects on non-target organisms and also foster environmental and human health concern [8,9], whereas, plant derived compounds are target specific and biodegradable [10]. Resistance to various synthetic insecticides [11] and detrimental effect on human health are compelling us to search for alternative weapons especially natural products of plant origin as vector controlling agents [12]. Many plant-based products are widely used for their insecticidal properties to control the vector mosquitoes [3,10]. In recent years, interest in phytochemicals has been revived because of the development of resistance, cross resistance and toxicity hazards associated with synthetic insecticides [4]. A large number of pant products have been reported to have mosquito larvicidal activity [12,13, 14]. This result may be observed due to presence of various active components like steroids, saponins, proanthocyanidins, glycosides and phenolic compounds etc. inside those plant extracts [15, 16].

The present endeavour is to envisage the larvicidal activities of Chloroform extract of green coffee beans, *Coffea arabica* L., methanol extract of green tea leaves, *Camellia sinensis* (L.) Kuntz and chloroform extract of pomegranate fruit peel, *Punica granatum* L., as, botanicals are likely to cause the least damage to anthropological environment in controlling this up surging vector of Dengue virus in the regional-national-international context [17,18,19].

2. MATERIALS AND METHODS

2.1 Procurement of Plant Parts

The three plants were selected randomly from a list of plants primarily sorted on the basis of their ethno medicinal value. Green tea leave and Pomegranate fruits were collected from local market. The Green coffee beans were procured from online market (Table 1).

2.2 Extraction Method of Plant Material

The extraction method of Freedman et al. [20] is followed here with few modifications.

Table 1. Common name and scientific name of three plants, parts used for bioassay and the extraction media

Common name	Botanical name	Parts used for extraction	Extraction medium
Green Coffee	*Coffea arabica* L.	Seed	Chloroform
Green Tea	*Camellia sinensis* (L.) Kuntz	Leaf	Methanol
Pomegranate	*Punica granatum* L.	Fruit peel	Chloroform

Green coffee beans were ground. An amount of 62.5 gm of green coffee bean dust was dissolved in 250 ml of chloroform and kept for 72 hours before getting filtrate. Then the filtrate was evaporated and dried. 1.25 gm of dry green coffee bean crude extract was collected in this process. The material was then dissolved in 95% ethanol. After ethanol extraction, post dried material was further sequentially extracted using distilled water with 5% ethanol for next 7 days. The extract was filtered using Whatmann No. 1 filter paper and collected.

Green tea leaves were ground in an electric grinder. Then the ground material was dissolved in 90% methanol (12.5 gm in 50 ml), stirred well and kept for 72 hours. Then the extract was filtered and the filtrate was kept for subsequent evaporation. We get 8.01 gm of crude extract of green tea from 50 gm of ground tea leaves.

The fruit peel of *Punica granatum* was prepared by macerating, dissolving in absolute ethanol for about 10-15 days. It was filtered using Whatmann No. 1 filter paper and dried in hot air oven. The material was then processed for chloroform extraction following the process as that of coffee bean extraction.

All crude dried extracts were kept in small vials in a deep freezer (-20^{o}C) until used.

2.3 Collection and Rearing of Mosquito

Eggs of *Aedes albopictus* mosquito were collected from natural habitat at Nalpur (22°31′45″N 88°11′10″E), Howrah, West Bengal, India. Larvae were reared inside the entomology laboratory of Maulana Azad College, with utmost precautions following WHO methodology [21]. Third instar/early fourth instar larvae were kept in a deep plastic container [400 larvae per 3L of rain water] in the Air conditioned room maintaining the temperature and humidity of 27±2^{o}C and 80±5% respectively. The pH of water was recorded as 6.5.

2.4 Preparation of Stock Solution

To prepare three separate stock solutions for three plant parts, 1g of each extract were added in three separate beakers containing 50 mL of 5% ethanol each and were considered as 2% stock solutions (20,000 ppm) [14].

2.5 Quantification of Larval Mortality Rates

Equal starting numbers of larvae (n = 30 larvae) were placed into each plastic bowl containing different concentrations of extract. We used pipette to measure the desired amount of plant extracts from stock solution. The concentrations for Green coffee bean extract were 0.4, 0.5, 0.6, 0.7 and 0.8 (%v/v which are equivalent to 80ppm, 100ppm, 120ppm, 140ppm and 160ppm) respectively; for Green tea leaves extract, concentration were 0.6, 0.7, 0.8, 0.9, 1.0, and 1.2 (%v/v which are equivalent to 120 ppm, 140 ppm, 160 ppm, 180 ppm, and 200 ppm, and 240 ppm) respectively and for Pomegranate fruit peel extract, concentration were 0.6, 0.7, 0.8, 0.9, and 1.0 (%v/v which are equivalent to 120ppm, 140ppm, 160ppm, 180ppm, and 200ppm) respectively. Mortality rates of treated larvae were quantified at 24hour and 48hour intervals. Each larva was examined and considered dead if it did not respond to probing with a dropper. Treatment-induced morphological deformities relative to control were analysed using light microscopy at 25x magnifications and recorded for further analysis.

2.6 Larvicidal Bioassay

The extracted plant materials were used in different concentration against *Aedes albopictus* and their efficacy was evaluated as per standard WHO method [7]. Each replicate contained 100ml of seasonal water (rain water) and above mentioned concentration of plant material in plastic bowls. Three replicas were conducted for each concentration and against each concentration along with a control were set [22]. Batches of 30 late 3rd instar/early 4th instar larvae were exposed in each container. The numbers of dead larvae were counted after 24 hour and 48 hour intervals. The experiment was conducted under laboratory condition at 27±2˚C and 80±5% RH.

2.7 Analysis of Data

The data, obtained in this experiment was analysed with special reference to Probit analysis, $LC_{50,}$ LC_{90}, Regression graph and homogeneity Chi-square using SPSS version 22.0.0.0 software.

3. RESULTS AND DISCUSSION

Larvae of *Aedes albopictus* were subjected against plant extracts of *Coffea arabica* (Green coffee), *Camellia sinensis* (Green tea), and *Punica granatum* (Pomegranate). Five different concentrations of crude plant extracts were tested. Table 2 and Graph 1 showed that *Coffea arabica* (Green coffee) was considered the best with LC_{50} values 0.08 with >90% mortality at 160ppm after 24 hours, followed by *Punica granatum* (Pomegranate) and *Camellia sinensis* (Green tea) with LC_{50} values 0.09 and 0.13 with 33% and 67% mortality at 200ppm and 240ppm respectively after 24 hours. The total mortality percentages of *Ae. albopictus* larvae at each concentration after 24 hours are shown in Fig. 1.

Table 2. Result summary of different plant extracts against *Aedes albopictus* larvae after 24 hours of exposure

LC_{50} -Lethal concentration 50 at which 50% of target population died.
LC_{90} - Lethal concentration 90 at which 90% of target population died.
P value - Level of significance $p \leq 0.05$, $p \geq 0.05$ non-significant
LFL = Lower fiducial limit UFL = Upper fiducial limit
SE = Standard Error, $\chi 2$ = Chi-square

Plant extract	Lethal concentration		LFL	UFL	Slope ±SE	χ^2	P-value	Regression equation
Green coffee	LC_{50}	0.08	-1.07	6.23	2.58±2.14	1.1	0.12	Y= - 0.53+2.58X
(*Coffea arabica*)	LC_{90}	0.14	-1.07	6.23	2.58±2.14	1.1	0.12	Y= - 0.53+2.58X
Pomegranate	LC_{50}	0.09	1.99	2.42	2.21±0.13	0.3	0.08	Y= - 0.0189+2.21X
(*Punica granatum*)	LC_{90}	0.17	1.99	2.42	2.21±0.13	0.3	0.08	Y= - 0.0189+2.21X
Green tea	LC_{50}	0.13	-0.28	4.49	2.1±1.67	1.2	0.07	Y= - 0.378+2.10X
(*Camellia sinensis*)	LC_{90}	0.24	-0.28	4.49	2.1±1.67	1.2	0.07	Y= - 0.378+2.10X

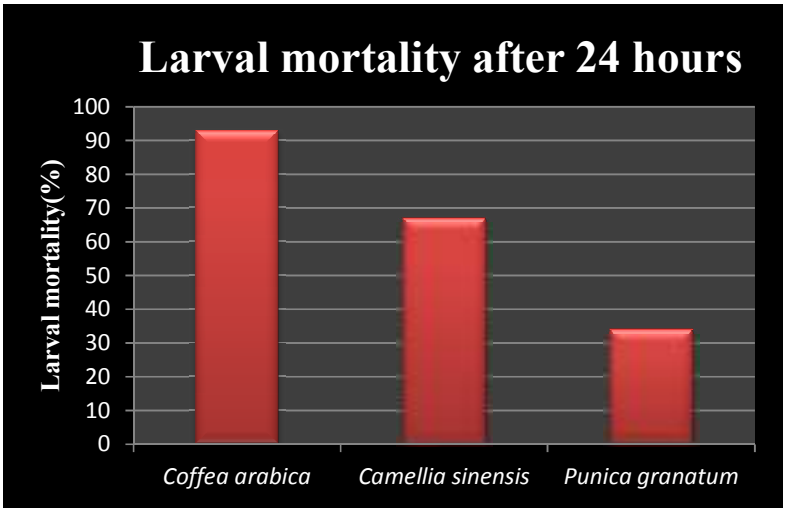

Fig. 1. Total larval mortality after 24 hours

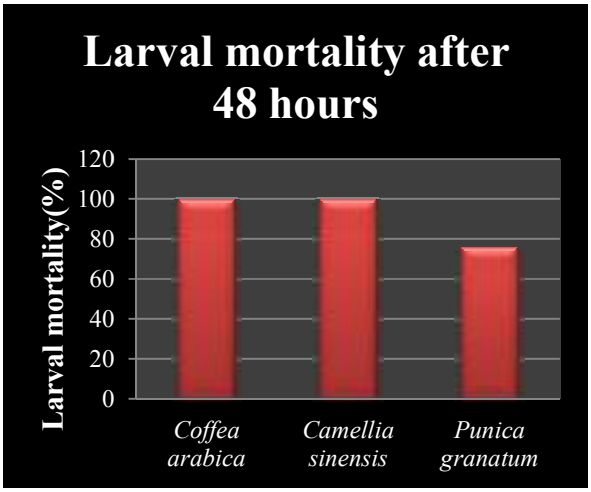

Fig. 2. Total larval mortality after 48 hours

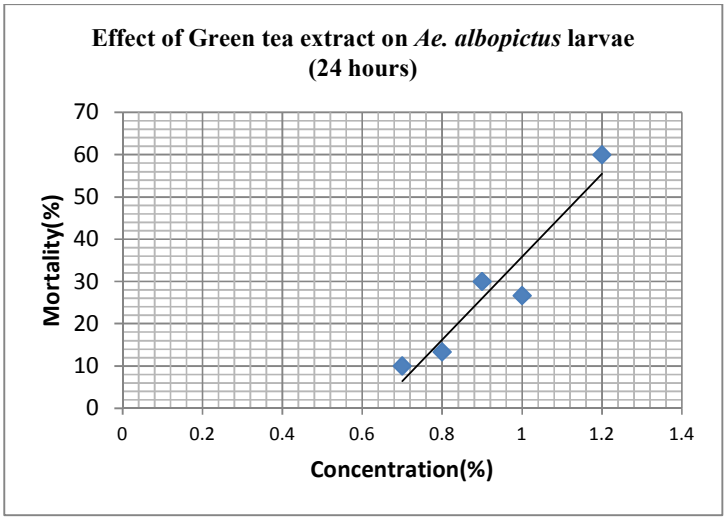

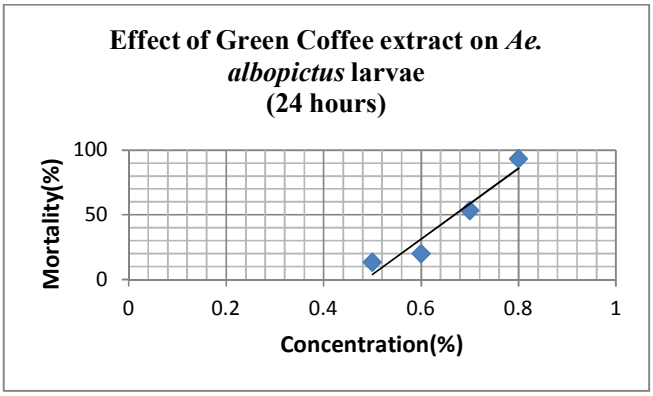

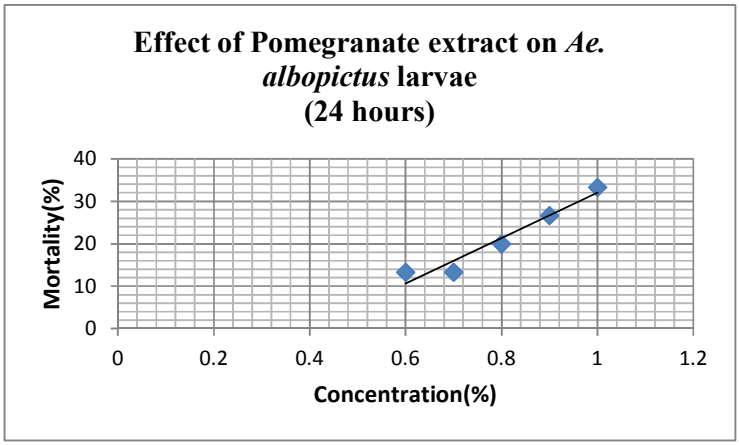

Graph 1. Regression of mortality on different concentration of three plant extract after 24 hours of exposure

The *Coffea arabica* (Green coffee) and *Camellia sinensis* (Green tea) were considered the best with LC_{50} values 0.06 and 0.06 respectively showing 100% mortality at 160ppm and 240ppm respectively after 48 hours, followed by *Punica granatum* (Pomegranate) with LC_{50} values 0.06 exhibiting 66% mortality at 200ppm after 48 hours of treatment (Table 3 and Graph 2). The total mortality percentage of *Ae. albopictus* larvae at each concentration of plant extract after 48 hours of exposure are shown in Fig. 2.

Table 3. Result summary of different plant extracts against *Aedes albopictus* larvae after 48 hours of exposure

LC_{50} -Lethal concentration 50 at which 50% of target population died.
LC_{90} - Lethal concentration 90 $_{at}$ which 90% of target population died.
P value - Level of significance $p \leq 0.05$, $p \geq 0.05$ non-significant
FL = Lower fiducial limit UFL = Upper fiducial limit
SE = Standard Error, χ 2 = Chi-square

Plant extract	Lethal concentration		LFL	UFL	Slope ±SE	χ^2	P-value	Regression equation
Green coffee	LC_{50}	0.06	0.79	5.1	2.95±1.26	0.23	0.02	Y= - 0.288+2.95X
(*Coffea arabica*)	LC_{90}	0.09	0.79	5.1	2.95±1.26	0.23	0.02	Y= - 0.288+2.95X
Pomegranate	LC_{50}	0.06	2.41	2.85	2.63±0.13	0.22	0.05	Y= - 0.0139+2.63X
(*Punica granatum*)	LC_{90}	0.30	2.41	2.85	2.63±0.13	0.22	0.05	Y= - 0.0139+2.63X
Green tea	LC_{50}	0.06	1.36	4.25	2.79±1.01	0.3	0.004	Y= - 0.266+2.79X
(*Camellia sinensis*)	LC_{90}	0.10	1.36	4.25	2.79±1.01	0.3	0.004	Y= - 0.266+2.79X

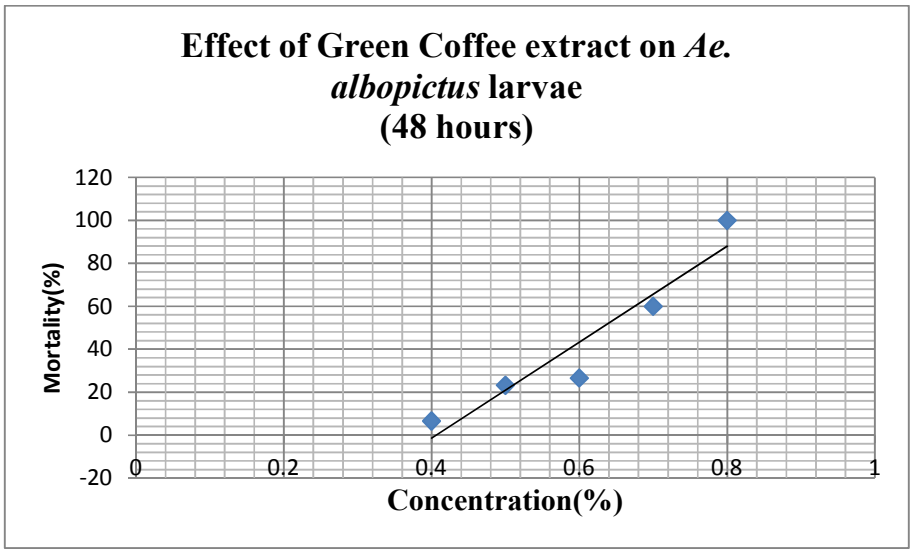

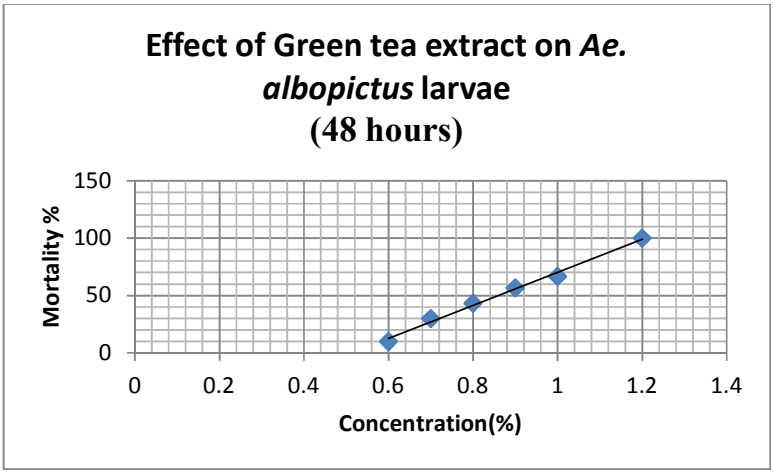

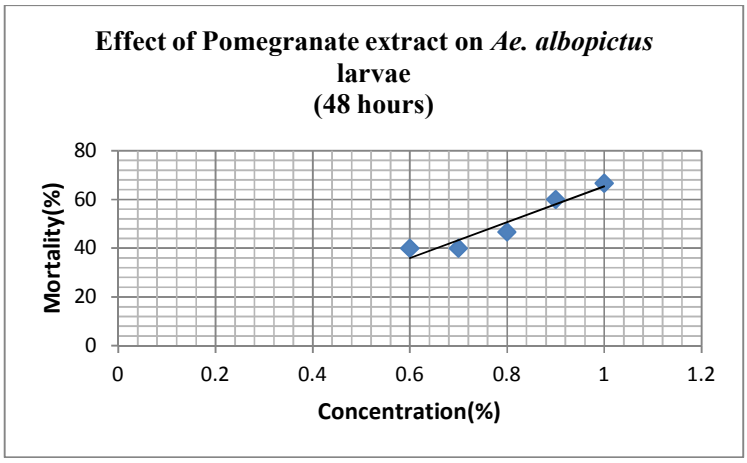

Graph 2. Regression of mortality on different concentration of three plant extract after 48 hours of exposure

Several authors [22,23,24] reported morphological aberrations in mosquito larvae induced by plant extracts. Saranya et al. [23] observed that aqueous leaf extract of *Spathodea campanulata* affect *Aedes aegypti* larval morphology such as dechitinized larva with damaged digestive tract and exuviae of the proceeding instar attached to the dead. Similarly, Arivoli and Tennyson [24] found that after treated with crude leaf extracts of *Abutilon indicum*, larvae of *Aedes aegypti*, *Anopheles stephensi*, and *Culex quinquefasciatus* had striated sclerotization, which appeared to be a feature of pupal cuticle. *Ae. albopictus* larvae in our experiment, when exposed to sub-lethal concentration of crude extract with special reference to green coffee bean showed severe deformities (Fig. 3A-D). Some of the distinct aberrations so far noticed were dechitinized larvae, damaged digestive tract with special reference to twisted digestive tract and appearance of early malformed pupae. During first 24 hours, larvae were flexing to clean their siphon with mouthparts & they stay at bottom of containers. Larvae also showed some kind of restless movement during 48 hours & after this they died in the treated solution.

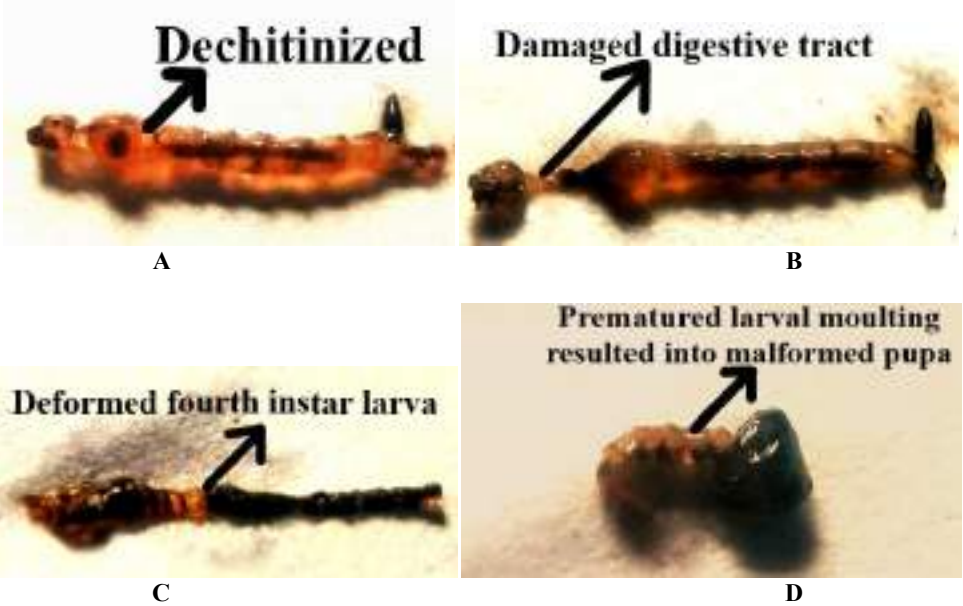

Fig. 3. *Aedes albopictus* larval deformities when treated with green coffee bean extract. A. Dechitinized larva B. Larva with deformed digestive tract. C. Deformed 4th instar larva. Exuviae of the proceeding instar attached to the dead larvae. D. Premature last larval moulting resulted in malformed pupa with some melanisation

4. CONCLUSION

A large number of pant products have been reported to have mosquito larvicidal activity. The present result revealed that chloroform extract of green coffee beans, *Coffea arabica* and methanol extract of green tea leaves, *Camellia sinensis* were the most effective against *Aedes albopictus* larvae showing 100% mortality after 48 hours of exposure. The overall larvicidal trend with reference to LC_{50} after 24 hours and 48 hours was green coffee > green tea > pomegranate. Larval survival and adult emergence was significantly reduced in different sub-lethal concentrations of above mentioned plant extracts over time. The result may be observed due to presence of phytochemicals, having mosquito lavicidal property. Exact phytochemical component and its mechanism of larvicidal activity can be studied further.

In present study, *Ae. albopictus* larvae, exposed to green tea, green coffee & pomegranate extract showed some kinds of deformities like browning of abdomen and twisted abdomen. During first 24 hours larvae were flexing to clean their siphon with mouthparts & they stay at bottom of containers. Larvae showed some kind of restless movement during 48 hours before they died. Exuviae of the late 3rd & late 4th instar larvae attached to the dead larvae were also observed. After 48 hours some dechitinized larvae were found with damaged digestive tract.

In search of alternative and safe methods for controlling larvae of Aedes *albopictus,* the potential vector of Dengue and Chikungunya, these eco-friendly phytochemicals especially green coffee bean extract might prove to be a good vector control tool as safe and cost effective chemicals over more resistant synthetic insecticides.

ACKNOWLEDGEMENT

Authors are grateful to Dr. Subir Chandra Dasgupta, Professor and Head, Department of Zoology, Maulana Azad College, Kolkata, West Bengal, India, for providing necessary laboratory facilities in the execution of this work. The authors also express their sincere thanks to Dr. D. K. Nath, Ex-State Entomologist, Government of West Bengal, for rendering his valuable technical expertise.

COMPETING INTERESTS

Authors have declared that no competing interests exist.

REFERENCES

1. Gratz NG. Critical review of the vector status of *Aedes albopictus.* Medical and Veterinary Entomology. 2004;18:215–227.
2. World Health Organisation: Dengue fact sheet . Available:http://www.searo.who.int/entity/vector_borne_tropical_diseases/data/data_factsheet/en/ 2018
3. Beula JM, Ravikumar S, Ali MS. Mosquito larvicidal efficacy of seaweed extracts against dengue vector of *Aedes aegypti*. Asian Pacific journal of Tropical Biomedicine. 2011;1(2):143-146.
4. Bharati M, Saha D. Insecticide susceptibility status and major detoxifying enzymes' activity in *Aedes albopictus* (Skuse), vector of dengue and chikungunya in Northern part of West Bengal, India. Acta Tropica. 2017;170:112-119.
5. Hawley WA. The biology of *Aedes albopictus*. J. Am. Mosq. Control Assoc. 1988;1:1-39.
6. Tandon N, Raychoudhury S. Reinvasion of Calcutta city by *Aedes albopictus*: the proven vector of Dengue in Suburban areas. Indian J Public Health. 1998;42(1):24–5. PMID: 10389503.
7. World Health Organisation: Insecticide resistance and vector control. XVII report of WHO Expert Committee on Insecticides. WHO Tech Rep Ser. 1970;443:279.
8. Das NG, Goswami D, Rabha B. Preliminary evaluation of mosquito larvicidal efficacy of plant extracts. Journal Vector Borne Disease. 2007;44:145-148.
9. Hayes JB Jr., Laws ER Jr. Handbook of pesticide toxicology. v.1. San Diego, CA: Academic Press; 1991.
10. Hamouda AB, Mechi A, Zarred K, Chaieb I, Laarif A. Insecticidal activities of fruit peel extracts of Pomegranate (*Punica granatum*) against red flour beetle *Tribolium castaneum.* Tunisian Journal of Plant Protection. 2014;9(1):91-100.
11. World Health Organization Global plan for insecticide resistance management in malaria program; 2012. Available:Http://www.who.int/malaria/publications/atoz/gpirm/en/
12. Mukhtar MU, Mushtaq S, Arslan A, Zaki AB, Hammad M, Bhatti A. Laboratory study on larvicidal activity of different plant extracts against *Aedes aegypti.* International Journal of Mosquito Research. 2015;2(3):127-130. ISSN: 2348-5906.

13. Mansour SA, Bakr RFA, Hamouda LSA, Mohamed RI. Toxic and synergistic properties of several botanical extracts against larval and adult stages of mosquito, *Anopheles pharoensis*. Biopestic. Int. 2010;6(2):129-145.
14. Murgan K, Murgan P, Noortheen A. Larvicidal and repellent potential of *Albizziaamara Boivin* and *Ocimum basilicum* Linn against dengue vector, *Aedes aegypti*. Bioresource Technology. 2007;98:198-201.
15. Bhandary SK, Sucheta Kumari N, Bhat VS, Sharmila KP, Bekal MP. Preliminary phytochemical screening of various extracts of *Punica granatum* peel, whole fruit and seeds. Nitte University Journal of Health Science, NUJHS. 2012; 2(4):34-38.
ISSN: 2249-7110.
16. Hostettmann K, Marson A. Saponins. Chemistry and pharmacology of natural products Cambridge: Cambridge University Press. 1995;132.
17. Rampurawala J, Vedamurthy AB, Joy Hoskeri H. A Report on a potent antihelminthic agent – Unbaked *Coffea arabica* bean extracts. Asian Journal of Pharmaceutical and Clinical Research. 2013;6(5):119-121.
18. Muema JM, Bargul JL, Nyanjom SG, Mutunga JM, Njeru SN. Potential of *Camellia sinensis* proanthocyanidines-rich fraction for controlling malaria mosquito populations through disruption of larval development. Parasites and Vectors. 2016;9:512.
19. Radwan SF, Sekina SE. Insecticidal activities of Pomegranate Peels and leave crude juices. Bulletin of Environment. Pharmacology and Life Sciences. 2016;5(3):68-75.
20. Freedman B, Nowak LJ, Kwalek WF, Berry EC, Gutnrie WD. A bioassay for plant derived pest control agents using the European corn borer. J. Econ. Entomol. 1979;72:541-545.
21. WHO. Guidelines for Laboratory and field testing of mosquito larvicides. 2005; WHO/CDS/WHOPES/GCDPP/2005.13.
22. Sharma P, Mohan L, Srivastava C. Phytoextract-induced developmental deformities in malaria vector. Bioresource Technology. 2006;97(14):1599-1604.
23. Saranya M, Mohanraj RS, Dhanakkodi B. Larvicidal, pupicidal activities and morphological deformities of *Spathodea campanulata* aqueous leaf extract against the dengue vector *Aedes aegypti*. Eur. J. Exp. Biol. 2013;3:205–213.
24. Arivoli S, Tennyson S. Larvicidal and adult emergence inhibition activity of *Abutilon indicum* (Linn.) (Malvaceae) leaf extracts against vector mosquitoes (Diptera: Culicidae). J. Biopestic. 2011;4:27–35.

UTTAR PRADESH JOURNAL OF ZOOLOGY

42(1): 40-50, 2021
ISSN: 0256-971X (P)

IMPACT OF UREA ON MONOGASTRIC MAMMALIAN SYSTEM: A SHORT TERM STUDY

SUJIT KUMAR BHOWAL[1*], SUBIR CHANDRA DASGUPTA[1], SUSANTA ROY KARMAKAR[1], ARNAB KAR[2], EERONDYUTI CHAKRABARTY[2], MONALISA GHOSH[2] AND POULAMI DEY[2]

[1]Department of Zoology, MaulanaAzad College, Kolkata -700013, India.
[2]Molecular Cell Biology Lab, Department of Zoology, Maulana Azad College, Kolkata -700013, India.

AUTHORS' CONTRIBUTIONS

This work was carried out in collaboration among all authors. Author SKB designed the study, performed the statistical analysis, wrote the protocol, and wrote the first draft of the manuscript. Authors SCD and SRK contributed in designing the experiments and in analysis of the study. Authors AK, EC, MG and PD managed the literature searches and writing portion of first draft. All authors read and approved the final manuscript.

Article Information

Editor(s):
(1) Dr. Rajib Deb, ICAR-Central Institute for Research, India.
Reviewers:
(1) Luciana Cristina Machado, University of São Paulo (USP), Brazil.
(2) Leandro dos Santos Machado, Universidade Federal Fluminense, Brazil.

Received: 18 November 2020
Accepted: 23 January 2021
Published: 08 February 2021

Original Research Article

ABSTRACT

Urea is a naturally occurring end product of amino acid metabolism in mammalian body. It is also a wide spread fertilizer and considered a nontoxic compound. However repeated exposure to urea has been reported to cause damage to vital body organs like liver, kidney etc. Present study was to evaluate the histopathological effects of urea on liver, kidney and testis as well as their correlation with serum biomarkers ALT, AST concentration as well as investigation of sperm head anomaly. For the study a total of 45 Swiss albino mice were taken and divided into 9 groups each consisting of 5 mice. Group I was kept as control group and given only a normal diet. Remaining groups of animals were given different doses of urea i.e. 50% and 75% of LD_{50} concentrations of urea at different hour intervals i.e. 24, 48, 72, 96 hours. All the animals were kept in standard experimental condition. There was gradual loss of body weight of treated mice with increased dose of urea. The tissue sections revealed histological alteration of the organs in the treatment group mice which may correlate with the increased concentration of serum ALT, AST and sperm head anomaly. The observations of the study also confirmed the toxic effects of the apparently non-toxic compound, urea at high and repeated doses. It is found that the test compound severely damages the histological architecture as well as function of the liver, kidney and testis.

Keywords: ALT; AST; histopathology; kidney; liver; mice; sperm head anomaly; urea.

**Corresponding author: Email: sujit.sb@gmail.com;*

1. INTRODUCTION

Urea (IUPAC name: Carbamide) is not only an acclaimed fertilizer but also a sought-after substitute of protein feed for ruminants as it induces an appreciable synthesis of amino acids in them due to microbial activity. In order to utilize urea as a protein replacement in ruminant diets, several studies were performed during the 1970s and 1980s, specially the effect of urea on intake of dry matter [1], fermentation in rumen [2,3], parameters regarding reproduction and milk yield [4,5]. However, it was concluded that in monogastric animals, on the contrary, the ingestion of urea causes malaise and serves no such effective purpose [6].

In humans, the nitrogen waste synthesized by protein and amino acid metabolism is removed from the body mainly by synthesis of urea via the process of Urea Cycle in the liver [7]. The kidney mainly removes from the blood and excretes through urine. It is one of the main nitrogen-containing metabolites. Various metabolic processes such as urea cycle, arginine and proline metabolism [8], protein metabolism, urea hydrolysis [9] are correlated with the urea production and regulation. In this cycle, ammonia and L-aspartate donates the amino groups that are converted to urea. It is dissolved in blood (in humans in a concentration of 2. 5 - 7. 5 mmol/liter) [10].

With the increase in use of urea as a fertilizer, the field runoffs contribute to the enhanced level of urea content in the water bodies adjacent to agricultural fields. It has been profoundly used in several places to make puffed rice or in fields of rice, vegetables. Consumption of such water and food is frequent by a lot of humans and even animals. Although considered a nontoxic compound, it is a matter to know whether consumption of the urea containing water on a regular basis has any effect on the normal body functioning. Thus, to understand the effect of urea on different visceral organs like liver, kidney, testes, body weight and other biochemical parameters of the body has become an urgent task. In order to evaluate the effect of urea on monogastric mammalian liver, kidney and testis, the following experimental studies were conducted in albino mice (*Mus musculus*).

2. MATERIALS AND METHODS

For the present study inbred strain of Swiss albino mice *(Mus musculus)* reared and maintained in the CPCSEA (Committee for the Purpose of Control and Supervision of Experiments on Animal) approved animal house of the Department of Zoology, Maulana Azad College, Kolkata served as experimental models. Mice were provided with food and water *ad libitum*. Food pellets and bread were provided as the usual food without any animal protein supplementation, unless mentioned otherwise. The experimental protocols were laid down in accordance with the guidelines by the CPCSEA approved Animal Ethics Committee, Maulana Azad College. In the present study for the induction of the test compound, urea (aqueous solution), force feeding method used by several workers was adopted [11]. The urea stock solution (aqueous) was prepared and force feeding was done by oral gavaging at the dose 5.75mg/gm of body weight and 8.625mg/gm of body weight for 50% and 75% of LD_{50} concentrations of urea respectively at 24, 48, 72, 96 hour intervals. The LD_{50} value for mouse i.e. 11500 mg/ kg body weight was noted from European chemical agency website. The body weight was noted and extensive histopathological studies were conducted for different treatment series following the method of Khuda-Bukhsh et al., 2011 [12]. Several biochemical markers, used in predictive risk factor assessment of toxicity, like serum Alanine transaminase(ALT), serum Aspartate transaminase (AST), were assayed (as per Autospan® Test Kit procedure) . In addition, cytological parameter like sperm head anomaly was also thoroughly studied.

Control and Treatment Series: A total of 45 healthy adult mice of either sex weighing between 25 and 30 grams were chosen for all experiments including histological, biochemical and cytological studies. Mice were divided into 9 groups (Group I, II, III, IV, V, VI, VII, VIII, IX) each group is consisted of 5 mice. Animals of each group were sacrificed at the end of each experimental schedule. Blood was collected by heart puncture after the animals were subjected to ether anesthesia before sacrificing them. Tissue fragments from the animals were collected immediately after sacrifice.

Control (Normal):- Group I, fed normal diet and each sacrificed at an interval of 24 hour (i.e. at 24, 48, 72, 96 hour), served as control series.

Treatment Series:-

Groups II, III, IV, V were treated with 50% of LD_{50} concentration.
Groups VI, VII, VIII, IX were treated with 75% of LD_{50} concentration.

Histological studies:-Liver, kidney and testis were taken from the animals immediately after their sacrifice for the study.

Biochemical and Patho-physiological Study:- Blood was collected in siliconized tube by heart puncture after the animals were subjected to ether anesthesia at

the end of an experimental schedule. Serum was isolated from the blood and was used for studying the biochemical and patho-physiological parameters.

Histopathological parameter:-

- **Body weight:**The total body weight of the mice was recorded with the help of a pan balance before they were sacrificed.

- **Preparation of Histology slides:** Histology slides of liver, kidney and testes were prepared. After the mice were sacrificed at different intervals liver, kidney, testes were dissected out immediately and cleaned properly with the help of clean forceps, normal saline (0.89% w/v) and blotting paper. The organs were put into formalin (4% v/v) for fixation. After fixation tissue was embedded in paraffin and then was sectioned in microtome. The standard double staining method using eosin and haematoxylin was followed [13].

2.1 Cytological Parameter

- **Sperm Head Anomaly**

Preparation of Slides: Both the epididymides of the male mice were dissected out and taken separately into 5 ml of 0.87% normal saline. The epididymides were made free of fats, vas deferens and other tissues. The inner content of each side of the epididymis was taken out in normal saline and the materials were thoroughly shaken to suspend the sperm in saline solution. To remove the debris the sperm suspension was filtered through silken cloth and the filtrate was collected in a graduated tube, more normal saline was added to make the volume 10 ml. The collected sperm suspension was put in the centre of a clean slide over which 0.02 ml methanol was added and was allowed to dry. The slide was stained with dilute Giemsa stock solution (6:1) was put on the material. The material was covered with a cover glass and sealed temporarily for observation as per the routine procedure described by Wyrobek 1984 [14]. The percentage of sperm head anomalies was calculated by the formula - No. of sperm with damaged head/ Total no. of sperm observed X100.

- **Patho-physiological parameters**

  - **Collection of blood and isolation of serum:-** Blood (approximately 2.0 ml from each mouse) was drawn from mice by heart puncture after the animals were subjected to ether anesthesia at the end of an experimental schedule using sterile disposable syringe and needle. Immediately it was collected in siliconized tube. Serum was obtained by centrifugation for use in determination of serum ALT and AST.
  - **Serum Alanine aminotransferase (ALT):-** Alanine transaminase (ALT) was analysed by AUTOSPAN® Liquid Gold ALT Test Kit (Ref. No. - 77LS200-60).
  - **Serum Aspartate aminotransferase (AST):-** Aspartate transaminase (AST) was analyzed by AUTOSPAN® Liquid Gold ALT Test Kit (Ref. No. - 77LS200-60).

2.2 Statistical Analysis

All values represented in the experiments are considered as mean ± standard error (S.E.) of five replicas. The mean values were compared between control and treated groups for evaluation of any significant changes by Tukey's Honest Significant Difference test followed by One-way Analysis of Variance test (ANOVA) by using the statistical software SPSS version 16.0 (SPSS Inc., IL, USA). $P < 0.001$ or $P < 0.01$ or 0.05 are considered statistically significant as the case may be.

3. RESULTS

Body weight:-Compared to the control group, body weight was significantly decreased in treated group animals. Both animals treated with 50% of LD_{50} and 75% of LD_{50} dose showed gradual reduction in body weight. At 96 hours of treatment group the body weight decreased significantly ($p<0.01$) (with treatment dose of 75% of LD_{50}) compared 24 hours of treatment. The details of body weight of different groups are demonstrated in Table 1 and Fig. 1.

ALT:-Serum ALT levels were significantly elevated in treated group mice compared to control group (Fig. 2). In the group treated with 50% of LD_{50}, serum ALT level gradually increased up to 72 hour of treatment and decreased after that. In 75% of LD_{50} groups the ALT level reached the highest point (78.32 IU/L) at 72 hours. The details of Serum ALT in all groups with statistical significance are listed in Table 2. Changes in the data in treated animals are significant when compared with the control ($p< 0.05$).

AST:-Serum AST levels were significantly elevated in treated group mice compared to control group (Table 3 and Fig. 3). In 75% of LD_{50} of urea group, serum AST level increased at maximum level at 24 hour (158.38 IU/ L) and gradually decreased after that. In 50% of the LD_{50} group of mice, the AST level gradually increased and reached the highest point of 144.22 IU/L at 72 hour and decreased to 121.80 IU/L at 96 hours. The details of Serum AST in all groups with statistical significance ($p<0.01$) are listed in Table 3.

Table 1. Summarized data of body weight (gm) as observed in 24, 48, 72 and 96 hours both with 50% of LD_{50} dose and 75% of LD_{50} dose of urea in control and treated mice. Data were statistical analysed with one way ANOVA (p< 0.01)**

Duration of treatment (Hour)	Body Weight (gm)		
	Control	50% of LD50	75% of LD50
24 Hr	26.06 ± 0.53	22.92 ± 0.51	22.76 ± 0.46**
48 Hr	26.06 ± 0.53	21.80 ± 0.53**	21.86 ± 0.64
72 Hr	26.06 ± 0.53	19.22 ± 0.43	19.36 ± 0.62**
96 Hr	26.06 ± 0.53	18.78 ± 0.33**	18.82 ± 0.52**

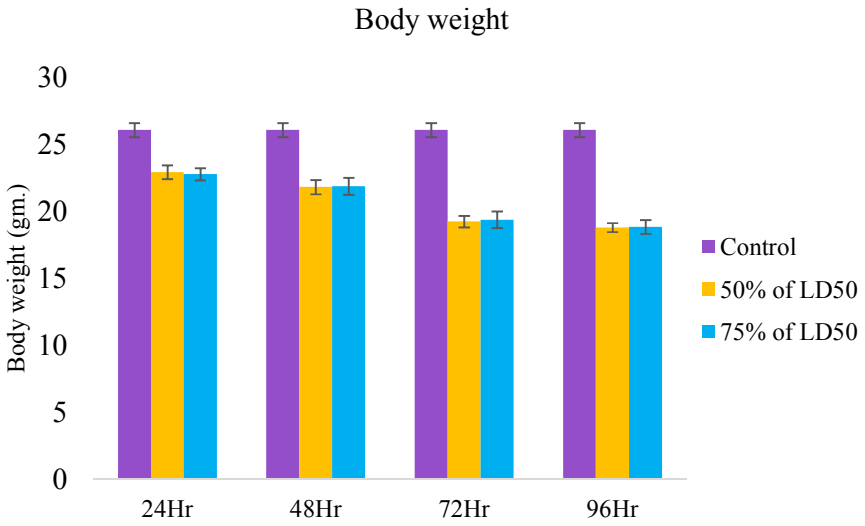

Fig. 1. Histogram of body weight (gm) in control group and 24, 48, 72 and 96 hours of treatment both with 50% of LD_{50} dose and 75% of LD_{50} dose of urea in mice

Table 2. Serum ALT level in control and treated group of animals in 24, 48, 72 and 96 hours both with 50% of LD_{50} dose and 75% of LD_{50} dose of urea. Data were statistical analysed with one way ANOVA (*p< 0.05)

Duration of treatment (Hour)	Serum ALT (Alanine aminotransferase) concentration (IU/L)		
	Control	50% of LD_{50}	75% of LD_{50}
24Hr	36.19 ± 2.32	69.52 ± 2.05*	75.46 ± 5.34
48Hr	36.18 ± 2.31	74.37 ± 2.10	73.38 ± 1.86*
72Hr	36.19 ± 2.32	77.26 ± 2.60*	78.32 ± 1.70
96Hr	36.19 ± 2.32	75.08 ± 4.99*	75.89 ± 3.19*

Table 3. Serum AST level in control and treated group of animals in 24, 48, 72 and 96 hours both with 50% of LD_{50} dose and 75% of LD_{50} dose of urea. Data were statistical analysed with one way ANOVA (p< 0.01)**

Duration of treatment (Hour)	Serum AST (Aspartate aminotransferase) concentration (IU/L)		
	Control	50% of LD_{50}	75% of LD_{50}
24 H	99.85 ± 3.07	117.58 ± 2.93**	158.38 ± 9.65**
48H	99.85 ± 3.07	126.08 ± 1.45	128.73 ± 1.34**
72H	99.85 ± 3.07	144.22 ± 1.06**	130.65 ± 1.01**
96H	99.85 ± 3.07	121.80 ± 1.40**	133.24 ± 1.47

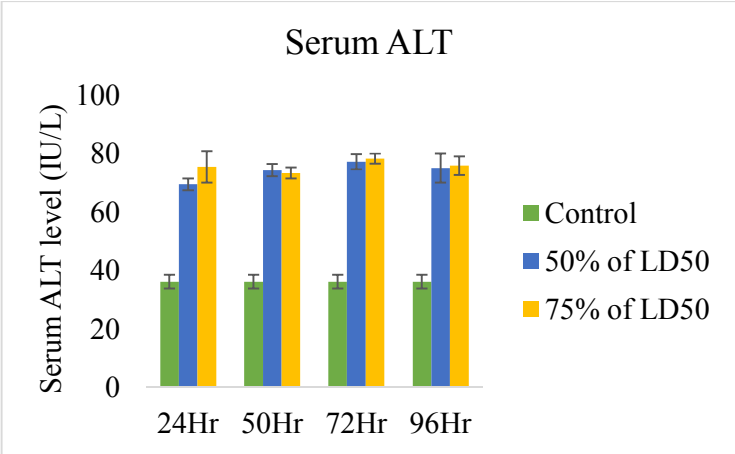

Fig. 2. Histogram of serum ALT in control and treated group of animals in 24, 48, 72 and 96 hours both with 50% of LD_{50} dose and 75% of LD_{50} dose of urea

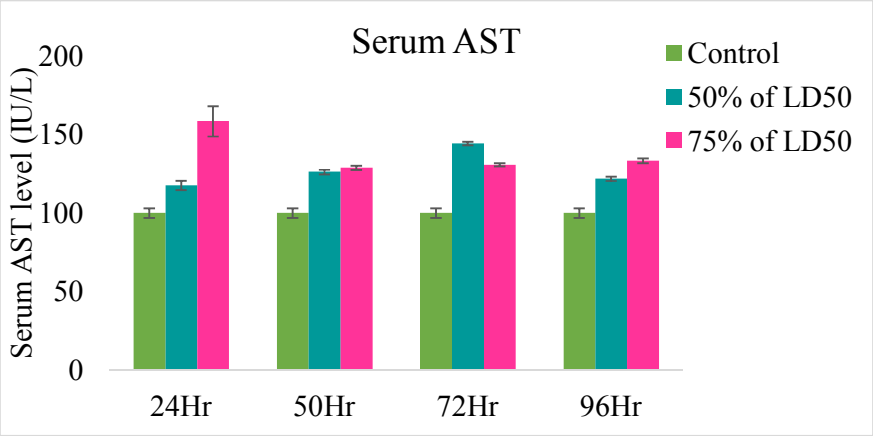

Fig. 3. Histogram of serum AST in control and treated group of animals in 24, 48, 72 and 96 hours both with 50% of LD_{50} dose and 75% of LD_{50} dose of urea

Sperm Head Anomaly:-In the control group of mice 2.88% sperm head anomaly was observed in all treatment duration. So, this could be considered as baseline data for the incidence of sperm head anomaly due to the effect of urea. The frequency of sperm head abnormality was raised gradually in both 50% of LD_{50} and 75% of LD_{50} group of mice (Fig. 4). The summarized data of sperm head anomaly in different groups with statistical significance ($p< 0.01$) are listed in Table 4.

Table 4. Summarized data of sperm head anomaly in control and treated group of animals in 24, 48, 72 and 96 hours both with 50% of LD_{50} dose and 75% of LD_{50} dose of urea. Data were statistical analysed with one way ANOVA (p< 0.01)**

Duration of treatment (Hour)	Percentage (%) of sperm head anomalies <u>No. of sperm with damaged head</u> X100. Total no. of sperm observed		
	Control	50% of LD_{50}	75% of LD_{50}
24Hr	2.88 ± 0.29	12.33 ± 0.84	19.78 ± 0.48**
48Hr	2.88 ± 0.29	18.89 ± 1.42**	24.22 ± 1.56**
72Hr	2.88 ± 0.29	26.56 ± 0.97**	38.33 ± 1.07**
96Hr	2.88 ± 0.29	35.00 ± 0.96**	45.44 ± 1.16**

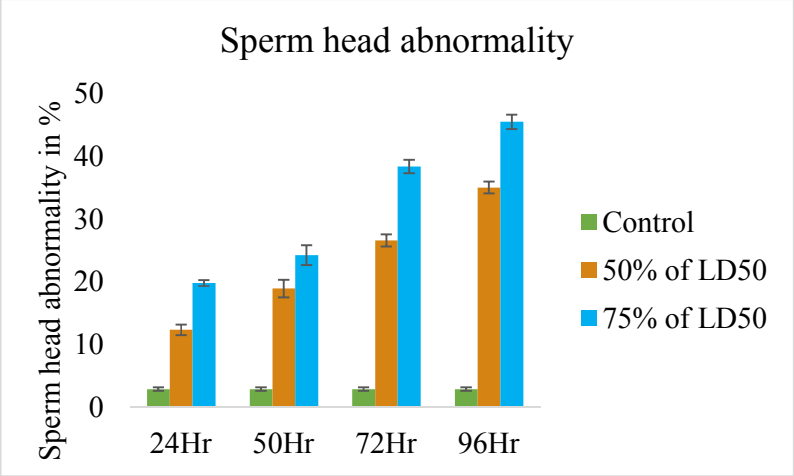

Fig. 4. Histogram of sperm head anomaly in control and treated group of animals in 24, 48, 72 and 96 hours both with 50% of of LD_{50} dose and 75% of of LD_{50} dose of urea. Data were statistical analysed with one way ANOVA (p< 0.01)**

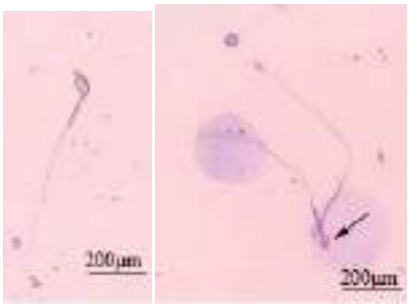

(a) **(b)**

Fig. 5. Photomicrograph of sperm of mouse isolated from control (a) and treated with urea at 96 hours with a concentration of 75% of LD_{50} dose of urea showing head abnormality in mice (b)

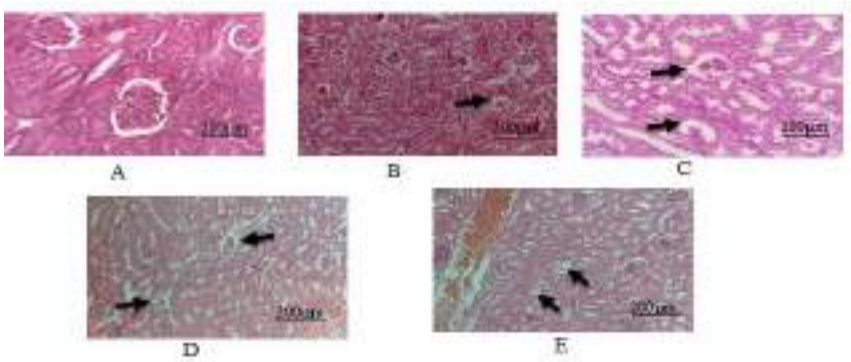

Fig. 6. Histopathological alterations in the cortex region of kidney (sections of kidney H&E stained) in different groups of mice. A) control group i.e. group I, B) Group II (treated with 50% concentration of LD 50 dose of at 24 hours interval), C) Group V (treated with 50% concentration of LD 50 dose of urea at 96 hours interval). D) Group VI (treated with 75% concentration of LD 50 dose of urea at 24 hours interval). E) Group IX (treated with 75% concentration of LD 50 dose of urea at 96 hours interval). The black arrows show the glomerular degradation

Table 5. Histopathological changes in the kidney of mice treated with 50% concentration of LD_{50} dose of urea at different hour intervals (24, 48, 72, 96 hours). +++ denotes the change that was more frequently found in all mice. ++ denotes the change that was less frequently found in all mice. + denotes the change that was rarely found in some mice. ± denotes the change that was very irregular

Histopathological Changes in kidney	Treatment (Dose 50% of LD_{50})			
	24Hr	48Hr	72Hr	96Hr
Glomerular shrinkage and atrophy	++	++	+++	++++
Tubular widened lumen	±	+	++	+++
Renal tubule degradation	±	+	++	+++

Table 6. Histopathological changes in the kidney of mice treated with 75% concentration of LD_{50} dose of urea at different hour intervals (24, 48, 72, 96 hours).++++ denotes the change that was most frequently found in all mice. +++ denotes the change that was more frequently found in all mice. ++ denotes the change that was less frequently found in all mice. + denotes the change that was rarely found in some mice

Histopathological Changes in kidney	Treatment (Dose 75% of LD_{50})			
	24Hr	48Hr	72Hr	96Hr
Glomerular shrinkage and atrophy	++	+++	++++	++++
Tubular widened lumen	+	++	+++	++++
Renal tubule degradation	+	++	+++	++++

3.1 Histological Alteration

Urea treatment induced remarkable changes in both liver and kidney. The following alterations were identified relative to the control group (Group I), which retained an absolute normal structure of both the organs.

Kidney alteration: Changes in glomeruli and tubules were observed. Glomeruli aberrations included degradation, shrinkage and atrophy (Fig. 6 B, C, D, E). For both the doses the severity of such degenerative alterations increased gradually with increase in duration of treatment, evidenced by the rise in the number of atrophied glomeruli at the 72 and 96 hour intervals. Tubules also exhibited degenerative changes involving renal tubule degradation followed by dilation of the tubular lumen. The damage aggravated with the increasing time interval for a particular concentration of dose.

For both the cases the propensity of severity is greater for the 75% of LD50 dose of urea than the 50% of LD50 dose. The observation of histopathological changes of kidney in different groups is listed in Table 5 and Table 6.

Liver alterations: Changes associated with the liver were distortion in the hepatic organization identified by the blurred trabeculae, hypertrophy of hepatocytes owing to cytoplasmic vacuolization (C.V.) and sporadically located necrotic hepatocytes (Fig. 7 B, C, D, E, F)). Among these the vacuolization of hepatocytes seemed to be the most pronounced effect. Compared to the 50% of LD_{50} dose, these negative effects heavily impacted the groups treated with 75% of LD_{50} dose. The onset of the changes occurred at early intervals at high dose and notably delayed at lower dose. The extent of damage apparently thrived by several folds with the increase in dose. The observation of histopathological changes of kidney in different groups is listed in Table 7 and Table 8.

Testis alterations: Due to urea administration various histopathological changes of testis such as apoptotic spermatogonia, irregular and distorted arrangement of spermatogenic cells and shedding of cellular material in the seminiferous tubules were observed in the treated group (Fig. 8). Vacuoles were also found in the seminiferous epithelium of testis. Changes were more prominent in the groups treated with 75% of LD_{50} than the changes in 50% of LD_{50} groups. The observations of histopathological changes in testis are summarized in Table 9 and Table 10.

4. DISCUSSION

Urea toxicity causes damages of tissues of various vital organs when they are administered through oral route in mouse. The study of body weight is one of the main criteria to gauge the toxic effects of the compound as changes in body weight may be attributed to alteration in biochemical reactions induced by treatment- induced toxicity [15]. The readings, obtained from the study shows a gradual decrease in the body weight of the treated groups of mice with increasing doses of urea. The significant decrease in body weight is also evident from the statistical evaluation ($p< 0.01$), whereas in control there is no such significant change. These outcomes

are in accordance with the studies conducted by Moqbel et al., 2017 in Albino mice [16].

The liver is susceptible to damage from direct exposure to toxic products because it participates in the metabolic detoxification of products and xenobiotics [17]. Alanine aminotransferase (ALT) and Aspartate aminotransferase (AST) are widely used as serum biomarker of hepatic injury. In rodents, the level of ALT and AST increased with body weight gain in normal condition [18]. But, in this study the significant elevation of ALT ($p<0.05$) and AST ($p<0.01$) in treatment group mice, compared to control group mice in both 50% and 75% of LD_{50} concentration may indicate to the damages related to permeability of hepatocyte membrane. After detailed microscopic observation it may be assumed that scattered necrotic liver cells [19] occurred along with cytoplasmic vacuolization of hepatocytes.

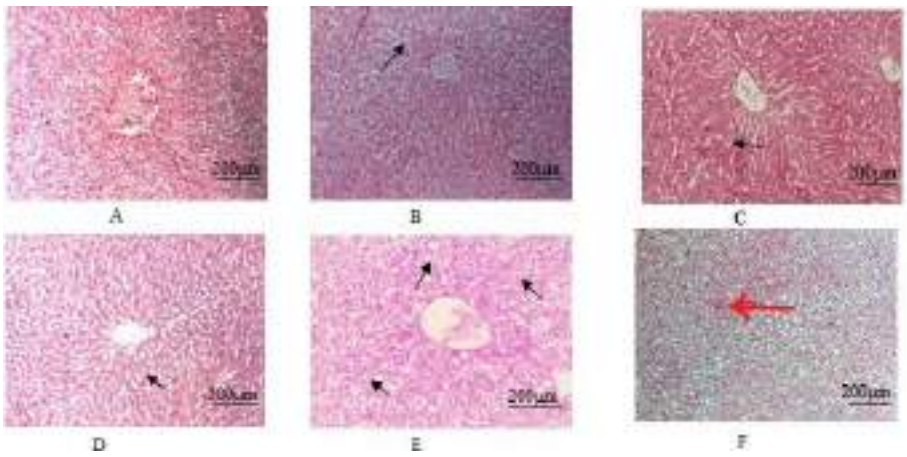

Fig. 7. Histopathological alteration of liver (sections of liver H&E stained) in different groups of mice. A) control group i.e. group I. B)Group II (treated with 50% concentration of LD_{50} dose of at 24 hours interval). C) Group V (treated with 50% concentration of LD_{50} dose of urea at 96 hours interval). D) group VI (treated with 75% concentration of LD_{50}dose of urea at 24 hours interval). E) and F) Group IX (treated with 75% concentration of LD_{50}dose of urea at 96 hours interval). The black arrows show the cytoplasmic vacuolization (C.V.) of hepatocytes and the red arrow shows the necrotic changes (N.C.) in hepatocyte

Table 7. Histopathological changes in liver of mice treated with 50% concentration of LD_{50} dose of urea at different hour intervals (24, 48, 72, 96 hours). +++ denotes the change that was more frequently found in all mice. ++ denotes the change that was less frequently found in all mice. + denotes the change that was rarely found in some mice. ± denotes the change that was very irregular

Histopathological Changes in liver	Treatment (Dose 50% of LD_{50})			
	24Hr	48Hr	72Hr	96Hr
Distortion in hepatic organization	++	+++	++++	++++
Cytoplasmic vacuolization of Hepatocyte	+++	+++	++++	++++
Necrotic changes in hepatocytes	++	+++	+++	++++

Table 8. Histopathological changes in the liver of mice treated with 75% concentration of LD_{50} dose of urea at different hour intervals (24, 48, 72, 96 hours). ++++ denotes the change that was most frequently found. +++ denotes the change that was more frequently found in all mice. ++ denotes the change that was less frequently found in all mice. + denotes the change that was rarely found in some mice

Histopathological Changes in liver	Treatment (Dose 75% of LD_{50})			
	24Hr	48Hr	72Hr	96Hr
Distortion in hepatic organization	±	+	+	++
Cytoplasmic vacuolization of Hepatocyte	+	++	++	+++
Necrotic changes in hepatocytes	±	+	++	+++

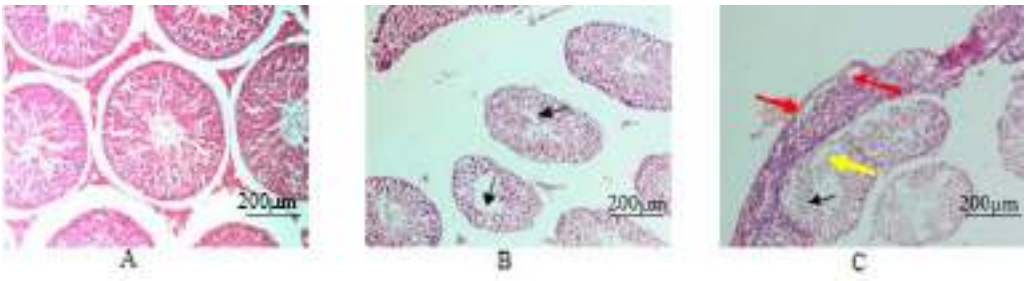

Fig. 8. Histopathological alterations in testis (sections of testis H&E staining) of different groups of mice. A) Control group i.e. group I, B) and C) Group IX (treated with 75% concentration of LD_{50} dose of urea at 96 hours interval). The black arrows show loss of spermatids in the seminiferous tubule, the red arrows show vacuole formation in epithelium and the yellow arrow shows the irregular and distorted arrangement of cells in seminiferous tubules

Table 9. Histopathological changes in testis of mice treated with 50% concentration of LD_{50} dose of urea at different hour intervals (24, 48, 72, 96 hours). +++ denotes the change that was more frequently found in all mice. ++ denotes the changes that was less frequently found in all mice. + denotes the change that was rarely found in some mice. ± denotes the change that was very irregular

Histopathological Changes in testis	Treatment (Dose 50% of LD_{50})			
	24 Hr	48Hr	72 Hr	96 Hr
Distorted arrangement of cells in the seminiferous tubule	+	++	+++	+++
Presence of vacuole in the epithelium of seminiferous tubule	±	+	++	+++
Loss of spermatid	+	++	+++	+++

Table 10. Histopathological changes in testis of mice treated with 75% concentration of LD_{50} dose of urea at different hour intervals (24, 48, 72, 96 hours). ++++ denotes the change that was most frequently found. +++ denotes the change that was more frequently found in all mice. ++ denotes the changes that was less frequently found in all mice

Histopathological Changes testis	Treatment (Dose 75% of LD_{50})			
	24 Hr	48Hr	72 Hr	96 Hr
Distorted arrangement of cells in the seminiferous tubule	++	+++	++++	++++
Presence of vacuole in the epithelium of seminiferous tubule	++	+++	+++	++++
Loss of spermatid	+++	+++	++++	++++

Kidney is an organ which is composed of renal tubule system, properly developed glomeruli and numerous renal corpuscles. The present study shows several histopathological alterations in kidney of urea treated mice including glomerular shrinkage and atrophy, tubular widened lumen and renal tubule degradation. The control group does not exhibit any kind of abnormalities in the structure of kidney. In another study it has been reported that the histological structures of kidney are severely affected in male albino rats treated with abamectin [20]. Detection of toxicity of various compounds on several animal tissues and organs can easily be evaluated by histopathological alterations [21].

Sperm quantity and quality are also found to be greatly affected in the treated mice compared to the control group. Damages in testicular tissues forming vacuoles in seminiferous tubules along with loss of spermatids are observed which increase along the elevating dose of urea. The statistical data is at par with the observations and indicates a significant difference in sperm count between treated and control groups ($p<0.01$).

The sperm head morphology of urea treated mice is observed viz amorphous head, short tail, hookless head and the data is similar to the kind of sperm head anomalies reported in gamma ray induced mice [22].

The frequency of sperm head anomaly is raised gradually in both 50% of LD_{50} and 75% of LD_{50} group of mice. From this study it can be observed that urea seems to have cytotoxic effects on various organs, tissues, cells and biochemical profiles under investigation in the experimental animal model, mouse.

5. CONCLUSION

The findings of this study indicate that oral intake of high urea concentration is capable of inducing adverse effects on visceral organs like liver, kidney, testis in mouse model which is further revealed by histopathological evidences. The significant decrease in the body weight of the treated animal indicates probable deleterious effect of urea in higher concentration. The marked changes in the levels of the liver biomarkers in the blood serum strengthen the fact that damage occurred due to acute toxicity in different time intervals. Elevated levels of ALT and AST in blood serum suggest the detrimental effect of urea in hepatic tissue. Urea also exhibits cytotoxic effects on the body as emanated from the lower sperm count in males, orally gavaged with urea solution and rise in sperm head anomalies. Higher concentration of urea also causes damage to the renal glomerular structure as well as to the renal tubules; thus, indicating a decreased effectiveness of kidney function. Necrotic damage and cytoplasmic vacuolization in the hepatic tissue are also observed which indicate possible reason for decline in the liver functionality. The test chemical on the other hand exerts damage in the testicular tissue by forming vacuoles in the germinal epithelium of the seminiferous tubules, loss of spermatogenic cells ultimately causing cellular irregularities in the seminiferous tubules. Therefore, it can be said that short term oral administration of aqueous solution of urea in this monogastric mammal has an acute deleterious effects on liver, kidney and testis which indicates to possibly cause such kind of deleterious effects in human also. Further study at biochemical and molecular level may reveal toxic impact of urea on cellular protein and associated genetic set up in mouse.

ETHICAL APPROVAL

The experimental protocols were laid down in accordance with the guidelines by the CPCSEA approved Animal Ethics Committee under the supervision of the Animal Ethics Committee vide F. No. – 25/250/2012-AWD, dated 26.02.2014.

ACKNOWLEDGEMENTS

We are privileged to convey our sincere gratitude to the principal, Maulana Azad College, Kolkata for providing laboratory facilities and financial support under DBT Star College Scheme to conduct the work. We also extend our thanks to Dr. A. Mukherjee, Asst. Professor, Maulana Azad College for assisting us in statistical analysis.

COMPETING INTERESTS

Authors have declared that no competing interests exist.

REFERENCES

1. Kertz A, Davidson L, Cordes B. Ruminal infusion of ammonium chloride in lactating cows to determine effect of pH on ammonia trapping. J Dairy Sci. 1983;66(12):2597-2601.
2. Wilson G, Martz F, Campbell J, Becker B. Evaluation of factors responsible for reduced voluntary intake of urea diets for ruminants. J Anim Sci. 1975;41(5):1431-1437.
3. Pisule Ski PM, Okorie AU, Buttery PJ, Haresign W, Lewis D. Ammonia concentration and protein synthesis in the rumen. J Sci Food Agric. 1981;32(8):759-766.
4. Ryder W, HillMan D, Huber J. Effect of feeding urea on reproductive efficiency in Michigan Dairy Herd Improvement Association herds. J Dairy Sci. 1972;55(9): 1290-1294.
5. Erb R, Brown C, Callahan C, Miller N, Hill D. Dietary urea for dairy cattle. II. Effect on functional traits. J Dairy Sci. 1976;59(4):656-667.
6. Ignarro LJ, Buga GM, Wei LH, Bauer PM, Wu G, del Soldato P. Role of the arginine-nitric oxide pathway in the regulation of vascular smooth muscle cell proliferation. Proc. Natl. Acad. Sci. 2001;98(7):4202–4208.
7. Berg JM, T JL, Stryer L. Biochemistry. 6th. W. H. Freeman and Company; New York. Protein Turnover and Amino Acid Catabolism. 2007;649-678.
8. Wu G, Morris SM. Jr. Arginine metabolism: nitric oxide and beyond. Biochem J. 1998;336:1–17.
9. Young VR, El-Khoury AE, Raguso CA, Forslund AH, Hambraeus L. Rates of urea production and hydrolysis and leucine oxidation change linearly over widely varying protein intakes in healthy adults. J Nutr. 2000;130(4):761–766.
10. Human Metabolism Database (HMBD). Available:http://www.hmdb.ca/metabolites/ HMDB0000294.
11. Bunyan J, Murrell EA, Shah PP. The introduction of obesity in rodents by means of

monosodium glutamate. Br. J. Nutr. 1976; 35:25-39.

12. Khuda-Bukhsh AR, Banerjee A, Biswas SJ, Karmakar SR, Banerjee P, Pathak S. An initial report on the efficacy of a millesimal potency Arsenicum Album LM 0/3 in ameliorating arsenic toxicity in humans living in a high-risk arsenic village. Zhong Xi Yi Jie He XueBao. 2011;9:596-604.
13. Bhowal SK, Lala S, Hazra A, Paira P, Banerjee S, Mondal NB, Chakraborty S. Synthesis and assessment of fertility-regulating potential of 2-(2″-chloroacetamidobenzyl)-3-(3′-indolyl) quinoline in adult rats as a male contraceptive agent. J. Contraception. 2008;77(3):214-222.
14. Wyrobek AJ, Watchmaker G, Gordon L, Handbook of Mutagenicity testing protocols Eds. Kilbey BJ, Legator M, Nicholas W, Ramel C. Elsevier Science. 1984;733-750.
15. Mansour SA, Mossa AH. Oxidative damage, biochemical and histopathological alteration in rat exposed to chlorpyrifos and the role of zinc as antioxidant. Pesticide Biochemistry and Physiology. 2010;96:14-23.
16. Fahmi S Moqbel, Mohammed AY Al-Eryani, Fahd M Abd Al Galil. Histopathological and biochemical effects of abamectin on kidney in male albino rats. Journal of Entomology and Zoology Studies. 2017;5(2):245-249.
17. Abd-Elhady K, Abou-Elghar E. Abamectin induced biochemical and histopathological changes in the albino rat, *Rattus norvegicus*. J. Plant Prot. Res. 2013;53:263–270.
18. Toita R, Kawano T, Fujita S, Murata M, Kang JH. Increased hepatic inflammation in a normal-weight mouse after long-term high-fat diet feeding. J Toxicol Pathol. 2018;31(1):43-47.
19. Khadhair AA, Majeed KS. Study the toxicity of digoxin on liver and their transaminase enzymes level in rat. Kufa Journal for Vet Medical Science. 2017;8(2):73-80.
20. Fahmi S Moqbel, Mohammed AY Al-Eryani, Fahd M Abd Al Galil. Histopathological and biochemical effects of abamectin on kidney in male albino rats. Journal of Entomology and Zoology Studies. 2017;5(2):245-249.
21. Khaldoun-Oularbi H, Richeval C, Djennas N, Lhermitte M, Humbert L. Effect of sub-acute exposure to abamectin ‘‘insecticide’’ on liver rats (*Rattus norvegicus*). Annales de Toxicologie Analytique. 2013;25:63-70.
22. Khan S, Adhikari JS, Rizvi M, Chaudhury MK. Radioprotective potential of melatonin against ^{60}Co γ-ray-induced testicular injury in male C57BL/6 mice. J. Biomedical Sci. 2015;22:61.

UTTAR PRADESH JOURNAL OF ZOOLOGY

42(3): 54-65, 2021
ISSN: 0256-971X (P)

CONSERVATION AND TRADITIONAL MANAGEMENT OF SACRED GROVES IN THE DISTRICT OF NADIA, WEST BENGAL, INDIA

SUJIT KUMAR BHOWAL[1*]
[1]Department of Zoology, Maulana Azad College, Kolkata, 700013, India.

AUTHOR'S CONTRIBUTION
The sole author designed, analysed, interpreted and prepared the manuscript.

Article Information

Editor(s):
(1) Dr. Tunira Bhadauria, Feroz Gandhi P.G. Degree College, India.
Reviewers:
(1) Matías Barceló, Pontificia Universidad Católica de Chile, Chile.
(2) Francisco Javier Rendón Sandoval, Universidad Nacional Autónoma de México (UNAM), Mexico.

Received: 17 December 2020
Accepted: 22 February 2021
Published: 08 March 2021

Original Research Article

ABSTRACT

Patches of socially protected forests or sacred groves (SGs) grown around places of local deities and/ or ancestral spirits are very ancient, and once was widespread in most parts of the state of West Bengal, including Nadia district. The causes of their dwindling count may be attributed to various reasons, most of them being anthropogenic. They are the rich biodiversity heritage of the state and play an important role in the religious and sociocultural life of the local people. Being self-ecosystems, they perform most of the ecological functions. Many threatened species have been found to be safely protected in the SGs. The district of Nadia in West Bengal is enriched with SGs for conserving local beliefs. Altogether 60 SGs were studied in different corners of Nadia, West Bengal. People across caste and creed are engaged in protecting age old faiths in old plants, their day to day medicinal uses and thus eventually conserving them. By doing this, they are also helping toward the sustenance of animals living on these old plant populations leading to the conservation of local biodiversity in such SGs. With continuous endeavour and active participation of women, the general people mostly from rural areas of the district are helping the state biodiversity conservation authority to conserve the heritage of these biodiversity sites across the district through financial and logistic aid. Conservation and judicious management of SGs are integral part of the aspiration of local population who are also got benefited from sharing of the resources from such areas.

Keywords: Benefit sharing; biodiversity; conservation; heritage site; sacred grove; traditional management.

1. INTRODUCTION

There are different traditional forms of worship of nature by various communities in India including West Bengal. One such significant tradition is that of providing protection to patches of forests dedicated to deities and/or ancestral spirits. These patches of forests are known as sacred groves (SGs) as defined

**Corresponding author: Email: sujit.sb@gmail.com;*

by Malhotra et al. [1]. The institution of SGs is very ancient and once was widespread in most parts of the state of West Bengal. About 670 SGs in this region have so far been reported. They play an important role in the religious and sociocultural life of the local people [2,3]. They are also rich biodiversity heritage sites of the state and are ecosystems by themselves and perform all the ecological functions. Many threatened, endangered and rare species find protection in such SGs [4-7]. The groves are rich in biological wealth of the state. Many threatened species are found to get safe refuge in these culturally protected areas [8,9]. The district of Nadia in West Bengal is a rich area of socio-cultural heritage pertaining to the maintenance of SGs for conserving local belief in supernatural existence. People across caste and creed are engaged in protecting age old faiths in old plants, their day to day medicinal uses and ultimately conserving them and thus providing valuable aid to the sustenance of animals living on these old plant population or forest patches [10-12]. Thus, existence of such SGs depends on the local faith of the people of the district. This also leads to the conservation of local biodiversity [13-15] associated with the SGs. Many investigatory work on SGs have been carried out such as their interactive association with the tribes of India as described by Das et al. [2], regarding wealth of SGs in Telangana, India [6] as well as ethnobotanical study of medicinal plants used in SGs of Kumaon Himalaya, Uttarakhand, India [10] and biodiversity management of SGs in the region of Western Himalaya [16]. There are reports on studies on SGs along the Western Ghats from Maharashtra and Goa [13,17], components of SGs of Karnataka [15], Manipur [18], Kerala [19,20], Andhra Pradesh [21] and Meghalaya [22]. Literature about biodiversity management of SGs [23] is also available including conservation tradition of SGs in India as described by Gokhale [24]. Significant role of SGs in conserving the local biodiversity was also studied by Khan et al. [25]. In this current work role of traditional practices of local people for conserving the SGs, their relationship with the vision of the local communities including characterization of the SGs spread across the district of Nadia are conducted.

2. MATERIALS AND METHODS

2.1 Study Area

Nadia is a vast district with an area of 3927.45 sq km and comprises 4.42% of total area of West Bengal. Total human population is 5,168,488 (2011 Census) and population density is 1,300/km^2. It is mainly a rural district with 17 blocks and having long international border with neighbouring country, Bangladesh [18,26]. The geographical boundary of Nadia district comprises Bangladesh in the East, Bardhaman and Hoogli district on the West, Murshidabad district on the North and North West and North 24 Parganas towards South and South East. Situated on the main rail route connecting Howrah/Kolkata the Nadia district is easily accessible by rail and also well connected by National Highway-34. Average elevation of the district land is 12-15 meters from sea level [26].

2.2 Drainage and River Basin

The district has a number of major rivers, bils (large freshwater bodies) as given in the following Chart 1.

Apart from these, there are numerous jheel, dighi (other large freshwater bodies) and various smaller water bodies spread throughout the district [27]. Drainage system is a very important component of SGs as many of them are located just beside or at the vicinity of a river or water body. Located in gangetic river basin the soil gets ample supply of water from the ground water sourced from river and associated drainage system. The vegetation and green pasture of the SGs require sufficient supply of water. The plants are at the bottom of the food chain of SGs and surrounding area. The faunal diversity of the area is also dependent on the availability of sufficient water.

2.3 Climate

The average temperature of the area varies from 9°C in winter to 42°C in summer. Average humidity range is 46% to 92%. Average annual rainfall varies from 167.0 to 994.1 mm.

Chart 1. Major rivers and water bodies of Nadia district

Nature	Name
1. River	Jalangi (Khore), Churni, Bhagirathi or Hoogly, Ichhamati, Jamuna, Mathabhanga, Anjana, Paglachandi, Jhor, Palda
2. Bil	Kulia, Khalsi, Chamta, Garar doah, Gazna bayor, Bathangachhi, Putikhali bil, Majher doah, Haldir bil, Horse bow lake, Hasadanga bil

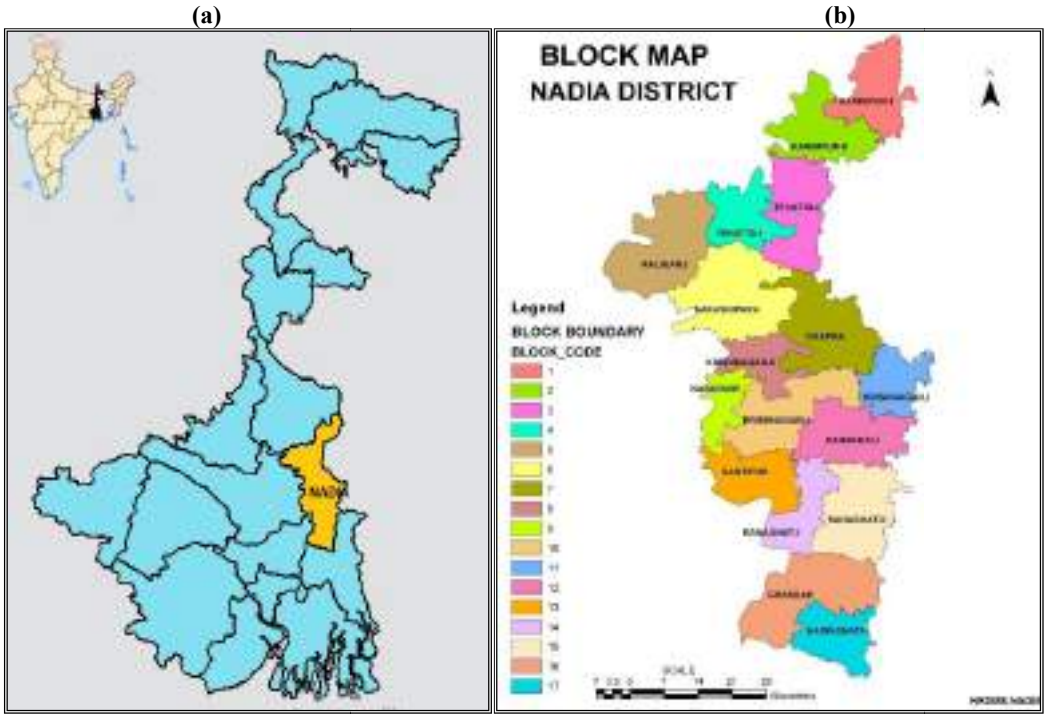

Plate 1. Map of West Bengal showing (a) location of Nadia district in West Bengal. (b) blocks in Nadia district.(www.nadia.nic.in/District_Profile/district_profile.html)
Map source: NRDMS/Nadia

2.4 Soil and Agriculture

Soil is the most important ingredient for vegetations to thrive. The soil type of Nadia district is Ganga flat land type. It is a mixture of clay and fine sand with sufficient content of dead biomass. At places subsoil still contain free calcium carbonate. The sand proportion is predominantly finer in size and whitish grey in colour [26]. This soil texture supports vegetation well. Nadia remains evergreen with canopy of large trees and seasonal field crops throughout the year for its plenty of underground water and soil type (new alluvium).

2.5 Culture

High birth rate among poor villagers and influx of people from neighbouring country rendered a considerable increase of human population in this district for last few decades. This, to some extent, imparts socio-cultural exchange. But the gradual increase in human population affected the ecological balance of many areas of this district. Moreover, establishment of new human habitat areas, sometime, required destruction of forest patches, adjacent to old dilapidated mansions or monuments (considered as SGs) might have disturbed and shrink these SGs for last few decades. Nadia district has a proud tradition in century old "Dochala" & "Charchala" & "Aatchala" terracotta temples [27].

2.6 Methods

1. **Interactive method:** Interaction, discussion and interviewing local people, temple committee, members of trustee boards of a temple developed at SGs. In general, the area surrounding these groves has been becoming populated by human habitation. Many of the endemic species of fauna and flora of rural Nadia districts decreased in abundance. Some are not even found today. The information was gathered by conversation with the local people, villagers or members of the temple committee if the sacred grove turned into a temple partly or as a whole. Photographs were taken of important SGs [17,19,23].
2. **Direct visit and observation of SGs:** Necessary information was also gathered by visiting the SGs including their direct observation.
3. **Collection of information:** Information regarding components and composition of SGs were collected along with their GPS location with the help of etrex model.

4. **Photographic documentation:** Photographs were taken with Canon DSLR camera.

Mode of transport: Hired taxi, two-wheeler motorcycle, cycle van, toto rickshaw were used for the purpose of visiting the sacred grove areas across Nadia district.

District Blocks covered for the study: Primary information of 75 sacred groves was gathered from various sources from 17 Blocks of Nadia district. The SGs were then separately visited and relevant information was gathered. After proper observation 60 such SGs were finally considered depending on their flora and fauna composition, historical perspective, and faith of the local people. The rest 15 SGs were excluded on the ground that either they comprise of a single old banyan, ashwatha or other tree or even the trees were shredded for infrastructural work like highway construction. These single tree SG-like areas also have a small temple or the tree itself is worshipped. Pictures of some of such old trees are given below in Plates 6 and 7.

Plate 2. Picture showing local people at Burimaa tala, Nakashipara, Nadia who gave information about the SG

Plate 3. GPS machine being used to collect GPS location of a SG

Plate 4. Portion of a sacred grove in Nadia

Plate 5. Part of Burima Talaa SG, Nakashipara, Nadia

Chart 2. List of 17 administrative blocks of Nadia district that were covered during survey

1.	Karimpur-1	9.	Krishmagar-2
2.	Karimpur-2	10.	Nabadwip
3.	Tehatta-1	11.	Shantipur
4.	Tehatta-2	12.	Krishnaganj
5.	Kaliganj	13.	Hanshkhali
6.	Nakashipara	14.	Ranaghat-1
7.	Chapra	15.	Ranaghat-2
8.	Krishnagar-1	16.	Chakdaha,
		17.	Haringhata.

Plate 6. A very old Banyan tree at Dhubulia, NH 34, Nadia

Plate 7. An isolated banyan tree beside Khedaitala Manasha Than, Chakdaha, Nadia

2.7 Identification of Plants and Animals

The study involves multi-taxa approach and the biodiversity components are studied on spatial and temporal (monsoon, pre-monsoon and post-monsoon) basis. Diversity of flora was assessed and identified by taxonomic expert or consulting taxonomy book or using standard monogrphs of Botanical Survey of

India (BSI), Kolkata [28,29]. In the same way faunal diversity was assessed by random sampling, visual encounter survey and focal count. Identifications of various taxa were carried out by following standard identification manuals. Large mammals were surveyed either by direct sighting or indirect evidences such as hoof mark/ pug mark, scat/ droppings scrape, sound and presence status from local people [30]. Smaller mammals such as rats and mice were surveyed by turning earth rocks, stones, bricks carefully using a torch light in case they were hiding in earth hole following Menon [31]. Bird watching was done mostly during morning time and also random surveys were carried out during other parts of day. Binocular (Olympus 8X40 DPSI) and Canon DSLR camera were used during the survey and identification was done by using Ali [32] and Grimmett et al. [33]. Amphibian and reptiles were surveyed by searching micro-habitats preferred by different species and identification was carried out by following Dutta et al. [34]. Butterflies are diurnal species and are hostspecific. Hence distribution of plants in a sacred grove is related to the butterfly diversity. Arachnids, such as spiders, scorpions etc. were recorded by searching them among bushes, on trees and on forest floor. Photographs were taken for identification and species level identification was carried out by following field guides and literatures such as Venkataraman [35] and Tikadar and Bustawade [36].

2.8 Biodiversity Assessment

The biodiversity between some selected sacred groves were evaluated using Shanon Weiner Index and Similarity Index using standard softwares and the data were analyzed to compare the diversity among different groves of Nadia district [30]. For calculating similarity index, I consider the most simple and widely used, the Jaccard index (Jaccard, 1912) to evaluate species similarity among different sites .Values for all indices vary from 0, least similar, to 1, most similar. The Jaccard index is calculated using the equation:

$$C_J = a / (a + b + c)$$

Where, a = the number of species common to both communities; b = the number of species in community B, but not A; c = the number of species in community A but not B [27].

2.9 Statistical Analysis

The computer statistical package Microsoft, SPSS version 16.0, SPSS Inc., IL, USA and Biodiversity pro 2.0 for Window Version 10 were used for statistical analysis [30].

3. RESULTS AND OBSERVATION

After detailed observation of sixty sacred groves documentation of biodiversity was carried out. In sixty out of seventy five sacred groves spread in seventeen blocks of the district of Nadia, West Bengal good diversity of fauna and flora was found. Maximum SGs were recorded in Krishnagar-1 block (ten) whereas minimum number was recorded in both Ranaghat-2 and Karimpur-2 blocks (each having one SG). Total of 151 species of plants that includes 72 species of trees, 33 species of herbs, 24 species of shrubs, 20 species of climbers and 2 species of orchids) and 7 species of lower plants (2 lichens and 3 bryophytes and 2 pterydophytes) were recorded from these sacred groves. Likewise 15 species of fungi were recorded from all the groves. The faunal diversity in the sacred groves includes 18 species of mammals, 57 species of birds, 15 species of reptiles, 8 species of amphibians, 31 species of butterflies, 12 species of arachnids, 17 species of other invertebrates. In total 9 species of rare, endangered or threatened flora and fauna were documented among all the groves according to their regional status. It was observed that maximum species variability was encountered in the SGs located away from the town areas. In this connection, SGs located in Nakashipara and Kaliganj blocks were found to have greater flora and faunal diversity than the rest.

Some common flora and fauna observed in sacred groves: Nadia district is a significant area in gangetic river basin that contains green pasture throughout the district. The natural flora is rich throughout the district including many SGs. The richness in vegetation supports diverse arrays of faunal population to a great extent. Many faunal species get safe refuge in these SGs. Some of the most important flora and faunal specimens are listed here:

Apart from these, various types of insects like ants and other hymenopteran insects, lepidopteran insects, and soil arthropods, are also found. Identification and taxonomic studies of fauna specimens being very tedious, describing them in detail is avoided in this article.

Key findings: Most of the sacred groves were found to be roosting and feeding site for birds and insectivorous birds like green bee-eaters, drongos, jungle bablers and mynas were commonly observed in these sacred groves. The undergrowth shrubs were found to be roosting and nesting sites for smaller birds like babblers. The larval host plants of most of the

butterfly species were recorded in these sacred groves, owing to good diversity of butterfly fauna. Sacred groves found amidst agricultural fields or barren lands or beside a water body and hence are chosen by birds for calling and displaying. Few invasive species of both flora and fauna like *Parthenium sp., Lantana sp., Eucatorium sp., Achatina sp. etc.* were found during survey. The data on flora and fauna diversity of the study region was made available to the WBBB management authority.

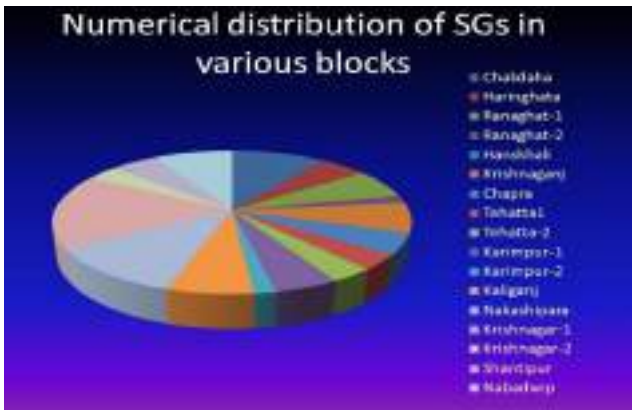

Plate 8. Simplified pie diagram showing relative distribution of SGs in various blocks of Nadia district, WB

Chart 3. List of some of the species of flora (in left column) and fauna (in right column). Scientific name is given in first bracket in each column

Local/ Scientific name of the flora	Local/ Scientific name of the fauna
Bamboo (*Bambusa balcooa, B. Bambos)*	Fox (*Vulpes bengalensis)*
Banyan (*Ficus bengalensis)*	Mongoose (*Herpestes sp.)*
Ashwtha *(Ficus religiosa)*	palm squirrel (*Funambulus sp.*)
Bakul *(Mimusops elengi)*	Field rat (*Bandicota bengalensis)*
Bel tree *(Aegle marmelos)*	Microchiroptera (*Pipistrellus sp.*)
Phani manasa *(Opuntia stricta)*	Bat (*Pteropus sp.)*
Bherenda (*Jatropha sp)*	Monkey (*Macaca sp.*)
Kadam *(Neolamarckia cadamba)*	Langur (*Semnopithecus sp.*)
Mango tree *(Mangifera indica)*	Owl (*Athene sp.*)
Neem *(Azadirachta indica)*	Pigeon (*Columba livia domestica*)
Jackfruit tree *(Artocarpus heterophyllus)*	Spotted dove (*Streptopelia chinensis)*
Tetul *(Tamarindus indica)*	White throated kingfisher (*Halcyon smyrnensis)*
Teak *(Tectona grandis)*	Tia (*Psittacula krameri*)
Sal tree *(Shorea robusta)*	Pond Heron *(Ardeola grayii)*
Tamal tree *(Cinnamomum tamala)*	Drongo *(Dicrurous adsimilis)*
Taal tree *(Borassus flabellifer)*	Green bee eater *(Merops orientalis)*
Date tree *(Phoenix dactylifera)*	Cormorrant (*Phalacrocorax niger)*
Sisu tree *(Dalbergia sissoo)*	Indian myna (*Acridotheres tristis)*
Shonajhuri *(Acacia auriculiformis)*	Jungle babbler (*Turdoides striatus)*
Babla tree *(Acacia nilotica)*	Spectacled cobra(*Naja naja*)
Lambu *(Dysoxylum costulatum)*	Monoceled cobra (*Naja kaouthia*)
Rubber tree (*Ficus elastic)*	Russel's viper (*Daboia russelii)*
Dumur *(Ficus hispida)*	Rat snake (*Ptyas mucosa)*
Nag keshar *(Mesua ferrea)*	Green vine snake (*Ahaetulla sp.*)
Champa *(Michelia champaca)*	Monitor lizard (*Varanus bengalensis*)
Bahera (*Terminalia bellirica)*	Toad (*Bufo sp.*)
Arjun *(Terminalia cuneata)*	Frog (*Rana sp.*)
Pituli *(Trewia nudiflora)*	Tree frog (*Hyla sp.*)
Kool *(Ziziphus mauritiana)*	etc.
Ashoka tree *(Saraca asoca) etc.*	

Species similarity index: A species similarity index was done using multi taxa analysis. Out of 60 sacred groves of Nadia district studied, species similarity index (even distribution of all species) of the 10 major sacred groves (in terms of area covered by them) was compared. The Jaccard index was calculated and the value was found to vary between 0.36 and 0.47. As all the similarity indices between the sites are below 50% level so it can be concluded that the sites' species composition are unique or heterogeneous in nature.

Shannon-Weiner Index: Diversity is a parameter of community structure which is related to the number of species (species richness) and abundance and evenness. Here, the species diversity of 10 sacred groves was compared and Sannon-Weiner Index was calculated. The Sannon-Weiner Index found to be in the range of 1.9 (Khisma Maniktala SG) - 3.1 (Burimatala SG, Nakashipara), which is a recognized range.

Ownership, religious faith and management of sacred groves: SGs in Nadia fall under following categories due to variation in the management status:

- SGs protected by government organizations like A.S.I. or Archaeological Survey of India (as in case of Terakota Temple, Palpara, Chakdaha; Ballal Dhipi, Bamanpukur, Mayapur)
- Privately owned SGs (Fakir bari/ mazaars)
- ISCKON temple, Mayapur
- Trustee Boards
- Village community / local committees / Samaj / Wakf Board
- Intra-village (by separate puja communities)

The human population of Nadia has increased to a considerable extent for last few decades especially due to influx of human population. Over the period the population migration not only brought in different human biological traits, but also a variety of cultural, religious, developmental and technological characteristics. Contemporary Nadia is an agglomeration of different endogamous groups of various religious faith chiefly composed of Hindus and Muslims. In other words, there is heterogeneity in the society in terms of religious beliefs, culture, and pattern of livelihoods. But majority of population in Nadia speaks in Bengali with minor exceptions of Urdu speaking muslims. In this connection, a few tentative inferences can be drawn from the information gathered: the sacred groves are found mainly among non-tribal Hindu groups. The absence of groves in the tribal areas is not clear. There is regional variation in terms of ethnic association. Moreover, the association with different castes is not clear. And habitat fragmentation occurs to the native fauna population due to anthropogenic activities.

3.1 Gender and Management of SGs

The role of gender in SGs can be analysed at least at four levels:

A majority of the SGs in Nadia are associated with female deities such as Maa Kali, Maa Chandi, Maa Manasha, Sri Radha, Maa Durga. But the deities of male god are also not scanty. Nadia is the birthplace of Chaitanya Mahaprabhu who preached the idea of nonviolence, speaking of love by the name of Lord Krishna. So, in many groves the idol of Lord Krishna along with Sri Radha, Sri Chaitanya Mahaprabhu, Jagannath-Balabhadra-Subhadra, Mahadeb or Lord Shiva are worshiped.

As far as the gender of the priest is concerned, it appears that without an exception the priesthood rests with males as also found in other states [24,37]. The access to men and women in various rituals, festivals, ceremonies that take place in the groves and harvest of biomass from the groves was studied. It appears that entry of both men and women of different age groups are permitted into the groves. In some SGs only married women's entry is observed to a large extent. Some information about the kind of role women plays in decision-making regarding management of SGs. Most SGs are associated with a temple or worship structure of other kinds and the worship is managed by a Puja Committee, Temple Committee or trustees which are mainly composed of male members in rural areas. It can be inferred that practically no significant role of women in the management of SGs are observed in Nadia District. It is highly recommended women are represented in the numerous trust bodies or committees that are managing SGs [38].

3.2 Participation of Local People for Protection of SGs

The role of sacred groves in the lives of the local people may be categorized into four features: religious belief, socio-political, socio-cultural and economic aspects. Sacred groves are live parts of the ecosystem. Local people maintain these groves as a part of their cultural tradition. This fact indicates that there are abundant scopes for strengthening this institution [37]. A lot more opportunities are required to be created in the form of workshops, conferences, exchange of views among a wide range of people of the different parts of the district by direct interaction with them. International agencies like UNESCO, the

World Bank and Ford Foundation have included SGs in their agenda [24]. The media is currently devoting a lot more space to this institution than before. The level of awareness among different sections of the population regarding the cultural and biological importance of SGs is increasing [39]. Realizing the cultural, biological and ecological importance of the SGs in our country and the threats faced by this ancient institution, the West Bengal Biodiversity Board, Kolkata (WBBB) has undertaken a number of activities in collaboration with many academic institutions, various panchayats, NGOs, and local human population. Travelling exhibitions using models, paintings, photographs of different components of SGs of our state may be organized to show the common people the importance of conservation of such SGs. Other objective of this is also to interact with local people and different organizations to learn more about SGs of the state and to strengthen the diverse SG-related local management practices and knowledge systems. Through growing awareness among village people living especially in the vicinity of SGs is very encouraging in the sense that these people are protecting the age-old trees of the area along with the beliefs and taboos associated with the SGs. The trees and other vegetation are safe house for many fauna. Thus, local people in one hand using the products and biproducts of the vegetations of the SGs; at the same time helping in protecting the flora and the fauna of the area, ultimately conserving the biodiversity of the SG ecosystem.

4. DISCUSSION

Sacred groves are segments of landscape, containing vegetation and other forms of life and geographical features that are delimited and protected by human societies under the belief to keep them in a relatively undisturbed state [16,40]. Various SGs constitute virgin vegetation, and are particularly enriched with various trees and associate groups of organisms, like epiphytes, amphibia, reptiles, birds, butterflies etc. With the continuing destruction of forest all around them, the SGs have become fragmented habitats housing a variety of genetic pools and became the safe refuge for many plant and animal species [23]. Today, unfortunately fewer plants are actually reported thriving in some SGs. Sacred groves also act as a nurturing ground for many ayurvedic and folk medicines. They are also of great forestry interest as indicators of the natural productivity of the region. Ecologically valuable species of *Ficus sp.* which conserve high amount of nitrogen, phosphorous, magnesium and calcium in their leaves, are found in several SGs [7,13,41]. Many SGs hold water resource in the form of freshwater ponds, lakes, dighi and jheels, streams or rivers. Not only has that, but the vegetative mass of the grove itself retains water and releasing it slowly in times of summer. It is evident that one of the important ecological roles of these groves is to provide a more dependable source of water for the organisms living in and around the SGs. In addition, transpiration from the SGs vegetation would increase atmospheric humidity and reduce temperature in the immediate vicinity [22]. In addition, diverse cultures recognize this association in different ways in relation to the sacred place and its elements [42]. The institution of SGs has been studied in different parts of Nadia district of the Indian state of West Bengal from anthropological as well as biological conservation points of view. Some of the SGs are on the verge of extinction for different reasons [43]. During interview, the local people reported that some animals are not seen today in the area which was found in these forest patches even few decades ago. This may be attributed to the uncontrolled destruction of habitat i.e. habitat fragmentation of these animals along with their killing for various purposes [25]. Some animals even did come out of these undisturbed forest patches and could be seen by villagers. The number of recently unseen animals is increasing gradually. This observation does not only indicate the extinction of these animals; rather these animals might have migrated to region where they found more secure habitat and abundant resources. Degradation of forests and destruction of habitat due to anthropogenic activities are the major causes of decline in the biodiversity profile of these SGs [25,43]. The biodiversity indices calculated in the SGs of the study area still point to the heterogeneity and richness of the species living in these groves. To preserve the species richness and diversity conservation practices are required to follow strictly and voluntarily by local people as found in Bonai forest division, Odisha [30]. Similarly, many traditional conservation practices of local people in many areas of the district of Nadia including daily worship and rituals in these grove areas [42], regular vigil by local believers, planting of many trees in the boundary of the groves, maintenance of taboos associated with these SGs contribute to the conservation and protection of biodiversity of SGs as encountered in various sacred groves in other part India [20] and abroad including Sri Lanka [14], Nepal [37]. These methods collectively belong to the traditional management practices of SGs in local level. Another important measure to protect the ancient institution of SGs in Nadia is to control indiscriminate access to SGs by cultural restriction and, thereby, reduced the human impact as reported in other parts of the country too [20,24,42]. The consequence of such restriction has been that SGs have evolved as important repository of

biological diversity and permitted diverse ecological processes to continue with least interference over long period of time [21]. Further attention toward the conservation of the SGs and their biological components is very much important, as they also serve as microhabitat for many significant fauna and flora which are essential components of larger ecosystem.

5. CONCLUSION

This article may draw attention of the conservationist so that these socio-ecological forest patches get their due attention for conservation. In general, the area surrounding these groves has been becoming populated by human habitation. Many of the endemic and rare species of fauna and flora in these areas of Nadia district decreased in abundance. Some are not even found today. Over the period, the population migration in this district brought together a variety of socio-cultural, religious, developmental, and technological characteristics. Contemporary Nadia is an agglomeration of different endogamous groups of various religious faiths. Keeping these faith conserved in the areas of SGs is an uphill task of the knowledgeable society because this would bring about the conservation of the biodiversity of these areas too. Conservation through traditional practices by indigenous people may result in sustainable development of the areas along with benefit sharing among stakeholder village conservationists thus converting these SGs into biodiversity heritage sites, not only of the district of Nadia but also of the whole country.

ACKNOWLEDGEMENTS

The author is extremely grateful to West Bengal Biodiversity Board (WBBB) for providing financial support. Sincere gratitude is also extended to Prof. S. Mukherjee, Dept. of Botany, Kalyani University and Dr. A. Mukherjee, Maulana Azad College respectively for their support in identification of plant species and statistical analysis.

COMPETING INTERESTS

Author has declared that no competing interests exist.

REFERENCES

1. Malhotra KC, Gokhale Y, Chatterjee S. Cultural and ecological dimensions of sacred groves in India. Published by: Indian National Science Academy**,** New Delhi & Indira Gandhi Rashtriya Manav Sangrahalaya, Bhopal; 2001.
2. Das K, Malhotra KC. Sacred groves among the tribes of India: A literature survey of ethnographic monographs, Mimeograph; 1998.
3. Deb D, Malhotra KC. Interface between biodiversity and tribal cultural heritage: an exploratory study, I. Human Ecology. 1997;8:157-163.
4. Jana P, Dasgupta S, Todaria NP. Impact and ecosystem service of forest and sacred grove as saviour of water quantity and quality in Garhwal Himalaya, India. Environ Monit Assess. 2017;189(9):477.
5. Tripathi OP. Study of distribution pattern and ecological analysis of major forest types of Meghalaya. Ph.D. Thesis, North-Eastern Hill University, Shillong, India. 2002;110-130.
6. Suthari S, Kandagalta R, Ragan A, Raju VS. Plant wealth of a sacred grove: Mallur Gutta, Telangana state, India. Int J Gen Med. 2016;9:369-381.
7. Amrithalingam M. Sthala vrikshas of Tamil Nadu, In: Krishna N and Prabhakaran J (eds.). The Ecological traditions of Tamil Nadu, C.P.R. Environment Education Centre**,** Chennai; 1998.
8. Mohapatra PP, Khandekar A, Dutta SK, Mahapatra C, Agarwal I. A novel, diminutive Hemiphyllodactylus Bleeker. 1860 (Squamata: Gekkonidae) from a sacred grove in Odisha, eastern India. Zootaxa. 2020;4852(4):6.
9. Dar JA, Subashree K, Raha D, Kumar A, Khare PK, Khan ML. Tree diversity, biomass and carbon storage in sacred groves of Central India. Environ Sci Pollut Res Int. 2019;26(36):37212-37227.
10. Singh H, Husain T, Agnihotri P, Pande PC, Khatoon SJ. An ethnobotanical study of medicinal plants used in sacred groves of Kumaon Himalaya, Uttarakhand, India. Ethnopharmacol. 2014;154(1):98-108.
11. Brandis D. Indigenous Indian forestry: sacred groves in Indian forestry. Oriental Institute. 1897;12-13.
12. Vartak VD, Gadg M, Dev R. An ethnobotanical study of the forests preserved on grounds of religious belief. Proceedings 60th Indian Science Congress, Abstracts. 1973;341.
13. Vartak VD, Gadgil M. Studies on sacred groves along the Western Ghats from Maharashtra and Goa: Role of beliefs and folklores. In: Jain SK (Editor) Glimpses of ethnobotany. Oxford University Press, Bombay. 1981;272-278.
14. Withanage H. Role of sacred groves in conservation and management of biodiversity in Sri Lanka. In: Ramakrishnan PS, Saxena

KG, Chandrashekara UM (Editors). Conserving the sacred for biodiversity management. UNESCO and Oxford-IBH Publishing, New Delhi. 1998;169-186.
15. Vasanth VKR, Shivprasad PV, Chandrashekar KR. Dipterocarps in a sacred grove at Nadikoor, Udupi Districts of Karnataka, India. In: Ganeshaiah KN, Uma Shaanker R, Bawa KS. (Editors) Tropical Ecosystems: Structure, Diversity and Human Welfare. Oxford and IBH Publishing, New Delhi. 2001;599-603.
16. Singh S, Youssouf M, Malik ZA, Bussmann RW. Sacred groves: myths, beliefs, and biodiversity conservation—a case study from Western Himalaya, India. International Journal of Ecology; 2017. Article ID 3828609 | Available:https://doi.org/10.1155/2017/3828609.
17. Chandran MDS, Gadgil M, Hughes JD. Sacred groves of the Western Ghats. In: Ramakrishnan PS, Saxena KG, Chandrasekara UM. (eds.) Conserving the sacred for biodiversity management. Oxford and IBH, New Delhi. 1998;211-232.
18. Khumbongmayum AD, Khan ML, Tripathi RS. Sacred groves of Manipur - Ideal centres for biodiversity conservation. Current Science. 2004;87(4):430-433.
19. Chandrashekara UM, Sankar S. Structure and function of sacred groves: case studies in Kerala, In: Ramakrishnan PS, Saxena KG, Chandrashekara UM (eds.) Conserving the sacred for biodiversity management. Oxford and IBH. Publishing Co, New Delhi. 1998;323-336.
20. Pushpangadan P, Rajendraprasad M, Krishnan RN. Sacred groves of Kerala: A synthesis on the state of art of knowledge, In: Ramakrishnan PS, Saxena KG, Chandrashekara UM.(eds.) Conserving the sacred for biodiversity management, Oxford and IBH Publishing Co., New Delhi. 1998;193-210.
21. WWF Andhra Pradesh. Sacred groves of Andhra Pradesh. World Wide Fund for Nature, Andhra Pradesh state Office, Hyderabad; 1996.
22. Tripathi OP, Tripathi RS, Pandey HN. Status of plant biodiversity in Mawlong Syiem sacred grove of Meghalaya, north-east India. In: Das AP. (Editor) Perspectives of plant biodiversity. Bishen Singh Mahendra Pal Singh, Dehradun. 2002;663-680.
23. Hughes JD, Subash Chandran MD. Sacred groves around the earth: an overview, In: Ramakrishnan PS, Saxena KG, Chandrashekara UM (eds.) Conserving the sacred for biodiversity management, Oxford and IBH Publishing Co., New Delhi. 1998; 69-46.
24. Gokhale Y. Sacred conservation tradition in India: An overview. Abstract**.** National Workshop on Community Strategies on the Management of Natural Resources. Bhopal; 2000.
25. Khan ML, Dei A, Khumbongmayum V, Tripathi RS. The sacred groves and their significance in conserving biodiversity: an overview. International Journal of Ecology and Environmental Sciences. 2008;34(3):277-291.
26. Chakravarti P, Chakravarti S. Soil of West Bengal. State Agricultural Research Institute, Kol- 700040; 1957.
27. Stiling P. Ecology: global insights and investigations. McGraw-Hill Inc, New York, 2012;369-370.
28. Roy D, Mukherjee SK. Diversity of trees in Kalyani township in West Bengal. J. Econ. Taxon. Bot. 2011;35(4):687-695.
29. Visalakshi N. Vegetation analysis of two tropical dry evergreen forests in Southern India. Tropical Ecology. 1995;36(1):117-127.
30. Mohapatra P, Dash PK, Palei HS, Debata S, Sarkar V, Mishra AK, Dutta SK. Ecological and social aspects of biodiversity conservation in sacred groves of bonai forest division, Odisha, India. In book: Biodiversity conservation and Wildlife Management, Publisher: North Orissa University. 2017;35-49.
31. Menon V. Indian mammals: a field guide. Hachette Book Publishing India Pvt. Ltd. Gurgaon. India. 2014.
32. Ali S. The book of Indian birds. BNHS India, Oxford university press, Oxford 13th Edn; 2017.
33. Grimmett R, Inskipp C, Inskipp T. Birds of the Indian Subcontinent. 2nd ed. London: Oxford University Press & Christopher Helm. 2011;1-528.
34. Dutta SK, Nair MV, Mohapatra PP, Mahapatra AK. Amphibians and reptiles of similipal biosphere reserve, regional plant research centre, ministry of environment and forests, Bhubaneswar, Odisha, India. 2009; 1-174.
35. Venkataraman MA Concise field guide to indian insects and arachnids. Simova Education and Research Publishers. 2012;570.
36. Tikadar BK, Bastawde BD. Scorpions (Scorpionida: Arachnida). The Fauna of India. (Edited by the Director). Calcutta Zoological Survey of India. 1983;3:671.

37. Nagendra H, Gokhale Y. Management regimes, property rights, and forest biodiversity in Nepal and India. Environ Manage. 2008;41(5):719-733.
38. Roy Burman JJ. The dynamics of sacred groves. I. Human Ecol. 1995;6:245-254.
39. Ogundiran A. Managing epidemics in ancestral yoruba towns and cities: Sacred Groves as Isolation Sites. Afr Archaeol Rev. 2020;1: 1-6.
40. Gupta AK. Policy and institutional aspects of sacred groves: Tending the spirit, sustaining and sacred, In: Ramakrishnan PS, Saxena KG, Chandrashekara, UM (eds.) Conserving the sacred for biodiversity management, Oxford and IBH Publishing Co., New Delhi. 1998;397-414.
41. Tripathi OP. Fragmentation and plant diversity status of major forest types in Meghalaya, North East India. Indian Forester. 2006;132:1598-1608.
42. Ramakrishnan PS. Conserving the sacred for biodiversity: The conceptual framework, In: Ramakrishnan PS, Saxena KG, Chandrashekara UM. (eds.) 1998. Conserving the sacred for biodiversity management, Oxford and IBH Publishing Co., New Delhi; 1998.
43. Kulkarni C, Finsinger W, Anand P, Nogué S, Bhagwat SA. Synergistic impacts of anthropogenic fires and aridity on plant diversity in the Western Ghats: Implications for management of ancient social-ecological systems. J Environ Manage. 2021;283:111957.

UTTAR PRADESH JOURNAL OF ZOOLOGY

42(6): 64-80, 2021
ISSN: 0256-971X (P)

ANTI-PROLIFERATIVE ACTIVITY OF INDOLES AND RELATED COMPOUNDS: A REVIEW

SUJIT KUMAR BHOWAL[1*]
[1]Department of Zoology, Maulana Azad College, Kolkata- 700013, India.

AUTHOR'S CONTRIBUTION
The sole author designed, analysed, interpreted and prepared the manuscript.

Article Information

Editor(s):
(1) Dr. Rajib Deb, ICAR-Central Institute for Research, India.
Reviewers:
(1) Surendra Kumar, Nehru Memorial College (Affiliated to Bharathidasan University), India.
(2) Noushin Ajmal, Pratap University, India.

Received: 18 January 2021
Accepted: 22 March 2021
Published: 30 March 2021

Review Article

ABSTRACT

Indoles, imidazole, indazole and carbazole are one of the most important biologically active natural compounds in living system which are even can be synthesized in laboratory. They are known to play functional role in cellular metabolism, cell division, cell growth as well as cellular signaling. The aim of this review is to amalgamate various information already available in the area of study of bio-activity of indole derivatives, including their ability to antagonize uncontrolled cellular proliferation in cancerous growth. An array of such compounds having central indole moiety and variation in their side chains have been synthesized and their bio-activities have been studied by various authors. Most of them show anti-cancer and anti-proliferative activities and functions through caspases 3/7/9, procaspase-3, cytochrome c, intracellular and extracellular apoptosis pathways and modulation of transcription pathways. These compounds are reportedly capable of neutralizing flagellar movements in sperms as well as of leishmanial protists. Reports show such compounds having anti-flagellated activities also seem to have anti-proliferative and anti-cancer properties.

Keywords: Anticancer; anti-proliferative properties; biological activities; caspases; indoles.

1. INTRODUCTION

Heterocyclic organic compounds are some of the most valuable sources of novel agents with diverse biological activities, mainly because of the unique ability of the resulting compounds to mimic the structure of peptides and to bind reversibly to proteins [1]. Indole derivatives are such heterocyclic compounds that have been extensively used as source for the preparation of large number of biologically relevant heterocycles [2,3]. Indole and other related compounds like indazole, imidazole and carbazole compounds are experimentally proven to be preventive agents against the flagellated protist, *Leishmania sp*. They are, hence termed as anti-flagellated agents also. Generally this anti-flagellated property is correlated with anti-tumorigenic or anticancer activities of these compounds [4]. Beside this, they are also, a very important category of compounds that play a key role in cell physiology and

**Corresponding author: Email: sujit.sb@gmail.com;*

are probable intermediates for numerous biological reactions. Indole derivatives correspond to scores of important modules of therapeutic agents such as anti-cancer [5,6], anti-oxidant, anti-rheumatoidal, anti-HIV [7], anti-microbial [8,9], anti-inflamatory [10], analgesic, anti-pyretic [4], anti-convulsant, anti-helmintic cardiovascular [11], selective COX-2(cyclooxygenase-2) inhibitory activities (which is an enzyme accountable for inflammation and pain) [12] and DNA binding ability [13]. Cancer is a proliferative property of cellular metabolism having a variety of other properties like limitless number of cell divisions, promoting angiogenesis, invasion of tissue and formation of metastasis, avoidance of apoptosis etc. as well as alteration in DNA binding ability [13]. Cancer is also a cellular abnormality with the potential to spread or invade other parts of the body. Benign tumors do not spread to other parts of the body, while malignant tumors are cancerous. According to a recent report by the World Health Organization, there are now more than 10 million cases of cancer per year worldwide. Cancer results from a multistage, multi-mechanism carcinogenesis process that involves mutagenic, cell death and epigenetic mechanisms, during the three distinguishable but closely allied stages: initiation, promotion and progression [14]. A considerable account of the role of indole compounds in cancer progression has been discussed by Ahmad et al., Gurkan-Alp and Patel et al. [15,16,17]. Intricate mechanism of the action of indole as potential drug against cellular proliferation has been analyzed by Patil et al. [18]. diindolylmethane (DIM), Indole-3-Carbinol (I_3C), Indole-3-acetic acid (I3AA) are similar compounds having plant and animal origin, have also been found to be active against various kinds of cancerous growth as studied by Del et al., 2010; Fares, 2014; Jeong et al., 2010 and Tilton et al. [19,20,21,22]. Similarly analogous compounds like imidazole, indazole and carbazole play remarkable role in controlling neoplastic cell proliferation in animal tissues which was discussed by Abbassi et al., Elsayed et al., Finlay et al., Jones et al., Romero et al. and Salahuddin et al. [23,24,25,26,27, 28].

2. MATERIALS

2.1 Chemical Compounds under Study

2.1.1 Indoles

Indole was first isolated by treatment of the indigo dye with oleum [18]. It is an organic compound (C_8H_7N) found in coal tar and produced in the gut by the bacterial decomposition of tryptophan.

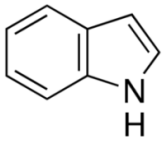

Indole moiety

Indole is an aromatic heterocycle, but exhibit very distinctive reactivity. Here are some general properties:

- The nitrogen is not basic (pKa -3.6)
- Indole can readily undergo aromatic electrophillic substitution.
- Highly ionic salts (e.g. Li+, K+) favours N substitution.
- When N is substituted, C-2 can be deprotonated [17].

Indole is an important heterocyclic system because it is built into proteins in the form of amino acid tryptophan, because it is the basis of drugs like indomethacin and because it provides the skeleton of indole alkaloids—biologically active compounds from plants including strychnine. The incorporation of indole nucleus, a biologically accepted pharmacophore in medicinal compound, has made it versatile heterocyclic possessing wide spectrum of biological activities. In the present study, we have also made an attempt to collect biological properties of imidazole nucleus reported in the new millennium [29]. One of the oldest and most reliable methods for synthesizing substituted indoles is the "Fischer Indole Synthesis", developed in 1883 by Emil Fischer (Fig. 1). This has also been accomplished in a one-pot synthesis using microwave irradiation [2].

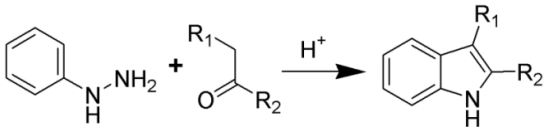

Fig. 1. Reaction mechanism of Fischer indole synthesis

2.1.2 Imidazoles and Indazoles

Imidazole is an organic compound with the formula $C_3N_2H_4$. It is a white or colourless solid that is soluble in water, producing a mildly alkaline solution. In chemistry, it is an aromatic heterocycle, classified as a diazole, and having non-adjacent nitrogen atoms. Many natural products, especially alkaloids, contain the imidazole ring. This ring system is present in important biological building blocks, such as

histidine and the related hormone histamine. Many drugs contain an imidazole ring, such as certain antifungal drugs, the nitroimidazole series of antibiotics, and the sedative midazolam. Imidazole is a planar 5-membered ring. It exists in two equivalent tautomeric forms, because the positive charge can be located on either of the two nitrogen atoms. Imidazole is a highly polar compound, as evidenced by its electric dipole moment of 3.67D. It is highly soluble in water.

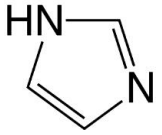

Imidazole moiety

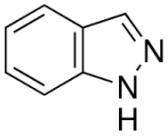

Indazole moiety

Indazole, also called isoindazole, is a heterocyclic aromatic organic compound. This bicyclic compound consists of the fusion of benzene and pyrazole. Indazoles are rare in nature. The alkaloids nigellicine, nigeglanine, and nigellidine are indazoles. Nigellicine was isolated from the widely distributed plant *Nigella sativa* L. (black cumin). Nigeglanine was isolated from extracts of *Nigella glandulifera*. Indazole derivatives display a broad variety of biological activities.

2.1.3 Carbazoles

Carbazole is an aromatic heterocyclic organic compound. It has a tricyclic structure, consisting of two six-membered benzene rings fused on either side of a five-membered nitrogen-containing ring. The compound's structure is based on the indole structure but in which a second benzene ring is fused onto the five-membered ring at the 2–3 position of indole (equivalent to the 9a–4a double bond in carbazole respectively).

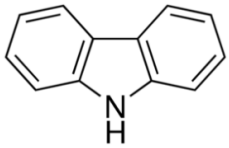

Carbazole moeity

2.2 Biological and Anti-Proliferative Activities

2.2.1 Indoles

Indole derivatives are found to contain several biological activities those including antimicrobial, antibiotic, anti-inflammatory, analgesic, anticonvulsant, antimalarial, anticancer, antiulcer & anti-leishmanial, contraceptive, antioxidant etc. The derivatives are also found to have agonistic effects on several receptors such as Liver x receptor, 5- HT1D receptor etc (Fig. 2) [18]. Indoles are probably the most widely distributed heterocyclic compounds in nature having medicinal importance. Tryptophan is an essential amino acid and as such is a constituent of most proteins; it also serves as a biosynthetic precursor for a wide variety of tryptamine-indole, and 2,3-dihydroindole containing secondary metabolites. In animals, serotonin (5-hydroxytrytamine) is a very important neurotransmitter in the CNS, and also in the cardiovascular and gastrointestinal systems. The structurally similar hormone melatonin is thought to control the diurnal rhythm of physiological functions [1].

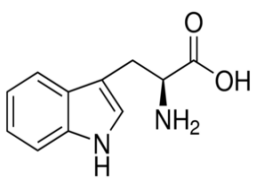

Tryptophan

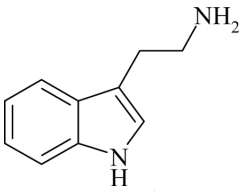

Tryptamine

Fig. 2. Structures of naturally occurring indoles

Many novel indole retinoid derivatives act as anti-cancerous agents like 2-substituted quinoxaline, triazolo (4,3-a) quinoxaline, 2-chloro-3(1-substituted indol-3-yl) quinoxaline, etc. 1-benzoyl-3-bromoacetyl indole, 2-Phenyl-1H indole, (Tetrazol-5-yl) methylindole, 2- thienyl-3-substituted indole, novel 1,3-diheterocycles indole, indole-3-carbinol, 4-(2-(4-bromophenyl)-1H-indol-3-yl)-2-methoxy-6-(4-bromophenyl) nicotinonitrile, etc. are some of the indole dervatives with anti-cancerous activities. Bis-indole derivatives and benzopyridoindoles possess anti-tumorous activities.

Indoles are natural compounds that can be found in numerous types of plant. They are, however more predominantly found in cruciferous vegetables. Cruciferous vegetables comprise of cauliflower, cabbage, turnip, broccoli and brussels sprouts. Indoles fit in a class of phytonutrient compounds (plant compounds with health- protecting qualities) which have been systematically proven to profit the body in a number of imperative ways. Consuming of cruciferous vegetables has been associated with reduced of the risk of colon, breast and prostate cancers. These vegetables are a rich source of many hytochemicals, including indole derivatives, dithiolethiones and sothiocyanates. Cruciferous vegetables are full of glucobrassicin (GB) which throughout metabolism, produce indole-3-carbinol,3,3'-diindolylmethane (DIM) and ascorbigen (ASC) [14].

Table 1. Some indole ring containing drugs and their applications

Drugs	Applications
Vincristine	Anticancer
Bufotenidine	Toxin
Vincamine	Vasodilator
Reserpine	Antihypertensive
Oxypertine	Antipsychotic
Amedalin	Antidepressant
Panobinostat	Anti-leukamic
Yohimbine	Sexual Disorder
Bucindolol	β-Blockers
Mitragynine	Opioid agonist
Oglufanide	Immunomodulatory

Table 2. Anti-proliferative activities of some indole derivatives

Name	Empirical formula	Anticancer activity	Other biological activities (if any)
Bis-indole derivatives	$C_{23}H_{15}N_3O_2$	Anti-tumor activity against several human cancer cell lines	Not reported yet
Indole-3-acetic acid (I3C)	$C_{10}H_9NO_2$	Apoptosis-inducing ligand in mammals	Induce cell elongation and cell division & acts as signaling molecule
2-substituted quinoxaline derivatives	$C_{23}H_{16}ClN_3$ [2-chloro-3-(1- benzyl indol-3- yl)quinoxaline]	Suppression of ovarian cancer in mice; tumor growth suppression in OVCAR3 and BG-1 cells	Antimicrobial activities
Indole-3-carbinol (I3C)	C_9H_9NO	Decreases tumor susceptibility in many cancer cell lines and demotes metastasis in liver	Antioxidant, and anti-atherogenic activities
Triazolo(4,3-a) quinoxaline derivatives	$C_{24}H_{17}N_5$ [4-(1-benzyl indol-3-yl)-(1,2,4)- triazolo(4,3- a) quinoxaline]	Tumor growth suppression in two human cancer cell lines- OVCAR3 and BG-1; and ovarian cancer cell line in mice	Antimicrobial activity
2-Phenyl-1H Indole	$C_{14}H_{11}N$	Anti-cancer activities in kidney, cervical and breast cancer cell lines	-
3,3'-Diindolylmethane (DIM)	$C_{17}H_{14}N_2$	Inhibit cell proliferation, cause cell cycle arrest at G1 phase and induce apoptosis in many cancer cell lines	Immuno-stimulant against human papilloma virus infection of the cervix
(Tetrazol-5-yl) methylindole	$C_{16}H_{13}N_5$ [1-[(2H- Tetrazol-5-yl)methyl]-2- phenyl-1H-indole]	Anti-cancer activity against human liver cancer cell line(HepG2)	Antimicrobial activity
2-thienyl-3-substituted indole	-	Antitumor activity against breast cancer cell line MCF-7	Anti-inflammatory, ulcerogenic and antimicrobial activity
Novel Indole Retinoid derivatives	-	Anti-proliferative activities in colon, breast and liver cancer cell lines.	-

2.2.2 Bis-indole derivative

Bis-indoles are produced in living organisms through dimerization of monomeric indole bases.

Derivatives like 3,3'-[pyridine-2,6-diylbis (methylene)] bis(1,3-dihydroindol-2-ones) and 3,6-Bis(2-oxo-1,2-dihydroindol-3-ylidene)piperazine-2,5-diones have anti-tumorous activity against a panel of many human tumor cell lines like bladder, colon, CNS, gastric, head-neck, lung, melanoma, ovarian, pancreas, breast, prostate, pleuramesothelioma, renal, uterus body. The pyridyl derivatives also have a high growth inhibitory effect against breast cancer cells and has a comparable

in vitro growth inhibitory activity to the known proteasome inhibitor MG-132 (Z-Leu-Leu-Leu-al) [4].

Bis-Indole Derivative

2.2.3 Indole-3-acetic acid or 3-IAA

It is the most common, naturally-occurring, plant hormone of the auxin class. On a larger scale, IAA serves as signaling molecule necessary for development of plant organs and coordination of growth. IAA is an apoptosis-inducing ligand in mammals. IAA, along with horseradish peroxidase, induces apoptosis in TCCSUP human urinary bladder carcinoma cells via both death receptor-mediated and mitochondrial apoptotic pathways. IAA/HRP activates p38 mitogen-activated protein (MAP) kinase and c-Jun N-terminal kinase(JNK) and also induces caspase-8 and caspase-9 activation, which results in caspase-3 activation and poly(ADP-ribose) polymerase (PARP) cleavage [21].

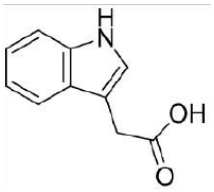

Indole-3-acetic acid

2.2.4 2-substituted quinoxaline derivatives

Conjugated indole-quinoxaline is vital for the antimicrobial activity and potential anti-cancer efficacy. Compounds like 3-(1- substituted indol-3-yl)quinoxalin-2(1H)ones, 2-(4-methyl piperazin-1-yl)-3-(1-substituted indol-3-yl) quinoxalines, 2-chloro3-(1-substituted indol-3-yl)quinoxalines, 2-(piperidin-1-yl)-3-(1- benzyl indol-3-yl)quinoxaline, 2-morpholino-3-(1-benzyl indol-3- yl)quinoxaline, etc. are derivatives of 2-substituted quinoxalines and have in vitro cytotoxic effect against OVCAR-3 and BG-1 cell lines in humans and also in vivo growth suppression of ovarian cancer xenografts in nude mice. Derivatives like 3-(1-substituted indol-3-yl)quinoxaline-2(1H)ones have anti-microbial activities against Gram-negative bacteria like *E. coli and P.aeruginosa*, 2-(4-methyl piperazin-1-yl)-3-(1-substituted indol-3-yl) quinoxalines show anti-microbial activity against Gram-negative bacteria *P. aeruginosa* and Gram-positive bacteria like *S. aureus* and *B. cereus*. Another derivative, 2-chloro-3-(1-substituted indol-3- yl)quinoxalines, show anti-microbial activity against a strain of fungi, *C. albicans* [30].

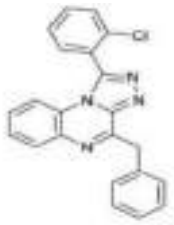

2-chloro-3-(1-substituted-indol-3-yl) quinoxalines

2.2.5 Indole-3-carbinol (I_3C) and 3,3'-Diindolylmethane (DIM)

Indole-3-carbinol is produced by the breakdown of the glucosinolate glucobrassicin, whichcan be found at relatively high levels in cruciferous vegetables such as broccoli, cabbage, cauliflower, brussels sprouts, collard greens and kale. 3,3′-Diindolylmethane (DIM) is a compound derived from the digestion of indole-3-carbinol, found in cruciferous vegetables such as broccoli, Brussels sprouts, cabbage and kale. The diet-derived indole derivatives, I3C and DIM, exert anticancer effects mediated through the regulation of cell cycle, induction of apoptosis, transcription, cell signal transduction, inhibiting angiogenesis and suppressing cell invasion. The activation of the mitochondrial pathway through releasing of Cytochrome C and activation of caspases, together with inactivation of hormonal, PI3K/Akt, MAPK, Bcl-2 and NF-kB pathways represent the possible molecular mechanism of these indole derivatives in their anticancer activity. The anti-cancer activity of I3C and DIM has been detected in various target organs including breast, prostate, colon, liver, cervix, endometrium, melanoma and lung using human cancer cell lines or various animal models. Furthermore, these derivatives have been evaluated in clinical trials phase I and phase II as potential chemopreventive agents against breast, ovary and colon cancer [20]. Indole-3-carbinol has the ability to alter estrogen metabolism and other cellular effects. Indole-3-carbinol can shift estrogen metabolism towards less estrogenic metabolites. It promotes liver cancer in trout when it is combined with aflatoxin B1 and promotes metastasis [22]. 3,3'-diindolylmethane acts as an immunostimulant against human papilloma virus infection of the cervix, but not a statistically significant level [19].

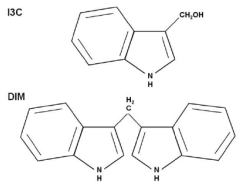

Indole-3-carbinol and 3,3'-diindolylmethe

2.2.6 Triazolo(4,3-a) quinoxaline derivatives

These compounds are 1-benzyl and 1-benzoyl-3-heterocyclic indole derivatives.4-(1-benzyl indol-3-l)-(1,2,4) - triazolo (4,3-a)quinoxaline, 4-(1-benzoyl indol-3-yl) -(1,2,4) -triazolo (4,3-a) quinoxaline, 1-methyl-4-(1- benzyl indol-3-yl)-(1,2,4)-triazolo(4,3-a)quinoxaline and 1-methyl-4-(1-benzoyl indol-3-yl)-(1,2,4) triazolo(4,3-a)quinoxalineare thederivatives of triazolo(4,3-a) quinoxalines, which are synthesized by treating 1-(2-(1-benzyl indol-3-yl)quioxalin-3-yl)hydrazine and 1-(2-(1-benzoyl indol-3-yl)quioxalin-3-yl)hydrazine with formic acid (25 mL) or acetic acid (25 mL) and allowed to stand at room temperature for 24 hours. These derivatives have *in vitro* cytotoxic effect against OVCAR-3 and BG-1 cell lines in humans and *in vivo* growth suppression of ovarian cancer xenografts in nude mice [30]. These indole derivatives also possess moderate level of antimicrobial activities.

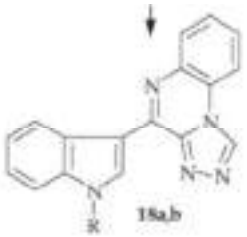

Triazolo(4,3-a) quinoxaline, a:R=CH_2Ph, b:R=COPh

2.2.7 2-Phenyl-1H Indole

Derivatives of 2-Phenyl-1H indole like 4-(2-(4-bromophenyl)-1H-indole-3-yl)-2-methoxy-6-phenyl nicotinonitrile,4-(2-(4-bromophenyl)-1H-indole-3-yl)-2-methoxy-6-(4-minophenyl)nicotinonitrile,4-(2-(4-bromophenyl)-1H-indole-3-yl)-2-methoxy-6-(2-hydroxyphenyl) nicotinonitrile,4-(2-(4-bromo- phenyl -1H-indole-3-yl)-2-methoxy-6-(4-hydroxyphenyl) nicotinonitrile,4-(2-(4-romophenyl)-1H-indole-3-yl)-2-methoxy-6-(4-bromophenyl) nicotinonitrile, 4-(2-(4-bromophenyl)-1Hindole-3-yl)-2-methoxy-6-(3-hydroxyphenyl) nicotinonitrile and 4-(2-(4-bromophenyl)-1H-indole-3-yl)-2-methoxy-6-(4-methylphenyl) nicotinonitrile have potent *in-vitro* anti-cancerous activities against HEK293 (Human Epidermal Kidney Cell Line), HELA (Cervical Cancer Cell Line) and MDA MB 468 (Breast Cancer Cell Line) [17]. Substitution at phenyl ring on 6th position of pyridine ring gives good anticancer activity as in the order of Br>NH2>CH3>OH>H. Absorbance of the samples was measured using a microplate (ELISA) reader. The wavelength to measure absorbance of the formazan product is between 550 and 600 nm according to the filters available for the ELISA reader, used . The percentage cell inhibition of the samples at different concentrations have been represented graphically below with the anticancer drug Methotrexate (MTX) as standard [31].

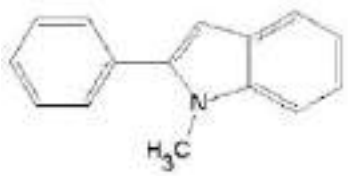

2-Phenyl-1H Indole

2.2.8 (Tetrazol-5-yl) methylindole

New (tetrazol-5-yl)methylindole derivatives are being synthesized from 2-phenylindole. Furthermore, the sugar acetyl hydrazones of the tetrazole derivatives as well as their derived acyclic *C*-nucleoside analogs show anticancer activity against human liver carcinoma cell line (HepG2). These indole derivatives reduce the expression of cyclooxygenase-2 in HepG2 cells and result in HepG2 cell death via apoptosis. These indole-containing compounds cause HepG2 cell cycle arrest at G0/G1 phase, thus preventing cell from entering S or G2/M phase and finally causing apoptosis. Sugar {5[(2-phenyl-1*H*-indol-1-yl)methyl]-2*H*tetrazol-2- yl} acetyl hydra- zones are the derivatives which are the most potent compounds and affect the cell viability in a dose dependent manner with IC_{50} values of 4.2 µg/mL [15]. These compounds also have potent antimicrobial activity against *Aspergillus Niger, Penicillium sp, Candida albican, Bacillus subtilis, Streptococcus lacti, Escherichia coli, Pseudomonas sp.*, and *Streptomyces sp*. [9].

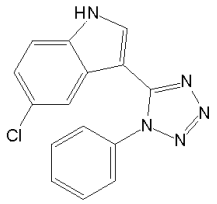

5-chloro-3-(1-phenyl-1H-tetrazol-5-yl)-1H-indole

2.2.9 2-thienyl-3-substituted indole

Derivatives of 2-thienyl-3-substituted indoles are potent antitumor agents against breast cancer cell line (MCF-7) along with antiinflammatory and ulcerogenic activities. About 23 new compounds have been synthesized from the parent 2-thienyl-3-substituted indole compound like N'-((2- (Thiophen-2-yl)-1H-indol-3-yl) methylene) acetohydrazide, 3-(2-methylhydrazono) methyl)-2-(Thiophen-2-yl)-1Hindole, 2-(Thiophen-2-yl)-1H-indole-3- carbaldehyde Oxime, 2- (2- (Thiophen-2-yl)-1H-indol-3-yl) methylene) hydrazine Carboxamide, 5- (2- (Thiophen-2-yl)-1h-indol-3-yl) methylene) pyrimidine-2,4,6 (1H,3h,5h)- trione, 4-oxo-4- (2- ((2- (Thiophen-2-yl) -1H-indol-3-yl) methylene) Hydrazinyl) Butanoic Acid, etc. All these synthesized compounds show good to moderate anti-tumor activity against breast cancer cell line (MCF-7) using doxorubicin as a standard drug (IC50=2.97 µg/ml), with the most potent one being N-cyclohexyl-2-(2-(Thiophen-2-yl)-1H-indol-3- yl)methylene) Hydrazine carboxamide(IC50 2.6 µg/ml) and Methyl 2- (2- ((2-(Thiophen-2- yl)-1H-indol-3-yl) methylene) Hydrazinyl) Acetate (IC50: 38.4 µg/ml) having the weakest activity. Compounds 2-(thiophen-2- yl)-1H-indole-3-carbaldehyde, 2- (2- ((2- (Thiophen-2- yl)-1H-indol-3-yl) methylene) hydrazine Carbonyl) benzoic Acid show high antiinflammatory activity against carrageenan induced oedema in albino rats against indomethacin as a reference standard but less ulcerogenic effect. While compounds like 4-amino- n'- ((2- (Thiophen-2-yl) -1H-indol-3-yl) methylene) benzo Hydrazide, 4-oxo-4- (2- ((2-(Thiophen-2-yl) - 1H-indol-3-yl) methylene) Hydrazinyl) Butanoic Acid and 2- (2- ((2- (Thiophen-2-yl)-1H-indol-3-yl) methylene) hydrazine Carbonyl) phenyl) carbamic Acid show anti-inflammatory activity but no ulcerogenic effect [10]. These compounds also show moderate level of antimicrobial activity [31].

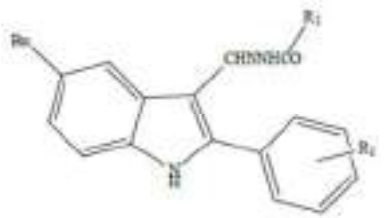

2-thienyl-3-substituted indole

2.2.10 Novel indole retinoid derivatives

Novel(E)-3-(5-substituted-1H-indol-3-yl)-1-(5,5,8,8-tetramethyl-5,6,7,8-tetrahydronaphtha len-2-yl)prop-2-en-1-one derivatives show *in vitro* anti-cancerous effects. Novel indole retinoid compounds like (E)-3-(1H-Indol-3-yl)-1-(5,5,8,8-tetramethyl-5,6,7,8-tetrahydronaphthalen-2-yl)prop-2-en-1-one, (E)-3-(5-Methoxy-1H-indol-3-yl)-1-(5,5,8,8- tetramethyl-5,6,7,8-tetrahydrona phthalen-2-yl)prop-2-en-1-one, (E)-3-(5-Chloro-1H-indol-3-yl)-1-(5,5,8,8-tetramethyl -5,6,7,8-etrahydronaphthalen-2-yl)prop-2-en-1-one and (E)-3-(5-Bromo-1H-indol-3-yl)-1-(5,5,8,8-tetra-methyl-5,6,7,8- etrahydrona phthalen-2- yl)prop-2-en-1-one have anti-proliferative capacity in liver, breast and colon cancer cell lines. Compound (E)-3-(1H-Indol-3-yl)-1-(5,5,8,8-tetramethyl-5,6,7,8- tetrahy dronaphthalen-2-yl)prop-2-en-1-one has the lowest IC50 level in cytotoxicity assays in breast cancer cell line panel, which includes ER-positive and ER-negative cell lines. Furthermore, it is also less toxic in MCF-12A, which is a normal-like breast epithelial cell line and induces apoptosis as a cause of anti-proliferative effect [16].

3. MECHANISM OF ANTI-PROLIFERATIVE ACTIVITY

Indole compounds act on a number of cellular signaling pathways leading to their observed biological effects (Fig. 3). Cancer progression involves up-regulation of signaling pathways that favour proliferation, angiogenesis, and invasion. Mechanisms of apoptosis stimulation of indole derivatives include- a) down-regulation of anti-apoptotic gene products such as Bcl-2 (B-cell lymphoma) and Bcl-XL (B-cell leukemia-extra large) b) down-regulation of the inhibitor of apoptosis proteins, e.g. CIAPs, X-chromosome linked inhibitor of apoptose protein (XIAP) and survival, c) up-regulation of pro-apoptotic factors such as *Bax* gene d) liberation of mitochondrial cytochrome C in addition to stimulating of caspase-9 and caspase-3 and e) inhibition of the NF-kB signaling pathway.

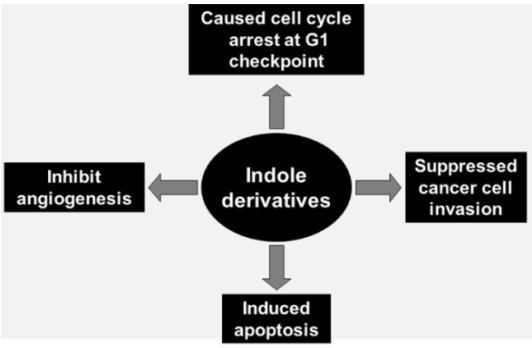

Fig. 3. Anti-proliferative activities performed by indole derivatives [20]

3.1 Mechanisms of Apoptosis Induction by Indoles Involve Two Pathways

3.1.1 Intrinsic and Extrinsic pathway

In the extrinsic pathway, signal molecules identified as ligands, which are released by the immune system's natural killer cells possess the Fas ligand (FasL) on their exterior to connect to transmembrane death receptors on the target cell (Fig. 4). After the binding of the death ligand to the death receptor the target cell triggers multiple receptors to aggregate together on the surface of the target cell. The aggregation of these receptors recruits an adaptor protein known as Fas-associated death domain protein (FADD) on the cytoplasmic side of the receptors. FADD, in turn, recruits Caspase-8. Caspase-8 will then be activated and will be now able to directly activate caspase-3 and caspase-7. The activation of caspase-3 will initiate the degradation of the cells. The intrinsic pathway is triggered by cellular strain, particularly mitochondrial stress caused by factors such as DNA damage from chemotherapy or UV exposure. Upon delivery of the stress signal, the pro-apoptotic proteins in the cytoplasm (Bcl-2-like protein 4 (BAX) and BAX-like Bcl-2 homology domain 3 protein (BID)) bind to the outer membrane of the mitochondria to signal the release of the internal content. The interaction between the pro-apoptotic (BAX and BID) and the antiapoptotic proteins (Bcl-2) on the surface of the mitochondria is thought to be important in the formation of the PT pores in the mitochondria, and hence, the release of cytochrome c and the intramembrane content from the mitochondria. Following the release, cytochrome c forms a multi protein complex [13].

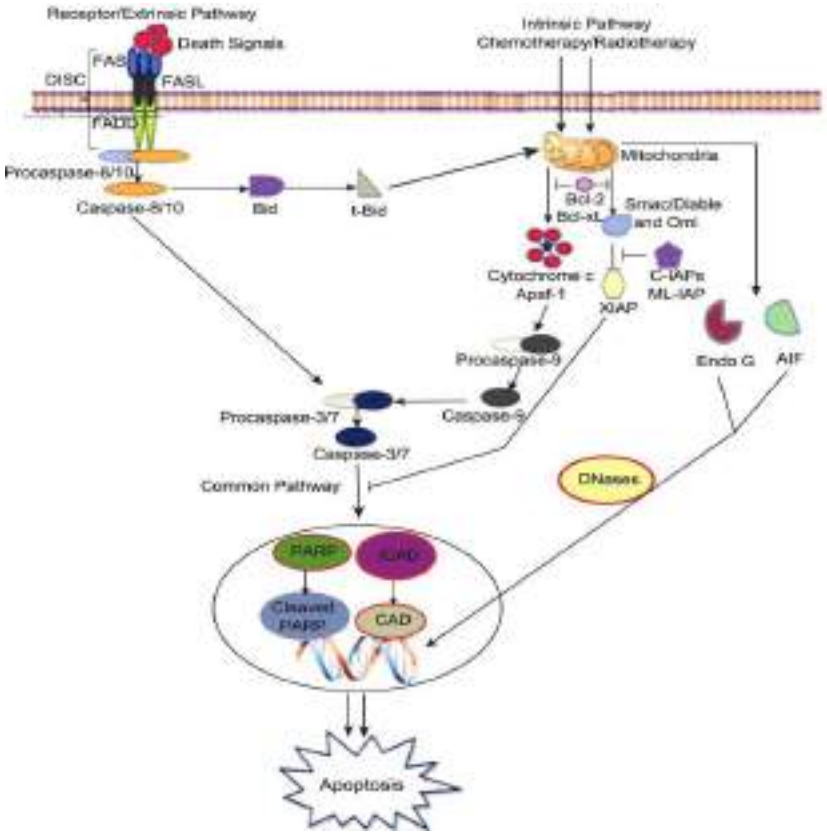

Fig. 4. Intrinsic and Extrinsic Pathways of Apoptosis activated by indoles [13] This is known as apoptosome which consists of cytochrome c, Apaf-1, procas-pase-9 and ATP. Following its formation, the complex will activate caspase-9. The activated caspase-9 will then turn the procaspase-3 and procaspase-7 into active caspase-3 and active caspase-7. These activated proteins initiate cell degradation or cell death. Besides the release of cytochrome C fromthe intramembrane space, the intramembrane also releases Smac/Diablo proteins to inhibit the inhibitor of apoptosis (IAP). IAP is a protein family which consists of 8-human derivatives. Their function is to stop apoptotic cell death by binding to caspase-3, caspase-7 and caspase-9 and inhibit them [13]

Tumor angiogenesis starts with cancerous tumor cells releasing molecules that post signals to the neighboring host tissues. This signaling activates definite genes in the host tissue that, in turn, build proteins to support growth of new blood vessels.

Indole compounds restrain the invasion of cancer cells and the expansion of new blood vessels (angiogenesis). Indole compounds adapt the cellular signaling pathways through chemosensitization leading to apoptosis and thus conquer the chemo-plus immune-resistance of well-known chemotherapeutic drugs (Fig. 5). Emerging evidence also documents the ability of indoles to reverse the process of EMT via regulation of key miRNAs. An efficient induction of apoptosis and reversal of EMT not only ensures increased sensitivity to conventional drugs (chemosensitization) but also results in significantly reduced invasion and metastasis [13,15].

Cancer progression involves upregulation of signaling pathways that favours proliferation, angiogenesis and invasion. NF-kB is activated and translocated to nucleus leading to transcriptional up-regulation of genes that play important roles in these processes. As efficient anticancer agents, indole compounds target an array of cellular pathways causing a reversal of pro-survival and invasion pathways and an efficient induction of apoptosis. As an example, indoles inhibit the upstream pathway (PI3-K-Akt) that regulates NF-kB signaling as well as block NF-kB activation and translocation to nucleus, thus preventing the generation of transcription of multiple target genes (Fig. 6). Such a multistep regulation ensures a much increased efficacy and underlines the efficacy of these compounds as effective anticancer agents [15].

I_3C-induced P450-dependent estrogen metabolism is responsible for the chemopreventive action of I_3C. In a study to compare the mechanisms of the action of I_3C in estrogen-responsive MCF-7 breast cancer cells and the estrogen- nonresponsive MDA-MB-231 breast cancer cells, it has been reported that I_3C was able to inhibit the growth of only estrogen-responsive cells with little effect on estrogen-nonresponsive cells. It has been reasoned that the inhibitory effects of I_3C may involve elective induction of estradiol metabolism and the related cytochrome P450 s y s t e m that may be limited to estrogen-sensitive cells. However, it was later shown that I_3C can suppress the growth of breast cancer cells independent of estrogen receptor signaling. It was shown that a combination of I_3C and tamoxifen inhibited MCF-7 cell growth more stringently than either agent alone [15].

I_3C signaling was observed to induce the G1 cell cycle arrest of MCF-7 cells. Furthermore, I_3C-mediated cell cycle arrest was also observed in estrogen receptor-negative MDA-MB-231 cells under conditions in which the antiestrogen tamoxifen had no effect on cell growth, thus demonstrating a more versatile effect of I_3C, independent of estrogen receptor signaling . This study implicated cyclin-dependent kinase 6 as a target for cell cycle control in human breast cancer cells. The first clue for the involvement of NF-kB pathway in I_3C action came from a study where the effect of I_3C was compared using estrogen receptor-a-negative MDA-MB-468 cells versus immortalized non- tumorigenic HBL100 cells. 73 In this study, phosphatidylinositol 3-kinase (PI3-K) and protein kinase B (PKB)/ Akt were identified as targets of I_3C. I_3C inhibits phosphory - lation and activation of PKB in MDA-MB-468 cells but not in the non- tumorigenic HBL100 cells. Because PKB can regulate NF-kB by the activation of IKK, resulting in increased phosphorylation of IkB and consequent release of NF-kB from the inhibitory complex, the effect of I_3C was tested on NF-kB and IKK. Despite inhibition of PKB, no decrease in IKK activity was observed in response to I_3C treatment. In support of this, nuclear levels of NF-kB (p65) were found to be unaltered. However, I_3C decreased NF-kB e DNA binding, as determined using electrophoretic mobility shift assay (EMSA). These results suggested that I_3C affected DNA binding of NF-kB protein family members, including p65 and p50, by a mechanism that does not involve the inhibition of IKK activity. I_3C is capable of inducing apoptotic cell death in MCF10A-derived cell lines with premalignant and malignant phenotypes but not in non-tumorigenic parental MCF10A cells. I_3C specifically inhibits Akt kinase activity and abrogates the epidermal growth factor (EGF)-induced activation of Akt in breast cancer cells. Transfection of Akt gene activates NF-kB directly, and such activation of NF- k B is completely abrogated by I_3C treatment. I_3C also directly inhibits the elastase-mediated proteolytic processing of CD40, which alters downstream signaling to disrupt NF-kB-induced cell survival and proliferative responses. DIM has similar activity against breast cancer cells as I_3C (Fig. 7). DIM can induce apoptosis processes in MCF10A-derived malignant cell lines but not in non-tumorigenic parental cells. DIM also specifically inhibits Akt kinase activity and abrogates the EGF-induced activation of Akt in breast cancer cells **(**Fig. 7), similar to those observed for I_3C. As a further mechanism, DIM can reduce the phosphorylation of IkBa, an inhibitor of NF-kB. Confocal studies revealed that DIM blocks the translocation of p65 subunit of NF-kB to the nucleus. Activation of NF-kB involves IkB kinase e-mediated kBa phosphorylation, which can be completely abrogated by DIM treatment [13,15,16,20].

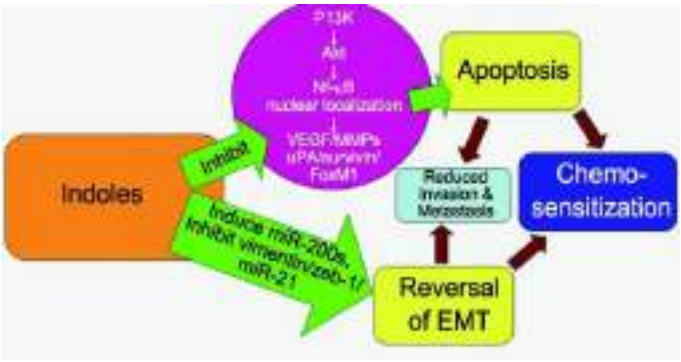

Fig. 5. Summary of mechanisms of anti-prliferative and chemosensitizing effects of indole compounds [13]

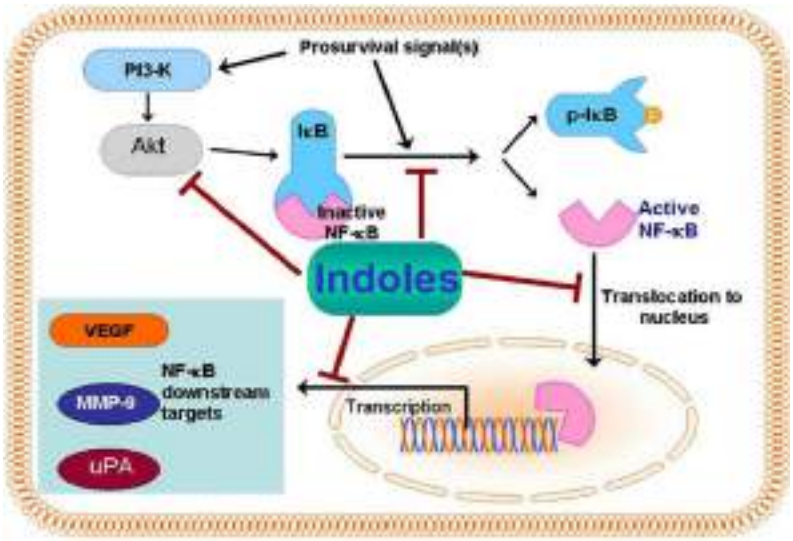

Fig. 6. Cellular effects of Indoles through regulation of NF-kB Signaling [15]

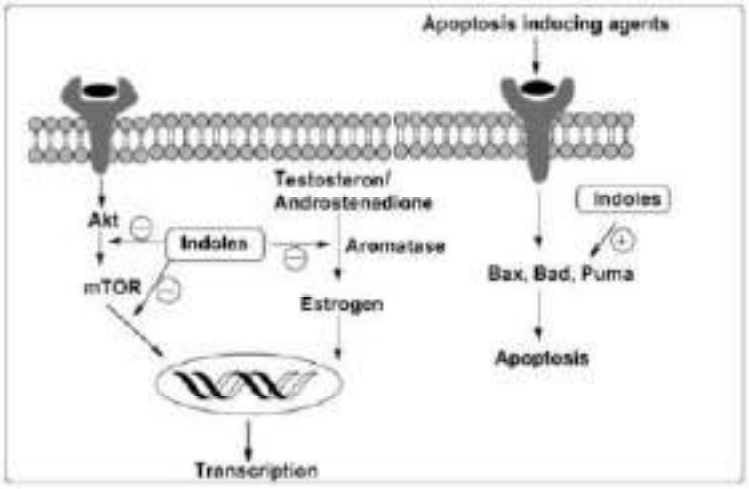

Fig. 7. I_3C-induced estrogen metabolism [20]

4. IMIDAZOLE AND INDAZOLE

Imidazole and its derivatives are reported to be physiologically and pharmacologically active and find applications in the treatment of several diseases. In the drug discovery the imidazole is the most important synthetic strategy. Many imidazoles are reported as pharmacological agents like Azomycine, Clotrimazole, Miconazole, Ergothionine, Clonidine and Moxonidine. One of the most important applications of imidazole derivatives is their usage as material for treatment of denture stomatities and in cancer [32].

Imidazoles come under the category of antimetabolite, which have specific mechanism of action in cancer. Antimetabolite is a type of chemical that inhibits the use of a metabolite. They have toxic effects on cells, such as halting cell growth and cell division, thereby making these compounds of use as chemotherapy for cancer. Antimetabolites can be used in cancer treatment, as they interfere with DNA production and therefore cell division and the growth of tumors. These are the chemicals which become the building blocks of DNA. They prevent these substances becoming incorporated in to DNA during the S phase of the cell cycle, stopping normal development and division. They also affect RNA synthesis because thymidine is used in DNA but not in RNA where uracil is used instead of cytosine, inhibition of thymidine synthesis via thymidylate synthase selectively inhibits DNA synthesis over RNA synthesis [30,31,33].

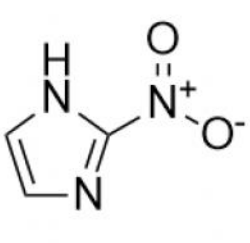

Azomycin

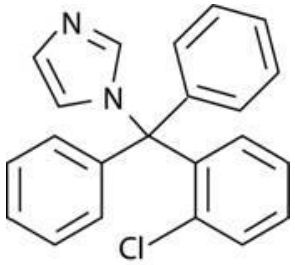

Clotrimazole

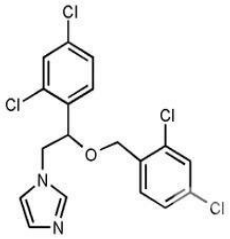

Miconazole

Table 3. Anti-proliferative activities of some imidazole and indazole compounds

Name	Empirical Formula	Anti-proliferative Activity
2-thioxoimidazolidine derivatives	C20H17N3O2S [1-[(1-benzyl indol-3-yl) carbomethyl]-2- thioxoi-midazolidine-4-one]	Tumor growth suppression in two human cancer cell lines-OVCAR3 and BG-1; and ovarian cancer cell line in mice.
Imidazolidine-2,4 dione derivatives	C20H17N303 [1-[(1- benzyl indol-3-yl) carbomethyl]imidazolidine- 2,4-dione]	Tumor growth suppression in two human cancer cell lines-OVCAR3 and BG-1; and ovarian cancer cell line in mice.
2-substituted-*N*-[4(1-methyl-4,5-diphenyl-1*H*- imidazole -2-yl) phenyl] acetamide derivatives	-	Cytotoxic activity against colon carcinoma cell line
Imidazole piperazines	-	Inhibition of tumor growth when human SW620 xenografts are dosed orally in nude mice
Imidazole pyrimidine amides	-	Anti-proliferative activity against a range of cancer cell lines
Benzimidazoles	C7H6N2	Potent anti-cancer activity against many human cancer cell lines
Indazole pyrimidine-based derivatives	-	VEGFR-2 kinase inhibitors; with varying levels of anticancer activity against NCI-60 cancer cell line panel
2-alkyl-6-nitroindazole derivatives	-	Trigger apoptosis; arrest cells in G2/M phase of the cell cycle.

5. CARBAZOLE

Carbazoles represent an important class of heterocycles. These have been reported toexhibitdiverse biological activities such as antimicrobial, antitumor, antiepileptic, antihistaminic, antioxidant, anti-inflammatory, antidiarrhoeal, analgesic, neuroprotective and pancreatic lipase inhibition properties.The carbazole derivatives have gained the attention of researchers due to their therapeutic potential against neurological disorders and cell proliferation. The biological profiles of these new generations of carbazole would represent a fruitful matrix for further development of carbazole nucleus, which can be a lead nucleus for future developments to get safer and effective anticancer therapeutic agents [34].

a) A number of new 1-substituted-6H-pyrido[4,3-b]carbazole derivatives have been synthesized by Beata Tylinska et al., 2013 and the compounds were subjected to preliminary *in vitro* cytostatic activity screening against murine leukemia (L1210), human lung cancer (A549) and human colon cancer (HT29) cell lines. One particular compound 6f exhibited over 20 times better activity against L1210 tumor cell line than the reference ellipticine [35].

b) Kumar, Sharma and Pathak, 2013 worked on the microwave assisted and parallel synthesis of novel substituted carbazole derivatives. The synthesized compounds were evaluated for their antibacterial and anticancer activity. Some of the synthesized carbazole derivatives exhibited significant cytotoxic activity against Ehrlich's Ascites Carcinoma (EAC) and HEP2 cell lines [36].

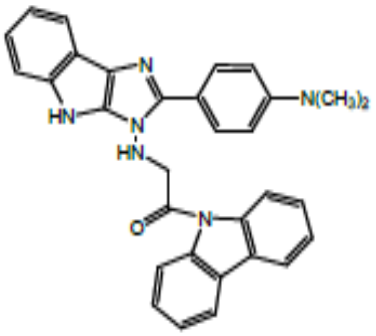

c) Kumar et al., 2014 synthesisized the 2,3-Dimethylindoles and Tetrahydrocarbazoles via Fisher Indole synthesis and evaluation of their anticancer properties. The differently substituted 2, 3-dimethylindoles and tetrahydrocarbazoles have reported to posses significant activity [37].

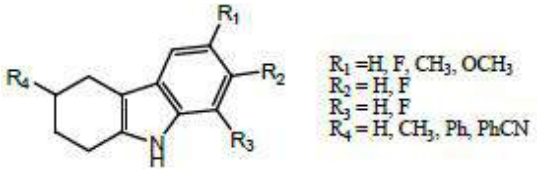

d) Nagarapu et al., 2010 carried out the Synthesis and cytotoxicity evaluation of 1-[3- (9H-carbazol-4-yloxy)-2-hydroxypropyl]-3-aryl-1H-pyrazole-5-carboxylic acid derivatives. The cytotoxicity of synthesized compounds was evaluated by a SRB (sulforhodamine B) assay against cancer cell such as SKeNeSH human neuroblastoma (NB), human A549 lung carcinoma and human breast cancer MCF-7 cell lines. The results showed that seven compounds can suppress SKeNeSH tumor cancer cell growth. Among them, compound 3d was the most effective small molecule in inhibiting SKeNeSH cell growth [38].

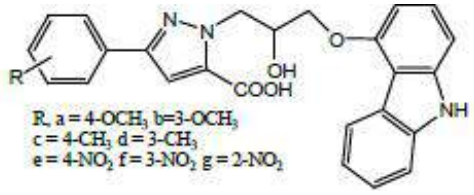

e) Shah et al., 2012 worked on the Design, Synthesis and Anticancer Evaluation of Carbazole Comprised With 1,3,4-Thiadiazole Derivative; All the synthesized compounds are evaluated for their anticancer activity by MTT assay and compared with standard drugs. The test compounds showed significant anticancer activity [39].

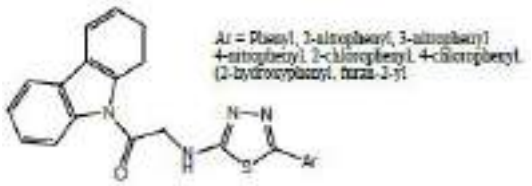

f) Haider et al., 2014 carried out the electrophilic substitution of Dimethyl 1- Methylcarbazole-2,3-dicarboxylate ie., synthesis of new b-Fused Carbazoles. Anti-proliferative activity of compounds was assessed using an XTT assay method [40].

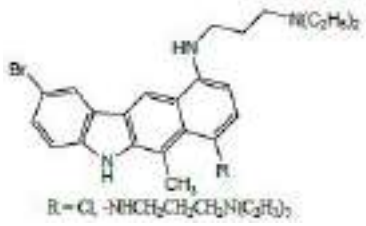

g) Tran Thi Thu Thuy et al carried out the Synthesis of novel derivatives of murrayafoline. A and their inhibitory effect on LPS-stimulated production of proinflammatory cytokines in bone marrow-derived dendritic cells. Results indicated that murrayafoline, a derivative containing 1,2,3-triazole nucleus, potentially possessed anti-inflammatory action through inhibiting production of IL-6, IL-12 p40 and TNF-α [41].

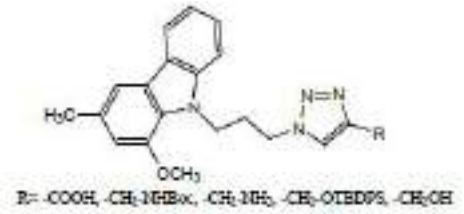

6. EXPERIMENTAL SCREENING OF ANTI-PROLIFERATIVE ACTIVITY

Some of the biological assays followed for the anticancer screening are as follows:-

6.1 Cell Culture Assay

A cell culture assay is any method which is used to assess the cytotoxicity of a material. This refers to the *in vitro* assessment of material to determine whether it releases toxic chemicals in sufficient quantities to kill cells either directly or indirectly through the inhibition of cell metabolic pathways. Cell culture assays are standardized by ASTM, ISO, and BSI (British Standards Institution). These assays can be performed in 3 methods- direct contact method, agar diffusion method and elution method. Most of the cell lines were grown in Dulbecco's modified Eagle's medium (DMEM) supplemented with 10% fetal calf serum (FCS) and 50 mg/ml penicillin/streptomycin [16].

6.2 Sulforhodamine B (SRB) Cytotoxicity Assay

The sulforhodamine B (SRB) assay is used for cell density determination, based on the measurement of cellular protein content. The method is optimized for the toxicity screening of compounds to adherent cells (104cells/well) in a 96-well format. After an incubation period, cell monolayers are fixed with 10% (wt/vol) trichloroacetic acid (TCA) and stained for 30 min, after which the excess dye is removed by washing repeatedly with 1% (vol/vol) acetic acid. The protein-bound dye is dissolved in 10 mM Tris base solution for OD determination at 510 nm using a microplate reader. The results are linear over a 20-fold range of cell numbers and the sensitivity is comparable to those of fluorometric methods [16,19].

6.3 Hoechst Staining

Hoechst stains are part of a family of blue fluorescent dyes used to stain DNA. These Bis-benzimides were originally developed by Hoechst AG and have three Hoechst stains: Hoechst 33258, Hoechst 33342, and Hoechst 34580. The dyes Hoechst 33258 and Hoechst 33342 are the ones most commonly used and they have similar excitation/emission spectra. Cancer cells (50.000 cells/well) are seeded into six-well plates and 24 h later the agents are applied. Apoptotic cells need to be visualized under a fluorescent microscope at 40 objective [16,17].

6.4 Flow Cytometry Analysis

Cancer cells have to be seeded at 5.105 cells/well onto 75 mm^2 tissue culture plates and incubated in humidified incubators at 37°C, with 5% CO2. The next day, cells are treated with two different concentrations of the anti-cancer agent (1.8 mM and 3.6 mM). On day 2 and day 4, 1.106 cells are to be sampled and stained with FITC Annexin V Apoptosis detection Kit (BD Pharmingen, Cat: 556570) according to the manufacturer's instructions. Control groups include corresponding DMSO concentrations as negative controls and CPT (5 mM) and 1% v/v hydrogen peroxide, as positive controls. Stained cells have to be kept from light on ice andanalyzed immediately using Becton Dickinson FACScalibur Flow Cytometer. Flow cytometry results are analyzed using WinMDI 2.9 software for differentially stained percentage of cells over controls and results are plotted and analyzed using GraphPad Prism version 5.00 (GraphPad Software, San Diego California USA) [16].

6.5 MTT Cytotoxicity Assay

The MTT assay is a colorimetric assay for assessing cell metabolic activity. NAD(P)H-dependent cellular oxidoreductase enzymes may, under defined conditions, reflect the number of viable cells present. These enzymes are capable of mitochondrial reduction of the yellow tetrazolium dye MTT 3-(4,5-dimethylthiazol-2-yl)-2,5-diphenyltetrazolium bromide to its insoluble formazan, which has a purple colour. Tetrazolium dye reduction is dependent on NAD(P)H- dependent oxidoreductase enzymes largely in the cytosolic compartment of the cell. Therefore, reduction of MTT and other tetrazolium dyes depends on the cellular metabolic activity due to NAD(P)H flux. Cells with a low metabolism such as

thymocytes and splenocytes reduce very little MTT. In contrast, rapidly dividing cells exhibit high rates of MTT reduction. IC50 is calculated for the samples and negative control (cells with vehicle) by the probit analysis using a simple t-test (SPSS statistical analysis software package/version 11.0, SPSS Inc., (IL), Chicago, USA) [31].

7. DISCUSSION

Heterocyclic compounds like indoles and related group of molecules are well studied by various workers and their role in myriad biological activities have been revealed. It has been observed that bulky geometry and better topology of the compounds increase their biological activities. Indole derivatives are known to perform important function as anticancer [5,6], anti-oxidant, anti-rheumatoidal, anti-HIV [7], anti-microbial [8,9], anti-inflamatory [10], analgesic, anti-pyretic [4], anti-convulsant, anti-helmintic cardiovascular [11], selective COX-2(cyclooxygenase-2) inhibitory agents [12] and also have DNA binding ability [13]. The plethora of research in medicinal biology and their anti proliferative as well as anti carcinogenic properties show enhanced anticancer activity of these chemical derivatives as compared to the standard drugs. Many novel indole retinoid derivatives like 2-substituted quinoxaline, triazolo (4,3-a) quinoxaline, 2-chloro-3(1-substituted indol-3-yl) quinoxaline, etc. 1-benzoyl-3-bromoacetyl indole, 2-Phenyl-1H indole, (Tetrazol-5-yl) methylindole, 2- thienyl-3-substituted indole, novel 1,3-diheterocycles indole, indole-3-carbinol,4-(2-(4-bromophenyl)-1H-indol-3-yl)-2-methoxy-6-(4-bromophenyl)nicotinonitrile etc. are some of the indole dervatives with anti-cancerous activities. Bis-indole derivatives and benzopyridoindoles also possess antitumorous activities. They can also be extracted from plants and are hence known as natural indoles and primarily found in cruciferous vegetables like cauliflower, cabbage, turnip, broccoli and brussels sprouts. Consuming cruciferous vegetables which are rich in phytonutrients including glucobrassicin, indole-3-carbinol,3,3'-diindolylmethane, ascorbigen, dithiolethiones and sothiocyanates has been associated with reduced risk of colon, breast and prostate cancers [14,29]. Similarly, imidazoles and indazoles are related heterocyclic compounds having specific mechanism of action against proliferative tissues. Antimetabolites like imidazoles and indazoles can be used in cancer treatment, as they impede DNA production and cell division as well as the growth in uncontrolled fashion within tumours. These are the chemicals which become the building blocks of DNA. They prevent normal nucleic acid building substances becoming incorporated into DNA during the S phase of the cell cycle, disrupting normal development and division. They also affect RNA synthesis because thymidine is used in DNA but not in RNA where uracil is used, thus causing inhibition of thymidine synthesis via thymidylate synthase selectively inhibiting DNA synthesis over RNA synthesis [31,33]. Carbazole heterocycles have also been reported to exhibit antitumor and anti neoplastic activities. The carbazole derivatives have gained the attention of researchers due to their therapeutic potential against neurological disorders and cell proliferation. The biological profiles of these new generations of carbazole like 1-substituted-6H-pyrido[4,3-b]carbazole, 2,3-Dimethylindoles and tetrahydrocarbazoles, 1- [3- (9H-carbazol-4-yloxy) -2-hydroxypropyl] -3-aryl- 1H- pyrazole-5 carboxylic acid derivatives, carbazole with 1,3,4-thiadiazole derivative etc. are under experimental investigations in murine model as well as other cell lines regarding their roles in controlling cellular proliferation [34,35,38,40]. Function of indole compounds are targeted on a number of cellular signaling pathways leading to their observed biological effects like cellular proliferation, cell cycle progression, cellular growth and development**.** All these metabolic functions are closely related to cancer progression involving up-regulation of signaling pathways associated with proliferation, angiogenesis, and invasion [42,43]. Mechanisms of apoptosis stimulation by the indole derivatives include down-regulation of anti-apoptotic gene products such as Bcl-2 and Bcl-XL as well as down-regulation of the inhibitor of apoptosis proteins, e.g. CIAPs, X-chromosome linked inhibitor of apoptose protein (XIAP) and survival. Up-regulation of pro-apoptotic factors such as *Bax* gene, liberation of mitochondrial cytochrome C in addition to stimulation of caspase-9 and caspase-3 and inhibition of the NF-kB signaling pathway are also essential steps [15,16,17]. In this connection a number of techniques like cell culture assay, sulforhodamine B (SRB) cytotoxicity assay, Hoechst staining assay, flow cytometry and MTT assay are being followed for the experimental screening of anti-proliferative activity of these chemicals [16].

8. CONCLUSION

From this work it has been revealed that various types of derivatives of indoles and the associated aromatic heterocyclic compounds can serve as future therapeutic leads for the discovery of antiproliferative agents including anticancer drugs. Apart from anticancer activity they have scores of other important applications as anti-oxidant, anti-rheumatoidal, anti-HIV, anti-microbial anti-inflamatory, analgesic, anti-pyretic, anti-convulsant and anti COX-2 agents. Thus

these classes of compounds certainly hold great promises in medicinal biology also. A further study to acquire more information concerning pharmacological activities of these compounds is in progress. The biological profiles of these new generations of indoles and the associated ones represent much progress with regard to the older compounds. The cellular mechanism of action of these compounds may even indoctrinate many unexplored areas of knowledge in the field of cancer biology.

ACKOWLEDGEMENTS

I would like to express my special thanks to Prof. C. R. Sahu, Professor of Zoology, University of Kalyani and Ms. S. Gupta for their whole-hearted cooperation in this work.

COMPETING INTERESTS

Author has declared that no competing interests exist.

REFERENCES

1. Kaushik NK, Kaushik N, Attri P, Kumar N, Kim CH, Verma AK, Choi EH. Biomedical Importance of Indoles. Molecules. 2013;18: 6620-6662.
2. Bratulescu G. A new and efficient one-pot synthesis of indoles. Tetrahedron Letters. 2008;49(6):984-986.
3. Sachdeva H, Mathur J, Guleria A. Indole derivatives as potential anticancer agents: A review. J. Chil. Chem. Soc. 2020;65(3):4900-4907.
4. Andreani A, Burnelli S, Granaiola M, Leoni A, Locatelli A, Morigi R, et al. Antitumor Activity of Bis-Indole Derivatives. J. Med. Chem. 2008;51:4563–4570.
5. El-Sayed WA, El-Kosy SM, Ali OM, Emselm HM, Abdel-Rahman AAH. Anticancer activity of new (Tetrazol-5-yl) methylindole derivatives and their acyclic c-nucleoside analogs. Acta Poloniae Pharmaceutica - Drug Research. 2012;4(69):669-677.
6. Patel H, Darji N, Pillai J, Patel B. Recent advance in anti-cancer activity of indole derivatives. Int. J. Drug Res. Tech. 2012;2(3): 225-230.
7. Xu H, Lv M. Developments of indoles as anti-HIV-1 inhibitors. Curr Pharm Des. 2009; 15(18):2120-2148.
8. Sundar L, Chang FN. Antimicrobial activity and biosynthesis of indole antibiotics produced by *Xenorhabdus nematophilus*. J Gen Microbiol. 1993;139(12):3139-3148.
9. El-Sayed WA, Megeid REA, Abbas HAS. Synthesis and antimicrobial activity of new 1-[(tetrazol-5-yl) methyl] indole derivatives, their 1,2,4-triazole thioglycosides and acyclic analogs. Arch Pharm Res. 2011;34(7):1085-1096.
10. El-Nakkady SS, Abbas SES, Roaiah HM, Ali IH. Synthesis, antitumor and anti-inflammatory activities of 2-thienyl-3-substitued indole derivatives. Global Journal of Pharmacology. 2012;6(3):166-177.
11. Nataraj KS, Venkateshwara Rao J, Jayaveera KN, Naresh K, Sruthi K. Antihelminthic and analgesic activity of some novel indole derivatives Pharmacologyonline. 2010; 2:60-67.
12. Bhat MA, Al-Omar MA, Raish M, Ansari MA, Abuelizz HA, Bakheit AH, et al. Indole Derivatives as Cyclooxygenase Inhibitors: Synthesis, Biological Evaluation and Docking Studies. Molecules. 2018;23(6):12-50.
13. El Sayed MT, Hamdy NA, Osman DA, Ahmed KM. Indoles as Anti-cancer Agents. Adv Mod Oncol Res. 2015;1(1):20-35.
14. Karikas GA. Chemoprevention molecular and biochemical mechanisms involved in cancer control and management. Health Science Journal. 2011;2(5):149-156.
15. Ahmad A, Sakr WA, Rahman KMW. Role of nuclear factor-kappa b signaling in anticancer properties of Indole compounds. Journal of Experimental and Clinical Medicine. 2011; 3(2):55-62.
16. Gurkan-Alp AS, Mumcuoglu M, Andac CA, Dayanc E, Cetin-Atalay R, Buyukbingol E. Synthesis, anticancer activities and molecular modeling studies of novel indole retinoid derivatives. European Journal of Medicinal Chemistry. 2012;58:346-354.
17. Patel HM, Darji N, Pillai J, Patel B. Design, Synthesis and anti-cancer activity of 2-Phenyl-1H Indole derivatives. International Journal of Institutional Pharmacy and Life Sciences. 2012;2(4):42-56.
18. Patil SS, Dandagvhal KR. Indole – an important scaffold in drug discovery. International Journal of Research in Pharmacy and Chemistry. IJRPC. 2016;6(2):301-311.
19. Del GP, Gudipudi DK, Montemarano N, Restivo AM, Malanowska-Stega J, Arslan AA. Oral diindolylmethane (DIM): Pilot evaluation of a nonsurgical treatment for cervical dysplasia. Gynecologic Oncology. 2010; 116(3):464–467.
20. Fares F. The anti-carcinogenic effect of Indole-3-Carbinol and 3,3'-Diindolylmethane and their

Mechanism of Action. Fares, Med Chem, 2014;1:1-8.
21. Jeong YM, Oh MH, Kim SY, Li H, Yun HY, Baek KJ, et al. Indole-3-acetic acid/horseradish peroxidaseinduces apoptosis in TCCSUP human urinary bladder carcinoma cells. Pharmazie. 2010;65(2):122-126.
22. Tilton SC, Hendricks JD, Orner GA, Pereira CB, Bailey GS, Williams DE. Gene expression analysis during tumor enhancement by the dietary phytochemical, 3,3'-diindolylmethane, in rainbow trout. Carcinogenesis. 2007;28(7): 1589-1598.
23. Abbassi N, Rakib ME, Chicha H, Bouissane L, Hannioui A, Aiello C, et al. Synthesis and antitumor activity of some substituted indazole derivatives. Arch Pharm (Weinheim). 2014; 347(6):423-431.
24. Elsayed NMY, El Ella DAA, Serya RAT, Tolba MF, Shalabya R, Abouzid KAM. Design, synthesis and biological evaluation of indazole – pyrimidine based derivatives as anticancer agents with anti-angiogenic and antiproliferative activities. Med Chem Comm. 2016;7:881-899.
25. Finlay MRV, Acton DG, Andrews DM, Barker AJ, Dennis M, Fisher E, et al. Imidazole piperazines: SAR and development of a potent class of cyclin-dependent kinase inhibitors with a novel binding mode. Bioorganic and Medicinal Chemistry Letters. 2008;18:4442–4446.
26. Jones CD, Andrews DM, Barker AJ, Bladesa K, Daunt P, East S, et al. The discovery of AZD5597, a potent imidazole pyrimidine amide CDK inhibitor suitable for intravenous dosing. Bioorganic and Medicinal Chemistry Letters. 2008;18:6369–6373.
27. Romero DH, Heredia VET, García-Barradas O, López MEM, Pavón ES. Synthesis of imidazole derivatives and their biological activities. Journal of Chemistry and Biochemistry. 2014;2(2):45-83.
28. Salahuddin, Shaharyar M, Mazumder A. Benzimidazoles: A biologically active compounds. Arabian Journal of Chemistry. 2012;1-17.
DOI: 10.1016 /j.arabjc.2012.07.017
29. Sharma V, Kumar P, Pathak D. Biological importance of the Indole nucleus in recent years: A comprehensive review. J. Heterocyclic Chem. 2010;47:491-502.
30. El-Sawy ER, Bassyouni FA, Abu-Bakr SH, Rady HM, Abdlla MM. Synthesis and biological activity of some new 1-benzyl and 1-benzoyl-3- heterocyclic indole derivatives. Acta Pharm. 2010;60:55–71.
31. El-Sawy ER, Abo-Salem HM, Mahmoud K, Zarie E. El-Metwally AM, Mandour AH. Synthesis, anticancer activity and molecular docking study of novel 1, 3-Diheterocycles Indole derivatives. International Journal of Pharmacy and Pharmaceutical Science. 2015; 6(7):377-385.
32. Baroniya S, Anwer Z, Sharma PK, Dudhe R, Kumar N. Recent advancement in imidazole as anti cancer agents: A review. Der Pharmacia Sinica. 2010;1(3):172-182.
33. Shalini K, Sharma PK, Kumar N. Imidazole and its biological activities: A review. Der Chemica Sinica. 2010;1(3):36-47.
34. Mounika KN, Jyothi AN, Raju GN, Nadendla RR. Carbazole derivatives in cancer treatment-A review. World Journal of Pharmacy and Pharmaceutical Sciences. 2015;12(4):420-428.
35. Tylińska B, Jasztold-Howorko R, Biaduń, B, Gębarowski T, Gasiorowski K. New pyridocarbazole derivatives. Synthesis and their in vitro anticancer activity. Acta Poloniae Pharmaceutica. 2013;70:823-832.
36. Kumar N, Sharma GK, Pathak D. Microwave assisted and parallel synthesis of novel substituted carbazole derivatives of biological interest. Int J Pharm Chem Sci. 2013;2:273-282.
37. Kumar T, Mahadevan K, Kumara MN. Synthesis and cytotoxic studies of 2, 3-dimethylindoles and tetrahydrocarbazoles. International Journal of Pharmacy and Pharmaceutical Sciences. 2014;6:137-140.
38. Nagarapu L, Gaikwad HK, Sarikonda K, Mateti J, Bantu R, Raghu PS, et al. Synthesis and cytotoxicity evaluation of 1-[3-(9H-carbazol-4-yloxy)-2-hydroxypropyl]-3-aryl-1H-pyrazole-5-carboxylic acid derivatives. Eur J Med Chem. 2010;45 (11):4720-4725.
39. Shah PB, Darji N, Patel B. Design, synthesis and anticancer evaluation of carbazole comprised with 1,3,4-thiadiazole derivative. International Journal of Institutional Pharmacy and Life Sciences. 2012;4:57-74.
40. Haider N, Marian B, Nagel T, Tarnai M, Tropper K. Electrophilic substitution of dimethyl 1-methylcarbazole-2,3-dicarboxylate: synthesis of new *b*-Fused carbazoles as potential antitumor agents. J. Braz. Chem. Soc. 2014;25(11):1965-1974.
41. Thuy TTT, Nguyen C, Toan QT, T Ngo, Bui T, Xuan NN, et al. Synthesis of novel derivatives of murrayafoline A and their inhibitory effect on LPS-stimulated production of pro-inflammatory cytokines in bone marrow-derived dendritic cells.

Archives of Pharmacal Research. 2013;36(7): 823-832.
42. Dan X, Zhi X. Indole alkaloids with potential anticancer activity. Current topics in medicinal chemistry, 2020;20 (21):1938-1949.
43. Li AL, Hao Y, Wang WY, Liu QS, Sun Y, Gu W. Design, synthesis, and anticancer evaluation of novel indole derivatives of ursolic acid as potential topoisomerase ii inhibitors. Int. J. Mol. Sci. 2020;21(8):2876.

UTTAR PRADESH JOURNAL OF ZOOLOGY

42(7): 56-68, 2021
ISSN: 0256-971X (P)

A BRIEF REVIEW ON THE THERAPEUTIC RESISTANCE AGAINST CANCER BY CANCER STEM CELL (CSC)

SUJIT KUMAR BHOWAL[1*]
[1]Department of Zoology, Maulana Azad College, Kolkata- 700013, India.

AUTHOR'S CONTRIBUTION
The sole author designed, analysed, interpreted and prepared the manuscript.

Article Information

Editor(s):
(1) Dr. Ana Cláudia Correia Coelho, University of Trás-os-Montes and Alto Douro, Portugal.
Reviewers:
(1) Homa mollaei, University of Birjand, Iran.
(2) Karima Al Salihi, Al Muthanna University, Iraq.
(3) Marcel Vasconcellos, Centro Universitário Serra dos Órgãos, Faculdade de Medicina, Brazil.

Received: 02 February 2021
Accepted: 07 April 2021
Published: 12 April 2021

Review Article

ABSTRACT

Cancer stem cells (CSCs) are small subpopulation of cells within tumours which possess characteristics associated with normal stem cell such as self-renewal and differentiation. CSCs play crucial role in cancer development by regulating the cancer cell survival, metastatic potential, disease relapse and poor prognosis. There are many cell markers like CD44, CD24, EpCAM, CD133, CXCR4, cMet, ALDH1 which can identify the CSCs.These cells are poorly regulated through cell cycle and also have metastatic ability as well as long life span. Chemotherapy is a part of successful cancer treatment. But the CSC's multidrug resistance mechanism (MDR) like high expression of ABC transporter, histone lysine demethylase, suppression of apoptosis, progesterone receptor membrane component-1(PGRMC1) and increased expression of aldehydrogenase-1 are responsible to resist chemotherapy. Combined therapies targeting CSCs and their progenies may represent the most promising approach for the future treatment of cancer patients. This review summarizes the characterisation and identification of CSCs, different multidrug resistance mechanism of CSCs and the advanced types of treatment mechanism.

Keywords: Cancer stem cell (CSC); CSC markers; disease relapse; metastasis; multidrug resistance; selective therapy; tumours.

1. INTRODUCTION

Cancer stem cell is a general term referring to the cancer cells capable of differentiation and self-renewal which is the role of CSCs chemotherapy resistance. The definition of CSCs does not determine their origin and the term "Cancer Stem Cell" does not mean that cancer begins from stem cell. CSCs are more differentiated than stem cells including a more limited spectrum of the cells existing in a tissue [1,2]. Some cells in a tumour may undergo some sort of genetic or epigenetic changes in the signalling pathway which results in phenotype similar to that of

**Corresponding author: Email: sujit.sb@gmail.com;*

stem cells [3,4]. These changes may happen in different types of cells such as stem cells, progenitors, and differentiated cells [5,6]. In 1994, CSCs were isolated for the first time. In 1855, German pathologist stated that cancers arise from the activation of dormant embryonic-like cells present in mature tissue and argued that cancer does not simply appear spontaneously [3,7]. One and half century later, Lapidot and colleagues came up with the CSC hypothesis [4]. The initial cell that develops cancer is not necessarily a cancer stem cell, though cancer-initiating cell and cancer stem cell are sometimes used interchangeably. The existence of CSCs was first proposed 40 years ago, though analysis of its details remains a mystery until the evolution of advanced research tools [2,8]. The best evidence to support the existence of CSCs came from the study of haematological malignancies [6]. Considering the role of embryonic stem cells and self-renewal in mature cells like blood cells, the definition of CSCs was revealed [7,9]. TPC (Tumour Propagating Cell) is the other term which has been used very often for cancer stem cells [8].

Tumour stem cell research is progressing rapidly in various fronts including studies of their origin, organization and characterization [2,10]. Cellular mechanism of their propagation, communication and signalling as well as immunological aspects are also discussed in detail after thorough studies [1,11-13]. The origin of human acute myeloid leukaemia is engraved in primitive hematopoietic cell [8,4]. The evolution of cancer stem cell has been described with detailed investigation in leukaemic cancer cells [7]. On the other hand, the nature and composition of tumour stem cells microenvironment is enlightened by Resetova et al. [14]. Cancer cells also exhibit cellular resistance against therapeutic avenues achieved through chemical and physical therapeutic modalities. In this connection, drug resistance by tumour stem cells in the form of chemoresistance is achieved by cancer stem cells [15,16]. Modulation of cell death pathways in such stem cells is also studied [17]. Thyroid cancer resistance to hemotherapeutic drugs via anticrime production of interleukin-4 and interleukin-10 is discussed by Stassi et al. [18]. Despite chemo resistance by cancer stem cells, various modalities have been under development to tame the uncontrolled propagation of stem cell populations hiding inside a cancerous tissue [19,20,21,22]. Ubiquitination is one of such pathways which is essential in targeted cancer therapy of cancer stem cell [3]. Targeting apoptosis pathways in cancer stem cells is another possibility [18]. So, cellular chemotherapy against cancer stem cellsis the need of the hour [20]. Detailed understanding and working on cancer stem cells is required to uproot the origin of the cancer cell population and thus also helpful for their management in cancer therapy [23].

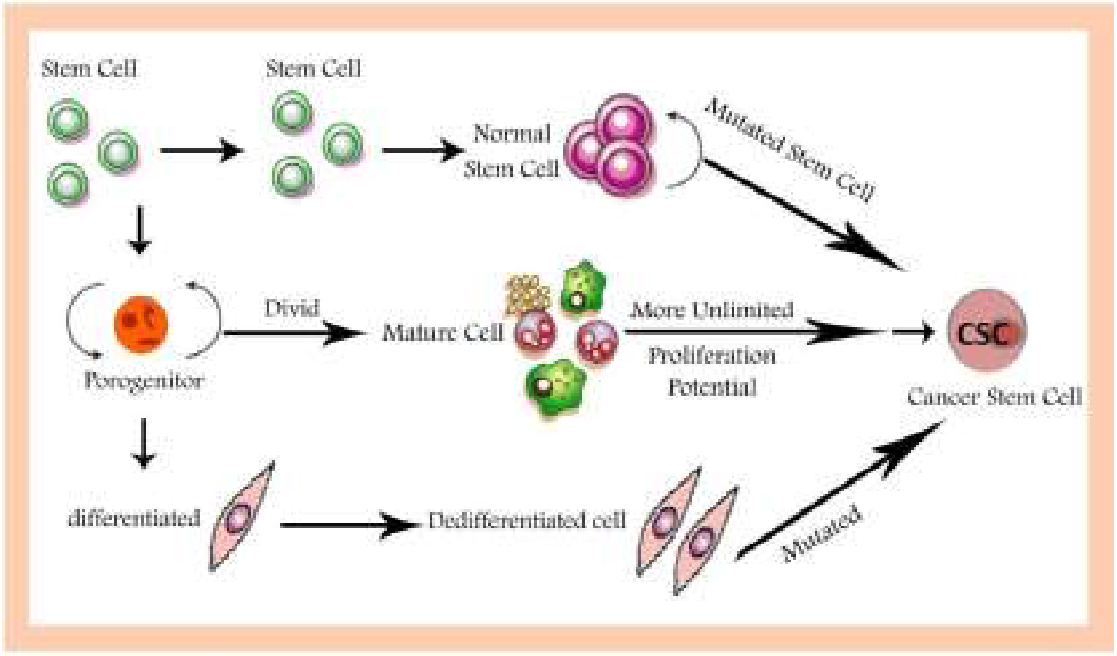

Fig. 1. Proposed model for the formation of cancer stem cells shows the origin of CSCs in different tissues [2]

2. CANCER STEM CELLS

Cells with stem-cell qualities have been identified in malignancies of haematopoietic origin and in some solid tumours. The existence of such a population would imply that the stem cell represents the cell of origin for the tumour, as illustrated in Figs. 1 and 2. One can predict that such cancer stem cells represent only a small fraction of a tumour, as they possess the capability to regenerate a tumour, and most cancer cells lack this regenerative capability. For example, when plated in soft agar or injected into mice, most tumour cells do not give rise to colonies. Similarly, in experiments performed in humans in the 1950s, unthinkable by today's ethical standards, 35 patients had an estimated one billion of their own tumour cells injected into their thigh or forearm. Only seven of these autotransplants resulted in tumour growth at the injection site. Furthermore, studies of acute myelogenous leukaemia have shown that only 0.1–1% of all cells have leukaemia-initiating activity. These leukaemia-initiating cells have many markers and properties of normal haematopoietic stem cells. So it is believed that leukaemia arises from a stem cellthat becomes transformed and gives rise to a large population of clones that proliferate but cannot self-renew or fully differentiate [12]. Similar populations of self renewing cells, such as those that carry the chromosomal translocation t(9; 22)(q34; q11), which forms the *bcr–abl*fusion gene, have also been identified in patients with chronic lymphocytic leukaemia and chronic myelogenous leukaemia (CML).

3. ISOLATION OF CSCS BY VARIOUS MARKERS

Long term cell culture, FACS (Fluorescence-activated cell sorting), and MACS (magnetic cell sorting) are the main techniques used to isolate CSCs. CSCs enrichment can be done using the FACS technique. We can also isolate cells based on the expression of special proteins of cellular-level, cell culture, epigenetic changes and expression pattern of such cellular-level markers as CD 24, CD133, ALDH1 and CD44. CSC characteristics can be determined through mRNA and miRNA expression analysis, copy number variation, etc. Then phenotypic and genotypic characteristics can be associated with *in-vitro* and *in-vivo* clinical data. Magnetic Cell Sorting (MACS) technology isolates cells with a high quality and is regarded as a standard method for cell isolation. This technique can isolate cells based on expression of special stem cell markers like CD133. Before isolation, cell markers are labelled using special monoclonal antibody or magnetic micro bead like anti

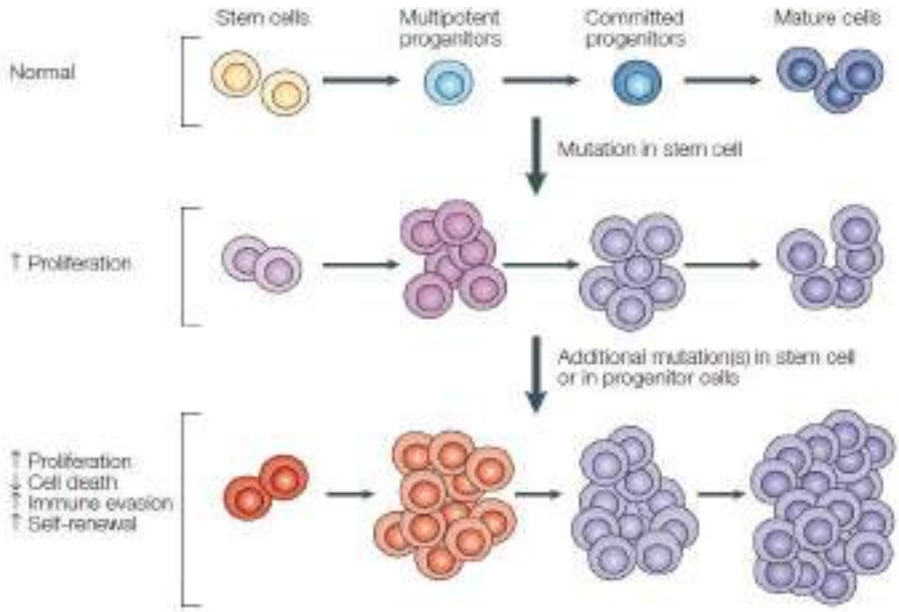

Fig. 2. Cancer stem cells and tumour progression, Normal stem cells give rise to multipotent progenitor cells, committed progenitors and mature, differentiated cells. Mutations in a stem cell give rise to a stem cell with aberrant proliferation and result in a pre-malignant lesion. Additional mutations lead to the acquisition of further increased proliferation, decreased apoptosis, evasion of the immune system, and further expansion of the stem-cell compartment that is typical of malignant tumours [7]

CD133 which is 106 times smaller than the cell's size. After labelling, magnetic isolation is carried out. Washing cells is the third step and after positive selection, marked cells are separated from unmarked ones. Positive selection is one of the best and most direct ways to isolate target cells from cell suspension. CSCs have a set of markers for detection and determination. For instance, CD133 known as Prominin 1 or AC133 is an intermembrane protein and a special surface antigen in blood stem cells and a marker for Murin neureopithelial. Although the function of CD133 is yet to be discovered, it is known as a marker for cancer tissues and isused individually or combined with other markers to isolate stem cells from many tumours like brain, prostate, colorectal, etc. In pancreatic cancer, surface markers such as ESA, CD24+, CD44+, etc. have been detected. The only selected marker identified for T ALL (T-acute Lymphoblastic Leukaemia) was CD34+ and further studies on T ALL cell lines have led to the detection of other markers like CD110 (C-MP1), CD90 (ty-1), CD44+, CD49+, CD133+ and the ALDH enzyme in colorectal cancer. ALDH1 is introduced as a stem cell marker (Table 1). Expression of ALDH1 may be associated with clinic pathologic feature in Esophageal squamous cel carcinoma patients. In the following table, some of the known markers are indicated [8,4].

4. CANCER STEM CELL RESISTANCE AGAINST DRUG AND CHEMO-THERAPY

The therapeutic strategies against cancer are facing too many problems. One of them is drug resistance. Recent researches have revealed that CSCs, especially pancreatic CSCs, play crucial roles in drug resistance which often impairs the successful use of chemotherapies. In pancreatic cancer stem-like cells were found to be more resistant to gemcitabine, commonly used against pancreatic carcinoma, and those cells were more invasive. Pancreatic CSCs were proved to contribute to drug resistance of gemcitabine as well. Another problem is that most therapies for pancreatic cancer do not affect pancreatic CSCs, which canthen re-establish tumours after treatment. The cancer stem cell developed many mechanisms to resist the drug and chemotherapy.

5. DRUG TRANSPORTERS IN STEM CELLS

Stem cells have many properties that separate them from mature, differentiated cells. In addition to their ability to self-renew and differentiate, they are quiescent, dividing infrequently. They also require specific environments comprising other cells, stroma and growth factors for their survival. One particularly intriguing property of stem cells is that they express high levels of specific ABC drug transporters. For example, haematopoietic stem cells express high levels of ABCG2, but the gene is turned off in most committed progenitor and mature blood cells [5,9]. The two ABC transporter-encoding genes that have been studied most extensively in stem cells are ABCB1, which encodes P-glycoprotein30, and ABCG2. Along with ABCC1, they represent the three principal multi drug-resistance genes that have been identified in tumour cells. These genes, members of the ABC-transporter super family, are promiscuous transporters of both hydrophobic and hydrophilic compounds (Table 2). These transporters also have important roles in normal physiology in the transport of drugs across the placenta and the intestine (more accurately, there tention of drugs in the intestinal lumen), and are important components of the blood–brain and blood–testis barriers. By using the energy of ATP hydrolysis, these transporters actively efflux drugs from cells, serving to protect them from cytotoxic agents. Mice deficient in either Abcg2, Abcb1 or Abcc1 are viable, fertile and have normal stem-cell compartments. This indicates that none of these genes are required for stem-cell growth or maintenance. However, these knockout mice are more sensitive to the effects of drugs such as vinblastine, ivermectin, topotecan and mitoxantrone, consistent with a role for these ABC transporters in protecting cells from toxins [9,24]. The drug-transporting property of stem cells conferred by these ABC transporters is an important marker in the isolation and analysis of haematopoietic stem cells. Most cells accumulate the fluorescent dyes Hoechst 33342 and rhodamine 123, but stem cells do not, as these compounds are effluxed by ABCG2 and ABCB1, respectively. Because they don't accumulate these fluorescent dyes, stem cells can be sorted by collecting cells that contain only a low level of Hoechst 33342 fluorescence. These cells are referred to as 'dull cells' or 'side population' (SP) cells. The term side population was coined because during flow-cytometry analysis, SP cells are visualized as a negatively stained 'side population' to one side of the majority of cells on a density dot plot. A large fraction of haematopoietic stem cells is found in the SP fraction40 and when isolated from mice and transplanted into irradiated mice, small numbers of these SP cells can reconstitute the bone marrow, demonstrating that these cells are pluripotent. SP cells can be isolated from many tissues including the brain, breast, lung, heart, pancreas, testes, skin and liver, and these cells might represent lineage- specific stem cells. Hoechst-33342 staining of bone marrow from ABCG2-null mice fails to detect SP cells. However, the lack of staining for SP cells occurs not because

Table 1. List of cell surface markers found on various tumour cells [4]

Tumour type	Cell surface marker references
Acute myeloid leukaemia (AML)	CD34+, CD38−
Breast cancer	EPCAM (ESA)+, CD44+, CD24−, ALDH, CD29, CD133
Ovarian cancer	CD133+, CD44+, CD117+, CD24+
Glioblastoma	CD133+, CD15+
Medulloblastoma	CD133+, CD15+
Small cell and non-small cell lung cancer	CD133+
Hepatocellular carcinoma	CD45−, CD90+
Colon cancer	CD133+, CD44+, CD26+, ALDH
Prostate cancer	CD44+, CD133+, CD49
Melonoma	CD20+, CD271+
Pancreas adenocarcinoma	CD44+, CD24+,
Renal carcinoma	CD133+
Head and neck squamous cell carcinoma (HNSCC)	CD44+, ALDH1
Lung cancer	CD133+, CD90, CD117, ALDH1

Table 2. List of ABC transporter proteins responsible for drug resistance [10]

ABC transporters involved in drug resistance			
Gene	**Protein/ alias**	**Chemotherapeutic drugs effluxed by transporter**	**Other drugs and substrates**
ABCA2	ABCA2	Estramustine	-
ABCB1	PGP/ MDR1	Colchicine, doxorubicin, etoposide, vinblastine, pacitaxel	Digoxin, saquinivir
ABCC1	MRP1	Doxorubicin, daunorubicin, vincristine, etoposide, colchicine, camptrothecins, methotrexate	Rhodamine
ABCC2	MRP2	Vinblastine, cisplatin, doxorubicin, methotrexate	Sulfinpyrazone
ABCC3	MRP3	Methotrexate, etoposide	-
ABCC4	MRP4	6-mercaptopurine, 6-thioguanine and metabolites; methotrexate	PMEA, Camp, cGMP
ABCC5	MRP5	6-mercaptopurine, 6-thioguanine and metabolites	PMEA, Camp, cGMP
ABCC6	MRP6	Etoposide	-
ABCC11	MRP8	5-fluorouracil	PMEA, Camp, cGMP
ABCG2	MXT/ BCRP	Mitoxantrone, topotecan, doxorubicin, daunorubicin, irinotecan, imatinib, methotrexate	Phenoforbide A, Hoechst 33342, rhodamine

ABC, ATP-binding cassette; BCRP, breast cancer resistance protein; cAMP, cyclic adenosine monophosphate; cGMP, cyclic guanosine monophosphate; MDR, multidrug-resistance-associated protein; MXR, mitoxantrone resistance protein; PMEA, 9-[2-(phosphonomethoxy)ethyl]adenine

these cells are absent, but because the lack of ABCG2 expression allows these cells to accumulate Hoechst dye and become fluorescence [24,10].

6. MULTIDRUG RESISTANCE MECHANISMS

6.1 Histone Lysine Demethylase and Cell Death Pathways in Cancer Stem Cells

His tone lysine demethylases promote tumourigenicity, they modulates cell death pathways in two possible ways-1) Epigenetic regulation by H3K4, H3K36 demethylation, thus repressing the transcription of pro-apoptotic or anti-proliferation related genes and H3K9, H3K27 demethylation, thereby activating anti-apoptotic or proliferation related genes; 2) Modulation of cell signalling pathways by direct lysine methylation mediated activation and inactivation of targeted proteins. His tone demethylases are known to repress mRNA expression of Bcl2, p21, ERBB2, CCNA2, BRCA1, miRlet-7e and regulate p53 functions [17].

6.2 Epigenetic Regulation of Cell Death and Proliferation

Epigenetic regulation of cell death and proliferation by histone lysine demethylases is mediated mainly

through repression of p21 by LSD1 and KDM5b. In MLL- AF9 leukaemia stem cells LSD1and p21 are essential for maintaining the properties of oncogenic potential and self-renewal. p21 is a cyclin-dependent kinase (cdk) inhibitor and is a key mediator of DNA damage induced p53-dependent cell cycle arrest and apoptosis. In leukaemic cells, p21 is necessary for self-renewal of leukaemia stem cells. LSD1 and KDM5b regulate mRNA expression of anti-apoptotic gene CDKN1 (p21). LSD1 also regulates expression of cellular proliferation genes CCNA2 and ERBB2 by binding directly to the promoters of these genes. KDM5b interacts with TFAP2C and Myc to form a complex leading to transcriptional repression of p21. As LSD1 represses the expression of p21, knockdown of LSD1 in MDA-MB 231 cell model decrease the occupancy of LSD1 on the p21 promoter and significantly increase in the repressive mark of methylated H3K9 on CCNA2 and ERBB2 promoter regions. CCNA2 encodes Cyclin A2 that functions as CDK2 kinase activator and promotes progression of cell through G1/S and G2/M phases of cell cycle. ERBB2 (HER2) is a member of epidermal growth factor (EGF) receptor family of receptor tyrosine kinases. It forms heterodimer with other members of EGF receptor family, stabilizing ligand binding and enhances downstream mitogen-activated protein kinase and phosphatidylinositol-3 kinase mediated downstream signalling pathways. Over-expression of cyclin A2 and ERBB2 corresponds to a drug resistant or aggressive phenotype of tumour cells. LSD1 can also be linked to the aberrant regulation of Wnt signalling pathways in cancer cells. Wnt signalling is important to maintain cancer stem cell state in various cancers. Treatment of colon cancer cells with LSD1 oligoamine inhibitor SL111144 led to increases in H3K4Me3, restoring expression of secreted frizzled-related proteins 2 (SFRP2). SFRP2 is a Wnt signalling pathway antagonist and it enhances the expression of the epithelial marker E-cadherine, through inhibition of the expression of SLUG, TWIST and SNAIL. SNAIL, SLUG and Twist are transcription factors involved in the epithelial mesenchymal transition (EMT) program. KDM6b act on H3K27 and is responsible for activation of anti-apoptotic gene Bcl2 transcription in hormone dependent breast cancers. Apart from normal antiapoptotic functions Bcl2 is thought to be involved in resistance to conventional cancer therapies, suggesting role of decreased apoptosis may play a role in the development of cancer. KDM5A-mediated H3K4 demethylase activity plays an important role in maintaining the proliferative capacity of breast cancer cells through repression of tumour suppressor genes, including BRCA1. Another histone lysine demethylase JARID1B leads to repression of let-7e which then increases expression of cyclin D1 [17,25]. Cycline D1 is a target gene of mir let-7e mediated gene regulation. JARID1B demethylase contributes to tumour cell proliferation through the epigenetic repression of a tumour suppressor miR let-7 that has been reported to be a direct regulator of RAS expression in human cells. In lung cancer patient samples, expression of RAS and let-7 showed reciprocal pattern, which has low let-7 and high RAS in cancerous cells, and high let-7 and low RAS in normal cells. Other targets of let-7 are some oncogenes like high mobility group A2 (HMGA2) and MYC. Histone lysine demethylase mediated epigenetic gene regulation thus can drive tumourigenesis in cancers and inhibit programmed cell death to support cancer stem cells state [26].

6.3 Non-Epigenetic Regulation of Cell Death and Proliferation

Non-epigenetic regulation by lysine histone demethylases is mediated by their potential to demethylate various cellular proteins. E2F1-p53 axis is the major target of non-epigenetic regulation of cell death and proliferation. p53 transcriptional activity is necessary to inhibit cancer stem cells growth and proliferation. His tone lysine-specific demethylase LSD1 interacts with p53 to repress p53-mediated transcriptional activetion and to inhibit p53 mediated apoptosis. LSD1 removes both mono and di-methylation at K370 of p53. Mono-methylation K370me1 represses p53 func- tion and prevents interaction of p53 with TP53BP1 (p53- binding protein 1), thus represses p53-mediated transcriptional activation in p53 negative cells (p53-/-) LSD1 removes methylation mark from E2F1 at lysine- 185. Lysine-185 methylation leads to E2F1 accumulation during DNA damage and activation of its pro-apoptotic target genes p73 and Bim (Fig. 3). E2F1 promotes DNA damage-induced apoptosis in p53 dependent as well as p53 independent manner. LSD1 mediated demethylation leads to dysregulation of the E2F1 function and promotes survival in many cancer cells [15,17].

7. INCREASED EXPRESSION OF ALDEHYDE DEHYDROGENASE IN CSC

Stem cell-like populations in normal female breast tissue are characterized by the expression of aldehyde dehydrogenase 1 (ALDH1). ALDH1, an enzyme responsible for oxidation of retinol to retinoic acid, is important for normal development and homoeostasis in several organs and is crucial during embryogenesis. Breast cancer stem cells also express ALDH1 and breast CSCs have been isolated on the basis of increased ALDH1 [24]. Indeed, expression of ALDH1 by breast tissue is considered to be a marker, in breast,

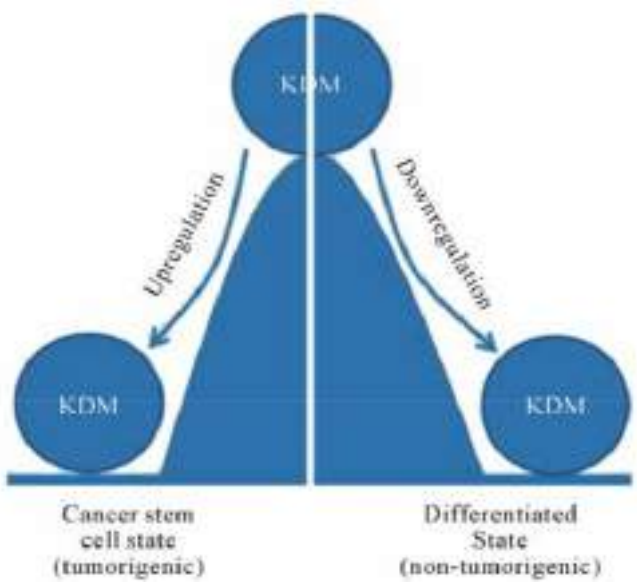

Fig. 3. General role of lysine histone demethylases in maintaining cancer stem cell state. Cancer stem cells over-express histone lysine demethylases and low expression is associated with differentiated state. KDM stands for lysine demethylase [17]

for both normal and malignant stem and progenitor cells. This finding appears to Breast cancer cells with a CD44+/CD24− phenotype have also been suggested to have tumour-initiating properties with stem cell-like features and have been shown to be associated with basal-like cancers and BRCA1 hereditary breast cancers in women [10]. The recent study showed increased invasion and tumourigenicity capacity of CD44+/CD24− breast cancer MCF7 cells *in vitro* and in nude mice [15]. A partial overlap between the CD44+/ CD24−/low population and the ALDH1+ population has been reported. The combined CD44+/ALDH1+ phenotype shows an especially high tumourigenic capacity, be- ing able to form tumours in nude mice from as few as 20 transplanted cells [10,15]. In this study, we are going to use CD44 and ALDH1 as cancer stem cell marker. The tumour microenvironment also affects cancer development and plays a significant role in prognosis. This appears to be true for the effect of stem/progenitor cells on the prognosis of human breast tumours. Stromal cells of breast tumours have been shown to be positive for ALDH1 [17]. Several studies have investigated the correlation between the expression of CSC markers and prognosis and drug resistance in female breast cancer. However, the expression of CSC markers in male breast cancer has not been well studied. Accordingly, in this study, the expression of two CSC markers—ALDH1 and CD44—in 19 male breast cancers, clinically important as ALDH1 expression has been associated with poor clinical outcome and resistance to chemotherapy in female [25].

8. ROLE OF PROGESTERONE RECEPTOR MEMBRANE COMPONENT (PGRMC1)

PGRMC1 is induced in a number of cancer types, including breast, ovarian and lung cancers, and a small study indicated that PGRMC1 is associated with poor survival in lung adenocarcinoma. PGRMC1 is also expressed in sebaceous carcinomas. PGRMC1 plays a causative role in cancer progression, because *in vitro*, PGRMC1 increases tumour cell proliferation, chemotherapy resistance and invasion, and *in vivo*, PGRMC1 increases tumour growth, angiogenesis and metastasis. There are a number of potential mechanisms through which PGRMC1 might promote tumour growth. PGRMC1 associates with the epidermal growth factor receptor (EGFR) and regulates susceptibility to the EGFR inhibitor erlotinib by increasing plasma membrane pools of EGFR. PGRMC1 also increases EGFR levels in Zebrafish. In lung cancer cells, the EGFR-PGRMC1 complex drives invasion, at least in part, by activating matrix metalloproteinases [19]. PGRMC1 is also detected in the nucleus in some cell types, where it regulates transcription and in the centromeric region of chromosomes during oocyte meiosis. PGRMC1 also localizes to the actin cytoskeleton and binds actin. In lung cancer cells, the prominent localization for PGRMC1 is cytoplasmic puncta, including early endoscopes, and numerous groups have reported similar findings in other cell types. Finally, PGRMC1 is secreted by lung cancer cells, where it has a pro-

proliferative function, and is detected in the plasma of lung cancer patients. There is a growing consensus that PGRMC1 is critical for the transport of specific receptors to the plasma membrane. The receptors include EGFR, GLP1R, glucagon-like peptide 1 receptor, and mPR1α, membrane progesterone receptor α. PGRMC1 binds to mPR1α and transports it to the plasma membrane. Indeed, PGRMC1 was originally identified as a putative hormone receptor or "receptor membrane component". Partially purified PGRMC1 binds to progesterone, and recently, progesterone binding by recombinant PGRMC1 was reported, suggesting a direct role for PGRMC1 in progesterone function. PGRMC1 has anestablished role in progesterone signalling, and in some diseases, such as breast cancer, this contributes to hormonal growth and anti-apoptotic signalling. However, PGRMC1 shares no homology with hormone receptors but has motifs that are structurally related to cytochrome *b5*, and PGRMC1 binds heme, an evolutionarily conserved function that is distinct from progesterone binding. According to the cancer stem cell theory, tumours contain a sub-population of cells with extended replicative potential that contribute to drug resistance. Cancer stem cells are thought to arise from mutations to either normal stem cells or transit amplifying cells, with key signalling contributions from the tumour microenvironment.PGRMC1 is detectable in amniotic-derived mesenchymal cells and has been identified as an important hormonal signalling intermediate in neuronal stem cells, but its expression and function in cancer-derived stem cells have not been determined. Is has been demonstrated that PGRMC1 is elevated in multiple tumour types, including head and neck cancer and in oral cancer. Using immunohistochemistry of paraffin-embedded tissue, we also confirm previous findings from western blots of frozen tissue that PGRMC1 staining correlated with survival in lung cancer patients. According to the stem cell theory, cancer stem cells are critical for the long term survival of a tumour population and its therapeutic resistance. We report here that PGRMC1 is abundant in lung cancer-derived stem cells from patients, and PGRMC1 inhibition triggered cell death in lung cancer stem cells where other therapeutic classes failed [25].

9. SUPPRESSION OF APOPTOSIS IN CSC

There are several methods of cancer treatment under discussion such as inhibiting kinases using small molecules, monoclonal antibodies, and other new treatment methods. These factors are designed individually or combined with chemotherapy to prevent the dysregulated signalling pathways which cause disorder through blocking the tumour growth or sensitizing cancer cells to death. One of the factors that let cancer cells overcome stress is their ability to avoid apoptosis. CSCs share some of their features with stem cells including dormancy, activation of DNA-repair machinery, expression of drug transporter (ABC), and natural resistance to apoptosis [19]. In thyroid cancer, therapy resistance leads to the induction of cell death, as a result of which the expression of anti-apoptotic proteins is increased along with the production of autocrine products such as (IL4) [27,14]. It has been proved that IL4 causes resistance to apoptosis in chronic lymphocytic Leukaemia and increases the anti-apoptotic proteins' expression in normal cells [18,28]. In pancreatic cancer, IL4 boosts the growth and its blockage has inhibitive effects [20]. The efficacy of chemotherapy may be enhanced when combined with anti-IL4 adjuvant treatment [29]. Several different molecular changes can regulate apoptosis among which are the activation of anti-apoptotic factors (Bcl-2, Bcl-xl, Bfl1/A1), inactivation of factors driving apoptosis such as p53. Most effective therapeutic strategies are based on special molecular biomarkers which respond to treatment in a group of patients. Apoptotic signal is a background that discovered in tumour biology and efforts have been made to activate organized death in CSCs [18,16]. According to the CSC hypothesis, manipulation of apoptotic machinery in order to eradicate tumour-initiating cells requires a huge therapeutic potential [28].

10. HEDGEHOG SIGNALLING AND CANCER

The Hedgehog molecules (SHH, IHH and DHH) are important signalling proteins in the development of embryonic stem cells and in the differentiation of many tissues. Hedgehog (HH) binds to the cell-surface receptor Patched (PTCH) and signals through the Smoothened (SMO) and GLI proteins. This pathway has a clear role in tumour formation in patients with nevoid basal-cell carcinoma syndrome, in which *PTCH* mutations have been described. Additional members of the HH pathway have also been found to be tumour suppressors or oncogene. Recently, components of the HH–PTCH pathway have been shown to be disrupted or over expressed in a large number of tumours, including sporadic medulloblastomas, breast, prostate, stomach, colon and pancreatic cancers. Most sporadic medulloblastomas have either germline *PTCH* mutations or *PTCH* silencing through methylation. Treatment of medulloblastomas with the SMO inhibitory compound cyclopamine resulted in reduced proliferation and changes in gene expression consistent with differentiation. Small-cell lung tumour cell lines show high expression of *SHH*, and their growth can be inhibited by SHH antibodies

orcyclopamine. Similarly high levels of HH expression and HH–PTCH pathway activation have been found in oesophageal, stomach, pancreatic, prostate and biliary tumours and in cell lines. Treatment with cyclopamine led to regression of pancreatic and prostatic tumours in mice, providing a model system for therapeutic development. HH over expression could lead to the unregulated growth of tissue stem cells (Fig. 4). This would result in a pre-malignant lesion in which abnormal stem-cell growth drives hyper proliferation. These unregulated stem cells would be the target for genetic events that drive the stem cells into the formation of tumour stem cells. Continued evolution of the tumour stem cells could occur to give rise to metastatic cells or further drug resistance [4,10].

11. RECENT APPROACHES FOR TARGETING PANCREATIC CSCs

Minnelide, a water-soluble prod rug of triptolide, is currently under phase I clinical trial. By decreasing CD133+tumour-initiate cells (TICs or CSCs) as well as non-TIC population, Minnelide could reduce tumour burden, which might point out a potential and effective therapy against PC [20]. Sulforaphane could inhibit the growth of pancreatic CSCs orthotopically implanted in NOD/SCID mice by inhibiting SHH pathway and also inhibits the marker of EMT in human pancreatic CSCs [16]. The dual endothelin1/VEGF signal peptide receptor, DEspR, is detected in micro vessels and tumour cells in PDAC. It can be found in CSCs isolated from PDAC-Panc1 cells as well. Researches demonstrated that DEspR inhibition could decrease Panc1-CSC xenograft tumour growth in nude rats by impacting CD133+ CSCs, suggesting that DEspR-inhibition defines a novel targeting therapy for pancreatic cancer [30]. Disulfiram, an irreversible inhibitor of ALDH, was found to play a key role in resistance to anticancer therapies for PDAC. Kim et al found human PDAC-derived cells, expressing high levels of ALDH, could show CSC features. Disulfiram is sensitive to this gemcitabine-resistant subpopulation and removes ALDH-high cancer cells and inhibits tumour growth [31]. CSCs are enriched in the side proportion (SP) cells, which over expresss stem cell markers as well as pluripotency maintaining factors, such as Nanog, Sox2, Oct4, c-Myc, signalling molecule Notch1, and drug resistant gene ABCG2. Some scientists established a combination of Sox2/Oct4/c-*myc* targeting agent, which could suppress all CSC properties and phenotypes, and reduce the tumourigenic capability of the SP cells and the resistance to conventional chemotherapy [32]. Inhibiting c-Met with XL184 or Alk-4/7 with SB431542 [33] reduces the number of CSCs in tumours and has synergistic effects with gemcitabine. While Gemcitabine treatment results in an increase of the c-Me-thigh CD44+ population, c-Met inhibition with XL184 leads to a decrease in c-Met high CD44+ cells. Combination treatment prevents the increase in the CSC population observed with Gemcitabine alone and also contributes toa decrease in c-Met high CD44+ population, suggesting that XL184 targets the CSC population specifically.

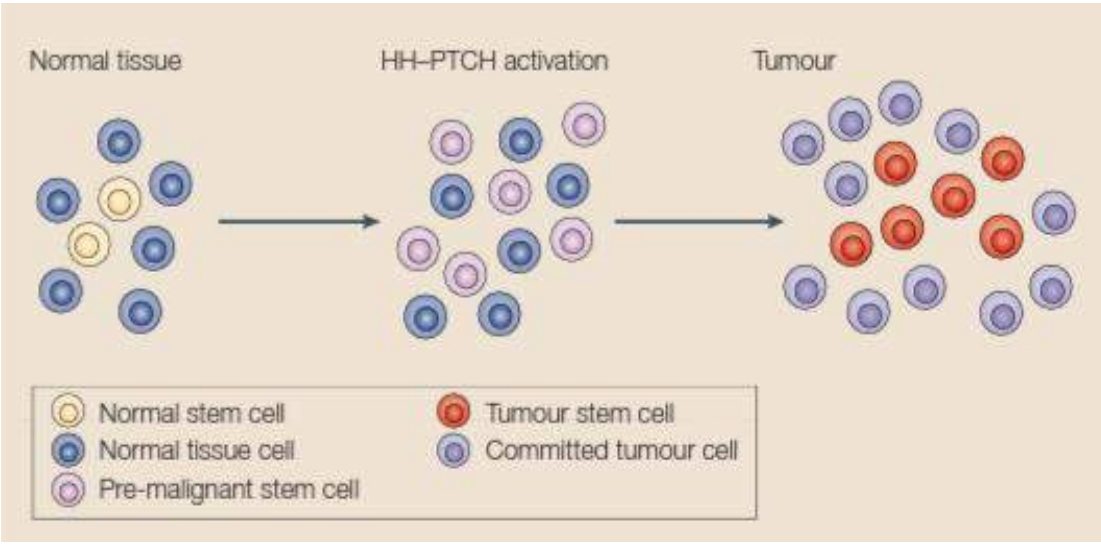

Fig. 4. In the above figure, normal stem cells (blue) undergo transformation to a stem cell with abnormal malignant. Subsequent genetic events give rise to a tumour stem cell (red) that can generate additional stem cells with abnormal signalling [10]

12. IMMUNOTHERAPY AGAINST CSCs

Nowadays, a series of immunotherapies are induced and directly targeting towards specific antigens expressed by tumour cells including CSCs. A recent study by Huang and colleges shows an anti-CD3/anti-CD133 bispecific antibody (BsAb) bounding with cytokine-induced killer (CIK) cells could target and kill CD133 high CSCs. The killing of CD133 high pancreatic (SW1990) by the effect cells (BsAb-CIK cells) was significantly ($p < 0.05$) higher than the killing by the parental CIK or by CIK cells bound only with anti-CD3 (CD3-CIK) and inhibited CD133 high tumour growth significantly. The findings introduce a novel immunotherapy for patients with cancer containing CD133 high CSCs by selectively targeting this population [23,34]. Immunotherapy with unconventional T cells such as $\gamma\delta$T cells is based on their potent HLA-nonrestricted cytotoxicity against different tumour entities and their additional capacity to recognize and present antigens to αβT cells [21,22]. Oberg demonstrated how bispecific antibodies that selectively recruit $\gamma\delta$T cells to tumour antigens expressed by cancer cells illustrate the tractable use of endogenous $\gamma\delta$T cells for immunotherapy [35]. They isolated $\gamma\delta$T cells from patients with PDAC tumour infiltrates lyse pancreatic tumour cells after selective stimulation with phosphorylated antigens and designed bispecific antibodies that bind CD3 or Vγ9 on $\gamma\delta$T cells andHer2/neu (ERBB2) expressed by pancreatic tumour cells [36,11]. Both antibodies enhanced $\gamma\delta$T-cell cytotoxicity with the Her2/Vg9 antibody also selectively enhancing release of granzyme B and perforin and reduced growth of pancreatic tumours grafted into SCID-Beige immunocompromised mice. As mentioned above, high level of ALDH was related with pancreatic CSCs. Visus et al. used ALDH asa marker for identifying and selectively targeting pancreatic CSCs as well [12,35,37]. They generated ALDH1A1-specificCD8+ T cells in order to eliminate ALDH+ CSCs, which induced growth inhibition of CSCs and reduction of metastasis. However, ALDH1A1-specific CD8+ T cells are not CSCs-specific. They could target normal ALDH+ stem cell as well [13].

13. DISCUSSION

Acquiring genetic change, clonal evolution, and the tumour microenvironment promote progression of cancer, metastasis and therapeutic resistance. These events correspond to the establishment of the great phenotypic heterogeneity and plasticity of cancer cells that contribute to tumour progression and resistance [23]. Cancer stem cells are likely to share many of the properties of normal stem cells that provide for a long lifespan, including relative quiescence, resistance to drugs and toxins through the expression of several ABC transporters, active DNA-repair capacity and resistance to apoptosis [38]. Therefore, tumours may have a built-in population of drug-resistant pluripotent cells that can survive chemotherapy [20] and repopulate the tumour. Cancer stem cells can acquire resistance to chemotherapy by a range of mechanisms, including the mutation or over expression of the drug target [31], inactivation of the drug, or elimination of the drug from the cell [15]. Typically, tumours that recur after an initial response to chemotherapy are resistant to multiple drugs (HDR) [6,15]. In the usual view of drug resistance, one or several cells in the tumour population obtain genetic alterations that confer drug resistance. These cells have a selective advantage that allows them to overtake the population of tumour cells following cancer chemotherapy [39]. Current therapies target proliferating cells and quickly achieve tumour mass reduction, but leave the CSCs unaffected and these, over time, originate tumour recurrence [23]. But, CSC-targeted therapies attack the root of the tumour by killing the CSCs. Since the rest of the tumour population, although highly proliferative, is short-lived and lacks self-replicative capability, eventually the tumour dries out and is cured [39]. Amalgamation of both kinds of approaches should be feasible to achieve quick reduction that would be also definitive. Cancer stem cells (CSC) are associated with the mechanisms of chemo resistance to different cytotoxic drugs or radiotherapy, as well as with tumour relapse and a poor prognosis [26]. Despite managing chemo resistance of cancer stem cells, various other modalities have also been under development to deal with the uncontrolled propagation of CSC populations hiding inside a cancerous tissue [19,20,21,22]. Ubiquitination is one of such pathways which is essential in targeted cancer therapy of cancer stem cell [3]. Targeting apoptosis pathways in cancer stem cells is another possibility [18]. So, cellular chemotherapy against cancer stem cells is the need of the hour [20]. Detailed understanding and working on cancer stem cells is required to uproot the origin of the cancer cell population and thus also helpful for their management in cancer therapy [23]. Some studies have shown that mitochondria sometimes play a central role in the propagation and maintenance of CSCs because of the ability of this organelle to modify cell metabolism, allowing survival and avoiding apoptosis clearance of cancer cells [40]. Thus, the whole mitochondrial cycle, from its biogenesis to its death, can be targeted by different drugs to reduce mitochondrial fitness, allowing for a restored or increased sensitivity to chemotherapeutic drugs. Once mitochondrial misbalance is induced by a specific drug in any of the processes of mitochondrial metabolism, an augmentation in reactive nitrogen/oxygen species is

achieved and, subsequently, activation of the intrinsic apoptotic pathway in such cells is accomplished [40].

14. CONCLUSION

Finally, it is to be expected that CSCs from different cancer types share many similarities in their basic biology, implying that similar therapeutic approaches could be used in many different cancers. The challenge is now to find a way to specifically target CSC without causing toxicity to normal cells. Cancer cells are themselves unique in their properties which confer them immortality and spreading ability throughout the body. Nonetheless the CSCs hiding inside cancer tissue microenvironment is much more lethal in such activities which ultimately make the tumours more destructive. Prevailing therapeutic procedures target only proliferating cell mass, thus quickly reducing the tumour, but leaving the CSCs untouched causing tumour recurrence over time. The repeated exposure of such chemotherapies may develop resistance in CSCs against an array of chemicals. Wining over or bypassing chemo resistance is one of the possible pathways to combat CSCs.

COMPETING INTERESTS

Author has declared that no competing interests exist.

REFERENCES

1. Li Y, Ajani J, Song S. Drug resistance and Cancer stem cells. Cell communication and signalling: CCS, 2021;19(1):19.
   DOI: 10.1186/s12964-020-00627-5
2. Bjerkvig R, Tysnes BB, Aboody KS, Najbauer J, Terzis AJ. Opinion: The origin of the cancer stem. cell: Current controversies and new insights. Nature Reviews Cancer. 2005;5:899-904.
3. Liu L, Yin S, Brobbey C, Gan W. Ubiquitination in cancer stem cell: Roles and targeted cancer therapy. STEMedicine. 2020; 1(3): e37.
   DOI: 10.37175/stemedicine. v1i3.37
4. Lapidot T, Sirard C, Vormoor J, Murdoch B, Hoang T, Caceres-Cortes J, Minden M, Paterson B, Caligiuri MA, Dick JE. A cell initiating human acute myeloid leukaemia after transplantation into SCID mice. Nature. 1994;367: 645-648.
5. Li Q, Wu J, Chen S, Zhao Y. Cancer stem cells: A new target for cancer therapy. Histology and Histopathology. 2018;33(12): 18004.
   DOI: 10.14670/HH-18-004
6. Soltanian S, Matin MM. Cancer stem cells and cancer therapy. Tumour Biology. 2012;32:425-440.
7. Huntly BJ, GillilandDG. Leukaemia stem cells and the evolution of cancer-stem-cell research. Nature Reviews Cancer. 2005;5:311-321.
8. Bonnet D, Dick JE. Human acute myeloid leukaemia is organized as a hierarchy that originates from a primitive hematopoietic cell. Nature Medicine. 1997;7:730-737.
9. Cammareri P, Lombardo Y, Francipane MG, Bonventre S, Todaro M, Stassi G. Isolation and culture of colon cancer stem cells. Methods in Cell Biology. 2008:311-324.
10. Atena M, Reza MA, Mehran G. A Review on the biology of cancer stem cell. Stem Cell Discovery. 2014;4:83-89.
11. Huang J, Li C, Wang Y, Lv HY, Guo YL, Dai H, et al. Cytokine-induced killer (CIK) cells bound with anti-cd3/anti-cd133 bispecific antibodies target cd133 (high) cancer stem cells in vitro and *in-vivo*. Clinical Immunology. 2013;149:156-168.
12. Himoudi N, Morgenstern DA, Yan M, Vernay B, Saraiva L, Wu Y, et al. Human γδT lymphocytes are licensed for professional antigen presentation by interaction with opsonized target cells. Journal of Immunology. 2012;188:1708-1716.
13. Braza MS, Klein B. Anti-Tumour immunotherapy with Vγ9Vδ2 T lymphocytes: From the bench to the bedside. British Journal of Haematology. 2013;160:123-132.
14. Resetkova E, Reis-Filho JS, JainRK, Mehta R, Thorat MA, Nakshatri H, et al. Prognostic impact of aldh1 in breast cancer: a story of stem cells and tumour microenvironment. Breast Cancer Research and Treatment. 2010;123(1):109-111.
15. Dean M, Fojo T, Bates S. Tumour stem cells and drug resistance. Nature Review Cancer. 2005;5:275-284.
16. Chuthapisith S. Cancer stem cells and chemoresistance. Cancer Stem Cells Theories and Practice, InTech, Shanghai; 2011.
    DOI: 10.5772/13789
17. Thakur R, Mishra D. Modulation of cell death pathways in cancer stem cells: targeting histone demethylases. Advances in Bioscience and Biotechnology. 2012;3:720-730.
18. Stassi G, Todaro M, Zerilli M, Ricci-VitianiL, Di Liberto D, Patti M, et al. Thyroid cancer resistance to hemotherapeutic drugs via

autocrine production of interleukin- 4 and interleukin-10. Cancer Research. 2003;63: 6784-6790.

19. Honeth G, Bendahl PO, Ringner M, Saal LH, Gruvberger-Saal SK, Lovgren K, et al. The CD44+/CD24- phenotype is enriched in basal-like breast tumours. Breast Cancer Research. 2008;10:53.
20. Rich JN, Bao SD. Chemotherapy and cancer stem cells. Cell Stem Cell. 2007;1:353-355.
21. Kim SK, Kim H, Lee DH, Kim TH, Kim T, Chung C, et al. Reversing the intractable nature of pancreatic cancer by selectively targeting ALDH-high, therapy-resistant cancer cells. PLoS ONE. 2013;8:e78130.
    Available:http://dx.doi.org/10.1371/journal.pone.0078130
22. Wang X, Liu Q, Hou B, Zhang W, Yan M., Jia H, et al. Concomitant targeting of multiple key transcription factors effectively disrupts cancer stem cells enriched in side population of human pancreatic cancer cells. PLoS ONE. 2013;8:e73942.
    Available:http://dx.doi.org/10.1371/journal.pone.0073942
23. Shenouda S, Kulkarni K, Abuetabh Y, Sergi C. Cancer Stem Cells and their Management in Cancer Therapy. Recent Patents on Anti-Cancer Drug Discovery. 2020; 15(3).
    DOI: 10.2174/1574892815666200713145931
24. Price JE, Tarin D. Low incidence of tumourigenicity in agarose colonies from spontaneous murine mammary tumours. Differentiation. 1989;41:202–207.
25. Ginestier C, Hur MH, Charafe-Jauffret E, Monville F, Dutcher J, Brown M, et al. ALDH1 is a marker of normal and malignant human mammary stem cells and a pre-dictor of poor clinical outcome. Cell Stem Cell. 2007;1(5): 555-567.
26. Ghasemi S, Xu S, Nabavi S, Amirkhani M, Sureda A, Tejada S, et al. Epigenetic targeting of cancer stem cells by polyphenols (cancer stem cells targeting). Phytotherapy Research; 2021.
    DOI: 10.1002/ptr.7059
27. YanW, ChenY, YaoY, Zhang H, WangT. Increased invasion and tumourigenicity capacity of CD44+/ CD24- breast cancer mcf7 cells *in-vitro* and in nude mice. Cancer Cell International. 2013;13(1):62.
28. Dancescu M, Rubio Trujillo M, Biron G, Bron D, Delespesse G, Sarfati M. Interleukin 4 protects chronic lymphocytic leukemic b cells from death by apoptosis and upregulates bcl-2 expression. Journal of Experimental Medicine. 1992;176:1319-1326.
29. Hampton KK, Stewart R, Napier D, Claudio P, Craven R. PGRMC1 levation in multiple cancers and essential role in stem cell survival. Adv Lung Cancer (Irvine). 2015;4(3): 37-51.
30. Signore M, Ricci-Vitiani L, De Maria R. Targeting apoptosis pathways in cancer stem cells. Cancer Letters. 2013;332: 374-382.
31. Avendaño C, Menéndez JC. Inhibitors of multidrug resistance to antitumour agents (MDR). Current Medicinal Chemistry. 2002;9: 159-193.
32. Banerjee S, Nomura A, Sangwan V, Chugh R, Dudeja V, Vickers SM, et al. CD133+ tumour initiating cells in a syngenic murine model of pancreatic cancer respond to minnelide. Clinical Cancer Research. 2014;20: 2388-2399.
33. Li SH, Fu J, Watkins DN, Srivastava RK, Shankar S. Sulforaphane regulates self-renewal of pancreatic cancer stem cells through the modulation of Sonic Hedgehog-GLI pathway. Molecular and Cellular Biochemistry. 2013;373:217-227.
34. Herrera VL, Decano JL, Tan GA, Moran AM, Pasion KA, Matsubara Y, et al. DE spRroles in Tumour vasculo-angiogenesis, invasiveness, CSC-Survival and anoikis resistance: A common receptor coordinator paradigm. PLoS ONE. 2014;9(1):e85821.
    Available:http://dx.doi.org/10.1371/journal.pone.0085821
35. Oberg HH, Peipp M, Kellner C, Sebens S, Krause S, Petrick D, et al. Novel bispecific antibodies increase γδT-cell cytotoxicity against pancreatic cancer cells. Cancer Research. 2014; 74:1349-1360.
36. Lonardo E, Hermann PC, Mueller MT, Huber S, Balic A, Miranda-Lorenzo I, et al. Nodal/activin signalling drives self-renewal and tumourigenicity of pancreatic cancer stem cells and provides a target for combined drug therapy. Cell Stem Cell. 2011; 9:433-446.
37. Visus C, Wang Y, Lozano-Leon A, Ferris RL, Silver S, Szczepanski MJ, et al. Targeting $ALDH^{bright}$ human carcinoma-initiating cells with ALDH1A1-specific CD8+ T cells. Clinical Cancer Research, 2011;17:6174-6184.

38. Miyoshi N, Mizusima T, Doki Y, Mori K. Biomarkers of Cancer Stem Cells in Cancer Therapy. 2019;51-59.
DOI: 10.1007/978-981-13-7295-7_5

39. Garcia-MayeaY, Mir C, Masson F, Paciucci R, Leonart M. Insights into new mechanisms and models of cancer stem cell multidrug resistance. Seminars in Cancer Biology. 2020;60:166-180.

40. García-Heredia J, Carnero A. Role of mitochondria in cancer stem cell resistance. Cell. 2020;9(7):1693.

UTTAR PRADESH JOURNAL OF ZOOLOGY

42(24): 988-993, 2021
ISSN: 0256-971X (P)

CHANGED INFECTIVITY OF GAMMA EXPOSED *Leishmania donovani*: LIGHT MICROSCOPIC VIEW

SANJUKTA MANNA [a*]

[a] Post Graduate Department of Zoology, Maulana Azad College, Kolkata, India.

AUTHOR'S CONTRIBUTION

The sole author designed, analysed, interpreted and prepared the manuscript.

Article Information

Editor(s):
(1) Dr. Osama Anwer Saeed, University of Anbar, Iraq.
Reviewers:
(1) Philip Asumang, Kwame Nkrumah University of Science and Technology, Ghana.
(2) Ferenc Orosz, Center for Natural Sciences, Hungary.

Received: 20 October 2021
Accepted: 26 December 2021
Published: 28 December 2021

Original Research Article

ABSTRACT

The use of γ-irradiated live attenuated *Leishmania donovani* parasites as a potential therapeutic agent against visceral leishmaniasis enhance the long-lasting protective immunity to host. Promastigotes of *L. donovani* exposed to gamma radiation (Co^{60} Source, Gammacell 220) at 20krad resulted in significant parasitisation of mononuclear phagocytic system *in vivo and in vitro*. Irradiation at this dose revealed altered parasitisation and optimum infection after acquiring the shape of amastigote-like organism. Few of them engulfed by macrophages and rest of the parasite remained side by side in the field as if they could not recognize the macrophages. Morphologic changes of *L. donovani* such as shrinkage of cytoplasm, loss of flagellum and progressive loss of motility, all were induced by 20 krad Gamma radiation (1.33MeV).

Keywords: Promastigotes; radiation; mononuclear; amastigote-like.

1. INTRODUCTION

Leishmania donovani, the causative organism of the dreaded disease 'kala-azar' in India and also other tropical countries have been known to impose its virulence and infectivity during its transformation from promastigote to amastigote stage within the host [1]. This disease is fatal if left untreated in over 95% cases. It remains one of the top parasitic diseases with outbreak and mortality potential [2]. All *Leishmania* spp. regardless of the disease syndrome, resulting from the infection, parasitize members of the host's mononuclear phagocyte system [3]. The development of modern vaccine technologies against various infectious diseases are in great hope and effective vaccine against infectious diseases like visceral leishmaniasis (VL) will be possible if various stress full conditions like the influence of heat shock, drugs and radiation impart transient effect on the parasite to elicit an enhanced immune response against those diseases. The literature on the effects of electromagnetic radiation upon *Leishmania* sp. is not extensive and mention only a few [4,5]. So far, many researchers attempted to develop a successful vaccine against the disease using killed attenuated parasites [6], recombinant protein vaccine [7], DNA vaccines

**Corresponding author: Email: sanjukta_manna@rediffmail.com;*

[8] etc. As the use of live non-attenuated parasites as vaccine candidates has a chance of reversion of virulence factors, it was recommended by WHO to develop more immunogenic radio-attenuated parasites without posing a risk of progressive infection [9]. The use of γ-irradiated live attenuated *Leishmania* sp. in the treatment of leishmaniasis has long been mentioned by different research groups [10,11,12]. Therefore, we have intended to investigate the nature of infection after inoculation with gamma irradiated live attenuated *Leishmania donovani* to hamster host. The light microscopic observations of *in vitro* and *in vivo* inoculation presented here offer a way to analyse the phenomena of attachment and internalization of gamma irradiated *Leishmania donovani* to hamster spleen macrophage.

2. MATERIALS AND METHODS

2.1 Parasite Culture and Exposed Doses

100 ml of *Leishmania donovani* (MHOM/IN/1983/AG83) culture ($3.7x10^7$ cells/ml) were exposed to gamma rays (Gammacell 220) at the dose of 20krads (12 krads/hr) at an exposure distance of 50 cm to the 100% radiation area and temperature maintained with 23°C.

2.2 Light Microscopic Study of Whole Cell

Few drops of nonirradiated and irradiated parasites were fixed on slides by methanol, stained with Geimsa and PBS (0.1 M, pH 7.2). The length and width of nonirradiated and irradiated parasites were determined by oculometer and photographs were taken in Carl Zeiss Axiolab Microscope under oil immersion. Irradiated cultures were taken on the Neubauer haemocytometer slide and the parasites were counted after Trypan blue exclusion method [13,14].

2.3 Attachment and Uptake of Promastigotes to Cultured Macrophages of Hamster (*Mesocricetus auratus*)

Macrophage collection and culture were followed after Chang and Dwyer [15]. The hamster's peritoneal exudate cells (macrophages) were harvested with RPMI-1640 and suspended in a polystyrene culture plate with nonirradiated and irradiated cell culture of *Leishmania donovani*. The cells were allowed to adhere for 2 hrs at 37°C in a humid atmosphere of 5% CO_2, 95% air. After 3 hours of incubation the culture medium was removed from each plate and was washed twice with Dulbecco's phosphate-buffered saline (PBS) to remove free parasites. The macrophages and phagocytosed parasites were fixed in methanol and then stained with Giemsa for determination of the intracellular parasite number. At least 100 cells were counted on a plate and the numbers of parasites per 100 infected cells were determined.

2.4 Endocytic Index

The endocytic index [16] was calculated by multiplying the percentage of infected macrophages and the mean number of parasites per infected cell.

$$\text{Endocytic index} = \frac{\text{Mean number of intracellular parasite}}{\text{infected macrophage}} \times \%\ \text{of infected macrophage}$$

$$\text{Mean number of intracellular parasites} = \frac{\text{Total numbr of intracellular parasite}}{\text{total number of macrophages}}$$

2.5 *In vivo* Study and Determination of Spleen Weight

Post irradiation *in vivo* studies was carried out by intracardial inoculation of nonirradiated and irradiated parasites to golden hamsters (*Mesocricetus auratus*). A group of 6 hamsters of about 200 g body weight were injected intracardially with nonirradiated and irradiated promastigotes. The animals were divided into two groups with three animals for infection with the nonirradiated parasites and with irradiated parasites. The animals were killed by cervical dislocation after 6 weeks from the inoculation. Spleens were dissected out from the treated hamsters and weighed.

2.6 Imprint Cytology and Endocytic Index

In imprint cytology, a monolayer of cells is formed and amastigotes are easily identifiable. A tissue specimen of the spleen was subjected to imprint cytology by the repeated pressing of its cut flat surface on microscopic slides. After staining with Giemsa, the parasite burden of the spleen was assessed [17].

The percentage of infected macrophages was determined by random examining at least 100 cells under high magnification of Trinocular Microscope, ZEISS. The mean number of intracellular parasites per infected macrophages was also determined and the endocytic index [16,18] was calculated. Experiments were repeated thrice.

3. RESULTS AND DISCUSSION

3.1 Morphological Changes

Nonirradiated parasites appeared slender, with along free anteriorly attached single delicate flagellum (20 µm) and posterior end gradually tapering to a point (Fig. 1a). There were no twists in the body. Promastigotes consistently showed a pale area of lightly stained cytoplasm within the cell. The deep coloured nucleus occupied a central position in the cell.

The irradiated parasites became ellipsoidal and the flagellar length became shorter (12 µm). The reservoir extended deeply into the cell's cytoplasm and the configuration was intermediate between promastigote and amastigote. After this exposure, a homogeneous population of amastigote-like forms or more or less sausage-shaped forms developed (Fig. 1b).

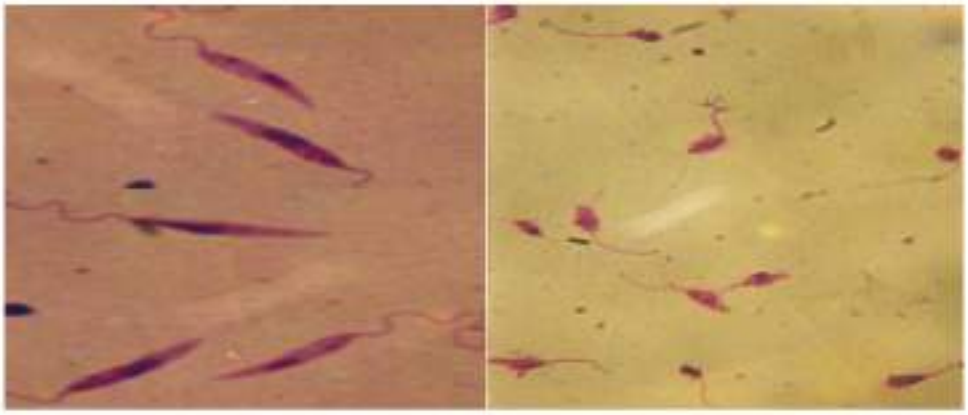

Fig. 1. (a) Nonirradiated Promastigote, (b) Irradiated Promastigote

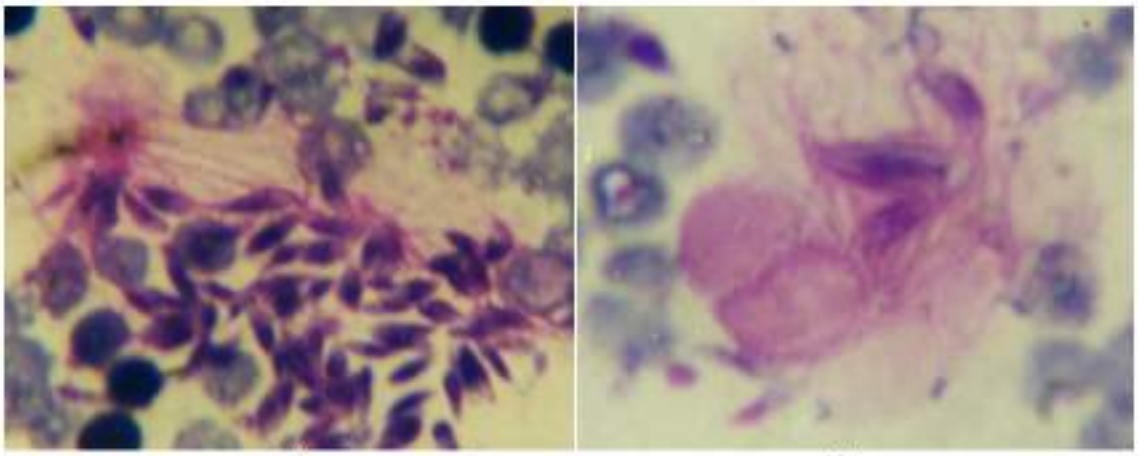

(a) (b)

Fig. 2. *In vitro* interaction of (a) nonirradiated promastigote and splenic macrophage (b) irradiated promastigote and splenic macrophage

Table 1. Endocytic index of non-irradiated and irradiated *L. donovani*

Radiation dose	Percentage of infected macrophages	Mean number of parasites per infected macrophages	Endocytic index
Non irradiated	22 ± 1.98	1.36 ± 0.09	29.9 ± 0.18
20 krad	30 ± 2.08	28 ± 0.12	84 ± 0.249

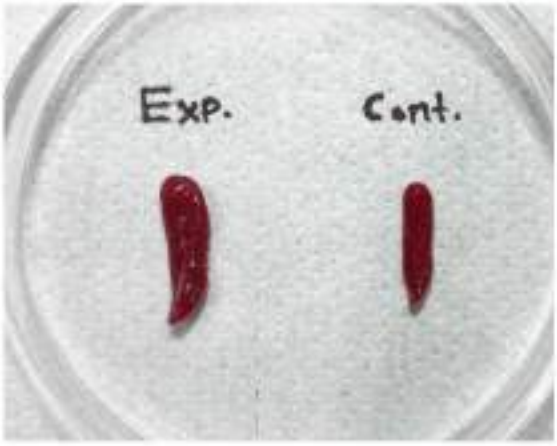

Fig. 3. Changes in spleen weight

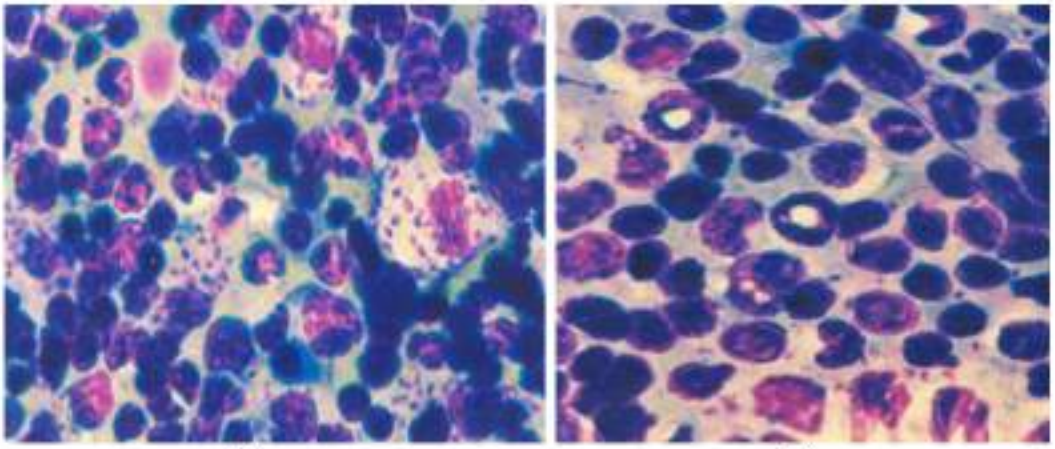

Fig. 4. Amastigotes in spleen macrophages inoculated with (a) nonirradiated promastigotes and (b) irradiated promastigotes

3.2 Mode of Attachment and Uptake of Nonirradiated and Irradiated Promastigotes by Macrophages (*In vitro*)

Morphologically distinct phagocytic events of macrophages were observed after promastigote binding, including the formation of tubular pseudopodia and cytoplasmic extension devoid of cell organelles in close contact with the parasites and ruffles. In case of nonirradiated promastigote, some macrophages containing promastigotes and others showing partially engulfed promastigotes had been clearly found (Fig. 2a). Contact between promastigotes and macrophages were generally random, although macrophage migration and eventual engulfment of promastigotes attached to the glass surface by macrophages through their flagellar tip was occasionally seen. Shortly after internalization most of the parasites were in very long, case-fitting phagosomes that exactly follow their outline suggests that ingestion mainly occurs by a zipper mechanism sequentially engulfing the different parts of the parasites. 5-6 promastigotes were attached with individual macrophage at a time.

In case of irradiated promastigotes, some notable features had been found. For 20 krad irradiated promastigotes, partially engulfed promastigotes were found. The engulfed promastigotes within the macrophage assumed an oval shape (Fig. 2b). Not total phagocytosis occurred, few irradiated promastigotes remained side by side in the field of macrophage suspension as if they could not recognize each other [19]. They were morphologically changed to amastigote-like form *in vitro*.

Endocytic index: In the case of inoculation with 20 krad irradiated promastigotes percentage of macrophage infection increased and so also the mean number of parasites per infected macrophages

resulting the endocytic index enhances at 20 krad radiation doses. The ratio of infected cells was approximately 8% greater in 20 krad irradiated cells than nonirradiated cells.

3.3 Engulfment of Nonirradiated and Irradiated Promastigotes by Macrophages (*in vivo*)

The masses of the spleen were 235 ± 20 and 300 ± 20.3 mg in weight infected with nonirradiated promastigotes and irradiated promastigotes at 20 krad respectively (Fig. 3). There was a heavy parasite load of macrophages in the spleen of hamster inoculated with nonirradiated promastigote and produced an early potency with a rapidly ascending parasitemia.

Microscopic examination of spleen smears from hamsters inoculated with parasites nonexposed and exposed at radiation dose revealed LD bodies. The hamsters inoculated with nonirradiated parasites showed normal infection and there was a peak parasitisation in parasitophorous vacuoles of macrophages after 42days. It showed that amastigotes occurred individually or in clusters (each macrophage with 3.5± 0.5 x 10^7 amastigotes) (Fig 4a). Few macrophages were ruptured and liberated the amastigotes in plasma. The parasite cytoplasm in the macrophage was stained as dark blue and only nuclear material could be seen. In case of 20 krad irradiated parasite limited number of macrophages were filled with amastigotes (each macrophage with 2.5± 0.5 x 10^7 amastigotes) (Fig. 4b). and rendered the organisms nonpathogenic while they were still active for receptor attachment.

4. CONCLUSION

The radio-attenuated pathogens are more immunogenic than their normal counterparts. The use of radio-attenuated *Leishmania* parasites is in practice for quite a long time now. In the present study, *Leishmania donovani*, an important protozoan for causing human health hazard kala-azar, were irradiated to get the attenuated condition of the parasite which might be proven to be a protective agent against infection. Earlier the organomegaly of the liver and spleen of the experimental BALB/c mice treated with attenuated parasites showed a reduction in the spleen and liver size at 100-Gy and 150-Gy, while animals infected with 50-Gy irradiated leishmania showed lesser response [20]. From the process of phagocytosis *in vitro* and *in vivo*, it was observed from our study that after acquiring the shape of amastigote-like form at 20 krad radiation doses, the promastigote cells infect the macrophage cells with slightly declined infectivity and could be developed into immunological markers of protection in animal models as higher radiation doses interfere their infectivity. This result was consistent with the use of γ-irradiated *Leishmania* sp. as a potential vaccine against cutaneous leishmaniasis in CBA mice by earlier treatises (12). The dose of radiation applied on *Leishmania* sp. is one of the important factors influencing the eventual level of protection although opinions differ regarding the optimum dose and source of radiation.

ETHICAL APPROVAL

The project is formulated following the guidelines of Institutional Animal Ethics Committee and got approval from the faculty Research Committee and hamsters had been killed for the present study following guidelines of the Committee (F.No.25/250/2012-AWD).

COMPETING INTERESTS

Author has declared that no competing interests exist.

REFERENCES

1. Tabbara KS. Progress towards *Leishmania* vaccine. Saudi Medical Journal. 2006;27:942-950.
2. Available:https://www.who.int/news-room/fact-sheets/detail/leishmaniasis. 8 January, 2022.
3. Miller HC, Twohy DW. Infection of macrophages in culture by Leptomonads of *Leishmania donovani*. Journal of Protozoology. 1969;14:781-789.
4. Lemma A, Cole L. *Leishmania enrrietti:* radiation effects and evaluation of radioattenuated organisms for vaccination. Experimental Parasitology.1974;35:161–169.
5. Datta S, Adak R, Chakraborty P, Haldar AK, Bhattacharjee S, Chakraborty A, Roy S, Manna M. Radio-attenuated leishmanial parasites as immunoprophylactic agent against experimental murine visceral leishmaniasis. Experimental Parasitology. 2012;130:39–47.
6. Okwor I, Liu D, Beverley SM, Uzonna JE. Inoculation of killed *Leishmania major* into immune mice rapidly disrupts immunity to a secondary challenge via IL-10-mediated process. Proceedings of National Academy of Science U S A. 2009;33:13951-13956.
7. Peters NC, Bertholet S, Lawyer PG, Charmoy M, Romano A, Ribeiro-Gomes FL, Stamper LW, Sacks DL. Evaluation of recombinant *Leishmania* polyprotein plus glucopyranosyl lipid A stable emulsion

vaccines against sand fly transmitted *Leishmania major* in C57BL/6 mice. Journal of Immunology. 2012;189:4832-4841.

8. Basu R, Bhaumik S, Basu JM, Naskar K, De T, Roy S. Kinetoplastid membrane protein-11 DNA vaccination induces complete protection against both pentavalent antimonial-sensitive and -resistant strains of *Leishmania donovani* that correlates with inducible nitric oxide synthase activity and IL-4 generation: evidence for mixed Th1- and Th2-like responses in visceral leishmaniasis. Journal of Immunology. 2005;174:7160-7171.
9. Demicheli MC, Reis BS, Goes AM, de Andrade AS. *Paracoccidioides brasiliensis*: attenuation of yeast cells by gamma irradiation.Mycoses. 2006;49:184-189. Available:http://dx.doi.org/10.1111/j.1439-0507.2006.01229.x
10. Alexander J, Russel DG. The interaction of *Leishmania* species with macrophages. Advances in Parasitology. 1992;31:175-253.
11. Howard JG, Stephen N, Hale C, Liew FY. Prophylactic immunization against experimental leishmaniasis: I. Protection induced in mice genetically vulnerable to fatal *Leishmania tropica* infection. Journal of Immunology. 1982;129:2206–2212.
12. Rivier D, Bovay P, Shah R, Didisheim S, Mauel J. Vaccination against *Leishmania major* in a CBA mouse model of infection: role of adjuvants and mechanism of protection. Parasite Immunology. 1999;21:461–473.
13. Freshney R. Culture of animal cells: A manual of basic technique. Alan R. Liss. Inc., New York. 1987;117.
14. Basu MK. Liposomal Delivery of Antileishmanial Agents. The Journal of Applied Research. 2005;5(1):221-236.
15. Chang KP, Dwyer DM. Multiplication of a human parasite (*Leishmania donovani*) in phagolysosomes of hamster macrophages *in vitro*. Science (Wash D.C.). 1976;193:678.
16. Bianco C, Griffen FM, Silverstein SC. Studies of the macrophage complement receptor, alteration of receptor function upon macrophage activation. Journal of Experimental Medicine. 1975;141:1278-1281.
17. Stauber LA, Franchino E, Grun J. An eight-day method for screening compounds against *Leishmania donovani* in golden hamster. Journal of Protozoology.1958;5:269-273.
18. Wales A, Kusel JR. Biochemistry of irradiated parasite vaccines: suggested models for their mode of action. Parasitology Today. 1992;8(11):358-63.
19. Manna S. Alteration In in -Vitro Infectivity of *Leishmania donovani* Exposed to Gamma Radiation. Asian Journal of Biomedical and Pharmaceutical Sciences. 2016;6(58):27-30.
20. Datta S, Manna M, Khanra S, Ghosh M, Bhar R, Chakraborty A, Roy S. Therapeutic immunization with radio-attenuated *Leishmania* parasites through i.m. route revealed protection against the experimental murine visceral leishmaniasis. Parasitology Research. 2012;111:361–369.

UTTAR PRADESH JOURNAL OF ZOOLOGY IMPACT OF Thelohanellus mrigalae TRIPATHI, 1952 ON Cirrhinus mrigala: PREVALENCE, HISTOPATHOLOGICAL AND HAEMATOLOGICAL ALTERATIONS

Research · May 2021

DOI: 10.13140/RG.2.2.25174.57924

CITATION
1

READS
179

2 authors:

Sanjukta Manna
Maulana Azad College,kolkata,India
12 PUBLICATIONS **46** CITATIONS
SEE PROFILE

Sudipta Naskar
University of Calcutta
4 PUBLICATIONS **21** CITATIONS
SEE PROFILE

UTTAR PRADESH JOURNAL OF ZOOLOGY

42(9): 41-49, 2021
ISSN: 0256-971X (P)

IMPACT OF *Thelohanellus mrigalae* TRIPATHI, 1952 ON *Cirrhinus mrigala*: PREVALENCE, HISTOPATHOLOGICAL AND HAEMATOLOGICAL ALTERATIONS

SANJUKTA MANNA[1*] AND SUDIPTA NASKAR[1]

[1]Department of Zoology, Maulana Azad College, 8 Rafi Ahmed Kidwai Road, Kolkata-700013, India.

AUTHORS' CONTRIBUTIONS

This work was carried out in collaboration between both authors. Author SM designed the study, performed the statistical analysis, wrote the protocol and wrote the first draft of the manuscript. Author SN managed the analyses of the study. Both authors read and approved the final manuscript.

Article Information

Editor(s):
(1) Dr. Angelo Mark P Walag, University of Science and Technology of Southern Philippines, Philippines.
Reviewers:
(1) Raquel Ivveth Ruiz Calderón, Universidad del Quindío, Colombia.
(2) Irom Bassey Okey, Cross River University of Technology, Nigeria.

Received: 20 February 2021
Accepted: 24 April 2021
Published: 01 May 2021

Original Research Article

ABSTRACT

Thelohanellus mrigalae Tripathi, 1952 is the important myxosporean parasites causing hemorrhagic thelohanellosis disease in *Cirrhinus mrigala*, a fresh water teleost. Infected fishes show profound swelling, formation of pus, cyst on gill filament and infiltration of pathogen into connective tissue. About 238 live specimens of *Cirrhinus mrigala* were examined and myxozoan parasite *T. mrigalae* were identified which implicates host specificity. Any significant infection was not observed in the sampling period of March-July, whereas prevalence of *T. mrigalae* was much higher in the period of November to February which is post-monsoon period in West Bengal. During monsoon, moderate infection was observed as rain water is the main factor for spreading spore. The plasmodia of *T. mrigalae* were located in the intrafilamental epithelial site of gill. The plasmodia were cylindrical and creamy-white patch and contained ellipsoidal spores as valvular shape. The spores were 20.4 – 22.1 (±6.34) µm in length and 8.5 – 10.2 (±0.87) µm in width. An oblong, irregularly shaped mass of protoplasm was observed between the polar capsule and spore capsule. The polar capsule was 10.2 – 13.5 (±0.05) µm in length and 3.4 – 4.25 (±0.5) µm in width containing a polar filament coiled perpendicular to the longitudinal axis of the spore body. Histology of gill filaments showed a series of nodules of various sizes distorting the normal architecture of the gill cartilage. Distention of the gill filament was pronounced and lamellae adjacent to the cyst were no longer present. Necrotic lesions and hyperplasia were extensively observed in the gill filaments. Infected fish had lower RBC counts, higher WBC counts and more fragile erythrocytes than control fish. Haemorrhaging was distinctly visible. The increase in number of mucous goblet cells on the gill lamellae of infected fish enhance the diffusion distance between water and blood haemoglobin and rapidly impair Oxygen (O_2) and Carbon dioxide (CO_2) exchange.

**Corresponding author: Email: sanjukta_manna@rediffmail.com;*

Keywords: Myxosporean; plasmodia; polar capsule; polar filament; gill lamella; goblet cells.

1. INTRODUCTION

Myxosporean pathogens are continually emerging and threatening the development of pisciculture. They cause production losses and some fish have to be discarded because they are unsightly and not considered to be fit for human consumption [1]. Different diseases are caused by this type of pathogen such as proliferative kidney disease, whirling disease, ulcerative disease etc in major carp. Therefore, the contribution to the knowledge of fish parasites is a prerequisite for healthy, rapid fish production and correct diagnosis of the disease agent of epizootics [2].

All myxozoans achieve transmission to new hosts by multicellular spores comprised of external valve cells that enclose infectious amoeboid cells (sporoplasms) and cells bearing polar capsules. The fish that attacked by myxozoan parasite showed in difficulties to breathe because it found the existence of a nodule or cyst on the gill filaments [3]. Upto now more than 108 species belonging to the genus *Thelohanellus* Kudo, 1933 [4] have been reported in the literature as parasites of freshwater and marine fishes in several geographical areas [5]. Members of this genus are highly host-specific and generally histozoic in various organs. Pathogenic *Thelohanellus* spp. causes "thelohanellosis", a disease characterized by severe hemorrhaging and first described by Yokoyama et al. [6] for *Thelohanellus hovorkai* Akhmerov, 1960 [7] in carp (*Cyprinus carpio*). Basu et al. [8] listed 32 Indian species of the genus *Thelohanellus* Kudo, 1933 [4]. In India, *Thelohanellus* spp. have been reported predominantly in three states namely West Bengal [9-11], Punjab [12,13] and Andhra Pradesh [14,15]. The presence of plasmodia of *T. mrigalae* was revealed as whitish cysts with microscopic spores. They were characterized by pyriform or broadly ellipsoidal spores (valvular view), which look slimmer in sutural view [16].

Since very scanty and infrequent information are available from *C. mrigala* infected by myxozoan parasites worldwide. Here we describe the genus *T. mrigalae* inhabiting *C. mrigala* in detail including its seasonal prevalence, morphometry, histopathological alterations of host tissue, histochemical analysis of mucous cells in gill filament and secondary lamellae and haematological alterations of fish to help farmers in taking appropriate measures to prevent heavy losses of Mrigal fish, an important carp.

2. MATERIALS AND METHODS

2.1 Sampling

238 *Cirrhinus mrigala* ranging from 750 to 850 g in weight and 30-35cm in length were purchased from Taltala market, near Maulana Azad College, Kolkata-13 throughout one year (2019). A parasitological survey was conducted on several organs and tissues, especially the gill filaments. Parasitized gill filaments from the infected host specimens were examined and analyzed using standard protocols [17-19].

2.2 Seasonal Variation and Prevalence

We have studied and examined the protozoan parasite *T.mrigalae* (Myxozoa: Myxosporea) and its prevalence throughout the year of 2019. Number of highly infected, moderately infected and noninfected (non-significant) fishes were identified and counted and infestation period categorized into March-June (Summar), July-October (Rainy) and November-February (Winter). Prevalence frequency index (PFI) was estimated following the formula given by Margolis et al. [20].

$$\text{Prevalence (\%)} = \frac{\text{Total number of infected X 100}}{\text{Total number of fish host examined}}$$

2.3 Morphometry

Macroscopically visible lesions or myxosporean cysts as plasmodia on gills were examined by naked eyes. For morphological and taxonomic measurements, at least one fresh plasmodium was taken from infected gill on slide and ruptured to release their spores. Spores were placed on a slide with normal saline and examined by using a high-resolving oil immersion objective with adjusted illumination of Trinocular Microscope, ZEISS and photographed with the Sony cyber shot DSC-T10 camera and calibrated by ocular micrometer. Smears of parasite spore were prepared, air-dried for 1h, fixed in absolute methanol and stained with Giemsa stain in phosphate buffer (pH 7.2) for 1 h. Presumptive *T. mrigalae* plasmodia were measured, cysts were crushed to obtain spores, and their total length, body length and width (in µm) were determined with ZEISS, Trinocular Microscope. Parasite identification was done according to Hoffman [19] and Feist & Longshaw [21]. Mean and standard deviations of each plasmodia and spore dimension were obtained from fresh mature spores.

2.4 Histopathological Examination

Tissue samples from highly infected, moderately infected and noninfected gills were fixed in 10 % formalin, then dehydrated in a series of alcohols, cleared in xylol, embedded in paraffin wax, and sectioned by a microtome at 6µm thick [22]. Tissue sections were stained with hematoxylin and eosin. The stained sections of gills were examined and photographed. This technique demonstrated the location of cysts within the gills.

2.5 Histochemical Analysis

Gill tissue sections were taken from the middle portion of the gill arches of highly infected, moderately infected and noninfected fishes. Tissue samples were fixed in 10 % formalin, then dehydrated in a series of alcohols, cleared in xylol, embedded in paraffin wax, and sectioned by a microtome at 5µm thickness. Sections were stained with combinations of Alcian Blue- Periodic acid-Schiff (AB-PAS) reagent at pH 2.6 for visualizing mucous goblet cells [23]. Mucous goblet cell counts were made under oil immersion (field size 0.20 mm) and the number of mucous cells containing glycoprotein was expressed as a percentage of the total cell population against pathogenic response.

2.6 Haematological Study

Blood samples were taken by caudal venipuncture after anaesthesizing both the highly infected, moderately infected and noninfected fishes. Total RBC and WBC counts were determined manually with the Neubauer counting chamber after the blood was diluted with Daice diluting fluid solution. Blood smears were prepared immediately by air dried, fixed in 95% methanol for 5mins then stained with Giemsa and observed through light microscope. Giemsa-stained blood smears were used for the measurement and assessment of any morphological alterations of blood cells. Blood cells were identified on the basis of morphology and dimensions using a stage and ocular micrometer.

3. RESULTS AND DISCUSSION

3.1 Seasonal Variation

During the study period a total of 238 numbers of live *Cirrhinus mrigala* were examined.

T. mrigalae is the most prevalent protozoa parasite of *C. mrigala* and were host specific because these were less infecting other major carp. From July to February (both monsoon and winter) plasmodia were detected on the gills of 650 to 750 g adult *C.mrigala* collected from Taltala Market, Entally, Kolkata-13. These protozoans were found mostly on gills. In winter season, the prevalence of *T.mrigalae* reached at 87.62% and gradually decreased in summer (17.64%) and monsoon (41.5%) (Table.1). This indicates that the winter was the most vulnerable period to get parasitic infestation. The water quality gets deteriorated and dissolved oxygen level become decreased during this period and the fishes were in stressed condition which favours the spreading several parasitic diseases. Mukherjee et al. [24], reported that low pH and low temperature were the major factor for spreading protozoan infection in fishes. Monsoon is the onset of myxosporean infection due to the availability of their intermediate host *Tubifex* sp, an oligochaete.

3.2 Light Microscopic Observations

Primary symptoms were mucus laden gills due to the presence of plasmodia within the entire length of the gill filament. Large, creamish milky white, elongated plasmodia present on the gill filament, 15-20 in number, containing1000-1500 microscopic *T.mrigalae* spores (Fig. 1b). The spores were ellipsoidal capsular structure with pointed anterior end and broad rounded posterior end with single valve. Spores (n=6) measured 20.4 – 22.1 (±6.34) µm in length and 8.5 – 10.2 (±0.87) µm in width. Valves were joined along a thickened straight suture line. A single polar capsule was situated anteriorly and occupied three fourth of the spore body cavity. It measured about 10.2–13.5 (±0.05) µm in length and 3.4 – 4.25 (±0.5) µm in width. Coiled polar filament arranged perpendicular to the polar capsule axis. The uninucleated crescentic sporoplasm was confined to a small portion behind the capsule. A medium sized vacuole occupied the vacant spaces of sporoplasm (Fig. 2).

3.3 Histopathological Changes

Histological studies showed that the noninfected gill lamellae have normal architecture (Fig. 3a) but in highly infected gill section the plasmodia were embedded partly or completely in the gill tissues (Fig. 3b). The growing curved plasmodia caused distortion of gill at their site of infection and also in the adjacent layers. The plasmodia produced the cysts by joining numerous small plasmodia (many- to-one type). The cysts containing plasmodia located in the central sinus of the gill filaments immediately adjacent to the gill filament cartilage. The cysts were spherical to elliptical in shape each containing more than 1000 parasites and surrounded by flattened epithelial cells.

Necrotic changes and hyperplasia were extensively observed in the gill arches in severe infection (Fig. 3c). Some of the cysts were also infiltrated by epithelial cells and macrophages (Fig. 3d). Epithelial desquamation and lamellar fusions were noticed. Swelling at the tips of secondary lamellae, curling, degeneration of secondary lamellae observed and oedema increased vacuolation and substituted by numerous growing plasmodia reducing the functional area of gill (Fig. 3e, f, g, h).

Table 1. Seasonal variations in PFI % age of *T. mrigalae* on *C. mrigala*

Parasite	Season's variations in PFI% age		
T.mrigalae	Summer (March-June)	Monsoon (July- October)	Winter (November-February)
	17.64	41.5	87.62

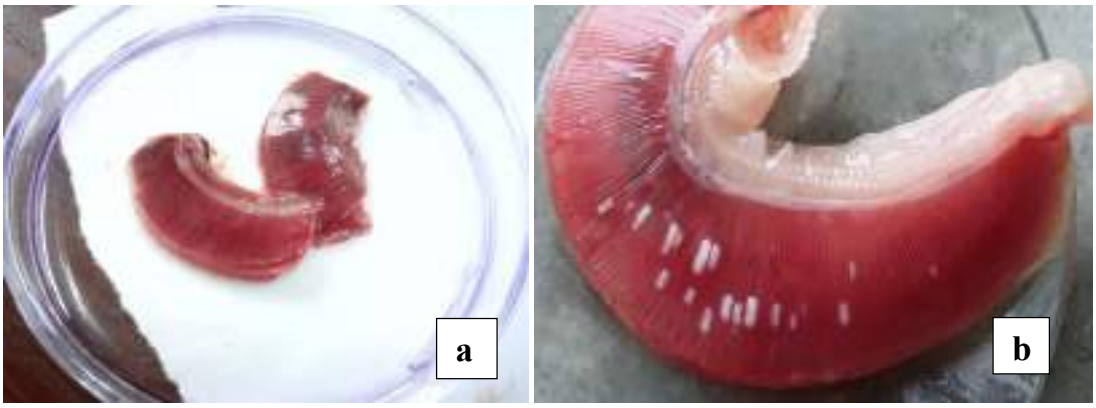

Fig 1(a) Noninfected gill and (b) Infected gill of *C. mrigala* with cyst

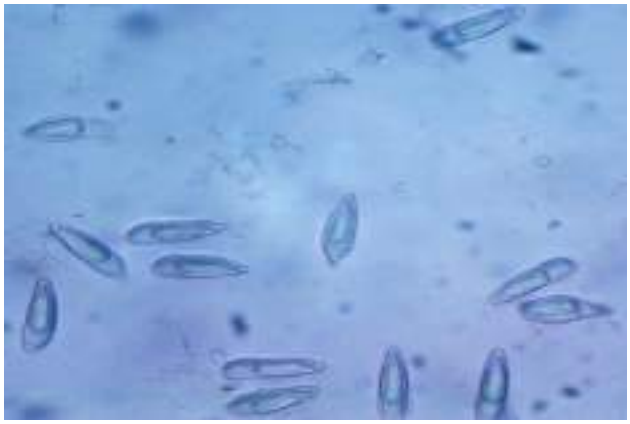

Fig. 2. *T. mrigalae* spores

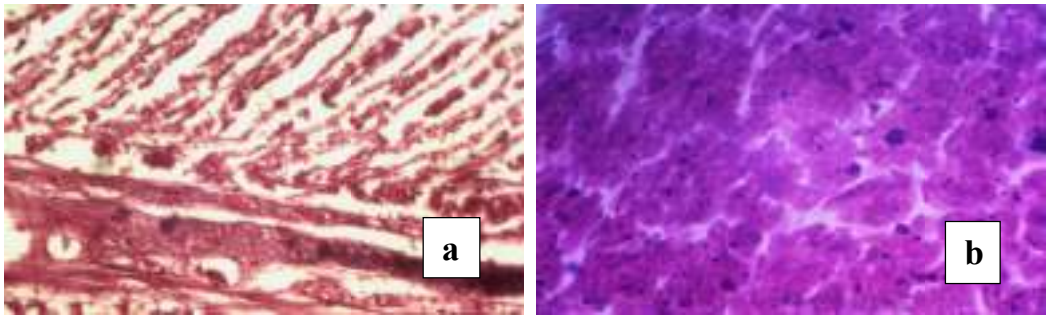

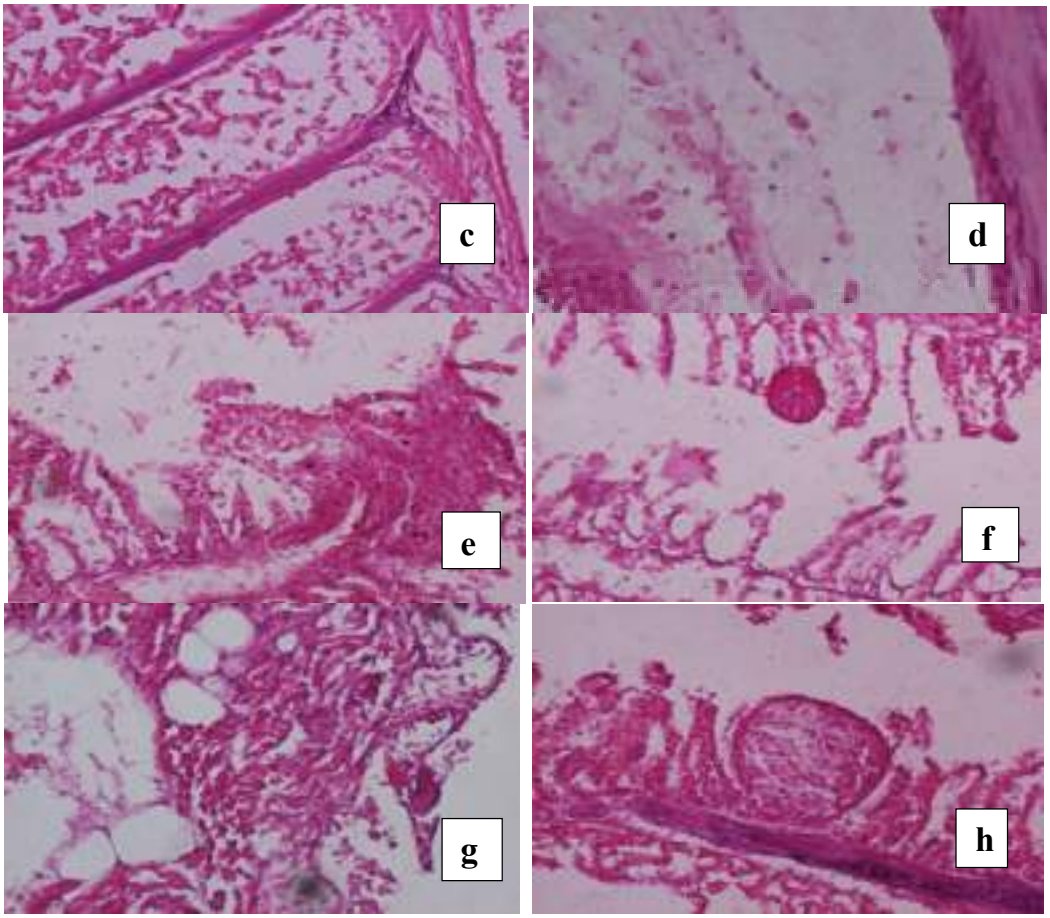

Fig. 3. Histopathology of gills of *C. mrigala* infected with *T.mrigalae* (a)Noninfected gill filament, (b)Intrafilamental plasmodia, (c)Necrotic changes, (d)Infiltration of macrophage cells, (e) Curling, (f)Degeneration of secondary lamellae, (g)Vacuolation, (h)Growing plasmodia

3.4 Histochemistry

Mucous goblet cells detected in the epithelium of gill filaments and their secretion may be a mechanism for adaptation to different stressed conditions of the aquatic environment. Mucous goblet cells counts were made under oil immersion (field diameter 124mm) and the number of goblet cells containing glycoprotein was expressed as a percentage of the total mucous cell population on 10 random fields in each section of gill lamella (Fig.4). With the combined Alcian Blue-Periodic Acid Schiff technique mucous goblet cells were stained magenta colour and demonstrated the presence of neutral and acid mucopolysaccharide groups. *T.mrigalae* infection resulted in hyperplasia and hypertrophy of these cells. During winter season infected fish gills showed higher proportion of magenta coloured secreted mucous goblet cells (Fig. 5b) in areas with lamellar epithelial hypertrophy compared to gill areas with healthy lamellar and filament morphology in moderately infected as well as with gills from uninfected groups (Fig. 5a). The mucosal barriers of the gill are the first line of defense for teleosts and contain a number of immunologically important factors, including immunoglobins, cytokines, proteases, lysozyme, antimicrobial peptides and complement factors [25]. The mucins, present in secreted mucous are mainly comprised of carbohydrates, which themselves can a□ect pathogen growth, virulence and adhesion to epithelia [26]. Jones et al. [27] and Powell et al. [28] observed that the production of the high amounts of glycoprotein within mucous cell populations had been shown in response to parasitic infection and deter the proliferation of pathogenic micro-organisms in freshwater fishes. A single type of mucous cell secretes the different acid and neutral glycoproteins which engaged in the prevention of epithelium damages and increase the water blood barrier for respiratory gases diffusion and consequently reduces O_2 uptake [29] and CO_2 excretion [30].

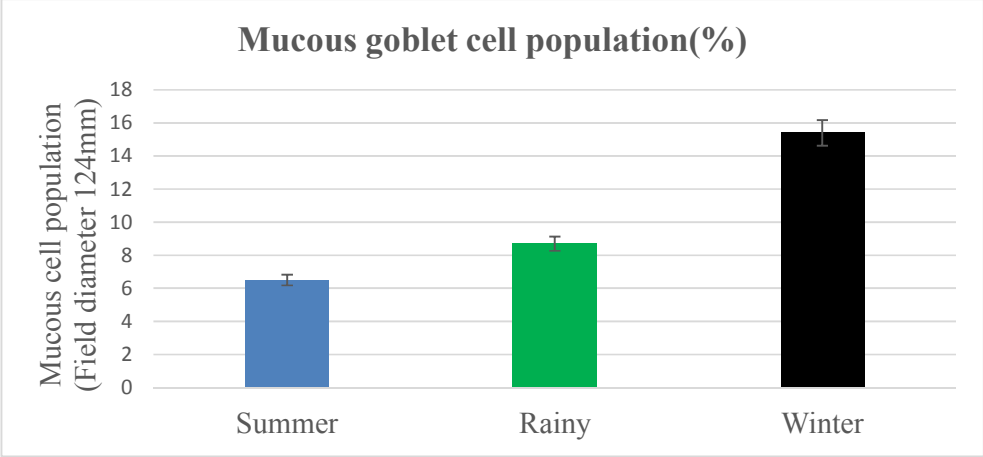

Fig. 4. Relative abundance ofsecreted mucous goblet cells with respect to season

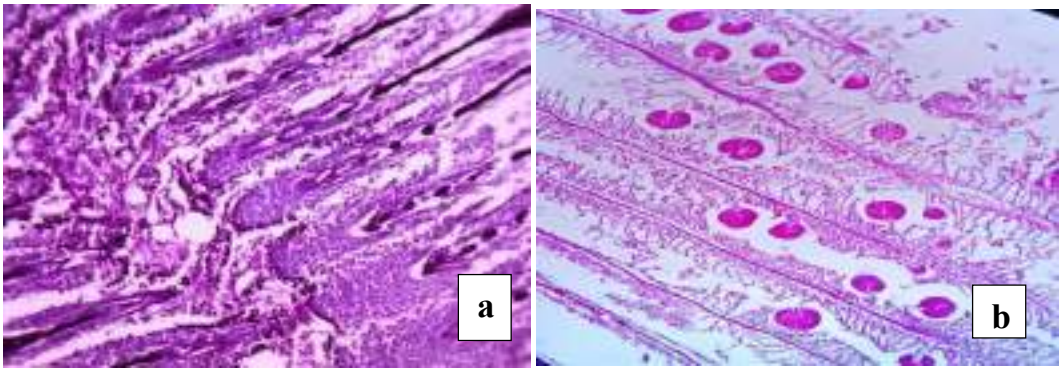

Fig. 5.(a)Noninfected healthy lamellae structure, (b) Infected lamellae with mucous goblet cells

3.5 Haematological Changes

In the Giemsa stained blood smear, deformed RBCs were evident. The deformities were mostly elongated erythrocytes measured 12.5±0.05µm in comparison to noninfected erythrocytes which measured 9.5±0.05 µm in length (Fig. 6a, b), chromatin condensation, hemolysis, membrane wrinkling, vacuolation of erythrocytes and basophilic stippling (Fig.6b). Erythrocyte counts in healthy noninfected *C.mrigala* were 3.90±0.5 × 10^6/mm^3. The highly infected *C.mrigala* during winter season revealed very low erythrocyte count (0.89±0.5 × 10^6/mm^3). Under diseased condition fish erythrocytes undergo amitotic divisions (Fig.6c). Large number of enucleated and ruptured RBCs as well as damaged leukocytes were evident. Swelling and amitotic division of circulating erythrocytes were found to have tendency to cause haemolytic anaemia in teleost fish.White blood cells significantly increased in highly infected fish (20±0.5 x10^6/mm^3) (Table.2) and differentiation into lymphocyte, eosinophil and basophil (Fig. 6d) were evident. However, no significant differences in RBC count occurred between the males and females of *C.mrigala* in case of both noninfected and infected fishes. Decreased RBC and increased WBC were reported due to epizootic ulcerative syndrome by heavy infestation of *T.mrigalae* Increased WBC was suggesting their importance in fish cell mediated immune response as they were the main component of inflammatorty exudate [31].

Table 2. Total counts of red blood cells (RBC), white blood cells (WBC) in noninfected, moderately infected and highly infected *C. mrigala*

	Blood parameters	Non infected (Control)	Moderate infection	High infection
Cirrhinus mrigala	RBC (×10^6)	3.9 ±0.5	1.49±0.5	0.89±0.5
	WBC (×10^6)	4.1± 0.05	16±0.25	20±0.5

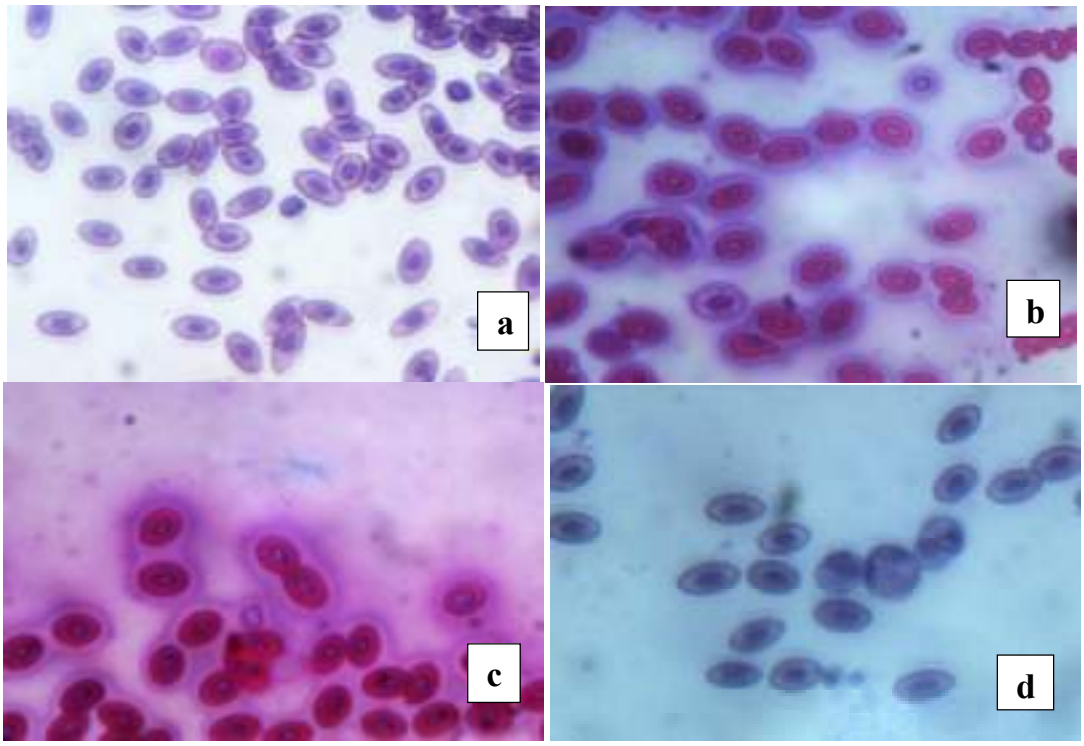

Fig. 6. (a)Blood smear of noninfected fish, (b)Infected fish blood smear with deformed RBC, chromatin condensation, vacuolation, basophilic stippling, (c)Amitotic division in diseased erythrocytes, (d)Leucocyte differentiation

4. CONCLUSION

This investigation concluded that the post monsoon season, i.e. winter season is most favorable for spreading *T.mrigalae* infection to *C.mrigala*. The probable reason for the availability of these parasites more in winter may be due to the unfavourable water condition for fishes.The plasmodia, sporogenic stages of Myxozoan parasite damaged more than 50% of the gills causing respiratory distress and suffocation. The curved plasmodia had tendency to expand the surface area in contact with adjacent gill lamellae facilitating the attainment of nutrients from the host. As the gill lamellae was was ruptured by growing cysts with necrotic lesions and hyperplasia, the normal respiratory function of the gill appeared to be impaired. The present tumour like cyst was studied histologically in an advanced stage of development with only mature spores found, earlier developmental stages awaite further study to evaluate whether the present plasmodia were transmitting from oligochaete. *T.mrigalae* infection gave the opportunity to other pathogenic microorganisms to enter the connective tissue through damaged gill lamellae and responsible for destruction of RBC and greater infiltration of WBC. Changes in the total number of and types of WBC can be used as an indicator of the presence of certain infectious diseases that occur in fish. Our work revealed that greater number of mucous cell population secreted by goblet cells can have roles in protozoan infection by preventing adhesion to gill lamella.

ETHICAL APPROVAL

Animal ethical care guidelines were followed as edible fishes were used in the study and did not require approval.

ACKNOWLEDGEMENTS

We are privileged to convey our sincere gratitude to Prof. Subir Chandra Das Gupta, Head of the Department, Post Graduate Department of Zoology, Maulana Azad College, Kolkata for providing laboratory facilities and financial support under DBT Star College Scheme to conduct the work.

COMPETING INTERESTS

Authors have declared that no competing interests exist.

REFERENCES

1. Kaur H, Singh R. Two new species of *Myxobolus* (Myxozoa: Myxosporea: Bivalvulida) infecting an Indian major carp and a cat fish in wetlands of Punjab, India. Journal of Parasitic Diseases. 2011;35(2):169–176. DOI:10.1007/s12639-011-0061-4.
2. Abdel-Ghaffar F, Morsy K, Bashtar AR, El-Ganainy S, Gamal S. *Thelohanellus niloticus* sp. nov. (Myxozoa:Myxosporea), a parasite of the Nile carp *Labeo niloticus* from the River Nile, Egypt. Parasitology Research. 2013; 112:379–383. DOI:10.1007/s00436-012-3148-7.
3. Maharshi G. Development of Spore Protein of *Myxobolus koi* as an Immunostimulant for Prevent of Myxobolusis on Gold Fish (*Cyprinus carpio* Linn) by Oral Immunisation. 2nd International Conference on Tropical and Coastal Region Eco Development 2016. IOP Conf. Series:Earth and Environmental Science. 2017; 55:012009. DOI:10.1088/1755-1315/55/1/012009.
4. Kudo R. A taxonomic consideration of myxosporidia. Transactions of the American Microscopical Society.1933;52:195-216. https://doi.org/10.2307/3222254
5. Zhang JY, Gu ZM, Kalavati C, Eiras JC, Liu Y, Guo QY, Molnar KA. Synopsis of the species of *Thelohanellus* Kudo, 1933 (Myxozoa: Myxosporea: Bivalvulida). Systematic Parasitology. 2013; 86:235–256. DOI :10.1007/s11230-013-9449-0.
6. Yokoyama H, Kiyanage YS, Sugai A, Wakabayashi H. Hemorrhagic thelohanellosis of color carp caused by *Thelohanelllus hovorkai* (Myxozoa: Myxosporea). Fish Pathology. 1998; 33:85–89. DOI: https://doi.org/10.3147/jsfp.33.85
7. Akhmerov AKH. Myxosporidia of fishes from the Amur River basin. Rybnoe Khozyaistvo Vnutrennykh Vodoemov Latvijskoi SSR. 1960;5, 240–307 (In Russian).
8. Basu S, Modak BK, Haldar DP. Synopsis of the Indian species of the genus *Thelohanellus* Kudo, 1933 along with description of *Thelohanellus disporomorphus* sp.n. Journal of Parasitology and Applied Animal Biology. 2006;15 (1&2):81 - 94.
9. Pagarkar AU, Das M. Two new species of myxozoa, *Thelohanellus caudatus* n. sp., and *Myxobolus serrata* n. sp., from the cultural carps. Journal of Inland Fisheries Society of India.1993;25:30–35.
10. Basu S, Haldar DP. Observations on two new thelohanellid species (Myxozoa:Bivalvulida) from Indian major carps of West Bengal, India. Journal of Parasitology and Applied Animal Biology. 2003; 12:15–24.
11. Acharya S, Dutta T. *Thelohanellus habibpuri* sp. n. (Myxozoa:Bivalvulida) from the tropical freshwater fish rohu, *Labeo rohita* (Hamilton-Buchanan, 1882) in West Bengal, India:Light and electron microscope observations. Animal Biology. 2007; 57:293–300.
12. Singh R, Kaur H. Biodiversity of myxozoan parasites infecting freshwater fishes of three main wetlands of Punjab, India. Protistology. 2012a; 7:79–89.
13. Singh R, Kaur H. *Thelohanellus* (Myxozoa: Myxosporea: Bivalvulida) infections in major carp fish from Punjab wetlands (India). Protistology. 2012b; 7:178–188.
14. Qadri SS. On a new myxosporidian *Thelohaenellus shortti* n. sp., from the freshwater fish, *Labeo fimbriatus* of Andhra Pradesh, India. Journal of Protozoology. 1967; 11:207–218
15. Lalitha Kumari PS. Studies on parasitic protozoa (Myxosporidia) of fresh water fishes of Andhra Pradesh, India. Rivista di Parassitologia. 1969; 30:153–226.
16. Lom J, Dykova I. Myxozoan genera:definition and notes on taxonomy, life cycle terminology and pathogenic species. Folia Parasitologica. 2006; 53:1-36. https://doi.org/10.14411/fp.2006.001.
17. Pritchard MH, Kruse GO. The collection and preservation of animal parasites. (Tech. Bull. 1). University of Nebraska Press (Lincoln), Nebraska, 1982. pp. 141.
18. Secretaría de Pesca. Proyecto de Norma Oficial Mexicana NOM020-PESC-1993, que acredita las técnicas para la identificación de agentes patógenos causales de enfermedad en los organismos acuáticos vivos cultivados, silvestres y de ornato en México. Diario Oficial 7 Diciembre (Primera Sección), México.1994.
19. Hoffman GL. Parasites of North American freshwater fishes. 2nd ed. Cornell University Press, Ithaca, New York. 1999;539.
20. Margolis L, Esch GW, Holmer JC, Kuris AM, Schad GA. The use of ecological terms in parasitology. Journal of Parasitology. 1982; 68:131-133.
21. Feist SW, Longswhaw M. Phylum Myxozoa. In:P.T.L. Woo (ed.). Fish diseases and disorders: Protozoan and metazoan infections. Cabi, Oxfordshire. 2006; 1:230- 296.
22. Stevens A. The Haematoxylins. In Bancroft, John; Stevens, Alan (eds.). The Theory and Practice of Histological Techniques (2nd ed.). Longman Group Limited.1982;109.

23. Jin C, Padra JT, Sundell K, Sundh H, Karlsson NG, Linden SK. Atlantic Salmon Carries a Range of Novel O-Glycan Structures Di□erentially Localized on Skin and Intestinal Mucins. Journal of Proteome Research. 2015; 14:3239–3251.
24. Mukherjee D, Soni M, Sanyal KB and Dash G. Prevalence of ectoparasitic infestation in Indian major carps during winter at different blocks of South 24-Parganas District, West Bengal, India. Journal of Fisheries Science. 2019; 1(1):7-14.
25. Valdenegro-Vega VA, Crosbie P, Bridle A, Leef M, Wilson R, Nowak BF. Di□erentially expressed proteins in gill and skin mucus of Atlantic salmon (*Salmo salar*) a□ected by amoebic gill disease. Fish Shellfish Immunol. 2014; 40:69–77.
26. Benktander J, Padra JT, Maynard B, Birchenough G, Botwright NA, McCulloch R, Wynne JW, Sharba S, Sundell K, Sundh H, Lindén SK. Gill mucus and gill mucin O-glycosylation in healthy and amebic gill disease-a□ected atlantic salmon. Microorganisms. 2020; 8:1871. DOI:10.3390/microorganisms8121871
27. Jones R, Baskerville A, Reid L. Histochemical identification of glycoproteins in pig bronchial epithelium:(a) normal and (b) hypertrophied from enzootic pneumonia. Journal of Pathology. 1975; II (6): I--II.
28. Powell MD, Ransome J, Barney M, Duijf RMM, Flik G. Effect of Dietary Inclusion of N-Acetyl Cysteine on Mucus Viscosity and Susceptibility of Rainbow Trout, *Oncorhynchus mykiss*, and Atlantic Salmon, *Salmo salar*, to Amoebic Gill Disease. Journal of the World Aquaculture Society. 2007; 38:435–442.
29. Fernandes MN, Perna SA, Moron SE. Chloride cell apical surface changes in gill epithelia of the armoured catfish *Hypostomus plecostomus* during exposure to distilled water. Journal of Fish Biology. 1998; 52:844–849.
30. Powell MD, Perry SF. Respiratory and acid – base disturbances in rainbow trout blood during exposure to chloramine-T under hypoxia and hyperoxia. Journal of Fish Biology. 1997; 50:418–428.
31. Martins ML, Mouriño JLP, Amaral GV, Vieira FN, Dotta G, Jatobá, AMB, Pedrotti FS, Jerônimo GT, Buglione-Neto CC, Pereira-Jr G. Haematological changes in Nile tilapia experimentally infected with *Enterococcus* sp. Brazilian Journal of Biology. 2008;68(3):657-661.

Brain Research Bulletin 156 (2020) 131–140

Contents lists available at ScienceDirect

Brain Research Bulletin

journal homepage: www.elsevier.com/locate/brainresbull

Research report

Alterations of thyroidal status in brain regions and hypothalamo-pituitary-blood-thyroid-axis associated with dopaminergic depletion in substantia nigra and ROS formation in different brain regions after MPTP treatment in adult male mice

Priyobrata Sinha[a,b], Nilkanta Chakrabarti[b,c,**], Nabanita Ghosh[a], Soham Mitra[a], Shauryabrota Dalui[a], Arindam Bhattacharyya[a,*]

[a] Immunology Lab, Department of Zoology, University of Calcutta, 35, Ballygunge Circular Road, Kolkata 700019, India
[b] Department of Physiology, University of Calcutta, 92, Acharya Prafulla Chandra Road, Kolkata 700009, India
[c] Centres with Potential for Excellence in Particular Areas (CPEPA, UGC), Centre for "Electrophysiology & Neuroimaging Studies Including Mathematical Modeling" India

ARTICLE INFO

Keywords:
MPTP
Dopaminergic neurons
ROS
Thyroidal status
Hypothalamo-pituitary-blood-thyroid axis
Different brain regions

ABSTRACT

MPTP produces oxidative stress, damages niagrostriatal dopaminergic neurons and develops Parkinsonism in rodents. Due to paucity of information, the thyroidal status in brain regions and peripheral tissues during different post-treatment days in MPTP-induced mice had been executed in the present study. MPTP depleted tyrosine hydroxylase protein expressions that signify the dopaminergic neuronal damage in substantia nigra. MPTP elevated ROS formation differentially in brain regions (cerebral cortex, hippocampus, substantia nigra) with maximal elevation at hippocampus. The changes in thyroid hormone (T_4 and T_3) levels indicate that brain regions might combat the adverse situation by keeping the levels of thyroid hormones either unchanged or in the elevated conditions in the latter phases (day-3 and day-7), apart from the depletion of thyroid hormones in certain brain regions (T_4 in SN and hippocampus, T_3 in hippocampus) as the immediate (day-1) effects after MPTP treatment. MPTP caused alterations of cellular morphology, RNA:Protein ratio and TPO protein expression, concomitantly depleted TPO mRNA expression and elevated TSH levels in the thyroid gland. Although T_4 levels changed differentially, T_3 levels remained unaltered in thyroid gland throughout the post-treatment days. Results have been discussed mentioning the putative role of T_4 and TSH in apoptosis and/or proliferation/differentiation of thyrocytes. In blood, T_4 levels remained unchanged while the changes in T_3 and TSH levels did not signify the clinical feature of hypo/hyperthyroidism of animals. In the pituitary, both T_4 and T_3 levels remained elevated where TSH differentially altered (elevated followed by depletion) during post-treatment days. Notably, T_4, T_3 and TSH levels did not alter in hypothalamus except initial (day-1) depletion of the T_4 level. Therefore, the feedback control mechanism of hypothalamo-pituitary-blood-thyroid-axis failed to occur after MPTP treatment. Overall, MPTP altered thyroidal status in the brain and peripheral tissues while both events might occur in isolation as well.

1. Introduction

1-methyl-4-phenyl-1,2,3,5-tetrahydropyridine (MPTP), a neurotoxin, causes induction of “Parkinson-like” tremor in rodents and humans (Bové et al., 2005). MPTP is metabolized to MPP^+ by monoamine oxidase B (MAO-B) in astrocytes. MPP^+ is actively secreted to the extracellular space via organic cation transporter (OCT-3) and then enters in catecholamine neurons selectively through dopamine transporter (DAT). MPP^+ causes (a) inhibition of complex-1 of mitochondrial electron transport chain that leads to generation of oxidative stress and induction of caspase-dependent apoptosis (b) direct oxidative damage of cytosolic targets that results in misfolding and oligomerization of alpha synuclein (co-chaperon proteins) and finally formation of Lewy bodies, (c) disrupting vesicles and release of excess dopamine to cytosol followed by auto-oxidation or MAO mediated oxidative deamination of dopamine, resulting in the formation of reactive oxygen species (ROS).

* Corresponding author.
** Corresponding author at: Department of Physiology, University of Calcutta, 92, Acharya Prafulla Chandra Road, Kolkata 700009, India.
E-mail addresses: ncphysiolcu@gmail.com (N. Chakrabarti), arindam19@yahoo.com (A. Bhattacharyya).

https://doi.org/10.1016/j.brainresbull.2019.12.013
Received 27 September 2019; Received in revised form 17 December 2019; Accepted 18 December 2019
Available online 28 December 2019
0361-9230/

MPTP intoxication is associated with inhibition of autophagy with unsettled mechanism, neuroinflammation through activation of microglial cells and glutamate induced calcium dependent exocitotoxicity, specifically in dopaminergic neurons (Blesa et al., 2012; Pasquali et al., 2014). Moreover, dopaminergic neurons have less defense mechanism against oxidative stress and therefore are more susceptible to damage by MPTP-induced toxicity (Datta and Bhonde, 2012). MPTP-induced rodent models of Parkinson's Disease (PD) using chronic, sub-acute and acute doses of MPTP exhibit the common features like niagrostiatal dopaminergic neuronal degeneration and motor dysfunction (Meredith and Rademacher, 2011).

Separate studies indicate that MPTP intoxication causes down-regulation of (a) DSCR1-like1 gene associated with apoptosis (Miller and Federoff, 2005) and (b) Rhes gene linked with dopaminergic neuroprotection via modulation of interneuronal (GABAergic neurons and aspiny cholinergic) activities, cellular signaling for cell proliferation/differentiation/survival, synaptic plasticity and learning/memory (Napolitano et al., 2017; Costa et al., 2018). Interestingly, DSCR1-like1 (Cao et al., 2002) and Rhes (Vargiu et al., 2001; Manzano et al., 2003) genes are responsive to thyroid hormone (TH). The expression of liver-X-receptor-beta (LXRβ) gene in microglia and astroglia in substantia nigra (SN) limits the MPTP-induced dopaminergic neuronal damage (Dai et al., 2012). The LXRβ suppresses the expression of genes for receptors of TH and TRH and, therefore coordinates the hypothalamic-pituitary-blood-thyroid axis (Miao et al., 2015). However, the status of TH in brain of experimental animals after MPTP treatment remains untouched.

TH controls energy-linked metabolism and has impact on antioxidant mechanism in brain and, therefore is supposed to relate with oxidative stress and neurodegeneration with undefined mechanism (Villanueva et al., 2013). Tetraiodothyronine (T_4), the abundant circulatory form of TH, enters the brain through blood-brain-barrier and CSF (Zibara et al., 2017; Zheng et al., 2003). T_4 is converted to T_3, the active form of TH at cellular level, by type-2 deiodinase (Dio2) in astrocytes (Roberts et al., 2015; De Castro et al., 2015). Both T_3 and T_4 are transported via monocarboxylate transporters (MCT) to nerve terminals (Roberts et al., 2015; Friesema et al., 2005). The enzyme type-3 deiodinase (Dio3) in neurons deactivates T_4 and T_3 to rT_3 and T_2 respectively (Friesema et al., 2005; van der Spek et al., 2017). Nerve terminals in adult rat brain accumulate T_3 (Sarkar and Ray, 1994) where T_3 alters activities of Na/K-ATPase (Sarkar and Ray, 1993), Ca/Mg–ATPase (Chakrabarti and Ray, 2002), nitric oxide synthase (Chakrabarti and Ray, 2000) and acetylcholine esterase (Chakrabarti et al., 2017). In adult mammalian brain, thyroid hormone is associated with calcium dependent neurotransmission (Chakrabarti and Ray, 2000; 2003), neurogenesis (Remaud et al., 2014; Fanibunda et al., 2018) and neuroprotection (Lin et al., 2011). Hypothyroidism and hyperthyroidism are reported to associate with neurodegeneration (Cortés et al., 2012; Villanueva et al., 2013; Ittermann et al., 2018).

In few cases, PD patients show clinical symptoms of hypothyroidism (Berger and Kelley, 1981; Johannessen et al., 1987; Tandeter and Shvartzman, 1993; Munhoz et al., 2004) along with either normal (Johannessen et al., 1987) or elevated serum thyroid stimulating hormone (TSH) level (García-Moreno and Chacón-Peña, 2003; Kawajiri et al., 2002). TH treatment is reported to improve the PD symptoms (Kawajiri et al., 2002; García-Moreno and Chacón-Peña, 2003). Hyperkinesia in PD patients appears to coexist with clinical symptoms of hyperthyroidism i.e. reduction of serum TSH level (Wingert and Hershman, 1979; Caradoc-Davies, 1986; Kim et al., 2005; Minár and Valkovič, 2014), elevated serum T_4 level (Caradoc-Davies, 1986; Aziz et al., 2011; Minár and Valkovič, 2014), elevated serum T_3 level (Minár and Valkovič, 2014; Kim et al., 2005). Restoring a euthyroid state may improve parkinsonian tremor (Minár and Valkovič, 2014). PD patients with thyrotoxicosis response to levodopa (Caradoc-Davies, 1986; Prakash and Kek, 2010). Alternatively, treatment of levodopa/carbidopa has no effect over thyroid function (Wingert and Hershman, 1979). The serum level of free T_4 is inversely related to cognitive performances in euthyroid early PD patients (Choi et al., 2014). TH controls mood and cognitive function in adults the exact mechanism of which is unclear (Bauer et al., 2002; Pilhatsch et al., 2011; Bocchetta et al., 2016). Therefore, case studies indicate that some PD patients share similar clinical features with the altered thyroidal conditions wherever the clear evidence of direct link is missing.

In periphery, MPTP-induced animal models of PD show depletion of sympathetic innervation in heart (Wallace et al., 1984; Fuller et al., 1988; Goldstein et al., 2003; Pasquali et al., 2014), intoxication in Leydig cells of testis, decrease in plasma testosterone level (Ruffoli et al., 2008), gut dysfunction (Pasquali et al., 2014) with duodenal ulceration (Keshavarzian et al., 1990) and gut microbiotadysbiosis (Lai et al., 2018). However, no report is available on MPTP-induced status of thyroid gland and hypothalamic-pituitary-blood-thyroid axis in experimental animal model.

Based on literature, a hypothesis has been drawn in the present study that MPTP treatment may impact on thyroidal status in brain and periphery (hypothalamic-pituitary-blood-thyroid axis) in mice. Therefore, the present study aims to unveil the status of TH (T_4 and T_3) in the tissues including brain regions like cerebral cortex (CC) and hippocampus (HC) associated with cognitive functions, substantia nigra (SN) as positive tissue for PD model and hypothalamus along with pituitary, blood and thyroid gland to execute the status of hypthalamo-pituitary-blood-thyroid axis during the MPTP treatment with acute dose in mouse model.

2. Materials and methods

2.1. Materials

MPTP and protease inhibitor cocktail were borrowed from Sigma Aldrich, Inc. (St. Louis, MO). ELISA kits of T_3, T_4, and TSH for mouse were purchased from Qayeebio International (China). Other chemicals were purchased in an analytical grade of the highest purity (India).

2.2. Ethical statement

All animal experiments were performed following the "Principles of Laboratory Animal Care" (NIH publication No. 85-23, revised 1985), and also abiding by the specific Indian law on "Protection of Animals" under the supervision of authorized investigators, "The Committee for the Purpose of Control and Supervision of Experiments on Animals (CPCSEA), Ministry of Environment, Forest and climate change, Government of India". All protocols of animal handling and research were duly approved by the Institutional Animal Ethics Committee (IAEC) under the guidelines of CPCSEA at the Department of Zoology, University of Calcutta, India (Registration number under CPCSEA is 885/GO/Re/S/05/CPCSEA).

2.3. Animal and treatment

Male Swiss albino mice (~25 ± 3 g body weight and 2–3 months of age) were obtained from the registered vendor in local area and housed in an animal facility maintaining at 25–28 [± 2] °C temperature, 55 [± 5] % relative humidity, and a 12 HR/12 HR light/dark cycle. All animals were provided rodent chow and filtered water *ad libitum*. The experimental mice were divided into four groups (n = 6 in each group) comprising vehicle (saline) treated control group and MPTP-treated groups (post-treated day-1, day-3 and day-7). Data were reproduced in second set (n = 6 in each group) of experiment. Separate animals (n = 3) were used for measurement of each parameter under a group of experiment. Animals received four consecutive subcutaneous injections of MPTP (18 mg/kg b.w., Sigma Aldrich, Inc. St. Louis, MO) at 2 -h interval in a single day; sacrificed at day-1, day-3, and day-7 after the last dose following the protocol published early (Jackson-

Lewis and Przedborski, 2007). Cerebral cortex (CC), hippocampus (HC), substantia nigra (SN) and hypothalamus were dissected from fresh brain tissue under ice-cooled condition, following the natural anatomical boundaries of mouse brain regions mentioned in the Paxinos and Franklin Mouse Brain Anatomy Atlas (Paxinos and Franklin, 2001). Pituitary and thyroid tissues were dissected from animals for further processing.

2.4. Histology

Thyroid histology had been performed by standard protocol of Haematoxyline/Eosine staining. In brief, thyroid tissues were fixed in formalin and processed for paraffin blocking. The serial sections of paraffin block of thyroid tissue having 5 µm thickness were used for staining with hematoxylin and eosin and mounted using DPX. Images were captured using a U-TVO 63× C microscope (Olympus Corp., Tokyo, Japan) using 400 times magnification.

2.5. Tissue processing

The weight (wet weight) of the tissue, collected just after dissection, was taken in digital balance. SN and thyroid gland were homogenized (20 % homogenate for SN and 10 % homogenate for thyroid) in an ice-cold RIPA lysis buffer (150 mM sodium chloride, 1.0 % TritonX-100, 50 mM Tris, 0.01 % SDS, 0.5 % sodium deoxycholate, pH 7.4) containing protease inhibitor cocktail (Sigma Aldrich, India). Then the homogenates were sonicated under ice and incubated at 4 °C for 30 min and centrifuged at 12,700 *g* or, 14,000 RPM in a CM-12 PLUS centrifuge (REMI Laboratory Instruments, Mumbai, India) for 20 min at 4 °C to collect post-mitochondrial fraction. The post-mitochondrial fractions were used for western blot analysis. For RT-PCR and Realtime PCR, thyroid tissues were homogenized in 100 µl Trizol reagent (Invitrogen) for extraction total RNA, following the kit (Invitrogen) protocol. 10 % (w/v) tissue homogenates in PBS (pH 7.4) were prepared for spectroflurometric analysis of ROS in brain tissue homogenates and ELISA of T_4, T_3 and TSH in all tissue (cerebral cortex, hippocampus, SN, hypothalamus, pituitary and thyroid) homogenates.

2.6. Protein estimation

Protein content of tissue samples were estimated using the Bradford reagent (Sigma-Aldrich Inc., USA) and subsequent measurement of absorbance at 595 nm in a UV-1700 Pharma Spec, Shimadzu spectrophotometer (Shimadzu Scientific Instruments, Columbia, MD).

2.7. RNA estimation

Thyroid tissues were weighed and homogenized in 100 µl Trizol reagent (Invitrogen) for RNA isolation. RNA purity was accessed with "MULTISKAN GO" microplate reader (Thermofisher Scientific, USA) using ratio of absorbance at 260 nm and 280 nm close to the value 2.0. The concentration of RNA was checked by the same microplate reader instrument.

2.8. Primer designing

Nucleic acid sequence of the primers specific for thyroid peroxidase (TPO) and housekeeping gene GAPDH were designed from the available mouse (*Mus musculus*) gene sequence (accession nos. NM_009417.2) in the "Gene" database of the National Center for Biotechnology Information (NCBI) of NIH, USA (https://www.ncbi.nlm.nih.gov/gene). Primers were finally designed by IDT (Integrated DNA Technology) and Primer Blast. Primer sequences were selected to optimally hybridized and amplify target cDNA sequences for polymerase chain reaction (PCR) assay. The sequences of primers used in the study are listed in the Table 1.The primers were purchased from Bioserve (India).

2.9. RT-PCR (Reverse Transcriptase PCR)

The RT-PCR was performed following the previous methods (Chakrabarti et al., 2008). Total RNA was converted to cDNA by using random hexamers and M-MLV reverse transcriptase provided in the cDNA preparation kit (Invitrogen, USA). Respective RNA samples (5 µg) were reverse transcribed simultaneously in the reaction mixture with final volume of 20 µl according to manufacturer's instruction (Invitrogen, USA). The cDNA was stored in −20 °C for future use regarding amplification by RT-PCR and real time PCR. The RT-PCR reaction was performed using 1 µl samples of cDNA in a 10 µl reaction volume containing Taq polymerase, dNTP, $MgCl_2$, primers (forward and reverse) and PCR buffer (pH 7.4). All the reagents for PCR were purchased from Promega (USA). The PCR was run as follows: 2 min at 95 °C for initial denaturation, followed by repeated 40 cycles of denaturation for 30 s at 95 °C, annealing for 30 s at 54 °C for TPO and 52 °C for GAPDH and, final extension for 7 min at 72 °C. PCR products were run on 2 % agarose gels and photographed using E-Gel imager (Life Technologies, USA). The relative expression of TPO genes was determined by real time PCR of their mRNAs after reverse transcription to cDNAs.

2.10. Real time PCR

The real time PCR was performed following the previous methods (Chakrabarti et al., 2008; Ghosh et al., 2019) by SYBR green detection system (Applied Biosystems, USA) with GAPDH as internal control. The cycle parameters were chosen as initial denaturation at 95 °C for 2 min, amplification and quantification with repeated 40 cycles (denaturation at 95 °C for 15 s, annealing at 52 °C temperature for 15 s, extension at 72 °C temperature for 30 s and fluorescence detection for 1 min during each cycle) of specific template for respective genes followed by reaction termination at 72 °C for 5 min and final hold at 4 °C. The quantification of the PCR product was done by the "delta-delta Ct method" (Livak and Schmittgen, 2001). The change in threshold values (Ct) for genes were obtained from 'StepOne v2.3' software of the qPCR machine (Applied Biosystems, USA). The ΔΔCt of the gene was calculated with respect to internal control GAPDH. Each experiment was repeated thrice.

2.11. Western blot

Western blot analysis had been done following the previous method (Ghosh et al., 2018) with slight modifications. In brief, the post-mitochondrial fraction isolated from SN and thyroid tissue with 40 µg and 30 µg of protein respectively from each sample of each group were loaded into the gel for electrophoresis and separated using 12 % and 10 % SDS-PAGE for tyrosine hydroxylase (TyrH) and TPO protein respectively and, electroblotted onto a PVDF membrane (Millipore, Merck, Germany). After blocking using 5 % non-fat dry milk for 1 h, the membranes were incubated with primary antibodies of anti-TyrH (Mouse Monoclonal,1:500, DSHB, IOWA university, USA), anti-TPO (Rabbit polyclonal, Abcam plc., 1:1000, Cambridge, UK) overnight at 4 °C, washed in TBS-Tween-20 (0.1 %) with respective cases. The part of the same membrane was processed with anti-GAPDH and anti-alpha-tubulin as loading control for TyrH and TPO respectively. Primary antibodies were detected against HRP-conjugated secondary antibodies using HRP substrate ECL solution. Then chemiluminescence had been performed in Chemidoc and the intensity of the TyrH and TPO proteins had been normalized against expression of respective reference proteins like GAPDH for TyrH and α-tubulin for TPO, using the 'ImageJ' software (NIH, USA).

Table 1
Details of the primers used for RT-PCR and real-time PCR.

Targeted genes	Sense	Antisense	Product details
GAPDH	5′CACGTGCAAATGCTCCAAAG3′	5′AAACTCCAGCAGGGACAAAG3′	99bp,Tm = 52 °C
TPO	5′GTGTTGGAGTCAGAGACTTGAG3′	5′CATTAGCCTTAGTGCGTAGGAG3′	143bp, Tm = 54 °C

2.12. Spectrofluorimetry

The spectrofluorimetric measurement of ROS had been done by following the previous protocol (Baek et al., 1999) with slight modification. In brief, DCFDA (Sigma Aldrich., India) dye was incubated with tissue homogenates (30 µg of protein) of CC, HC and SN in phosphate buffer saline (NaCl-8.5 g/litre, Na_2HPO_4-1.91 g/litre, KH_2PO_4-0.38 g/litre; Himedia Laboratories, Mumbai, India) at 37 °C for 30 min. The spectrofluorimetric measurements had been taken after 10 min and 30 min of the incubation period. The amount of DCF formed had been expressed in "DCF formed/min./mg of protein".

2.13. ELISA of T_3, $T_4$and TSH

ELISA was used to measure T_3 and T_4 in brain regions, blood, thyroid and pituitary. TSH was measured in blood, thyroid, hypothalamus and pituitary. Commercialized sandwich ELISA kit had been used to measure T_3, T_4 and TSH according to the manufacturer's protocol (Qayeebio International, China). As per declaration from manufacturer company, the kits were manufactured for measuring total content of T_3, T_4 and TSH in blood plasma, tissue homogenates as well as in cell lysates. The OD values were read in a microplate reader at 450 nm. The content was calculated against the respective standard curves generated with the supplied standards in the kit and expressed in pg/mg of tissue weight and µg/dl or ng/ml in blood.

2.14. Statistical analysis

All values are represented as mean ± SEM. The pairwise analysis had been done using ANOVA followed by Tukey HSD post hoc analysis considering the significance levels at $p < 0.001$, $p < 0.01$, $p < 0.05$ and $p < 0.10$ in respective cases. The data analysis had been done using R-language. The Pearson correlation had been analyzed using 'SPSS Statistics 17.0′.

3. Results

3.1. Differential changes of TyrH expression in SN during different days after MPTP treatment

TyrH expression remained significantly in lower levels during post-treated days compared to that of control whereby the biphasic pattern of changes appeared during those days (day1 to day7). TyrH expression level significantly decreased at day-1 followed by amelioration at day-3 and finally decreased at day-7 to the level which appeared to be intermediate level compared to the levels of day-1 and day-3 (Fig. 1)

3.2. Increase in levels of ROS during different days after MPTP treatment

ROS significantly increased in the brain regions during post-treated days of experimental observations. ROS in CC and HC achieved maximum level at day-3 and in SN at day-7. ROS level ameliorated at day-7 in CC and HC and, at day-3 in SN (Fig.2). Interestingly, maximum elevation of ROS level had been found in HC at day-3 after MPTP treatment.

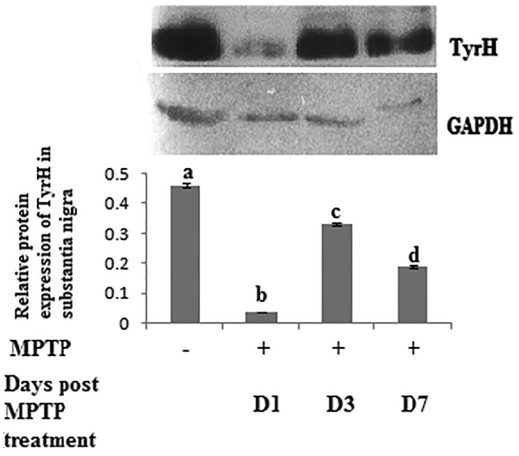

Fig. 1. Changes in protein expression of TyrH in substantia nigra after MPTP treatment. The expression of TyrH proteins (bar graphs) are represented as relative expressions based on densitometry of Western blot images (upper panels) of TyrH during different post-treated days compared to that of loading control GAPDH. Data are expressed as mean ± SEM. The signs (+) and (-) represent tissues collected from animals treated with and without MPTP respectively. The post-treated days of Day-1, Day-3 and Day-7 are indicated by D1, D3 and D7 respectively. Letters (a, b, c, d) imply significant differences among different conditions of experiments. Significant level is set as $p < 0.05$. The details of experimental procedures are described in "Materials and Methods".

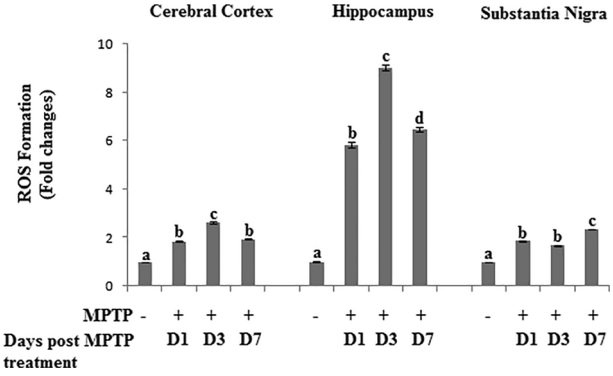

Fig. 2. Changes in the status of reactive oxygen species (ROS) in different brain regions after MPTP treatment. The levels of ROS are represented as "fold changes" of the spectrofluorimetric measurement of DCFDA dye during different days after MPTP treatment compared to that in control animals. Data are expressed as mean ± SEM. The signs (+) and (-) represent tissues collected from animals treated with and without MPTP respectively. The post treated days of Day-1, Day-3 and Day-7 are indicated by D1, D3 and D7 respectively. Letters (a, b, c, d) imply significant differences among different conditions of experiments. Significant level is set as $p < 0.05$. The details of experimental procedures are described in "Materials and Methods".

3.3. Changes in thyroid gland: thyroid morphology, weight of thyroid gland, contents of total protein and RNA of thyroid tissue and, expression of TPO (gene and protein) during different days after MPTP treatment

The cellular atrophy in thyroid gland and disruption of colloids were observed during day-1 to day-3 after MPTP treatment. The

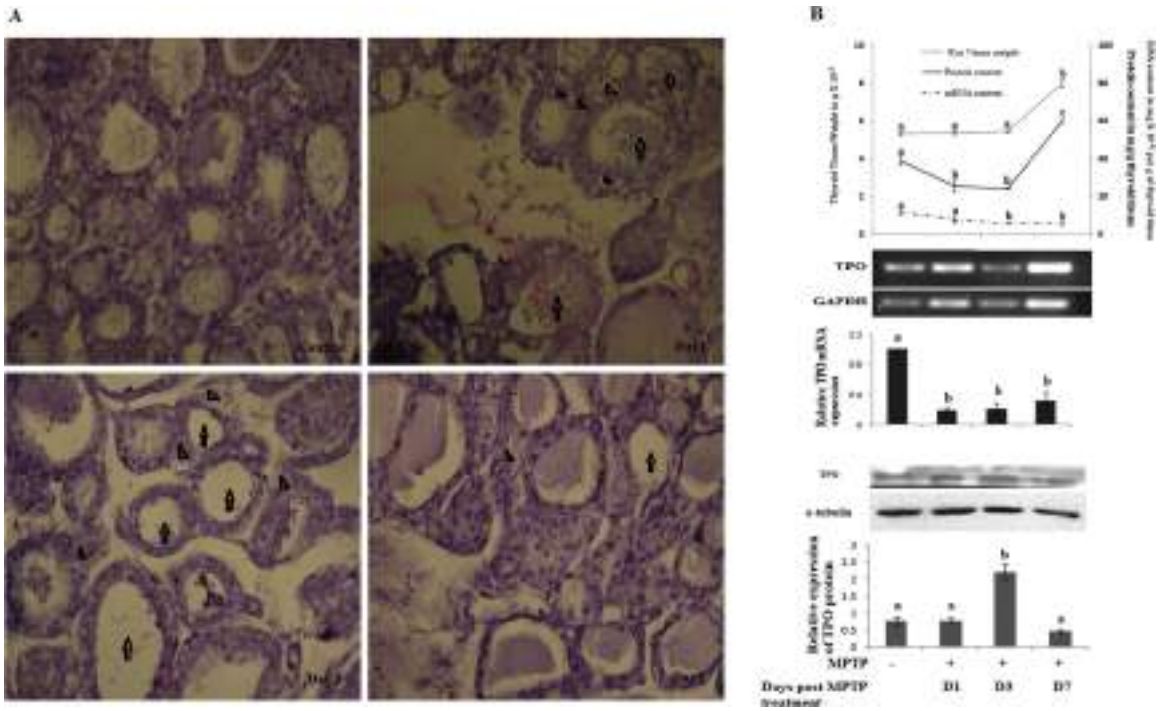

Fig. 3. Changes in status of thyroid tissue in different days after MPTP treatment. (A): Microscopic images (magnification with ×400) of the thyroid tissues stained with hematoxyline/eosin (H&E) indicates the morphological changes including cellular atrophy (arrowhead) and damages of colloids (arrow) in thyroid gland of control and MPTP treated (day-1, day-3, day-7) animals (B):Line graphs represent the weight of the wet thyroid tissue, protein content per gram of thyroid tissue and mRNA content per gram of thyroid tissue during different experimental conditions. Bar graphs and images denote relative expressions of mRNA (middle panel) and protein (lower panel) of thyroid peroxidase (TPO) in thyroid tissues during different experimental conditions. The mRNA expressions of TPO (bar graphs in middle panel) are represented as relative expressions based on densitometry of images (top to the bar graphs in middle panel) of PCR products of TPO during different post-treated days compared to that of loading control GAPDH. The expressions of TPO proteins are represented as relative expressions (bar graphs in lower panel) based on densitometry of Western blot images (top to the bar graphs in lower panel) of TPO during different post-treated days compared to that of loading control α-tubulin. Data are expressed as mean ± SEM. The signs (+) and (-) represent tissues collected from animals treated with and without MPTP respectively. The post treated days of Day-1, Day-3 and Day-7 are indicated by D1, D3 and D7 respectively. Letters (a, b, c) imply significant differences among different conditions of experiments. Significant level is set as $p < 0.05$. The details of experimental procedures are described in "Materials and Methods".

regaining of thyroid morphology with colloidal reappearance had been found in day-7 (Fig.3A).

The tissue weight (wet weight) of thyroid gland increased significantly at day-7 after MPTP treatment whereby the thyroid tissue wet weight remained unaltered during initial days (day-1 and day-3) after MPTP treatment (Fig.3B, upper panel). Although the protein content of thyroid tissue decreased significantly at day-1 and day-3, the same increased at day-7 compared to that of control after MPTP treatment whereby the protein contents of thyroid tissue at day-7 appeared to be significantly greater levels compared to that of day-1 and day-3 after MPTP treatment (Fig.3B, upper panel). The total RNA content of thyroid tissue remained unaltered during day-1 whereby the same decreased at day-3 and day-7 after MPTP treatment compared to that of control values (Fig. 3B, upper panel). Consequently, the RNA:protein ratio remained unaltered at day-1 (0.033 ± 0.011) and day-3 (0.024 ± 0.005) and, decreased significantly ($p < 0.10$) at day-7 (0.009 ± 0.001) compared to that of control value (0.030 ± 0.003).

The fold change of TPO m-RNA expression in thyroid remained in decreased condition throughout the study period (day-1 to day-7) after MPTP treatment compared to that of control values (Fig. 3B, middle panel). However, TPO protein expression significantly increased at day-3 and remained unaltered during other days of studies (Fig. 3B, lower panel).

3.4. Differential changes in contents of thyroid hormone (T_3, T_4) in brain tissues and thyroid hormone (T_3, T_4) as well as TSH in blood, thyroid gland, pituitary, and hypothalamus during different days after MPTP treatment

The blood T_4 levels remained unaltered during post-treated study periods. The blood T_3 level significantly decreased at day-1 followed by amelioration to control level (day-3) and finally increased at day-7 after MPTP treatment. The blood TSH level remained unaltered at day-1 that significantly increased during day-3 and day-7 after MPTP treatment (Fig. 4A).

T_3 levels remained unaltered in hypothalamus and thyroid whereas increased significantly in pituitary after MPTP treatment. The T_4 level in hypothalamus significantly decreased initially at day-1 after MPTP treatment followed by amelioration to normal levels thereafter. A sustained increase in T_4 levels had been found during allover study periods (day-1 to day-7) after MPTP treatment in pituitary. In case of thyroid, the T_4 level significantly increased at day-1 followed by attenuation to the normal level at day-3 that finally and significantly decreased at day-7 after MPTP treatment. The TSH level remained unchanged in the hypothalamus whereas elevated levels of TSH had been found throughout the study periods (day-1-day-7) in thyroid after MPTP treatment. In pituitary, the TSH level decreased at day-1, ameliorated to normal levels during other days after MPTP treatment (Fig. 4B).

T_3 level remained unaltered in cerebral cortex after MPTP treatment. In the hippocampus, T_3 level significantly decreased at day-1 followed by amelioration to normal levels during other post-treated days. T_3 level significantly increased in day-7 keeping the levels in normal condition during other days (day-1 and day-3) in SN. The T_4

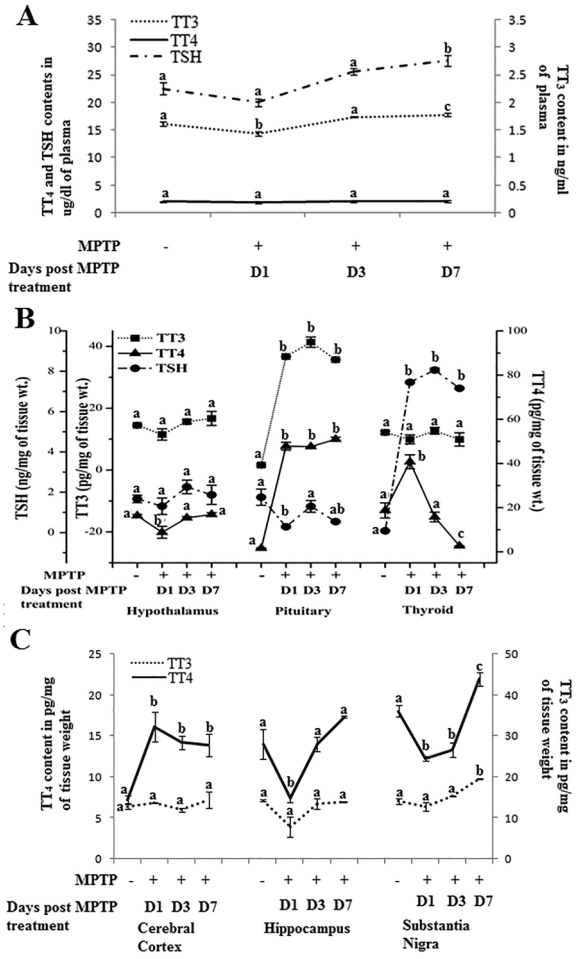

Fig. 4. Changes in levels of thyroid hormone (T_4 and T_3) and TSH in peripheral tissues and different regions of brain after MPTP treatment. (A): The blood levels of total T_3 (TT_3), total T_4 (TT_4) and TSH are expressed as μg/dl of plasma (B): The content of TT_3 and TT_4 are expressed as pg/mg of tissue weight and TSH are represented as ng/mg of tissue weight in hypothalamus, pituitary and thyroid gland. (C): The content of TT_3 and TT_4 are represented as pg/mg of tissue weight in the cerebral cortex (CC), hippocampus (HC) and substantia nigra (SN). Data are expressed as mean ± SEM. The signs (+) and (-) represent tissues collected from animals treated with and without MPTP respectively. The post treated days of Day-1, Day-3 and Day-7 are indicated by D1, D3 and D7 respectively. Letters (a, b, c) imply significant differences among different conditions of experiments. Significant level is set as $p < 0.05$. The details of experimental procedures are described in "Materials and Methods".

levels remained in significantly elevated conditions during post-treated days in cerebral cortex. In hippocampus, T_4 level significantly decreased at day-1, followed by amelioration to control levels at day-3 and day-7 after MPTP treatment. In SN, T_4 levels at day-1 and day-3 significantly decreased which gained significantly elevated level at day-7 after MPTP treatment (Fig.4C).

The significant and positive correlation have been found in the (a) alterations of plasma T_3 levels with alterations of T_3 levels in hippocampus ($r = 0.731$) and substantia nigra ($r = 0.750$). In addition, the alterations of levels of T_4 in hippocampus ($r = 0.584$) and substantia nigra ($r = 0.767$) appear as significantly and positively correlated with T_3 levels of respective brain tissues.

4. Discussion

The present study reports, for the first time, the status of thyroid hormone in periphery and brain in association with the status of hypothalamo-pituitary-blood-thyroid axis in MPTP treated mice. The results indicate that MPTP treatment caused (a) alterations of thyroidal status in blood and thyroid gland without having the clear indication of altered thyroidal status (hypo- or hyper-thyroidism), (b) failure of the feed-back control mechanism of hypothalamo-pituitary-blood-thyroid axis, (c) variation in the levels of thyroid hormone in the brain regions (cerebral cortex, hippocampus and substantia nigra) with different days of post-treatment conditions. Interestingly, the results for the first time, infer that the changes in levels of T_3 in blood during different post-treatment days are significantly and positively correlated with that in two regions of brain i.e., HC and SN.

4.1. MPTP induced depletion of TyrH protein expression in SN and ROS formation in different regions of brain

MPTP treatment reduces the expression of TyrH, the rate limiting enzyme of the dopamine synthesis pathway and a well-known dopaminergic neuronal cell marker in SN and shows symptoms of Parkinson's disease (Tabrez et al., 2012; Huang et al., 2017). In the present study, the acute dose of MPTP treatment caused depletion of TyrH expression in SN during post-treated days where maximum depletion had been found at day-1 followed by amelioration at day-3 and attainment of the intermediate level at day-7 after MPTP treatment. Notably, the biphasic pattern of changes of TyrH protein expressions in SN during post-MPTP-treated different days found in the present study are consistent with previous reports (Jackson-Lewis et al., 1995; Bian et al., 2008) the exact explanation of which needs further studies. The separate studies indicate that glucagon-like-peptide-1 or GLP-1 (Li et al., 2009), opioid receptors like sigma receptor-1 (Francardo et al., 2014; Hong et al., 2015) and neurotropic factor (Airavaara et al., 2012) are supposed to involve in neuroprotective and neurorestoration mechanism after MPTP treatment in rodent models. The differential pattern of status of astrogliosis (Aoki et al., 2009; Huang et al., 2017) and number of apoptotic neuronal cells (Aoki et al., 2009) in SN have been reported during different days after MPTP treatment in mouse model. Neurogenesis has been found in SN after MPTP treatment in mouse (Zhao et al., 2003). Notably, MPTP treatments ranging from acute to chronic doses with different study protocols have been executed to find the levels of neuroprotective/neurorestorative facts after MPTP treatment as mentioned above.

It is reported that the acute dose of MPTP with multiple injections in a single day has been found to be associated with oxidative stress induced dopaminergic neurodegenerations through non-apoptotic pathway (Kim et al., 2009; Tatton and Kish, 1997). Previous report indicates that MPTP treatment alters antioxidant enzymes including superoxide dismutase (SOD) and catalase differentially in several brain regions of young adult mice. The above mentioned study indicates that activities of SOD decrease whereas catalase increases in SN, SOD increases in cerebellum and striatum whereas catalase decreases in cerebellum without any changes in striatum (Thiffault et al., 1995). In the present study, the acute dose of MPTP-treatment caused rise in ROS levels in CC, HC and SN of mice brain during post-treated days with maximum elevation at day-3 in CC and HC and, day-7 in SN (Fig. 2). Interestingly, HC showed greatest level of elevated ROS compared to that of other brain regions whereby the similar levels of elevated ROS had been found in CC and SN. Rodent studies indicate that hippocampus appears to have greater levels of antioxidant defence system and defensive signalling molecules (heat shock protein expression) to keep inactive the cycloxygenase pathway of inflammatory damage and therefore is less susceptible to oxidative damage compared to cerebral cortex (Zlatković et al., 2014; Vandresen-Filho et al., 2015). It is well documented that ROS are associated with both physiological and pathophysiological effects in hippocampus. The physiological effects of ROS in hippocampus include diverse signalling pathways for synaptic plasticity and learning-memory formation. The pathophysiological effects of ROS in hippocampus cause deleterious consequences of cellular death and cognitive failure (Salim, 2017; Beckhauser et al.,

2016).Therefore the differential pattern of elevation of ROS in SN, HC and CC, in our present study, indicates that MPTP-treatment might have diverse impacts on brain regions in mice. MPTP-induced oxidative stress might cause dopaminergic neuronal damage in SN. Concomitantly, MPTP-induced oxidative stress in HC and CC might be involved in alterations of cognitive functions. Notably, thyroid hormone is reported to regulate the oxidative status in hippocampus, amygdale (Cano-Europa et al., 2008) and cerebral cortex (Mano et al., 1995; Das and Chainy, 2004) of adult mammalian brain. Therefore, it is postulated that MPTP-treated ROS formation might have relation to thyroidal status in brain regions.

4.2. MPTP induced changes of thyroidal status in brain regions (cerebral cortex, hippocampus and substantia nigra)

The level of T_4 and T_3 in brain depends on the peripheral supply of T_4, the metabolic conversion of T_4 to T_3 in astrocytes by deiodinase-type-II activity and the inactivation of T_3 to T_2 or T_4 to rT_3 by deiodenase-type-III activity in neurons (Zheng et al., 2003; Zibara et al., 2017; Friesema et al., 2005; Roberts et al., 2015; De Castro et al., 2015; van der Spek et al., 2017). In the present study, MPTP treatment caused elevation of T_4 levels while T_3 levels remained unaltered during post-treated days in cerebral cortex. The thyroid hormone levels appeared to be depleted in hippocampus (T_4 at day-1; Fig.4C) and substantia nigra (T_4 in day-1 to day-3; Fig. 4C) as the immediate effect of MPTP treatment. Both T_4 and T_3 levels in substantia nigra elevated and T_4 level in hippocampus attended normal level at day-7 after MPTP treatment. Our results indicate that the peripheral supply of T_4 and activities of deiodinase enzymes (type-II and type-III) might act to alter the levels of TH in brain regions after MPTP treatment. Interestingly, the alterations of T_3 levels in hippocampus and substantia nigra have been found to be significantly and positively correlated with alterations of plasma T_3 levels. In addition, the alterations of levels of T_4 in hippocampus and substantia nigra are significantly and positively correlated with T_3 levels of respective brain tissues. Such correlations of the status of thyroid hormone among brain tissues and plasma vs. brain tissues signify the functional importance of thyroidal status in both periphery and brain during MPTP treated mice model of Parkinsonism.

4.3. MPTP induced changes of thyroidal status in Blood

The disorder of thyroid function is diagnosed by measuring blood level of thyroid stimulating hormone (TSH) and thyroid hormone, mainly free-T_4 level. The low levels of blood free-T_4 and free-T_3 is reported at overt-hypothyroidism and the rise of these parameters happens during overt-hyperthyroidism. However, blood TSH level is reported as the most prevalent parameter to diagnose both subclinical and overt thyroid dysfunctions. The blood TSH level rises during hypothyroidism and decreases during hyperthyroidism (Sheehan, 2016). In the present study, blood T_4 level remained unaltered during the post treatment days. Blood TSH level remained unaltered at initial and middle phases (day-1 to day-3) but increased at last phase (day-7) of post-treatment days. T_3 level in blood decreased initially (day-1), became normal in the middle phase (day-3) and increased finally (day-7) after MPTP treatment (Fig. 4). Therefore, the blood levels of TSH, T_4 and T_3 found in the present study did not signify the actual status of thyroid dysfunction (hypothyroidism or hyperthyroidism) in MPTP-treated mice.

4.4. MPTP induced changes in thyroid gland: Effects on levels of thyroid hormone, TPO expression (protein and mRNA) and TSH

In the present study MPTP treatment caused the damage of histomorphological structure of thyroid gland with disappearances of colloids at day-1. The gradual regaining of the histomophological structure of thyroid gland had been found in the following days like day-3 and day-7 with reappearance of colloids in follicles at day-7 after MPTP treatment. Notably, the weight of the thyroid gland did not change during day-1 and day-3, but increased in day-7 after MPTP treatment (Fig. 3B). In the present study, the content of total protein and RNA in thyroid tissues altered during post-treated days (Fig. 3B) in such a way that the RNA:protein ratio in thyroid gland remained unaltered during day-1 and day-3 and, reduced significantly at day-7 after MPTP treatment. The RNA:protein ratio indicates the ribosomal capacity, capacity of protein synthesis and cellular growth in tissue which signify the status of multiple steps including transcriptional efficiency of RNA synthesis, rate of RNA degradation, translational efficiency of protein synthesis and posttranslational modification of proteins during physiological and pathophysiological conditions (Brown et al., 1983; Lewis et al., 1984; Attaix et al., 1988; Preedy et al., 1990; Tesseraud et al., 1996; Tujioka et al., 2017). The depletion of the level of RNA:protein ratio in association with cellular growth is supposed to associate with the expression of those proteins which are constitutively expressed and condition of cellular growth where the rate of cellular growth for a fixed nutritional capacity is independent of abundance of protein (Scott et al., 2010). The low RNA:protein ratio of $\leq$ 1:50 is reported to facilitate the accumulation of core domain of p53, a tumour suppressor protein, in cells whereby the cells are in stressed or damaged condition and p53 is found to arrest cell cycle or causes apoptosis (Kovachev et al., 2017). Interestingly, the RNA:protein ratio had been found as 50 % of 1:50 during day-7 after MPTP treatment in the present study. Therefore, the rise of thyroid weight, alterations of RNA:protein ratio and regaining of histomorphological structure with reappearance of colloid in thyroid follicles indicate that the cellular proliferation and differentiation might happen during day-7 after MPTP treatment.

TSH stimulates cellular proliferation in cooperation with other factors including IGF (Dumont et al., 1992; Kimura et al., 2001; Kang et al., 2017) and also promotes cellular differentiation (Morgan et al., 2016) to produce different cell types in thyroid gland. Cell culture studies indicate that TSH exhibits cellular death (Speight et al., 1968). Alternatively, the *in vitro* studies indicate that TSH inhibits apoptosis of primary human thyrocytes (Kawakami et al., 1997; Feldkamp et al., 1999). Antibody studies in autoimmunity during Graves diseases indicate that TSH has two separate receptors coupled with different subunits of G-proteins while activation of one receptor through Gs and Gq/11 coupled signalling pathways potentiates cellular proliferation as well as thyroid hormone synthesis/secretion and subsequently inhibits action of another receptors linked with $G_{s\alpha}$ subunit for oxidative stress dependent cellular apoptosis (Morshed et al., 2013). In the present study, thyroid gland appeared to have sustained levels of elevated TSH (Fig. 4B) during post-treated days. Noteworthy, the elevated TSH levels in post-treated days in the present study might combat the cellular damage by its anti-apoptotic action during day-1 and subsequently potentiate regaining histomorphological structure by cellular proliferation and/or differentiation during days-3 to day-7.

TSH acts on its receptor present in thyroid follicular cells and enhances the machinery including TPO expression for thyroid hormone production and release in thyroid gland (Mondal et al., 2016; Sarapura and Samuel, 2017; Carvalho and Dupuy, 2017). In the present study, the protein expression of TPO increased extensively on day-3 keeping the levels at control levels in other days after MPTP treatment (Fig.3B). Contrarily, TPO mRNA-expression remained repressed during post-treated days. In the other study, the diminution of TPO mRNA expression in thyroid gland has been reported during low dose of iodine (potassium iodide) treatment in hyperthyroid (goitrogen treated and iodine deprived) dogs which have had both elevated serum TSH level and concomitantly reestablishment of synthesis as well as release of thyroid hormone (Uyttersprot et al., 1997). Noteworthy, the presence of two or more forms of mRNA through alternative splicing of TPO gene (Ohtaki et al., 1996), sensitivity of TPO gene to iodine compared to TSH (Collison et al., 1989; Ohtaki et al., 1996; Uyttersprot et al., 1997; Luo et al., 2014) and differential dynamics of mammalian mRNA vs. protein

levels due to complexity of post-transcriptional as well as post-translational modification (Liu et al., 2016; Cheng et al., 2016) are indispensable for the complete understanding the pattern of expression of mRNA vs. protein of TPO during different pathophysiological conditions.

In rodents, thyroid gland produces equal amount of T_4 and T_3 (Chanoine et al., 1993; van der Spek et al., 2017). In the present study, T_3 levels remained unaltered in thyroid gland throughout the post-MPTP-treatment days (Fig.4). T_4 level elevated at day-1 followed by attenuation to control levels at day-3 and finally depleted at day-7 after MPTP treatment. It is reported that T_4 acts as anti-apoptotic factor in cancer cell lines (Lin et al., 2015). Therefore, it is worthwhile to mention that thyroid gland might try to combat the adverse situation of cellular death with the elevated levels of TSH and T_4 through their anti-apoptotic actions, during initial days (day-1 to day3) after MPTP treatment.

In human, Dio-1 in thyroid gland contributes 6 % of circulatory T_3 in healthy condition that increases to 57 % in severe hyperthyroidism (Maia et al., 2011). In rat, deiodenase type-I is abundant in thyroid gland (Schoenmakers et al., 1995) which is responsive to TSH but not to T_4 (Erickson et al., 1982) and have ability to convert T_4 to T_3 in thyroid gland even during selenium-deficient condition (Chanoine et al., 1993). The synthesis of thyroglobulin is reported to be low in thyrocytes of follicles filled with large amount of colloids and such follicles are engaged in release of thyroid hormone preferably (Suzuki et al., 2011; Luo et al., 2014; Rajab et al., 2017). In day-7 after MPTP treatment of the present study, appearance of more follicles filled with large amount of colloid (Fig.3A) and depletion of T_4 level in thyroid gland (Fig.4B) indicate that T_4 in thyroid gland might be converted to T_3 which might be released to blood resulting elevation of T_3 in blood (Fig.4A) keeping the T_3 level normal in thyroid gland (Fig.4B).

4.5. MPTP induced changes of thyroidal status in Hypothalamus and Pituitary

Hypothalamus releases thyrotropin releasing hormone (TRH) which acts through TRH-receptor-2 linked G-protein-PKC pathway and stimulates the synthesis and release of TSH from thyrotrophs in anterior pituitary. T_4 and T_3 effort feed-back control and regulate synthesis and release of TSH, and TRH at their sources and the expression of TRH-receptor at pituitary level (Mullur et al., 2014; De Castro et al., 2015; Joseph-Bravo et al., 2015; Sarapura and Samuel, 2017). In the present study, pituitary appeared to have elevated levels of T_4 and T_3 all over the post-MPTP treated days. TSH levels in pituitary decreased in day-1, attended normal level in day-3 and finally remained at intermediate level in day-7. The oscillation of TSH levels in pituitary (Fig. 4B) and elevated levels of TSH in blood (Fig. 4A) during post-treated days indicate that TSH might have been synthesized and released from pituitary while the feed-back inhibition of elevated thyroid hormone levels might have been counterbalanced in pituitary during those days. In hypothalamus, T_4 level decreased initially (day-1) after MPTP treatment followed by amelioration to control level at later phases while the levels of T_3 and TSH remained unaltered in hypothalamus. Therefore, the results imply that hypothalamic TRH and its receptor in pituitary might have significant role to counterbalance the feed-back inhibition of elevated thyroid hormone levels for TSH synthesis and release in pituitary. In brief, the normal feed-back mechanism on hypothalamus and pituitary axis failed to perform after MPTP treatment.

5. Conclusion

Overall, the present study refers the novel findings related to the changes in thyroidal status in MPTP-treated (acute dose) mice. The changes in blood levels of thyroid hormone (T_4 and T_3) and TSH did not designate whether the animal developed status of hypothyroid or hyperthyroid condition after MPTP treatment. MPTP affected thyroid gland and altered the thyroidal status in other peripheral tissues including hypothalamus, pituitary and blood where feedback regulation mechanism of hypothalamus-pituitary-blood-thyroid axis failed to explain the facts of MPTP-induced changes found in the present study. Therefore, the findings of the present study claim that screening of thyroidal status in peripheral tissues involving with hypothalamo-pituitary-blood-thyroid axis is necessary during MPTP-induced model of Parkinsonism. MPTP altered the levels of thyroid hormone differentially in three regions of brain like substantia nigra (positive tissue for Parkinsonism), cerebral cortex and hippocampus (two regions associated with cognitive function). Noteworthy, both T_4 and T_3 appeared to be either in elevated or in unchanged condition at latter phase of post-MPTP-treated days in brain regions which depict that thyroid hormone might have role on brain during neurodegeneration.

CRediT authorship contribution statement

Priyobrata Sinha: Methodology, Data curation, Writing - original draft. **Nilkanta Chakrabarti:** Conceptualization, Writing - review & editing. **Nabanita Ghosh:** Methodology, Software, Validation. **Soham Mitra:** Conceptualization, Visualization, Investigation. **Shauryabrota Dalui:** Validation, Software. **Arindam Bhattacharyya:** Supervision.

Declaration of Competing Interest

There is no conflict of interests exist.

Acknowledgement

I sincerely thank all the lab members of Immunology Laboratory, Department of Zoology, University of Calcutta for their help. Special thanks to Dr. Sougata Roy Chowdhury for helping in the statistical analysis. This work is supported by University of Calcutta and funded by Neuroscience Taskforce, DBT, Govt. of India (BT/PR3986/MED/30/677/2011).

References

Airavaara, M., Harvey, B.K., Voutilainen, M.H., Shen, H., Chou, J., Lindholm, P., Lindahl, M., Tuominen, R.K., Saarma, M., Hoffer, B., Wang, Y., 2012. CDNF protects the nigrostriatal dopamine system and promotes recovery after MPTP treatment in mice. Cell Transplant. 21 (6), 1213–1223.

Aoki, E., Yano, R., Yokoyama, H., Kato, H., Araki, T., 2009. Role of nuclear transcription factor kappa B (NF-kappaB) for MPTP (1-methyl-4-phenyl-1,2,3,6-tetrahyropyridine)-induced apoptosis in nigral neurons of mice. Exp. Mol. Pathol. 86, 57–64.

Attaix, D., Aurousseau, E., Bayle, G., Rosolowska-Huszcz, D., Arnal, M., 1988. Respective influences of age and weaning on skeletal and visceral muscle protein synthesis in the lamb. Biochem. J. 256 (3), 791–795.

Aziz, N.A., Pijl, H., Frölich, M., Roelfsema, F., Roos, R.A., 2011. Diurnal secretion profiles of growth hormone, thyrotrophin and prolactin in Parkinson's disease. J. Neuroendocrinol. 23, 519–524.

Baek, B.S., Kwon, H.J., Lee, K.H., Yoo, M.A., Kim, K.W., Ikeno, Y., Yu, B.P., Chung, H.Y., 1999. Regional difference of ROS generation, lipid peroxidation, and antioxidant enzyme activity in rat brain and their dietary modulation. Arch. Pharm. Res. 22 (4), 361–366.

Bauer, M., Heinz, A., Whybrow, P.C., 2002. Thyroid hormones, serotonin and mood: of synergy and significance in the adult brain. Mol. Psychiatry 7, 140–156.

Beckhauser, T.F., Francis-Oliveira, J., De Pasquale, R., 2016. Reactive oxygen species: physiological and physiopathological effects on synaptic plasticity. J. Exp. Neurosci. 10 (S1), 23–48.

Berger, J.R., Kelley, R.E., 1981. Thyroid function in Parkinson disease. Neurology. 31 (1), 93–95.

Bian, M., Yu, M., Yang, S., Gao, H., Huang, Y., Deng, C., Gao, Y., Sun, F., Huang, F., 2008. Expression of Cbl-interacting protein of 85 kDa in MPTP mouse model of Parkinson's disease and 1-methyl-4-phenyl-pyridinium ion-treated dopaminergic SH-SY5Y cells. Acta Biochim Biophys Sin (Sanghai). 40 (6), 505–512.

Blesa, J., Phani, S., Jackson-Lewis, V., Przedborski, S., 2012. Classic and new animal models of Parkinson's disease. J. Biomed. Biotechnol. 2012.

Bocchetta, A., Traccis, F., Mosca, E., Serra, A., Tamburini, G., Loviselli, A., 2016. Bipolar disorder and antithyroid antibodies: review and case series. Int. J. Bipolar Disord. 4 (1), 5.

Bové, J., Prou, D., Perier, C., Przedborski, S., 2005. Toxin-induced models of Parkinson's disease. NeuroRx. 2 (3), 484–494.

Brown, J.G., van BUEREN, J., Millward, D.J., 1983. The effect of tri-iodothyronine administration on protein synthesis in the diabetic rat. Biochem. J. 214 (2), 637–640.
Cano-Europa, E., Perez-Severiano, F., Vergara, P., Ortiz-Butrón, R., Ríos, C., Segovia, J., Pacheco-Rosado, J., 2008. Hypothyroidism induces selective oxidative stress in amygdala and hippocampus of rat. Metab. Brain Dis. 23 (3), 275–287.
Cao, X., Kambe, F., Miyazaki, T., Sarkar, D., Ohmori, S., Seo, H., 2002. Novel human ZAKI-4 isoforms: hormonal and tissue-specific regulation and function as calcineurin inhibitors. Biochem. J. 367 (2), 459–466.
Caradoc-Davies, T.H., 1986. Resolution of dyskinesia and the "on-off" phenomenon in thyrotoxic patients with Parkinson's disease after antithyroid treatment. Br Med J (Clinical Res Ed.). 293, 38–39.
Carvalho, D.P., Dupuy, C., 2017. Thyroid hormone biosynthesis and release. Mol. Cell. Endocrinol. 458, 6–15.
Chakrabarti, N., Ray, A.K., 2000. Rise of intrasynaptosomal Ca^{2+} level and activation of nitric oxide synthase in adult rat cerebral cortex pretreated with 3-5-3′-L-triiodothyronine. Neuropsychopharmacology. 22 (1), 36–41.
Chakrabarti, N., Ray, A.K., 2002. Stimulation of Ca2+/Mg2+-ATPase activity in adult rat cerebrocortical synaptosomes by 3-5-3′-L-triiodothyronine. Neurosci. Res. Commun. 31 (3), 193–201.
Chakrabarti, N., Ray, A.K., 2003. Stimulation of AChE activity in relation to changes in electronmicroscopic structure of adult rat cerebrocortical synaptosomes pretreated with 3-5-3′-triiodo-L-thyronine. Neuroreport. 14 (11), 1497–1501.
Chakrabarti, N., Subbarao, T., Sengupta, A., Xu, F., Stouffer, R.L., Sridaran, R., 2008. Expression of mRNA and proteins for GnRH I and II and their receptors in primate corpus luteum during menstrual cycle. Mol. Reprod. Dev. 75 (10), 1567–1577.
Chakrabarti, N., Datta, S., Samanta, D., Chaudhuri, A.G., Ray, A.K., 2017. Alterations in cerebrocortical synaptosomal acetylcholinesterase activity and histomorphology of thyroid gland of adult rat during different thyroidal conditions. Indian J. Exp. Biol. 55, 201–208.
Chanoine, J.P., Braverman, L.E., Farwell, A.P., Safran, M., Alex, S., Dubord, S., Leonard, J.L., 1993. The thyroid gland is a major source of circulating T_3 in the rat. J. Clin. Invest. 91 (6), 2709–2713.
Cheng, Z., Teo, G., Krueger, S., Rock, T.M., Koh, H.W., Choi, H., Vogel, C., 2016. Differential dynamics of the mammalian mRNA and protein expression response to misfolding stress. Mol. Syst. Biol. 12 (1), 855.
Choi, S.M., Kim, B.C., Choi, K.H., Nam, T.S., Kim, J.T., Lee, S.H., Park, M.S., Kim, M.K., Cho, K.H., 2014. Thyroid status and cognitive function in euthyroid patients with early Parkinson's disease. Dement. Geriatr. Cogn. Disord. 38 (3-4), 178–185.
Collison, K.S., Banga, J.P., Barnett, P.S., Kung, A.W.C., McGregor, A.M., 1989. Activation of the thyroid peroxidase gene in human thyroid cells: effect of thyrotrophin, forskolin and phorbol ester. J. Mol. Endocrinol. 3 (1), 1–5.
Cortés, C., Eugenin, E., Aliaga, E., Carreño, L.J., Bueno, S.M., Gonzalez, P.A., Gayol, S., Naranjo, D., Noches, V., Marassi, M.P., Rosenthal, D., 2012. Hypothyroidism in the adult rat causes incremental changes in brain-derived neurotrophic factor, neuronal and astrocyte apoptosis, gliosis, and deterioration of postsynaptic density. Thyroid. 22, 951–963.
Costa, G., Pinna, A., Porceddu, P.F., Casu, M.A., Di Maio, A., Napolitano, F., Usiello, A., Morelli, M., 2018. Rhes counteracts dopamine neuron degeneration and neuroinflammation depending on gender and age. Front. Aging Neurosci. 10, 163.
Dai, Y.B., Tan, X.J., Wu, W.F., Warner, M., Gustafsson, J.Å., 2012. Liver X receptor β protects dopaminergic neurons in a mouse model of Parkinson disease. Proc. Natl. Acad. Sci. U.S.A. 109 (32), 13112–13117.
Das, K., Chainy, G.B.N., 2004. Thyroid hormone influences antioxidant defense system in adult rat brain. Neurochem. Res. 29 (9), 1755–1766.
Datta, I., Bhonde, R., 2012. Can mesenchymal stem cells reduce vulnerability of dopaminergic neurons in the substantianigra to oxidative insult in individuals at risk to Parkinson's disease? Cell Biol. Int. 36 (7), 617–624.
De Castro, J.P., Fonseca, T.L., Ueta, C.B., McAninch, E.A., Abdalla, S., Wittmann, G., Lechan, R.M., Gereben, B., Bianco, A.C., 2015. Differences in hypothalamic type 2 deiodinase ubiquitination explain localized sensitivity to thyroxine. J. Clin. Invest. 125, 769–781.
Dumont, J.E., Lamy, F., Roger, P., Maenhaut, C., 1992. Physiological and pathological regulation of thyroid cell proliferation and differentiation by thyrotropin and other factors. Physiol. Rev. 72 (3), 667–697.
Erickson, V.J., Cavalieri, R.R., Rosenberg, L.L., 1982. Thyroxine-5'-deiodinase of rat thyroid, but not that of liver, is dependent on thyrotropin. Endocrinology. 111 (2), 434–440.
Fanibunda, S.E., Desouza, L.A., Kapoor, R., Vaidya, R.A., Vaidya, V.A., 2018. Thyroid hormone regulation of adult neurogenesis. Vitam. Horm. 106, 211–251.
Feldkamp, J., Pascher, E., Perniok, A., Scherbaum, W.A., 1999. Fas-mediated apoptosis is inhibited by TSH and iodine in moderate concentrations in primary human thyrocytes in vitro. Horm. Metab. Res. 31 (06), 355–358.
Francardo, V., Bez, F., Wieloch, T., Nissbrandt, H., Ruscher, K., Cenci, M.A., 2014. Pharmacological stimulation of sigma-1 receptors has neurorestorative effects in experimental parkinsonism. Brain. 137 (Pt7), 1998–2014.
Friesema, E.C., Jansen, J., Visser, T.J., 2005. Thyroid hormone transporters. Biochem. Soc. Trans. 33, 228–232.
Fuller, R.W., Hemrick-Luecke, S.K., Robertson, D.W., 1988. Comparison of 1-methyl-4-phenyl-1, 2, 3, 6-tetrahydropyridine (MPTP) and 1-methyl-4-phenylpyridinium (MPP+) effects on mouse heart norepinephrine. Biochem. Pharmacol. 37 (17), 3343–3347.
García-Moreno, J.M., Chacón-Peña, J., 2003. Hypothyroidism and Parkinson's disease and the issue of diagnostic confusion. Mov. Disord. 18 (9), 1058–1059.
Ghosh, N., Mitra, S., Sinha, P., Chakrabarti, N., Bhattacharyya, A., 2018. TNFR2 mediated TNF-α signaling and NF-κB activation in hippocampus of 1-methyl-4-phenyl-1, 2, 3, 6-tetrahydropyridine-treated mice. Neurosci. Res. 137, 36–42.
Ghosh, N., Mitra, S., Sinha, P., Chakrabarti, N., Bhattacharyya, A., 2019. Study of Microglial and astroglial alterations induced by acute 1-Methyl-4-Phenyl-1, 2, 3, 6-Tetrahydropyridine treatment in mouse brain. Proc. Zool. Soc. 1–8.
Goldstein, D.S., Li, S.T., Holmes, C., Bankiewicz, K., 2003. Sympathetic innervation in the 1-methyl-4-phenyl-1, 2, 3, 6-tetrahydropyridine primate model of Parkinson's disease. J. Pharmacol. Exp. Ther. 306, 855–860.
Hong, J., Sha, S., Zhou, L., Wang, C., Yin, J., Chen, L., 2015. Sigma-1 receptor deficiency reduces MPTP-induced parkinsonism and death of dopaminergic neurons. Cell Death Dis. 6 (7), e1832.
Huang, D., Xu, J., Wang, J., Tong, J., Bai, X., Li, H., Wang, Z., Huang, Y., Wu, Y., Yu, M., Huang, F., 2017. Dynamic changes in the nigrostriatal pathway in the MPTP mouse model of Parkinson's disease. Parkinsons Dis. 2017, 9349487.
Ittermann, T., Wittfeld, K., Nauck, M., Bülow, R., Hosten, N., Völzke, H., Grabe, H.J., 2018. High thyrotropin is associated with reduced hippocampal volume in a population-based study from Germany. Thyroid. 28 (11), 1434–1442.
Jackson-Lewis, V., Jakowec, M., Burke, R.E., Przedborski, S., 1995. Time course and morphology of dopaminergic neuronal death caused by the neurotoxin 1-methyl-4-phenyl-1, 2, 3, 6-tetrahydropyridine. Neurodegeneration 4 (3), 257–269.
Jackson-Lewis, V., Przedborski, S., 2007. Protocol for the MPTP mouse model of Parkinson's disease. Nat. Protoc. 2 (1), 141–151.
Johannessen, A.C., Boye, A., Pakkenberg, H., 1987. Thyroid function in patients with Parkinson's disease. Acta Neurol. Scand. 75, 364–365.
Joseph-Bravo, P., Jaimes-Hoy, L., Uribe, R.M., Charli, J.L., 2015. 60 years of neuroendocrinology: TRH, the first hypophysiotropic releasing hormone isolated: control of the pituitary–thyroid axis. J. Endocrinol. 226 (2), T85–T100.
Kang, H.S., Kumar, D., Liao, G., Lichti-Kaiser, K., Gerrish, K., Liao, X.H., Refetoff, S., Jothi, R., Jetten, A.M., 2017. GLIS3 is indispensable for TSH/TSHR-dependent thyroid hormone biosynthesis and follicular cell proliferation. J. Clin. Invest. 127 (12), 4326–4337.
Kawajiri, M., Ohyagi, Y., Furuya, H., Araki, T., Inoue, N., Esaki, S., Yamada, T., Kira, J., 2002. A patient with Parkinson's disease complicated by hypothyroidism who developed malignant syndrome after discontinuation of etizolam. Rinsho Shinkeigaku = Clinical neurology 42, 136–139.
Kawakami, A., Eguchi, K., Matsuoka, N., Tsuboi, M., Urayama, S., Kawabe, Y., Tahara, K., Ishikawa, N., Ito, K., Nagataki, S., 1997. Modulation of Fas-mediated apoptosis of human thyroid epithelial cells by IgG from patients with Graves' disease (GD) and idiopathic myxoedema. Clin. Exp. Immunol. 110 (3), 434–439.
Keshavarzian, A., Haydek, J.M., Zepeda, D.O., Stinneford, J.G., Fields, J.Z., 1990. Gastroduodenal ulcers in rats induced by 1-methyl-4-phenyl-1, 2, 5, 6-tetrahydropyridine (MPTP): requirement for gastric acid secretion and the role of prostaglandins. Res. Commun. Chem. Pathol. Pharmacol. 70 (1), 21–48.
Kim, H.T., Edwards, M.J., Narsimhan, R.L., Bhatia, K.P., 2005. Hyperthyroidism exaggerating parkinsonian tremor: a clinical lesson. Parkinsonism Relat. Disord. 11, 331–332.
Kim, S., Moon, M., Park, S., 2009. Exendin-4 protects dopaminergic neurons by inhibition of microglial activation and matrix metalloproteinase-3 expression in an animal model of Parkinson's disease. J. Endocrinol. 202 (3), 431–439.
Kimura, T., Van Keymeulen, A., Golstein, J., Fusco, A., Dumont, J.E., Roger, P.P., 2001. Regulation of thyroid cell proliferation by TSH and other factors: a critical evaluation of in vitro models. Endocr. Rev. 22 (5), 631–656.
Kovachev, P.S., Banerjee, D., Rangel, L.P., Eriksson, J., Pedrote, M.M., Martins-Dinis, M.M.D., Edwards, K., Cordeiro, Y., Silva, J.L., Sanyal, S., 2017. Distinct modulatory role of RNA in the aggregation of the tumor suppressor protein p53 core domain. J. Biol. Chem. 292 (22), 9345–9357.
Lai, F., Jiang, R., Xie, W., Liu, X., Tang, Y., Xiao, H., Gao, J., Jia, Y., Bai, Q., 2018. Intestinal pathology and gut microbiota alterations in a methyl-4-phenyl-1, 2, 3, 6-tetrahydropyridine (MPTP) mouse model of Parkinson's disease. Neurochem. Res. 43 (10), 1986–1999.
Lewis, S.E.M., Kelly, F.J., Goldspink, D.F., 1984. Pre-and post-natal growth and protein turnover in smooth muscle, heart and slow-and fast-twitch skeletal muscles of the rat. Biochem. J. 217 (2), 517–526.
Li, Y., Perry, T., Kindy, M.S., Harvey, B.K., Tweedie, D., Holloway, H.W., Powers, K., Shen, H., Egan, J.M., Sambamurti, K., Brossi, A., Lahiri, D.K., Mattson, M.P., Hoffer, B.J., Wang, Y., Greig, N.H., 2009. GLP-1 receptor stimulation preserves primary cortical and dopaminergic neurons in cellular and rodent models of stroke and Parkinsonism. Proc. Natl. Acad. Sci. U.S.A. 106 (4), 1285–1290.
Lin, H.Y., Davis, F.B., Luidens, M.K., Mousa, S.A., Cao, J.H., Zhou, M., Davis, P.J., 2011. Molecular basis for certain neuroprotective effects of thyroid hormone. Front. Mol. Neurosci. 4, 29.
Lin, H.Y., Glinsky, G.V., Mousa, S.A., Davis, P.J., 2015. Thyroid hormone and anti-apoptosis in tumor cells. Oncotarget. 6 (17), 14735–14743.
Livak, K.J., Schmittgen, T.D., 2001. Analysis of relative gene expression data using real-time quantitative PCR and the $2^{-\Delta\Delta CT}$ method. Methods. 25 (4), 402–408.
Liu, Y., Beyer, A., Aebersold, R., 2016. On the dependency of cellular protein levels on mRNA abundance. Cell. 165 (3), 535–550.
Luo, Y., Ishido, Y., Hiroi, N., Ishii, N., Suzuki, K., 2014. The emerging roles of thyroglobulin. Adv Endocrinol. 2014.
Maia, A.L., Goemann, I.M., Souza Meyer, E.L., Wajner, S.M., 2011. Type 1 iodothyronine deiodinase in human physiology and disease. J. Endocrinol. 209 (3), 283–297.
Mano, T., Sinohara, R., Sawai, Y., Oda, N., Nishida, Y., Mokuno, T., Asano, K., Ito, Y., Kotake, M., Hamada, M., Nakai, A., 1995. Changes in lipid peroxidation and free radical scavengers in the brain of hyper-and hypothyroid aged rats. J. Endocrinol. 147 (2), 361–365.
Manzano, J., Morte, B., Scanlan, T.S., Bernal, J., 2003. Differential effects of triiodothyronine and the thyroid hormone receptor β-specific agonist GC-1 on thyroid hormone target genes in the brain. Endocrinology. 144 (12), 5480–5487.

Meredith, G.E., Rademacher, D.J., 2011. MPTP mouse models of Parkinson's disease: an update. J. Parkinsons Dis. 1 (1), 19–33.
Miao, Y., Wu, W., Dai, Y., Maneix, L., Huang, B., Warner, M., Gustafsson, J.Å., 2015. Liver X receptor β controls thyroid hormone feedback in the brain and regulates browning of subcutaneous white adipose tissue. Proc. Natl. Acad. Sci. U.S.A. 112 (45), 14006–14011.
Miller, R.M., Federoff, H.J., 2005. Altered gene expression profiles reveal similarities and differences between Parkinson disease and model systems. Neuroscientist. 11 (6), 539–549.
Minár, M., Valkovič, P., 2014. Thyroid-induced worsening of parkinsonian tremor resistant to drugs and subthalamic nucleus deep brain stimulation. Case Rep. Neurol. Med. 2014, 489275.
Mondal, S., Raja, K., Schweizer, U., Mugesh, G., 2016. Chemistry and biology in the biosynthesis and action of thyroid hormones. Angew. Chem. Int. Ed. Engl. 55 (27), 7606–7630.
Morgan, S.J., Neumann, S., Marcus-Samuels, B., Gershengorn, M.C., 2016. Thyrotropin stimulates differentiation not proliferation of normal human thyrocytes in culture. Front Endocrinol (Lausanne). 7, 168.
Morshed, S.A., Ma, R., Latif, R., Davies, T.F., 2013. How one TSH receptor antibody induces thyrocyte proliferation while another induces apoptosis. J. Autoimmun. 47, 17–24.
Mullur, R., Liu, Y.Y., Brent, G.A., 2014. Thyroid hormone regulation of metabolism. Physiol. Rev. Suppl. 94, 355–382.
Munhoz, R.P., Teive, H.A., Troiano, A.R., Hauck, P.R., Leiva, M.H., Graff, H., Werneck, L.C., 2004. Parkinson's disease and thyroid dysfunction. Parkinsonism Relat. Disord. 10 (6), 381–383.
Napolitano, F., Warren, E.B., Migliarini, S., Punzo, D., Errico, F., Li, Q., Thiolat, M.L., Vescovi, A.L., Calabresi, P., Bezard, E., Morelli, M., 2017. Decreased Rhes mRNA levels in the brain of patients with Parkinson's disease and MPTP-treated macaques. PLoS One 12 (7), e0181677.
Ohtaki, S., Nakagawa, H., Nakamura, M., Kotani, T., 1996. Thyroid peroxidase: experimental and clinical integration. Endocr. J. 43 (1), 1–14.
Pasquali, L., Caldarazzo-Ienco, E., Fornai, F., 2014. MPTP neurotoxicity: actions, mechanisms, and animal modeling of Parkinson's disease. Handbook of Neurotoxicity 237–275.
Paxinos, G., Franklin, K.B.J., 2001. The Mouse Brain in Stereotaxic Coordinates, 2nd edn. Academic Press, San Diego.
Pilhatsch, M., Marxen, M., Winter, C., Smolka, M.N., Bauer, M., 2011. Hypothyroidism and mood disorders: integrating novel insights from brain imaging techniques. Thyroid Res. 4 (1), S3.
Prakash, K.M., Kek, P.C., 2010. Hyperthyroidism "masked" the levodopa response in newly diagnosed Parkinson's disease patients. Parkinsonism Relat. Disord. 16, 691–692.
Preedy, V.R., Paska, L., Sugden, P.H., Schofield, P.S., Sugden, M.C., 1990. Protein synthesis in liver and extra-hepatic tissues after partial hepatectomy. Biochem. J. 267 (2), 325–330.
Rajab, N.M.A., Ukropina, M., Cakic-Milosevic, M., 2017. Histological and ultrastructural alterations of rat thyroid gland after short-term treatment with high doses of thyroid hormones. Saudi J. Biol. Sci. 24 (6), 1117–1125.
Remaud, S., Gothié, J.D., Morvan-Dubois, G., Demeneix, B.A., 2014. Thyroid hormone signaling and adult neurogenesis in mammals. Front Endocrinol (Laussane) 5, 62.
Roberts, S.C., Bianco, A.C., Stapleton, H.M., 2015. Disruption of type 2 iodothyroninedeiodinase activity in cultured human glial cells by polybrominated diphenyl ethers. Chem. Res. Toxicol. 28, 1265–1274.
Ruffoli, R., Giambelluca, M.A., Scavuzzo, M.C., Pasquali, L., Giannessi, F., Fornai, F., 2008. MPTP-induced Parkinsonism is associated with damage to Leydig cells and testosterone loss. Brain Res. 1229, 218–223.
Salim, S., 2017. Oxidative stress and the central nervous system. J. Pharmacol. Exp. Ther. 360 (1), 201–205.
Sarapura, V.D., Samuel, M.H., 2017. Thyroid-stimulating hormone. The Pituitary. Academic Press, pp. 163–201.
Sarkar, P.K., Ray, A.K., 1993. Synaptosomal action of thyroid hormone: changes in Na+-K+-ATPase activity in adult rat cerebral cortex. Horm. Metab. Res. 25 (01), 1–3.
Sarkar, P.K., Ray, A.K., 1994. Synaptosomal T3 content in cerebral cortex of adult rat in different thyroidal states. Neuropsychopharmacology. 11 (3), 151–155.
Schoenmakers, C.H., Pigmans, I.G., Visser, T.J., 1995. Investigation of type I and type III iodothyroninedeiodinase in rat tissues using N-bromoacetyliodothyronine affinity labels. Mol. Cell. Endocrinol. 107 (2), 173–180.
Scott, M., Gunderson, C.W., Mateescu, E.M., Zhang, Z., Hwa, T., 2010. Interdependence of cell growth and gene expression: origins and consequences. Science. 330 (6007), 1099–1102.
Sheehan, M.T., 2016. Biochemical testing of the thyroid: TSH is the best and, oftentimes, only test needed–a review for primary care. Clin. Med. Res. 14 (2), 83–92.
Speight, J.W., Baba, W.I., Wilson, G.M., 1968. The effect of propylthiouracil and thyroid-stimulating hormone on the survival of rat thyroid cells in vivo and in vitro. J. Endocrinol. 41 (4), 577–591.
Suzuki, K., Kawashima, A., Yoshihara, A., Akama, T., Sue, M., Yoshida, A., Kimura, H.J., 2011. Role of thyroglobulin on negative feedback autoregulation of thyroid follicular function and growth. J. Endocrinol. 209, 169–174.
Tabrez, S., Jabir, N.R., Shakil, S., Greig, N.H., Alam, Q., Abuzenadah, A.M., Damanhouri, G.A., Kamal, M.A., 2012. A synopsis on the role of tyrosine hydroxylase in Parkinson's disease. CNS Neurol. Disord. Drug Targets. 11 (4), 395–409.
Tandeter, H.B., Shvartzman, P., 1993. Parkinson's disease camouflaging early signs of hypothyroidism. Postgrad. Med. 94 (5), 187–190.
Tatton, N.A., Kish, S.J., 1997. In situ detection of apoptotic nuclei in the substantia nigra compacta of 1-methyl-4-phenyl-1,2,3,6-tetrahydropyridine-treated mice using terminal deoxynucleotidyl transferase labelling and acridine orange staining. Neuroscience. 77 (4), 1037–1048.
Tesseraud, S., Peresson, R., Chagneau, A.M., 1996. Age-related changes of protein turnover in specific tissues of the chick. Poult. Sci. 75 (5), 627–631.
Thiffault, C., Aumont, N., Quirion, R., Poirier, J., 1995. Effect of MPTP and L-deprenyl on antioxidant enzymes and lipid peroxidation levels in mouse brain. J. Neurochem. 65 (6), 2725–2733.
Tujioka, K., Yamada, T., Yokogoshi, H., Akiduki, S., Hishida, Y., Tsutsui, K., Hayase, K., 2017. Changes in thyroid hormone are not involved in regulating brain protein synthesis in adults rats fed ornithine. J Nutri Sci Vitaminol. 63 (6), 389–395.
Uyttersprot, N., Pelgrims, N., Carrasco, N., Gervy, C., Maenhaut, C., Dumont, J.E., Miot, F., 1997. Moderate doses of iodide in vivo inhibit cell proliferation and the expression of thyroperoxidase and Na+/I− symporter mRNAs in dog thyroid. Mol. Cell. Endocrinol. 131 (2), 195–203.
van der Spek, A.H., Fliers, E., Boelen, A., 2017. The classic pathways of thyroid hormone metabolism. Mol. Cell. Endocrinol. 458, 29–38.
Vandresen-Filho, S., Martins, W.C., Bertoldo, D.B., Mancini, G., De Bem, A.F., Tasca, C.I., 2015. Cerebral cortex, hippocampus, striatum and cerebellum show differential susceptibility to quinolinic acid-induced oxidative stress. Neurol. Sci. 36 (8), 1449–1456.
Vargiu, P., Morte, B., Manzano, J., Perez, J., de Abajo, R., Sutcliffe, J.G., Bernal, J., 2001. Thyroid hormone regulation of rhes, a novel Ras homolog gene expressed in the striatum. Brain Res. Mol. Brain Res. 94 (1-2), 1–8.
Villanueva, I., Alva-Sánchez, C., Pacheco-Rosado, J., 2013. The role of thyroid hormones as inductors of oxidative stress and neurodegeneration. Oxid. Med. Cell. Longev. 2013, 218145.
Wallace, R.A., Boldry, R., Schmittgen, T., Miller, D., Uretsky, N., 1984. Effect of 1-methyl-4-phenyl-1, 2, 3, 6 tetrahydropyridine (MPTP) on monoamine neurotransmitters in mouse brain & heart. Life Sci. 35 (3), 285–291.
Wingert, T.D., Hershman, J.M., 1979. Sinemet® and thyroid function in Parkinson disease. Neurology. 29 (7), 1073.
Zhao, M., Momma, S., Delfani, K., Carlen, M., Cassidy, R.M., Johansson, C.B., Brismar, H., Shupliakov, O., Frisen, J., Janson, A.M., 2003. Evidence for neurogenesis in the adult mammalian substantia nigra. Proc. Natl. Acad. Sci. U.S.A. 100 (13), 7925–7930.
Zheng, W., Deane, R., Redzic, Z., Preston, J., Segal, M., 2003. Transport of l-[125 I] thyroxine by in situ perfused ovine choroid plexus: inhibition by lead exposure. J Toxicol Environ Health A. 66 (5), 435–451.
Zibara, K., Zein, N.E., Sabra, M., Hneino, M., Harati, H., Mohamed, W., Kobeissy, F.H., Kassem, N., 2017. Thyroxine (T4) Transfer from blood to cerebrospinal fluid in sheep isolated perfused choroid plexus: role of multidrug resistance-associated proteins and organic anion transporting polypeptides. Front. Neurol. 8 (214), 1–10.
Zlatković, J., Todorović, N., Bošković, M., Pajović, S.B., Demajo, M., Filipović, D., 2014. Different susceptibility of prefrontal cortex and hippocampus to oxidative stress following chronic social isolation stress. Mol. Cell. Biochem. 393 (1-2), 43–57.

Article

Journal of
Nanoscience and Nanotechnology
Vol. 20, 3404–3414, 2020
www.aspbs.com/jnn

Gold Nanoparticles (AuNPs) Conjugated with Andrographolide Ameliorated Viper (*Daboia russellii russellii*) Venom-Induced Toxicities in Animal Model

Sourav Ghosh[1], Subir Chandra Dasgupta[2], Anjan Kumar Dasgupta[3], Aparna Gomes[4], and Antony Gomes[1,*]

[1] *Laboratory of Toxinology and Experimental Pharmacodynamics, Department of Physiology, University of Calcutta, Kolkata 700009, India*
[2] *Post Graduate Department of Zoology, Maulana Azad College, Kolkata 700013, India*
[3] *Department of Biochemistry, University of Calcutta, Kolkata 700019, India*
[4] *Council of Scientific & Industrial Research-Indian Institute of Chemical Biology, Kolkata 700032, India*

Andrographolide, a diterpenoid compound found in the aerial parts of *Andrographis paniculata* (a well known anti snake venom plant) was conjugated with gold nanoparticle (andrographolide-AuNPs) and its efficacy against *Daboia russellii russellii* venom (DRRV) induced local damage, organ toxicity and inflammatory response was evaluated in animal models. Ethical clearance was obtained before animal experiments. Andrographolide-AuNPs was formed by adsorption method. Physico-chemical characterization of particle was done by dynamic light scattering (DLS), field emission scanning electron microscopy (FE-SEM), transmission electron microscopy (TEM) and X-ray diffraction (XRD). Swiss albino male mice were divided into 5 groups: Gr. 1-Sham control, Gr. 2-DRRV control, Gr. 3-anti snake venom serum treated, Gr. 4-andrographolide treated and Gr. 4-andrographolide-AuNPs treated. 1/5th minimum lethal dose of DRRV (10 μg/*s.c.*/20 g mice) was induced in animals of group 2, 3, 4 and 5 animals, followed by treatment with anti snake venom serum (2 mg/20 g mice, *i.v.*) andrographolide (50 μg/20g mice, *i.p.*) and andrographolide-AuNPs (50 μg/20 g mice, *i.v.*) in group 3, 4 and 5 animals, respectively. Blood was collected after 18 h, serum was prepared and organ toxicity markers (transaminases, phosphatases, lactate dehydrogenase, creatine phosphate, urea, creatinine, Ca^{2+}, phosphorous), inflammatory markers (interleukin 1β, 6, 17a, 10, tumor necrosis factor α) and local damage testings (defibrination, edema, hemorrhage) were assessed. Values were expressed as mean $\pm$ SEM ($n = 4$), one way analysis of variance was done, $P < 0.05$ was considered as statistically significant. Formed andrographolide-AuNPs were pink in color with hydrodynamic diameter 30–50 nm, polydispersity index 0.412 and zeta potential -16.21 mV. XRD data confirmed the presence of crystalline gold in andrographolide-AuNPs. TEM (20–50 nm) and FE-SEM (20–25 nm) indicated the presence of nearly spherical particle. DRRV envenomation followed by treatment with andrographolide-AuNPs provided protection against venom induced edema, hemorrhage, defibrination, organ toxicity and inflammation in animal model. Venom neutralization by andrographolide-AuNPs was > andrographolide, which confirmed the increased efficacy of andrographolide after gold nanoparticle conjugation, may be due to anti-oxidant/anti-inflammatory activity of andrographolide, showing increased efficacy after gold nanoparticle tagging. Thus, andrographolide-AuNPs may serve as a supportive therapy in snakebite (against venom induced local damage, organ toxicity and inflammatory response) subject to further detail studies.

Keywords: *Andrographis paniculata*, Andrographolide, Gold Nanoparticle, *Daboia russellii russellii* Venom, Venom Toxicity, Inflammation, Oxidative Stress.

*Author to whom correspondence should be addressed.

 1533-4880/2020/20/3404/011 doi:10.1166/jnn.2020.17421

1. INTRODUCTION

Gold nanoparticles (AuNPs) have many physical properties that make them suitable for biomedical applications such as biological imaging, drug delivery, disease treatment, diagnostic assay, radiotherapy, biosensors, thermal ablation, chemical sensing etc. [1, 2]. AuNPs have been found to be anticancer, hematopoietic, hepatoprotective, antioxidant, anti-inflammatory, anti-arthritic, etc. [3–8]. Gold conjugated with anti-snake venom herbs (*Vitex negundo*) and herbal compounds (2-hydroxy-4-methoxy benzoic acid and curcumin) showed better efficacy in neutralizing snake venom in animal models [9–13]. C60 fullerene nanoparticle has been found to be effective against rattle snake venom proteins in cricket model [14].

Andrographis paniculata (AP) is a medicinally important herb of family *Acanthaceae*, widely distributed around the world including Bangladesh, China, Hong Kong, India, Indonesia, Malaysia, Pakistan, Philippines and Thailand [15, 16]. Extract from aerial parts of AP contains diterpenoids, diterpene glycosides, lactones, flavonoids, and flavonoid glycosides, which makes it one of the most widely used herbs in traditional medicines [15, 17]. The folk and traditional use of AP against snake bite, bug bite, diabetes, dysentery, fever, and malaria is well known for a long time [18]. Its efficacy against snake bite, cardiovascular diseases, cancer, cytotoxicity, diarrhoea, hepatitis, hepatotoxicity, HIV, hyperglycemia, inflammation, microbial growth, malaria and oxidative stress has been well documented [19–32]. In the present study, andrographolide (a diterpenoid compound present in the aerial parts of *Andrographis paniculata*) has been conjugated with gold nanoparticles, its physico-chemical characterization and efficacy against *Daboia russellii russellii* venom (DRRV) was evaluated in animal models.

2. EXPERIMENTAL DETAILS

2.1. Materials

All the chemicals used in the present communication were of analytical grade, unless otherwise mentioned. The following chemicals were used in the present study—5,5′dithiobis (2-nitrobenzoic acid) (Sigma, USA), acid phosphatase biochemical kit (Spinreact, Spain), alanine aminotransferase biochemical kit (Spinreact, Spain), alkaline phosphatase biochemical kit (Spinreact, Spain), andrographolide (Sigma-Aldrich, USA), anti snake venom serum I.P. (Vins Bioproducts Limited, India, Batch No. 01AS15045), aspartate aminotransferase biochemical kit (Spinreact, Spain), calcium chloride (SRL, India), calcium biochemical kit (Spinreact, Spain), creatinine biochemical kit (Spinreact, Spain), disodium hydrogen phosphate (SRL, India), ethylenediaminetetraacetic acid (SRL, India), gold salt (Sigma-Aldrich, USA), interleukin 10 enzyme linked immunosorbent assay (ELISA) kit (R&D, USA), interleukin 17a ELISA kit (R&D, USA), interleukin 1β ELISA kit (R&D, USA), interleukin 6 ELISA kit (R&D, USA), lactate dehydrogenase biochemical kit (Spinreact, Spain), phosphorous biochemical kit (Spinreact, Spain), potassium dihydrogen phosphate (SRL, India), pyrogallol (SRL, India), sodium bicarbonate (SRL, India), sodium chloride (SRL, India), sodium dihydrogen phosphate (SRL, India), thiobarbituric acid (SRL, India), tricarboxylic acid (SRL, India), tris-aminomethane (SRL, India), tumor necrosis factor α ELISA kit (R&D, USA), urea biochemical kit (Spinreact, Spain), γ-glutamyl transferase biochemical kit (Spinreact, Spain).

2.2. Conjugation of Gold Nanoparticle with Andrographolide

Andrographolide was procured from Sigma-Aldrich, USA (Catalogue No.: 365645; Lot No.: MKBN8939V). It was dissolved in 3% ethanol to make 1 mg/ml solution. Gold salt ($HAuCl_4$) was purchased from Sigma-Aldrich, USA (Catalogue No.: 484385). Gold Nanoparticles (AuNPs) were synthesized by citrate reduction method after Sengupta et al. [33]. Milli-Q water (25 ml) was brought to boil, an aqueous solution of 10 mM gold salt (625 μl) was added to it in dark with continuous stirring at 450 rpm. Freshly prepared 100 mM trisodium isocitrate (750 μl) was added quickly to it which brought change in the solution color from pale yellow to bluish followed by deep red in about 15 min. The solution was allowed to be cooled in room temperature with continuous stirring (450 rpm). Gold nanoparticle prepared was then conjugated with andrographolide to synthesize andrographolide-conjugated gold nanoparticles (andrographolide-AuNPs) by adsorption method. 0.5 mL of andrographolide (1 mg/mL) was added slowly to 1.0 mL of freshly prepared AuNPs on a vortex mixture, kept at 4 °C for further use, and termed as andrographolide-AuNPs.

2.3. Animals and Animal Grouping

Swiss albino male mice (20 ± 2 gm) were obtained from authorized animal suppliers of the University of Calcutta. The animals were housed in polypropelene cages in a well ventilated room with controlled atmosphere (temperature: 24 ± 1 °C, humidity: 50 ± 5% and 12–12 h light-dark cycle). The animals were provided with green vegetables, balanced pellet, and water *ad libitum*. A quarantine period of 7 days was allowed before the experiments. The experimental designs described in this research article were approved by the animal ethical committee of the Department of Physiology, University of Calcutta (Reference number: IAEC/Revised Proposal/AG-01/2012; dt: 01.02.2013) and the animals were maintained as per the guidelines of the Committee for the Purpose of Control and Supervision of Experiments on Animal (CPCSEA), Government of India.

Animals ($n = 6$) were randomly divided into group 1: control, group 2: *Daboia russellii russellii* venom (DRRV) control, group 3: anti snake venom serum (ASVS)

treated, group 4: andrographolide treated and group 5: andrographolide-AuNPs treated. Group 2, 3, 4 and 5 animals were injected with DRRV (10 μg/20 g mice/*s.c.*, i.e., 1/6th of minimum lethal dose in *s.c.* route). Group 3, 4 and 5 animals were treated with ASVS (2 mg/20 g/*i.v.*), andrographolide (50 μg/20 g/*s.c.*) and andrographolide-AuNPs (50 μg/20 g/*s.c.*), respectively.

2.4. Snake Venom Preparation

The lyophilized *Daboia russellii russellii* venom (DRRV) was obtained from Irula Snake Catcher's Cooperative, Chennai, India, preserved in desiccators at 8 °C. It was dissolved in 0.9% saline and centrifuged at 3000 rpm for 10 min. The supernatant was used as venom and kept at 4 °C for further use. Venom concentration was expressed in terms of dry weight (mg/ml).

2.5. DRRV Toxicity Markers

The intravenous (*i.v.*) and subcutaneous (*s.c.*) lethal toxicity of DRRV was assessed by administrating different concentrations of venom in 0.2 ml 0.9% saline in Swiss albino male mice (20 ± 2 g). The neutralizing potency of andrographolide-AuNPs was assessed by *s.c.* injection of venom into mice followed immediately by the various doses of ASVS, andrographolide and andrographolide-AuNPs (*s.c.*). The minimum hemorrhagic dose (MHD) of DRRV was defined as the least amount of venom which, when injected intradermally (*i.d.*) into mice, resulting in a hemorrhagic lesion of 10 mm diameter after 24 h. Neutralization of the hemorrhagic activity was estimated after injecting 1 MHD of DRRV (*i.d.*) followed by various doses of ASVS, andrographolide and andrographolide-AuNPs (*s.c.*), and the hemorrhagic lesion was measured after 24 h. The minimum defibrinogenating dose (MDD) of venom was defined as the least amount of DRRV which, when injected (*i.v.*) into male albino mice, produced incoagulable blood 4 h later. Neutralization of the defibrinogenating activity was estimated after injecting 1 MDD of DRRV (*i.v.*) followed by various amounts of ASVS, andrographolide and andrographolide-AuNPs (*s.c.*), and the nature of blood was recorded after 4 h [11]. DRRV induced *in vitro* phospholipase A2 (PLA2) and minimum clotting dose of plasma (MCDP) was estimated [11].

2.6. Organ Toxicity Markers

Animals of group 2, 3, 4 and 5 were injected with DRRV (10 μg/*s.c.*/20 g mice, i.e., 1/6th of MLD in *s.c.* route), followed by treatment with ASVS (2 mg/20 g/*i.v.*), andrographolide (50 μg/20 g/*s.c.*) and andrographolide-AuNPs (50 μg/20 g/*s.c.*) in group 3, 4 and 5 animals, respectively. Blood from all the animals were collected after 18 h of DRRV induction, serum was prepared and aspartate aminotransaminase (AST), alanine aminotransaminase (ALT), γ-glutamyl transaminase (γGT), acid phosphatase (ACP), alkaline phosphatase (ALP), lactate dehydrogenase (LDH), creatinine phosphate, urea, creatinine, Ca^{2+}, phosphorous were assessed by using biochemical kits.

2.7. Paw Edema Induced by DRRV

Paw edema in mice was induced by DRRV and measured after Trebien and Calixto [34]. The minimum edema dose (MED) of DRRV was defined as the least amount of DRRV which, when injected in mouse paw, produced edema of 100% at 4 hours. Group 2, 3, 4 and 5 animals were injected with 2 μg DRRV (subplanter), followed by treatment with ASVS (2 mg/20 g/*i.v.*), andrographolide (50 μg/20 g/*s.c.*) and andrographolide-AuNPs (50 μg/20 g/*s.c.*) in group 3, 4 and 5 animals, respectively. Paw edema was measured using digital caliper (Mitutoyo, Japan).

2.8. *In Vivo* Inflammatory Markers

Animals of group 2, 3, 4 and 5 were injected with DRRV (10 μg/20 g mice/*s.c.*, i.e., 1/6th of MLD in *s.c.* route), followed by treatment with ASVS (2 mg/20 g/*i.v.*), andrographolide (50 μg/20 g/*s.c.*) and andrographolide-AuNPs (50 μg/20 g/*s.c.*) in group 3, 4 and 5 animals, respectively. Blood from all the animals were collected after 18 h of DRRV induction, serum was prepared and interleukin 17a, tumor necrosis factor α, interleukin 1β, interleukin 6, interleukin 10 assays were estimated by using enzyme linked immunosorbent assay (ELISA) kit (R&D Products, U.S.A.) and ELISA reader (Biotec, USA).

2.9. *In Vivo* Stress Markers

Animals of group 2, 3, 4 and 5 were injected with DRRV (10 μg/20 g mice/*s.c.*, i.e., 1/6th of MLD in *s.c.* route), followed by treatment with ASVS (2 mg/20 g/*i.v.*), andrographolide (50 μg/20 g/*s.c.*) and andrographolide-AuNPs (50 μg/20 g/*s.c.*) in group 3, 4 and 5 animals, respectively. Blood was collected after 18 h of DRRV induction, serum was prepared and reduced glutathione (expressed as μM/mg protein), superoxide dismutase (IU/mg protein) and lipid peroxidation (MDA/mg protein) were estimated from the serum [35–37]. Serum protein was estimated after Lowry et al. [38]. Blood (in presence of heparin as an anticoagulant) was centrifuged for 15 min at 3000 rpm and 1% aqueous solution of packed cell volume was used as red blood corpuscle (RBC) lysate. Using this lysate, catalase activity (μM/mg hemoglobin) was estimated [39].

2.10. Statistical Analysis

Statistical significance between two groups was done by one way analysis of variance (ANOVA) and $P < 0.05$ was considered as statistically significant. Values were expressed as mean $\pm$ standard error of mean ($n = 6$).

3. RESULTS

3.1. Formation and Characterization of Andrographolide-AuNPs

Pink colored andrographolide conjugated gold nanoparticle (andrographolide-AuNPs) was formed by adsorption method. The particle was visibly stable at room temperature (26 ± 2 °C) for 45 ± 5 days, incubator (37 ± 1 °C) for 45 ± 5 days and refrigerator (6 ± 1 °C) for 75 ± 4 days. Andrographolide-AuNPs had zeta potential of about −16.21 mV, indicating it as moderately stable. Maximum absorbance (λ_{max}) of andrographolide and andrographolide-AuNPs was found to be 420 nm and 540 nm, respectively. Andrographolide emit fluorescence when excited at its maximum absorbances. Andrographolide-AuNPs showed a quenching in fluorescence activity after excited at 420 nm. Hydrodynamic diameter of andrographolide-AuNPs was 30–50 nm with polydispersity index 0.412. X-ray diffraction (XRD) analysis indicated the presence of crystalline gold in andrographolide-AuNPs. The field emission scanning electron microscopy (FESEM) data of andrographolide-AuNPs showed that the particle size was 20–25 nm with nearly spherical shape (Fig. 1). Transmission electron microscopy of andrographolide-AuNPs revealed the size (20–50 nm) and shape (nearly hexagonal) of particles (Fig. 2).

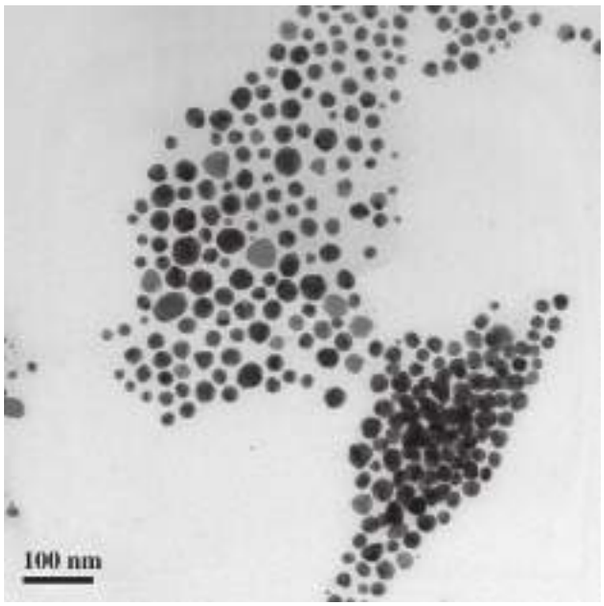

Figure 2. Transmission electron microscopy of andrographolide-AuNPs. The size of andrographolide-AuNPs was found to be 20–50 nm with nearly spherical in shape.

3.2. *Daboia russellii russellii* Venom (DRRV) Neutralization Studies

3.2.1. *Neutralization of DRRV Induced Minimum Lethal Dose*

Minimum lethal dose (MLD) of *Daboia russellii russellii* venom (DRRV) in intravenous (*i.v.*) route and subcutaneous (*s.c.*) route was found to be 5 μg/20 gm/*i.v.* and 60 μg/20 gm/*s.c.*, respectively in male albino mice. Anti snake venom serum (ASVS) showed 1 fold protection against DRRV induced MLD in *i.v.* and *s.c.* route. Andrographolide and andrographolide-AuNPs did not show protection against DRRV-induced lethality in male albino mice through *i.v.* and *s.c.* route (Table I).

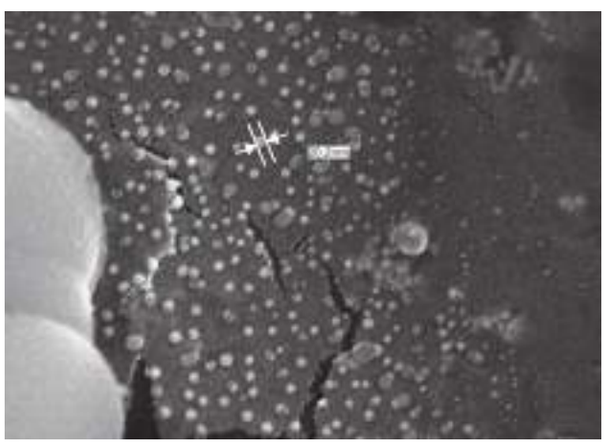

Figure 1. Field emission scanning electron microscopy (FESEM) of andrographolide-AuNPs. FESEM diameter of andrographolide-AuNPs was found to be 20–25 nm with nearly spherical shape.

3.2.2. *Neutralization of DRRV Induced Minimum Edema Dose*

In vivo minimum edema dose (MED) of DRRV was found to be 2 μg/20 gm/inter-planter in male albino mice. ASVS showed no protection against DRRV induced MED. Andrographolide-AuNPs offered 3 fold protection, as compared with andrographolide (1 fold protection). The edema induced by DRRV over a time period of 24 hrs was significantly neutralized by andrographolide-AuNPs as compared with andrographolide (Table I).

3.2.3. *Neutralization of DRRV Induced Minimum Hemorrhagic Dose*

In vivo minimum hemorrhagic dose (MHD) of DRRV was found to be 20 μg/20 gm/*i.d*/24 hrs in male albino mice. ASVS showed no protection against DRRV induced MHD. Andrographolide (50 μg) failed to offer any protection against DRRV induced hemorrhage, whereas andrographolide-AuNPs gave 1 fold protection against DRRV induced haemorrhagic lesion in male albino mice (Table I and Figs. 3(A–E)).

3.2.4. *Neutralization of DRRV Induced Minimum Defibrinogenating Dose*

Minimum defibrinating dose (MDD) of DRRV was found to be 3 μg/*i.v.* Treatment with ASVS and andrographolide offered no protection in DRRV induced defibrinogenating

Table I. *Daboia russellii russellii* venom (DRRV) neutralization by andrographolide-AuNPs in animal model. P = protection, NP = no protection.

DRRV neutralizing experiments	DRRV	DRRV + ASVS	DRRV + Andrographolide	DRRV + Andrographolide-AuNPs
Minimum lethal dose (MLD) (*i.v.*)	5 μg (1 MLD)	5 μg (1 fold) P 7.5 μg (1.5 fold) NP	5 μg (1 fold) NP	5 μg (1 fold) NP
Minimum lethal dose (MLD) (*s.c.*)	60 μg (1 MLD)	60 μg (1 fold) P 66 μg (1.1 fold) NP	60 μg (1 fold) NP	60 μg (1 fold) NP
Minimum edema dose (MED)	2 μg (1 MED)	2 μg (1 fold) NP	2 μg (1 fold) P	2 μg (1 fold) P 4 μg (2 fold) P 6 μg (3 fold) P 8 μg (4 fold) NP
Minimum hemorrhagic dose (MHD)	20 μg (1 MHD)	20 μg (1 fold) NP	20 μg (1 fold) NP	20 μg (1 fold) P 30 μg (1.5 fold) NP
Minimum defibrination dose (MDD)	3 μg (1 MDD)	3 μg (1 fold) NP	3 μg (1 fold) NP	3 μg (1 fold) P 4 μg (1.33) NP
Minimum clotting dose of plasma (MCDP)	1 μg (1 MCDP)	1 μg (1 fold) NP	1 μg (1 fold) P 1.5 μg (1.5 fold) NP	1 μg (1 fold) P 1.5 μg (1.5 fold) P 2 μg (2 fold) NP
PL A2	1 μg (1 unit)	1 μg (1 fold) NP	1 μg (1 fold) NP	1 μg (1 fold) P 1.5 μg (1.5 fold) NP

activity, whereas treatment with andrographolide-AuNPs offered 1 fold protection against DRRV induced defibrinogenating activity.

3.2.5. Neutralization of DRRV Phospholipase A2 Activity

In *in vitro* study, DRRV (1 μg) possessed 1 unit of phospholipase A2 (PLA2) activity. ASVS and andrographolide failed to neutralize DRRV induced PLA2 activity. Andrographolide-AuNPs offered 1 unit (1 μg) protection against DRRV induced PLA2 neutralization.

3.2.6. Neutralization of DRRV Induced Minimum Clotting Dose of Plasma

DRRV induced minimum clotting dose of plasma (MCDP) was found to be 1 μg. ASVS offered no protection against DRRV induced MCDP activity. Andrographolide offered 1 fold protection and andrographolide-AuNPs offered 1.5

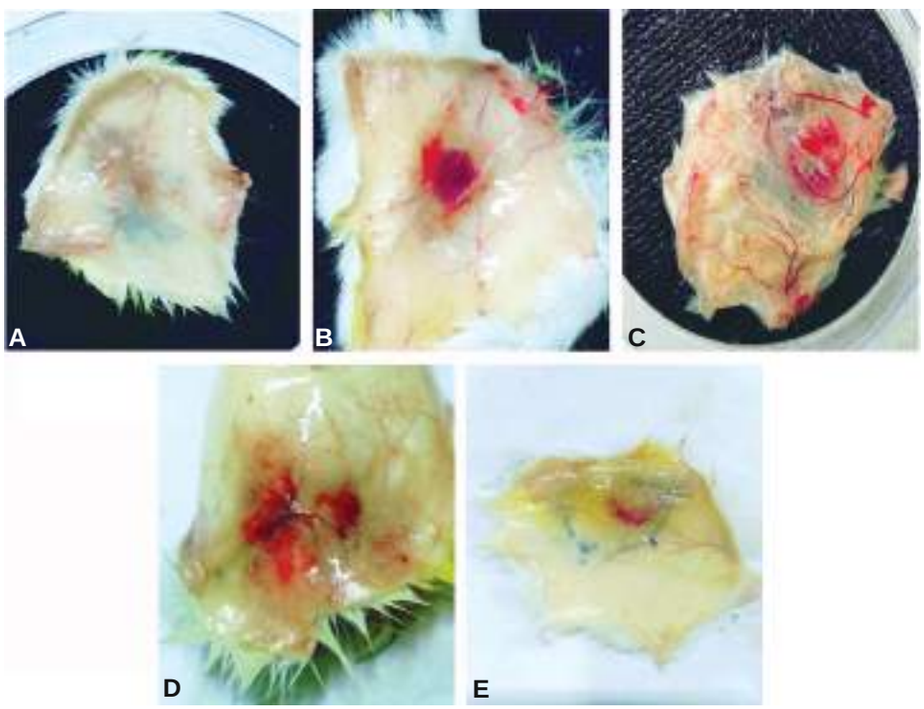

Figure 3. Protection of *Daboia russellii russellii* venom (DRRV) induced hemorrhage after treatment with andrographolide-AuNPs: (A) Sham control, (B) DRRV control, (C) ASVS treated (100 mg/kg), (D) andrographolide treated (50 mg/kg), (E) andrographolide-AuNPs treated (5 ml/kg).

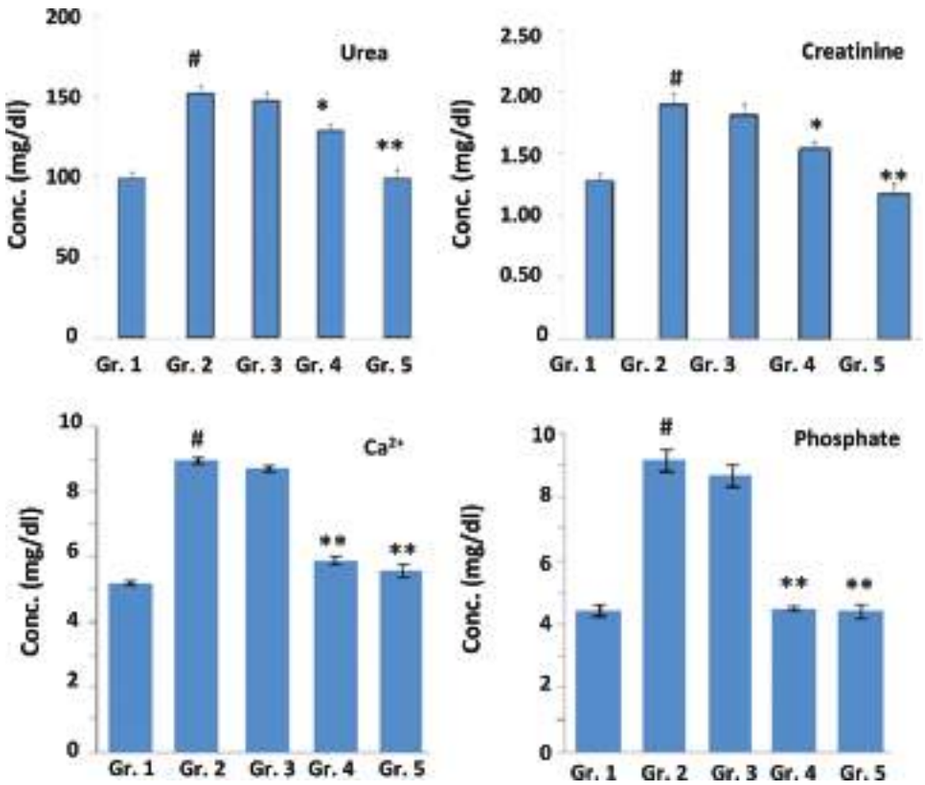

Figure 4. Effect of andrographolide-AuNPs in *Daboia russellii russellii* venom (DRRV) induced changes in nephrotoxicity markers in animal model. Significant change was observed in serum urea, creatinine, calcium and phosphate after treatment with andrographolide-AuNPs in DRRV-induced animals. $^{\#}P < 0.05$ when compared to group 1 animals, $^{*}P < 0.05$ when compared to group 2 animals; $^{**}P < 0.01$ when compared to group 2 animals. Values were expressed as mean ± SEM; Gr. 1-sham control, Gr. 2-DRRV control, Gr. 3-ASVS treated, Gr. 4-andrographolide treated, Gr. 5-andrographolide-AuNPs treated.

unit (1.5 μg) protection of DRRV induced MCDP activity (Table I).

3.2.7. Neutralization of DRRV Induced Organ Toxicity

There was significant increase in serum urea, creatinine, calcium and phosphate in group 2 DRRV control animals, when compared to group 1 sham control animals, showing DRRV-induced nephrotoxicity. There was no change in serum urea, creatinine, calcium and phosphate in group 3 ASVS treated animals when compared to group 2 DRRV control animals. Treatment with andrographolide in group 4 animals and andrographolide-AuNPs in group 5 animals caused significant decrease in serum urea, creatinine, calcium and phosphate level as compared with group 2 DRRV control animals (Fig. 4).

There was significant increase in serum aspartate aminotransaminase (AST), alanine aminotransaminase (ALT), γ-glutamyl transaminase (γGT), acid phosphatase (ACP) and alkaline phosphatase (ALP) in group 2 DRRV control animals, when compared to group 1 sham control animals, showed DRRV-induced hepatotoxicity. There was no change in serum AST, ALT, γGT, ACP and ALP in group 3 ASVS treated animals when compared to group 2 DRRV control animals. Treatment with andrographolide in group 4 animals and andrographolide-AuNPs in group 5 animals caused significant decrease in serum AST, ALT, γGT, ACP and ALP level as compared with group 2 DRRV control animals (Fig. 5).

There was significant increase in serum lactate dehydrogenase (LDH) in group 2 DRRV control animals, when compared to group 1 sham control animals, showing DRRV-induced myotoxicity. There was no change in serum LDH in group 3 ASVS treated animals when compared to group 2 DRRV control animals. Treatment with andrographolide in group 4 and andrographolide-AuNPs in group 5 animals caused significant decrease in serum LDH level as compared with group 2 venom control animals (Fig. 5).

3.2.8. Neutralization of DRRV Induced Inflammation

There was significant increase in serum proinflammatory cytokines (interleukin 17a, interleukin 1β, interleukin 6, tumor necrosis factor α), and decrease in serum anti-inflammatory cytokine (interleukin 10) in group 2 DRRV control animals, when compared to group 1 sham control animals, showing DRRV-induced inflammation. There was no change in serum proinflammatory cytokines and anti-inflammatory cytokine in group 3 ASVS treated

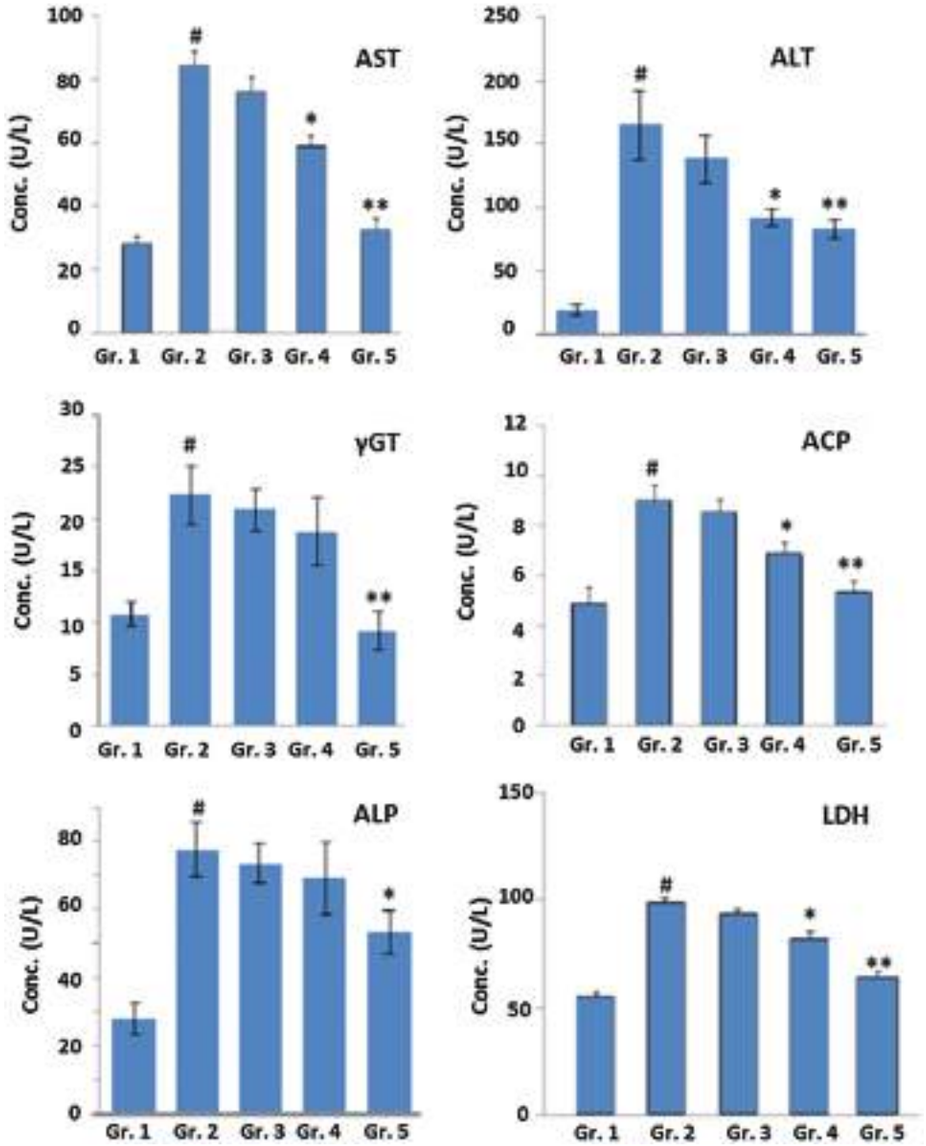

Figure 5. Effect of andrographolide-AuNPs in *Daboia russellii russellii* venom (DRRV) induced changes in hepatotoxicity and myotoxicity markers in animal model. Significant change was observed in serum AST, ALT, γGT, ACP, ALP and LDH after treatment with andrographolide-AuNPs in DRRV-induced animals. $^{\#}P < 0.05$ when compared to group 1 animals, $^{*}P < 0.05$ when compared to group 2 animals; $^{**}P < 0.01$ when compared to group 2 animals. Values were expressed as mean ± SEM; Gr. 1-sham control, Gr. 2-DRRV control, Gr. 3-ASVS treated, Gr. 4-andrographolide treated, Gr. 5-andrographolide-AuNPs treated.

animals when compared to group 2 DRRV control animals. Treatment with andrographolide in group 4 animals and andrographolide-AuNPs in group 5 animals caused significant decrease in serum IL 17a, IL 1β, TNF α, IL 6 and increase in serum IL 10 level as compared with group 2 DRRV control animals (Table II).

3.2.9. Neutralization of DRRV Induced Oxidative Stress

There was significant increase in prooxidant (lipid peroxidation) and decrease in serum anti-oxidant parameters (reduced glutathione, superoxide dismutase, catalase) in group 2 DRRV control animals, when compared to group 1 sham control animals, showing DRRV-induced oxidative stress in animal model. There was no change in antioxidants (reduced glutathione, superoxide dismutase, catalase) and prooxidation (lipid peroxidation) in group 3 ASVS treated animals when compared to group 2 DRRV control animals. Treatment with andrographolide in group 4 animals and andrographolide-AuNPs in group 5 animals caused significant decrease in lipid peroxidation and increase in reduced glutathione, superoxide dismutase, catalase as compared with group 2 DRRV control animals (Table II).

Table II. Effect of andrographolide-AuNPs in *Daboia russellii russellii* venom (DRRV) induced changes in inflammatory and oxidative stress markers in animal model. Significant decrease was observed in serum interleukin 17a, IL 1β, IL 6, TNF α and increase in serum interleukin 10 after treatment with andrographolide-AuNPs in DRRV-induced animals. Significant decrease in lipid peroxidation (LPO) and increase in reduced glutathione (GSH), superoxide dismutase (SOD), catalase was observed after treatment with andrographolide-AuNPs in DRRV-induced animals. $^{\#}P < 0.05$ when compared to group 1 animals, $^{*}P < 0.05$ when compared to group 2 animals; $^{**}P < 0.01$ when compared to group 2 animals. Values were expressed as mean ± SEM; Gr. 1-sham control, Gr. 2-DRRV control, Gr. 3-ASVS treated, Gr. 4-andrographolide treated, Gr. 5-andrographolide-AuNPs treated.

	Anti-inflammatory markers					Oxidative stress markers			
	IL 1β	TNF α	IL 6	IL 17a	IL 10	GSH (μM/mg protein)	SOD (IU/mg protein)	Catalase (μM/mg Hb)	LPO (MDA/mg pro)
Gr. 1	6.97 ± 0.64	160.98 ± 20.58	12.3 ± 1.65	18.98 ± 2.29	105.97 ± 11.54	157.32 ± 18.71	31.26 ± 3.48	42.29 ± 4.94	7.29 ± 1.04
Gr. 2	19.64 ± 2.98$^{\#}$	398.24 ± 48.97$^{\#}$	45.91 ± 5.21$^{\#}$	94.64 ± 10.32$^{\#}$	54.64 ± 6.89$^{\#}$	71.93 ± 8.91$^{\#}$	13.62 ± 2.55$^{\#}$	20.62 ± 3.55$^{\#}$	18.51 ± 2.35$^{\#}$
Gr. 3	18.21 ± 1.36	374.86 ± 42.73	43.61 ± 7.32	89.43 ± 7.09	51.68 ± 7.73	75.38 ± 6.98	15.42 ± 2.97	23.82 ± 4.64	17.57 ± 3.02
Gr. 4	18.98 ± 2.16	365.46 ± 35.24	39.94 ± 3.97	56.68 ± 5.09**	68.43 ± 8.87*	111.65 ± 15.62*	19.83 ± 3.98*	29.96 ± 3.64*	14.98 ± 1.92*
Gr. 5	10.21 ± 3.94**	294.87 ± 29.89*	26.61 ± 4.16**	49.97 ± 4.18**	81.59 ± 9.23*	141.78 ± 13.91**	26.51 ± 3.52**	38.71 ± 5.03**	10.35 ± 1.84**

4. DISCUSSIONS

In the recent times it has been observed that application of nanotechnology in snake venom research is coming up rapidly to solve the emerging issues of snake envenomation [12]. Use of gold nanoparticle in experimental biology and biomedical research is significant in (a) increased physical and chemical stability and high biocompatibility when compared to other metal nanoparticles, (b) possible fictionalization with bioactive organic molecules and (c) remarkable optical characteristics due to surface Plasmon resonance [40–42]. It has been established that conjugation of gold nanoparticle with herbal compound increase the efficacy of the herbal compound [7]. The present communication was an attempt to establish the anti-snake venom potential of andrographolide after conjugation with gold nanoparticle.

The physicochemical characterizations of andrographolide conjugated gold nanoparticle (andrographolide-AuNPs) were done to study its stability, shape, size and conjugation of the particle. Zeta potential, the potential difference between the dispersing liquid and the nanoparticle surfaces, determines the stability of the particle in the solution. In the study, andrographolide-AuNPs bear negative charges; higher negative charge increases the stability of the particle because there will be more repulsion force between the particles. Ultraviolet/visible-spectrum is the reflection of nanoparticle's shape, size, local refractive index and its interaction with solvent medium [43]. Andrographolide emits fluorescence when excited at its maximum absorbance, which was quenched after adsorption in nanoparticles, indicating the conjugation between herbal compound and the nanoparticle [44]. Dynamic light scattering of andrographolide-AuNPs measured the hydrodynamic diameter, surface distribution profile and fluctuation of scattered light intensity of nanoparticles in suspension [45]. Low polydispersity index confirmed the formation of monodispersive andrographolide-AuNPs. X-ray diffraction analysis indicated the presence of crystalline gold in andrographolide-AuNPs. The field emission scanning electron microscopy (FESEM) and transmission electron microscopy (TEM) of andrographolide-AuNPs also confirmed the size and shape of the particles. There was a difference between hydrodynamic diameter (obtained from dynamic light scattering of the particle) and TEM diameter, because hydrodynamic diameter measures the solvent and other solute molecules attached with the particle, whereas the TEM diameter measures the particle's actual diameter.

Daboia russellii russellii (commonly known as Russell's viper), mostly found in South-East Asia, Indian subcontinent and China causing a number of casualties. The lethality of *Daboia russellii russellii* venom (DRRV) is the result of venom induced pre-synaptic neurotoxicity, hemolysis, hemorrhage, vasodialation, rhabdomyolysis and cardiovascular shock [46]. DRRV contains high phospholipase content (around 70% of protein), which is mainly associated with high number of deaths [46, 47]. Zinc-dependent metalloproteinases in DRRV are hemorrhagic toxins which rupture the microvessels and causes profuse bleeding, local necrosis, edema and blisters [48–50]. Anti snake venom serum (ASVS) cannot protect against these local damages caused by viper venom [10]. Several herbal compounds showing interesting leads as an alternatives of ASVS and to protect against the venom induced local damages.

Andrographolide present in the aerial parts of *Andrographis paniculata* is a labdane diterpenoid with several medicinal properties. In earlier studies, it has been shown to inhibit viper venom induced metalloproteinases and protein kinase C [51, 52]. The present study has emphasized on the increase of the efficacy of andrographolide by conjugating with gold nanoparticle. Although andrographolide-AuNPs did not offer protection against viper venom induced mortality, but it neutralized venom induced defibrination, edema and hemorrhage. Study of DRRV induced *in vitro* minimum clotting dose of plasma (MCDP) and phospholipase A2 (PLA2) activity simulates the clinical symptoms of viper bite. Andrographolide-AuNPs offered significant protection in viper venom induced phospholipase A2 activity and minimum clotting dose of plasma. *Daboia russellii russellii* envenomation causes nephrotoxicity, hepatotoxicity

and myotoxicity in animal model [10]. Elevated levels of urea, creatinine, calcium, phosphate (for nephrotoxicity), AST, ALT, γGT, ACP and ALP (for hepatotoxicity) and LDH (for myotoxicity) were seen in viper venom control animals, which were significantly reduced after treatment with andrographolide-AuNPs indicating that andrographolide-AuNPs inhibited venom induced organ damages (kidney, liver, muscle) in animal models. *Daboia russellii russellii* activates inflammatory cascade in clinical cases. Increased proinflammatory cytokines (interleukins 1β, 6, 17a, 10, tumor necrosis factor α) and decreased anti-inflammatory cytokine (interleukin 10) were observed in DRRV control animals, which were significantly changed after treatment with andrographolide-AuNPs, indicating that andrographolide-AuNPs inhibited venom induced inflammatory response. Elevated pro-oxidant (lipid peroxidation) and decreased antioxidants (reduced glutathione, superoxide dismutase, catalase) were observed in viper envenomation [53]. Treatment with andrographolide-AuNPs decreased viper venom induced oxidative stress level in animal models. Although anti snake venom serum (ASVS) protected venom induced lethality, but it did not neutralized venom induced local damage, organ toxicity, inflammatory response and oxidative stress.

The molecular mechanism of neutralization of DRRV by andrographolide-AuNPs is difficult to understand at this stage, although, the *in vitro* and *in vivo* studies showed interesting data confirming the neutralization efficacy of andrographolide-AuNPs against viper venom induced local effects, organ toxicity, inflammatory response and oxidative stress. Andrographolide-AuNPs may act by (a) inhibition of viper venom PLA2 activity, (b) increased targeting of DRRV receptors by andrographolide-AuNPs, (c) decreased availability of DRRV proteins at the target site, (d) inhibition of pro-oxidant activity of DRRV, and thereby neutralizing the venom induced damages at the vascular bed, (e) interference with the cellular and molecular markers (proinflammatory markers, antioxidants etc.), and (f) increased cellular uptake of andrographolide-AuNPs.

5. CONCLUSION

The present study confirmed the successful conjugation of gold nanoparticle with andrographolide. The gold conjugation increased the neutralizing efficacy of andrographolide-AuNPs against viper venom-induced physiological changes (local damage, organ toxicity, inflammatory response and oxidative stress) in animal models. This study may provide clue for supportive therapy of andrographolide-AuNPs against snake bite and may be used along with ASVS treatment for better protection. It may open a new domain of biomedical research in developing anti snake venom antidote using nanotechnology and herbal resources.

Conflict of Interest

The authors declare no conflict of interest among them.

Acknowledgment: Indian Council of Medical Research, Government of India, India has been acknowledged for providing financial support and Research Associate-A fellowship to Dr. Sourav Ghosh (Ref. No. 58/32/2012-BMS). University Grants Commission, Government of India, New Delhi has been acknowledged for providing Emeritus fellowship to Professor Antony Gomes. Center for Research in Nanoscience and Nanotechnology, University of Calcutta, India has been acknowledged for instrumental facilities.

References and Notes

1. Cabuzu, D., Cirja, A., Puiu, R. and Grumezescu, A.M., **2015**. Biomedical applications of gold nanoparticles. *Current Topics in Medicinal Chemistry*, *15*(16), pp.1605–1613.
2. Zhang, X., **2015**. Gold nanoparticles: Recent advances in the biomedical applications. *Cell Biochemistry and Biophysics*, *72*(3), pp.771–775.
3. Connor, D.M. and Broome, A.M., **2018**. Gold nanoparticles for the delivery of cancer therapeutics. *Advances in Cancer Research, 139*, pp.163–184.
4. Ghosh, S., Sengupta, J., Saha, K., Dasgupta, S.C., Gomes, A. and Gomes, A., **2017**. Green synthesis of gold nanoparticle using hygrophila spinosa T. Anders leaf extract and evaluation of hematopoietic-antioxidant properties in swiss albino male mice. *Materials Focus*, *6*(1), pp.47–53.
5. Ghosh, S., Sengupta, J., Datta, P. and Gomes, A., **2014**. Hematopoietic and antioxidant activities of gold nanoparticles synthesized by aqueous extract of fenugreek (*Trigonella foenum-graecum*) seed. *Advanced Science, Engineering and Medicine*, *6*(5), pp.546–552.
6. Ghosh, S. and Gomes, A., **2016**. Hepatoprotective efficacy of gold nanoparticle synthesized by green method using *Trigonella foenum-graecum* seed extract. *Translational Medicine, 6*, pp.190–194.
7. Gomes, A., Ghosh, S., Sengupta, J., Datta, P. and Gomes, A., **2014**. Herbonanoceuticals: A new step towards herbal therapeutics. *Medicinal and Aromatic Plants*, *3*(162), pp.162–170.
8. Gomes, A., Sengupta, J., Datta, P., Ghosh, S. and Gomes, A., **2016**. Physiological interactions of nanoparticles in energy metabolism, immune function and their biosafety: A review. *Journal of Nanoscience and Nanotechnology*, *16*(1), pp.92–116.
9. Saha, K., Ghosh, S., Ghosh, S., Dasgupta, S.C. and Antony, G., **2015**. Neutralization of Naja kaouthia venom induced toxicity and stress response by Vitex negundo-gold nanoparticle (VN-GNP) in experimental animal model. *Journal of Toxins*, *2*, p.8.
10. Saha, K. and Gomes, A., **2017**. Russell's viper venom induced nephrotoxicity, myotoxicity, and hepatotoxicity—Neutralization with gold nanoparticle conjugated 2-hydroxy-4-methoxy benzoic acid *in vivo*. *Indian Journal of Experimental Biology, 55*(1), pp.7–14.
11. Gomes, A., Sengupta, J., Ghosh, S. and Gomes, A., **2016**. Application of gold nanoparticle conjugation with 2-hydroxy-4-methoxy benzoic acid (HMBA) from hemidesmus indicus root enhancing neutralization of snake (Viper) venom activity. *Journal of Nanoscience and Nanotechnology*, *16*(8), pp.8322–8329.
12. Gomes, A., Ghosh, S., Sengupta, J., Saha, K. and Gomes, A., **2018**. Nanotechnology in snake venom research—An overview. *Indian Journal of Experimental Biology*, 56(10), pp.707–715.
13. Ghosh, S. and Gomes, A., **2016**. Russell's viper (*Daboia russelli russelli*) venom toxicity neutralizing efficacy of curcumin-gold nanoparticle (C-GNP) in experimental animal model. *Journal of Toxins*, *3*(2), pp.6–11.

14. Karain, B.D., Lee, M.K.H. and Hayes, W.K., **2016**. C60 fullerenes as a novel treatment for poisoning and envenomation: A proof-of-concept study for snakebite. *Journal of Nanoscience and Nanotechnology*, *16*(7), pp.7764–7771.

15. Akbar, S., **2011**. *Andrographis paniculata*: A review of pharmacological activities and clinical effects. *Alternative Medicine Review*, *16*(1), pp.66–77.

16. Kabir, M.H., Hasan, N., Rahman, M.M., Rahman, M.A., Khan, J.A., Hoque, N.T., Bhuiyan, M.R.Q., Mou, S.M., Jahan, R. and Rahmatullah, M., **2014**. A survey of medicinal plants used by the Deb barma clan of the Tripura tribe of Moulvibazar district, Bangladesh. *Journal of Ethnobiology and Ethnomedicine*, *10*(1), pp.19–46.

17. Hossain, M., Urbi, Z., Sule, A. and Rahman, K.M., **2014**. *Andrographis paniculata* (Burm. f.) Wall. ex Nees: A review of ethnobotany, phytochemistry, and pharmacology. *The Scientific World Journal*, *2014*, p.274905.

18. Burkill, I.H., **1966**. *A Dictionary of the Economic Products of the Malay Peninsula*, 2nd edn., Kuala Lumpur, Malaysia, Ministry of Agriculture and Co-Operatives. Vol. 2.

19. Kumarapppan, C., Jaswanth, A. and Kumarasunderi, K., **2011**. Antihaemolytic and snake venom neutralizing effect of some Indian medicinal plants. *Asian Pacific journal of Tropical Medicine*, *4*(9), pp.743–747.

20. Premendran, S.J., Salwe, K.J., Pathak, S., Brahmane, R. and Manimekalai, K., **2011**. Anti-cobra venom activity of plant *Andrographis paniculata* and its comparison with polyvalent anti-snake venom. *Journal of Natural Science, Biology, and Medicine*, *2*(2), pp.198–204.

21. Hsieh, Y.L., Shibu, M.A., Lii, C.K., Viswanadha, V.P., Lin, Y.L., Lai, C.H., Chen, Y.F., Lin, K.H., Kuo, W.W. and Huang, C.Y., **2016**. *Andrographis paniculata* extract attenuates pathological cardiac hypertrophy and apoptosis in high-fat diet fed mice. *Journal of Ethnopharmacology*, *192*, pp.170–177.

22. Zhou, J., Zhang, S., Choon-Nam, O. and Shen, H.M., **2006**. Critical role of pro-apoptotic Bcl-2 family members in andrographolide-induced apoptosis in human cancer cells. *Biochemical Pharmacology*, *72*(2), pp.132–144.

23. Nanduri, S., Nyavanandi, V.K., Thunuguntla, S.S.R., Kasu, S., Pallerla, M.K., Ram, P.S., Rajagopal, S., Kumar, R.A., Ramanujam, R., Babu, J.M. and Vyas, K., **2004**. Synthesis and structure-activity relationships of andrographolide analogues as novel cytotoxic agents. *Bioorganic & Medicinal Chemistry Letters*, *14*(18), pp.4711–4717.

24. Rasool, U., Priya, S., Parveen, A., Sah, S.K. and Hemalatha, S., **2018**. Efficacy of *Andrographis paniculata* against extended spectrum β-lactamase (ESBL) producing *E. coli. BMC Complementary and Alternative Medicine*, *18*(1), pp.244–258.

25. Chen, H., Ma, Y.B., Huang, X.Y., Geng, C.A., Zhao, Y., Wang, L.J., Guo, R.H., Liang, W.J., Zhang, X.M. and Chen, J.J., **2014**. Synthesis, structure-activity relationships and biological evaluation of dehydroandrographolide and andrographolide derivatives as novel anti-hepatitis B virus agents. *Bioorganic & Medicinal Chemistry Letters*, *24*(10), pp.2353–2359.

26. Singh, D.P., Awasthi, H., Luqman, S., Singh, S. and Mani, D., **2015**. Hepatoprotective effect of a polyherbal extract containing *Andrographis paniculata*, Tinospora Cordifolia and Solanum Nigrum against paracetamol induced hepatotoxicity. *Pharmacognosy Magazine*, *11*(Suppl. 3), pp.375–379.

27. Niranjan Reddy, V.L., Malla Reddy, S., Ravikanth, V., Krishnaiah, P., Venkateshwar Goud, T., Rao, T.P., Siva Ram, T., Gonnade, R.G., Bhadbhade, M. and Venkateswarlu, Y., **2005**. A new bis-andrographolide ether from *Andrographis paniculata* nees and evaluation of anti-HIV activity. *Natural Product Research*, *19*(3), pp.223–230.

28. Borhanuddin, M., Shamsuzzoha, M. and Hussain, A.H., **1994**. Hypoglycaemic effects of *Andrographis paniculata* Nees on non-diabetic rabbits. *Bangladesh Medical Research Council Bulletin*, *20*(1), pp.24–26.

29. Chua, L.S., **2014**. Review on liver inflammation and antiinflammatory activity of *Andrographis paniculata* for hepatoprotection. *Phytotherapy Research*, *28*(11), pp.1589–1598.

30. Rahman, M.M., Ahmad, S.H., Mohamed, M.T.M. and Ab Rahman, M.Z., **2014**. Antimicrobial compounds from leaf extracts of Jatropha curcas, Psidium guajava, and *Andrographis paniculata*. *The Scientific World Journal*, *2014*, pp.1–8.

31. Govindarajan, M. and Sivakumar, R., **2012**. Adulticidal and repellent properties of indigenous plant extracts against Culex quinquefasciatus and Aedes aegypti (Diptera: Culicidae). *Parasitology Research*, *110*(5), pp.1607–1620.

32. Liang, E., Liu, X., Du, Z., Yang, R. and Zhao, Y., **2018**. Andrographolide ameliorates diabetic cardiomyopathy in mice by blockage of oxidative damage and NF-κB-mediated inflammation. *Oxidative Medicine and Cellular Longevity*, *2018*.

33. Sengupta, J., Datta, P., Patra, H., Dasgupta, A.K. and Gomes, A., **2013**. *In vivo* interaction of gold nanoparticles after acute and chronic exposures in experimental animal models. *Journal of Nanoscience and Nanotechnology*, *13*(3), pp.1660–1670.

34. Trebien, H.A. and Calixto, J.B., **1989**. Pharmacological evaluation of rat paw oedema induced by Bothrops jararaca venom. *Agents and Actions*, *26*(3–4), pp.292–300.

35. Ellman, G.L., **1959**. Tissue sulfhydryl groups. *Archives of Biochemistry and Biophysics*, *82*(1), pp.70–77.

36. Pryor, W.A., **1973**. Free radical reactions and their importance in biological systems. *Federation Proceedings, 32*, pp.1862–1869.

37. Buege, J.A. and Aust, S.D., **1978**. Microsomal lipid peroxidation. *Methods in Enzymology, 52*, pp.302–310.

38. Lowry, O.H., Rosebrough, N.J., Farr, A.L. and Randall, R.J., **1951**. Protein measurement with the Folin phenol reagent. *Journal of Biological Chemistry*, *193*(1), pp.265–275.

39. Beers, R.F. and Sizer, I.W., **1952**. A spectrophotometric method for measuring the breakdown of hydrogen peroxide by catalase. *Journal of Biological Chemistry*, *195*(1), pp.133–140.

40. Dykman, L.A. and Khlebtsov, N.G., **2011**. Gold nanoparticles in biology and medicine: Recent advances and prospects. *Acta Naturae* *3*(2) pp.34–55.

41. Zhao, Y. and Nalwa, H.S., eds., **2007**. *Nanotoxicology: Interactions of Nanomaterials with Biological Systems*, California, USA, American Scientific Publishers. Vol. 19.

42. Singh, S. and Nalwa, H.S., **2007**. Nanotechnology and health safety-toxicity and risk assessments of nanostructured materials on human health. *Journal of Nanoscience and Nanotechnology*, *7*(9), pp.3048–3070.

43. Aromal, S.A. and Philip, D., **2012**. Green synthesis of gold nanoparticles using *Trigonella foenum-graecum* and its size-dependent catalytic activity. *Spectrochimica Acta Part A: Molecular and Biomolecular Spectroscopy*, *97*, pp.1–5.

44. Joshi, P., Shewale, V., Pandey, R., Shanker, V., Hussain, S. and Karna, S.P., **2011**. Site specific interaction between ZnO nanoparticles and tryptophan: A first principles quantum mechanical study. *Physical Chemistry Chemical Physics*, *13*(2), pp.476–479.

45. Kaszuba, M., McKnight, D., Connah, M.T., McNeil-Watson, F.K. and Nobbmann, U., **2008**. Measuring sub nanometre sizes using dynamic light scattering. *Journal of Nanoparticle Research*, *10*(5), pp.823–829.

46. Warrell, D.A., **1989**. Snake venoms in science and clinical medicine 1. Russell's viper: Biology, venom and treatment of bites. *Transactions of the Royal Society of Tropical Medicine and Hygiene*, *83*(6), pp.732–740.

47. Jayanthi, G.P. and Gowda, T.V., **1988**. Geographical variation in India in the composition and lethal potency of Russell's viper (Vipera russelli) venom. *Toxicon*, *26*(3), pp.257–264.

48. Gutiérrez, J.M., Rucavado, A., Escalante, T. and Díaz, C., **2005**. Hemorrhage induced by snake venom metalloproteinases: Biochemical and biophysical mechanisms involved in microvessel damage. *Toxicon*, *45*(8), pp.997–1011.

49. Bjarnason, J.B. and Fox, J.W., **1994**. Hemorrhagic metalloproteinases from snake venoms. *Pharmacology & Therapeutics*, *62*(3), pp.325–372.

50. Markland, F.S., **1998**. Snake venoms and the hemostatic system. *Toxicon*, *36*(12), pp.1749–1800.

51. Luo, W., Liu, Y., Zhang, J., Luo, X., Lin, C. and Guo, J., **2013**. Andrographolide inhibits the activation of NF-κB and MMP-9 activity in H3255 lung cancer cells. *Experimental and Therapeutic Medicine*, *6*(3), pp.743–746.

52. Yen, T.L., Chen, R.J., Jayakumar, T., Lu, W.J., Hsieh, C.Y., Hsu, M.J., Yang, C.H., Chang, C.C., Lin, Y.K., Lin, K.H. and Sheu, J.R., **2016**. Andrographolide stimulates p38 mitogen-activated protein kinase-nuclear factor erythroid-2-related factor 2-heme oxygenase 1 signaling in primary cerebral endothelial cells for definite protection against ischemic stroke in rats. *Translational Research*, *170*, pp.57–72.

53. Sebastin Santhosh, M., Hemshekhar, M., Thushara, R.M., Devaraja, S., Kemparaju, K. and Girish, K.S., **2013**. Vipera russelli venom-induced oxidative stress and hematological alterations: Amelioration by crocin a dietary colorant. *Cell Biochemistry and Function*, *31*(1), pp.41–50.

Received: 2 November 2018. Accepted: 27 August 2019.

Visual and olfactory cues for mate recognition in male pumpkin beetle, Aulacophora foveicollis

Abhishek Mukherjee & Abhisek Makal

International Journal of Tropical Insect Science

e-ISSN 1742-7592

Int J Trop Insect Sci
DOI 10.1007/s42690-020-00262-0

Springer

International Journal of Tropical Insect Science
https://doi.org/10.1007/s42690-020-00262-0

ORIGINAL RESEARCH ARTICLE

Visual and olfactory cues for mate recognition in male pumpkin beetle, *Aulacophora foveicollis*

Abhishek Mukherjee [1] · Abhisek Makal [1]

Received: 7 February 2020 / Accepted: 14 September 2020

Abstract

Visual and olfactory mediated cues play a major role in mate selection in different groups of insects. This study aimed to observe if there is any role of mate color (under different wavelengths) and/or cuticular hydrocarbons in mate selection of *Aulacophora foveicollis*. In this study, visual cues and olfactory cues showed a vital role for male *A. foveicollis* to find mates. Males preferred (81%) orange (similar body colour) coloured glass model than white (52%) and black (49%) under the visible spectrum; whereas under the UV spectrum white coloured model was more preferred (77%) than orange (60%) and black (48%) coloured. In contrast, unresponsive males were very high though white coloured model was still preferred (36.67%) than orange (24.44%) or black (22.22%) coloured under IR spectrum. It was also observed that body surface waxes can play alone an olfactory cue for male mate selection (attraction was 67%) from short distance. Under the visual spectrum, when both visual and olfactory cues were presented, attraction of males toward all orange (93%), white (74%), and black (71%) coloured glass bead model increased. Even under UV and IR spectra attraction increased when body surface extract of female was applied on the glass models though the preference was more towards white coloured model than orange as previous. Male *A. foveicollis* showed less preference towards black colour. These works provide evidence that both visuals and olfactory cues can act separately as well as synergistically to find mates for male insects. These findings will be helpful for sustainable pest management program.

Keywords Red pumkin beetle · Visible spectrum · Cuticular hydrocarbons · Mate choice

Introduction

Aulacophora foveicollis Lucas (Coleoptera: Chrysomelidae) is a gregarious polyphagous pest of Cucurbitaceae (like pumpkin, bottle gourd, sponge gourd, etc) in India, Bangladesh, and Vietnam (Karmakar et al. 2016, 2017; Karmakar and Barik 2016; Khan et al. 2011; Rahaman and Prodhan 2007). Both adults and larvae of this pest cause damage to its host plants. Larvae pupate in the soil and before pupation (12–13 days) feed on young and healthy roots of the host plant. After completing the pupal stage (11–12 days), newly emerged adults rapaciously consume leaves, flowers and flower buds for 8–9 weeks which kills branches and shoots and reduces crop production (Mukherjee et al. 2017). Numbers of literature indicates that *A. foveicollis* showed attraction toward volatiles and colour cues from host like *Momordica cochinchinensis* and *Solena amplexicaulis* plants (Karmakar et al. 2016, 2017; Karmakar and Barik 2016) which established that as many other phytophagous insects, *A. foveicollis* also relies on olfactory and visual information to find host plants but stimuli which affect sexual recognition are still poorly understood.

Visual, acoustic, olfactory, gustatory, and tactile sensory signals play an important role in mate recognition of insects (Greenspan and Ferveur 2000). Colour vision is another essential cue (visual-based) for leaf beetle insects for mate selection and recognition (Piñero 2018). Further, for different wavelengths different behavior for the same colour object exists in leaf beetles (Kühnle and Müller 2011). The natural light of sun content both ultraviolate (UV) and infrared (IR) spectrum along with visible spectrum so, it is important to observe the role of colour under different wavelengths (UV, visible, and IR) for mate recognition of *A. foveicollis*. Pheromones, long-range volatile substances, influence mating behaviours over long distances of insects (Holdcraft et al. 2016; Rodstein et al. 2009; Roelofs and Rooney 2003) while

✉ Abhishek Mukherjee
2007.mukherjee@gmail.com

[1] Maulana Azad College, 8, Rafi Ahmed Kidwai Rd, Taltala, Kolkata, West Bengal 700013, India

cuticular hydrocarbons (CHCs) being low volatile substances present in the insect body surface act as close-range contact pheromone and play a vital role in mate identification in beetles (Barbour et al. 2007; Fukaya et al. 2000; Ferveur 2005; Ginzel and Hanks 2003; Howard and Blomquist 2005; Peterson et al. 2007; Sugeno et al. 2006; Xue et al. 2016). Pheromonal communication between male and female of the beetle, *A. foveicollis* has been demonstrated by Kumar and Nadarajan (2008) but the role of body surface waxes as cues (olfactory) in mate selection of this insect has not been evaluated. So it is of considerable interest whether *A. foveicollis* uses cuticular hydrocarbons for mate recognition after the arrival of the close-range of the opposite sex. Hence, overall the objectives of this study were to elucidate the role of colour cue under the different spectrum of wavelengths for mate identification and the role of CHCs in the sexual selection. It may contribute to sustainable pest management strategies by preparing baited traps (CHCs as a lure for the trap) with specific colour under specific wavelength which will be more efficient to manage this insect pest.

Materials and methods

Insects

Adults of *A. foveicollis* were collected from the bottle gourd [*Lagenaria siceraria* (Molina) Standl.] plants growing in the Crop Research Farm (CRF), The University of Burdwan, and maintained in 1-l glass jars, containing bottle gourd leaves covered with fine-mesh nylon nets at 27 ± 1 °C, 70 ± 5% r.h., and L12: D12 photoperiod in a 'BOD' incubator. To keep leaves in a natural condition, a moist piece of cotton was placed around cut ends of bottle gourd leaves followed by wrapping with aluminium foil to prevent moisture loss, and fresh leaves were given daily by replacing the previous one. For extraction of surface waxes from adults, each female/male (6 days old) was individually kept in a glass jar (2.5 cm diameter, 2 cm height), and placed at −20 °C for freeze kill. The number of insects used was 25 for both male and female.

For the behavioural studies, newly emerged males and females were separated from the stock culture (newly emerged males and females mate after 5–6 days of emergence). Two separate stock cultures (one for male and another for female) were maintained in separate glass jars (12 cm diameter, 10 cm high) and they were provided fresh bottle gourd leaves daily. During courtship behaviour, the male showed sudden alertness and vibrate antennae up and down as it approached the female. In case of a positive response from the female, the male bends their abdomen and exerts aedeagus for copulation. Males that showed abdominal bending behaviour towards females during courtship behaviour were selected for assay (Barbour et al. 2007; Fukaya et al. 2004).

Extraction of body surface waxes

To extract the body surface waxes, the freeze killed females were dipped in distilled ether (1.5 ml/female) for 1 min. Further, the extract was dried over anhydrous Na_2SO_4 and the solvent was removed under nitrogen flow. The concentrate was then dissolved in 2.5 ml methylene chloride (CH_2Cl_2) and stored below −20 °C for future use. For extraction and storage of male body surface waxes, same procedures were followed as female.

Glass-bead models

Three types of models were prepared by painting glass beads (7 mm length × 4 mm diameter): orange [Cadmium Orange (#150)], white [Titanium White (#432)] and black [Ivory Black (#244)] acrylic paints, respectively (Liquitex, Piscataway, NJ, USA) (Fig. 1). These were prepared at least 1 day before use (Fukaya et al. 2004; Barbour et al. 2007). For bioassays, the surfaces of the beads were added with 1 female or male equivalent (from here on "female equivalent" = FE and "male equivalent" = ME) body extract (0.227 mg/female; 0.1696 mg/male) in 100 μl of CH_2Cl_2 solution.

Y-tube olfactometer set-up

The behavioural responses of *A. foveicollis* were evaluated in a glass Y-shaped olfactometer (5 cm long stem and arms; 0.6 cm radius, and 45°Y-angle between two arms), similar to that used in our previous study (Mukherjee et al. 2017). Each arm of the olfactometer was connected to a glass-made microkit adapter fitted into a glass vial (3 cm long and 1 cm radius). One glass vial contained a piece (1 cm^2) of Whatman no. 41 filter paper of the same size moistened with one FE/ME surface extract (dissolved in 100 μl of methylene chloride), while the other glass vial contained a filter paper of the same size moistened with the same amount of the control solvent

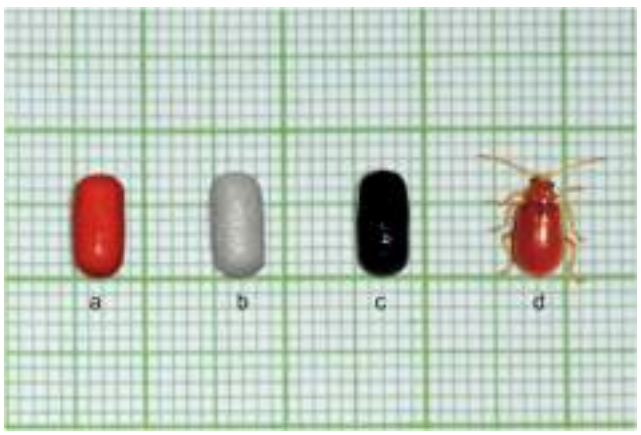

Fig. 1 Orange (**a**), white (**b**), and black (**c**) glass-bead models (size: 7 mm length, 4 mm diameter) and an adult *A. foveicollis* male (**d**)

(methylene chloride). The stem of the olfactometer was connected to a porous glass vial (3 cm long and 1 cm radius) in which test insects were released. Charcoal-filtered air was pushed into the system at 300 ml min^{-1}. All the connections between different parts of the set-up consisted of teflon tubing.

Y-tube olfactometer bioassays

The behavioural responses of adult male *A. foveicollis* (6 days old) towards one FE body surface waxes and adult female *A. foveicollis* (6 days old) towards one ME body surface waxes were evaluated to find attractiveness in both sexes respectively.

Wind tunnel bioassays

The wind tunnel consisted of a Plexiglas observation chamber (30 cm × 15 cm × 15 cm) with attachments for filtering, regulating the speed, channelling, and expelling of the air. Charcoal-filtered air was passed through the chamber at 0.10 m s^{-1} with air temperature 27 ± 1 °C and 70 ± 5% relative humidity. Sides and floor of the observation chamber were covered with black poster board to insulate insects in the chamber from external visual stimuli. The visible light source, i.e., CFL (Compact Fluorescent Lamp) [as a source of visual spectrum 400–700 nm], UV tube [as a source of Ultraviolet spectrum 100–280 nm], IR blub [as a source of Infrared spectrum 700–1000 nm] was mounted over the wind tunnel of the observation chamber. The light intensities were kept at a constant value of 1.68–2.00 μWcm^{-2} by using neutral density filters (Reisenman et al. 2000). A Plexiglas platform 7 cm above the floor of the chamber was used for the release of the test insect, whereas a Plexiglas platform 3.5 cm above the floor of the chamber was used for attachment of female body or glass models (Fig. 2). Six days old adult males were used in this study because males started to mate after the 5-6th day of emergence (Mukherjee et al. 2015). They were provisioned with only water for 12 h prior to use in olfactory assays. All tests with male insects were carried out between 10:00 and 17:00 h (Karmakar et al. 2017). A beetle was introduced into the wind tunnel, observed for 15 min, and then recaptured. The following bioassays were performed: (i) attraction of the males towards the dead female insect's body, with or without surface waxes, under different wavelengths of light, (ii) the effect of visual cue on the males towards different coloured models (orange, white, and black) under different wavelengths of lights, (iii) the olfactory responses of males towards female body extract in combination with different coloured glass models under different spectrum. Each bioassay was performed with 90 insects. Each insect was used once and discarded. After testing five insects, the Plexiglas observation chamber and release platform were cleaned with deionised water and the chamber was ventilated for 15 min before the next assay. The bioassays were conducted under UV or visible or IR light regimes, respectively.

i. **Behavioural response of males towards dead body of females with or without surface waxes**

A freeze killed female body with or without surface waxes was fixed horizontally 20 cm from the upwind end on the smaller Plexiglas platform (3.5 cm) in the observation chamber and the test insect was released 25 cm from the upwind end on the taller Plexiglas platform (7 cm) to observe the response of male *A. foveicollis*. All assays were done under UV, visible and IR spectra separately to observe the preferences for the same freeze killed female body (with or without surface waxes).

ii. **Behavioural response of males towards coloured glass-bead models (no-choice test)**

A single glass-bead coloured with any of the one (orange, white and black) was placed centrally 20 cm from the upwind end on the smaller Plexiglas platform (3.5 cm) in the observation chamber, and a male *A. foveicollis* was released 25 cm from the upwind end on the taller Plexiglas platform (7 cm) to observe the attraction of males toward the colored glass-beads. The entire choice assays were done under UV, visible and IR spectrum separately.

iii. **Behavioural response of males towards two different coloured glass-bead models (two-choice test)**

To determine which colour (i.e., orange, white, and black) was more attractive to males, two choice tests were conducted with two different colored glass beads (orange vs. white, orange vs. black and white vs. black) with a gap of 5 cm between them. Activities of male towards the colours were repeated separately under different wavelengths like UV, visible and IR.

iv. **Behavioural response of males towards glass-bead models with female body surface extract**

One FE body surface waxes was applied on the three types of colour beads (orange, white and black) separately. In this assay, a colored glass bead (either orange or white or black) was placed 20 cm from the upwind end on the smaller Plexiglas platform (3.5 cm) of the observation chamber and the test insect was released 25 cm from the upwind end on the taller Plexiglas platform (7 cm). The female body surface waxes were used as odour cue, in combination with coloured glass beads (visual cue). The tests were repeated separately under UV, visible and IR spectrum.

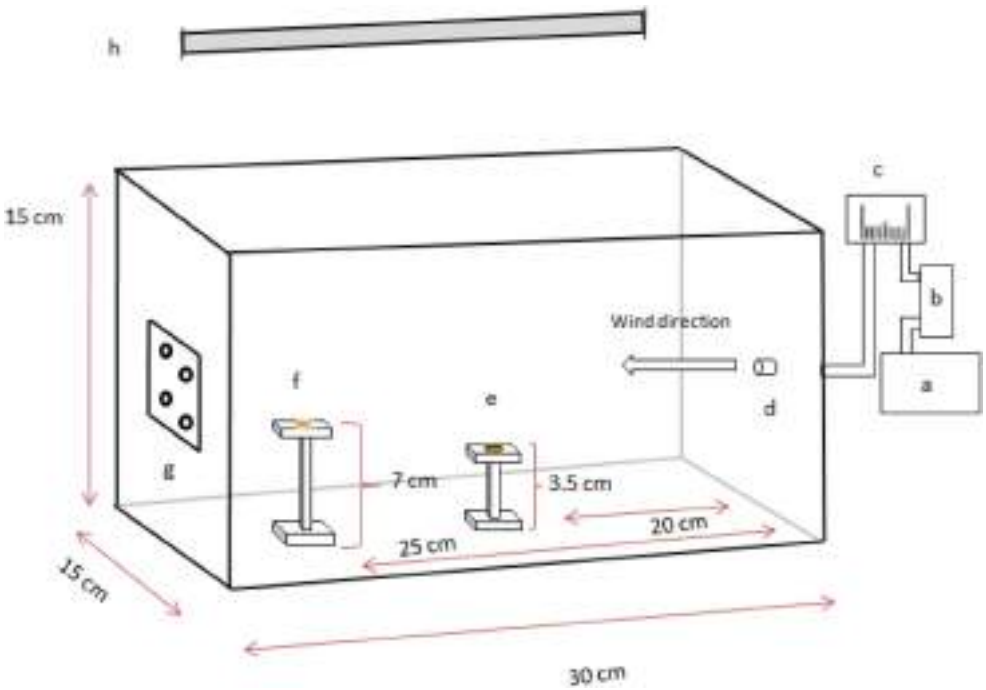

Fig. 2 Schematic diagram of the wind tunnel: (**a**) air pump, (**b**) air purifier, (**c**) flow meter to control the air flow, (**d**) air inlet, (**e**) smaller Plexiglas platform (3.5 cm) for attachment of female body or glass models, (**f**) taller Plexiglas platform (7 cm) for release of the test insect, (**g**) air expelling vent, (**h**) illumination set up

Statistical analysis

In olfactometer bioassays, response of test insects (male and female) were analyzed by a χ^2 test on the null hypothesis that the probability of scores for the test compound(s) or control solvent is equal to 50% (Koschier et al. 2000; Roy et al. 2012). Insects which did not respond by selecting any arm of the olfactometer were not included in the analyses.

For wind tunnel assays, one way ANOVA was done first between the preferences of male mate choice under a specific wavelength on different coloured models and again between the preferences for a specific coloured model under different wavelengths. Tukey's Honest Significant Difference test was conducted followed by ANOVA for comparing the variables with other in SPSS16 (SPSS Inc., IL, USA).

For two-choice test again χ^2 test was done on the same null hypothesis as previous that the probability of scores for the two test subjects (i.e. two models with two different colours) is equal to 50% (Koschier et al. 2000; Roy et al. 2012).

Results

Male response to female body surface extracts in Y-tube olfactometer bioassays

Virgin males showed attraction ($p = 0.0016$,df = 1) (67%) towards the odour from one FE surface extract compared to the control solvent (Fig. 3).

Female response to male body surface extracts in Y-tube olfactometer bioassays

Virgin females could not distinguish between one ME surface extract compared to the control solvent ($p = 0.834$, df = 1) (Fig. 3).

Male response to freshly killed female insect and surface waxes removed dead female insect in the wind tunnel

When the freshly killed female body was placed in the wind tunnel they showed (in ANOVA analysis) significant (F =

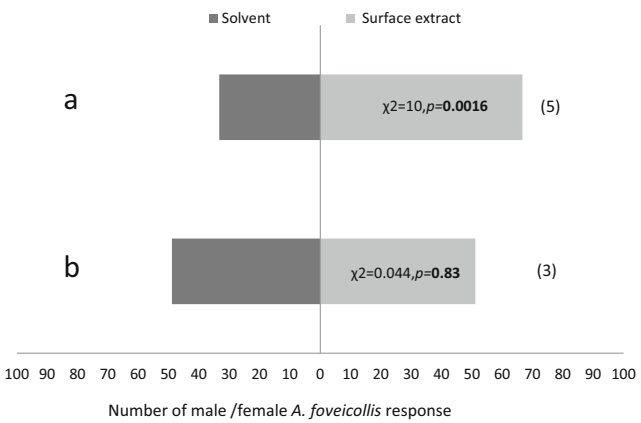

Fig. 3 **a** Behavioral responses of male *A. foveicollis* towards female body surface extract; **b** female *A. foveicollis* responses towards male body surface extract. Numbers in parentheses indicate the numbers of insects that did not respond to either treatment ($N = 90$ in each bioassay)

123.95; $P < 0.0001$) difference in preference while choosing under the different spectrum. The positive response was highest (97.78%) under the visible spectrum. The response towards the female dead body under UV and IR spectrum was 73.33% and 34.44% respectively. When the body surface waxes were removed from the freshly killed female body it also showed (in ANOVA analysis) a significant ($F = 58.27$; $P < 0.0001$) difference in response. Attraction under UV, visible and IR spectrum was 61.11%, 83.33%, and 26.67% respectively. Though the responses of male insects were lower towards surface waxes removed dead female body than the freshly killed female body, still preference was higher under visible spectrum than the other two spectrum (Table 1).

Male response to glass-bead model [no choice] under different spectrum [i.e. UV, visible and IR spectrum] in the wind tunnel

Specific wavelength vs. different colour response

Orange, white and black coloured glass model when separately placed under UV light, 60%, 77%, and 48% male showed attraction respectively. Greater preference under UV light was observed for the white coloured model compared to the orange and black. ANOVA analysis showed an overall difference ($F = 9.29$; $df = 2$; $P = 0.015$) in male's preferences among the orange, white and black coloured model under UV light (Table 2) but post hoc Tukey's test revealed that there was no significant difference in preference between orange and black ($p = 0.243$) as well as white and orange coloured model ($p = 0.105$) only difference in preference was present between the white and black coloured model ($p = 0.012$).

In the visible spectrum, the orange coloured model becomes the most preferred colour model by (81%) male insects whereas white and black coloured were preferred by only 52% and 49% male insects respectively. ANOVA analysis showed a significant difference ($F = 36.33$; $P < 0.0001$; $df = 2$) in the preference of male insects under visible wavelength for different coloured models (i.e. either orange or white or black coloured models). Post hoc Tukey's test revealed that under visible spectrum orange coloured (own body colour) model was most preferred because a significant difference in preference was present ($p = 0.001$) between orange and white as well as orange and black coloured model. Whereas the choice between white and black coloured model have no significant ($p = 0.716$) difference which indicates the preference under visible spectrum was same for the white and black coloured model (Table 2).

Under the IR spectrum preferences of male insects were slightly high for white glass model (37%) than the orange and black coloured model (24% and 22% respectively) though the numbers of unresponsive insects were higher in every case than UV and visible spectrum (Table 2). ANOVA between the response of male insects under IR wavelength and different coloured models showed a significant difference ($F = 7.35$; $P = 0.0241$; $df = 2$) among the choices (Table 2). When post hoc Tukey's test was conducted it showed that under IR light there was no difference ($p = 0.851$) in preference of male insect between the orange and black coloured model. No significant difference was also present in the male's selection between the white and orange coloured model ($p = 0.054$). While the choice between the white and black coloured model had a significant ($p = 0.028$) difference.

Specific colour vs. different wavelength response

When preference of male insects for a particular colour (i.e either orange or white or black) under different wavelengths (UV, visible, and IR) were compared by ANOVA it showed a significant difference in male responses for orange coloured glass bead model ($F = 117.24$; $df = 2$; $P < 0.0001$). Again preference for the white and black coloured model under different spectrum showed a significant difference ($F = 23.04$; $P = 0.002$ and $F = 17.96$; $P = 0.003$) in ANOVA (Table 3).

A significant difference ($p = 0.003$) was present when we compared the preferences of male insects through Tukey's test for the orange coloured model under UV and visible light. There was also a significant difference in choice for the same

Table 1 Behavioral responses of male *A. foveicollis* towards freshly killed female insect and waxes extracted dead female insect under different spectrum (no choice) in wind tunnel ($n = 90$ males tested in each bioassay)

Assays	Spectrum	% of insects responded	No. of unresponsive insects	df	F value	*P* value
Freshly killed female dead body	UV	73.33% (66*)	8	2	123.95	<0.0001
	Visible	97.77% (88)	5			
	IR	34.44% (31)	22			
Surface waxes extracted female dead body	UV	61.11% (55)	12	2	58.27	<0.0001
	Visible	83.33% (75)	9			
	IR	26.67% (24)	27			

*In the bracket the digits designate the actual number of male insects showed positive response

Table 2 Behavioral responses of male *A. foveicollis* under each spectrum [i.e. UV/visible/IR spectrum] to specific coloured glass bead models (no choice) added with or without *A. foveicollis* female insect surface extract in a wind tunnel (n = 90 males tested in each bioassay)

Assays	Extract present	Spectrum	Colour of model	% of insects responded	No. of unresponsive insects	df	F value	P Value
Glass model	N	UV	Orange	60% (54*)	9	2	9.29	0.015
			White	76.67% (69)	5			
			Black	47.78% (43)	11			
	N	Visible	Orange	81.11% (73)	4	2	36.33	<0.0001
			White	52.22% (47)	4			
			Black	48.89% (44)	7			
	N	IR	Orange	24.44% (22)	27	2	7.35	0.024
			White	36.67% (33)	22			
			Black	22.22% (20)	30			
Glass model	Y	UV	Orange	71.11% (64)	7	2	7.038	0.027
			White	85.56% (77)	5			
			Black	67.78% (61)	9			
	Y	Visible	Orange	93.33% (84)	8	2	17.45	0.003
			White	74.44% (67)	10			
			Black	71.11% (64)	12			
	Y	IR	Orange	31.11% (28)	26	2	8.615	0.017
			White	40% (36)	22			
			Black	26.67% (24)	25			

*In the bracket the digits designate the actual number of male insects showed positive response

orange coloured model under UV light and IR as well as visible light and IR ($p < 0.0001$ in both cases). Hence, the orange coloured model was most attracted by male insects under visible light than UV and IR light.

Further when we tested white coloured model under different wavelengths it showed that male insects has more ($p = 0.025$) attraction towards white model under UV light than visible light. Insects also had more ($p = 0.002$) attraction towards white model under UV than IR spectrum but no significant ($p = 0.130$) difference of choice was observed towards the white model under visible spectrum and IR light i.e. choice of white glass model under visible light and IR both had less preference than UV.

Table 3 Behavioral responses of male *A. foveicollis* to specific coloured (orange/white/black) glass-bead models [no choice] under different spectrum [i.e. UV, visible and IR spectrum] added with or without *A. foveicollis* female insect surface extract in a wind tunnel (n = 90 males tested in each bioassay)

Assays	Extract present	Colour of model	Spectrum	% of insects responded	No. unresponsive insects	df	F value	P value
Glass model	N	Orange	UV	60% (54*)	9	2	117.24	<0.0001
			Visible	81.11% (73)	4			
			IR	24.44% (22)	27			
	N	White	UV	76.67% (69)	5	2	17.96	0.003
			Visible	52.22% (47)	4			
			IR	36.67% (33)	22			
	N	Black	UV	47.78% (43)	11	2	23.04	0.002
			Visible	48.89% (44)	7			
			IR	22.22% (20)	30			
Glass model	Y	Orange	UV	71.11% (64)	7	2	92.923	<0.0001
			Visible	93.33% (84)	8			
			IR	31.11% (28)	26			
	Y	White	UV	85.56% (77)	5	2	80	<0.0001
			Visible	74.44% (67)	10			
			IR	40% (36)	22			
	Y	Black	UV	67.78% (61)	9	2	97.563	<0.0001
			Visible	71.11% (64)	7			
			IR	26.67% (24)	34			

*In the bracket the digits designate the actual number of male insects showed positive response

Again preference for black coloured model was tested under different spectrum it showed no significant differences in preference under UV and visible light ($p = 0.966$) but it showed a significant difference when we compare responses under UV and IR light ($p = 0.003$) as well as visible light with the IR light ($p = 0.002$).

Male response to glass-bead model with female body surface extract [no choice] under different spectrum [i.e. UV, visible and IR sepectrum] in the wind tunnel

Specific wavelength vs. different coloured model added with female body surface extract

Orange, white, and black coloured glass-bead models when added with one FE body surface extract, under UV light, the preferences of male insects were 71%, 86%, and 68% respectively. A significant difference ($F = 7.038$;$df = 2$; $P = 0.027$) was observed in ANOVA analysis in male insect's preference among orange, white and black coloured model under UV light (Table 2). It means that adding surface waxes increases the overall attraction for all coloured models but the sequence of preference for colours remains the same under UV light as previous. Post hoc Tukey's test, under UV light, reveals that male's preference for the orange coloured and black coloured glass model (surface waxes added) had no difference ($p = 0.969$), i.e. both have same responsiveness. While preference between the white and orange coloured models, both added with surface waxes extract, had a significant difference ($p = 0.047$), i.e. white was more preferred than orange coloured model. A significant difference ($p = 0.035$) was also present in the attraction between the white and black coloured models (both added with surface waxes extract).

Under visible spectrum, preference of male insects' for the orange coloured model added with one FE surface extract was 93% whereas the white and black coloured models were only 74% and 71% respectively. ANOVA analysis showed, under the visible spectrum, male insects' preferences for the orange, white and black coloured models added with surface waxes had a significant difference ($F = 17.45$; $P = 0.003$;$df = 2$) (Table 2). Post hoc Tukey's test showed a significant difference in male insects preference between the orange and black coloured model (both added with one FE surface extract) ($p = 0.004$) and also between the orange and white coloured model (both added with one FE surface extract) ($p = 0.008$) whereas preference between the black coloured model and white coloured model (both added with one FE surface extract) did not show any significant difference statistically ($p = 0.705$).

Under IR added with surface extract, preference of male insects' were 31%, 40%, and 27% for the orange, white and black coloured model respectively. ANOVA among the choices of the orange, white, and black coloured model (added with one FE surface extract) in IR spectrum showed a significant ($F = 8.615$, $df = 2$, $P = 0.017$) difference (Table 2). Again the Tukey's test elucidated that preference for male insects between one FE surface waxes added orange and black coloured models ($p = 0.417$), as well as orange and white models ($p = 0.77$), had no significant differences. But male insects' choice for the black and white coloured model (added with one FE surface waxes) was significant ($p = 0.015$).

Specific colouered model added with female body surface extract vs. different wavelength

Again when male insects' attraction for the orange coloured glass bead model (added with one FE surface waxes) were compared (by ANOVA analysis) for different spectrum (i.e either under UV or visible or IR spectrum) it showed a significant ($F = 92.923$; $df = 2$; $P < 0.0001$) difference in response (Table 3).

When we compare (by Tukey's test) the orange coloured model under UV and visible spectrum a significant difference ($p = 0.007$) was observed because insects were more attracted towards orange coloured model under the visible spectrum than UV. A significant difference was also present in choice for the same orange coloured model under the UV and IR spectrum as well as the visible and IR spectrum ($p < 0.0001$ in both cases).

While separate ANOVA, revealed significant differences ($F = 97.563$; $P < 0.0001$ and $F = 80$; $P < 0.0001$) under different wavelengths (i.e under UV, visible, and IR spectrum separately) for both white and black coloured models (added with one FE surface extract) (Table 3).

Again when we compared the response of male insects towards the white coloured model (added with one FE surface extract) Tukey's test showed no significant difference ($p = 0.056$) in male insects preference between UV and visible light response. While comparing the responses of male insects under the IR and visible spectrum and under the UV and IR spectrum for the same white coloured model (one FE surface waxes added) a significant difference ($p < 0.0001$ in both cases) was observed (Table 3).

When the black coloured model was compared (in Tukey's test) for UV and visible spectrum it showed no significant ($p = 0.950$) difference in response but a significant difference was present between UV and IR spectrum as well as visible and IR spectrum ($p < 0.0001$ in both case) (Table 3).

Male response towards two different coloured glass-bead models [two-choice] under different spectrum [i.e. UV, visible and IR spectrum] in the wind tunnel

In chi-square test, under UV spectrum white coloured model was preferred (66.67%) significantly ($\chi^2 = 10$, $df = 1$, $p = 0.00156$) more than the orange coloured (33.33%) model.

But under visible spectrum the preference shifted toward orange coloured glass model (73.33%) significantly ($\chi^2 = 19.6$, df = 1, $p < 0.0001$) than white coloured model (26.67%).Under IR spectrum again white was more preferred colour (62.22%) than orange colour (37.78%) and significant level was $\chi^2 = 5.38$, df = 1, $p < 0.02037$ (Fig. 4).

In the two choice test between white and black coloured model under UV spectrum male insect preferred white (73.33%) than black coloured model (26.67%) and a significant difference ($\chi^2 = 19.6$, df = 1, $p < 0.0001$) was also present in chi-square test. In visible spectrum white was also preferred (72.22%) than black coloured (27.78%) and the significant difference was $\chi^2 = 17.78$, df = 1, $p < 0.0001$. Under IR spectrum white coloured model was again preferred (62.22%) than black coloured model (37.78%) ($\chi^2 = 5.38$, df = 1, $p < 0.02037$) (Fig. 5).

Again in two choice test between orange and black coloured model, orange was more preferred than black by male insects in every wavelength i.e. UV (67.78%), visible (82.22%), and IR (62.22%) spectrum. Chi-square analysis also showed significant difference for each wavelength (UV, visible, and IR) separately $\chi^2 = 11.37$ df = 1, $p < 0.00074$; $\chi^2 = 37.37$ df = 1, $p < 0.00002$; and $\chi^2 = 5.38$ df = 1, $p < 0.02037$ between orange and black coloured model (Fig. 6).

Discussion

Insects can efficiently employ multiple cues to recognize the mature conspecifics of opposite sex (Candolin 2003). In many species of insects, visual cues play an important role for host recognition as well as mate selection (Hausmann et al. 2004; Lu et al. 2007; Stenberg and Ericson 2007; Szentesi et al. 2002). In a previous study, it was observed that *A. foveicollis* females employ visual cues to discriminate between white and white-yellow artificial flowers (Karmakar et al. 2016), but till date no report is available on the role of visual cue in mate selection by *A. foveicollis* males. In this study, we observed that *A. foveicollis* males could distinguish between three clours: orange (their body colour), white (reflect and scatter all the visible wavelengths of light) and black (the total absorption of visible light) under visible spectrum, and males showed preference significantly towards the orange coloured glass model than the white and black coloured glass models. A significant preference towards the orange coloured glass model by *A. foveicollis* males also provide evidence that a single visual cue is sufficient to locate mate (Kühnle and Müller 2011; Stenberg and Ericson 2007). As the natural body colour of *A. foveicollis* male is orange thus the preference for its own body colour, indicating that visual cues help to locate mates by males in the crop field (Fukaya et al. 2004; Szentesi et al. 2002). The surface waxes extracted female dead body and the orange glass-bead model induced the same behavioural responses suggested the importance of visual cue in mate selection by males (Fukaya et al. 2004). The current research provides an evidence that preference by males were reduced towards both orange coloured model and surface waxes extracted female dead body under UV light, whereas white coloured glass model was the most preferred under the same UV spectrum. Many insects could perceive the UV light as a unique color (Koshitaka et al. 2008), and its reflectance in white substrate could influence the preference (Shimoda and Honda 2013). In IR spectrum, the white coloured model was the most preferred, but the numbers of unresponsive male insects were very high and also the overall preference towards all coloured models were much lower than the other two spectrums, which may be due to their restricted activities in the IR spectrum, i.e., IR spectrum may not elicit a good chemical response in photoreceptor pigments (Otálora-Luna and Dickens 2011). Thus, this study suggested that male *A. foveicollis* can discriminate between

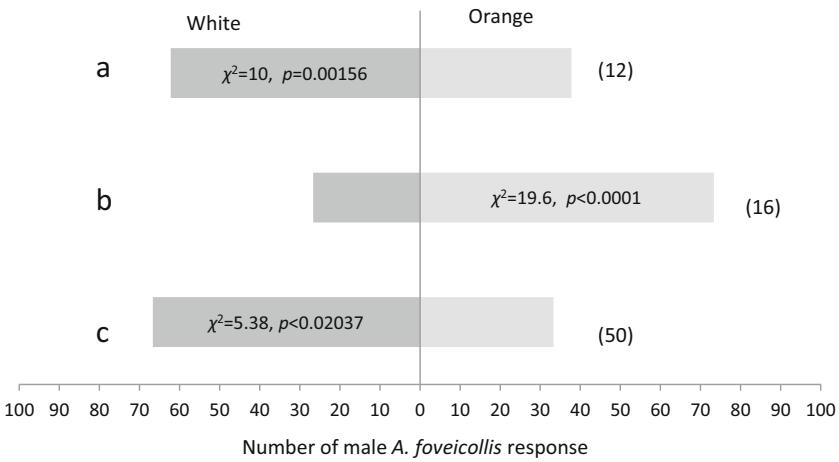

Fig. 4 Behavioral responses of *A. foveicollis* males [two choice test] to white vs orange coloured glass-bead models under different wavelengths [i.e. a = UV spectrum, b = visible spectrum, c = IR spectrum] in a wind tunnel. Numbers in brackets are the number of insects that did not respond to either treatment (N = 90 in each bioassay)

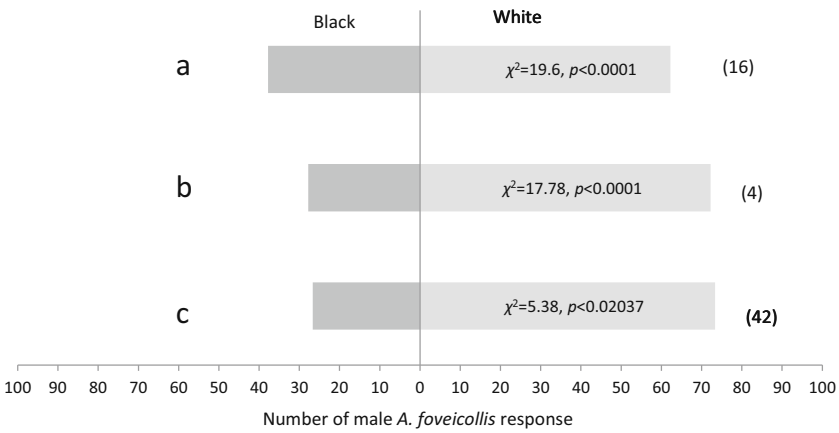

Fig. 5 Behavioral responses of male *A. foveicollis* [two choice test] to black vs white coloured glass-bead models different wavelengths [i.e. a = UV spectrum, b = visible spectrum, c = IR spectrum] in a wind tunnel. Numbers in brackets are the number of insects that did not respond to either treatment (N = 90 in each bioassay)

the conspecific colour and other two colours (white and black) under visible spectrum, though the different spectrums of light can change its preference (under UV spectrum) or overall activity (under IR spectrum) (Otálora-Luna and Dickens 2011).

In natural environment, where different colour combinations are available, only visual cues are not sufficient to recognize mates by an insect. They usually rely on more than one cue to find its mate (Candolin 2003). Kumar and Nadarajan (2008) demonstrated that *A. foveicollis* females emit volatile pheromones, which could attract the male towards them but the role of surface waxes has not been observed till now. This study revealed that visual cues along with olfactory cues from surface waxes play a vital role in male mate recognition. The Y-tube assays showed that one FE surface waxes was sufficient to induce short-range olfactory cues by a male to find it's mate, but the females did not show attraction towards one ME surface waxes. There are large numbers of evidences in insect species indicating the active role of surface waxes as short-range olfactory cues by males to recognize females for mating recognition (Peterson et al. 2007; Thomas and Simmons 2010; Zhang et al. 2014; Xue et al. 2016) our result also akin with them. Attraction of *A. foveicollis* males towards freshly killed female insect (i.e. surface waxes unaltered dead body) compared to dewaxed female insect, and female surface waxes added in glass bead models of different colours compared to without surface waxes added coloured glass bead models provides evidence that surface waxes as olfactory cue together with the visual cues play a vital role for attraction of the males. A number of literatures indicated synergistic effects between olfactory and visual cues for attraction of insects (Fukaya et al. 2004; Karmakar et al. 2017; Piñero 2018; Zhou et al. 2011).

In conclusion, this work clearly represents that both visual and olfactory cues have a significant role in mate choice by the male pumpkin beetle, *A.foveicollis.* A combination of short-range (5 cm) olfactory cue and visual stimuli acted synergistically on males to locate females in the natural context. It was

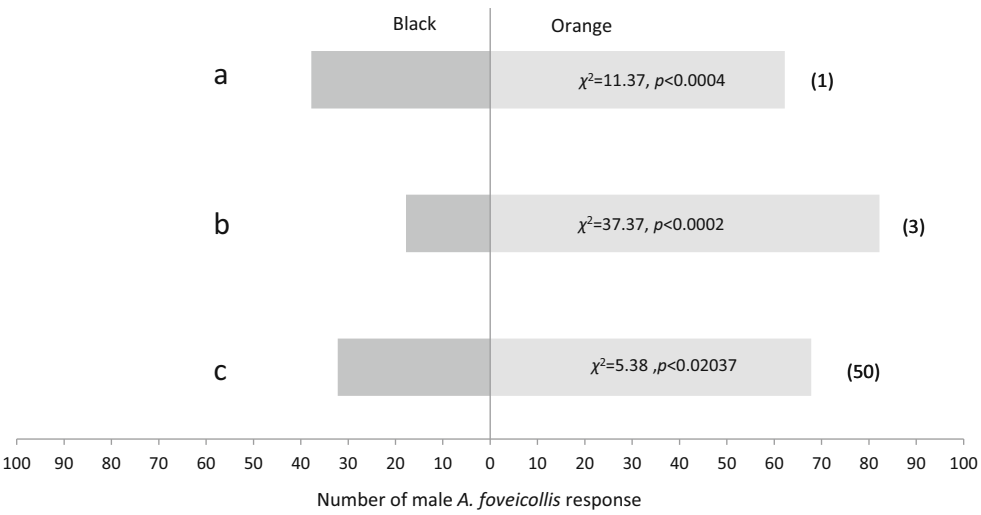

Fig. 6 Behavioral responses of *A. foveicollis* males [two choice test] towards black vs orange coloured glass-bead models under different wavelengths [i.e. a = UV spectrum, b = visible spectrum, c = IR spectrum] in a wind tunnel. Numbers in brackets are the number of insects that did not respond to either treatment (N = 90 in each bioassay)

also suggested that the behavioral responses of males change in UV and IR spectrum compared to visible spectrum. All this information can be helpful in behavioural manipulation methods of pest-management. Future investigations on the behavioral responses of *A. foveicollis* males to the cues in the field condition should be a topic for future research.

Acknowledgements We are grateful to Prof. Anandamay Barik for helpful suggestions during this work. We are very much thankful to Dr. Poorani Janakiraman, National Bureau of Agriculturally Important Insects (formerly PDBC), Karnataka, India for identifying the insect. We are also thankful to Prof. Subir Chandra Dasgupta, HOD department of Zoology of Mualna Azad College for providing us the departmental facilities. DBT star college scheme for providing different instrumental facilities to complete the work.

Compliance with ethical standards

Conflict of interest The authors declare that they have no conflict of interest.

References

Barbour JD, Lacey ES, Hanks LM (2007) Cuticular hydrocarbons mediate mate recognition in a species of longhorned beetle (Coleoptera: Cerambycidae) of the primitive subfamily Prioninae. Ann Entomol Soc Am 100:333–338

Candolin U (2003) The use of multiple cues in mate choice. Biol Rev 78: 575–595

Ferveur JF (2005) Cuticular hydrocarbons: their evolution and roles in Drosophila pheromonal communication. Behav Genet 35:279–295

Fukaya M, Akino T, Yasuda T, Wakamura S, Satoda S, Senda S (2000) Hydrocarbon components in contact sex pheromone of the white-spotted longicorn beetle, *Anoplophora malasiaca* (Thomson) (Coleoptera: Cerambycidae) and pheromonal activity of synthetic hydrocarbons. Entomol Sci 3:211–218

Fukaya M, Akino T, Yasuda T, Yasui H, Wakamura S (2004) Visual and olfactory cues for mate orientation behaviour in male white-spotted longicorn beetle, *Anoplophora malasiaca*. Entomol Exp Appl 111: 111–115

Ginzel MD, Hanks LM (2003) Contact pheromones as mate recognition cues of four species of longhorned beetles (Coleoptera: Cerambycidae). J Insect Behav 16:181–187

Greenspan RJ, Ferveur JF (2000) Courtship in Drosophila. Annu Rev Genet 34:205–232

Hausmann C, Samietz J, Dorn S (2004) Visual orientation of overwintered *Anthonomus pomorum* (Coleoptera: Curculionidae). Environ Entomol 33:1410–1415

Holdcraft R, Rodriguez-Saona C, Stelinski LL (2016) Pheromone autodetection: evidence and implications. Insects 7:17

Howard RW, Blomquist GJ (2005) Ecological, behavioral, and biochemical aspects of insect hydrocarbons. Annu Rev Entomol 50:371–393

Karmakar A, Barik A (2016) *Solena amplexicaulis* (Cucurbitaceae) flower surface wax influencing attraction of a generalist insect herbivore, *Aulacophora foveicollis* (Coleoptera: Chrysomelidae). Int J Trop Insect Sc 36:70–81

Karmakar A, Malik U, Barik A (2016) Effects of leaf epicuticular wax compounds from *Solena amplexicaulis* (lam.) Gandhi on olfactory responses of a generalist insect herbivore. Allelopathy J 37:253–272

Karmakar A, Mitra S, Barik A (2017) Systemically released volatiles from *Solena amplexicaulis* plant leaves with color cues influencing attraction of a generalist insect herbivore. Int J Pest Manage 64:210–220

Khan MMH, Alam MZ, Rahaman MM (2011) Host preference of red pumpkin beetle in a choice test under net case condition. Bangladesh J Zool 39:231–234

Koschier EH, Kogel WJD, Visser J (2000) Assessing the attractiveness of volatile plant compounds to western flower thrips *Frankliniella occidentalis*. J Chem Ecol 26:2643–2655

Koshitaka H, Kinoshita M, Vorobyev M, Arikawa K (2008) Tetrachromacy in a butterfly that has eight varieties of spectral receptors. Proc R Soc Lond B 275:947–954

Kühnle A, Müller C (2011) Relevance of visual and olfactory cues for host location in the mustard leaf beetle *Phaedon cochleariae*. hysiol. Entomol 36:68–76

Kumar SK, Nadarajan L (2008) Evidence of female–produced sex pheromone in red pumpkin beetle, *Aulacophora foveicollis* Lucas (Coleoptera: Chrysomelidae). Curr Sci 94:1369–1371

Mukherjee A, Sarkar N, Barik A (2015) *Momordica cochinchinensis* (Cucurbitaceae) leaf volatiles: semiochemicals for host location by the insect pest, *Aulacophora foveicollis* (Coleoptera: Chrysomelidae). Chemoecology 25:93–104

Mukherjee A, Karmakar A, Barik A (2017) Bionomics of *Aulacophora foveicollis* (Coleoptera: Chrysomelidae) by feeding on *Momordica cochinchinensis*. Proc Zool Soc 70:81–87

Lu W, Wang Q, Tian M Y, He X Z, Zeng X L , Zhong Y X (2007) Mate location and recognition in *Glenea cantor* (Fabr.) (Coleoptera: Cerambycidae: Lamiinae): Roles of host plant health, female sex pheromone, and vision. Environ Entomol 36:864–870

Otálora-Luna F, Dickens JC (2011) Spectral preference and temporal modulation of photic orientation by Colorado potato beetles on a servosphere. Entomol Exp Appl 138:93–103

Peterson MA, Dobler S, Larson EL, Juarez D, Schlarbaum T, Monsen KJ, Francke W (2007) Profiles of cuticular hydrocarbons mediate male mate choice and sexual isolation between hybridizing Chrysochus (Coleoptera: Chrysomelidae). Chemoecology 17:87–96

Piñero JC (2018) A comparative assessment of the response of two species of cucumber beetles (Coleoptera: Chrysomelidae) to visual and olfactory cues and prospects for mass trapping. J Econ 111:1439–1445

Rahaman MA, Prodhan MDH (2007) Effects of net barrier and synthetic pesticides on red pumpkin beetle and yield of cucumber. Int J Sustain Crop Prod 2:30–34

Reisenman CE, Lorenzo-FigueirasA NL, Giurfa M, Lazzari CR (2000) Interaction of visual and olfactory cues in the aggregation behaviour of the haematophagous bug *Triato mainfestans*. J Comp Physiol 186:961–968

Rodstein J, Mc Elfresh JS, Barbour JD, Ray AM, Hanks LM, Millar JG (2009) Identification and synthesis of a female-produced sex pheromone for the cerambycid beetle *Prionus californicus*. J Chem Ecol 35:590–600

Roelofs WL, Rooney AP (2003) Molecular genetics and evolution of pheromone biosynthesis in Lepidoptera. Proc Natl Acad Sci U S A 100:9179–9184

Roy N, Laskar S, Barik A (2012) The attractiveness of odorous esterified fatty acids to the potential biocontrol agent, Alticacyanea. J Asia-Pacific Entomol 15:277–282

Shimoda M, Honda K (2013) Insect reactions to light and its applications to pest management. Appl Entomol Zool 48:413–421

Stenberg JA, Ericson L (2007) Visual cues override olfactory cues in the host-finding process of the monophagous leaf beetle *Altica engstroemi*. Entomol Exp Appl 125:81–88

Sugeno W, Hori M, Matsuda K (2006) Identification of the contact sex pheromone of *Gastrophysa atrocyanea* (Coleoptera: Chrysomelidae). Appl Entomol Zool 41:269–276

Szentesi A, Weber DC, Jermy T (2002) Role of visual stimuli in host and mate location of the Colorado potato beetle. Entomol Exp Appl 105: 141–152

Thomas ML, Simmons LW (2010) Cuticular hydrocarbons influence female attractiveness to males in the Australian field cricket, *Teleogryllus oceanicus*. J Evol Biol 23:707–714

Xue HJ, Zhang B, Segraves KA, Wei JN, Nie RE, Song KQ, Liu J, Li WZ, Yang XK (2016) Contact cuticular hydrocarbons act as a mating cue to discriminate intraspecific variation in *Altica* flea beetles. Anim Behav 111:217–224

Zhang B, Xue HJ, Song KQ, Liu J, Li WZ, Nie RE, Yang XK (2014) Male mate recognition via cuticular hydrocarbons facilitates sexual isolation between sympatric leaf beetle sister species. J Insect Physiol 70:15–21

Zhou ZS, Guo JY, Guo W, Wan FH (2011) Synergistic effects of olfactory and tactile cues in short range mate finding of *Ophraella communa*. Entomol Exp Appl 138: 48–54

Role of Artificial Intelligence in 21st Century Cancer Research: A Review

[1]Arnab Kar, [2]Susanta Roy Karmakar, [3]Subir Chandra Dasgupta, [4]Sujit Kumar Bhowal*
[1]Post Graduate student of Zoology, [2,4]Assistant Professor of Zoology, [3]Professor of Zoology
[1, 2, 3, 4]Department of Zoology,
Maulana Azad College, Kolkata- 700013, India

Abstract: From the last century scientists from all over the globe have researched tirelessly to defeat the deadly disease, Cancer. In the past few years Artificial Intelligence left a satisfactory impression in some fields of medical science. Nowadays, Artificial Intelligence have fascinating role in cancer detection, molecular nature of cancer, which varies patient to patient, high resolution medical imaging, genomic profiling, dose detection during chemo- and radiotherapy, calculation of survival rate etc. Machine learning, especially deep learning, has the ability to discover malignancies and decision making capacity, which helps in drug design. Technical development of computer science, technologies, statistics continuously improve the accuracy of such analysis which is far better than traditional analysis. Recent development of algorithms and Deep Neural Networks help in cancer prognosis and diagnosis. The problem arising in research also discussed here. However, we are hopeful that in the near future we will be able to modify this system to diagnose cancer as early as possible and treat cancer in the most severe stage; to make it the most popular strategy in cancer treatment.

Index Terms **- Algorithm; Artificial Intelligence; Cancer; Deep learning; Deep Neural Network; Dose detection; Machine learning.**

I. INTRODUCTION:

Cancer after its discovery diverts our maximum attention towards it due to its high fatality rate and complex treatment procedure. According to the World Health Organization (WHO), the global cancer burden is estimated to have risen to 18.1 million new cases and 9.6 million deaths in 2018. One in 5 men and one in 6 women worldwide develop cancer during their lifetime, and one in 8 men and one in 11 women die from the disease (*WHO, 2018)*. Cancer has some unique property such as it can avoid therapies due to its drug resistant property; it interacts with its micro environment and maintains a cancer stem cell niche which is very much difficult to destroy. For this reason cancer relapses within some days after treatment stopped. Another problem associated with cancer is that it is very much difficult to detect a cancer at the early stage of growing. Following this complexity, researchers are now trying hard to develop strategies that are hard to be avoided by cancer.

Artificial intelligence (AI) was first coined by John McCarty (Fig.1) in a conference at Dartmouth College. This new technology, which originated from extensive interlinking between engineering, computer science and other applied sciences, is developing main fields of applied research with technology transfer in robotics, natural language processing, machine learning, computer vision etc. (*Coccia, 2019)*. Development of Metal Oxide Semiconductor and very large scale integration helped to build Artificial Neural Network in around 1980s and improve machine learning efficiency. Around the 1970s a system called MYCIN developed which has a significant role in medical applications. In 2010, IBM (International Business Machines) introduced a supercomputer called WATSON that helps in cancer detection and treatment recommendation like a virtual oncologist. Moreover, there are several AI systems developed for this structure.

Actually, AI analyzes a huge amount of data that cannot be perceived by the human brain, and makes decisions based on its previous experiences. The bigger no. of data makes more accurate decisions. It is also used for non-invasive cancer detection with high accuracy in melanoma, cervical cancer, uterine cancer, breast cancer. The basic work of AI is done by Artificial Neural Network (ANN) which acts like a biological neural network; it performs as a nonlinear data analysis tool where complex relationships between input and output are modelled. ANN is the foundation of machine learning (ML) which is a type of AI, not explicitly programmed to perform a specific task used to construct predictive algorithm models that learn logical patterns from mass historical data so as to predict the survival rate of a patient. ML has been used extensively for improving prognosis. The more data an ML model

is exposed to, the better it performs over time (*Huang, et al.,* 2019).

Deep learning (DL) which is a subset of ML (Fig.2) has attracted more attention in the last few years. DL uses ANN to design an algorithm from a large amount of input data like the human brain. DL often makes decisions based on Medical imagery like CT scan, Magnetic Resonance Imaging (MRI) etc. AI also gained huge popularity in non-invasive cancer detection and advanced multi drug systems in recent days. There is a huge prospect of artificial intelligence combined with nanotechnology which makes a major breakthrough in cancer research.

II. TYPE OF MACHINES:

Machine Learning (ML) algorithm is the important tool which is used in nearly all AI applications in cancer research at first the machine is learnt by huge amounts of input data (Fig.3). Machine learning has 2 types:-

2.1 Supervised Learning

Supervised learning is used to train ML algorithms with a labelled dataset of inputs and outputs. An algorithm makes itself familiar with general rules that map input to output. Supervised ML algorithms can learn patterns hidden in inputted data for categorical outputs (classification) and continuous data (regression).

2.2 Unsupervised Learning

Unsupervised ML algorithms use unlabeled data, with an attempt to discover any structure in the input data. Usually Unsupervised ML algorithms help to simplify (dimensionality reduction) or organize (clustering) data.

Usually, in cancer prediction and prognosis ML algorithm uses supervised learning. However, this supervised learning acts as classifiers that classify on the basis of conditional probabilities (*Wishart et al., 2006*). There are some major types of conditional algorithms, such as:-

1) Artificial neural networks (ANN – *Rummelhart et al.,1986*).
2) Genetic algorithms (GA – *Holland, 1975*).
3) Decision trees (DT – *Quinlan, 1986*).
4) Linear discriminant analysis (LDA) methods.
5) k-nearest neighbor algorithms

III. Artificial Intelligence in Cancer Prognosis Prediction:

One of the major obstacles that clinicians face in cancer prevention is that cancer gone unnoticed in most cases because they have nothing but their work experience for diagnosis of cancer and in numerous cases patients die due to treatment stress. So, in recent years with the development of modern AI technologies and machine algorithm prognosis, prediction of a specific cancer has become more accurate (Fig.4).

3.1 In Brain Cancer:

Brain malignancies predicted by an AI method MIRSPSO (mutual information and rough set of particle swarm optimization) which uses Support Vector Machine (SVM) algorithm and Random Forest (RF) algorithm separately. Both of these algorithms make predictions based on learned patterns (inputs). When examined in 700 brain cancer patients this method predicted with 88.5% accuracy i.e. far better than conventional statistical methods (*Zhao et al.,2019).*

3.2 In Oral Cancer:

Oral squamous cell carcinoma is a challenging problem in third world countries. Prognosis of this disease can successfully be done using AI technologies. In a study (*Zain et al., 2013*) uses a combination of ANFIS (Adaptive neuro- fuzzy inference system), artificial neural network, support vector machine, logistic regression to predict death rate after a particular treatment. Clinicopathologic variables from the OCRCC database and genomic variables from Immunohistochemistry (IHC) staining are inputted into the algorithmic model. Three features viz. drink, invasion and *p63* achieved the best accuracy (accuracy= 93.81%; AUC= 0.90) for prognosis of the oral cancer.

In another study (*Rajpoot et. al., 2019*) developed a digital marker using an abundance of tumor infiltrating lymphocyte (Fig.5) biomarkers as prognostic indicator. five state-of-the-art convolutional neural network models

ResNet50, DenseNet, Inception, Xception and MobileNet acts as classifier and the total no. of disease free survival predicted using Kaplan-Meier (KM) curves and Cox hazard analyses by conducting univariate and multivariate analysis of digital, clinical, and pathological parameters (Fig.6).

3.3 In Breast Cancer:

There are several studies conducted by several researchers to utilize AI in predictive prognosis of breast cancer. Most of the research concentrated on the use of Deep Neural Network (DNN) to analyze multidimensional data. (*Ching et al., 2018)* developed a new ANN framework known as Cox-net (a neural network extension of the Cox regression model) to predict patient survivability from high throughput transcriptomics data. Cox-net digs out extensive biological information, at both the gene levels and cellular pathway, by analyzing features represented in the hidden layer nodes in Cox-net.

Chi et al., 2007 designed MDNNMD (multimodal DNN by integrating multi-dimensional data) for the prognosis of breast cancer (Fig.7). The design of the method's architecture and the fusion of multi- dimensional data are the novelties of this system and make this system fruitful. The results of the comprehensive performance evaluation reflect that this proposed method outperformed all the other prediction methods using single dimensional data.

3.4 In Prostrate Cancer:

Urologists are able to develop AI technology based on DNN algorithms to monitor prostate cancer. For an independent test dataset three criteria of a malignant tissue i.e. its presence, extent, and Gleason grade (used to determine aggressiveness of prostate cancer) (Fig.8) were predicted by the DNN. *Strom et al., 2020* developed this algorithm when digitized 6682 slides from needle core biopsies from 976 randomly selected participants aged 50–69 in the Swedish prospective and population-based STHLM3 diagnostic study and another 271 from 93 men from outside the study. The captured images were used to train deep neural networks to analyze prostate biopsies.

Whole slide images were classified through a segmentation algorithm based on Laplacian filtering to identify the region corresponding to tissue sections. Two convolutional DNN ensembles (each consisting of 30 inception V3 models) were used which were pre-trained on ImageNet with classification layers adapted to expectable outcome.

3.5 In Cervical Cancer:

The National Cancer Institute developed a ML algorithm to predict cervical cancer. In normal, Visual Inspection after Application (VIA) of acetic acid has been done to visualize precancerous and cancerous cells in the cervix. Sometimes in very complicated stages cervical cytology (Pap tests) and colposcopy have been done. The deep learning algorithm Faster R- CNN (Faster Region based convolutional neural network) was used and the machine was trained by images collected by cervicography from a population-based longitudinal cohort of 9406 women, all of whom ages 18–94 years in Guanacaste, Costa Rica *(Schiffman et. al., 2019).* The patients were subdivided into two groups (Fig.9). In one group (cases) more severe patients CIN2+ and CIN2 were kept, in another group patients with <CIN2 were kept. For training set images from 189 images from cases and 555 images from control fed to the machine to design algorithm. Therefore validation test last images taken from women during follow up used; 82 from cases and 242 from control. Lastly for screening test at first images used from 85 women in the case group and 8,174 from the control group. The ML algorithm complete the screening with higher accuracy (area under the curve [AUC] = 0.91, 95% confidence interval [CI] = 0.89 to 0.93) than original cervigram interpretation (AUC = 0.69, 95% CI = 0.63 to 0.74; P <.001) or conventional cytology(AUC = 0.71, 95% CI = 0.65 to 0.77; P<.001).

3.5 In Gastric Cancer:

ANN has been shown to be a more powerful statistical tool for predicting the survival rate of gastric cancer like all other cancer prediction system patients compared to the Cox proportional hazard regression model. *Oh et al., 2018* used a survival recurrent network (SRN) to predict survival rate, and the results corresponded closely with actual survival. The American Joint Committee on Cancer (AJCC) also certified this system as a powerful tool to make predictions for gastric cancer. SRN model provides an individualized prediction based on numerous factors rather than only tumor factors followed by TNM staging in traditional models; basically, patient grouping is not necessary in SRN technique. *Biglarian et al., 2011,* analyzed 436 registered gastric cancer patients who had had surgery between 2002 and 2007 at the Taleghani Hospital, Tehran (Iran), to predict the survival time using Cox proportional hazard and ANN techniques. Moreover, the Cox regression analysis also revealed that the survival rates significantly associated with the patient's age at the time of diagnosis, high-risk behaviors like extent of wall penetration, distant metastasis, and tumor stage. Actually, using these features the system makes almost true

predictions which are 83.1%accurate.

3.6 In Lung Cancer:

In most of the cases it is very difficult to understand the survivability of lung cancer patient after treatment. *Lynch et al., 2017* used a supervised learning procedure to SEER (Surveillance, Epidemiology, and End Results) program database to classify lung cancer patients in terms of survival. The database uses different algorithms including linear regression, Decision Trees, Gradient Boosting Machines (GBM), Support Vector Machines (SVM), and a custom ensemble. For this study, researchers chose linear regression, Decision Trees, ensemble learning algorithms, Random Forest and Generalized Boosting Machines as logic-based methods, Support Vector Machine (SVM) using a polynomial kernel function as a non-probabilistic method; and at the final stage of prediction, custom ensemble method used a weighting function to sum the prediction of each of the five individual models. The final result showed that the GBM algorithm is the best ML procedure to perform the task.

IV. ARTIFICIAL INTELLIGENCE IN CANCER DIAGNOSIS AND IMAGING:

Due to the limited ability of the human brain to analyse large amounts of data AI models are used to make cancer diagnosis more accurate. Clinicians are very much dependent on their work experience and personal knowledge to diagnose cancer but in AI technology Integrative processing and extraction can allow more accurate disease diagnosis due to the efficiency and effectiveness of learning and training large samples. Different AI setups are able to state the molecular nature and the treatment sensitivity of a tumour.

Deep Convolutional Neural Network (DNCC) used to diagnose thyroid cancer; and shows high sensitivity and increased specificity compared to radiologists. DNCC has diagnosed the tumour from sonographic images taken during clinical trials *(Li ei al., 2019).*

Orringer et al., 2020 studied about the efficiency of AI technique in intraoperative brain tumour diagnosis. Actually, in the traditional way H-E staining of processed tissue was done which is time and labour consuming. DNCC aided technique can complete diagnosis within 3 minutes and replace traditional methods which took 40 minutes. To develop ML algorithms the machine was trained with 2.5 million Stimulated Raman Histology (SRH) images. They repeated the same method multiple times to every common type of brain tumour and got an overall success (Fig.10).

Prior to AI, dermatologists depend only on biopsy results to confirm melanoma. But use of CNN helps a lot to diagnose melanoma through noninvasive ways. *Uhlmann et al., 2018* have studied to train CNN, validate and test the DL algorithm for the diagnostic classification of dermoscopic images of lesions of melanocytic origin. The researchers use Google's Inception v4 CNN architecture and train the machine with 300 images test set (comprises 20% melanoma image and 80% benign tumor image). Main outcome measures were sensitivity, specificity and diagnostic classification. The efficiency of the machine was compared with the knowledge of 58 international dermatologists.

In another study *Phillip et al., 2019* studied to examine the accuracy of artificial intelligence neural network DERM (Deep Ensemble for Recognition of Melanoma) to detect malignant melanoma from dermoscopic images of pigmented skin lesions (Fig.11) and to show how this outperforms doctors' ability of detection assessed by meta-analysis. Particularly those deep learning techniques which identify and assess features of pigmented lesions that are associated with malignant melanoma used to develop DERM. The novelty of deep learning is that it can learn and auto-determines features which are associated with malignant melanoma directly from the data; unlike earlier machine learning methods which learn features pre-determined by researchers. The algorithm was experienced and accepts a dataset of archived dermoscopic images of skin lesions, using 10- fold cross-validation. This preliminary analysis demonstrates the ability of an AI-based system i.e. DERM algorithm to learn features of a skin lesion that are associated with malignant melanoma, which can then be applied to the identification of malignant melanoma (Fig.12)

In *Qiu et al., 2017* employed an AI system known as to develop and test computer-aided diagnosis (CAD) scheme of mammograms (Fig.13) for classifying between malignant and benign masses. An image dataset involving 560 regions of interest (ROIs) extracted from digital mammograms was used. In the algorithm setup an 8 layer deep learning network consists of 3 pairs of convolution- max-pooling layers for automatic feature extraction and a multiple layer perceptron (MLP) classifier which help in feature categorization were implied to each ROI to process the DL.

To improve the feature robustness each convolutional layer is connected with a max pooling layer. The output comes from the sixth layer mix totally connected with a MLP classifier which then generates a classification score to prognosticate the likelihood of malignancy of a particular ROI. Again, a four-fold cross validation method was applied to train and test this deep learning network for better accuracy.

This study demonstrates the feasibility of applying a CAD scheme based on deep learning to categorize

malignant and benign breast masses without a lesion segmentation, image feature computation and selection process.

V. AI AND GENOME ANALYSIS IN CANCER:

Implication of AI to classify cancer is a modern approach, where expression of relevant genes involved in various types of cancer is detected using ML algorithms. This system is also helpful to detect the origin of cancer in a patient's body when cancer is detected in a critical stage.

The ML algorithm trained with features subsets (features correlated with the cancer class) to build a mathematical model. ML evaluates features subsets in two ways called filter method, and wrapper method. General characteristics of training data set considered by filter while, wrapper approaches measure biases of ML algorithm (*Mewes et al., 2005*).

AlphaGo (*Hassabis et al., 2016*) object recognition is a deep learning algorithm that outperforms human analytical power. DL used to find out complex structures in massive data set like splice site promoters and enhancers. More accuracy may come if convolutional neural networks are used in DL methods. (*Sun et al., 2019*) develop genomic deep learning (GDL) algorithm to classify cancer based on relationship of mutation (at oncogene or tumor suppressor gene) and cancer. To develop GDL algorithm researchers used 6083 WES (whole exon sequencing) files from 12 different types of cancer from TCGA (The Cancer Genome Atlas) and 1991 WES of healthy samples from IGSR (International Genome Sample resource). After that, 12 specific models were prepared which can distinguish a specific cancer from others 97.47% accurately; a mixture model to distinguish between all 12 types of cancer based on GDL, 70.08% accurately and a total specific model which can identify healthy and cancer tissue 94.7% accurately.

AI IN PERSONALISED MEDICINE DESIGNING:

In the age of high-throughput, data-intensive biomedical research assays, it is necessary for researchers to develop strategies for analyzing, integrating, and explaining the massive amounts of data generated. Given how important data-intensive assays are to reveal appropriate intervention targets and strategies for treating an individual with a disease, AI can play a significant role in the development of personalized medicines (Fig.14).

Different approaches like SVM, DL, NLP (Neural Language Processing) may be integrated to translate high dimensional data into clinically actionable data which acts as a foundation tool in precision medicine. Next generation sequencing has revolutionized medical research and enable multilayer studies that integrate genomic data of high dimensionality such as DNA- seq, RNA- seq and multi- omics data such as proteome, epigenome and micro-biome *(Chari et al., 2010)*. The integrative analysis done by several AI technologies such as BIOXCEL Therapeutics, XTALPI AI etc. help in designing and development of precise medicine.

In the recent past, Microsoft has built up collaboration with research groups of Jackson Laboratory to develop a database called the Clinical Knowledgebase (CKB). A machine learning called JAX researchers can curate CKB, which stores information about genetic mutations that impulse cancer and drug responses in cancer patients. The database helps oncologists find out what matches exist between a patient's known cancer-related genomic mutations and drugs that target them, allowing providers to choose the most appropriate treatments (*Kent, 2019*).

VI. AI TO DESIGN DRUG DELIVERY SYSTEM:

Over the last decades, targeted delivery of therapeutics with maximal efficiency and minimal side effects through different systems has attracted a growing interest. Target fishing (TF) is a technique which helps to link biological targets with novel drug compounds as well as rapid prediction and identification of biological targets. To design the control system neural networks, fuzzy logic, integrators, and differentiators may be applied. Drugs may be delivered using focused ultrasound, micropump mechanism, and targeted delivery by micro-robots (Fig.15).

Advance wireless communication systems also provide a high degree of flexibility to the entire drug delivery system and receive and send data from external sources to monitor and control drug delivery. Microfluidic technology permits the development of smart drug delivery systems, like Janus micro- or nanoparticles capable of delivery of multiple drugs *(Staples et al., 2006)*. For programmed drug delivery, electronic components, wireless communication hardware, and power supply have been embedded in a microchip implant (MicroCHIPS, Inc.) followed by a pulsatile release for about six months.

Information technology, wireless communication, and artificial neural networks (ANNs) contribute to modelling smart drug delivery systems that are very helpful for overcoming the limitations of conventional treatment strategies. ANN helps to monitor the factor responsible for cytotoxicity when a nanoemulsion system is applied.

Model neurons are stimulated to create interconnected processing element of ANNs which are helpful to generate software for mimicking the biological processes, generating the control algorithms, Pharmacodynamic/ pharmacokinetic modeling, controlled drug delivery, and evaluating the effectiveness of treatment strategies (*Murtoniemi et al., 1994*). Ligand based targets are predicted by ML approaches which give rise of Target Fishing (TF) in which ligand dataset , target protein, and relationship between the ligands may be used to predict protein targets of novel compounds with biological activities *(Sherrif et al., 2004).*

VII. CONCLUSION:

World famous scientist Stephen Hawking once said, "The development of full artificial intelligence could spell the end of the human race. Once humans develop artificial intelligence, it will take off on its own and redesign itself at an ever-increasing rate. Humans, who are limited by slow biological evolution, couldn't compete and would be superseded." Though AI is the ultimate solution in some complicated cases, more clinical trials should be done to make it successful; in the sense compatible otherwise it will get an opportunity to destroy the entire human race. Now human employment is standing before a question mark due to rapid implementation of AI. Both the Government and Private sectors should make a brief policy to restrict its use. Another existing problem is the "black-box problem", i.e. our knowledge cannot be able to detect how AI makes a particular inference. Still AI depends on other techniques for learning; it can learn about cancer patterns by itself and this drawback can raise questions about its authenticity. However, scientists should strictly follow the ethical guideline. Designing algorithms obviously is a tough work and should be done under proper surveillance. As prevention is better than cure so we should give more attention towards cancer diagnosis than treatment. Hope in the near future we can make a cancer free world with the help of both human and artificial intelligence.

VIII. FIGURS AND GRAPHS:

Figure 1- John McCarty (1927- 2011)

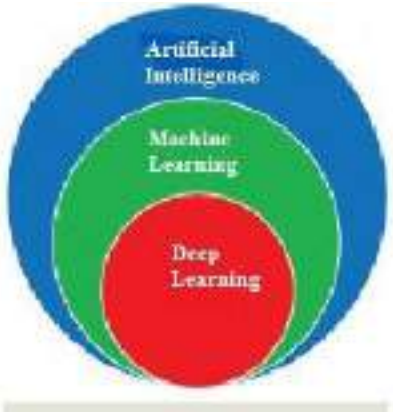

Figure 2- relationship between artificial intelligence, machine learning, deep learning

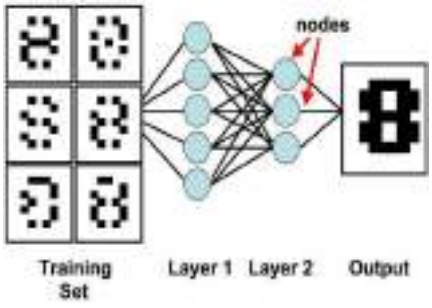

Figure3-an example of how a machine learner is trained to recognize images using a training set

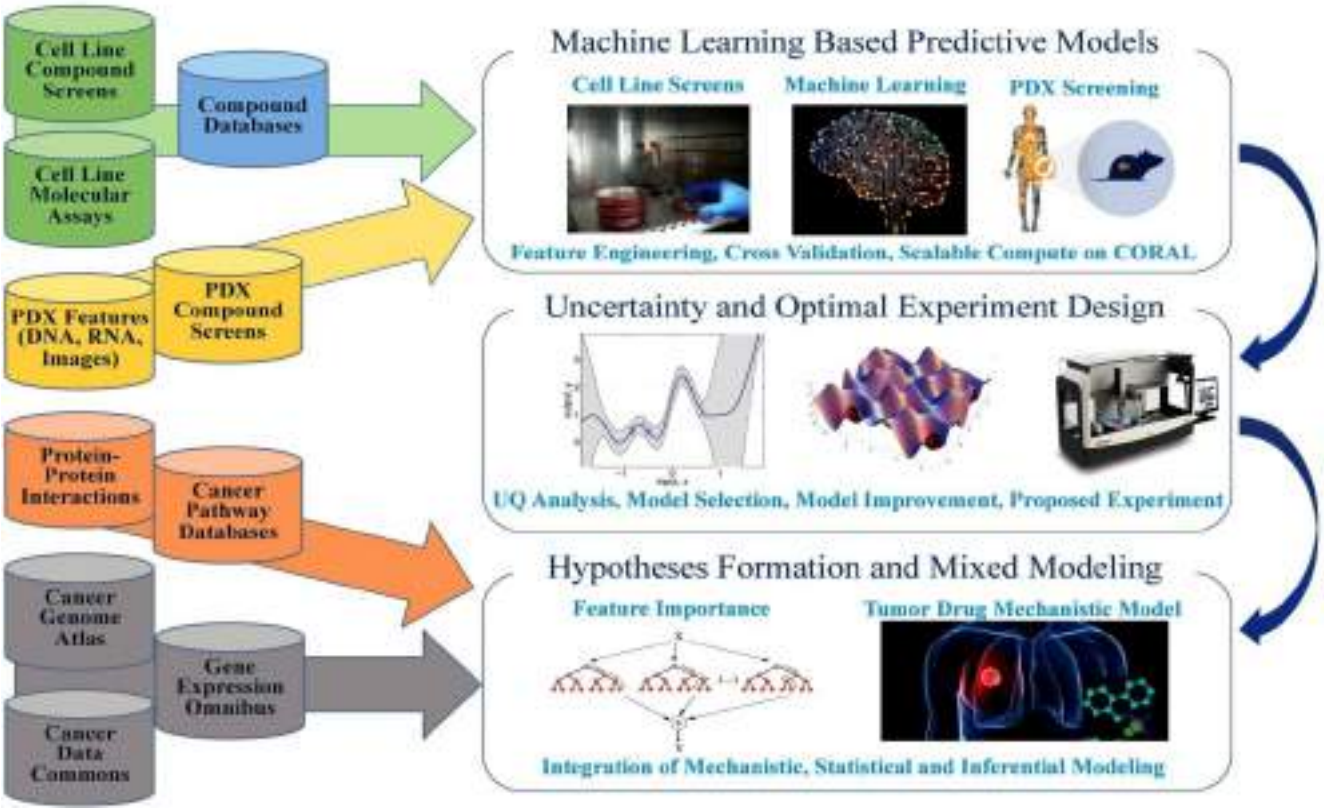

Figure 4-general work flow of AI for making prediction

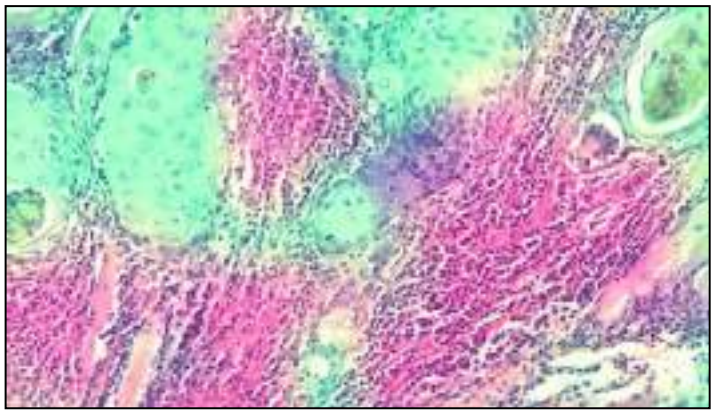

Figure 5- tumour infiltrating lymphocyte

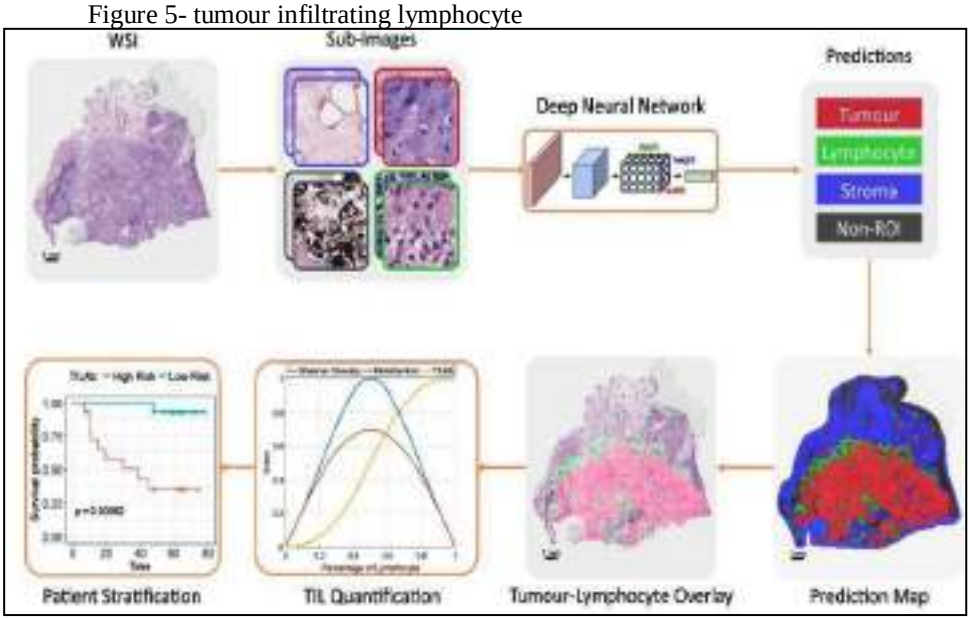

Figure-6 - a novel digital score for abundance of tumour infiltrating lymphocytes predicts disease free survival in oral squamous cell carcinoma

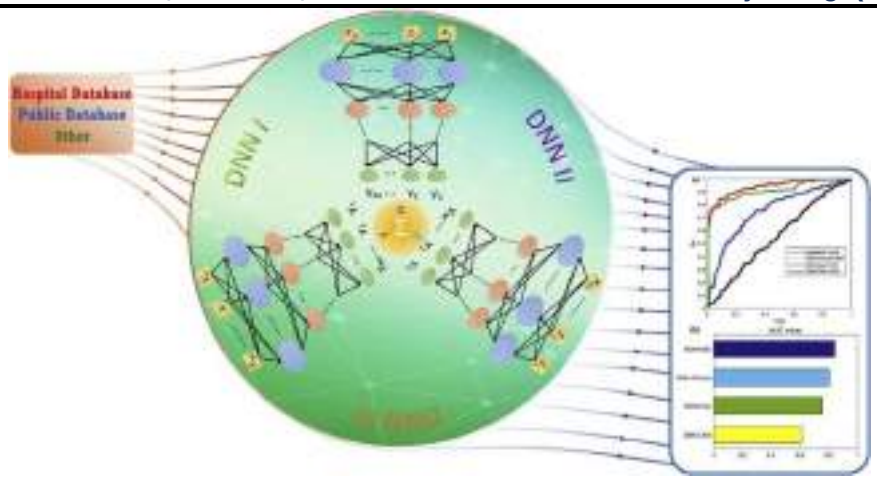

Figure-7- multimodal DNNs to predict human breast cancer prognosis by integrating multi-dimensional data including gene expression profile, copy no. alteration (CAN) profile, and clinical data. The model consist of a triple modal DNN and it is combined predictive scores from each independent model. The graphical representations (*A. Li et al, 2018)* show a comparison of the ROC curve and AUC value. The results indicated that combining different data types and ensemble DNN methods is an efficient way to improve human breast cancer prognosis prediction performance.

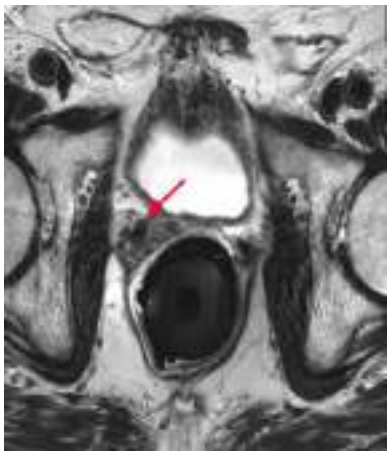

Figure 8- prostrate cancer

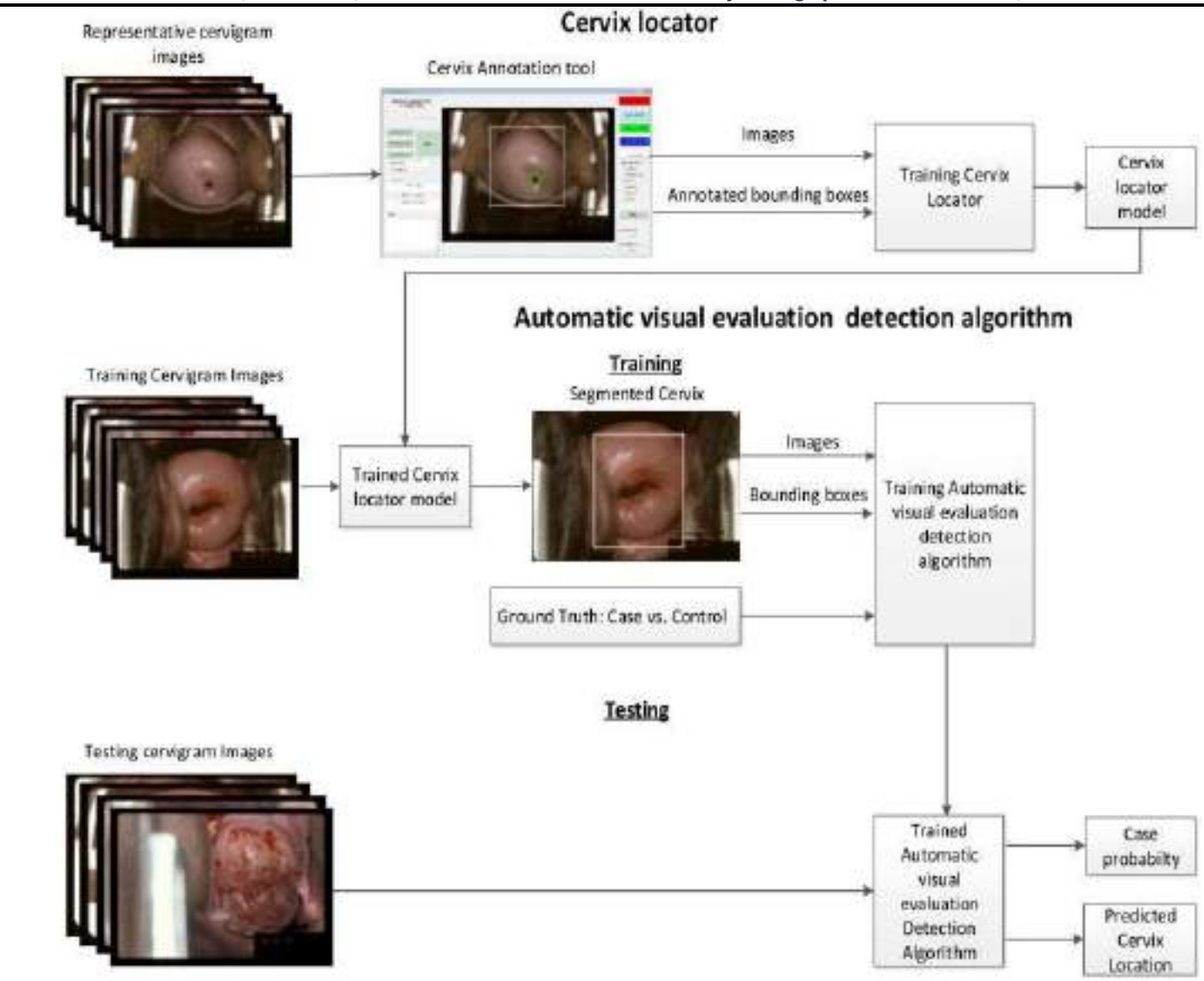

Figure 9 - the basic design of automated visual evaluation algorithm. Two models are trained: a cervix locator (top), and the automated visual evaluation detection algorithm (bottom). The final validation algorithm incorporated both cervix locator and automated visual evaluation.

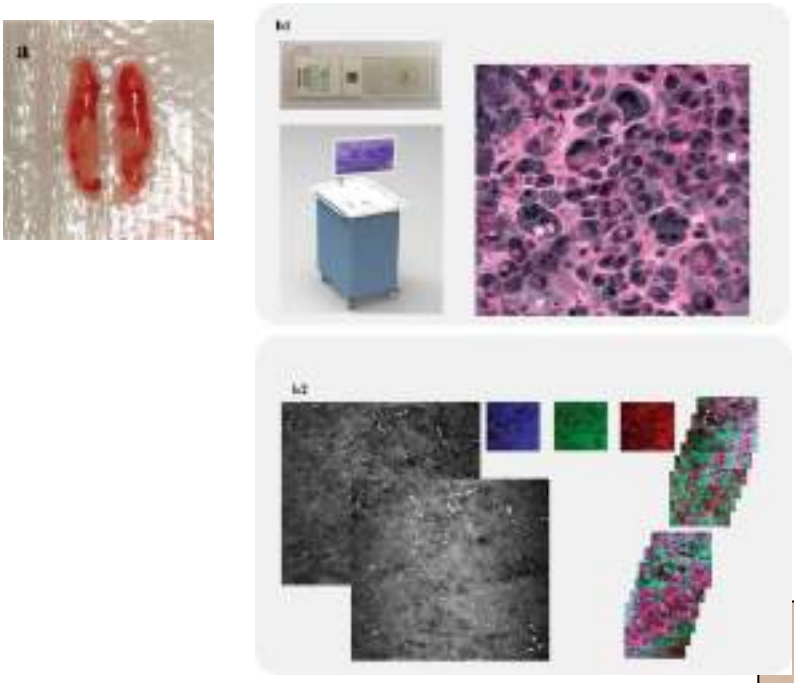

Figure 10: (a) fresh surgical specimen; (b1) image acquisition; (b2) image processing; (c) intra-

Figure 11-melanoma diagnosis by machine

Figure 12-ML algorithm can diagnose skin cancer from scanned image

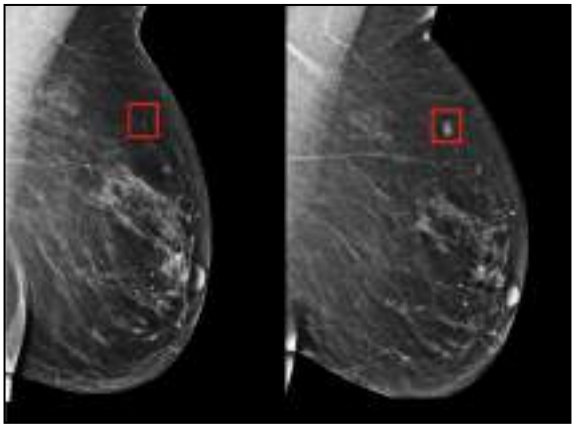

Figure 13- diagnosis of breast cancer by DL algorithm

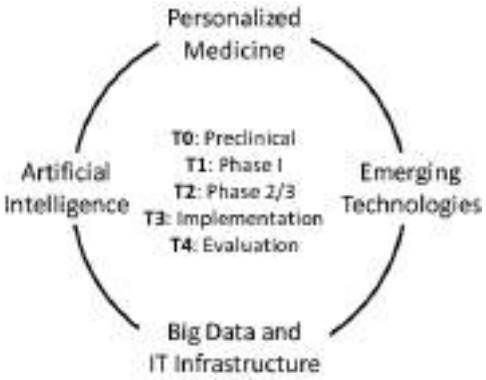

Figure 14- basic pathway to develop personalized medicine

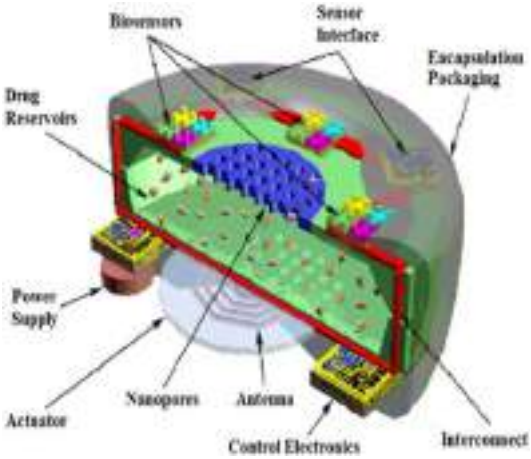

Figure 15- basic design of nano-drug delivery system.

IX. ACKNOWLEDGMENT:

The authors would like to thank The Principal, Maulana Azad College to his kind support. The authors are also thankful to all teaching staffs and non-teaching staffs of Maulana Azad College for their kind help.

X. REFERENCES:

[1] Alessandra, M., Maria, D.D., Gulia, L., 2010. Oral pulsatile delivery: rationale and chrono-pharmaceuticle formulation, *Int. J. Pharm, 398*, p:1-8

[2] Bhattacharya, T., Brettin, T., Doroshow, J.H., Evrard, Y.A., Greenspan, E.J., Gryshuk, A.L., Hoang, T.T., Lauzon, C.B.V., 2019. AI Meets Exascale Computing: Advancing Cancer Research With Large-Scale High Performance Computing. *Front Oncol. 9*, p:984 doi:10.3389/fonc.2019.00984

[3] Biglarian, A., Hajizadeh, E., Kazemnejad, A., Zali, M., 2011. Application of artificial neural network in predicting the survival rate of gastric cancer patients. *Iran J Public Health*. 40(2)p:80–86.

[4] Chang, S.W., Abdul-Kareem, S., Merican, A.F., Zain, R.B., 2013. Oral cancer prognosis based on clinicopathologic and genomic markers using a hybrid of feature selection and machine learning methods. *BMC Bioinformatics*.14,p: 170. doi: 10.1186/1471-2105-14-170

[5] Chari, R., Coe, B.P., Vucic, E.A., Lockwood, W.W., Lam, W.L., 2010. An integrative multi-dimensionalgenetic and epigenetic strategy to identify aberrant genes and pathways in cancer. *BMC Syst. Biol*., 4,p:67. doi:10.1186/1752-0509-4-67

[6] Chi, C. L., Street, W. N., & Wolberg, W. H., 2007. Application of artificial neural network-based survival analysis on two breast cancer datasets. *AMIA Annual Symposium proceedings. AMIA Symposium*, *2007*, p: 130–134.

[7] Ching T, Zhu X, Garmire LX (2018) Cox-nnet: An artificial neural network method for prognosis prediction of high-throughput omics data. PLoS Comput Biol 14(4): e1006076. doi:- 10.1371/journal.pcbi.1006076

[8] Coccia, M., 2019. Artificial intelligence technology in oncology: a new technological paradigm, Yale University School of Medicine, *Global Oncology*.

[9] Cruz, J. A., Wishart, D. S., 2006. Applications of Machine Learning in Cancer Prediction and Prognosis, *Cancer Informatics*: 2, p: 59–78

[10] Haenssle, H. A., Fink, C., Schneiderbauer, R., Toberer, F., Buhl, T., Blum, A., Kalloo, A., Hassen, A., Thomas, L., Enk, A., Uhlmann, L., Reader study level-I and level-II Groups, Alt, C., Arenbergerova, M., Bakos, R., Baltzer, A., Bertlich, I., Blum, A., Bokor-Billmann, T., Bowling, J., Zalaudek, I., 2018. Man against machine: diagnostic performance of a deep learning convolutional neural network for dermoscopic melanoma recognition in comparison to 58 dermatologists. *Annals of oncology: official journal of the European Society for Medical Oncology*. 29(8), p:1836–1842

[11] Hassanzadeh, P., Atyabi, F., & Dinarvand, R., 2019. The significance of artificial intelligence in drug delivery system design. *Advanced drug delivery reviews*, *151-152*, p:169–190. doi:10.1016/j.addr.2019.05.001.

[12] healthitanalytics.com/news/microsoft-using-ai-to-accelerate-cancer-precision-medicine

[13] Heneghan, H. M., Miller, N., Kelly, R., Newell, J., & Kerin, M. J., 2010. Systemic miRNA-195 differentiates breast cancer from other malignancies and is a potential biomarker for detecting noninvasive and early stage disease. *The oncologist*, *15*(7), p:673–682. doi:10.1634/theoncologist.2010-0103

[14] Herrero, R., Schiffman, M. H., Bratti, C., Hildesheim, A., Balmaceda, I., Sherman, M. E., Greenberg, M., Cárdenas, F., Gómez, V., Helgesen, K., Morales, J., Hutchinson, M., Mango, L., Alfaro, M., Potischman, N. W., Wacholder, S., Swanson, C., Brinton, L. A., 1997. Design and methods of a population-based natural history study of cervical neoplasia in a rural province of Costa Rica: the Guanacaste Project. *Revista panamericana de salud publica, Pan American journal of public health*, *1*(5),p:362–375.

[15] Hollon, T. C., Pandian, B., Adapa, A. R., Urias, E., Save, A. V., Khalsa, S., Eichberg, D. G., D'Amico, R. S., Farooq, Z. U., Lewis, S., Petridis, P. D., Marie, T., Shah, A. H., Garton, H., Maher, C. O., Heth, J. A., McKean, E. L., Sullivan, S. E., Hervey-Jumper, S. L., Patil, P. G., Orringer, D. A., 2020. Near real-time intraoperative brain tumor diagnosis using stimulated Raman histology and deep neural networks. *Nature medicine*, *26*(1), p:52–58.doi:10.1038/s41591-019-0715-9

[16] Hsu, E. R., Klemm, J. D., Kerlavage, A. R., Kusnezov, D., Kibbe, W. A. (2017). Cancer Monoshot Data and Technology Team: Enabling a National Learning Healthcare System for Cancer to Unleash the Power of Data. *Clinical pharmacology and therapeutics*, *101*(5), p:613–615. doi:10.1002/cpt.636

[17] https://en.m.wikipedia.org.

[18] https://i0.wp.com/images-prod.healthline.com

[19] https://warwick.ac.uk/newsandevents/pressreleases/ai_can_predict/

[20] https://www.cancernetwork.com/sites/default/files/1902review-ai-fig1.png

[21] https://www.futuresplatform.com

[22] https://www.itnonline.com.

[23] https://media.springernature.com.

[24] https://in.pcmag.com/news/130541/this-mit-ai-predicts-breast-cancer-risk-up-to-5-years-in-advance

[25] https://www.nibib.nih.gov.

[26] https://www.thechemicalengineer.com/media/15213/939aihero.jpg?width=960

[27] https://www.theguardian.com/society/2018/may/29/skin-cancer-computer-learns-to-detect-skin-cancer-more-accurately-than-a-doctor

[28] Hu, L., Bell D.,Antani, S., Xue Z., Yu, K., Horning P.M., Gachuhi, N., Wilson, B., Jaiswal, M.S., Befano, B., Long, L.R., Herrero, R., Einstein, M.H., Burk, R. D., Demarco, M., Gage, J. C., Cecilia A., Rodriguez, Wentzensen, N., Schiffman, M., 2019. An Observational Study of Deep Learning and Automated Evaluation of Cervical Images for Cancer Screening, *JNCI: Journal of the National Cancer Institute*, 111(9), p:923–932,doi:10.1093/jnci/djy225

[29] Hua, K. L., Hsu, C. H., Hidayati, S. C., Cheng, W. H., & Chen, Y. J. 2015. Computer-aided classification of lung nodules on computed tomography images via deep learning technique. *OncoTargets and therapy*, *8*, 2015–2022. doi:10.2147/OTT.S80733

[30] Huang S., Yang J., Fong S., Zhao Q., 2019.Mining Prognosis Index of Brain Metastases Using Artificial Intelligence, *Cancers, 11*, 1140; doi:10.3390/cancers11081140

[31] Jhajharia, S., Varshney, H.K., Verma, S., Kumar, R., 2016. A neural network based breast cancer prognosis model with pca processed features. In: 2016 Int. Con. on Adv. in Computing, Communications and Informatics (ICACCI), p: 1896–1901

[32] Kann, B.H., Thomas, R. C., Thompson, R., Artificial Intelligence in Oncology: Current Applications and Future Directions, *Oncology (Williston Park). 33(2),* p:46-53.

[33] Levine, A.B., Schlosser, C., Grewal, J., Coope, R., Jones, S.J.M., Yip, S., 2019. Rise of the machines: advances in deep learning for cancer diagnosis. *Trends Cancer, 5*, p:157–169. doi:10.1016/j.trecan.2019.02.002

[34] Li, X. Zhang, S., Zhang, Q., Wei, X., Pan, Y., Zhao, J., Xin, X., Qin, C., Wang, X., Li, J., Yang, F., Zhao, Y., Yang, M., Wang, Q., Zheng, Z., Zheng, X., Yang, X., Whitlow, C.T., Gurcan, M.N., Zhang, L., Wang, X., Pasche, B.C., Gao, M., Zhang, W., Chen K., 2019, Diagnosis of thyroid cancer using deep convolutional neural network models applied to sonographic images: a retrospective, multicohort, diagnostic study, *Lancet Oncol. 20,* p:193–201.

[35] Lusci A, Pollastri G, Baldi P. Deep architectures and deep learning in chemoinformatics: The prediction of aqueous solubility for drug-like molecules. *J. Chem. Inf. Model, 53*, p:1563-75.

[36] Ly, D. Q., Paramonov, L., Davidson, C., Ramsden, J., Wright, H., Holliman, N., Hagon, J., Heggie, M., Makatsoris, C., 2011 *Nanotechnol. Percept*. 7, p:199–217

[37] Lynch, C. M., Abdollahi, B., Fuqua, J. D., de Carlo, A. R., Bartholomai, J. A., Balgemann, R. N., van Berkel, V. H., & Frieboes, H. B., 2017. Prediction of lung cancer patient survival via supervised machine learning classification techniques. *International journal of medical informatics*, *108*, p:1–8. doi:10.1016/j.ijmedinf.2017.09.013

[38] media.springernature.com

[39] Murtoniemi, E., Merkku, P., Kinnunen, P., Leivisk, K., Yliruusi, J., 1994. Effect of neural network topology and training end point in modelling the fluidized bed granulation process, *Int. J. Pharm*. 110, p:101– 108

[40] Oh, S. E., Choi, M. G., & Seo, S. W., 2019. ASO Author Reflections: Use of the Survival Recurrent Network for Prediction of Overall Survival in Patients with Gastric Cancer. *Annals of surgical oncology*, *26*(Suppl 3), p:539–540.doi.10.1245/s10434-018-7044-y

[41] Padovani de Souza, K., Setubal, J. C., Ponce de Leon F de Carvalho, A. C., Oliveira, G., Chateau, A., Alves,R. 2019. Machine learning meets genome assembly. *Briefings in bioinformatics*, *20*(6), p: 2116–2129. doi: 10.1093/bib/bby072

[42] Phillips, M., Greenhalgh, J., Marsden, H., Palamaras, I. 2019. Detection of Malignant Melanoma Using Artificial Intelligence: An Observational Study of Diagnostic Accuracy. *Dermatology practical & conceptual*, *10*(1), e2020011. doi:10.5826/dpc.1001a11

[43] Press release (N- 263), The International Agency for Research on Cancer (IARC), World Health Organization, 2018.

[44] Qiu, Y., Yan, S., Gundreddy, R. R., Wang, Y., Cheng, S., Liu, H., & Zheng, B. 2017. A new approach to develop computer-aided diagnosis scheme of breast mass classification using deep learning technology. *Journal of X-ray science and technology*, *25*(5), p: 751–763.doi:10.3233/XST-16226

[45] Quinlan, J.R., 1986, Induction of decision trees. *Mach Learn*, 1, p:81–106. doi: 10.1007/BF00116251

[46] Ramesh, K., Gupta, S. Ahmed, S., Kakkar, V., 2016. A Comprehensive Study on Design Trends and Future Scope of Implantable Drug Delivery Systems. *Int. J. of BioScience and Biotech. 8*, p:11-20. doi: 10.14257/ijbsbt.2016.8.6.02.

[47] Sacha, G.M., Varona, P., 2013. Artificial intelligence in nanotechnology. *Nanotechnology*. 24, p:1–13.

[48] Shaban, M., Khurram, S. A., Fraz, M. M., Alsubaie, N., Masood, I., Mushtaq, S., Hassan, M., Loya, A., & Rajpoot, N. M. (2019). A Novel Digital Score for Abundance of Tumour Infiltrating Lymphocytes Predicts Disease Free Survival in Oral Squamous Cell Carcinoma. *Scientific reports*, *9*(1), 13341.doi:-10.1038/s41598-019-49710

[49] Sherriff, A., Ott, J., & ALSPAC Study Team, 2004. Artificial neural networks as statistical tools in epidemiological studies: analysis of risk factors for early infant wheeze. *Paediatric and perinatal epidemiology*, *18*(6), p:456–463. doi:-10.1111/j. p:1365-3016.

[50] Silver, D., Huang, A., Maddison, C., Guez, A.,Sifre, L., Driessche, G., Schrittwieser, J., Antonoglou, I., Panneershelvam, V., Lanctot, M., Dieleman, S., Grewe, D., Nham, J., Kalchbrenner, N., Sutskever, I., Lillicrap, T., Leach, M., Kavukcuoglu, K., Graepel, T., Hassabis, D. (2016). Mastering the game of Go with deep neural networks and tree search. *Nature. 529*. p:484489. doi: 10.1038/nature16961.

[51] Staples, M., & Daniel, K., Cima, M.J., Langer, R. 2006. Application of Micro- and Nano Electromechanical Devices to Drug Delivery. *Pharmaceutical research. 23*. p:847-63. doi: 10.1007/s11095-006-9906-4.

[52] Ström, P., Kartasalo, K., Olsson, H., Solorzano, L., Delahunt, B., Berney, D. M., Bostwick, D. G., Evans, A. J., Grignon, D. J., Humphrey, P. A., Iczkowski, K. A., Kench, J. G., Kristiansen, G., van der Kwast, T. H., Leite, K., McKenney, J. K., Oxley, J., Pan, C. C., Samaratunga, H., Srigley, J. R., Eklund, M., 2020. Artificial intelligence for diagnosis and grading of prostate cancer in biopsies: a population-based, diagnostic study. *The Lancet. Oncology*, *21*(2), p:222–232. doi:10.1016/S1470-2045(19)30738-7

[53] Sun D., Wang M., Li A., 2018. A multimodal deep neural network for human breast cancer prognosis prediction by integrating multi-dimensional data, IEEE ACM Trans. *Comput. Biol. Bioinform.* 16 (3), p:841–850. doi:10.1109/TCBB.2018.2806438

[54] Sun, Y., Zhu, S., Ma, K., Liu, W., Yue, Y., Hu, G., Lu, H., Chen, W., 2019. Identification of 12 cancer types through

genome deep learning. *Sci Rep*, 9, 17256. doi:10.1101/528216.

[55] Sutradhar, K. B., Sumi, C. D., 2016. Implantable microchip: the futuristic controlleddrug delivery system. *Drug delivery*, *23*(1),1–11.doi:10.3109/10717544.2014.903579

[56] Wang, Y., Tetko, I.V., Hall, M.A., Frank, E., Facius, A., Mayer, K.F.X., Mewes, H.W., 2005, Gene selection from microarray data for cancer classification- a machine learning approach, Computational Biology and chemistry, 29(1), p: 37-46

[57] Xu, J., Yang, P., Xue, S., Sharma, B., Sanchez-Martin, M., Wang, F., Beaty, K. A., Dehan, E., & Parikh, B. 2019. Translating cancer genomics into precision medicine with artificial intelligence: applications, challenges and future perspectives. *Human genetics*, *138*(2), p:109–124. doi: 10.1007/s00439-019- 01970-5

[58] Zen, K., Zhang, C.Y., 2012. Circulating microRNAs: a novel class of biomarkers to diagnose and monitor human cancers. *Med Res Rev*, *32*, p:326–48.

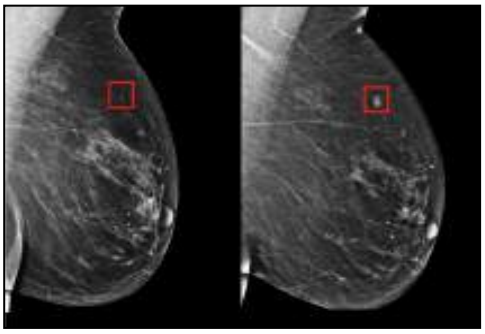

a

b2

b1

LR-4420
[1-7]

RESEARCH ARTICLE Legume Research - An International Journal

Interrelation between Surface Wax Alkanes from Red Kidney Bean (*Phaseolus vulgaris* L.) Seeds and Adzuki Bean Weevil [*Callosobruchus chinensis* (F.)] (Coleoptera: Bruchidae)

A. Mukherjee, A. Sengupta, S. Shaw, S. Sarkar, D. Pal[1], U.K. Das[1] 10.18805/LR-4420

ABSTRACT

Background: *Callosobruchus chinensis* (Fabricius) (Coleoptera: Bruchidae) is one of the major insect pests of *Phaseolus vulgaris* L. grains, commonly known as rajma seeds, in Europe and Asia including India. Infestations of these insects destroy majority of legume seeds including rajma which causes a great economic loss. Hence, a proper sustainable pest management measures are necessary for storage of rajma seeds. For this, the study aims to identify and quantify the *n*-alkane profile from the surface waxes of rajma seeds and their role as olfactory cue in *C. chinensis*. Individual synthetic alkane followed by the synthetic blends mimicking rajma seed surface wax *n*-alkanes as olfactory cue was also evaluated.

Methods: Collected rajma seeds were solvent extracted to isolate surface waxes. The extract then fractioned by thin-layer chromatography and followed by gas chromatography-mass spectrometry analyses to purify, quantify and identify *n*-alkanes.

Result: Rajma seeds' surface waxes analysis revealed 18 *n*-alkanes between *n*-C_{15} and *n*-C_{33}. The predominant alkanes were *n*-octacosane and *n*-hexadecane. *n*-Octadecane was the least abundant alkane in seeds. Total alkane content was 3502.67±12.82µg from 100 g (number 200 ± 5.13) seeds. Adult female *C. chinensis* elicited attraction towards the surface wax alkanes at concentrations of 0.5, 1, 2, 4 and 6 seed(s) equivalent of rajma seed(s) in the Y-tube olfactometer bioassay, but the highest attraction was observed at 6 seeds equivalent. Hence, a synthetic alkane blend resembling of 6 seeds equivalent, present in seeds' surface wax alkane or a combination of nine (which elicited positive response) synthetic alkane blend resembling 6 seeds equivalent could be used as lures in developing baited trap in insect pest management programme.

Key words: Alkanes, *Callosobruchus chinensis*, Olfactory bioassay, *Phaseolus vulgaris* seed, Surface wax, Y-tube olfactometer.

INTRODUCTION

Phaseolus vulgaris, commonly known as red kidney bean or rajma bean, belongs to the family Fabaceae. It is a valuable grain legume in Europe, American, tropical and subtropical regions including India (Gepts, 1990; Toro *et al.*, 1990; Dutta *et al.*, 2016). The rajma bean is an important source of dietary protein for millions of people in India (Marwein and Ray, 2019).

It is cultivated in both *Rabi* and *Kharif* seasons throughout India, covering an area of ca. 9.4 million ha (Rawal and Navarro, 2019).

Callosobruchus chinensis (F.) (Coleoptera: Bruchidae) is one of the major destructive pests of legumes including rajma seeds (red kidney bean). Female *C. chinensis* lay eggs on the surface of rajma seeds where the larvae hatch and burrow inside them. After 23-30 days, adults emerge from the seeds passing through the larval and pupal stages (Chakraborty and Mondal, 2015). Infestation of this insect can cause enormous food value loss of legume seeds (nearly 50-60%) (Caswell, 1973). Therefore, proper control measures are necessary for storage of the seeds. Major disinfestants used to control this pest have harmful effects on the environment and human health, for this, the uses of disinfestants have been restricted from 2015 under the policy of Montreal Protocol (United Nations Environment Programme, 1998). Therefore, it is necessary to find alternative methods to control *C. chinensis* as a pest of stored rajma seeds.

Alkanes are the most abundant group of secondary compounds present in most of the plant's or seed's surface wax, though the composition and amount vary among different species (Baker, 1982; Jetter *et al.*, 2000; Nietupski *et al.*, 2005; Shao *et al.*, 2007; Nawrot *et al.*, 2010). For wide range of insects, alkanes act as attractants (Schiestl *et al.*, 1999; Dutton *et al.*, 2000; Roy and Barik, 2012; Sarkar

Ecology Research Laboratory, Zoology Department, Maulana Azad College, 8, Rafi Ahmed Kidwai Rd, Taltala, Kolkata-700 013, West Bengal, India.
[1]Ramakrishna Mission Vidyamandira, P.O. Belur Math, Howrah-711 202, West Bengal, India.

Corresponding Author: A. Mukherjee, Ecology Research Laboratory, Zoology Department, Maulana Azad College, 8, Rafi Ahmed Kidwai Rd, Taltala, Kolkata-700 013, West Bengal, India. Email: 2007.mukherjee@gmail.com

How to cite this article: Mukherjee, A., Sengupta, A., Shaw, S., Sarkar, S., Pal, D., Das, U.K. (2021). Interrelation between Surface Wax Alkanes from Red Kidney Bean (*Phaseolus vulgaris* L.) Seeds and Adzuki Bean Weevil [*Callosobruchus chinensis* (F.)] (Coleoptera: Bruchidae). Legume Research. 10.18805/LR-4420

Submitted: 18-05-2020 **Accepted:** 21-10-2020 **Online:** 16-01-2021

et al., 2013a; Mukherjee *et al.*, 2013; Mitra *et al.*, 2019; Das *et al.*, 2019; Mitra *et al.*, 2020) as well as ovipositional stimulants or both (Eigenbrode and Espelie, 1995; Srinivasan *et al.*, 2006; Mitra *et al.*, 2019; Mitra *et al.*, 2020). Long-chain alkanes such as heneicosane, docosane, tricosane, tetracosane, pentacosane, hexacosane and heptacosane elicited attraction to *Andrena nigroaenea* (Kirby) Miller (Schiestl *et al.*, 1999). Pentadecane, octadecane, docosane, pentacosane, heptacosane, octacosane, nonacosane, tritriacontane also display attraction in *Aphis craccivora* females (Mitra *et al.*, 2020). Furthermore, a dose of 14.54, 11.02, 17.99 and 5.92 µg/ml of docosane, tricosane, pentacosane and heptacosane attracts *Lema praeusta* (Fab.) female (Das *et al.*, 2019). D-catechin from the *P. vulgaris* seeds has been shown to act as ovipositional stimulants in *C. chinensis* (Ueno *et al.*, 1990), but till date no information is available on the surface wax alkanes and its role in insect response from rajma seed. For this reason, the *n*-alkane profile from the surface waxes of rajma seeds was identified and quantified and their role as olfactory cue in *C. chinensis* to find the host was studied under laboratory conditions. We also observed the role of individual synthetic alkanes followed by the synthetic blends mimicking rajma seed surface wax alkanes in *C. chinensis* as olfactory cues.

MATERIALS AND METHODS

The whole experiment was performed from June to August, 2019 at the Ecology Research Laboratory, Department of Zoology, Maulana Azad College (West Bengal, India), while the chromatographic analysis was performed in the Chemical-Ecology laboratory, The University of Burdwan, Burdwan, West Bengal, India. Rajma seeds (Arun) were used throughout the study as it is commonly available in market of Burdwan district, West Bengal. Rajma seeds were collected from the market of Burdwan, West Bengal for this study.

n-Alkanes extraction from seed surface

The surface waxes were extracted from 100 g of uninfected and healthy (number 200 ± 5.13) [mean ± standard error (SE)] rajma seeds. One hundred gram seeds were dipped in 2 L *n*-hexane for 1min in room temperature (27°C) for extraction of surface waxes (Barik *et al.*, 2004; Roy *et al.*, 2012a; Sarkar *et al.*, 2013a; Adhikari *et al.*, 2014, Mitra *et al.*, 2020) and the crude extract was filtered through a Whatman (Maidstone, UK) No. 41 filter paper followed by evaporation of the solvent using reduced pressure. The extract was further passed through a column of aluminium oxide (Alcoa, Frankfurt, Germany: F-20 grade) and eluted with petroleum ether. The eluent was then fractioned by TLC on silica gel G (Sigma St. Louis, MO, USA) layers (thickness 0.5 mm) [prepared using a Unoplan coating apparatus (Shandon, London)] with carbon tetrachloride (mobile phase).The TLC plate was air-dried after the appearance of a light yellowish band. The Rf value of this TLC plate was compared and confirmed with the Rf (0.87) value of a standard mixture of alkanes between *n*-C_{15} and *n*-C_{33}. The single yellowish band was eluted from the TLC plate using chloroform. This purified sample does not show presence of any detectable functional groups in IR spectroscopy. The extraction and purification process were repeated three times separately. Half portion of each sample was used for quantification of the alkane compounds by gas chromatography (GC) and identification with coupled gas chromatography-mass spectrometry (GC-MS) while the second portion was used for the olfactory bioassay. GR grade (from E. Merck, India Pvt. Ltd) solvents were used throughout this study.

n-Alkanes quantification by Gas chromatography (GC)

Extracts of rajma seeds (three separate) were analyzed by a Tech comp GC (Em Macau, Rua De Pequim, Nos. 202A-246, Centro Financeiro F7, Hong Kong) model 7900 attached with an HP-1 capillary column (Agilent, USA; length: 30 m×0.25 mm × 0.25-mm film thickness) and a flame ionization detector (FID). Initially the oven temperature programme was 170°C held for 1 min, then raised at 4°C/ min to 300°C and finally held for 15 min (Barik *et al.*, 2004; Sarkar *et al.*, 2013a; Mukherjee *et al.*, 2013; Adhikari *et al.*, 2014; Das *et al.*, 2019; Mitra *et al.*, 2019; Mitra *et al.*, 2020). The flow rate of carrier gas (nitrogen) was 18.5 ml/min. The volume of sample injected was 1 µl with a split ratio of 1:10. The limit of detection of the GC instrument is $\leq 5 \times 10^{-12}$ g/s (*n*-hexadecane). The peaks were identified by comparing the retention times with those of standard *n*-alkanes from *n*-C_{15} through *n*-C_{33} and the areas of each peak were quantified by using internal standard *n*-tricosane (*n*-C_{23}). Each *n*-alkane (>99% purity) was purchased from Sigma Aldrich (between *n*-C_{15} to *n*-C_{33}).

n-Alkanes identification with coupled gas chromatography-mass spectrometry (GC-MS)

The extracts were also analyzed with an Agilent 6890 GC coupled to a 5973 Mass Selective Detector for confirmation. The temperature programme and column (HP-1) configuration were same as mentioned in GC analysis. The MS parameters were 280°C at the interface, ionization energy 70 eV and scan speed approximately 1 s over the mass range of 40-600 mass units. Helium was the carrier gas. Alkanes were verified by comparing the diagnostic ions and GC retention times with respective standards (between *n*-C_{15} to *n*-C_{33}).

Test insects

Adult *C. chinensis* were collected from the local storehouses containing rajma seeds of Kolkata. They were maintained in glass jars (1 L) covered with fine-mesh nylon nets at 27 ± 1°C temperature, 65 ± 10% relative humidity (r. h.) and 12 L:12 D photoperiod in a 'Biological Oxygen Demand' incubator. Newly emerged females (4^{th} generation) were separated from the stock cultures and were kept in separate glass jars without rajma seeds. The behaviour of 90 females

to 0.5,1, 2, 4 and 6 seed(s) equivalent of surface wax alkanes and a control solvent was observed for 3 min in preliminary assays. Virgin females (olfactory responses of virgin or mated females to alkanes odor were same in the preliminary study) were used throughout the olfactory bioassays. Females were used in the bioassays as females are guided by olfactory cues for oviposition on a proper host.

Y-tube olfactory bioassay

Second half of purified alkanes from the surface of rajma seeds were dissolved in petroleum ether to make five different concentrations of 0.5, 1, 2, 4 and 6 seed(s) equivalent for olfactory bioassays. The highest dose of the alkanes was used 6 seeds equivalent for olfactory bioassays as the insect produced the highest significant ($P<0.00001$) attraction. Synthetic mixtures of alkanes were also prepared by maintaining the combinations and amounts of alkane present in the rajma seeds at 0.5, 1, 2, 4 and 6 seed(s) equivalent. Individual synthetic alkanes mimicking the amount present in each concentration of seed surface waxes were used for olfactory bioassays. The behavioural responses of *C. chinensis* females were observed in a glass Y-tube olfactometer (5 cm long stem and arms; 0.6 cm radius and 45° Y-angle between two arms). Each arm of the olfactometer was connected to a glass-made micro kit adapter fitted into a 1 cm radius 3 cm long glass vial. One glass vial contained a piece (1 cm^2) of Whatman No. 41 filter paper added with particular concentration of alkanes, whilst the other glass vial contained a filter paper of same size moistened with petroleum ether (control solvent). An air-flow of 450 ml min^{-1} was passed through charcoal and the charcoal filtered air was pushed into the system at 150 ml min^{-1}. The air was sucked from the porous glass vial at a rate of 100 ml min^{-1}, which was connected to the stem of the olfactometer. Silicon rubber tubes were used to connect different parts of the set-up. To evaluate the role of alkanes as attractant, laboratory condition was maintained at 27 ± 1°C, r. h. at 70 ± 3% and light intensity at 150 lux. One adult female *C.chinensis* was introduced into the porous glass vial, which was then attached with the stem of the olfactometer and exposed to a particular odor. Insects were not attracted towards the control solvent (petroleum ether) in preliminary assays. The behaviour of each female was observed for 3 min and considered to have made a choice if it reached at the end of either arm. The insect was removed from the Y-tube and the choice made was recorded as a positive response or negative response by one unit, respectively. “No response” was noted when the female remained in the common arm of the Y-tube (Koschier *et al.*, 2000; Mukherjee *et al.*, 2013, 2014; Sarkar *et al.*, 2013a,b; Das *et al.*, 2019; Mitra *et al.*,2019; Mitra *et al.*, 2020). For experiment with one alkane sample, a group of 90 naïve female insects were used and after testing five insects, the olfactometer set-up was cleaned with petroleum ether followed by acetone. To avoid the positional bias the position of two arms was systematically changed.

Statistical analyses

The data obtained on the responses of *C. chinensis* in olfactometer assays for the different concentrations of seed surface wax alkanes, synthetic mixtures of alkanes and individual synthetic alkanes were analysed by a Chi-square test (Sokal and Rohlf, 1995; Koschier *et al.*, 2000; Roy *et al.*, 2012b; Sarkar *et al.*, 2013a,b; Das *et al.*, 2019; Mitra *et al.*, 2020). Insects that did not respond by selecting either arm of the olfactometer were not included in the analyses.

RESULTS AND DISCUSSION

_n_-Alkane profiles in rajma seed surface

The extraction of 100 g rajma seeds yielded 3.50 ± 0.012 mg of seed surface wax alkanes which is ca. 10% of the total crude extract of surface waxes. Table 1 and Fig. 1 shows 18 *n*-alkanes in the surface waxes of rajma seeds. Octacosane (*n*-C_{28}) was the predominant *n*-alkane, accounting for 846.67±17.64µg. Heneicosane (*n*-C_{21}) was the second most abundant alkane followed by *n*-tritriacontane (*n*-C_{33}) in the surface waxes of rajma seeds. *n*-Hexadecane (*n*-C_{16}) and *n*-pentadecane (*n*-C_{15}) were the least abundant alkanes in rajma seeds. The rest 13 *n*-alkanes displayed different patterns in the surface waxes of rajma seeds.

Y-tube olfactometer bioassay

The results obtained in the series of olfactometric bioassays showing effectiveness of *C.chinensis* towards alkanes isolated from *P. vulgaris* L. seeds surface waxes are presented in Table 2. Alkanes from the rajma seed surface

Table 1: Amount of alkanes (µg/100 g seeds) in *P. vulgaris* L. seeds surface waxes.

Name of alkanes	Amount of alkanes (µg) (mean ± SE, N = 3)
n-pentadecane (C15)	56.33 ± 3.18
n-hexadecane (C16)	32.33 ± 2.29
n-heptadecane (C17)	65.33 ± 2.03
n-octadecane (C18)	165.67 ± 2.73
n-nonadecane (C19)	252±6.11
n-icosane (C20)	226.67±8.82
n-henicosane (C21)	463.33±8.82
n-docosane (C22)	147±2.31
n-tetracosane (C24)	164±4.36
n-pentacosane (C25)	227.67±8.69
n-hexacosane(C26)	93±5.03
n-heptacosane (C27)	84.33±3.76
n-octacosane (C28)	846.67±17.64
n-nonacosane (C29)	74.33±2.73
n-triacontane (C30)	91±2.31
n-hentriacontane (C31)	157.33±3.28
n-dotriacontane (C32)	58.67±2.85
n-tritriacontane (C33)	297±9.07
Total	3502.67±12.82

attracted the insect significantly at 0.5 seed equivalent (63.33%; χ^2=6.4; df =1; P<0.05), 1 seed equivalent (68.89%; χ^2=12.84; df =1; P< 0.001), 2 seeds equivalent (73.33%; χ^2=19.6; df =1; P< 0.001), 4 seeds equivalent (81.11%; χ^2=34.84; df =1; P<0.00001) and 6 seeds equivalent (86.67%; χ^2=48.4; df =1; P<0.00001). Insects' did not respond towards 0.25 seed equivalent.

Bioassays with the mixtures of synthetic alkanes mimicking the surface wax alkanes of *P. vulgaris* L. seeds are also summarized in Table 2. Insects showed attraction towards a mimic of 0.5 seed equivalent (61.11%; χ^2=4.4; df =1; P<0.05), 1 seed equivalent (66.67%; χ^2=10; df =1; P< 0.01), 2 seeds equivalent (70%; χ^2=14.4; df =1; P< 0.001), 4 seeds equivalent (78.89%; χ^2=30.04; df =1; P<0.00001) and 6 seeds equivalent (84.44%; χ^2=42.71; df =1; P<0.00001).

Table 3 represents the results of olfactory bioassays of *C.chinensis* for individual synthetic alkanes mimicking the surface wax alkanes of *P. vulgaris* L. seeds. The insect responded positively to *n*-C_{21} at 1.16 µg (58.89%; χ^2=4.4; df =1; P=0.09), 2.32 µg (63.33%; χ^2=6.4; df =1; P=0.011), 4.64µg (64.44%; χ^2=7.51; df =1; P<0.01), 9.28 µg (67.78%; χ^2=11.38; df =1; P<0.001) and 13.92 µg (70%; χ^2=14.4; df =1; P<0.001). Females also showed positive responses towards *n*-C_{25} at 0.569 µg (58.89%; χ^2=4.4; df =1; P=0.09), 1.138 µg (64.44%; χ^2=7.51; df =1; P<0.01), 2.276 µg (66.67%; χ^2=10; df =1; P=0.001), 4.552 µg (67.78%; χ^2=11.38; df =1; P<0.001) and 6.828 µg (70%; χ^2=14.4; df =1; P<0.001). A positive response was also recorded for *n*-C_{15} at 0.564 µg (62.22%; χ^2=5.37; df =1; P=0.02) and the response for the same was the highest at 1.692 µg (66.67%; χ^2=10; df =1; P=0.001). Females showed attractions towards *n*-C_{16} at 1.938 µg (60%; χ^2=3.6; df =1; P=0.057), *n*-C_{20} at 1.692 µg (56.67%; χ^2=1.6; df =1; P=0.2), *n*-C_{22} at 2.94 µg (60%; χ^2=3.6; df =1; P=0.057) and 4.41 µg (62.22%; χ^2=5.37; df =1; P=0.02), *n*-C_{24} at 4.92 µg (61.11%; χ^2=4.4; df =1; P<0.05), *n*-C_{31} at 4.72 µg (61.11%; χ^2=4.4; df =1; P<0.05) and *n*-C_{32} at 1.17 µg (63.33%; χ^2=6.4; df =1; P=0.011) and

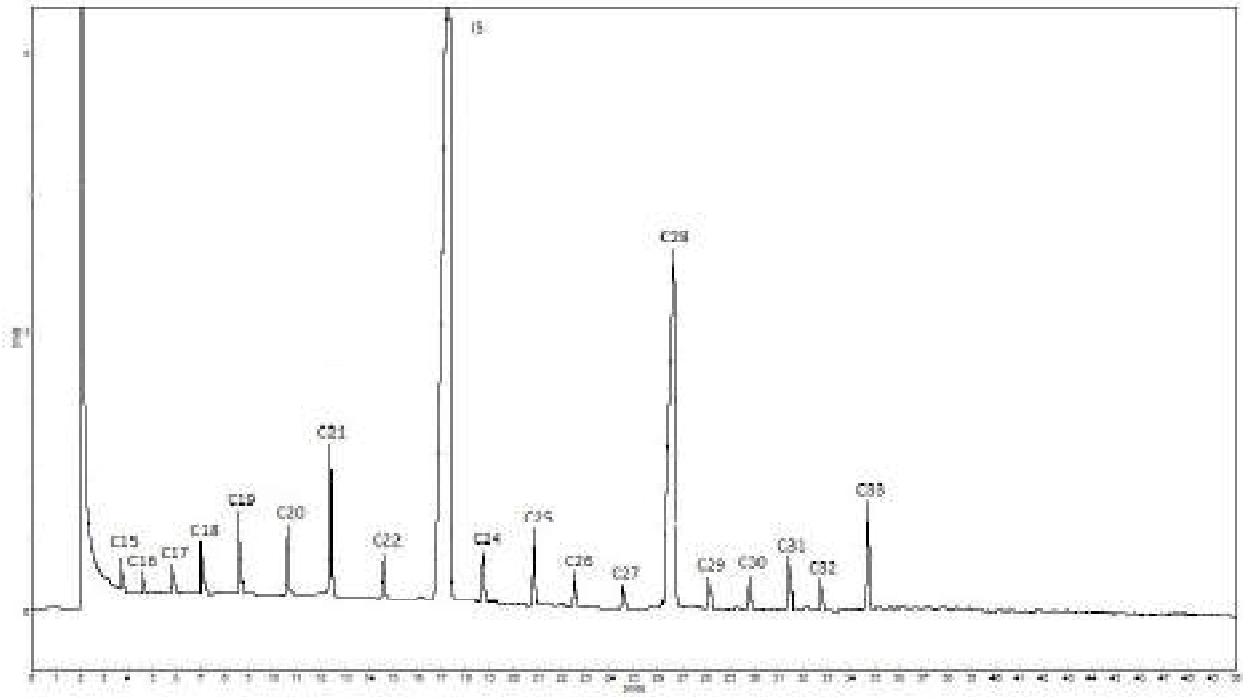

Fig 1: GC-FID chromatogram of rajma seeds surface wax alkanes (IS= Internal Standard, C_x= Carbon chain length).

Table 2: Attractiveness of extracted surface alkanes from *P. vulgaris* L. seeds to *C. chinensis* choosing odour arm (%) in olfactometer bioassay. (N = 90 in each bioassay).

Amount of alkanes used for bioassay	% of insects attracted towards the surface alkanes	% of insects attracted towards the synthetic alkanes mimicking surface waxes
6 seeds equivalent (105 µg)#	86.67%*****	84.44%*****
4 seeds equivalent(70 µg)	81.11%*****	78.89%*****
2 seeds equivalent(35 µg)	73.33%*****	70%***
1 seed equivalent (17.5 µg)	68.89%***	66.67%**
0.5 seed equivalent (8.75 µg)	63.33%**	61.11%*

The actual amount (µg) of each alkane represented in the bioassay.

*Significant level for p is *p<0.05,**p<0.01,*** p<0.001, ****p<0.0001,***** p<0.00001.

Table 3: Attractiveness of individual and mixtures of synthetic alkanes mimicking the amount present in seed(s) surface waxes of *P. vulgaris* L. to *C. chinensis* choosing odour arm (%) in olfactometer bioassay (N = 90 in each bioassay).

Alkanes	Concentrations				
	0.5 seed equivalent	1 seed equivalent	2 seeds equivalent	4 seeds equivalent	6 seeds equivalent
n-C15 (a)	NR[a](0.141µg)[#]	56.67%(0.28165 µg)	62.22%* (0.564 µg)	64.44%*** (1.128 µg)	66.67%***(1.692 µg)
n-C16 (b)	NR (0.1615 µg)	NR (0.323 µg)	NR (0.646 µg)	55.56% (1.292 µg)	60%* (1.938 µg)
n-C20 (c)	NR (0.5665 µg)	NR (1.133 µg)	NR (2.266 µg)	NR (4.532 µg)	56.67% (6.798 µg)
n-C21 (d)	58.89% (1.16 µg)	63.33%** (2.32 µg)	64.44%** (4.64 µg)	67.78%*** (9.28 µg)	70%**** (13.92 µg)
n-C22 (e)	NR (0.3675 µg)	NR (0.735 µg)	56.67% (1.47 µg)	60%* (2.94 µg)	62.22%** (4.41 µg)
n-C24 (f)	NR (0.41 µg)	NR (0.82 µg)	NR (1.64 µg)	NR (3.28 µg)	61.11% *(4.92 µg)
n-C25 (g)	58.89.% (0.569 µg)	64.44%**(1.138 µg)	66.67%** (2.276 µg)	67.78%*** (4.552 µg)	70%**** (6.828 µg)
n-C31 (h)	NR (0.3935 µg)	NR (0.787 µg)	NR (1.574 µg)	55.56% (3.148 µg)	61.11% *(4.722 µg)
n-C32 (i)	NR (0.1465 µg)	NR (0.293 µg)	NR (0.586 µg)	63.33%** (1.172 µg)	67.78%***(1.758 µg)
[a+b+c+d+e+f+g+h+i]	60%	65.56%**	68.89%***	76.67%*****	80%*****

[a] NR= No response

[#] The actual amount (µg) of each alkane represented in the bioassay.

*Significant level for p is *p<0.05, **p<0.01, *** p<0.001, ****p<0.0001, ***** p<0.00001.

1.76 µg (67.78%; χ^2=11.38; df =1; P<0.001). Rest of the alkanes did not show attraction in the bioassays. A combination of nine alkane's mixture mimicking the amounts present in the seed surface waxes showed 65.56, 68.89, 76.67 and 80% attraction at 1 seed equivalent (χ^2=8.71; df =1; P<0.01), 2 seeds equivalent (χ^2=12.84; df =1; P<0.001), 4 seeds equivalent (χ^2=25.6; df =1; P<0.00001) and 6 seeds equivalent (χ^2=32.4; df =1; P<0.00001), respectively.

Alkanes are the most common component in plant and seed surface waxes. They have different roles in plant insect interactions such as attractants for feeding (Dutton *et al.*, 2000; Tasin *et al.*, 2005; Sarkar *et al.*, 2013a; Mukherjee *et al.*, 2013; Sarkar and Barik, 2014; Mitra *et al.*, 2019) or stimulants for oviposition (Eigenbrode and Espelie, 1995; Li and Ishikawa, 2006; Das *et al.*, 2019; Mitra *et al.*, 2020). A study by Parr *et al.* (1998) on chickpea seed surface wax showed that heptacosane (*n*-C_{27}) and nonacosane (*n*-C_{29}) were the most abundant *n*-alkanes. *n*-Alkanes with chain lengths from *n*-C_{15} to *n*-C_{32} were present in the surface waxes of khesari seeds among four variety. Further, *n*-C_{19} was the most predominant alkane in surface waxes of four varities of khesari seeds (Adhikary *et al.*, 2014). However in our study, *n*-C_{28} was the most predominant alkane in the surface waxes of rajma seeds.

The olfactory bioassay study provides evidence that the long-chain alkanes can act as close range attractant for *C.chinensis.* Different studies by previous authors demonstrated the importance of surface wax alkanes in different insects (Schiestl *et al.*, 1999; Tasin *et al.*, 2005; Roy and Barik, 2012; Mukherjee *et al.*, 2013; Sarkar *et al.*, 2013a; Adhikary *et al.*, 2014; Mitra *et al.*, 2020). Kotze *et al.* (2010) showed that alkanes from flowers of *Acacia cyclops* A. Cunn.ex G. Don are used by a gall midge, *Dasineura dielsi* Rübsaamen for finding its host. *Aulacophora foveicollis* Lucas females elicited attraction to a synthetic blend of *n*-C_{19}, *n*-C_{27} and *n*-C_{29} alkanes mimicking the amounts present in 6 mg surface wax alkanes of *Momordicacochin chinensis* Spreng flowers (Mukherjee *et al.*, 2013). Adhikary *et al.*, (2014) showed that a blend of *n*-C_{15}, *n*-C_{18}, *n*-C_{19}, *n*-C_{21}, *n*-C_{23} and *n*-C_{25} with the amount of 0.33, 0.20, 1.16, 0.94, 0.75 and 0.56 µg, respectively attracted the *C. maculatus*. *Aphis craccivora* females showed attraction towards a synthetic blend of pentadecane, octadecane, docosane, pentacosane, heptacosane, octacosane, nonacosane resembling the amounts present in the leaf surface waxes of BIO L 212 Ratan (BIO) and Nirmal B-1 (NIR) cultivars of *Lathyrus sativus* (Mitra *et al.*, 2020). In the present study, a clear positive attraction (P<0.01) of the insect was recorded at 0.5 seed equivalent surface wax alkanes from rajma seeds, but the highest attraction was recorded (P < 0.00001) at 6 seeds equivalent. In general, our results provide evidences that *C.chinensis*, is highly attracted towards 6 seeds equivalent surface wax alkane of rajma seeds and also a synthetic blend of alkane mixture produced same response (P<0.00001) as 6 seeds equivalent surface wax alkanes. We also identified the specific alkanes and their quantity in the surface wax of rajma seeds and suggest that a synthetic blend of nine alkanes (*n*-C_{15}, *n*-C_{16}, *n*-C_{20}, *n*-C_{21}, *n*-C_{22}, *n*-C_{24}, *n*-C_{25}, *n*-C_{31} and *n*-C_{32}) mimicking 6 seeds equivalent may be applied in lures to develop baited trap to control the outbreak of this insect. Different oviposition-deterrent and toxic effects of various botanicals like *Azadirachta indica, Milletiaie ferrnginea* and *Chrysanthemum cineraraefolium* oil had been already known (Mulatu and Gebremedhin, 2000) but no such compounds are available, which can be used as baited trap to control this insect pest. However, further experiment is needed to evaluate the response of the blend combined with those nine synthetic alkanes towards *C.chinensis* in storage condition.

ACKNOWLEDGEMENT

We are thankful to Prof Subir Chandra Dasgupta (HOD) and Principal of Maulana Azad College for providing laboratory facility in Ecology Laboratory at Maulana Azad College and DBT Star College Scheme for providing instrumental facilities. We are also grateful to Dr. Anandamay Barik, Professor, Department of Zoology, University of Burdwan for providing the facility to conduct the sample analyses.

REFERENCES

Adhikary, P., Mukherjee, A. and Barik, A. (2014). Role of surface wax alkanes from *Lathyrus sativus* L. seeds for attraction of *Callosobruchus maculatus* (F.) (*Coleoptera: Bruchidae*). Journal of Stored Products Research. 59: 113-119.

Baker, E.A. (1982). Chemistry and morphology of plant epicuticular waxes. In: *The Plant Cuticle*. Academic Press, London. pp. 139-165.

Barik, A., Bhattacharya, B., Laskar, S. and Banerjee, T.C. (2004). The determination of *n*-alkanes in the cuticular wax of leaves of *Ludwigia adscendens* L. Phytochemical Analysis. 15: 109-111.

Caswell, G.H. (1973). The impact of infestation on commodities. Tropical Stored Products Information. 19: 25.

Chakraborty, S. and Mondal, P. (2015). Studies on the biology of pulse beetle (*Callosobruchus chinensis* Linn.) infesting cowpea. International Journal of Current Research. 7: 23512-23515.

Das, S., Koner A. and Barik, A. (2019). A beetle biocontrol agent of rice-field weeds recognizes its host plants by surface wax long-chain alkanes and free fatty acids. Chemoecology. 29: 155-170.

Dutta, S.K., Chatterjee, D., Sarkar, D., Singh, S.B., Boopathi, T., Kuotsu, R., Vikramjeet, K., Akoijam, R.S., Saha, S., Vanlalhmangaiha, Malsawmzuali, Chowdhury, S. and Lungmuana (2016). Common bean (*Phaseolus vulgaris* L., Fabaceae), landraces of Lushai hills in India: Nutrients and antioxidants source for the farmers. Indian Journal of Traditional Knowledge. 15: 313-320.

Dutton, A., Mattiacci, L. and Dorn, S. (2000). Plant-derived semiochemicals as contact host location stimuli for a parasitoid of leaf miners. Journal of Chemical Ecology. 26: 2259-2273.

Eigenbrode, S.D. and Espelie, K.E. (1995). Effects of plant epicuticular lipids on insect herbivores. Annual Review of Entomology. 40: 171-194.

Gepts, P. (1990). Biochemical evidence bearing on the domestication of Phaseolus (Fabaceae) beans. Economic botany. 44: 28-38.

Jetter, R., Schäffer, S. and Riederer, M. (2000). Leaf cuticular waxes are arranged in chemically and mechanically distinct layers: evidence from *Prunus laurocerasus* L. Plant, Cell and Environment. 23: 619-628.

Koschier, E.H., Kogel, W.J.D. and Visser, J.H. (2000). Assessing the attractiveness of volatile plant compounds to western flower thrips *Frankliniella occidentalis*. Journal of Chemical Ecology. 26: 2643-2655.

Kotze, M.J., Jürgens, A., Johnson, S.D. and Hoffmann, J.H. (2010). Volatiles associated with different flower stages and leaves of *Acacia cyclops* and their potential role as host attractants for *Dasineura dielsi* (Diptera: Cecidomyiidae). South African Journal of Botany. 76: 701-709.

Li, G. and Ishikawa, Y. (2006). Leaf epicuticular wax chemicals of the Japanese knotweed *Fallopia japonica* as ovipositional stimulants for *Ostrinia latipennis*. Journal of Chemical Ecology. 32: 595-604.

Marwein, Y. and Ray, L.I.P. (2019). Performance of rajma (*Phaseolus vulgaris*) cultivars under organic mulches in Meghalayan Plateau of North Eastern India. Legume Research-An International Journal. 42: 114-118.

Mitra, P., Mobarak, S.H., Debnath, R. and Barik, A. (2019). The role of *Lathyrus sativus* flower surface wax in short-range attraction and stimulant for nymph laying by an adult viviparous aphid. Bulletin of Entomological Research. 110: 231-241.

Mitra, P., Das S. and Barik, A. (2020). Leaf waxes from *Lathyrus sativus*: short×range attractant and stimulant for nymph laying in a viviparous insect. Chemoecology. 30: 117-129.

Mukherjee, A., Sarkar, N. and Barik, A. (2013). Alkanes in flower surface waxes of *Momordica cochinchinensis* influence attraction of *Aulacophora foveicollis* Lucas (Coleoptera: Chrysomelidae). Neotropical Entomology. 42: 366-371.

Mukherjee, A., Sarkar, N. and Barik, A. (2014). Long-chain free fatty acids from *Momordica cochinchinensis* leaves as attractants to its insect pest, *Aulacophora foveicollis* Lucas (*Coleoptera: Chrysomelidae*). Journal of Asia-Pacific Entomology. 17: 229-234.

Mulatu, B. and Gebremedhin, T. (2000). Oviposition-deterrent and toxic effects of various botanicals on the adzuki bean beetle, *Callosobruchus chinensis* L. International Journal of Tropical Insect Science. 20: 33-38.

Nawrot, J., Gawlak, M., Szafranek, J., Szafranek, B., Synak, E., Warchalewski, J.R., Piasecka-Kwiatkowska, D., Błaszczak, W., Jelinski, T. and Fornal, J. (2010). The effect of wheat grain composition, cuticular lipids and kernel surface microstructure on feeding, egg-laying and the development of the granary weevil, *Sitophilus granarius* (L.). Journal of Stored Products Research. 46: 133-141.

Nietupski, M., Szafranek, B., Ciepielewska, D., Synak, E., Fornal, Ł. and Szafranek, J. (2005). Correlation between bean seed surface lipids and *Acanthoscelides obtectus* Say development. Journal of Plant Protection Research. 45: 125-133.

Parr, M.J., Tran, B.M.D., Simmonds, M.S.J., Kite, G.C. and Credl, P.F. (1998). Influence of some fatty acids on oviposition by the bruchid beetle, *Callosobruchus maculatus*. Journal of Chemical Ecology. 24: 1577-1593.

Rawal, V. and Navarro, D.K. (2019). The Global Economy of Pulses. FAO, Rome, Italy. pp. 41.

Roy, N. and Barik, A. (2012). Alkanes used for host recognition by the arctiid moth, *Diacrisiaca signetum* Kollar. Journal of the Entomological Research. 36: 345-350.

Roy, N., Laskar, S. and Barik, A. (2012a). Determination of *n*-alkane profile through developmental state of sunflower leaves. The South Pacific Journal of Natural Science. 30: 72-76.

Roy, N., Laskar, S. and Barik, A. (2012b). The attractiveness of odorous esterified fatty acids to the potential biocontrol agent, *Altica cyanea*. Journal of Asia-Pacific Entomology. 15: 277-282.

Sarkar, N. and Barik, A. (2014). Alkanes from bitter gourd as allelochemicals in olfactory responses of *Epilachna dodecastigma* (Wied.). Allelopathy Journal. 33: 43-51.

Sarkar, N., Mukherjee, A. and Barik, A. (2013a). Long-chain alkanes: allelochemicals for host location by the insect pest, *Epilachna dodecastigma* (*Coleoptera: Coccinellidae*). Applied Entomology and Zoology. 48: 171-179.

Sarkar, N., Mukherjee, A. and Barik, A. (2013b). Olfactory responses of *Epilachna dodecastigma* (*Coleoptera: Coccinellidae)* to long-chain fatty acids from *Momordica charantia* leaves. Arthropod Plant Interaction. 7: 339-348.

Schiestl, F.P., Ayasse, M., Paulus, H.F., Löfstedt, C., Hansson, B.S., Ibarra, F. and Francke, W. (1999). Orchid pollination by sexual swindle. Nature. 399: 421-422.

Shao, S., Meyer, C.J., Ma, F., Peterson, C.A. and Bernards, M.A. (2007). The outermost cuticle of soybean seeds: chemical composition and function during imbibition. Journal of Experimental Botany. 58: 1071-1082.

Sokal, R.R. and Rohlf, F.J. (1995). Biometry: the Principles and Practice of Statistics in Biological Research, 3rd Edn. WH Freeman, New York.

Srinivasan, R., Uthamasamy, S. and Talekar, N.S. (2006). Characterization of oviposition attractants of *Helicoverpa armigera* in two solanaceous plants, *Solanum viarum* and *Lycopersicon esculentum*. Current Science. 90: 846-850.

Tasin, M., Anfora, G., Ioriatti, C., Carlin, S., De Cristofaro, A., Schmidt, S., Bengtsson, M., Versini, G. and Witzgall, P. (2005). Antennal and behavioural responses of grapevine moth *Lobesis botrana* females to volatiles from grapevine. Journal of Chemical Ecology. 31: 77-87.

Toro, O., Tohme, J. and Debouck, D. G. (1990). Wild bean (*Phaseolus vulgaris* L.): description and distribution. Centro Internacional de Agricultura Tropical, Cali, Colombia. pp.106.

Ueno, T., Kuwahara, Y., Fujii, K., Taper, M.L., Toquenaga, Y. and Suzuki, T. (1990). D-Catechin: An oviposition stimulant of azuki bean weevil *Callosobruchus chinensis* in the Host Azuki Bean. Journal of Pesticide Science. 15: 573-578.

United Nations Environment Programme (1998). Montreal Protocol on Substances that Deplete the Ozone Layer, 1998: Assessment of Alternatives to Methyl Bromide. Methyl Bromide Alternatives Committee, Nairobi, Kenya.

Avens Publishing Group
J Toxins
August 2019 Volume 5, Issue 1

Open Access Research Article

Journal of Toxins

Effect of Aqueous Extract of *Naja naja Sp.* Shedded Skin in Pregnant Female Rats and its Role on the Growth and Development in the Pups

Mukherjee S[1], Gomes A[2] and Das Gupta SC[1*]

[1]*Department of Zoology Maulana Azad College, Rafi Ahmed Kidwai Road, India*
[2]*Laboratory of Toxinology & Experimental Pharmacodynamics, Deptartment of Physiology, Calcutta University, India*

***Address for Correspondence**
Das Gupta SC, Department of Zoology Maulana Azad College, 8, Rafi Ahmed Kidwai Road, Kolkata 700013, India, Tel: 91-33-2226 0995; Fax-91-33--2226-0995; Mobile: + 91-9830471981; E-mail: subirdgupta@gmail.com

Submission: 27 May, 2019
Accepted: 31 July, 2019
Published: 03 August, 2019

Keywords: Pregnancy; Prenatal toxicity; Snake shed skin; SSS

Abstract

Snake shed skins are widely used in the folk and traditional medicine of various cultures since ancient time. In ancient Chinese and Levantine medicinal system snake shed skin is used in the treatment of several diseases viz. glaucoma, hernia, psoriasis etc. Indian traditional and folk medicinal system make use of the ash of snake shed skin for inducing labour in pregnant women, which lacks scientific validation. Mukherjee et al., 2013 reported that *N. naja* shedded skin caused temporary cessation of the estrous cycle. However no scientific evidence is present regarding its role on pregnant animals. Thus, the present study was commenced for scientifically validating the role of *Naja naja* shed skin aqueous extract on the pregnant rats.

In the present study, SSS altered the urinary volume, calcium, magnesium levels, as well as altered the urinary creatinine output. SSS also altered serum 17-β estradiol level, progesterone and C-reactive protein level. In a dose-dependent manner, SSS exposure towards pregnant mother retarded the growth and development in the pups. At the highest dose SSS lead to fetal resorption. The present study for the first reports the prenatal toxicity and teratogenicity of SSS.

Abbreviations

b.w: Body Weight; P4: Progesterone; s.c: subcutaneous; SSS: *Naja naja* Shedded Skin aqueous extract; SSS(1): *Naja naja* Shedded Skin aqueous extract 1 $mg.kg^{-1}$ b.w.; SSS(10): *Naja naja* Shedded Skin aqueous extract 10 $mg.kg^{-1}$ b.w.; SSS(5): *Naja naja* Shedded Skin aqueous extract 5 $mg.kg^{-1}$ b.w.

Introduction

Snake and its body parts, are studied extensively in the folk and traditional medicine of various cultures, since primeval time for therapeutic benefits [1-3]. Evidences based studies in Chinese and Levantine medicinal system revealed the use of snake shed skin for treatment of several diseases. In the Indian traditional medicine, snake shed skin is used for labour induction in pregnant women [4]. Though largely used by traditional naturopaths for treating various female reproductive disorders, there is no scientific evidence regarding the bioactivity of the snake shed skin on female reproductive system.

Reported for the first time the role of aqueous *Naja naja* shed skin extract on the estrous cycle of female mice [4]. The *Naja naja* shedded skin aqueous extract caused cessation of the estrous cycle for 10 days by altering hormone (LH, FSH, 17-β estradiol, progesterone) and cytokine (IL-1β, TNF-α, IL-12) profiles. Although the role of the aqueous extract on the estrous cycle of mice are quite extensively studied, but its role on the pregnant female rats remains vague. Therefore, the present study is embarked to evaluate the role of *Naja naja* shed skin aqueous extract on pregnant female rats, and subsequently its effect on pups.

Materials and Methods

Chemicals and reagents

The following kits were use for the present study: Calcium, creatinine, magnesium were purchase from Ecoline Merck (India). 17-β Estradiol (E_2), progesterone (P_4), C-Reactive Protein (CRP) Elisa kits were purchase from Cusabio (China).

Collection of *N. naja* shedded skin- Fresh *Naja naja* shedded skins of both sexes was collected from North 24-Parganas, West Bengal, India through field collection as per the permission granted by the Ministry of Forests & Wild Life, Govt. of West Bengal, India (2105/ WL/4R-1 (PI-IX)) and identified by the Zoological Survey of India. The shedded skins were store in desiccator at room temperature and later subjected to aqueous extraction.

Animals and experimental design

Sexually matured male and female Wistar rats were purchase from the enlisted supplier of Maulana Azad College, Kolkata. During breeding and until gestation day, rats were housed in polypropylene cages at 22±3 °C; relative air humidity 45 to 55% with 12.00 h light & dark cycle and provided with standard diet and tap water ad libitum. The rats were acclimatized for one week in the laboratory conditions, before being used in the experiment. Virgin female rats (approximately120-130 g) were bred overnight with untreated adult males of the same strain (one male: two females) [5]. The day on which sperm were visualized in the vaginal smear was designated 0 day pregnant. Sperm positive females were randomly assigned to test groups according to their day 0 of gestation. All experimental protocols described in the present study are approved by institutional animal ethics committee (CPCSEA), Govt. of India (Institutional Sanction No: 25/ 250/ 2012 - AWD).

Preparation of aqueous extract of *Naja naja* Shed Skin (SSS) and protein estimation

ISSN: 2328-1723

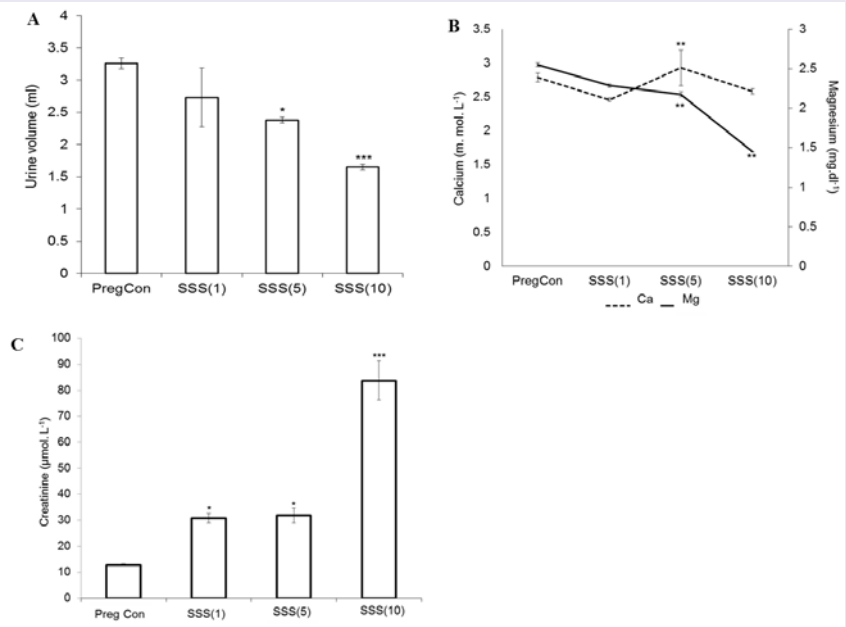

Figure 1: Effect of SSS on urinary biochemical markers.
0 day pregnant rats were treated with SSS(1) (1 mg.kg-1 body weight, X 10 days, s.c), SSS(5) (5 mg.kg-1 body weight, X 10 days, s.c) and SSS(10) (10 mg.kg-1 body weight, X 10 days, s.c) . (A) SSS(1) did not produce significant change in the urinary volumes on day 20 of gestation in pregnant rat as compared with pregnant control rat. SSS(5) and SSS(10) produced significant decrease in the urinary volumes on day 20 of gestation in pregnant rat as compared with pregnant control rat.
(B) SSS(1) did not produce significant change in the urinary calcium and magnesium level on day 20 of gestation as compared with control pregnant rat. SSS(5) produced significant increase in urinary calcium on day 20 of gestation but SSS(10) did not produced significant change in urinary calcium as compared with control pregnant rat. SSS(5) and SSS(10) produced significant decrease in urinary magnesium on day 20 of gestation as compared with control pregnant.
(C) SSS(1) SSS(5) and SSS(10) produced significant increase in the urinary creatinine on day 20 of gestation in pregnant rat as compared with control pregnant rat Values were represented as mean±SEM (n=4).*P< 0.05, ***P< 0.001,*** P< 0.001 (Significant).

Freshly powdered *Naja naja* shedded skin was soaked in physiological mammalian saline overnight at 4 °C. It was strained, and centrifuged at 5000 rpm at 4 °C for 20 min. Supernatant was collected and expressed in terms of protein content [6]. The supernatant was used for the experimental study.

Treatment regime- For study with aqueous extract of snake shed skin extract (SSS) and control animals were randomized into 4 groups (n=4): Control pregnant, SSS(1) (1 $mg.kg^{-1}$ b.w.) , SSS(5) (5 $mg.kg^{-1}$ b.w.) and SSS(10) (10 $mg.kg^{-1}$ b.w.). SSS(1), SSS(5) and SSS(10) were administered sub cutaneously (s.c.) from day 0 to day 9 of gestation (total of 10 exposure).

Effect of SSS on urinary biochemical markers- Urine was collected on day 20 (final trimester), urinary volume was measured, calcium, magnesium, creatinine were assayed.

Effect of SSS on serum biochemical markers- On day 21 blood was collected from retro-orbital plexus of the rats, and the serum was separated. From the serum; hormones (E_2, P_4), and inflammatory marker (CRP) were assayed by Elisa (Biotek, USA; Model No. EL×800 MS) according to the manufacturers protocols. The concentration of these hormones and CRP were calculated from their respective standard curves.

Biomorphometry of pups- Gestational period of the pregnant female rats were monitored after prenatal exposure of SSS (1,5&10 $mg.kg^{-1}$ body weight X 10 exposure, s.c.) in pregnant rat. Following gestational period and the birth of pups, the bio-morphometric features (body weight, head length, head diameter, neck width and tail length) were monitored and measured every 5 days interval (using digital calliper Mitutoyo, Japan), until the weaning period (21 days) is completed.

Statistical analysis- Statistical analysis was done by Graph Pad InStat software (La Jolla, CA, USA). Data were expressed as mean±SEM (n=4) unless otherwise mentioned. The differences between the treated and untreated control group were analyzed by one-way ANOVA and post-test was done using Tukey's multiple comparison tests to determine the significant levels. *p<0.05, **p<0.01, ***p<0.001 were considered significant.

Results

The protein content of *Naja naja* aqueous extract (SSS) was found to be 6±1 $mg.ml^{-1}$.

Effect of SSS on urinary biochemical markers

SSS(1) treatment did not produced significant change in the urinary volume on day 20 of gestation as compared with pregnant control rat. SSS(5) and SSS(10) treatment produced significant decrease in the urinary volume on day 20 of gestation as compared with pregnant control rat (Figure 1a). SSS(1) treatment did not produce significant change in urinary calcium level on day 20 of gestation as compared with pregnant control rat. SSS(5) treatment produced significant increase in the urinary calcium level on day 20 of gestation as compared with pregnant control rat. SSS(10) did

ISSN: 2328-1723

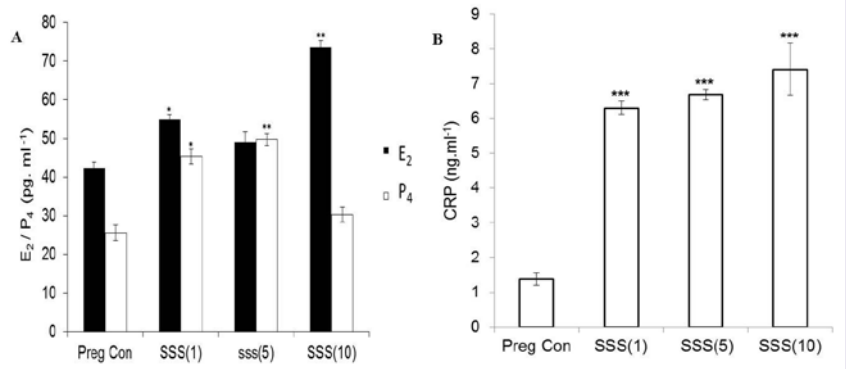

Figure 2: Effect of SSS on serum biochemical markers.
0 day pregnant rats were treated with SSS(1) (1 mg.kg-1 body weight, X 10 days, s.c), SSS(5) (5 mg.kg-1 body weight, X 10 days, s.c) and SSS(10) (10 mg.kg-1 body weight, X 10 days, s.c) . (A) SSS(1) produced significant increase in serum E2 and P4 on day 21 of gestation as compared with control pregnant rat. SSS(5) did not produce significant change in serum E2 and produced significant increase in serum P4 on day 21 of gestation as compared with pregnant control rat. SSS(10) produced significant increase in serum E2 level and did not produced significant change in serum P4 on day 21 of gestation as compared with control pregnant rat.
(B) SSS(1), SSS(5) and SSS(10) produced significant increase in serum CRP on day 21 of gestation as compared with control pregnant rat.
Values were represented as mean±SEM (n=4).*P< 0.05, ***P< 0.001,*** P< 0.001 (Significant).

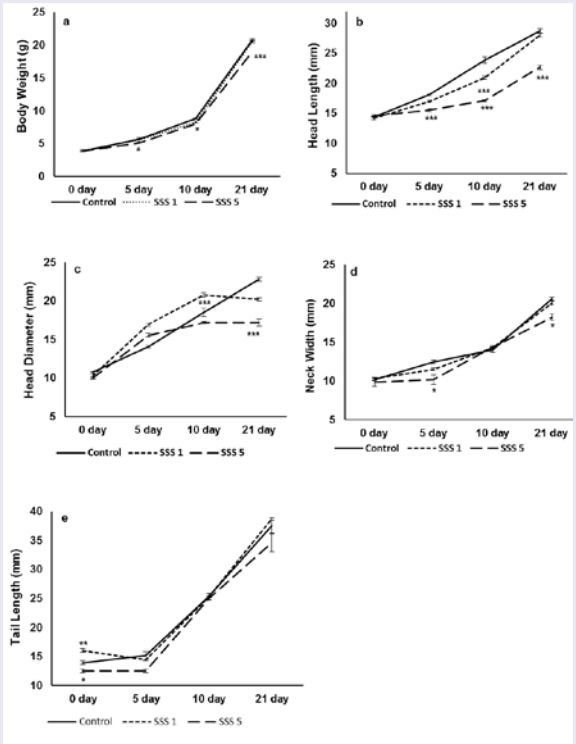

Figure 3: Effect of SSS on the biomorphometric parameters of pups.
0 day pregnant rats were treated with SSS(1) (1 mg.kg-1 body weight, X 10 days, s.c), SSS(5) (5 mg.kg-1 body weight, X 10 days, s.c) and SSS(10) (10 mg.kg-1 body weight, X 10 days, s.c) . a: body weight in g; b: head length in mm, c: head diameter in mm, c: neck width in mm, d: tail length in mm.
Values were represented as mean±SEM (n=7).*P< 0.05, ***P< 0.001,*** P< 0.001 (Significant).

not produce significant change in the urinary calcium level on day 20 of gestation as compared with pregnant control rat (Figure 1b). SSS(1) treatment did not produce significant change in the urinary magnesium level on day 20 of gestation as compared with pregnant control rat. SSS(5) and SSS(10) treatment produced significant decrease in urinary magnesium level on day 20 of gestation as compared with pregnant control rat (Figure 1b). SSS(1), SSS(5) and SSS(10) treatment produced significant increase in the urinary creatinine level on day 20 of gestation as compared with pregnant control rat (Figure 1c).

Effect of SSS on serum biochemical markers- SSS (1) treatment produced significant increase in the serum E2 level on day 21 of gestation as compared with pregnant control rat. SSS(5) treatment did not produce significant change in serum E2 level on day 21 of

ISSN: 2328-1723

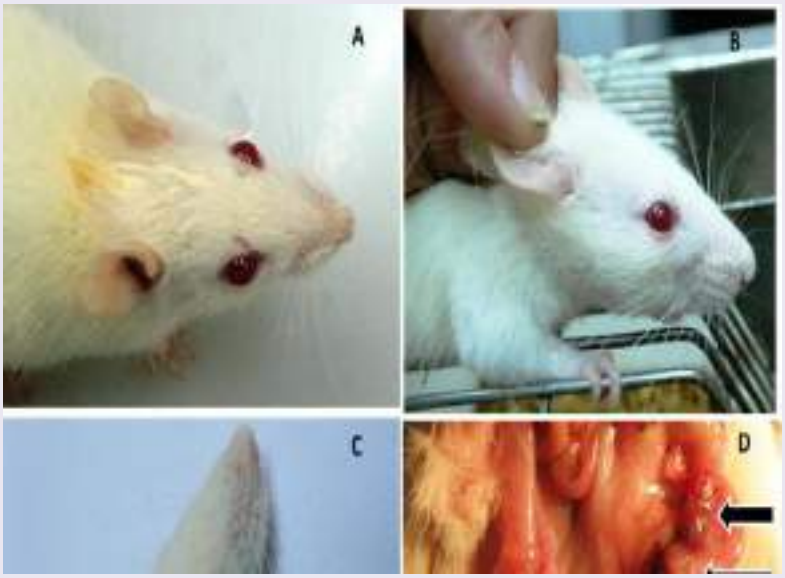

Figure 4: Effect of SSS treatment on pregnant femats and its consequence on the pups.
0 day pregnant rats were treated with SSS(1) (1 mg.kg-1 body weight, X 10 days, s.c), SSS(5) (5 mg.kg-1 body weight, X 10 days, s.c) and SSS(10) (10 mg.kg-1 body weight, X 10 days, s.c) . (A) Control Pups: showed normal development including no impairment in eye (B) SSS(1) treated pups: showed normal development including no impairment in eye, (C) SSS(5) treated pups showed: developmental toxicity as is evident improper development of the eye. (D) a. SSS(10) caused fetal resorption. SSS(10) treated pregnant rats showed sites of implantation sites even on 30 post gestation days. Data shown here were from one of the four repeated experiment showing similar results.

gestation as compared with pregnant control. SSS(10) treatment produced significant increase in serum E2 level on day 21 of gestation as compared with pregnant control rat (Figure 2a). SSS(1) and SSS(5) treatment produced significant increase in serum P4 level on day 21 of gestation as compared with pregnant control rat. SSS(10) treatment did not produce significant change serum P4 level on day 21 of gestation as compared with pregnant control (Figure 2a). SSS(1), SSS(5) and SSS(10)treatment produced significant increase in of serum C-reactive protein (CRP) level on day 21 of gestation as compared with pregnant control rat (Figure 2b).

Effect of SSS on biomorphometry and physiological parameters of the pups- SSS(1) treatment did not produce significant change in body weight, head diameter, neck width and tail length of the pups on day 0 up to day 21 as compared with control pups. SSS(1) treatment produced significant decrease in the head length of the pups on day 5, on day 10 which returned to control level as compared with control pups. (Figure 3a and 3b).

SSS(5) treatment caused growth impairment in the pups. It led to malformation in the head region. The eyes were not well developed (Figure 4c), but no malformation was observed in the four digits in the front and hind limb. SSS(5) treatment did not produce significant change in body weight from day 0 to day 15, but it significantly decreased on day 21 as compared with control pups (Figure 3a). SSS(5) treatment produced significant decrease in the head length on day 0 up to day 21 as compared with control pups (Figure 3b). SSS(5) treatment did not produce significant change in head diameter observed on day 0 to day 15, but significantly decreased on day 21 as compared with control pups (Figure 3c). SSS(5) treatment did not produce significant change in neck width from day 0 to day 15, but significantly decreased on day 21 as compared with control pups (Figure 3d). SSS(5) treatment did not produced significant change in tail length on day 0 to day 21 as compared with control pups (Figure 3e).

SSS(10) treatment caused fetal resorption, and absence of birth of new born pups as was evident from the sites of implantation upon examination of the uterus. (Figure 4d).

Discussion

The present study was designed to evaluate the role of *Naja naja* shed skin aqueous extract on pregnant female rats. In the present study, SSS decreased urinary volume in a dose dependent manner. SSS(5) increased urinary calcium output, SSS(5) and SSS(10) decreased urinary magnesium and increased urinary creatinine output. During normal pregnancy, urinary volume is increased at second and third trimester which is mediated by angiotensin-(1-7) [7]. This is associated with increased water intake, decreased plasma vasopressin and down regulation of kidney Aquaporin 1 (AQP1) [8]. Mineral metabolism is regulated by the demand of the fetus and placenta, which together pulled calcium and other minerals from the maternal circulation for the growth, development and various enzymatic reactions across feto-placental barriers [9,10]. During pregnancy creatinine acted as one of the most important indices for muscle mass loss [11]. From the above result it can be concluded that SSS altered normal mineral status as well as water balance indicating it altered normal pregnancy condition (Figure 1a-1d).

Pregnancy remained under the influence of two major steroidal hormones; estrogen and progesterone. Progesterone was mainly required for maintaining the quiescent endometrium preventing preterm delivery. Just prior to labour there was increase in the level of estrogen 100-1000 folds and in turn shifted the uterus from quiescent

ISSN: 2328-1723

to rhythmically contractile state. In the present study SSS(1) and SSS(5) treatment produced significant rise in 17-β estradiol and decreased progesterone as compared with pregnant control rat [12]. SSS(10) treatment showed decrease in estradiol and an increase in progesterone due to fetal resorption (Figure 2a). Serum C-reactive protein is a major acute phase inflammatory protein. During normal pregnancy, an increase in the level C-reactive protein in labour indicated muscle damage and tearing associated with parturition, but a very high and elevated level was associated with preterm delivery, fetal growth restriction and preeclamsia [13,14]. SSS(1) and SSS(5) treatment produced dose dependent increase in the C-Reactive Protein (CRP) at term as compared with pregnant control supported that SSS had activated the inflammatory pathway associated with parturition. SSS(10) treatment caused a further increase in CRP due to fetal resorption where membrane damage was more pronounced.

In the pups SSS(1) did not produce significant change in body weight, head diameter, neck width and tail length but decreased head length; and SSS(5) decreased body weight, head diameter, neck width and head length of the pups. In the SSS(5) treated pups, the eyes were not developed indicating that SSS had passed feto-placental barrier, caused growth restriction and hampered the developmental process. SSS(10) due to feto-placental passage caused fetal resorption by recruiting the inflammatory markers [15,16].

The above study reflected that SSS is associated with reproductive toxicity in pregnant rat associated with developmental toxicity and teratogenic effect.

References

1. Costa-Neto EM (2005) Animal-based medicines: biological prospection and the sustainable use of zootherapeutic resources. An Acad Bras Cienc 77: 33-43.
2. Soewu DA (2008) Wild animals in ethnozoological practices among the Yorubas of southwestern Nigeria and the implications for biodiversity conservation. Afr J Agric Res 6: 421-427.
3. Lev E (2003) Traditional healing with animals (zootherapy): medieval to present-day Levantine practice. J Ethnopharmacol 85: 107-118.
4. Mukherjee S, Dasgupta SC, Gomes A (2013) Effect of *Naja naja* Laurenti shed skin extract on estrous cycle, hormone - cytokine profiles, histopathology of ovary and uterus of Swiss albino mice. Indian J Exp Biol 51: 235-240.
5. Hellwig J, Liberacki AB (1997) Evaluation of the pre-, peri-, and postnatal toxicity of monoethanolamine in rats following repeated oral administration during organogenesis. Fundam Appl Toxicol 40: 158-162.
6. Lowry OH, Rosebrough NJ, Farr AL, Randall RJ (1951) Protein measurement with the Folin phenol reagent. J Biol Chem 193: 265-275.
7. Lubrano Rosales A, Chesa Ponce N (1999) Study of urinary outflow in pregnancy. Actas Urol Esp 23: 763-768.
8. Joyner J, Neves LA, Stovall K, Ferrario CM, Brosnihan KB (2008) Angiotensin-(1-7) serves as an aquaretic by increasing water intake and diuresis in association with downregulation of aquaporin-1 during pregnancy in rats. Am J Physiol Regul Integr Comp Physiol 294: R1073-R1080.
9. Kovacs CS, Gel-H F (2006) Calcium and bone disorders during pregnancy and lactation. Endocrinol Metab Clin North Am 35: 21-51.
10. Kovacs CS (2013) Bone metabolism in the fetus and neonate. Pediatr Nephrol 29: 793-803.
11. Phillips DI (1995) Relation of fetal growth to adult muscle mass and glucose tolerance. Diabet Med 12: 686-690.
12. Hendrick V, Altshuler LL, Suri R (1998) Hormonal changes in the postpartum and implications for postpartum depression. Psychosomatics 39: 93-101.
13. Ernst GD, de Jonge LL, Hofman A, Lindemans J, Russcher H, et al. (2011) C-reactive protein levels in early pregnancy, fetal growth patterns, and the risk for neonatal complications: the Generation R Study. Am J Obstet Gynecol 205: 132.e1-e12.
14. van den Hooven EH, de Kluizenaar Y, Pierik FH, Hofman A, van Ratingen SW, et al. (2012) Chronic air pollution exposure during pregnancy and maternal and fetal C-reactive protein levels: the Generation R Study. Environ Health Perspect 120: 746-751.
15. Konopka CK, Morais EN, Naidon D, Pereira AM, Rubin MA, et al. (2013) Maternal serum progesterone, estradiol and estriol levels in successful dinoprostone-induced labor. Braz J Med Biol Res 46: 91-97.
16. Kovacs CS, Kronenberg HM (1997) Maternal-fetal calcium and bone metabolism during pregnancy, puerperium, and lactation. Endocr Rev 18: 832-872.

Acknowledgement

We thankfully acknowledge University Grant Commission, New Delhi, India for partial financial assistance (Ref No: F 38-130 (SR), dated 19.12.2009 and we are thankful to the Dept. of Forests & Wild Life, Govt. of West Bengal, India (2105/WL/4R-1(PI- IX)) for kind permission of collection of the shed snake skin.

Proc Zool Soc
https://doi.org/10.1007/s12595-019-00296-4

RESEARCH ARTICLE

Study of Microglial and Astroglial Alterations Induced by Acute 1-Methyl-4-Phenyl-1,2,3,6-Tetrahydropyridine Treatment in Mouse Brain

Nabanita Ghosh[3] · Soham Mitra[1] · Priyobrata Sinha[2] · Nilkanta Chakrabarti[2] · Arindam Bhattacharyya[1]

Received: 23 December 2017 / Revised: 13 May 2019 / Accepted: 22 May 2019

Abstract The precise mechanism(s) of Parkinson's disease, a progressive neurodegenerative disorder affecting a large number of people worldwide, is far from clearly understood. For disease induction in mouse model, 1-methyl-4-phenyl-1,2,3,6-tetrahydropyridine (MPTP) is used that specifically destroys those neurons of basal ganglia and the substantia nigra that are involved in Parkinsonism. However, the effect of MPTP treatment on glial cells that play significant role in maintaining brain homeostasis remains unexplored. In view of this, the present study was designed to investigate the status of microglia and astrocytes in substantia nigra as well as in hippocampus, the region related to memory processing and cognition, in mouse brain upon MPTP administration. We examined the neuropathological alterations in hippocampus and substantia nigra upon MPTP administration by using western blot, quantitatitative PCR, immunohistochemistry and immunofluorescence. Subcutaneous administration of MPTP in Swiss mice resulted in degeneration of nigrostriatal dopaminergic neurons. In addition, there was marked microglial activation and neuroinflammation in both the substantia nigra and the hippocampus. Astrocytes also showed activation at early phase (day 1 post treatment), but it was substantially reduced in substantia nigra at day 3 post treatment. However, the number of astrocytes remained reduced in the hippocampus throughout the post-treatment period. Consistent microglial activation and neuroinflammation with gradual decline in the number of astrocytes in both substantia nigra and hippocampus appear causally associated with MPTP-induced progressive degeneration of mouse brain.

Keywords MPTP · Substantia nigra · Hippocampus · Microglia · Astrocytes

Introduction

Parkinson's disease (PD), one of the most commonly occurring age related progressive neurodegenerative disorders, is characterized by dopaminergic (DA) neurodegeneration in substantia nigra pars compacta (SNpc) and dopamine depletion in striatum, cytoplasmic inclusions of aggregated proteins [Lewy bodies (LBs)], and chronic neuroinflammation (McGeer and McGeer 2008). Neuroinflammation may not be the primary trigger for neurodegeneration, but, with reference to epidemiological and preclinical data of PD, chronic neuroinflammation may be referred to as the "silent driver" of neuronal dysfunction and death during disease progression. Microglia and astrocytes are identified as glial cell populations of the central nervous system (Huang et al. 2017). Microglia constitute 5–20% of total population of glial cells in the rodent brain. The basal ganglia and SN are reported to have the highest population of microglia (Lawson et al. 1990). They are the primary cells to respond to infection and injury, as the resident macrophages in the central nervous system (CNS) (Saijo and Glass 2011; Kettenmann et al. 2011; Suzumura 2013). Microglia when activated produce

✉ Arindam Bhattacharyya
arindam19@yahoo.com

1 Immunology Lab, Department of Zoology, University of Calcutta, 35, Ballygunge Circular Road, Kolkata 700019, India

2 Department of Physiology, University of Calcutta, 92, Acharya Prafulla Chandra Road, Kolkata 700009, India

3 Department of Zoology, Maulana Azad College, 8, Rafi Ahmed Kidwai Road, Kolkata 700013, India

many proinflammatory factors (cytokines, chemokines, reactive oxygen species etc.) that promote neurodegeneration (Saijo and Glass 2011). Reactive microglia were identified in the SNpc of postmortem human brain suggesting its involvement in neuroinflammation during PD (McGeer et al. 1988; Wang et al. 2015). Microglial activation, characterized by an increase in the number of CD11b expression (Liu et al. 2015), was observed in the striatum and the SN 12 h after acute MPTP treatment (Furuya et al. 2004; L'Episcopo et al. 2012). Compared to microglia, astrocytes are the most abundant glial cells in the adult brain (Lee et al. 2009). It plays crucial role in maintaining brain homeostasis by forming the blood brain barrier, restoring water ion homeostasis, secreting neurotrophins required for neuronal health (Kimelberg and Nedergaard 2010). In response to inflammatory stimuli, astrocytes are reported to produce an array of pro- and anti-inflammatory mediators, antioxidants, and neurotrophic factors. Astrocytes are reported to promote the dopaminergic neuron survival and maintenance by secreting various neurotrophic factors in the SN (Huang et al. 2017). Astrocytic activation is characterized by increase in number of Glial fibrillary acidic protein (GFAP) positive astrocytes. Reactive astrogliosis has been observed in striatum and SN of patients with PD (Yamada et al. 1992; Langston et al. 1999). However, their behavior and activation status are altered under acute, subacute and chronic stress in different regions of brain. In experimental subacute MPTP induced PD in mice model, the striatal GFAP level was found to increase by 3.7-fold at 3 days after MPTP administration (Yu et al. 2013). Reactive astrogliosis is one of the major causes of neurodegeneration during chronic neuroinflammation (Huang et al. 2017). Nevertheless, condition of astrocyte in brain during acute MPTP administration is not clear till date.

Hippocampus, another important part of the brain, has been at the forefront of research related to the neurobiology of memory. Moreover, the discovery of place cells, head direction cells, and grid cells in the rodent hippocampal formation has brought forward that hippocampus plays a pivotal role in the various sensory, emotional, and cognitive components of brain (Knierim. 2015). Not only that, hippocampus is also a home of neural stem cells in an adult brain (Kempermann et al. 2015). Since in PD, besides motor dysfunctions, nonmotor symptoms (NMS) also appear in the early, often premotor, phase of the disease, (Watson and Leverenz 2010), the condition of hippocampus during PD is a topic of major concern. The status of glial cells, both microglia and astrocytes in hippocampus during PD remains elusive till date. The main objective of this study is to investigate the activation status of microglia and astrocytes in hippocampus and SN upon acute MPTP administration that represents acute phase of PD.

Materials and Methods

Materials and Reagents

MPTP-HCl was procured from Sigma (St Louis, MO, USA). Primary antibodies anti-GFAP (3670S), anti-tyrosine hydroxylase (2792S) and anti-beta actin (4967S) were procured from Cell Signaling Technologies and secondary antibodies HRP conjugated anti-mouse secondary (SKU:HPO6) and anti-rabbit secondary (SKU:HPO3) were purchased from Genei (Bangalore, India). FITC conjugated rat anti-mouse CD11b antibody (553310) was purchased from BD Biosciences (India). Immunohistochemistry kit was procured from Genei (Bangalore, India). All additional chemicals used were of highest experimental grade available.

Animals

Male Swiss albino mice, 3–4 months of age, weighing approximately 25–35 g, were procured from NIN, Hyderabad. They were acclimatized under laboratory conditions for 2 weeks before commencement of the experiments. Three mice were kept per cage to avoid overcrowding. The animals were maintained in a standard diet, water *ad libitum* and were subjected to 12 h light and dark cycles. This work has approval from Animal Ethical Committee, Department of Zoology, University of Calcutta (Registration Number of CPCSEA—885/GO/Re/S/05/CPCSEA).

MPTP Administration Protocol and Establishment of Disease Model

Mice were randomly divided into different groups (each group containing 5 mice) comprising (A) vehicle (0.9% normal saline) treated control and (B) MPTP-treated set. MPTP-HCl was dissolved in the vehicle (0.9% normal saline) and administered at a dose of 18 mg/kg b.w. (Jackson-Lewis and Przedborski 2007). Two sets of MPTP treated mice (n = 5 each) were taken for time dependent sacrifice. The MPTP treated sets received four subcutaneous injections of MPTP solution (over the shoulders, into the loose skin over the neck) at 2 h interval on day 0. The animals were euthanized following the procedure approved by the Committee for the Purpose of Control and Supervision of Experiments on Animals (CPCSEA) on day 1 and day 3 post MPTP administration (Jackson-Lewis and

Przedborski 2007). Brain tissues were dissected out and processed for further analyses as described in the various assays below.

RNA Extraction and Quantitative Real Time PCR

RNA was extracted using TRIzol reagent, following the manufacturer's protocol (Invitrogen, Carlsbad, CA). The purity of RNA was measured spectrophotometrically at 260/280 nm (Thermoscientific Multiskan GO, USA). The conc. of RNA (μg/μl) was calculated as 40 × OD at 260 nm × dilution factor/1000. 5 μg of RNA from each sample was converted to cDNA using random hexamer (Thermo Scientific) and MMLV reverse transcriptase (Promega Corporation). For qPCR, the expressions of mature mRNA and gene in tissue samples were performed by SYBR green detection system with GAPDH as internal control. The cycle parameters was chosen as- initial denaturation at 94 °C for 2 min, 35 cycles of denaturation at 94 °C for 15 s and annealing, extension and fluorescence detection for 1 min each cycle at specific annealing temperature for respective genes and final hold at 4 °C. The $\Delta\Delta C_T$ of each gene was calculated with respect to internal control GAPDH. Each experiment was performed thrice. The primer sequences of the genes used in this work are listed below.

Gene	Primer sequence (5′ to 3′)	Annealing temperature (°C)	Amplicon size (bp)
GFAP	Fp: CCAAACTGGCTGATGTCTAC	56	206
	Rp: ATCTGCCTCCTGTCTATACG		
CD11b	Fp: ACAGTGCTCACCTGGAATATG	56	150
	Rp: GGAAGGGAGTCTTTCCACTTAC		
GAPDH	Fp: CTCCCTCACAATTTCCATCC	52	99
	Rp: GGGTGCAGCGAACTTTAT		

Tissue Handling

The brains were carefully dissected out and kept on ice. Substantia nigra from each mouse brain was cut according to the Paxinos Mouse Brain Anatomy Atlas. Those were isolated and protein lysates were prepared for western blot.

Protein Lysate Isolation from Tissue Samples

Total cell lysate for western blot analysis were performed according to Ghosh et al. (2018). Briefly, different brain regions were homogenized in ice-cold RIPA lysis buffer (composition—150 mM sodium chloride, 50 mM Tris buffer at pH 8.0, 0.5% sodium deoxycholate, 1.0% TritonX-100, 0.01% SDS) with protease inhibitor cocktail (Sigma-Aldrich Inc., USA) at 4 °C. The tissues were then incubated on ice for 30 min, and centrifuged at 14,000 rpm for 15 min at 4 °C. Protein content was estimated according to Bradford method and optical density was measured at 595 nm in a UV-1700 Pharma Spec, Shimadzu spectrophotometer (Shimadzu Scientific Instruments, Columbia, MD).

Western Blot Analysis

Western blot analysis was done according to Ghosh et al. (2018). Briefly, 50 micrograms of total protein extracts of each sample were resolved in a 9–12% polyacrylamide gels, electro blotted onto polyvinylidenedifluoride membrane (Amersham Biosciences, Piscataway, NJ), and the membranes were blocked with 5% nonfat dry milk for 1-h. The membranes were incubated with primary antibodies (Anti-tyrosine hydroxylase antibody at dilution 1:1000, Anti-beta actin antibody 1:2500), overnight at 4 °C, washed in TBS-Tween-20 (0.01%). Primary antibodies were detected against HRP-conjugated secondary antibodies (1:5000 dilution) using the HRP substrate ECL solution. The band intensity was measured by densitometry (Gel Doc™ XR + System, BioRad Laboratories, USA).The expressions of targeted proteins were normalized with expressions of reference proteins (β-actin) in the same gel.

Immunohistochemistry (IHC)

IHC was performed according to Mitra et al. (2015). After formalin fixation of dissected brains, sagittal sections (5 μm thick) were cut from paraffin-embedded brain tissue and mounted on slides. Tissues were deparaffinized, dehydrated through graded ethanol, and then endogenous peroxidase was quenched in a 3% hydrogen peroxide solution. Background staining was inhibited with 5% BSA. Sections were incubated in a humid chamber overnight at 4 °C with primary antibodies (Anti-GFAP antibody at 1:100 dilution). After three washes in PBS-Tween20, sections were sequentially incubated in horseradish peroxidase (HRP)-conjugated anti-sera specific for those antigens in Tris-buffered saline containing

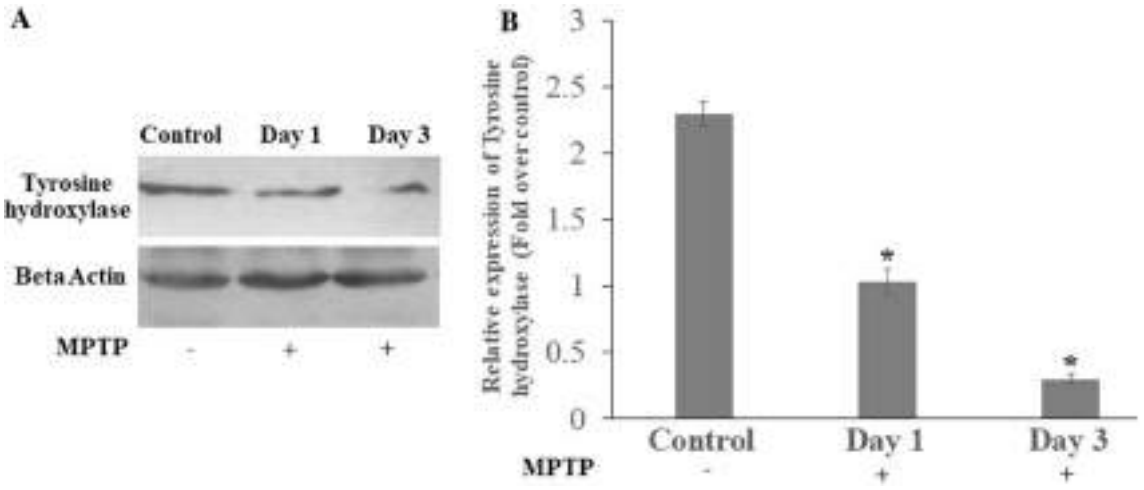

Fig. 1 Effect of MPTP on tyrosine hydroxylase immunoreactivity in substantia nigra. Representative image of immunoblot analysis of tyrosine hydroxylase from whole tissue lysate of mouse SN of all three groups (**a**). Histogram showing tyrosine hydroxylase expression relative to respective loading controls in all experimental groups (**b**). Beta-actin was used as a normalization control. Presence and absence of MPTP in control and treatment groups is indicated by $^{+/-}$ sign. Data in the histogram plot is represented as the mean ± SEM of three independent experiments. Asterisks indicate significant change in treated groups compared to control ($p < 0.05$)

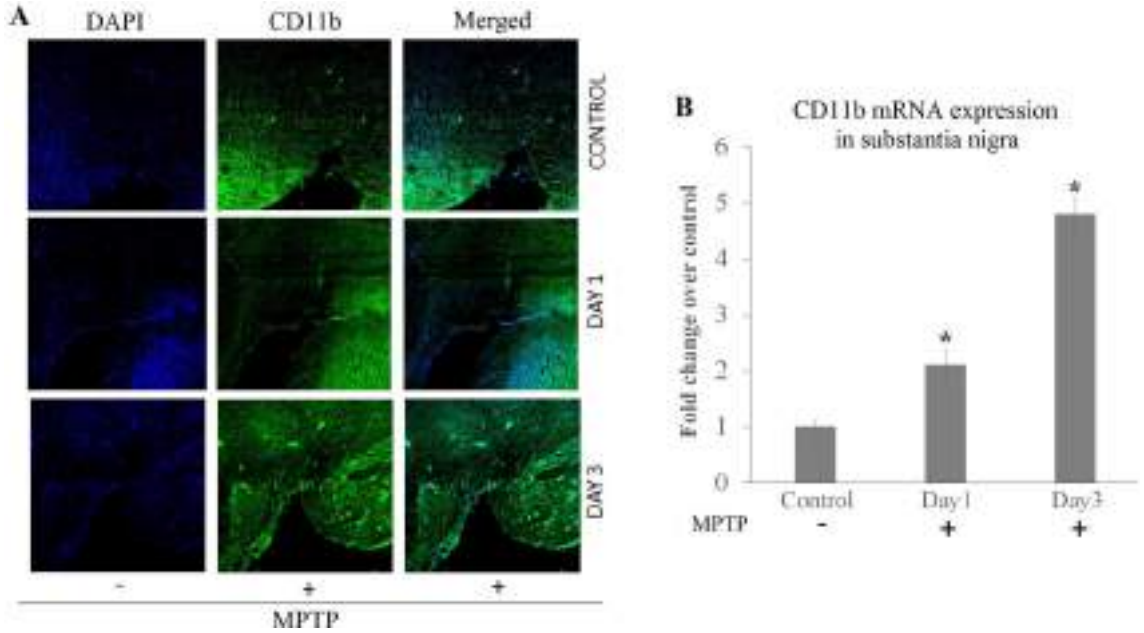

Fig. 2 Effect of MPTP on CD11b expression as a marker of microglial activation in substantia nigra. Different days of sacrifice post-MPTP treatment are indicated by day 1 and day 3. Representative image of immunoflourescence detection of the CD11b expression in substantia nigral sections at ×20 magnifications (**a**). Histogram showing the fold change in mRNA expression of CD11b with respect to loading control (GAPDH) in substantia nigra (**b**). Presence and absence of MPTP in control and treatment groups is indicated by +/− sign. Data in the histogram plot is represented as the mean ± SEM of three independent experiments. Asterisks indicate significant difference ($p < 0.05$) in values for different doses compared to control

0.3% Triton-X and 0.5% blocking agent for 2 h at room temperature. Immunoreactive complexes were then detected using a DAB system of GeNei Pvt. Ltd. (Bangalore, India). Sections were then dehydrated through graded ethanol, cleared in xylene, and cover slipped with DPX mounting medium. Slides that received no primary antibody served as negative controls. Images were captured in U-TVO 63 × C microscope (Olympus Corp., Tokyo, Japan) using 10× lens.

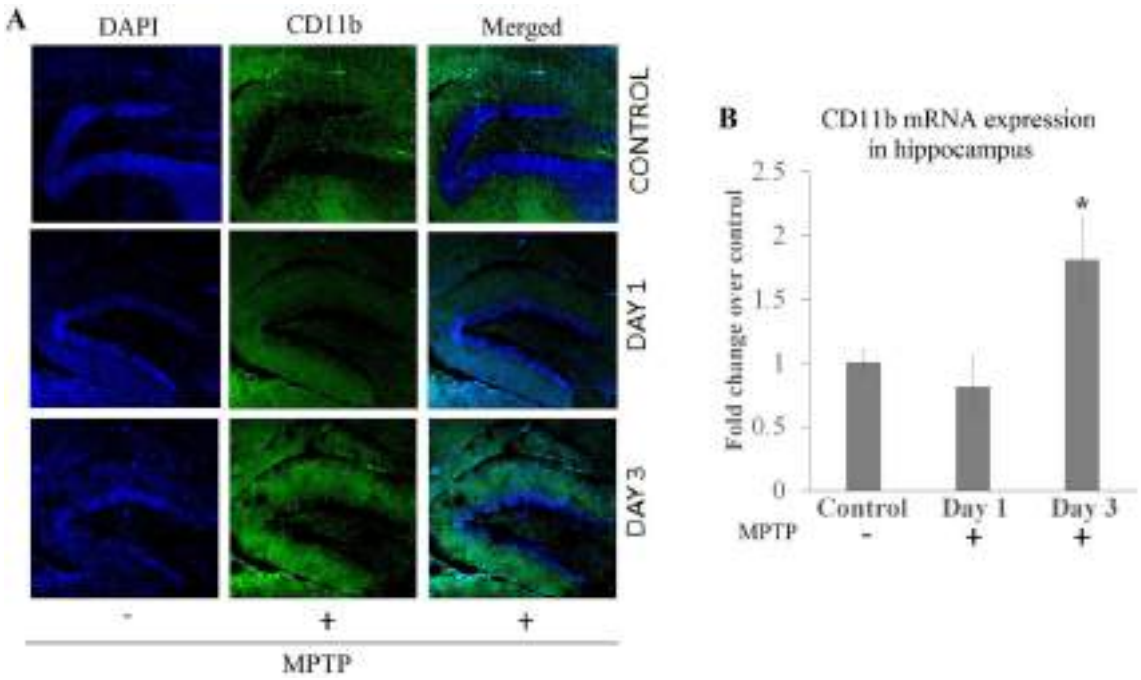

Fig. 3 Effect of MPTP on CD11b expression as a marker of microglial activation in mouse hippocampus. Different days of sacrifice post-MPTP treatment are indicated by day 1 and day 3. Representative image of immunoflourescence detection of the CD11b expression in hippocampal sections at ×20 magnifications (**a**). Histogram showing the fold change in mRNA expression of CD11b with respect to loading control (GAPDH) in substantia nigra (**b**). Presence and absence of MPTP in control and treatment groups is indicated by +/− sign. Data in the histogram plot is represented as the mean ± SEM of three independent experiments. Asterisks indicate significant difference ($p < 0.05$) in values for different doses compared to control

Immunofluorescence

The immunofluorescence procedure was carried out on sections incubated in blocking buffer (0.3–0.5% Triton X-100, 5% BSA in TBS) for 30 min at room temp followed by an overnight incubation with primary antibody. After three washes in TBS-T, primary antibody was revealed by incubating the sections in FITC-conjugated anti-sera specific for those antigens and diluted at a 1:30 ratio in Tris-buffered saline containing 0.3% Triton-X and 0.5% blocking agent for 2 h at room temperature followed by TBS washing. The tissue sections were counterstained with a nuclear counterstain (DAPI by Vector Laboratories Inc. Burlingame, CA, USA) and mounted with DPX resin. Images were captured in Olympus Flouview FV1000 confocal microscope (Olympus Corp., Tokyo, Japan) by 10× lenses.

Statistical Analysis

Results are expressed as mean ± SEM. Statistical evaluation of data has been done by one-way analysis of variance (ANOVA) followed by pairwise comparison of means using post hoc Tukey test. Results were considered significant at $p < 0.05$.

Results

MPTP Treatment Reduced Tyrosine Hydroxylase Immunoreactivity in Substantia Nigra (SN)

To examine whether MPTP elicits dopaminergic neurodegeneration in substantia nigra (SN), we performed western blot to assess tyrosine hydroxylase expression (the rate limiting enzyme for dopamine synthesis) in SN. Compared with control, the tyrosine hydroxylase enzyme expression was appreciably reduced in the SN of treated mice with maximum reduction at 72 h post treatment. It confirms dopaminergic neurodegeneration in SN after acute MPTP treatment (Fig. 1).

MPTP Treatment Causes Microglial Activation in Both Substantia Nigra and Hippocampus

To investigate the status of microglial cells in mouse hippocampus and substantia nigra post-MPTP treatment, we checked the mRNA as well as immunofluorescence of CD11b, the surface marker of activated microglial cells (Roy et al. 2006). Both mRNA and protein expression of CD11b showed significant increase in SN of treated mice at 24 and 72 h post treatment. The increment was most

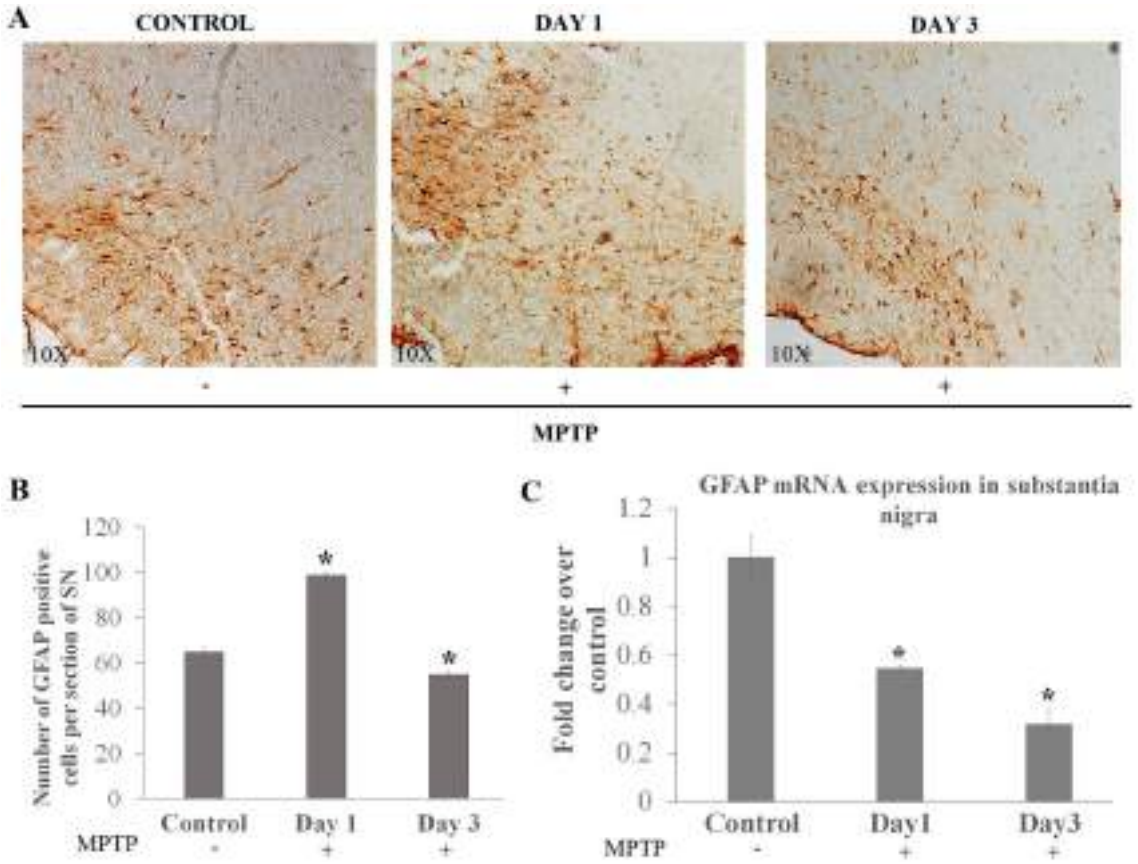

Fig. 4 Effect of MPTP on GFAP expression as a marker of astrocytic status in mouse substantia nigra. Different days of sacrifice post-MPTP treatment are indicated by day 1 and day 3. Representative image of immunohistochemical detection of GFAP expression in substantia nigral sections at ×10 magnifications (**a**). Histogram showing the number of GFAP positive cells per substantia nigral section as counted by ImageJ software (**b**). Fold change in mRNA expression of GFAP with respect to loading control (GAPDH) in substantia nigra (**c**). Presence and absence of MPTP in control and treatment groups is indicated by +/− sign. Data in the histogram plot is represented as the mean ± SEM of three independent experiments. Asterisks indicate significant difference ($p < 0.05$) in values for different doses compared to control

noticeable at 72 h (Fig. 2). In hippocampus, the increase in CD11b expression was recorded only at 72 h post-MPTP treatment indicating microglial activation (Fig. 3).

Acute MPTP Treatment Causes Differential Alteration in Astrocytic Status in Substantia Nigra and Hippocampus

To study the status of astrocytes in mouse SN and HC post-MPTP treatment, we first checked the mRNA expression of glial fibrillary acidic protein (GFAP), the cell surface marker of activated astrocytes (Jang et al. 2013), and then performed immunohistochemistry for the same cell surface marker. In substantia nigra, the number of GFAP positive cells significantly increased at 24 h but decreased at 72 h post-MPTP treatment (Fig. 4A) cell surface markers of activated astrocytes Glial fibrillary acidic protein (GFAP) (Jang et al. 2013), acquired from different experimental groups and then performed immunohistochemistry for the same cell surface marker. In substantia nigra, the number of GFAP positive cells significantly increased at 24 h post-MPTP treatment and decreased at 72 h post-MPTP treatment (Fig. 4A). In contrast, the GFAP mRNA expression of SN progressively reduced at both 24 h and 72 h post-MPTP treatment when compared with that of vehicle-treated controls (Fig. 4B). In MPTP treated HC, the number of GFAP- positive cells reduced both at 24 h and 72 h in comparison with controls (Fig. 5A). Although the GFAP mRNA expression was unchanged at 24 h, it was significantly reduced at 72 h post-MPTP treatment (Fig. 5B).

Discussion

In the present study, we used an acute MPTP- induced Parkinsonism model in Swiss albino mice to investigate the status of glial cells, both astrocytes and microglia, in substantia nigra and hippocampus at day 1 and day 3 post-

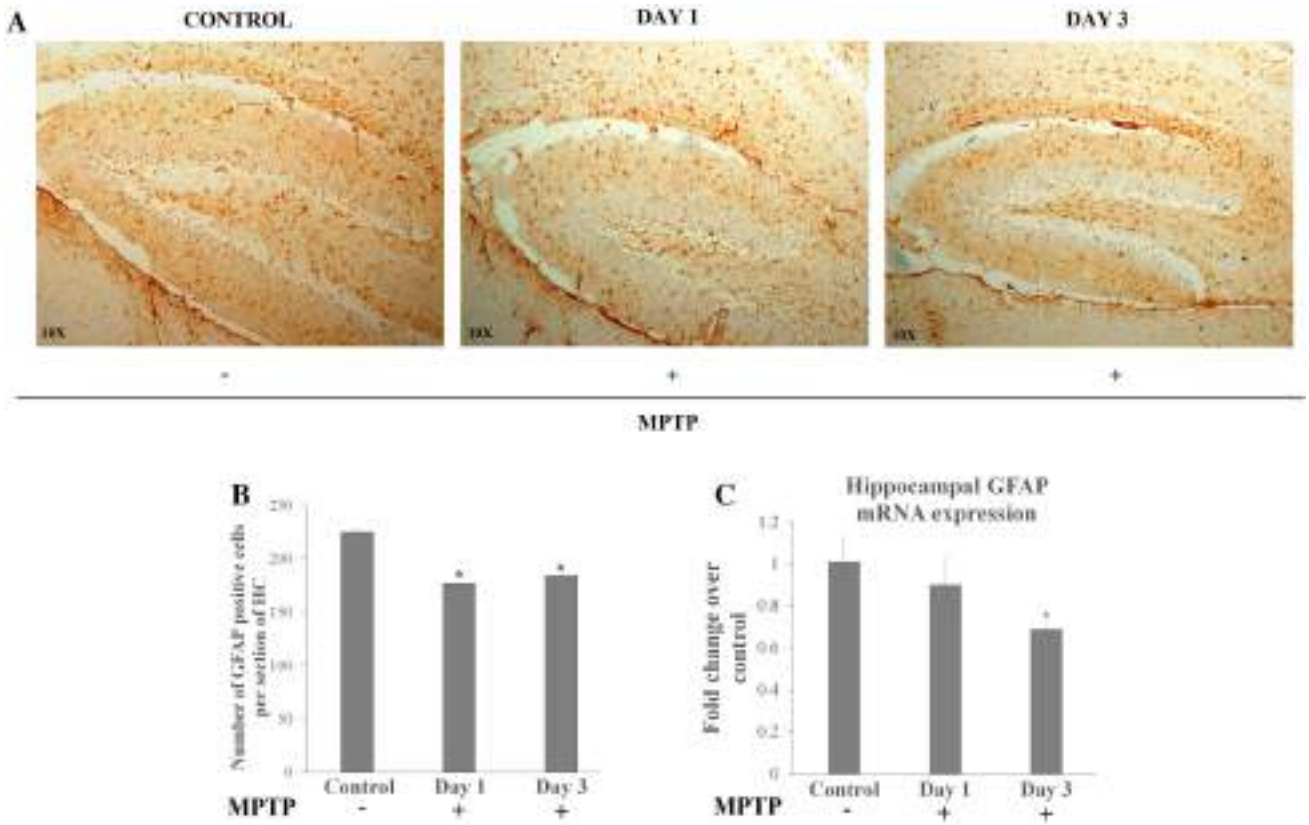

Fig. 5 Effect of MPTP on GFAP expression as a marker of astrocytic status in mouse hippocampus. Different days of sacrifice post-MPTP treatment are indicated by day 1 and day 3. Representative image of immunohistochemical detection of GFAP expression in hippocampal sections at ×10 magnifications (**a**). Histogram showing the number of GFAP positive cells per hippocampal section as counted by ImageJ software (**b**). Fold change in mRNA expression of GFAP with respect to loading control (GAPDH) in hippocampus (**c**). Presence and absence of MPTP in control and treatment groups is indicated by +/− sign. Data in the histogram plot is represented as the mean ± SEM of three independent experiments. Asterisks indicate significant difference ($p < 0.05$) in values for different doses compared to control

MPTP treatment. We selected these 2 days for acute study because on day 3 post MPTP treatment, the dopaminergic neurodegeneration was maximum.

During PD, the crosstalk among astrocytes, microglial cells and neurons is crucial for maintenance of nigrostriatal axis. Astrocytes promote survival and maintenance of dopaminergic neurons by secretion of different neurotrophic factors in the substantia nigra. Microglia cells monitor the brain microenvironment and engulf cellular debris. Therefore, both astrocytes and microglia are required for neuroprotection. However, their involvement is not sufficient for the protection of dopaminergic neurons of substantia nigra during PD (Glass et al. 2010; Rodrigues et al. 2014). The effects of augmented inflammatory responses on microglia are considered detrimental (Saijo et al. 2009). However, there are controversies surrounding the activities of reactive astrocytes. While some investigators have reported induction of oxidative stress and inflammation triggering dopaminergic neuronal death (Glass et al. 2010), others have demonstrated suppression of neuroinflammation and amelioration of neuronal damage by reactive astrocytes in animal models of PD via release of neurotrophic factors (Saijo et al. 2009; Yan et al. 2015). Likewise, the exact role and status of both the cell types in hippocampus is debatable. In our study we observed persistent microglial activation on day 3 post MPTP treatment in both the regions of interest. Such activated microglia in SN brings about further degeneration of dopaminergic neurons, confirmed by reduced tyrosine hydroxylase expression. The effect of activated microglia in hippocampus is not yet clear. As for astrocytes, in substantia nigra, sharp increase in astrocyte count on day 1 post treatment was noticed, which further declined on day 3. This indicates that, in SN on day 3, the number of astrocytes declined and microglial expression increased bringing about uninterrupted neuroinflammation worsening the condition of dopaminergic neurons. On the other hand, in hippocampus, on both day 1 and day 3 post MPTP treatment, the astrocyte count declines from the control level. This may indicate that the protective action of

astrocytes is absent in hippocampus during MPTP treatment. But the avid microglial activation as noticed in this region might promote neuroinflammation in hippocampus affecting its health. Such hippocampal inflammation in turn may cause cognitive decline and memory deficit observed in some cases of PD (Sy et al. 2010). This study shows that the glial cells behave differently in the hippocampus and substantia nigra in mouse brain upon acute MPTP administration promoting progressive neuroinflammation.

Acknowledgements The authors are grateful to Neuroscience Taskforce, Department of Biotechnology (Govt. of India) for funding this work and providing fellowship support (Project Sanction No. BT/PR3986/MED/30/677/2011). Authors are grateful to the Animal Ethical Committee for providing the ethical clearance to execute the animal experiments. Authors are thankful to Maulana Azad College, Dept. of Zoology, for assistance in Gel Documentation and Light microscopy. Authors express their sincere thanks to all lab members and friends for lending their helping hands in animal maintenance and other assistance whenever necessary.

Compliance with Ethical Standards

Conflict of interest The authors declare that they have no conflict of interest.

References

Furuya, T., H. Hayakawa, M. Hayakawa, K. Yoshimi, S. Hisahara, M. Miura, Y. Mizuno, and H. Mochizuki. 2004. Caspase-11 mediates inflammatory dopaminergic cell death in the 1-methyl-4-phenyl-1,2,3,6-tetrahydropyridine mouse model of Parkinson's disease. *J Neurosci* 8: 1865–1872.

Ghosh, N., S. Mitra, P. Sinha, N. Chakrabarti, and A. Bhattacharyya. 2018. TNFR2 mediated TNF-α signaling and NF-κB activation in hippocampus of 1-methyl-4-phenyl-1,2,3,6-tetrahydropyridine-treated mice. *Neurosci Res* 137: 36–42.

Glass, C.K., K. Saijo, B. Winner, M.C. Marchetto, and F.H. Gage. 2010. Mechanisms underlying inflammation in neurodegeneration. *Cell* 6: 918–934.

Huang, D., J. Xu, J. Wang, J. Tong, X. Bai, H. Li, Z. Wang, Y. Huang, Y. Wu, M. Yu, and F. Huang. 2017. Dynamic changes in the nigrostriatal pathway in the MPTP mouse model of Parkinson's disease. *Parkinsons Dis* 2017: 9349487.

Jackson-Lewis, V., and S. Przedborski. 2007. Protocol for the MPTP mouse model of Parkinson's disease. *Nature Protocols* 1: 141–151.

Kempermann, G., H. Song, and F.H. Gage. 2015. Neurogenesis in the adult hippocampus. *Cold Spring Harb Perspect Biol* 9: a018812.

Kettenmann, H., U.K. Hanisch, M. Noda, and A. Verkhratsky. 2011. Physiology of microglia. *Physiol Rev* 2: 461–553.

Kimelberg, H.K., and M. Nedergaard. 2010. Functions of astrocytes and their potential as therapeutic targets. *Neurotherapeutics* 4: 338–353.

Knierim, J.J. 2015. The hippocampus. *Curr Biol* 23: R1116–R1121.

Langston, J.W., L.S. Forno, J. Tetrud, A.G. Reeves, J.A. Kaplan, and D. Karluk. 1999. Evidence of active nerve cell degeneration in the substantia nigra of humans years after 1-methyl-4-phenyl-1,2,3,6-tetrahydropyridine exposure. *Ann Neurol* 4: 598–605.

Lawson, L.J., V.H. Perry, P. Dri, and S. Gordon. 1990. Heterogeneity in the distribution and morphology of microglia in the normal adult mouse brain. *Neuroscience* 1: 151–170.

Lee, S., J.Y. Park, W.H. Lee, H. Kim, H.C. Park, K. Mori, and K. Suk. 2009. Lipocalin-2 is an autocrine mediator of reactive astrocytosis. *J Neurosci* 1: 234–249.

L'Episcopo, F., C. Tirolo, N. Testa, S. Caniglia, M.C. Morale, M. Deleidi, M.F. Serapide, S. Pluchino, and B. Marchetti. 2012. Plasticity of subventricular zone neuroprogenitors in MPTP (1-methyl-4-phenyl-1,2,3,6-tetrahydropyridine) mouse model of Parkinson's disease involves cross talk between inflammatory and Wnt/β-catenin signaling pathways: functional consequences for neuroprotection and repair. *J Neurosci* 6: 2062–2085.

Liu, J., D. Huang, J. Xu, J. Tong, Z. Wang, L. Huang, Y. Yang, X. Bai, P. Wang, H. Suo, Y. Ma, M. Yu, J. Yu, and F. Huang. 2015. Tiagabine protects dopaminergic neurons against neurotoxins by inhibiting microglial activation. *Sci Rep* 5: 15720.

McGeer, P.L., and E.G. McGeer. 2008. Glial reactions in Parkinson's disease. *Mov Disord* 4: 474–483.

McGeer, P.L., S. Itagaki, B.E. Boyes, and E.G. McGeer. 1988. Reactive microglia are positive for HLA-DR in the substantia nigra of Parkinson's and Alzheimer's disease brains. *Neurology* 8: 1285–1291.

Mitra, S., N. Ghosh, P. Sinha, N. Chakrabarti, and A. Bhattacharyya. 2015. Alteration in nuclear factor-kappaB pathway and functionality of estrogen via receptors promote neuroinflammation in frontal cortex after 1-Methyl-4-Phenyl-1,2,3,6-tetrahydropyridine treatment. *Sci Rep* 5: 13949.

Rodrigues, M.C., P.R. Sanberg, L.E. Cruz, and S. Garbuzova-Davis. 2014. The innate and adaptive immunological aspects in neurodegenerative diseases. *J Neuroimmunol* 1–2: 1–8.

Saijo, K., and C.K. Glass. 2011. Microglial cell origin and phenotypes in health and disease. *Nat Rev Immunol* 11: 775–787.

Saijo, K., B. Winner, C.T. Carson, J.G. Collier, L. Boyer, M.G. Rosenfeld, F.H. Gage, and C.K. Glass. 2009. A Nurr1/CoREST pathway in microglia and astrocytes protects dopaminergic neurons from inflammation-induced death. *Cell* 1: 47–59.

Suzumura, A. 2013. Neuron-microglia interaction in neuroinflammation. *Curr Protein Pept Sci* 1: 16–20.

Sy, H.N., S.L. Wu, W.F. Wang, C.H. Chen, Y.T. Huang, Y.M. Liou, C.S. Chiou, C.R. Pawlak, and Y.J. Ho. 2010. MPTP-induced dopaminergic degeneration and deficits in object recognition in rats are accompanied by neuroinflammation in the hippocampus. *Pharmacol Biochem Behav* 2: 158–165.

Wang, Q., Y. Liu, and J. Zhou. 2015. Neuroinflammation in Parkinson's disease and its potential as therapeutic target. *Transl Neurodegener* 4: 19.

Watson, G.S., and J.B. Leverenz. 2010. Profile of cognitive impairment in Parkinson's disease. *Brain Pathol* 3: 640–645.

Yamada, T., T. Kawamata, D.G. Walker, and P.L. McGeer. 1992. Vimentin immunoreactivity in normal and pathological human brain tissue. *Acta Neuropathol* 2: 157–162.

Yan, Y., W. Jiang, L. Liu, X. Wang, C. Ding, Z. Tian, and R. Zhou. 2015. Dopamine controls systemic inflammation through inhibition of NLRP3 inflammasome. *Cell* 1–2: 62–73.

Yu, M., H. Suo, M. Liu, L. Cai, J. Liu, Y. Huang, J. Xu, Y. Wang, C. Zhu, J. Fei, and F. Huang. 2013. *Neurobiol Aging* 3: 916–927.

Malaria Protein As A Cure To Cancer

Dr Sanjukta Manna[1] and Souradeep Das[2]

[1] Assistant Professor, Post Graduate Department of Zoology, Maulana Azad College, Kolkata, India,
[2] Post graduate Student of Zoology, Maulana Azad College, Kolkata, India,

Corresponding author

Dr Sanjukta Manna
Assistant Professor, Post Graduate Department of Zoology, Maulana Azad College, Kolkata, India.

Abstract **--** Cancer is the most important health issue in recent times. Despite development of several Circulating Tumor Cell (CTC) isolation and detection technique detection and molecular characterization of cancer has remained a challenge. Malaria research has led to the discovery of oncofetal chondroitin sulfate, which appears to be shared between placental trophoblasts and cancer cells and can be detected by malaria protein VAR2CSA. Interestingly, using recombinant VAR2CSA (rVAR2) to target oncofetal chondroitin sulfate shows promise for novel cancer diagnostics and therapeutics. In this review, it was documented that rVAR2 efficiently captures CTCs carcinoma patients with minimal contamination by specific chondroitin sulphate signature and rVAR2 is found to deliver target specific drug delivery.

Keywords- metastatic; chondroitin sulfate; trophoblasts; recombinant VAR2CSA

INTRODUCTION

Every sixth death in this world is caused by cancer hence it's called the king of all maladies. Along with this it has still limited satisfactory understanding of diagnosis and cure. Cancer is an effective family of more than 100 unique conditions and is collectively characterized by the presence of cell populations that undergo uncontrolled division that displays the potential to invade other tissues. Cancer will not be recovered until it is understood and knowing the unique alterations that identify normal cells from tumor cells. The combination of different strategies can be used to improve the precision of drug delivery, leading to a more effective personalized therapy [1].

The deadly disease of malaria came as a sudden cure to another deadly disease cancer when, a team of researchers accidentally discovered a new protein called malaria protein,**Variant Surface antigen 2-CSA (VAR2CSA)**, produced by the mosquito-borne parasite *Plasmodium falciparum*. VAR2CSA binds to a particular type of sugar molecule present in the placenta, which is also found on the majority of cancer cell types. It was found that, by attaching toxins to VAR2CSA, over 90 per cent of tumor cell lines were effectively cured across a broad array of cancer types such as brain, blood, gastric, lung, skin, prostate, ovarian, pancreatic, bladder, and breast cancers [2]. In this article we discussed about the role of malaria protein in fighting cancer as per the latest research finding.

In 16th August, 2018, researchers from the University of Copenhagen have discovered a method of diagnosing a broad range of cancers at their early stages by utilizing a particular malaria protein- VAR2CSA, which sticks to cancer cells in blood samples. The researchers hope that this method can be used in cancer screenings in the near future (*Source:* University of Copenhagen The Faculty of Health and Medical Sciences). In Cancer, metastasis

is the process in which malignant cells spread from the primary tumor to distant sites, is of key importance. Up to 90% of cancer-related deaths are related to the metastatic spread of cancer cells. This complex process is vital to cancer progression and involves intravasation of cancer cells into the blood stream. The cancer cells traveling in the blood are called circulating tumor cells (CTCs) and a subset of these has increased metastatic capacity. CTCs have spurred increasing clinical interest since their levels in the blood were shown to be predictive of overall outcome for patients' carcinomas. This novel technique is seen to effectively detect CTC in blood before and after metastasis. In Case of Malaria, **Pregnancy Associated Malaria (PAM)** has severe consequences for both mother and child. PAM is caused by *P. falciparum* in which infected red blood cells that bind to receptors in the placenta. By adhesion to the placental tissue (sequestration), the parasites avoid being filtered through the spleen where they would have been killed [3]. To avoid host clearance, the parasite expresses adhesion proteins on the surface of infected erythrocytes, which effectively anchor these cells to specific receptors in the host vasculature [4]. The anchor protein, VAR2CSA, mediates binding of infected erythrocytes to placental syncytiotrophoblasts [5], [6]. This is the key event underlying placental malaria pathogenesis.

The Glycosaminoglycans (GAG) is the link between cancer and malaria

Glycosaminoglycans (GAGs) are carbohydrate modifications attached to proteins in the cell membrane. Changes in expression and composition of GAGs have been reported in cancer over the past three decades. Chondroitin sulfate (CS) is a major cancer-associated GAG that also has a key role in malaria pathogenesis. The malaria parasite *Plasmodium falciparum* has evolved a protein, called **VAR2CSA** that mediates attachment of infected erythrocytes to a distinct type of CS in the placental syncytium. CS chains comprise repeated disaccharide units, made up of glucoronic acid and N acetyl galactosamine (GalNAc) residues. As part of the cellular glycocalyx, GAGs are believed to control the information flow from ECM to signal transduction pathways stemming from plasma membrane. While the function and mechanical contribution of GAGs in cancer are not fully understood, it is clear that they act as key regulators of malignant phenotypes.

Chondroitin Sulfate (CS) plays the key role in both Cancer and Malaria

Most cancer cells express a distinct CS GAG epitope that is normally restricted to trophoblastic calls in placenta. These oncofetal CS chains, previously termed placental type CS, are expressed on CS-modified proteoglycans (CSPGs) of tumor and tumor-infiltrated stromal cells across multiple types of malignancies, indicating a possible broad functional importance of CS for the disease pathology. CPGs have been associated with proliferation, migration, invasion, angiogenesis and metastasis. VAR2CSA binds a distinct chondroitin sulphate (CS) glycosaminoglycan (GAG) chain A (CSA). Importantly, VAR2CSA expressing malaria parasites bind only to a distinct placental specific CS subtype. The placental CS subtype is thought to play roles in trophoblast cell proliferation and invasion, features also shared by cancer cells. This led to investigate whether human cancer cells also express the placental CS subtype.

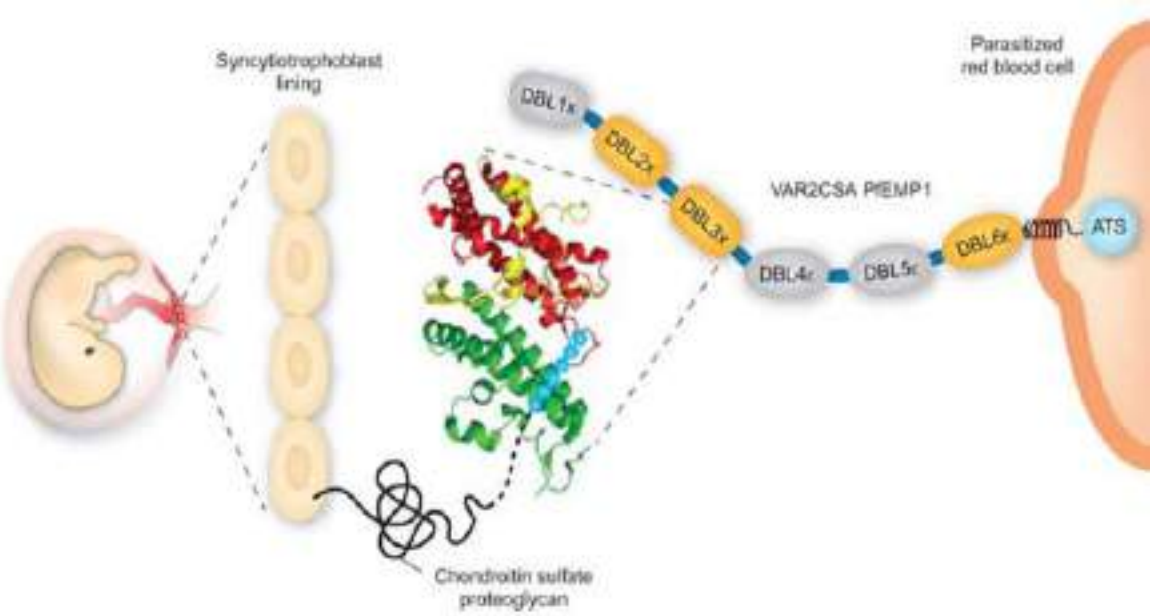

Figure 1. A schematic representation of the VAR2CSA PfEMP1 variant anchored to the membrane of the infected erythrocyte. The DBL3x domain, illustrated as an enlargement in ribbon form. The subdomains 1, 2 and 3 are colored yellow, red and green, respectively. VAR2CSA binds to the CSA moiety of placental chondroitin sulfate proteoglycan present on the surface of the syncytiotrophoblast cells in the placenta.\ The CSA ligand is shown schematically as hexagons (blue), positioned over the region covering subdomains 2 and 3 [7].

Intriguingly, this specific chondroitin sulfate (CS) turned out to be not only of interest to researchers trying to develop protective vaccines against pregnancy-associated malaria, it also became the path to discover a novel oncofetal marker. As per the latest research findings of [2] Salanti et al., 2015 it was revealed that the carbohydrate that the malaria parasite attaches itself to an oncofetal chondroitin sulfate (CSA) – which is expressed in the placenta is the same as the one displayed on proteoglycans in cancerous cells (the placental and malignant compartments display a common CS signature that binds malarial protein, VAR2CSA).

The Oncofetal Hypothesis: Trophoblasts and Cancer Cells

In 1902, embryologist John Beard [8] first proposed the trophoblastic theory of cancer. The hypothesis stated that, during early embryonic development, these cells rapidly multiply and create their own blood supply. Furthermore, they invade the surrounding maternal tissue and resist immune surveillance. Interestingly, all of these trophoblastic characteristics are also essential traits of cancer cells. Regardless of whether Beard's hypothesis conforms to reality, the phenotypic comparison of cancer cells with trophoblasts remains intriguing.

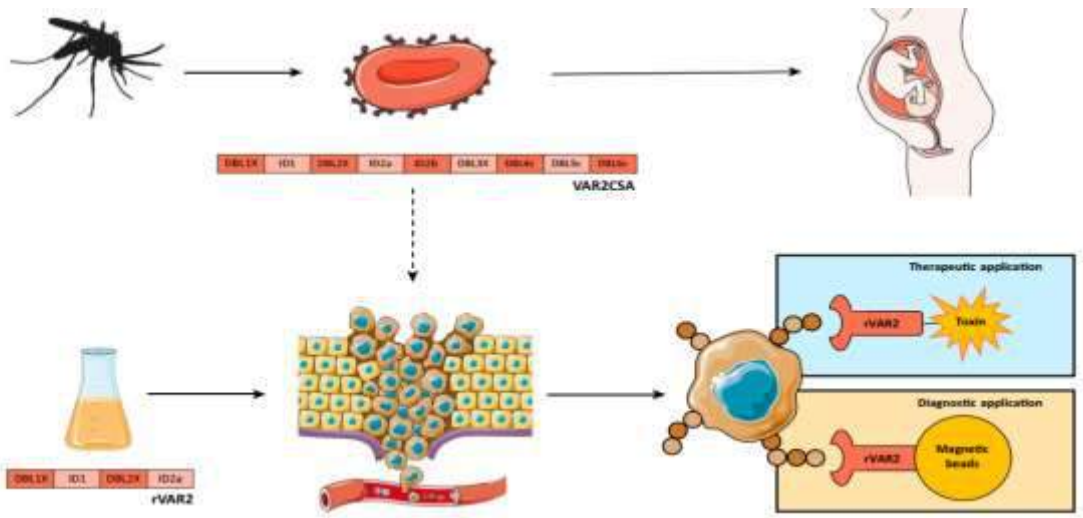

Figure 2. Using the Malaria Protein VAR2CSA for Cancer Therapeutic and Diagnostic Purposes. During pregnancy-associated malaria, the malaria parasites express a protein called VAR2CSA, which is displayed on the surface of the infected erythrocytes. VAR2CSA enables specific anchoring of the erythrocytes to the syncytiotrophoblast in the placenta by binding to oncofetal chondroitin sulfate (of CS). Intriguingly, of CS is also expressed by tumors, and VARCSA-expressing parasites or recombinant VAR2CSA (rVAR2) can specifically bind to a wide range of cancer cell lines and tissues of hematopoietic, epithelial, and mesenchymal origin. This can, for example, be exploited for cancer therapeutics by conjugating a toxin to rVAR2, or for cancer diagnostics by using rVAR2-coupled magnetic beads to capture circulating tumor cells in a blood sample. This figure was created using templates from Servier Medical Art website (https://smart.servier.com/).

VAR2CSA

VAR2CSA, a member of the PfEMP1 variant surface antigen family. VAR2CSA is a large protein (350 kDa) that is structurally composed of six Duffy binding-like (DBL) domains (DBL1X, DBL2X, DBL3X, DBL4ε, DBL5ε, and DBL6ε) among them, three mediate binding to chondroitin sulfate A (CSA) [9] (Figure5). VAR2CSA has extracellular, transmembrane, and intra-cytoplasmic regions, and its extracellular region is uniquely structured among PfEMP1 family members. The extracellular region of VAR2CSA which includes an N-terminal sequence, 6 cysteine-rich Duffy binding like (DBL) domains, and inter-domain (ID) regions, appear to play a key role in adhesion and immunogenicity of recombinant VAR2CSA protein fragments [10] (Figure 5).VAR2CSA expressing parasites only adhere in the placental chondroitin sulfate (CS) and do not bind to CS expressed elsewhere in the body[7],[2]. To examine the idea of using VAR2CSA as a common marker of placental and malignant cell, the researchers [2] separated the malaria protein (VAR2CSA), which attaches itself to the carbohydrate (CSA) and chemically conjugated it to a diphtheria toxin forming **recombinant VAR2CSA or rVAR2.**

Recombinant Malarial VAR2CSA (rVAR2) in Action

Salanti et. al.,2015 examined the interaction between *P. falciparum*-infected erythrocytes and CS in the placenta, by an immunohistochemistry assay with V5- tagged recombinant VAR2CSA (rVAR2) or control protein (rContr) and human tissue specimens. The rVAR2 protein efficiently bound to placental tissue only and not to any control tissue (Figure 3) showing that rVAR2 detects only placental like Chondroitin Sulphate or pl-CS (Figure 3) exclusively.

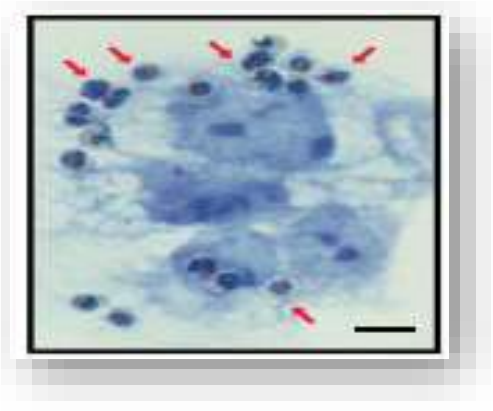

Figure 3. Representative images of indicated tissue specimens incubated with anti-V5 + anti-mouse HRP alone (anti-V5-HRP) or in combination with recombinant [2]

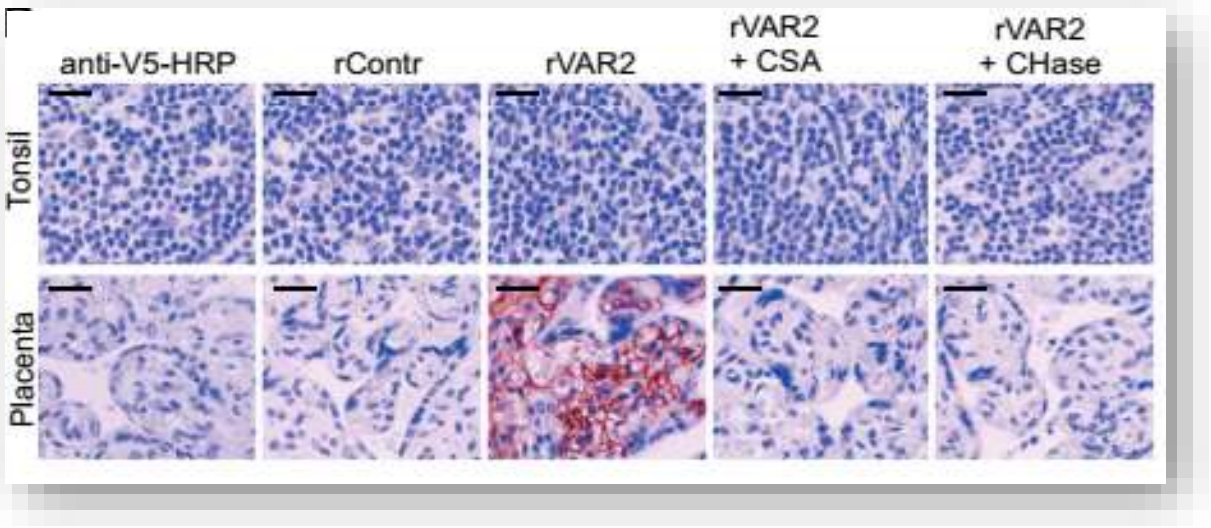

Figure 4. Representative image of *P.falciparum* -infected, VAR2CSA-expressing erythrocytes bound to the plasma membrane (red arrows) of trophoblastic cells [2]

The Chondroitin Sulfate Proteoglycan (CSPG) component of the placenta has been associated with the ability of the placental cells to maintain high proliferation rates and the capacity of the villous trophoblasts to invade into uterine tissue during implantation [11], [12]. Invasion and enhanced proliferation are phenotypes shared with cancer cells. Therefore, it is hypothesized (Oncofetal hypothesis) that the placental and malignant compartments display a common CS signature that binds malarial VAR2CSA. Accordingly, it was showed that VAR2CSA expressing *P. falciparum* infected erythrocytes displayed binding to human cancer cell lines in vitro, with 95% success rate using patient-derived human cancer cell lines of hematopoietic, epithelial, and mesenchymal origin (Figure 4). This proved the oncofetal hypothesis as, placenta like chondroitin sulfate (pl-CS) is also expressed on most human cancer cells.

Targeting and Treating Cancer Cell

Now the question was whether rVAR2 could be used as a pl-CS-specific tumor targeting system, to answer this scientists [2] were genetically fused the cytotoxic domain of Diphtheria toxin (DT388) to rVAR2, creating a recombinant rDT388-VAR2 (rVAR2-DT) fusion protein. *In vitro*, the rVAR2-DT protein efficiently killed tumor cell lines of both epithelial and mesenchymal origin. The experiment was carried out on mice model prostate cancer cell line with success (Figure 5). The results revealed that rVAR2 can facilitate efficacious CS dependent delivery of a cytotoxic compound to cancer cell in vivo with no morphologic evidence of adverse effects on normal tissues. Researchers [13] chemically conjugated a hemiasterlin analog (KT886) to rVAR2. The rVAR2- KT886 drug conjugate (VDC886) carried an average of three toxins per rVAR2 molecule. All cancer cell line tested were effectively killed in vitro by the VDC886. Subsequent testing of the VDC886 in showed the treatment significantly inhibited growth of tumors as compared to the control groups which demonstrate that VDC886 can target diverse human tumor types *in vivo.*

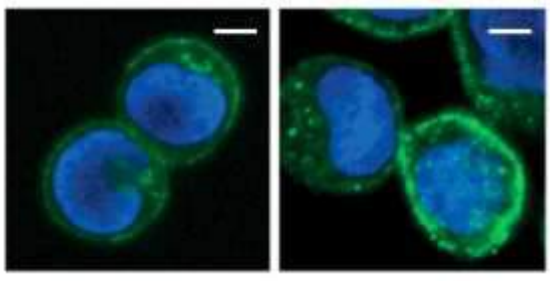

Figure. 5- Colon carcinoma cells analyzed by confocal microscopy 5 (left) and 30 (right) min after addition of rVAR2-FITC (green) and Cancer cell (blue) [2].

Conclusion

This review sheds light on, how recombinant versions of the evolutionarily refined malaria protein VAR2CSA can broadly detect pl-CS on trophoblastic cells as well as in human tumors. It also illustrates the new horizon which has been opened by the unconventional therapeutic technique for diagnosing cancer at its initial stages which has been ever so difficult from the decent of this deadly disease. With this conjugate of malaria protein and toxin, it possible to produce a treatment to capture and kill only the cancer cells in the body.

The human trial and further research on this novel diagnostic tool is still at its infant stage and needs to be done elaborately. Along with diagnosis VAR2CSA is also used as drug conjugated with an anticancer toxin (VDC886) that has been also successful to kill cancer cell specifically in mice. And in mice implanted with three types of human tumors - the drug also showed varying degrees of success. The use of VAR2CSA *in vivo* on mice also has been successfully administered on tumor cell which showed evidence to cure even after metastasis which is quite intriguing.

The biggest questions are, whether it'll work in the human body, and if the human body can tolerate the doses needed without developing side effects? Further researches in animal models are needed to review the pathophysiological pattern of this conjugate before human trials can commence.

References

[1] Bazak, R., Houri, M., El Achy, S., Kamel, S., Refaat, T. Cancer active targeting by nanoparticles: a comprehensive review of literature. J Cancer Res Clin Oncol 141(5):769-84, 2015.

[2] Salanti, A., Clausen, T.M., Agerbæk, M.Ø., Al Nakouzi, N., Dahlbäck, M., O.O, H.Z., Lee, S., Gustavsson, T., Rich, J.R., Hedberg, B.J., Mao, Y., Barington, L., Pereira, M.A., LoBello, J., Endo, M., Fazli, L., Soden, J., Wang, C.K., Sander, A.F., Dagil, R., Thrane, S., Holst, P.J., Meng, L., Favero, F., Weiss, G.J., Nielsen, M.A., Freeth, J., Nielsen, T.O., Zaia, J., Tran, N.L., Trent, J., Babcook, J.S., Theander, T.G., Sorensen, P.H., Daugaard, M. Targeting human cancer by a glycosaminoglycan binding malaria protein. Cancer Cell 28(4): 500-514, 2015.

[3] Andersen, P., Nielsen, M.A., Resende, M., Rask, T.S., Dahlbäck, M., Theander, T., Lund, O., Salanti, A. Structural insight into epitopes in the pregnancy-associated malaria protein VAR2CSA. PLoS Pathog 4(2): e42. doi: 10.1371/ journal. ppat.0040042, 2008.

[4] Baruch DI, Pasloske BL, Singh HB, Bi X, Ma XC, Feldman M, Taraschi TF, Howard RJ.,1995. Cloning the *P. falciparum* gene encoding PfEMP1, a malarial variant antigen and adherence receptor on the surface of parasitized human erythrocytes. Cell. 82(1):77-87, 1995 Jul 14

[5] Salanti, A., Staalsoe, T., Lavstsen, T., Jensen, A.T., Sowa, M.P., Arnot, D.E., Hviid, L., and Theander, T.G. Selective upregulation of a single distinctly structured var gene in chondroitin sulphate A-adhering *Plasmodium falciparum* involved in pregnancy-associated malaria. Mol. Microbiol. 49: 179–191, 2003.

[6] Salanti, A., Madeleine, D., Louise,T., Nielsen M.A, Barfod,L., Magistrado, P., Jensen, A.T.R, Lavstsen,T., Ofori M.F., Marsh K, Hviid,L., Theander,TG., Evidence for the involvement of VAR2CSA in pregnancy associated malaria. J. Exp. Med. 200: 1197–1203, 2004.

[7] Bentley GA, Gamain B. How does Plasmodium falciparum stick to CSA? Let's see in the crystal. Nat Struct Mol Biol. 15(9):895-7. doi: 10.1038/nsmb0908-895, 2008 Sep.

[8] Beard J. Cancer genesis. Lancet. 1:1447-1448, 1904.

[9] Clausen, T.M., Christoffersen, S., Dahlbäck, M., Langkilde, A.E., Jensen, K.E., Resende, M., Agerbæk, M.O., Andersen, D., Berisha, B., Ditlev, S.B., Pinto VV, Nielsen MA, Theander TG, Larsen S, Salanti A. Structural and functional insight into how the *Plasmodium falciparum* VAR2CSA protein mediates binding to chondroitin sulfate A in placental malaria. J. Biol. Chem. 287: 23332–23345, 2012.

[10] Fried, M., and Duffy, P.E. Adherence of *Plasmodium falciparum* to chondroitin sulfate A in the human placenta. Science. 272: 1502–1504, 1996.

[11] Baston-Bust, D.M., Gotte, M., Janni, W., Krussel, J.S., and Hess, A.P. Syndecan-1 knock-down in decidualized human endometrial stromal cells leads to significant changes in cytokine and angiogenic factor expression patterns. Reprod. Biol. Endocrinol. 8: 133, 2010.

[12] Van Sinderen M, Cuman C, Winship A, Menkhorst E, Dimitriadis E. The chrondroitin sulfate proteoglycan (CSPG4) regulates human trophoblast function. Placenta. 34: 907-12, 2013.

[13] Holtan SG, Creedon DJ, Haluska P, Markovic SN. Cancer and pregnancy: parallels in growth, invasion, and immune modulation and implications for cancer therapeutic agents. Mayo Clin Proc. 84: 985-1000. 2009.

Proc Zool Soc
https://doi.org/10.1007/s12595-018-0271-1

RESEARCH ARTICLE

Variations in Composition of Alkanes and Free Fatty Acids in *Aulacophora foveicollis* Lucas (Coleoptera: Chrysomelidae) on Exposure to Monocrotophos

Amarnath Karmakar[1] · Saubhik Mitra[1] · Abhishek Mukherjee[1] · Anandamay Barik[1]

Received: 16 January 2018 / Revised: 13 July 2018 / Accepted: 6 August 2018

Abstract *Aulacophora foveicollis* Lucas (Coleoptera: Chrysomelidae) is an important herbivore pest of cucurbitaceae, which is currently controlled by insecticides in southeast Asia. The insect cuticle is the first line of defence against insecticides. So, we investigated the variations in the composition of *n*-alkanes and free fatty acids (FFAs) in cuticular and internal lipids of *A. foveicollis* males and females exposed to monocrotophos compared to untreated adults. Both sexes of *A. foveicollis* adults were dipped in petroleum ether for 1 min at room temperature for extraction of surface waxes, and the insects were further kept in dichloromethane for 15 days for extraction of internal lipids. *n*-Alkanes and FFAs of cuticular and internal lipids were identified and quantified by GC–MS and GC–FID analyses. Higher quantities of cuticular lipids were observed in males and females exposed to monocrotophos than untreated males and females. Twenty *n*-alkanes were identified between *n*-C_{15} and *n*-C_{36} in cuticular lipids of untreated *A. foveicollis* adults; whereas 21 *n*-alkanes were detected in cuticular lipids of treated adults. Nineteen FFAs were recorded between C10:0 and C22:0 in cuticular lipids of untreated adults; whereas 21 and 19 FFAs were recorded in cuticular lipids of treated males and females, respectively. Hentriacontane and palmitoleic acid were the predominant *n*-alkane and FFA in the cuticular lipids of treated males and females, respectively. This study revealed that change of alkanes and FFAs in cuticular lipids of *A. foveicollis* males and females are linked to exposure to monocrtophos, which might result in increasing resistance of *A. foveicollis*.

Keywords Monocrotophos · Cuticular lipids · Internal lipids · Alkanes · Free fatty acids

Introduction

Aulacophora foveicollis Lucas (Coleoptera: Chrysomelidae) is an important herbivorous pest of cucurbitaceae, which feeds on leaves and flowers of squash, pumpkin, cucumber, bottle gourd, luffa, spine gourd, creeping cucumber and water melons (Singh and Gill 1979; Raman and Annadurai 1985; Mukherjee et al. 2014, 2015a; Karmakar et al. 2016a; Sarkar et al. 2016). The insect is widely distributed in Asia, Africa, Australia and South Europe. In India, it is noted throughout the country, especially in north western parts. The larvae of *A. foveicollis* pass through four instars (12–13 days) on roots to complete larval development. After pupation (12–13 days), adults feed on leaves for 8–9 weeks (Mukherjee et al. 2017). The adults makes irregular holes in leaves and flowers, whilst neonate larvae damage young and healthy roots of its host plant, which ultimately kills the branches and shoots, and retard growth of its hosts and leads to delayed maturation of crop (Singh and Gill 1979). The insect can withstand a wide range of humidity and temperature, and within the same growing season, it can switch from one crop to another. This makes the control of this pest very difficult. Application of bio-control agents such as a tachinid fly *Medinodexia morgani* (Hardy), mite *Histiostoma* sp. and reduviid bug *Rhinocoris fuscipes* Fabr. to control *A. foviecollis* are not yet

Electronic supplementary material The online version of this article (https://doi.org/10.1007/s12595-018-0271-1) contains supplementary material, which is available to authorized users.

✉ Anandamay Barik
anandamaybarik@yahoo.co.in

[1] Ecology Research Laboratory, Department of Zoology, The University of Burdwan, Burdwan, West Bengal 713104, India

successful (Waterhouse and Norris 1987). Recent studies have indicated that allelochemicals (alkanes, free fatty acids and volatile organic compounds) from different host plants might act as attractants of *A. foviecollis* adults, and subsequently, might be used for development of baited traps in integrated pest management program (Mukherjee et al. 2013, 2014, 2015a, b; Mukherjee and Barik 2014; Karmakar and Barik 2016; Karmakar et al. 2016a, b; Sarkar et al. 2016). However, still growers are forced to apply chemical-based insecticides such as organophospahtaes (monocrotophos, diazinon-60EC) and carbamates (carbofuran) to control outbreaks of this insect pest (Sinha and Chakrabarti 1983; Rahaman and Prodhan 2007).

Monocrotophos is (class Ib highly hazardous according to WHO) a broad-spectrum, fast-acting, contact and systemic insecticide, which is used to control a wide range of pests, including sucking, chewing and boring insects such as aphids, caterpillars, bollworms, mites, moths, jassids, budworms, stem borers and locusts. The toxic effect of this insecticide is achieved by inhibiting acetyl cholinesterase, an essential enzyme for normal nerve impulse transmission, causing rapid twitching of voluntary muscles and finally paralysis of insects (Skripsky and Loosli 1994). The use of monocrotophos has resulted in contamination of the soil as well as surface and ground water (Jabbar et al. 1993; Tariq et al. 2004; WHO 2009; Dujaković et al. 2010). Furthermore, monocrotophos is toxic to fish (Remia et al. 2008; Velmurugan et al. 2007; Pamanji et al. 2015), aquatic species (Mundhe and Pandit 2014; Simpson and Roger 1995; Vijayavel et al. 2006; Agrahari et al. 2007; Vijay Kumar and Prasad 2013), soil microbes (Rangaswamy et al. 1989; Gundi et al. 2005; Majumder and Das 2016), rats (Joshi and Rajini 2012; Kazi and Oommen 2012; Sankhwar et al. 2013) and humans (Rupa et al. 1988; Skripsky and Loosli 1994; Singh et al. 2004; Chakravarthi et al. 2009; WHO 2009). After the Rotterdam Convention in the year 1998, the amount of monocrotophos used for pest control significantly decreased due to increased resistance to this insecticide to other pests, and inhalation or absorption through the skin or oral entry in the human being through vegetables may result in excessive sweating, headache, weakness, giddiness, nausea, vomiting, hypersalivation, abdominal cramps, diarrhoea, blurred vision and slurred speech (WHO 2009). But it is still used in India, China, Bangladesh and Malaysia.

The lipid layer on the insect cuticle, which consists mainly of hydrocarbons like free fatty acids, alkanes, alcohols and ketons, serves as the primary barrier against the entry of pesticides and other chemicals from the environment (Lockey 1988), and subsequently, without this barrier insecticides entry will be increased in the insect body via integument. Hence, it would be interesting to observe the effects of monocrotophos exposure on the cuticular lipids of *A. foveicollis* adults. We analyzed composition of *n*-alkanes and free fatty acids (FFAs) from cuticular and internal lipids (as alkanes and FFAs are the major compounds of the surface wax) of natural *A. foveicollis* males and females, and monocrotophos exposed *A. foveicollis* adults. The *n*-alkanes and FFAs compositions were identified and quantified by gas chromatography–mass spectrometry (GC–MS) and GC–FID (flame ionisation detector) analyses.

Materials and Methods

Insects

A stock culture of *A. foveicollis* was maintained for five generations at 27 °C and 80 ± 5% relative humidity (RH) under a 14 h: 10 h (light: dark) photoperiod in a biochemical oxygen demand (BOD) incubator (ADS Instruments and Tech., Calcutta) on *Momordica cochinchinensis* (roots and leaves for larvae and adults, respectively) by our previously described method of Mukherjee et al. (2017). From the sixth generation, newly emerged adult males and females were separated from the colony. Both males and females of same age (8th day old) were used throughout the experiment. The insects were exposed to direct contact of monocrotophos. The aqueous solution of monocrotophos (Sigma Aldrich, Steinheim, Germany; CAS: 6923-22-4) were applied to a 9 cm diameter Whatman 41 filter paper [concentration: 0.69 µg/cm^2 (0.044 mg per Petri dish)] followed by air-drying in room temperature, and subsequently, each filter paper was placed into a glass Petri dish. The concentration of monocrotophos was chosen on the basis of 24-h LC_{25} by our laboratory trial studies [We also tested the insecticide at a concentration of 0.157 µg/cm^2 (0.01 mg per Petri dish), i.e., 24-h LC_{10}, and 1.57 µg/cm^2 (0.1 mg per Petri dish), i.e., 24-h LC_{50} in laboratory to determine the 24-h LC_{25} used in the present study. The basis for not choosing 24-h LC_{10} was that only 10% females were dead; while 50% of the adults died at 24-h LC_{50}. So, we provided a sublethal dose of 24-h LC_{25} to observe the effects of acclimatization to monocrotophos on lipids of *A. foveicollis*]. Ten *A. foveicollis* males or females were separately exposed for 24-h to monocrotophos (24-h LC_{25}) in each Petri dish ($N = 10$ for males or females). After exposure, the living adults were frozen immediately in liquid nitrogen and stored at − 80 °C until assay. Dead *A. foveicollis* males or females were discarded from the assay. *Aulacophora foveicollis* males and females were separately exposed for 24-h to filter papers treated with distilled water only as control.

Extraction of Cuticular and Internal Lipids

Aulacophora foveicollis males or females (2 g) were dipped in 400 ml petroleum ether followed by shaking for 1 min at room temperature for extraction of surface waxes from the insects (extracts I), and the insects were collected for extraction of internal alkanes and FFAs. The collected insects after extraction of surface waxes were further extracted by 400 ml of dichloromethane for 15 days (extracts II). The crude extracts of extracts I and II were separately passed through Whatman No. 41 filter paper (Maidstone, UK), and the solvent was evaporated at room temperature (27 °C) to obtain dried crude extracts. Three dried crude extracts of either extracts I or extracts II were separately collected and weighed, which was obtained from three batches of 2 g males or females. Each dried crude extract I was then dissolved in 20 ml petroleum ether and divided into two equal fractions (each fraction equivalent to 1 g insect), and the first and second fractions were used for identification and quantification of alkanes and FFAs, respectively. Similarly, each dried crude extract II was then dissolved in 20 ml dichloromethane and used for identification and quantification of alkanes and FFAs.

Identification and Quantification of Cuticular and Internal Alkanes

The first portion of each dried crude extract (extracts I or II) was fractioned by thin layer chromatography (TLC) on silica gel G (Sigma St. Louis, MO, USA) layers (thickness 0.5 mm), which had been prepared using a Unoplan coating apparatus (Shandon, London), with carbon tetrachloride as the mobile phase (Sarkar et al. 2014; Mitra et al. 2017). The purified alkane samples were used for gas chromatography–mass spectrometry (GC–MS) and gas chromatography–flame ionization detector (GC–FID) for identification and quantification, respectively. For quantification of compounds, three separate extracts were analyzed by a Techcomp GC model 7900 (Em Macau, Rua De Pequim, Nos. 202A-246, Centro Financeiro F7, Hong Kong) fitted with a SE-30 capillary column (Agilent, USA; column length 30 m × 0.32 mm × 0.25 µm film thickness) and a flame ionization detector. The oven temperature programme was initially 170 °C held for 1 min, then raised at 4 °C/min to 300 °C and finally held for 15 min (Mitra et al. 2017). The carrier gas was nitrogen with a flow rate of 18 ml/min. The volume of the sample injected was 1 µl with a split ratio of 1:10. The peaks were identified by comparison of their retention times with those of standard *n*-alkanes from *n*-C_{15} through *n*-C_{36}, and the area of each peak was converted into quantities of *n*-alkanes based on internal standard tricosane (*n*-C_{23} at 1 µg/µl, in preliminary studies of extracts from both males and females did not indicate presence of *n*-C_{23}). All *n*-alkanes (> 99% purity) between *n*-C_{15} and *n*-C_{36} were purchased from Sigma Aldrich (Supplementary material S1).

Identification and Quantification of Cuticular and Internal Free Fatty Acids (FFAs)

The second portion of each dried crude extract (extracts I or II) was mixed with diethyl ether and filtered through Whatman No. 41 filter paper. The extract was purified by TLC on silica gel G layers (thickness 0.5 mm), which had been prepared using a Unoplan coating apparatus (Shandon, London), with *n*-butanol: acetic acid: water (4:1:5 v/v/v; this mixture (v/v/v) was shaken and water was separated from this mixture by a separating funnel and discarded) as the mobile phase (Sarkar and Barik 2015; Malik and Barik 2015). The band was eluted from the silica gel layer with diethyl ether, and diethyl ether was removed under reduced pressure to get purified free fatty acids. The purified free fatty acids were esterified with 3 ml BF_3-methanol followed by warming for 5 min in a hot water bath at 50–60 °C temperature, and cooled. Hexane (30 ml) was added to this mixture followed by washing with saturated NaCl twice in a separating funnel. The aqueous layer of each sample was discarded and the hexane fraction was passed through 50 g anhydrous Na_2SO_4 twice. One portion of each esterified sample (hexane fraction) was used for GC–MS and another for GC–FID. The remaining part of the esterified fatty acids (three separate samples from either extracts I or II) were analyzed using a Techcomp Gas Chromatograph model 7900 fitted with a SE-30 capillary column (Agilent, USA; length: 30 m × 0.32 mm × 0.25-µm film thickness) and a flame ionization detector. The oven temperature program was initially held at 160 °C for 2 min, then raised at the rate of 3 °C/min to 220 °C and finally held at 220 °C for 18 min (Mitra et al. 2017).The injector port temperature was 280 °C. The carrier gas was nitrogen with a flow rate of 18 ml/min (Sarkar and Barik 2015; Malik and Barik 2015). The volume of the sample injected was 1 µl with a split ratio of 1: 10. The peaks were identified by comparison of their retention times with those of standard esterified fatty acids. The percentage composition of FFAs was computed from the GC peak area and the area of each peak was converted into quantities of fatty acids based on reference standard methyl tricosanoate (C23:0 at 1 µg/µl) (Supplementary material S2).

Statistical Analysis

The data on amounts of individual *n*-alkanes and FFAs from cuticular and internal lipids of *A. foveicollis* males and females with or without exposure to insecticide were log (x + 1) transformed prior to performing statistical

analyses. The data were subjected to Levene's test for homogeneity of variance with respect to treatments followed by multivariate analysis of variance [MANOVA using amounts of *n*-alkanes and FFAs as dependent variable, and sex (male and female) and treatments (untreated cuticular, untreated internal, treated cuticular and treated internal lipids) as fixed factors] to determine whether there is any effect of production of alkanes and FFAs among the treatments (Zar 2010). Furthermore, the amounts of individual alkanes and FFAs from cuticular and internal lipids of *A. foveicollis* males and females with or without exposure to insecticide were subjected to principal component analysis (PCA) to reduce the redundancy of the data and portray the relationship among the variables in a biplot (Adhikary et al. 2015; Malik et al. 2016). A series of one-way ANOVA were conducted to compare the effects on total and individual *n*-alkanes and FFAs in *A. foveicollis* males or females with or without exposure to insecticide. In case of significant *F*-values of one-way ANOVA, the data were subjected to post hoc Tukey test using SPSS software (SPSS 10.0; SPSS Inc., Chicago, IL, USA) (Zar 2010).

Results

Extraction of Lipids from *A. foveicollis* Adults with or Without Exposure to Monocrotophos

The petroleum ether extracts (extracts I) of *A. foveicollis* males yielded higher content of cuticular lipids (10.75 mg/g body weight, 0.261 mg/insect) when exposed to monocrotophos compared to untreated males (7.21 mg/g body weight, 0.195 mg/insect). Similarly, the petroleum ether extracts of *A. foveicollis* females produced higher content of cuticular lipids (11.65 mg/g body weight, 0.322 mg/insect) when exposed to monocrotophos compared to untreated females (8.39 mg/g body weight, 0.261 mg/insect).

A much higher quantity of internal lipids was obtained from dicholoromethane extracts (extracts II) of treated *A. foveicollis* males (47.49 mg/g body weight, 1.15 mg/insect) compared to untreated males (39.60 mg/g body weight, 1.07 mg/insect). The quantities of internal lipids from females (53.22 mg/g body weight, 1.47 mg/insect) were also higher than untreated females (43.90 mg/g body weight, 1.36 mg/insect).

Total alkanes represented 11.23% of total cuticular lipids of untreated *A. foveicollis* males, whilst it was higher (12.86%) in total cuticular lipids of males exposed to monocrotophos; whereas total alkanes accounted for 11.59% of total cuticular lipids of untreated *A. foveicollis* females, which was also higher (17.35%) in treated *A. foveicollis* females. A much higher concentration of FFAs, i.e., 35.11% of total cuticular lipids were observed in *A. foveicollis* males after exposure to insecticide compared to untreated males (8.86%). Similarly, the amounts of FFAs were much higher in treated *A. foveicollis* females (39.87% of total cuticular lipids) compared to untreated females (11.10% of total cuticular lipids).

The Levene's test for homogeneity of variance indicated that data set for the amounts of individual *n*-alkanes and FFAs from cuticular and internal lipids of *A. foveicollis* males and females with or without exposure to insecticide were homogenous conforming to application of ANOVA (Supplementary Table S1). The multivariate analysis revealed that *n*-alkane and FFAs productions were different among the treatments [treatments (for cuticular and internal lipids of untreated and treated males and females: Pillai's trace, value: 2.998, $F = 668.208$, hypothesis $df = 16$, error $df = 9$, $P < 0.0001$; between sex and cuticular and internal lipids of males and females: Pillai's trace, value: 2.999, $F = 51.126$, hypothesis $df = 48$, error $df = 9$, $P < 0.0001$], but for sex (i.e., between male and female) there was no significant difference [Pillai's trace, value: 0.999, $F = 48.489$, hypothesis $df = 16$, error $df = 1$, $P = 0.112$] (Supplementary Table S1). The PCA revealed that two factors F1 and F2, explained more than 69% of the variation in the observed abundance of *n*-alkanes and FFAs (Fig. 1, Supplementary Table S2). The biplot represented the spatial orientation of variables against two extracted factors and all the variables showed loading for the first two factors (Supplementary Table S2). The communalities of the variables considered were > 0.6 with the lowest value shown by arachidonic acid (Supplementary Table S2). The factor loadings and the contribution of the variables to the factors were shown in Supplementary Table S2.

n-Alkanes in Cuticular and Internal Lipids of *A. foveicollis*

Total alkanes in cuticular and internal lipids of untreated *A. foveicollis* males represented 808.92 ± 38.03 and 128.91 ± 7.27 µg/g body weight, respectively, and among the total amounts of alkanes, 398.01 ± 18.23 and 49.39 ± 3.08 µg/g body weight accounted for identified *n*-alkanes in cuticular and internal lipids of untreated *A. foveicollis* males, respectively (Table 1) and the rest were branched-chain alkanes (Supplementary Table S3). Total alkanes in cuticular and internal lipids of treated males were 1381.52 ± 58.51 and 89.44 ± 6.63 µg/g body weight, respectively, and among the total amounts of alkanes, 1228.64 ± 53.47 and 63.45 ± 4.37 µg/g body weight represented identified *n*-alkanes in cuticular and internal lipids of treated *A. foveicollis* males, respectively

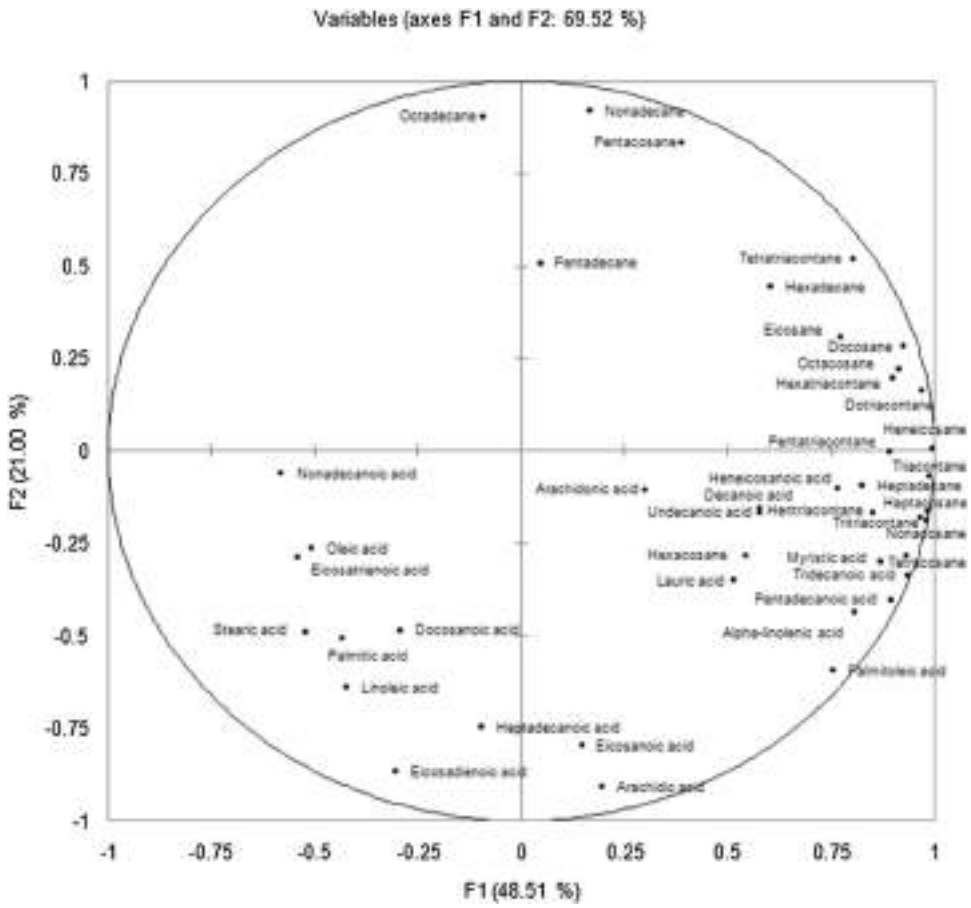

Fig. 1 The biplot showing the ordination of *n*-alkanes and free fatty acid compounds

(Table 1) and the rest were branched-chain alkanes (Supplementary Table S3). Twenty and 15 *n*-alkanes were detected between *n*-C_{15} and *n*-C_{36} alkanes in cuticular and internal lipids of untreated males, respectively; whilst 21 and 14 *n*-alkanes were detected in the cuticular and internal lipids of treated males, respectively (Table 1, Supplementary Figure S1). Pentacosane (*n*-C_{25}) was predominant followed by nonadecane (*n*-C_{19}) among the *n*-alkanes in cuticular lipids of untreated males; whereas hentriacontane (*n*-C_{31}) was predominant followed by tritriacontane (*n*-C_{33}) in cuticular lipids of treated males. Nonadecane (*n*-C_{19}) was the most abundant among the alkanes of internal lipids of untreated males; whereas *n*-C_{31} was the most abundant among the alkanes of internal lipids of treated males. Among the branched-chain alkanes, methyl branch of *n*-C_{31} predominated in cuticular lipids of untreated and treated *A. foveicollis* males, representing for 135.63 ± 6.76 and 35.22 ± 1.49 µg/g insect, respectively; whereas methyl branch of *n*-C_{21} and *n*-C_{19} were predominant in internal lipids of untreated and treated males, accounting for 71.57 ± 3.73 and 13.17 ± 0.80 µg/g insect, respectively (Supplementary Table S3). Hexadecane (*n*-C_{16}), octacosane (*n*-C_{28}), triacontane (*n*-C_{30}), dotriacontane (*n*-C_{32}) and teratriacontane (*n*-C_{34}) were detected among the cuticular alkanes of untreated and treated males but not in internal lipids. Eicosane (*n*-C_{20}) was unique to cuticular lipids of males with exposure to insecticide. Hexacosane (*n*-C_{26}) was not detected in internal lipids of treated males. Pentadecane (*n*-C_{15}), octadecane (*n*-C_{18}), nonadecane (*n*-C_{19}) and *n*-C_{25} were detected in higher amounts in cuticular lipids of untreated males compared to treated *A. foveicollis* males. *n*-C_{21}, docosane (*n*-C_{22}), tetracosane (*n*-C_{24}), *n*-C_{26}, heptacosane (*n*-C_{27}), octacosane (*n*-C_{28}), nonacosane (*n*-C_{29}), *n*-C_{30} (triacontane), *n*-C_{31}, dotriacontane (*n*-C_{32}), *n*-C_{33}, pentatriacontane (*n*-C_{35}) and hexatriacontane (*n*-C_{36}) were higher in cuticular lipids of treated males compared to untreated males. *n*-C_{15}, *n*-C_{27}, *n*-C_{29}, *n*-C_{31} and *n*-C_{35} were higher in internal lipids of treated *A. foveicollis* males compared to internal lipids of untreated males; whereas *n*-C_{18}, *n*-C_{21}, *n*-C_{22}, *n*-C_{24} and *n*-C_{36} were higher in internal lipids of untreated males compared to treated males.

The total alkanes in cuticular and internal lipids of untreated *A. foveicollis* females accounted for 971.73 ± 49.80 and 182.87 ± 7.96 µg/g body weight, respectively, and among the total amounts of alkanes, 474.28 ± 24.94 and 62.59 ± 3.01 µg/g body weight accounted for identified *n*-alkanes in cuticular and internal

Table 1 Composition of *n*-alkanes (μg/g insect) in cuticular and internal lipids of *Aulacophora foveicollis* males (untreated) and *A. foveicollis* males after exposure to monocrotophos (treated) (Mean ± SE, $N = 3$)

n-Alkanes	Untreated		Treated		$F_{3,11}$
	Cuticular	Internal	Cuticular	Internal	
Pentadecane (*n*-C_{15})	1.41 ± 0.11^{a}	0.27 ± 0.03^{b}	0.79 ± 0.04^{c}	0.59 ± 0.06^{d}	53.583
Hexadecane (*n*-C_{16})	0.35 ± 0.04	–	0.36 ± 0.02	–	
Heptadecane (*n*-C_{17})	1.74 ± 0.04^{a}	0.57 ± 0.04^{b}	2.09 ± 0.16^{a}	0.51 ± 0.05^{b}	86.818
Octadecane (*n*-C_{18})	22.23 ± 1.22^{a}	0.66 ± 0.04^{b}	0.99 ± 0.07^{c}	0.41 ± 0.04^{d}	311.084
Nonadecane (*n*-C_{19})	63.06 ± 2.67^{a}	9.74 ± 0.45^{b}	26.66 ± 1.01^{c}	9.13 ± 0.57^{b}	295.269
Eicosane (*n*-C_{20})	–	–	3.09 ± 0.08	–	
Heneicosane (*n*-C_{21})	57.51 ± 3.05^{a}	2.73 ± 0.23^{b}	215.44 ± 8.59^{c}	0.94 ± 0.08^{d}	490.650
Docosane (*n*-C_{22})	56.63 ± 2.91^{a}	3.97 ± 0.18^{b}	104.06 ± 5.93^{c}	2.36 ± 0.23^{d}	215.655
Tetracosane (*n*-C_{24})	7.37 ± 0.27^{a}	6.12 ± 0.40^{a}	13.40 ± 0.53^{b}	4.85 ± 0.44^{c}	81.245
Pentacosane (*n*-C_{25})	78.75 ± 4.31^{a}	0.84 ± 0.05^{b}	36.15 ± 2.10^{c}	0.88 ± 0.05^{b}	241.978
Hexacosane (*n*-C_{26})	2.38 ± 0.13^{a}	4.65 ± 0.23^{b}	5.50 ± 0.30^{c}	–	154.006
Heptacosane (*n*-C_{27})	3.15 ± 0.42^{a}	1.98 ± 0.12^{b}	19.24 ± 1.17^{c}	12.74 ± 0.87^{d}	116.601
Octacosane (*n*-C_{28})	2.94 ± 0.26^{a}	–	6.82 ± 0.47^{b}	–	144.241
Nonacosane (*n*-C_{29})	3.68 ± 0.17^{a}	1.76 ± 0.13^{b}	119.28 ± 7.52^{a}	11.57 ± 0.83^{b}	226.314
Triacontane (*n*-C_{30})	1.32 ± 0.14^{a}	–	10.15 ± 0.65^{b}	–	–
Hentriacontane (*n*-C_{31})	11.58 ± 0.47^{a}	9.32 ± 0.13^{b}	276.53 ± 9.99^{c}	13.39 ± 0.71^{a}	695.210
Dotriacontane (*n*-C_{32})	3.66 ± 0.13^{a}	–	8.93 ± 0.45^{b}	–	–
Tritriacontane (*n*-C_{33})	12.46 ± 0.68^{a}	1.71 ± 0.19^{b}	245.69 ± 10.55^{c}	1.29 ± 0.16^{b}	518.439
Tetratriacontane (*n*-C_{34})	3.64 ± 0.23	–	4.01 ± 0.39	–	
Pentatriacontane (*n*-C_{35})	34.21 ± 1.35^{a}	1.63 ± 0.13^{b}	81.46 ± 3.42^{c}	4.54 ± 0.35^{d}	401.709
Hexatriacontane (*n*-C_{36})	29.92 ± 1.53^{a}	3.47 ± 0.26^{b}	48.02 ± 2.37^{c}	0.26 ± 0.04^{d}	257.311
Total	398.01 ± 18.23^{a}	49.39 ± 3.08^{b}	1228.64 ± 53.47^{c}	63.45 ± 4.37^{d}	380.112

Different superscript letters in the same entry indicate significant differences ($P < 0.05$) by Tukey test

lipids of untreated females, respectively (Table 2) and the remaining were branched-chain alkanes (Supplementary Table S4). Alkanes in the cuticular and internal lipids of treated females represented 2022.32 ± 91.67 and 118.23 ± 5.38 μg/g body weight, respectively, and among the total amounts of alkanes, 1777.66 ± 82.35 and 85.04 ± 3.66 μg/g body weight represented identified *n*-alkanes in cuticular and internal lipids of treated females, respectively, (Table 2) and the rest were branched-chain alkanes (Supplementary Table S4). Twenty and 16 *n*-alkanes were identified between *n*-C_{15} and *n*-C_{36} alkanes in cuticular and internal lipids of untreated females, respectively; whilst 21 and 13 *n*-alkanes were detected in the cuticular and internal lipids of treated females, respectively (Table 2, Supplementary Figure S1). *n*-C_{25} and *n*-C_{31} were predominant among the *n*-alkanes in cuticular lipids of untreated and treated females, respectively; whereas *n*-C_{31} and *n*-C_{19} were predominant among the internal alkanes of untreated and treated females, respectively. Among the branched-chain alkanes, methyl branch of *n*-C_{31} and *n*-C_{29} were the most abundant in cuticular lipids of untreated and treated *A. foveicollis* females, representing for 170.08 ± 8.91 and 64.03 ± 3.61 μg/g insect, respectively; whereas methyl branch of *n*-C_{21} and *n*-C_{19} were predominant in internal lipids of untreated and treated females, accounting for 89.47 ± 3.62 and 17.10 ± 0.65 μg/g insect, respectively (Supplementary Table S4). *n*-C_{16}, *n*-C_{20}, *n*-C_{30}, *n*-C_{32} and *n*-C_{34} were not identified in internal lipids of untreated and treated females, while *n*-C_{15}, *n*-C_{18} and *n*-C_{28} were not detected among the alkanes of internal lipids of treated females. *n*-C_{17} was not detected in cuticular lipids of untreated females. *n*-C_{15}, *n*-C_{18}, *n*-C_{19} and *n*-C_{25} alkanes were higher in cuticular lipids of untreated females compared to treated females; whereas *n*-C_{21}, *n*-C_{22}, *n*-C_{24}, *n*-C_{26}, *n*-C_{27}, *n*-C_{28}, *n*-C_{29}, *n*-C_{30}, *n*-C_{31}, *n*-C_{32}, *n*-C_{33}, *n*-C_{35} and *n*-C_{36} were higher in cuticular lipids of treated females compared to untreated females. The amounts of *n*-C_{21} and *n*-C_{26} were higher in internal lipids of untreated females than internal lipids of treated females; whereas *n*-C_{17}, *n*-C_{19}, *n*-C_{27}, *n*-C_{29}, *n*-C_{31} and *n*-C_{35} alkanes were higher internal lipids of treated females compared to internal lipids of untreated females.

Table 2 Composition of *n*-alkanes (μg/g insect) in cuticular and internal lipids of *Aulacophora foveicollis* females (untreated) and *A. foveicollis* females after exposure to monocrotophos (treated) (Mean ± SE, $N = 3$)

n-Alkanes	Untreated		Treated		$F_{3,11}$
	Cuticular	Internal	Cuticular	Internal	
Pentadecane (n-C_{15})	1.61 ± 0.21^{a}	1.46 ± 0.05^{a}	0.83 ± 0.06^{b}	–	42.898
Hexadecane (n-C_{16})	1.83 ± 0.12	–	2.17 ± 0.33	–	3.550
Heptadecane (n-C_{17})	–	0.49 ± 0.03^{a}	2.77 ± 0.19^{b}	1.30 ± 0.21^{c}	74.991
Octadecane (n-C_{18})	31.03 ± 1.26^{a}	1.22 ± 0.04^{b}	2.80 ± 0.20^{c}	–	547.398
Nonadecane (n-C_{19})	75.81 ± 3.47^{a}	3.97 ± 0.20^{b}	28.09 ± 1.23^{c}	13.75 ± 0.36^{d}	295.978
Eicosane (n-C_{20})	3.61 ± 0.33	–	3.81 ± 0.31	–	5.375
Heneicosane (n-C_{21})	60.12 ± 3.47^{a}	6.49 ± 0.29^{b}	275.61 ± 10.48^{c}	0.98 ± 0.08^{d}	548.329
Docosane (n-C_{22})	79.89 ± 3.91^{a}	2.48 ± 0.26^{b}	156.87 ± 7.54^{c}	3.01 ± 0.12^{b}	301.273
Tetracosane (n-C_{24})	3.37 ± 0.23^{a}	8.06 ± 0.32^{b}	21.76 ± 1.26^{c}	8.56 ± 0.57^{b}	120.669
Pentacosane (n-C_{25})	84.99 ± 6.04^{a}	2.87 ± 0.25^{b}	51.08 ± 3.40^{c}	2.29 ± 0.20^{b}	134.578
Hexacosane (n-C_{26})	4.41 ± 0.33^{a}	5.99 ± 0.39^{b}	6.80 ± 0.51^{b}	0.66 ± 0.09^{c}	56.990
Heptacosane (n-C_{27})	4.26 ± 0.43^{a}	2.82 ± 0.16^{b}	26.71 ± 1.11^{c}	12.40 ± 0.47^{d}	289.473
Octacosane (n-C_{28})	5.64 ± 0.25^{a}	0.63 ± 0.05^{b}	11.77 ± 1.09^{c}	–	95.823
Nonacosane (n-C_{29})	6.13 ± 0.34^{a}	2.25 ± 0.12^{b}	186.43 ± 9.41^{c}	13.06 ± 0.82^{d}	360.457
Triacontane (n-C_{30})	1.89 ± 0.11^{a}	–	10.42 ± 0.77^{b}	–	118.780
Hentriacontane (n-C_{31})	15.51 ± 0.90^{a}	10.49 ± 0.36^{b}	315.29 ± 14.42^{c}	13.34 ± 0.56^{d}	436.731
Dotriacontane (n-C_{32})	3.39 ± 0.21^{a}	–	8.69 ± 0.22^{b}	–	302.187
Tritriacontane (n-C_{33})	12.72 ± 0.64^{a}	2.86 ± 0.15^{b}	313.73 ± 13.55^{c}	2.56 ± 0.22^{b}	515.141
Tetratriacontane (n-C_{34})	3.88 ± 0.28	–	4.79 ± 0.37	–	5.746
Pentatriacontane (n-C_{35})	33.27 ± 1.41^{a}	3.31 ± 0.23^{b}	243.12 ± 12.82^{c}	5.27 ± 0.35^{d}	319.631
Hexatriacontane (n-C_{36})	40.91 ± 2.17^{a}	7.20 ± 0.35^{b}	104.13 ± 6.31^{c}	7.86 ± 0.66^{b}	183.742
Total	474.28 ± 24.94^{a}	62.59 ± 3.01^{b}	1777.66 ± 82.35^{c}	85.04 ± 3.66^{d}	351.313

Different superscript letters in the same entry indicate significant differences ($P < 0.05$) by Tukey test

Free Fatty Acids (FFAs) in Cuticular and Internal Lipids of *A. foveicollis*

Nineteen and 18 FFAs between C10:0 and C22:0 fatty acids were detected in cuticular and internal lipids of untreated *A. foveicollis* males, accounting for 639.32 ± 33.52 and 5741.45 ± 191.67 μg/g body weight, respectively; whereas 21 and 18 FFAs were represented for 3772.80 ± 182.55 and 2180.72 ± 107.81 μg/g body weight in cuticular and internal lipids of treated males, respectively (Table 3, Supplementary Figure S2). Palmitic acid (C16:0) was predominant followed by linoleic acid (C18:2) in cuticular lipids of untreated males; whereas palmitoleic acid (C16:1) was predominant fatty acid followed by arachidic acid (C20:0) in cuticular lipids of *A. foveicollis* males with exposure to insecticide. Linoleic acid (C18:2) was the most abundant followed by C20:0 fatty acid in the internal lipids of untreated males; whereas arachidonic acid (C20:4) was predominant followed by palmitoleic acid (C16:1) in the internal lipids of treated males. Decanoic acid (C10:0) was unique among the cuticular lipids of treated males. Undecanoic acid (C11:0) and heneicosanoic acid (C21:0) were not detected in internal lipids of untreated and treated males. α-Linolenic acid (C18:3) was not detected in cuticular lipids of untreated males. C11:0, lauric acid (C12:0), tridecanoic acid (C13:0), myristic acid (C14:0) and pentadecanoic acid (C15:0), C16:1, C18:1, stearic acid (C18:0), eicosadienoic acid (C20:2), eicosanoic acid (C20:1), C20:0 and C21:0 fatty acids were much higher in cuticular lipids of treated males compared to cuticular lipids of untreated males; whereas C19:0 fatty acids was higher among cuticular lipids of untreated males compared to cuticular lipids of treated males. C18:3, C18:1, C20:4 and C20:3 fatty acids were higher among fatty acids on internal lipids of treated males compared to untreated males; whereas C12:0, C13:0, C15:0, C16:1, C16:0, C17:0, C18:2, C19:0, C20:2, C20:1, C20:0 and C22:0 fatty acids were higher among the internal lipids of untreated males compared to treated males.

Nineteen and 18 free fatty acids (FFAs) were detected in cuticular and internal lipids of untreated *A. foveicollis* females, accounting for 931.51 ± 46.21 and 6321.58 ± 253.26 μg/g body weight, respectively;

Table 3 Composition of free fatty acids (μg/g insect) in cuticular and internal lipids of *Aulacophora foveicollis* males (untreated) and *A. foveicollis* males after exposure to monocrotophos (treated) (Mean ± SE, $N = 3$)

Fatty acid	Untreated		Treated		$F_{3,11}$
	Cuticular	Internal	Cuticular	Internal	
Decanoic acid (C10:0)	–	–	26.67 ± 1.54	–	–
Undecanoic acid (C11:0)	2.07 ± 0.14^a	–	178.03 ± 8.11^b	–	470.866
Lauric acid (C12:0)	5.99 ± 0.48^a	49.75 ± 2.88^b	241.39 ± 13.18^c	18.44 ± 0.99^d	263.715
Tridecanoic acid (C13:0)	1.94 ± 0.08^a	12.31 ± 1.12^b	122.52 ± 7.25^c	9.12 ± 0.58^d	244.593
Myristic acid (C14:0)	25.59 ± 1.27^a	27.12 ± 1.40^a	158.08 ± 9.22^b	26.74 ± 1.07^a	192.979
Pentadecanoic acid (C15:0)	5.50 ± 0.58^a	31.99 ± 1.39^b	151.67 ± 6.73^c	18.55 ± 0.97^d	374.192
Palmitoleic acid (C16:1)	43.89 ± 2.47^a	539.08 ± 21.49^b	1065.70 ± 67.07^c	339.57 ± 22.59^d	135.180
Palmitic acid (C16:0)	179.03 ± 7.60^a	659.18 ± 27.21^b	185.58 ± 10.88^a	156.61 ± 7.60^c	242.564
Heptadecanoic acid (C17:0)	14.54 ± 1.39^a	71.80 ± 3.46^b	16.25 ± 1.47^a	10.67 ± 0.56^c	207.238
Alpha-linolenic acid (C18:3)	–	63.37 ± 3.27^a	417.86 ± 20.15^b	129.64 ± 7.80^c	285.250
Linoleic acid (C18:2)	127.88 ± 10.04^a	1816.94 ± 61.07^b	106.15 ± 8.15^a	17.85 ± 0.91^d	772.783
Oleic acid (C18:1)	18.98 ± 1.35^a	112.73 ± 6.35^b	35.90 ± 2.19^c	266.04 ± 13.12^d	232.028
Stearic acid (C18:0)	25.42 ± 1.15^a	185.76 ± 10.19^b	38.21 ± 2.34^c	172.28 ± 11.35^b	121.547
Nonadecanoic acid (C19:0)	18.98 ± 1.03^a	45.39 ± 2.32^b	11.25 ± 1.10^c	14.73 ± 0.66^d	118.775
Arachidonic acid (C20:4)	17.27 ± 1.15^a	38.83 ± 2.10^b	15.24 ± 0.63^a	546.21 ± 23.67^c	482.542
Eicosatrienoic acid (C20:3)	23.83 ± 1.51^a	102.69 ± 5.75^b	20.90 ± 1.67^a	170.14 ± 7.24^c	225.205
Eicosadienoic acid (C20:2)	3.75 ± 0.51^a	122.99 ± 6.58^b	39.29 ± 2.11^c	40.02 ± 1.26^c	206.130
Eicosanoic acid (C20:1)	2.43 ± 0.25^a	28.82 ± 1.43^b	39.10 ± 2.01^c	19.55 ± 0.82^d	142.063
Arachidic acid (C20:0)	48.11 ± 4.01^a	1074.43 ± 39.01^b	719.28 ± 27.16^c	185.23 ± 7.57^d	389.430
Heneicosanoic acid (C21:0)	13.67 ± 1.15^a	–	112.78 ± 8.72^b	–	127.046
Docosanoic acid (C22:0)	60.46 ± 4.02^a	758.26 ± 26.52^b	70.94 ± 3.78^a	39.34 ± 1.77^c	668.610
Total	639.32 ± 33.52^a	5741.45 ± 191.67^b	3772.80 ± 182.55^c	2180.72 ± 107.81^d	230.723

Different superscript letters in the same entry indicate significant differences ($P < 0.05$) by Tukey test

whereas 19 and 18 FFAs represented 4646.02 ± 215.18 and 2638.85 ± 101.73 μg/g body weight in cuticular and internal lipids of treated females, respectively (Table 4, Supplementary Figure S2). C16:0 fatty acid was predominant followed by C18:1 in cuticular lipids of untreated females; whilst C16:1 predominated followed by arachidic acid (C20:0) in cuticular lipids of treated females. C18:2 fatty acid was predominant fatty acid followed by C20:0 in internal lipids of untreated females; whereas C16:1 fatty acid predominated followed by C20:0 fatty acid in internal lipids of treated females. C11:0 fatty acid was unique to cuticular lipids of untreated females; whereas C18:3 was not detected in cuticular lipids of untreated females. C21:0 fatty acid was detected in cuticular lipids of untreated and treated females. C12:0, C13:0, C14:0, C15:0, C16:1, C17:0, C18:2, C20:4, C20:2, C20:1, C20:0, C21:0 and C22:0 fatty acids were higher in cuticular lipids of treated females compared to cuticular lipids of untreated females; whereas C16:0, C18:1, C18:0 and C19:0 fatty acids were higher in cuticular lipids of untreated females compared to cuticular lipids of treated females. C14:0, C15:0, C16:1, C18:3 and C20:3 fatty acids were higher in internal lipids of treated females compared to internal lipids of untreated females; whereas C12:0, C13:0, C16:0, C17:0, C18:2, C18:1, C18:0, C19:0, C20:4, C20:2, C20:1, C20:0 and C22:0 fatty acids were higher in internal lipids of untreated females compared to internal lipids of treated females.

Discussion

Lipids are synthesized in specialized cells called oenocytes, and subsequently transported to the cuticle of the insect, which serve various biological functions such as cell membrane structure, signaling and energy storage (Reue 2011; Yen et al. 2008). The present study demonstrated that internal lipids were higher in untreated *A. foveicollis* females compared to untreated males because females possess more lipids than males as lipids are essential substrate for egg development. Cuticular lipids serve important roles in restriction of water transpiration from the insect body, protection against microorganisms and chemical communication between species (Blomquist and Bagnères 2010; Chung and Carroll 2015; Gibbs 1998, 2002, 2007;

Table 4 Composition of free fatty acids (μg/g insect) in cuticular and internal lipids of *Aulacophora foveicollis* females (untreated) and *A. foveicollis* females after exposure to monocrotophos (treated) (Mean ± SE, $N = 3$)

Fatty acid	Untreated		Treated		$F_{3,11}$
	Cuticular	Internal	Cuticular	Internal	
Undecanoic acid (C11:0)	1.69 ± 0.19	–	–	–	–
Lauric acid (C12:0)	6.64 ± 0.57^{a}	48.29 ± 3.29^{b}	21.74 ± 1.85^{c}	12.81 ± 0.99^{d}	86.711
Tridecanoic acid (C13:0)	0.89 ± 0.02^{a}	26.28 ± 1.52^{b}	124.64 ± 6.96^{c}	17.21 ± 1.01^{d}	241.432
Myristic acid (C14:0)	10.63 ± 0.47^{a}	23.55 ± 1.48^{b}	159.49 ± 7.96^{c}	65.75 ± 3.09^{d}	240.811
Pentadecanoic acid (C15:0)	3.33 ± 0.48^{a}	35.58 ± 1.83^{b}	152.68 ± 7.65^{c}	59.94 ± 3.11^{d}	229.920
Palmitoleic acid (C16:1)	35.48 ± 2.54^{a}	620.53 ± 22.19^{b}	1511.18 ± 53.28^{c}	724.45 ± 26.63^{d}	363.894
Palmitic acid (C16:0)	254.06 ± 13.34^{a}	529.77 ± 22.30^{b}	146.51 ± 8.05^{c}	62.92 ± 2.84^{d}	220.974
Heptadecanoic acid (C17:0)	4.09 ± 0.39^{a}	57.48 ± 3.81^{b}	44.12 ± 1.96^{c}	12.77 ± 0.94^{d}	132.195
Alpha-linolenic acid (C18:3)	–	122.38 ± 8.98^{a}	447.09 ± 26.66^{b}	277.14 ± 13.53^{c}	153.972
Linoleic acid (C18:2)	136.35 ± 6.32^{a}	2449.15 ± 72.29^{b}	199.79 ± 11.79^{c}	18.92 ± 0.69^{d}	1009.141
Oleic acid (C18:1)	189.47 ± 10.37^{a}	286.81 ± 10.28^{b}	129.43 ± 9.81^{c}	221.94 ± 11.64^{d}	38.724
Stearic acid (C18:0)	148.91 ± 10.01^{a}	717.09 ± 29.12^{b}	35.22 ± 2.33^{c}	227.73 ± 7.08^{d}	359.771
Nonadecanoic acid (C19:0)	45.53 ± 3.20^{a}	39.60 ± 1.04^{a}	17.76 ± 1.24^{b}	28.61 ± 1.02^{c}	43.402
Arachidonic acid (C20:4)	8.15 ± 0.48^{a}	35.26 ± 1.90^{b}	519.95 ± 22.37^{c}	17.24 ± 0.90^{d}	495.487
Eicosatrienoic acid (C20:3)	27.44 ± 1.18^{a}	51.89 ± 2.59^{b}	27.20 ± 1.68^{a}	173.39 ± 7.68^{c}	279.233
Eicosadienoic acid (C20:2)	1.63 ± 0.12^{a}	112.58 ± 8.21^{b}	41.31 ± 2.56^{c}	32.39 ± 1.40^{d}	116.011
Eicosanoic acid (C20:1)	2.64 ± 0.17^{a}	68.91 ± 3.67^{b}	35.37 ± 1.56^{c}	10.97 ± 0.79^{d}	213.262
Arachidic acid (C20:0)	40.84 ± 3.21^{a}	998.85 ± 54.42^{b}	936.84 ± 62.29^{b}	653.32 ± 22.94^{c}	103.873
Heneicosanoic acid (C21:0)	5.22 ± 0.48^{a}	–	30.13 ± 1.27^{b}	–	337.205
Docosanoic acid (C22:0)	8.52 ± 0.47^{a}	97.58 ± 4.96^{b}	65.57 ± 4.57^{c}	21.36 ± 1.60^{d}	139.191
Total	931.51 ± 46.21^{a}	6321.58 ± 253.26^{b}	4646.02 ± 215.18^{c}	2638.85 ± 101.73^{d}	179.418

Different superscript letters in the same entry indicate significant differences ($P < 0.05$) by Tukey test

Hadley 1994; Paszkiewicz et al. 2016). Both *A. foveicollis* males and females had higher amount of cuticular lipids when exposed to monocrotophos compared to untreated males and females, implicating that change of cuticular lipids are linked to exposure to insecticide (Paszkiewicz et al. 2016; Pedrini et al. 2009). Similar resistance-related cuticle differences by exposing to chloropyrifos insecticide were obtained from *Blatta germanica* males (Paszkiewicz et al. 2016). Pedrini et al. (2009) demonstrated that pyrethroid-resistant insects contain higher amounts of surface hydrocarbons than pyrethroid-susceptible insects. The current study indicated that cuticles of *A. foveicollis* females are more resistant to monocrotophos compared to males as cuticular lipids are higher in treated *A. foveicollis* females (exposed to monocrotophos) compared to treated males.

In the current study, substantial variations of individual *n*-alkanes were observed in cuticular and internal lipids of untreated *A. foveicollis* males and females as well as both males and females when exposed to monocrotophos (Nelson et al. 2002; Nelson and Charlet 2003; Golebiowski et al. 2012). *n*-Alkanes with longer chains have lower volatility due to higher boiling points, which results in better adaptation of insects to warmer climates (Gibbs and Pomonis 1995). Exposure to monocrotophos resulted increase of higher amounts of n-C_{35} and n-C_{36} in the cuticular lipids of both *A. foveicollis* males and females, implicating that fitness of *A. foveicollis* adults may be altered at higher temperature. Cuticular hydrocarbons especially alkanes play an important role as contact pheromones to identify friends or foes (Akino et al. 2004; Nawrot et al. 2010). Hence, change of surface hydrocarbons from both *A. foveicollis* males and females when exposed to monocrotophos may affect communication of *A. foveicollis* adults.

The FFAs in insect cuticles may change in composition and quantity, depending on the species and their diet and developmental stage (Stanley-Samuelson et al. 1988). The FFAs found in our study ranged between C10 and C22, and similar profiles were recorded in different insects (Gołębiowski et al. 2010, 2012; Paszkiewicz et al. 2016). Cuticular fatty acids may protect insects against fungal attack (Gołębiowski et al. 2008), but sometime may also enhance growth of fungus on insects such as palmitoleic acid promotes mycelial growth; on the other hand it is toxic to the conidia of *Erynia variabilis* (Kerwin 1984).

However, the toxic effects of palmitoleic acid can be lowered by the presence of a sufficient amount of oleic acid (Kerwin 1984). This study revealed an increase in total FFAs concentrations in the cuticular and internal lipids of *A. foveicollis* males and females when exposed to monocrotophos, implicating that amounts of FFAs in cuticular lipids can protect insects from penetration of insecticides into the body of adult *A. foveicollis* males and females. A higher concentration of total free fatty acids concentrations in the cuticular and internal lipids was observed in *B. germanica* males exposed to chloropyriphos compared to untreated males (Paszkiewicz et al. 2016).

In conclusion, the current study clearly indicates that a higher content of cuticular lipids in terms of alkanes and FFAs in the *A. foveicollis* males and females after exposure to monocrotophos compared to the males and females that were not exposed, indicating that both *A. foveicollis* males and females are showing increasing resistance to the insecticide. Kranthi et al. (2001) demonstrated 16, 2 and 4 strains of *Helicoverpa armigera*, *Earias vittella* and *Spodoptera litura* were resistant to monocrotophos due to wide use in cotton pest management in India, respectively. The strains of *H. armigera* were susceptible to monocrotophos in china till 1993 (Wu et al. 1995), but they showed resistance by 1995 (Wu et al. 1996). Furthermore, *H. armigera* populations also showed resistance against monocrotophos in Pakistan (Ahmad et al. 1995). However, it remains to be seen whether there are any changes in remaining compounds of the cuticular and internal lipids of *A. foveicollis* males and females after exposure to monocrotophos. Future research is needed to know the protecting mechanism of cuticular hydrocarbons of *A. foveicollis* males and females against exposure to monocrotophos.

Acknowledgements We thank Dr. Janakiraman Poorani, Principal Scientist, National Research Centre for Banana, Tamilnadu for identifying the insect. We are thankful to DST PURSE Phase-II for providing necessary instrumental facilities.

References

Adhikary, P., A. Mukherjee, and A. Barik. 2015. Attraction of *Callosobruchus maculatus* (F.) (Coleoptera: Bruchidae) to four varieties of *Lathyrus sativus* L. seed volatiles. *Bulletin of Entomological Research* 105: 187–201.

Agrahari, S., K.C. Pandey, and K. Gopal. 2007. Biochemical alteration induced by monocrotophos in the blood plasma of fish, *Channa punctatus* (Bloch). *Pesticide Biochemistry and Physiology* 88: 268–272.

Ahmad, M., I.M. Arif, and Z. Ahmad. 1995. Monitoring insecticide resistance of *Helicoverpa armigera* (Lepidoptera: Noctuidae) in Pakistan. *Journal of Economic Entomology* 88: 771–776.

Akino, T., K. Yamamura, S. Wakamura, and R. Yamaoka. 2004. Direct behavioral evidence for hydrocarbons as nestmate recognition cues in *Formica japonica* (Hymenoptera: Formicidae). *Applied Entomology and Zoology* 39: 381–387.

Blomquist, G.J., and A.-G. Bagnères. 2010. *Insect Hydrocarbons: Biology, Biochemistry, and Chemical Ecology*. Cambridge: Cambridge University Press.

Chakravarthi, B.K., R. Naravaneni, G.H. Philip, and C.S. Reddy. 2009. Investigation of monocrotophos toxic effects on human lymphocytes at cytogenetic level. *African Journal of Biotechnology* 8: 2042–2046.

Chung, H., and S.B. Carroll. 2015. Wax, sex and the origin of species: Dual roles of insect cuticular hydrocarbons in adaptation and mating. *BioEssays* 37: 822–830.

Dujaković, N., S. Grujić, M. Radisić, T. Vasiljević, and M. Lausević. 2010. Determination of pesticides in surface and ground waters by liquid chromatography–electrospray–tandem mass spectrometry. *Analytica Chimica Acta* 678: 63–72.

Gibbs, A., and J.G. Pomonis. 1995. Physical properties of insect cuticular hydrocarbons: The effects of chain-length, methyl-branching and unsaturation. *Comparative Biochemistry and Physiology—Part B: Biochemistry and Molecular Biology* 112: 243–249.

Gibbs, A.G. 1998. Water-proofing properties of cuticular lipids. *American Zoologist* 38: 471–482.

Gibbs, A.G. 2002. Lipid melting and cuticular permeability: New insights into an old problem. *Journal of Insect Physiology* 48: 391–400.

Gibbs, A.G. 2007. Waterproof cockroaches: The early work of J. A. Ramsay. *Journal of Experimental Biology* 210: 921–922.

Gołębiowski, M., M.I. Boguś, M. Paszkiewicz, and P. Stepnowski. 2010. The composition of the free fatty acids from *Dendrolimus pini* exuviae. *Journal of Insect Physiology* 56: 391–397.

Gołębiowski, M., M.I. Boguś, M. Paszkiewicz, W. Wieloch, E. Włóka, and P. Stepnowski. 2012. The composition of the cuticular and internal free fatty acids and alcohols from *Lucilia sericata* males and females. *Lipids* 47: 613–622.

Gołębiowski, M., E. Malinski, M.I. Boguś, J. Kumirska, and P. Stepnowski. 2008. The cuticular fatty acids of *Calliphora vicina*, *Dendrolimus pini* and *Galleria mellonella* larvae and their role in resistance to fungal infection. *Insect Biochemistry and Molecular Biology* 38: 619–627.

Gundi, V.A.K.B., G. Narasimha, and B.R. Reddy. 2005. Interaction effects of insecticides on microbial populations and dehydrogenase activity in a black clay soil. *Journal of Environmental Science and Health B* 40: 269–283.

Hadley, N.F. 1994. *Water Relations of Terrestrial Arthropods*. San Diego: Academic Press.

Jabbar, A., S.Z. Masud, Z. Parveen, and M. Ali. 1993. Pesticide residues in cropland soils and shallow groundwater in Punjab Pakistan. *Bulletin of Environmental Contamination and Toxicology* 51: 268–273.

Joshi, A.K.R., and P.S. Rajini. 2012. Hyperglycemic and stressogenic effects of monocrotophos in rats: Evidence for the involvement of acetylcholinesterase inhibition. *Experimental and Toxicologic Pathology* 64: 115–120.

Karmakar, A., and A. Barik. 2016. *Solena amplexicaulis* (Cucurbitaceae) flower surface wax influencing attraction of a generalist insect herbivore, *Aulacophora foveicollis* (Coleoptera: Chrysomelidae). *International Journal of Tropical Insect Science* 36: 70–81.

Karmakar, A., U. Malik, and A. Barik. 2016a. Effects of leaf epicuticular wax compounds from *Solena amplexicaulis* (Lam.) Gandhi on olfactory responses of a generalist insect herbivore. *Allelopathy Journal* 37: 253–272.

Karmakar, A., A. Mukherjee, and A. Barik. 2016b. Floral volatiles with colour cues from two cucurbitaceous plants causing attraction of *Aulacophora foveicollis*. *Entomologia Experimentalis et Applicata* 158: 133–141.

Kazi, A.I., and A. Oommen. 2012. Monocrotophos induced oxidative damage associates with severe acetylcholinesterase inhibition in rat brain. *NeuroToxicology* 33: 156–161.

Kerwin, J.L. 1984. Fatty acid regulation of the germination of *Erynia variabilis* conidia on adults and puparia of the lesser housefly, *Fannia canicularis*. *Canadian Journal of Microbiology* 30: 158–161.

Kranthi, K.R., D.R. Jadhav, R.R. Wanjari, S. Shakir Ali, and D. Russell. 2001. Carbamate and organophosphate resistance in cotton pests in India, 1995 to 1999. *Bulletin of Entomological Research* 91: 37–46.

Lockey, K.H. 1988. Lipids of the insect cuticle: Origin, composition and function. *Comparative Biochemistry and Physiology—Part B: Comparative Biochemistry* 89: 595–645.

Majumder, S.P., and A.C. Das. 2016. Phosphate-solubility and phosphatase activity in Gangetic alluvial soil as influenced by organophosphate insecticide residues. *Ecotoxicology and Environmental Safety* 126: 56–61.

Malik, U., and A. Barik. 2015. Free fatty acids from the weed, *Polygonum orientale* leaves for attraction of the potential biocontrol agent, *Galerucella placida* (Coleoptera: Chrysomelidae). *Biocontrol Science and Technology* 25: 593–607.

Malik, U., A. Karmakar, and A. Barik. 2016. Attraction of the potential biocontrol agent *Galerucella placida* (Coleoptera: Chrysomelidae) to the volatiles of *Polygonum orientale* (Polygonaceae) weed leaves. *Chemoecology* 26: 45–58.

Mitra, S., N. Sarkar, and A. Barik. 2017. Long-chain alkanes and fatty acids from *Ludwigia octovalvis* weed leaf surface waxes as short-range attractant and ovipositional stimulant to *Altica cyanea* (Weber) (Coleoptera: Chrysomelidae). *Bulletin of Entomological Research* 107: 391–400.

Mukherjee, A., and A. Barik. 2014. Long-chain free fatty acids from *Momordica cochinchinensis* Spreng flowers as allelochemical influencing the attraction of *Aulacophora foveicollis* Lucas (Coleoptera: Chrysomelidae). *Allelopathy Journal* 33: 255–266.

Mukherjee, A., A. Karmakar, and A. Barik. 2017. Bionomics of *Momordica cochinchinensis* fed *Aulacophora foveicollis* (Coleoptera: Chrysomelidae). *Proceedings of the Zoological Society* 70: 81–87.

Mukherjee, A., N. Sarkar, and A. Barik. 2013. Alkanes in flower surface waxes of *Momordica cochinchinensis* influence attraction to *Aulacophora foveicollis* Lucas (Coleoptera: Chrysomelidae). *Neotropical Entomology* 42: 366–371.

Mukherjee, A., N. Sarkar, and A. Barik. 2014. Long-chain free fatty acids from *Momordica cochinchinensis* leaves as attractants to its insect pest, *Aulacophora foveicollis* Lucas (Coleoptera: Chrysomelidae). *Journal of Asia-Pacific Entomology* 17: 229–234.

Mukherjee, A., N. Sarkar, and A. Barik. 2015a. *Momordica cochinchinensis* (Cucurbitaceae) leaf volatiles: semiochemicals for host location by the insect pest, *Aulacophora foveicollis* (Coleoptera: Chrysomelidae). *Chemoecology* 25: 93–104.

Mukherjee, A., N. Sarkar, and A. Barik. 2015b. Leaf surface *n*-alkanes of *Momordica cochinchinensis* Spreng as short-range attractants for its insect pest, *Aulacophora foveicollis* Lucas (Coleoptera: Chrysomelidae). *Allelopathy Journal* 36: 109–122.

Mundhe, A.Y., and S.V. Pandit. 2014. Assessment of toxicity of monocrotophos in freshwater bivalve, *Lamellidens marginalis*, using different markers. *Toxicology International* 21: 51–56.

Nawrot, J., M. Gawlak, J. Szafranek, B. Szafranek, E. Synak, J.R. Warchalewski, D. Piasecka-Kwiatkowska, W. Błaszczak, T. Jeliński, and J. Fornal. 2010. The effect of wheat grain composition, cuticular lipids and kernel surface microstructure on feeding, egg-laying, and the development of the granary weevil, *Sitophilus granarius* (L.). *Journal of Stored Products Research* 46: 133–141.

Nelson, D.R., and L.D. Charlet. 2003. Cuticular hydrocarbons of the sunflower beetle, *Zygogramma exclamationis*. *Comparative Biochemistry and Physiology—Part B: Biochemistry and Molecular Biology* 135: 273–284.

Nelson, D.R., D.L. Olson, and C.L. Fatland. 2002. Cuticular hydrocarbons of the flea beetles, *Aphthona lacertosa* and *Aphthona nigriscutis*, biocontrol agents for leafy spurge (*Euphorbia esula*). *Comparative Biochemistry and Physiology—Part B: Biochemistry and Molecular Biology* 133: 337–350.

Pamanji, R., M.S. Bethu, B. Yashwanth, S. Leelavathi, and J.V. Rao. 2015. Developmental toxic effects of monocrotophos, an organophosphorous pesticide, on zebrafish (*Danio rerio*) embryos. *Environmental Science and Pollution Research* 22: 7744–7753.

Paszkiewicz, M., A. Sikora, M.I. Boguś, E. Włóka, P. Stepnowski, and M. Gołębiowski. 2016. Effect of exposure to chlorpyrifos on the cuticular and internal lipid composition of *Blattella germanica* males. *Insect Science* 23: 94–104.

Pedrini, N., S.J. Mijailovsky, J.R. Girotti, R. Stariolo, R.M. Cardozo, A. Gentile, and M.P. Juárez. 2009. Control of pyrethroid-resistant Chagas disease vectors with entomopathogenic fungi. *PLoS Neglected Tropical Disease* 3: e434.

Rahaman, M.A., and M.D.H. Prodhan. 2007. Effects of net barrier and synthetic pesticides on red pumpkin beetle and yield of cucumber. *International Journal of Sustainable Crop Production* 2: 30–34.

Raman, K., and R.S. Annadurai. 1985. Host selection and food utilization of the red pumpkin beetle, *Raphidopalpa foveicollis* (Lucas) (Chrysomelidae: Coleoptera). *Proceedings: Animal Sciences* 94: 547–556.

Rangaswamy, V., P.B. Charyulu, and K. Venkateswarlu. 1989. Effect of monocrotophos and quinalphos on soil population and nitrogen-fixing activity of *Azospirillum* sp. *Biomedical and Environmental Science* 2: 305–311.

Remia, K.M., S. Logaswamy, K. Logankumar, and D. Rajmohan. 2008. Effect of an insecticide (monocrotophos) on some biochemical constituents of the fish *Tilapia mossambica*. *Pollution Research* 27: 523–526.

Reue, K. 2011. A thematic review series: Lipid droplet storage and metabolism: From yeast to man. *Journal of Lipid Research* 52: 1865–1868.

Rupa, D.S., P.V. Lakshman Rao, P.P. Reddy, and O.S. Reddi. 1988. In vitro effect of monocrotophos on human lymphocytes. *Bulletin of Environmental Contamination and Toxicology* 41: 737–741.

Sankhwar, M.L., R.S. Yadav, R.K. Shukla, D. Singh, R.W. Ansari, A.B. Pant, D. Parmar, and V.K. Khanna. 2013. Monocrotophos induced oxidative stress and alterations in brain dopamine and serotonin receptors in young rats. *Toxicology and Industrial Health* 32: 422–436.

Sarkar, N., and A. Barik. 2015. Free fatty acids from *Momordica charantia* L. flower surface waxes influencing attraction of *Epilachna dodecastigma* (Wied.) (Coleoptera: Coccinellidae). *International Journal of Pest Management* 61: 47–53.

Sarkar, N., A. Karmakar, and A. Barik. 2016. Volatiles of *Solena amplexicaulis* (Lam.) Gandhi leaves influencing attraction of two generalist insect herbivores. *Journal of Chemical Ecology* 42: 1004–1015.

Sarkar, N., U. Malik, and A. Barik. 2014. *n*–alkanes in epicuticular waxes of *Vigna unguiculata* (L.) Walp. leaves. *Acta Botanica Gallica* 161: 373–377.

Simpson, I.C., and P.A. Roger. 1995. The impact of pesticides on non-target aquatic invertebrates in wetland ricefields: A review. In *Impact of pesticides on farmer health and the rice environment*, ed. P.L. Pingali and P.A. Roger, 249–270. Philippines: IRRI Editions.

Singh, D., and C.K. Gill. 1979. Estimation of losses in growth and yield of muskmelon due to *Aulacophora foveicollis* Lucas. *Indian Journal of Entomology* 44: 294–295.

Singh, S., A. Ranjit, S. Parthasarathy, N. Sharma, and P. Bambery. 2004. Organophosphate induced delayed neuropathy: Report of two cases. *Neurology India* 52: 525–526.

Sinha, S.N., and A.K. Chakrabarti. 1983. Effect of seed treatment with carbofuran on the incidence of red pumpkin beetle, *Raphidopalpa foveicollis* Lucas on cucurbits. *Indian Journal of Entomology* 45: 145–151.

Skripsky, T., and R. Loosli. 1994. Toxicology of monocrotophos. *Reviews of Environmental Contamination and Toxicology* 139: 13–39.

Stanley-Samuelson, D.W., R.A. Jurenka, C. Crips, G.J. Blomquist, and M. de Renobales. 1988. Fatty acids in insects: composition, metabolism and biological significance. *Archives of Insect Biochemistry and Physiology* 9: 1–33.

Tariq, M.I., S. Afzal, and I. Hussain. 2004. Pesticides in shallow groundwater of Bahawalnagar, Muzafargarh, D.G. Khan and Rajan Pur districts of Punjab, Pakistan. *Environment International* 30: 471–479.

Velmurugan, B., M. Selvanayagam, E.I. Cengiz, and E. Unlu. 2007. The effects of monocrotophos to different tissues of freshwater fish *Cirrhinus mrigala*. *Bulletin of Environmental Contamination and Toxicology* 78: 450–454.

Vijay Kumar, B., and N.V. Prasad. 2013. Effect of the pesticide monocrotophos on the osmoregulation of a brackish water oligochaete, *Pontodrilus bermudensis* (Beddard) in relation to salinity variations. *International Journal of Bioassays* 2: 964–970.

Vijayavel, K., E.F. Rani, C. Anbuselvam, and M.P. Balasubramanian. 2006. Interactive effect of monocrotophos and ammonium chloride on the freshwater fish *Oreochromis mossambicus* with reference to lactate/pyruvate ratio. *Pesticide Biochemistry and Physiology* 86: 157–161.

Waterhouse, D.F., and K.R. Norris. 1987. *Biological Control: Pacific Prospects*. Melbourne: Inkata Press.

WHO 2009. Health implications from monocrotophos use: a review of the evidence in India.

Wu, Y., J. Shen, J. Chen, X. Lin, and A. Li. 1996. Evaluation of two resistance monitoring methods in *Helicoverpa armigera*: Topical application and leaf dipping method. *Journal of Plant Protection* 22: 3–6.

Wu, Y., J. Shen, F. Tan, and Z. You. 1995. Mechanism of fenvalerate resistance in *Helicoverpa armigera* (Hübner). *Journal of Nanjing Agricultural University* 18: 63–68.

Yen, C.-L.E., S.J. Stone, S. Koliwad, C. Harris, and R.V. Farese Jr. 2008. Thematic review series: glycerolipids. DGAT enzymes and triacylglycerol biosynthesis. *Journal of Lipid Research* 49: 2283–2301.

Zar, J.H. 2010. *Biostatistical Analysis*. New Jersey: Prentice Hall.

Tissue and Cell 56 (2019) 14–22

Contents lists available at ScienceDirect

Tissue and Cell

journal homepage: www.elsevier.com/locate/tice

Anti-fibrotic effect of black tea (*Camellia sinensis*) extract in experimental pulmonary fibrosis

Kaustav Chakraborty[a,1], Avijit Dey[b,1], Arindam Bhattacharyya[a], Subir Chandra Dasgupta[b,*]

[a] Immunology Laboratory, Department of Zoology, University of Calcutta, 35, Ballygunge Circular Road, Kolkata, 700019, West Bengal, India
[b] Department of Zoology, Maulana Azad College, 8, Rafi Ahmed Kidwai Road, Kolkata, 700013, West Bengal, India

ARTICLE INFO

Keywords:
Pulmonary fibrosis
Lung
Bleomycin
Black tea extract

ABSTRACT

There is no effective therapy exists for Idiopathic pulmonary fibrosis (IPF) till now. Few studies have been done on protective effects of green tea in pulmonary fibrosis but there is no single report on black tea extract (BTE) in pulmonary fibrosis so far. This study aims to investigate the anti-fibrotic effect of BTE against experimental pulmonary fibrosis. Four groups of animals were selected for this study. Group 1: control group mice. Group 2: mice exposed to bleomycin for 21 days, Group 3 and Group 4: bleomycin exposed mice treated with 25 mg BTE/kg b.w./day, p.o and 50 mg BTE/kg b.w./day, p.o. respectively for 21 days. Bleomycin exposed mice showed increased collagen deposition and wet/dry weight ratio, which were attenuated upon 50 mg BTE/kg b.w. treatment. The increased level of histopathological parameters in bleomycin-induced mice was significantly decreased after 50 mg BTE/kg b.w. treatment. Furthermore, 50 mg BTE/kg b.w. administration also decreased the expression of α-SMA in bleomycin-induced mice. This treatment with 50 mg BTE/kg b.w. also down regulated the expression of TGF-β and up regulated IFN-γ expression in experimental pulmonary fibrosis. The results of the present study put-forward BTE as a potential anti-fibrotic agent due to its attenuating effect on potential fibrotic markers.

1. Introduction

Idiopathic pulmonary fibrosis (IPF) is a devastating disease of the lung for which no effective therapy exists (Mason et al., 1999; Gross and Hunninghake, 2001). It is a progressive disorder characterized by the excessive proliferation of fibroblasts and deposition of extracellular matrix, which destroy normal tissue architecture and function (O'Connell et al., 2011). Abnormal repair of lung tissues is a serious pathological condition in pulmonary fibrosis. Chronic inflammation and progressive fibrosis of the pulmonary interstitial tissues are the main features for pulmonary fibrosis (Green, 2002). It is believed that lung inflammation initiates lung fibrosis; however, the exact pathophysiology of this disease has not yet been fully demonstrated (Janssen et al., 2013). Therefore, it is crucial to find new therapeutic strategies for pulmonary fibrosis.

Bleomycin-induced pulmonary fibrosis in rodents is popular and has been used as a surrogate model for human lung fibrosis (Giri et al., 2002). Many research groups have reported that during the early stages of bleomycin-induced lung damage, several biochemical and functional changes occurs such as inflammatory cell infiltration, increased collagen content, reduced lung volume and compliance (Osanai et al., 1991; Zia et al., 1992; Usuki and Fukuda, 1995) that resembles human pulmonary fibrosis.

Tea brew and its bioactive components have been attracting much attention with regard to human health. For last few decades several studies have concluded their effectiveness and potential applicability in disease prevention or therapy. Both green tea and black tea are cardio protective (Riemersma et al., 2001; Davies et al., 2003; Hirata et al., 2004; Stangl et al., 2007; Jochmann et al., 2008; Singh et al., 2009), antioxidant and anti-inflammatory (Roy et al., 2008; de Mejia et al., 2009), have anti-cancer effects (Zhang et al., 2007; Kurahashi et al., 2008; Chen et al., 2008; Tang et al., 2009; Boehm et al., 2009; Wang et al., 2010; Larsen et al., 2010; Henning et al., 2011; George et al., 2011; Shih et al., 2016), anti-obese effects (Klaus et al., 2005; Chen

Abbreviations: IPF, Idiopathic Pulmonary Fibrosis; BIPF, Bleomycin-induced Pulmonary Fibrosis; BTE, Black Tea Extract; TGF-β, Transforming Growth factor-β; TNF-α, Tumor Necrosis Factor-α; IFN-γ, Interferon-γ; IL-, Interleukin; α-SMA, α-Smooth Muscle Actin; BALF, Broncho-Alveolar Lavage Fluid; DAB, 3,3'-diaminobenzidine; p.o., per oral

* Corresponding author.
E-mail address: subirdgupta@gmail.com (S.C. Dasgupta).
[1] Contributed equally in this research paper.

https://doi.org/10.1016/j.tice.2018.11.006
Received 22 August 2018; Received in revised form 27 November 2018; Accepted 28 November 2018
Available online 29 November 2018
0040-8166/

et al., 2009; Grove and Lambert, 2010), neuroprotective effects (Yamada et al., 2007; Hamaguchi et al., 2009; Skrzypczak-Jankun and Jankun, 2010). In last few years scientist are looking for therapeutic effects of tea and its active components in lung diseases. Few studies have been done so far mainly on green tea and its active component epigallocatechin-3-gallate (EGCG) on pulmonary fibrosis (Donà et al., 2003; Kim et al., 2006; Sriram et al., 2008, 2009; Hamdy et al., 2012; You et al., 2014). However, there is no report on protective nature of black tea extract (BTE) in experimental pulmonary fibrosis till now.

To full-fill our objective, we have checked different parameters such as wet/dry weight ratios, quantification of hydroxyproline, collagen staining, expression of pro- and anti-fibrotic molecules, immunohistochemistry for EMT marker α-SMA after BTE treatment in bleomycin-induced pulmonary fibrosis. Apart from these, we also performed IHC to see the effect of BTE on apoptotic markers in lung fibrosis. It has been demonstrated that Bax plays an important role in the pathogenesis of bleomycin-induced pulmonary fibrosis as well as transgenic TGF-β1 (Kang et al., 2007). The function of the Bcl-2 family of proteins is modulation of cell survival (Reed, 1994; Oltvai et al., 1993; Boise et al., 1993). Bax protein is an endogenous antagonist of Bcl-2, which binds to and inactivates this protein (Oltvai et al., 1993). So, the balance between Bax and Bcl-2 is the key determining factor for susceptibility of a cell to apoptosis. Therefore, this study is the first attempt to evaluate the protective effect of BTE against bleomycin-induced pulmonary fibrosis.

2. Materials and methods

2.1. Chemicals

Absolute alcohol (ethanol) and Methanol (Merck, India), anti-mouse Bax, Bcl2, caspase-3 (Santa Cruz Biotechnology, United States) for immunohistochemistry, Avitin-Biotin Conjugate (Thermo Fisher Scientific, United States) for immunohistochemistry, Biotin-conjugated anti-mouse secondary antibodies (Thermo Fisher Scientific, United States) for immunohistochemistry, DAB substrate and diluent (Thermo Fisher Scientific, United States) for immunohistochemistry, DPX (LOBA Chemie, India), Di-sodium hydrogen phosphate (SRL, India), Sodium di-hydrogen phosphate (SRL, India), Eosin (Sigma, USA), Formaldehyde solution 37–41% w/v (Merck, India), Giemsa's stain (Himedia, India), Glacial Acetic Acid (Merck, India), Glycerol anhydrous (Milli-Mark, India), Hematoxylin (Merck, Germany), mice ELISA kits for TGF-β, TNF-α, IL-1β and IL-10 (RayBiotech, USA), Multistrix SG Paraffin wax 56–58 °C (Merck, India), Picric Acid (Merck, India), Potassium hydroxide (Merck, India), Salt mixture H.M.W. (SRL, India), Sodium chloride (SRL, India), Tri-sodium citrate (Merck, India), Xylene (Merck, India).

2.2. Animals

Male (25 ± 1 g) swiss albino mice were obtained from the enlisted supplier of CPCSEA (Committee for the Purpose of Control and Supervision of Experiments on Animal), India. They were housed in polypropylene cages (290 × 220 × 140 mm) at controlled temperature (25 ± 2°), with light conditions (12 h light and dark cycle) and relative humidity (65 ± 5%). The animals were provided with pellet diet (Ashirwad Industries, Chandigarh, India), green vegetables, gram and water *ad libitum*. All animals for this experiment were kept in CPCSEA approved animal house (vide F. No.- 25/250/2012-AWD, dated 26.2.2014) of Maulana Azad College, Kolkata. Experiments described in this study were done by following the guideline of the CPCSEA, Government of India.

2.3. Collection of black tea

Fresh black tea (C.T.C., Assam) was purchased from authenticated tea supplier M/S. Subodh Brothers Pvt. Ltd., Kolkata-700012, India.

2.4. Preparation of black tea extract and treatment schedule

Black tea extract (BTE) was prepared after Dey et al., 2017 (Dey et al., 2017). First, 1 g black tea was added into 100 ml of boiled drinking water, was kept covered for 5 min, filtered by tea strainer and cooled down to 40 °C. The dry weight of one cup of black tea liquor was calculated by evaporating the water from 100 ml freshly prepared BTE. For treatment in experimental mice, BTE was produced in the same way by adding 1 g of black tea in 6 ml boiled drinking water. 100 µl and 200 µl BTE was administered orally by oral gavage to BTE treatment group of mice to attain the doses of 25 mg and 50 mg BTE/kg b.w./day, p.o. These two doses are equivalent to 2.5 cup and 5 cup BTE respectively in human considering 60 kg as average body weight of an adult human. BTE was expressed in terms of dry weight. Freshly prepared BTE was administered orally by the help of oral gavage to the bleomycin-treated mice groups for 21 days.

2.5. Bleomycin-induced pulmonary fibrosis in mice

Animals were anesthetized with ketamine and given intratracheal injections of 50 µL of bleomycin (5 mg/kg body weight) diluted in normal saline on Day 0 (Chakraborty et al., 2017). For experiments, mice were sacrificed on day 21 and lung samples were collected.

2.6. Experimental design

Four groups of animals were selected for this study (n = 15 per group). Group 1: control group mice were treated with 0.9% sterile saline. Group 2: mice exposed to bleomycin for 21 days, Group 3 and Group 4: bleomycin exposed mice treated with 25 mg BTE/kg b.w./day, p.o and 50 mg BTE/kg b.w./day, p.o respectively for 21 days. BTE was orally administered by using oral gavage for mice. All four experimental groups of mice were provided with pellet diet, green vegetables, gram and drinking water *ad libitum*.

2.7. Determination of wet/dry weight ratios

The wet/dry (W/D) method was used to measure pulmonary edema. After a thoracotomy, the lungs were collected and weighed before and after drying in the incubator at 60 °C for 72 h.

2.8. Histopathology

For morphological observation by light microscopy, lungs from all experimental groups were collected on day 21. The tissues were fixed in 10% neutral buffered formalin for 24 h and then dehydrated in graded (50–100%) ethanol followed by paraffin block preparation. Xylene was used to deparaffinise the paraffin sections, then the sections were stained with haematoxyiln-eosin and Masson's trichrome. Histological changes were observed with a bright field microscope (ZEISS, Germany) and photographs were captured using ZEISS AxioCam ICc1 and Zen software (Zen2 lite) at 100X magnification. The Ashcroft score was used for the quantitative histologic analysis (Ashcroft et al., 1988).

2.9. Immunohistochemistry

For immunohistochemistry (IHC), lungs tissue sections were mounted on poly-L-Lysine coated slides. Sections were deparaffinised, dehydrated through graded alcohols, antigen retrieval was done by 10 mM sodium citrate and endogenous peroxidase was quenched by 3% hydrogen peroxide (H_2O_2). After blocking with 1% foetal calf serum (FCS) in tris-buffer saline (TBS), the sections were incubated in a humid chamber overnight at 4 °C with primary antibodies like anti-mouse Bax, Bcl2, caspase-3 (Santa Cruz Biotechnology, United States). After

washing in wash buffer (1% Tween 20 in TBS or 1X TBST), sections were incubated in biotin-conjugated anti-mouse secondary antibodies (Thermo Fisher Scientific, United States) diluted in Tris-buffered saline (TBS) for 2 h at room temperature. After washing in 1X TBST sections were incubated in Avitin-Biotin Conjugate (ABC) (Thermo Fisher Scientific, United States) for 30 min. Immunoreactivity was detected using a DAB system (Thermo Fisher Scientific, United States). Sections were then counterstained briefly in hematoxylin, dehydrated through graded alcohols, cleared in xylene, and cover-slipped with DPX (Jungbluth et al., 2003; Ataee et al., 2010). Images were captured and changes were observed with bright field microscope (ZEISS, Germany) and photographs were taken by using ZEISS AxioCam ICc1 and Zen software (Zen2 lite) at 100X magnification.

2.10. Hydroxyproline assay

The collagen content in the lung homogenates was examined by a hydroxyproline (HYP) colorimetric assay kit (BioVision). All steps of the HYP assay were performed according to the manufacturer's instructions. The absorbance of each sample at 560 nm wavelength was read by a microplate reader (Thermo Fisher Scientific, USA).

2.11. Broncho-alveolar Lavage fluid (BALF) and serum collection

After sacrifice, trachea of mice was exposed and a plastic cannula was inserted into the trachea. 1 ml of 0.9% saline solution was injected into the lungs by a syringe and was then withdrawn. This injection procedure was repeated five times. The BALF was centrifuged at 1500 rpm for 8 min at 4 °C. The BALF supernatant was collected after centrifugation and stored at −80 °C before the cytokine assay (Chakraborty et al., 2014). For serum preparation blood was collected by cardiac puncture and was kept in a siliconized vial in room temperature for 15 min, 15 min in 4 °C and then was centrifuged at 3000 rpm for 15 min in 4 °C.

2.12. Cytokine assay

TGF-β, TNF-α, IL-1β and IL-10 levels in BALF and serum were measured using ELISA kits according to the manufacturer's protocol (RayBio® Mouse ELISA kit). The absorbance at 450 nm (A450) was determined using a 96-well bichromatic microplate reader (eBioscience, USA).

2.13. Reverse transcription PCR and quantitative PCR analysis

Total RNA was extracted from lung tissues using an RNAase Mini Kit (Promega). The RNA was then reverse transcribed to cDNA according to Chakraborty et al. (2014) (Chakraborty et al., 2014). Real-time PCR amplifications were performed in triplicate using the PowerUp™SYBR Green Master Mix and were carried out using ABI PRISM 7000 Sequence Detection System (Applied Biosystems). The threshold cycle (Ct) was obtained from the PCR curves and expression levels of the target genes were quantified in terms of the Ct values corresponding to the untreated and treated samples and were normalized against GAPDH (internal control). Fold change of gene expression was quantified in terms of $2^{-\Delta\Delta Ct}$ (Chakraborty et al., 2018). Subsequently, the expressions of GAPDH, TGF-β, IFN-γ, CTGF and PGE2 transcripts were determined. Primer sequences were designed using the NCBI-Primer BLAST online tool and Primer-quest from Integrated DNA Technologies. Primer sequences were as follows:

TGF-β (F) 5'-GGTGGTATACTGAGACACCTTG-3'
TGF-β (R) 5'-CCCAAGGAAAGGTAGGTGATAG-3'
IFN-γ (F) 5'- GGCCATCAGCAACAACATAAG-3'
IFN-γ (R) 5'- GTTGACCTCAAACTTGGCAATAC-3'
GAPDH (F) 5'- TCTCCCTCACAATTTCCATCC-3'
GAPDH (R) 5'- GGGTGCAGCGAACTTTATTG-3'

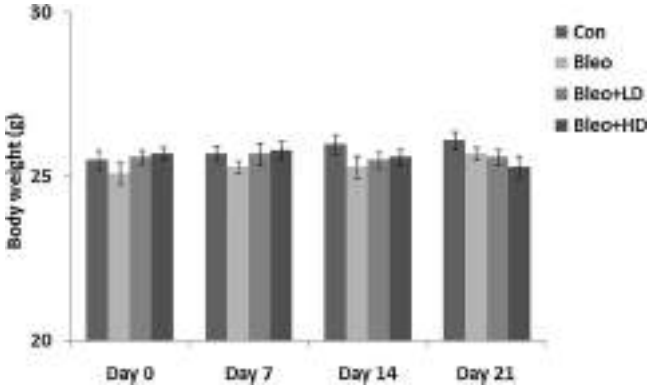

Fig. 1. Body weight changes after BTE treatment in experimental pulmonary fibrosis. The bar graph shows body weight of mice in all the experimental groups on different experimental days. Data represent the mean ± standard deviation (n = 5).

2.14. Statistical analysis

The data generated on various parameters were subjected to statistical analysis for reporting group means and standard deviation (mean ± SD) with significance between the controls and the treated. Collected data were subjected to one-way analysis of variance (ANOVA) considering p-values of < 0.05 were considered as significant. SPSS 17.0 software (IBM Corporation, United States) was used for statistical analysis.

3. Results

3.1. Effect of BTE on body weights of lung fibrosis mice

First of all, we examined the effect of BTE on the body weight of bleomycin-treated mice groups up to day 21. But, we didn't observe any significant change among all the experimental groups (Fig. 1).

3.2. BTE ameliorates fibrosis in experimental lung fibrosis

Histopathological examinations of lung showed that inflammation persisted in bleomycin-treated mice (Fig. 2B). Bleomycin + 25 mg BTE/kg b.w./day, p.o. treated mice showed slight reduction in inflammation whereas bleomycin + 50 mg BTE/kg b.w./day, p.o. treated mice expressed a significant reduction in lung inflammation (Fig. 2C,D) with respect to bleomycin-treated mice. We also found that the total number of leukocytes and number of inflammatory cell such as neutrophils were more infiltrated in bleomycin-treated group and bleomycin + 25 mg BTE/kg b.w./day, p.o. treated mice group (Sup. Fig. 1A,B). But there was significantly decreased quantity of leukocytes and neutrophils observed after 50 mg BTE/kg b.w./day, p.o. treatment (Sup. Fig. 1A,B). Severe fibrosis was found in bleomycin-treated mice (Fig. 2F). Fibrosis even existed in bleomycin + 25 mg BTE/kg b.w./day, p.o. treated mice group (Fig. 2G). In contrast, lung fibrosis was markedly alleviated in bleomycin + 50 mg BTE/kg b.w./day, p.o. treated mice group (Fig. 2H). The collagen content was tested using a hydroxyproline (HP) assay, which showed that bleomycin induced an increase in the HP content in lung. But, BTE bleomycin + 50 mg BTE/kg b.w./day, p.o. significantly reduced the HP content compared to bleomycin-treated and bleomycin + 25 mg BTE/kg b.w./day, p.o. (Fig. 2J). Likewise, compared with the bleomycin-treated mice without BTE, the mice treated with bleomycin + 50 mg BTE/kg b.w./day, p.o. showed a significant reduction in the lung Wet/Dry weight ratio (Fig. 3). Although, the mice treated with bleomycin + 25 mg BTE/kg b.w./day, p.o. didn't show any significant change.

Further, we checked the expression of α-SMA which is known to be

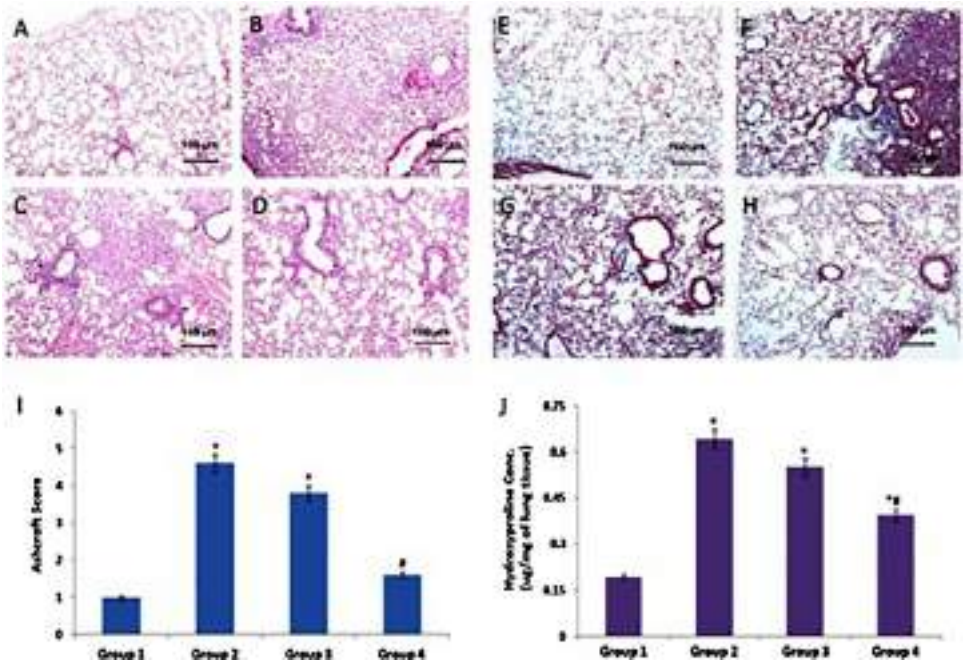

Fig. 2. The anti-fibrotic effects of therapeutic treatment with BTE on experimental pulmonary fibrosis. Histopathological changes in mouse lungs observed under light microscope with **(A–D)** Haematoxylin-Eosin and **(E–H)** Masson's trichrome staining on day 21. Magnification = 100 × . Indicated scale bars signify 100 µm distances. **(I)** Comparison of the Ashcroft score among the experimental groups. (*J*) Severity of fibrosis was quantified by hydroxyproline assay. The levels of lung hydroxyproline concentration in all four experimental mice groups on day 21 are represented as bar graph. Data are represented as mean ± SD (n = 5) where *P < 0.05 compared with control (saline-treated) group; #P < 0.05 compared with bleomycin-treated group. Group 1: control group, Group 2: Bleomycin-treated, Group 3 and Group 4: bleomycin exposed mice treated with 25 mg BTE/kg b.w./day, p.o and 50 mg BTE/kg b.w./day, p.o respectively.

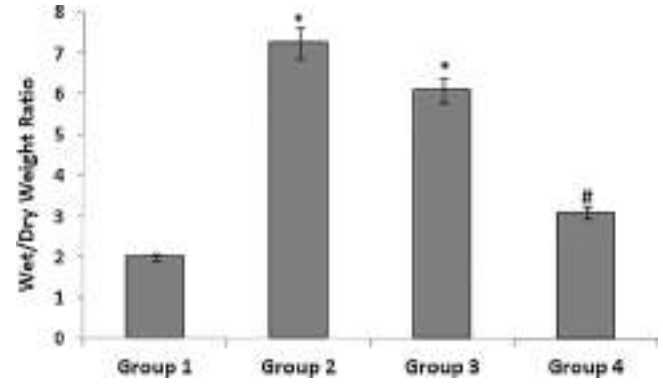

Fig. 3. BTE treatment affects Wet/Dry weight ratio of lung in pulmonary fibrosis. The degree of lung injury was assessed by W/D ratio. Data are represented as mean ± SD (n = 5) where *P < 0.05 compared with control (saline-treated) group; #P < 0.05 compared with bleomycin-treated group. Group 1: control group, Group 2: Bleomycin-treated, Group 3 and Group 4: bleomycin exposed mice treated with 25 mg BTE/kg b.w./day, p.o and 50 mg BTE/kg b.w./day, p.o respectively.

critical for pulmonary fibrosis (Ou et al., 2008). Fig. 4 revealed that there was increased expression of α–SMA in bleomycin-treated mice group. After BTE treatment, there was a trend of reduction of α-SMA expression in bleomycin + 25 mg BTE/kg b.w./day, p.o. and especially in bleomycin + 50 mg BTE/kg b.w./day, p.o. All these findings demonstrated that 50 mg BTE/kg b.w./day, p.o. reduces experimental lung fibrosis.

3.3. Expression of pro- and anti-fibrotic markers after BTE treatment in lung fibrosis

As TGF-β is one of the important pro-fibrotic factors which drive fibrosis, we checked its expression after BTE treatment in bleomycin-treated lung fibrosis. By qPCR analysis, we found that TGF-β expression was significantly downregulated in bleomycin + 50 mg BTE/kg b.w./day, p.o. treated mice with compared to bleomycin-treated and bleomycin + 25 mg BTE/kg b.w./day, p.o. treated mice (Fig. 5A).

We also determined the expression of anti-fibrotic molecule such as IFN-γ. BTE treatment induced IFN-γ expression with compared to control and bleomycin-treated groups. Both bleomycin + 25 mg BTE/kg b.w./day, p.o. and bleomycin + 50 mg BTE/kg b.w./day, p.o. treated mice showed significant increase in the expression of IFN-γ with compared to bleomycin-treated groups (Fig. 5B).

3.4. Role of BTE on apoptotic markers in bleomycin-induced lung fibrosis

We examined by IHC the expression of Bax, Caspase3 and Bcl-2 in bleomycin-induced pulmonary fibrosis after BTE treatment. Our findings suggested that the increased expression of Bax (Fig. 6A) and Caspase3 (Fig. 6C) in bleomycin-treated mice was reduced upon 50 mg BTE/kg b.w. treatment. 25 mg BTE/kg b.w. treatment reduced the expression level of Bax and Caspase3 in comparison to bleomycin-treated group but not much reduced as in bleomycin + 50 mg BTE/kg b.w./day, p.o. treated group (Fig. 6A and 6C). No such significant changes were observed for Bcl-2 protein among the experimental groups (Fig. 6B).

3.5. Effect of BTE on pro- and anti-inflammatory cytokines in experimental lung fibrosis

The expression of key pro-inflammatory and anti-inflammatory cytokines from both BALF and serum showed significant changes. TNF-α level was higher in bleomycin-treated mice compared to other groups. The level of TNF-α was significantly reduced in bleomycin + 50 mg BTE/kg b.w./day, p.o. treated mice compared to bleomycin-treated and bleomycin + 25 mg BTE/kg b.w./day, p.o. treated group (Fig. 7A,B). Expression of another important pro-inflammatory cytokine IL-1β was increased in bleomycin-treated mice. Furthermore, IL-1β level was significantly dropped down in treated mice compared to bleomycin-treated and bleomycin + 25 mg BTE/kg b.w./day, p.o. treated mice in both BALF and serum sample (Fig. 7C,D).

Anti-inflammatory cytokine such as IL-10 level was also higher in bleomycin-induced lung fibrosis. BTE treatment showed significant decrease in secretion of IL-10 compared to bleomycin-treated group. Level of IL-10 was most significantly decreased in BALF and serum sample of bleomycin + 50 mg BTE/kg b.w./day, p.o. treated mice, almost equivalent to the level found in control group (Fig. 7E,F). TGF-β has dual role in lung fibrosis. It is pro-fibrotic as well as anti-

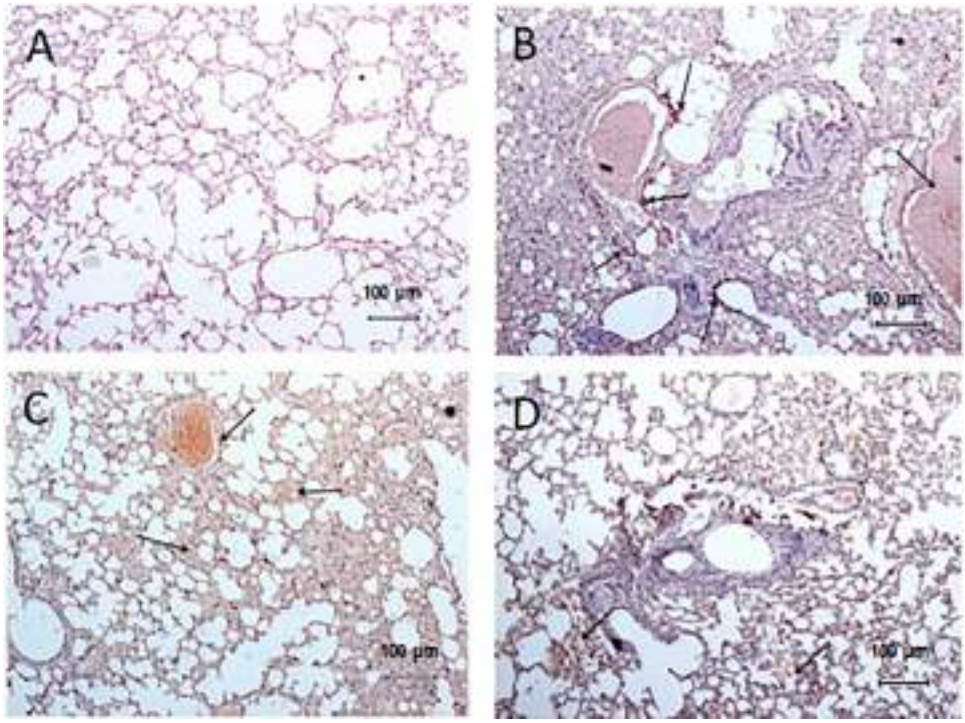

Fig. 4. BTE reduces α-SMA expression in experimental pulmonary fibrosis. Immunohistochemistry for α-SMA marker in lung tissue sections from all experimental mice groups. Magnification = 100 × . Indicated scale bars signify 100 µm distances. **(A)** Group 1: control group, **(B)** Group 2: Bleomycin-treated, **(C)** Group 3 and **(D)** Group 4: bleomycin exposed mice treated with 25 mg BTE/kg b.w./day, p.o and 50 mg BTE/kg b.w./day, p.o respectively.

inflammatory cytokine in nature. In our study we found that TGF-β level was significantly higher in bleomycin treated mice compared to other groups. TGF-β level was significantly decreased bleomycin + 50 mg BTE/kg b.w./day, p.o. treated mice compared to bleomycin-treated and bleomycin + 25 mg BTE/kg b.w./day, p.o. treated mice (Fig. 7G,H).

4. Discussion

To the best of our knowledge, there is no single report on anti-fibrotic property of black tea or any of its active components against pulmonary fibrosis. There are few reports on green tea and its active component EGCG in experimental pulmonary fibrosis. For example, Hamdy et al. (2012) used green tea extract (GTE) to see its protective nature in cyclophosphamide-induced pulmonary fibrosis. They found GTE (150 mg/kg b.w.) administered orally for 14 days, significantly reduced the expression of TGF-β and concentration of hydroxyproline which were otherwise higher in cyclophosphamide-treated pulmonary fibrosis (Hamdy et al., 2012).

Green tea leaves undergo minimal oxidation and retain the majority of catechins. Rich content of catechins representing approximately 90% of the polyphenolic fraction in green tea. Main catechins found in green tea are: catechin (C), epicatechin (EC), gallocatechin (GC), epicatechin gallate (ECG), epigallocatechin (EGC), epigallocatechin gallate (EGCG) among which EGCG is the major catechin fraction studied most extensively among the active components of green tea In black tea due to full oxidation, catechins polymerised to theaflavins and thearubigins (Unilever Report, 2011). Only about 15% catechins from green tea remain unchanged, and most of them transformed into theaflavins and thearubigins (Boehm et al., 2009). Fully fermented black tea has a dark brown hue and a sweet aroma of malt sugar. The typical black tea brew is consist of a number of small molecules, mostly alkaloids (theobromine and caffeine), carbohydrates, aminoacids (like theanine) and glycosylated flavonoids, together accounting for 30–40% of the dry

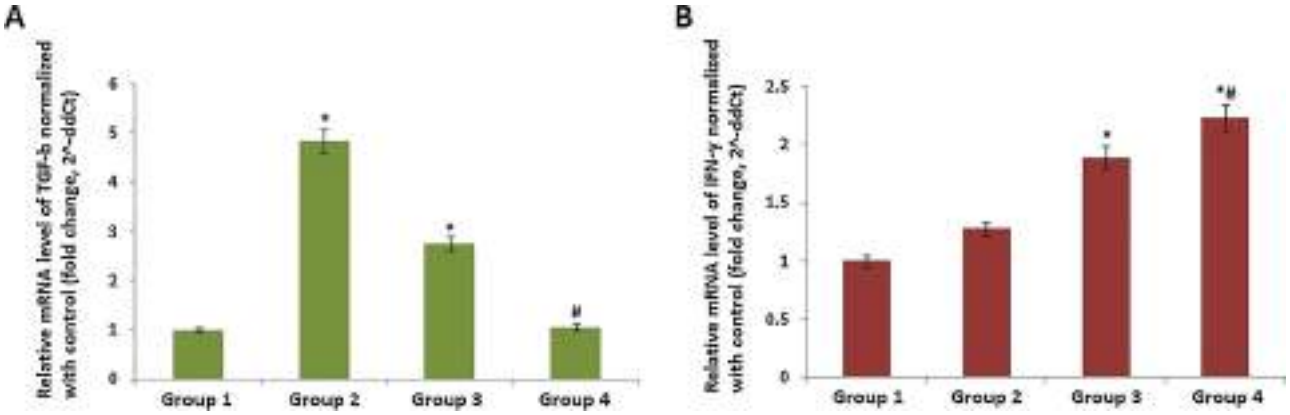

Fig. 5. BTE treatment decreases pro-fibrotic factors expression and increases anti-fibrotic factors expression. Relative mRNA expression level of **(A)** TGF-β, **(B)** IFN-γ in mice lungs were assessed by real-time PCR in all experimental mice groups on day 21. Data are represented as mean ± SD (n = 5) where *P < 0.05 compared with saline-treated control group; #P < 0.05 compared with bleomycin-treated group. GAPDH used as a loading control. Group 1: control group, Group 2: Bleomycin-treated, Group 3 and Group 4: bleomycin exposed mice treated with 25 mg BTE/kg b.w./day, p.o and 50 mg BTE/kg b.w./day, p.o respectively.

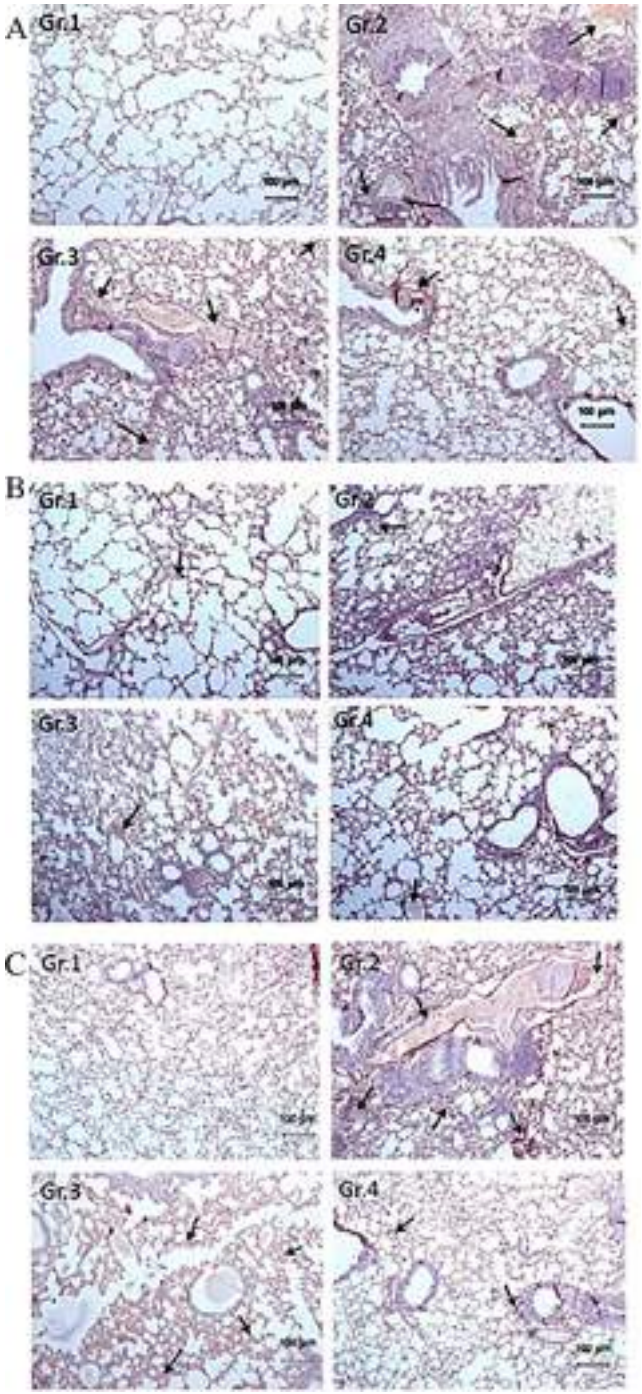

Fig. 6. A Effect of BTE on Bax in bleomycin-induced pulmonary fibrosis. Immunohistochemistry for Bax in lung tissue sections from all experimental mice groups. Magnification = 100 × . Indicated scale bars signify 100 µm distances. Gr.1: control group, Gr.2: Bleomycin-treated, Gr.3 and Gr.4: bleomycin exposed mice treated with 25 mg BTE/kg b.w./day, p.o and 50 mg BTE/kg b.w./day, p.o respectively. **B Expression of Bcl-2 in bleomycin-induced pulmonary fibrosis after BTE treatment.** Immunohistochemistry for Bax in lung tissue sections from all experimental mice groups. Magnification = 100 × . Indicated scale bars signify 100 µm distances. Gr.1: control group, Gr.2: Bleomycin-treated, Gr.3 and Gr.4: bleomycin exposed mice treated with 25 mg BTE/kg b.w./day, p.o and 50 mg BTE/kg b.w./day, p.o respectively. **C Effect of BTE on Caspase3 in bleomycin-induced pulmonary fibrosis.** Immunohistochemistry for Bax in lung tissue sections from all experimental mice groups. Magnification = 100 × . Indicated scale bars signify 100 µm distances. Gr.1: control group, Gr.2: Bleomycin-treated, Gr.3 and Gr.4: bleomycin exposed mice treated with 25 mg BTE/kg b.w./day, p.o and 50 mg BTE/kg b.w./day, p.o respectively.

weight. Remaining 60–70% consists of fermentation products, poorly characterized polyphenolic fractions in that number oxytheotannins further subdivided into theaflavins and thearubigins. Theaflavins which is a mixture of theaflavin-3-gallate, theaflavin-3´-gallate and theaflavin-3,3´-digallate possess benzotropolone rings with dihydroxy or trihydroxy aromatic moieties as substituents and a characteristic yellow-orange color (Vermeer et al., 2008). More than 5000 individual compounds construct the red-brown or dark brown thearubigins which retaining chiral properties of flavanols and theaflavins while prone to aggregation in aqueous solution. Their structures and bioavailability are still not well characterized (Kuhnert, 2010). Among the dry weight of black tea 3–6% is theaflavins and 12–18% is thearubigins which gives the strong, bitter flavor and characteristic dark color (Menet et al., 2004). Comparison of a content of the basic compounds in crude black and green tea extract is given in Table 1 (Kuroda and Hara, 1999). The most important flavonols in black tea are myricetin, quercetin, kaempferol and ruthin, similar as in green tea. Black tea contains phenolic acids, caffeine (almost one third the amount typical for coffee) and amino acids including theanine which occurs only in the tea leaves. Theanine or γ -glutamylethylamine accounts almost 50% of its aminoacid content and also gives the tea a unique brothy taste.

Our findings suggested that BTE (50 mg/kg b.w.) significantly downregulated the expression of pro-fibrotic molecule for example TGF-β and significantly upregulated the expression of anti-fibrotic molecule such as IFN-γ. BTE (50 mg/kg b.w.) also significantly reduced the level of pro-inflammatory cytokines such as TNF-α and IL-1β as well as anti-inflammatory cytokines such as IL-10 and TGF-β in both BALF and serum samples. Sriram et al. (2008 & 2009) demonstrated the anti-fibrotic nature of Epigallocatechin-3-gallate (EGCG) which is the major green tea component in bleomycin-induced pulmonary fibrosis. Intraperitoneal administration of EGCG at a dose of 20 mg/kg body weight significantly improved the body weight, considerably decreased the W/D ratio and hydroxyproline levels, which proved EGCG as a potential anti-fibrotic agent due to its attenuating effect on pulmonary fibrosis (Sriram et al., 2008, 2009). You et al. (2014) also reported that green tea extract EGCG inhibits irradiation-induced pulmonary fibrosis in adult rats (You et al., 2014). Our results suggested that BTE (50 mg/kg b.w.) treatment significantly decreased wet to dry lung weight ratio accompanied by reduced hydroxyproline concentration. H—E staining showed improved lung architecture and less collagen deposition evident in Masson's Trichrome staining. We also found that BTE (50 mg/kg b.w.) remarkably reduced the expression of α-SMA. However, we did not find any significant change in body weight in all experimental groups.

Presence of microscopic areas of epithelial cell dropout is a common feature of IPF. Epithelial cells apoptosis is key event in pathogenesis of this disease. Previous study confirmed that apoptotic hyperplastic epithelial cells are present in patients with IPF and that the expression of pro-apoptotic markers like bax and caspase-3 appears to be up-regulated and anti-apoptotic marker bcl-2 down-regulated in these cells. The increased expression of pro-apoptotic markers in epithelial cells of IPF patients are responsible for inadequate and delayed re-epithelialisation which ultimately leads to fibroblast proliferation (Plataki et al., 2005). Our IHC data showed similar situation in bleomycin-induced pulmonary fibrosis. After BTE (50 mg/kg b.w.) treatment, there was down-regulation of the expression of Bax and Caspase3 whereas the Bcl-2 expression remains unchanged in all experimental groups.

In our study, 50 mg BTE/kg b.w./day, p.o. dose shows some anti-fibrotic properties in experimental pulmonary fibrosis. Our results suggest the possibility of using BTE as protective agent for lung fibrosis. Thus, this study confirms the beneficial use of BTE in experimentally induced lung fibrosis. Further studies are warranted to establish the exact molecular mechanism of action of BTE and its active components which provide protection against pulmonary fibrosis and could be used as therapy to cure pulmonary fibrosis. It may have a wide application in

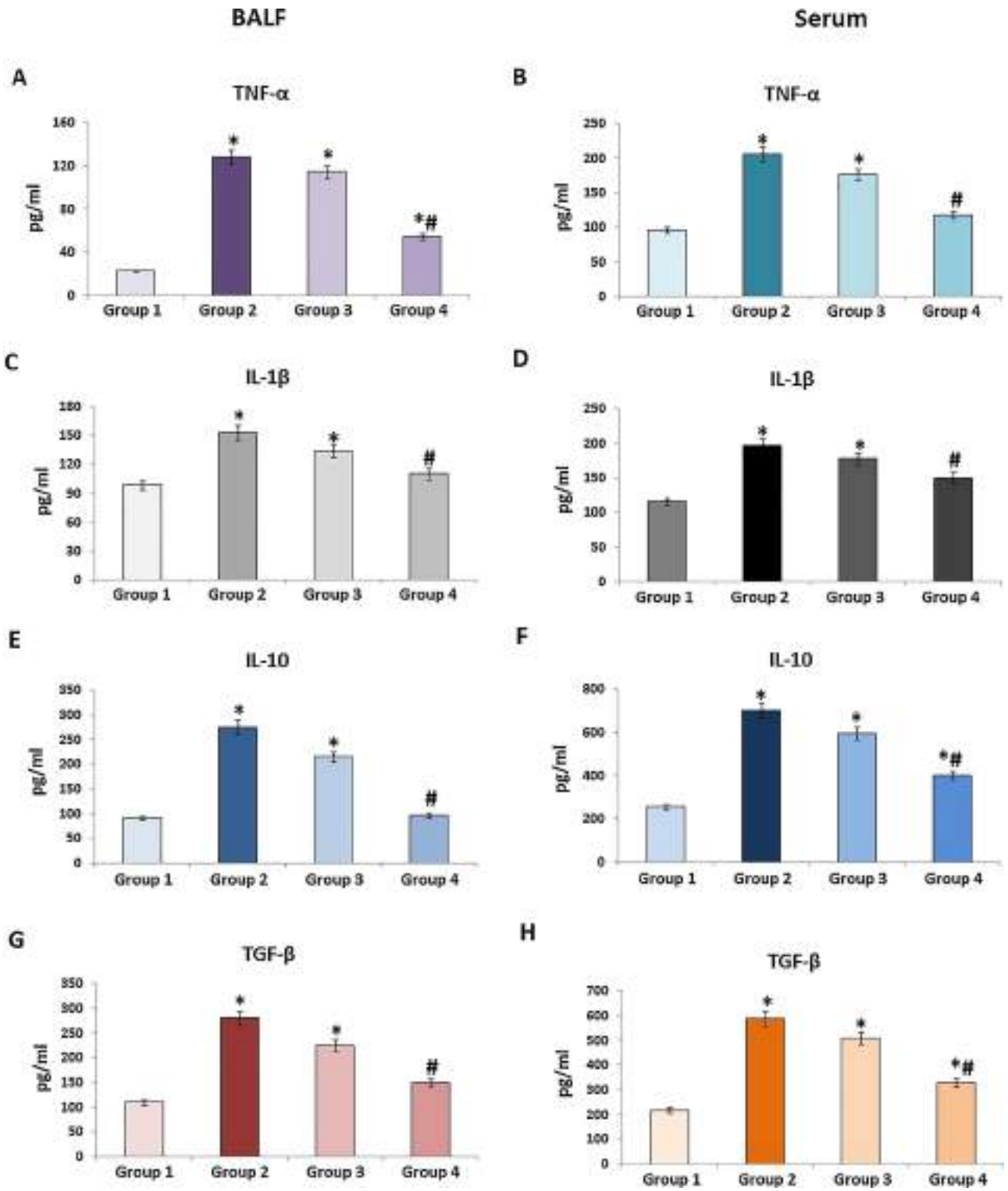

Fig. 7. Cytokine assay of pro- and anti-inflammatory markers. Pro-inflammatory cytokines **(A–B)** TNF-α, **(C–D)** IL-1β and anti-inflammatory cytokines **(E–F)** IL-10, **(G–H)** TGF-β level in BALF and serum were assayed using ELISA kit in all experimental groups. Group 1: control group, Group 2: Bleomycin-treated, Group 3 and Group 4: bleomycin exposed mice treated with 25 mg BTE/kg b.w./day, p.o and 50 mg BTE/kg b.w./day, p.o respectively.

suppressing drug- or chemical-induced lung injury.

5. Conclusion

In conclusion, BTE has the potential anti-fibrotic effects which protect and cure pulmonary fibrosis in experimental animals.

Author disclosures

KC and AD carried out the research and drafted the manuscript. KC and AD participated during all the experiments. SCD and AB designed and supervised all the experiments. All authors read and approved the final manuscript.

Conflict of interests

The authors declare there is no conflict of interests exists.

Funding source

This research work was supported by the National Tea Research Foundation, Tea Board, India (Code No. NTRF: 164/2014; Ref No. NTRF: 17(305)/2013/4423 dated 11th March 2014) and Council of Scientific & Industrial Research [No. 27(0323)/17/EMR-II, dated 12/04/2017], Government of India.

Acknowledgements

Authors would like to thank the Post Graduate Department of Zoology, Maulana Azad College, Kolkata and Immunology Laboratory, Department of Zoology, University of Calcutta, Kolkata for instruments facility. Authors also like to thank the University Grant Commission [UGC/1057E/Jr. Fellow (Upgradation), dated 21/08/2014], Government of India and National Tea Research Foundation, Tea Board, India for providing fellowship to the fellow.

Appendix A. Supplementary data

Supplementary material related to this article can be found, in the online version, at doi:https://doi.org/10.1016/j.tice.2018.11.006.

References

Ashcroft, T., Simpson, J.M., Timbrell, V., 1988. Simple method of estimating severity of pulmonary fibrosis on a numerical scale. J. Clin. Pathol. 41, 467–470.

Ataee, R., Ajdary, S., Zarrindast, M., Rezayat, M., Hayatbakhsh, M.R., 2010. Anti-mitogenic and apoptotic effects of 5-HT1B receptor antagonist on HT29 colorectal cancer cell line. J. Cancer Res. Clin. Oncol. 136 (10), 1461–1469. https://doi.org/10.1007/s00432-010-0801-3.

Boehm, K., Horneber, M., Borrelli, F., Ernst, E., 2009. Green Tea (Camellia Sinensis) for the Prevention of Cancer (Protocol). The Cochrane Collaboration: John Wiley & Sons, Ltd, pp. 1–7.

Boise, L., Gonzalez-Garcia, M., Postema, C.E., Ding, L., Lindsten, T., Turka, L.A., Mao, X., Nuñez, G., Thompson, C.B., 1993. Bcl-x, a bcl-2-related gene that functions as a dominant regulator of cell death. Cell 74 (4), 597–608.

Chakraborty, K., Chatterjee, S., Bhattacharyya, A., 2014. Modulation of phenotypic and functional maturation of murine bone-marrow-derived dendritic cells (BMDCs) induced by cadmium chloride. Int. Immunopharmacol. 20, 131–140.

Chakraborty, K., Chatterjee, S., Bhattacharyya, A., 2017. Modulation of CD11c+ lung dendritic cells in respect to TGF-β in experimental pulmonary fibrosis. Cell Biol. Int. 41, 991–1000.

Chakraborty, K., Chatterjee, S., Bhattacharyya, A., 2018. Impact of Treg on other T cell subsets in progression of fibrosis in experimental lung fibrosis. Tissue Cell 53, 87–92.

Chen, D., Milacic, V., Chen, M.S., Wan, S.B., Lam, W.H., Huo, C., Landis-Piwowar, K.R., Cui, Q.C., Wali, A., Chan, T.H., Dou, Q.P., 2008. Tea polyphenols, their biological effects and potential molecular targets. Histol. Histopathol. 23 (4), 487–496.

Chen, N., Bezzina, R., Hinch, E., Lewandowski, P.A., Cameron-Smith, D., Mathai, M.L., Jois, M., Sinclair, A.J., Begg, D.P., Wark, J.D., Weisinger, H.S., Weisinger, R.S., 2009. Green tea, black tea, and epigallocatechin modify body composition, improve glucose tolerance, and differentially alter metabolic gene expression in rats fed a high-fat diet. Nutr. Res. 29, 784–793.

Davies, M.J., Judd, J.T., Baer, D.J., Clevidence, B.A., Paul, D.R., Edwards, A.J., Wiseman, S.A., Muesing, R.A., Chen, S.C., 2003. Black tea consumption reduces total and LDL cholesterol in mildly hypercholesterolemic adults. Am. Socie. Nutr. Sci. 133, 3298S–3302S.

de Mejia, E.G., Ramirez-Mares, M.V., Puangpraphant, S., 2009. Bioactive components of tea: cancer, inflammation and behaviour. Brain Behav. Immun. 23, 721–731.

Dey, A., Gomes, A., Dasgupta, S.C., 2017. Black tea (*Camellia sinensis*) extract induced prenatal and postnatal toxicity in experimental albino rats. Phcog. Mag. 13 (52), S769–S774.

Donà, M., Dell'Aica, I., Calabrese, F., Benelli, R., Morini, M., Albini, A., Garbisa, S., 2003. Neutrophil restraint by green tea: inhibition of inflammation, associated angiogenesis, and pulmonary fibrosis. J. Immunol. 170 (8), 4335–4341.

George, J., Singh, M., Srivastava, A.K., Bhui, K., Roy, P., Chaturvedi, P.K., Shukla, Y., 2011. Resveratrol and black tea polyphenol combination synergistically suppress mouse skin tumors growth by inhibition of activated MAPKs and p53. PLoS One 6, e23395.

Giri, S.N., Biring, I., Nguyen, T., Wang, Q., Hyde, D.M., 2002. Abrogation of bleomycin-induced lung fibrosis by nitric oxide synthase inhibitor, aminoguanidine in mice. Nitric Oxide 7, 109–118.

Green, F.H., 2002. Overview of pulmonary fibrosis. Chest. 122, 334S–339S.

Gross, T.J., Hunninghake, G.W., 2001. Idiopathic pulmonary fibrosis. N. Engl. J. Med. 345, 517–525.

Grove, K.A., Lambert, J.D., 2010. Laboratory, epidemiological, and human intervention studies show that tea (*Camellia sinensis*) may Be useful in the prevention of obesity. J. Nutr. 140, 446–453.

Hamaguchi, T., Ono, K., Murase, A., Yamada, M., 2009. Phenolic compounds prevent Alzheimer's pathology through different effects on the amyloid-beta aggregation pathway. Am. J. Pathol. 175 (6), 2557–2565.

Hamdy, A.M., El-Maraghy, S.A., Kortam, M.A., 2012. Modulatory effects of curcumin and green tea extract against experimentally induced pulmonary fibrosis: a comparison with N-Acetyl cysteine. J. Biochem. Mol. Toxicol. 26 (11), 461–468.

Henning, S.M., Wang, P., Heber, D., 2011. Chemopreventive effects of tea in prostate cancer: green tea versus black tea. Mol. Nutr. Food Res. 55, 905–920.

Hirata, K., Shimada, K., Watanabe, H., Otsuka, R., Tokai, K., Yoshiyama, M., Homma, S., Yoshikawa, J., 2004. Black tea increases coronary flow velocity reserve in healthy male subjects. Am. J. Cardiol. 93, 1384–1388.

Janssen, W., Pullamsetti, S.S., Cooke, J., Weissmann, N., Guenther, A., Schermuly, R.T., 2013. The role of dimethylarginine dimethylaminohydrolase (DDAH) in pulmonary fibrosis. J. Pathol. 229, 242–249.

Jochmann, N., Lorenz, M., Krosigk, A., Martus, P., Böhm, V., Baumann, G., Stangl, K., Stangl, V., 2008. The efficacy of black tea in ameliorating endothelial function is equivalent to that of green tea. Br. J. Nutr. 99, 863–868.

Jungbluth, A.A., Stockert, E., Huang, H.J.S., Collins, V.P., Coplan, K., Iversen, K., Kolb, D., Johns, T.J., Scott, A.M., Gullick, W.J., Ritter, G., Cohen, L., Scanlan, M.J., Cavenee, W.K., Old, J.L., 2003. A monoclonal antibody recognizing human cancers with amplification overexpression of the human epidermal growth factor receptor. Proc. Natl. Acad. Sci. U. S. A. 100 (2), 639–644.

Kang, H., Cho, S.J., Lee, C.G., Homer, R.J., Elias, J.A., 2007. TGF-β1 stimulates pulmonary fibrosis and inflammation via a bax-dependent, bid activated pathway that involves matrix Metalloproteinase-12. JBC.

Kim, H.R., Park, B.K., Oh, Y.M., Lee, Y.S., Lee, D.S., Kim, H.K., Kim, J.Y., Shim, T.S., Lee, S.D., 2006. Green tea extract inhibits paraquat-induced pulmonary fibrosis by suppression of oxidative stress and endothelin-l expression. Lung 184 (5), 287–295.

Klaus, S., Pültz, S., Thöne-Reineke, C., Wolfram, S., 2005. Epigallocatechin gallate attenuates diet-induced obesity in mice by decreasing energy absorption and increasing fat oxidation. Int. J. Obes. 29, 615–623.

Kuhnert, N., 2010. Unraveling the structure of the black tea thearubigins. Arch. Biochem. Biophys. 501, 37–51.

Kurahashi, N., Sasazuki, S., Iwasaki, M., Inoue, M., Tsugane, S., 2008. Green tea consumption and prostate Cancer risk in japanese men: a prospective study. Am. J. Epidemiol. 167 (1), 71–77.

Kuroda, Y., Hara, Y., 1999. Antimutagenic and anticarcinogenic activity of tea polyphenols. Mutat. Res. 436, 69–97.

Larsen, C.A., Dashwood, R.H., Bisson, W.H., 2010. Tea catechins as inhibitors of receptor tyrosine kinases: mechanistic insights and human relevance. Pharmacol. Res. 62, 457–464.

Mason, R.J., Schwarz, M.I., Hunninghake, G.W., Musson, R.A., 1999. NHLBI Workshop Summary. Pharmacological therapy for idiopathic pulmonary fibrosis. Past, present, and future. Am. J. Respir. Crit. Care Med. 160, 1771–1777.

Menet, M.-C., Sang, S., Yang, C.S., Ho, C.-T., Rosen, R.T., 2004. Analysis of theaflavins and thearubigins from black tea extract by MALDITOF mass spectrometry. J. Agric. Food Chem. 52, 2455–2461.

O'Connell, O.J., Kennedy, M.P., Henry, M.T., 2011. Idiopathic pulmonary fibrosis: treatment update. Adv. Ther. 28, 986–999.

Oltvai, Z., Milliman, C., Korsmeyer, S., 1993. Bcl-2 heterodimerizes in vivo with a conserved homolog, bax, that accelerates programmed cell death. Cell 74, 609–619.

Osanai, K., Takahashi, K., Sato, S., Iwabuchi, K., Ohtake, K., Sata, M., Yasui, S., 1991. Changes of lung surfactant and pressure volume curve in bleomycin-induced pulmonary fibrosis. J. Appl. Physiol. 70, 1300–1308.

Ou, X.M., Feng, Y.L., Wen, F.Q., Huang, X.Y., Xiao, J., Wang, K., Wang, T., 2008. Simvastatin attenuates bleomycin-induced pulmonary fibrosis in mice. Chin. Med. J. (Engl.) 121, 1821–1829.

Plataki, M., Koutsopoulos, A.V., Darivianaki, K., Delides, G., Siafakas, N.M., Bouros, D., 2005. Expression of apoptotic and antiapoptotic markers in epithelial cells in idiopathic pulmonary fibrosis. Chest 127 (1), 266–274.

Reed, J., 1994. Bcl-2 and the regulation of programmed cell death. J. Cell Biol. 124, 1–6.

Riemersma, R.A., Rice-Evans, C.A., Tyrrell, R.M., Clifford, M.N., Lean, M.E.J., 2001. Tea flavonoids and cardiovascular health. QJM: Int. J. Med. 94, 277–282.

Roy, D.K., Kumar, K.T., Karmakar, S., Pal, S., Samanta, S.K., Adhikari, D., Sen, T., 2008. Pharmacological studies on indian black tea (leaf variety) in acute and chronic inflammatory conditions. Phytother. Res. 22, 814–819.

Shih, L.J., Lin, Y.R., Lin, C.K., Liu, H.S., Kao, Y.H., 2016. Green tea (-)-epigallocatechin gallate induced growth inhibition of human placental choriocarcinoma cells. Placenta 41, 1–9.

Singh, D.K., Banerjee, S., Porter, T.D., 2009. Green and black tea extracts inhibit HMG-CoA reductase and activate AMP kinase to decrease cholesterol synthesis in hepatoma cells. J. Nutr. Biochem. 20, 816–822.

Skrzypczak-Jankun, E., Jankun, J., 2010. Theaflavin digallate inactivates plasminogen activator inhibitor: could tea help in Alzheimer's disease and obesity? Int. J. Mol. Med. 26, 45–50.

Sriram, N., Kalayarasan, S., Sudhandiran, G., 2008. Enhancement of antioxidant defense system by Epigallocatechin-3-gallate during bleomycin induced experimental pulmonary fibrosis. Biol. Pharm. Bull. 31 (7), 1306–1311.

Sriram, N., Kalayarasan, S., Sudhandiran, G., 2009. Epigallocatechin-3-gallate exhibits anti-fibrotic effect by attenuating bleomycin-induced glycoconjugates, lysosomal hydrolases and ultrastructural changes in rat model pulmonary fibrosis. Chem. Biol.

Interact. 180 (2), 271–280.
Stangl, V., Dreger, H., Stangl, K., Lorenz, M., 2007. Molecular targets of tea polyphenols in the cardiovascular system. Cardiovasc. Res. 73, 348–358.
Tang, N., Wu, Y., Zhou, B., Wang, B., Yu, R., 2009. Green tea, black tea consumption and risk of lung cancer: a meta-analysis. Lung Cancer 65, 274–283.
Unilever Report, 2011. Tea, Flavonoids and Cardiovascular Health (September). .
Usuki, J., Fukuda, Y., 1995. Evolution of three patterns of intra-alveolar fibrosis produced by bleomycin in rats. Pathol. Int. 45, 552–564.
Vermeer, M.A., Mulder, T.P.J., Molhuizen, H.O.F., 2008. Theaflavins from black tea, especially Theaflavin-3-gallate, reduce the incorporation of cholesterol into mixed micelles. J. Agric. Food Chem. 56, 12031–12036.
Wang, P., Aronson, W.J., Huang, M., Zhang, Y., Lee, R.-P., Heber, D., Henning, S.M., 2010. Green tea polyphenols and metabolites in prostatectomy tissue: implications for Cancer prevention. Cancer Prev. Res. Phila. (Phila) 3 (8), 985–993.
Yamada, T., Terashima, T., Wada, K., Ueda, S., Ito, M., Okubo, T., Juneja, L.R., Yokogoshi, H., 2007. Theanine, r-glutamylethylamide, increases neurotransmission concentrations and neurotrophin mRNA levels in the brain during lactation. Life Sci. 81, 1247–1255.
You, H., Wei, L., Sun, W.L., Wang, L., Yang, Z.L., Liu, Y., Zheng, K., Wang, Y., Zhang, W.J., 2014. The green tea extract epigallocatechin-3-gallate inhibits irradiation-induced pulmonary fibrosis in adult rats. Int. J. Mol. Med. 34 (1), 92–102.
Zhang, M., Holman, C.D.J., Huang, J.-P., Xie, X., 2007. Green tea and the prevention of breast cancer: a case-control study in Southeast China. Carcinogenesis 28 (5), 1074–1078.
Zia, S., Hyde, D.M., Giri, S.N., 1992. Development of a bleomycin hamster model of subchronic lung fibrosis. Pathology 24, 155–163.

ISSN 2348-313X (Print)
International Journal of Life Sciences Research ISSN 2348-3148 (online)
Vol. 6, Issue 3, pp: (239-248), Month: July - September 2018, Available at: www.researchpublish.com

Acute Toxicity of Hexavalent Chromium in Adult *Channa punctatus* (Bloch, 1793) with regard to changes in Erythrocytic and Leucocytic Profiles

[1]Samudra Gupta, [2*]Rajarshi Ghosh

[1] Student of B.Sc. (Hons.) in Zoology
[2*]Assistant Professor in Zoology (WBES)
[1, 2] Department of Zoology, Maulana Azad College, Kolkata-700013, West Bengal, India

Abstract: **The tannery industries and drainage from urban and agricultural areas add chromium as one of the heavy metals to the aquatic environment and thereby imposing negative effects on the aquatic fauna. In the present study, the haematological alterations produced on short-term exposure to sublethal concentration of chromium (25 mg L^{-1}) were investigated in fresh water air-breathing fish, *Channa punctatus* (Bloch) for 24h, 48h and 72h respectively. The 96h LC_{50} of chromium salt, potassium dichromate was determined to be 34.59 mg/L. The results revealed statistically significant decrease in erythrocytic parameters like TEC (Total Erythrocytic Count), Hb (Haemoglobin) content and Haematocrit (Hct %) values in all experimental groups compared to the control with an increase of exposure periods. On the contrary, leucocytic parameters such as TLC (Total Leucocytic Count), Leucocrit (Lct %) and neutrophil populations were significantly increased during acute exposure. Acute lymphocytopenia was also recorded. The absolute corpuscular values like MCH (Mean Cell Haemoglobin) and MCHC (Mean Cell Haemoglobin Concentration) also exhibited significant increase in fishes of experimental groups while MCV (Mean Cell Volume) exhibited a fluctuating pattern. The depression of erythrocytic parameters clearly indicated that the fishes became anaemic due to acute toxicity of chromium.**

***Keywords: Channa punctatus*, hexavalent chromium, erythrocytic parameters, leucocytic parameters, neutrophilia, lymphocytopenia.**

I. INTRODUCTION

A wide range of adverse effects on freshwater fishes have been observed due to various heavy metals entering aquatic ecosystem through effluents which are regularly discharged from industries, tanneries, sewage treatment plants [1]. Heavy metals are important pollutants because they are not eliminated from the aquatic ecosystem by natural processes easily. The wastewater generated by tanneries is a major source of chromium (Cr^{6+}) and their indiscriminate introduction in the aquatic ecosystem pose a serious threat to the growth and survival of the fish population [2]. The chromium discharged into water get into food chain very easily from the environment. By entering into biological systems, it can perturb the biochemical processes leading to health abnormalities. A considerable amount of experimental data on chromium toxicity to aquatic life was reviewed [3] but the data on chromium toxicity to Indian freshwater air-breathing teleosts are scarce and are mostly limited to the effects on biochemical, immunological or enzymological profiles [4], [5]. Blood is an excellent bio-indicator which can be used as a sensitive index in understanding various physiological processes in fish. The present work was undertaken to investigate the short-term toxicity of chromium (Cr^{6+}) to adult freshwater spotted murrel, *Channa punctatus* (family: Channidae) with regard to the alterations in the erythrocytic parameters viz.TEC, Hb content, Hct %, MCH, MCHC and MCV and leucocytic parameters like TLC, Lct % and DWBC% (Differential count of WBC). The morphological abnormalities of erythrocytes were also analyzed under light microscopic study.

ISSN 2348-313X (Print)
International Journal of Life Sciences Research ISSN 2348-3148 (online)
Vol. 6, Issue 3, pp: (239-248), Month: July - September 2018, Available at: www.researchpublish.com

II. MATERIALS AND METHODS

A. Collection of specimens and acclimatization

The adult fresh-water air-breathing *Channa punctatus* (Bloch) of both sexes (13.78 ± 0.33 cm in length and 39.36 ± 2.35 g in weight) were procured from clean and unpolluted local freshwater pond sources in Kolkata and transported to the laboratory of Department of Zoology, Maulana Azad College, Kolkata-700013, West Bengal. They were treated with 0.05% $KMnO_4$ solution for 2 minutes to avoid dermal infection, if any and kept in glass aquaria filled with clean dechlorinated tap water (pH: 7.2 ± 0.05; water temperature: 23 ± 2° C; total hardness: 225.8 ± 5 mg L^{-1}as $CaCO_3$; dissolved oxygen: 3.8 ± 1 mg L^{-1}) under continuous aeration. The fish were acclimatized for 5 days prior to experimentation. The physico-chemical parameters of tap water were monitored using standard procedures of APHA [6]. Fish were fed with commercial dry pellets during the acclimatization period only. Approximately 50 % of water in aquaria was renewed daily in order to remove unutilized food or metabolic waste products to minimize the level of ammonia excreted as well as maintaining the dissolve oxygen level.

B. Detection of LC50 dose

Analytical grade potassium dichromate ($K_2Cr_2O_7$) by BDH (India) was used as a metal toxicant in the present experiment and for the determination of LC_{50} dose of chromium at 96 h using probit analysis [7]. Six test concentrations of narrow range viz. 25, 30, 35, 40, 45 and 50 mg L^{-1} respectively and a control (without chromium) were selected to estimate the LC_{50} dose at 96 h. 8 fish specimens were placed in each of the aquarium and triplicates were maintained for each of the six treatment groups as well as for control. The required concentrations were prepared in distilled water and maintained in respective aquaria by renewing the water every day. Both sexes of fish were used during experiments. Dead fishes were removed from the aquaria immediately. The behavioural pattern and percentage of mortality was recorded at 96 h interval for each of the test concentrations. The LC_{50} value of $K_2Cr_2O_7$ for adult *C. punctatus* was estimated to be 34.59 mg L^{-1} at 96 h exposure period.

C. Experimental design

For short-term study, the live fish samples were divided into four groups each containing 8 individuals. One Group was kept as control, and other three groups were exposed to chosen sublethal dose of $K_2Cr_2O_7$ (25 mg L^{-1}) for 24, 48 and 72 h respectively after determining 96h LC_{50} value. The whole exposure medium was changed every day in both the control as well as treatment groups to maintain the desired concentration of chromium salt. After stipulated exposure periods, blood was collected from control and experimental fishes by severing the caudal peduncle of fish without using anaesthesia for haematological investigations. After collection the blood was immediately transferred to glass vials containing 3.8 % Sodium citrate solution (anticoagulant).

D. Estimation of erythrocytic and leucocytic parameters

Total Erythrocytic Count (TEC) and Total Leucocytic Count (TLC) were determined using Neubaur's improved double chamber haemocytometer (Fein-OPTIK, Blankenburg, G.D.R.) using Hayem's solution as diluting fluid. Haemoglobin (Hb) percentage was determined using Sahli's Haemometer. The Haematocrit and Leucocrit values were estimated by microhaematocrit method using Wintrobe's tube [8]. Differential Count (DWBC %) of leucocytes was made by staining thin air-dried blood film with Leishman's stain. The count of leucocytes and morphology of erythrocytes were observed under oil immersion magnification in a research microscope (Magnus MLX-DX, Olympus India Pvt. Ltd.). The red cell indices, such as Mean Corpuscular Volume (MCV), Mean Corpuscular Haemoglobin (MCH) and Mean Cell Haemoglobin Concentration (MCHC) were calculated from TEC, Hb % and Haematocrit values using standard formulae [9], [10].

E. Statistical analysis

The results were expressed as mean and standard error (mean ± S.E.). Student's *t*- test was used to distinguish between means of significant differences [11]. Treatments were taken to be significantly different where $P < 0.05$ and highly significant where $P < 0.01$.

III. RESULTS

The majority of the fishes exposed to sublethal concentration (25 mg L^{-1}) of $K_2Cr_2O_7$ especially for 48 and 72 h exhibited abnormal behaviour like loss of equilibrium, erratic swimming and loss of appetite. The exposed fishes were found to swim to the water surface and excess mucous secretion was observed from the body. The fishes also stood motionless in the bottom of the aquarium, hanging in a vertical orientation.

In the present study, significant alterations in the haematological parameters were observed in fishes exposed to sublethal concentration of chromium during the exposure period, viz. 24, 48 and 72 h along with some morphological changes in RBC of exposed fishes. The TEC ($\times 10^6$ mm^{-3}) and haemoglobin values (g %) exhibited a highly significant decrease ($P < 0.01$) especially after 48 h and 72 h exposure periods compared to control whereas the Haematocrit values exhibited a sharp decline ($P < 0.01$) from the onset of the exposure period compared with control (TABLE I). As shown in TABLE II, MCV values were significantly decreased ($P < 0.05$) after 24 h exposure but a sharp increment was observed after 72 h ($P < 0.05$). There were significant fluctuations in the MCH values throughout the exposure periods but after 72 h of exposure, a significant increase in the value ($P < 0.05$) was found. MCHC values were found to be very high ($P < 0.01$) especially after 24 and 48 h of exposure periods.

Several cellular and nuclear abnormalities of peripheral RBCs were also studied in fish population exposed to sublethal dose of chromium. Three types of nuclear abnormalities viz. nuclear extrusion (Fig.1), notched nuclei (Fig.2) and bilobed nuclei (Fig.3) were observed along with four types of cellular abnormalities such as spindle-shaped cells (Fig.3), budding erythrocytes (Fig.1), vacuolated cells (Fig.4) and deformed erythrocytes (Fig.5). These morphological abnormalities were found to increase after 72 h of exposure.

Highly significant increase ($P < 0.01$) in TLC ($\times 10^3$ mm^{-3}) and Lct % values were observed initially and at the end (TABLE III). A significant decrease ($P < 0.05$) of both leucocytic parameters was observed in the middle of the exposure periods. The differential count of leucocytes showed highly significant alterations throughout the exposure periods (TABLE IV). A gradual increase in neutrophil and monocyte population was observed throughout the experimental period which was highly significant ($P < 0.01$) after 72 h compared to control. On the contrary, a significant decrease ($P < 0.05$) was observed in eosinophil (EO) population especially after 48 h of exposures. The populations of large lymphocytes (LL) and small lymphocytes (SL) also showed the opposite trend to that of the neutrophil (NEU). Both lymphocytes (SL and LL) exhibited a steep decline ($P < 0.01$).after 72 h of exposure (Lymphocytopenia). No significant deviation was found in the basophil cell population (B) throughout the short-term exposures.

IV. DISCUSSION

The present study reveals that the fishes exposed to hexavalent chromium showed significant decrease in erythrocytic parameters during experimental period. This result indicates anaemic condition associated with erythropenia. The reduction in TEC coupled with low haemoglobin count may be due to disruptive metabolic and haemopoietic activities of the fish exposed to sublethal concentration of $K_2Cr_2O_7$. The incidence of erythropenia in fishes under heavy metal exposure was reported earlier [12], [13], [14].The impairment of haemopoietic organs by heavy metals resulted slower erythropoiesis and subsequent reduction in TEC [15], [16], [17], [18]. The reduced RBC count coupled with low haemoglobin count also may be due to destructive action of chromium on erythrocytes. The damage of RBC in *Catla catla* exposed to $K_2Cr_2O_7$ was described [19]. Accumulation of several heavy metals in kidney, the major erythropoietic organ in fishes has been reported by various authors [20], [21]. Haemolysis of RBC after dichromate exposure in a marine fish, *Dicentrachus labrax* was reported [22]. Drop in TEC and haemoglobin percentage were also reported in the fish, *Heteropneustes fossilis* under exposure of nickel sulphate for 15 days [23]. Impairment of iron uptake in the intestine and defective iron metabolism might be one of the reasons behind the reduced percentage of haemoglobin in the experimental fishes exposed to sublethal doses of heavy metals [24]. The present study is in the line with the earlier works which suggests that the decrease in the level of TEC, haemoglobin and haematocrit value is due to the haemodilution mechanism because of gill damage or impaired osmoregulation and increased destruction in the circulating RBCs [25], [26], [27], [28], [29], [30], [31]. Contrastingly, significant increase in TEC and haemoglobin content has been reported after exposure to copper in *Cyprinus carpio* [32] which suggested that hypoxic condition induced by heavy metal accumulation stimulated the spleen for erythropoiesis and release of stored and immature erythrocytes into the circulation [33].

The anaemic condition of the experimental fish groups were further detected by Haematocrit study. Significant changes were recorded in the mean value of MCV, MCH and MCHC and similar results have been reported in *Labeo rohita* which was exposed to chromium [34]. Cells released from the affected spleen would have lowered MCV values initially, as observed in the present study. This present result is well in agreement with the observation [35], which suggested that the initial decrease in the MCV value may be due to high percentage of immature RBCs in the circulation released from the spleen. A similar kind of observation was reported in *Cyprinus carpio* after cadmium exposure [36]. However, an increasing trend on the MCV and MCH values were more or less observed in the present study. These haematological alterations might be due to haemopoietic or erythrocyte mobilization response to hypoxia induced by heavy metals [14]. Moreover, the elevation in MCV and MCH value may also be due to release of large erythrocytes into the circulation [37], [38]. The observed low concentration of MCHC after 48 and 72 h indicates a decrease in haemoglobin synthesis due to toxic action of $K_2Cr_2O_7$.

Increase in the TLC and Leucocrit (Lct %) values as observed in present study might be due to the adaptation to meet stressful toxic condition by exposed organisms. This observation is in agreement with the earlier reports [39], [40], [41],[42],[43]. In the present experiment, leucocytes showed an initial rise due to elevated levels of neutrophil and monocytes followed by leucopenia (especially lymphocytopenia) after 48 h of chromium exposure. This observation is in the line with the earlier observation [12] where similar kind of results were reported in leucocytes of teleosts under the exposure of sublethal dose of chromium. The increase in number of WBCs appears to be associated with the increased circulatory levels of granulocytes, especially neutrophils, which may play an important role in immunological defence system during heavy metal exposure [33]. This observation suggests the development of certain degree of tolerance during toxicant stress condition. The elevation in neutrophil population (neutrophilia) can be correlated with the earlier findings [44] where *Brycon amazonica* were exposed to low concentration of phenol in laboratory condition. This condition indicates hypersensitivity to toxic effluents [45]. On the contrary, the drop in lymphocyte population is probably due to the mobilization of lymphocytes from the peripheral blood to accumulate in the lymphoid tissue [45], [46]. According to some other reports, this decrease in lymphocyte count can also be correlated with the elevated level of corticosteroid hormone, whose secretion is a nonspecific immune response in fishes to any environmental stressor [47], [48].

7 types of erythrocytic abnormalities were observed in the present study. The increase in frequency of erythrocytic abnormalities depends upon the exposure time of heavy metal toxicant. In intracellular condition, chromium undergoes reduction from Cr^{+6} to Cr^{+3} and generates reactive oxygen species (ROS) as highly reactive free radicals which react and disrupt the DNA. Similar works reported by other authors suggested that the blebbed and lobed nuclei are caused by nuclear budding during interphase and this entire mechanism occurs probably by elimination of amplified genes from the nucleus [49], [50]. These abnormalities may also be raised due to formation of free radicals under oxidative stress by heavy metal toxicants [51]. According to some previous reports, binucleated cells and notched nuclei are formed by the aneugenic effect of heavy metals which exerts their action by creating aneuploidy which is produced due to failure in tubulin aggregation [52],[53]. The abnormal shapes of erythrocytes are probably produced by hypoxic condition which results in depression of ATP [54].The vacuolated condition of erythrocytes is most probably due to the interruption in the lipid solubility of erythrocyte membranes caused by heavy metals, ultimately leading to the apoptosis [55]. These changes in erythrocytes of fishes induced by chromium are non-reversible and these cytotoxic damages lead to the mortality of fishes.

V. CONCLUSION

Fish haematology has now become an important biomonitoring tool for the assessment of aquatic pollution as it creates a direct link between the environmental condition and physiological status of organisms. In present study, changes observed in the behavioural and haematological parameters of adult *C. punctatus* exposed with chosen sublethal dose (25 mg L^{-1}) of hexavalent chromium were described. The non-specific immune responses to heavy metal over the short-term exposure periods can be interpreted as initial increase in WBC, perhaps due to the increase in circulating neutrophils and monocytes coupled with stress-mediated reduction in leucocytes (especially lymphocytes) in the middle. The depression in most of the erythrocytic parameters was observed which possibly reflect the relative magnitude of stress due to exposure of chromium. The result obtained from this study clearly indicates that the industrial effluents containing heavy metals have

potential to alter the physiological as well as biochemical processes in the exposed organisms. The formation of erythrocytic abnormalities also reveals the genotoxic potential of chromium. Thus, these haematological parameters can be treated as good biomarker for monitoring the impact of industrial effluents containing heavy metals in aquatic environment. Being an edible freshwater fish, there might be a chance of accumulation of heavy metals in many non-target organisms mainly in human. Thus, a continuous monitoring with regard to the discharge of the industrial effluents into the water body is mostly important and it is suggested that the effluents should be passed through the treatment plant before being discharged into the aquatic body.

ACKNOWLEDGEMENT

This work is financially supported by Department of Biotechnology, Star College scheme (CHS/GIA/0107/2011-2012 dt 15.06.2011) that has been granted to Maulana Azad College, Kolkata. The authors express their gratitude to Professor S.C. Dasgupta, Head of the Department of Zoology, for providing the necessary infrastructural facilities.

REFERENCES

[1] Jordao CP, Pereira MG, Bellato CR, Pereira JL, Matos AT (2002). Assessment of water systems for contaminants from domestic and industrial sewages. Environ Monit Assess 79: 75-100.

[2] Mishra AK, Mohanty B (2008).Acute toxicity impacts of hexavalent chromium on behavior and histopathology of gill, kidney and liver of the freshwater fish, *Channa punctatus* (Bloch). Environ Toxicol Pharmacol 26(2): 136-141.

[3] Irwin RJ, VanMouwerik M, Stevens L, Seese MD, Basham W (1997). Chromium VI (Hexavalent chromium). Environmental Contaminants Encyclopedia. National Park Service, Water Resources Division, Fort Collins, Colorado.

[4] Sastry KV, Tyagi S (1982). Toxic effects of chromium in a freshwater teleost fish, *Channa punctatus*. Toxicol lett 11(1-2): 17-21.

[5] Vutukuru SS (2003).Chromium induced alterations in some biochemical profile of the Indian major carp, *Labeo rohita* (Hamilton). Bull Environ Contam Toxicol 70: 118-123.

[6] APHA (2005). Standard Methods for the Examination of Water and Wastewater. 21st ed. American Public Health Association, Washington D.C.

[7] Finney DJ (1947). Probit analysis: a statistical treatment of the sigmoid response curve. Cambridge: Cambridge University Press, pp. 256.

[8] Wintrobe MM (1967). Clinical haematology. Philadelphia: Lea and Febiger, pp. 281.

[9] Hepler, OE (1963). Manual of clinical laboratory methods. Illinois: Springfield.

[10] Dacie JV, Lewis SN (1984). Practical haematology. 6th ed. Edinburg: Churchill Livingstone.

[11] Zar JH (1999). Biostatistical Analysis. 4th ed. Delhi: Pearson Education, Inc.

[12] Srivastava AK, Mishra S (1979). Blood dyscrasia in a teleost, *Colisa fasciatus* after acute exposure to sublethal concentration of lead. J Fish Biol 14: 199-203.

[13] Goel KA, Gupta K (1985). Haematobiochemical characteristics of *Heteropneustes fossilis* under the stress of zinc. Indian J Fish 32: 256-259.

[14] Bhatkar NV (2011). Chromium (III) induced haematological alterations in Indian common carp, *Labeo rohita* (Ham.). J Appl & Nat Sci 3 (2): 258 -263.

[15] Santhakumara M, Balaji M, Amudu K (2000).Adaptive changes in respiratory movements of an air breathing fish *Anabus testudineus* exposed to organophosphate pesticide monocroptophos. Eco Env Conserv 6(1): 67-69.

[16] Mazon AF, Monteiro EA, Pinheiro GH, Fernandes MN (2002). Hematological and physiological changes induced by short-term exposure to copper in the freshwater fish, *Prochilodus scrofa*. Braz J Biol 62: 621-631.

[17] Gupta K, Sachar A, Gupta K, Raina S (2009) Effect of lindane on haematological parameters of minor carp, *Labeo boga* (Ham.). Biosci Biotechnol Res Asia 6(2):695-702.

[18] Sharma J, Langer S (2014).Effect of manganese on haematological parameters of fish *Garra gotyla gotyla*. J Entomol Zool Stud 2(3): 77-81.

[19] Christy I (1995). Respiratory and histopathological responses of *Catla catla*,exposed to heavy metal,chromium. J Ecotoxicol Environ Monit 5 (4): 263-268.

[20] Rana KS, Raizada S (2000). Histopathological alterations induced by tannery and textile dyeing effluents in the kidney of *Labeo rohita* (Ham.). J Environ Biol *21* (4): 301-304.

[21] Dhanapakiam P, Ramaswamy VK (2001). Toxic effects of copper and zinc mixtures on some haematological and biochemical parameters in common carp, *Cyprinus carpio* (Linn). J Environ Biol *22* (2): 105-111.

[22] Roche H, Bogé G (1993). Effects of Cu, Zn and Cr salts on antioxidant enzyme activities in vitro of red blood cells of a marine fish, *Dicentrarchus labrax.* Toxic in vitro 7: 623-629.

[23] Nanda P, Behera MK (1996). Nickel induced changes in some haemato-biochemical parameters of a cat fish *Heteroneustes fossilis* (Bloch). Environ Ecol 14(1): 82-85.

[24] Kothari S, Saxena G (1997). Cadmium toxicity in the intestinal bulb of a teleost *Punctius sophere* (Ham), A histoenzymological study. In: Rao KS, editor. Recent advances in fresh water biology. Amol Pub. New Delhi, pp. 299-313.

[25] Smit GL, Hattingh J, Burger AP (1979).Haematological assessment of the effects of the anaesthetic MS222 in natural and neutralized form in three fresh water fish species: Interspecies differences. J Fish Biol 15: 633-643.

[26] Karuppasamy R (2000).Impact of phenyl mercuric acetate (PMA) on the biomodel respiration in an airbreathing fish, *Channa punctatus* (Bloch). J Environ Pollut 7(4): 287-293.

[27] Tyagi A, Srivastava N (2005). Haematological changes in fish *Channa punctatus* (Bloch) to chronic zinc exposure. J Environ Biol 26(2): 429-432.

[28] Gupta K (2008). Copper induced toxicity on haematological and haemopoietic profile of *Puntius sophore* (Ham.). MPhil, University of Jammu, Jammu and Kashmir, India.

[29] Olanike K, Funmilola A, Olufemi B, Olajide O (2008).Sub lethal concentrations toxicity and blood profile of adult *Clarias gariepinus* exposed to lead nitrate. Int J Hematol 4: 2-10.

[30] Witeska M, Kondera E, Szymanska M , Ostrysz M (2010). Hematological changes in common carp (*Cyprinus carpio* L.) after short–term Lead (Pb) exposure. Polish J of Environ Stud 19(4): 825-831.

[31] Kaoud HA, Zak MM, El-Dashan AR, Saeid S , El Zorba HY(2011). Amelioration the Toxic effects of cadmium-exposure in Nile Tilapia (*Oreochromis niloticus*) by using *Lemna gibba* L. Life Sci J 8(1): 185-195.

[32] Witeska M (2005).Stress in fish: Haematological and Immunological effects of heavy metals. Electron J Ichthyol 1: 35-41.

[33] Kori-Siakpere O, Ubogu EO (2008).Sublethal haematological effects of zinc on the freshwater fish, *Heteroclarius* sp. (Ostheichthys: Clariidae). Afr J Biotechnol 7(12):2068-2073.

[34] Venkatachalam T, Natarajan AV (2014).Haematological investigation on freshwater teleost *Labeo rohita* (Ham.) following aquatic toxicities of Cr (III) and Cr (VI). Int J Res Biosciences 3(3): 1-14.

[35] Saravanan M, Prabhu Kumar K, Ramesh M (2011).Haematological and biochemical responses of freshwater teleost fish *Cyprinus carpio* (Actinopterygii: Cypriniformes) during acute and chronic sublethal exposure to lindane. Pest Biochem Physiol 100(3):206–211.

[36] Koyama J, Ozaki H (1984).Haematological changes of fish exposed to low concentrations of cadmium in the water. Bull Jpn Soc Sci Fish 50: 199-203.

[37] Hardig J, Hoglund LB (1983). On accuracy in estimating fish blood variables. Comp Biochem Physiol 75(1):35– 40.

[38] Wepener V, Van Vuren JHJ, Du Preez HH (1992). The effect of hexavalent chromium at different pH values on the haematology of *Tilapia sparrmanii* (Cichlidae) Comp Biochem Physiol C Toxicol Pharmacol 10l (2): 375–381.

[39] Haniffa MA, Porchelvi M (1985). Effects of distillery effluents on oxygen consumption of freshwater fish, *Sarotherodon mossambicus*. J Environ Biol 6: 17-23.

[40] Garg VK, Garg SK, Tyagi SK (1989). Haematological parameters of fish, *Channa punctatus* under the stress of manganese. Environ Ecol *7*: 752-755

[41] Hota S (1995). Toxic effect of arsenic on haemato-biochemical abnormalities in *Channa punctatus* (Bloch) J Ecotoxicol Environ Monit 5 (4): 249-255.

[42] Ray D, Banerjee SK (1998). Hematological and histopathological changes in *Clarias batrachus* (Linn) exposed to Nickel and Vanadium. Environ Ecol 16 (1): 151-156.

[43] Ali SS, Hussain A, Shakoori AR (2000). Haematological effects of hexavalent chromium in freshwater teleost *Oreochromis mossambicus.* J Ecotoxicol Environ Monit 10 (1): 3-10.

[44] Hori TSF, Avilez IM , Iwama GK, Johnson SC, Moraes G, Afonso LOB (2008). Impairment of the stress response in matrinxa juveniles (*Brycon amazonicus)* exposed to low concentrations of phenol. Comp Biochem Physiol C Toxicol Pharmacol 147: 416-423.

[45] Akinrotimi OA, Orlu EE, Gabriel UU (2013). Haematological responses of *Tilapia guineensis* treated with industrial effluents. Appl Ecol Env Sc 1(1):10-13.

[46] Ajani F, Olukunle OA, Agbede SA (2007). Hormonal and haematological responses of *Clarias gariepinus* to nitrite toxicity. J Fish Int 2(1):48-53.

[47] Iwama GK, Greer GL, Larkin PA (1976). Changes in some hematological characteristics of Coho Salmon (*Oncorhynchus kisutch*) in response to acute exposure to dehydroabietic acid (DHAA) at different exercise levles. J Fish Res Board Can 33: 285-289.

[48] Ellis AE (1981). Stress and modulation of defense mechanisms in fish. In: Pickering AD, editor. Stress and Fish, chap. 7, Academic press, New York.

[49] Shimizu N, Itoh N, Utiyama H, Wahl GM (1998). Selective entrapment of extrachromosomally amplified DNA by nuclear budding and micronucleation during S phase. J Cell Bio 140: 1307-1320.

[50] Crott JW, Mashiyama SD, Ames BC, Fenech M (2001). The effect of folic acid deficiency and MTHFR C677T polymorphism on chromosome damage in human lymphocytes *in vitro*. Cancer Epidemiol Biomark Prevent 10: 1089-1096.

[51] Von Sonntag C (1987).The Chemical Basis of Radiation Biology. New York: Taylor and Francis, pp. 516.

[52] Ventura BC, Angelis DF, Marin-Molares MA (2008). Mutagenic and genotoxic effects of the atrazine herbicide in *Oreochromis nilotics* (Perciformes, Cichlidae) detected by the micronuclei test and the comet assay. Pest Biochem Physiol 90: 42-51.

[53] Fernandes TCC, Mazzeo DEC,Marin-Molares MA (2007). Mechanism of micronuclei formation in polyploidizated cells of *Allium cepa* exposed to trifluralin herbicide. Pest Biochem Physiol 88: 252-259.

[54] Ateeq B, Farah MA, Ali MN, Ahmed W (2002). Induction of micronuclei and erythrocyte alterations in the catfish, *Clarias batrachus* by 2,4-dichlorophenoxyacetic acid and butachlor. Mutat Res 518:135-144.

[55] Walia GK, Handa D, Kaur H, Kalotra R (2013). Erythrocyte abnormalities in a freshwater fish, *Labeo rohita* exposed to tannery industry effluent. Int J Pharm Biol Sc 3 (1):287-295.

ISSN 2348-313X (Print)
International Journal of Life Sciences Research ISSN 2348-3148 (online)
Vol. 6, Issue 3, pp: (239-248), Month: July - September 2018, Available at: www.researchpublish.com

APPENDICES - A

TABLE I: Changes in erythrocytic parameters (TEC, Hb and Hct) of freshwater fish, *Channa punctatus* exposed to sublethal dose of hexavalent chromium (25 mg L^{-1}).

Erythrocytic parameters	Control	Exposure period		
		24h	48h	72h
TEC ($\times 10^6$ mm^{-3})	3.07 ± 0.11	2.66 ± 0.41	2.15 ± 0.03 **	1.43 ± 0.13**
Hb (g %)	11.3 ± 0.35	10.12 ± 0.47	8.63 ± 0.46**	7.5 ± 0.11**
Hct (%)	24.43 ± 0.04	15 ± 0.73**	14 ± 0.57**	14.25 ±0.65**

Values are expressed as Mean ± S.E., n = 8, ** = highly significant at *P* < 0.01 level. TEC = Total Erythrocytic Count, Hb = Haemoglobin,

Hct = Haematocrit.

TABLE II: Changes in erythrocytic parameters (MCV, MCH and MCHC) of freshwater fish, *Channa punctatus* exposed to sublethal dose of hexavalent chromium (25 mg L^{-1}).

Erythrocytic parameters	Control	Exposure period		
		24h	48h	72h
MCV (fl)	79.91 ± 2.25	63.21 ± 3.02*	65.16 ± 9.02	102.88 ± 7.58*
MCH (pg)	37.09 ± 2.08	45.53 ± 6.86	40.22 ± 2.47	54.92 ± 5.41*
MCHC (gL^{-1})	46.28 ± 1.42	68.55 ± 5.0**	61.81 ± 2.79**	53.24 ± 2.81

Values are expressed as Mean ± S.E., n = 8. * = significant at *P* < 0.05 level, ** = significant at *P* < 0.01 level. MCV: Mean Corpuscular Volume, MCH: Mean Corpuscular Haemoglobin, MCHC: Mean Cell Haemoglobin Concentration.

TABLE III: Changes in leucocytic parameters (TLC and Lct %) of freshwater fish, *Channa punctatus* exposed to sublethal dose of hexavalent chromium (25 mg L^{-1}).

Erythrocytic parameters	Control	Exposure periods		
		24h	48h	72h
TLC ($\times 10^3$ mm^{-3})	32.33 ± 0.73	47.75 ± 0.66**	37.54 ± 1.32*	58.12 ± 1.04**
Lct (%)	1.48 ± 0.01	1.75 ± 0.03**	1.45 ± 0.08*	2.9 ± 0.18**

Values are expressed as Mean ± S.E., n = 8.* = significant at p < 0.05 level, ** = significant at p < 0.01 level. TLC: Total Leucocytic Count, Lct: Leucocrit.

TABLE IV: Changes in the relative population of leucocytes (DWBC %) of freshwater fish, *Channa punctatus* exposed to sublethal dose of hexavalent chromium (25 mg L^{-1})

DWBC%	Control	Exposure Periods		
		24 h	48 h	72 h
NEU	34.55 ± 2.38	35.31 ± 1.13	38.52 ± 0.91	47.66 ± 2.93**
EO	1.88 ± 0.17	2 ± 0.11	1.4 ± 0.17*	1.84 ± 0.22
B	3.8 ± 0.49	3.97 ± 0.36	3.56 ± 0.12	3.1 ± 0.29
LL	18.09 ± 3.32	11.5 ± 0.86	13.16 ± 1.32	6.64 ± 0.39**
SL	39.92 ± 6.17	33.75 ± 2.14	34.62 ± 2.01	28.83 ± 3.14**
M	9.65 ± 0.66	10.81 ± 0.96	14.23 ± 1.64**	17.29 ± 1.08**

Values are expressed as Mean ± S.E., n = 8. * = significant at p < 0.05 level, ** = significant at p < 0.01 level. NEU: Neutrophil, EO: Eosinophil, B: Basophil, LL: Large Lymphocyte, SL: Small Lymphocyte, M: Monocyte.

ISSN 2348-313X (Print)
International Journal of Life Sciences Research ISSN 2348-3148 (online)
Vol. 6, Issue 3, pp: (239-248), Month: July - September 2018, Available at: www.researchpublish.com

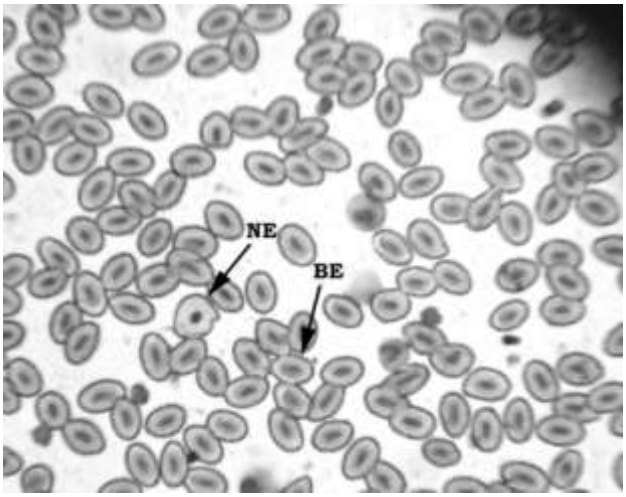

Fig 1: Peripheral blood smear (× 450) of *C. punctatus* exposed to sublethal dose (25 mg L^{-1}) of chromium (VI) at 72 h showing nuclear extrusion (NE) and budding erythrocytes (BE)

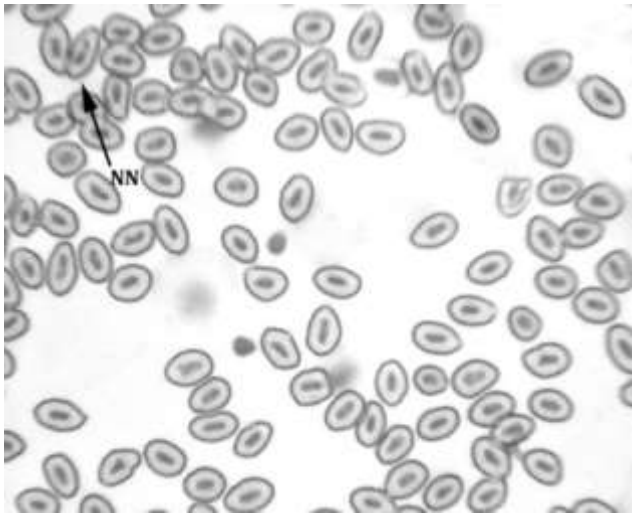

Fig 2: Peripheral blood smear (× 450) of *C. punctatus* exposed to sublethal dose of chromium (VI) at 72 h showing notched nucleus (NN)

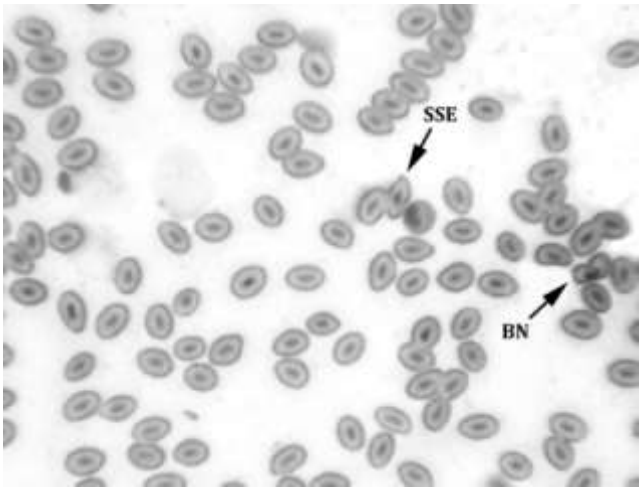

Fig 3: Peripheral blood smear (× 450) of *C. punctatus* exposed to sublethal dose of chromium (VI) at 72 h showing spindle-shaped erythrocyte (SSE) and bilobed nucleus (BN)

ISSN 2348-313X (Print)
International Journal of Life Sciences Research ISSN 2348-3148 (online)
Vol. 6, Issue 3, pp: (239-248), Month: July - September 2018, Available at: www.researchpublish.com

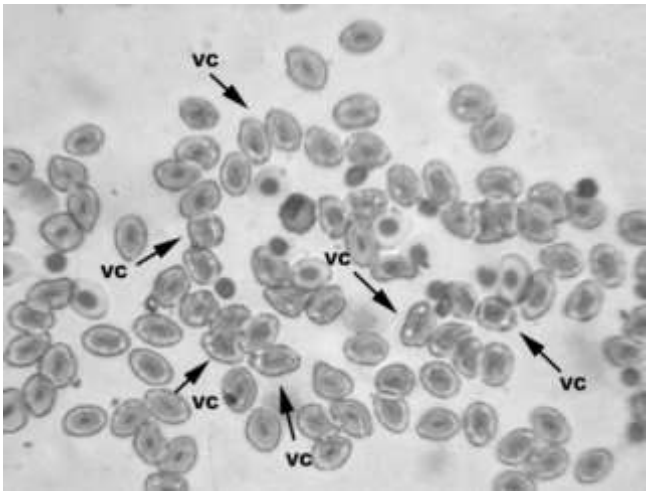

Fig 4: Peripheral blood smear (× 450) of *C. punctatus* exposed to sublethal dose of chromium (VI) at 72 h showing vacuolated cells (VC)

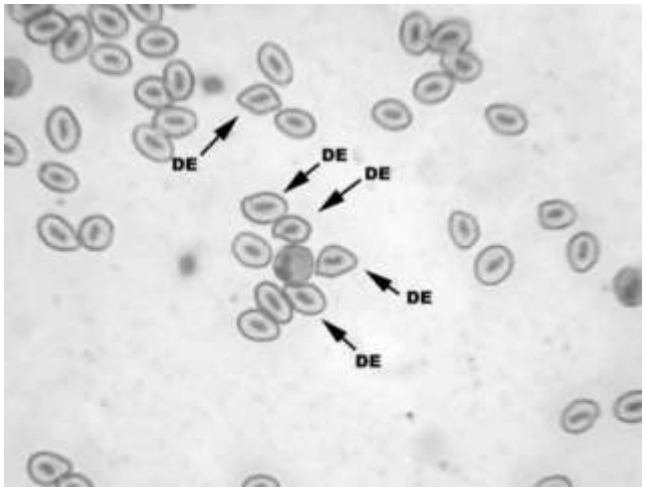

Fig 5: Peripheral blood smear (×450) of *C. punctatus* exposed to sublethal dose of chromium (VI) at 72 h showing deformed erythrocytes (DE)

Title: TNFR2 mediated TNF-α signaling and Nf-κB activation in hippocampus of 1-methyl-4-phenyl-1,2,3,6-tetrahydropyridine-treated mice

Authors: Nabanita Ghosh, Soham Mitra, Priyobrata Sinha, Nilkanta Chakrabarti, Arindam Bhattacharyya

PII: S0168-0102(17)30687-9
DOI: https://doi.org/10.1016/j.neures.2018.02.007
Reference: NSR 4155

To appear in: *Neuroscience Research*

Received date: 15-11-2017
Revised date: 21-2-2018
Accepted date: 22-2-2018

Please cite this article as: Ghosh, Nabanita, Mitra, Soham, Sinha, Priyobrata, Chakrabarti, Nilkanta, Bhattacharyya, Arindam, TNFR2 mediated TNF-α signaling and Nf-κB activation in hippocampus of 1-methyl-4-phenyl-1,2,3,6-tetrahydropyridine-treated mice.Neuroscience Research https://doi.org/10.1016/j.neures.2018.02.007

TNFR2 mediated TNF-α signaling and Nf-κB activation in hippocampus of 1-Methyl-4-Phenyl-1,2,3,6-Tetrahydropyridine-treated mice

Nabanita Ghosh[1], Soham Mitra[1], Priyobrata Sinha[2], Nilkanta Chakrabarti[2], Arindam Bhattacharyya[1*]

[*]Address for correspondence

[1]Immunology Lab
Department of Zoology
University of Calcutta
35, Ballygunge Circular Road
Kolkata-700019
India
E-mail ID – arindam19@yahoo.com

[2]Department of Physiology
University of Calcutta
92, Acharya Prafulla Chandra Road
Kolkata-700009
India

Highlights

- MPTP treatment causes increase in TNF-alpha expression in mouse hippocampus
- TNF-alpha activates TNFR2 mediated signaling cascade
- NF-κB subunits p65 and p52 translocate and dimerize in nucleus of mouse hippocampus
- Hippocampal neuronal population was unaltered upon MPTP treatment
- p65-p52 dimer has role in protecting hippocampus during MPTP induced neuroinflammation

Abstract:

1-Methyl-4-Phenyl-1,2,3,6-Tetrahydropyridine (MPTP) -induced neuroinflammation and its impact in hippocampus remain elusive till date. Our present study includes the time dependent changes of inflammatory molecules in mouse hippocampus during MPTP treatment. MPTP treatment increased level of TNF-α, enhanced expression of TNFR2 along with PI3 kinase (PI3K) induced phosphorylation of Akt resulting in persistent nuclear factor-κB (NF-κB) activation. The expressions gradually increased from Day1 post-MPTP treatment, maximally at Day3 post-treatment. MPTP induced translocation of p65 and p52, two subunits of NF-κB family, to nucleus where they had been found to dimerize. Therefore, MPTP induced TNF-α signaling through TNFR2 mediated pathway and recruited p65-p52 dimer in hippocampal nucleus which is reported to have protective effect on hippocampal neurons indicated by unchanged neuronal count in hippocampus in treated groups with respect to control. Our finding suggests that this unique NF-κB dimer plays some role in providing inherent protection to hippocampus during MPTP-treatment.

Keywords: Hippocampus; MPTP; TNF-α; TNFR2; p65/p52

1. Introduction:

Neuroinflammation is one of the key factors bringing about non-specific cell death and neurodegeneration in most of the neurodegenerative disorders. Parkinson's disease (PD) is one such progressive neurodegenerative disease characterized by decreased dopamine levels in the striatum and

loss of pigmented dopamine neuronal cells in the substantia nigra pars compacta followed by cognitive and motor impairments. Many environmental toxins are used to induce PD like disorders with alternative pathological features in animal model. Among them, 1-methyl-4-phenyl-1,2,3,6-tetrahydropyridine (MPTP) appears to target the dopaminergic neurons and is used most widely in animal model of idiopathic PD.

The mostly affected area in PD is substantia nigra pars compacta since it is rich in dopaminergic neurons and hence prone to MPTP induced oxidative stress. Identifying environmental factors that predispose to the development of idiopathic PD via oxidative stress, mitochondrial dysfunction, Lewy pathology remains elusive (Beitz 2014).The major secondary cause of the disease that prolongs the disease progression is neuroinflammation. Role of neuroinflammation in the pathophysiology of PD is supported by both epidemiological and genetic studies. Furthermore, studies of post mortem samples from PD patients confirm the involvement of innate as well as adaptive immunity and association of microglial/astroglial cells in the affected brain regions (Hirsch et al. 2012; Hunot and Hirsch 2003). In MPTP model of PD, other regions are also affected due to this bystander neuroinflammation. Previously MPTP induced neuroinflammation has been widely studied in substantia nigra and frontal cortex (Mitra et al. 2015b; Mitra et al. 2016). But its effect on hippocampus is elusive till date. According to a study with post mortem PD brains, hippocampal volume and cell number remains unaltered in PD patients (Joelving et al. 2006). The reason behind this inherent protection of hippocampus from PD induced neuroinflammation is an unresolved mystery.

It is previously reported that TNF-α, one of the potent proinflammatory cytokine, hugely increases in substantia nigra, frontal cortex and hippocampus in mouse model of PD induced by Paraquat and Rotenone mediated neuroinflammation (Mitra et al. 2011; Mitra et al. 2015a). TNF-α level was also reported to increase in striatum of 6-OHDA treated mice of PD model (Zhao et al. 2007), substantia nigra and cerebral cortex of MPTP treated mice (Mitra et al., 2015b). TNF-α has pleiotropic action depending on different type of receptor activation. It exerts proinflammatory and pro-apoptotic effect when it acts via TNFR1, whereas, it becomes anti-inflammatory and neuroprotective when it activates TNFR2 (Probert 2015). TNF-α also exerts distinctive region specific effect on brain. In substantia nigra and striatum it promotes neurodegeneration whereas it promotes neuroprotection in hippocampus (Sriram et al. 2006). However the exact role of TNFR2 in providing protection to hippocampus is elusive till date. TNFR2 is specifically expressed on few neuronal subtypes, oligodendrocytes, microglia and astrocytes in the brain .TNFR2 acts through PI3K-Akt pathway or by recruitment of NIK which ultimately leads to Nf-κB activation (Beyer and MacBeath 2012). Nf-κB activation causes dimerization of p65/p65, p65/p50, p65/p52, p52/RelB and c-Rel/p50. Depending on the dimer type,

different pro-inflammatory and anti-inflammatory functions are executed (Hayden and Ghosh, 2014). The neuroprotective and anti-apoptotic effect of GDNF in MN9D cells exposed to 6-OHDA involves p65 / p52 dimer activation (Cao et al. 2013). But whether NF-κB signaling pathway is responsible for the selective protection of hippocampus from MPTP induced damage is far from clear.

In this study we investigated the effect of MPTP on mouse hippocampus in time dependent manner. We found that TNF-α activates TNFR2 mediated signaling pathway and recruits p65-p52 heterodimer in the nucleus which has some plausible protective role selectively on mouse hippocampus.

2. Materials and Methods:

2.1. Materials

MPTP, was purchased from Sigma Aldrich, Inc. (St. Louis, MO). Among the antibodies used, primary antibodies anti-TNF Receptor Type 2 (TNFR2) (#3727), anti-PI3K (#4249), anti-pAkt (#5012), p65 (#8242), p52 (#4882), were procured from Cell Signaling Technology, Inc. (Danvers, MA, USA). Anti-Lamin B1 antibody was procured from Santa Cruz Biotechnology (# sc-20682) and anti-β-Actin antibody procured from Abcam (#8227, Abcam, Inc. Cambridge, UK). The secondary antibodies like goat anti-rabbit IgG-HRP (horseradish peroxidase) and rabbit anti-mouse IgG-HRP were purchased from Bangalore GeNei Pvt. Ltd. (Bangalore, India). For TNF-α estimation, commercial mouse TNF-α ELISA Kit was procured from Ray Biotech (Cat nos. - ELM-TNFa-1). The remaining chemicals were purchased in analytical grade of highest purity (India).

2.2. Animal and treatment

Swiss albino mice (~25 g each; five mice in each group) were obtained from the National Institute of Nutrition (Hyderabad, India). Each was housed in an animal facility (maintained at 25-28 [± 2]°C; with 55 [± 5]% relative humidity, and a 12 hour/12 hour light/dark cycle) located at the Animal Housing Unit in the Department of Zoology, University of Calcutta. All animals were provided rodent chow (National Institute of Nutrition) and filtered water *ad libitum.* All animal experiments were performed following the "Principles of Laboratory Animal Care" (NIH publication No. 85-23, revised 1985), as well as by following specific Indian law on "Protection of Animals" under the supervision of authorized investigators.

For the experiments, the mice (n=5) were randomly divided into different groups comprising (A) vehicle (0.9% normal saline) treated control and (B) MPTP-treated set. We had two sets of MPTP treated mice (n=5 each) for time dependent sacrifice. The MPTP treated sets received four subcutaneous injection of MPTP (18 mg/kg b.w.) at 2 hours interval in a single day and were sacrificed

at Day1and Day3 for time chase experiment (Jackson-Lewis and Przedborski 2007). The brain tissue of sacrificed animals were then harvested for analyses as described in the various assays below.

2.3. Tissue handling

After sacrifice, brains were dissected out by decapitation aseptically. Isolated hippocampi were harvested for analyses as described in the assays below. Mice brain sections were cut according to the Paxinos Mouse Brain Anatomy Atlas.

2.4. Preparation of cell lysate

Total cell lysate for western blot analysis were performed according to Mitra et al, (Mitra et al. 2012). Briefly, brain region hippocampus was dissected out immediately after dissection of sagittal sections of whole brain. Tissues were homogenized in ice-cold RIPA lysis buffer (150 mM sodium chloride, 1.0% TritonX-100, 50 mM Tris pH 8.0, 0.01% SDS, 0.5% sodium deoxy cholate) containing 1 mM PMSF (phenyl methane sulfonyl fluoride or phenylmethylsulfonyl fluoride) (SRL, India), 1 µg/ml aprotinin, 1 µg/ml leupeptin and 1 µg/ml pepstatin (Sigma-Aldrich Inc., USA). The samples were sonicated and incubated on ice for 30 min, and centrifuged 3 times at 14,000 rpm for 15 min at 4°C. A portion of the supernatant was reserved for protein determination using the Bradford reagent (Sigma-Aldrich Inc., USA) and subsequent measurement of absorbance was done at 595 nm in a UV-1700 Pharma Spec, Shimadzu spectrophotometer (Shimadzu Scientific Instruments, Columbia, MD). The remaining supernatant was stored at -80°C.

2.5. Nuclear Extract Preparation

Nuclear extract from mice brain was prepared according to Mitra *et al*. (Mitra et al. 2015b). Briefly, mouse brain tissue pellets were suspended in 1.5 ml of buffer A (10 mM Hepes, pH 7.9, 1.5 mM $MgCl_2$, 10 mM KCl, and 1 mM EDTA) supplemented with 1 mM dithiothreitol, 1 mM phenylmethylsulfonyl fluoride, 0.5 µg/ml leupeptin and 1 µM pepstatin, and left on ice for 10 min. The nuclei were separated from the cytosol fraction by centrifugation at 4°C at 800g for 15 mins. Supernatants containing cytosolic protein were discarded. The pellets containing nuclei were suspended in 1.2 ml of buffer B (20 mM Hepes, pH 7.9, 1.5 mM $MgCl_2$, 420 mM KCl, 25% glycerol, and 0.2 mM EDTA) supplemented with 1 mM dithiothreitol, 1 mM phenylmethylsulfonyl fluoride, 0.5 µg/ml leupeptin, and 1 µM pepstatin, homogenized and left on ice for 30 min. Samples were centrifuged at 12,000g for 20 min at 4°C. The supernatant, containing nuclear proteins, was transferred to a micro centrifuge tube. The

supernatant (10 µl) was used for a Bradford assay and the remainder was stored at -80°C and used for further experiments.

2.6. Western blot analysis

Western blot analysis was done according to Sinha *et al.* (Sinha et al. 2015). Briefly, 50 micrograms of total protein extracts, cytosolic and nuclear protein extracts of each sample of each day of sacrifice were separated on a 9-12% polyacrylamide gels, electro blotted onto polyvinylidenedifluoride membrane (Amersham Biosciences, Piscataway, NJ), and the membranes were blocked with 5% nonfat dry milk for 1-hr. The membranes were incubated with primary antibodies, anti-TNFR2, anti-PI3K, anti-pAkt, p65, p52 [Cell Signaling Technology, Inc. (Danvers, MA, USA)] at dilutions of 1:1000, overnight at 4°C, washed in TBS-Tween-20 (0.01%). Primary antibodies were detected against HRP-conjugated secondary antibodies using the HRP substrate ECL solution. The band intensity was measured by densitometry (Gel Doc™ XR+ System, Bio-Rad Laboratories, USA).The cytosolic and membrane proteins (TNFR2, PI3K and pAkt) were normalized with β-Actin and nuclear proteins (p65 and p52 were normalized with Lamin B1.

2.7. Immunoprecipitation

Immunoprecipitation was done according to Mitra *et al.* (Mitra et al. 2016). Briefly, for immunoprecipitation, clear lysate mouse hippocampus were prepared and about 100 µg of protein were immunoprecipitated using 10 µl of anti-p65 antibody (Cell Signaling Technology, Inc. Danvers, MA, USA) for overnight at 4°C with gentle rotation. 25 µl Protein G CL-Agarose (Bangalore Genei, India) was added to the previous mixture, depending on the experiment and allowed it to mix for 4 hours at 4°C with gentle rotation. It was then centrifuged at 3000 rpm for 2 min. The immunoprecipitates were washed extensively with sterile PBS and separated by SDS-PAGE, followed by western blot analyses with anti-p52 antibody (Cell Signaling Technology, Inc. Danvers, MA, USA) as described above.

2.8. ELISA

Cell lysates were prepared from dissected brain regions of control and MPTP treated mice. Dissected brain regions were homogenized in specialized lysis buffer for ELISA, containing 25 mM HEPES, 0.1% Tween-20, 5mM magnesium chloride, 1.3 mM EDTA, 1 mM EGTA and protease inhibitors (1 mM phenylmethylsulfonyl fluoride, 0.5 µg/ml leupeptin, 1 µM pepstatin). The expression level of TNF-α from hippocampal protein lysate was analyzed using commercial enzyme-linked immunosorbent assay (ELISA) kit [Ray Bio (Cat no. - ELM-TNFα-1)] according to the manufacturer's

protocol. The OD values were read in a microplate reader at 450 nm. The concentration of TNF-α in samples were calculated against the standard curve generated using recombinant TNF-α supplied with the kit.

2.9. Immunohistochemistry

Immunohistochemistry was performed according to Mitra et al. (Mitra et al. 2013); briefly, sagittal brain sections (5 μm thick) were cut from paraffin-embedded brain tissue and mounted on positively charged Super frost slides (Export Mengel CF, Menzel, Braunschweig, Germany). Tissues were de-paraffinized, dehydrated through graded alcohols, and then endogenous peroxidase was quenched in a 3% hydrogen peroxide solution. Background staining was inhibited with 5% bovine serum albumin [BSA] (Sisco Research Laboratories Pvt. Ltd. [SRL], Mumbai, India). The sections were incubated in a humid chamber overnight at 4°C with primary antibody (anti-NeuN) (diluted 1:50 in solution containing 5% BSA). After three washes in PBS-Tween20, sections were sequentially incubated in horseradish peroxidase (HRP)-conjugated anti-sera specific for those antigens and were diluted at a 1:30 ratio in Tris-buffered saline containing 0.3% Triton-X and 0.5% blocking agent for 2 hours at room temperature. Immunoreactive complexes were then detected using a DAB system of Bangalore GeNei Pvt. Ltd. (Bangalore, India). Sections were then dehydrated through graded alcohols, cleared in xylenes, and cover slipped with DPX mounting medium. Slides that received no primary antibody served as negative controls. Images were captured using a Zeiss Axiovert X-100 microscope (Jena, Germany) using 10X lens. The cell count of the IHC sections were done with the help of ImageJ software.

2.10. RNA extraction and Quantitative real time PCR

RNA was extracted using the TRIzol reagent, following the manufacturer's protocol (Invitrogen, Carlsbad, CA). The amount of RNA was measured spectrophotometrically using Nano drop (Thermo Scientific Multiskan GO). 5 μg of RNA from each sample was converted to cDNA using random hexamer (Thermo Fisher Scientific) and MMLV reverse transcriptase (Promega Corporation). For qPCR, the expressions of mature mRNA and gene in tissue samples were performed by SYBR green detection system with GAPDH as internal control. Each experiment was performed thrice. The primer sequences of the genes used in this work are listed in Table 1.

2.11. Statistical analysis

Results are expressed as mean ± SEM. Statistical evaluation of data has been done by one-way analysis of variance (ANOVA) followed by pairwise comparison of means using post hoc Tukey test. Results were considered significant at $p < 0.05$.

3. Results:

3.1. MPTP treatment increased the expression of TNF-α and TNFR2 in mouse hippocampus

TNF-α protein expression was found to be significantly increased ($p<0.05$) upon MPTP treatment (Figure.1A) on both Day1and 72 hours; with maximum increase at Day3post-treatment ($p<0.05$) with respect to control. Protein expression of TNFR2 increased significantly on Day1and Day3post-MPTP treatment in comparison to vehicle treated groups (Figure.1B) ($p<0.05$). Figure.1C graphically shows relative intensities of TNFR2 in mouse hippocampus normalized with β-actin. These results indicate TNFR2 upregulation upon increased expression of TNF-α in mouse hippocampus in our model of study.

3.2. MPTP-treatment results in TNF-α-TNFR2 mediated Nf-κB activation in mouse hippocampus

To investigate the downstream signaling of TNFR2 in our model of study, we first looked into the status of PI3K and p-Akt by western blot with respective antibodies in whole cell lysates. PI3K expression showed significant increase at both Day1and Day3of MPTP treatment ($p<0.05$) (Figure.2A, first panel). Significant increase in phosphorylation of Akt ($p<0.05$) was also seen at both the treatment conditions with maximum increase on Day3 post MPTP treatment with respect to vehicle treated control (Figure.2A, second panel). Figure.2B graphically shows relative intensities of PI3K and p-Akt in mouse hippocampus normalized with β-actin. Immunoblot results of p65 and p52 in nuclear extract showed gradual and significant increase ($p<0.05$) in expression of both p65 (Figure.2C, upper panel) and p52 (Figure.2C, lower panel) from Day1to Day3 post-MPTP treatment with respect to control. Graphical presentation of the relative intensities of p65 and p52 normalized with β-actin is given in Figure.2D. This indicates activation of two Nf-κB subunits (p65 and p52) and their subsequent nuclear translocation upon induction of TNFR2 mediated signaling post-MPTP treatment in mouse hippocampus.

3.3. MPTP treatment causes subsequent dimerization of p65 and p52 subunits in the nucleus of mouse hippocampus

To investigate any plausible interaction between p65 and p52 in nucleus, immunoprecipitation experiment was performed with nuclear extract of mouse hippocampus. Immunoprecipitation was done using anti-p65 antibody followed by immunoblotting with anti-p52 antibody. Significantly increased ($p<0.05$) dimerization of p65 with p52 in nuclear extract was observed during MPTP treatment with respect to control in both Day1and Day3 groups with maximum interaction in Day3 group (Figure 3A). Graphical presentation of relative levels of p52 bound p65 in control and treatment groups is shown in Figure 3B. This result indicates that p65-p52 heterodimer may act as a transcription factor, playing crucial role to prevent neuronal loss in mouse hippocampus in our model of study.

3.4. MPTP treatment altered NeuN mRNA expression but NeuN protein expression remained unaltered

To investigate the neuronal status in hippocampus post MPTP treatment, the expression of NeuN was studied at both transcription and protein level. It was found that, after Day1 post MPTP treatment the NeuN mRNA expression significantly reduced ($p<0.05$) with respect to control, but, on Day3, it was found to be increased again restoring its status like control (Figure. 4A). However, the NeuN protein expression or NeuN positive cell count showed no significant alterations in MPTP treated groups with respect to control groups (Figure. 4B). Figure. 4C shows percentage population of NeuN positive cells in mouse hippocampus in control and all treatment groups.

4. Discussion

In the present study, we provide an experimental platform to investigate the status of TNFR2 mediated signaling cascade in mouse hippocampus after MPTP treatment. We report a gradual and significant increase in TNF-α expression in mouse hippocampus on both Day1and Day3 post-MPTP treatment. In addition, a consistently heightened expression of TNFR2 in hippocampus was also observed on both Day1 and Day3 post-MPTP treatment with respect to control groups. Release of pro-inflammatory cytokine TNF-α is reported to be linked with PD pathology resulting in loss of dopaminergic neurons in substantia nigra and striatum (Sriram et al. 2002; Sriram and O'Callaghan 2007). However, TNF-α exerts differential effect on brain regions; promoting neurodegeneration in substantia nigra and striatum whereas promoting neuroprotection in hippocampus (Sriram et al. 2006). However the process of neuroprotection in hippocampus is a puzzle till date. In our study, TNF-α triggered TNFR2 mediated signaling cascade via PI3K/Akt activation. Akt does not have any role in modulating gene expression by acting as a transcription factor itself, rather, it recruits NF-κB, an extensively expressed transcription

factor, that plays a key role in regulating gene expression involved in several cellular processes, including cell survival and proliferation (Wang et al. 1996). Meanwhile, NF-κB is believed to be activated by Akt upon phosphorylation (Kalechman et al. 2003; Kawasaki et al. 2003). However, it is still not clear whether the NF-κB signaling pathway is involved in TNFR2 mediated neuroprotection of hippocampal neurons upon MPTP treatment. In the present study, NF-κB has been hypothesized and preliminarily identified as a downstream target of a signaling pathway initiated by TNF-α via TNFR2 in mouse hippocampus. Our observation supports the previously reported fact by others that TNF-α induces NF-κB activation in TNFR2 mediated pathway providing neuroprotection to primary cortical neurons from glutamate induced excitotoxicity (Marchetti et al. 2004). In our study, it was observed that, in mouse hippocampus upon MPTP treatment, TNFR2 activation recruited PI3-Kinase which phosphorylated Akt. This p-Akt releases p52 from inactive precursor p100 [NIK phosphorylates IKKα which in turn phosphorylates p100 and results in release of active subunit p52 (Hayden and Ghosh, 2014)]. In our study, the nuclear translocation of two NF-κB subunits p65 and p52 was enhanced. Briefly, our present findings indicate that TNF-α activated the PI3K/Akt signaling pathway via TNFR2 which subsequently upregulated NF-κB signaling pathway in mouse hippocampus.

NF-κB proteins can form homo- or heterodimers, such as p65/p65, p65/p50, p65/p52, p52/RelB and c-Rel/p50, having different dynamics and DNA target specificities (Chen et al. 1998;Escalante et al. 2002; Fusco et al. 2009). Upon activation, in canonical pathway of NF-κB activation, TNF-α activates TNFR1 and induces dimerization of p65/p50 which subsequently functions as transcription factor of various target genes responsible for progressive inflammation (Hayden and Ghosh 2014). p65/p52 heterodimer is reported to be involved in GDNF mediated neuroprotection of dopaminergic neurons of substantia nigra in rat model of early PD (Cao et al. 2008). But it is an unsolved riddle till date as to which NF-κB dimer is responsible for TNFR2 mediated signaling in hippocampus. In our study, p65 and p52 had been found to dimerize in the nuclei of mouse hippocampus after MPTP treatment. Our study reports for the first time that p65/p52 heterodimers appeared to be involved in the activation of the NF-κB signaling pathway upon TNFR2 stimulation in mouse hippocampus. It is worthwhile to mention that the formation of p65/p50 heterodimer was not found in our present study (data not shown). This result further confirms absence of pro-inflammatory gene transcription via canonical NF-κB pathway in mouse hippocampus post- MPTP treatment. The NeuN mRNA expression was found to reduce on Day1 post MPTP treatment but was recovered on Day3 post MPTP treatment. Whereas the NeuN positive cell count was found to be unaltered on both the experimental groups with respect to control. This result shows that the initially lowered rate of NeuN mRNA synthesis was recovered in the later stage of the study indicating some upstream protective action to restore neuronal health in

hippocampus. We also checked the overall neuronal status of substantia nigra and tyrosine hydroxylase expression (rate limiting enzyme of dopamine synthesis) in our model of study and found progressive reduction in both their expression confirming neurodegeneration in substantia nigra post MPTP treatment (Supplementary figure).

Therefore, our present study reveals that TNF-α stimulated TNFR2 activation in mouse hippocampus triggered PI3K/Akt mediated NF-κB pathway activation resulting in nuclear translocation of p65 and p52 and, their subsequent dimerization. The unaltered NeuN positive cell number in hippocampus confirms lack of neuronal loss in hippocampus in our study.

5. Conclusion

Our study infers that MPTP-treatment caused elevation of TNF-α, triggering TNFR2 upregulation and subsequent activation of TNFR2 mediated signaling cascade that ultimately recruited p65 and p52 in the nucleus resulting in their dimerization. This TNF-α triggered TNFR2 mediated downstream signaling cascade is considered to be associated with inherent protection of hippocampus from MPTP mediated damage. Therefore, the pleiotropic cytokine TNF-α by means of TNFR2 mediated signaling becomes a boon to hippocampus instead of being a death inducer.

Acknowledgement:

The authors are grateful to Neuroscience Taskforce, Department of Biotechnology (Govt. of India) for funding this work and providing fellowship support (Project sanction No. - BT/PR3986/MED/30/677/2011). Authors are grateful to the Animal Ethical Committee for providing the ethical clearance to execute the animal experiments. Authors are thankful to Dept. of Zoology, Maulana Azad College, Kolkata, for assistance in Gel Documentation and microscopy. Authors express their sincere thanks to all lab members and friends for lending their helping hands in animal maintenance and other assistance whenever necessary.

Author Contributions:

The work is an outcome of the cumulative effort of the whole team. All the authors have contributed in various degrees to execute and communicate this work.

More specific author contributions are as follows:

- **Study conception and design: Nabanita Ghosh, Arindam Bhattacharyya**
- **Acquisition of data: Nabanita Ghosh, Soham Mitra, Priyobrata Sinha**
- **Analysis and interpretation of data: Nabanita Ghosh, Nilkanta Chakrabarti**
- **Drafting of manuscript: Nabanita Ghosh**
- **Critical revision: Nilkanta Chakrabarti, Arindam Bhattacharyya**

Declaration for Animal Ethical Approval:

Our Lab is registered under CPCSEA (Committee for the Purpose of Control and Supervision of Experiments on Animals), Ministry of Environment, Forest and Climate change, Govt. of India. All animal experiments executed during this work are approved by CPCSEA.

Registration number of our Lab under CPCSEA – 885/GO/Re/S/05/CPCSEA.

Declaration of Conflict of Interest:

There exists no conflict of interest among authors.

References:

Beitz, J.M., 2014. Parkinson's disease: a review. Front Biosci (Schol Ed). 6, 65-74.

Beyer, E.M., MacBeath G., 2012. Cross-talk between receptor tyrosine kinase and tumor necrosis factor-alpha signaling networks regulates apoptosis but not proliferation. Mol Cell Proteomics. 11:M111 013292.

Cao, J.P., Niu, H.Y., Wang, H.J., Huang, X.G., Gao, D.S., 2013. NF-kappaB p65/p52 plays a role in GDNF up-regulating Bcl-2 and Bcl-w expression in 6-OHDA-induced apoptosis of MN9D cell. Int J Neurosci. 123, 705-710.

Cao, J.P., Wang, H.J., Yu, J.K., Liu, H.M., Gao, D.S., 2008. The involvement of NF-kappaB p65/p52 in the effects of GDNF on DA neurons in early PD rats. Brain Res Bull. 76, 505-511.

Chen, F.E., Huang, D.B., Chen, Y.Q., Ghosh, G., 1998. Crystal structure of p50/p65 heterodimer of transcription factor NF-kappaB bound to DNA. Nature. 391, 410-413.

Escalante, C.R., Shen, L., Thanos, D., Aggarwal, A.K., 2002. Structure of NF-kappaB p50/p65 heterodimer bound to the PRDII DNA element from the interferon-beta promoter. Structure. 10, 383-391.

Fusco, A.J., Huang, D.B., Miller, D., Wang, V.Y., Vu, D., Ghosh, G., 2009. NF-kappaB p52:RelB heterodimer recognizes two classes of kappaB sites with two distinct modes. EMBO Rep. 10, 152-159.

Hayden, M.S., Ghosh, S., 2014. Regulation of NF-kappaB by TNF family cytokines. Semin Immunol. 26, 253-266.

Hirsch, E.C., Vyas, S., Hunot, S., 2012. Neuroinflammation in Parkinson's disease. Parkinsonism Relat Disord. 18 Suppl 1, S210-212.

Hunot, S., Hirsch, E.C., 2003. Neuroinflammatory processes in Parkinson's disease. Ann Neurol. 53 Suppl 3, S49-58; discussion S58-60.

Jackson-Lewis, V., Przedborski, S., 2007. Protocol for the MPTP mouse model of Parkinson's disease. Nat Protoc. 2, 141-151.

Joelving, F.C., Billeskov, R., Christensen, J.R., West, M., Pakkenberg, B., 2006. Hippocampal neuron and glial cell numbers in Parkinson's disease--a stereological study. Hippocampus. 16, 826-833.

Kalechman, Y., Sredni, B., Weinstein, T., Freidkin, I., Tobar, A., Albeck, M., Gafter, U., 2003. Production of the novel mesangial autocrine growth factors GDNF and IL-10 is regulated by the immunomodulator AS101. J Am Soc Nephrol. 14, 620-630.

Kawasaki, K., Smith, R.S., Jr., Hsieh, C.M., Sun, J., Chao, J., Liao, J.K., 2003. Activation of the phosphatidylinositol 3-kinase/protein kinase Akt pathway mediates nitric oxide-induced endothelial cell migration and angiogenesis. Mol Cell Biol. 23, 5726-5737.

Marchetti, L., Klein, M., Schlett, K., Pfizenmaier, K., Eisel, U.L., 2004. Tumor necrosis factor (TNF)-mediated neuroprotection against glutamate-induced excitotoxicity is enhanced by N-methyl-D-aspartate receptor activation. Essential role of a TNF receptor 2-mediated phosphatidylinositol 3-kinase-dependent NF-kappa B pathway. J Biol Chem. 279, 32869-32881.

Mitra, S., Chakrabarti, N., Bhattacharyya, A., 2011. Differential regional expression patterns of alpha-synuclein, TNF-alpha, and IL-1beta; and variable status of dopaminergic neurotoxicity in mouse brain after Paraquat treatment. J Neuroinflammation. 8, 163.

Mitra, S., Chakrabarti, N., Dutta, S.S., Ray, S., Bhattacharya, P., Sinha, P., Bhattacharyya, A., 2015a. Gender-specific brain regional variation of neurons, endogenous estrogen, neuroinflammation and glial cells during rotenone-induced mouse model of Parkinson's disease. Neuroscience. 292, 46-70.

Mitra, S., Ghosh, N., Sinha, P., Chakrabarti, N., Bhattacharyya, A., 2015b. Alteration in Nuclear Factor-KappaB Pathway and Functionality of Estrogen via Receptors Promote Neuroinflammation in Frontal Cortex after 1-Methyl-4-Phenyl-1,2,3,6-Tetrahydropyridine Treatment. Sci Rep. 5, 13949.

Mitra, S., Ghosh, N., Sinha, P., Chakrabarti, N., Bhattacharyya, A., 2016. Alteration of nuclear factor-kappaB pathway promote neuroinflammation depending on the functions of estrogen receptors in substantia nigra after 1-methyl-4-phenyl-1,2,3,6-tetrahydropyridine treatment. Neurosci Lett. 616, 86-92.

Mitra, S., Keswani, T., Dey, M., Bhattacharya, S., Sarkar, S., Goswami, S., Ghosh, N., Dutta, A., Bhattacharyya, A., 2012. Copper-induced immunotoxicity involves cell cycle arrest and cell death in the spleen and thymus. Toxicology. 293, 78-88.

Mitra, S., Keswani, T., Ghosh, N., Goswami, S., Datta, A., Das, S., Maity, S., Bhattacharyya, A., 2013. Copper induced immunotoxicity promote differential apoptotic pathways in spleen and thymus. Toxicology. 306, 74-84.

Probert, L., 2015. TNF and its receptors in the CNS: The essential, the desirable and the deleterious effects. Neuroscience. 302, 2-22.

Sinha, K., Sadhukhan, P., Saha, S., Pal, P.B., Sil, P.C., 2015. Morin protects gastric mucosa from nonsteroidal anti-inflammatory drug, indomethacin induced inflammatory damage and apoptosis by modulating NF-kappaB pathway. Biochim Biophys Acta. 1850, 769-783.

Sriram, K., Matheson, J.M., Benkovic, S.A., Miller, D.B., Luster, M.I., O'Callaghan, J.P., 2002. Mice deficient in TNF receptors are protected against dopaminergic neurotoxicity: implications for Parkinson's disease. FASEB J. 16, 1474-1476.

Sriram, K., Matheson, J.M., Benkovic, S.A., Miller, D.B., Luster, M.I., O'Callaghan, J.P., 2006. Deficiency of TNF receptors suppresses microglial activation and alters the susceptibility of brain regions to MPTP-induced neurotoxicity: role of TNF-alpha. FASEB J. 20, 670-682.

Sriram, K., O'Callaghan, J.P., 2007. Divergent roles for tumor necrosis factor-alpha in the brain. J Neuroimmune Pharmacol. 2, 140-153.

Wang, C.Y., Mayo, M.W., Baldwin, A.S. Jr., 1996. TNF- and cancer therapy-induced apoptosis: potentiation by inhibition of NF-kappaB. Science. 274, 784-787.

Zhao, C., Ling, Z., Newman, M.B., Bhatia, A., Carvey, P.M., 2007. TNF-alpha knockout and minocycline treatment attenuates blood-brain barrier leakage in MPTP-treated mice. Neurobiol Dis. 26, 36-46.

Figure legends:

Figure. 1: Effect of MPTP on pro-inflammatory cytokine TNF-α and its receptor (TNFR2) as an indication of neuro-inflammatory status of mouse hippocampus post-MPTP administration. Mice were administered with vehicle (Control) and MPTP (18mg kg^{-1}). Different days of sacrifice post-MPTP treatment are indicated by Day1 and Day3. (A) ELISA analysis of TNF-α expression from whole lysate of mouse hippocampus of all three groups (pg/mg tissue). Note that, TNF-α expression significantly increased in mouse- hippocampus post-MPTP treatment on both Day1 (178.34 ± 13.6 pg/ml) and Day3 (373.5 ± 55.7 pg/ml); with maximum increase on Day3 post-treatment ($p<0.05$) with respect to control (112.72 ± 1.59 pg/ml). (B) Immunoblot analysis of TNFR2 from whole lysate of mouse hippocampus of all three groups. Note that, TNFR2 expression steadily increased on Day1 and Day3 with respect to control. Beta-actin was used as a normalization control. (C) Densitometry analysis of TNFR2 protein

expression in mouse hippocampus. Presence and absence of MPTP in control and treatment groups is indicated by -/+ sign. Data in the densitometry analysis are represented as the mean ± SEM of three independent experiments. Asterisks (*) indicate significant difference ($p < 0.05$) in values for different doses compared to control.

Figure. 2: Effect of MPTP on activation of TNFR2 mediated downstream signaling cascade and on NFκB activation in mouse hippocampus post-MPTP administration. Mice were administered with vehicle (Control) and MPTP (18mg kg^{-1}). Different days of sacrifice post-MPTP treatment are indicated by Day1 and Day3. (A) Immunoblot analysis of PI3K and p-Akt from whole tissue lysate of mouse hippocampus of all three groups. Beta-actin was used as a normalization control. Note that, both PI3K and p-Akt expression increased significantly on Day3 in comparison to control. (B) Densitometry analysis of PI3K and p-Akt western blots. Significant increase in PI3K expression was indicated by asterisks (*) and in p-Akt was indicated by hash (#) ($p<0.05$) on different days compared to control. (C) Immunoblot analysis of p65 and p52 from nuclear extract of mouse hippocampus of all three groups. Lamin-B1 was used as normalizing control in this case. Note that, nuclear translocation of both p65 and p52 increased gradually post-MPTP treatment, with maximum nuclear expression on Day3. (D) Densitometry analysis of p65 and p52 western blots. Significant increase in p65 nuclear translocation was indicated by asterisks (*) and in p52 was indicated by hash (#) ($p<0.05$) on different days compared to control. Presence and absence of MPTP in control and treatment groups is indicated by -/+ sign. Data in the densitometry analysis are represented as the mean ± SEM of three independent experiments.

Figure. 3: Evaluation of the binding status of p65 and p52 after nuclear translocation by MPTP treatment done by immunoprecipitation experiments. (A) MPTP treatment increased the binding of p65 to p52 on both Day 1 and Day 3 treatment groups compared to control groups. Blots were normalized by immunoblot of p52 in the same samples (input). (B) Graph showing relative levels of p52 bound p65 in control and treatment groups. Data in the densitometry analysis are represented as the mean ± SEM of three independent experiments. Asterisks (*) indicate significant difference ($p < 0.05$) in values for different doses compared to control. Presence and absence of MPTP in control and treatment groups is indicated by -/+ sign.

Figure. 4: Effect of MPTP on NeuN expression as an indication of overall neuronal status in mouse hippocampus. (A) Fold change in NeuN mRNA expression over respective control samples normalized with GAPDH mRNA expression in hippocampus of all treatment groups. NeuN mRNA expression on Day1 showed 1.5 times reduction than Control; but was restored on Day3. (B) Immunohistochemical

detection of NeuN positive cells in mouse hippocampal sections of control, Day1 and Day3 at 10X magnification. (C) Histogram of % population of NeuN positive cells in hippocampus shows no significant alterations on Day1 and Day3 with respect to control. Presence and absence of MPTP in control and treatment groups is indicated by -/+ sign. Data are represented as the mean ± SEM of three independent experiments. Asterisks (*) indicate significant change in treated groups compared to control ($p < 0.05$).

FIGURES:

Figure. 1:

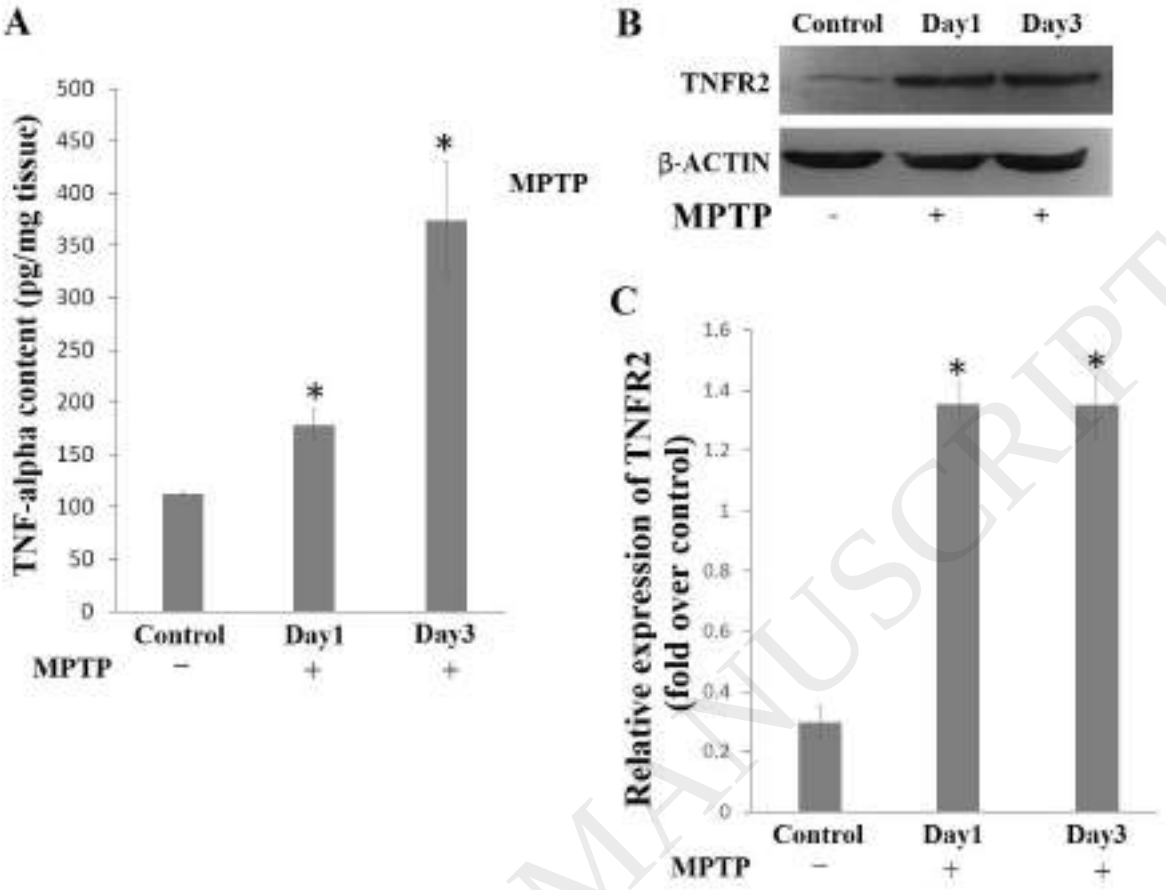

Figure. 2:

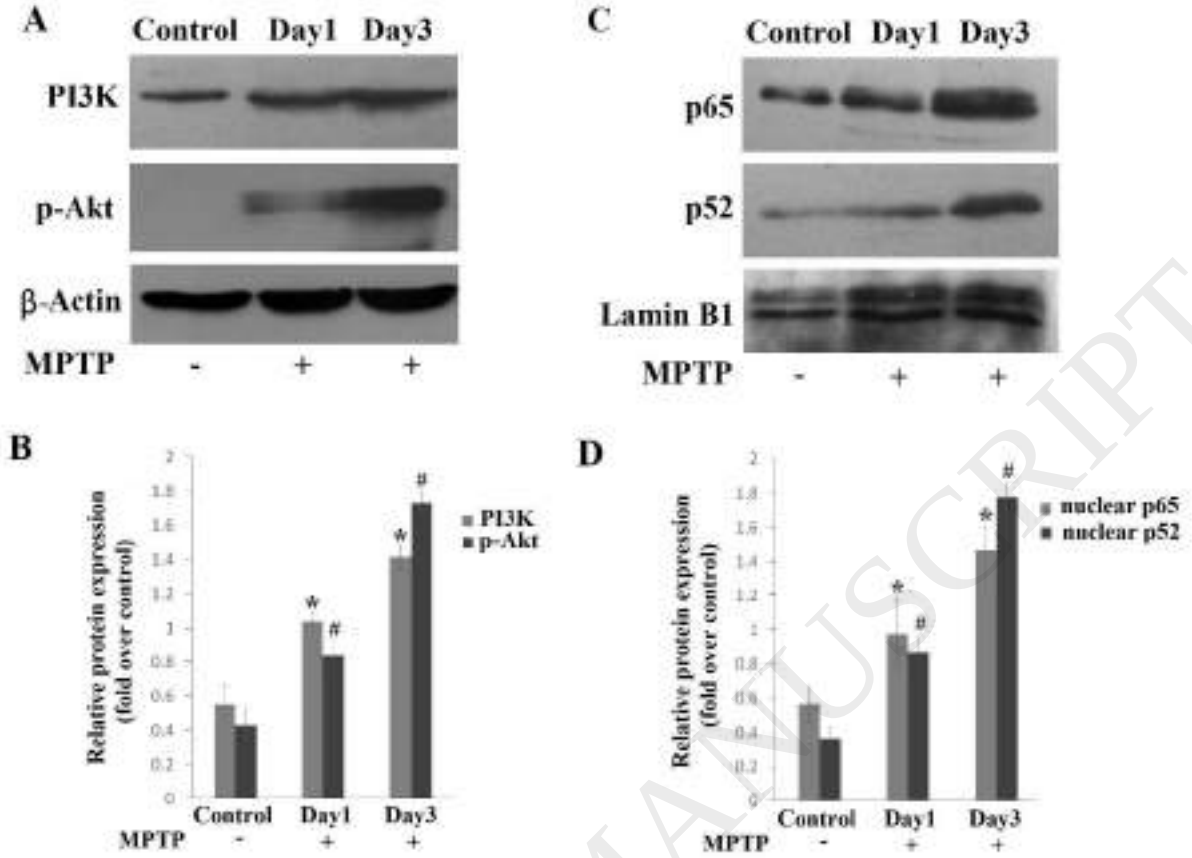

Figure. 3:

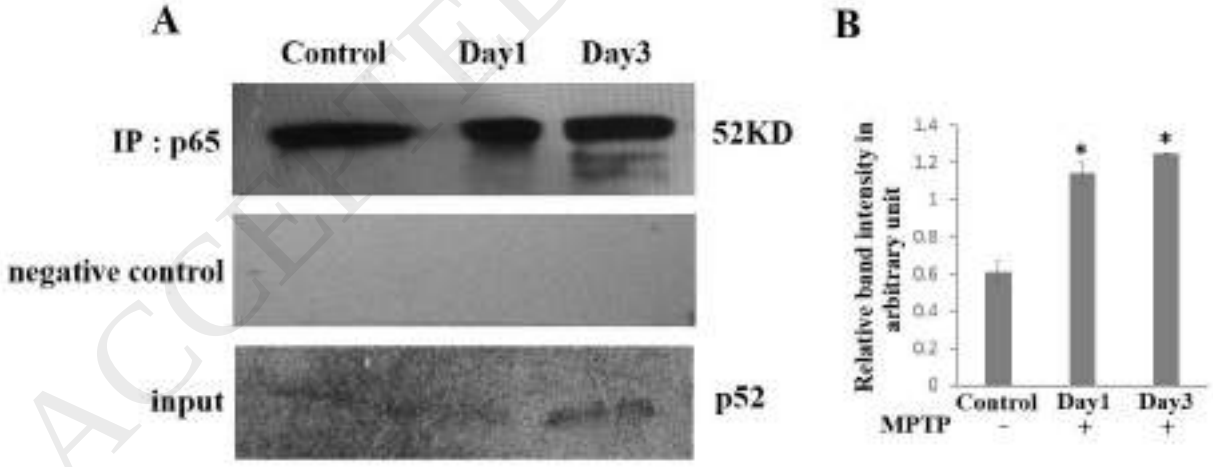

Figure. 4:

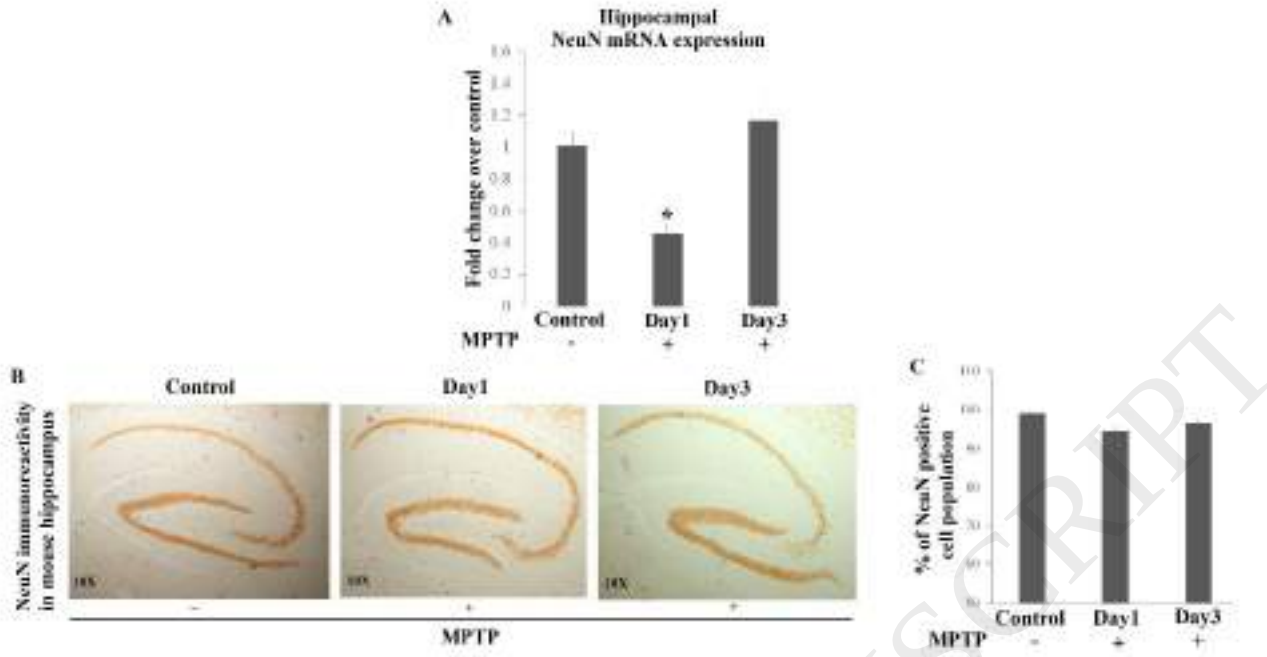

Table 1: Details of Primers used in this study:

Gene	Primer sequence (5' to 3')	Annealing temperature (°C)	Amplicon size
NeuN	Fp: CCCAAGGTTACCCTGTATTG Rp: CCAGAGGAAGGAAGGTGATA	56	206
GAPDH	Fp: CTCCCTCACAATTTCCATCC Rp: GGGTGCAGCGAACTTTAT	52	99

Proc Zool Soc
DOI 10.1007/s12595-016-0199-2

RESEARCH ARTICLE

Qualitative and Quantitative Evaluation of Gall Induced by *Pseudophacopteron alstonium* Yang et Li 1983 (Hemiptera: Psyllidae: Phacopteronidae) as Plant Parasite, in *Alstonia scholaris* Leaves

Sanjukta Manna[1] · Sriza Hazra[1] · Abhishek Mukherjee[1]

Received: 8 July 2016 / Revised: 20 October 2016 / Accepted: 28 October 2016

Abstract *Alstonia scholaris* (Dr C. Alston, 1685–1760) (Family Apocynaceae) (Chattim tree), commonly known as devil tree, is an evergreen tropical tree. The tree is native to India and also found in Sri Lanka, Southern China, throughout Malaysia to northern Australia. This plant is seriously damaged by formation of tumor like galls across the Kolkata city,West Bengal which affects its ornamental and medicinal value. Gall is formed by ovipositing adults of *Pseudophacopteron alstonium* Yang et Li 1983 (Hemiptera: Psyllidae: Phacopteronidae) and results in destruction of host plant. The nymphal stage undergoes moulting through first instar to third instar to reach the adult within galls. It is observed that highly infested leaves can bear 60–80 galls. The gallmaker *Pseudophacopteron* sp. stresses the host organ, and the host counters it with physiological activities supplemented by newly differentiated tissues. In infested leaves, chlorophyll and carbohydrate contents decreased sequentially with the age of the gall. There were no significant changes in protein and total amino acid content in gall tissue. But total lipid content was highest in mature galled leaves. Increased phenolic content after psylloid herbivory, which exerted oxidative stress on the host plants, was observed in gall infested leaves as compared to fresh ungalled leaves of *Alstonia scholaris.* Moisture content was highest in ungalled healthy leaves than the young galled, mature galled and perforated galled leaves.

✉ Sanjukta Manna
sanjukta_manna@rediffmail.com

[1] Post Graduate Department of Zoology, Maulana Azad College, Kolkata 700 013, India

Keywords *Alstonia scholaris* galls · *Pseudophacopteron* · Hypertrophy · Hyperplasy · Chlorophyll

Introduction

Alstonia scholaris (Apocynaceae) (local name, chatim) is an evergreen, tropical tree native to the Indian Subcontinent and used for treating skin disorder, malarial fever, urticaria, chronic dysentery, diarrhoea and in snake bites. Galls are developed by hypertrophy and hyperplasy, usually under the influence of a parasitic organism, like viruses, bacteria, fungi, algae, higher plants, nematodes, mites or insects (Mani 1964). Insects of the orders Thysanoptera, Hemiptera, Diptera and Hymenoptera, and in some cases those of Lepidoptera and Coleoptera, are responsible for gall making (Raman et al. 2009). Leaves of *Alstonia* sp. are common to found infested with insect-caused galls. Species of the genus *Pseudophacopteron alstonium* Yang et Li 1983 (Hemiptera: Psylloidea), commonly called psyllids, produce leaf galls on *Alstonia* and alters the differentiation processes of the leaves, modifying architecture to its advantage (Yang and Li 1983). Psyllid galls usually contain only one nymph per chamber, but some galls have been found to contain more than one nymph (Albert et al. 2011). Psyllid galls may have either simple or complex structures, and can be found either isolated or aggregated (Hodkinson 1984; Raman 2003). Most of the earlier literatures (Price et al. 1998; Christiano et al. 2003) on gall formation induced by *Pseudophacopteron* sp. were limited to identification and gall morphology. Raman (2003) provided valuable information on plant galls in India and cecidogenetic behavior of some gall inducing insects and morphogenesis of their galls. However, the anatomical,

biochemical and developmental (ontogenesis) aspects of leaf galls induced by many insects still remain unexplored in India. Hence an attempt has been made to study the histological and biochemical changes in leaf galls induced by psylloid herbivores from their normal counterparts on *Alstonia scholaris.* We studied the changes in chlorophyll, total carbohydrate, protein, lipid, amino acid, total phenol and moisture contents in *A. scholaris* leaves due to gall formation. Experimental findings were validated statistically.

Material and Methods

Collection of Plant Samples

The ungalled healthy, young galled, mature galled and perforated galled leaves of *A. scholaris* were collected periodically at an interval of 5–7 days from Panchasayar region, New Garia, Kolkata, West Bengal. All categories of leaves were taken from the same tree. Gall developmental stages were determined using diameter as a small spot bulged on the leaf blade and were taken to laboratory for morphological and anatomical analysis. Populations of eggs, immatures and adults of gall maker were obtained from the galls that were sampled. The plant was identified with the help of the herbarium kept in the archive of Acharya Jagadish Chandra Bose Indian Botanic Garden, Botanical Survey of India, West Bengal, India.

Morphological Analysis of Gallmaker and Host Plant Parts

Galls were observed morphologically under dissecting microscope in the laboratory. Leaves bearing eggs were collected from the infested trees. Individual galls were slit ($n = 50$) along the middle using a razor blade and the occupying immature stages were extracted and transferred to 70% ethanol. Each gall was categorized according to age based on the developmental stage of the extracted immatures. Live adult stages of the insect were collected from the leaf bed and were aspirated into microfuge tube containing 70% ethanol. First to third instars (each stage $n = 50$) and adult insects ($n = 50$) were dehydrated with the ethanol series and were prepared for permanent mounting by transferring them to warm 10% KOH solution ($\sim$60 °C) until turned translucent. These specimens were rinsed in 10% acetic acid and mounted in DPX. Prepared slides were examined under microscope. All the stages were photographed with the help of a Sony cyber shot DSC-T10 camera. The insect was identified as *Pseudophacopteron alstonium* Yang et Li 1983, a Psyllidae. The characterisation of adult insects and morphological terminology used in the descriptions were combined from Ossiannilsson (1992), Oliveira et al. (2011), and Burckhardt and Queiroz (2012).

Histopathological Analysis of Host Plant

Thin transverse sections of gall chamber of young, mature and perforated gall were dissected to observe the nature of host damage as well as for histological analysis. These sections were stained in Safranin and Light Green (Sass, 1951) and then observed under microscope. Photographs were taken by a Sony cyber shot DSC-T10 camera.

Biochemical Assay

Fresh samples were used for biochemical analyses and leaves were categorized into: (a) ungalled (b) young galled (c) mature galled and (d) perforated galled leaves.

The degree of infestation was ascertained by subjecting 1 g of fresh ungalled, young galled, mature galled and perforated galled leaves to various biochemical analyses: total carbohydrates (Dubois et al. 1956), total chlorophyll content (Arnon 1949), proteins (Lowry et al. 1951), total lipids (Folch et al. 1957), total amino acids (Moore and Stein 1948) and total phenol content (Bray and Thorpe 1954).

Statistical Analysis

One way ANOVA (analysis of variance) followed by Tukey test using SPSS were performed on the data of biochemical analyses of ungalled, young, mature and perforated galled leaves of infested plants. Means associated with all the data for each biochemical parameter were separated using Tukey's test when significant values were obtained (Zar 1999).

Results

Developmental Stages of Insect

The adults of *Pseudophacopteron* sp. oviposit mainly on abaxial surface of new leaves. Life cycle of *Pseudophacopteron* sp. can be divided into egg, nymph and adult stages. Eggs were laid singly or in clump (Fig. 1a). Nymphal stage comprises of three instars collected from young and mature galled leaves which was yellowish in colour with one pair of red rosette shaped compound eyes. Body was ovate, divided into head, thorax and abdomen. Three pairs of thoracic appendages were observed. First and second instar nymph were more or less similar in structure with exception of length (Fig. 1b, c). The third instar

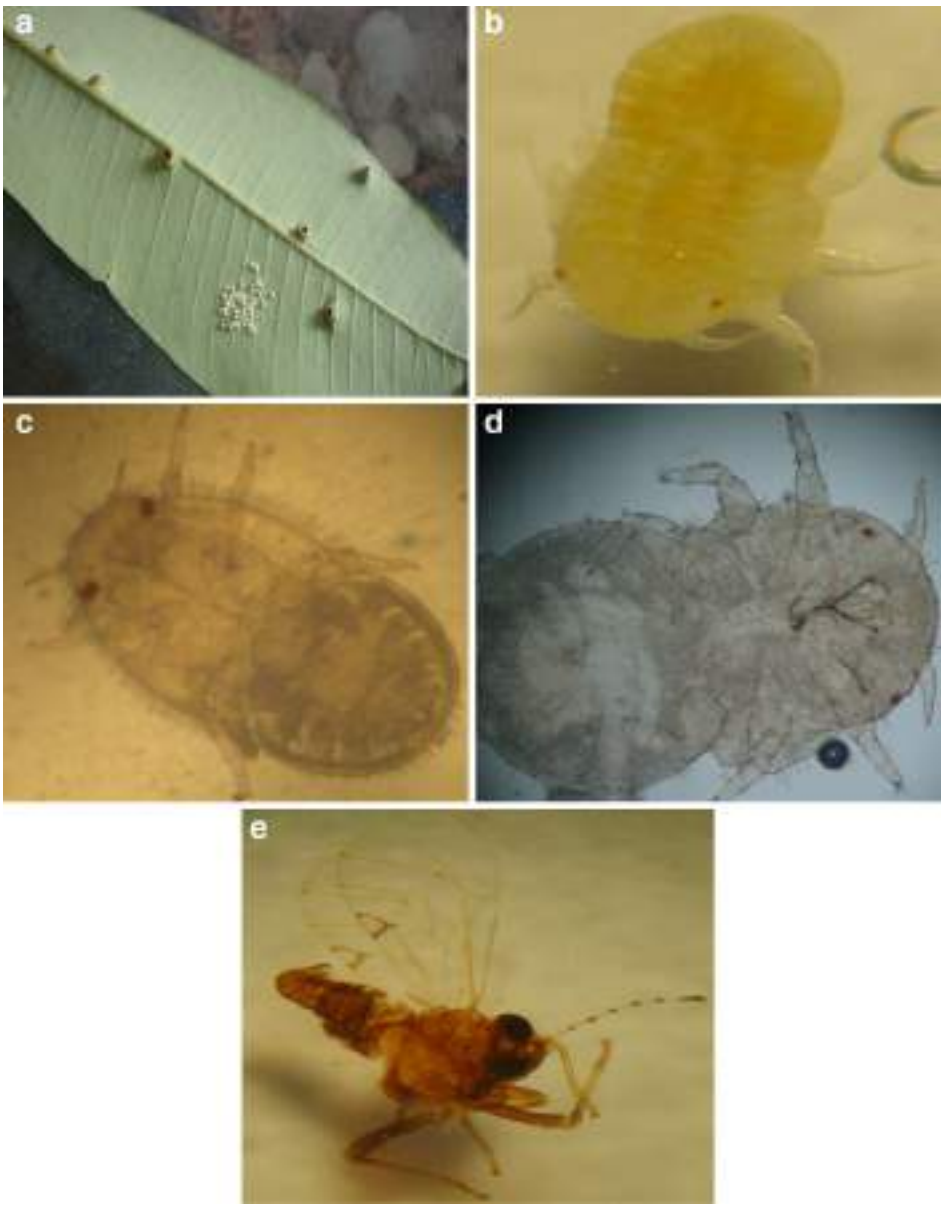

Fig. 1 Life cycle of *Pseudophacopteron* sp.; **a** Eggs are laid in groups, **b**, **c** and **d** first, second and third instar stages respectively, **e** adult stage

looked similar to adult. Bristles were present along the head and thorax (Fig. 1d). Antennae were short and filiform, present in all the instar. Adult was soft bodied, yellowish, winged, one pair of large, red, compound bulging eyes and with tapering antennae. The wings were large, crossveinless and covered with bristles (Fig. 1e).

Morphological Alterations in the Leaf

Morphological and anatomical structures of *A.scholaris* galls showed completely deformed cells and compression to form a concave nymphal cavity. Galls were formed on both abaxial and adaxial surface of the leaves (Fig. 2a, b) but they were abundant on the abaxial surface. The mature galls were unilocular with a single chamber or multilocular with 3–4 chambers (Fig. 2c). It was sub cylindrical, concolorous with the host leaf, except at the apex which is yellowish. The wall of mature gall was thick and succulent. The galls were persistent remaining on leaves long after the escape of adults. Diameter of the gall chamber (inner cavity) ranges from 0.1 cm to 1 cm. Initiation of the gall formation resulted from the oviposition by female insects on the leaves. First initial change of leaf was decolourisation followed by a large outgrowth on abaxial side where the gall appeared, enlarged and placed in a depression or a small circular pit. At initial stage, galls grew towards the abaxial side of the leaf but later on its growth was on the adaxial surface. A little bulge appeared on the adaxial side of the leaf which further developed into dome shaped structure. The cavity of gall was lined by closely packed

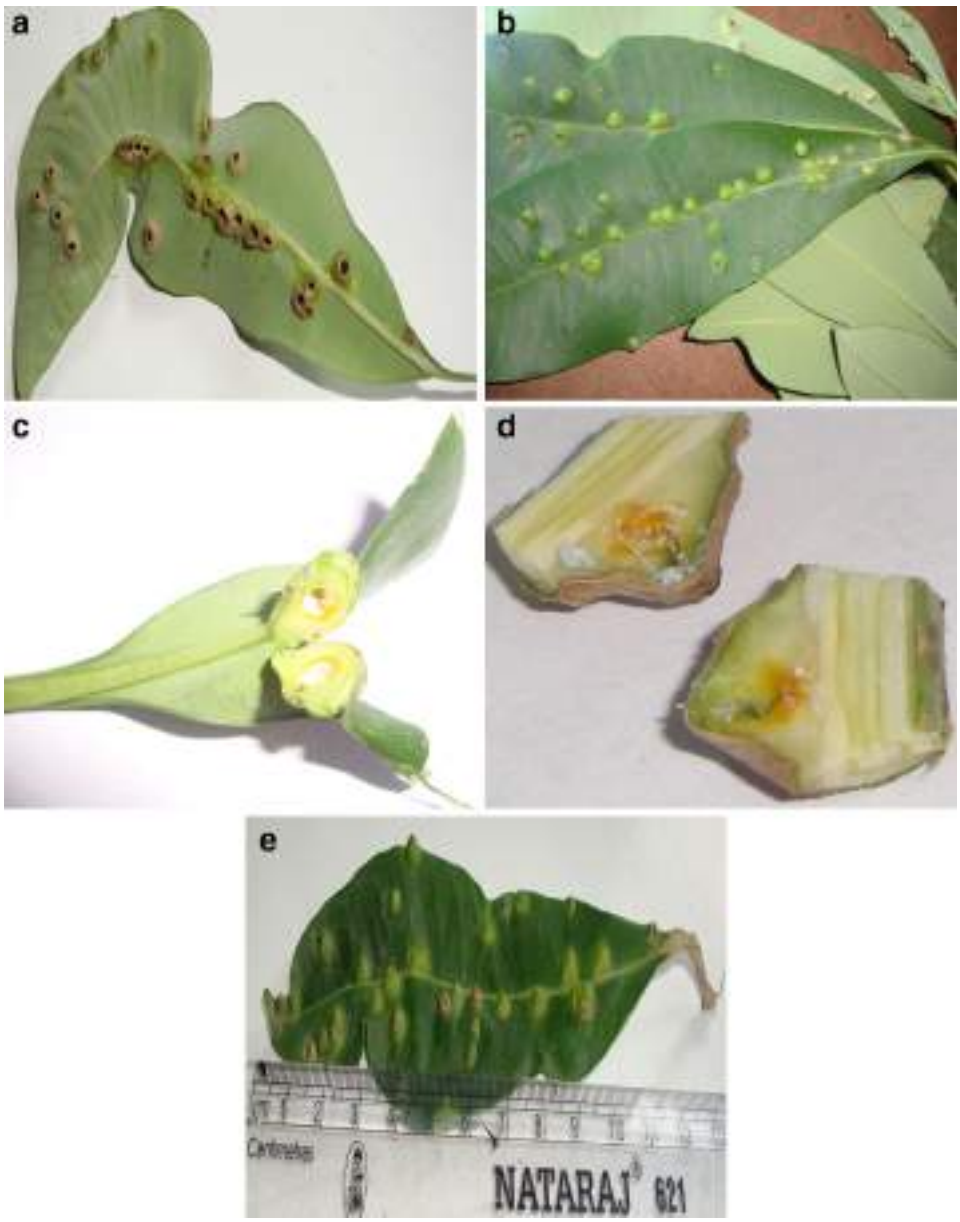

Fig. 2 Morphological alterations in the leaf; **a** Leaf appears crumbled and completely deformed, **b** Galls on both abaxial and adaxial surface, **c** Matured unilocular gall chamber, **d** Succulent wall with yellowish apex, **e** 12 cm long leaf bearing 30 galls

mass of chlorophyll- lacking cells. The adult emerged from a small circular opening formed in the centre of the gall. It was the senescent stage of gall which was characterised by the presence of small orifices on the gall surface with a yellowish brown rim (Fig. 2d). These matured leaves can bear approximately 20–30 galls (Fig. 2e). Highly infested leaves contained between 60 and 80 galls. Such leaves appeared crumbled and completely deformed.

Histopathological Observation

After hatching, the first-instar psyllid nymph inserted its stylets into epidermal cells, and continues inducing the cell alterations started by the egg's presence. The gall formation was initiated by divisions of the cells of the abaxial epidermis and of the adjacent parenchyma (Fig. 3a). There was no welding, but only overlapping of parenchyma. No stomata were observed. During second instar stage, parenchymal cells of gall chambers became homogeneous with rapid division resulting in an increase in gall size (Fig. 3b). Some cells of the parenchyma redifferentiated into procambial strands. The abaxial portion of the gall was not vascularized, and had isodiametric epidermal and parenchyma cells. In case of the mature nymphal (third) stage, groups of neoformed parenchyma cells transformed into procambial strands within the gall chamber as meristamatic activity induced. There was only one collateral vascular bundle in the gall's wall with the phloem facing the lumen of the chamber which appears as fissure (Fig. 3c). In mature galls, the phloematic bundles were arranged in the

Table 1 Results of biochemical analysis of ungalled, young galled, mature galled and perforated galled leaf

Biochemical parameters	Ungalled leaf	Young galled leaf	Mature galled leaf	Perforated galled leaf	$F_{3,8}$	*P*
Carbohydrate (μg/g)	8.05 ± 0.14[a]	3.93 ± 0.15[b]	2.46 ± 0.14[c]	1.9 ± 0.12[d]	25.108	0.000
Protein (μg/g)	1.80 ± 0.1[a]	1.82 ± 0.07[a]	1.85 ± 0.05[a]	1.9 ± 0.03[a]	0.351	0.790
Lipid (μg/g)	20.07 ± 0.82[a]	30.13 ± 0.43[b]	53.93 ± 0.93[d]	41.93 ± 0.79[c]	368.173	0.000
Amino acid (μg/g)	0.35 ± 0.02[a]	0.355 ± 0.02[a]	0.366 ± 0.012[a]	0.373 ± 0.01[a]	0.358	0.785
Phenol (μg/g)	8.05 ± 0.14[a]	3.79 ± 0.14[b]	3.26 ± 0.05[b]	13.65 ± 0.5[c]	314.531	0.000
Moisture (%)	80.08 ± 1.15[a]	72.077 ± 1.5[b]	72.43 ± 1.3[b]	77.43 ± 0.87[c]	10.213	0.004
Chlorophyll-a (μg/g)	0.303 ± 0.01[a]	0.243 ± 0.04[b]	0.201 ± 0.01[c]	0.251 ± 0.03[b]	9.270	0.006
Chlorophyll-b (μg/g)	0.466 ± 0.02[a]	0.261 ± 0.01[b]	0.068 ± 0.01[c]	0.215 ± 0.03[b]	102.906	0.000
Total Chlorophyll (μg/g)	0.772 ± 0.02[a]	0.504 ± 0.01[b]	0.265 ± 0.01[d]	0.467 ± 0.04[c]	86.853	0.000

Within the row means followed by same letter(s) are not significantly different by Tukey's test ($P < 0.05$)

lower part of the wall, very close to the lumen. The periderm coated most of the gall. The gall surfaces also showed intense undulating patterns and the mesophyll was totally homogenous. In the folded region of the gall, some loss of fibre walls was noted. The gall in the third nymphal stage reached its definitive dome shape. The cortical cells undergo hypertrophy and became larger and more vacuolated than the medullar region. During the adult emergence, differentiated epidermis gave rise to the region of the gall opening and fissures corresponding to the rupture of the epidermis were observed (Fig. 3d). The adult gall-makers made an exit channel with their mouthparts and left the waste in the chamber. In the senescent phase, the adults were emerged out in the environment. Major anatomical alterations in this phase were the absence of trichomes, and suberization occurs in the opening region of the gall chamber (Fig. 3e). The abaxial portion of the gall degraded rapidly, and its tissues were disorganized. Later the gall tissues disintegrated after inducer's emergence, but the periderm remains almost intact until leaf abscission.

Biochemical Assay

The significant changes in different biochemical parameters (viz. carbohydrate, protein, lipid, chlorophyll etc.) in noninfested and infested leaves are provided in Table 1. Total carbohydrate was highest in ungalled healthy leaves but least in mature galled and perforated galled leaves (Table 1). The protein content was increased 5.5% in perforated galled leaves than in ungalled, young galled, mature galled leaves. Lipid content was highest in mature galled than normal ungalled, young and perforated leaves. The ungalled, young, mature and perforated galled leaves showed no significant differences in free amino acids. Phenol concentration was highest in perforated galled leaves followed by ungalled, young galled and mature galled leaves. The moisture content recorded in the leaf reduced corresponding to the severity of infestation. The galled tissues showed a decrease in the chlorophyll content (65.6%) with the increase in the growth of the gall becoming very low level in the mature gall.

Discussion

Gall is essentially a neoplastic growth. Neoplastic growths are pathological structures due to feeding or ovipositional stimuli caused by insect feeding ranging from nearly normal to the highly complex, abnormal outgrowths, characterized by cellular hypertrophy and hyperplasy. In gall induced mature tissues, cell redifferentiation is necessary, generating specialized tissues (Oliveira and Isaias, 2009). In response to the stimuli of gall induction, the parenchyma cells recover their ability to divide and hypertrophy. We observed that larval penetration led to homogenization of the parenchyma, cell hypertrophy and hyperplasia, enlarging giant cells and resulted in destruction to the epidermis and some portions of vascular bundles. According to Carneiro and Isaias (2015), galls at induction stage have hypertrophic and hyperplasic cells, with thin primary walls, sometimes fragmented vacuoles. Phloematic bundles indicates the establishment of a photosynthetates drain to the gall tissues (Rohfritsch 1992). At gall senescence, around the insect chamber and the exit channel, the necrotic tissue resembles the protective layer of the abscission zone of the leaves. This gall morphogenesis seems to be associated with the inducer's nutritional physiology and protective shelter (Bronner 1992; Mani 1973; Rohfritsch 1992). Gall development involves two contracting events: the insect stresses the host organ, and the host counters it with new physiological activities supplemented by newly differentiated tissues (Albert et al. 2013). *Alstonia* sp. host exhibited remarkable biochemical changes after psylloid herbivory. It is well known that carbohydrate deficiency results in reduction of general vitality, activity, and growth of insects even though

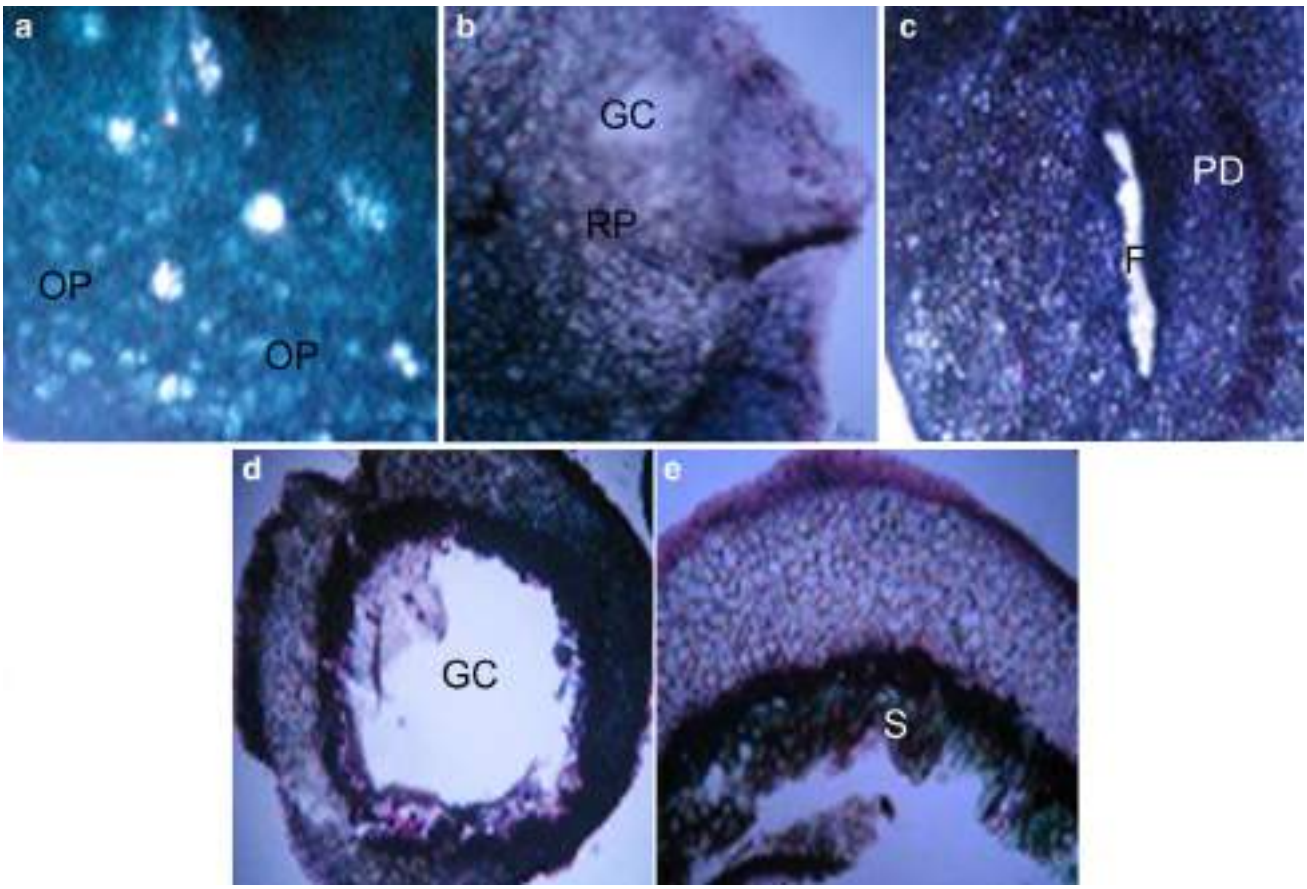

Fig. 3 Photomicrographs of sections of ungalled and galled leaves (Safranin and *Light Green*); **a** Initiation of gall formation during first instar (young gall), **b** Increase in gall size during second instar (mature gall), **c** Fissure development during third instar (mature gall), **d** Gall opening and rupture of epidermis during adult emergence (perforated gall) **e** Suberization during senescent phase. *E* epidermis, *OP* overlapping parenchyma, *GC* gall chamber, *RP* redifferentiated parenchyma, *F* fissure, *PD* periderm, *S* suberization (colour figure online)

proteins and lipids serve as an alternative source of energy (Harborne 2003; Schoonhoven et al. 2005). A steady decrease in carbohydrate content was noticed in the galled leaves. It can be hypothesized that growth of gall tissues was always associated with the changes in the levels of host plant cellular contents such as carbohydrates, proteins, lipids and other secondary chemicals. Galled leaves showed no significant changes in protein and total amino acid contents as compared to their normal ungalled leaves. There was a reduced total protein in the highly infested leaf which might be due to the lower protein requirement and host plant would reach the saturated level in secretion of proteins (Raman et al. 1997). Lipid content was significantly increased in mature and perforated galled leaves as a sink. This lipid source acting as precursors of ecdysteroid moulting hormone for *Pseudophacopteron* sp., and provides structural role in cellular membranes of this insect (Mukherjee et al. 2016).

Generally, when a plant is infested, its phenol content increases as a consequence of a defense reaction to the infestation. Phenols are formed in response to the ingress of insects and their appearance is considered as part of an active defence response in plant to protect from invaders (biotic stress) or stress factors (abiotic stress) and are believed to be an adaptive response to the altered conditions. Our findings showed that levels of total phenolic content in perforated galled leaves were significantly higher than ungalled ones. It indicates that psylloid herbivory, exerted oxidative stress on the host plants which led to increased antioxidant enzyme activities and serve as a chemical defense mechanism in plants against pathogen attack (Felton et al. 1989). However, gall inducing insects have evolved ways to hijack plant defenses to their own benefit, by sequestering these chemicals and using them to protect themselves from predators, parasitoids, pathogens and other herbivores. This notion has been termed the enemy hypothesis (Price et al. 1987; Schultz 1992; Hartley 1998).

A steady state reduction in moisture content was observed in gall infested leaves. This may be due to the fact that the gall insects are known to extract moisture content and nutrients from the leaf tissue of host plant cell (Meyer

1987) for the formation of gall on the leaf tissue. Hence the increased infestation leads to lower the water content in the leaf. We observed net chlorophyll content in fresh ungalled leaves of *Alstonia* sp much higher than of galled leaves. This loss of chlorophyll was due to disappearance of chloroplast and redifferentiation of mesophyll (Albert et al. 2011). The stress imposed by the galling herbivore lowered the photosynthetic rate.

The present study has shown that the galls of *Alstonia* sp. caused by *Pseudophacopteron* sp. are not uncontrolled tumor growth. Their ontogeny follows a well-defined sequence, and produce well-defined morpho-anatomical structure for exploring the coevolution between gall-inducing insects as parasite and the host plants.

Acknowledgements We convey our sincere gratitude to Prof. Subir Das Gupta, Head of the Department, for providing laboratory facilities to conduct the work. Authors are also grateful to Prof. Samiran Chakraborti, Emeritus Fellow (UGC), for identification of insects.

References

Albert, S., A. Padhiar, D. Gandhi, and P. Nityanand. 2011. Morphological, anatomical and biochemical studies on the foliar galls of *Alstonia scholaris* (Apocynaceae). *Revista Brasileria de Botanica* 34(3): 343–358.

Albert, S., S. Rana, and D. Gandhi. 2013. Anatomy and ontogenesis of foliar galls induced by *Odinadiplosis Odinae* (Diptera: Cecidomyiidae) on *Lannea Coramandelica* (Anacardiaceae). *Acta Entomologica Serbica* 18(1/2): 161–175.

Arnon, D.J. 1949. Copper enzymes in isolated chloroplasts. *Plant Physiology* 24: 1–25.

Bronner, R. 1992. The role of nutritive cells in the nutrition of cynipids and cecidomyiids. In *Biology of insect induced galls*, ed. J.D. Shorthouse, and O. Rohfritsch, 118–140. Oxford: Oxford University Press.

Bray, H.G., and W.V. Thorpe. 1954. Analysis of phenolic compounds of interest in metabolism. *Methods Biochemical Analysis* 1: 25–52.

Burckhardt, D., and D.L. Queiroz. 2012. Checklist and comments on the jumping plant-lice (Hemiptera: Psylloidea) from Brazil. *Zootaxa* 3571: 26–48.

Carneiro, R.G.S., and R.M.S. Isaias. 2015. Gradients of metabolite accumulation and redifferentiation of nutritive cells associated with vascular tissues in galls induced by sucking insects. *AoB Plants*. doi:10.1093/aobpla/plv086.

Christiano, J.C.S., R.M.S. Isaias, and J.E. Kraus. 2003. Características foliares relacionadas ao estabelecimento do sistema Aspidosperma australe (Apocynaceae)—Pseudophacopteron sp. (Phacopteronidae). *Resumos do 54 Congresso Nacional de Botânica, Belém* 1: 1.

Dubois, M., K.A. Gilles, J.K. Hamilton, P.A. Rebers, and F. Smith. 1956. Colorimetric method for determination of sugars and related substances. *Analytical Chemistry* 28: 350–356.

Felton, G.W., K. Donato, R.J. Del Vecchio, and S.S. Duffey. 1989. Activation of plant foliar oxidases by insect feeding reduces nutritive quality of foliage for noctuid herbivores. *Journal of Chemical Ecology* 15: 2667–2694.

Folch, J., M. Lees, and G.H. Sloane-Stanley. 1957. A simple method for the isolation and purification of total lipids from animal tissues. *The Journal of biological chemistry* 226: 497–509.

Harborne, J.B. 2003. *Introduction to ecological biochemistry*. London: Academic Press.

Hartley, S.E. 1998. The chemical composition of plant galls: are level of nutrients and secondary compounds controlled by the gall-former. *Oecologia* 113: 492–501.

Hodkinson, I.D. 1984. The biology and ecology of the gall-forming Psylloidea (Homoptera). In *Biology of gall insects*, ed. T.N. Ananthakrishnan, 59–77. London: Arnold.

Lowry, O.H., N.J. Rosebrough, A.L. Farr, and R.J. Randall. 1951. Protein measurement with the folin phenol reagent. *The Journal of biological chemistry* 193: 265–275.

Mani, M.S. 1964. *Ecology of plant galls*. The Hague: Dr.W. Junk Publishers.

Mani, M.S. 1973. *Plant galls of India*, 354. New Delhi, India: The Macmillan Company of India.

Meyer, J. 1987. *Plant galls and gall inducers*. Berlin: Gerbruder Borntraeger.

Moore, S., and W.H. Stein. 1948. Photometric ninhydrin method for use in the chromatography of amino acids. *The Journal of biological chemistry* 176: 367–388.

Mukherjee, A., A. Karmakar, and A. Barik. 2016. Bionomics of *Momordica cochinchinensis* fed *Aulacophora foveicollis* (Coleoptera: Chrysomelidae). *Proceedings of the Zoological Society*. doi:10.1007/s12595-016-0166-y.

Oliveira, D.C., and R.M.S. Isaias. 2009. Influence of leaflet age in anatomy and possible adaptive values of the midrib gall of *Copaifera langsdorffii* (Fabaceae: Caesalpinioideae). *Revista de Biologıa Tropical* 57: 293–302.

Oliveira, D.C., R.M.S. Isaias, A.S.F.P. Moreira, T.A. Magalhães, and J.P. de Lemos-Fillho. 2011. Is the oxidative stress caused by *Aspidosperma* spp. galls capable of altering leaf photosynthesis? *Plant Science* 180: 489–495.

Ossiannilsson, F. 1992. The psylloidea (Homoptera) of Fennoscandia and Denmark. *Fauna Entomologica Scandinavica* 26: 1–346.

Price, P.W., G.W. Fernandes, and G.L. Waring. 1987. Adaptive nature of insect galls. *Environmental Entomology* 16: 15–24.

Price, P.W., G.W. Fernandes, A.C.F. Lara, J. Brawn, H. Barrios, M.G. Wright, S. Ribiero, and N. Rothcliff. 1998. Global patterns in local number of insect galling species. *Journal of Biogeography* 25: 581–591.

Raman, A. 2003. Cecidogenetic behavior of some gallinducing thrips, pyllides, coccids, and gall midges, and morphogenesis of their galls. *Oriental Insects* 37: 359–413.

Raman, A., R.N. Singh, and A. Maryanska-Nadachowska. 1997. Biology and Karyology of a Cecidogenous Psylloid, *Trioza fletcheri minor* (Homoptera: Psylloidea) and Morphogenesis of galls on the leaves of *Terminalia tomentosa* and *T. arjuna* (Combretaceae). *Insecta Matsumurana* 53: 117–134.

Raman, A., R. Beiderbeck, and W. Herth. 2009. Early subcellular responses of susceptible and resistant Vitis taxa to feeding by grape Phylloxera *Daktulosphaira vitifoliae*. *Botanica Helvetica* 119: 31–39.

Rohfritsch, O. 1992. Patterns in gall development. In *Biology of insect induced galls*, ed. J.D. Shorthouse, and O. Rohfritsch, 60–86. New York: Oxford University Press.

Sass, J.E. 1951. *Botanica Microtechnique*, *2* ed, 228. Ames, IA, USA: The Iowa State College press.

Schultz, B.B. 1992. Insect herbivores as potential causes of mortality and adaptation in gall forming insects. *Oecologia* 90: 297–299.

Schoonhoven, L.M., J.J.A. van Loon, and M. Dicke. 2005. *Insect-plant biology*. New York: Oxford University Press.

Yang, C.K., and F.S. Li. 1983. A preliminary study on Chinese *Pseudophacopteron* with descriptions of three new species (Homoptera: Psyllidae). *Wuyi Science* 3: 120–128.

Zar, J.H. 1999. *Biostatistical analysis*. New Jersey: Prentice Hall.

International Journal of Engineering, Science and Mathematics
Vol. 7 Issue 4(2), April 2018,
ISSN: 2320-0294 Impact Factor: 6.765
Journal Homepage: http://www.ijmra.us, Email: editorijmie@gmail.com
Double-Blind Peer Reviewed Refereed Open Access International Journal - Included in the International Serial Directories Indexed & Listed at: Ulrich's Periodicals Directory ©, U.S.A., Open J-Gage as well as in Cabell's Directories of Publishing Opportunities, U.S.A

Ultrastructural Changes of Radioattenuated *Leishmania donovani,* The Causative Organism of Human Kala-azar Disease

Sanjukta Manna*

Abstract

The promastigotes of *Leishmania donovani* which were exposed above 20krad gamma radiation (Gammacell 220, Co^{60} source at 23^0C) looked like amastigotes by shedding their flagella and became round in shape. With the increasing doses of radiation, the number of amastigote like structures increased. At higher doses, abnormalities included shrinkage, rounding, loss of flagellum, aggregation, vacuolation, progressive loss of motility and these changes occurred producing an almost endless variety of morphological forms. From the electron micrograph it was revealed that the most effected organelles after irradiation were mitochondria, kinetoplast and flagellum. Irradiated cells have different levels of injury; ones with less damage recover quickly and have opportunity to modify antigenic profile while those with more damage repaired later. This result was also supported by the alteration in microtubular structure of plasma membrane. Nucleus showed a larger relative volume in 30 krad irradiated promastigotes. The relative volume of the kinetoplast does not appear to differ so much. It was evident that flagellar pocket was much dilated in case of promastigote irradiated at 20 and 30 krad radiation doses. Although this damage did not always contribute to cell death but the damages were irrepairable. These findings will be crucial for the outcome of modified infection and probable vaccine development.

Keywords:

Leishmania donovani,
gamma radiation,
irradiated promastigotes,
kinetoplast

Author correspondence:
Dr. Sanjukta Manna
E-mail: sanjukta.manna77@gmail.com
Tel: +91-33-24155928
Post Graduate Department of Zoology, Maulana Azad College, 8 Rafi Ahmed Kidai Road, Kolkata-700013

1. Introduction

A comparative study and comprehensive understanding of the effect of gamma radiation on *Leishmania donovani* promastigotes *in vitro* and *in vivo* at subsequent morphological, biochemical and immunological level is lacking. Visceral leishmaniasis (VL or kala-azar) caused by *Leishmania donovani* is the most dreaded disease and devastating among various forms of leishmaniasis. The disease has gained significance because of high mortality rate particularly amongst the children and poor people. In India high incidence has been reported from the states of Bihar, Assam, West Bengal and Eastern Uttar Pradesh where resistance and relapse are on increase [1]. According to official figures, in 2010 over 28,000 new cases were reported in Nepal, Bangladesh and India [2]. However, this figure is an underestimation of the real number of cases [3] and falls far from the objective set by the regional governments to eliminate VL from the Indian subcontinent by 2020.

Leishmania donovani, an intracellular protozoan parasite causes kala-azar in India. The parasite is transmitted by various species of female sandflies (*Phlebotomus* sp.). It exists in two morphological forms: the promastigotes, residing in the gut of female sandflies, and the amastigote, living in the reticuloendothelial system of the mammalian hosts. The promastigotes possess a full–length, free-flagellum whereas it is rudimentary in amastigotes. Gamma radiation had interesting effects on leishmanial cells allowing both sterilization and immune enhancement, without introduction of new epitopes in the preparation, but parasites

presented unequal radiosensitivity, related to their flagellar disposition and kinetoplast-mitochondrial organization. Although studies on fine structural properties of normal promastigotes and amastigotes and also of some stressed leishmanial cells have been published [4,5,6,7,8], yet structural comparison between normal and irradiated cells have not been analyzed. For that, the study was undertaken to demonstrate the ultrastructural changes, as they occur *in vitro*, produced by gamma radiation exerted upon promastigotes.

2. Research Method

Media and Chemicals

Glutaraldehyde, paraformaldehyde were from Mark, cacodylate buffer, epoxy resin, uranyl acetate and lead citrate, bovine serum (FBS, heat inactivated) were from Difco (Detroit, Michigan); M199, penicillin, streptomycin, and gentamycin were from Gibco Laboratories (Grand Island, New York). All other reagents used were of analytical grade.

Leishmania Stock

Promastigotes of *Leishmania donovani* (MHOM/IN/1983/AG83) were grown at 22^0 C in medium 199 (pH 7.4) supplemented with 10% heat inactivated fetal bovine serum, 2mM L-glutamine, 100U of penicillin G sodium and 100µg of streptomycin sulfate per ml and subcultured in the same medium at an average density of $2x10^6$ cells/ml.

Radiation Exposure

The stationary phase cell culture ($3.7x10^6$cells/ml) was taken for radiation exposure and exposed to a ^{60}Co gamma source for irradiation at 23^0 C using doses in the range of 10, 20, 30, 40 and 50 krad (Gammacell 220) which delivered a radiation dose at the rate of approximately 12 krads/hr at an exposure distance of 50 cm to the 100% radiation area. The dose rate (12 krad/hr) was calibrated with Fricke dosimeter[9]. The irradiated promastigotes were harvested from culture by centrifugation at 1000 x g at 4^0 C and taken for the experiment.

Scanning Electron Microscopic Study of Whole Cell

The technique was followed from standard research methods [10,11]. We use the HITACHI S530 Scanning Electron Microscope to observe the surface structure and the photographs were taken by MAMIYA 6X7 camera using NOVA 120 ASA films.

Transmission Electron Microscopic Study of Whole Cell

The standard protocol was followed [11,12]. The internal structure of *Leishmania donovani* was observed through Philips CM-10 Transmission Electron Microscope at an accelerating voltage of 80 kV with 15,000 to 20,000 magnifications.

Morphometric Analysis

Ultrathin sections (70 nm thick) of promastigote (photographed under 25,000 magnification) were calibrated. The outlines of the whole cell and of the different organelles (nucleus, mitochondrion, pocket flagellum, kinetoplast) were manually contoured using the Leica Quantimed 500IW image analysis program to obtain the area. The volumes of the cell and organelles were obtained by multiplying the total area by the section thickness. The relative volume of each organelle was obtained by dividing the organelle volume by the total cell volume.

3. Results and Analysis

Scanning Electron Microscopic Study

The non-irradiated parasites were spindle-shaped with elongated anteriorly attached distinct flagellum and rough contour. Membrane folds were evident along the same longitudinal axis as the microtubules of the cytoskeleton. In addition, cells contained membrane indentations which resembled pores After exposure to gamma radiation the shape of cells became a more homogeneous mixture of spherical forms as gradually swelling at 10 and 20 krad radiation doses (Figs.1). A reduction in the depth of membrane folds of irradiated parasites paralleled the expansion of cells. At 30, 40 and 50 krad radiation doses, morphological alterations occurred which lead to the formation of amastogote-like organisms (Fig.1). The shortening and almost

complete disappearance of flagellum, as well as a transformation from long, slender, motile cells into nonmotile, ellipsoidal organisms were observed.

Fig. 1: Scanning Electron Micrograph

Normal promastigote

10krad irradiated

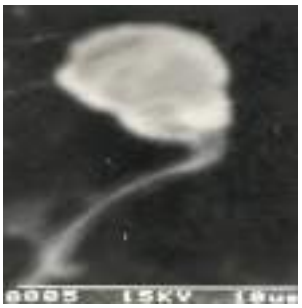

20krad irradiated

30krad irradiated

40krad irradiated

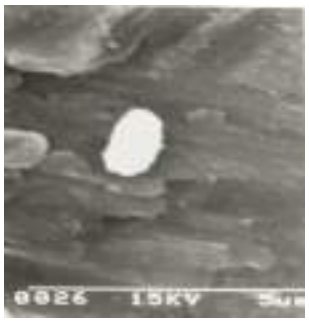

50krad irradiated

Transmission Electron Microscopic Study

A. Non irradiated parasite

The motile cylindrical promastigote was upto 18 µm long with a single flagellum. Flagellum was surrounded by a plasma membrane, arising from a basal body lying close to the kinetoplast was noted at the anterior end of the parasite. The flagellar pocket with desmosome-like plaques was not distended and enclosed the flagellum loosely. The vesicular nucleus was elliptical in shape in cross section. A relatively rod shaped, deeply stained kinetoplast was located at the anterior end of the organism near the point of emergence of the flagellum. The granular cytoplasm with ribosomal particles distributed throughout the cell. Two subcellular organelles, the glycosomes and polyphosphate containing bodies were found. The paraxial rod has the appearance of a cross hatched paracrystalline structure with nine pairs of peripheral axonemal doublets encircling a central pair. The mitochondrion appeared as tubular form. The cytoplasm was granular and homogeneous throughout the cell (Fig .2).

B. Irradiated parasite

10 krad

In this case, mostly the irradiated parasites were somewhat stumpy but virtually all had a conspicuous kinetoplast. Flagella remains attached (Fig.2). Other changes were associated with dilation of the flagellar pocket, enlargement of cytoplasmic bodies (multivesiculate bodies and lipid droplets) and a decrease in ribosomal content of the cells. When parasites were exposed with 10 krad gamma radiation, damage of the cell organelles were not so prominent. Flagellar pocket was usually distended and the distance between kinetoplast and this pocket had been increased. Membrane damage was not so significantly visible and structural organization remain more or less unaltered. The distinct kinetoplast had been found to send off long mitochondrial branches deep into the cytoplasm. Nucleus with distinct nuclear membrane and heterochromatin was also observed.

20 krad

On exposure to 20 krad radiation doses the promastigotes tended to be aflagellate, sausage-shaped and mostly immotile (Fig.2). Mitochondria appeared swollen. The double membrane surrounding the kinetoplast became poorly resolved in these treated cells and increased volume fraction occupied by kinetoplast was also evident. Some parasite displayed short flagella that were most often restricted to the flagellar pocket. The flagellar pocket was distended. The cytoplasm was not so dense as in the normal cell. The cytoplasm contained lipid droplets and frequently large electron dense inclusions. Dilated nucleus and scattered chromatin organization were found.

30 krad

Parasites exposed to 30 krad remain large, stunted and except for the appearance of lipoidal droplets in an occasional parasite there was little further evidence of any significant cell activity other than obvious deterioration. More ovoid forms appeared (Fig. 2). Mitochondria broke into two parts, extended throughout the periphery and appeared as elongated bulbous structure which is. related to autolytic processes. The kinetoplast lost its shape and the DNA material acquired less compact appearance. Small vacuoles were visible in the fine granular cytoplasm. The flagellar pocket as well as desmosome-like plaques disappeared. Disorganization of nucleus, nuclear membrane, dispersion of heterochromatin material was evident.

40 krad

Many have to undergo a kind of abortive development, some parasites reached the stage characterized by an opaqueness of protoplasm and the presence of much lipid inclusions before an extensive vacuolization, shrinkage away from the plasma membrane (Fig 2). The parasite was continued to increase greatly in size. Dyskinetoplastic situation occurred, that is kinetoplast was impaired but still present. Definite nuclear structure disappeared. Significantly, some cells contained megasome-like structure which were identified by their electron density. Parasites displayed large vacuoles which appeared to fuse with each other, as well as with the distended flagellar pocket.

50 krad

The promastigotes rounded up and lost their motility because the flagellum with flagellar pocket had been desolated. The cells were scarcely larger than the normal, while lipoidal granules continued to persist in a deteriorated and patchy protoplasmic mass. The kinetoplast was changed almost beyond recognition (Fig. 2). Numerous large lipid like volutin bodies were evident throughout the cell. The assembly of mitochondria seemed to involve changes linked to the development of membranous whorl formation, as well as the transformation of such structures into lysosomal bodies which eventually could be converted in myelin like figures and undergone autodigestion. Some flattened sacs with rough surfaced membrane filled with unidentified material were also evident. The plasma membrane of many of the parasites exposed at this dose developed a kind of bleb.

Fig.2: Transmission Electron Micrograph

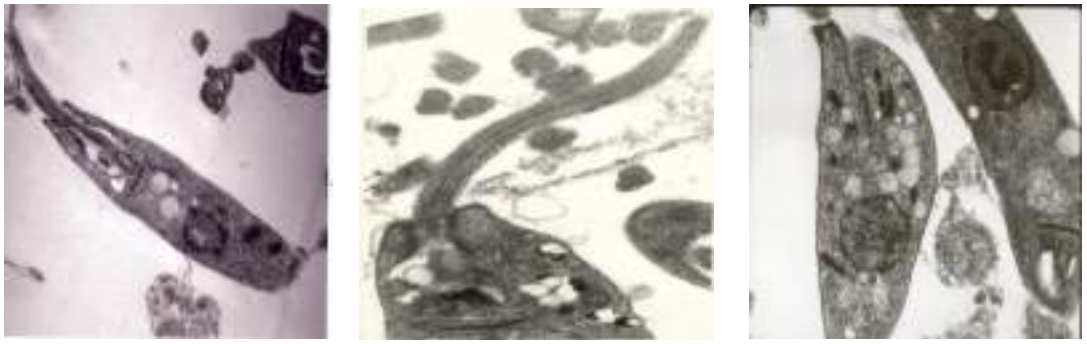

Normal promastigote 10krad irradiated 20krad irradiated

30krad irradiated

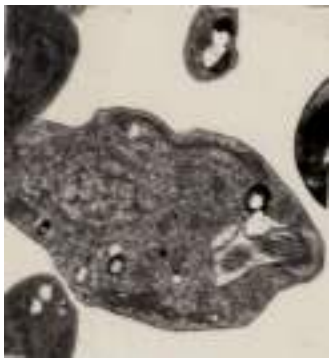

40krad irradiated

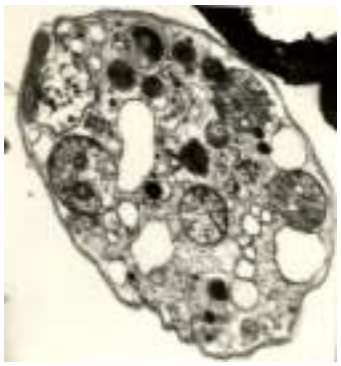

50krad irradiated

Morphometric Analysis

After exposed to gamma radiation at different doses, the normal promastigote transformed to amastigote-like form and there was an increase in the absolute cellular volume from 30.43 μm^3 in the nonirradiated promastigote to 33.23 μm^3 (average) in the irradiated promastigote. The relative volumes occupied by the nucleus were 8.72%, 8.8%, 6.32%, 10.5%, 9.5% and 3.8% in nonirradiated and irradiated promastigotes at 10, 20, 30, 40, 50 krad radiation doses respectively (Table 1). Nucleus showed a larger relative volume in 30 krad irradiated promastigotes. The relative volumes of kinetoplast were 3.13%, 3.8%, 3.8%, 4.23%, 2.02%, 1.02% in nonirradiated and irradiated promastigotes at 10, 20, 30, 40, 50 krad radiation doses respectively. In contrast, the relative volume of the kinetoplast does not appear to differ so much. Most other organelles, including flagellar pocket, mitochondria to varying degrees, showed not much larger relative volume in irradiated promastigotes when compared to nonirradiated promastigotes. The relative volumes of flagellar pocket occupied were 5%, 6.5%, 7.92%, 8.1%, 5.37% and 1.7% in normal and irradiated promastigote at 10, 20, 30, 40 and 50 krad radiation doses respectively. It was evident that flagellar pocket was much dilated in case of promastigote irradiated at 20 and 30 krad radiation doses.

Table 1 : Morphometric Analysis (Relative volume percentages)

Radiation doses	Nucleus	Kinetoplast	Mitochondria	Flagellar pocket
Non irradiated	8.72 ± 1.98	3.13 ± 0.5	7.09 ± 0.5	5 ± 0.25
10 krad	8.8 ± 0.11	3.8 ± 1.1	6.85 ± 0.3	6.5 ± 0.3
20 krad	6.32 ± 0.13	3.8 ± 0.5	5.75 ± 1	7.92 ± 0.5
30 krad	10.5 ± 1.5	4.23 ± 1.2	5.06 ± 0.4	8.1 ± 0.9
40 krad	9.543±0.89	2.02 ± 0.5	5.2 ± 0.1	5.37 ± 1.1
50 krad	3.81 ± 0.85	1.02 ± 0.2	5.73 ± 1.2	1.7 ± 1.1

4. Conclusion

Axenic, amastigote-like cells are advantageous in that they can be used as an in vitro model to study parasite development that occurs *in vivo*.

The ultrastructure of nonirradiated *L. donovani* in the present study is similar with the earlier observations [13,14]. It included several features such as trilaminate cell membrane, pellicular microtubules, structure of the flagellum with 9+2 arrangement of axoneme, desmosome, kinetoplast in a dilation of the mitochondrial tube. The reduction in the depth of membrane folds paralleled with the formation of amastigote-like form was evident from the scanning electron micrograph. In irradiated promastigote, membrane became more pronounced as cells shriveled along the longitudinal axis of their microtubule cytoskeleton. Since normal promastigotes are motile due to the active motion of a long flagellum, the paraxial rod along the axoneme may be important for the vigorous flagellar motility of the organisms which are in agreement with the observation of Pan and Pan (1986). The desmosome-like plaques acted as a sphincter for closing off the

flagellar pocket [15]. Their formation was believed to maintain the integrity of the flagellum and parasite body as a motile unit.

Higher radiation doses caused condensation of the *L. donovani* and morphologic changes such as shrinkage of cytoplasm, dispersion of nuclear and kinetoplast material into an amorphous mass, ballooning of the membrane, loss of flagellum, aggregation, vacuolation and progressive loss of motility leading to eventual death and degradation. These changes were observed in a large percentage of the parasites and appeared earlier when high doses (30-50 krad) were applied. Above this dose, the paraxial rod of flagellum had been destroyed and the organisms remained static. The physiological regeneration with the condensation of the nucleus and reorganization of some of the organelles was induced by 20 krad doses and these irradiated promastigotes regenerated seemingly at the same rate as nonirradiated. In the groups exposed above 30-50 krad particularly the changes occurred with nearly explosive rapidity and produce an almost endless variety of morphological effects such that it was virtually impossible to find any consistent pattern or sequence to the changes which occurred. Mitochondria broke into two parts which was related to autolytic processes [16]. Numerous small vacuoles were distributed at random throughout the cell, flagella detached and desmosome-like plaques disappeared. The promostigotes irradiated at 30 krad, resembled true amastigotes in morphology and ultrastructure. The dyskinetoplastic situation occurred above 40 krad radiation doses. It had been postulated that kinetoplast was a self dependent DNA containing orgenelle, found in flagellates of the families Trypanosomatidae, was responsible in the morphogenesis of mitochondria and essential for the transformation occurring from one stage to another in the complex life cycles of these parasites[17]. Support for the latter statement comes from the present study that dyskinetoplastic *Leishmania donovani*, though able to live, cannot be propagated *in vitro*. It is obvious, therefore, that above 40 krad radiation doses practically all the developmental processes of the parasite had been effectively arrested. Above 40 krad irradiated parasite the cytoplasm became altered (as shown in electron micrograph), then visibly vacuolated and finally became myelinated. As the myelination occurred the entire cell disintegrated. Doses much less than those immediately lethal stopped cell division or retarded it and caused loss of kinetoplast. It was evident that much lower doses were needed to suppress division (to transform or kill ultimately) than for immediate death. The results were consistent with the observation on sporogenous cycle of *Plasmodium gallinaceum* [18].Terzian demonstrated that parasites exposed to 5, 10, 20 and 30 krad showed the characteristic vacuole formation. The surface membrane of parasites exposed to 30 krad developed a kind of bleb and remained stunted. Parasites exposed above 20 krad never reached maturity and characteristic lipoidal droplets appreared in large numbers. Some observer observed the agglutination of trypanosomes exposed to gamma radiation and morphologic changes such as shrinkage of cytoplasm, condensation of nuclear and kinetoplast material into an amrophous mass, ballooning of the membrane and loss of flagellum [19].

After exposed to gamma radiation, the absolute cellular volume of normal promastigotes increased from 30.43 μm^3 to 33.23 μm^3 in the irradiated promastigotes. It was evident in the present study, that the volume percentage of flagellar pocket of 30 krad irradiated promastigote occupied was increased in comparison to other radiation doses. Therefore, the flagellar distension was proved with respective higher radiation doses. Similar previous observation is lacking. From this experiment it was successful to bring the radio attenuated condition of *Leishmania donovani* which could be developed into vaccine candidates and useful as immunological markers of protection in both animal models and humans and to draw up a general framework for development of live attenuated *Leishmania* vaccines. This study would give some valuable information of attenuation dose at 10-20 krad which can be utilised in future study as a vaccine tool.

References

[1] Dube, A., Singh, N., Sundar, S, and Singh, N., "Refractoriness to the treatment of sodium stibogluconate in Indian kala-azar field isolates persist in in vitro and in vivo experimental models", *Parasitology Research*, vol 96(4) pp.216–223, 2005.

[2] Picado, A., Dash, A.P., Bhattacharya, S. and Boelaert, M., "Vector control interventions for visceral leishmaniasis elimination initiative in South Asia 2005–2010", *Indian Journal Medical Research* vol. 136 pp. 22–31, 2012.

[3] Singh, S.P., Reddy, D.C.S., Rai, M., Sundar, S., "Serious underreporting of visceral leishmaniasis through passive case reporting in Bihar, India", *Tropical Medical International Health*, vol 11pp. 899–905, 2006.

[4] Chang, K.P., "*Leishmania donovani*: promastigote-macrophage surface interactions *in vitro", Experimental Parasitology*, vol.48 pp. 175-189, 1979.

[5] Alexander, J. and Vickerman, K. "Fusion of host cell secondary lysosomes with the parasitophorous vacuoles of *Leishmania mexicana* infected macrophages", *Journal of Protozoology*, vol. 22, pp. 502-508, 1975.

[6] Datta, S., Adak, R. Chakraborty,P.,Haldar, A. K., Bhattacharjee, S., Chakraborty, A., Roy, S. and Manna, M., "Radio-attenuated leishmanial parasites as immunoprophylactic agent against experimental murine visceral leishmaniasis", *Experimental Parasitology*, vol 130, Issue 1,pp. 39-47, January 2012.

[7] Chaoqun, Y., Upasna, G. D., Jason, H., Lynn, M. T., Laurie, L.H., John, E. D. and Mary, E. W., "Attenuation of *Leishmania infantum chagasi* Metacyclic Promastigotes by Sterol Depletion", *Infection and Immunity*, vol. 81 no. 7 pp.2507-2517 July 2013.

[8] Banerjee,A., Bhattacharya, P., Dagur, P. K., Karmakar, S., Ismail, N., Joshi, A. B.,. Akue, A. D., KuKuruga M., Philip J.M. Jr., Dey R. and. Nakhasi, H.L., "Live Attenuated *Leishmania donovani* Centrin Gene–Deleted Parasites Induce IL-23–Dependent IL-17–Protective Immune Response against Visceral Leishmaniasis in a Murine Model", *Journal of Immunology*, vol 200 (1) pp.163-176, January 2018.

[9] Spinks, J.W.T. and Woods, R.J. An introduction to radiation chemistry. 2nd Ed., Wiley, N.Y., pp. 43-45, 1976.

[10] Colley, C., Fedrick, J.L.K., Zaman, V., Canning, C.V.,"Light and Electron microscopic study of *Nosema eurytremae", Journal of. Invertebrate. Pathology*, vol 26 ,pp 11-20. 1975.

[11] De Souza, W., Sant'Anna, C., and Cunha-e-Silva, N.L., "Electron microscopy and cytochemistry analysis of the endocytic pathway of pathogenic protozoa". *Progress in Histochemica and Cytochemica*, vol 44pp 67–124, 2009.

[12] Benchimol, B, Piva, B, Campanati, L, and De Souza, W., "Visualization of the funis of *Giardia lamblia* by high-resolution field emission scanning electron microscopy — new insights". *Journal of Structural Biology*, 147: 102–115,2004.

[13] Killick-Kendrick, R. and Molyneux, D.H.. "Transmission of Leishmaniasis by the bite of phlebotomine sandflies :possible mechanisms". *Transaction of Royal Society,*vol 75pp. 152-154, 1981.

[14] Pan, A.A. and Pan, S.C, "*Leishmania mexicana* comparative fine structure of amastigotes and promastigotes *in vitro* and *in vivo", Experimental. Parasitology,* vol 62 pp. 254-265, 1986.

[15]]Molyneux, D.H., Killick-Kendrick, R. and Ashford, R.W., "*Leishmania* in phlebotomid sandflies. III. The ultrastructure of *Leishmania mexicana amazonensis* in the midgut and pharynx of *Lutzomyia longipalpis." Proceedings of Royal Society London*, B190 ,pp. 341-357, 1975.

[16] Gardener, P.J., Shchory, L. and Chance, M.L., "Species differentiation in the genus *Leishmania* by morphometric studies with the electron microscope", *Annals of Tropical and Medical Parasitology,* vol 71 pp. 147-155, 1977.

[17] Rudzinska, M.A., D'Alesandro, P.S. and Trager, W., "The fine structure of *Leishmania donovani* and the role of the kinetoplast in the *Leishmania*-leptomonad transformation." *Journal of Protozoology,*vol 11 pp. 166-191,1964.

[18] Terzian, L.A.,. "Morphological changes produced by gamma radiation on the sporogenous cycle of *Plasmodium gallinaceum*." *Experimental. Parasitology,.*vol 11, pp 102-110, 1961.

[19] Martinez-Silva, R., Lopez, V.A., Colon, J.I. and Chiriboga, J. , "*Trypanosoma cruzi* : effects of gamma radiation on growth and infectivity", *Experimental Parasitology,*vol 25 pp. 162-170, 1969.

ISSN 0970-4450

PRANIKEE

Journal of Zoological Society of Orissa

Volume- XXX
2018

ISSN 0970-4450

PRANIKEE

Journal of Zoological Society of Orissa

Post Graduate Department of Zoology
Utkal University, Vani Vihar
Bhubaneswar - 751 004, Odisha, India

Volume XXX, 2018

Pranikee - Journal of Zoological Society of Orissa, ISSN 0970-4450
Volume XXX, 2018, pp 15-28

MODULATORY EFFECTS OF INDOLYL QUINOLINE ON FUNCTIONAL FERTILITY OF MALE RATS (*RATTUS RATTUS)*

SK Bhowal[1] and CR Sahu [2*]

[1] Post Graduate Department of Zoology, Maulana Azad College, Kolkata- 700013, India.
[2]Department of Zoology, University of Kalyani, WB – 741235, India.

*Corresponding Author
E mail: crsahu344@gmail.com

ABSTRACT

Functional fertility of indolyl quinoline 2-(2″-chloroacetamidobenzyl)-3-(3′-indolyl quinoline) was evaluated in male rats (*Rattus rattus*) treated by oral gavages for 12 weeks followed by mating exposures to proven proestrus females. Fertility rate, percentage of pregnancy and some biochemical parameters were assessed in the model. Further, male steroid hormone testosterone and serum gonadotropin (FSH and LH) levels were also evaluated to test the efficacy of the compound. Routine histological analysis of epididymis and testis were considered to examine any discrepancy arises out of the effect of the compound. Functional fertility in treated animals was decreased significantly as was evidenced by reduction in the fertility and pregnancy rates in the female rats which were mated with treated male rats. Level of testosterone hormone, protein, glycogen content as well as epididymal glycerophosphorylcholin (GPC) decreased whereas concentration of LH and FSH, alkaline phosphatase and cholesterol increased significantly. Histological examination revealed depletion in the number of different germinal cells, disruptions both in epididymal and testicular architecture as well as scanty spermatozoa. The results were discussed in the light of severity of the histological and biochemical responses made by the compound. The significant results revealed from the study indicate infertility activity of the said chemical agent on male rats.

Keywords: Male rat, indolyl quinoline, male reproductive rgans, infertility, gonadotropin, biochemical parameters, histological analysis, glycerophosphorylcholin.

Abbreviations: GnRH: Gonadotropic-Releasing Hormone; SRL: Sisco Research Laboratory; mL: milli litre; ANOVA: Analysis of Variance; NS: Not Significant; GPC: Glycerophosphorylcholine

INTRODUCTION

To fight the grave situation of population explosion in countries like India, effective family planning is need of the hour. A significant step towards this is the fertility management by means of contraception (Allag and Rangari, 2002). Though some extremely successful contraceptive modalities have been developed for females, yet no or very modest effective method of systemic contraception has been worked out for males till now. An array of synthetic chemicals and plant derived compounds in addition to the infertility inducing methods of hormonal, chemical and immunological approach have been explored for a long time (Gottwald et al., 2006, Kopf, 2008, Etribi et al., 1982, Vannucchi et al., 2015). Use of hormonal steroids or gonadotropic-releasing hormone (GnRh) agonists/ antagonists causing acute oligospermia or azoospermia is under investigation (Paulsen et al., 1994, Edwards et al., 2013). But these methods affect either secondary sex characters in male or are not cost effective. On the other hand a

number of nitrogen heterocyclic compounds derived from indole have been explored for their anti flagellated activities. Imidazole, carbazole, indazole, ornidazole are examples of such compounds. They also demonstrated anti proliferative as well as antispermatogenic activity or *vice versa* (Grima et al., 2001). The imidazole group of compounds which are clinically used in treatment against flagellated protozoa and anaerobic bacteria for genital tract infections of both men and women have also been experimentally demonstrated to possess potential antifertility activity in male rat (Lohiya et al., 2005, Gupta et al., 2011). Meanwhile, antispermatogenic and antisteriodogenic properties of some traditionally used contraceptive agents have also been reported (Corsi et al., 1976, Silvestrini et al., 1984). Other allied compounds have been reported as anti-spermatogenic (Dhanapal et al., 2012, Mishra and Singh, 2009, Singla et al., 2013). So exploring effective anti-spermatogenic agents that could rely on alternative methods to the hypothalamo-pituitary gonadal axis may appear to become effective in the development of male systemic contraceptive. The compound 2-(2″-chloroacetamidobenzyl) - 3-(3′-indolyl) quinoline or indolyl quinoline contains indole, and quinoline moieties that match with all of the mentioned compounds structurally and functionally (Cooper et al., 1997, Grima et al., 2001, Bone et al., 2000, Chakrabarty et al., 1999). The above information was the main thrust behind this effort of evaluating modulatory effects of the compound on the functional fertility in male rats.

MATERIALS AND METHODS

Chemicals:

Analytical grade chemicals and reagents were purchased from Merck India Ltd. Staining reagents were from SRL India Ltd., Mumbai, India. The tested chemical compound has been synthesised through the application of Friedel-Crafts reaction (Mahato et al., 1994). The purity of the compound was verified and the bioactivity was determined (Bhowal et al., 2008).

Animals:

All experiments on laboratory animals were performed as per the guidelines of the animal ethics committee of the University. Rats (*Rattus rattus*) from random bred colonies were housed on a fourteen hours light and ten hours dark cycle under standard husbandry conditions (temp. 22^0 C ± 2^0 C, relative humidity 55 % ± 5%) and were provided standard pellet food and sterile water *ad libitum.*

Design of experiment, mating and fertility tests

Eight different groups consisting of 5 animals in each group were allocated from a population of 80 male rats, where 50% of the total was considered as control without any treatment. The test material was orally gavaged to different groups of rats for 2, 4, 8 and 12 weeks at a dose of 250 mg / kg of body weight (5g/kg per day did not cause lethality, (unpublished observation). Mating schedules were designed to examine the infertility effect by the compound accurately as well as monitoring their health and weight throughout the experimental period. The males were kept in a cage with the cyclic females (at pro estrous stage) as 1:1 ratio to observe any copulation plug or the presence of spermatozoa in the vaginal smear on the next morning and in successful mating it was considered as Day -1 of pregnancy. Accordingly, the percentage of successful mating was considered with the number of sperm positive females per

number of exposed female. The so called successful mating females were separated on next morning while food and water was given *ad libitum.*

On day 10 of gestation, laparotomy of female rats was performed under ether anesthesia (through inhalation) and their ovaries were excised, uteri were exposed including counting of corpora lutea, implantation sites and number of normal live fetuses was done. Fertility rates were calculated by the percentage of implantation sites per number corpora lutea (representing the number of eggs ovulated) and pregnancy rate was considered to be the number of viable fetuses per female mated.

Histology of testis and epididymis

The tunica albugenia of one of the two testes was nicked at both the ends after immersing in Bouin's fixative for 12 hours and continued the fixation process for another 12 hours. Epididymides of five rats per group were fixed in Bouin's fixative. Tissues were dehydrated in ethanol following several changes in upgrades of alcohol, thereafter, embedded in paraffin for section cuttings (6-µm thick) and microscopic studies. The tissue slides were processed for staining through eosin-hematoxylin and finally photomicrographs were taken.

Estimation of Testosterone hormone

Testosterone was quantitated by Radio Immuno Assay (RIA) using the commercial Coat-A-Count total testosterone RIA kit. There was 3.3% cross-reactivity of the anti-sera with dihydrotestosterone. The sensitivity of the assay was found to be 4 ng/dl (0.14 nmol/L) and that of intra-assay coefficient of variation was 4.85%. The study samples were assayed in duplicate.

Estimation of FSH and LH

Concentrations of serum FSH and LH were estimated by RIA with the help of second antibody precipitation. Carrier-free I125 was used for iodination of hormone. Pure rat FSH (NIDDK-FSH-1-9) and LH (NIDDK-rLH-1-9) has been iodinated using chloramine- T (Greenwood et al., 1963). NIDDK-anti-rFSH-S-11 and anti-rLH-S-11 anti-sera were used at a final tube dilution of 1:125,000, 1:750,000 and 1:437,500 or greater, respectively. The sensitivities of the assays have been found to be 1 ng/ml for FSH and 0.75 ng/ml for LH. The intra-assay coefficients of variation for all assays were <10%. Hormone concentrations were expressed in terms of NIDDK reference preparations, RP-2 in the case of rFSH and RP-3 in the case of rLH.

Biochemical profiles

For estimation of protein, testicular tissue (100 mg/test) was homogenized in 2ml ice cold 0.02 mol/L Tris-HCl buffer (pH 7.8), centrifuged at 800×g for 10 min at 4°C. Protein concentration was estimated from the precipitate which was collected at 4°C from the supernatant with 2 ml of 10% (w/v) trichloro acetic acid. The precipitate was dried, dissolved in 1 N NaOH solution and was estimated spectrophotometrically at 660 nm (Lowry et al., 1951).

Homogenized testicular tissue in 2 mL of ice cold 0.02 mol/L Tris-HCl buffer (pH 9.0) was used for estimation of alkaline phosphatase concentration. The homogenate was centrifuged at 800×g for 10 min at 4°C. The supernatant was taken for estimation at 420 nm spectrophotometrically by paranitrophenol phosphate method (Chakraborty and Lala, 1998).

Cholesterol was extracted from testicular tissue (100 mg) homogenizing in 2 ml of glacial acetic acid; after centrifugation the supernatant fraction was taken for cholesterol estimation spectrophotometrically at 626 nm by the ferric chloride method (Chakraborty and Lala, 1998).

Glycogen was extracted from 100 mg of testicular tissue dissolved in 30% (w/v) potassium hydroxide solution in a boiling water bath. The solution was then cooled, glycogen precipitated with 2 volumes of ethanol, centrifuged, washed with ethanol and finally dried on a water bath. The precipitate was dissolved in 1 mL distilled water. The resultant solution was filtered through glass wool to remove extraneous polysaccharides. From this solution, glycogen was estimated spectrophotometrically at 490 nm using 80% (v/v) phenol and concentrated sulphuric acid (Chakraborty and Lala, 1998).

Glycerophosphorylcholine (GPC) was estimated from epididymis. One of the two epididymis was quickly placed in icecoldnormal saline 0.9% (w/v) and was used for extraction of GPC. Spermatozoa were taken out through puncture of the tubules with a needle and the epididymis was then chopped with a fine scissors and finally mixed in 2 ml normal saline, centrifuged at 550×g for 10 min at 4ºC. The supernatant was oxidized to formaldehyde by periodate. The formaldehyde was quantitatively converted to a purple colour compound by adding chromotropic acid and then measured spectrophotometrically at 580 nm (Chakraborty and Lala, 1998).

Statistical analysis

Results were expressed as mean ± standard deviation of mean of five repeated determination for 5 rats in each of the 4 groups of rats. The significance of difference in the mean data obtained were analysed and were compared using one-factor ANOVA. Values were considered significant when $P<0.05$ or less.

RESULTS

Effects on fertility status of the rats

The fertility status of the female rats mated with a normal male rat not underwent any treatment showed a normal implantation site (Fig.1 A). A significant reduction related to time of exposure in functional fertility as indicated by rate of pregnancy was noticed due to the introduction of the compound. The female rats mated with the compound treated male rats during treatment period showed a decreased numbers of implantation sites from 5.20 to 0.0 (Figs.1 B, C) whereas the females mated with control males showed average number of implantation site from 13.6 to 14.0 (Fig.1A). While the pregnancy rate for the control varied from 2.72 to 2.80 (Table 1) during the experiment period, the treated group of rats showed a value ranges between 1.04 and 0.0 in 12 weeks treatment period. Thus, pregnancy rate of treated female animals showed decreased value compared to control group animals (Figs. 4 A, B). However, there is a very little change in percentage of mating.

Effects on testicular histology

The section of the testis of control rats showed seminiferous tubules of variable size with spermatocytes in the lumen at different stages of maturation (Fig. 2 A). The cellular interstitial connective tissue was prominent. A few blood vessels were also visible in the interstitial region. In contrast to the control the section of the testis of compound treated male rats demonstrate a structural disorganization of the seminiferous tubules along with loss in number of differentiating germinal cells in 8 weeks of treatment (Fig. 2B). In addition to, hyperpycnotic nuclei in many cells and vacuolated cytoplasm were prominent features encountered in the treated section of the testis during 8 and 12 week. The tubules were found to be devoid of spermatozoa. However, no anomalies in the morphology of sperm were noticed.

Effects on epididymal histology

The epididymis in the section of the control groups revealed a lumen with normal cellular structure containing basal cells. The lumen also contains mature sperm cells (Fig. 3A). The treatment with the compound after 3 weeks revealed slightly smaller tubular diameters along with thicker tubular epithelium. Few spermatozoa were observed in treated animals compared to the controls. The degree of effects was very pronounced during 8 to 12 weeks (Fig. 3B).

Effects on hormonal profile

The effects of administration of the compound to male rats on the concentrations of reproductive hormone levels are shown in Fig 5. Serum FSH and LH increased significantly during the experimental period. On the other hand testosterone level declined significantly and the percentage of reduction is shown in Table 2 and Fig.5. Percentage of increase in FSH and LH concentration is also demonstrated in Table 2 and Fig. 5.

Effects on biochemical profile

The effects of treatment with the compound on the testicular and epididymal biochemistry of male rats are shown in Table 2. On treatment with the compound testicular cholesterol levels increased significantly (Fig. 7). There was decline in total protein concentration and increase in concentration of testicular alkaline phosphatase (Fig. 6). On the other hand reduction in testicular glycogen and epididymal GPC levels (Fig. 7) was observed. Percentages of change in other biochemical parameters of protein concentration and concentration of testicular alkaline phosphatase are given in Fig. 6 where as percentages of change in other biochemical parameters such as testicular cholesterol, glycogen and epididymal GPC concentration are given in Fig. 7.

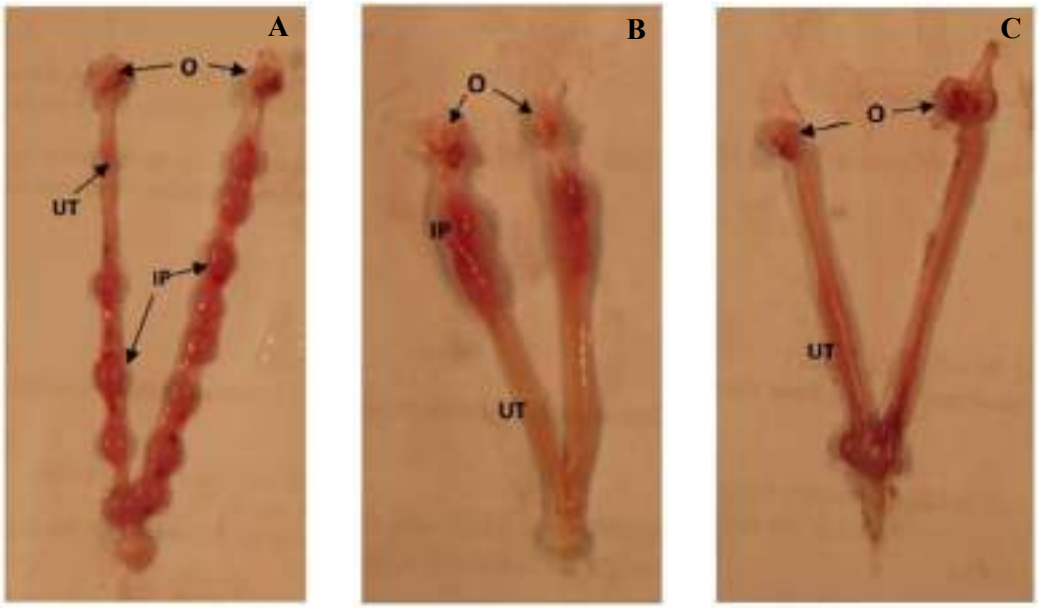

Fig. 1 (A) Normal implantation site in a normal female mated with normal male rat, (B) More reduction of implant site in a normal female mated with 4 weeks Indolyl quinoline treated male rat, (C) Few of implant sites in a normal female mated with 12 weeks indolyl Quinoline treated male rat. (IP: implantation site, O: ovary, UT: uterine tube)

Table 1 Percentage of pregnancy, number of implantation site, number of corpus luteum, fertility rate and pregnancy rate of female rats mated with male treated with indolyl quinoline at a dose of 250 mg / kg per day for 2, 4, 8 and 12 weeks.

Parameters	Experimental Groups	Treatment period			
		2 weeks	4 weeks	8 weeks	12 weeks
Percentage (%) of mating	Control	100	100	100	100
	Treated	100	75	75	75
No. of implantation sites (IP)	Control	13.6 ± 1.18	11.6 ±1.14	13.6 ±1.94	14.0 ± 1.58
	Treated	5.20 ±0.83	2.60 ±0.54	0.80 ±0.83	0.00±0.00
No. of corpus luteum (CL)	Control	13.9 ± 1.02	13.2 ± 0.90	14.5±1.23	15.3±1.24
	Treated	13.2 ± 1.03	12.2 ± 1.15	11.4±0.81	10.6±0.72*
Fertility rate	Control	97.84± 5.33	87.87± 6.17	93.79± 5.27	91.50± 8.02
	Treated	39.39± 2.01	21.31± 1.88	7.01± 0.24*	0
Pregnancy rate	Control	2.72± 0.16	2.64± 0.25	2.72± 0.19	2.80± 0.12
	Treated	1.04± 0.05*	0.65± 0.03	0.20± 0.01	0

Each value is expressed as the mean ± SD (n = 5 per group). Results were statistically analyzed with one-way ANOVA and compared with the control group. *P < 0.01 or 0.05; @ at P < 0.001, NS = Not significant.

Table 2 Hormonal and Biochemical profile expressed as percentage value of increase or decrease after treatment with indolyl quinoline for 2, 4, 8, 12 weeks.

Hormonal and Biochemical Parameters	Treatment period			
	2 weeks	4 weeks	8 weeks	12 weeks
Testicular testosterone	Percentage (%) of reduction control vs treated			
	41.27	43.06	46.51	43.57
Serum FSH	Percentage (%) of increase control vs treated			
	26.53	28.42	29.77	27.36
Serum LH	Percentage (%) of increase control vs treated			
	22.12	18.75	17.85	20.53
Testicular protein	Percentage (%) of reduction control vs treated			
	27.02	32.42	38.85	37.73
Alkaline phosphatase	Percentage (%) of increase control vs treated			
	67.10	58.82	57.50	55.73
Cholesterol	Percentage (%) of increase control vs treated			
	13.43	28.67	31.43	31.68
Glycogen	Percentage (%) of reduction control vs treated			
	48.42	43.13	43.21	38.36
Epididymal GPC	Percentage (%) of reduction control vs treated			
	52.94	34.90	33.38	33.33

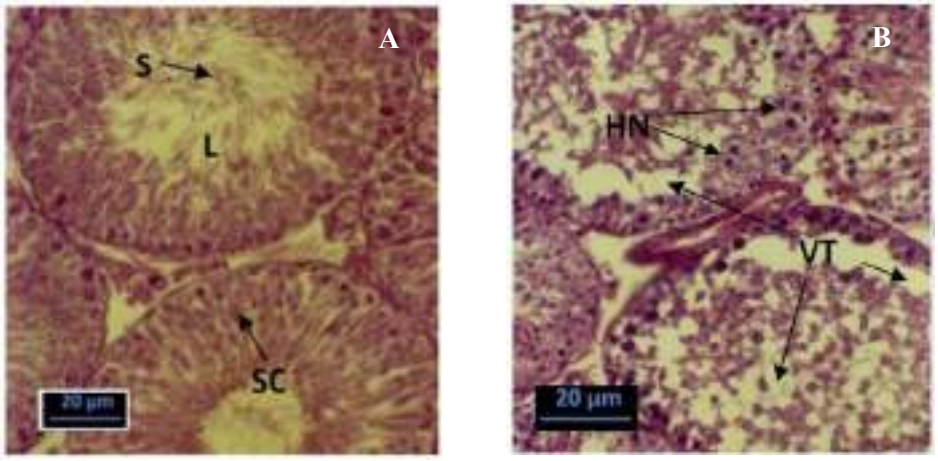

Fig. 2 (A) T. S. of the testis of normal rat showing normal architecture of the seminiferous tubules with differentiating spermatogenic cells. (B) T.S. of testis of 8 weeks indolyl quinoline treated male rat showing loss of differentiating germ cells. (HN: hyperpycnotic nuclei, L: lumen of seminiferous tubule, S: spermatozoa, SC: Sartoli cell, VT: vacuolated tubule)

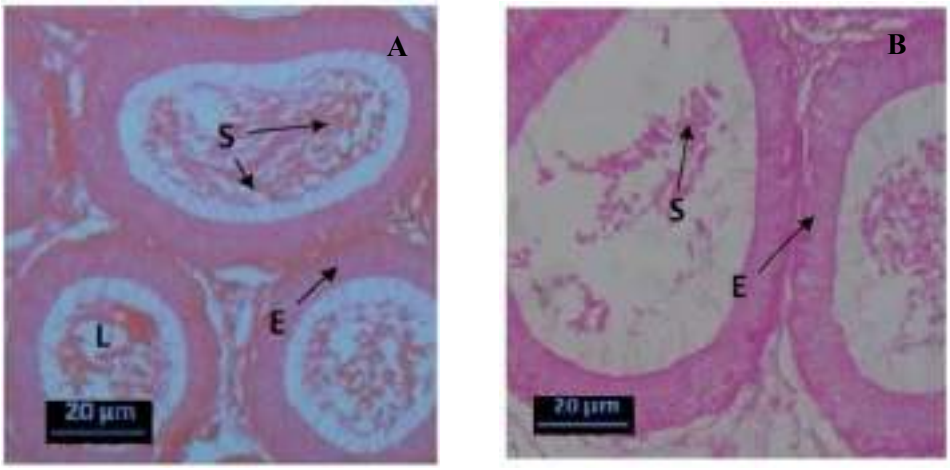

Fig. 3 (A) T.S. of epididymis of control rat showing normal architecture of tubules and spermatozoa. (B) T.S. of epididymis of 6 weeks indolyl quinoline treated male rat showing thicker epithelium. Note less number of spermatozoa. (E: epithelium, L: lumen of epididymis S: spermatozoa)

.

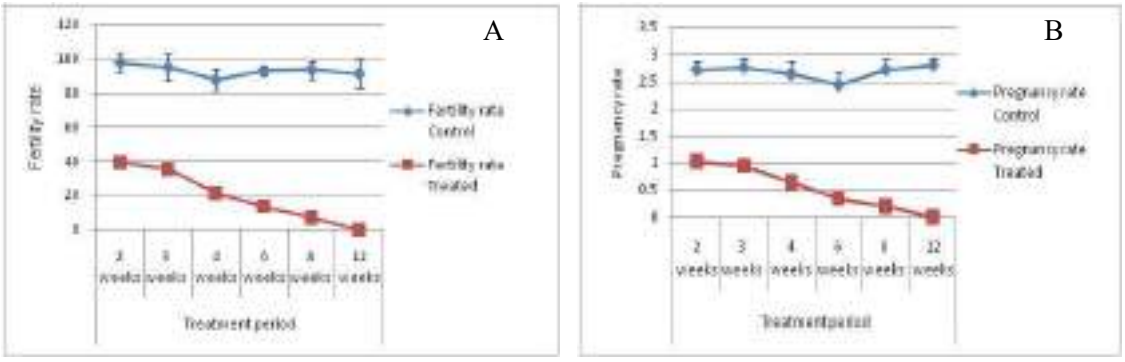

Fig 4 Fertility (A) and pregnancy rate (B) of control and treated animals administered with indolyl quinoline during the experiment period at a dose of 250 mg/kg in male rats.

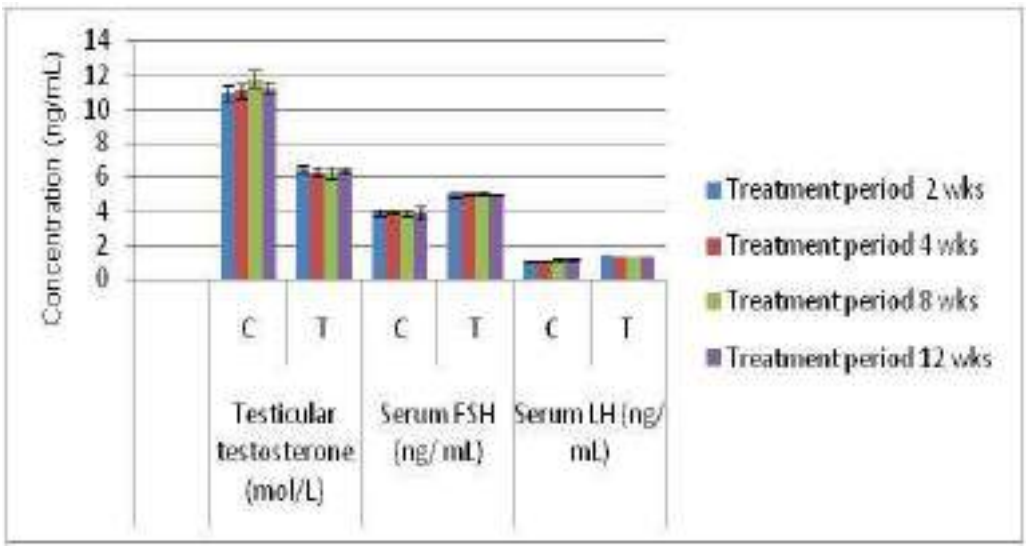

Fig 5 Testosterone, FSH and LH hormone profiles of control (C) and 2, 4, 8, 12 weeks indolyl quinolone treated (T) male rats.

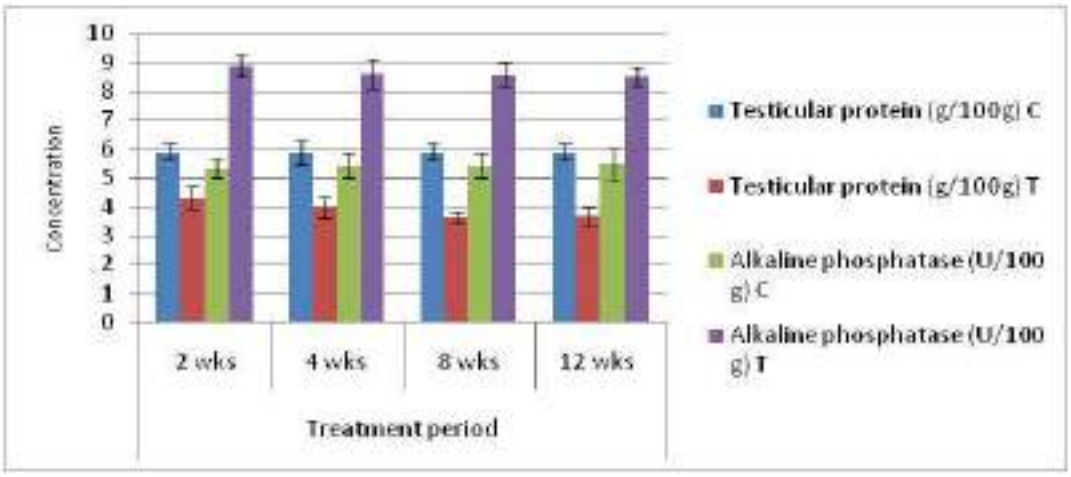

Fig 6 Biochemical profiles of protein and alkaline phosphatase that show % of reduction in treated (T) animals compared to control (C) after indolyl quinoline treatment for 2, 4, 8 and 12 weeks at a dose of 250 mg / kg in male rats.

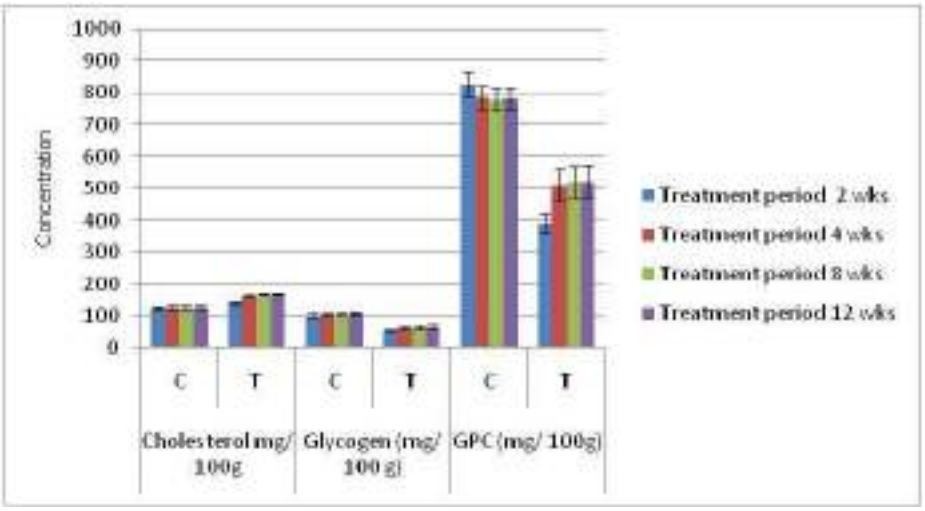

Fig 7 Biochemical profiles of cholesterol, glycogen and GPC that show % increase in treated (T) animals compared to control (C) after indolyl quinoline treatment for 2, 4, 8 and 12 weeks at a dose of 250 mg / kg in male rats.

DISCUSSION

Spermatogenesis is a process of both mitotic and meiotic divisions where spermatogonia divide to produce spermatocytes and subsequently haploid spermatids. Further, the spermatids undergo a notable change during their development through a process of spermiogenesis where the round shaped structure of the spermatids turned into elongating spermatids that transform into spermatozoa through certain steps. The whole process occurs into the seminiferous tubular lumen. The compound of interest studied here is capable of inducing harm to seminiferous epithelium of rat and thus changing the process of spermatogenesis along with other reproductive parts in question causing infertility.

Functional infertility was induced in male rats by the compound through exposed time period as substantiated by reduced fertility and the rate of pregnancy. To examine the compound to have an effect on which phase of spermatogenic process, epididymal maturation and or testicular events of spermatogenesis, a periodical mating schedule followed by sacrifice of the male rats has been planned. It is known that for maturation of spermatozoa the epididymis plays a very crucial role and a cascade of reactions take place in epididymal fluid during transportation of the sperm through the convoluted ductus system of the epididymis. The fertilizing ability of the sperm (Robaire and Viger, 1995, Dacheux et al., 2003, Gatti et al., 2004, Turner et al, 1995, Metayer et al., 2002, Blobel, 2000) is ensured by the factors derived from the epididymal fluid that rearrange and reorganize lipids and proteins in the spermatozoal membrane (Yanagimachi, 1994) Decline in GPC level, an indicator of epididymal function (Setchel et al., 1994), morphological changes in epididymis and sperm count indicate that epididymal dysfunction could be one of the causes of infertility induced by the compound during treatment period. Moreover, no distinct morphological change in the shape and structure of the epididymal sperms as seen under light

microscope indicates that the tested compound does not cause antifertility through morphological disruption of sperms.

Contrary to this, no significant change is observed in the mating rates between the control and treated rats, suggesting no harmful effects of the tested compound on the copulating potential of the rats. It has further been studied that the inhibition of spermatogenesis by the compound is attributed to the elevated levels of gonadotrophins. The events of spermatogenesis are mainly regulated by testosterone and the role of gonadotrophin also could not be ruled out (Clearmont and Hervay, 1965, Meitrich et al., 1994, McLachlan et al., 1994 a, b, O'Donnel et al., 1996, McLachlan et al., 1996).

The possible cause of induction of infertility by the tested compound might be a reduction in the level of testosterone, though the other possibilities may not be ruled out. The beginning and continuation of spermatogenesis in pre-pubertal and pubertal rats is LH and FSH dependant. Negative feedback regulation of FSH, LH and sex hormone to this process has also been studied extensively (Everett, 1994) and it has been shown that high level of FSH and LH are detrimental as sub- normal level (Kerr and Sharpe, 1989, Sharpe, 1994). Histological assessment in the present study is a useful parameter that offers a sensitive indicator of damage to the epididymis and the testis cells. The treatment made thereof through different weeks also provides information on the marked cells and degree of toxicity. FSH acts as a mitotic factor for Sertoli cells (Sharpe, 1994). Further, cooperation of testosterone and FSH brings about the binding of spermatids with the Sertoli cells. This is an indispensible step in the process of spermiogenesis (Muffy et al., 1993). Sertoli cells do not divide in adult under normal conditions. But it has also been shown that the terminally differentiated Sertoli cells can re-start mitotic cycle even after attaining maturity (Chaudhury et al., 2005). Thus it can be clearly stated that the compound imposed some change in the overall reproductive physiology that could lead to the inhibition of spermatogenesis. Therefore, the action of the test compound on the spermatozoa pursuing epididymal maturation suggests a condition of functional infertility during the treatment period.

ACKNOWLEDGEMENT

Our thanks goes to the Principal, Maulana Azad College, Kolkata-700013 for providing necessary infrastructural assistance; to UGC and DBT for providing financial assistance for the research work.

REFERENCES

Allag I and Rangari K (2002) Extragenomic action of steroids on spermatozoa Prospects for regulation of fertility. *Health Popul*, 25 (1):38-44.

Bhowal SK, Lala S, Hazra A, Paira P, Banerjee, Mondal NB and Chakraborty S (2008) Synthesis and assessment of fertility-regulating potential of 2-(2″-chloroacetamidobenzyl)-3-(3′-indolyl) quinoline in adult rats as a male contraceptive agent. *Contraception,* 77:214-222.

Blobel CP (2000). Functional processing of fertilin; evidence for a critical role proteolysis in sperm maturation and activation. *Rev Reprod*, 5:75-83.

Bone W, Jones NG, Kamp G, Yeung CH and Cooper TG (2000) Effect of ornidazole on fertility of male rats: inhibition of a glycolysis-related motility pattern and zona binding required for fertilization in vitro. *J Reprod Fertil*, 118:127-135.

Chakrabarty G, Basu A, Manna PP, Mahato SB, Mandal NB and Bandyopadhyay S (1999) Indolylquinoline derivatives are cytotoxic to *Leishmania donovani* promastigotes and amastigotes in vitro and are effective in treating murine visceral leishmaniasis. *J Antimicrob Chemother*, 43:359-366.

Chakraborty S and Lala S (1998) Assessment of the antifertility effect of phaseolinone, an anti-leishmanial agent, in male rats. *Contraception*, 58:183-191.

Chaudhury I, Sadler-Rggleman I, Ague JM and Skinner MK (2005) The helixloop-helix inhibitor of differentiation (ID) proteins induce post-mitotic terminally differentiated Sertoli cell to re-enter the cell cycle and Proliferate. *Biol Reprod*, 72:1205-1217.

Clearmont Y and Hervay SG (1965) Duration of the cycles of the epithelium of normal, hypophysectomized and hypophysectomized hormone treated albino rats. *Endocrinology*, 76:80-89.

Cooper TG, Yeung CH, Skupin R and Haufe G (1997) Antifertility potential of ornidazole analogues in rats. *J Androl*, 18:431-438.

Corsi G, Palazzo G, Germani C, Barcellona S and Silvestrini B (1976) 1-Halobenzyl-1H-indazole –3-carboxylic acids. A new class of antispermatogenic agents. *J Med Chem*, 19:778-783.

Dacheux JL, Gatti JL and Dacheux F (2003) Contribution of epididymal secretory proteins for spermatozoa maturation. *Microsc Res Tech*, 61:7-17.

Dhanapal R, Ratna JV, Saratchandran I and Gupta M (2012) Reversible antispermatogenic and antisteroidogenic activities of *Feronia limonia* fruit pulp in adult male rats. *Asian Pac J Trop Biomed*, 2(9): 684-690.

Edwards B, Smith A and Skinner DC (2013) Dose and durational effects of the gonadotropin-releasing hormone agonist, deslorelin: the malerat (*Rattus norvegicus*) as a model. *J. Zoo Wildl Med*, 44 (4 Suppl):S97-101.

Etribi A, Ibrahim A, Mahmoud K, El-Haggar S, Hamada T and El-Ahmadi I (1982) Antisperm antibodies and human infertility. *Fertil Steril*., 37(2):236-239.

Everett JW (1994) Pituitary and hypothalamus: perspective and overview. In: Knobil E, Neill JD, editors. The physiology of reproduction. New York: Raven Press; pp 1509-1526.

Gatti JL, Castella S, Dacheux F, Ecroyd H, Métayer S, Thimon V and Dacheux JL (2004) Post-testicular sperm environment and fertility, *Anim Reprod Sci*, 82-83:321-339.

Gottwald U, Davies B, Fritsch M and Habenicht U (2006) New approaches for male fertility control: HE6 as an example of a putative target. *Mol Cell Endocrinol*, 250(1-2): 49-57

Greenwood FC, Hunter WM and Glover JS (1963) The preparation of 131I labeled human growth hormone of high specific activity. *Biochemistry,* 89:114–123.

Grima J, Silvestrini B and Cheng Y (2001) Reversible inhibition of spermatogenesis in rats using a new male contraceptive, 1-(2,4′-dichlorobenzyl)- indazole-3-carbohydrazide, *Biol. Reprod*, 64:1500-1508.

Gupta RS, Saxena P, Gupta R and Kachhawa JB (2011) Evaluation of reversible contraceptive activities of *Cuminum cyminum* in male albino rats. *Contraception*, 84(1):98-107.

Kerr JB and Sharpe RM (1989) Focal disruption of spermatogenesis in testis of adult rats after a single administration of human chorionic gonadotrophin. *Cell Tissue Res*, 257:163-169.

Kopf G (2008) Approaches to the identification of new nonhormonal targets for male contraception. *Contraception*, (4):S18-22

Lohiya NK, Mishra PK, Pathak N, Manivannan B, Bhande SS, Panneerdoss S and Sriram S (2005) Efficacy trial on the purified compounds of the seeds of *Carica papaya* for male contraception in albino rat. *Reprod Toxicol*, 20(1):135-148.

Lowry OH, Rosebrough NJ, Farr AL and Randall RJ (1951) Protein measurement with the Folin phenol reagent. *J. Biol. Chem*, 193(1):265-275.

Mahato SB, Mandal NB, Chattopadhyay S, Nandi G, Luger P and Weber M (1994) Synthesis of indolylquinolines under Friedel–Crafts reaction conditions. *Tetrahedron*, 50: 10803-10812.

McLachlan RI, Wereford NG, deKrester M and Robertson DM (1994a) Testosterone effect on spermatogenesis in the gonadotropin-releasing hormone immunized rat. *Biol Reprod*, 50:271-280.

McLachlan RI, Wereford NG, Donnel L, de Krester M and Robertson D (1996) The endocrine regulation of spermatogenesis: independent roles for testosterone and FSH. *J Endocrinol*, 148:1-9.

McLachlan RI, Wereford NG, Tgouts C, de Krester M and Robertson DM (1994b) Effects of testosterone on spermatogenic cell populations in the adult rat. *Biol Reprod*, 51:945-955.

Meitrich ML, Wilson G, Ye WS, Kurdglu B, Parchuri N and Terry NHA (1994) Hormonal protection from procarbazine-induced testicular damage is selective for survival and recovery of stem spermatogonia. *Can Res*, 54:1027-1034.

Metayer S, Dacheux F, Dacheux JL and Gatti JL (2002) Comparison, characterization, and identification of protease and protease inhibitors in epididymal fluids of domestic animals. Matrix metalloproteinases are major fluid gelatinase. *Biol Repod*, 66:1219-1229.

Mishra RK and Singh SK (2009) Reversible antifertility effect of aqueous rhizome extract of *Curcuma longa* L. in male laboratory mice. *Contraception*, 79 (6):479-487.

Muffy KE, Nazian S and Cameron DF (1993) Junction-related Sertoli cell cytoskeleton in testosterone-treated hypophysectomized rats. *Biol Reprod*, 49:1122-1132.

O'Donnel L, McLachlan RJ, and Wereford NG (1996) Testerone withdrawal promotes stage specific detachment of round spermatid from the rat seminiferous epithelium. *Biol Repord*, 55: 895-901.

Paulsen C, Christensen R and Bagatell C (1994) Status of male contraception: hormonal approach. In: Corson SL, Derman RJ, Tyner LB, editors. Fertility control. 2nd ed. London: Golden Publishers; 281-292.

Robaire B and Viger RS (1995) Regulation of epididymal epithelial cell function. *Biol Reprod*, 52: 226-236.

Setchel BP, Maddocks S and Brooks DE (1994) Anatomy, vasculature, enervation and fluids of the male reproductive tract. In: Knobil E, Neill JD, editors. The physiology of reproduction. New York: Raven Press, pp 1063-1175.

Sharpe RM (1994) Regulation of spermatogenesis. In: Knobil E, Neill EK, editors. The Physiology of Reproduction. New York: Raven Press, pp 1363-1434.

Sharpe RM (1994) Toxicity of spermatogenesis and its detection. In: Kenneth SK, editor. Reproduction and development. New York: Marcel Dekker, Inc; pp 625-635.

Silvestrini B, Palazzo G and De Gregario M (1984) Lonidamine and related compounds. *Prog Med Chem,* 21:110-135

Singla N, Kaur G, Babbar BK and Sandhu BS (2013) Potential of triptolide in reproductive management of the house rat, *Rattus rattus*. *Integr Zool*, 8(3):260-276.

Turner TT, Miller DW and Avery EA (1995) Protein synthesis and secretion by the rat caput epididymis in vivo: influence of the luminal microenvironment. *Biol Reprod*, 52:1012-1019.

Vannucchi C, Angrimani D, Eyherabide A, Mazzei C, Lucio C and Maiorka P (2015) Effects of intratesticular administration of zinc gluconate and dimethyl sulfoxide on clinical, endocrinological, and reproductive parameters in dogs. *Theriogenology*, 84(7):1103-1110

Yanagimachi R (1994) Fertility of mammalian spermatozoa: its development and relativity. *Zygote*, 2:371–372.

ISSN: 0976-3031

Available Online at http://www.recentscientific.com

CODEN: IJRSFP (USA)

International Journal of Recent Scientific Research
Vol. 12, Issue, 03 (B), pp. 41220-41227, March, 2021

International Journal of Recent Scientific Research

DOI: 10.24327/IJRSR

Research Article

ASYMPTOMATIC SARS-CoV-2: INFECTION AND CHALLENGES IN INDIA

Sanjukta Manna*, Anish Pal and Pradip Bhattacharjee

Department of Zoology, Maulana Azad College, 8 Rafi Ahmed Kidwai Road, Kolkata 700 013, India

DOI: http://dx.doi.org/10.24327/ijrsr.2021.1203.5848

ARTICLE INFO

Article History:

Received 13th December, 2020
Received in revised form 11th January, 2021
Accepted 8th February, 2021
Published online 28th March, 2021

Key Words:

SARS CoV-2, IgM, circadian clock, asymptomatic, viral shedding

ABSTRACT

The outbreak of severe acute respiratory syndrome coronavirus 2 (SARS-CoV-2) has become a global pandemic. Asymptomatic carriers have mild or non-symptoms but with positive test for viral nucleic acid of SARS-CoV-2 or with positive test for serum specific IgM antibody. The study was made to focus on the asymptomatic infection and transmission of COVID-19 (belonging to beta genera of Coronaviridae family). The patients who have a weak immune reaction are generally being affected by SARS CoV-2. The immune system efficiently shields the body against infectious agents but eventually may fail or overreact with harsh outcomes for the infected person. The viral infections impact the circadian clock circuitry of the infected organism that in turn, interacts with the molecular components of the infecting pathogens. The transmission of corona virus may take place from the asymptomatic patients but the rate of transmission is generally lower as the patients does not have usual cough and sneezing. The immune system of the host plays a very important role in determining whether the infection will be symptomatic or asymptomatic. In asymptomatic individual the immune system fails to exaggerate against the virus and thus fails to generate the inflammation and does not show the popular clinical manifestations indicated by other respiratory viruses. Asymptomatic spread occurs when a person infects others in the days before their symptoms develop. They had a significantly longer duration of viral shedding than the symptomatic group. The virus-specific IgG levels in the asymptomatic group were significantly lower relative to the symptomatic group in the acute phase. The reduction in IgG and neutralizing antibody levels in the early convalescent phase of asymptomatic patient might have implications for immunity strategy and serological surveys.

INTRODUCTION

Coronaviruses are a group of viruses that belong to the Coronaviridae family. Coronaviridae is a family of enveloped, single-stranded, positive-sense RNA virus. The Coronaviridae family can be divided into four genera: alpha(α), beta(β), gamma(γ), and delta(δ). The coronaviruses of the α and β genera generally infect mammals and humans, while the coronaviruses of the γ and δ genera mainly infect birds. 229E (HCoV-229E), OC43 (HCoV-OC43), NL63 (HCoV-NL63), HKU1 (HCoV-HKU1), SARS-CoV, and MERS-CoV, SARS-CoV-2 can affect human beings (Nickbakhsh *et al*., 2020). In 2003, an outbreak of the coronavirus strain SARS-CoV caused more than 8000 infections worldwide, and led to 774 deaths from SARS (Severe Acute Respiratory Syndrome). In 2012, another virulent strain of coronavirus was identified. The outbreak of this virus, named MERS-CoV, began in Saudi Arabia and caused hundreds of deaths from Middle East Respiratory Syndrome (MERS). SARS-CoV2 is the third terrible variety of coronavirus that causes the more commonly known COVID-19, which stands for Coronavirus Disease 2019. It causes severe symptoms and significant mortality, similar to the SARS and MERS coronavirus strains. Several cases of pneumonia from COVID-19 were reported in Wuhan, China on December 2019. A novel coronavirus was identified in a bronchoalveolar fluid sample isolated from a patient in the Wuhan Seafood Market (Wu *et.al*., 2020). This infection is characterized by a broad spectrum of clinical syndromes, ranging from mild influenza-like symptoms to severe pneumonia and acute respiratory distress syndrome (Raoult *et.al*., 2020).

On February 11, 2020, the virus was named severe acute respiratory syndrome coronavirus 2 (SARS-CoV-2) by the International Committee on Taxonomy of Viruses (ICTV) (Drosten *et.al*., 2003; Ksiazek *et.al*., 2003). The ability of a single virus to cause different pathological manifestations is due to multiple contributory factors including the quantity of viral inoculum, the genetic background of patients and the presence of concomitant pathological conditions. The first case of COVID-19 in India, which originated from China, was

Corresponding author:* **Sanjukta Manna
Department of Zoology, Maulana Azad College, 8 Rafi Ahmed Kidwai Road, Kolkata 700 013, India

reported on 30 January 2020 (Perappadan, 2020). India currently has the largest number of confirmed cases in Asia, and has the second highest number of confirmed cases in the world after the United States with more than 10.3 million reported cases of COVID-19 infection and more than 154,000 deaths as of February 2, 2021(MyGov.in., 2021). The per day cases peaked mid-September in India with over 90,000 cases reported per day and have since come down to below 15,000 as of 2021 January (Press Information Bureau,2021).

In this review, we explored the knowledge that supports the SARS-CoV-2 immunity among persons with asymptomatic specifically, whether full or partial immunity develops in these persons, how long protective immunity lasts, and if it is possible to be immune from reinfection but still asymptomatically transmit SARS-CoV-2 while in a carrier state. This valuable correspondence will assist infection control practices during this pandemic.

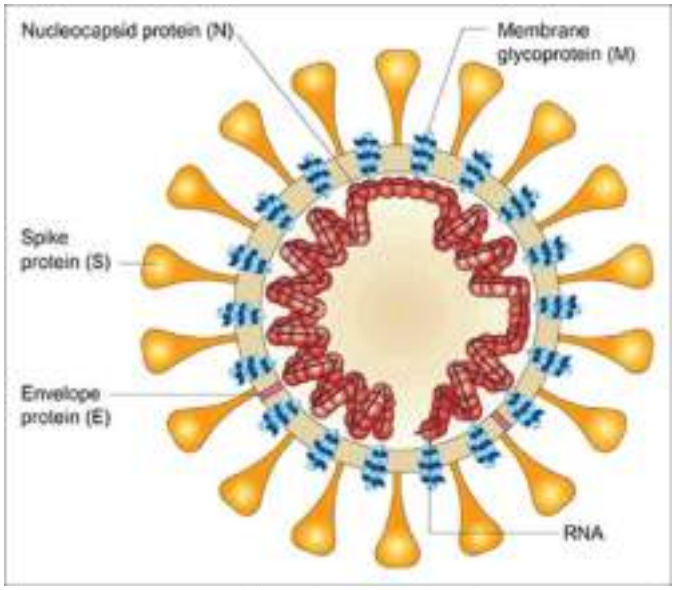

Fig 1 Etiology of SARS-Corona virus (https://www.nature.com/articles/nm1143)

SUVIVALITY OF SARS-COV-2

Entry of the virus

The S protein on the surface of coronavirus can recognize and bind to the receptor and then invade the host cell through clathrin-mediated endocytosis. Different coronaviruses can use different cell receptors to complete the invasion (Atkinson and Petersen, 2020). The receptor of SARS-CoV2 is ACE2. Many coronaviruses utilize peptidases as their cellular receptor but it is unclear why peptidases are used, as entry occurs even in the absence of the enzymatic domain of these proteins. Then through a series of process the virus genome is released into the cytosol.

Replicase protein expression

The next step is the translation of the replicase gene from the virion genomic RNA. Initiated by replicase gene several NSPS are formed which assemble into the replicase–transcriptase complex (RTC) to create an environment suitable for RNA synthesis, and ultimately are responsible for RNA replication and transcription of the sub-genomic RNAs.

Replication and transcription

Viral RNA synthesis which produces both genomic and sub genomic RNAs, follows the translation and assembly of the viral replicase complexes.

Assembly and Release

After replication and sub-genomic RNA synthesis, the viral structural proteins are translated and inserted into the endoplasmic reticulum (ER). These proteins move along the secretory pathway into the endoplasmic reticulum–Golgi intermediate compartment (ERGIC). The viral genomes encapsulated by N protein bud into membranes of the ERGIC containing viral structural proteins, forming mature new virus (Gudbjartsson *et.al*., 2020).

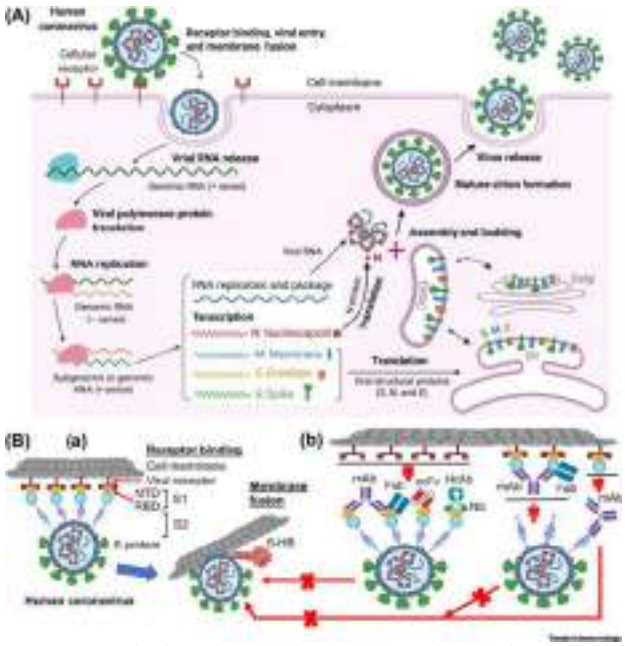

Fig 2 Mechanism of action of Corona virus (Jiang et.al., 2020)

Distinction of SARS-COV 2 from other respiratory illness

Numerous coronaviruses first discovered in domestic poultry in the 1930s, cause respiratory, gastrointestinal, liver, and neurologic diseases in animals. Only 7 coronaviruses are known to cause disease in humans. Four of the seven coronaviruses most frequently cause symptoms of the common cold. Three of the seven coronaviruses cause much more severe, and sometimes fatal, respiratory infections in humans and have caused major outbreaks of deadly pneumonia in the 21st century:

- SARS-CoV2 is a novel coronavirus identified as the cause of coronavirus disease 2019 (COVID-19) that began in Wuhan, China in late 2019 and spread worldwide.
- MERS-CoV was identified in 2012 as the cause of Middle East respiratory syndrome (MERS).
- SARS-CoV was identified in 2003 as the cause of an outbreak of severe acute respiratory syndrome (SARS) that began in China near the end of 2002.

Fig 3 Difference among the COVID-19, Flu and Cold (Medical News Today, May 19, 2020)

Asymptomatic persons: a major role in the transmission

There are two classes of asymptomatic cases with SARS-CoV-2 infection: first, cases with little or mild symptoms within the incubation period but with symptoms onset in the coming 14-day quarantine period or typical changes on the chest-radiograph. At present, fever as one of the dominant symptoms of COVID-19 was identified in only 40% of the patients in India, while 60% of patients developed fever after hospitalization indicating that some asymptomatic COVID-19 cases before admission may develop symptoms and tested positive for viral nucleic acid or antibodies during the hospitalization. The transmission appears to have occurred during the incubation period in these index patients. The asymptomatic persons are potential sources of COVID 19 infection may warrant a reassessment of transmission dynamics of the current outbreak. On April 21, 2020 Raman R. Gangakhedkar, Head of Epidemiology and Communicable Diseases, ICMR said that during contact tracing one positive patient may be turned out from on an average three or four asymptomatic patients. The attack rate (number of people exposed who are sick divided by the number of people exposed) per million, taken by age, was highest among those aged 50-69 yrs. (63.3%) and was lowest among those under 10 yrs. (6.1%). The attack rate was higher among males (41.6%) than females (24.3%). Asymptomatic patient reinforces the value of measures that prevent the spread of SARS-CoV-2 by infected persons who may not exhibit illness despite being infectious.

Viral shedding

Nasopharyngeal swab testing also revealed that the asymptomatic patients shed the virus of 19 days. The asymptomatic group had a significantly longer duration of viral shedding than the symptomatic group (viral shedding was 6 d). The duration of viral shedding was 14 d in patients with mild symptoms.

Asymptomatic vs Symptomatic: Cross-reactive antibody responses

During the incubation period, a specific adaptive immune response elicited to eliminate the virus and developed an endogenous protective immune response. to preclude disease progression to severe stages. Therefore, strategies to boost immune responses (anti-sera or pegylated IFNα) at this stage are certainly important. Genetic differences are well-known to contribute to individual variations in the immune response to pathogens. However, when a protective immune response is impaired, virus will propagate and massive destruction of the affected tissues will occur. The damaged cells induce innate inflammation in the lungs that is largely mediated by proinflammatory macrophages and granulocytes. T-cell antigen receptors, on CD4+ or CD8+ T cells recognize the conformational structure of the antigen-binding-grove together with the associated antigen peptides. Therefore, different HLA haplotypes (HLA-loci variability) are associated with distinct disease susceptibilities.

T cell reactivity was highest against proteins other than the coronavirus spike protein, but T cell reactivity was also detected against spike. The SARS-CoV-2 T cell reactivity was mostly associated with CD4+ T cells, with a smaller contribution by CD8+ T cells (Grifoni *et. al*.,2020).

Earlier reports ((Bert *et.al*., 2020) demonstrated that substantial T cell reactivity exists in many unexposed people and speculated that the SARS-CoV-2-specific T cells in unexposed individuals might originate from memory T cells derived from exposure to 'common cold' coronaviruses (CCCs), such as HCoV-OC43, HCoV-HKU1, HCoV-NL63 and HCoV-229E, which widely circulate in the human population and are responsible for mild self- limiting respiratory symptoms. T cell reactivity was highest against a pool of SARS-CoV-2 spike peptides that had higher homology to CCCs in more than 90% of the human population(Sette and Crotty 2020). Substantial CD4+ T cell,CD8+ T cell, and neutralizing antibody responses develop to acute SARS-CoV-2 infection, and some of the T and B cells are retained long term as immunological memory and protective immunity against SARS-CoV-2 infection (Guo *et.al*.,2020; Li *et.al*.,2008).While most acute infections result in the development of protective immunity, available data for SARS-CoV-2suggest the possibility that substantive adaptive immune responses can fail to occur (Choe *et.al*.,2017;Okba *et.al*.,2019;Zhao *et.al*.,2017) and robust protective immunity can fail to develop (Callow *et.al*.,1990). A failure to develop protective immunity could occur due to a T cell and/or antibody response of insufficient magnitude or durability, with the neutralizing antibody response being dependent on the CD4+ T cell response (Zhao *et.al*., 2016).

T cell responses are strongly biased toward certain viral proteins, and the targets can vary substantially betweenCD4+ and CD8+ T cells (Moutaftsi *et.al*., 2010;Tian *et.al*., 2020). Knowledge of SARS-CoV-2 proteins and epitopes recognized by human T cell responses is of immediate relevance, as it will allow for monitoring of COVID-19 immune responsesin laboratories worldwide. Epitope knowledge will also assist candidate vaccine design and facilitate evaluation of vaccine candidate immunogenicity. Almost all of the current COVID-19 vaccine candidates are focused on the spike protein. Spike accounting for 50% and N accounting for 36% of the defined

epitopes. In a large study of humanSARS-CoV-2 responses, spike was reported as essentially the only target of CD8+ T cell responses (Li *et.al*., 2008). The spike prote in was a target of human SARS-CoV-2 CD8+ T cell responses, but it is not dominant.

Immunopathogenesis in COVID-19 is a serious concern. It is most likely that an early CD4+ and CD8+ T cell response against SARS-CoV-2 is protective, but an early response is difficult to generate because of efficient innate immune evasion mechanisms of SARS-CoV-2 in humans (Blanco-Melo *et.al*., 2020). Immune evasion by SARS-CoV-2 is likely exacerbated by reduced myeloid cell antigen-presenting cell (APC) function.

Asymptomatic infection may be associated with subclinical lung abnormalities, as detected by computed tomography. It has been reported that only a specific mild immune response is caused by the SARS-CoV-2 invasion in asymptomatic patients. A lower level of angiotensin-converting enzyme 2 (ACE2) as its receptor and weaker binding capacity with SARS-CoV-2 should be a major factor that leads to the absence of any clinical manifestations for asymptomatic infections (Zhou *et.al*., 2020).

Table 1 Clinical characteristics of asymptomatic infections of COVID-19

Type	General Clinical characteristics	RT-PCR test
Asymptomatic	No clinical symptoms and chest imaging findings.	Positive
Mild	Mild clinical symptoms, such as fever, fatigue, cough, anorexia, malaise, muscle pain, sore throat, dyspnea, nasalcongestion, headache. No abnormal chest imaging findings.	Positive
Moderate	Mild or moderate clinical features. Chest imaging showed mild pneumonia and infestation	Positive
Severe	Suspected respiratory infection, Shortness of breath, RR - 30 breaths/min; At rest, oxygen saturation -93%; PaO_2/FiO_2- 300 mmHg, Chest imaging showed the lesions significantly	Positive
Critical	Rapid progress of disease, Respiratory failure, and need mechanical ventilation; Shock; Combined with other organ failure requires ICU monitoring treatment	Positive

RT-PCR, reverse transcriptase-polymerase chain reaction; RR, respiratory rate; PaO_2, arterial partial pressure of oxygen; FiO_2, oxygen concentration; ICU, intensive care unit.

Chest imaging (CT scan) showed no pleural effusions, air bronchogram signs or enlarged lymph nodes, which were typical changes seen in critically symptomatic patients. Above all, age and body condition may play an important role in the severity of COVID-19, and this is related to different immune responses and other potential pathogenesis. It was reported that asymptomatic cases were more common in middle-aged people in India.

Levels of virus specific IgG and IgM in asymptomatic individuals

Asymptomatic COVID-19 patients had significantly lower levels of SARS-CoV-2-specific immunoglobulin G (IgG) antibodies compared with symptomatic patients during the acute phase of the illness. In the asymptomatic group, 81.1% (30/37) tested positive for IgG, and 83.8% (31/37) of the symptomatic group tested positive for IgG approximately 3–4 weeks after exposure. Moreover, 62.2% of the asymptomatic group were positive for IgM, whereas 78.4% of the symptomatic group were IgM positive (Long *et.al*., 2020). Interestingly, IgG levels in the symptomatic group were significantly higher than those in the asymptomatic group in the acute phase. Sustained IgG levels were maintained for more than 2 years after SARS-CoV-2infection (Guo *et.al*., 2020).

Several studies revealed that COVID-19 convalescent individuals have detectable neutralizing antibodies, which correlate with the numbers of virus-specific T cells characterizing adaptive immune response (Ni *et.al*., 2020).

Brouwer *et al*., 2020 observed that convalescent COVID 19 patients showed strong anti-SARS-CoV2 S protein specific B cell responses and developed memory and antibody producing B cells that may have participated in the control of infection and establishment of humoral immunity. They isolated 19 Neutralised antibody (NAbs) that target a diverse range of antigenic sites on spike protein and have neutralizing activities against SARS-Cov-2 virus. The reduction in IgG and neutralizing antibody levels in the early convalescent phase might have implications for immunity strategy and serological surveys.

Cytokine storm: Symptomatic vs Asymptomatic patients of SARS-CoV2

COVID-19 infection is accompanied by an aggressive inflammatory response with the release of a large amount of pro-inflammatory cytokines in an event known as "Cytokine storm." cytokine storm correlated directly with lung injury, multiorgan failure, and unfavourable prognosis of severe COVID-19.

Elevated concentrations of 18 pro- and anti-inflammatory cytokines were observed in the symptomatic group as compared to the asymptomatic group. During an innate immune response to a Corona virus infection, pattern recognition receptors (PRRs) recognize different pathogen associated molecular patterns (PAMPs) in host body. Binding of PAMPs to PRRs triggers the inflammatory response against the invading virus resulting in the activation of several signalling pathways and subsequently transcription factors which induce the expression of genes responsible for production several pro-inflammatory cytokines. These transcription factors induce the expression of genes encoding inflammatory cytokines, chemokines and adhesion molecules. This sequence of events results in recruitment of leukocytes and plasma proteins to site of infection where they perform various effector functions that serve to combat the triggering infection (Thompson *et.al*., 2011). Three of the most important pro-inflammatory cytokines of the innate immune response are IL-1, TNF- α, and IL-6. Cytokines like tumour necrosis factor-related apoptosis-inducing ligand (TRAIL) ($P = 3.39 \times 10^{-14}$), macrophage colony-stimulating factor (M-CSF) ($P = 5.08 \times 10^{-13}$), growth-regulated oncogene-α (GRO-α) ($P = 1.5 \times 10^{-10}$), granulocyte colony-stimulating factor (G-CSF) ($P = 2.05 \times 10^{-9}$) and interleukin 6 (IL-6) ($P = 6.33 \times 10^{-9}$) observed in symptomatic patients(Long *et.al*.,2020).

The "cytokine storm" results from a sudden acute increase in circulating levels of different pro-inflammatory cytokines including IL-6, IL-1, TNF- α, and interferon. This increase in cytokines results in influx of various immune cells such as macrophages, neutrophils, and T cells from the circulation into the site of infection resulting into destabilization of endothelial cell to cell interactions, damage of vascular barrier, capillary

damage, diffuse alveolar damage, multiorgan failure, and ultimately death. Lung injury is one consequence of the cytokine storm that can progress into acute lung injury (Ragab *et.al*., 2020). So, cytokine storm (CS) is a critical life-threating condition and one of the common causes of mortality in the recently declared pandemic of COVID19.

In viral infections, the aberrant release of pro-inflammatory factors leads to lung epithelial and endothelial cell apoptosis which damages the lung microvascular and alveolar epithelial cell barrier, leading to vascular leakage, alveolar oedema and hypoxia. The uncontrolled production of pro-inflammatory factors, containing IL-6, IL-8, IL-1β, and GM-CSF, and chemokines such as CCL2, CCL-5, IP-10, and CCL3, together with reactive oxygen species cause ARDS leading to pulmonary fibrosis and death (Reghunathan *et.al*., 2005). Significantly higher levels of stem cell factor (SCF) (P = 1.48 × 10−9), IL-13 (P = 3.75 × 10−7), IL-12 p40 (P = 7.08 × 10−6) and leukemia inhibitory factor (LIF) (P = 1.33 × 10−3) were observed in the asymptomatic group (Long *et.al*.,2020).Many observers showed that the asymptomatic individuals had a reduced inflammatory response characterized by low circulating concentrations of cytokines and chemokines.

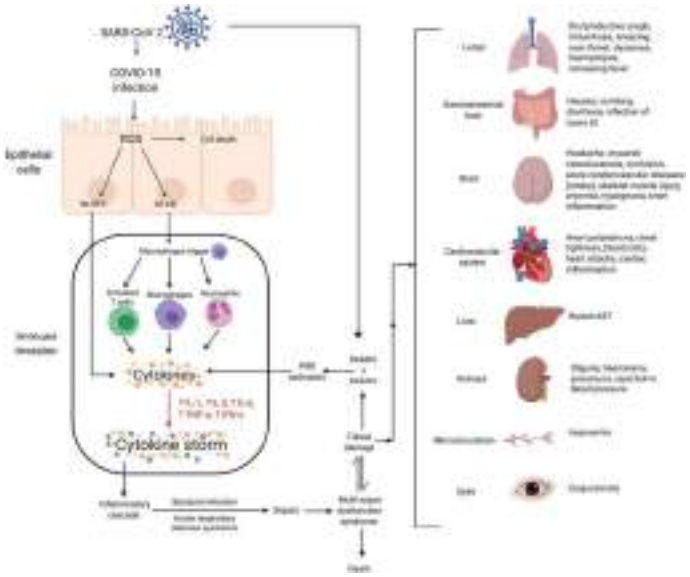

Fig 4 Pathogenic inflammatory cytokine storm and associated damages in SARS-CoV-2 infections. Infection with SARS-CoV 2 can stimulate a hyperinflammatory immune response wherein epithelial-cell-mediated production of reactive oxygen species (ROS) can cause cell death. ROS can also stimulate the synthesis of NLRP3 and NF-κB which contribute to increased cytokine levels, and thus, the cytokine storm. This essentially causes immune invasion which can lead to clinically relevant conditions such as ARDS, sepsis, MODS and potentially even death. The organs affected as a result of MODS, and their associated symptoms, have been shown. Lower gastrointestinal (GI) is rich in ACE2 receptors and hence at higher risk of infection due to COVID-19. Twenty percent of COVID-19 patients have diarrhea as symptoms. SARS-CoV-2, severe acute respiratory syndrome coronavirus 2; COVID-19, coronavirus disease 2019; ROS, reactive oxygen species; NLRP3, (NOD)-like receptor protein 3 inflammasome; NF-κB, nuclear factor kappa-light-chain-enhancer of activated B cells; IL, interleukin; TNF, tumor necrosis factor; IFN, interferon; PAMPs, pathogen-associated molecular patterns; DAMPs, damage-associated molecular patterns; PRR, pattern recognition receptors; AST, aspartate aminotransferase; MODS, multiple organ dysfunction syndrome.

Treatment of asymptomatic infections: Controversy

- Antiviral therapy could fasten viral clearance on asymptomatic infections(Hu *et.al*.,2020)
- Isolation and close observation are enough forasymptomatic infections
- Antiviral treatments not suggested for asymptomatic infections as antiviral drugs (lopinavir/ritonavir) did not seem to be effective(Luo *et.al*.,2020).
- Recommended to continue the isolation management, and health examinations for 14 days
- Recommended to screen for high-risk populations such as close contacts, especially in one confined space with diagnosed or suspected infected patients to control this global epidemic effectively.
- The extent of presymptomatic or asymptomatic SARS-CoV-2 infection should be clarified by studies using serial virologic data, serologic data, or a combination of both in observational cohorts or surveillance systems.
- Knowledge of SARS-CoV-2 immunity among persons with asymptomatic SARS-CoV-2 infection is needed;
- Specifically, whether full or partial immunity develops in these persons, how long protective immunity lasts, and if it is possible to be immune from reinfection but still asymptomatically transmit SARS-CoV-2 while in a carrier state.

Profiles of those who tested COVID-19 positive in India in the time frame

1. Symptomatic international travellers: 523 cases (1.3 %)).
2. Symptomatic contacts of laboratory confirmed cases: 4,257 cases (10.6 %)).
3. Symptomatic healthcare workers 947 cases (2.4 %)).
4. Hospitalised Severe Acute Respiratory Infection (SARI) patients: 4,204 cases (10.5 %)
5. Asymptomatic direct and high risk contacts of laboratory confirmed case-family members: 10,160 cases (25.3 %)).
6. Asymptomatic healthcare workers in contact with confirmed case without adequate protection: 1,135 cases (2.8 %)).
7. ILI (Influenza-like illness) identified in hot zones: 1,199 cases (3.0 %)).

The ICMR has advised states to conduct sero-survey to identify asymptomatic individuals exposed to coronavirus infection. A sero-survey involves testing of blood serum of a group of individuals for the presence of antibodies against that infection to know who has been infected in the past and has now recovered. A new study has estimated that at least 28 per cent of 40,184 people, who had tested positive for COVID-19 between January 22 and June30 in India, were asymptomatic.

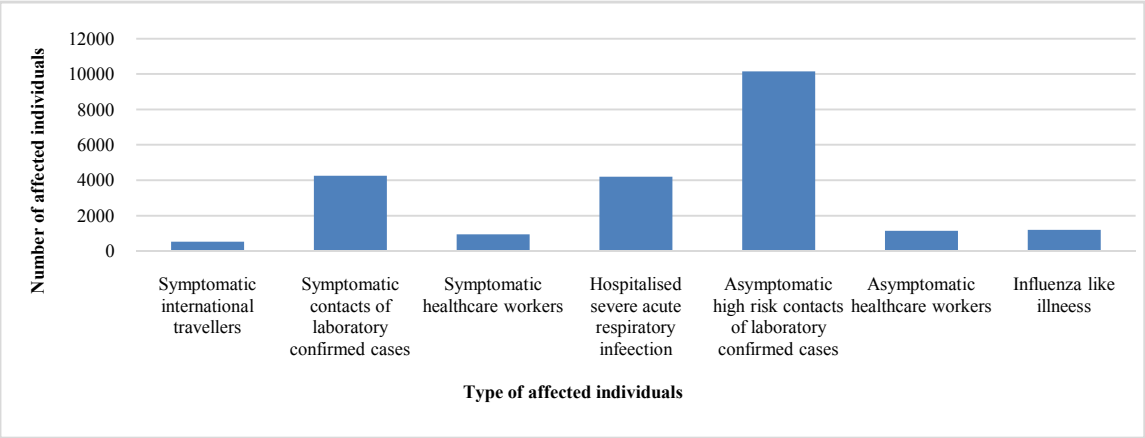

Fig 5 A general comparison between number of symptomatic and asymptomatic affected individuals in India

Circadian Coordination between symptomatic and asymptomatic SARS-CoV2

The homeostatic processes between SARS-CoV-2 and circadian rhythms and sleep may significantly modify the susceptibility to infection as well as the overall clinical manifestation of the disease. These circadian rhythms are synchronized by external cues, such as environmental light and temperature, and feeding times and are resilient to temperature fluctuations within the physiological range.

The implementation of healthy sleep measures as a protective strategy against infection, and early detection of patients at risk for more severe disease (e.g., night-shift workers) may enable improved implementation of supportive measures and lead to better outcomes. There are clear reciprocal dependencies between sleep duration and quality and the immune responses against viral, bacterial, and parasitic pathogens, the latter altering in turn sleep patterns (Zhang *et.al*., 2020). Thus, it is likely that improved sleep quality and duration in the population may mitigate the propagation and severity of disease induced by SARS-CoV-2 infection.

When a viral agent enters the body, it alters the biological processes of the infected cells in order to favour its replication and to spread to various tissues. Diseases caused by viruses, rickettsiae, bacteria, fungi or parasites continue to represent primary cause of morbidity. Infections by viruses rework the biological processes of infected cells to facilitate replication and spread and thus the molecular interplay between the mechanisms of the biological clock, immune system, and virus infection can influence disease outcomes. Comorbid persons are more vulnerable to virus infection as their altered circadian rhythm be involved in the metabolic syndrome, which involves obesity and increased the risk for diabetes and heart disease. Melatonin is well-known hormone of the circadian system with 24hrs rhythmicity by the pineal gland and has been associated with improved response against the virus (Zhang *et.al*., 2020).

COVID-19 outbreak is affecting physical health as well as mental health. Mental illnesses have been reported to alter immunity, thus increasing the vulnerability to diseases. Normal daily routines of both asymptomatic and symptomatic patients are inevitable to maintain normal rhythms and to prevent transmission of SARS-CoV-2.

Although, the virus mainly affects lungs to cause severe to moderate pneumonia, it may adversely impact mental health to develop stress, anxiety and depression.

CONCLUSION

COVID-19 is a rapidly spreading global threat that has been declared as a pandemic by the WHO. Due to the higher transmissibility and infectiousness, asymptomatic infection, and lack of effective treatment options and vaccine, fatalities and morbidities are increasing day by day globally. Although, grooming evidences suggest possible transmission of SARS-CoV-2 from asymptomatic cases, WHO declared coronavirus have relatively low risk transmitted through asymptomatic cases from past experience in the middle east respiratory syndrome (MERS). Asymptomatic cases are unlikely the major driver of transmission in COVID-19, otherwise, more cases of infection would have been presented. Besides, the process of viral shedding of asymptomatic patients is limited by the lack of symptoms such as coughing and sneezing, reduced the risk of infection. The relatively low viral loads of asymptomatic patient also limit its capacity of transmission and being the so-called super-spreader.

The asymptomatic patients infected by SARS-CoV-2 might have favorable clinical outcomes. Patients who have a contact history of COVID-19 should be monitored and tested for SARS-CoV-2 in anal and throat swabs to rule out infection, even if they are asymptomatic.

ACKNOWLEDGEMENTS

We would like to express our gratitude to Prof. Subir Chandra Das Gupta, Head of the Department, Post Graduate Department of Zoology, Maulana Azad College, Kolkata for his encouragement to prepare this review.

REFERENCES

1. Atkinson, B. and Petersen, E.(2020).SARS-CoV-2shedding and infectivity. Lancet, 395, 1339–1340. DOI:10.1016/S0140-6736(20)30868-0.
2. Bert, NL., Tan, A., Kunasegaran, K., Tham, Y.L.C., Hafezi, M., Chia, A. *et al*. (2020). Different pattern of pre-existing SARS-COV-2 specific T cell immunity in SARS-recovered and uninfected individuals. Bio Rxiv, DOI: https://doi.org/10.1101/2020.05.26.115832.

3. Blanco-Melo, D., Nilsson-Payant, B.E., Liu, W.C., Møller, R., Panis, M., Sachs, D., Albrecht, R.A., Oever, B.R. (2020). SARS-CoV-2 launches a unique transcriptional signature from in vitro, ex vivo, and in vivo systems. bioRxiv, DOI: https://doi.org/10.1101/2020.03.24.004655.
4. Brouwer PJM, Caniels TG, StratenK vd, SnitselaarJL, AldonY, Bangaru S, Torres J L, *et al*.,(2020). Potent neutralizing antibodies from COVID-19 patients define multiple targets of vulnerability. Science, DOI: 10.1126/science.abc5902.
5. Callow, K.A., Parry, H.F., Sergeant, M., Tyrrell, D.A.J (1990). The time course of the immune response to experimental coronavirus infection of man. Epidemiology and Infection, 105, 435-446. DOI: https://doi.org/10.1017/S0950268800048019.
6. Choe, P.G., Perera, R.A.P.M., Park, W.B., Song, K.H., Bang, J.H., Kim, E.S., Kim, H.B., Ko, L.W.R., Park, S.W., Kim, N.J. *et al.* (2017). MERS-CoV antibody responses 1 year after symptom onset, South Korea. EmergingInfectiousDiseases, 23, 1079–1084. DOI: https://doi.org/10.3201/eid2307.170310
7. Drosten, C., Gunther, S., Preiser, W., van der W.S., Brodt, H.R., Becker, S., Rabenau, H., Panning, M., Kolesnikova, L., Fouchier, R.A., (2003). Identification of a novel coronavirus in patients with severe acute respiratory syndrome.The New England Journal of Medicine, 348: 1967–1976.
8. Grifoni, A., Weiskopf, D., Ramirez, S.I.,Mateus, J. *et al*. (2020). Targets of T cell responses to SARS-CoV-2 coronavirus in humans with COVID-19 disease and unexposed individuals. Cell, 181,1489–150.DOI:10.1016/j.cell.2020.05.015.
9. Gudbjartsson, D. F., Helgason, A., Jonsson, H., Magnusson, O.T., Melsted, P., Norddahl, G.L., Saemundsdottir, J. *et al*. (2020). Spread of SARS-CoV-2 in the Icelandic population. *The New England Journal of Medicine*, DOI: https://doi.org/10.1056/ NEJMoa2006100.
10. Guo, T., Fan, Y., Chen, M., Wu, X., Zhang, L., He, T., *et al*. (2020). Cardiovascular implications of fatal outcomes of patients with coronavirus disease 2019 (COVID-19). JAMA Cardiology, DOI:10.1001/jamacardio.2020.1017. https://www.nature.com/articles/nm1143.
11. Hu, Z., Song C, Xu C, Jin G, Chen Y, Xu X, *et al*. (2020). Clinical characteristics of 24 asymptomatic infections with COVID-19 screened among close contacts in Nanjing, China. Science China Life Sciences. 63,706–711.DOI: https://doi.org/10.1007/s11427-020-1661-4.
12. IndiaFightsCorona COVID-19"MyGov.in. Govt of India. Retrieved 2 January 2021.
13. Jiang X, Luo M, Zou Z, Wang X, Chen C, Qiu J. (2020) Asymptomatic SARS-CoV-2 infected case with viral detection positive in stool but negative in nasopharyngeal samples lasts for 42 days. *Journal of Medical Virology*, DOI:10.1002/jmv.25941.
14. Ksiazek, T.G., Erdman, D., Goldsmith, C.S., Zaki, S.R., Peret, T., Emery, S., Tong, S., Urbani, C., Comer, J.A., Lim, W. *et al*. (2003). A novel coronavirus associated with severe acute respiratory syndrome. The New England Journal of Medicine, 348, 1953–1966.
15. Li, C.K., Wu, H., Yan, H., Ma, S., Wang, L., Zhang, M., Tang, X., Temperton, N.J., Weiss, R.A., Brenchley, J.M. *et al*. (2008). T cell responses to whole SARS coronavirus in humans. *Journal of Immunology*, 181, 5490–5500. DOI: 10.4049/jimmunol.181.8.5490.
16. Long, Q., Tang, X., Shi, Q. *et al*. (2020). Clinical and immunological assessment of asymptomaticSARS-CoV-2infections. Nature Medicine. DOI: https://doi.org/10.1038/s41591-020-0965-6.
17. Luo, S.H., Liu, W., Liu, Z.J., Zheng, X.Y., Hong, C.X. *et al*. (2020). A confirmed asymptomatic carrier of 2019 novel coronavirus. ChineseMedicalJournal,133(9), 1123-1125.DOI:10.1097/CM9.0000000000000798.
18. Medical News Today, May 19, 2020.
19. Moutaftsi, M., Tscharke, D.C., Vaughan, K., Koelle, D.M., Stern, L., Calvo-Calle, M., Ennis, F., Terajima, M., Sutter, G., Crotty, S. etal. (2010). Uncovering the interplay between CD8, CD4 and antibody responses to complex pathogens. FutureMicrobiology, 5, 221-239. DOI:10.2217/fmb.09.110.
20. Ni, L.,Ye,F.,Cheng,M.L.,Deng Y-Q,Zhao,H *et al*. (2020). Detection of SARS-CoV-2-specific humoral and cellular immunity in COVID-19 convalescent individuals. Immunit,. DOI: https://doi.org/10.1101/2020.03.17.20037713.
21. Nickbakhsh, S., Ho, A., Marques, D. F.P., McMenamin, J., GunsonR. R. *et al*. (2020). Epidemiology of Seasonal Coronaviruses: Establishing the Context for the Emergence of Coronavirus Disease (2019). *Journal of Infectious Disease,* 359, 1091–9.DOI: 10.1093/infdis/jiaa185.
22. Okba, N.M.A., Raj, V.S., Widjaja, I., Geurtsvan-Kessel, E., C.H., Kessel, E., de Bruin, Chandler, F.D., Park, W.B., Kim, N.J., Farag, E.A.B.A., Al-Hajri, M. *et al*. (2019). Sensitive and Specific Detection of Low-Level Antibody Responses in Mild Middle East Respiratory Syndrome Coronaviru Infections. Emerging Infectious Diseases, 25(10), 1868-1877. DOI: 10.3201/eid2510.190051.
23. One of the highest globally, India's Recovery Rate now nearly 97%"Press Information Bureau. 28 January 2021.
24. Perappadan, Bindu Shajan (30 January 2020). "India's first coronavirus infection confirmed in Kerala". The Hindu. ISSN 0971-751X. Retrieved 24 February 2021.
25. Ragab, D., Salah, H., Taeimah, M., Khattab, R., Salem, R. (2020). The COVID-19 Cytokine Storm; What We Know So Far. Frontiersin. Immunology, 11,1446. DOI:10.3389/fimmu.2020.01446.
26. Raoult, D., Zumla, A., Locatelli, F., Ippolito, G., Kroemer, G. (2020). Coronavirus infections: Epidemiological, clinical and immunological features and hypotheses. Cell Stress, 4(4), 66–74. DOI:10.15698/cst2020.04.216.
27. Reghunathan, R, Jayapal, M, Hsu, LY, Chang HH, Tai, D. *et al*. (2005). Expression profile of immune response genes in patients with Severe Acute Respiratory Syndrome. BMC Immunology, 6,2. DOI: 10.1186/1471-2172-6-2.
28. Sette, A. and Crotty, S. (2020). Pre-existing immunity to SARS-CoV-2: the knowns and unknowns. Nature

Reviews Immunology,20, 457–458. DOI: https://doi.org/ 10.1038/s41577-020-0389-z.
29. Thompson, M, Kaminski, J, Kurt-Jones, E, Fitzgerald, K. (2011). Pattern recognition receptors and the innate immune response to viral infection. Viruses, 3:920–40. DOI: 10.3390/v3060920.
30. Tian X, Li A, Huang S, Xia S, Lu Z. *et al*. (2020). Potent binding of 2019 novel coronavirus spike protein by a SARS coronavirus-specific human monoclonal antibody. Emerging Microbes and Infections, 9(1), 382–385.
31. Wu F,ZhaoS, YuB, ChenYM, WangW, SongZG *et al*. (2020). A new coronavirus associated with human respiratory disease in China. Nature, 579, 265–369. DOI: 10.1038/s41586-020-2008-3.
32. Zhang R, Wang X, Ni L, Di X, Ma B, Niu S, Liu C, Reiter RJ. (2020). COVID-19: Melatonin as a potential adjuvant treatment. Life Science. 23, 117583. DOI: 10.1016/j.lfs.2020.117583.
33. Zhao J, ZhaoJ, MangalamAK, ChannappanavarR, FettC. *et al*. (2016). Airway memory CD4(+) T cells mediate protective immunity against emerging respiratory coronaviruses. Immunity, 44,1379–1391. DOI: 10.1016/j.immuni.2016.05.006.
34. Zhao J, Alshukairi AN, Baharoon SA, Ahmed WA, Bokhari AA, Nehdi AM. *et al*. (2017). Recovery from the Middle East respiratory syndrome is associated with antibody and T-cell responses. Science Immunology, 2(14), DOI: 10.1126/sciimmunol.aan5393.
35. Zhou P, Yang XL, Wang XG, Hu B, Zhang L, Zhang W. *et al*. (2020). A pneumonia outbreak associated with a new coronavirus of probable bat origin. Nature, DOI: https://doi.org/10.1038/s41586-020-2012-7.

How to cite this article:

Sanjukta Manna *et al*.2021, Asymptomatic Sars-Cov-2: Infection and Challenges In India. *Int J Recent Sci Res.* 12(03), pp. 41220-41227. DOI: http://dx.doi.org/10.24327/ijrsr.2021.1203.5848

****

ISSN: 0976-3031

Available Online at http://www.recentscientific.com

CODEN: IJRSFP (USA)

International Journal of Recent Scientific Research
Vol. 11, Issue, 07 (B), pp. 39147-39151, July, 2020

International Journal of Recent Scientific Research

DOI: 10.24327/IJRSR

Research Article

GLUTEN INDUCED INFLAMMATORY RESPONSES IN MURINE MODEL: AN OVERVIEW

Sanjukta Manna*, Taniya Mondal and Ayantika Mitra

Post Graduate Department of Zoology, Maulana Azad College, 8 Rafi Ahmed Kidwai Road, Kolkata 700 013, India

DOI: http://dx.doi.org/10.24327/ijrsr.2020.1107.5450

ARTICLE INFO

Article History:

Received 06th April, 2020
Received in revised form 14th May, 2020
Accepted 23rd June, 2020
Published online 28th July, 2020

Key Words:

allergy, enteropathy, gluten, IgE, wheat

ABSTRACT

The prevalence of wheat allergy has reached significant levels in many countries. Immunoglobulin E (IgE)-mediated food allergy is the most common type of adverse reaction towards wheat proteins. Increased intestinal permeability after gluten exposure occurs in all individuals. Both genetic and environmental factors influence the nature of reactivity to gluten and phenotypic expression of enteropathy. Gluten can trigger adverse inflammatory, immunological and autoimmune reactions in some people. It can produce abroad spectrum of gluten related disorders. This comprehensive review explored to identify the strengths, challenges, and future prospects of animal models in basic and applied wheat protein allergy evidenced from clinical trials and its role as potential pathogenic co-factor.

INTRODUCTION

Among major allergic foods, wheat is the most cultivated basic staple food crop in the world, causing food allergies ranging severity. The prevalence of wheat allergy has reached significant levels in many countries. Therefore, wheat is a major global food safety and public health issue. Several researchers reveal that a family of protein in wheat may be responsible for activating inflammation in chronic health conditions. Food allergens in general are water/saline soluble proteins. However, wheat contains four different classes of protein allergens: water soluble (albumin), saline (globulin), alcohol soluble (gliadin), and acid soluble (gluten) protein allergens. The total protein content in wheat flour ranges from 8% to 12% (Yokooji *et al*., 2018). The term gluten includes both gliadin and glutenin. gliadins contribute to the cohesiveness and extensibility of the gluten, whereas glutenin plays a role in the maintenance of the elasticity and strength of the gluten (Wieser,2007). Gliadins are represented as single chain polypeptides, and are divided into four major groups: α-, β-, γ-, and ω-gliadins and connected to each other through intrachain disulfide bonds. Glutenins consist of high molecular weight glutenin subunits (HMW-GS) and low molecular weight glutenin subunits (LMW-GS). These polymeric forms contribute to the strength of gluten and improves dough quality. There is extensive evidence in the literature that food processing like fermentation and enzyme treatment can alter the allergenicity of food proteins (Verhoeckx *et al*.,2015; Ortiz *et al*., 2016; Vanga *et al*., 2017; Phromraksa,2008). However, thermal processing does not reduce or eliminate allergenicity of wheat allergens. In this review we have summarized the knowledge on classification, properties, structure and role of gluten proteins in the pathogenesis of gluten intolerance manifestations.

Types of Gluten Proteins

Gluten proteins are wheat storage proteins constituting about 10% of wheat and give wheat dough its functional properties such as water absorption capacity, viscosity and elasticity which contribute to the unique baking properties. Gluten is the product of a ball of wheat flour dough that has been exhaustively washed in tap water, and the baking qualities of the wheat depends on its ability to trap carbon dioxide in dough. Gluten proteins are among the most complex proteins in nature containing hundreds of components as monomers, oligomers and polymers. No nutritional value has been attributed to gluten. Based on their physical characteristics (water/saline insoluble), gluten proteins can be divided into gliadin and glutenin. Gliadin family proteins are monomeric and can be genetically classified into α/β, γ-ω,1,2- and ω5-gliadins. The glutenin family proteins are divided into low and high molecular weight glutenin (Yokooji *et al*., 2018).Some fragments of gluten are toxic and others are immunogenic (Fig1).

Corresponding author:* **Sanjukta Manna
Post Graduate Department of Zoology, Maulana Azad College, 8 Rafi Ahmed Kidwai Road, Kolkata 700 013, India

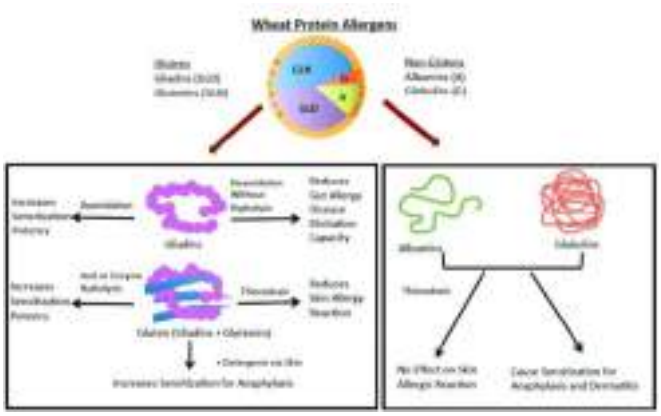

Fig 1 Schematic overview of wheat allergens: effect of molecular modifications on wheat allergenicity in animal models.

Gluten can trigger adverse inflammatory, immunological and autoimmune reactions in some people. Gluten can produce abroad spectrum of gluten related disorders. Two pathways have been hypothesized to be triggered by these peptides: one is the direct effect on the epithelium that involves the innate immune response (Schuppan *et al*.,2003), the other represents the adaptive immune response involving CD4 + T cells in the lamina propria that recognize processed gluten epitopes (Schuppan, 2000). The initial development and maintenance of tolerance to gluten when interrupted can lead to several diseases. Gluten related diseases such as wheat allergy, celiac disease and gluten intolerance are widespread in the globe in genetically pre-disposed individuals. Marsh (1992) observed that gluten absorption in the intestinal revealed five interrelated lesions (preinfiltrative, infiltrative, hyperplastic, destructive, and hypoplastic) that were interpreted as cell-mediated immunologic responses. Gluten peptides can cross the basement membrane to directly interact with immune cells present in the lamina propria. In this regard, intestinal epithelial cells have been shown to release exosome-like vesicles morphologically similar to those secreted by professional antigen presenting cells(Ciccocioppo,2005).In 1979 Zioudrou *et al*. reported the opioid activity of gluten after pepsin digestion of wheat. It is well documented that opioid peptide influence the central nervous system by modulating the release of hormones and neurotransmitter via opioid receptors. Takahasi *et al*.(2000) observed that an opioid peptide derived from wheat gluten, gluten exorphin A5(Gly-Tyr-Tyr-Pro-Thr) had effects on central nervous system of mammal as evidenced by memory loss and emotional distraction.

Types of Gluten Allergies

Wheat allergies are of two types: IgE-dependent reactions and IgE-independent but eosinophil dependent reactions, however most wheat allergies are IgE-dependent reactions (Fig 2). The IgE-mediated wheat allergies include three groups of disorders: (i) Occupational allergies, such as allergic rhinitis (AR), allergic conjunctivitis (AC), bakers' asthma (BA), and contact urticaria (CU); (ii) wheat food allergy (WFA), such as atopic dermatitis (AD), gastrointestinal allergic disease, andsystemic anaphylaxis; and (iii) wheat-dependent exercise-induced anaphylaxis (WDEIA). The IgE independent but eosinophil mediated wheat allergies include eosinophilic esophagitis (EOE) and eosinophilic gastritis (EOG) (Jin *et al*., 2019).

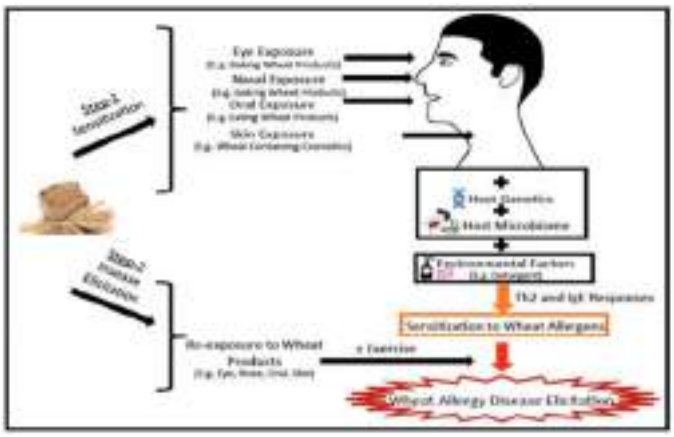

Fig 2 The genesis of wheat allergy: sensitization and elicitation of disease.

Wheat allergies are often confused with celiac disease and nonceliac gluten sensitivity. In contrast to wheat allergies that are mediated by IgE antibodies celiac disease is an autoimmune disease in which gluten in the diet triggers WBC to attack the villi that line the small intestine leading to erosions and prevention of absorption of some nutrients (malsorption).The non-celiac gluten sensitivity is mediated by the over-active innate immune system.

Insights to Various Types of Inflammatory Responses to Gluten

Several mouse models of wheat allergy have been developed and studied upon for greater insights on its allergenicity.Kozai *et al*. (2006) developed a mouse model to explain the molecular mechanisms of wheat dependent exercise-induced anaphylaxis (WDEIA) (Table 1).

Table 1 Major lessons learnt from animal models on wheat protein allergenicity

Species	Wheat Allergen Exposure	Route	Sensitization	Elicitation of Reaction
Dog	Gliadins	IP	IgE	Vomiting, Skin
	Glutenins	Oral	IgE	reaction,
	Albumins+ Globulins	Skin	IgE	Diarrhoea
Mouse	Gliadins			Anaphylaxis, EIA
	Gluten			No Anaphylaxis
	Gluten+ Detergent	IP	IgE	Anaphylaxis
		Skin	No IgE	Increased
	Acid-Hydrolyzed gluten (AHG) + Detergent	Skin	IgE	Anaphylaxis
		Skin	Increased IgE	Anaphylaxis
		IP	IgE	Dermatitis (Th1, Th2, Th17 Cytokines + Allergenic Chemokines)
	Albumins + Globulins			
Rat	Gluten and AHG	IP	IgE	EIA
		Skin	IgE	
		Oral	IgE	
	Enzyme Hydrolyzed Gluten	Oral	IgE	EIA

Abbreviations: IP = intraperitoneal injection; EIA = exercise-induced anaphylaxis

They sensitized mice with albumin/ globulin, gliadin and glutenin fractions. Then, they tested the effect of exercise (treadmill) after oral feeding with each protein fraction. This

model showed that: (i) gliadins and glutenins not only elicited sensitization, but also caused WDEIA; (ii) salt-soluble proteins neither caused sensitization nor WDEIA; (iii) exercise caused mucosal lesions after oral challenge with wheat proteins and the leakage of gliadin and glutenin proteins into the liver. Thus, gluten proteins (gliadin and glutenin) were linked to WDEIA. Although ω-5-gliadin was linked to WDEIA, whether it can cause anaphylaxis independent of exercise was unknown.

According to Galipeau *et al*. (2015), intestinal microbiota modulates gluten induced immunopathology in mice. They investigated whether specific microbiota compositions influence immune responses to gluten in mice expressing the human DQ8 gene, which confers moderate celiac disease (CD) genetic susceptibility. Germ-free mice, clean specific-pathogen-free (SPF) micecolonized with a microbiota devoid of opportunistic pathogens and proteobacteria, and conventional SPFmice that harbor a complex microbiota that includes opportunistic pathogens were used. Clean SPF mice had attenuated responses to gluten compared to germ-free and conventional SPF mice. Germ-free mice developed increased intraepithelial lymphocytes, markers of intraepithelial lymphocyte cytotoxicity, gliadin-specifi cantibodies, and a proinflammatory gliadin-specific T-cell response. Antibiotic treatment, leading to Proteobacteria expansion, further enhanced gluten-induced immunopathology in conventional SPF mice Protection against gluten-induced immunopathology in clean SPF mice was reversed after supplementation with a member of the proteobacteria phylum, an enteroadherent *Escherichia coli* isolated from a CD patient.

Deamidation of gluten is a common practice used by the food industry because this modification of gluten increases its solubility, thus making it a preferred form of gluten to use as a food ingredient and in cosmetics. However, there are concerns on the potentially enhanced allergenicity of such modified gluten. Studies show that deamidated gliadin (DG) sensitizes mice more effectively than the native gliadin and that the DG elicited IgE profile in mice was very similar to that seen in wheat allergic human (Fig 3).

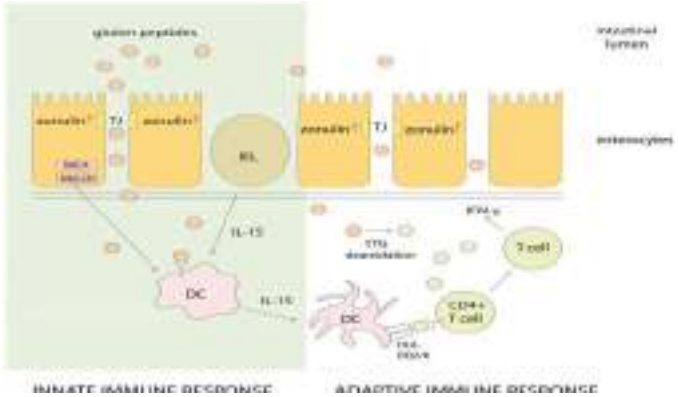

Fig 3 Schematic representation of major pathways in celiac disease (CD) pathogenesis. MICA,NKG2D-stress molecules on enterocytes, IEL-intraepithelial lymphocyte, DC-dendritic cell (Balakireva and Zamyatnin, Jr.,2016).

After gluten enters (Fig 3) into the digestive system, glutamine and proline-rich gluten composing proteins are partially hydrolyzed by proteases presented in the gastrointestinal tract. The upregulation of intestinal peptide zonulin, involved in tight junction regulation, appears to be partly responsible for the increased permeability characteristic of the gut. As a result, generated gluten-derived peptides reach the lamina propria (mucosa) by transcellular or paracellular transport where they are modified by tissue transglutaminase (tTG) enhancing their affinity to MHC II molecules, and thereby making them toxic and immunogenic in HLA-DQ2 or DQ8 (human leukocyte antigen Class II with DQ2 and/or DQ8 molecules on antigen-presenting cells) containing patients . The repetitive presence of glutamine and proline residues determines the gluten-derived peptides as a preferred substrate for tTG. tTG-mediated modifications occur in two ways: deamidation or more frequently transamidation. Further peptides presentation by HLA-DQ2/DQ8 protein subunits in the surface of dendritic cells to gluten-specific T cells induces two levels of immune response: the innate response and the adaptive (T-helper cell mediated) response with the production of interferon-γ and IL-15. As a result, it causes immune-mediated enteropathy, intestinal inflammation, followed by the atrophy of villi, crypt hyperplasia and increased infiltration by intraepithelial lymphocytes. It also produces weight loss and chronic diarrhea.

Gourbeyre *et al*. (2012) used the Balb/c mouse model to test this hypothesis. They found that: i) Native gliadin elicited a higher T helper 1 type of immune response and the deamidated gliadin (DG) elicited a higher T helper 2 or allergic immune response and histamine response. However, both types of proteins elicited anaphylaxis to the same extent; ii) native gliadin elicited IgE against all five gliadins (α/β, γ-, ω 1,2-, and ω5-). However, these antibodies did not bind to DG. In contrast, DG elicited IgE against all five deamidated gliadins, which also bound the native gliadin. These data support that DG is more allergenic than the native gliadin.

Yokooji *et al*. (2018) elucidated the role of Aspirin in facilitating intestinal absorption of the wheat allergen gliadin. They performed concentration checks on the plasma of gliadin after oral administrations by gavage or administration into a closed intestinal loop. They found that aspirin increased plasma concentrations of gliadin after oral administration but had no effect in the closed intestinal loop study. Aspirin increased the absorption of intact and pepsin digested gliadin via the paracellular pathway maintaining their allergenicity.

Verdu *et al*. (2007) used HLA-DQ8 mice to investigate the effects of gliadin sensitization on innate immune markers and on neuromotor and epithelial cell secretory functions in the gut to provide symptoms in humans without celiac disease. CD3+ intraepithelial lymphocyte, macrophages and FOX-P3 positive cell counts were determined. Acetylcholine release, small intestinal contractility, and epithelial ion transport were measured and compared with controls to find recruitment of intraepithelial lymphocyte, macrophages and FOX-P3 cells in G/G (gliadin sensitized and gavaged with gliadin), but not in control mice. This was paralleled by increased acetylcholine release from the myenteric plexus, muscle hypercontractility, and increased active ion transport in G/G mice. Gluten sensitivity in HLA-DQ8 mice induces immune activation in the absence of intestinal atrophy. This is associated with cholinergic dysfunction and a prosecretory state that may lead to altered water movements and dysmotility.

Dietary gluten reduces the number of intestinal regulatory T cells in mice. Ejsing-Duun *et al*. (2008) hypothesized that

gluten is responsible for mediating its effect on T1D (type 1 diabetes) through the influence on T_{reg} development independent of gluten-induced *Lactococci*. Dietary gluten significantly decreased the occurrence of T_{regs} by 10–15% in mice compared with those fed a standard diet. The prevalence of T_{reg} was 5- to 10-fold more abundant in the Peyer's patches than in the spleen. They concluded that the dietary gluten has a significant negative quantitative impact on the generation of T_{reg} in mice, independent of gluten-induced *Lactococcus garvieae*, and T_{reg} are far more abundant in Peyer's patches than in the spleen.

Vijakrishnaraj *et al*. (2017) developed a wheat gluten induced BALB/c model for addressing wheat gluten related disorders by sensitizing the wheat gluten through route of intraperitoneal and oral challenge in prolonged days. They found that prolonging sensitization of gluten can moderate the antigen-specific inflammatory markers such as IL-1β, IL-4, IL-15, IL-6, IFN-γ, and TNF-α level in mice sera. Histopathology staining of jejunum sections indicated that enterocyte degeneration in the apical part of villi and damage of tight junction in G+ (gliadin and gluten) sensitized murine model.

CONCLUSION

Wheat allergies are a significant public health problem and food safety issue at the global level. Untreated gluten-sensitive enteropathy manifests diarrhea, abdominal distention, developmental delay, severe malnutrition, dental enamel defects and ultimately celiac diseases. Fundamental mechanisms underlying this problem are incompletely understood at present. A number of valuable animal models have been developed for wheat food allergy and anaphylaxis, but not for other types of wheat-induced allergies. Currently, animal models are markedly underutilized to advance mechanistic knowledge on wheat allergies. There are ample opportunities for further improvement of current models as well as to develop new models.

This review work provides insight into the IgEepitope structure of wheat allergens, effects of detergents and other chemicals on wheat allergenicity, and the role of genetics, microbiome, and food processing in wheat allergenicity. This study can also serve as source of experimental models useful for pre-clinical testing tools to develop safer genetically modified wheat, hypoallergenic wheat products, pharmaceuticals and vaccines. The great deal of research work done on gluten allergies and the findings have shed light on newer aspects and approaches towards this greater health issue. Though the detailed mechanism of IgE independent reactions of wheat allergies and uses of less used physiological routes (skin, eyes, airways, oral) of exposure to wheat proteins to elicit sensitization seem to be less explored till now. Treatment of gluten-sensitive enteropathy remained empiric until the middle of the 20th century when patients were noted to improve dramatically after wheat was removed from their diet.

The currently prevalent type 1 diabetes (T1D) and celiac disease (CD) and with their increasing incidence, the potential effects of gliadin intolerance of T1D are alarming. This very common dietary intolerance may increase T1D risks (Galipeau *et al*., 2011) at many folds. A person with gluten intolerance should eliminate gluten from their diet. Specific microbiota-based therapies may aid in prevention in gluten induced enteropathy and the pathobionts are capable of modulating gluten sensitization by increased T cell proliferation and proinflammatory cytokines production.

ACKNOWLEDGEMENTS

We are privileged to convey our sincere gratitude to Prof. Subir Chandra Das Gupta, Head of the Department, Post Graduate Department of Zoology, Maulana Azad College, Kolkata for providing laboratory facilities and financial support under DBT Star College Scheme to conduct the work.

REFERENCES

Balakireva, A.V. and Zamyatnin, A.A.Jr. (2016). Properties of Gluten Intolerance: Gluten Structure, Evolution, Pathogenicity and Detoxification Capabilities. *Nutrients*, 8(10): 644. DOI: 10.3390/nu8100644.

Ciccocioppo, R.,Sabatino, A. D. and Corazza, G. R. (2005). The immune recognition of gluten in coeliac disease. *Clinical and Experimental Immunology*, 140: 408–416. DOI:10.1111/j.1365-2249.2005.02783x

Ejsing-duun, M., Josephsen, J.,Aasted, B.,Buschard, K.and Hansen, A.K.(2008). Dietary Gluten Reduces the Number of Intestinal Regulatory T Cells in Mice.*Scandinavian Journal of Immunology*, 67: 553–559. DOI: 10.1111/j.1365-3083.2008. 02104.x

Galipeau, H.J., Justin, L., Carville, M.,Huebener, S., Litwin, O., Meisel, M.,Jabri, B., Sanz, Y.,Murray, J.A., Jordana, M.,Alaedini, A.,Chirdo, F.Gand Verdu E F. (2015).Intestinal Microbiota Modulates Gluten-Induced Immunopathology in Humanized Mice. *The American Journal of Pathology***,** 185(11): 2969-2982.DOI: 10.1016/j.ajpath.2015.07.018

Galipeau, H.J., Rulli, N.E., Jury, J., Huang, X., Araya, R., Murray, J.A.,David, C.S., Chirdo, F.G., McCoy, K.D., Verdu, E.F. (2011).Sensitization to Gliadin Induces Moderate Enteropathy and Insulitis in Nonobese Diabetic-DQ8 Mice. *Journal of Immunology,*187 (8):4338-4346.DOI: 10.4049/jimmunol.1100854

Gourbeyre, P.,Denery-Papini, S., Larre, C., Gaudin, J.C., Brossard, C.andBodinier, M. (2012). Wheat gliadins modified by deamidation are more efficient than native gliadins in inducing a Th2 response in Balb/c mice experimentally sensitized to wheat allergens. *Molecular Nutrition and Food Research*, 56(2), 336–344. DOI:10.1002/mnfr.201100353

Jin, Y., Acharya H. G., Acharya,D., Jorgensen,R., Gao,H., Secord,J., Ng,P.K.W. and Gangur,V. (2019). Advances in Molecular Mechanisms of Wheat Allergenicity in Animal Models: A Comprehensive Review. *Molecules*, 24, 1142.DOI:10.3390/molecules24061142.

Kozai, H., Yano, H., Matsuda, T., Kato, Y. (2006). Wheat-dependent exercise-induced anaphylaxis in mice is caused by gliadin and glutenin treatments. *Immunological Letter*, 102(1), 83–90.DOI: 10.1016/j.imlet.2005.07.007.

Marsh, M.N.(1992). Gluten, major histocompatibility complex, and the small intestine. *Gastroenterology*, 102:330–54.

Ortiz, T.,Para, R., Gonipeta, B., Reitmeyer, M., He, Y., Srkalovic, I., Ng, P.K.W and Gangur, V. (2016). Effect of extrusion processing on immune activation properties

of hazelnut protein in a mouse model. *International Journal of Food Science and Nutrition*, 67(6), 660–669. DOI: 10.1080/09637486.2016.1191445

Phromraksa, P.,Nagano, H., Boonmars, T., Kamboonruang, C. (2008). Identification of proteolytic bacteria from thai traditional fermented foods and their allergenic reducing potentials. *Journal of FoodScience*, 73, M189–M195. DOI: 10.1111/j.1750-3841.2008.00721.x

Schuppan, D.,Esslinger, B. and Dieterich, W. (2003). Innate immunity and coeliac disease. *Lancet*, 362(9377), 3–4. DOI: 10.1016/S0140-6736(03)13843-3

Schuppan, D. (2000) Current concepts of celiac disease pathogenesis. *Gastroenterology,*119(1), 234–42. DOI:10.1053/gast.2000.8521.

Takahasi, M., Fukunaga, H., Kaneto, H., Fukudome, S., and Yoshikawa, M.(2000). Behavioral and Pharmacological Studies on Gluten Exorphin A5a newly Isolated Bioactive Food Protein Fragment, in Mice. *Japanese Journal ofPharmacology*,84(3),259-264.DOI:10.1254/jjp.84.259

Vanga, S.K., Singh, A. and Raghavan, V.(2017). Review of conventional and novel food processing methods on food allergens. *Critical Reviews in Food Science and Nutrition*, 57(10),2077–2094. DOI: 10.1080/10408398.2015.1045965

Verdu, E.F.,Huang, X., Natividad, J., Lu, J., Blennerhassett, P. A., David, C.S., McKay, D. M. and Murray, J. A. (2007).Gliadin-dependent neuromuscular and epithelial secretory responses in gluten-sensitive HLA-DQ8 transgenic mice. *American Physiological Society-Gastrointestinal Liver Physiology*,294, G-217-225**.**DOI:10.1152/ajpgi.00225.2007

Verhoeckx, K.C.M., Vissers, Y.M., Baumert, J.L., Faludi, R.,Feys, M., Flanagan, S., Herouet-Guicheney, C.,Holzhauser, T.,Shimojo, R.,Van der Bolt, N. *et al*.(2015). Food processing and allergenicity. *Food and Chemical Toxicology*, 80, 223–240. DOI:10.1016/j.fct.2015.03.005

Vijaykrishnaraj, M., Mohan, B.V., Muthukumar, S.P., Kurrey, N.K., and Prabhasankar, P. (2017).Antigen-specific gut inflammation and systemic immune responses induced by pro-longing wheat gluten sensitization in BALB/c murine model.*Journal of Proteome Research*, DOI: 10.1021/acs.jproteome.7b00199

Wieser, H. (2007). Chemistry of gluten proteins. *Food Microbiology*, 24, 115–119. DOI: 10.1016/j.fm.2006.07.004

Yokooji, T., Fukushima T, Hamura K, Ninomiya N, Ohashi R, Taogoshi T, Matsuo H. (2018). Intestinal absorption of wheat allergen gliadin in rats. *Allergology International*, DOI:10.1016/j.alit.2018.11.005

Zioudrou, C.,Streaty,R.A. and Klee, W. A.(1979). Opioid peptides derived from foood proteins, the exorphins. *Journal of Biological Chemistry*, 254(7),2446-2449.PMID: **372181.**

How to cite this article:

Sanjukta Manna, Taniya Mondal and Ayantika Mitra.2020, Gluten Induced Inflammatory Responses in Murine Model: an Overview. *Int J Recent Sci Res.* 11(07), pp. 39147-39151. DOI: http://dx.doi.org/10.24327/ijrsr.2020.1107.5450

****

MEDWIN PUBLISHERS
Committed to Create Value for Researchers

Advances in Clinical Toxicology
ISSN: 2577-4328

Black Tea (*Camellia sinensis*) Extract Induced Changes on Placenta can Alter Fetal and Neonatal Bone Health in Experimental Animal Model

Dey A[1], Gomes A[2], Chakraborty K[3] and Dasgupta SC[4]*

[1]Department of Zoology, Ramakrishna Mission Vidyamandira, Belur Math, India
[2]Department of Physiology, University of Calcutta, India
[3]Department of Zoology, S.B.S. Government College, Hili, India
[4]Department of Zoology, Maulana Azad College, India

Research Article
Volume 5 Issue 4
Received Date: December 10, 2020
Published Date: December 24, 2020
DOI: 10.23880/act-16000201

***Corresponding author:** Subir Chandra Dasgupta, Professor & Head, Post Graduate Department of Zoology, Maulana Azad College, 8, Rafi Ahmed Kidwai Road, Kolkata 700013, West Bengal, India, Tel: +919830471981; Email: subirdgupta@gmail.com

Abstract

Tea (*Camellia sinensis*) being the most consumed beverage worldwide. The safety evaluation of tea needs to be monitored during pregnancy, prenatal and postnatal developmental period beside its beneficial roles toward health and disease. Retardation of growth of fetus and neonates are common in preeclampsia. Present study was to evaluate the role of Black Tea extract (BTE) on placental and apoptotic markers in pregnant Wister albino rats and to correlate it the growth of fetus and pups. Among three experimental groups, Group 1 was pregnant female rats treated with saline, were the control group. Group 2 and Group 3 were pregnant female rats treated with 50 mg and 100 mg BTE/kg/day, p.o. respectively throughout prenatal and postnatal periods. Expressions of BMP-7, MMP-2 and VEGFR2 in placenta were examined by flow cytometry; Bax, Bcl-2 and caspase-3 expressions in uteri and placenta were observed by IHC. Bone health of fetus and pup were checked by histology, bone-cartilage double staining and estimation of bone mineral density by ICP-MS. Experimental data were subjected to the ANOVA; expressed as mean ± standard deviation with significance ($P < 0.05$) between the controls and the treated groups ($n = 6$). BTE increased the level of MMP-2, Bax and caspase-3; decreased the level of BMP-7 in placenta. In fetus and pups, BTE significantly decreased the concentration of Ca^{2+}, P, Mg^{2+} and Zn^{2+} in bone and decreased the rate of ossification were observed. This study confirmed BTE induced preeclampsia retarded the fetal and neonatal bone health in experimental animal model.

Keywords: Black Tea Extract; Pregnancy; Preeclampsia; Fetal-Neonatal Bone Health

Abbreviations: BTE: Black tea extract; FACS: Fluorescence-activated cell sorting; ICP-MS: Inductively coupled plasma-mass spectrometry; PBS: Phosphate buffered saline; FCS: Fetal calf serum; IHC: Immunohistochemistry.

Introduction

Tea (*Camellia sinensis*) is native to the different Asian countries like China, India, Laos, Thailand, Vietnam, and Myanmar [1]. Tea is one of the most widely consumed beverages in the world, with a global market comprising of four major zones: Asia-Pacific, Europe, North America and Africa [2,3]. The tea is second only to water in terms of worldwide consumption and presently tea is cultivated in over thirty countries around the world [4,5]. Tea is classified into three types; green tea, black tea and oolong tea. The classification of tea is based on the fermentation and oxidation of the polyphenols in the tea leaves during production [6]. Green

tea is the non-fermented form of tea, in which the oxidation of the tea polyphenols called catechins is prevented and thus, most of the catechins are preserved during its processing. Black tea and oolong tea are respectively fully fermented and semi-fermented tea leaves. In black tea and oolong tea, leaf polyphenolics are allowed for aerobic oxidation and the catechins are enzymatically catalysed to form theaflavins and thearubigins [4,7]. In case of black tea the reaction is carried out to maximize the oxidation (fermentation) but for oolong tea reaction is stopped usually half-way before it is completely oxidised. There are two main types of black tea; orthodox (rolling) black tea and CTC (crushing, tearing and curling) black tea, produced through various stages including withering, rolling, drying and grading [8]. Tea and its bioactive components have the potential in disease prevention and are effective in therapy. Both green tea and black tea are cardio protective [9,10], antioxidant and anti-inflammatory [11,12], has anti-cancer effects [13,14], anti-obese effects [15], neuroprotective effects [16]. Despite the increasing demand for tea and its active constituents, few studies have reported their safety. Tea has numerous beneficial roles towards health and disease but its safety evaluation during pregnancy and prenatal as well as in postnatal developmental period need to be monitored. Very few studies have been reported regarding tea extract consumption and its effect during pregnancy in animal models [17,18]. Pu-erh black tea a highly fermented version of black tea is associated with development of fetal toxicity at a high concentration [19]. Preeclampsia is a disease of late pregnancy characterized by increased maternal blood pressure, proteinuria, increase in pro-inflammatory cytokine and decrease in anti-inflammatory cytokine [20,21]. According to Dey, et al. [22] black tea induced preeclampsia in experimental Wister albino rat [22]. In the present study, an attempt has been made to assess the effect of varying doses of black tea extract (BTE) on some placental and apoptotic markers that caused preeclamsia in pregnant rats which may further leads to retardation of growth in fetus and pups.

Materials and Methods

Chemicals

Absolute alcohol (ethanol) and Methanol (Merck, India), Alcian blue 8GX (Sigma-Aldrich, USA), Alizarin Red S (Sigma-Aldrich, USA), Anti-rat Alexa Fluor 488-MMP-2 (Novus Biologicals, USA) for FACS, Anti-rat Bax, Bcl2, caspase-3 (Santa Cruz Biotechnology, United States) for immunohistochemistry, Anti-rat FITC BMP-7 (Milli-Mark, USA) for FACS, Anti-rat PE VEGFR2 (BioLegend, USA) for FACS, Avitin-Biotin Conjugate (Thermo Fisher Scientific, United States) for immunohistochemistry, Benzyl alcohol (Milli-Mark, India), Biotin-conjugated anti-rat secondary antibodies (Thermo Fisher Scientific, United States) for immunohistochemistry, Collagenase (type IV) (Himedia, India), DAB substrate and diluent (Thermo Fisher Scientific, United States) for immunohistochemistry, DPX (LOBA Chemie, India), Di-sodium hydrogen phosphate (SRL, India), Sodium di-hydrogen phosphate (SRL, India), Eosin (Sigma, USA), Fetal calf serum (Sigma-Aldrich, USA), Formaldehyde solution 37-41% w/v (Merck, India), Glacial Acetic Acid (Merck, India), Glycerol anhydrous (Milli-Mark, India), Hematoxylin (Merck, Germany), Hydrogen peroxide (Milli-Mark, India), Paraffin wax 56-58°C (Merck, India), Nitric acid (Milli-Mark, India), Potassium hydroxide (Merck, India), Salt mixture H.M.W. (SRL, India), Sodium chloride (SRL, India), Tri-sodium citrate (Merck, India), Trizma® base (SRL, India), Tween-20 (Milli-Mark, India), Xylene (Merck, India).

Animals

Male (150±10 g) and female (120±10 g) wister albino rats were obtained from the enlisted supplier of CPCSEA (Committee for the Purpose of Control and Supervision of Experiments on Animal), India. Rats were kept in polypropylene cages (421×290×190mm) at controlled temperature (25±2°), light condition (12h light and dark cycle) and relative humidity (65±5%). The animals were provided with pellet diet, green vegetables, gram and water *ad libitum*. All animals for this experiment were kept in CPCSEA approved animal house (vide F. No. - 25/250/2012-AWD, dated 26.2.2014) of Maulana Azad College, Kolkata. Experiments described in this study were done by following the guideline of the CPCSEA, Government of India.

Collection of Black Tea

Fresh black tea (C.T.C., Assam) was purchased from authenticated tea supplier M/S. Subodh Brothers Pvt. Ltd., Kolkata-700012, India.

- **Preparation of black tea extract and treatment schedule**

Black tea extract (BTE) was prepared after Dey, et al. [22]. First, 1 g black tea was added into 100 ml of boiled drinking water, was kept covered for 5 minutes, filtered by a tea strainer. The dry weight of 100 ml freshly prepared BTE was calculated by evaporating the water from which is equivalent to one cup of black tea liquor. Dry weight of BTE/ml was also calculated in the same way by adding 1 g of black tea in 6 ml boiled drinking water. 50 mg and 100 mg BTE/kg b.w./day, p.o. were the two doses selected for treatment which are equivalent to 5 cup and 10 cup BTE respectively in human considering 60 kg as average body weight of an adult human. 1 g of black tea was added in 6 ml boiled drinking water, was kept covered for 5 minutes, filtered and cooled down to 40°C.

200 µl and 400 µl BTE from this liquor was administered orally to achieve respective dose of 50 mg and 100 mg BTE/kg b.w./day. The doses were administered orally by the help of oral gavage to the pregnant rats throughout their prenatal (21 days) and postnatal periods of time (21days).

Experimental Design

The pregnant rats were selected by pairing a pro-estrous female overnight with two male rats of proven fertility and determining the vaginal sperm count on the following day (9:00 to 9:30 a.m.) using an improved Neubauer haemocytometer. Rats with vaginal sperm counts >45×10^6/ml were selected and considered as at day 0 of pregnancy. For this study three animal groups were chosen (n=8 per group). Group 1 was the control group where the pregnant female rats were treated with saline. Group 2 and Group 3 were pregnant female rats treated with 50 mg and 100 mg BTE/kg body weight/day, p.o. respectively. Both the doses of BTE were administered in the pregnant rats throughout their prenatal (21 days) and postnatal periods (21days) of time. All three groups of rats were provided with pellet diet, gram, green vegetables and drinking water *ad libitum*.

Isolation of Placenta and Uterus

Pregnant rats (on day 20) of three different groups were euthanized according to CPCSEA approved procedures. Uterine horns were picked up, collected by using scissors at each distal end, placed in a petri dish filled with PBS and place on ice, washed several times with PBS before isolating the placenta. The endometrial tissue was carefully peeled out surrounding the embryo conceptuses. Isolated conceptuses were placed in a new petri dish with PBS on ice and continue until all conceptuses have been freed from the endometrium. Conceptuses were transferred to a new petri dish with PBS placed under the microscope and with two forceps peel the decidua away from the placenta. Yolk sacs, excess giant cell tissue at the edges of the placenta were removed in order to minimize cell clumping during preparation of single-cell suspension. Placentas for FACS analysis were collected in a 15-ml Falcon tube, with PBS+5% FCS and on ice [23]. Uteri and placenta of different groups were fixed in 10% neutral buffered formalin for immunohistochemistry.

- **Study of placental BMP-7, MMP-2 and VEGFR2 positive cells population by flow cytometry**

0.1% Collagenase solution in PBS with 10% FCS was prepared and was added into placenta (5ml/placenta). 16-G needle fitted on a 5-ml syringe was used to mechanically disrupt the tissue by passaging the collagenase solution and placenta through the needle 3 times. It was repeated with an 18-G needle. The mixture was placed in a 37°C, 5% CO_2 incubator for 45 minutes. After that the cell solution was passed through a 20-G needle, and incubate for an additional 45 minutes, in 37°C. After the 1.5 hr total incubation in collagenase, cell solution was passed through 22-G and 25-G needles 3 times with each needle [23]. Placental digests were filtered through a 40µm nylon cell-strainer and red blood cells were removed by centrifuging the placental digests at 4°C for 5 minutes at 2000 rpm using RBC lysis buffer solution. Next cells were washed, counted and re-suspended in PBS to make single-cell suspension. Accurate cell count was taken and then cells were divided into aliquots having 10^6cells/100 µl of cell staining buffer (CSB), containing 3% foetal calf serum (FCS). Further the cells were incubated with the titrated amount of anti-rat PE (Phycoerythrin dye)-CD309 (VEGFR2, Flk-1), FITC (Fluorescein isothiocyanate dye) BMP-7, Alexa Fluor 488 – MMP-2, fluorochrome-conjugated primary antibody in the dark, and incubated for 1 h [24]. Finally the cells were washed and the pellets were resuspended in 100µl CSB and were analyzed using BD FACSVerse flow cytometer and BD FACSuite ™ Software.

- **Immunohistochemistry of placental Bax, Bcl-2 and caspase-3**

For immunohistochemistry (IHC) Uteri and placenta of different groups were fixed in 10% neutral buffered formalin. Tissues were then dehydrated in graded (50-100%) ethanol followed by clearing in xylene. Paraffin (56°C-58°C) embedding was done at 58±1°C for 4 h, followed by paraffin block preparation. 4µm thick paraffin embedded section was cut with a rotary microtome (Weswox model MT-1090, India). Tissue sections were mounted on poly-L-Lysine coated slides. Sections were deparaffinised, dehydrated through graded alcohols, antigen retrival was done by 10mM sodium citrate and endogenous peroxidase was quenched by 3% hydrogen peroxide (H2O2). After blocking with 1% foetal calf serum (FCS) in tris buffer saline (TBS), the sections were incubated in a humid chamber overnight at 4°C with primary antibodies like anti-rat Bax, Bcl2, caspase-3 (Santa Cruz Biotechnology, United States). After washing in wash buffer (1% Tween 20 in TBS or 1X TBST), sections were incubated in biotin-conjugated anti-rat secondary antibodies diluted in Tris-buffered saline (TBS) for 2 hours at room temperature. After washing in 1X TBST sections were incubated in Avidin-Biotin Conjugate (ABC) for 30 minutes. Immunoreactivity was detected using a DAB system. Sections were then counterstained briefly in hematoxylin, dehydrated through graded alcohols, cleared in xylene, and cover-slipped with DPX [25,26]. Images were captured and changes were observed with bright field microscope (ZEISS, Germany) and photographs were taken by using ZEISS AxioCam ICc1 and Zen software (Zen2 lite) at 100X magnification. Quantification of Bax, Bcl2, caspase 3

positive cells was calculated by ImageJ software. Percentage of placental cells positive for Bax, Bcl-2 and caspase 3 was calculated separately by ImageJ. An average of 20 fields was observed for three different groups. The ratios of the Bax : Bcl-2 was calculated.

Bone and Cartilage Double Staining of Pups

Day 0 pups of three different groups were collected etherized and were put into 4% NaCl solution for overnight at 4°C. On next day fetuses were skinned and eviscerated, the cervical and dorsal muscles gently removed. The specimens were immediately placed in the acid staining solution (pH 2.8) for at least 24 hr at room temperature. It was then dehydrated in ethanol 96% for at least 6 hr. Maceration of soft tissues was performed by placing specimens in the basic staining solution for 30 hr at room temperature, while renewing the solution at least three times. Clearing and hardening was performed by placing specimens in the cleaning solution for at least 8 hr. Conservation of double-stained fetuses was performed in a 1:1 ethanol 70% and glycerin mixture [27].

The acid staining solution (pH 2.8) made up of 5 parts 0.14% Alcian blue (dissolved in 70% ethanol, filtered),1 part of 0.12% Alizarin red S (dissolved in 96% ethanol, filtered), 8 parts glacial acetic acid and 50 parts 70% ethanol. On the other hand the basic staining solution consisted of 250 parts 0.7% KOH (dissolved in distilled water) and 1part 0.5% Alizarin red S (dissolved in distilled water, filtered). The clearing solution consisted of 2 parts 70% ethanol, 2 parts glycerin and 1 part benzyl alcohol.

Estimation of Bone Mineral Density of Pups

Left femur was collected from day 20 foetus and day 21 pups of three different groups. Bone marrow was cleaned out from the bones. Bone (left femur) ash was prepared in a muffle furnace (700°C×6 h) [28] and dissolved in 5% HNO_3. Bone minerals (Ca^{2+}, P, Mg^{2+} and Zn^{2+}) were measured by using Inductively Coupled Plasma – Mass Spectroscopy (ICP-MS) (ThermoFisher-Scientific X-series 2, Massachusetts, USA). The samples were ran with respect to previously known concentrations of the elements to determine their respective values. Measurement of samples were carried using standard curves having regression values greater than 0.99.

Histology of Femur of Pups

Femurs were dissected out from day 21 pups of three different groups; bone marrow was washed out by flushing double distilled water through femur. Then the bones were suspended in osteomoll for decalcification [29]. After the tissue became soft the tissues were fixed in 10% neutral buffered formalin for 24 h. Tissues were then dehydrated in graded (50-100%) ethanol followed by clearing in xylene. Paraffin (56°C-58°C) embedding was done at 58±1 °C for 4 h, followed by paraffin block preparation. 4µm thick paraffin embedded section was cut with a rotary microtome (Weswox model MT-1090, India). Xylene was used to deparaffinise the paraffin sections, and then counter stained with haematoxyiln-eosin and was mounted in DPX with a cover slip. Images were captured and changes were observed with bright field microscope (ZEISS, Germany) and photographs were taken by using ZEISS AxioCam ICc1 and Zen software (Zen2 lite) at 100X magnification.

Statistical Analysis

The data generated on various parameters were subjected to statistical analysis were expressed as means and standard deviation (mean ± SD) or mean ± SEM with significance between the controls and the treated. Collected data were subjected to one-way analysis of variance (ANOVA) considering p-values of <0.05 were considered as significant. SPSS 17.0 software (IBM Corporation, United States) was used for statistical analysis.

Results

Expression of BMP7+VEGFR2+ and MMP2+VEGFR2+ Double Positive Cell Population

FACS analysis showed no significantly ($p<0.05$) changes were found in BMP7+VEGFR2+ cell population of three different experimental groups (Figure 1A,B). Interestingly, the percentage of BMP7+ cells is significantly ($p<0.05$) decreased in group 3 as compared to control group (Figure 1A,C). On the other hand, BTE (100 mg /kg body weight/day, p.o.) significantly ($p<0.05$) decreased MMP2+VEGFR2+ cell population compared to control group (Figure 2 A,B) whereas administration of BTE (100 mg /kg body weight/day, p.o.) significantly ($p<0.05$) increased MMP2+ cells percentage in group 3 compared to control group (Figure 2 A,C).

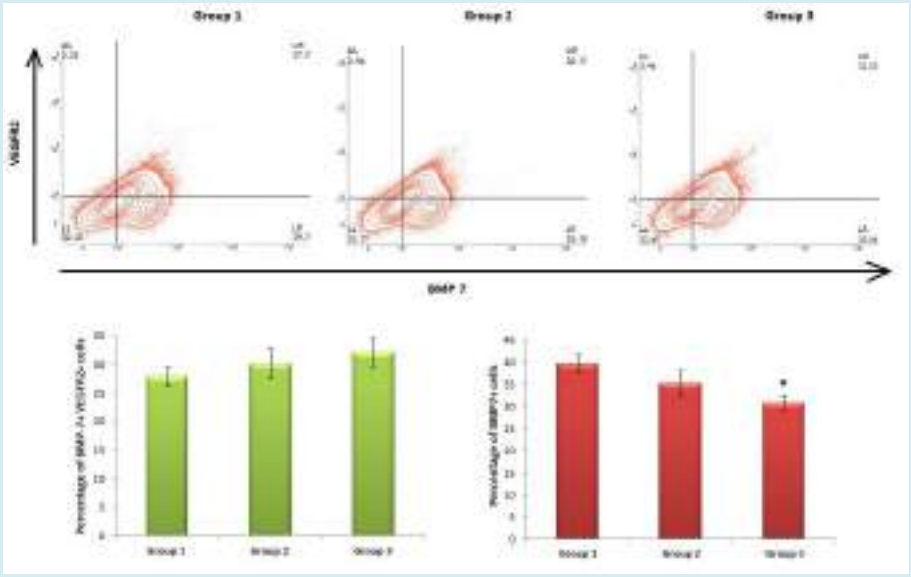

Figure 1: Expression pattern of BMP7+VEGFR2+ double positive cell population. (A) Contour plots of BMP7-VEGFR2 were obtained from the single cell suspension prepared from placenta. (B) Bar diagram representing percentage of BMP7+VEGFR2+ double positive cells. (C) Bar diagram representing percentage of BMP7+ positive cells. Data represent the mean±SD (n=6). *p< 0.05 when compared to animals of group 1. Gr. 1: control group, Gr. 2: pregnant female rats treated with BTE (50 mg BTE/kg body weight/day, p.o.), Gr.3: pregnant female rats treated with BTE (100 mg BTE/kg body weight/day, p.o.).

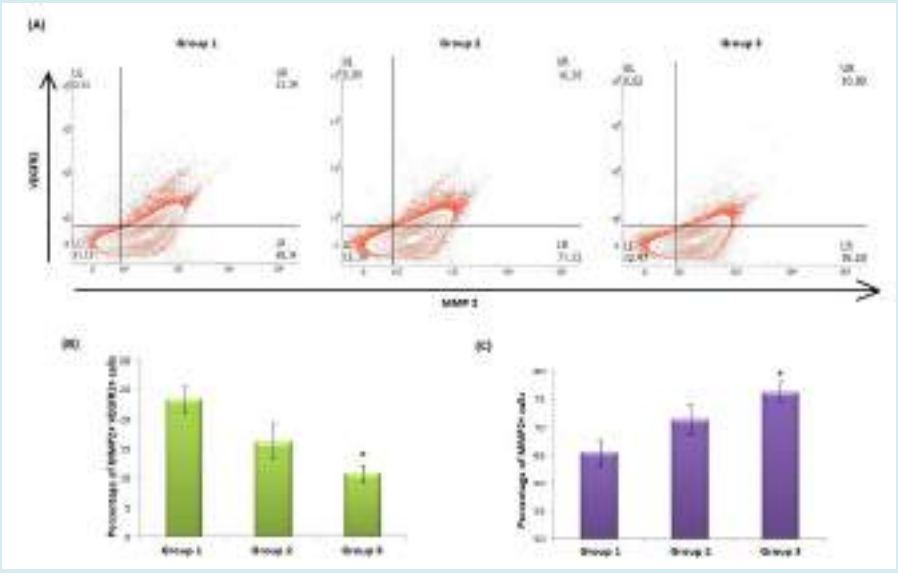

Figure 2: Expression pattern of MMP2+VEGFR2+ double positive cell population. (A) Contour plots of MMP2-VEGFR2 were obtained from the single cell suspension prepared from placenta. (B) Bar diagram representing percentage of MMP2+VEGFR2+ double positive cells. (C) Bar diagram representing percentage of MMP2+ positive cells. Data represent the mean±SD (n=6). *p< 0.05 when compared to animals of group 1. Gr. 1: control group, Gr. 2: pregnant female rats treated with BTE (50 mg BTE/kg body weight/day, p.o.), Gr.3: pregnant female rats treated with BTE (100 mg BTE/kg body weight/day, p.o.).

Expression of Bax, Bcl-2 and Caspase-3

Immunohistochemistry showed BTE (100 mg /kg body weight/day, p.o.) increased the expression of Bax, Bcl-2 and caspase-3 in placenta and uteri compared to control group. Orange coloured dots indicate the antibody binding region. BTE (50 mg /kg body weight/day, p.o.) showed no significant changes in placenta and uteri (Figures 3 & 4).

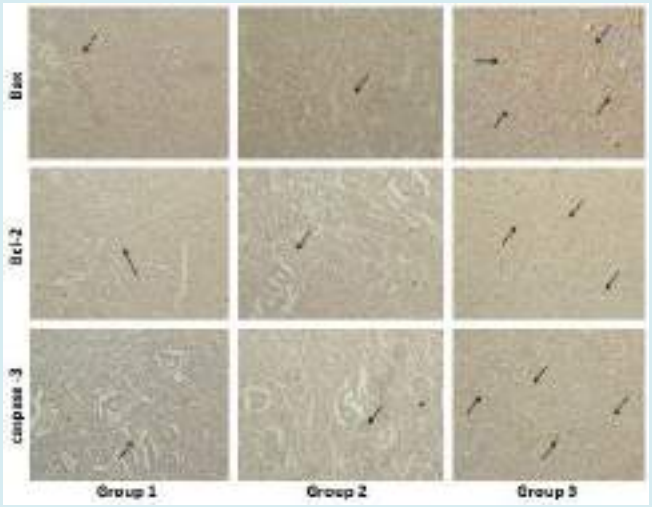

Figure 3: Localization of Bax, Bcl-2 and caspase-3 positive cells in placenta examined by immunohistochemistry (100X magnification). Gr. 1: control group, Gr. 2: pregnant female rats treated with BTE (50 mg /kg body weight/ day, p.o.), Gr.3: pregnant female rats treated with BTE (100 mg /kg body weight/day, p.o.). Black arrow indicating the expression of respective antibodies in placenta of three different groups of mothers on day 20.

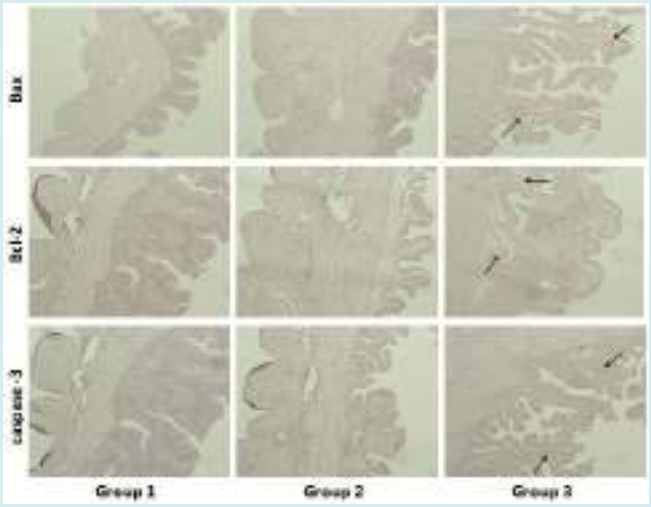

Figure 4: Localization of Bax, Bcl-2 and caspase-3 positive cells in uteri examined by immunohistochemistry (100X magnification). Gr. 1: control group, Gr. 2: pregnant female rats treated with BTE (50 mg /kg body weight/day, p.o.), Gr.3: pregnant female rats treated with BTE (100 mg / kg body weight/day, p.o.). Black arrow indicating the expression of respective antibodies in uteri of three different groups of mothers on day 20.

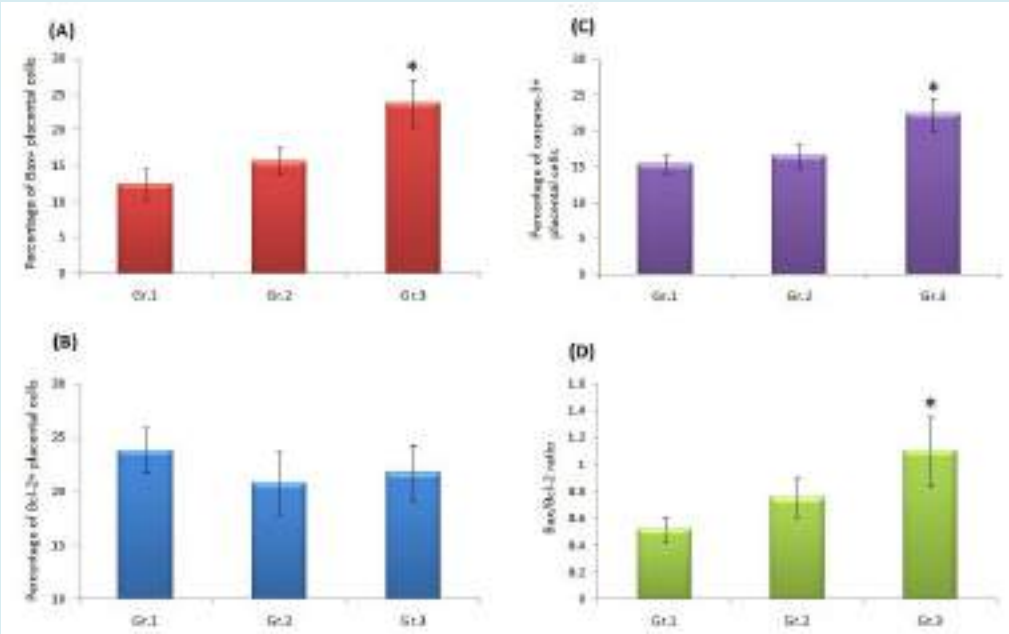

Figure 5: Quantitative expression of Bax, Bcl-2 and caspase-3 positive cells in placenta. (A) Histogram showing the percentage of Bax+ placental cell population, (B) Percentage of Bcl-2+ placental cell population, (C) Percentage of caspase-3+ placental cell population, (D) Bax/Bcl-2 ratio of placental cell population in three different groups. Data represent the mean±SD (n=6). *p< 0.05 when compared to animals of group 1. Gr. 1: control group, Gr. 2: pregnant female rats treated with BTE (50 mg /kg body weight/day, p.o.), Gr.3: pregnant female rats treated with BTE (100 mg /kg body weight/day, p.o.).

Quantitative analysis by ImageJ software showed percentage of Bax+ and caspase-3+ placental cell population were significantly ($p<0.05$) increased in Group 3 mother compared to Group 1 (Figure 5 A,C). There was no significant alteration in Bcl-2+ placental cell population in all experimental groups (Figure 5B). The Bax/Bcl-2 ratio was also significantly ($p<0.05$) increased in Group 3 placenta compared to Group 1 (Figure 5 D).

Effect of BTE on Bone and Cartilage

Bone and cartilage double staining of day 0 pups showed rate of ossification of carpus, metacurpus, phalanges of fore limbs and tarsus, metatarsus, phalanges of hind limbs was lesser in Gr.2 and Gr.3 pups compared to Gr.1 pups. An unstained gap was found between parietal bones of skull in pups of Gr.2 and Gr.3 mothers. Parietal bones were complete and no gap was found in Gr.1 pups (Figure 6).

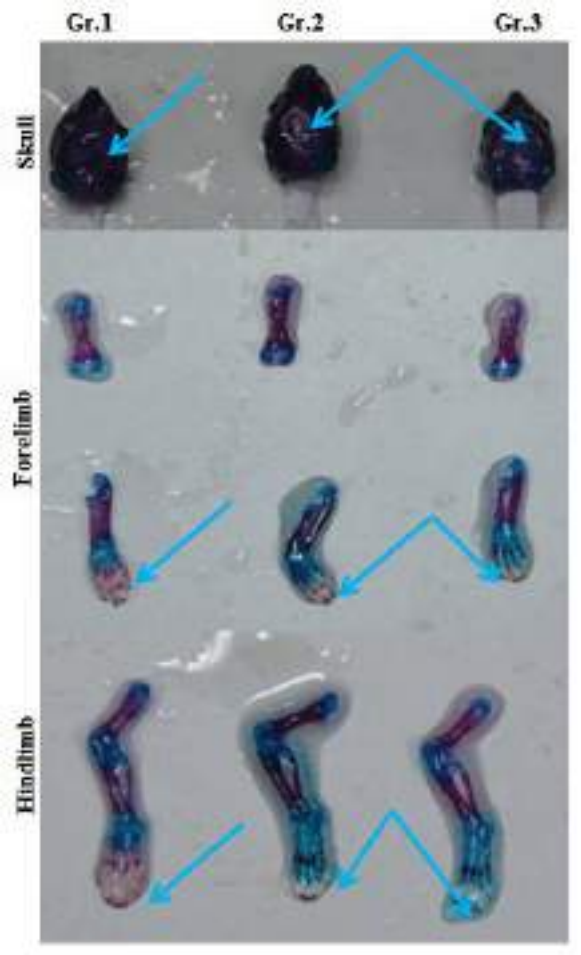

Figure 6: Bone and cartilage double staining of day 0 pups (Alcian blue- Alizarin red counterstaining). Blue colour indicates cartilaginous part and red colour indicates ossified part. Gr. 1: pups of control group, Gr. 2: pups of pregnant female rats treated with BTE (50 mg /kg body weight/day, p.o.), Gr.3: pups of pregnant female rats treated with BTE (100 mg /kg body weight/day, p.o.). Blue arrows are indicating the changes in rate of ossification in different regions of skeleton of pups of three experimental groups.

Effect of BTE in Bone Mineral Density of Pups

Inductively Coupled Plasma-Mass Spectroscopy data showed Ca^{2+}, P, Mg^{2+} and Zn^{2+} levels were significantly decreased ($p<0.05$) in day 20 fetus and day 21 pups of Group 2 (50 mg BTE /kg body weight/day, p.o.) and Group 3 (100 mg BTE/kg body weight/day, p.o.) mothers compared to Group 1 (Table 1).

Group of animals	Bone minerals of day 20 fetus (µg/g) (Prenatal Period)				Bone minerals of day 21 pup (µg/g) (Postnatal Period)			
	Ca^{+2}	P	Mg^{+2}	Zn^{+2}	Ca^{+2}	P	Mg^{+2}	Zn^{+2}
Group 1	2.862±0.077	13.234±0.276	2.297±0.121	0.328±0.05	59.475±2.173	222.241±5.938	3.395±0.237	3.269±0.218
Group 2	1.661±0.036*	9.443±0.12*	1.409±0.008*	0.298±0.005	40.475±0.812*	150.45±2.148*	2.471±0.046*	2.705±0.124*
Group 3	1.225±0.01*	6.8625±0.067*	1.151±0.025*	0.186±0.009*	36.665±0.93*	134.7±3.153*	2.055±0.09*	1.934±0.058*

Table 1: Effect of BTE on bone minerals in fetus and pups different groups of female albino rats.
Values shown are Mean±SEM (n = 8), *p < 0.05, Gr. 1: control group, Gr. 2: pregnant rats treated with BTE (50 mg BTE/kg body weight/day, p.o.), Gr.3: pregnant rats treated with BTE (100 mg BTE/kg body weight/day, p.o.).

Histological changes in femur

BTE (100 mg BTE/kg body weight/day, p.o.) remarkably altered the zone of proliferation (zp) region and zone of hypertrophy (zh) with reduced epiphyseal growth plate (egp) in the femur of group 3 pups compared to group 1 pups on day 21 of lactation. No significant changes were found in the group 2 pups (Figure 7).

Figure 7: Histology of femur of pups on day 21 of lactation period (H-E counterstaining, 40X magnification). Zp= zone of proliferation, zh=zone of hypertrophy, egp= epiphyseal growth plate. Gr. 1: pups of control group, Gr. 2: pups of pregnant female rats treated with BTE (50 mg /kg body weight/day, p.o.), Gr.3: pups of pregnant female rats treated with BTE (100 mg /kg body weight/day, p.o.).

Discussion

Preeclampsia is linked to alterations of placental function leading to stress and apoptotic signalling which can lead to defects in the offspring. Apoptotic and stress signalling are augmented in preeclampsia placenta and cord tissue that alter the intrauterine environment and activates the detrimental signaling that is transported to fetus [30]. In the present study, IHC of placenta and uteri showed BTE (100 mg BTE/kg body weight/day, p.o.) increased the expression of Bax and caspase-3 which may be an indication of preeclampsia. BTE (100 mg BTE/kg body weight/day, p.o.) also increased the Bax/Bcl-2 ratio compared to control group.

Matrix metalloproteinase is a family of proteolytic enzymes, able to degrade extracellular matrix & basement membrane components. Activity and localization of MMP2 and 9 in vitro systems (tissue culture and amniotic fluid) were examined in several studies. Omran, et al. (2011) found strong MMP-2 protein expression in the majority of the preeclamptic placentas. MMP-2 also restricted intrauterine growth which may lead to remarkable low mean birth weight in patients with preeclampsia [31]. It was found that before the appearance of clinical symptoms, the plasma concentrations of MMP-2 was elevated in preeclamptic women. MMP-2 may play a role in causing hypertension during pregnancy through multiple complex pathways [32]. On the other hand, Bone Morphogenetic Protein 7 (BMP-7) is the member of the transforming growth factor β superfamily. In an experiment, BMP-7 was found to be a potent apoptotic signals for the undifferentiated limb mesoderm which was a potent inhibitory factor for joint formation exhibit an intense expression in the perichondrium of the developing cartilages [33]. BMP7 is an important factor during the process of implantation that contributes to healthy embryonic development [34]. The primary receptor for vascular endothelial growth factor (VEGF) is vascular endothelial

growth factor receptor 2 (VEGFR-2), a crucial receptor involved in normal endothelial function. Significantly decrease in VEGFR-2 transcript and protein levels were found in preeclamptic placentae. Nevo, et al. (2013) showed a novel hypoxia-induced and preeclampsia-related down-regulation of VEGFR-2 in the human placenta. In hypoxic conditions and preeclampsia, sFlt-1 (Soluble fms-like tyrosine kinase-1) was found to be increased by which the VEGFR-2 expression and signaling get attenuated. A direct interaction between sFlt-1 and VEGFR-2 was involved in VEGFR-2 regulation, inhibition of VEGFR-2-mediated processes during placentation and also a novel platform to examine the onset of preeclampsia [35]. In the present study we found, BTE (100 mg /kg body weight/day, p.o.) significantly ($p<0.05$) increased MMP2+ placental cells but MMP2+VEGFR2+ and BMP7+ cell populations were decreased compared to control group. So it was clear that BTE (100 mg /kg body weight/day, p.o.) induced higher expression of MMP-2 and decreased level of BMP-7 causing preeclampsia and restriction in intrauterine growth. There was a further trigger of the apoptotic signal which might be responsible for increased the expression of Bax and caspase-3 and also increased the Bax/Bcl-2 ratio in BTE (100 mg /kg body weight/day, p.o.) treated rats compared to control group.

It was established the principal caffeine metabolism enzyme, cytochrome CYP1A2, is absent in the placenta and fetus [36]. Caffeine which is also a constituent of tea can freely passes through the placental barrier from the mother to the fetus and hence, maternal caffeine intake during pregnancy directly influences fetal caffeine exposure levels [37,38]. Fetal exposure to caffeine increases circulating catecholamine concentrations, which might subsequently lead to fetoplacental vasoconstriction and hypoxia [19] and eventually affect fetal growth and development [40-42]. In a study, pu-erh black tea a highly fermented version of black tea is associated with development of fetal toxicity at a high concentration [19]. Though in another study there was no heat-sterilized green tea catechins (GTC-H) related fetal malformations or developmental variations [42].

Dey, et al. biomorphometric parameters like cranial length, cranial diameter, neck width, craniosacral length and tail length showed BTE retards the growth of pups but no significant changes were found in terms of time taken to open eyes, eruption of incisors and appearance of fur [22]. In present study, it was found that BTE decreased the bone mineral density of fetus and pups. It was clearly evident that BTE significantly decreased the concentration of Ca^{2+}, P, Mg^{2+} and Zn^{2+} in bone in dose dependent manner and decreased the rate of ossification. BTE (100 mg BTE/kg body weight/day, p.o.) remarkably altered the normal growth of bone as the zone of proliferation (zp) region and zone of hypertrophy (zh) with reduced epiphyseal growth plate (egp) in the femur of pups were noticed. These findings also supported the proposed findings. The animal results are also applicable to human. This study is the first time effort to establish the effect of Black tea extract at high dose on mother and pups during pregnancy and lactation period. Till now it is not clear which active component(s) of black tea is/are responsible for this negative action. On the other hand black tea constituents vary with internal and external factors. So different black tea varieties may affect prenatal and postnatal health in different level. The usage of different pesticides and herbicides in the tea gardens should not be ignored which may alter the health and hygiene of tea consumers. Further studies are warranted to establish the BTE induced changes at molecular level and physiological changes during pregnancy and development of embryos.

Conclusion

In conclusion, BTE increased the level of MMP-2, Bax and caspase-3 whereas decreased the level of BMP-7 in placenta which was an indication of preeclampsia. In fetus and pups, BTE significantly decreased the bone mineral density and the rate of ossification which were the outcomes of preeclampsia. This study confirmed BTE induced preeclampsia during pregnancy retarded the bone growth of fetus and pups in experimental animal model.

Acknowledgements

Authors would like to thank the Post Graduate Department of Zoology, Maulana Azad College, Kolkata for instruments facility and Department of Zoology and West Bengal State University for assisting in flow cytometry and its data analysis. Authors also thankful to the National Tea Research Foundation, Tea Board, India for financial assistance to carry out the present investigation. This research work was supported by the National Tea Research Foundation, Tea Board, India [Code No. NTRF: 164/2014; Ref No. NTRF: 17(305)/2013/4423 dated 11th March, 2014].

Conflict of Interests

The authors declare there is no conflict of interests exists.

References

1. Balentine DA, Harbowy ME, Graham HN (1998) Tea: The plant and its manufacture; chemistry and consumption of the Beverage. In: Spiller GA (Eds), Caffeine. Boca Raton, CRC Press, pp: 37-68.

2. Modder WWD, Amarakoon AMT (2002) Tea and Health. Tea Research Institute, Talawakelle, Sri Lanka, pp: 1-179.

3. Skotnicka M, Chorostowska-Wynimko J, Jankun J, Skrzypczak-Jankun E (2011) The Black tea bioactivity: an overview. Cent Eur J Immunol 36(4): 284-292.

4. Graham HN (1992) Green tea composition, consumption, and polyphenol chemistry. Prev Med 21(3): 334-350.

5. Wong CC, Cheng K, Chao J, Peng X, Zheng Z, et al. (2009) Analytical methods for bioactive compounds in teas. In: Ho CT, ett al. (Eds.), Tea and tea products: Chemistry and health-promoting properties. Boca Raton, CRC Press, pp: 77-110.

6. Hara Y (2001) Green tea: Health benefits and applications. Marcel Dekker Inc, New York.

7. Wan X, Li D, Zhang Z (2009) Green tea and black tea manufacturing and consumption. In: Ho CT, et al. (Eds.), Tea and tea products: Chemistry and health promoting properties. Boca Raton, CRC Press, pp: 1-8.

8. Astill C, Birch MR, Dacombe C, Humphrey PG, Martin PT (2001) Factors affecting the caffeine and polyphenol contents of black and green tea infusions. J Agric Food Chem 49(11): 5340-5347.

9. Jochmann N, Lorenz M, Krosigk A, Martus P, Bohm V, et al. (2008) The efficacy of black tea in ameliorating endothelial function is equivalent to that of green tea. Br J Nutr 99(4): 863-868.

10. Singh DK, Banerjee S, Porter TD (2009) Green and black tea extracts inhibit HMG-CoA reductase and activate AMP kinase to decrease cholesterol synthesis in hepatoma cells. J Nutr Biochem 20(10): 816-822.

11. Roy DK, Kumar KT, Karmakar S, Pal S, Samanta SK, et al. (2008) Pharmacological studies on Indian black tea (leaf variety) in acute and chronic inflammatory conditions. Phytother Res 22(6): 814-819.

12. de Mejia EG, Ramirez-Mares MV, Puangpraphant S (2009) Bioactive components of tea: cancer, inflammation and behaviour. Brain Behav Immun 23(6): 721-731.

13. Larsen CA, Dashwood RH, Bisson WH (2010) Tea catechins as inhibitors of receptor tyrosine kinases: mechanistic insights and human relevance. Pharmacol Res 62(6): 457-464.

14. Shih LJ, Lin YR, Lin CK, Liu HS, Kao YH (2016) Green tea (-)-epigallocatechin gallate induced growth inhibition of human placental choriocarcinoma cells. Placenta 41: 1-9.

15. Grove KA, Lambert JD (2010) Laboratory, Epidemiological, and Human Intervention Studies Show That Tea (*Camellia sinensis*) May Be Useful in the Prevention of Obesity. J Nutr 140(3): 446-453.

16. Skrzypczak-Jankun E, Jankun J (2010) Theaflavin digallate inactivates plasminogen activator inhibitor: Could tea help in Alzheimer's disease and obesity? Int J Mol Med 26(1): 45-50.

17. Isbrucker RA, Edwards JA, Wolz E, Davidovich A, Bausch J (2006) Safety studies on epigallocatechin gallate (EGCG) preparations. Part 3: teratogenicity and reproductive toxicity studies in rats. Food Chem Toxicol 44(5): 651-661.

18. Fan YC, Chan WH (2014) Epigallocatechin gallate induces embryonic toxicity in mouse blastocysts through apoptosis. Drug Chem Toxicol 37(3): 247-254.

19. Wang D, Meng J, Xu K, Xiao R, Xu M, et al. (2012) Evaluation of oral subchronic toxicity of Pu-erh green tea (*Camellia sinensis var. assamica*) extract in Sprague Dawley rats. J Ethnopharmacol 142(3): 836-844.

20. Saudan P, Brown MA, Buddle ML, Jones M (1998) Does gestational hypertension become pre-eclampsia? Br J Obstet Gynaecol 105(11): 1077-1084.

21. Hennessy A, Pilmore HL, Simmons LA, Painter DM (1999) A Deficiency of Placental IL-10 in Preeclampsia. J Immunol 163(6): 3491-3495.

22. Dey A, Gomes A, Dasgupta SC (2018) Black Tea (*Camellia sinensis*) Extract Induced Prenatal and Postnatal Toxicity in Experimental Albino rats. Pharmacogn Mag 13(Suppl 4): S769-S774.

23. Gekas C, Rhodes KE, Mikkola HKA (2008) Isolation and Analysis of Hematopoietic Stem Cells from the Placenta. J Vis Exp 16: 742.

24. Chakraborty K, Chatterjee S, Bhattacharyya A (2017) Modulation of CD11c+ lung dendritic cells in respect to TGF-β in experimental pulmonary fibrosis. Cell Biol Int 41(9): 991-1000.

25. Jungbluth AA, Stockert E, Huang HJS, Collins VP, Coplan K, et al. (2003) A monoclonal antibody recognizing human cancers with amplification/overexpression of the human epidermal growth factor receptor. Proc Natl Acad Sci 100(2): 639-644.

26. Ataee R, Ajdary S, Zarrindast M, Rezayat M, Hayatbakhsh MR (2010) Anti-mitogenic and apoptotic effects of 5-HT1B receptor antagonist on HT29 colorectal cancer cell line. J Cancer Res Clin Oncol 136(10): 1461-1469.

27. Menegola E, Broccia ML, Giavini E (2001) Atlas of Rat

Fetal Skeleton Double Stained for Bone and Cartilage. Teratology 64(3): 125-133.

28. Gomes A, Haldar S, Giri B, Mishra R, Saha A, et al. (2009) Experimental osteoporosis induced in female albino rats and its antagonism by Indian black scorpion (*Heterometrus bengalensis* C.L.Koch) venom. Toxicon 53(1): 60-68.

29. Nunes JS (2016) Musculoskeletal System. In: Parker GA, Picut CA (Eds.) Atlas of Histology of Juvenile Rat 1st (Edn.), Academic Press, Cambridge, pp: 29-43.

30. Afroze SH, Kalagiri RR, Reyes M, Zimmerman JD, Beeram MR, et al. (2016) Apoptotic and stress signaling markers are augmented in preeclamptic placenta and umbilical cord. BBA Clin 6: 25-30.

31. Omran OM, Shokry M, Ismail H, Omar G, Rezk M (2011) Expression of matrix metalloproteinases 2 and 9 in human trophoblasts of normal and preeclamptic placentas. Int J Health Sci 5(2 Suppl 1): 21-23.

32. Palei ACT, Granger JP, Tanus-Santos JE (2013) Matrix Metalloproteinases as Drug Targets in Preeclampsia. Cur Drug Targets 14(3): 325-334.

33. Macias D, Ganan Y, Sampath TK, Piedra ME, Ros MA, et al. (1997) Role of BMP-2 and OP-1 (BMP-7) in programmed cell death and skeletogenesis during chick limb development. Development 124(6): 1109-1117.

34. Monsivais D, Clementi C, Peng J, Fullerton PT, Prunskaite-Hyyrylainen R, et al. (2017) BMP7 Induces Uterine Receptivity and Blastocyst Attachment. Endocrinology 158(4): 979-992.

35. Nevo O, Lee DK, Caniggia I (2013) Attenuation of VEGFR-2 Expression by sFlt-1 and Low Oxygen in Human Placenta. Plos One 8(11).

36. Aldridge A, Aranda JV, Neims AH (1979) Caffeine metabolism in the newborn. Clin Pharmacol Ther 25(4): 447-453.

37. Weathersbee PS, Lodge JR (1977) Caffeine: its direct and indirect influence on reproduction. J Reprod Med 19(2): 55-63.

38. Arnaud MJ, Bracco I, Sauvageat JL, Clerc MF (1983) Placental transfer of the major caffeine metabolite in the rat using 6-amino-5[N-formylmethylamino]1,3[Me-14C]-dimethyluracil administered orally or intravenously to the pregnant rat. Toxicol Lett 16(3-4): 271-279.

39. Kirkinen P, Jouppila P, Koivula A, Vuori J, Puukka M (1983) The effect of caffeine on placental and fetal blood flow in human pregnancy. Am J Obstet Gynecol 147(8): 939-942.

40. Jarosz M, Wierzejska R, Siuba M (2012) Maternal caffeine intake and its effect on pregnancy outcomes. Eur J Obstet Gynecol Reprod Biol 160(2): 156-160.

41. Rhee J, Kim R, Kim Y, Tam M, Lai Y, et al. (2015) Maternal Caffeine Consumption during Pregnancy and Risk of Low Birth Weight: A Dose-Response Meta-Analysis of Observational Studies. PLOS ONE 10(7).

42. Morita O, Knapp JF, Tamaki Y, Stump DG, Moore JS, et al. (2009) Effects of green tea catechin on embryo/fetal development in rats. Food Chem Toxicol 47(6): 1296-1303.

ISSN: 0976-3031

Available Online at http://www.recentscientific.com

CODEN: IJRSFP (USA)

International Journal of Recent Scientific Research
Vol. 11, Issue, 08 (B), pp. 39479-39482, August, 2020

International Journal of Recent Scientific Research

DOI: 10.24327/IJRSR

Research Article

LACERATED MYIASIS BY BLOWFLY ON *Bufo melanostictus* SCHNEIDER, 1799 IN WEST BENGAL, INDIA

Sanjukta Manna*

Post Graduate Department of Zoology, Maulana Azad College,8 Rafi Ahmed Kidwai Road, Kolkata 700 013, India

DOI: http://dx.doi.org/10.24327/ijrsr.2020.1108.5511

ARTICLE INFO

Article History:

Received 14th May, 2020
Received in revised form 29th June, 2020
Accepted 05th July, 2020
Published online 28th August, 2020

Key Words:

Maggots, Calliphoridae, Cephalopharyngeal Skeleton, Spiracle.

ABSTRACT

Larvae of blowflies can cause obligatory myiasis on common toad but it is the first report of flesh-eating behavior of maggots of Calliphoridaeon *Bufo melanostictus* from South 24 Parganas West Bengal, India. We documented the blowfly maggot infestation with the morphometry of larvae.The larvae are nearly transparent, usually more or less flattened. They were identified with their twelve body segments and internal chitinous cephalopharyngeal skeleton having oral hooks and characteristically recessed posterior spiracles. Two strongly sclerotized posterior spiracles with narrow peritremal ring appeared as finger like projection. The larvae sizes are in the range of 7.0 to 12.0 mm. in length with the average of about 10.0 ± 0.1 mm.The warm climate of March is the best suited for incubation of myiasis producing maggots on toads.

INTRODUCTION

Myiasis in anurans is usually caused by the larvae of diptera from the Calliphoridae, Sarcophagidae, Chloroidae, and Muscidae families (Eizemberg *et al*. 2008) and can cause substantial mortality (Dasgupta 1962; Reichenback-Klinke and Elkan 1965). These dipterans have been reported as an obligate parasite of amphibians, particularly *Bufo melanostictus*.Mainly blowflies of Calliphoridae show a special type of ectoparasitism on *Bufo melanostictus* that causes myiasis. It has been known for a long time that *Lucilia* sp. of Calliphoridae which is Nearctic and Palaearctic in distribution, is parasitic on toads causing myiasis (Dasgupta 1962). Hall (1948) included *L. bufonivora* Moniez 1876., *L. silvarum*Meigen 1826 and *L. elongata* Shannon 1924 are the main species parasitic on toad.These flies lay eggs on healthy hosts with first instar larvae penetrating the skin causing primary myiasis or if the larvae penetrate previous wounds causing secondary myiasis. The larvae feed on the living tissue of their host and initiating myiasis as a result (Stevens and Wall 1997). Adult flies are not parasitic and resemble house flies. They were saprophagous and had tendency to migrate in search of soft fleshy part of the haunch. Extensive histological changes of the skin took place due to larval infestation. The epidermal cells were dissolved by alkaline proteolytic enzyme (Zumpt 1965).

The myiasis from Indian Anurans are not extensively recorded except Dasgupta (1962) who had drawn attention on lesions on hind leg of *Bufo melanostictus* collected from Siliguri district, West Bengal and identified the flies as *Lporphyrina* Walker 1856.The obligate myiasis-causing blow-fly parasites have evolved from an ancestral saprophagous stage, with flies occasionally being attracted to decaying tissue or wounded animals. This later involved into flies which relied more on living tissue until obligate parasites evolved (Zumpt1967; Mc Donagh 2009). Till date no comprehensive data of myiasis on *Bufo melanostictus*are available with morphometric support from India.The present study registers the infestation of blowfly maggot causing dermal myiasis on common toad *Bufo melanostictus* collected from Jaynagar, South 24 Parganas, West Bengal, India. In this research work myiasis causing larvaewere identified on the basis of morphometry with host and locality (Szpila2010).

Experimental Section

Bufomelanostictus, the common Indian toad, were collected from paddy fields which was its natural habitatat Jaynagar, South 24-Parganas District, West Bengal, India in the month of March, 2018. We observed three *Bufo melanostictus* with external lacerated wound on one of the hind legs out of six specimens collected. Toads with external lesions on limbs were

Corresponding author:* **Sanjukta Manna
Post Graduate Department of Zoology, Maulana Azad College,8 Rafi Ahmed Kidwai Road, Kolkata 700 013, India

separated and anaesthetized and wound parts were placed in petri dish with normal saline at room temperature. Total 65maggots were obtained from the wound after three to four hours. The maggots were preserved in 70% ethanol and examined microscopically (Trinocular Microscope, ZEISS). All the larvae were photographed with the help of a Sony Cyber Shot DSC-T10 camera.

RESULTS AND DISCUSSION

It was found that infected toads were usually motionless, probably due to extensive destruction of their muscular tissues as the maggots burrowed the lesion, congregated and fed the flesh as a group (Fig1).It was observed that the larvae or maggots were crawling down in saline from open wound and actively seeking a suitable area to pupate (Fig 2).

Fig 1 Maggots burrowed the lesion on hind limb of *Bufo melanostictus*

Fig 2 Second instar larva

The larvae emerged from the toad within a day of collection and possess the typical characteristics of the genus *Lucilia* sp. They were in the range of 7.0 to 12.0 mm long with the average of about 10.0 ± 0.1 mm.The maggots were nearly transparent, usually more or less flattened. They were identified with their twelve body segments, cephalopharyngeal skeleton and characteristically recessed posterior spiracles. The anterior end bore a pair of oral hooks (Fig3) that were connected to the internal, chitinous, cephalopharyngeal skeleton.

Fig 3 A pair of oral hook

Fig 4 Spinose bands with cuticular spines

The 1st instar larvae emerged from hatched eggs on the host and the larvae commence feeding immediately. They rapidly develop into second and third instar after consuming liquid protein from blood and muscle from the host. They moved independently about the surface. All segments of larvae had pronounced ridges and with rings of small dark spinose bands with cuticular spines (Fig4). The tip of spines was single and arranged in irregular rows (Fig5). The span of the posterior spinose bands increases towards the end of the body whereas reverse trends was observed in case of body segment. Similar observation was reported by Szpila (2010). The first segment corresponded to the head and was small, membranous. The cephalopharyngeal sclerites, also known as the cephalopharyngeal skeleton consisted of two oral hooks, two dental sclerites, the hypostomal sclerites, the pharyngeal sclerites, the ventral cornu,the dorsal cornu, and broad vertical plate as shown in (Fig6). The dorsal cornu was longer than ventral cornu. The ventral cornu ended with pigmented area.The two halves of the skeleton had a transverse connecting

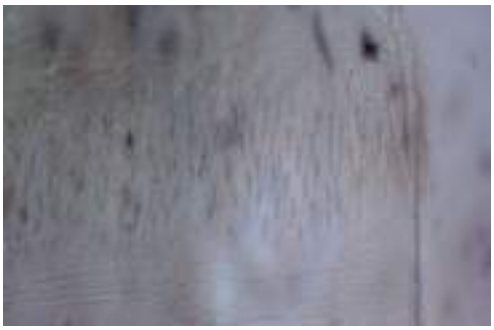

Fig 5 Irregular arrangement of the spines

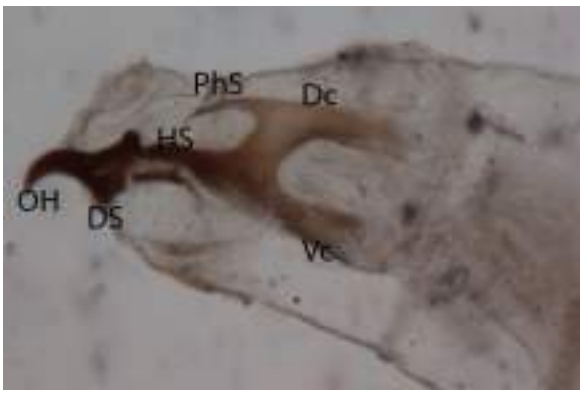

Fig 6 Cephalopharyngeal skeleton with two oral hooks (OH), two dental sclerites (DS), the hypostomal sclerites (HS), the pharyngeal sclerites (PhS), the ventral cornu (Vc), the dorsal cornu (Dc)

Dorsal bridge, giving the skeleton an H-shaped configuration.The twelfth segment was modified by the presence of the anus which was a simple aperture surrounded by a chitinous ring. Two strongly sclerotized posterior spiracles situated in the depressed area of the twelfth segment and were orientated in a ventral-caudal direction. They appeared as finger like projection microscopicallyandwere placed superficially. Posterior spiracle with narrow peritremal ring showed an inner projection between two slits (Fig7). Tubercles of last segment were relatively small (Fig8). With these characters the larvae were recognized as *Luciliabufonivora*, atoad blowfly.

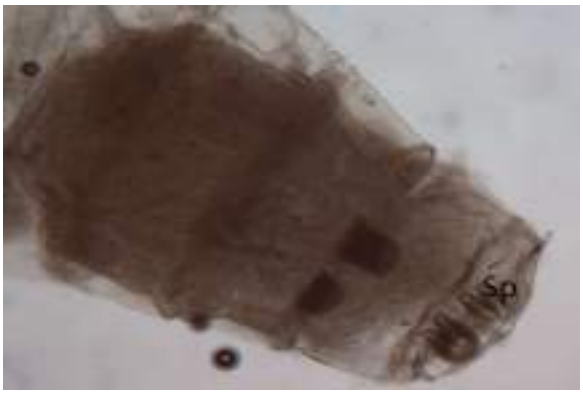

Fig 7 Sclerotized posterior spiracles with narrow peritremal ring

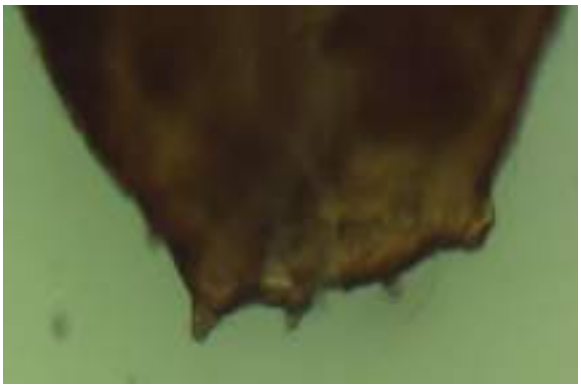

Fig 8 Tubercles in the posterior segment

The blowfly larvaefeed upon living tissues at least for a period of time to make"punched out" ulcers which frequently merge to produce larger ulcers with scalloped edges.Third stage larvae have developed mouthparts capable of rasping the skin and inflicting considerable damage (Monzu 1978).In present investigation it was observed that blowfly larvae of Calliphoridae feed readily on muscles and blood of living toad like the flesh fly (Sarcophagids).*Luciliabufonivora* has been reported as the cause of myiasis in a range of amphibian hosts; however, most reports relate to infestations of the common toad, *Bufobufo* (Anura: Bufonidae). and have been reported to occur in the nasal cavities of their host (WeddelingandKordges 2008; Martín *et al*. 2012). Toad myiasis due to *L. silvarum* have been reported to occur in the back, neck, legs and parotid glands of the host (Bolekand Coggins 2002).*L.bufonivora* and *L. silvarum* were considered separately and genetically studied by Arias-Robledo *et al*. 2018 and confirmed their taxonomic status although these two are morphologically similar.

The Calliphorid blowfly *Lucilia*sp. composedlargely of saprophagous and obligatory agentsof myiasis. In Europe many species are involved in myiasis of sheep,goat, pigsetc. Most cases of toad myiasis by *L. bufonivora* have been reported to in the nasal cavities of their host (van Diepenbeek. andHuijbregts 2011; Martín *et al*.2012) and toad myiasis due to *L.silvarum* developing in thenasal cavities ((Bolekand Coggins 2002).

Body myiasis tended to occur when warm wet conditions coincided with high fly abundance. In warm temperatures toads are more active and can travel more quickly. This may influence the seasonal activity and development of blowfly population as the heat activated reactions provide energy to move muscles which are best suited for incubation of myiasis producing maggots (Zabala *et al*.2014). Preventing the spread of this myiasis-causing species is of great importance in ecological balance as well as epidemiological surveillance.

Acknowledgement

I convey my sincere gratitude to Prof. Subir Chandra Das Gupta, Head of the Department, Zoology and Coordinator of DBT Star Programme, Maulana Azad College for providing necessary infrastructure required for the study.

Compliance with Ethical Standards

Ethics approval and consent to participate

The project is formulated following the guidelines of Institutional Animal Ethics Committee and got approval from faculty Research Committee and toad has been killed for the present study following guidelines of the Committee (F.No.25/250/2012-AWD). The authors declare that the study was conducted on naturally infected animals in the field. No experimental infection was established during this research work.

References

Arias-Robledo G, Stark T, WallRL, Stevens JR(2019) The toad fly *Luciliabufonivora*: its evolutionary status and molecular identification. Med Vet Entomol 33(1): 131-139

Bolek MG,Coggins JR (2002) Observations on myiasis by the calliphorid, *Bufo luciliasilvarum*, in the Eastern American toad (*Bufo americanusamericanus*) from southeastern Wisconsin. J Wild Dis 38: 598–603

Dasgupta B (1962) On the myiasis of the Indian toad *Bufo melanostictus*. Parasitol 52:63–66

Eizemberg R, Sabagh LT, Mello RS (2008) First record of myiasis in *Aplastodiscusarildae* (Anura: Hylidae) by *Notochaetabufonivora* (Diptera: Sarcophagidae) in the Neotropical area. Parasitol Res 102: 329-33

Hall DG(1948) The Blow-flies of North America.The Thomas Say Foundation, USA, pp. 215.

Zabala J, Dı´azB, Salon˜ a-BordasMI (2014) Seasonal Blowfly Distribution and Abundance in Fragmented Landscapes. Is It Useful in Forensic Inference about Where a Corpse Has Been Decaying? PLOS ONE 9(6): 1-11

Martín BD, OteizaAG,BordasMIS (2012)Confirmación de la presencia de *Luciliabufonivora*Moniez, 1876 (Diptera: Calliphoridae) en la penínsulaIbérica. Boletín de la Asociación Española de Entomología36: 433–438

Mcdonagh LM (2009) *Assessing patterns of genetic and antigenic diversity inCalliphoridae* (blowflies). Phd thesis, University of Exeter

Monzu N(1978) Some basic facts about primary blowflies. Journal of the Department of Agriculture, Western Australia 19(3):93-95

Reichenback-KlinkeG, Elkan E(1965) The principal diseases of lower vertebrates. Diseases of amphibians. Academic Press Inc., London, England, pp. 381

Stevens J,Wall R(1997) The evolution of ectoparasitism in the genus *Lucilia* (Diptera: Calliphoridae). *International J Parasitol*27 (1): 51-59

SzpilaK (2010) Key for the Identification of Third Instars of European Blowflies (Diptera: Calliphoridae) of Forensic Importance. Current Concepts in Forensic Entomology, Edn 1 Springer pp.43-56

van Diepenbeek A,Huijbregts H(2011) De pad enzijnkwelgeest [The toad and his torturer]. RAVON 41: 64-70

Weddeling K,Kordges T(2008)*Luciliabufonivora* infestation (myiasis) in amphibians in North Rhine-Westphalia – distribution, host species, ecology and phenology. Zeitschriftfür Feldherpetologie 15: 183–202

Zumpt F (1965) Myasis in man and animals in the Old World. Butterworths, London [Ch. albiceps]

Zumpt F,Ledger J(1967) A malign case of myiasis caused by *Hemipyrelliafernandica* (Macquart) (Diptera Calliphoridae) in a cape hedgehog (*Erinaceus frontalis* A. Smith). *Acta Zoologica et Pathologica Antverpiensia*43: 85-91.

How to cite this article:

Sanjukta Manna.2020, Lacerated Myiasis by Blowfly on Bufomelanostictus Schneider, 1799 in West Bengal, India. *Int J Recent Sci Res.* 11(08), pp. 39479-39482. DOI: http://dx.doi.org/10.24327/ijrsr.2020.1108.5511

****

ISSN: 0976-3031

Available Online at http://www.recentscientific.com

CODEN: IJRSFP (USA)

International Journal of Recent Scientific Research
Vol. 11, Issue, 10 (C), pp. 39928-39932, October, 2020

International Journal of Recent Scientific Research

DOI: 10.24327/IJRSR

Research Article

OVERVIEW OF PLANT NEMATODES AS AN AGRICULTURAL NEMESIS

Sanjukta Manna* and Souradeep Das

Post Graduate Department of Zoology, Maulana Azad College, Kolkata, India

DOI: http://dx.doi.org/10.24327/ijrsr.2020.1110.5591

ARTICLE INFO

Article History:

Received 6th July, 2020
Received in revised form 15th August,, 2020
Accepted 12th September, 2020
Published online 28th October, 2020

Key Words:

Phytonematodes, Stylet, Salicylic acid, Jasmonic acid, ROS

ABSTRACT

Phytonematodes are a major part of soil community that plays a vital role in soil nutrient cycling and primary productivity. They are obligate, biotrophic pathogens of numerous plant species. These organisms cause dramatic changes in the morphology and physiology of their hosts. Cyst nematodes invade roots and piercing vascular bundles with their stylets and disrupting cells as they go. The root-knot nematodes, are biotrophic and induce complex feeding structures in the roots of their hosts which supply the nematode with a rich and long-lasting food source. Root lesion nematodes are worm-like and mobile, and can infect host plant roots or storage organs forming lesions, necrotic areas, browning and cell death, often followed by root rotting from secondary attack. Plant Parasitic Nematodes are able to induce and modulate different signaling pathways in plants with the help of their effect or proteins. These effectors can not only induce the auxin and cytokine in signaling for the development of nematode feeding sites but can also suppress the salicylic acid and jasmonic acid signaling to avoid host defense responses. Plant parasitic nematode could regulate different defense pathways, e.g., ROS production to establish compatible interactions with the plant hosts.

INTRODUCTION

The nematodes are highly diversified, probably one of the most numerous multicellular animals on earth. The species parasitic on plants are of considerable agricultural importance. Nematodes are ubiquitous members of the soil faunal community that can have a significant impact on nutrient cycling and primary productivity in many ecosystems. Nematode ecology gained recent attention because it has been noticed that nematode population can respond to ecological changes and soil status hence can be considered as sensitive indicators.

Plant and soil nematodes are a major threat to agriculture as the cost to world agriculture of nematode parasitism was estimated recently to be US$ 125 billion annually. Application of ecological approaches and knowledge of biological suppression of nematode affected plant disease in natural ecosystems is receiving more attention as environmental concerns mount for the longevity and quality of natural resources.

The importance of Plant Parasitic Nematodes(PPN) can be seen in two ways broadly-(1) biological and cultural approaches to enhance the habitat and effectiveness of natural enemies of plant-parasitic nematodes to control the agricultural damage caused by it and (2) the use of nematodes as biological indicators of soil quality (Neher, 2010).

PLANT AND NEMATODE ECOLOGY

Nutrient mineralization

Nematodes ingest more nutrients than required, and the excesses are excreted in readily mineralize able form such as amino acids, NH_4^+ and PO_4^{3-}. This nutrient accounts for almost 25% of total mineralized soil nutrient which can be even greater in rhizosphere soil. Bacterial feeder and omnivorous nematodes are major contributor of nitrogen mineralization whereas fungal feeders contribute towards phosphate mineralization.

Redistribution of other microorganisms involved in nutrient cycling

Nematodes are quite non-motile in soil that moves within centimeters over few days. But they can also be easily moved across ecosystems either in river systems, flood water and irrigation water or phoretically on insects. Based on the fact that nematodes themselves can phoretically transport bacterial and fungal spores, hence nematodes can redistribute and inoculate microbes into new soil patches. *Caenorhabditis elegans* will transfer the N_2-fixing bacterium *Sinorhizobium meliloti* to the roots of *Medicago truncatula* under the control of plant derived volatile chemical signals (Horiuchi *et al.*, 2005). Bacterial-feeding nematodes were also vectoring for

Corresponding author:* **Sanjukta Manna
Post Graduate Department of Zoology, Maulana Azad College, Kolkata, India

four strains of beneficial rhizobacteria to wheat roots (Knox *et al*., 2003). Unfortunately, harmful bacteria can be transmitted in this way as well. For example, *Salmonella* can be transmitted by bacterial-feeding nematodes to fruits and vegetables in contact with the soil and coliform bacteria in municipal water supply.

DIFFERENT TYPES OF PHYTONEMATODES

Predatory nematodes

The majority of predatory nematodes belong to four major taxonomic groups of nematodes, Mononchida, Dorylaimida, Diplogasterida and Aphelenchida. Each group has its own type of feeding apparatus, feeding mechanisms and food preferences.

Mononchid predators

Mononchids possess a strongly sclerotized buccal cavity, which is often armed with one tooth, more large puncturing teeth, numerous small grasping teeth, or both. Several of commonly occurring mononchids feed extensively, though not exclusively, on plant parasitic and other nematodes (Bilgrami *et al*., 1986).

Dorylaimid predators

Dorylaimids possess a hollow stylet, properly called odontostyle, which is used to puncture the prey organisms and to feed through (Linford and Oliviera,1937).When feeding on other nematodes, the large odontostyle of these predators disorganizes the internal organs of the prey to quickly render it immobile. *Nygolaimoidea* and *Sectonema* have a large, slender, protrusible tooth called mural tooth with which they pierce or slit their prey. This tooth is not hollow and food is sucked up through the oral aperture. Dorylaimid predators are the most ubiquitous group of predatory nematodes, occurring in all types of soils, climates and habitats.

Diplogasterid predators

Diplogasterid predators possess comparatively smaller buccal cavity than those of mononchids but armed with teeth. They feed on nematodes, bacteria and other soil microorganisms. Diplogasterids are generally found abundantly in decomposing organic manure. Diplogasterid predators appear to be more prey-selective than other groups. This targeted prey-predator relation is of significant interest because it is useful for targeted bio-management of harmful parasitic nematodes by chemotaxis behavior towards attractants from prey nematodes (Bilgrami and Jairajpuri, 1988;Bilgrami and Jairajpuri, 1989).

Aphelenchid predators

The genus *Seinura* are predatory among aphelenchids. Feeding apparatus is typical aphelenchid stylet. These predators penetrate the cuticle of prey nematodes with their fine needle-like stylet and inject digestive enzymes into the prey body, which paralyses the prey almost instantly. Ingestion of prey body contents then takes place. These species are generally small in size but capable of feeding on larger preys than their own body size by injecting enzymes (Linford and Oliviera, 1937).

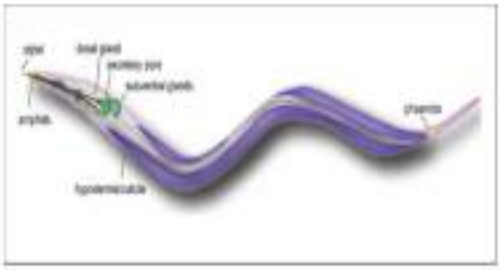

Fig.1 Schematic overview of a plant-parasitic nematode. Amphids and phasmids are chemosensory organs. The stylet is a protrusible, hollow puncturing device, that is used to penetrate plant cell walls (Shanya et al., 2013)

Fig.2 Life cycle of mitotic parthenogenetic root-knot nematode

Plant Pathogenic Nematodes

Root-knot, lesion and cyst nematodes pose a serious threat to main agricultural crops such as potato, sugar beet, and soybean. The order Tylenchida constitute the economically most detrimental group of plant parasitic nematodes. Root-knot nematodes such as *Meloidogyne incognita*, *Meloidogyne hapla*, and *Meloidogyne chitwoodi*, are most polyphagous, being able to infect almost all domesticated plants worldwide (Trudgill and Blok 2001). *Pratylenchus* is a genus of nematodes commonly known as lesion nematodes and notorious parasite in crops such as potato and tomato as well as a range of cereals and legumes. Lesion nematodes are migratory endoparasites and provide other opportunistic soil bacteria and fungi access to the plant root. The invasion of plant roots by root-knot and cyst nematodes lead to the formation of nematode feeding sites. In case of sedentary endoparasites, establishment of so called 'giant cells' or 'syncytia' (root-knot and cyst nematodes, respectively) is considered as one of the most sophisticated adaptations of plant parasitism. Upon the injection of nematode secretions, parasitized cells rapidly become larger, hypertrophied and multinucleated. Feeding sites, giant cells or syncytia, are used till the end of the nematode life cycle and serve as sink tissues to which nutrients are imported in a symplastic or apoplastic manner (Hoth *et al*., 2008). On the other hand, migratory endoparasites, such as *Pratylenchus* species move freely through the root to feed and reproduce, creating numerous local tissue lesions, which are used as an entrance by the secondary pathogens such as bacteria or fungi. The feeding takes place mostly in the root cortex, but root hair feeding is observed for younger life stages as these are unable to perforate thicker epidermal cell wall (Zunke 1990).

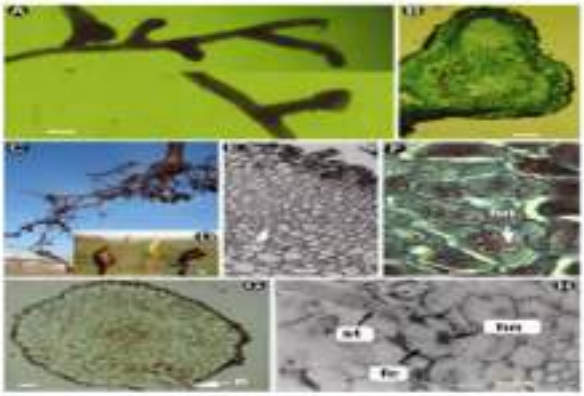

Fig 3 Morphogenesis caused by ectoparasite root nematodes. *Paratrichodorus teres* (A,B): (A) Apical-root galls on wheat. (B) Cross-section of apical-root wheat gall (Source: N. Vovlas). *Xiphinema index* (C–F): (C, D) Apicalroot galls in grapevine. (E,F) Cross-sections showing multinucleate cells with hypertrophied nucleus (hn) induced by nematode parasitism. *Helicotylenchus oleae* (G,H): Cross-sections of olive roots showing the nematode feeding on a parenchymatic feeding cell (fc) with hypertrophied nucleus (hn) (Vovlas et al., 2005). fc, feeding cell; hn, hypertrophied nucleus; n, nematode; st, stylet. Scale bars: A,D = 1,000 µm; B = 200 µm; E = 10 µm; F,H = 20 µm; G = 100 µm.

PLANT NEMATODE INTERACTION

Morphogenesis Induced by Nematodes

Plant ectoparasites comprise a broad range of nematode families. The feeding habit of these nematodes, their secretions, the population densities, the type of cell selected, and the time of interaction within these cells are important factors in the development of different cell and root structures.Trichodorid nematodes preferably feed on epidermal cells in the elongation regions of rapidly growing roots; they tend to aggregate at the root's apex and stop root growth through gregarious feeding (Wyss, 2010). Usually, they induce abnormal growth of lateral roots and the proliferation of branched roots (Agrios, 2005). Severely infected roots show a smaller root system than non-infected plants, with the presence of fewer roots exhibiting short, stubby, swollen root branches (Figure 3; Agrios, 2005).

Meloidogyne, plant endoparasiteis a genus including more than 90 species. Only a few of them are considered as major pests (*M. incognita*, *M. javanica*, *M. arenaria*, and *M. hapla*; Jones *et al.*, 2013). One of their main characteristics is that they are extremely polyphagous (Moens *et al.*, 2009). Root-knot nematodes (RKN) initiate a subtle interaction with their hosts through intercellular migration after sensing chemical gradients of root diffusates (Teillet *et al.*, 2013). Second-stage juvenile (J2), the infective parasitic form of RKNs, enters the elongation zone of the root and using cell wall hydrolytic enzymes such as endoglucanases,endoxylanase, ectatelyases, etc., from their sub ventral glands secreted into the apoplast (Perry and Moens, 2011). They reach the vascular cylinder by entering through the root meristem area. In this way, they considerably reduce mechanical damage to the plant cells as compared to other nematode groups, such as cyst nematodes (CN). Once established, a group of five to eight cells in the vascular cylinder develop into feeding cells, called giant cells (GCs) (Figures 4 B,D,F,G,H,I; Escobar *et al.*, 2015).

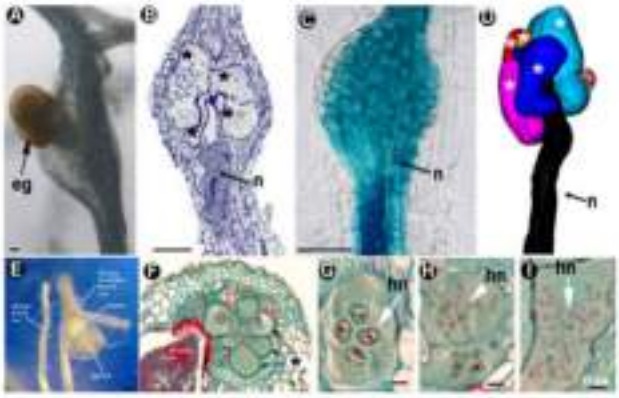

Fig 4 Morphogenesis in root knot nematodes forming galls. *Meloidogyne* spp. (A–I): (A) Egg mass (eg) protruding from a gall in a *Cucumis sativus* root infected by *Meloidogyne javanica*. (B) Longitudinal section of a gall from *Arabidopsis thaliana* showing multinucleate giant cells (*) and anterior region of the nematode (n). (C) Vascular tissue of a gall with GUS intense signal from an *Arabidopsis* transgenic marker line. (D) 3D reconstruction of giant cells (*) from *Arabidopsis thaliana* (Source: C. Escobar). *Meloidogyne artiellia* (E–I): (E) Healthy and *M. artiellia*-infected chickpea roots, showing the prominent adult female covered by the egg mass. (F) Cross-section of *M. artiellia*-infected root showing the typical feeding site with giant cells (Palomares-Rius et al., 2011). (G–I) Detail of multinucleate giant cells induced by *M. artiellia*, *M. arenaria*, and *M. javanica* in chickpea roots, respectively (Vovlas et al., 2005). *, multinucleate giant cell; eg, egg-mass; hn, hypertrophied nucleus; n, nematode. Scale bars: A–C,E = 100µm; F–I = 20 µm.)

Signal Transduction in Plants

Plants and pathogens are continuously engaged in co-evolution in the struggle for dominance between hosts and pathogens. The plant cell wall is the first physical barrier encountered by pathogens including plant parasitic nematodes (PPNs), fungi, bacteria, and viruses. Once the physical barrier is crossed by the pathogen, the host cytoplasm serves as the battleground where a war is fought between host and pathogen molecules. Next to the cell wall, there are membrane-localized pattern recognition receptors (PRRs) that recognize often conserved pathogen/microbe-associated molecular patterns (PAMPs/MAMPs) such as proteins, lipids, carbohydrates, and cell wall derivatives. As a consequence of the recognition of PAMPs/MAMPs, PRRs initiate a conserved downstream cellular signaling cascade referred to as PAMP-triggered immunity (PTI) inside the cytoplasm of the host cell. The responses include the activation of mitogen-activated protein kinases (MAPKs), the production of reactive oxygen species (ROS), and the induction of signaling pathways via salicylic acid (SA) and jasmonic acid (JA) (Ali *et al.*,2018)

Nematode-Associated Molecular Patterns (NAMPs) and Signaling for Nematode Resistance

The first detailed study on NAMPs highlighted the perception of nematode-produced ascarosides by plant cells, triggering the gene expressions associated with MAMP-triggered immunity and the activation of MAPKs as well as JA and SA signaling (Manosalva, 2015). Ascarosides are small molecules acting as pheromones in the social behavior of nematodes. In spite of diverse nematode phylogeny and ecology, ascaroside biosynthesis and signaling are highly conserved among nematodes (Choe, 2012). In *Caenorhabditis elegans* (a free-living nematode) and many other species, ascarosides are involved in social signaling, finding mating partners, and coordinating nematode behaviors (Kaplan, 2011).Ascarosides are secreted by nematodes into their environment. Structurally,

they are derivatives of the 3, 6-dideoxy-L-sugar, ascarylose, modified with fatty acid-derived side chains, and they are classified according to the number of carbons in their side chains.

Ascarosides featuring an 11-carbon side chain is the most abundant among three genera of plant parasitic nematodes including root knot and cyst-forming nematodes. Ascarosides are believed to be possible NAMPs perceivable by plant for basal defence mechanism.

Phytoalexin Pathway and NAMP-Triggered Immunity (NTI)

PPNs genes involved in the early events of defense responses in plants. Phytoalexins are important defense-related plant metabolites in the initial stages of plant–nematode interactions. The biosynthesis of these metabolites is a key component of the innate immune system and involves a series of signaling events. The transcription factor, *WRKY33*, is considered to be the key player in the activation of camalexin-based PTI (PAMP triggered immunity) in plants. This type of PTI comprises signal perception by transmembrane receptors followed by the commencement of signaling cascades through various MAPKs (Mitogen activated protein kinases) such as MPKs, MKKs, MKKKs, etc., involving several phosphorylation and dephosphorylation event. These signaling cascades lead to the upregulation of the *WRKY33* protein that in turn activates the PAD3 (phytolexin deficient 3) gene to induce camalexin production (Ali *et al*.,2018).

MANAGEMENT OF PHYTONEMATODES

Many deferent genera and species of nematodes can be important to crop production in Florida. In many cases a mixed community of plant-parasitic nematodes is present in a field, rather than having a single species occurring alone. Most cucurbits are extremely susceptible to root nematodes and also are often damaged by sting nematodes; other nematodes occasionally cause some losses.

General IPM Considerations

Integrated pest management (IPM) for nematodes requires (1) determining whether pathogenic nematodes are present within the field; (2) determining whether nematode population densities are high enough to cause economic loss; and (3) selecting a profitable management option. Attempts to manage nematodes may be unprofitable unless all of the above IPM procedures are considered and carefully followed. Similarly, some management methods pose risks to people and the environment. Therefore, it is important to know that their use is justified by actual conditions in a field and that certified applicators are overseeing their use.

Chemical Control

All of the nonfumigant nematicides currently registered for use in cucurbits are soil applied. Nimitz, a new no fumigant nematicide that became commercially available in 2015, is still actively under assessment in fled trial evaluations. All of the non-fumigant nematicides must be incorporated with soil or carried by water into soil to be effective. As the name implies, they are specific to nematodes, have limited residual activity, and require integrated use of other cultural or chemical pest control measures to manage other weed and disease pests.

Use of broad spectrum fumigants effectively reduces nematode populations and increases vegetable crop yields, particularly when compared with no fumigant nematicides. Since these products must diffuse through soil as gases to be effective, the most effective fumigations occur when the soil is well drained, in seedbed condition, and at temperatures above 60°F. Fumigant treatments are most effective in controlling root-knot nematode when residues of the previous crop are either removed or allowed to decay.

Biocontrol

Laboratory studies showed the presence of significant juvenile hatching inhibitive potential of botanical extract against *M. incognita*, however was concentration dependent, that is the hatching of the nematode decreased with increased extract concentration. Among the tested botanicals, Mexican marigold, bitter leaf, lantana, baker tree and neemseed extracts were effective in reducing *M. incognita* egg hatching. The mechanisms of plant extracts action may include denaturing and degrading of proteins, inhibition of enzymes and interfering with the electron flow in respiratory chain or with ADP phosphorylation (Susan and Noweer, 2005).

Biocontrol potential and efficacy of predatory nematodes vary with their types. Among the different types of predators, diplogasterids are the most suited for biocontrol of nematodes. Prey specificity is an important factor in biocontrol. Mononchids generally lack prey specificity, they feed on all types of nematodes, rotifers, protozoa, oligocheates and other invertebrates (Bilgrami *et al*., 1986). As extreme generalist predators, the prospects of using mononchids effectively to control specific pest species seemed remote. On the other hand high degree of prey-predator specificity was seen in Diplogasterids and Monoacids where juveniles of endoparasitic nematodes being preferred over ectoparasitic species. Dorylaimids are also better candidates for biocontrol since they are widely and abundantly distributed in the field and their population may be elevated in the field by adding organic nutrients. However, their long life cycle and low rate of fecundity are causes of concern.

CONCLUSION

Nematode biology and ecological studies open a new vista in understanding ecosystem better. It has a huge impact on the soil ecology and it is of high agricultural importance. Nematodes have beneficial as well as harmful effect on agricultural crop yield. They are found useful in pest control as well as under certain circumstances they increase Nitrogen and Carbon fixation in soil. Sedentary endoparasitic nematodes establish an intimate relationship with their host plants, inducing the redifferentiation of root cells into specialized feeding cells. The whole new level of food web is also of considerable interest. In India, nematode ecology is not vastly studied but as an agro-economic country the understanding of nematode biology is very important. Most economically important plants in India are quite vulnerable for nematode pathogenesis. The trend is now shifting towards better management. The molecular players involved in plant- nematode interaction is also started to unveil. In future, still unveiled aspects of nematode biology will provide a better management for soil and ecological dynamics as well. It will be helpful in reducing agricultural economic loss and increase in crop yield. In this review an

overview on phytonematodes is done briefly, from perception to molecular interaction to management.

ACKNOWLEDGEMENT

We convey our sincere gratitude to Prof. Subir Chandra Das Gupta, Head of the Department, Zoology and Coordinator of DBT Star Programme, Maulana Azad College for providing necessary infrastructure required for the study.

REFERENCES

1. AgriosGN(2005). Plant Pathology. London: Elsevier, Academic Press.
2. Ali MA,Anjam MS, Nawaz MA, Lam HM, ChungG (2018). Signal Transduction in Plant–Nematode Interactions. *Int. J. Mol. Sci.* 19(6),1648; https://doi.org/10.3390/ijms19061648
3. Bilgrami AL, AhmadI, JairajpuriMS (1986).A study on the intestinal contents of some mononchs. Rev. Ne´matol. 17, 339–340.
4. Bilgrami AL, & Jairajpuri MS (1988). Aggregation of *Mononchoideslongicaudatus* and *M. fortidens* (Nematoda: Diplogasterida) at feeding sites. Nematologica. 34, 119–121.
5. Bilgrami AL, & Jairajpuri MS (1989). Resistance of prey to predation and strike rate of the predators *Mononchoideslongicaudatus* and *M. fortidens* (Nematoda: Diplogastgerida). Revue de Nematologie, 12, 45–49.
6. Choe A,Reuss SHvon, KoganD,Gasser RB., Platzer EG, SchroederFC and SternbergP W(2012).Ascaroside signaling is widely conserved among nematodes. *Curr. Biol.* 22, 772–780 .
7. Escobar C, Barcala M, Cabrera J, Fenoll C (2015). Overview of root-knot nematodes and giant cells. Adv. Bot. Res. 73, 1–32. DOI:10.1016/bs.abr.2015.01.001
8. Horiuchi J, Prithiviraj B, Bais HP, Kimball BA, Vivanco JM (2005). Soil nematodes mediate positive interactions between legume plants and rhizobium bacteria. Planta 222(5), 848-857. DOI: 10.1007/s00425-005-0025-y
9. Hoth S, Stadler R, Sauer N et al (2008) Differential vascularization of nematode-induced feeding sites. Proc Natl Acad Sci USA 105, 12617–12622.
10. Jones JT, Haegeman A, Danchin EGJ, Gaur HS, Helder J, Jones MGK, et al. (2013). Top 10 plant-parasitic nematodes in molecular plant pathology. Mol. Plant Pathol. 14, 946–961. 10.1111/mpp.12057
11. KaplanF, Srinivasan J, Mahanti P, Ajredini R, DurakO,et al.(2011) Ascaroside Expression in *Caenorhabditiselegans* Is Strongly Dependenton Diet and Developmental Stage. *PLoS ONE.6*, e17804.
12. Knox OGG, KillhamK, MullinsCE and WilsonMJ (2003). Nematode enhanced microbial colonization of the wheat rhizosphere. FEMS Microbiol. Lett. 225, 227–233.
13. LinfordMB, OlivieraJM. (1937). The feeding of hollow-spear nematodes on other nematodes. Science 85, 295–297.
14. Manosalva P, Manohar M, von ReussSH, Chen S, Koch A, Kaplan F, ChoeA, MicikasRJ, Wang X, Kogel KH. et al. (2015) Conserved nematode signalling molecules elicit plant defenses and pathogenresistance.*Nat. Commun. 6*, 7795.
15. Moens M, Perry R, Starr J. (2009). *Meloidogyne* species a diverse group of novel and important plant parasites, in Root-knot nematodes, eds. Perry R. N., Moens M., Starr J. L. (Wallingford: CABI publ.), 1–13.
16. Neher DA.(2010) Ecology of plant and free-living nematodes in natural and agricultural soil. Annu Rev Phytopathol.48:371-94. doi: 10.1146/annurev-phyto-073009-114439
17. Palomares-Rius JE, CastilloP, Navas-CortésJA, Jiménez-DiazRM, and TenaM. (2011). A proteomic study of in-root interactions between chickpea pathogens: the root-knot nematode *Meloidogyne artiellia* and the soil-borne fungus *Fusarium oxysporum* f. sp. *ciceris* race 5. *J. Proteomics* 74, 2034–2051.
18. Perry R, Moens M. (2011). Introduction to plant-parasitic nematodes; modes of parasitism, in Genomics and molecular genetics of plant-nematode interactions, eds Jones J., Gheysen G, Fenoll C. (Amsterdam: Springer;), 3–20.
19. Shinya R, Morisaka H, Kikuchi T, Takeuchi Y, Ueda M, Futai K (2013) Secretome Analysis of the Pine Wood Nematode *Bursaphelenchus xylophilus* Reveals the Tangled Roots of Parasitism and Its Potential for Molecular Mimicry. PLoS ONE 8(6): e67377.https://doi.org/10.1371/journal.pone.0067377
20. Susan AH and Noweer EM (2005). Management of Root-Knot Nematode *Meloidogyne incognita* on Eggplant with some Plant Extracts. *Egypt. J. Phytopathol.* 3
21. Teillet A, Dybal K, Kerry BR, MillerAJ, Curtis RHC, & HeddenP. (2013). Transcriptional changes of the root–knot nematode *Meloidogyne incognita* in response to *Arabidopsis* thaliana root signals. *PLoS ONE, 8*, e61259. DOI:10.1371/journal.pone.0061259.
22. Trudgill DL, Block VC (2001) Apomictic, polyphagous root-knot nematodes: exceptionally successful and damaging biotrophic root pathogens. Annu Rev Phytopathol 39, 53–77
23. Vovlas N, Rapoport HF, Jiménez Diaz RM, Castillo P. (2005). Differences in feeding sites induced by root-knot nematodes, *Meloidogyne* spp., in chickpea. Phytopathology 95, 368–375. 10.1094/PHYTO-95-0368
24. Wyss U. (2010). Feeding behaviour of plant-parasitic nematodes, in The Biology of Nematodes, ed Lee D. L. (Boca Ratón: Taylor & Francis Group;), 462–513.
25. Zunke U. (1990) Ectoparasitic feeding behaviour of the root lesion nematode, *Pratylenchus penetrans*, on root hairs of different host plants. *Revue Nématol.* 13, 331–337.

UTTAR PRADESH JOURNAL OF ZOOLOGY

41(11): 122-127, 2020
ISSN: 0256-971X (P)

IMPACT OF URBANIZATION ON ABUNDANCE OF SOIL ARTHROPODS

SANJUKTA MANNA[1*] AND ARNAB KAR[1]

[1]Department of Zoology, Maulana Azad College, 8 Rafi Ahmed Kidwai Road, Kolkata 700 013, India.

AUTHORS' CONTRIBUTIONS

This work was carried out in collaboration between both authors. Author SM designed the study, performed the statistical analysis, wrote the protocol and wrote the first draft of the manuscript. Author AK managed the analyses of the study and literature searches. He was involved in sample collection and experimentation. Both authors read and approved the final manuscript.

Article Information

Editor(s):
(1) Dr. Rajib Deb, ICAR-Central Institute for Research, India.
Reviewers:
(1) A. K. Sharma, ICAR-IVRI, India.
(2) Tuo Yalamoussa, Université Peleforo Gon Coulibaly, Côte d'Ivoire.

Received: 10 July 2020
Accepted: 15 September 2020
Published: 24 September 2020

Short Communication

ABSTRACT

Arthropods have important role in maintaining the soil fertility. The major contribution of arthropods to soil is through decomposition and humification of all organic matter. Both micro and macro arthropods were collected using standard Tullgren extractions on fortnightly intervals from five different sites selected on the basis of habitat differences, identified up to the level of order and counted during rainy season. Soil temperature was noted on the field sites while analysis for soil pH, texture, and soil moisture contents were done in the laboratory. This study suggested that rapid urbanization of Kolkata has led to a drastic change in land use and destruction of natural ecosystems which was also observed in a site, Digha (adjacent to Ramnagar), Purba Midnapore, West Bengal where unplanned urbanization hampers local biodiversity. Uncontrolled and unplanned tourism of Digha deteriorate the biodiversity and population dynamics of soil arthropods mainly of order Mesostigmata, Collembola and Coleoptera. Egra (Habitat E), adjacent to Digha showed highest diversity (as obtained from the calculated diversity indices) in June-July (monsoon) as it was favorable and resourceful for their breeding, proper growth and survival. The soil's physical condition was correlated with changes in soil moisture and soil pH which in turn correlated with soil fauna. To understand the comparative biodiversity richness between the study areas, Shannon diversity index was calculated. Increasing soil alkalinity and decreasing moisture levels lowered the Shannon diversity index and accelerated the biological degradation to some extent in case of Egra and Ramnagar area. This study revealed that the metro city, Kolkata, with high pollution threats, can nonetheless harbor a large number of Prostigmata. Increased precipitation in June and July, 2018 and 2019, acted favorable on these mite population. By understanding soil arthropod communities will prove useful in developing management plans for both rural and urban ecosystems.

Keywords: Arthropods; urbanization; Mesostigmata; Collembola; Coleoptera.

**Corresponding author: Email: sanjukta_manna@rediffmail.com;*

1. INTRODUCTION

Arthropods represent as much as 85% of the soil fauna in species richness [1]. They are dominant in upper stratum of soil which is normally rich with soil organic matter. They comprise a large proportion of meso and macrofauna of the soil. Macrofauna contribute to improve soil structure, aeration and water infiltration. They predate on soil organism and help to maintain the biological equilibrium in soil. The soil's physical condition, which includes structure and density, can have a big impact on the diversity of soil organisms that regulate fertility. Heavy, wet soils with little porosity can inhibit the existence of many beneficial aerobic organisms. On the other hand, sandy soils often lack enough moisture to support significant populations of beneficial organisms. Meso and macrofauna play a fundamental role in establishing biogeochemical cycles and are involved in forming the structure of a soil [2]. This is because soil microbial activity has a direct influence in ecosystem stability [3]. The study of soil animals has been neglected field for a long time particularly in India [4]. Little attention has been given to ecological studies of the soil insects, particularly on their seasonal occurrence, site specific diversity/ distribution, species diversity, population dynamics and community structure of the soil fauna [5]. The present study was designed to document the diversity of soil arthropod in the garden of three urban regions such as Maulana Azad College campus, Vivekananda Road and Maniktala, Kolkata, and two rural areas of Egra and Ramnagar, near Digha, the famous tourist spot situated in Purba Midnapore, West Bengal to understand the impact of urbanization on polluted and non-polluted region. The aim of the study was to investigate the dominance and diversity of soil arthropod communities in these highly humid climatic regions to observe the lowland variation in faunal composition.

2. MATERIALS AND METHODS

Soil samples were collected from three sites of Kolkata and two from Purba Midnapore, West Bengal, India during June and July, 2018 and 2019 as mentioned below. The soil samples were collected at fortnightly interval by a shovel from each site and brought by a polythene packet to the laboratory. Arthropods were collected from the soil samples by keeping the soil samples (500 gm) in Tullgren funnel and put on the light (100W) overnight [6]. In winter, generally the abundance of Collembola, mites, ants, and millipedes, the major contributors to the soil arthropod decreased dramatically in temperate regions [7] and also it was reported that [8] soil arthropod numbers increased in the middle of the rainy season than in the early or late periods of the rainy season as a whole.

Survey and documentation of arthropods from five different habitats viz.

Habitat- A (Road side soil of Vivekananda Road area, Kolkata-700006, West Bengal, India)
Habitat- B (Garden of a house near Maniktala, Kolkata-700054, West Bengal, India)
Habitat - C (Garden of Maulana Azad College, Kolkata-700013, West Bengal, India)
Habitat - D (Soil of ditch near Ramnagar, Near Digha, Purba Midnapore, West Bengal, India)
Habitat- E (Soil besides a pond bank at Egra, Purba Midnapore, West Bengal, India)

The arthropods were collected with 30% alcohol in the vials fitted at the mouth of the Tullgren funnel. Then the collected specimens were examined under Trinocular Microscope, ZEISS and photographed with the Sony cyber shot DSC-T10 camera. Specimens collected were identified to order level and quantified to estimate soil arthropods distribution and diversities of these habitats.

Separate soil samples were taken in polythene bags from each site for the chemical analysis of soil parameters. While collecting soil samples, the temperature, moisture and pH were measured. For the measurement of temperature, a thermometer was inserted into the soil up to 30 cm. in depth [9]. Soil moisture was determined by an oven dry method [10]. The pH value was determined by a glass electrode in free suspension of soil in water by the means of pH meter (Systronics). International pipette method was employed for carrying out mechanical analysis of soil for the determination of soil texture [11]. The diversity of soil arthropod of five sites were determined by calculating relative abundance and the index of general diversity [12], the following formula was used

$$H' = -\sum_{i=1}^{R} p_i \, ln \, p_i$$

Here,

H' = Shannon's Biodiversity Index
p_i= Proportions of individuals founds in species i
n = the number of species present in the population of the particular habitat

Data pertaining to the soil factors and population density were subjected to statistical assessment with the number of soil arthropods in relation to each of the

variables (temperature, pH, moisture and soil texture) considered in this investigation.

3. RESULTS AND DISCUSSION

A total of over 415 (average) soil arthropods were collected from five different highly humid environments throughout the survey period. The orders Collembola and Mesostigmata had higher dominance. Other orders had either low population or irregular occurrence. Soil factors in the study sites exhibited fairly wide range of variation. In the habitat A and D (Table 1) minimum population were observed where sandy texture of soil with high pH (Fig 5) and low organic matter was noticed.

It was evident from the Table 1 that group diversity increases with the increase of soil moisture and improved soil texture. Different soil factors like temperature, pH, moisture and structural components in the study sites exhibited fairly wide range of variation during the months of the study period (Fig. 4). Throughout the period of study, the average temperature of soil in these five habitats exhibited a decline with urbanization and moisture content of soil (Fig. 2) in each habitat showed wide range of variation and exhibited a higher value outside Kolkata.

The Shannon diversity index(H) was used to characterize species diversity in arthropod community of five habitats. The diversity in habitat D and E (Ramnagar and Egra) were much higher than in the habitat from highly disturbed, polluted site (A, B, C). The highly humid, low land of Egra not only has greater number of arthropod present, but the individuals in the community are distributed more equitably among these specimens (Fig. 1).

Table 1. The number of soil arthropod in each habitat

Arthropods (Frequency%)	Habitat				
	A	B	C	D	E
Order: Collembola	42	35	19	45	39
Order: Prostigmata	33	26	29	20	5
Order: Coleoptera	-	-	-	10	14
Order: Mesostigmata	25	39	48	15	-
Order: Cryptostigmata	-	-	14	10	9
Order: Hemiptera	-	-	-	-	16
Order: Isoptera	-	-	-	-	5
Order: Acarina	-	-	-	-	11
Order: Anomis	-	-	-	-	2

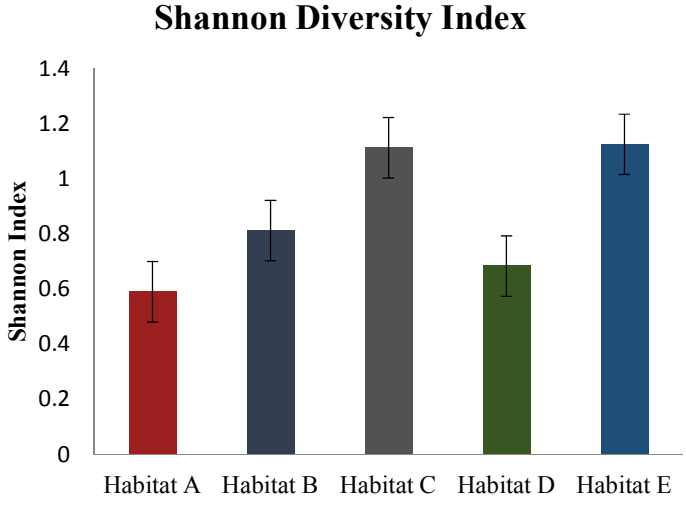

Fig. 1. Distribution and diversity index of soil arthropod community in five sites

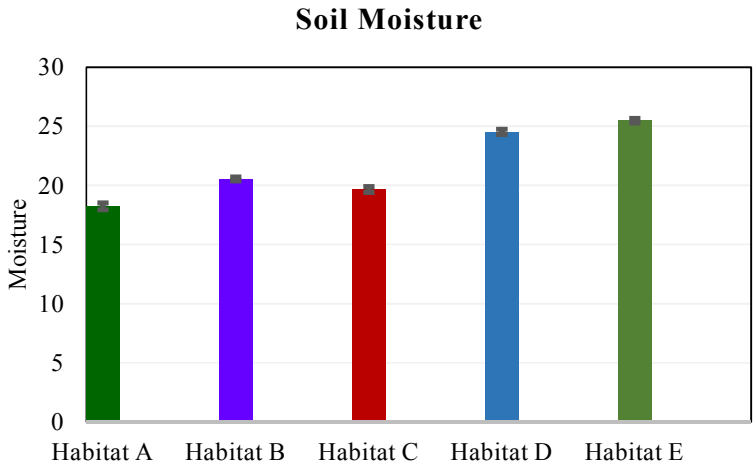

Fig. 2. Moisture content of soil of five sites during collection

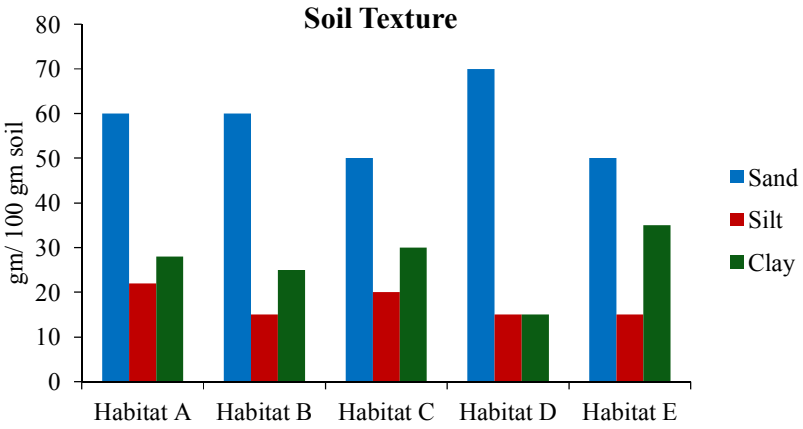

Fig. 3. Soil texture of five sites

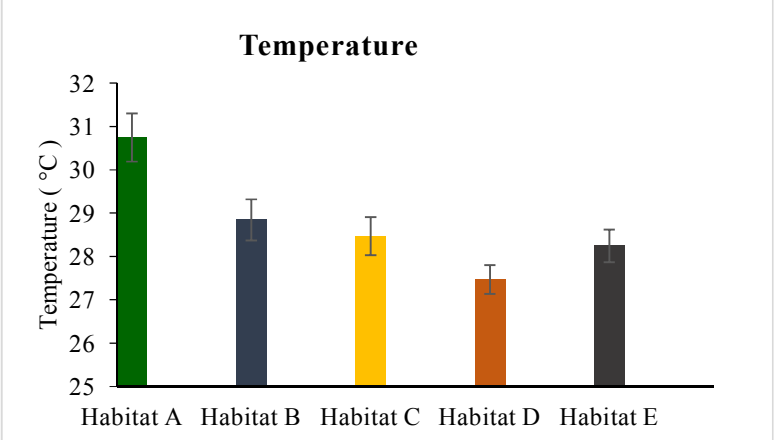

Fig. 4. Temperature of soil during survey time

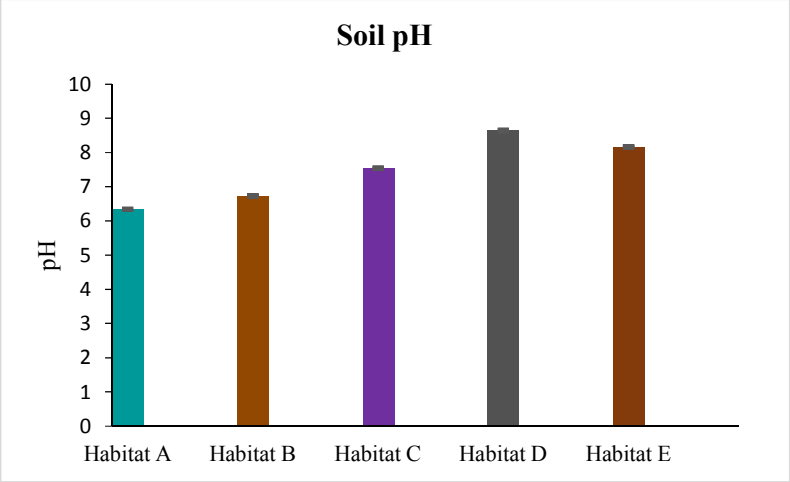

Fig. 5. pH of soil of five sites during study

The arthropod diversity is usually proportional to the stability of the ecosystem: The greater the diversity the greater the stability. Diversity is therefore a factor in successful conservation management. The soil sample collected from the habitat A and B (Table 1), most polluted area of central Kolkata have very low biodiversity (Fig. 1). Pollution often reduces the arthropod diversity by favoring a few dominant species. The concrete materials, brick dust, cements, contaminated water makes the soil unhealthy for living the arthropods naturally. The soil sample of habitat C, garden of Maulana Azad College (Table 1) revealed comparatively greater biodiversity (Fig. 1) than Site-A which is also a most polluted area of Kolkata. This showed most stable communities with diverse insect population. The garden is well maintained with proper fertilizer, water and other equipment by the college authority. But as it is present at the urban area so the polluting agents decreases so far, the population size. Habitat D is the soil sample which collected from Ramnagar area where the pollution level was very low. But the study showed that biodiversity of soil insect was very low here. Ramnagar is located at the coastal region of Bay of Bengal. The soil was very sandy (Fig. 3) and with very low amount of humus. But it was due to natural condition and also growing tourist spot with dynamic estuarine network. The most stable communities of soil arthropods was observed in the soil collected from a pond bank of Egra (Habitat E).There was no polluting agent and no urban factors left any impact. Collembola, Coleoptera and Mesostigmata were the dominant arthropods in each habitat (Fig. 6).

(a) **(b)** **(c)**

Fig. 6. Dominant arthropods in survey site belonging to order (a) Collembola (b) Coleoptera (c) Mesostigmata

4. CONCLUSION

Our observations revealed the order wise faunal abundance, diversity and distribution of soil arthropods which increased with the increase of soil moisture and decrease of pH. The habitat E shows maximum richness in faunal diversity in comparison to other four habitats. The present study demonstrated that habitat A, B and C and D were less diverse in arthropod population. Monsoon was the time when maximum beetles and springtails were found. Which thrive in rich organic matter content soil. As soil moisture and rainfall were generally strongly correlates with densities of arthropods as it was favorable for their breeding and survival. Only three orders namely, Collembola Mesostigmata, and Coleoptera (Fig. 6) covered most of the collected arthropods and had the highest dominant degree. The soil arthropods comprised of insects, millipedes, centipedes, collembolans, symphylans, acaris, mites etc. Among them the Collembola Mesostigmata and Coleoptera (Fig. 6) have the ability to survive in virtually every habitat because of their tremendous adaptive diversity. They are perhaps the most successful of all the invaders of the terrestrial habitat. And the roadside soil is mostly polluted by vehicular exhausts, which has enormous effects on the community of soil arthropods. Though being an area of central Kolkata and concrete jungle, Maulana Azad College Campus has a large expanse of gardens with diverse floral composition, that is varieties of trees, shrubs, bushes and medicinal plants providing diverse habitat that can support a large group of arthropods.

ETHICAL APPROVAL

As per international standard or university standard ethical approval has been collected and preserved by the authors.

ACKNOWLEDGEMENTS

We are privileged to convey our sincere gratitude to Prof. Subir Chandra Das Gupta, Head of the Department, Post Graduate Department of Zoology, Maulana Azad College, Kolkata for providing laboratory facilities and financial support under DBT Star College Scheme to conduct the work.

COMPETING INTERESTS

Authors have declared that no competing interests exist.

REFERENCES

1. Bagyaraj DJ, Nethravathi CJ, Nitin KS. Soil biodiversity and arthropods: Role in soil fertility. Economic and Ecological Significance of Arthropods in Diversified Ecosystems, Springer Science & Business Media Singapore, A. K. Chakravarthy, S. Sridhara (Eds.). 2016;17-51.
DOI: 10.1007/978-981-10-1524-3_2
2. Harris JA, Birch P. Soil microbial activity in opencast coal mine restorations. Soil Use and Management. 1989;5:155–160.
3. Smith JL, Halvorson JJ, Papendick RI. Using multiple-variable indicator kriging for evaluating soil quality. Soil Sci Soc Am J. 1993;57:743–749.
4. Kumar U, Singh R. Soil Fauna: A retrospection with reference to Indian soil. International Journal of Research Studies in Zoology. 2016;2(3):1-22.
5. Ghosh SN, Chattopadhyay A, Bhattacharyya DK. Studies on roadside soil of ants (Hymenoptera: Formicidae) of Kolkata with reference to the effects of lead emitted through automobile exhaust. Rec. Zool. Surv. India. 2007;257:1-149.
6. Macfadyen A. Notes methods for the extraction of soil arthropods. Journal of Animal Ecology. 1953;22:65-77.
7. Shakir MM, Ahmed S. Seasonal abundance of soil arthropods in relation to meteorological and edaphic factors in the agroecosystems of Faisalabad, Punjab, Pakistan. International Journal of Biometeorology; 2014.
DOI: 10.1007/s00484-014-0874-9
8. Zhu X, Gao B, Yuan S, Hu Y. Community structure and seasonal variation of soil arthropods in the forest-steppe ecotone of the mountainous region in Northern Hebei, China. Journal of Mountain Science. 2010;7(2):187–196.
9. Ochsner TE, Logsdon S, Clay D, Moore D, Tsegaye T. Measuring soil temperature. ACSESS Publications; 2008.
DOI: 10.2136/2008.soilsciencestepbystep.c18
10. Dowdeswell WH. Practical animal ecology. Methuen Educational Ltd., London. 1959;265.
11. Daji JA, Kadam JR, Patil ND. A text book of soil science. Media Promoters and Publishers Pvt. Ltd., Bombay; 1996.
12. Shannon CE, Weaner W. The mathematical theory of communication. Urbana: University of Illinois Press; 1963.

UTTAR PRADESH JOURNAL OF ZOOLOGY

41(22): 1-8, 2020
ISSN: 0256-971X (P)

MORPHOGENESIS AND HISTOPATHOLOGY OF FRUIT GALLS INDUCED BY *Pseudophacopteran* sp. ON *Alstonia scholaris*

SANJUKTA MANNA[1*]

[1]Department of Zoology, Maulana Azad College, Kolkata, 700013, India.

AUTHOR'S CONTRIBUTION

The sole author designed, analysed, interpreted and prepared the manuscript.

Article Information

Editor(s):
(1) Dr. Ana Cláudia Correia Coelho, University of Trás-os-Montes and Alto Douro, Portugal.
Reviewers:
(1) Adiss Kamal Issifou Fatiou, University of Abomey-Calavi, Benin Republic.
(2) Işılay Lavkor, Biological Control Research Institute, Turkey.

Received: 15 September 2020
Accepted: 21 November 2020
Published: 14 December 2020

Original Research Article

ABSTRACT

Alstonia scholaris (Chatim Tree) invites attention of the researchers worldwide as these plants are seriously damaged by insect galls which affect its ornamental and medicinal value. Plant galls are pathologically developed cells, tissues and organs of plants which induced by influence of a parasitic organism, like viruses, bacteria, fungi, algae, nematodes, mites or insects. Hence an attempt has been made to study the histological and biochemical changes in fruit galls induced by *Pseudophacopteran* sp., a psylloid herbivores on *Alstonia scholaris*. The adult insect was yellowish in colour, winged and with bulging eyes. The nymph undergoes moulting to reach the adult stage inside the fruit chamber. Hyperplasia in the pericarp was very distinctly noticed. The pericarp proliferated to form a "covering gall". Chlorophyll content in the gall tissue decreased. A steady increase of carbohydrate content in galled fruit was due to the manipulation of plant cell metabolism in galls. Increased phenolic content exerted oxidative stress in response to pathogen in the fruit cell lineages thus inhibited seed formation.

Keywords: *Alstonia scholaris;* carbohydrate; chlorophyll; pericarp; phenolic content; *Pseudophacopteran* sp.

1. INTRODUCTION

Alstonia scholaris is an elegant evergreen tree, found in most parts of India. In Ayurveda it is used as a bitter and as an astringent herb for treating skin disorders, malarial fever, urticaria, chronic dysentery, diarrhoea, in snake bite and for upper purification process of Panchakarma [1]. Small, green yet fragrant flowers of *Alstonia* appear in Autumn that develop into schizocarp fruit of 7-40 cm long. Fruits are pendulous, two lobed, dehiscent follicles, brown or green, spindle shaped and contain numerous flat, oblong brown seeds (Fig. 1). Nowadays in India, the *Alstonia scholaris* is very much infested by *Pseudophacopteran* sp (Hemiptera: Psyllidae: Phacopteronidae) forming abnormal outgrowth of

**Corresponding author: Email: sanjukta_manna@rediffmail.com;*

plant tissues known as gall similar to benign tumors or warts in animals. The insect induces perturbation in the growth mechanisms and differentiation process of the host plant, modifying the plant's architecture to its advantage [2].

Plant galls are pathologically developed cells, tissues and organs of plants like tumor, which mostly develop by hypertrophy and hyperplasy, usually under the influence of insects [3]. Growth of all gall tissues are associated with the changes in the levels of their cellular contents such as carbohydrate, proteins, nucleic acids, phenols, IAA and enzymes [4]. The Psyllidae, the gall inducing species, generally exhibit a high level of affinity to *A. scholaris*. The gall-inducing species of the Psylloidea induce different types of galls: leaf-roll galls, e.g., *Lauritrioza alacris* (Flor) [= *Trioza alacris*] (Triozidae) on *Laurus nobilis* L. (Lauraceae) [5], pit galls, e.g., *Trioza ocoteae* Houard on *Ocotea acutifolia* (Nees) Mez. (Lauraceae) [6], spherical, pouch galls, e.g., *Pseudophacopteron tuberculatum* (Crawford) (Phacopteronidae) on *Alstonia scholaris* (L.) R. Br. (Apocynaceae) [7] and spherical, closed galls, e.g., *Trioza jambolanae* Crawford on *Syzygium cumini* L. (Myrtaceae) [8]. Since, very scanty and infrequent information are available from *A. scholaris* fruit infected by psylloid herbivore worldwide. The present work revealed the structure of entomogenous fruit gall in *A. scholaris* induced by *Pseudophacopteron* sp and the histopathological changes during gall development as well as biochemical alterations of host plant tissues which respond to challenges imposed by insects as parasite in beneficial or detrimental ways [9].

2. MATERIALS AND METHODS

2.1 Collection of Developmental Stages of Insect from Galled Fruit

Fruit samples for the study were collected from the *A. scholaris* plants during July-April, consecutively two years (2017-2018, 2018-2019). Fruit samples were categorized into gall infested fruit and ungalled (healthy) fruit. Fresh and mature galled fruits were taken more or less same aged trees of the same cultivar. The galled fruits were slit along the median axis and the occupying immature nymphal stages were extracted. The live adult stages were aspirated into microfuge vials containing 70% ethanol. The nymphal stages and adult insects were prepared for permanent mounting by transferring them to warm 10% KOH solution (~ 60°C) until they turned translucent. These specimens were rinsed in 10% acetic acid and mounted in DPX and all the stages were examined microscopically (Trinocular Microscope, ZEISS).

2.2 Morphological and Histopathological Analysis of Galled Fruit

To observe nature of host damage, thin transverse sections of galled fruit were obtained for histological analysis. The thin sections were stained in Safranin & Light Green [10] and then observed under microscope (Trinocular Microscope, ZEISS).

2.3 Biochemical Assay

2.3.1 Preparation of fruit extract

For each set of experiment, one gram of ungalled and infested galled fruits (excluding the insect) were washed carefully with distilled water. The fruits were ground separately to a fine paste with a mortar and pestle and filtered through cheese clothes. Distilled water was added to each set of experiment to one gram of ground galled and ungalled fruits to reach a final volume of 10 ml for biochemical assays.

2.3.2 Total soluble sugar content

The total soluble sugar content was estimated by anthrone method [11]. In this method one gram of fresh galled and ungalled fruits were heated in 95% ethanol and homogenized. The fruit extract was filtered through charcoal. In this filtered extract, 4 ml of anthrone and sulphuric acid was added and final volume was made up to 10ml.The absorbance of the resultant blue–green solution was measured at 625 nm in the UV–visible spectrophotometer (Shimadzu UV-1800). The amount of soluble carbohydrates present in the supernatant was calculated using a standard curve prepared with D–glucose.

2.3.3 Quantitative analysis of total chlorophyll

Total chlorophyll content was estimated following standard method [12]. One gram of fresh galled and ungalled fruit samples was taken in a test tube and acetone was added to it. The tissue was ground in a mortar and pestle in the presence of excess acetone. Then the mixture was boiled for 30 minutes in water bath until the extract was free from pigment. Supernatant was collected in a separate tube and repeated the tissue extraction with acetone. Then the extract was filtered on a funnel and made up to 10ml. Measurement of chlorophyll a and b made by direct determination of absorbance at different wavelengths, using a Shimadzu Spectrophotometer. OD was measured at 645 and 663 nm and the total chlorophyll was calculated.

Fig. 1. Galled fruits of *A. Scholaris*

2.3.4 Total phenol content

The phenolic content of the fresh and infested fruits of *A. scholaris* were determined using a freshly prepared ethanolic extract of fruits and sodium carbonate and Folin-ciocalteau's reagent [13]. After reaction they were subjected to colorimetric analysis (650 nm). All experiments were repeated five times. The amount of phenol present in solution was calculated using a standard curve prepared with pyrochatechol.

2.4 Statistical Analysis

The data collected was subjected to statistical analysis using OriginLab software and their mean values were calculated. The results were presented as the mean ± S.D.

3. RESULTS AND DISCUSSION

3.1 Developmental Stages of Insect

The adult insect lays eggs on the surface of the developing fruits. Eggs are laid grouped at more than one place. The eggs appear white in colour. It is presumed that the insect along with the egg deposits some physiologic fluid which acts as a stimulant for the initiation of the gall. Lysis of the cells occurs leading to the formation of a depression. This process stimulates hypertrophic response resulting in cell division and subsequent formation of the gall. Psyllidae are hemimetabolous insects. All the instars were developed inside the fruit chamber. At the time of emergence, the exit hole was made and ultimately ruptured the fruit (Fig. 2). The nymph secreted a characteristic white waxy secretion within the gall chamber. The body of nymph was ovate with distinct thorax and abdomen. Eyes were not bulging out in immature insect (Fig. 3). The adult insect was yellowish in colour, winged and with bulging eyes (Fig. 4). Antenna in adults were filiform, tapering and straight. The terminal segment of the adult antenna included two unequal terminal setae. The wings were large and cross vein less and covered with bristles.

3.2 Morphoanatomical Changes in Fruit

The first visible change was a slight decolorization on the areas where the eggs were deposited on fruit. Chemical stimulus brought about degeneration of surrounding cells forming a small chamber within which the egg lies. Gradually the decolorized area increased in size and formed a small bulging outgrowth where the gall appeared enlarged dome shaped structure. With an increase in number of gall chambers along the fruits transformed the normal bean shaped to completely deformed knot like, gouty and tumor like structure (Fig. 5).

3.3 Histopathological Changes in Fruit

Both transverse and radial sections of ungalled healthy fruits showed a curved endosperm. Fruits were multilocular. The locules were surrounded by the pericarp and radiating to each seed. In the galled fruits, we observed many deformities. The nymph secreted resinous substances which fill the whole fruit chambers (Fig. 6). The patterns of tissue polarization and expansion in relation to their host organs through cell redifferentiation resulted in changes their functionality. During nymphal stages, the pericarp proliferated to form a "covering gall" into spherical knot like shape. Basically, a concentric chamber with hyperplasia was formed surrounding each gall maker due to rapid proliferation of pericarp (Fig. 7). The adult gall-makers opened galleries (exit channel), cutting the gall tissues with their mouthparts and leaving a fissure like structure in fruit histology (Fig. 8).

Fig. 2. Ruptured gall

Fig. 3. Nymphal stage

Fig. 4. Adult insect

Fig. 5. Fruits transformed to tumor like stucture

Fig. 6. Nymph secreted resinous substances

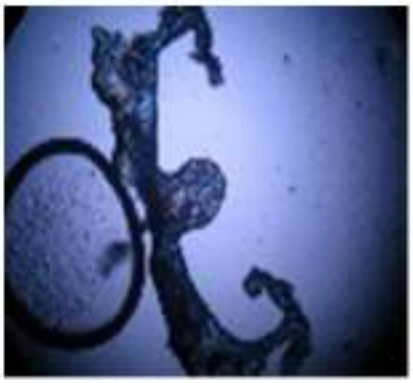

Fig. 7. Proliferation of pericarp

Fig. 8. Adult gall-makers opened galleries

3.4 Biochemical Changes

3.4.1 Chlorophyll content

The galled tissues showed a decrease in the chlorophyll content (Fig. 9) as growth of gall chamber progressed. It indicated that gall tissues typically have low photosynthetic rate and was responsible for the decolorization of the fruit. The low chlorophyll content in galled tissues was due to the loss of palisade tissues and disappearance of chloroplast [7].

3.4.2 Total sugar content

The level of sugar in the ungalled fruits and galled fruits showed a marked variation. A steady increase of sugar content was noticed in the galled fruits than in the normal fruits (Fig. 10). The galled tissue

surrounding the nymphal chamber accumulated more sugar than ungalled tissue.

3.4.3 Phenol content

Phenol concentration (Fig. 11) was higher in perforated galled fruits than ungalled healthy fruits.

Significant changes in mean of all the variables of galled fruit were noticed. The mean values of carbohydrate and phenolics were increased with the stages of galled fruits and on the other hand, chlorophyll contents were found to decrease with the maturation of the gall. The initiation and development of galls, mediated by psylloid herbivory, exposes the host plants to high oxidative stress and increases phenolic content [14-16] that may induce the production of oxidative enzymes as a defense against natural enemies.

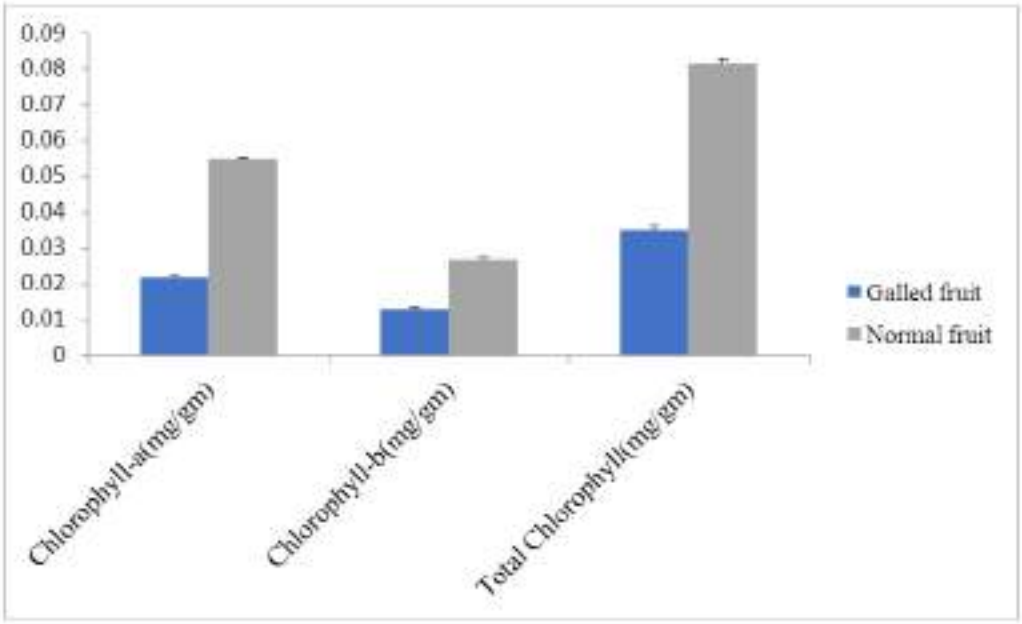

Fig. 9. Chlorophyll content of galled and normal fruit

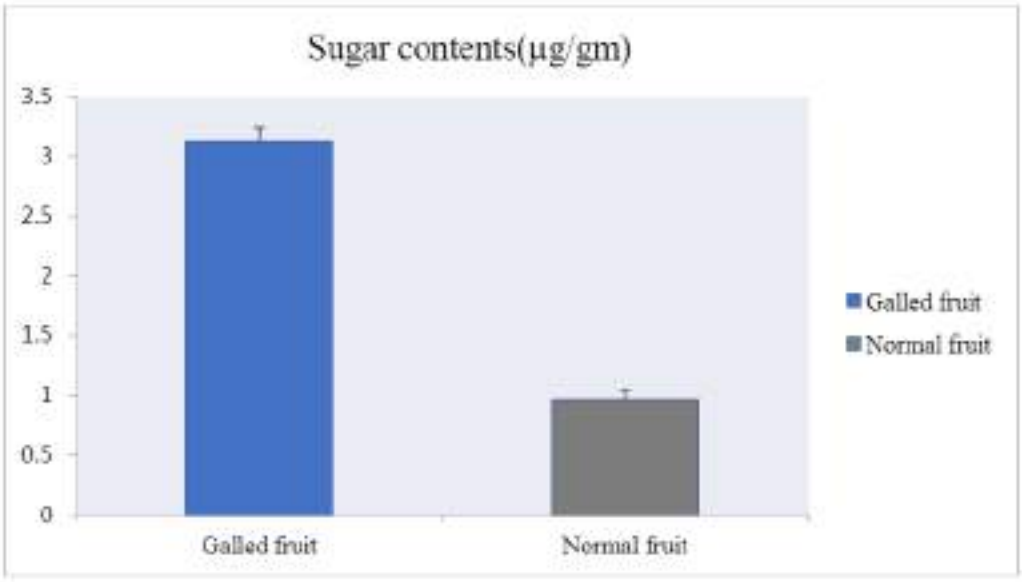

Fig. 10. Sugar content of galled and normal fruit

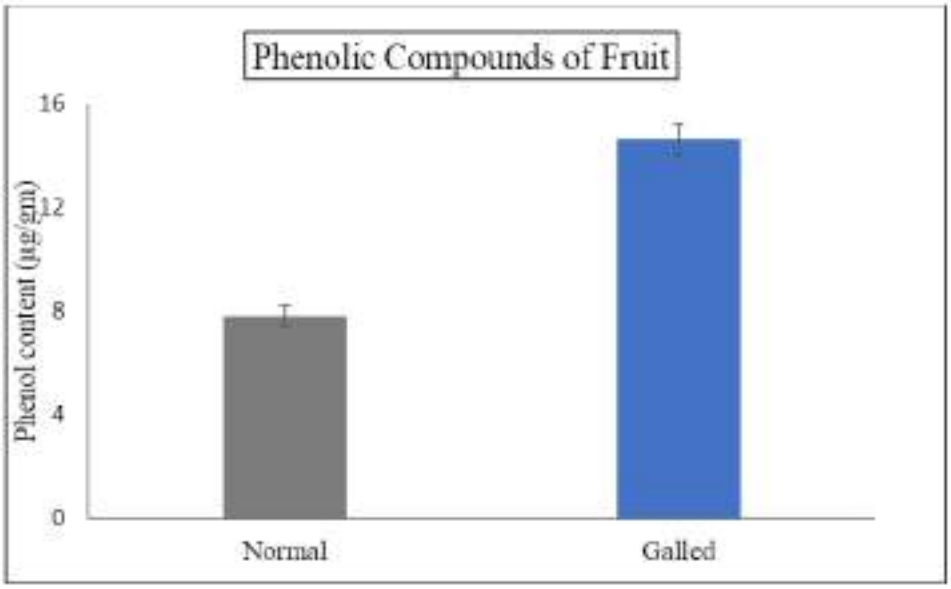

Fig. 11. Phenol content of healthy normal fruit and mature galled fruit

4. CONCLUSION

The gall insects exhibit a very large degree of specificity not only with the reference to host plants, but also to plant organs and tissues and they take advantage of host plant cellular contents mainly carbohydrates, chlorophyll and other secondary metabolites. By inducing a gall, the insect ensures nutrition and shelter for shorter or longer periods of its life. This investigation reports the biology of a psyllidae that induces gouty, ostiolate galls in fruits. This species completes one generation in six months. Feeding action of the nymph initiates the gall and morphogenetic gradients become apparent around the feeding site. The gall attains its near final gouty, knot like shape which remains plugged with some secretory resinous material. Shrinkage and dying up of cells lining the opening in the mature gall facilitates the adult emergence.

Accumulation of more sugar in gall chamber implies that these cells may be functioning as the nutritive tissues. The stimulus from gall maker redirects growth and differentiation of cells which act as a sink of nutritive substances from the host plants. Chlorophyll content of gall tissues showed a decrease as growth progressed. The low chlorophyll content in galled tissues was due to the loss of palisade tissues and is responsible for the decolorization of fruit.

The galls are not an uncontrolled tumor growth but produce an equally well-defined morphoanatomical structure and 'enemy-free', highly specialized nutritive habitat for insect parasite.

DISCLAIMER

The products used for this research are commonly and predominantly use products in our area of research and country. There is absolutely no conflict of interest between the authors and producers of the products because we do not intend to use these products as an avenue for any litigation but for the advancement of knowledge. Also, the research was not funded by the producing company rather it was funded by personal efforts of the authors.

COMPETING INTERESTS

Author has declared that no competing interests exist.

REFERENCES

1. Pratyush K, Misra CS, James J, Lipin Dev MS, Thaliyil Veettil AK, Thankamani V. Ethnobotanical and pharmacological study of *Alstonia* (Apocyanaceae)- a Review. Journal of Pharmaceutical Sciences and Research. 2011;3:1394-1403.
2. Raman A. Insect-induced plant galls of India: unresolved questions. Current Science. 2007; 92:748-757.
DOI:https://www.jstor.org/stable/24097803.
3. Mani MS. The ecology of plant galls. The Hague. The Netherlands: Walter Junk Publishers; 1964.
ISBN: 9789401762304 9401762309.
OCLC Number: 617637684: 434 pp.
4. Arya HC, Vyas GS, Tandon P. The problem of tumor formation in plants. In Form, structure

and function in plants; Prof. B.M.Johri commemoration volume (H.Y. Mohan ram, J.J.Shah and C.K.Shah,eds.). Sarita publishers, India. 1975;270-279.
5. Bouyjou B, Nguyen TX. Observations sur la morphogenèse et la structure de la galle de Trioza alacris Flor (Homoptera – Psyllidae) sur Laurus nobilis L. — Marcellia. 1974;38: 49–56.
6. Meyer J. Plant Galls and Gall Inducers. Gebrüder Borntträger, Stuttgart. 1987;291.
7. Albert S, Padhiar A, Gandhi D, Nityanand P. Morphological, anatomical and biochemical studies on the foliar galls of *Alstonia scholaris* (Apocynaceae). Revista Brasileira de Botanica. 2011;34:343–358. DOI:https://doi.org/10.1590/S0100-84042011000300009.
8. Raman A. Gall induction by hemipteroid insects. Journal of Plant Interactions. 2012;7: 29–44. DOI:https://doi.org/10.1080/17429145.2011.630847.
9. Bostock RM, Karban R, Thaler JS, Weyman PD, Gilchrist D. Signal interactions in induced resistance to pathogens and insect herbivores. European Journal of Plant Pathology. 2001;107(1):103–111. DOI:https://doi.org/10.1023/A:1008703904253
10. Sass JE. Botanica Microtechnique, 2nd Ed. The Iowa State College press, Ames , Iowa, USA. 1951;228.
11. Yemn EW, Willis AJ. The estimation of carbohydrates in plant extracts by anthrone. Biochemical Journal. 1954;57:508-514. DOI: 10.1042/bj0570508.
12. Arnon DJ. Copper enzymes in isolated chloroplasts. Plant Physiology. 1949;24:1-25. DOI: 10.1104/pp.24.1.1.
13. Bray HG, Thorpe WV. Analysis of phenolic compounds of interest in metabolism. Methods of Biochemical Analysis. 1954;1:25-52.
14. De Oliveira DC, Isaias RMS. Redifferentiation of leaflet tissues during gall midrib gall development in *Copaifera langsdorffii* (Fabaceae). South African Journal of Botany. 2010;76:239-248. DOI:10.1016/j.sajb.2009.10.011.
15. De Oliveira DC, Magalhaes TA, Carneiro RGS, Alvim MN, Isaias RMS. Do Cecidomyiidae galls of *Aspidosperma spruceanum* (Apocynaceae) fit the pre-established cytological and histochemical patterns? Protoplasma. 2010;242:81-93. DOI:10.1007/s00709-010-0128-6.
16. Shorthouse JD, Rohfritsch O (eds.). Biology of insect induced galls. Oxford University Press, New York; 1992.